Top 3 Differentials in Radiology

A Case Review

William T. O'Brien Sr.



Thieme

Top 3 Differentials in Radiology

A Case Review

Top 3 Differentials in Radiology

A Case Review

William T. O'Brien Sr., DO
Clinical Instructor in Radiology
Division of Neuroradiology
University of Cincinnati
Cincinnati, Ohio

Thieme
New York • Stuttgart

Thieme

Thieme Medical Publishers, Inc.
333 Seventh Ave.
New York, NY 10001

Executive Editor: Timothy Hiscock
Managing Editor: J. Owen Zurhellen IV
Editorial Director: Michael Wachinger
Vice President, Production and Electronic Publishing: Anne T. Vinnicombe
Production Editor: Heidi Grauel, Dovetail
Vice President, International Marketing: Cornelia Schulze
Chief Financial Officer: Peter van Woerden
President: Brian D. Scanlan
Compositor: ICC Macmillan
Printer: Everbest Printing Co.

Library of Congress Cataloging-in-Publication Data

Top 3 differentials in radiology : a case review / edited by William T. O'Brien.
p. ; cm.
Includes bibliographical references and index.
ISBN 978-1-60406-226-7
1. Diagnosis, Radioscopic. 2. Diagnosis, Differential. I. O'Brien, William T. II. Title: Top three differentials in radiology.
[DNLM: 1. Radiography--Case Reports. 2. Diagnosis, Differential--Case Reports. WN 180 T673 2009]
RC78.T66 2009
616.07'572--dc22
2009014853

Copyright © 2010 by Thieme Medical Publishers, Inc. This book, including all parts thereof, is legally protected by copyright. Any use, exploitation, or commercialization outside the narrow limits set by copyright legislation without the publisher's consent is illegal and liable to prosecution. This applies in particular to photostat reproduction, copying, mimeographing or duplication of any kind, translating, preparation of microfilms, and electronic data processing and storage.

Important note: Medical knowledge is ever-changing. As new research and clinical experience broaden our knowledge, changes in treatment and drug therapy may be required. The authors and editors of the material herein have consulted sources believed to be reliable in their efforts to provide information that is complete and in accord with the standards accepted at the time of publication. However, in view of the possibility of human error by the authors, editors, or publisher of the work herein or changes in medical knowledge, neither the authors, editors, nor publisher, nor any other party who has been involved in the preparation of this work, warrants that the information contained herein is in every respect accurate or complete, and they are not responsible for any errors or omissions or for the results obtained from use of such information. Readers are encouraged to confirm the information contained herein with other sources. For example, readers are advised to check the product information sheet included in the package of each drug they plan to administer to be certain that the information contained in this publication is accurate and that changes have not been made in the recommended dose or in the contraindications for administration. This recommendation is of particular importance in connection with new or infrequently used drugs.

Some of the product names, patents, and registered designs referred to in this book are in fact registered trademarks or proprietary names even though specific reference to this fact is not always made in the text. Therefore, the appearance of a name without designation as proprietary is not to be construed as a representation by the publisher that it is in the public domain.

Printed in China

5 4 3 2 1

ISBN 978–1-60406–226–7

Dedicated to the memory of

Robert L. Meals, DO

March 12, 1928 – June 9, 2005



© 2005 by Susan Schary

For decades, Dr. Meals inspired thousands of students while serving as:

Academic Chairman, Department of Radiology
Philadelphia College of Osteopathic Medicine
Philadelphia, Pennsylvania

Dr. Meals was more than an instructor; he was a mentor and a true friend.
To those who chose to pursue a career in radiology, he will always be a legend.
He is sorely missed but will never be forgotten.

Contents

Foreword viii

Preface ix

Acknowledgments x

Contributors xi

Section I. Chest and Cardiac Imaging 1
Editor, Bang Huynh

Section II. Gastrointestinal Imaging 53
Editor, Robert A. Jesinger

Section III. Genitourinary Imaging 105
Editor, Todd M. Johnson

Section IV. Musculoskeletal Imaging 157
Editor, Michael A. Tall

Section V. Head and Neck Imaging 209
Editor, William T. O'Brien Sr.

Section VI. Brain and Spine Imaging 261
Editor, Paul M. Sherman

Section VII. Pediatric Imaging 313
Editor, Karen M. Ayotte

Section VIII. Ultrasound Imaging 365
Editor, David J. Weitz

Section IX. Fetal Imaging 417
Editors, Erika Rubesova and Laura J. Varich

Section X. Vascular and Interventional Radiology 469
Editor, David D. Gover

Section XI. Nuclear Medicine 521
Editor, Kamal D. Singh

Section XII. Breast Imaging 573
Editor, Jessica W.T. Leung

Section XIII. Roentgen Classics 625
Editor, Grant E. Lattin Jr.

Appendix 677

Index of Differential Diagnoses 697

Index of Key Findings 705

Foreword

Technological advances are forever offering new modalities to image, reveal, and diagnose disease. Given the sheer volume of information available, residents can quickly become overwhelmed and find themselves challenged with the task of determining which knowledge is most pertinent to acquire in preparation for board examinations and general practice. With the demands of residency and daily practice, the favored books are those that are concise, take the least amount of time to read, and are most informative. Dr. O'Brien and colleagues have done exemplary work incorporating the imaging findings and developing the Top 3 differential diagnoses for the more common cases and pathology encountered in daily practice. Each case is packed with high-yield information regarding the top differential diagnoses for key radiographic findings. Further details regarding each case can be found in more comprehensive texts and review articles used as references.

Residents preparing to navigate through the oral and computer-based board examinations will find this review book rewarding and continue to refer to it throughout their careers. Seasoned radiologists will find the book a valuable asset for refreshing their memories prior to tackling recertification examinations. It is most impressive that Dr. O'Brien conceptualized and began work on this book while in residency and fellowship training. Residents, staff radiologists, and patients will certainly benefit from his tremendous accomplishment.

Peter S. Palka, DO
Chairman, Department of Diagnostic Imaging
David Grant USAF Medical Center
Travis Air Force Base, California

Preface

This case-based review book is intended primarily for radiology residents and staff physicians preparing for the initial general radiology board certification examinations, as well as more senior radiologists preparing for recertification. The case-based approach most closely resembles the format of the oral and computer-based examinations and allows for development of a reasonable list of differential diagnoses based on key imaging findings.

The book is organized into 12 core sections based on specific radiology subspecialties. Each core section is comprised of 25 unknown cases. On the first page of each case, readers are presented with radiographic images from a patient whose diagnosis is as yet unknown, along with a clinical history and image description. The first image for each case is meant to illustrate a key radiographic finding, which is the basis for the case discussion. Subsequent images may narrow the list of differential diagnoses or even lead to a single diagnosis. The second page lists the key finding, from which a list of differential diagnoses is broken down into the Top 3, along with additional diagnostic considerations. As this is primarily a board review book, the Top 3 differential diagnoses are intended for a board-type setting. Although these are also the three most common entities in the vast majority of cases, this is not always the case. The discussion section of each case provides a brief but comprehensive review of all entities on the list of differential diagnoses, making this a high-yield reference for board review. The final diagnosis for each case is provided but is not the focus of this review book. In fact, some cases have a final diagnosis which is not considered in the Top 3 differentials. Imaging pearls are provided at the end of each case to allow for a quick review of key teaching points.

The final section, titled "Roentgen Classics," contains 25 cases representing each of the previous core sections. The cases in this section have imaging findings that are so characteristic that only one diagnosis should be entertained. A detailed discussion regarding the diagnosis follows.

The concept of this book originated when I was preparing for the oral board and pilot computer-based examinations. I preferred the case-based approach but felt that most review books available at that time were lacking in terms of providing differential diagnoses. Most review books provided images and then jumped directly to a final diagnosis without describing the findings or providing differential diagnoses. The remainder provided differential diagnoses but based the entire discussion on the final diagnosis or provided only a cursory review of the other diagnoses.

I was looking for a case-based board review book that focused on the development of differential diagnoses based upon key findings and offered a high-yield discussion regarding each entity on the list of differentials. Since no such reference was available, I began compiling a list of key findings for which I would look up appropriate differential diagnoses (with help from colleagues) and then break them down into the Top 3.

Once this list was developed for all of the radiology subspecialties, it became apparent that this would make for a terrific comprehensive case-based review book. Therefore, I recruited assistance from my former residency program (David Grant USAF Medical Center) and other institutions in California that participated in the mock oral board examination we sponsored annually, including the University of California, Davis; University of California, San Francisco; and Stanford University. I also recruited a few individuals from the University of Cincinnati where I completed my neuroradiology fellowship. The end result of much hard work and dedication is this comprehensive case-based board review book.

I hope that you find this book useful. My goal was to design the book that I wish I had when preparing for the board examinations. Thanks to the efforts of all of the contributors, I believe we accomplished that goal.

I wish you the best of luck on your board examinations and your future endeavors in radiology.

William T. O'Brien Sr., DO

Acknowledgments

First and foremost, I would like to thank the section editors and case authors for the time and effort they put into this project. Nearly all contributors have a current or past affiliation with David Grant USAF Medical Center; University of California, Davis; University of California, San Francisco; Stanford University; and the University of Cincinnati. This book would not have been possible without their significant contributions. They offered their time and expertise to create a tremendous reference for residents and staff radiologists preparing to take the board examinations.

In addition, I would like to thank the individuals and institutions who volunteered images for cases throughout this text. In particular, I would like to thank Drs. Ronald Cohen, Bamidele Kammen, Kenneth Martin, and Paul Nancarrow from the Children's Hospital and Research Center Oakland and Drs. Rebecca Cornelius and Cristopher Meyer from the University of Cincinnati for contributing numerous cases from their personal teaching files. I would also like to thank the radiology departments at the University of Cincinnati and Cincinnati Children's Hospital Medical Center for contributing images from their department teaching files, particularly Drs. Jonathan Moulton, Susan Braley, and the late Howard Fiegelson. Several of the section editors supplied images not only for their section but for other sections, especially Drs. Robert Jesinger and Paul Sherman who contributed numerous cases from their personal teaching files.

Several individuals assisted with researching and verifying differential diagnoses for the key radiographic findings. These include Drs. Grant Lattin, Jr., Jeffrey Tan, Edward Yi, Paul DiDomenico, Evan Moser, John Lichtenberger, Arash Momeni, James Odone, Brian Johnston, and Henry Woods. Mr. Gil Gardner, medical illustrator, created illustrations used to highlight teaching points within selected cases. The cover is adapted from a proposal by Mrs. Asseneth Singh, graphic designer, who volunteered her time and talents to design the original cover of this text, focusing on the concept of the Top 3 differential diagnoses.

I believe that one of the noblest contributions radiologists can make to our profession is to pass along their knowledge and expertise to the next generation of radiologists. To that end, I wish to thank the late Robert L. Meals, DO, for inspiring me to pursue a career in radiology. I am also indebted to the radiology staff where I completed my residency (David Grant USAF Medical Center) and fellowship (University of Cincinnati and Cincinnati Children's Hospital Medical Center) training. It was an honor to train at such exemplary institutions.

Last and most importantly, I am forever grateful to my family for their continuous love and support, as well as the sacrifices they made during the completion of this project. I have been blessed with a wonderful wife; two sons, Patrick and William (Liam); and a daughter, Shannon. Annie is the love of my life, and I cherish each moment we have together. We are fortunate to have three children who make us proud to be their parents on a daily basis. I will never be able to thank you enough for all that you do.

Contributors

M. Jason Akers, MD
Clinical Instructor in Radiology
University of Cincinnati
Cincinnati, Ohio

Karen M. Ayotte, MD*
Chief, Pediatric Imaging
David Grant USAF Medical Center
Travis AFB, California

Natasha Brasic, MD
Department of Radiology and Biomedical Imaging
University of California, San Francisco
San Francisco, California

Cam Chau, MD
Department of Diagnostic Imaging
UC Davis Medical Center
Sacramento, California

Chloe M. Chhor, MD
Department of Radiology
University of California, San Francisco
San Francisco, California

Boon Chye Ching, MBBS, FRCR (UK), MMED
Diagnostic Imaging
National Cancer Centre
Singapore

Daniel G. Church, MD
Clinical Fellow in Radiology
Lucile Packard Children's Hospital
Stanford, California

Matthew R. Denny
Department of Biology
Washington University
St. Louis, Missouri

Paul B. DiDomenico, MD*
Department of Diagnostic Imaging
David Grant USAF Medical Center
Travis AFB, California

Eva Escobedo, MD
Professor of Radiology
UC Davis Medical Center
Sacramento, California

Hedieh K. Eslamy, MD
Clinical Fellow in Radiology
Lucile Packard Children's Hospital
Stanford, California

Cameron C. Foster, MD
Assistant Professor of Radiology
UC Davis Medical Center
Sacramento, California

Sonia Kaur Ghei, MD
Department of Diagnostic Imaging
UC Davis Medical Center
Sacramento, California

David D. Gover, MD*
Chief, Vascular and Interventional Radiology
David Grant USAF Medical Center
Travis AFB, California

Philip Granchi, MD
Department of Diagnostic Imaging
UC Davis Medical Center
Sacramento, California

Bo Yoon Ha, MD
Clinical Fellow in Radiology
Lucile Packard Children's Hospital
Stanford, California

Bang Huynh, MD*
Chief, Thoracic Imaging
David Grant USAF Medical Center
Travis AFB, California

Robert A. Jesinger, MD*
Director, Radiology Residency Program
David Grant USAF Medical Center
Travis AFB, California

Todd M. Johnson, MD*
Chief, Abdominal Imaging
David Grant USAF Medical Center
Travis AFB, California

Brian S. Johnston, MD*
Department of Diagnostic Imaging
David Grant USAF Medical Center
Travis AFB, California

Michael C. Kuo, MD
Clinical Fellow, Abdominal Imaging
UC Davis Medical Center
Sacramento, California

Grant E. Lattin Jr., MD*
Assistant Professor of Radiology
Uniformed Services University of the Health Sciences
Bethesda, Maryland

Jessica W.T. Leung, MD
Medical Director, Breast Health Center
California Pacific Medical Center
San Francisco, California

John P. Lichtenberger III, MD*
Department of Diagnostic Imaging
David Grant USAF Medical Center
Travis AFB, California

Shaun Loh, MD, MBA
Department of Diagnostic Imaging
UC Davis Medical Center
Sacramento, California

Michael A. Mahlon, DO*
Department of Diagnostic Imaging
Landstuhl Regional Medical Center
Landstuhl, Germany

Frederick R. Margolin, MD
Breast Health Center
California Pacific Medical Center
San Francisco, California

Arash J. Momeni, MD*
Department of Diagnostic Imaging
David Grant USAF Medical Center
Travis AFB, California

Wayne L. Monsky, MD, PhD
Assistant Professor of Radiology
UC Davis Medical Center
Sacramento, California

Matthew J. Moore, MD
Clinical Instructor in Neuroradiology
University of Cincinnati
Cincinnati, Ohio

Sima Naderi, MD
Assistant Professor of Radiology
UC Davis Medical Center
Sacramento, California

Vicki E. Nagano, MD
Department of Nuclear Medicine
Kaiser Sacramento
Sacramento, California

William T. O'Brien Sr., DO
Clinical Instructor in Radiology
University of Cincinnati
Cincinnati, Ohio

James B. Odone, MD*
Department of Diagnostic Imaging
David Grant USAF Medical Center
Travis AFB, California

Eleanor L. Ormsby, MD, MPH
Chief Resident, Diagnostic Imaging
UC Davis Medical Center
Sacramento, California

Anokh Pahwa, MD
Department of Diagnostic Imaging
UC Davis Medical Center
Sacramento, California

Chirag V. Patel, MD
Assistant Professor of Radiology
UC Davis Medical Center and
Children's Hospital
Sacramento, California

Glade E. Roper, MD
Department of Diagnostic Imaging
UC Davis Medical Center
Sacramento, California

Erika Rubesova, MD
Clinical Assistant Professor of
Radiology
Lucile Packard Children's Hospital
Stanford, California

Thomas Ray S. Sanchez, MD
Assistant Professor of Radiology
UC Davis Medical Center and
Children's Hospital
Sacramento, California

Paul M. Sherman, MD*
Chief, Neuroradiology
David Grant USAF Medical Center
Travis AFB, California

Kamal D. Singh, MD*
Chief, Nuclear Medicine
David Grant USAF Medical Center
Travis AFB, California

Arvind Sonik, MD
Department of Diagnostic Imaging
UC Davis Medical Center
Sacramento, California

Rebecca Stein-Wexler, MD
Director, Radiology Residency
Program
UC Davis Medical Center
Sacramento, California

Corinne D. Strickland, MD
Department of Diagnostic Imaging
University of Arizona College of
Medicine
Tucson, Arizona

Joyce F. Sung, MD
Maternal Fetal Medicine Fellow
Lucile Packard Children's Hospital
Stanford, California

Michael A. Tall, MD*
Chief, Magnetic Resonance Imaging
Wilford Hall Medical Center
Lackland AFB, Texas

Jeffrey P. Tan, MD*
Department of Diagnostic Imaging
48th Medical Group
RAF Lakenheath, United Kingdom

Adrianne K. Thompson, MD*
Chief, Body Imaging
Wilford Hall Medical Center
Lackland AFB, Texas

Charles A. Tujo, MD*
Deputy Chief of Radiology
Landstuhl Regional Medical Center
Landstuhl, Germany

Laura J. Varich, MD
Clinical Associate Professor of Radiology
Lucille Packard Children's Hospital
Stanford, California

David J. Weitz, MD*
Chief, Ultrasound Imaging
David Grant USAF Medical Center
Travis AFB, California

Sandra L. Wootton-Gorges, MD
Director of Pediatric Imaging
UC Davis Medical Center and
Children's Hospital
Sacramento, California

Charlyne Wu, MD
Department of Diagnostic Imaging
UC Davis Medical Center
Sacramento, California

Philip Yen, MD
Department of Diagnostic Imaging
UC Davis Medical Center
Sacramento, California

Adam J. Zuckerman, DO
Clinical Instructor in Neuroradiology
University of Cincinnati
Cincinnati, Ohio

* The views expressed in this material are those of the authors and do not reflect the official policy or position of the U.S. government, the Department of Defense, the Department of the Air Force, or the Department of the Army.

Section I Chest and Cardiac Imaging

Case 1

Arash J. Momeni

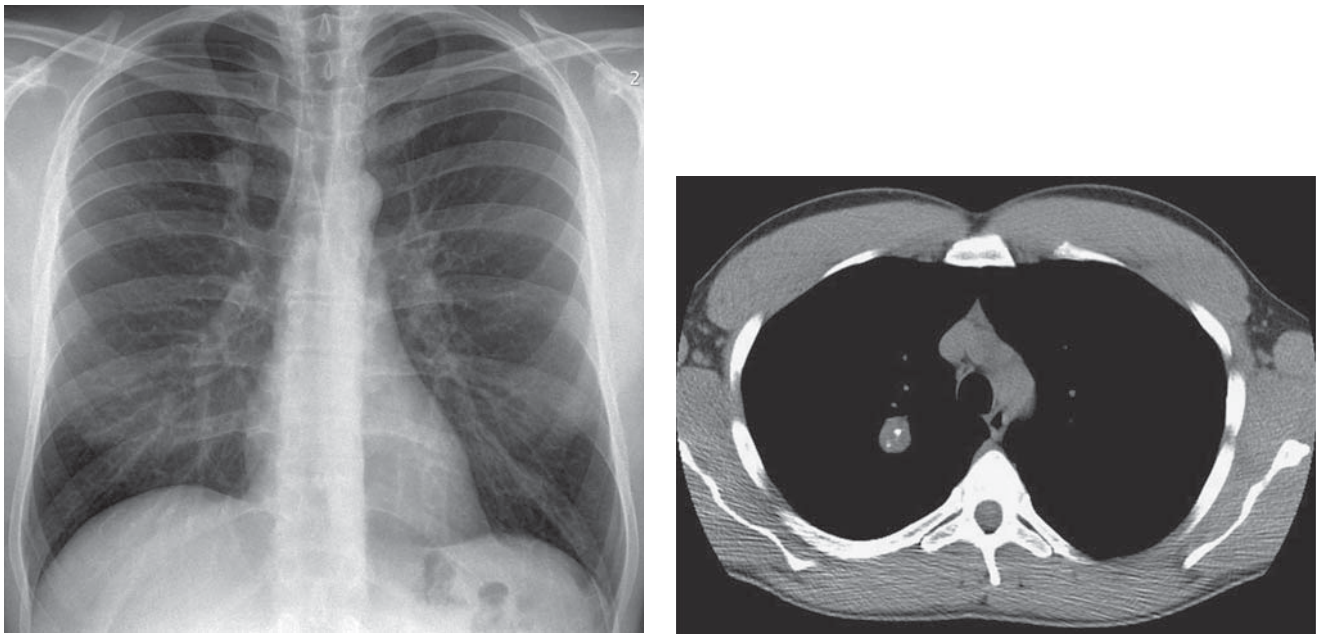


Fig. 1.1 **(A)** Frontal radiograph of the chest demonstrates a circumscribed pulmonary nodule within the right upper lobe. **(B)** Unenhanced computed tomography image through the upper chest reveals a circumscribed right upper lobe pulmonary nodule with regions of coarse calcification and macroscopic fat. (Courtesy of Matthew D. Duncan, MD.)

Clinical Presentation

A 43-year-old asymptomatic man presents for preoperative evaluation (**Fig. 1.1**).

Key Imaging Finding

Solitary pulmonary nodule

Top 3 Differential Diagnoses

- **Granuloma.** Granulomas are produced secondary to an infectious or inflammatory process, such as tuberculosis, fungal disease, or vasculitides. They present radiographically as solitary or multiple pulmonary nodules. If benign patterns of calcification are identified (central, diffuse, popcorn, or laminated), no further workup is necessary. Eccentric or speckled calcifications, by contrast, are suspicious for a neoplastic process until proven otherwise. Calcified hilar and mediastinal lymph nodes are commonly seen with granulomatous disease.
- **Neoplasm.** Both primary bronchogenic carcinoma and metastatic disease may present as a solitary pulmonary nodule or mass (>3 cm). Irregular borders or suspicious calcifications suggest neoplasm over granulomatous disease. Adenocarcinoma (including its subtype bronchioloalveolar carcinoma) characteristically presents in a peripheral location and is considered the most common primary malignant lung neoplasm. Squamous cell and small cell carcinoma are associated with smoking and tend to occur centrally. Squamous cell carcinoma has a proclivity to cavitate. Small cell carcinoma typically presents as a perihilar mass with associated lymphadenopathy. Large cell carcinoma is relatively uncommon and presents peripherally. Although typically multiple, metastatic disease may present as a solitary pulmonary nodule.
- **Hamartoma.** Hamartomas are composed of normal tissue assembled in a disorganized fashion. They are the most common benign tumor of the lung, accounting for 5 to 10% of solitary pulmonary nodules. Classically, they are well-defined, solitary masses <4 cm in diameter. Focal deposits of macroscopic fat, in addition to a benign pattern of calcification (typically popcorn), are most helpful in making the diagnosis.

Additional Differential Diagnoses

- **Round pneumonia.** Typically seen in pediatric patients younger than 8 years of age, pneumonia may have a rounded masslike appearance. It is due to centrifugal spread of the rapidly replicating bacteria through the pores of Kohn and canals of Lambert from a single primary focus in the lung.
- **Arteriovenous malformation (AVM).** AVMs are fistulous vascular communications between a pulmonary or systemic artery and a pulmonary vein. When multiple, nearly 90% are associated with Osler-Weber-Rendu disease (hereditary hemorrhagic telangiectasis), characterized clinically by epistaxis, telangiectasia of the skin and mucous membranes, and gastrointestinal bleeding. Although usually congenital, AVMs may be acquired in the setting of cirrhosis, trauma, or certain infections. Radiographically, they are well-defined, avidly enhancing nodules or masses with an enlarged feeding artery and a draining vein. It is critical to prospectively identify AVMs, because inadvertent biopsy can have catastrophic consequences. These lesions are typically treated with embolization (coils or detachable balloons).

Diagnosis

Hamartoma

✓ Pearls

- Benign calcification patterns for a pulmonary nodule are central, diffuse, popcorn, and laminated.
- Malignant features are irregular borders, suspicious calcifications, and eccentric soft tissue mass.
- Evaluation for fat should rely on visible fat, not Hounsfield values, which may be falsely low from averaging with air.

Suggested Readings

Collins J, Stern EJ. Chest Radiology: The Essentials. Philadelphia: Lippincott Williams & Wilkins; 2007

McLoud TC. Thoracic Radiology: The Requisites. St. Louis: Mosby; 1998

Case 2

Philip Yen

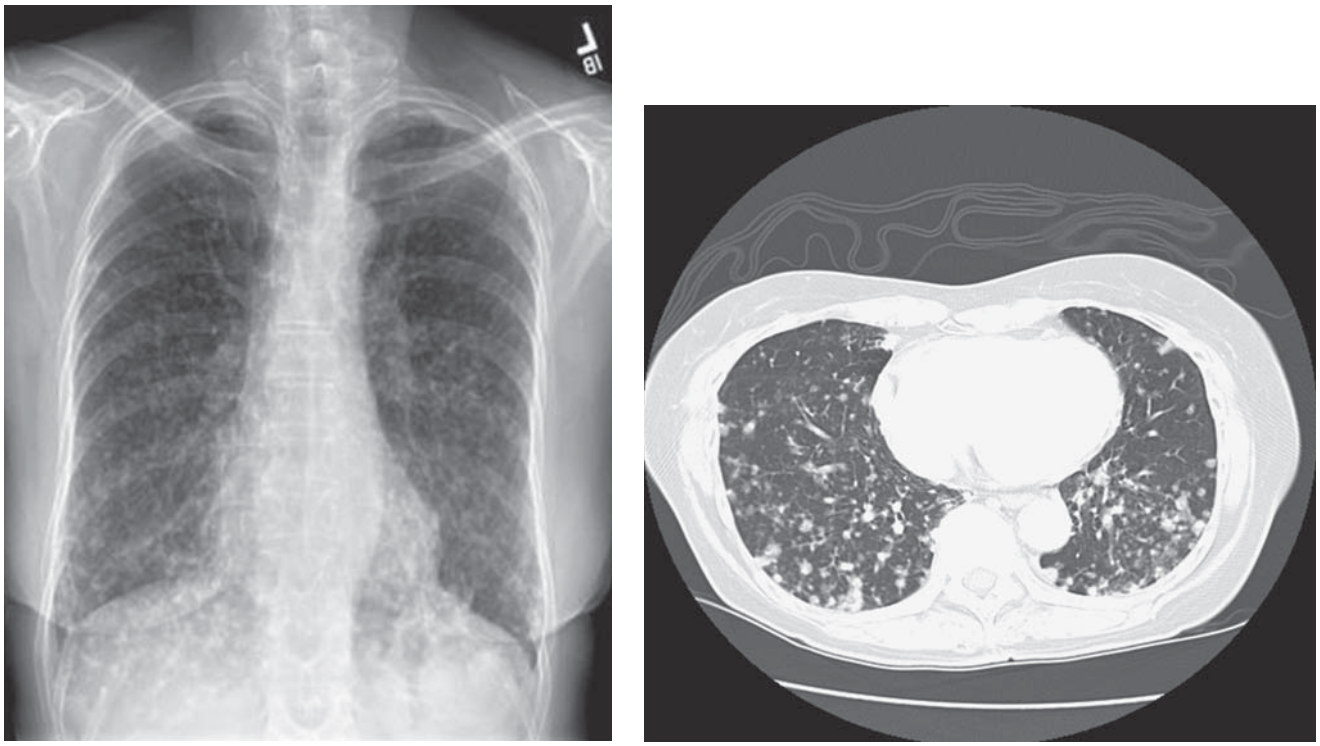


Fig. 2.1 **(A)** Posteroanterior chest radiograph shows multiple diffuse bilateral nodules in all lobes. **(B)** Contrast-enhanced axial computed tomography image in the lung window demonstrates multiple lung nodules of varying sizes.

Clinical Presentation

A 56-year-old man presents with a cough (**Fig. 2.1**).

Key Imaging Finding

Multiple pulmonary nodules

Top 3 Differential Diagnoses

- **Metastatic disease.** The majority of patients with multiple metastatic nodules have a known primary neoplasm. Although nodules can be found anywhere in the lung, as they are primarily spread hematogenously, they tend to favor the lung bases due to the increased blood flow seen there as compared with the upper lobes. Many times nodules may vary in size reflecting separate episodes of metastases or varying growth rates. Nodules can be small and numerous or large "cannonball" lesions, which are generally seen with gastrointestinal and genitourinary primary malignancies.
- **Granulomatous disease (tubercular or fungal).** Mycobacterium tuberculosis is an aerobic bacterium that disseminates by inhalation of airborne respiratory droplets. Primary and secondary (reactivation) patterns of pulmonary involvement may be seen. Hematogenous spread of the disease results in multiple 1 to 2 mm nodules dispersed in a random distribution. Common fungal causes of multiple granulomatous nodules include histoplasmosis and coccidioidomycosis, both of which may manifest with a miliary pattern accompanied by hilar and/or mediastinal adenopathy.
- **Septic emboli.** Patients usually have a concomitant history of intravenous drug abuse, bacterial endocarditis, or other source of systemic infection. Patients present with multiple bilateral nodules that tend to be peripheral and well defined. A vessel may be identified coursing directly into the center of a nodule, termed the "feeding vessel sign" thought to represent the hematogenous source of the nodule. This sign is not specific for septic emboli, as it may also be seen in metastatic disease.

Additional Differential Diagnoses

- **Wegener syndrome.** Wegener granulomatosis is a vasculitis that affects multiple organs, including the kidneys, upper and lower airways, and lungs. Detection of serologic markers such as antineutrophil cytoplasmic antibodies (c-ANCAs) frequently aids in diagnosis. Pulmonary manifestations include multiple lung nodules that may range from 2 to 10 cm. These nodules may cavitate and appear thick-walled with air-fluid levels. A history of multiple sinus infections is common.
- **Rheumatoid arthritis (RA).** The most common pulmonary manifestation of RA is a pleural effusion. Rheumatoid nodules are not a common presentation of RA, but when they do occur, they can be as small as 2 mm or as large as 5 cm. Nodules may be solitary or multiple and usually are peripheral and well defined. Of particular note is the tendency to disappear with successful therapy as subcutaneous rheumatoid nodules heal.

Diagnosis

Metastatic disease

✓ Pearls

- Due to blood flow, hematogenous spread (whether of infection or neoplasm) tends to favor lower lobes.
- Tuberculosis (TB) and fungal infections can have very similar imaging features; TB may be primary or secondary.
- Septic emboli occur in patients with intravenous drug abuse, endocarditis, or systemic infections and may cavitate.
- The majority of RA patients have musculoskeletal manifestations prior to pulmonary involvement.

Suggested Readings

Collins J, Stern EJ. Chest Radiology: The Essentials. Philadelphia: Lippincott Williams & Wilkins; 2007

Mettler FA. Essentials of Radiology. Philadelphia: Saunders; 2005

Webb R, Higgins C. Thoracic Imaging: Pulmonary and Cardiovascular Radiology. Philadelphia: Lippincott Williams & Wilkins; 2005

Case 3

Philip Yen

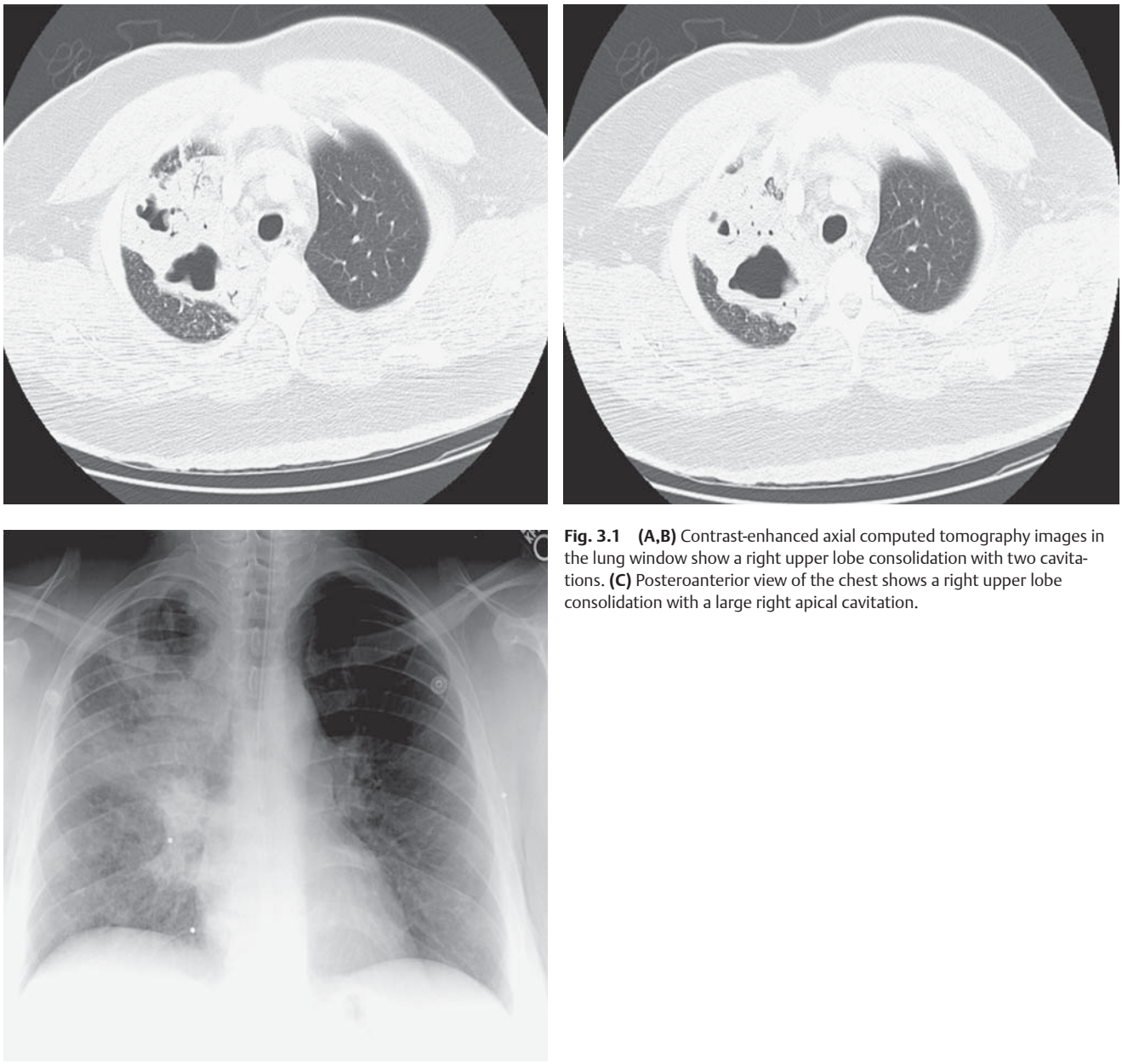


Fig. 3.1 **(A,B)** Contrast-enhanced axial computed tomography images in the lung window show a right upper lobe consolidation with two cavitations. **(C)** Posteroanterior view of the chest shows a right upper lobe consolidation with a large right apical cavitation.

Clinical Presentation

A 40-year-old man presents with fever, night sweats, hemoptysis, and weight loss (**Fig. 3.1**).

Key Imaging Finding

Cavitary pulmonary mass

Top 3 Differential Diagnoses

- **Tuberculosis (TB).** Primary TB may be asymptomatic or present with lobar air-space consolidations. Cavitations are unusual in this phase but can occasionally be found. Reactivation disease presents clinically with night sweats, fever, and weight loss. Radiographically, this phase manifests as multiple cavitations, reflecting the increased inflammation and necrosis. These are predominantly in the upper lobes, where the higher oxygen tension enables the aerobic bacterium to thrive and where lymphatic clearance is less than that of the lower lobes.
- **Fungal disease.** The most common fungal causes of cavitary lesions are the endemic fungi. Histoplasmosis is endemic to the Ohio and Mississippi River valleys. It particularly favors the nitrogen-rich soil found in bat or avian guano-laden areas, such as caves and chicken houses. Coccidioidomycosis, a soil-born fungus, is endemic to the southwestern United States and is spread by inhalation.
- **Squamous cell carcinoma (primary or metastatic).** Approximately 30% of all primary lung cancers arise from primary squamous cell carcinoma (SCC). It is typically located centrally with involvement of hilar or mediastinal lymph nodes. Patients frequently have a history of smoking. Metastatic SCC originates from a head and neck primary or cervical cancer in women. SCC commonly cavitates.

Additional Differential Diagnoses

- **Pyogenic infection (pulmonary abscess, septic emboli).** Staphylococcus aureus is the most common bacterial infection to result in cavitation. It typically causes a widespread consolidation and may lead to cavitation and abscess formation. In the setting of multiple widespread cavities, a source of showering septic emboli should be considered.
- **Wegener disease.** Wegener disease is a multiorgan vasculitis that affects the airways, lungs, and kidneys. Patients present with sinus disease, along with cough and hemoptysis. Serum antineutrophil cytoplasmic antibodies (c-ANCAs) are frequently detected. The most common pulmonary manifestations are multiple lung nodules, followed by air-space consolidations, ground glass opacities, and thick-walled cavitations.
- **Rheumatoid arthritis (RA).** Although not a common manifestation, RA occasionally can present with well-defined pulmonary nodules that tend to cavitate. The lesions commonly regress with treatment of the underlying disease process.

Diagnosis

Reactivation TB

✓ Pearls

- Cavitation within the upper lobes and superior segment involvement is associated with postprimary TB.
- SCC has a stronger association with smoking than does adenocarcinoma.
- SCC (primary or secondary) commonly cavitates.
- Wegener disease is a vasculitis that affects the airways, lungs, and kidneys; pulmonary nodules cavitate.

Suggested Readings

Collins J, Stern EJ. Chest Radiology: The Essentials. Philadelphia: Lippincott Williams & Wilkins; 2007

Erasmus JJ, Connolly JE, McAdams HP, et al. Solitary pulmonary nodules: 1. Morphologic evaluation for differentiation of benign and malignant lesions. Radiographics 2000;20:43-58

Webb R, Higgins C. Thoracic Imaging: Pulmonary and Cardiovascular Radiology. Philadelphia: Lippincott Williams & Wilkins; 2005

Case 4

John P. Lichtenberger III

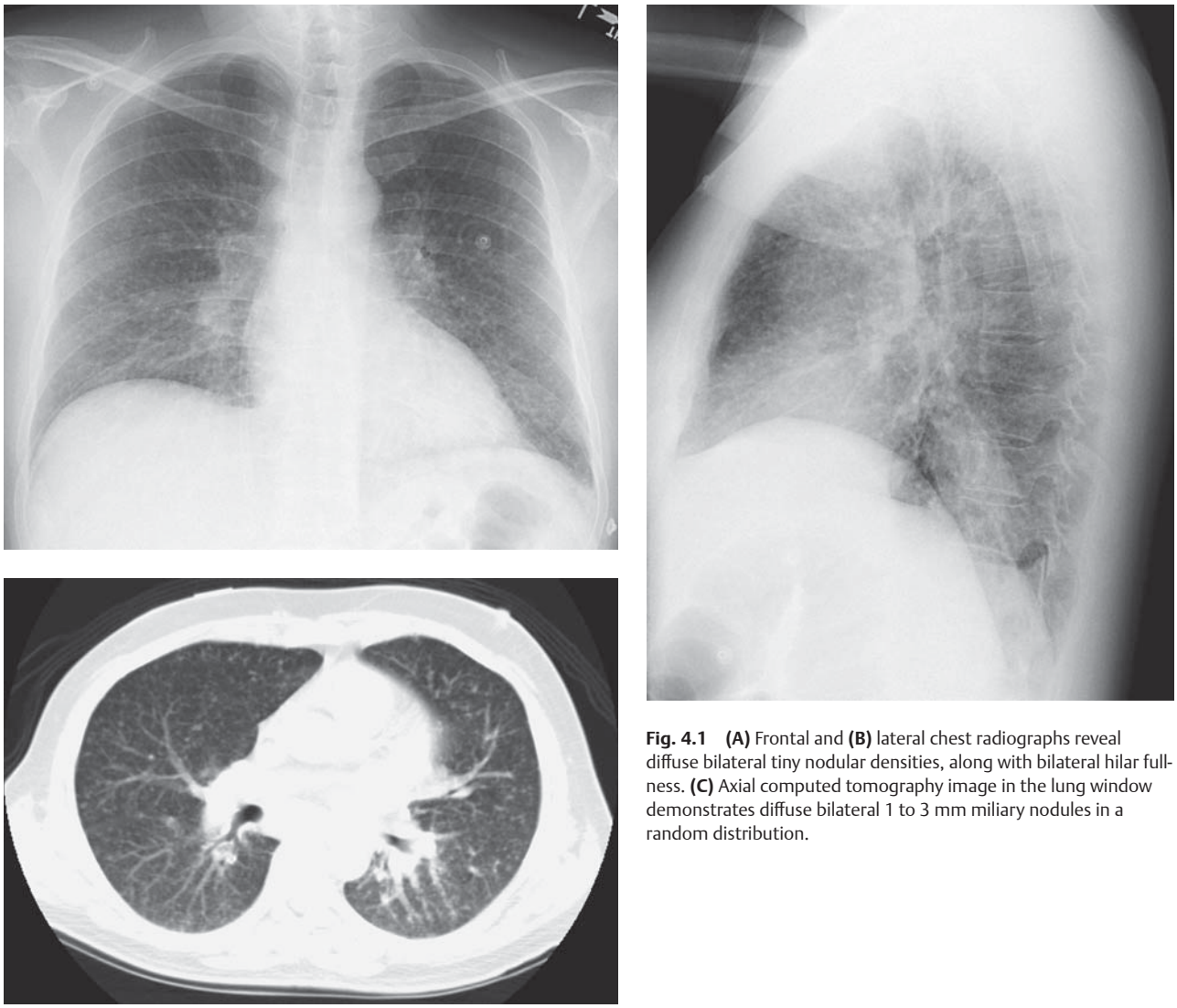


Fig. 4.1 **(A)** Frontal and **(B)** lateral chest radiographs reveal diffuse bilateral tiny nodular densities, along with bilateral hilar fullness. **(C)** Axial computed tomography image in the lung window demonstrates diffuse bilateral 1 to 3 mm miliary nodules in a random distribution.

Clinical Presentation

A 28-year-old immunocompromised patient presents with a chronic cough (**Fig. 4.1**).

Key Imaging Finding

Miliary pulmonary nodules

Top 3 Differential Diagnoses

- **Tuberculosis (TB).** Pulmonary infection with mycobacterium TB is classified as primary or reactivation based on clinical and radiographic features. Primary TB is predominantly a lower lobe air-space disease; mediastinal lymphadenopathy and pleural effusions are typical radiographic manifestations of primary infection. Reactivation TB, on the other hand, characteristically presents as upper lobe consolidation with regions of cavitation and fibrosis or endobronchial spread with ill-defined centrilobular opacities in a "tree in bud" configuration. Hematogenous spread presents with randomly distributed 1 to 3 mm nodules, referred to as a miliary pattern. The miliary pattern is more common in children, the elderly, and immunocompromised patients (human immunodeficiency virus, transplant, etc.).
- **Fungal disease.** Fungal infection in the lung encompasses both primary infection in immunocompetent patients (e.g., *Histoplasma, Coccidioides,* and *Blastomycosis*) and opportunistic infection in immunosuppressed patients (e.g., *Aspergillus, Candida,* and *Cryptococcus*). Although radiographic features are somewhat organism dependent, disseminated fungal infection can result in a miliary pattern identical to miliary TB.
- **Metastatic disease.** Although hematogenous metastases to the lung may occur with numerous primary malignancies, thyroid carcinoma, renal cell carcinoma, and melanoma are the most common primary malignancies to produce a miliary pattern of dissemination in the chest.

Additional Differential Diagnoses

- **Pneumoconiosis.** Pneumoconiosis results from inhalation of particulate matter as a result of occupational exposure. Silicosis and coal workers' pneumoconiosis are among the most common entities. Radiographic findings consist of multiple upper lobe fibrotic nodules ranging from 1 to 10 mm in size. When small, the appearance mimics that of miliary disease processes. As the disease progresses, fibrosis ensues, and the nodular densities coalesce. Eggshell calcifications may be seen within hilar and mediastinal lymph nodes. A late complication referred to as progressive massive fibrosis presents radiographically as upper lobe masslike opacities in the setting of underlying fibrosis. Patients are at an increased risk of superinfection, especially TB.
- **Healed varicella.** Acute varicella pneumonia is a severe form of primary infection that occurs primarily in children and pregnant women. The infection presents as multifocal regions of patchy air-space disease, and affected patients are very ill. Healed varicella presents radiographically as calcified miliary pulmonary nodules in a random distribution.

Diagnosis

Fungal disease (Coccidioidomycosis)

✓ Pearls

- Miliary spread of TB is most common in children, the elderly, and immunocompromised patients.
- Disseminated fungal disease may present with a miliary pattern; coccidioidomycosis can cavitate.
- Thyroid carcinoma, renal cell carcinoma, and melanoma are the most common primary neoplasms with a miliary pattern.
- There is a fulminant form of silicosis, silicoproteinosis, but most cases develop decades after exposure.

Suggested Readings

Collins J, Stern EJ. Chest Radiology: The Essentials. Philadelphia: Lippincott Williams & Wilkins; 2007

McLoud TC. Thoracic Radiology: The Requisites. St Louis: Mosby; 1998

Case 5

Paul B. DiDomenico

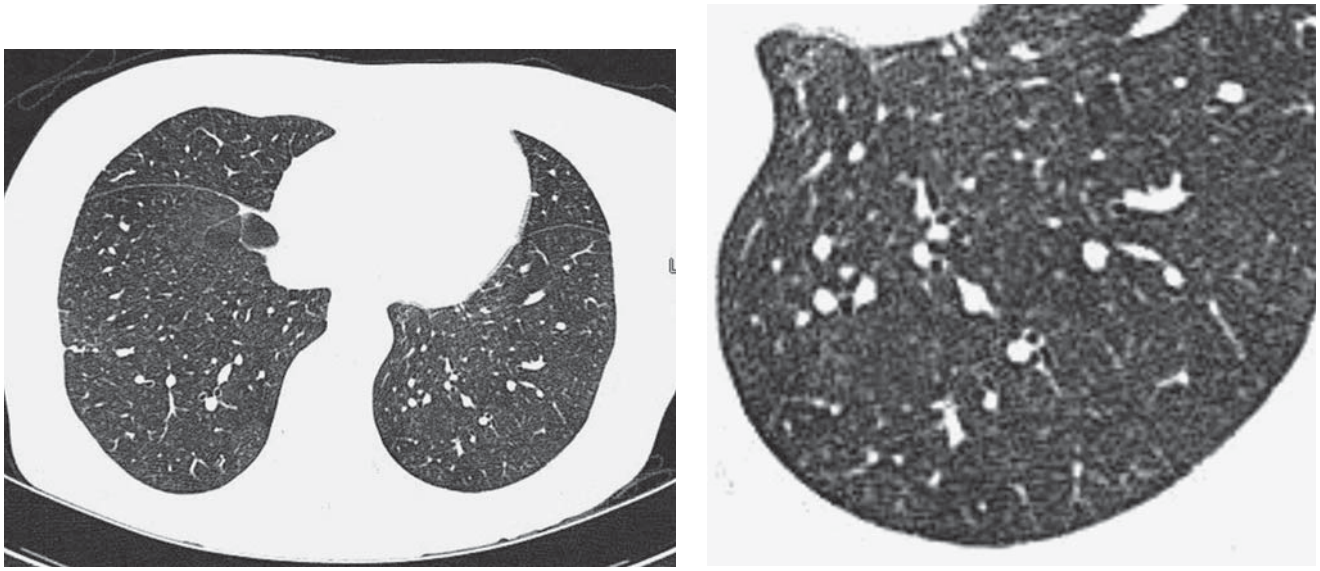


Fig. 5.1 **(A)** Axial computed tomography image through the chest and **(B)** coned-down view of the left lower lobe in the lung window reveal diffuse bilateral ill-defined centrilobular ground-glass nodules. (Courtesy of Cristopher Meyer, MD, University of Cincinnati.)

Clinical Presentation

A 50-year-old woman presents with a cough and shortness of breath (**Fig. 5.1**).

Key Imaging Finding

Centrilobular pulmonary nodules

Top 3 Differential Diagnoses

- **Infectious bronchiolitis (*Mycobacterium avium-intracellulare* [MAI], tuberculosis [TB]).** Infection from both tuberculous and nontuberculous mycobacterial (NTMB) organisms may manifest as numerous small nodular opacities centered on the bronchiole of the secondary pulmonary lobule with sparing of the subpleural space (centrilobular nodules). Numerous species of mycobacteria are ubiquitous in the environment, but MAI and *Mycobacterium kansii* account for most nontuberculous infections. A pattern of clustered nodules with branching opacities (so-called tree in bud pattern) in the lingula and right middle lobe is typical of MAI and is often seen in elderly women; this pattern is termed "Lady Windermere" syndrome. NTMB infections may be indistinguishable from postprimary (reactivation) TB.
- **Hypersensitivity pneumonitis (HP).** Also known as extrinsic allergic alveolitis, HP results from exposure to environmental antigens inhaled as dust particles. Varying sources of organic dusts may result in farmer's lung (moldy hay), bird fancier's lung (avian proteins), or humidifier lung (thermophilic bacteria), which are indistinguishable radiographically. Following exposure, the acute phase may exhibit fine nodular or ground-glass opacities. Centrilobular nodules with ground-glass opacities are typical of the subacute phase of the disease, most often in the middle to lower lung zones. If exposure continues, there may be progression to end-stage lung disease with fibrosis.
- **Endobronchial spread of tumor.** Metastatic spread of tumors within the chest may take a variety of routes, including direct, hematogenous, lymphatic, and endobronchial spread. Although hematogenous spread is the most common form of widespread dissemination, endobronchial spread is also possible in late stages of disease and may manifest as centrilobular nodules in any part of the lung.

Additional Differential Diagnoses

- **Respiratory bronchiolitis–associated interstitial lung disease (RB-ILD).** RB-ILD is usually seen in smokers 30 to 50 years of age. Findings on computed tomography include either upper lobe predominant or diffuse centrilobular nodules, representing accumulated pigmented macrophages, with patchy ground-glass opacities.
- **Pneumoconiosis.** Silicosis and coal workers' pneumoconiosis result from occupational exposure and present as upper lobe–predominant interstitial lung diseases. Either perilymphatic or centrilobular nodules may be present, which may eventually coalesce to form masslike opacities and may calcify. Involved lymph nodes may also calcify peripherally, resulting in a characteristic "eggshell" appearance. Late findings may include fibrosis with peripheral emphysema (progressive massive fibrosis).

Diagnosis

Hypersensitivity pneumonitis

✓ Pearls

- Mycobacteria are common causes of infectious bronchiolitis; a "tree in bud" appearance is characteristic.
- HP results from exposure to inhaled antigens; centrilobular nodules and ground-glass opacities are typical.
- Endobronchial spread of tumor occurs in late stages of malignancy and may involve any part of the lung.
- RB-ILD is a smoking-related process with diffuse or upper lobe–predominant centrilobular nodules.

Suggested Readings

Collins J, Stern EJ. Chest Radiology: The Essentials. Philadelphia: Lippincott Williams & Wilkins; 2007

Webb WR, Muller NL, Neidich DP. High-Resolution CT of the Lung. Philadelphia: Lippincott Williams & Wilkins; 2000

Case 6

John P. Lichtenberger III

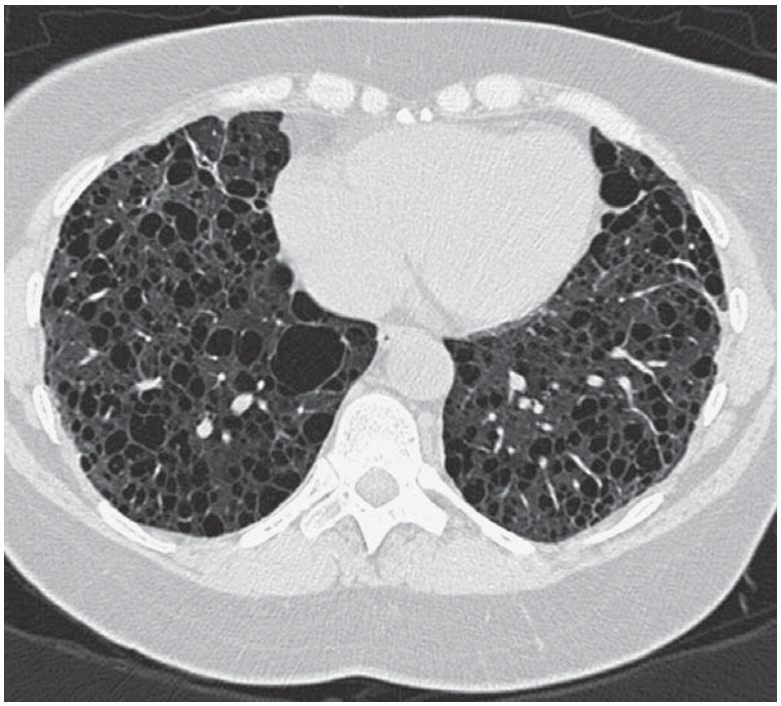


Fig. 6.1 Unenhanced axial computed tomography image through the chest in the lung window reveals numerous bilateral thin-walled cysts, most of which are similar in size. The intervening lung is normal.

Clinical Presentation

A 31-year-old woman with a history of smoking presents with a chronic cough and shortness of breath (**Fig. 6.1**).

Key Imaging Finding

Cystic lung disease

Top 3 Differential Diagnoses

- **Emphysema.** Emphysema is characterized by nonfibrotic enlargement of the airways distal to the terminal bronchioles with destruction of the alveolar walls. Computed tomography (CT) further characterizes this process based on the location of these cystic spaces at the lobular level. Centrilobular emphysema involves the central portion of the secondary pulmonary lobule with upper lobe predominance and is highly associated with cigarette smoking. Panlobular emphysema involves the entire lobule and is classically associated with alpha-1 antitrypsin deficiency. Paraseptal emphysema is predominantly subpleural, involving the alveolar ducts and sacs.
- **Lymphangioleiomyomatosis (LAM).** A relatively rare disease affecting women of reproductive age, LAM is characterized by proliferation of smooth muscle cells around bronchioles. This results in air trapping and characteristic thin-walled lung cysts. The cysts are typically uniform in size. Air trapping predisposes patients to pneumothoraces. A similar process involving the lymphatics results in chylous pleural effusions. LAM may occur as an isolated abnormality or be associated with tuberous sclerosis.
- **Pulmonary Langerhans cell histiocytosis (LCH).** Seen predominantly in young and middle-aged adults and almost exclusively in smokers, pulmonary LCH is an idiopathic disease of mature histiocyte proliferation. On imaging, numerous small (<1 cm) upper lobe–predominant nodules, many of which demonstrate cavitation, are eventually replaced by irregular, thin-walled cysts of varying sizes. Associated pneumothoraces are common. Occasionally, LCH may progress to interstitial fibrosis and honeycombing with characteristic sparing of the costophrenic sulci.

Additional Differential Diagnoses

- **Pneumocystis pneumonia.** The most common cause of diffuse pneumonia in immunocompromised patients, pneumocystis pneumonia classically results in central ground-glass opacities with or without reticulonodular interstitial thickening on plain radiographs. CT most commonly demonstrates ground-glass opacification with abnormal air spaces, to include thin-walled cysts, pneumatoceles, and pneumothoraces, as well as interlobular septal thickening.
- **Lymphocytic interstitial pneumonitis (LIP).** Lymphocytic infiltration of the alveolar septa characterizes LIP, a lower lobe–predominant hyperplasia of bronchus-associated lymphoid tissue. A reticulonodular interstitial pattern on plain radiographs is better characterized on CT as centrilobular nodules with thin-walled cystic air spaces and regions of ground-glass opacification. LIP is commonly seen in the setting of Sjögren syndrome and acquired immunodeficiency syndrome (AIDS), particularly in children.

Diagnosis

Lymphangioleiomyomatosis

✓ Pearls

- Cysts and emphysema can coexist but are distinct processes; centrilobular emphysema is most common.
- Cysts must be distinguished from bronchiectasis by establishing a lack of continuity with the airways.
- LAM occurs almost exclusively in women of childbearing age; chylous pleural effusions may be seen.
- LCH is seen almost exclusively in smokers and tends to spare the costophrenic sulci.

Suggested Readings

Collins J, Stern EJ. Chest Radiology: The Essentials. Philadelphia: Lippincott Williams & Wilkins; 2007

Koyama M. Chronic cystic lung disease: diagnostic accuracy of high-resolution CT in 92 patients. AJR Am J Roentgenol 2003;180:827–835

Case 7

William T. O'Brien Sr.

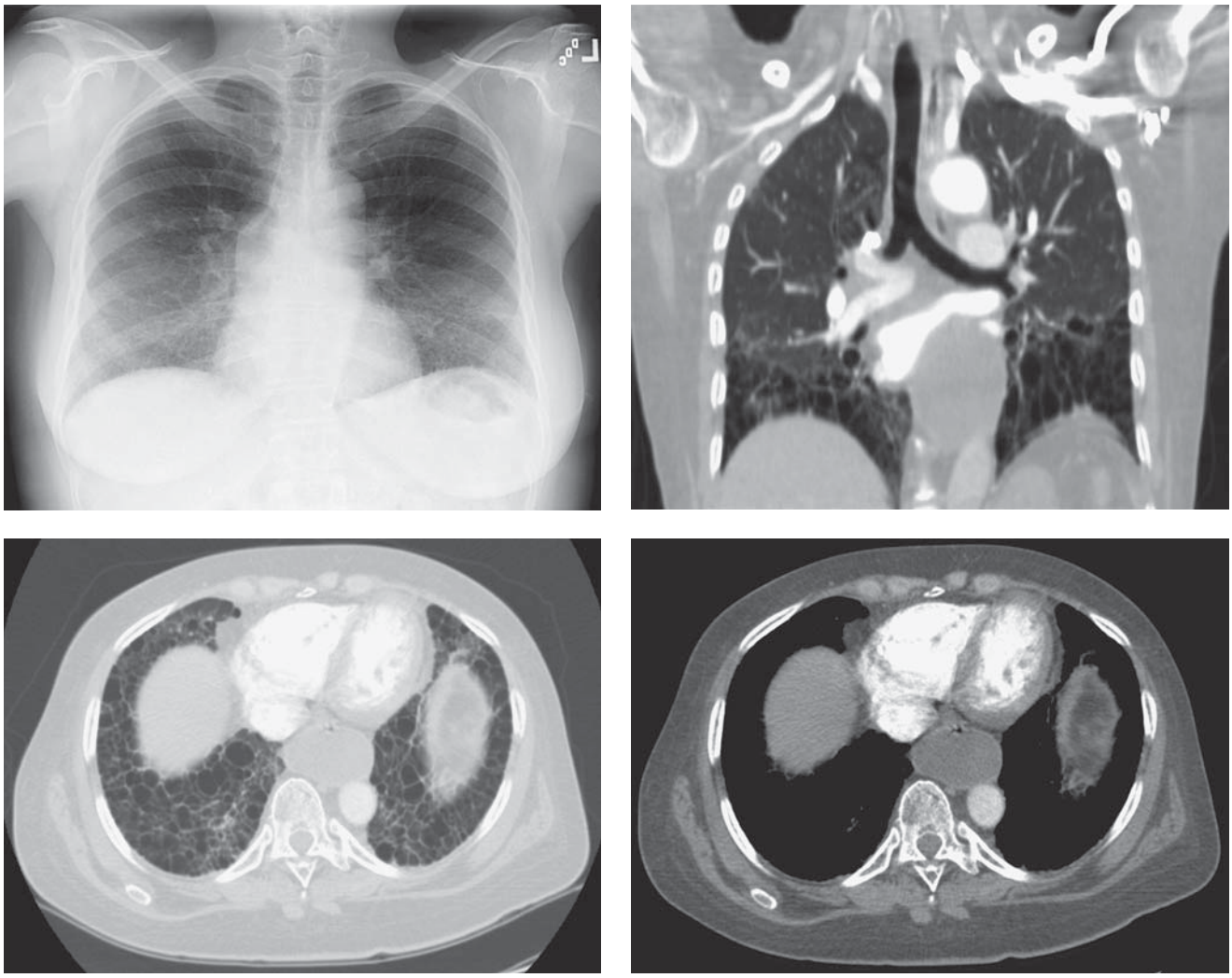


Fig. 7.1 **(A)** Frontal chest radiograph demonstrates coarsened interstitial lung markings predominantly at the lung bases. **(B)** Coronal and **(C)** axial CT images in the lung window reveal end-stage fibrotic changes with honeycombing throughout the lower lobes with sparing of the upper lobes. **(D)** Axial CT image in the soft tissue window shows a dilated, patulous, fluid-filled esophagus.

Clinical Presentation

A 50-year-old woman presents with chronic shortness of breath and difficulty swallowing (**Fig. 7.1**).

Key Imaging Finding

Lower lobe interstitial lung disease (ILD)

Top 3 Differential Diagnoses

- **Usual interstitial pneumonia (UIP).** UIP is a relatively common cause of fibrotic lung disease. Patients often present with worsening, progressive cough and shortness of breath. Plain radiographs reveal increased interstitial markings at the lung bases with normal to low lung volumes. On high-resolution computed tomography (CT), UIP presents as irregular septal thickening along the peripheral aspect of the lower lobes with subpleural honeycombing and traction bronchiectasis in advanced cases. Occasionally, ground-glass opacities may been seen, which correlate with regions of active alveolitis. Median survival once diagnosed is approximately 3 years. About 70% of UIP cases have no identifiable cause, in which case they are referred to as idiopathic pulmonary fibrosis (IPF).
- **Collagen vascular diseases.** Collagen vascular diseases, which include scleroderma, rheumatoid arthritis (RA), and systemic lupus erythematosus (SLE), involve the lungs to varying degrees. Scleroderma is a systemic process that affects young women and involves many organ systems, including the lungs, esophagus, and musculoskeletal system. Pulmonary findings include pneumonitis and ILD with a striking lower lobe predominance. High-resolution CT reveals irregular septal thickening and subpleural honeycombing. Secondary findings include a dilated, patulous esophagus. RA is a systemic disease that most severely affects articular surfaces. Pulmonary involvement may be seen in up to 50% of cases. Unilateral pleural effusion is the most common presentation of RA within the chest. Additional manifestations include lower lobe ILD, necrobiotic pulmonary nodules, and pericarditis. Caplan syndrome refers to coal workers' pneumoconiosis superimposed upon RA. SLE is a systemic process that occurs in young women. Pleural and pericardial effusions are the most common manifestation of SLE in the chest.
- **Asbestos-related disease.** This group of diseases results from occupational exposure, as can be seen in former shipyard workers and mechanics. The clinical and radiographic manifestations usually present 20 years after the initial exposure. Pleural thickening and pleural plaques are the most common radiographic manifestation and are typically bilateral, involving predominantly the lower thorax. The plaques often calcify. A benign exudative pleural effusion may also occur. Rounded atelectasis is a common finding and presents as a rounded mass that abuts the pleura in a region of underlying pleural thickening. Vessels can be seen "swirling" into the lesion. High-resolution CT findings include subpleural lines and parenchymal bands extending to the pleura. Lung involvement can include lower lobe septal thickening and subpleural honeycombing. When there is pulmonary fibrosis, it is called asbestosis.

Additional Differential Diagnoses

- **Drug toxicity.** Drug toxicity from chemotherapeutic agents or elicit drug abuse may rarely result in predominantly lower lobe ILD characterized by irregular septal thickening and subpleural honeycombing. Other patterns of injury are pulmonary edema, pulmonary hemorrhage, and hypersensitivity pneumonitis. Bleomycin and busulfan are the most common chemotherapeutic agents that cause lower lobe ILD. Amiodarone may also result in lower lobe ILD, along with characteristic dense opacities.

Diagnosis

Connective tissue disorder (scleroderma)

✓ Pearls

- UIP is the histologic and imaging descriptor of many diseases; when the cause is unknown, it is referred to as IPF.
- Scleroderma is the most common collagen vascular disease that produces lower lobe fibrosis.
- Asbestos exposure and asbestosis are related but different; asbestosis is defined by interstitial fibrosis.
- Chemotherapeutic agents may cause lower lobe–predominant ILD; amiodarone produces dense opacities.

Suggested Readings

Kazerooni EA, Gross BH. Cardiopulmonary Imaging. Philadelphia: Lippincott Williams & Wilkins; 2004

McLoud TC. Thoracic Radiology: The Requisites. St. Louis: Mosby; 1998

Case 8

Bang Huynh

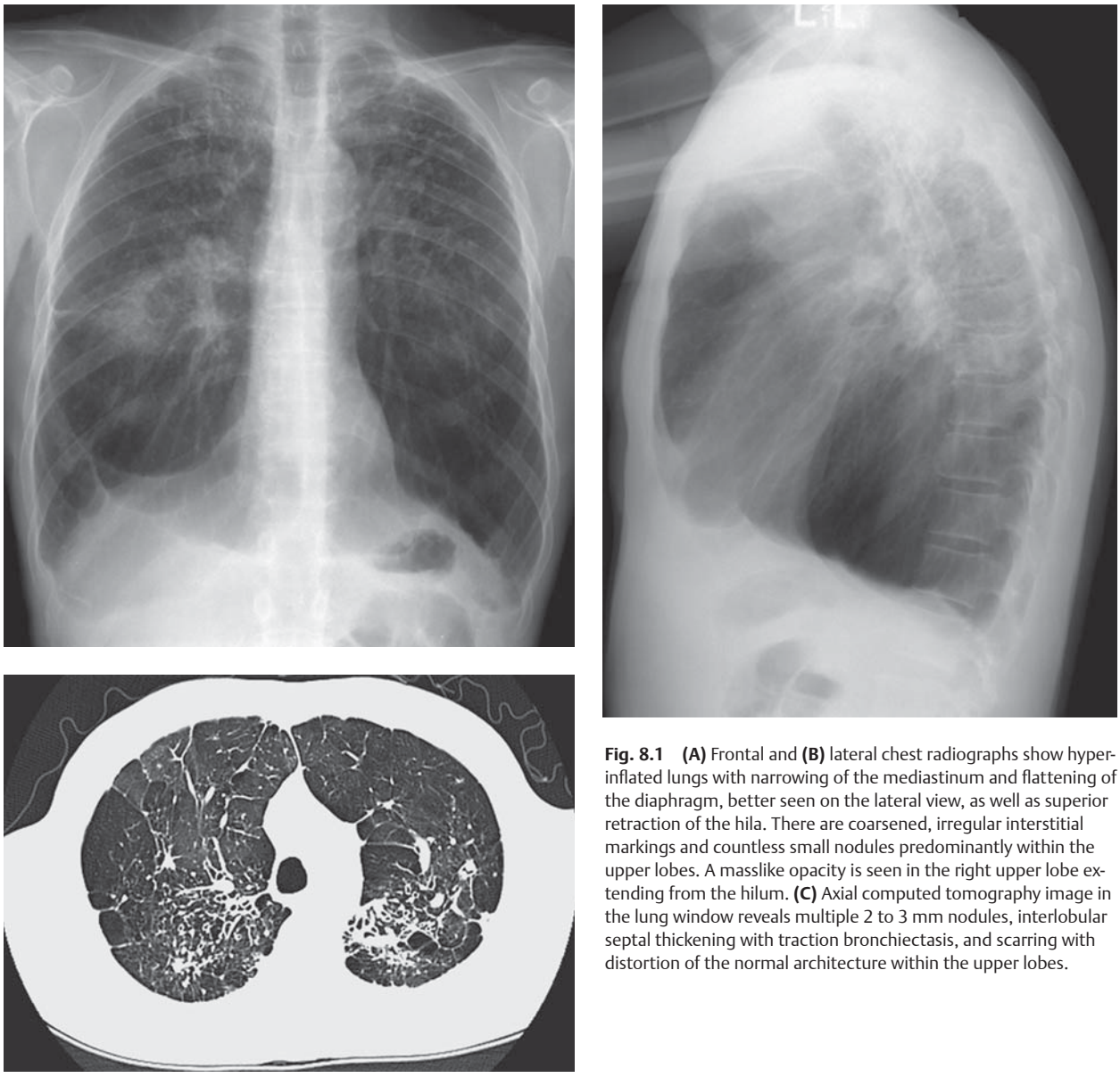


Fig. 8.1 **(A)** Frontal and **(B)** lateral chest radiographs show hyperinflated lungs with narrowing of the mediastinum and flattening of the diaphragm, better seen on the lateral view, as well as superior retraction of the hila. There are coarsened, irregular interstitial markings and countless small nodules predominantly within the upper lobes. A masslike opacity is seen in the right upper lobe extending from the hilum. **(C)** Axial computed tomography image in the lung window reveals multiple 2 to 3 mm nodules, interlobular septal thickening with traction bronchiectasis, and scarring with distortion of the normal architecture within the upper lobes.

Clinical Presentation

An elderly man presents with chronic progressive shortness of breath (**Fig. 8.1**).

Key Imaging Finding

Upper lobe interstitial lung disease

Top 3 Differential Diagnoses

- **Postprimary tuberculosis (TB).** Primary TB can have a broad range of presentations but is typically characterized by mediastinal and unilateral hilar lymphadenopathy (sometimes of low attenuation). Parenchymal involvement can range from poorly defined opacities to lobar consolidations. Pleural effusions are not uncommon. Nodal calcification is present in about one third of cases. There is no distribution preference, and cavitation, though possible, is not common. In contrast, postprimary TB favors the posterior segments of the upper lobes or superior segments of the lower lobes primarily due to higher oxygen tension and less efficient lymphatic clearance. Cavitation and fibrosis are distinct features of postprimary TB. Other manifestations of TB are miliary and endobronchial patterns.
- **Sarcoidosis.** Sarcoidosis is a systemic disease of unknown etiology characterized by noncaseating granulomas. Thoracic disease may include mediastinal/hilar and parenchymal involvement. Hilar adenopathy is often bilateral and symmetric. Parenchymal involvement usually consists of countless 2 to 4 mm centrilobular and subpleural (perilymphatic) nodules. There is an upper lobe and peribronchovascular distribution. Sarcoid granulomas can resolve completely; however, they occasionally cause severe and extensive fibrosis that resembles progressive massive fibrosis seen in complicated silicosis.
- **Cystic fibrosis (CF).** CF is a genetic disorder affecting Caucasian children and young adults. The lungs and gastrointestinal tract are most affected, with thick secretions from exocrine glands. Pulmonary involvement occurs in more than 90% of patients. Viscous secretions result in upper lobe–predominant mucous plugging, air trapping, bronchial wall thickening, and bronchiectasis.

Additional Differential Diagnoses

- **Silicosis/coal workers' pneumoconiosis.** *Pneumoconiosis* is a broad term that describes reactions of the lungs to inhaled dust particles. Coal workers' pneumoconiosis and silicosis are pathologically different but have very similar radiographic appearances. Silicosis is caused by the inhalation of free silica, a compound associated with mining of heavy metal, sandblasting, and stonework. Patients may present acutely following heavy exposure whereby silicoproteinosis develops or, more commonly, with chronic silicosis from decades of exposure. The chronic form is associated with cyclic inflammation, resulting in fibrosis with an upper lobe predominance. Complicated silicosis is an extreme progression in which the fibrosis coalesces into masslike opacities, a process called progressive massive fibrosis.
- **Langerhans cell histiocytosis (LCH).** Pulmonary LCH is characterized by abnormal histiocyte proliferation and is seen predominantly in young and middle-aged smokers. Imaging findings include numerous small upper lobe (mainly) nodules, many of which cavitate, and irregular cysts of varying sizes.

Diagnosis

Complicated silicosis

✓ Pearls

- Postprimary TB may result in upper lobe cavitary pulmonary nodules and fibrosis.
- Sarcoidosis presents with symmetric hilar adenopathy; perilymphatic pulmonary nodules may also be seen.
- Pulmonary manifestations of CF include upper lobe mucous plugging, air trapping, and bronchiectasis.
- Silicoproteinosis is a unique form of silicosis that is acute and indistinguishable from alveolar proteinosis.

Suggested Readings

Collins J, Stern EJ. Chest Radiology: The Essentials. Philadelphia: Lippincott Williams & Wilkins; 2007

Mueller-Mang C, Grosse C, Schmid K, et al. What every radiologist should know about idiopathic pneumonias. Radiographics 2007;27:595–615

Pipavath S, Godwin JD. Imaging of interstitial lung disease. Clin Chest Med 2004;25(3):455–465

Case 9

Arash J. Momeni

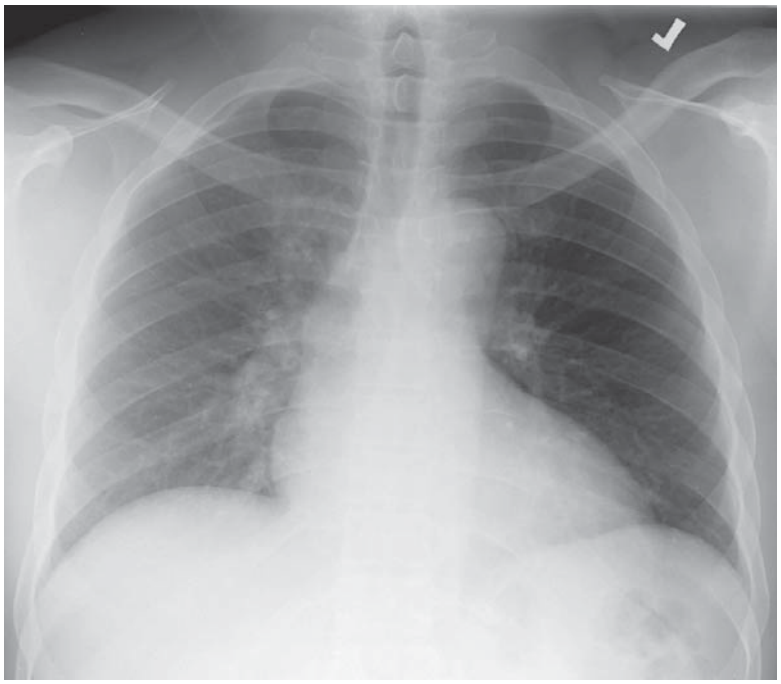


Fig. 9.1 Frontal chest radiograph demonstrates hyperlucency of the left hemithorax. Lung volumes are symmetric.

Clinical Presentation

A 40-year-old man presents with occasional dyspnea on exertion (**Fig. 9.1**).

Key Imaging Finding

Hyperlucent lung

Top 3 Differential Diagnoses

- **Chest wall abnormality.** Several chest wall abnormalities may result in a hyperlucent lung. For example, mastectomy results in relative radiolucency on the side of the breast removal. Poland syndrome is characterized by a spectrum of abnormalities ranging from isolated absence of the pectoralis major muscle to additional abnormalities of the ipsilateral extremity, such as syndactyly, brachydactyly, and rib anomalies.
- **Swyer-James syndrome.** Swyer-James, or MacLeod, syndrome is a form of obliterative bronchiolitis that occurs following an insult, classically viral, to the developing lung. This process affects small bronchi and bronchioles. The portions of the lung ventilated by abnormal airways remain inflated by collateral air drift. Chest radiographs demonstrate unilateral hyperlucency due to reduced lung perfusion. Air trapping may be seen on expiratory radiographs/computed tomography (CT). Lung volumes on the affected side may be normal or decreased. On CT, additional findings may include bronchiectasis and attenuated vessels in areas of decreased lung attenuation.
- **Acute asthmatic attack.** Hyperlucency in asthma is secondary to bronchoconstriction and compensatory vasoconstriction of hypoventilated portions of the lung. As this is usually a more central process, findings are commonly bilateral but may be asymmetric.

Top 3 Differential Diagnoses You Cannot Afford to Miss

- **Airway obstruction.** The hallmark of airway obstruction in children is air trapping, which is manifested as failure of the lung to decrease in volume, and subsequently increase in opacification, on expiratory chest radiographs. The mediastinum may shift to the contralateral side. Air trapping occurs when an endobronchial lesion causes a check valve type of obstruction. In children, this is usually secondary to foreign body aspiration. Expiratory views, decubitus views, and fluoroscopy may be helpful.
- **Pulmonary embolism.** Oligemia of the lung beyond the occluded pulmonary vessel, or the Westermark sign, is a helpful but not commonly encountered sign of pulmonary embolism. A large unilateral thrombus, whether bland, septic, or neoplastic, can result in a unilateral hyperlucent lung.
- **Pneumothorax.** A pneumothorax results in hyperlucency of the ipsilateral hemithorax and may present with central displacement of the visceral pleural line, absence of lung markings distal to the displaced pleural line, and contralateral shift of the mediastinum. In a supine patient, a pneumothorax may collect anteromedially, in the nondependent portion of the thorax. This will result in the pneumothorax presenting as a lucency in the anteromedial chest rather than as a pleural line. A tension pneumothorax is a true emergency.

Diagnosis

Chest wall abnormality (Poland syndrome)

✓ Pearls

- Swyer-James syndrome is usually a unilateral process in which the affected lung is reduced in size.
- Expiratory views, decubitus views, and fluoroscopy may be helpful in evaluating for foreign bodies.
- Always consider pulmonary embolism and pneumothorax (in a supine patient) with a hyperlucent lung.

Suggested Readings

Collins J, Stern EJ. Chest Radiology: The Essentials. Philadelphia: Lippincott Williams & Wilkins; 2007

Reid L, Simon G. Unilateral lung transradiancy. Thorax 1962;17:230–239

Stern EJ, Frank MS. Small airway diseases of the lungs: findings at expiratory CT. AJR Am J Roentgenol 1994;163:37–41

Case 10

Bang Huynh

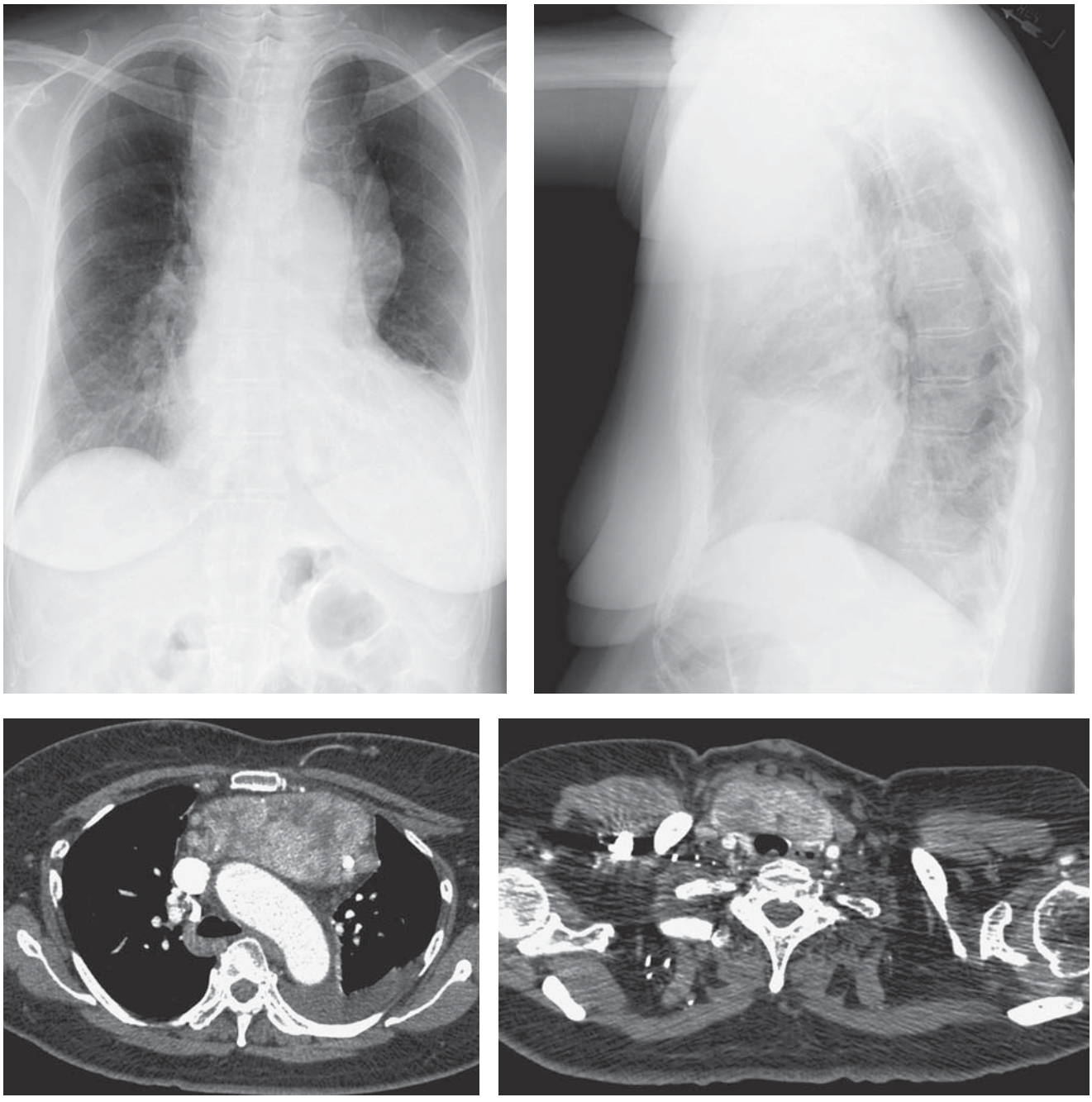


Fig. 10.1 **(A)** Posteroanterior radiograph shows a lobulated mediastinal mass that does not silhouette the aortic arch. **(B)** Lateral radiograph shows that the retrosternal clear space is obscured. Enhanced axial computed tomography images reveal **(C)** a heterogeneously enhancing anterior mediastinal mass with coarse foci of calcification that is contiguous with **(D)** the thyroid gland.

Clinical Presentation

A middle-aged woman presents for an employment physical (**Fig. 10.1**).

Key Imaging Finding

Anterior mediastinal mass

Top 3 Differential Diagnoses

- **Lymphoma.** Lymphoma is a primary neoplasm of the lymphoreticular system that is divided into two main types: Hodgkin disease (HD) and non-Hodgkin lymphoma (NHL). Although HD is the less common of the two types, it is more likely to involve the thorax (up to 85% of HD cases as compared with 40 to 50% of NHL cases). Of the HD cases with thoracic involvement, nearly all (98%) involve superior mediastinal nodes (i.e., aortopulmonary, prevascular, and paratracheal). The percentage of superior mediastinal node involvement in HD is so high that normal superior mediastinal nodes in the setting of thoracic involvement make HD unlikely. Calcification does not occur prior to treatment. In HD, the anatomical extent of disease correlates well with prognosis. In contrast, prognosis of NHL is better predicted by histopathologic classification.
- **Thymic lesion.** The normal thymus increases from birth to puberty, after which it begins to involute over a 5- to 15-year period. Thymic tissue is progressively replaced by fat. By the age of 60, little thymic tissue remains. Abnormalities of thymic origin can be due to several processes. The thymus itself may be abnormally enlarged, as in thymic hyperplasia or rebound, or abnormally infiltrated, as in lymphoid follicular hyperplasia. Several masses and tumors can arise from the thymus, including thymoma, thymic carcinoma, thymic carcinoid, cysts, lipomas, and lymphoma. Thymomas (most common) most often occur in the third and fourth decades of life and may be associated with myasthenia gravis.
- **Thyroid lesion.** Thyroid masses account for ~10% of mediastinal masses. The majority (80%) are in the anterior mediastinum. Mediastinal masses of thyroid origin are almost always contiguous with the thyroid. A truly ectopic mediastinal mass without a connection to the thyroid is possible but uncommon. Radiographically, mediastinal thyroid masses often cause tracheal deviation. On computed tomography, normal thyroid tissue has a characteristic appearance, being high attenuation relative to adjacent soft tissue on noncontrast studies and enhancing avidly postcontrast. Calcifications may be present, but in the end, differentiation between goiter and thyroid carcinoma is difficult unless lymphadenopathy or metastasis is present.

Additional Differential Diagnoses

- **Germ cell neoplasm (GCN).** GCNs, which account for ~10% of primary mediastinal masses, arise from primitive germ cells that have arrested in the mediastinum during embryologic migration. The majority of such neoplasms are located in the anterior mediastinum and present during the second through fourth decades of life. GCNs can be benign or malignant, but the majority (80%) are benign. They include teratomas, seminomas, embryonal carcinoma, yolk sac tumors, choriocarcinoma, and mixed cell types. Imaging findings are broad. Solid and cystic components may be present. Teratomas, which contain elements of all germinal layers, can include skin, hair, fat, and bones if well differentiated.

Diagnosis

Thyroid lesion (goiter)

✓ Pearls

- HD presents as noncalcified mediastinal adenopathy involving the anterior and superior mediastinum.
- Thymic lesions include thymomas (most common), invasive thymomas, carcinomas, lipomas, and cysts.
- Thyroid lesions are contiguous with the thyroid gland, result in tracheal deviation, and avidly enhance.
- GCNs most commonly present in the second through fourth decades of life; the majority are benign.

Suggested Readings

Collins J, Stern EJ. Chest Radiology: The Essentials. Philadelphia: Lippincott Williams & Wilkins; 2007

Reed JC. Chest Radiology: Plain Film Patterns and Differential Diagnoses. St. Louis: Mosby; 1991

Webb WR, Higgins CB. Thoracic Imaging. Philadelphia: Lippincott Williams & Wilkins; 2005

Case 11

Bang Huynh

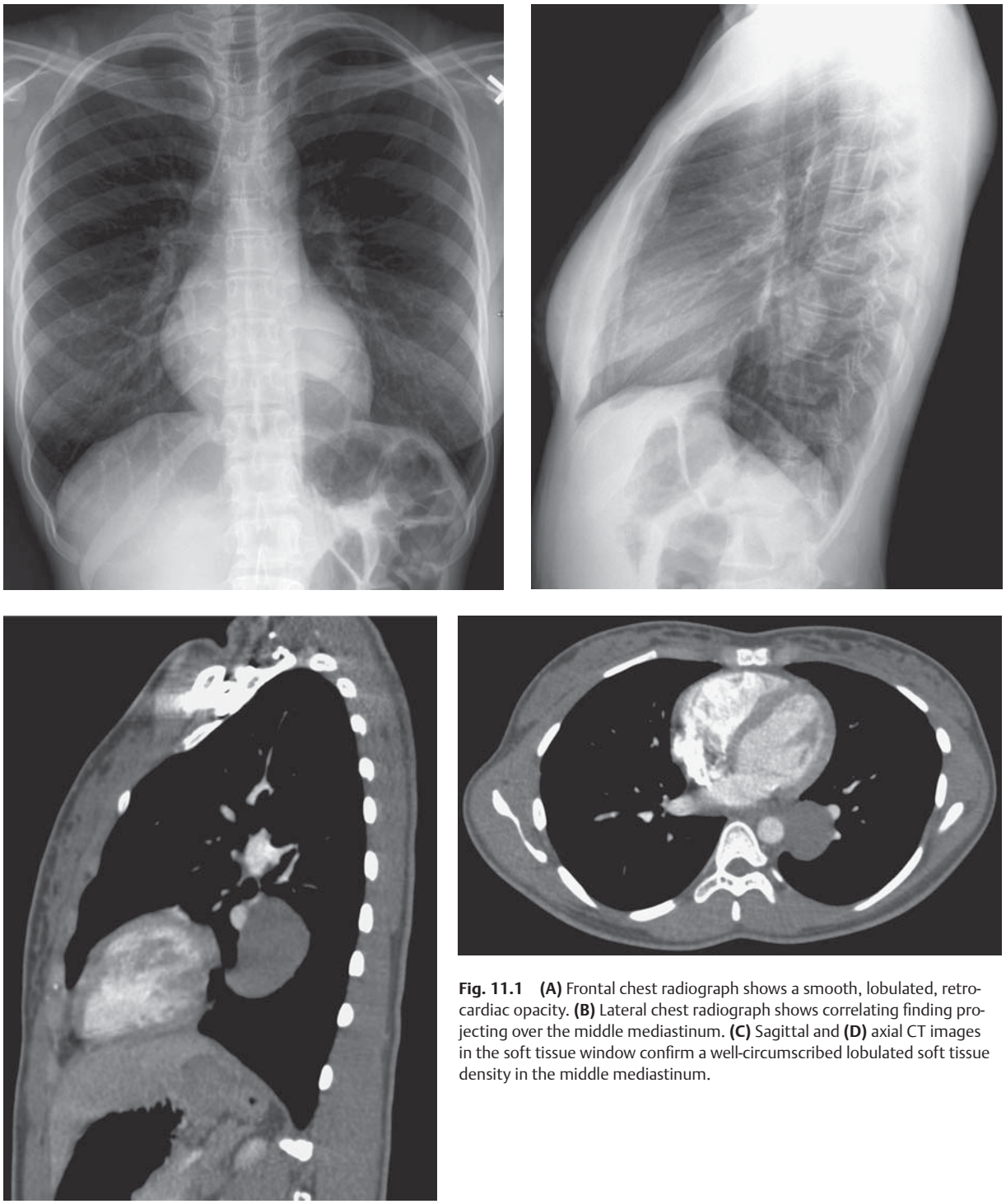


Fig. 11.1 **(A)** Frontal chest radiograph shows a smooth, lobulated, retrocardiac opacity. **(B)** Lateral chest radiograph shows correlating finding projecting over the middle mediastinum. **(C)** Sagittal and **(D)** axial CT images in the soft tissue window confirm a well-circumscribed lobulated soft tissue density in the middle mediastinum.

Clinical Presentation

An asymptomatic patient presents for a preemployment physical chest radiograph (**Fig. 11.1**).

Key Imaging Finding

Middle mediastinal mass

Top 3 Differential Diagnoses

- **Lymphadenopathy.** The presence of lymphadenopathy is often not specific to an etiology. Lymphoma is high on the list of differential diagnoses, and metastasis, particularly if the patient has a known primary, must be considered. There are some secondary features, best evaluated by computed tomography (CT), that may help narrow the differentials. Low attenuation nodes may reflect necrosis in the setting of tuberculosis (TB), fungal infection, or metastasis and lymphoma. Enhancing nodes may be seen in the setting of Castleman disease, hypervascular metastases, TB, and sometimes sarcoid. Pattern of nodal calcification may also narrow the differential diagnosis.
- **Vascular abnormality.** Vascular abnormalities must always be considered in the differential diagnoses of a middle mediastinal mass, particularly if they are in proximity to the aorta. Possible causes of abnormal aortic and middle mediastinal contours are thoracic aortic aneurysm, penetrating aortic ulcers, and pseudoaneurysms. CT or magnetic resonance imaging is helpful in the evaluation. Aortic aneurysms (diameter >4 cm) can be described by their shape (fusiform or saccular) and by the extent of wall involvement (true or false aneurysm). Saccular aneurysms are associated with infections and are at high risk for rupture, whereas fusiform aneurysms are more often associated with atherosclerosis. Pulmonary artery aneurysms are less common vascular causes of middle mediastinal masses. Etiologies include primary and secondary causes of pulmonary artery hypertension, as well as trauma, neoplasm, and infection.
- **Congenital cyst.** Duplication cysts are the most common congenital cysts in the middle mediastinum and result from abnormalities in foregut development. Among the various types, bronchogenic cysts are the most common. Although they may present in any part of the mediastinum, most are in contact with the tracheobronchial tree and within 5 cm of the carina; thus, most are in the middle mediastinum. On radiographs, they often appear as smooth, sharply circumscribed lobular or round densities. On CT, about half have simple fluid attenuation; the remainder of cysts have varying attenuation, depending on proteinaceous or blood content. When they are of higher attenuation, they can appear solid but will not enhance. If a wall is seen, it is thin unless the cyst is infected. Rarely, the wall will calcify. Most bronchogenic cysts are asymptomatic, but they can increase in size over time to become symptomatic by compression of adjacent structures. Pericardial cysts are less common and result from failure of fusion of a portion of the pericardium. Most are located at the cardiophrenic angle, right greater than left. Management of congenital cysts tends to be surgical, though more recent options include percutaneous or transbronchial aspiration.

Additional Differential Diagnoses

- **Hiatal hernia.** A hiatal hernia is a protrusion of the part of the stomach through the diaphragmatic hiatus. A gas or gas–fluid level may be seen with a hiatal hernia. Radiographically, esophageal carcinoma can mimic a hernia, as both can present with subtle abnormal bowing of the azygoesophageal recess.

Diagnosis

Congenital cyst (bronchogenic)

✓ Pearls

- Mediastinal lymphadenopathy is most often due to lymphoma, metastases, infectious process, or sarcoid.
- Vascular enlargement of the thoracic aorta or pulmonary arteries may result in a middle mediastinal mass.
- Bronchogenic duplication cysts are the most common congenital cysts in the middle mediastinum.
- When a congenital cyst is rapidly enlarging, suspect infection or hemorrhage.

Suggested Readings

Collins J, Stern EJ. Chest Radiology: The Essentials. Philadelphia: Lippincott Williams & Wilkins; 2007

Reed JC. Chest Radiology: Plain Film Patterns and Differential Diagnoses. St. Louis: Mosby; 1991

Webb WR, Higgins CB. Thoracic Imaging. Philadelphia: Lippincott Williams & Wilkins; 2005

Case 12

Thomas Ray S. Sanchez

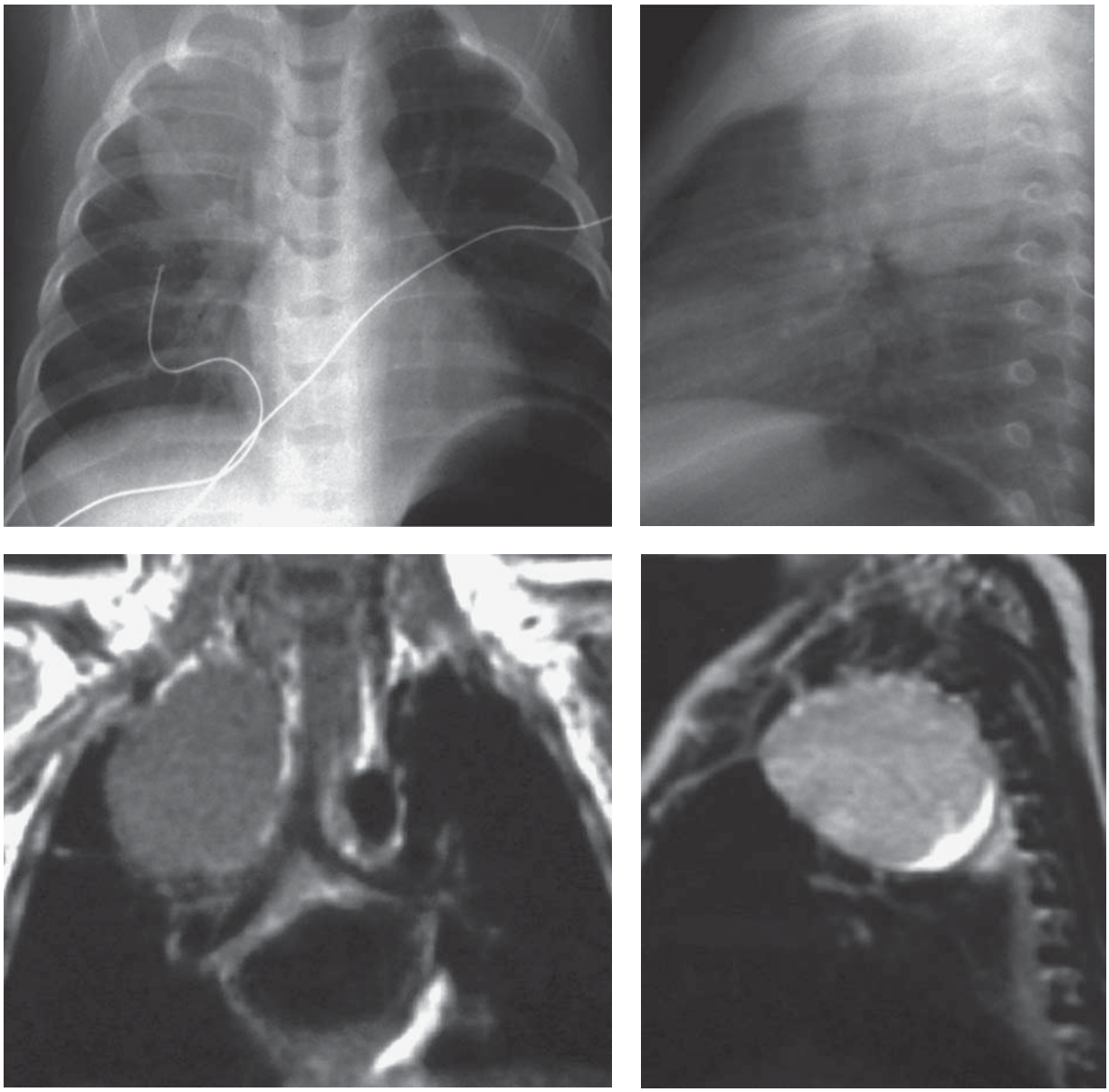


Fig. 12.1 **(A)** Posteroanterior and **(B)** lateral chest radiographs show a well-defined right paraspinal mass that arises from the posterior mediastinum. **(C)** Coronal T1-weighted image shows a homogeneous and isointense right paraspinal/paratracheal solid mass. **(D)** Sagittal T2-weighted image demonstrates a homogeneously hyperintense mass with a crescent area of necrosis or cystic degeneration posteriorly. There is no evidence of intraspinal extension or bony involvement. (Courtesy of Leonard E. Swischuk, MD.)

Clinical Presentation

A 3-month-old boy presents with respiratory distress (**Fig. 12.1**).

Key Imaging Finding

Posterior mediastinal mass

Top 3 Differential Diagnoses

- **Neurogenic tumor.** Neuroblastic tumors arise from the sympathetic tissues that are found from the neck down to the pelvis. Neuroblastomas are the most immature form and are considered malignant. On the other end of the spectrum, ganglioneuromas contain mature neurogenic cells and are considered benign. Plain film findings, such as posterior mediastinal location, intratumoral calcification (present in ~30–50%), rib splaying, and associated bony erosion or metastasis, are highly suggestive of this disease. Computed tomography (CT) scan and/or magnetic resonance imaging (MRI) will better delineate its exact origin, the presence of vascular encasement, and intraspinal extensions (dumbbell tumors), which are all important findings with regards to treatment planning.
- **Lymphoma.** Although the anterior mediastinum is the usual location classically infiltrated by lymphoma, the posterior mediastinal nodes can rarely be involved as well. Homogeneous masses with lobulations and the absence of necrosis or calcification in untreated cases will help differentiate it from other posterior mediastinal masses.
- **Developmental cyst.** Neurenteric, duplication, and bronchogenic cysts can be grouped together under the heading of bronchopulmonary foregut cysts/malformations. They are difficult to differentiate from one another and basically look the same on most imaging studies. They are well marginated round/oval masses that are cystic in nature (low density on CT and high intensity on T2-weighted MR images) and have thin walls. The presence of infection or hemorrhage can complicate matters; hence they can mimic a solid lesion or abscess formation. Neurenteric cysts have associated spinal malformations, which, when present, suggest the diagnosis.

Additional Differential Diagnoses

- **Extramedullary hematopoiesis.** In patients with severe and chronic anemia (usually associated with sickle cell disease, thalassemia, or hypersplenism), extramedullary hematopoiesis may occur as a result of the body's attempt to produce more red blood cells. Extramedullary hematopoiesis presents as bilateral but often asymmetric paraspinal masses. Associated findings include trabecular coarsening of the adjacent vertebrae. Tissue correlation will sometimes be needed to rule out malignancy.
- **Mediastinal hematoma.** Mediastinal widening with associated pleural effusion (more commonly on the left) are the most common signs of mediastinal/vascular injury. A history of trauma, vascular catheterization, or central line placement will further strengthen the suspicion. Because plain radiographs are often nonspecific, contrast-enhanced CT scan will be needed in suspected cases and will clearly differentiate it from other mediastinal masses.

Diagnosis

Neurogenic tumor (neuroblastoma)

✓ Pearls

- Rib involvement (erosion or splaying) confirms the posterior mediastinal location of a mass on chest radiograph.
- Mediastinal neuroblastoma is seen almost exclusively in young children under the age of 5 years.
- Management of congenital cysts tends to be surgical; percutaneous aspiration is an option in some cases.
- Extramedullary hematopoiesis often presents as bilateral but asymmetric posterior mediastinal masses.

Suggested Readings

Collins J, Stern EJ. Chest Radiology: The Essentials. Philadelphia: Lippincott Williams & Wilkins; 2007

Reed JC. Chest Radiology: Plain Film Patterns and Differential Diagnoses. St. Louis: Mosby; 1991

Case 13

Bang Huynh

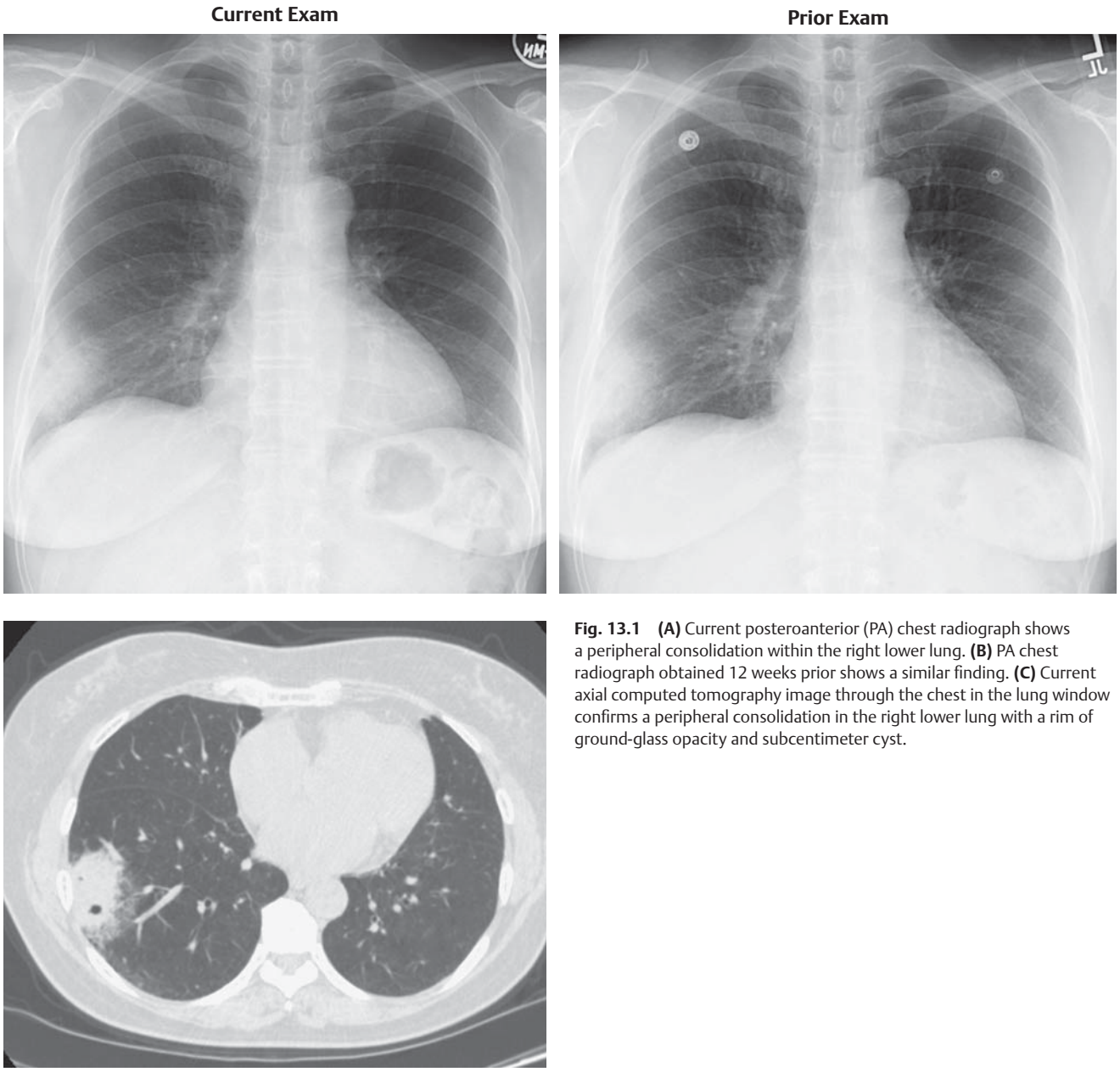


Fig. 13.1 **(A)** Current posteroanterior (PA) chest radiograph shows a peripheral consolidation within the right lower lung. **(B)** PA chest radiograph obtained 12 weeks prior shows a similar finding. **(C)** Current axial computed tomography image through the chest in the lung window confirms a peripheral consolidation in the right lower lung with a rim of ground-glass opacity and subcentimeter cyst.

Clinical Presentation

Follow-up examination of a patient with suspected pneumonia treated 12 weeks ago (**Fig. 13.1**).

Key Imaging Finding

Chronic air-space disease

Top 3 Differential Diagnoses

- **Cryptogenic organizing pneumonia (COP).** COP refers to the idiopathic clinical syndrome reflected by imaging and histopathologic findings of organizing pneumonia (OP). Patients typically present with cough and dyspnea. They are often treated for infectious pneumonia at initial presentation but fail to improve with treatment. When OP is later considered and the patient is treated with steroids, findings finally improve. OP is primarily an intra-alveolar process, manifesting with patchy and peribronchial consolidations. There is often a lower lobe predominance. In some patients, the distribution can be peripheral, a pattern similar to that seen in chronic eosinophilic pneumonia. Ground-glass opacities are also commonly seen on computed tomography (CT).
- **Pulmonary alveolar proteinosis (PAP).** PAP is a disease characterized by the filling of the alveolar air spaces with protein. In most cases, there is no known etiology, but some cases are thought to be due to exposure to dust (particularly silica). Symptoms are often mild for the degree of radiographic change. On radiographs, PAP manifests as bilateral, diffuse, or patchy hazy opacities. On CT, the classic pattern is smooth interlobular septal thickening on a background of ground-glass opacities ("crazy paving"); however, crazy paving is not specific to PAP and includes a differential. PAP can also present as patchy ground-glass opacities or consolidations with an abrupt margin separating normal from involved lung.
- **Bronchioloalveolar carcinoma (BAC).** BAC is a well-differentiated subtype of adenocarcinoma that makes up 5 to 30% of bronchogenic carcinomas. It most commonly presents as a nodule of ground-glass opacity (60%). The remaining 40% of cases present as diffuse or patchy consolidations/ground-glass opacities. In some cases, pseudocavitation can be seen. The CT angiogram sign (a low-attenuating consolidation of the lung parenchyma with enhancing pulmonary vessels) has been described with BAC but is not specific.

Additional Differential Diagnoses

- **Chronic eosinophilic pneumonia.** Chronic eosinophilic pneumonia is an idiopathic process characterized by alveolar and interstitial infiltration of inflammatory cells. Patients also usually have increased eosinophils in the peripheral blood. Radiographically, homogeneous peripheral consolidations are present, in a pattern reminiscent of the photographic negative of pulmonary edema. Consolidation may also be patchy, sometimes with an upper lobe predominance. On CT, crazy paving can be seen. As is often the case, the classic presentation is not so common. Patients respond rapidly to the administration of steroids.
- **Lipoid pneumonia.** Lipoid pneumonia is the result of chronic aspiration of products that contain oil or fat. On radiographs, there are consolidations with a lower lobe distribution. The classic CT finding is consolidations with low attenuation (−40 to −100). Crazy paving may also be seen but is not specific. As this is usually a long-standing process, fibrosis, necrosis, and even cavitations may be present.

Diagnosis

Bronchioloalveolar adenocarcinoma

✓ Pearls

- Organizing pneumonia is a common cause of chronic air-space disease; symptoms improve with steroids.
- CT findings associated with PAP are classically described as "crazy paving"; however, this is nonspecific.
- BAC may present as a ground-glass nodule (most common) or chronic air-space disease.

Suggested Readings

Leung AN, Miller RR, Muller NL. Parenchymal opacification in chronic infiltrative lung diseases: CT pathologic correlation. Radiology 1993;188:209–214

Mathieson JR, Mayo JR, Staples CA, et al. Chronic diffuse infiltrative lung disease: comparison of diagnostic accuracy of CT and chest radiography. Radiology 1989;171:111–116

Webb WR, Higgins CB. Thoracic Imaging. Philadelphia: Lippincott Williams & Wilkins; 2005

Case 14

John P. Lichtenberger III

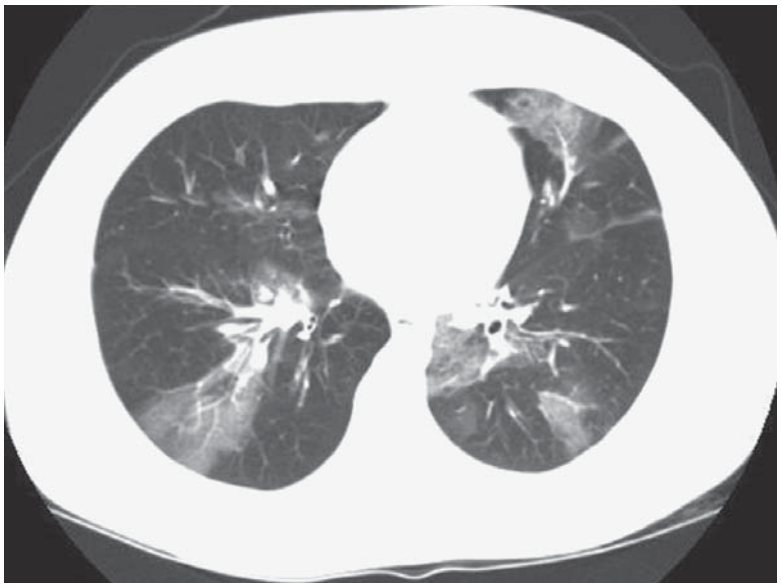


Fig. 14.1 Axial computed tomography image through the chest in the lung window reveals multiple bilateral regions of peripheral air-space disease. (Courtesy of Cristopher Meyer, MD, University of Cincinnati.)

Clinical Presentation

A patient presents with a chronic cough (**Fig. 14.1**).

Key Imaging Finding

Peripheral air-space disease

Top 3 Differential Diagnoses

- **Cryptogenic organizing pneumonia (COP).** A nonspecific inflammatory response resulting in alveolar space fibrosis, COP is characterized by focal areas of chronic lower lobe–predominant peripheral consolidation, which often spares the subpleural space. Diffuse and bronchovascular nodules may also be seen. Lung volumes are often normal radiographically.
- **Eosinophilic pneumonia.** Eosinophilic lung disease encompasses a wide range of disorders characterized by tissue or blood eosinophilia and pulmonary involvement, typically differentiated by integrating clinical presentation with imaging findings. Acute eosinophilic pneumonia typically demonstrates a pattern similar to pulmonary edema, and chronic eosinophilic pneumonia is suggested by homogeneous peripheral consolidations that radiographically may be seen as a photographic negative of pulmonary edema. Upper lobe predominance and a protracted course may distinguish chronic eosinophilic pneumonia from other entities, such as Churg-Strauss (granulomatous vasculitis associated with asthma) and Löffler (eosinophilia and transient and migratory consolidations) syndromes.
- **Pulmonary infarct.** Although bronchial circulation may be protective in the more proximal airways, occlusion of distal pulmonary arteries from embolic sources, malignancy, or interstitial edema may lead to focal, peripheral pulmonary hemorrhage and infarct. This is seen radiographically as wedge-shaped peripheral regions of consolidation. Most pulmonary emboli are multiple, with a lower lobe predominance, and result from deep venous thrombosis. Causes of venous thrombosis are extensive but include trauma, malignancy, hypercoagulable states, and central venous line placement. A Hampton hump refers to a wedge-shaped peripheral opacity along the diaphragm and is highly suggestive of pulmonary embolism. Heart failure is an important predisposing factor for pulmonary infarction in general.

Additional Differential Diagnoses

- **Pulmonary contusion.** In the setting of trauma, hemorrhage into the alveolar space can result in peripheral nonsegmental consolidations, typically adjacent to sites of thoracic injury along the rib cage. These pulmonary contusions usually resolve rapidly if parenchymal injury is not complicated by pneumatocele, laceration, hematoma, or infection.
- **Alveolar sarcoidosis.** Sarcoidosis most commonly presents as bilateral symmetric hilar and mediastinal lymphadenopathy with or without parenchymal involvement. The most common parenchymal manifestations are perilymphatic nodules and architectural distortion with an upper lobe predominance. Peripheral consolidations associated with mediastinal and bilateral hilar adenopathy in an asymptomatic patient may be a rare presentation of alveolar sarcoidosis.

Diagnosis

Eosinophilic pneumonia

✓ Pearls

- COP results in chronic peripheral lower lobe consolidations that can spare the subpleural space.
- Eosinophilic pneumonia can present as a photographic negative of pulmonary edema with eosinophilia.
- Pulmonary infarcts from emboli may present with wedge-shaped peripheral lower lobe consolidations.
- Pulmonary contusions present as nonsegmental consolidations along the chest wall at sites of injury.

Suggested Readings

Collins J, Stern EJ. Chest Radiology: The Essentials. Philadelphia: Lippincott Williams & Wilkins; 2007

Frazier AA, Galvin JR, Franks TJ, et al. From the archives of the AFIP: pulmonary vasculature—hypertension and infarction. Radiographics 2000;20(2):491–524

Jeong YJ, Kim KI, Seol J, et al. Eosinophilic lung diseases: a clinical, radiologic, and pathologic overview. Radiographics 2007;27:617–637

Case 15

John P. Lichtenberger III

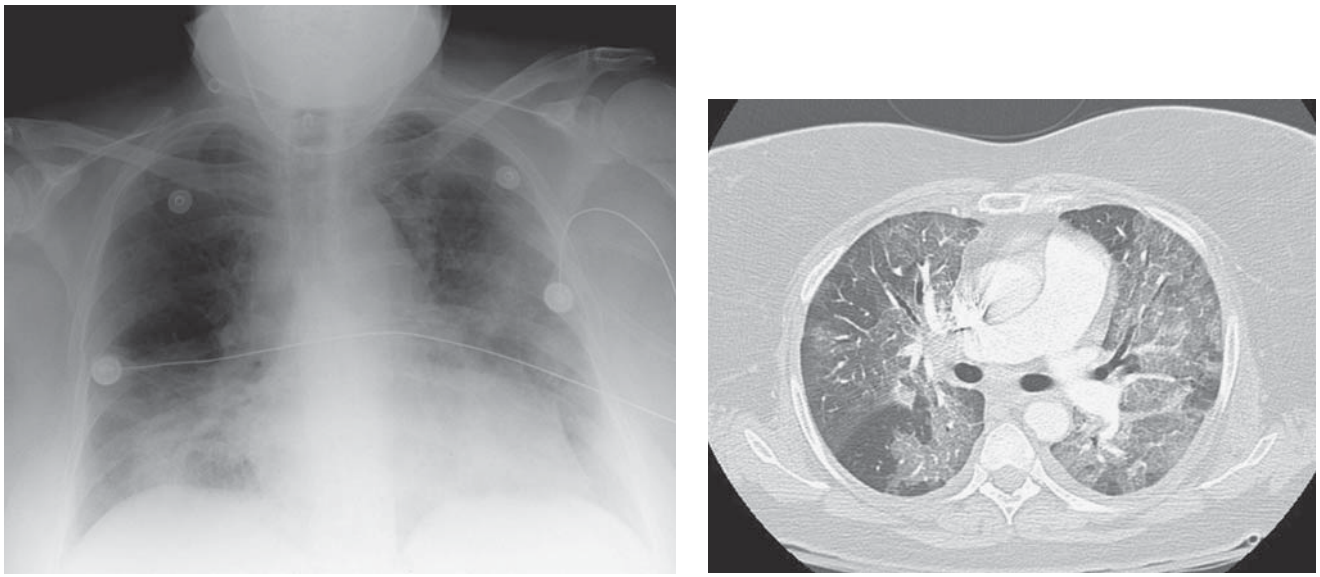


Fig. 15.1 **(A)** Frontal chest radiograph shows lower lung–predominant bilateral patchy air-space disease. **(B)** Contrast-enhanced axial CT image of the chest demonstrates ground-glass opacities in a geographic distribution with sharp margins, as well as smooth interlobular septal thickening, referred to as "crazy paving." Pulmonary vessels are normal in size.

Clinical Presentation

A multitrauma patient presents with shortness of breath (**Fig. 15.1**).

Key Imaging Finding

Ground-glass opacification

Top 3 Differential Diagnoses

- **Pulmonary edema.** Pulmonary edema follows a natural progression that involves interstitial edema with Kerley B lines, cephalization of flow, and resultant air-space disease (ground-glass opacities with regions of consolidation). The central and perihilar lungs are involved early with patchy opacities in a batwing configuration. Cardiomegaly and pleural effusions are seen in the setting of cardiogenic pulmonary edema.
- **Atypical infection.** Pneumocystis, cytomegalovirus, and respiratory syncytial virus pneumonias may account for ground-glass opacities, particularly in an immunocompromised patient. Invasive aspergillosis may elicit a ground-glass halo around a focal region of consolidation that represents pulmonary hemorrhage. A panlobular distribution is more typical of pneumocystic pneumonia.
- **Pulmonary hemorrhage.** Air-space disease secondary to pulmonary hemorrhage may manifest as ground-glass opacities, as well as ground-glass nodules. Common etiologies are trauma and vasculitis.

Additional Differential Diagnoses

- **Acute respiratory distress syndrome (ARDS).** Diffuse lung parenchymal injury resulting in pulmonary opacification and hypoxia characterizes ARDS. Common causes of ARDS are trauma, sepsis, toxic inhalation, and near drowning. Although ARDS remains a clinical diagnosis, the underlying pathology leads to ground-glass opacities with regions of consolidation. The lack of cardiomegaly and pleural effusions helps distinguish this entity from cardiogenic pulmonary edema. Pneumothorax is a frequent complication.
- **Alveolar proteinosis.** An idiopathic disease predominantly affecting middle-aged men, alveolar proteinosis results from chronic accumulation of excessive proteinaceous material in the alveoli. Radiographic features may mimic pulmonary edema, although cardiomegaly and pleural effusions are not characteristic. On computed tomography, ground-glass opacities are distributed geographically with sharp margination and associated smooth septal thickening. Juxtaposition of normal and involved lung parenchyma has been termed "crazy paving," which in and of itself is a nonspecific finding. Treatment consists of bronchoalveolar lavage.
- **Vasculitis.** Perivascular inflammation within the lung secondary to a vasculitic process may appear as ground-glass opacities. Common causes are Wegener granulomatosis and systemic lupus erythematosus. Symptomatic patients are treated with steroids during acute flares.

Diagnosis

Acute respiratory distress syndrome

✓ Pearls

- Pulmonary edema progresses from interstitial to air-space disease; cardiomegaly and effusions are typical.
- Atypical infections may present with ground-glass opacities, especially in immunocompromised patients.
- ARDS results from diffuse lung injury; it mimics pulmonary edema but lacks cardiomegaly or effusions.
- Alveolar proteinosis presents with ground-glass opacities and septal thickening; it is treated with lavage.

Suggested Readings

Park CM, Goo JM, Lee HJ, et al. Nodular ground-glass opacity at thin-section CT: histologic correlation and evaluation of change at follow-up. Radiographics 2007;27:391–408

Reed JC. Chest Radiology: Plain Film Patterns and Differential Diagnoses. St. Louis: Mosby; 1991

Case 16

Arash J. Momeni

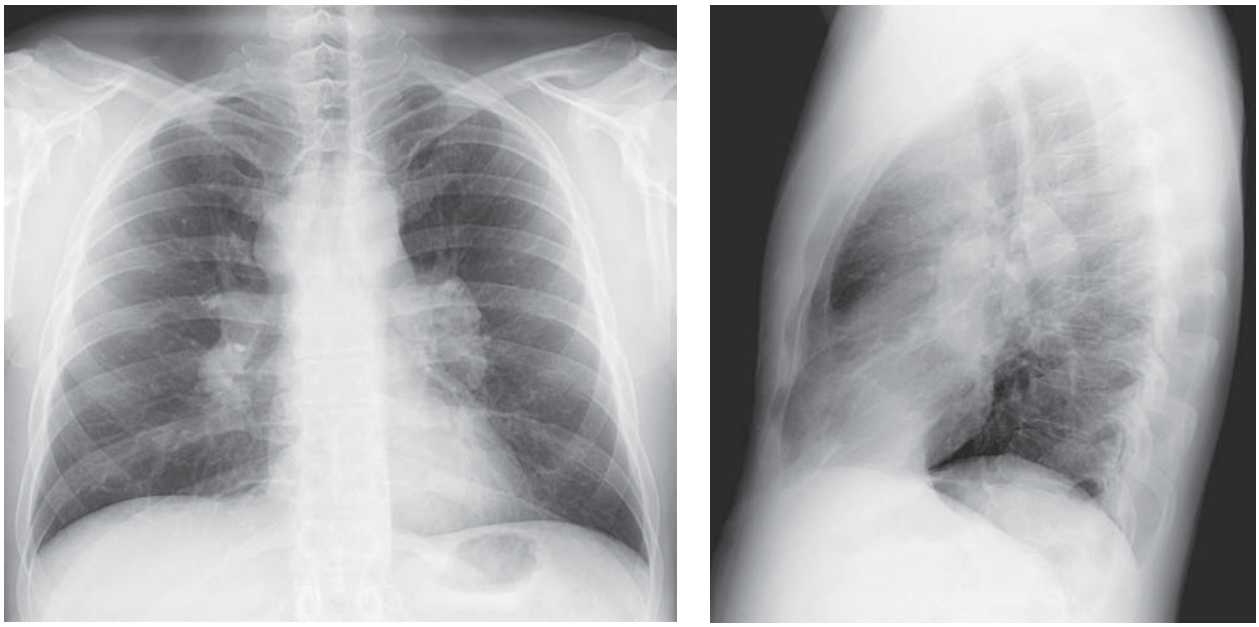


Fig. 16.1 **(A)** Frontal and **(B)** lateral chest radiographs demonstrate bilateral symmetric hilar and right paratracheal lymphadenopathy.

Clinical Presentation

A 34-year-old African American man presents with long-standing shortness of breath (**Fig. 16.1**).

Key Imaging Finding

Mediastinal/hilar lymphadenopathy

Top 3 Differential Diagnoses

- **Infection.** Reactive lymphadenopathy from an infectious etiology, such as tuberculosis (TB), fungal disease, or bacterial pneumonia, is the most common cause of mediastinal lymph node enlargement. Coexistent pulmonary disease, including granuloma formation and air-space disease, is commonly seen. Calcified lymph nodes may be seen in the setting of TB and fungal disease, including histoplasmosis and coccidioidomycosis. Mycobacterial infection may present with low-attenuation lymph nodes.
- **Lymphoma.** Thoracic involvement of lymphoma is usually associated with Hodgkin disease. It typically presents as superior mediastinal lymphadenopathy, resulting in mediastinal widening on chest radiographs. On computed tomography (CT), lymphoma may present as multiple discrete masses located in known lymph node sites, conglomerate lymphadenopathy, or an anterior mediastinal mass. Calcification in the absence of treatment is exceedingly rare. Lymphoma is the second most common intrathoracic malignancy associated with human immunodeficiency virus (HIV) infection, in which it is usually aggressive, widely disseminated, and associated with extranodal disease.
- **Sarcoidosis.** Sarcoidosis is a systemic disease of unknown etiology characterized by noncaseating granulomas. It characteristically affects African American women between 20 and 40 years of age. Lymphadenopathy is the most common intrathoracic manifestation and occurs in 75 to 80% of patients at some point in their illness. The classic pattern is bilateral hilar and right paratracheal nodal enlargement, the so-called 1-2-3 sign. Sarcoidosis may be classified according to its appearance on the chest radiograph as normal (stage 0), lymphadenopathy only (stage I), nodal enlargement and parenchymal disease (stage II), parenchymal disease only (stage III), or end-stage pulmonary fibrosis (stage IV).

Additional Differential Diagnoses

- **Metastatic disease.** Primary neoplasms may present with mediastinal or hilar lymph node enlargement. Neoplasms prone to mediastinal or hilar metastases include lung, breast, head and neck, and genitourinary tract carcinomas, as well as melanoma.
- **Pneumoconiosis.** Pneumoconioses are occupational diseases caused by inhalation of dust particles, including coal and silica. In addition to upper lobar parenchymal disease, scarring, and subpleural micronodules, silicosis and coal workers' pneumoconiosis characteristically present with calcified hilar and mediastinal lymph nodes in a characteristic "eggshell" configuration. These patients are prone to superimposed infection, especially TB, and are at increased risk of developing lung cancer.

Diagnosis

Sarcoidosis

✓ Pearls

- Reactive lymphadenopathy is common with infection; nodes may calcify with TB and fungal disease.
- Absence of superior mediastinal lymphadenopathy makes Hodgkin disease an unlikely consideration.
- Sarcoidosis classically presents with right paratracheal and bilateral hilar lymphadenopathy ("1-2-3" sign).
- Pneumoconioses are occupational diseases that present with calcified nodes in an "eggshell" pattern.

Suggested Readings

Collins J, Stern EJ. Chest Radiology: The Essentials. Philadelphia: Lippincott Williams & Wilkins; 2007

McLoud TC. Thoracic Radiology: The Requisites. St Louis: Mosby; 1998

Case 17

Bang Huynh



Fig. 17.1 Axial CT image through the chest in the bone window shows unilateral thick, uniform pleural calcification along the posterior pleural surface of the left hemithorax. The ipsilateral hemithorax is small compared with the right.

Clinical Presentation

History withheld (**Fig. 17.1**).

Key Imaging Finding

Calcified pleural disease

Top 3 Differential Diagnoses

- **Asbestos-related pleural disease.** Manifestations of asbestos exposure include pleural plaques, pleural thickening, and pleural effusion. Of these, pleural plaques are the most common. Plaques develop 10 to 20 years after exposure. On computed tomography, plaques have a "squared" profile. Calcifications are seen in ~20% of cases, typically of the parietal surface. Most cases tend to be bilateral, but they are not necessarily symmetric. The apices and costophrenic sulci are often spared. As a side note, asbestos exposure, asbestosis, and mesothelioma may be related, but they are distinct entities. Asbestosis is the interstitial pulmonary fibrosis that occurs as a result of asbestos exposure, and mesothelioma is a malignancy.
- **Fibrothorax secondary to infection or hemorrhage.** Fibrothorax is the result of an organizing pyothorax, hemothorax, or effusion. If extensive enough, it can cause lung restriction. Pleural calcifications can develop in the setting of fibrosis, regardless of the cause. Calcifications are often seen in patients with healed tuberculosis, prior bacterial empyema, or prior hemothorax. Unlike plaques of asbestos exposure, these etiologies tend to be unilateral.
- **Iatrogenic (pleurodesis).** Talc pleurodesis is the intentional creation of fibrosis for symptomatic malignant pleural effusions, chylous effusions, or recurrent spontaneous pneumothoraces. As with other causes of pleural fibrosis, calcification can occur. Talc pleurodesis can mimic true pleural calcification by the accumulation of talc in the pleural space. In such instances, deposits of high-density talc can coat the visceral and parietal surface. If an effusion is present, a variant of the "split pleura" sign may be seen.

Diagnosis

Fibrothorax (secondary to prior tuberculous pleuritis)

✓ Pearls

- Asbestos-related pleural disease usually develops 10 to 20 years after onset of exposure.
- "Rounded atelectasis" is commonly seen with pleural disease of asbestos exposure.
- Fibrothorax presents as pleural calcifications and restriction in a patient with prior infection or hemorrhage.
- Talc pleurodesis is used to treat recurrent pleural effusions or pneumothoraces.

Suggested Readings

Choi J, Hong KT, Oh Y, et al. CT manifestations of late sequela in patients with tuberculosis pleuritis. AJR Am J Roentgenol 2001;176:441–445

Murray JG, Patz EF Jr, Erasmus JJ, Gilkeson RC. CT appearance of pleural space after talc pleurodesis. AJR Am J Roentgenol 1997;169:89–91

Case 18

Thomas Ray S. Sanchez

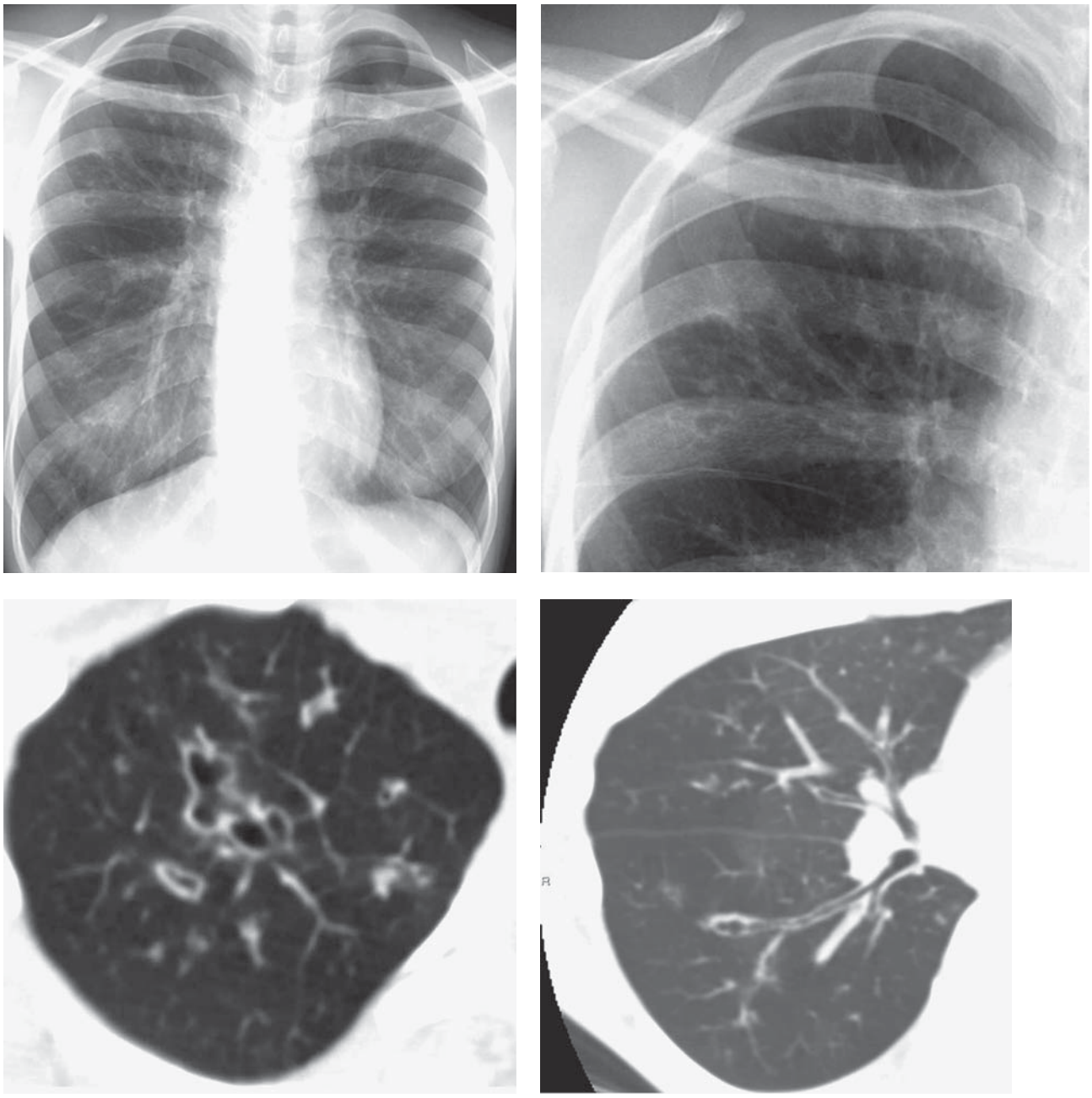


Fig. 18.1 **(A)** Posteroanterior radiograph of the chest shows pulmonary hyperaeration with diffuse peribronchial thickening. **(B)** Coned-down view of the right upper lobe demonstrates thickened and dilated bronchi, as well as clusters of cystic spaces. **(C)** Coned-down axial high-resolution CT image through the right upper lobe in the lung window shows findings compatible with bronchiectasis: dilated and thickened airways; mucous plugging of the distal airways, giving rise to the "tree in bud sign"; and the "signet ring" sign, with the bronchial diameter larger than the accompanying blood vessel. **(D)** Coned-down axial high-resolution CT image through the right lower lobe in the lung window reveals dilated and thickened bronchioles with a lack of distal tapering, the "tram track" sign.

Clinical Presentation

A 20-year-old woman presents with a history of chronic cough, asthma-like symptoms, and severe sinusitis (**Fig. 18.1**).

Key Imaging Finding

Bronchiectasis

Top 3 Differential Diagnoses

- **Postinfectious.** The most common cause of bronchiectasis is postinfectious, resulting from poorly treated or necrotizing infections, to include bacterial, viral, and mycobacterial etiologies. The bronchial walls are damaged not only from the infectious organism itself but also by the host's immune response. The end result is peribronchial injury, impaired clearance of secretions, and further colonization of pathogenic agents. Although pulmonary involvement can be diffuse, more often it is focal. Tuberculosis typically involves the upper lobes; *Mycobacterium avium* complex (MAC) characteristically affects the lingula and right middle lobe in older women ("Lady Windermere" syndrome).
- **Cystic fibrosis.** Cystic fibrosis is the most common life-limiting genetic disorder in Caucasian children and young adults. It is a multisystem disorder predominantly involving the respiratory and gastrointestinal tracts, causing thick mucous secretions of the exocrine gland. Pulmonary involvement occurs in more than 90% of patients and can sometimes be the only manifestation of cystic fibrosis. The viscous secretions cause mucous plugging, leading to bacterial infections, chronic inflammation, and tissue destruction reminiscent of postinfectious bronchiectasis. In contradistinction, the pulmonary involvement is more diffuse but often predominates in the upper lobes. High-resolution computed tomography has been proven to be sensitive and specific in demonstrating small airway disease, such as air trapping, mucous plugging, and bronchiectasis.
- **Allergic bronchopulmonary aspergillosis (ABPA).** ABPA is a type of hypersensitivity reaction to *Aspergillus fumigatus*. Hence, it is commonly associated with asthma. Patients will present with asthma-like symptoms but fail to respond to conventional antiasthma therapy. Bronchiectasis results from the bronchial wall damage caused by mucous plugs containing immune complexes, inflammatory cells, and hyphal elements of the fungus. As with cystic fibrosis, the pattern of bronchiectasis is more diffuse but predominates centrally. Mucous plugging of the central dilated bronchi results in the characteristic "finger in glove" opacities, which are typically of increased attenuation (>100 HU).

Additional Differential Diagnoses

- **Obstructive lesion/mass.** Postobstructive bronchiectasis is often due to aspiration, hilar adenopathy, or endobronchial tumors. The retained secretions become breeding grounds for infections and eventual tissue damage. The pattern of bronchiectasis is often focal and, in cases of chronic aspirations, usually involves the lower lobes.
- **Ciliary dyskinesia.** Ciliary dyskinesia is a group of genetic disorders of cilia motility, resulting in poor mucociliary clearance, chronic infections, and bronchiectasis. Kartagener syndrome is a variant of this disease characterized by sinusitis, bronchiectasis, infertility, and situs inversus.

Diagnosis

Cystic fibrosis

✓ Pearls

- A variety of infections may lead to bronchiectasis; MAC classically involves the right middle lobe and lingula.
- Bronchiectasis associated with cystic fibrosis tends to be central and involve the upper lobes.
- Mucous plugging within dilated central bronchi ("finger in glove") is classically seen with ABPA.
- Kartagener syndrome is characterized by sinusitis, bronchiectasis, infertility, and situs inversus.

Suggested Readings

Grenier P, Maurice F, Musset D, et al. Bronchiectasis: assessment by thin-section CT. Radiology 1986;161:95–99

Kuhlman JE, Reyes BL, Hruban RH, et al. Abnormal air-filled spaces in the lung. Radiographics 1993;13:47–75

Case 19

Paul B. DiDomenico

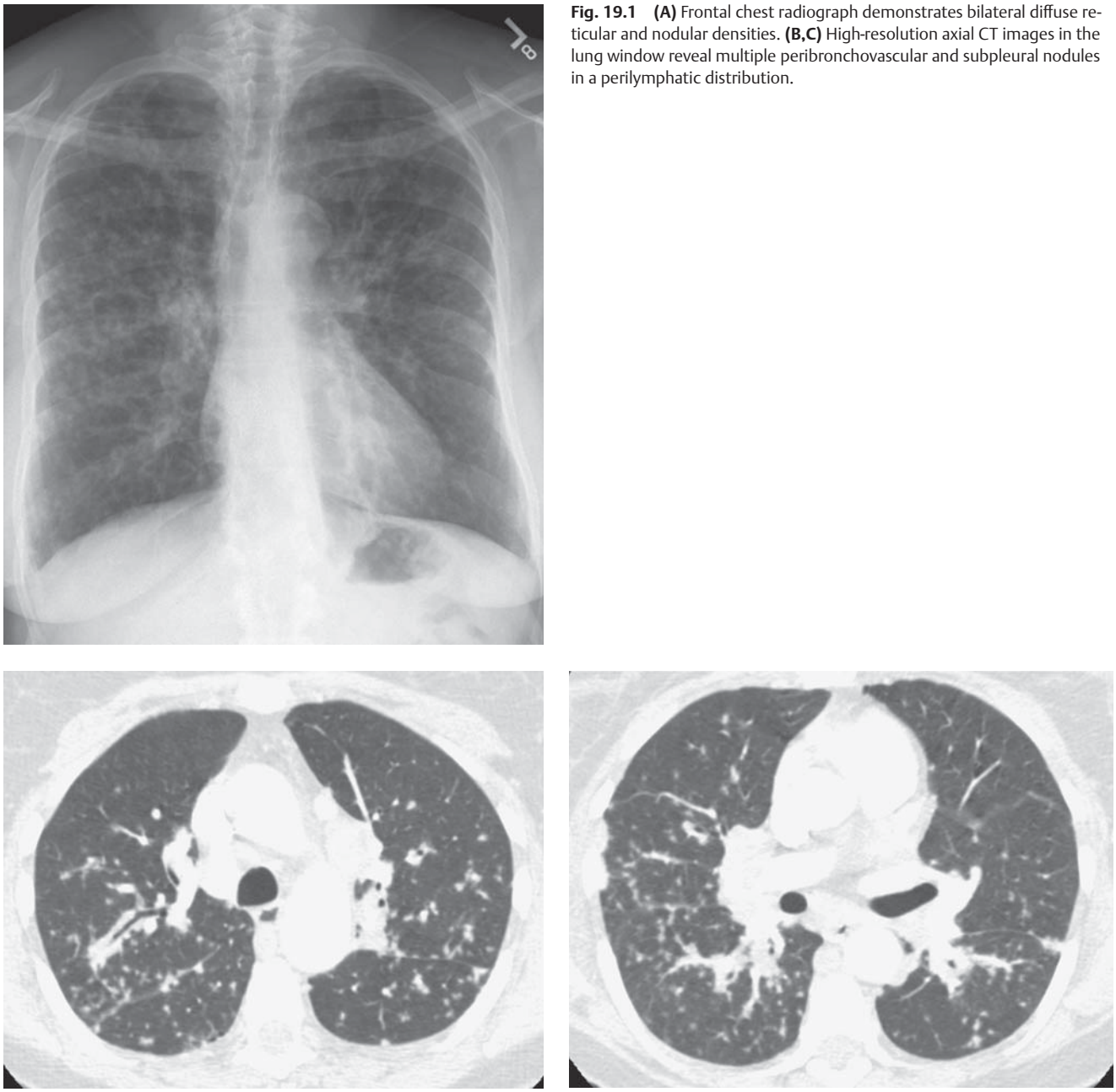


Fig. 19.1 **(A)** Frontal chest radiograph demonstrates bilateral diffuse reticular and nodular densities. **(B,C)** High-resolution axial CT images in the lung window reveal multiple peribronchovascular and subpleural nodules in a perilymphatic distribution.

Clinical Presentation

A middle-aged woman presents with fatigue (**Fig. 19.1**).

Key Imaging Finding

Perilymphatic pulmonary nodules

Top 3 Differential Diagnoses

- **Sarcoidosis.** Sarcoidosis is an idiopathic granulomatous disease that more commonly occurs in African Americans. It is a systemic disease, although the lung is the most commonly involved organ system. Chest radiographs may demonstrate mediastinal lymphadenopathy with a bilateral upper lobe–predominant interstitial pattern of reticulonodular opacities. The high-resolution computed tomography (CT) appearance is that of multiple 1 to 5 mm nodules in a peribronchovascular and subpleural (perilymphatic) distribution with irregular interlobular septal thickening and regions of architectural distortion. Additional chest findings may include enlarged mediastinal lymph nodes, alveolar opacities, and fibrotic changes with peripheral honeycombing in late-stage disease.
- **Lymphangitic spread of tumor.** Also known as lymphangitic carcinomatosis, this refers to neoplastic infiltration of the pulmonary lymphatics either from direct invasion by a primary lung neoplasm, retrograde extension of hilar nodal disease, or metastatic hematogenous emboli that have invaded the lymphatic system. A perilymphatic nodular pattern is characteristic but is usually unilateral or asymmetric if bilateral, possibly with pleural effusions. These features may help distinguish the appearance from sarcoidosis. Common tumors include bronchogenic, breast, renal, gastrointestinal, and thyroid carcinomas, as well as melanoma.
- **Pneumoconiosis.** Silicosis and coal workers' pneumoconiosis result from occupational exposure and present as upper lobe–predominant interstitial lung diseases, owing to decreased lymphatic drainage of the upper lobes. Either perilymphatic or centrilobular nodules may be present, which may eventually coalesce to form masslike opacities and may calcify. Involved lymph nodes may also calcify peripherally, resulting in a characteristic "eggshell" appearance. Late findings may include fibrosis with peripheral emphysema (progressive massive fibrosis).

Additional Differential Diagnoses

- **Lymphoproliferative disorder.** Lymphoproliferative disorders, including lymphoma, posttransplant lymphoproliferative disorder (PTLD), and lymphocytic interstitial pneumonitis (LIP), may manifest as a perilymphatic pulmonary nodular pattern. Correlation with clinical history is helpful, as PTLD occurs in up to 8% of lung transplant patients, and LIP is associated with human immunodeficiency virus/acquired immunodeficiency syndrome (HIV/AIDS) in children, as well as Sjögren syndrome in adults.

Diagnosis

Sarcoidosis

✓ Pearls

- Parenchymal involvement of sarcoidosis can manifest as multiple bilateral perilymphatic nodules.
- Lymphangitic carcinomatosis presents most commonly as a unilateral perilymphatic nodular pattern.
- Pneumoconioses are inhalational diseases that may reveal perilymphatic or centrilobular nodules.
- Lymphoproliferative disorders (lymphoma, PTLD, and LIP) most often occur in predisposed patients.

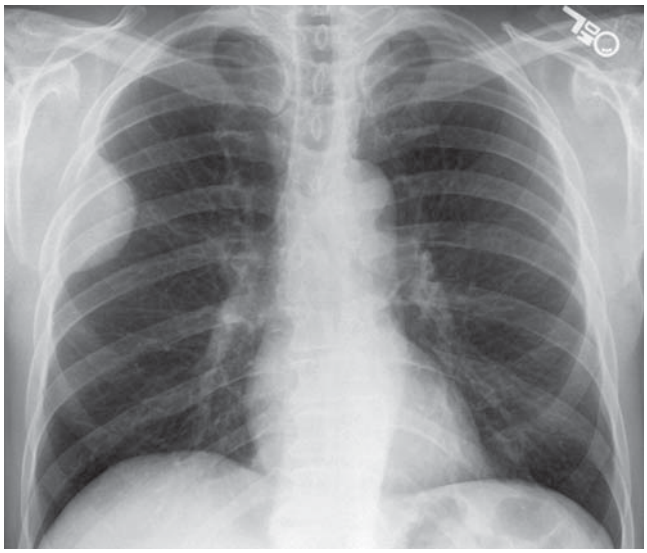
Suggested Readings

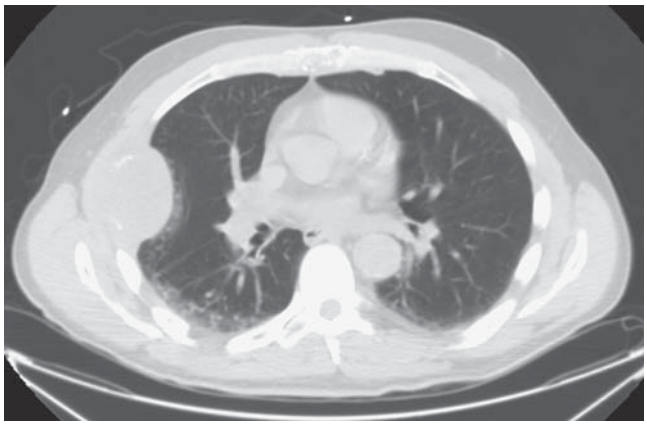
Collins J, Stern EJ. Chest Radiology: The Essentials. Philadelphia: Lippincott Williams & Wilkins; 2007

Webb WR, Muller NL, Neidich DP. High-Resolution CT of the Lung. Philadelphia: Lippincott Williams & Wilkins; 2000

Case 20

John P. Lichtenberger III





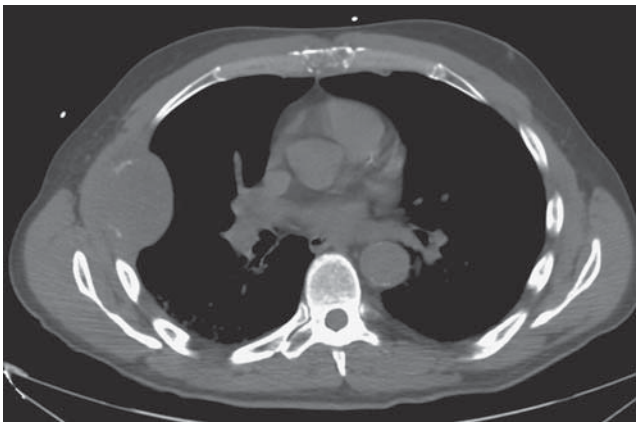


Fig. 20.1 **(A)** Posteroanterior radiograph of the chest shows a smooth, peripheral, well-demarcated mass with a broad base and obtuse angles to the chest wall. The appearance is reminiscent of a "ball under a blanket." Subtle rib erosive changes were evident on close inspection. Axial unenhanced CT images through the chest in **(B)** soft tissue and **(C)** bone window confirms the pleural and extrapleural location of the mass with a smooth interface with lung parenchyma. Rib erosive changes are better seen on CT.

Clinical Presentation

A patient presents with dyspnea and chest pain (**Fig. 20.1**).

Key Imaging Finding

Pleural-based mass

Top 3 Differential Diagnoses

- **Pleural metastases.** The most common neoplasm of the pleura is metastatic disease, usually from adenocarcinoma of the lung and breast, lymphoma, or invasive thymoma. Although effusion is the most common presentation of metastatic pleural disease, metastases can also cause both diffuse pleural thickening and pleural seeding with nodular thickening and plaques. The metastatic foci may involve the pleura directly or extend into the pleura from chest wall involvement, to include the ribs. Irregular pleural thickening and chest wall invasion/erosive changes are suggestive of an aggressive process.
- **Empyema.** Defined as pulmonary parenchymal infection extending to the pleural surface, empyema is most frequently the result of bacterial pneumonia, recent surgery, or trauma. Important complications include bronchopleural fistulas and fibrous loculation. Drainage into the chest wall, termed empyema necessitatis, is most often seen in tuberculosis, although other considerations include fungal infection in immunocompromised patients, as well as malignancy. Radiographically, loculated collections with obtuse margins may be lenticular and compress the adjacent lung. Air–fluid levels may be seen in both empyema and lung abscess. Pleural collections tend to have different sizes and configurations on frontal and lateral projections, whereas parenchymal abscesses typically have a similar appearance on frontal and lateral views.
- **Mesothelioma.** Although rare, mesothelioma is the most common primary pleural neoplasm and is associated with prior asbestos exposure. Radiologic features suggesting mesothelioma are irregular, nodular pleural thickening (>1 cm), involvement of the mediastinal pleura, volume loss of the involved hemithorax, and calcification. Pleural effusions are also relatively common. Mesothelioma and pleural metastases, however, are not reliably differentiated based on imaging findings.

Additional Differential Diagnoses

- **Fibrous tumor of the pleura.** Localized fibrous tumor of the pleura is a solitary, lobular, encapsulated tumor arising from either the visceral (80%) or parietal pleura. These tumors may be quite large at presentation, and when pedunculated they may demonstrate pathognomonic positional mobility. Important associated clinical features are hypertrophic osteoarthropathy (HOA) and episodic hypoglycemia. Characteristic findings on computed tomography include contrast enhancement and heterogeneity related to central necrosis and/or hemorrhage. Fibrous content may result in low signal intensity on T1- and T2-weighted magnetic resonance sequences.
- **Fibrothorax.** Etiologies of focal or diffuse fibrosis of the pleura are hemothorax, tuberculous or pyogenic empyema, asbestos-related pleural disease, and inflammatory conditions such as rheumatoid effusions. Pleural thickening in fibrothorax is usually <1 cm and may calcify; the mediastinal pleura is usually spared.

Diagnosis

Pleural metastases

✓ Pearls

- Metastases are the most common pleural neoplasm; look for chest wall involvement and erosive changes.
- Empyemas often result from bacterial infection; bronchopleural fistulas and loculations are complications.
- Mesothelioma is the most common primary pleural malignancy and is associated with asbestos exposure.
- Fibrous tumors of the pleura may be large and pedunculated; HOA and episodic hypoglycemia may occur.

Suggested Readings

McLoud TC. Thoracic Radiology: The Requisites. St. Louis: Mosby; 1998

Webb WR, Higgins CB. Thoracic Imaging. Philadelphia: Lippincott Williams & Wilkins; 2005

Case 21

William T. O'Brien Sr.

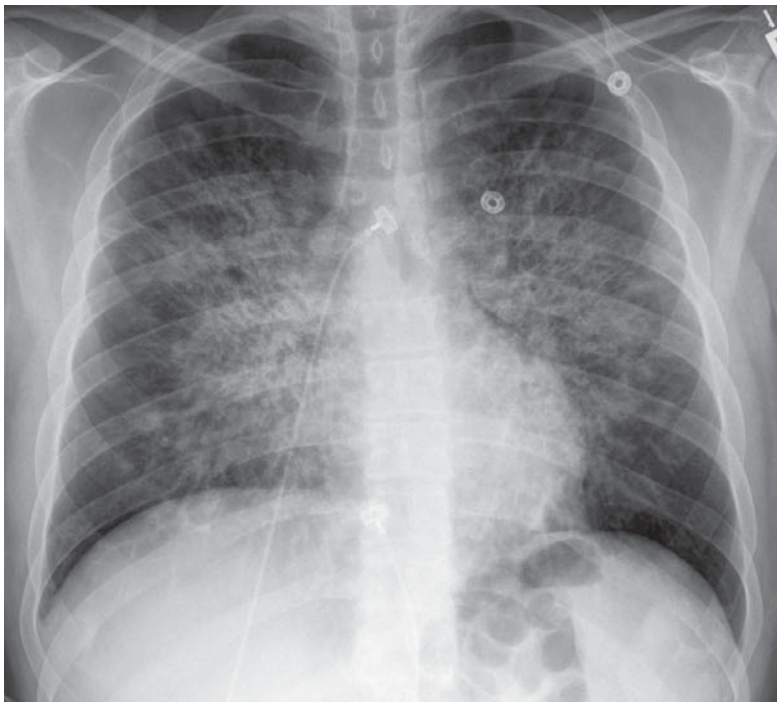


Fig. 21.1 Frontal chest radiograph reveals perihilar opacities in a reticulonodular pattern, along with scattered ground-glass opacities.

Clinical Presentation

A 32-year-old man who is positive for human immunodeficiency virus (HIV) presents with a several-week history of shortness of breath, fever, and nonproductive cough (**Fig. 21.1**).

Key Imaging Finding

Parenchymal disease in a patient with HIV

Top 3 Differential Diagnoses

- ***Pneumocystis carinii (jiroveci)* pneumonia (PCP).** Patients with HIV with CD4 (cluster of differentiation 4) counts <200 are at increased risk of acquiring PCP; it is the most common opportunistic infection in this population. The disease course is indolent, with patients presenting with several weeks of dyspnea, fever, and cough. The most common imaging findings are confluent regions of ground-glass opacities with or without reticulonodular septal thickening. Cysts may be present in up to one third of cases.
- **Tuberculosis (TB).** The clinical and radiographic findings of TB in the HIV population depend largely on the CD4 count. In patients with a CD4 count >200, the findings are similar to reactivation TB in immunocompetent hosts, including upper lobe consolidations, upper lobe cavitary lesions, and centrilobular pulmonary nodules in a "tree in bud" configuration. In patients with CD4 counts <200, the findings are more reflective of primary TB, including a miliary pattern, consolidations, and lymphadenopathy.
- **Fungal infection.** Histoplasmosis and coccidioidomycosis infection in the HIV population consists predominantly of a miliary pattern due to hematogenous dissemination of the disease. With severe infection, pulmonary consolidations may occur.

Additional Differential Diagnoses

- **Invasive aspergillosis.** Invasive aspergillosis is an aggressive infection (mortality rate 70–90%) that presents with multiple pulmonary nodules with a surrounding ground-glass halo secondary to hemorrhage. Cavitation is common. An "air crescent" sign is seen in the recovery or healing phase.
- **Kaposi sarcoma.** Kaposi sarcoma is the most common malignancy in the United States related to acquired immunodeficiency syndrome (AIDS). Nearly all patients with Kaposi sarcoma have skin involvement. Pulmonary involvement consists of nodular peribronchovascular septal thickening, as well as lymphadenopathy and pleural effusions.
- **Pulmonary lymphoma.** AIDS-related lymphoma is of the non-Hodgkin variant and typically presents as multiple nodules or masses (up to 5 cm). Less common radiographic manifestations are air-space consolidation and reticulonodular septal thickening. Lymphocytic interstitial pneumonitis (LIP) is a lymphoproliferative disorder that may rarely evolve into lymphoma. LIP presents in immunocompromised patients as centrilobular pulmonary nodules, smooth or nodular septal thickening, and ground-glass opacities.

Diagnosis

Pneumocystis carinii (jiroveci) pneumonia

✓ Pearls

- PCP is the most common opportunistic infection in HIV; ground-glass opacities are most often seen.
- In immunocompromised patients, TB most often presents with air-space disease, miliary nodules, and lymphadenopathy.
- Invasive aspergillosis presents as nodules with a ground-glass halo; the "air crescent" sign occurs with healing.
- Pulmonary involvement of Kaposi sarcoma is usually preceded by cutaneous or visceral involvement.

Suggested Readings

Marchiori E, Mueller NL, Souza AS, et al. Pulmonary disease in patients with AIDS: high-resolution CT and pathologic findings. AJR Am J Roentgenol 2005;184:757–764

Reed JC. Chest Radiology: Plain Film Patterns and Differential Diagnoses. St. Louis: Mosby; 1991.

Case 22

Bang Huynh

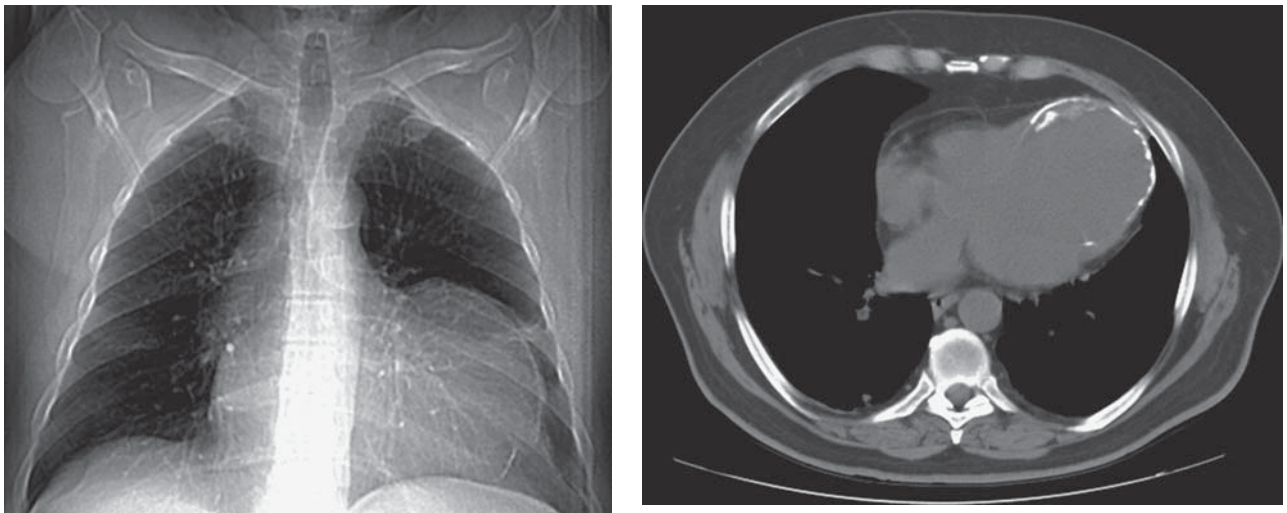


Fig. 22.1 **(A)** Scout CT image shows an abnormally enlarged left ventricular contour with a rim of peripheral calcification. **(B)** Unenhanced CT image of the chest in the soft tissue window reveals a wide-neck out-pouching with myocardial calcifications.

Clinical Presentation

An older man presents with chest pain (**Fig. 22.1**).

Key Imaging Finding

Abnormal left ventricular contour

Top 3 Differential Diagnoses

- **True left ventricular aneurysm.** A true ventricular aneurysm is the result of a myocardial infarction. Unlike false aneurysms (which are contained ruptures), true aneurysms have a true myocardial wall. The wall can be thinned and akinetic or dyskinetic with paradoxical bulging during systole. As with scarring of any cause, it can partially calcify. Most true aneurysms involve the anterolateral wall or apex of the left ventricle. A more reliable distinguishing feature of false aneurysms is the presence of a wide neck (>50% of the aneurysm diameter). Most true aneurysms are treated medically unless they are felt to cause arrhythmias or exacerbate heart failure. Thrombus may form in the aneurysm, requiring more aggressive management, as left-sided emboli may result in systemic end-arterial occlusions.
- **False left ventricular aneurysm.** A false ventricular aneurysm is a pseudoaneurysm that maintains communication with the ventricular cavity. It is a rupture of the myocardium contained by pericardial adhesions and hematoma, a rare complication of myocardial infarction. Differentiation between a true and false aneurysm is important, because false aneurysms have a propensity to rupture. For that reason, false aneurysms are usually resected. A progressively enlarging abnormal ventricular contour should alert to the possibility of an expanding false aneurysm. False aneurysms tend to occur on the posterior or diaphragmatic surface of the heart, but the location alone is not a reliable discriminator. On computed tomography (CT) or magnetic resonance imaging (MRI), the more reliable finding is a narrow neck (<50% of the aneurysm diameter).
- **Pericardial cyst/mass.** Pericardial cysts or masses should be included in the differential of an abnormal cardiac contour on radiograph. On CT or MRI, a pericardial mass or cyst should be readily distinguishable from a ventricular aneurysm. Pericardial cysts are usually fluid attenuation on CT. Occasionally, proteinaceous fluid can cause it to be of higher attenuation. On MRI, pericardial cysts follow fluid signal characteristics. When proteinaceous, the fluid can be high signal on T1-weighted sequences. A pericardial mass will be morphologically different from an aneurysm. Gradient echo and postcontrast imaging are helpful in distinguishing thrombus from tumor.

Additional Differential Diagnoses

- **Calcific pericarditis.** Calcific pericarditis is mentioned not because it results in a ventricular contour abnormality but because the associated pericardial calcifications can mimic calcifications in infarcted or aneurysmal myocardium on radiographs. Tuberculosis (TB) is a relatively common cause of pericardial calcifications. Other causes are viral and uremic pericarditis.

Diagnosis

True ventricular aneurysm

✓ Pearls

- True aneurysms involve all myocardial layers, have a wide neck, and commonly involve the cardiac apex.
- False aneurysms are contained ruptures that commonly occur along the diaphragmatic cardiac surface.
- Pericardial cysts and masses may produce an abnormal cardiac contour on radiographs.
- Calcific pericarditis results from TB, viral, or uremic pericarditis and may mimic ventricular calcifications.

Suggested Readings

Konen E, Merchant N, Gutierrez C, et al. True versus false left ventricular aneurysm: differentiation with MR imaging—initial experience. Radiology 2005;236:65–75

Webb WR, Higgins CB. Thoracic Imaging. Philadelphia: Lippincott Williams & Wilkins; 2005

Case 23

Bang Huynh

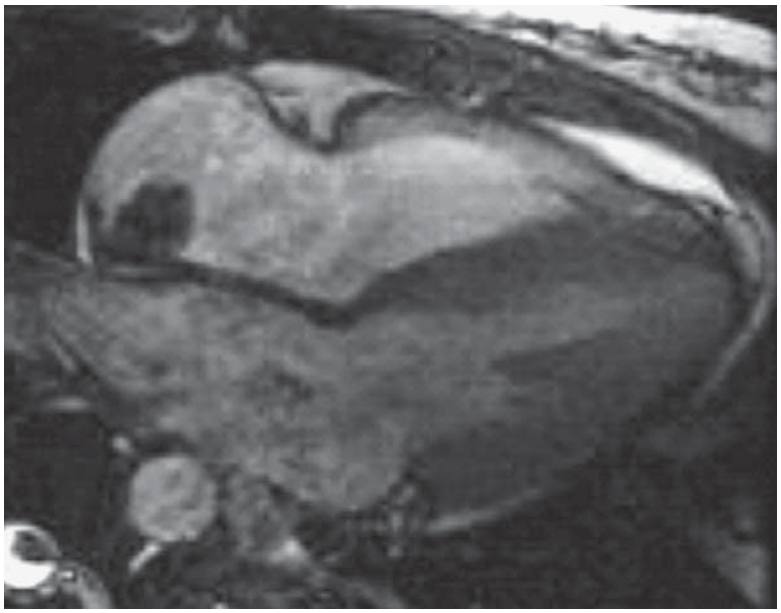


Fig. 23.1 Four-chamber gradient echo image reveals a circumscribed hypointense mass within the right atrium along the interatrial septum. (Courtesy of Cristopher Meyer, MD, University of Cincinnati.)

Clinical Presentation

A patient presents with intermittent chest pain, palpitations, and shortness of breath (**Fig. 23.1**).

Key Imaging Finding

Cardiac mass

Top 3 Differential Diagnoses

- **Thrombus.** Thrombus is the most common cardiac mass and should be high in the list of differential diagnoses for a nonenhancing cardiac filling defect. Left ventricular thrombi are usually associated with ventricular aneurysms. Left atrial thrombi are often associated with atrial fibrillation. Though often seen on computed tomography (CT), magnetic resonance imaging (MRI) is the modality of choice for distinction between a thrombus and a tumor. Tumors enhance, whereas thrombi do not. MRI signal characteristics can be helpful, particularly on gradient echo (GRE), where thrombi tend to be low in signal. That said, myxomas can also be dark on GRE, and fresh thrombi may not yet be low signal on GRE. Thrombi in the left chambers can embolize to cause stroke or end-organ ischemia/infarct.
- **Metastases.** Cardiac metastases are far more common than primary cardiac neoplasms. Melanoma, leukemia, and lymphoma are frequent culprits, but any malignancy can find its way to the heart, including breast and lung carcinoma. Routes to the heart include hematogenous seeding, lymphatic spread, and direct extension. MRI is helpful in revealing the extent and location of the metastasis and thus helps in assessing resectability.
- **Benign primary cardiac neoplasm.** Although far less common than metastases, benign primary cardiac tumors are more common than malignant primary cardiac tumors by a ratio of 4:1. Although benign in the sense that they do not metastasize or locally invade, they can still cause significant morbidity and mortality by interfering with normal cardiac function. Such masses can cause arrhythmias, abnormal myocardial contraction/relaxation, and obstruction of normal coronary flow. Among the benign cardiac primaries, myxomas are the most common and typically occur in young to middle-aged adults (more common in women). Myxomas are usually in the left atrium (70%), pedunculated, and attached to the interatrial septum. They can be large and cause symptoms secondary to outflow obstruction or systemic emboli. On gradient echo cine MR images, myxomas are hypointense; they are isointense to cardiac muscle on T1 sequences and heterogeneously enhance. Calcifications may be seen. Rhabdomyomas are the most common primary benign cardiac neoplasms in children and are associated with tuberous sclerosis. They more commonly originate along the interventricular septum and may be multiple.

Additional Differential Diagnoses

- **Malignant primary cardiac neoplasm.** About 20% of primary cardiac tumors are malignant. Of those, sarcomas are the most common, followed by primary cardiac lymphomas. Although the absence of aggressive features does not exclude malignancy, the presence of the following features makes malignancy likely: irregular margins, disruption of normal boundaries (extension into vessels and/or outside the heart into the mediastinum), central necrosis, multichamber involvement, pericardial effusion, and evidence of metastases.

Diagnosis

Thrombus

✓ Pearls

- Thrombus is the most common cardiac mass; left-sided thrombi can embolize, causing end-organ ischemia.
- Metastases are by far the most common cardiac neoplasms; MRI helps determine the extent of disease.
- Myxomas are the most common benign primary cardiac neoplasms in adults; rhabdomyomas are the most common in children.
- Malignant primary cardiac tumors are the least common neoplasms; sarcomas are the most common type.

Suggested Readings

Araoz PA, Eklund HE, Welch TJ, et al. CT and MR imaging of primary cardiac malignancies. Radiographics 1999;19:1421–1434

Chiles C, Woodard PK, Gutierrez FP. Metastatic involvement of the heart and pericardium: CT and MR imaging. Radiographics 2001;21:439–449

Grebenc ML, Rosado de Christenson ML, Burke AP, et al. Primary cardiac and pericardial neoplasms: radiologic-pathologic correlation. Radiographics 2000;20:1073–1103

Case 24

Bang Huynh



Fig. 24.1 Delayed postgadolinium imaging demonstrates a region of abnormal delayed enhancement within the inferior cardiac wall. The abnormal enhancement involves more than 50% of the thickness of the myocardium. (Courtesy of Cristopher Meyer, MD, University of Cincinnati.)

Clinical Presentation

A patient presents with chest pain (**Fig. 24.1**).

Key Imaging Finding

Delayed myocardial enhancement

Top 3 Differential Diagnoses

- **Infarction/scar.** Use of gadolinium chelates in cardiac magnetic resonance imaging (MRI) includes assessment of early perfusion (first pass) and delayed enhancement pattern. Delayed images are typically acquired 10 to 20 minutes postinjection. Normal myocardium enhances early, whereas infracted myocardium or scar tissue demonstrates delayed enhancement. Distinction between viable and nonviable myocardium is important for clinical decisions. Viable tissue, such as hibernating or stunned myocardium, does not have delayed enhancement. In contrast, infarcted tissue enhances in a delayed fashion. The delayed enhancement is typically subendocardial or transmural in a coronary artery vascular distribution. The extent of mural scarring is important as well; in general, myocardial scarring or fibrosis involving more than 50% of the wall thickness is unlikely to recover contractile function following revascularization.
- **Myocarditis.** Myocarditis is an inflammation of the myocardium resulting from a large variety of causes, such as infections, drugs, toxins, and systemic diseases. The specific cause often remains unknown. Like infarctions, myocarditis can result in delayed myocardial enhancement. Unlike infarcts, the enhancement pattern tends to involve the midportion of the myocardium, rather than subendocardial or transmural involvement. Additionally, myocarditis often does not correspond to a coronary artery vascular distribution. The enhancement pattern of myocarditis has been described as becoming less intense and more diffuse over a period of weeks to months. That said, the distinction between myocarditis and infarction often cannot be made by imaging alone.
- **Cardiac mass.** Metastases to the heart are far more common than primary cardiac tumors. Cardiac neoplasms (metastatic or primary) usually enhance and sometimes have delayed enhancement. The presence and pattern of delayed enhancement are usually not helpful in characterizing the histology of the mass. Morphologic features of the mass and clinical history help distinguish cardiac neoplasms from other etiologies of delayed myocardial enhancement.

Additional Differential Diagnoses

- **Infiltrative disease.** Amyloidosis is perhaps the most common infiltrative disease process involving the myocardium. It is caused by deposition of fibrillar proteins and can result in a restrictive cardiomyopathy. In addition to causing cardiac dysfunction, amyloidosis can reveal areas of delayed enhancement on MRI. The delayed enhancement is often diffuse and heterogeneous and does not correspond to a vascular distribution. Glycogen storage diseases may have similar findings. Abnormal enhancement can also be seen with other infiltrative processes, such as sarcoidosis and lymphoma, which typically reveal more focal regions of heterogeneous delayed myocardial enhancement.

Diagnosis

Infarction/scar

✓ Pearls

- Infarction presents as subendocardial or transmural delayed enhancement in a vascular distribution.
- Myocarditis typically involves the midportion of the myocardium and does not follow a vascular territory.
- Cardiac masses may demonstrate delayed enhancement but will be masslike in a nonvascular distribution.
- Infiltrative diseases cause restrictive physiology and diffuse or focal delayed heterogeneous enhancement.

Suggested Readings

Araoz PA, Eklund HE, Welch TJ, et al. CT and MR imaging of primary cardiac malignancies. Radiographics 1999;19:1421–1434

Vogel-Claussen J, Rochitte CE, WuK C, et al. Delayed enhancement MR imaging: utility in myocardial assessment. Radiographics 2006;26:795–810

Case 25

Bang Huynh

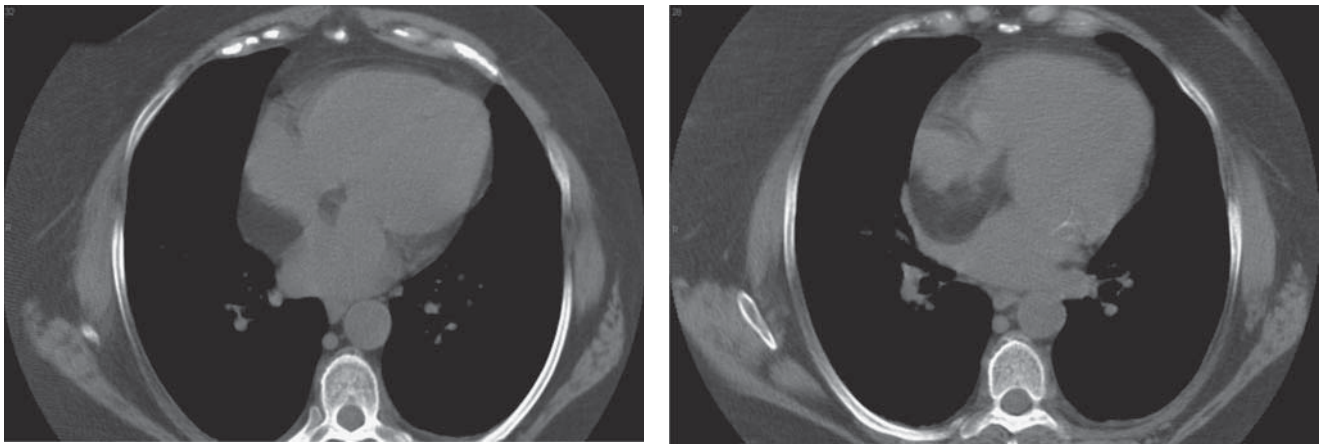


Fig. 25.1 **(A,B)** Unenhanced axial CT images in the soft tissue window demonstrate fat attenuation within the interatrial septum with sparing of the fossa ovalis.

Clinical Presentation

History withheld (**Fig. 25.1**).

Key Imaging Finding

Cardiac wall fat

Top 3 Differential Diagnoses

- **Lipoma.** Lipomas are soft masses composed of encapsulated mature adipose cells. As such, they have attenuation on computed tomography (CT) and signal characteristic on magnetic resonance imaging (MRI) identical to subcutaneous fat. On MRI, lipomas will have high signal on T1 sequences; the signal will suppress with fat saturation. Most are homogeneous and occasionally contain thin septations. Lipomas do not enhance following the administration of intravenous contrast. Common locations are the right atrium and atrial septum.
- **Lipomatous hypertrophy of the interatrial septum.** Despite having a fat composition similar to lipomas, this is a distinct entity. Unlike lipomas, lipomatous hypertrophy is not encapsulated. Instead, the fat insinuates the interatrial septum around the fossa ovalis. It is not a true neoplasm. Associated symptoms include supraventricular arrhythmias.
- **Arrhythmogenic right ventricular dysplasia (ARVD).** ARVD is a cardiomyopathy of unknown etiology characterized by fibrofatty infiltration of the right ventricular myocardium. Possible associated findings include right ventricular wall motion abnormalities (either focal or global), wall thinning, and focal aneurysm. Clinically, ARVD is associated with arrhythmias and sudden death in otherwise healthy patients. Diagnosis of ARVD is based on a combination of major and minor criteria. MRI alone is not sufficient for diagnosis but provides important information regarding the right ventricular wall motion, myocardial thinning, dilatation, and fibrofatty replacement.

Diagnosis

Lipomatous hypertrophy of the intra-atrial septum (LHIS)

✓ Pearls

- Lipomas are well-encapsulated lesions that most commonly occur in the right atrium and atrial septum.
- Lipomatous hypertrophy of the interatrial septum may present with supraventricular arrhythmias.
- ARVD results in fatty infiltration of the right ventricular wall, wall thinning, and abnormal wall motion.
- ARVD is associated with arrhythmias and sudden cardiac death in otherwise healthy patients.

Suggested Readings

Attili AK, Chew FS. Imaging of cardiac masses and myocardial disease: self-assessment module. AJR Am J Roentgenol 2007;188:S21–S25

Gaerte SC, Meyer CA, Winer-Muram HT, et al. Fat-containing lesions of the chest. Radiographics 2002;22:S61–S78

Miller SW. Cardiac Imaging: The Requisites. Philadelphia: Elsevier Mosby; 2005

Section II Gastrointestinal Imaging

Case 26

Robert A. Jesinger

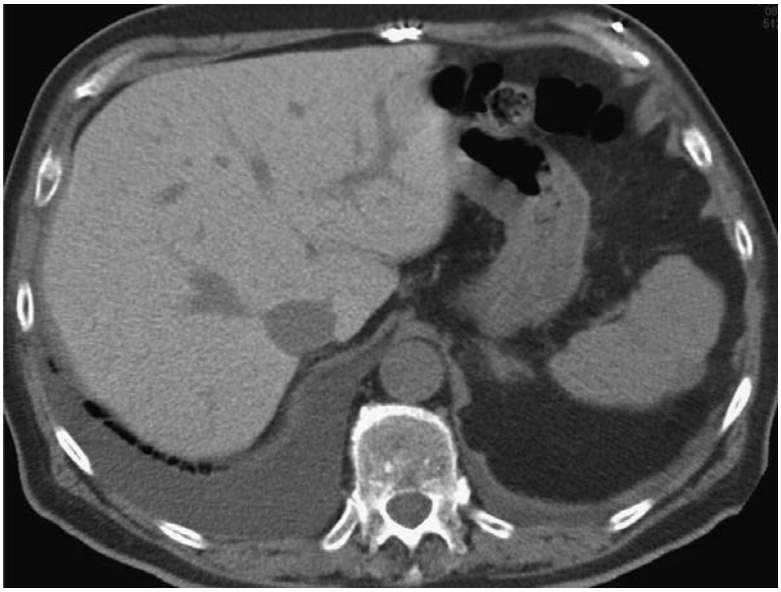


Fig. 26.1 Unenhanced computed tomography image of the liver demonstrating diffusely increased attenuation (>80 HU). Small layering bilateral pleural effusions are noted, as is metallic artifact from the anterior chest wall.

Clinical Presentation

A 65-year-old man presents with recurrent congestive heart failure (**Fig. 26.1**).

Key Imaging Finding

Hyperdense liver

Top 3 Differential Diagnoses

- **Iron deposition.** Iron deposition in the liver, commonly in the reticuloendothelial system, can be seen as a consequence of increased oral intake, multiple blood transfusions (usually in the setting of dialysis or chronic anemia), ineffective erythropoiesis (thalassemia or sideroblastic anemia), or from the more rare disorder of primary hemochromatosis. Hepatic enlargement, increased parenchymal attenuation (>80 HU), and cirrhotic liver morphology can be key visual markers, as can laboratory markers of impaired hepatic function. Careful detection of liver masses is important due to increased risk of hepatocellular carcinoma. Classic magnetic resonance imaging (MRI) features include decreased hepatic parenchymal signal intensity on T2-weighted imaging sequences due to the superparamagnetic effect of iron. Decreased myocardial and pancreatic parenchymal T2 signal intensity is a classic MRI feature in primary hemochromatosis, and decreased T2 signal intensity in the spleen is characteristic of secondary hemochromatosis.
- **Amiodarone therapy.** Amiodarone is an antiarrhythmic medication that is 40% iodine by weight. It has primary hepatic and biliary metabolism and is slowly excreted into bile by the liver. Hence, chronic amiodarone therapy increases hepatic parenchymal attenuation; normalization occurs over weeks to months after the medication is discontinued. In addition to a hyperdense liver, amiodarone therapy is associated with lower lobe pulmonary interstitial lung disease, as well as focal pulmonary infiltrates with characteristically increased attenuation.
- **Glycogen storage disease.** There are multiple subtypes of glycogen storage disease, many of which can result in decreased liver density similar to hepatic steatosis. Types I (von Gierke) and IV, however, are subtypes that are associated with increased hepatic attenuation. Type IV in particular may result in cirrhosis with an increased incidence of hepatocellular carcinoma. Unlike hemochromatosis, the classic MRI feature is increased hepatic parenchymal signal on T1-weighted imaging sequences.

Additional Differential Diagnoses

- **Gold therapy.** Intramuscular gold therapy was commonly used to treat patients with rheumatoid arthritis until the 1990s. Agents with less toxicity are now routinely used for rheumatoid arthritis in place of gold therapy. Chronic accumulation of gold salts results in a hyperdense liver.
- **Thoratrast.** Thoratrast is a radioactive material (alpha emitter) that was used as a contrast agent for several decades (1920s–1950s). The agent is taken up by the reticuloendothelial system, resulting in dense opacities within the liver, spleen, and lymph nodes. There is an increased risk of malignancy, especially angiosarcoma.

Diagnosis

Amiodarone therapy

✓ Pearls

- Primary hemochromatosis affects the pancreas, and secondary hemochromatosis affects the spleen.
- Amiodarone may cause a hyperdense liver, high attenuation pulmonary infiltrates and ILD.
- Hepatoma and angiosarcoma may arise in the setting of a hyperdense liver.

Suggested Readings

Federle MP, Jeffrey RB, Desser TS, et al. Diagnostic Imaging: Abdomen. Salt Lake City, UT: Amirsys; 2004

Guyader D, Gandon Y, Deugnier Y, et al. Evaluation of computed tomography in the assessment of liver iron overload: a study of 46 cases of idiopathic hemochromatosis. Gastroenterology 1989;97(3):737–743

Pomerantz S, Siegelman ES. MR imaging of iron depositional disease. Magn Reson Imaging Clin N Am 2002;10(1):105–120

Tani I, Kurihara Y, Kawaguchi A, et al. MR imaging of diffuse liver disease. AJR Am J Roentgenol 2000;174(4):965–971

Case 27

Robert A. Jesinger

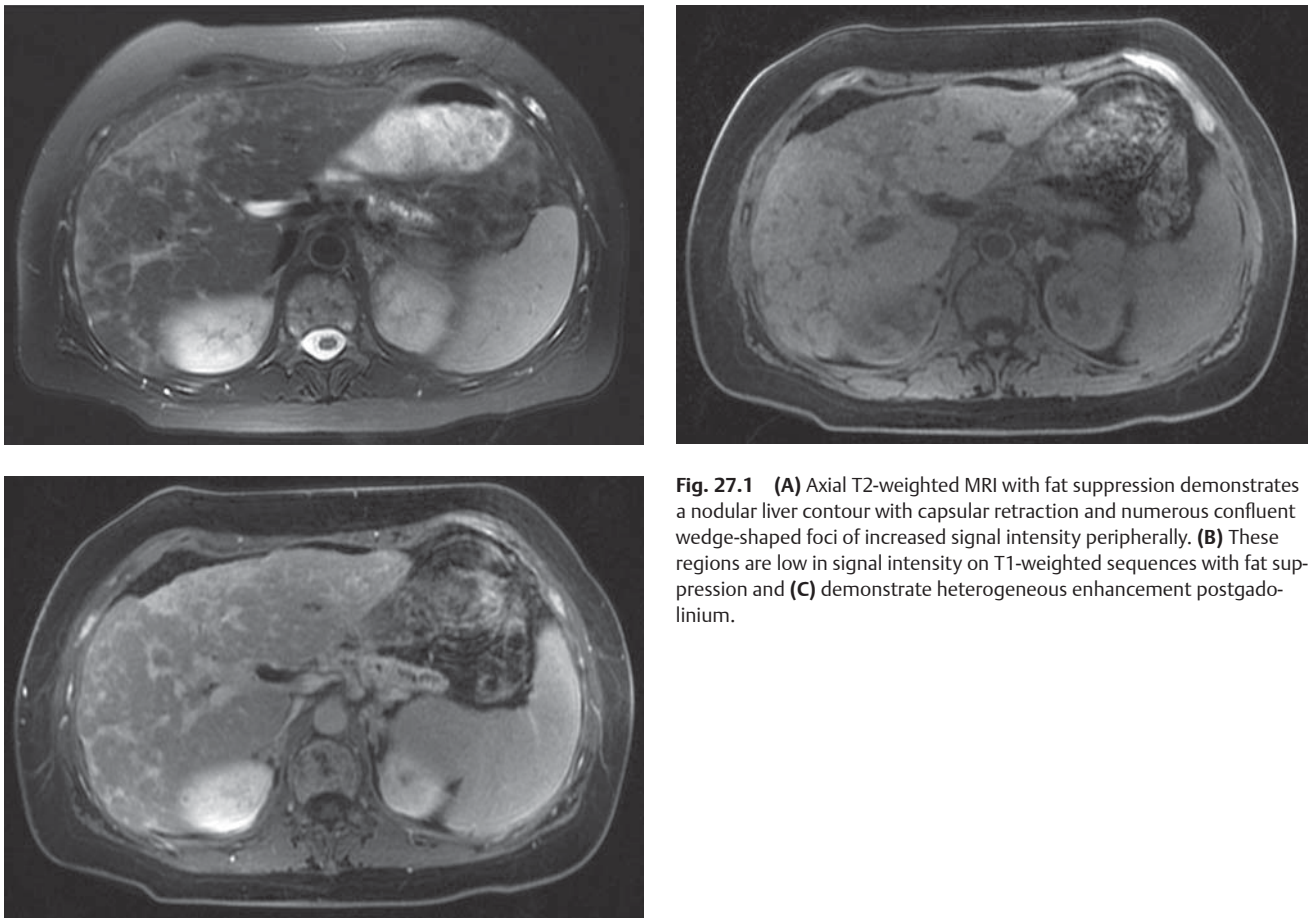


Fig. 27.1 **(A)** Axial T2-weighted MRI with fat suppression demonstrates a nodular liver contour with capsular retraction and numerous confluent wedge-shaped foci of increased signal intensity peripherally. **(B)** These regions are low in signal intensity on T1-weighted sequences with fat suppression and **(C)** demonstrate heterogeneous enhancement postgadolinium.

Clinical Presentation

A 67-year-old woman presents with chronic liver enzyme elevation and a history of breast cancer (**Fig. 27.1**).

Key Imaging Finding

Nodular liver contour

Top 3 Differential Diagnoses

- **Cirrhosis.** Cirrhosis is a chronic liver disease characterized by hepatic fibrosis and regenerative hepatic nodules. Common causes include alcohol (micronodular cirrhosis), chronic viral hepatitis (macronodular cirrhosis), autoimmune hepatitis, and chronic metabolic conditions (primary biliary cirrhosis, primary hemochromatosis, Wilson disease, alpha-1 antitrypsin deficiency). Imaging findings include nodular liver surface contour, distorted hepatic architecture with atrophy, and stigmata of portal hypertension (enlarged main portal vein with slow flow, flow reversal, or occlusion; varices; splenomegaly; gallbladder/bowel wall thickening; and ascites). Magnetic resonance imaging (MRI) of liver nodules helps distinguish regenerative nodules (low T2 signal) from neoplastic nodules (high T2 signal).
- **Treated metastases.** Chemotherapy treatment of liver metastases (commonly from breast, lung, and colorectal cancer) can result in scarring of hepatic tumor implants. Liver parenchyma, between these areas of scarring, can be normal or regenerative. The overall imaging appearance simulates macronodular cirrhosis and hence is referred to as "pseudocirrhosis." Correlation with appropriate history is helpful.
- **Budd–Chiari syndrome.** Chronic hepatic venous occlusive disease can result in a nodular liver contour, usually as a consequence of regenerative nodules. In chronic Budd–Chiari syndrome, these nodules are usually small, multiple, and hypervascular, and the number of nodules is often underestimated on computed tomography (CT) imaging. Large regenerative hypervascular nodules may be seen and are usually hyperintense on T1-weighted MRI sequences. There is no evidence that large regenerative nodules degenerate into malignancy. A central scar in nodules > 1 cm can be seen. Caudate hypertrophy occurs as a result of its separate venous drainage into the inferior vena cava, which may simulate a dominant nodule.

Additional Differential Diagnoses

- ***Schistosoma japonicum.*** *S. japonicum,* a major cause of hepatic schistosomiasis, is highly associated with hepatic fibrosis. Calcified eggs along the portal tracts produce the pathognomonic "turtleback" calcification. The size and shape of the liver can be preserved, but fibrosis and portal tract calcification often result in a nodular liver contour.
- **Confluent hepatic fibrosis.** Confluent hepatic fibrosis may occur in the setting of chronic liver disease. The most common appearance is a wedge-shaped hypodense region on CT that extends from the hilum. The anterior segment of the right hepatic lobe and medial segment of the left hepatic lobe are the most common sites of involvement. There is overlying capsular retraction and no or little enhancement.

Diagnosis

Treated breast metastases (pseudocirrhosis)

✓ Pearls

- MR signal intensity and vascularity can help in differentiating regenerative and malignant hepatic nodules.
- Pseudocirrhosis is most commonly seen with treated breast, lung, and colorectal metastases.
- The "turtleback" appearance of the liver is most commonly associated with schistosomiasis.

Suggested Readings

Brancatelli G, Federle MP, Grazioli L, Golfieri R, Lencioni R. Benign regenerative nodules in Budd-Chiari syndrome and other vascular disorders of the liver: radiologic-pathologic and clinical correlation. Radiographics 2002;22(4):847–862

Dodd GD III, Baron RL, Oliver JH III, Federle MP. Spectrum of imaging findings of the liver in end-stage cirrhosis: 1. Gross morphology and diffuse abnormalities. AJR Am J Roentgenol 1999;173(4):1031–1036

Federle MP, Jeffrey RB, Desser TS, et al. Diagnostic Imaging: Abdomen. Salt Lake City, UT: Amirsys; 2004

Yang DM, Kim HS, Cho SW, Kim HS. Pictorial review: various causes of hepatic capsular retraction: CT and MR findings. Br J Radiol 2002;75(900):994–1002

Case 28

Robert A. Jesinger



Fig. 28.1 Lateral view from an upper gastrointestinal examination demonstrates a large contrast-filled outpouching along the posterior aspect of the cervical esophagus.

Clinical Presentation

A 75-year-old woman presents with difficulty swallowing (**Fig. 28.1**).

Key Imaging Finding

Esophageal diverticulum

Top 3 Differential Diagnoses

- **Proximal esophageal pulsion diverticulum.** Pulsion (from the Latin, meaning "pushing outward") diverticula of the esophagus are thought to develop due to increased intraluminal pressures combined with focal areas of weakness in the esophageal wall. The more common Zenker diverticulum is a midline defect that occurs in the posterior cervical esophagus above the level of the cricopharyngeal muscle (upper esophageal sphincter). A Zenker diverticulum occurs through Killian dehiscence, which is at the junction of the cricopharyngeal and inferior pharyngeal constrictor muscles. A Killian–Jamieson diverticulum is a lateral defect that occurs in the cervical esophagus at the level of the cricopharyngeal muscle. Both typically occur in older patients, and presenting complaints include dysphagia, halitosis, and intermittent coughing from aspiration. An additional proximal pulsion diverticulum is the lateral hypopharyngeal diverticulum, which occurs more cephalad within the hypopharynx. It is commonly seen in older patients with chronic obstructive pulmonary disease, as well as at a younger age in workers such as glassblowers and wind instrument musicians. They are associated with laryngoceles.
- **Distal esophageal pulsion diverticulum.** Diverticula in the distal esophagus (lower 6–10 cm), termed epiphrenic diverticula, usually occur in the setting of an underlying esophageal motility disorder (achalasia, diffuse esophageal spasm, etc.). Most patients have minimal symptoms, but surgical diverticulectomy is indicated in severely symptomatic patients.
- **Midesophageal traction diverticulum.** Diverticula of the midesophagus commonly develop by "traction" effects from an inflammatory process within the adjacent mediastinum (e.g., tuberculosis and histoplasmosis). Midesophageal diverticula can also be seen in the spectrum of foregut duplications/malformations and in the postsurgical setting after tracheoesophageal fistula repair.

Additional Differential Diagnoses

- **Intramural pseudodiverticulosis.** Intramural pseudodiverticulosis is a rare condition in which numerous 1 to 4 mm saccular outpouchings form within the esophageal wall secondary to inflammatory dilatation of esophageal submucosal glands. Most patients have an associated motility disorder or underlying esophageal strictures.

Diagnosis

Proximal esophageal pulsion diverticulum (Zenker diverticulum)

✓ Pearls

- A Zenker diverticulum is a posterior midline defect that occurs above the level of the cricopharyngeal muscle.
- A Killian–Jamieson diverticulum is a lateral defect that occurs at the level of the cricopharyngeal muscle.
- Mediastinal inflammatory processes that scar can create an esophageal traction diverticulum.

Suggested Readings

Duda M, Serý Z, Vojácek K, Rocek V, Rehulka M. Etiopathogenesis and classification of esophageal diverticula. Int Surg 1985;70(4):291–295

Federle MP, Jeffrey RB, Desser TS, et al. Diagnostic Imaging: Abdomen. Salt Lake City, UT: Amirsys; 2004

Sydow BD, Levine MS, Rubesin SE, Laufer I. Radiographic findings and complications after surgical or endoscopic repair of Zenker's diverticulum in 16 patients. AJR Am J Roentgenol 2001;177(5):1067–1071

Case 29

Eleanor L. Ormsby

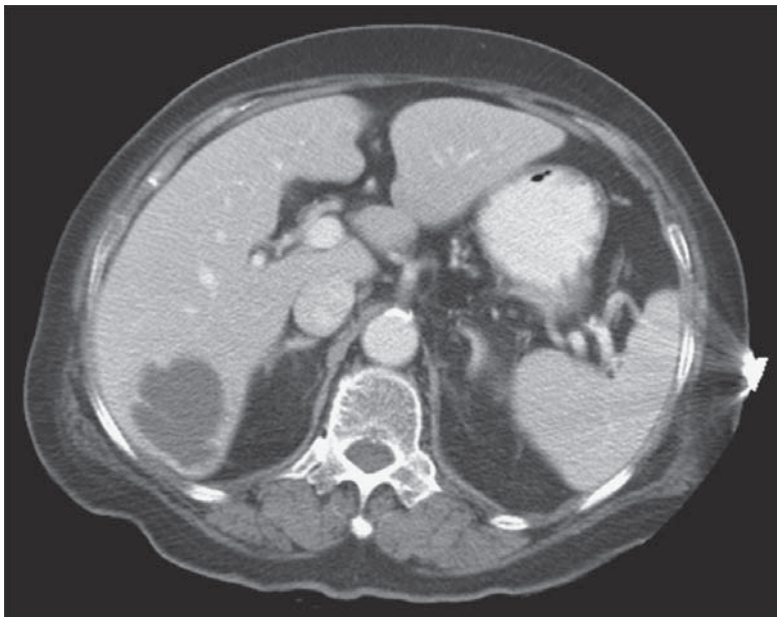


Fig. 29.1 Axial contrast-enhanced CT image demonstrates a well-defined hypodense lobular mass in the posterior right lobe of the liver. The mass has a peripheral rim and septal enhancement. On delayed imaging (not shown), there was no contrast filling in of the mass.

Clinical Presentation

A 73-year-old woman presents with a history of right upper quadrant pain (**Fig. 29.1**).

Key Imaging Finding

Solitary hypodense, hypovascular liver mass

Top 3 Differential Diagnoses

- **Hepatic cyst.** Hepatic cysts are thought to be congenital lesions arising from developmental defects of the biliary ducts. They are well circumscribed with very thin or imperceptible walls. They rarely cause symptoms and typically do not result in abnormal liver function tests. Simple cysts do not enhance.
- **Solitary metastasis.** The most common appearance of hepatic metastases on computed tomography is a low-density lesion with respect to the liver. There may be a degree of peripheral rim enhancement. Calcifications may be seen in mucinous adenocarcinomas of the colon, stomach, or ovary. Hypovascular metastatic masses are best seen on portal venous phase images. Smaller lesions may fill in on delayed images.
- **Hepatic abscess.** Hepatic abscesses are most commonly pyogenic usually from ascending cholangitis, hematogenous spread, or direct extension from adjacent sites of infection. They may also occur as a complication after surgery or traumatic events involving the liver. Hepatic abscesses are hypodense with peripheral enhancement. Pyogenic abscesses are commonly multilocular. Amebic abscesses appear similar to pyogenic abscesses but tend to be unilocular. They are common worldwide and have a tendency to rupture. Echinococcal infection (hydatid cyst) can be very large with rimlike calcification. Daughter cysts within the larger cyst are pathognomonic. Mycotic abscesses are typically multiple and small.

Additional Differential Diagnoses

- **Peripheral cholangiocarcinoma.** Intrahepatic cholangiocarcinomas are hypodense on arterial and portal venous phase imaging and characteristically demonstrate delayed (>10 minutes) peripheral to central enhancement. Overlying capsular contraction is due to fibrosis. The masses tend to be infiltrative with irregular borders. Biliary ductal dilatation is common peripherally to the tumor.
- **Biliary cystadenoma.** Biliary cystadenomas are uncommon, multilocular, well-defined cystic masses arising from the bile ducts. They typically occur in middle-aged women who complain of chronic abdominal pain. Malignant transformation to cystadenocarcinoma can occur. The cyst wall may enhance.
- **Hepatic laceration (trauma).** Blunt abdominal trauma to the liver commonly results in solitary or multiple lacerations. They are usually of low density relative to enhanced liver parenchyma. Blood clots may appear hyperdense within a lacerated liver.

Diagnosis

Hepatic abscess (pyogenic)

✓ Pearls

- Delayed imaging with intravenous contrast is helpful in differentiating hepatic cysts from hypodense metastases.
- Amebic abscesses in the liver are fairly common worldwide and have a tendency to rupture.
- Delayed imaging (>10 minutes) is helpful in the diagnosis of cholangiocarcinoma.
- Linear hypodense liver lesions are suspicious for liver lacerations in the setting of trauma.

Suggested Readings

Brancatelli G, Federle MP, Grazioli L, Carr BI. Hepatocellular carcinoma in noncirrhotic liver: CT, clinical, and pathologic findings in 39 U.S. residents. Radiology 2002;222(1):89–94

Halpert RD, Feczko PJ. Gastrointestinal Radiology: The Requisites. 2nd ed. Philadelphia: Mosby; 1999

Lim JH. Cholangiocarcinoma: morphologic classification according to growth pattern and imaging findings. AJR Am J Roentgenol 2003;181(3):819–827

Case 30

Robert A. Jesinger

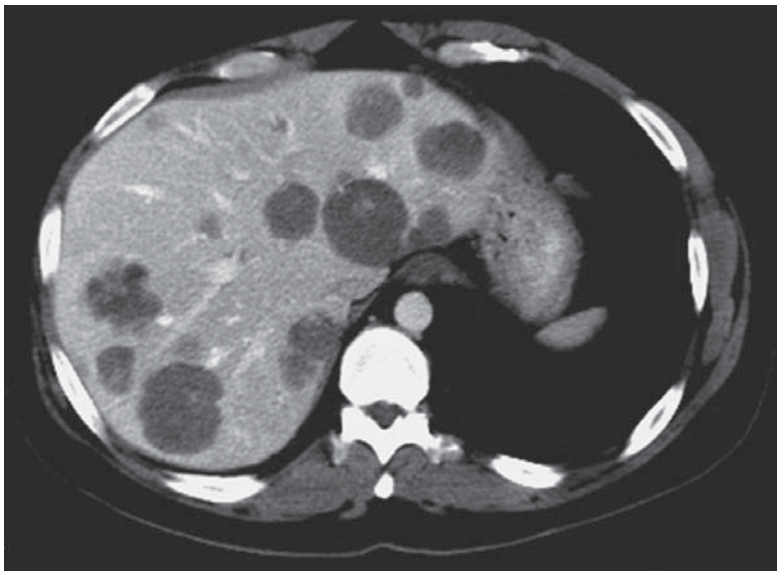


Fig. 30.1 Contrast-enhanced axial CT image of the liver demonstrates multiple hypoattenuating hepatic lesions with regions of internal enhancement.

Clinical Presentation

A 55-year-old man presents with weakness and weight loss (**Fig. 30.1**).

Key Imaging Finding

Multiple hypoattenuating hepatic lesions

Top 3 Differential Diagnoses

- **Hepatic cysts.** Small isolated hepatic cysts are commonly seen on routine abdominal computed tomography (CT) and ultrasound. Hepatic cysts are well-circumscribed, homogeneous masses of near water attenuation value (−20 to +20 HU) that show no enhancement after intravenous (IV) contrast administration. When multiple hepatic cysts are seen, polycystic kidney and/or liver disease, biliary hamartomas, and Caroli disease should be considered. Caroli disease is characterized by dilated biliary ducts surrounding an enhancing portal vein and hepatic artery, which is referred to as the central dot sign. When a large solitary liver cyst is noted, hepatic cystadenoma, biloma, and/or hydatid cyst should be considered. Usually hepatic cysts are not associated with biliary obstruction, nor is spontaneous cyst rupture common.
- **Metastatic disease.** Liver metastases rank second to lymph node metastases in cancer patients. Virtually any primary malignant neoplasm can produce liver metastases, but the most common primary tumor sites are the colon, lung, breast, stomach, and pancreas. In children, the most common primary tumors producing hypoattenuating liver metastases are neuroblastoma, Wilms tumor, and leukemia. Most metastatic lesions enhance after IV contrast administration, but their visual conspicuity usually results from normally enhancing adjacent liver parenchyma. Surgical resection of isolated metastatic liver lesions has been found to increase survival time in certain cancers (e.g., colon cancer).
- **Multiple hepatic abscesses.** Hepatic abscesses are relatively rare, but when they are encountered, they typically fall into three categories: pyogenic (80%), amebic (10%), and fungal (10%). Historically, pyogenic hepatic abscesses were found in the setting of appendicitis, but currently, diverticulitis and sepsis are more common causes. Amebic abscesses are prone to rupture. Imaging findings include thick-walled, hypoattenuating liver masses with internal septations, peripheral lesion enhancement, and gas in up to 20% of cases. Untreated, liver abscesses have a high mortality rate. However, image-guided catheter drainage has improved mortality rates significantly.

Additional Differential Diagnoses

- **Cholangiocarcinoma.** A rare cancer of the bile ducts, cholangiocarcinoma typically presents as multiple hypoattenuating infiltrative lesions, paralleling the bile ducts and causing biliary obstruction. Risk factors include primary sclerosing cholangitis, parasitic liver flukes (e.g., *Clonorchis sinensis*), choledochal anomalies, and prior thoratrast exposure. Delayed enhancement (>10 minutes) is a key distinguishing feature. Most patients present late, when curative surgical resection is contraindicated.

Diagnosis

Metastatic disease (angiosarcoma)

✓ Pearls

- Hepatic cysts rarely rupture, whereas dominant hepatic amebic abscesses can be more prone to rupture.
- Multiple irregularly shaped hypoattenuating lesions in the liver are concerning for metastases.
- Delayed enhancement (> 10 minutes) is important in diagnosing hepatic cholangiocarcinomas.

Suggested Readings

Federle MP, Jeffrey RB, Desser TS, et al. Diagnostic Imaging: Abdomen. Salt Lake City, UT: Amirsys; 2004

Martin DR, Semelka RC. Imaging of benign and malignant focal liver lesions. Magn Reson Imaging Clin N Am 2001;9(4):785–802

Mortelé KJ, Ros PR. Cystic focal liver lesions in the adult: differential CT and MR imaging features. Radiographics 2001;21(4):895–910

Case 31

Chirag V. Patel

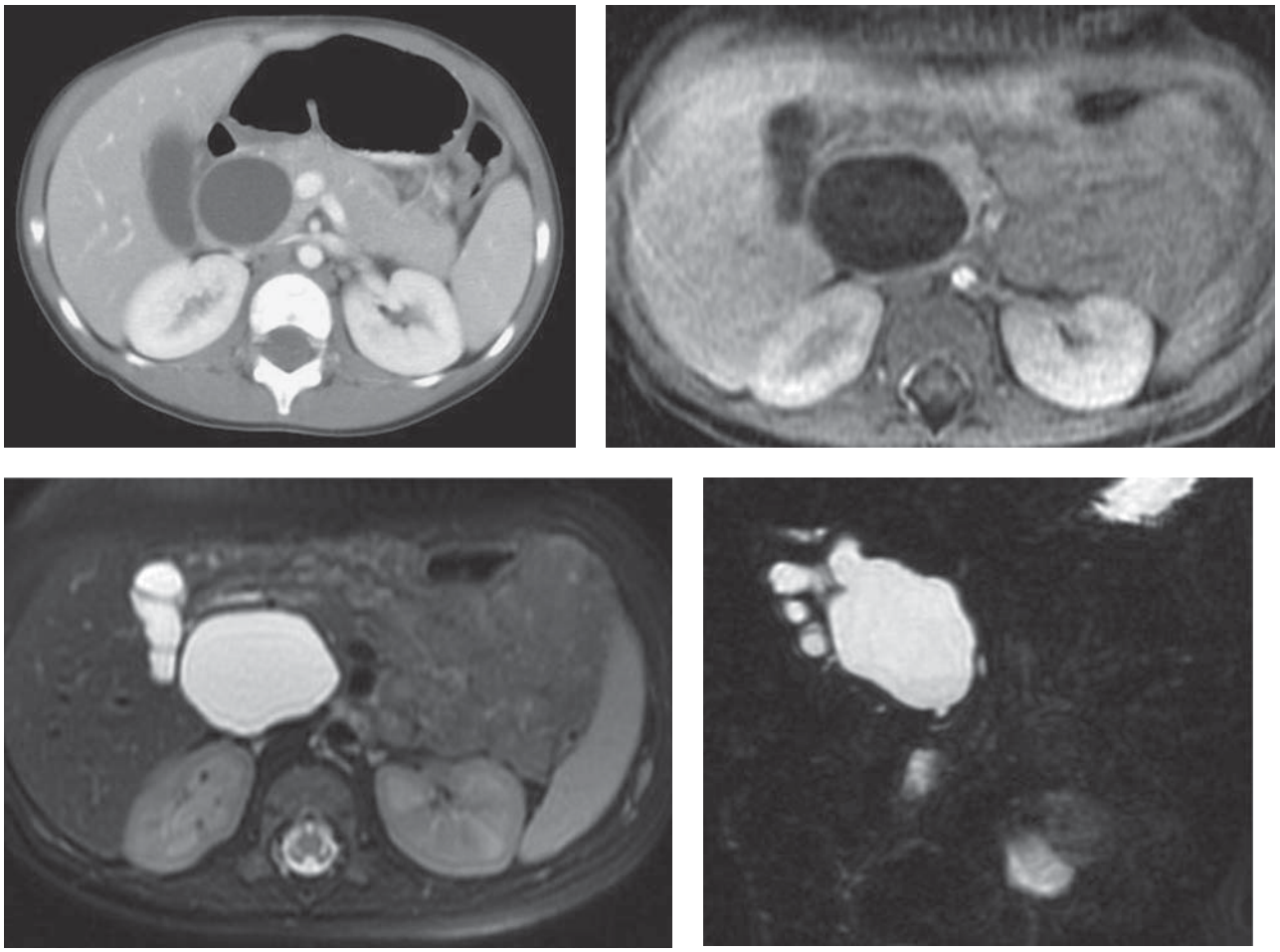


Fig. 31.1 **(A)** Axial contrast-enhanced CT image demonstrates a cystic mass in the right upper quadrant medial to the gallbladder. **(B)** Axial postcontrast T1-weighted three-dimensional spoiled gradient recalled echo, **(C)** T2-weighted single-shot fast spin echo, and **(D)** magnetic resonance cholangiopancreatography in a different patient with a right upper quadrant abdominal mass, showing cystic dilatation of extrahepatic biliary ducts. (**[A]** courtesy of Children's Hospital and Research Center, Oakland, California.)

Clinical Presentation

A 3-year-old boy presents with early satiety and intermittent postprandial emesis (**Fig. 31.1**).

Key Imaging Finding

Right upper quadrant cystic mass in a child

Top 3 Differential Diagnoses

- **Choledochal anomaly.** Congenital cystic enlargement of the bile ducts is referred to as a choledochal anomaly. Choledochal cysts are classified as five different types. Type 1 is the most common, accounting for 80 to 90% of cases, and represents cystic or fusiform dilatation of the common bile duct. Most choledochal cysts become symptomatic in the first decade of life, with a palpable right upper quadrant mass, jaundice, and pain being the classic triad of symptoms. Presentation is more insidious in older children and adults. On imaging, demonstration of cystic or fusiform dilatation of the extra hepatic bile duct is enough for diagnosis. However, magnetic resonance cholangiopancreatography or endoscopic retrograde cholangiopancreatography may be of further help in preoperative evaluation. Types 2 through 5 consist of a common bile duct diverticulum, a choledochocele, extrahepatic ductal dilatation, and intrahepatic ductal dilatation (Caroli disease), respectively.
- **Pancreatic pseudocyst.** Pseudocyst is the most common cystic lesion of the pancreas in children, accounting for 75% of all cystic lesions. Blunt trauma and pancreatitis are the most common etiologies. The diagnosis on imaging is based on the exclusion of communication with the biliary ducts (choledochal cyst) and bowel (enteric duplication cyst or diverticulum) and demonstrating a true intrapancreatic location of the cystic lesion. In the absence of a history of acute pancreatitis, careful evaluation for septation or papillary growth should be undertaken to rule out a rare cystic pancreatic malignancy. Correlation for a history of trauma (accidental or nonaccidental) should always be considered.
- **Gastrointestinal (GI) duplication cyst/diverticulum.** GI duplication cysts can occur anywhere in the GI tract; however, the stomach and duodenum are rare locations, whereas the ileum and esophagus are the most common locations. Diverticula commonly occur within the duodenum. Demonstration of continuity of the cyst with the GI tract and visualization of gut signature on ultrasound aid in diagnosis. There may be fluid–debris levels.

Additional Differential Diagnoses

- **Ovarian cystic lesion.** An ovarian cystic lesion can sometimes present as an abdominal mass. When large, demonstrating the organ of origin may be difficult. In girls younger than 17 years, cystic ovarian teratoma is the most common cystic lesion. Mature cystic teratoma is the most common subtype (90%) and demonstrates fat and/or calcification within a predominantly cystic mass. Simple ovarian cysts also may occur in children, especially in the prenatal and postnatal period while under maternal estrogen stimulation.
- **Mesenteric cyst.** Mesenteric cysts represent lymphangiomas localized to the mesentery. On ultrasound, they are seen as single or multiple cysts with thin, imperceptible walls and may or may not have septations. On computed tomography, the attenuation coefficient of the cystic content ranges from water density to fat density, depending on the proportion of the chylous component. Mesenteric cysts are usually homogeneous. When complicated by infection or hemorrhage, the cysts can show atypical features, with thick walls and inhomogeneous cystic content.

Diagnosis

Choledochal anomaly (type 1)

✓ Pearls

- Fusiform dilatation of the extrahepatic common bile duct is the most common choledochal anomaly.
- The diagnosis of pancreatic pseudocyst in a child requires assessment for nonaccidental trauma.
- Duplication cysts commonly communicate with the bowel and have gut signature on ultrasound.

Suggested Readings

Dohke M, Watanabe Y, Okumura A, et al. Anomalies and anatomic variants of the biliary tree revealed by MR cholangiopancreatography. AJR Am J Roentgenol 1999;173(5):1251–1254

Govil S, Justus A, Korah I, Perakath A, Zachariah N, Sen S. Choledochal cysts: evaluation with MR cholangiography. Abdom Imaging 1998;23(6):616–619

Case 32

Shaun Loh

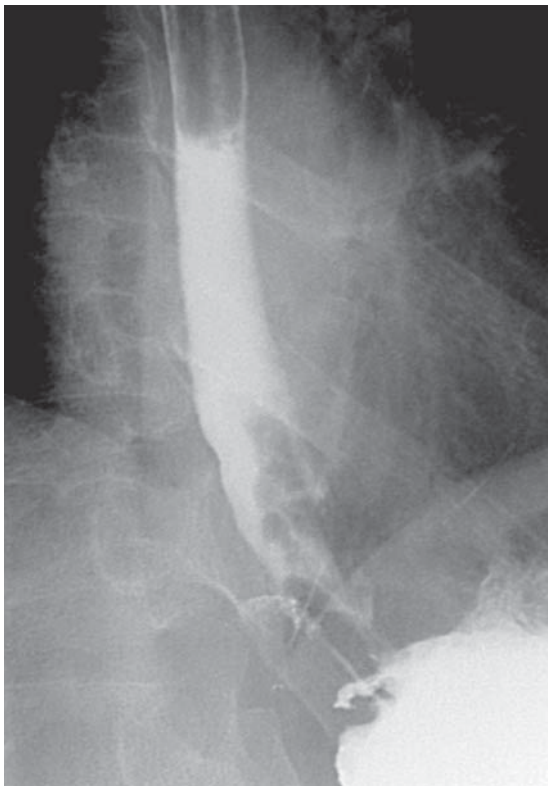


Fig. 32.1 Esophogram demonstrates tortuous longitudinal submucosal filling defects in the distal esophagus.

Clinical Presentation

A 40-year-old man presents with a 2-week history of food "sticking" in his throat (**Fig. 32.1**).

Key Imaging Finding

Esophageal submucosal masses/thickened folds

Top 3 Differential Diagnoses

- **Varices.** Varices are a common sequela of portal hypertension, often secondary to chronic liver disease. They are classified according their pathophysiology as either uphill or downhill. Uphill varices are more common and involve the distal portion of the esophagus. They form as a result of portal hypertension, where increased pressures cause upward flow of blood from the portal vein through collateral flow through the azygous vein to the superior vena cava. Uphill varices commonly cause gastrointestinal bleeding. Downhill varices, in contrast, are rarer and involve the proximal esophagus. An obstruction of the superior vena cava results in downward flow through the azygous vein to the inferior vena cava and portal vein. Common causes of superior vena cava obstruction are lung cancer, mediastinitis, retrosternal goiters, and thymomas. Downhill varices may present with symptoms of superior vena cava syndrome, including facial, periorbital, or neck swelling. In an esophogram, varices typically appear as longitudinal, serpentine, radiolucent filling defects that vary in size with changes in patient positioning and phase of respiration.
- **Reflux esophagitis.** The inflammatory changes and submucosal edema in esophagitis may appear as thickened, tortuous folds, much like varices. The thickened folds in the setting of esophagitis, however, will remain fixed in appearance. An adequate clinical history combined with endoscopy will readily differentiate between the two.
- **Varicoid esophageal carcinoma.** Esophageal carcinoma is a common malignancy of the gastrointestinal tract. Advanced esophageal carcinomas may present as infiltrating, polypoid, ulcerative, or varicoid lesions. The varicoid lesion is the least common subtype and appears on esophograms as a thickened, rigid, serpentine, longitudinal filling defect due to the submucosal spread of tumor. Varicoid lesions are frequently confused for varices but differ in that varicoid tumors have fixed configurations and do not change their appearance in response to esophageal peristalsis, respiratory maneuvers, or repositioning of the patient. Diagnosis is confirmed with endoscopic biopsy.

Additional Differential Diagnoses

- **Lymphoma.** Lymphoma rarely involves the esophagus, but when it does, signs of lymphoma are seen in other parts of the body. Most cases of esophageal lymphoma are from contiguous spread from the gastric cardia or fundus. When lymphoma infiltrates in a submucosal fashion, it produces fixed, tortuous, longitudinal folds. Endoscopic biopsy will help aid in the diagnosis.

Diagnosis

Esophageal varices

✓ Pearls

- Portal hypertension causes uphill esophageal varices, whereas superior vena cava obstruction causes downhill varices.
- Esophageal varices will vary in size and appearance with patient positioning; they enhance avidly.
- Reflux esophagitis may present with mucosal abnormalities and thickened folds.
- Varicoid esophageal carcinoma is the least common tumor subtype.

Suggested Readings

Federle MP, Jeffrey RB, Desser TS, et al. Diagnostic Imaging: Abdomen. Salt Lake City, UT: Amirsys; 2004

Kim YJ, Raman SS, Yu NC, To'o KJ, Jutabha R, Lu DS. Esophageal varices in cirrhotic patients: evaluation with liver CT. AJR Am J Roentgenol 2007;188(1):139–144

Matsumoto A, Kitamoto M, Imamura M, et al. Three-dimensional portography using multislice helical CT is clinically useful for management of gastric fundic varices. AJR Am J Roentgenol 2001;176(4):899–905

Case 33

Paul B. DiDomenico

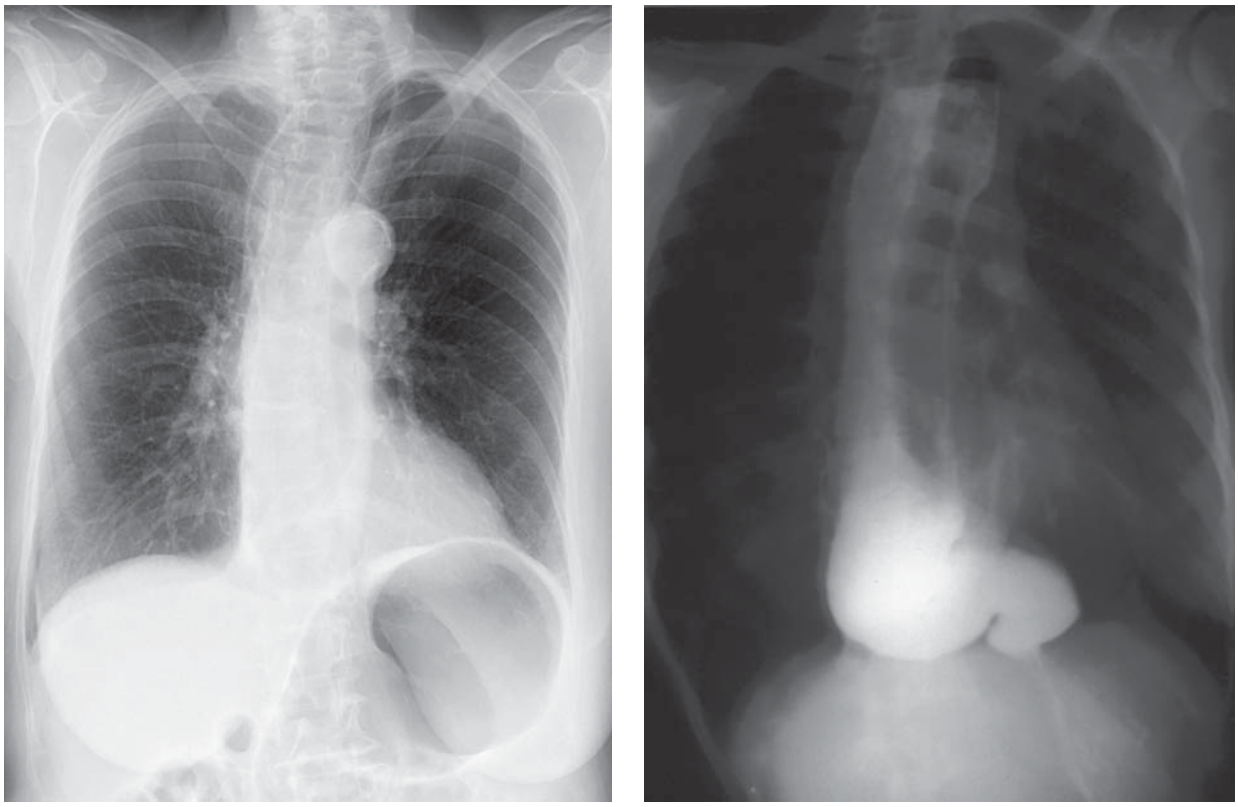


Fig. 33.1 **(A)** A posteroanterior chest radiograph demonstrates a widened mediastinum with lucency and smooth borders. **(B)** A slightly obliqued frontal view from an esophagram reveals a dilated esophagus that tapers to a "bird's beak" appearance distally at the gastroesophageal junction, causing a static column of barium.

Clinical Presentation

Patient presents with chronic dysphagia (**Fig. 33.1**).

Key Imaging Finding

Esophageal dilatation

Top 3 Differential Diagnoses

- **Achalasia.** Achalasia is a disease of the myenteric plexus of the esophagus that results in failure of relaxation of the lower esophageal sphincter (LES). Persistent contraction of the LES results in smooth distal tapering with a classic "bird's beak" appearance, proximal dilatation on barium esophagram, and diminished or absent peristalsis. Primary (idiopathic) achalasia is thought to be due to degeneration of the myenteric plexus; secondary achalasia results from destruction of the plexus by infiltrating tumor or infection, such as Chagas disease or fungal infection. Treatment options include calcium channel blockers, pneumatic dilatation, and Heller myotomy.
- **Scleroderma.** Scleroderma is a collagen vascular disease in which smooth muscle becomes fibrotic. This affects the distal two thirds of the esophagus, which is lined by smooth muscle, resulting in dysmotility and dilatation. The LES becomes incompetent, and there is patulous dilation of the gastroesophageal junction, which may help distinguish this disorder from achalasia. The resulting chronic reflux, however, may cause a peptic stricture that may mimic achalasia.
- **Esophageal/gastric carcinoma.** Malignancy of either the distal esophagus or the gastric cardia may cause mass effect at the gastroesophageal junction, resulting in a tapered narrowing of the lower esophagus with dysmotility and dilatation. Irregularity of the mucosa, "shouldering" mass effect, and correlation with history may suggest malignancy, though final diagnosis would be made via endoscopy and biopsy.

Additional Differential Diagnoses

- **Esophagitis with stricture.** Long-standing reflux, often with a coexisting hiatal hernia, may result in a peptic stricture at the distal esophagus with narrowing of a short distal segment seen on barium esophagram. Esophageal motility is usually normal, and there is minimal dilatation of the esophagus.
- **Postsurgical changes (vagotomy).** Vagotomy has been reported as a secondary cause of achalasia secondary to neuronal damage or fibrosis at the gastroesophageal junction. These changes result in focal narrowing of the distal esophagus with proximal dilatation.

Diagnosis

Achalasia

✓ Pearls

- Smooth tapering of the distal esophagus on esophagram ("bird's beak") is a key finding in achalasia.
- Scleroderma often scars the distal esophagus, resulting in a patulous gastroesophageal junction and chronic reflux.
- Irregular tapering of the distal esophagus on esophagram is a concerning finding for carcinoma.

Suggested Readings

Federle MP, Jeffrey RB, Desser TS, et al. Diagnostic Imaging: Abdomen. Salt Lake City, UT: Amirsys; 2004

Levine MS, Rubesin SE. Diseases of the esophagus: diagnosis with esophagography. Radiology 2005;237(2):414–427

Woodfield CA, Levine MS, Rubesin SE, Langlotz CP, Laufer I. Diagnosis of primary versus secondary achalasia: reassessment of clinical and radiographic criteria. AJR Am J Roentgenol 2000;175(3):727–731

Case 34

Eleanor L. Ormsby

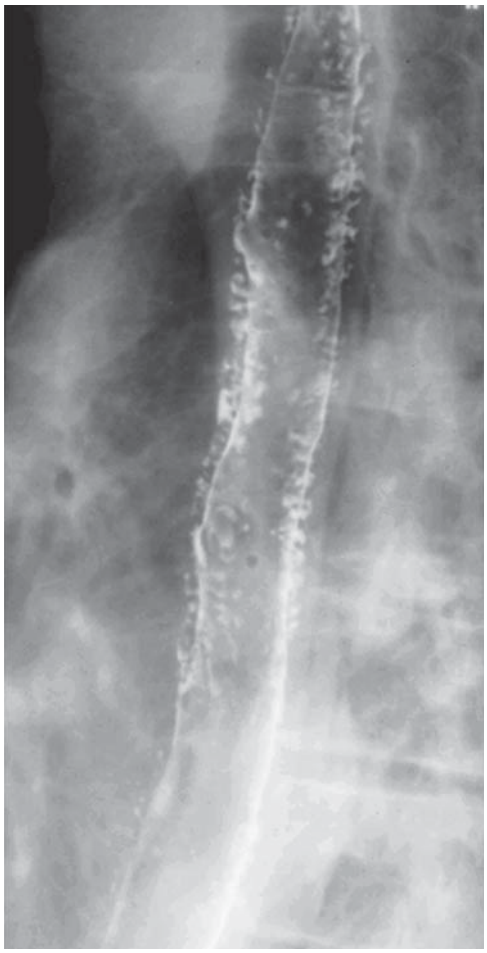


Fig. 34.1 Oblique image from an esophagram demonstrates multiple contrast outpouchings along the midesophageal wall, consistent with intramural pseudodiverticula. (Courtesy of the Department of Radiology, University of Cincinnati.)

Clinical Presentation

A 42-year-old man presents with odynophagia (**Fig. 34.1**).

Key Imaging Finding

Esophageal pseudodiverticula

Top 3 Differential Diagnoses

- **Reflux esophagitis.** Pseudodiverticula are flask-shaped outpouchings of contrast-filling dilated mucous glands in the esophageal wall. They are the sequelae of chronic irritation and esophagitis. Reflux esophagitis usually affects the distal esophagus as a result of irritation of esophageal mucosa by gastric acid. An esophagram demonstrates thickened distal folds, ulcers (which are usually linear), benign strictures (which classically begin immediately above the gastroesophageal junction), and/or intramural pseudodiverticula. Hiatal hernias are commonly associated with gastroesophageal reflux.
- ***Candida* esophagitis.** *Candida* is often cultured in esophageal pseudodiverticulosis, likely due to chronic esophagitis. It is most commonly seen in immunosuppressed patients, especially in the setting of acquired immunodeficiency syndrome (AIDS). Patients with esophageal stasis, such as those with achalasia or scleroderma, are also at risk for developing *Candida* esophagitis. An esophagram may demonstrate diffuse mucosal nodularity and ulceration, longitudinally oriented plaques, and pseudodiverticula.
- **Superficial spreading carcinoma.** Superficial spreading carcinoma is an unusual form of squamous cell carcinoma, which is characterized by small plaquelike mucosal nodularities on an esophagram. Focal necrosis and ulceration can also be seen, as can pseudodiverticula. Endoscopic biopsy confirms the diagnosis.

Additional Differential Diagnoses

- **Drug-induced esophagitis.** In most patients with drug-induced esophagitis, there is no underlying esophageal disease. A wide range of drugs can cause esophagitis, including tetracycline, ascorbic acid, and iron sulfate. An esophagram may show single or multiple shallow ulcerations with possible associated fold thickening at the level of the aortic arch or the distal esophagus where a transient delay in the passage of bolus occurs. Occasionally, pseudodiverticula may occur. Repeat esophagrams usually demonstrate complete healing following withdrawal of the medication.

Diagnosis

Candida esophagitis

✓ Pearls

- Transmural inflammation in the esophagus may dilate mural glands and result in pseudodiverticula.
- Candidiasis presents in immunosuppressed patients with mucosal plaques and pseudodiverticula.
- Endoscopy is performed to exclude superficial spreading carcinoma in the setting of pseudodiverticulosis.

Suggested Readings

Creteur V, Laufer I, Kressel HY, et al. Drug-induced esophagitis detected by double-contrast radiography. Radiology 1983;147(2):365–368

Halpert RD, Feczko PJ. Gastrointestinal Radiology: The Requisites. 2nd ed. Philadelphia: Mosby; 1999

Lee SS, Ha HK, Byun JH, et al. Superficial esophageal cancer: esophagographic findings correlated with histopathologic findings. Radiology 2005;236(2):535–5441

Levine MS, Moolten DN, Herlinger H, Laufer I. Esophageal intramural pseudodiverticulosis: a reevaluation. AJR Am J Roentgenol 1986;147(6):1165–1170

Case 35

Robert A. Jesinger

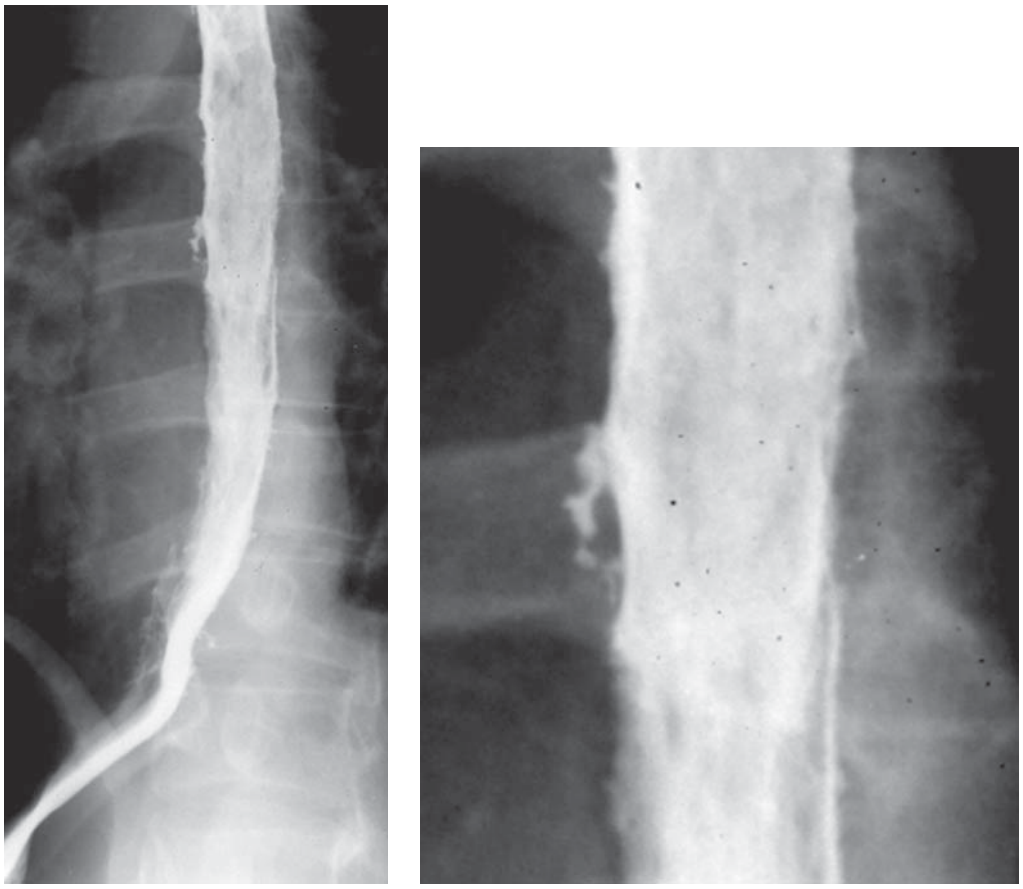


Fig. 35.1 **(A)** Single-contrast fluoroscopic image and **(B)** coned-down view of the esophagus from a barium swallow examination demonstrate a large midesophageal ulcer, as well as smaller ulcerations and thickening of the longitudinal folds. (Courtesy of the Department of Radiology, University of Cincinnati.)

Clinical Presentation

A 35-year-old man presents with chest pain and odynophagia (**Fig. 35.1**).

Key Imaging Finding

Esophageal ulcers

Top 3 Differential Diagnoses

- **Reflux esophagitis.** Erosions and ulcerations can form in the distal esophagus as a result of irritation of esophageal mucosa from gastric acid. Key imaging findings of esophageal inflammation are longitudinal fold thickening, pooling of contrast in mucosal erosions or ulcers, poor peristalsis, and poor esophageal distention in the region of inflammation. Midesophageal strictures may be seen in severe chronic reflux. Careful visual assessment for Barrett metaplasia, hiatal hernia, and reflux on fluoroscopy can aid in assessment.
- **Viral esophagitis (cytomegalovirus [CMV], human immunodeficiency virus [HIV], and herpes simplex virus [HSV]).** Discrete ulcers against otherwise normal background mucosa are the hallmark of viral esophagitis. Viral esophagitis typically occurs in immunosuppressed patients, especially in the setting of HIV. HSV ulcers tend to be multiple, small, discrete, and focal, whereas ulcers caused by CMV and HIV are typically large. Although imaging characteristics may suggest the underlying source of ulceration, serology or biopsy is often used for definitive diagnosis and treatment
- **Drug-induced esophagitis.** Esophageal injury and ulceration may occur from ingested medications if the tablets become trapped in the esophageal lumen. Typically, esophageal dysmotility or an obstructing lesion is present with subsequent ulcer formation from prolonged direct contact with the esophageal mucosa. Medications that can cause mucosal injury include antimicrobial medications (e.g., doxycycline, tetracycline, and clindamycin), anti-inflammatory agents, and supplements (e.g., potassium chloride and vitamin C).

Additional Differential Diagnoses

- **Caustic esophagitis.** Caustic esophagitis is the consequence of contact injury usually with an alkaline substance. Numerous household and garden chemicals (alkalis), when ingested, can cause both superficial and deep liquefaction necrosis in the esophagus, leading to ulceration and long segment scarring. Acid burns are less frequently encountered and typically lead to less severe superficial mucosal burns.
- **Esophageal carcinoma.** Malignancy should always be considered in the differential diagnoses of mucosal irregularity and ulceration. Both primary squamous cell carcinoma and adenocarcinoma in the setting of Barrett metaplasia can ulcerate. Aggressive midesophageal malignancies can erode into the tracheobronchial tree, resulting in fistula formation. Metastases and lymphoma may also mimic esophageal carcinoma.

Diagnosis

Viral esophagitis (CMV)

✓ Pearls

- Mucosal ulcers, fold thickening, poor peristalsis, and poor distensibility are key findings in esophagitis.
- HSV typically causes multiple small ulcers; CMV and HIV commonly present as large ulcers.
- Contact injury from prolonged retention of medications in the esophagus can cause a focal ulcer.
- Esophageal carcinoma and lymphoma should always be considered as a potential cause for an ulcer.

Suggested Readings

Berkovich GY, Levine MS, Miller WT Jr. CT findings in patients with esophagitis. AJR Am J Roentgenol 2000;175(5):1431–1434

Federle MP, Jeffrey RB, Desser TS, et al. Diagnostic Imaging: Abdomen. Salt Lake City, UT: Amirsys; 2004

Levine MS, Rubesin SE. Diseases of the esophagus: diagnosis with esophagography. Radiology 2005;237(2):414–427

Case 36

Brian S. Johnston

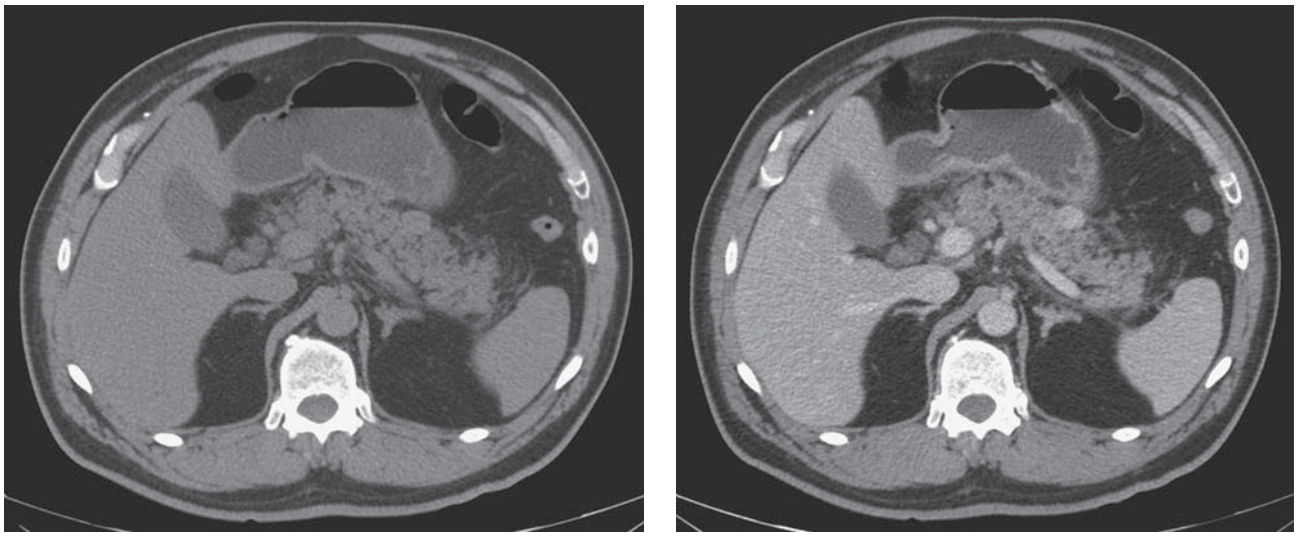


Fig. 36.1 **(A)** Unenhanced and **(B)** enhanced axial CT images through the level of the pancreas demonstrate a solid, round enhancing mass at the junction of the pancreatic body and tail.

Clinical Presentation

A 45-year-old woman presents with fatigue and laboratory abnormalities (**Fig. 36.1**).

Key Imaging Finding

Solid pancreatic mass

Top 3 Differential Diagnoses

- **Pancreatic adenocarcinoma.** Ductal epithelial adenocarcinoma is the most common primary tumor of the pancreas and typically occurs in older males. This malignancy grows in an infiltrative manner with poorly defined margins, often mimicking pancreatitis. Vascular encasement and narrowing are common findings, especially involving the splenic vein and superior mesenteric artery. Imaging findings include a hypovascular pancreatic mass with distal pancreatic ductal dilatation and parenchymal atrophy. Prognosis is typically poor.
- **Islet cell tumor.** In contrast to pancreatic adenocarcinoma, islet cell tumors (and their metastases) are hypervascular. Peritumoral neovascularity is common, and vascular encasement and narrowing are not typically seen. The tumors are classified by the hormones they produce. Insulinoma is the most common subtype and is most often benign. Gastrinoma, nonfunctioning islet cell tumor, glucagonoma, VIPoma (vasoactive intestinal polypeptide tumor), and somatostatinoma represent less common subtypes of islet cell tumors that tend to have more malignant characteristics. Gastrinoma results in hypersecretion of gastric acid and results in multiple gastric and duodenal (typically postampullary) ulcers. They are commonly associated with Zollinger–Ellison syndrome. Islet cell tumors may be seen as part of multiple endocrine neoplasia (MEN) syndrome type 1.
- **Solid and papillary epithelial neoplasm (SPEN).** SPEN is a rare pancreatic tumor that is mostly seen in young women. Imaging findings include a large, well-circumscribed noncalcified mass, usually containing both solid and cystic areas. Necrosis and hemorrhage are common. These neoplasms have a good prognosis after resection. In young children, pancreatoblastoma can have a similar appearance.

Additional Differential Diagnoses

- **Lymphoma.** Lymphoma may involve the pancreas, typically from local spread of the non-Hodgkin variant. Associated abdominal or pelvic lymphadenopathy is typically present, which would support the diagnosis. Vascular encasement is less common in contrast to adenocarcinoma.
- **Metastases.** Colorectal and gastric malignancies most commonly involve the pancreas by local invasion. Numerous tumors can result in hematogenous pancreatic metastases, including melanoma, breast cancer, lung cancer, and renal cell carcinoma metastases. Metastatic disease involving peripancreatic lymph nodes can simulate a primary pancreatic tumor.

Diagnosis

Islet cell tumor

✓ Pearls

- A hypovascular pancreatic mass encasing and narrowing adjacent vessels is pathognomonic of cancer.
- The most common hypervascular islet cell tumor of the pancreas is an insulinoma.
- SPEN is a rare solid and cystic pancreatic tumor that occurs in young women.
- Hypervascular pancreatic metastases include melanoma, breast cancer, and renal cell carcinoma.

Suggested Readings

Federle MP, Jeffrey RB, Desser TS, et al. Diagnostic Imaging: Abdomen. Salt Lake City, UT: Amirsys; 2004

McNulty NJ, Francis IR, Platt JF, Cohan RH, Korobkin M, Gebremariam A. Multidetector row helical CT of the pancreas: effect of contrast-enhanced multiphasic imaging on enhancement of the pancreas, peripancreatic vasculature, and pancreatic adenocarcinoma. Radiology 2001;220(1):97–1021

Schueller G, Schima W, Schueller-Weidekamm C, et al. Multidetector CT of pancreas: effects of contrast material flow rate and individualized scan delay on enhancement of pancreas and tumor contrast. Radiology 2006;241(2):441–448

Case 37

Brian S. Johnston

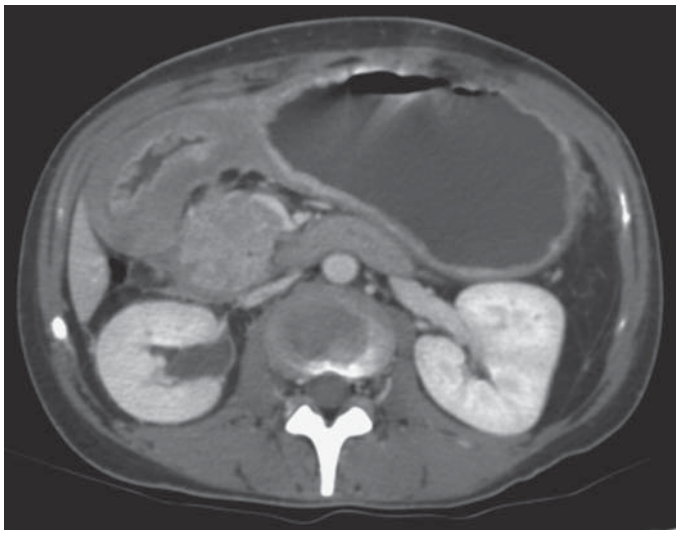


Fig. 37.1 Contrast-enhanced axial CT image through the upper abdomen demonstrates diffuse circumferential antral wall thickening with narrowing of the gastric lumen.

Clinical Presentation

A 45-year-old woman presents with weight loss and heartburn (**Fig. 37.1**).

Key Imaging Finding

Linitis plastica

Top 3 Differential Diagnoses

- **Gastric carcinoma**. Diffuse infiltrative gastric wall thickening, in association with a rigid, contracted, narrowed stomach ("linitis plastica" appearance), is the second most common appearance for gastric carcinoma after focal irregular wall thickening with ulceration. Poorly differentiated tumor types and poor prognoses are often found in association with the linitis plastica type of gastric carcinoma. Key imaging findings include gastric antral wall thickening with possible fundal sparing, absent peristalsis, and loss of normal gastric fold pattern.
- **Metastatic disease.** A common presentation of gastric metastases is diffuse infiltrative wall thickening, with breast and lung cancers representing the most common primary neoplasms. The infiltrative tumor results in a rigid, contracted stomach. Pancreatic adenocarcinoma can invade the distal stomach by contiguous spread, also producing the linitis plastica appearance.
- **Lymphoma.** Primary gastric lymphoma accounts for <15% of gastric malignancies. Secondary gastric involvement, however, is not uncommon in systemic lymphomas, especially the non-Hodgkin variant. Diffuse infiltration of the tumor results in a desmoplastic response and subsequent gastric luminal rigidity and narrowing.

Additional Differential Diagnoses

- **Crohn disease.** Severe gastric involvement with Crohn disease can produce a rigid, contracted, narrowed distal stomach, which is referred to as the "ram's horn" appearance. By the time the stomach is involved with Crohn disease, there is typically more pronounced small bowel (usually terminal ileum) and/or colonic involvement as well.

Diagnosis

Metastatic disease (breast cancer)

✓ Pearls

- Linitis plastica with a rigid gastric wall is the second most common appearance of gastric carcinoma.
- Diffuse infiltrative metastatic breast and lung cancers may produce linitis plastica.
- Lymphoma in the gastric wall is often secondary to diffuse systemic disease involvement.
- Postinflammatory scarring of the distal stomach in Crohn disease is termed the "ram's horn" appearance.

Suggested Readings

Ba-Ssalamah A, Prokop M, Uffmann M, Pokieser P, Teleky B, Lechner G. Dedicated multidetector CT of the stomach: spectrum of diseases. Radiographics 2003;23(3):625–644

Halpert RD, Feczko PJ. Gastrointestinal Radiology: The Requisites. St. Louis: Mosby; 1999

Horton KM, Fishman EK. Current role of CT in imaging of the stomach. Radiographics 2003;23(1):75–87

Case 38

Robert A. Jesinger

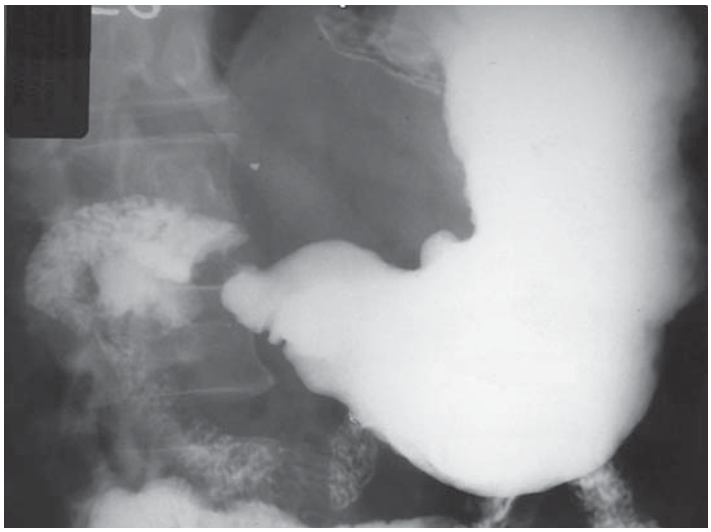


Fig. 38.1 Single-contrast fluoroscopic image from an upper gastrointestinal examination demonstrates a focal smooth outpouching of contrast along the lesser curvature of the stomach. The contrast collection extends beyond the margins of the stomach wall. (Courtesy of the Department of Radiology, University of Cincinnati.)

Clinical Presentation

A 34-year-old man presents with epigastric pain (**Fig. 38.1**).

Key Imaging Finding

Gastric ulcer

Top 3 Differential Diagnoses

- **Peptic ulcer disease.** Benign gastric ulcers typically occur in the gastric antrum and appear as a contrast "outpouching" beyond the margin of the gastric wall. The margins of the ulcer are smooth, and the adjacent fold pattern is typically normal. *Helicobacter pylori* infection has been found to be a major causative factor. Nonsteroidal antiinflammatory drugs (NSAIDs) are another but less common cause of benign gastric ulcers.
- **Gastric carcinoma.** Focal gastric wall thickening with ulceration is the most common presentation of gastric carcinoma. Malignant gastric ulcers may occur anywhere within the stomach but most commonly are located in the antrum. In contrast to benign ulcers, malignant ulcers appear as a contrast "inpouching" due to contrast filling an ulcerated gastric mass. The margins of the ulcer are irregular. Diagnosis is confirmed with endoscopic biopsy.
- **Lymphoma.** Primary gastric lymphoma accounts for <15% of gastric malignancies. Secondary gastric involvement, however, is not uncommon in systemic disease (e.g., non-Hodgkin lymphoma). Gastric lymphoma may mimic both the diffuse infiltrative type (linitis plastica) and the focal ulcerative variant of gastric adenocarcinoma.

Additional Differential Diagnoses

- **Metastatic disease.** A mural gastric mass with central ulceration may be secondary to metastatic disease. The more common primary neoplasms are breast and lung cancers, as well as malignant melanoma. Pancreatic adenocarcinoma can involve the distal stomach (usually distal greater curvature) by contiguous spread, and central ulceration of the invading mass can occur.
- **Zollinger–Ellison syndrome.** Zollinger–Ellison syndrome consists of multiple gastric and duodenal (classically postbulbar) ulcers secondary to marked gastric hypersecretion caused by a gastrinoma. The majority of gastrinomas occur within the pancreas (islet cell tumors), but 15% can be found in the duodenum. An association with multiple endocrine neoplasia (MEN) syndrome type 1 occurs in 25% of cases. Clinical features of gastric hypersecretion and diarrhea mimic Ménétrier disease. The majority of gastrinomas (60%) are malignant, with a propensity for early liver and lymph node metastases. Hepatic metastases are hypervascular.

Diagnosis

Peptic ulcer disease

✓ Pearls

- Contrast "outpouching" suggests a benign gastric ulcer; "inpouching" suggests a malignant ulcer.
- Ulcer margin and adjacent fold pattern are important in distinguishing benign from malignant ulcers.
- Postbulbar duodenal ulcers are highly suspicious for being caused by Zollinger–Ellison syndrome.

Suggested Readings

Federle MP, Jeffrey RB, Desser TS, et al. Diagnostic Imaging: Abdomen. Salt Lake City, UT: Amirsys; 2004

Halpert RD. Gastrointestinal Imaging: The Requisites. 3rd ed. Philadelphia: Elsevier; 2006

Pattison CP, Combs MJ, Marshall BJ. *Helicobacter pylori* and peptic ulcer disease: evolution to revolution to resolution. AJR Am J Roentgenol 1997;168(6):1415–1420

Rubesin SE, Furth EE, Levine MS. Gastritis from NSAIDS to *Helicobacter pylori*. Abdom Imaging 2005;30(2):142–159

Case 39

Robert A. Jesinger

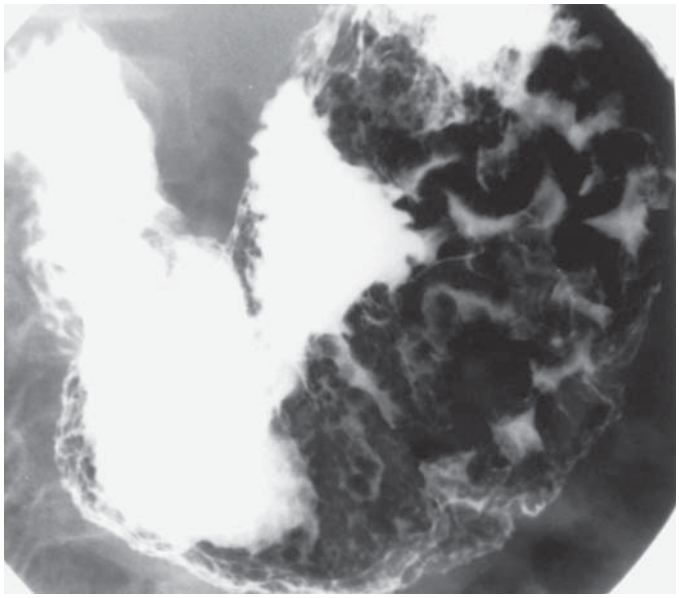


Fig. 39.1 Fluoroscopic image of the stomach from an upper gastrointestinal examination demonstrates marked gastric fold thickening in the regions of the fundus and antrum of the stomach.

Clinical Presentation

A 45-year-old man presents with weight loss, abdominal pain, and diarrhea (**Fig. 39.1**).

Key Imaging Finding

Gastric fold thickening

Top 3 Differential Diagnoses

- **Gastritis.** Chronic inflammation is the most common cause of gastric fold thickening. Common causes include *Helicobacter pylori* infection, nonsteroidal antiinflammatory medications, alcohol abuse, and hypersecretion of acid. Secondary imaging findings suggesting gastritis as the cause of gastric fold thickening include small mucosal ulcerations, thickening of the areae gastricae in the distal stomach, and decreased gastric peristalsis.
- **Gastric carcinoma.** Focal gastric wall thickening, in association with irregular thickened folds and ulceration, is the most common appearance for gastric carcinoma. There is overlap to the imaging features of gastritis and gastric carcinoma, which may delay diagnosis. Endoscopy with biopsy is often required for definitive diagnosis. Gastric carcinoma may metastasize to the liver (most common). Ovarian metastases (Krukenberg tumors) tend to occur late and in more advanced cases.
- **Lymphoma.** Primary gastric lymphoma accounts for <15% of gastric malignancies. Secondary gastric involvement, however, is not uncommon in systemic lymphomas (e.g., non-Hodgkin lymphoma). Focal nodular gastric fold thickening secondary to lymphoma can produce an exaggerated desmoplastic reaction and simulate gastric carcinoma.

Additional Differential Diagnoses

- **Metastatic disease.** Focal irregular gastric fold thickening may be secondary to metastatic disease. The more common primary neoplasms include breast and lung cancers. Pancreatic adenocarcinoma can involve the distal stomach (usually distal greater curvature) by contiguous spread.
- **Ménétrier disease.** Hyperplastic hypersecretory gastropathy is a rare condition of uncertain etiology that can affect adults and children. Findings include thickened proximal gastric folds in association with hypersecretion of mucus, protein loss, and low gastric acid output. Enlarged proximal gastric folds and dilution of barium on fluoroscopy secondary to hypersecretion of fluid are key imaging findings. There is an increased risk of gastric cancer, which should prompt periodic cancer screening. Severe cases have been treated with partial gastrectomy.

Diagnosis

Ménétrier disease

✓ Pearls

- Chronic gastritis is the most common cause of gastric fold thickening (*H. pylori* screening needed).
- Gastric cancer or metastatic breast and lung cancers may present with nodular gastric fold thickening.
- Patients with Ménétrier disease are at increased risk for gastric cancer.

Suggested Readings

Federle MP, Jeffrey RB, Desser TS, et al. Diagnostic Imaging: Abdomen. Salt Lake City, UT: Amirsys; 2004

Halpert RD. Gastrointestinal Imaging: The Requisites. 3rd ed. Philadelphia: Elsevier; 2006

Rubesin SE, Furth EE, Levine MS. Gastritis from NSAIDS to *Helicobacter pylori.* Abdom Imaging 2005;30(2):142–159

Wolfsen HC, Carpenter HA, Talley NJ. Ménétrier's disease: a form of hypertrophic gastropathy or gastritis? Gastroenterology 1993;104(5):1310–1319

Case 40

Brian S. Johnston

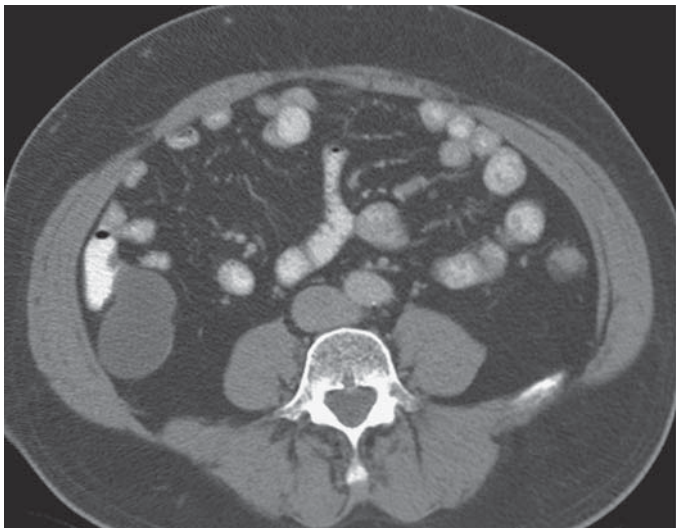


Fig. 40.1 Contrast-enhanced axial CT image of the abdomen demonstrates a hypoattenuating mass in the right lower quadrant of the abdomen that appears to arise from the right cecum.

Clinical Presentation

A 44-year-old man presents with abdominal pain in the right lower quadrant (**Fig. 40.1**).

Key Imaging Finding

Cecal mass

Top 3 Differential Diagnoses

- **Appendicitis/appendiceal abscess.** An obstructed, dilated appendix or an encapsulated abscess due to perforated appendicitis can present as a focal cecal mass on imaging. Key findings are nonenhancing fluid (pus), fat stranding from inflammation, and an obstructing appendicolith. Careful visual and clinical analysis for rupture is important, as emergent surgery is typically avoided after rupture in favor of percutaneous management. Focal calcification usually represents an appendicolith, which can occasionally be seen in the dependent portion of an abscess after perforation.
- **Cecal/appendiceal carcinoma.** Imaging findings in cecal adenocarcinoma depend on the extent of invasion. As the cecum usually allows for significant tumor growth before development of symptoms (e.g., obstruction), neoplasms in this region are typically large at the time of presentation, with transmural invasion, pericolonic adenopathy, and occasionally distant metastases. Pericolonic fat stranding is uncommon, as is desmoplastic reaction, which is a finding that is more commonly seen with carcinoid tumor.
- **Mucocele of the appendix.** Mucocele of the appendix is a descriptive term for an appendix that is distended by mucus. Causes include mucinous cystadenoma or cystadenocarcinoma, mucosal hyperplasia, and mucous retention cyst. A mucocele can also occur secondary to occlusion of the appendiceal lumen by an intrinsic or extrinsic benign or malignant mass. Computed tomography imaging findings include a typically well-encapsulated cystic mass occasionally with mural calcification. Ultrasound shows a simple to minimally complex cyst in the region of the appendix. Most appendix mucoceles are asymptomatic, but rupture can lead to pseudomyxoma peritonei.

Additional Differential Diagnoses

- **Lymphoma.** Although colonic lymphoma is relatively rare, the most common site of involvement is the cecum. The cecum can also be secondarily involved from direct spread of lymphoma from the terminal ileum, which is a common site of lymphomatous involvement. Imaging findings mimic those of cecal adenocarcinoma. Non-Hodgkin lymphoma predominates in adults; Burkitt lymphoma is a subtype more commonly seen in children and young adults.
- **Adnexal mass.** Right lower quadrant (RLQ) pain or mass effect in women is commonly due to ovarian or adnexal pathology. These processes may involve or abut the cecum, mimicking a cecal-origin mass. Common etiologies include simple or complex ovarian cysts, endometriosis, tubo-ovarian abscesses, and benign or malignant ovarian neoplasms.

Diagnosis

Mucocele of the appendix

✓ Pearls

- Periappendiceal inflammation or abscess can present as a focal cecal mass.
- Cecal carcinomas are typically large at presentation due to delayed onset of obstructive symptoms.
- Rupture of a mucocele of the appendix leads to pseudomyxoma peritonei.
- Distinguishing ovary from cecum is important in a woman with a painful RLQ mass.

Suggested Readings

Federle MP, Jeffrey RB, Desser TS, et al. Diagnostic Imaging: Abdomen. Salt Lake City, UT: Amirsys; 2004

Halpert RD. Gastrointestinal Imaging: The Requisites. 3rd ed. Philadelphia: Elsevier; 2006

Kim SH, Lim HK, Lee WJ, Lim JH, Byun JY. Mucocele of the appendix: ultrasonographic and CT findings. Abdom Imaging 1998;23(3):292–296

Case 41

Robert A. Jesinger

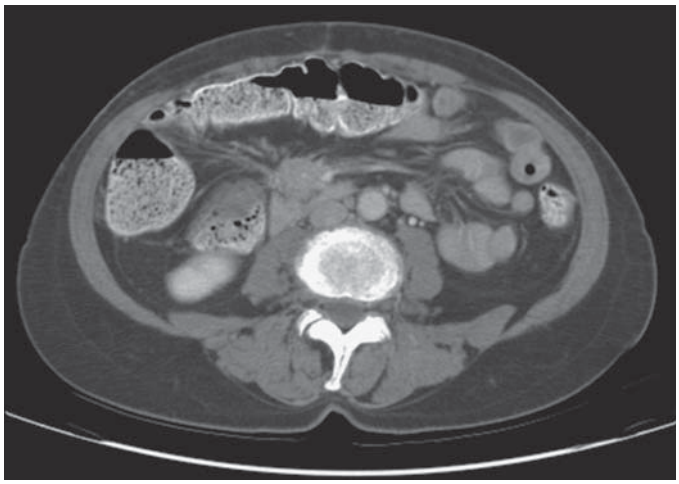


Fig. 41.1 Enhanced axial CT image through the lower abdomen demonstrates a solid enhancing mass in the small bowel mesentery. There is retraction of mesenteric vessels toward the mass suggestive of a desmoplastic reaction. A tiny calcification is noted in the center of the mass.

Clinical Presentation

A 48-year-old man presents with chronic abdominal pain (**Fig. 41.1**).

Key Imaging Finding

Mesenteric mass

Top 3 Differential Diagnoses

- **Metastatic disease.** Metastatic disease to the bowel mesentery can occur via direct spread (pancreatic and colon carcinomas), hematogenous dissemination (breast and lung carcinomas), lymphatic spread (lymphoma), or peritoneal seeding (gastric and ovarian carcinomas). Enhanced computed tomography (CT) is the modality of choice for assessing the number of lesions, margins (round vs irregular), internal components (soft tissue, fluid, calcification, etc.), and enhancement characteristics, as well as identification of the primary source of neoplasm.
- **Carcinoid tumor.** Gastrointestinal carcinoid tumor is a slow-growing hypervascular lesion arising from neuroendocrine cells within the bowel. Mesenteric involvement incites a desmoplastic response, resulting in a spiculated mesenteric mass with intense reactive scarring. Calcifications are visible in up to 70% of these cases. Mesenteric involvement is typically secondary, with the primary neoplasm most commonly within the appendix or ileum. A negative oral contrast agent (water) is helpful in detecting the primary tumor.
- **Desmoid tumor/fibrosing mesenteritis.** Mesenteric desmoid tumors consist of focal regions of masslike fibrosis. They are most commonly associated with familial adenomatous polyposis and cranial osteomas (Gardner syndrome). CT reveals a circumscribed or stellate soft tissue mesenteric mass. Larger lesions may undergo central necrosis, and calcification may be seen following treatment. A related entity referred to as fibrosing mesenteritis is similar to desmoid tumor both radiographically and pathologically; however, it occurs in the absence of familial adenomatous polyposis and is a diagnosis of exclusion.

Additional Differential Diagnoses

- **Reactive lymphadenopathy.** Reactive lymphadenopathy may present as a mesenteric mass and is typically due to an infectious process within the abdomen. Although virtually any abdominal infection may result in conglomerate lymphadenopathy, mycobacterium tuberculosis, *Mycobacterium avium-intracellulare* (MAI), and *Tropheryma whippelei* (Whipple disease) are particularly prone to lymph node enlargement. In particular, these infectious agents result in characteristic lymphadenopathy with central low attenuation.
- **Abdominal mesothelioma.** Abdominal mesothelioma arises from the serosal lining of the peritoneal cavity and is associated with a history of asbestos exposure. Classic CT findings are ascites and serosal soft tissue masses, mimicking peritoneal carcinomatosis. Correlation with chest imaging for pleural thickening and calcification is helpful in establishing the diagnosis, although peritoneal involvement may occur in the absence of pleural disease.

Diagnosis

Carcinoid tumor

✓ Pearls

- Masses in the bowel mesentery should prompt a careful search for a primary tumor or polyp syndrome.
- Carcinoid tumor incites a desmoplastic reaction and commonly calcifies.
- Mesenteric adenopathy with central low attenuation is concerning for tuberculosis, MAI, and Whipple disease.
- Reactive adenopathy can be related to routine gastroenteritis, but lymphoma should always be considered.

Suggested Readings

Federle MP, Jeffrey RB, Desser TS, et al. Diagnostic Imaging: Abdomen. Salt Lake City, UT: Amirsys; 2004

Halpert RD. Gastrointestinal Imaging: The Requisites. 3rd ed. Philadelphia: Elsevier; 2006

Pantongrag-Brown L, Buetow PC, Carr NJ, Lichtenstein JE, Buck JL. Calcification and fibrosis in mesenteric carcinoid tumor: CT findings and pathologic correlation. AJR Am J Roentgenol 1995;164(2):387–391

Sheth S, Horton KM, Garland MR, Fishman EK. Mesenteric neoplasms: CT appearances of primary and secondary tumors and differential diagnosis. Radiographics 2003;23(2):457–473, quiz 535–536

Case 42

Paul B. DiDomenico

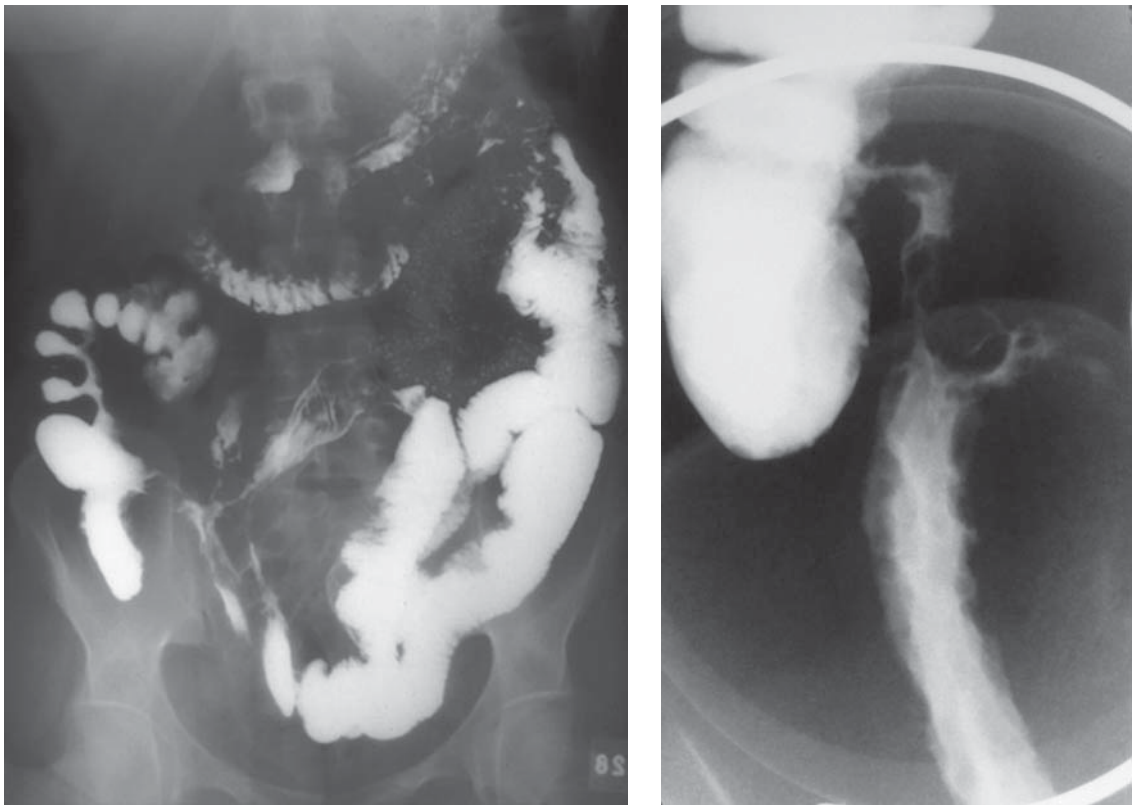


Fig. 42.1 **(A)** Overhead and **(B)** right lower quadrant spot compression views from a small bowel follow-through study demonstrate irregularity and thickening of the terminal ileum with stricture formation. Image **A** demonstrates fistula formation between bowel loops, as well as general separation of the loops.

Clinical Presentation

A young adult man presents with diarrhea and abdominal pain (**Fig. 42.1**).

Key Imaging Finding

Terminal ileal wall thickening

Top 3 Differential Diagnoses

- **Inflammatory bowel disease.** Of the two main types of idiopathic inflammatory bowel disease (ulcerative colitis and Crohn disease), Crohn disease characteristically involves the terminal ileum, causing transmural inflammation, thickening, and deep fissuring ulcers. Proliferation of mesenteric fat ("creeping fat") may cause the bowel loops to appear separated on a small bowel follow-through study. Fistulas and sinus tracts are a hallmark of the disease secondary to transmural involvement, and skip (discontinuous) lesions are characteristic. These findings are in contrast to those of ulcerative colitis, which is characterized by continuous involvement of the colon beginning distally and progressing proximally. Ulcerative colitis may cause dilatation of the distal ileum, termed "backwash" ileitis, in ~25% of cases.
- **Infection.** Certain infections have a predilection for the terminal ileum, among them salmonella, campylobacter, yersinia, and mycobacterium tuberculosis. Immunosuppressed patients (i.e., those with human immunodeficiency virus [HIV] and acquired immunodeficiency syndrome) are also at increased risk for opportunistic infection from *Cryptosporidium* and cytomegalovirus (CMV). Imaging features of these infections are generally nonspecific, and the diagnosis is usually made through stool analysis, mucosal biopsy, and/or response to empiric antimicrobial therapy.
- **Lymphoma.** Non-Hodgkin lymphoma affects the small bowel in approximately one third of cases, with the ileum being the most common site of involvement. Imaging appearance is variable; however, lymphoma typically manifests as nodular/polypoid or diffuse infiltrative small bowel wall thickening. When the terminal ileum is involved, the bowel wall may be thickened with a narrow lumen, resembling Crohn disease.

Additional Differential Diagnoses

- **Ischemia.** Ischemia of the superior mesenteric artery territory can result in bowel wall thickening due to edema and occasionally hemorrhage. There may be gas in the bowel wall (pneumatosis), which may also be seen in the mesenteric and portal venous system on computed tomography imaging. Intravenous contrast material may aid in visualization of the site of occlusion due to clot or atherosclerotic disease.
- **Metastatic disease.** Metastatic spread of carcinoma can involve the terminal ileum through contiguous or peritoneal spread (gastrointestinal or genitourinary primary neoplasms), as well as hematogenous spread (malignant melanoma and lung and breast carcinomas). Metastatic spread to the small bowel is less common than primary small bowel lymphoma.

Diagnosis

Crohn disease

✓ Pearls

- Crohn disease classically involves the distal ileum, with chronic inflammation leading to strictures/fistulas.
- CMV or *Cryptosporidium* involvement of the terminal ileum should prompt an evaluation for HIV.
- Nodular ileal wall thickening is concerning for malignancy, including lymphoma and metastatic disease.

Suggested Readings

Federle MP, Jeffrey RB, Desser TS, et al. Diagnostic Imaging: Abdomen. Salt Lake City, UT: Amirsys; 2004

Furukawa A, Saotome T, Yamasaki M, et al. Cross-sectional imaging in Crohn disease. Radiographics 2004;24(3):689–702

Halpert RD. Gastrointestinal Imaging: The Requisites. 3rd ed. Philadelphia: Elsevier; 2006

Macari M, Balthazar EJ. CT of bowel wall thickening: significance and pitfalls of interpretation. AJR Am J Roentgenol 2001;176(5):1105–1116

Case 43

Robert A. Jesinger

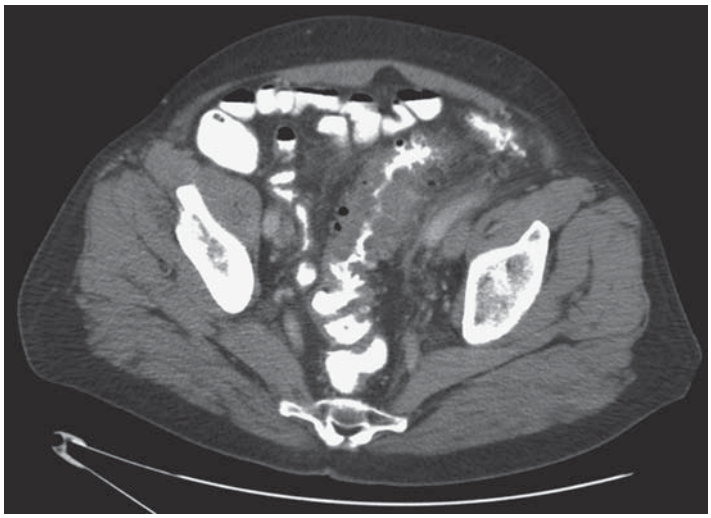


Fig. 43.1 Contrast-enhanced axial CT image through the pelvis demonstrates circumferential wall thickening of the sigmoid colon with pericolonic fat stranding. There is the suggestion of focal gas within the bowel wall.

Clinical Presentation

A 58-year-old man presents with abdominal pain (**Fig. 43.1**).

Key Imaging Finding

Colonic wall thickening

Top 3 Differential Diagnoses

- **Infectious colitis.** Infectious colitis is the most common cause of focal bowel wall thickening and is frequently the sequela of diverticulitis. Most cases are caused by gram-negative bacteria. Immunosuppressed patients not only are susceptible to typical infectious causes of colitis but also are prone to severe atypical infections, especially in the setting of neutropenia (neutropenic colitis). Antibiotic therapy may occasionally alter the normal bacterial flora of the colon, allowing for overgrowth of *Clostridium difficile*, which is the causative organism of pseudomembranous colitis. Classic imaging findings of infectious colitis are colonic air–fluid levels, wall thickening, and increased mucosal enhancement.
- **Inflammatory bowel disease.** Crohn disease and ulcerative colitis (UC) are idiopathic conditions leading to transmural (Crohn) or mucosal (UC) bowel wall inflammation. UC begins in the rectum and progresses proximally without skip lesions; Crohn disease, in contrast, may involve any portion of the gastrointestinal tract from the esophagus to the anus (most commonly the terminal ileum) and routinely demonstrates skip lesions. Early imaging findings reveal mucosal inflammation ("granular" mucosal appearance and edematous haustra). Diffuse bowel wall thickening is typically a later finding. Strictures and fistulas are seen in Crohn disease secondary to transmural involvement, whereas chronic UC often leads to fixed colonic dilatation ("lead pipe" appearance). Both entities involve the terminal ileum: Crohn disease results in strictures, and UC results in dilatation due to backwash ileitis. Patients with UC have an increased risk (up to 10%) of colon cancer.
- **Colon carcinoma.** Colon carcinoma may present as focal short segment bowel wall thickening and pericolonic fatty infiltration, mimicking colitis. Secondary findings that suggest underlying malignancy are regional lymphadenopathy and distant metastases, most commonly within the liver. Appropriate cancer screening (e.g., colonoscopy) should be confirmed.

Additional Differential Diagnoses

- **Ischemic colitis.** Ischemic bowel disease is commonly the result of atherosclerotic or embolic disease, but it may also occur in the setting of hypoperfusion. Watershed areas (splenic flexure) are the most susceptible regions to decreased blood flow. Enhanced computed tomography is ideal for assessment of bowel wall enhancement and mesenteric artery patency. Complications include bowel necrosis, which may lead to pneumatosis and portal venous gas.

Diagnosis

Infectious colitis

✓ Pearls

- Infection, ischemia, and inflammatory conditions are common causes of colonic wall thickening.
- Ischemic bowel necrosis may lead to pneumatosis, portal venous gas, and sepsis.
- Colonoscopy and biopsy are often used to help exclude malignancy in the setting of bowel wall thickening.

Suggested Readings

Federle MP, Jeffrey RB, Desser TS, et al. Diagnostic Imaging: Abdomen. Salt Lake City, UT: Amirsys; 2004

Halpert RD. Gastrointestinal Imaging: The Requisites. 3rd ed. Philadelphia: Elsevier; 2006

Macari M, Balthazar EJ. CT of bowel wall thickening: significance and pitfalls of interpretation. AJR Am J Roentgenol 2001;176(5):1105–1116

Thoeni RF, Cello JP. CT imaging of colitis. Radiology 2006;240(3):623–638

Case 44

Eleanor L. Ormsby

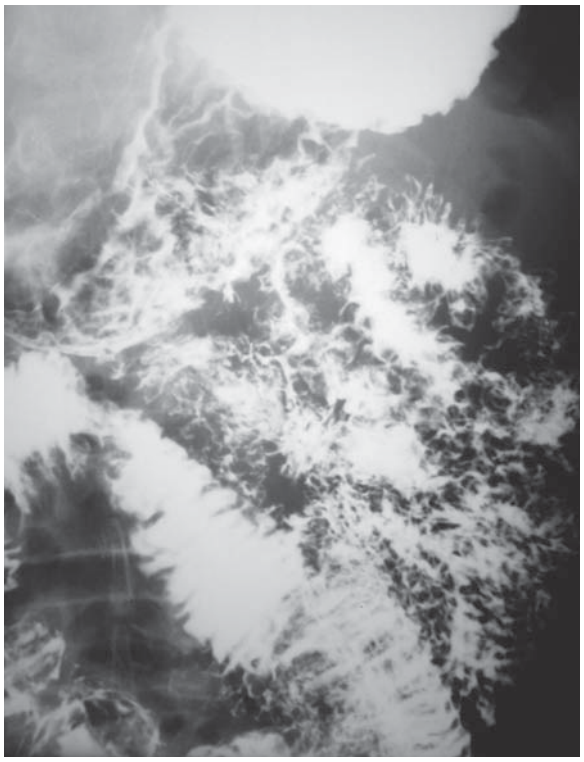


Fig. 44.1 Frontal view from a small bowel follow-through examination reveals multiple regions of nodular small bowel wall thickening. The findings are most pronounced within the left upper quadrant.

Clinical Presentation

A patient presents with abdominal pain (**Fig. 44.1**).

Key Imaging Finding

Small bowel wall thickening

Top 3 Differential Diagnoses

- **Crohn disease.** On small bowel follow-through examinations, Crohn disease presents as irregularly thickened folds associated with mucosal ulceration (early) and strictures (late). The findings are usually seen in the terminal ileum. The "string" sign has been used to describe marked segmental narrowing of bowel loops. In contrast to ulcerative colitis, lesions in Crohn disease can be scattered in the small bowel ("skip lesions"), with normal bowel interposed between involved segments. On computed tomography, bowel wall thickening and mesenteric stranding are the most common findings. The fibrofatty proliferation seen in the mesentery is referred to as "creeping fat."
- **Lymphoma.** Small bowel lymphoma can occur with or without predisposing factors, such as immunodeficiency syndromes, celiac sprue, and Crohn disease. There are different types of imaging findings, including nodular bowel wall thickening, bowel wall infiltration with loss of bowel markings, and intraluminal polypoid masses. There may be associated luminal narrowing or characteristic aneurysmal dilatation, which is more common with diffuse infiltration.
- **Small bowel hemorrhage.** Small bowel is the most common site of intramural hemorrhage and may be due to trauma, mesenteric ischemia, vasculitis, coagulopathy, anticoagulant medication, or Henoch-Schönlein purpura. Short segment, uniformly thickened small bowel folds with "stack of coins" appearance is the typical finding. Appropriate clinical history helps to differentiate the cause, as the imaging findings are nonspecific.

Additional Differential Diagnoses

- **Metastases.** Metastases to the small bowel commonly present as multiple masses with nodular bowel wall thickening, which may result in fold tethering or ulceration. Metastases can be from intraperitoneal seeding, hematogenous spread, lymphatic spread, or direct extension from a contiguous neoplasm. Clinical correlation with a known history of primary cancer or enteropathy is important.
- **Amyloidosis.** In amyloidosis, extracellular deposits of amyloid occur throughout the body, including the gastrointestinal tract. Small bowel folds may be diffusely thickened and nodular. Although this may be a primary disease, most often, it occurs in patients with underlying multiple myeloma or chronic inflammatory conditions.
- **Whipple disease.** Whipple disease is a rare, chronic, systemic disease caused by a bacterial infection (gram-positive bacilli with periodic acid–Schiff stain). Patients present with chronic diarrhea, arthralgias, and malabsorption. Thickened proximal small bowel folds with micronodularity (1–2 mm) and low-density mesenteric lymphadenopathy are characteristic findings.

Diagnosis

Lymphoma

✓ Pearls

- Mucosal ulceration, mesenteric fibrofatty proliferation, and strictures are key findings in Crohn disease.
- In the setting of trauma, smooth small bowel fold or wall thickening is concerning for mural hemorrhage.
- Bowel lymphoma or metastases should be considered when nodular small bowel fold thickening is seen.

Suggested Readings

Federle MP, Jeffrey RB, Desser TS, et al. Diagnostic Imaging: Abdomen. Salt Lake City, UT: Amirsys; 2004

Furukawa A, Saotome T, Yamasaki M, et al. Cross-sectional imaging in Crohn disease. Radiographics 2004;24(3):689–702

Case 45

Shaun Loh



Fig. 45.1 Single-contrast esophagram demonstrates a long, narrow stricture involving the distal esophagus, as well as mucosal irregularity within the midesophagus.

Clinical Presentation

A 40-year-old man presents with dysphagia (**Fig. 45.1**).

Key Imaging Finding

Esophageal stricture

Top 3 Differential Diagnoses for Short Segment Stricture

- **Reflux esophagitis.** Reflux esophagitis is one of the most common causes of esophageal strictures. The stricture typically appears as an area of smooth, tapered narrowing in the distal esophagus. Asymmetric scarring can occur, resulting in a more eccentric stricture. Sacculations may be present between multiple strictures.
- **Drug-induced stricture.** The two most common agents implicated in drug-induced esophagitis, tetracycline and doxycycline, typically cause superficial ulceration that heals without stricture formation. Other drugs such as quinidine, potassium chloride, alendronate, and nonsteroidal antiinflammatory drugs, may cause larger ulcerations and strictures in the proximal to midesophagus areas. Tablet medications may lodge in the esophagus due to extrinsic compression from adjacent structures, such as the aortic arch and left mainstem bronchus.
- **Esophageal carcinoma.** Squamous cell carcinoma accounts for ~80% of all cases of esophageal cancer. Risk factors include smoking, alcohol abuse, caustic ingestions, achalasia, and Plummer-Vinson syndrome. Adenocarcinoma from Barrett esophagitis comprises the majority of the remaining cases. The most common finding is a fixed narrowing of the esophageal lumen. The tumor may also appear as an annular constricting lesion causing a long segment stricture with prominent shoulders. Another pattern is that of a polypoid intraluminal filling defect. Prognosis is poor, with a 5% 5-year survival rate.

Top 3 Differential Diagnoses for Long Segment Stricture

- **Iatrogenic (nasogastric tube).** Nasogastric intubation prevents the lower esophageal sphincter from closing, allowing the acidic gastric contents to bathe the lumen of the distal esophagus. Mucosal injury and stricture formation can ensue. Strictures are most commonly seen with prolonged intubations.
- **Caustic ingestion.** Ingestion of strong acids or more commonly bases causes long, symmetric esophageal strictures, usually months to years after the initial injury. The stricture may appear "threadlike," with a diffuse, long segmental narrowing, irregular contours, and ulcerations. Treatment entails either esophageal dilation or esophagectomy. There is an increased risk of malignancy after the initial injury.
- **Radiation changes.** Radiation changes occur within the radiotherapy field during the treatment of thoracic and cervical neoplasms. The strictures are often long, smooth, concentric, and tapered.

Diagnosis

Iatrogenic stricture from a nasogastric tube

✓ Pearls

- Strictures from reflux esophagitis commonly are seen as smooth areas of narrowing in the esophagus.
- Tablet medications may lodge in the esophagus and incite ulceration and stricture formation.
- Irregular areas of stricturing in the esophagus are concerning for esophageal carcinoma.
- Prolonged nasogastric tube placement can result in mucosal injury to the esophagus and stricture formation.

Suggested Readings

Federle MP, Jeffrey RB, Desser TS, et al. Diagnostic Imaging: Abdomen. Salt Lake City, UT: Amirsys; 2004

Luedtke P, Levine MS, Rubesin SE, Weinstein DS, Laufer I. Radiologic diagnosis of benign esophageal strictures: a pattern approach. Radiographics 2003;23(4):897–909

Case 46

Robert A. Jesinger

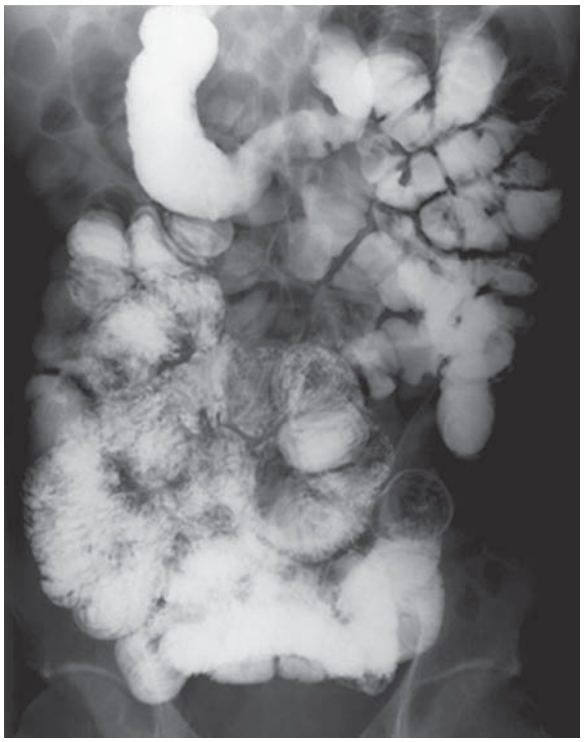


Fig. 46.1 Single-contrast small bowel follow-through image demonstrates dilatation of small bowel loops with reversal of the jejunal and ileal fold pattern.

Clinical Presentation

A 29-year-old man presents with weight loss and chronic abdominal pain (**Fig. 46.1**).

Key Imaging Finding

Small bowel dilatation

Top 3 Differential Diagnoses

- **Small bowel obstruction.** Small bowel dilatation (>3 cm diameter), air–fluid levels, and prominent thinned folds are key findings in mechanical small bowel obstruction. Common causes include focal adhesions, hernia, intussusception, volvulus, and obstructing mass (lymphoma). Abdominal radiographs and enhanced computed tomography (CT) are standard in the initial evaluation and help guide the need for surgical intervention. Obstruction may be complete or partial. In complete obstruction, a transition point may be found with decompression of bowel loops beyond the level of obstruction. Closed loop obstructions are considered a surgical emergency due to the increased risk of ischemic necrosis and subsequent perforation. Clinically, patients present with nausea and vomiting and demonstrate high-pitched bowel sounds on auscultation.
- **Adynamic ileus.** Adynamic ileus results in bowel dilatation secondary to a lack of peristalsis. In comparison to mechanical obstruction, ileus usually results in fluid-filled loops of the small and large bowel without a transition point or decompression of distal bowel loops. Common causes of ileus are medications (analgesics, anticholinergics, etc.), neurologic insult, and inflammatory or infectious processes. Focal ileus may be seen adjacent to sites of inflammation, such as in the setting of pancreatitis or appendicitis. Clinically, bowel sounds are decreased or absent due to lack of peristalsis.
- **Celiac sprue.** Celiac sprue is an autoimmune disorder caused by a hypersensitivity to wheat gluten, resulting in damage to the mucosal lining of the small intestine. Clinical symptoms are related to malabsorption and hypersecretion of fluid. Fluoroscopic findings include small bowel dilatation, reversal of the jejunal and ileal fold patterns ("ilealization" of the jejunum and "jejunization" of the ileum), and dilution of barium due to hypersecretion. Transient intussusceptions are commonly seen, which may further increase small bowel dilatation. Patients with celiac sprue are at increased risk for the development of malignancies, including lymphoma and adenocarcinoma. Diagnosis is confirmed with duodenal biopsy, along with various serologic studies. Approximately 70% of patients have symptomatic improvement within 2 weeks of starting a gluten-free diet.

Additional Differential Diagnoses

- **Scleroderma.** Scleroderma is a chronic disease thought to represent a type of autoimmune dysfunction that results in excessive deposition of collagen in various organ systems. The deposition of collagen within the small bowel results in diffuse scarring. Radiographic manifestations include small bowel dilatation with crowding of folds ("hidebound" bowel) and antimesenteric small bowel pseudosacculations.

Diagnosis

Celiac sprue

✓ Pearls

- Common causes of dilated small bowel loops are mechanical obstruction and dysmotility (ileus).
- Bowel dilation from mural scarring can be seen in scleroderma and celiac sprue.
- Patients with celiac sprue are at increased risk for bowel lymphoma and adenocarcinoma.

Suggested Readings

Federle MP, Jeffrey RB, Desser TS, et al. Diagnostic Imaging: Abdomen. Salt Lake City, UT: Amirsys; 2004

Furukawa A, Yamasaki M, Furuichi K, et al. Helical CT in the diagnosis of small bowel obstruction. Radiographics 2001;21(2):341–355

Case 47

William T. O'Brien Sr.

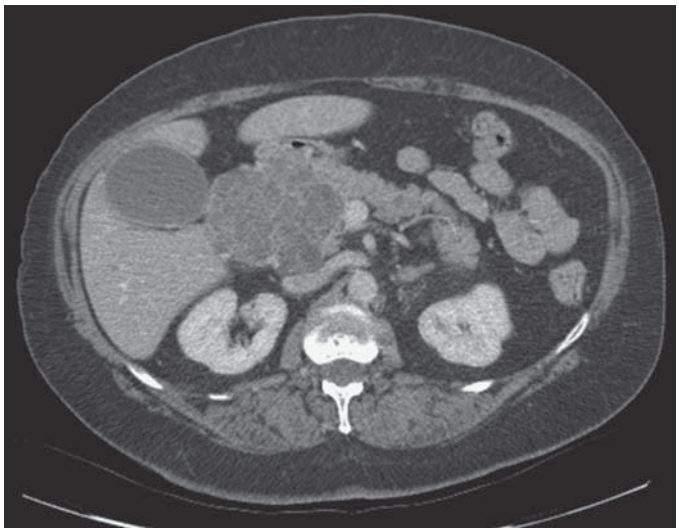


Fig. 47.1 Contrast-enhanced axial CT image through the upper abdomen demonstrates a multiloculated cystic mass with thin internal septations within the head of the pancreas.

Clinical Presentation

A 42-year-old woman presents with early satiety and abdominal discomfort with meals (**Fig. 47.1**).

Key Imaging Finding

Cystic pancreatic mass

Top 3 Differential Diagnoses

- **Pancreatic pseudocyst.** Pancreatic pseudocysts are the most common cystic pancreatic lesions, accounting for ~90% of all cases, and are a complication of pancreatitis. Although they may be found throughout the abdomen, they occur most frequently within the pancreatic parenchyma. Pseudocysts are contained within a fibrous capsule, and they may be unilocular or multilocular. The cystic components have a high amylase content. Some of these lesions may communicate with the pancreatic duct. Pseudocysts should be suspected in a patient with a history or secondary imaging findings of prior pancreatitis.
- **Mucinous cystadenoma.** Mucinous cystadenomas are benign pancreatic neoplasms that are commonly found in middle-aged to elderly patients, with a strong female predominance. They contain large (>2 cm) mucin-containing cysts and are commonly seen in the tail of the pancreas. Peripheral calcifications may be seen in ~20% of cases. On magnetic resonance imaging, the lesions are hyperintense on T2-weighted sequences and have a variable appearance on T1, depending on the amount of mucin. The more mucin, the brighter the signal intensity on T1-weighted sequences. These lesions cannot be differentiated from a malignant mucinous cystadenocarcinoma on imaging; therefore, the lesions are usually resected.
- **Serous cystadenoma.** Serous cystadenomas are benign pancreatic neoplasms that usually occur in middle-aged women. They may occur anywhere in the pancreas but are commonly located in the pancreatic head. These lesions consist of numerous small cysts (<2 cm) with thin intervening septations. Central calcifications are seen in up to half of all cases. There is a very small risk of malignancy (<5%); the vast majority of these lesions can be safely followed with imaging. There is an association with von Hippel–Lindau disease.

Additional Differential Diagnoses

- **Intraductal papillary mucinous neoplasm (IPMN).** Unlike mucinous and serous cystadenomas, IPMNs communicate with the pancreatic duct. They occur equally in men and women and typically present in the 6th decade. They may affect the main duct with segmental or diffuse ductal dilatation, or they can affect side branches and mimic mucinous or serous cystadenomas. On endoscopy, mucus can be seen emanating from the ampulla. The lesions will fill with contrast on endoscopic retrograde cholangiopancreatography (ERCP).
- **Solid and papillary epithelial neoplasm (SPEN).** SPEN is an uncommon malignant pancreatic neoplasm that characteristically occurs in young women (often in the 3rd decade). They are composed of cystic and solid components and predominantly occur in the pancreatic tail. Cystic components may be complex due to hemorrhage. The malignant nature of these lesions necessitates surgical resection.

Diagnosis

Microcystic (serous) cystadenoma

✓ Pearls

- Pancreatic pseudocysts secondary to pancreatitis account for the majority of cystic pancreatic lesions.
- Mucinous cystadenomas occur in middle-aged to elderly women, most commonly in the pancreatic tail.
- Serous cystadenomas occur in middle-aged women, most commonly in the head of the pancreas.
- Mucus emanating from the pancreatic duct (ampulla) on ERCP is suspicious for IPMN as the cause.

Suggested Readings

Federle MP, Jeffrey RB, Desser TS, et al. Diagnostic Imaging: Abdomen. Salt Lake City, UT: Amirsys; 2004

Kim YH, Saini S, Sahani D, Hahn PF, Mueller PR, Auh YH. Imaging diagnosis of cystic pancreatic lesions: pseudocyst versus nonpseudocyst. Radiographics 2005;25(3):671–685

Case 48

William T. O'Brien Sr.

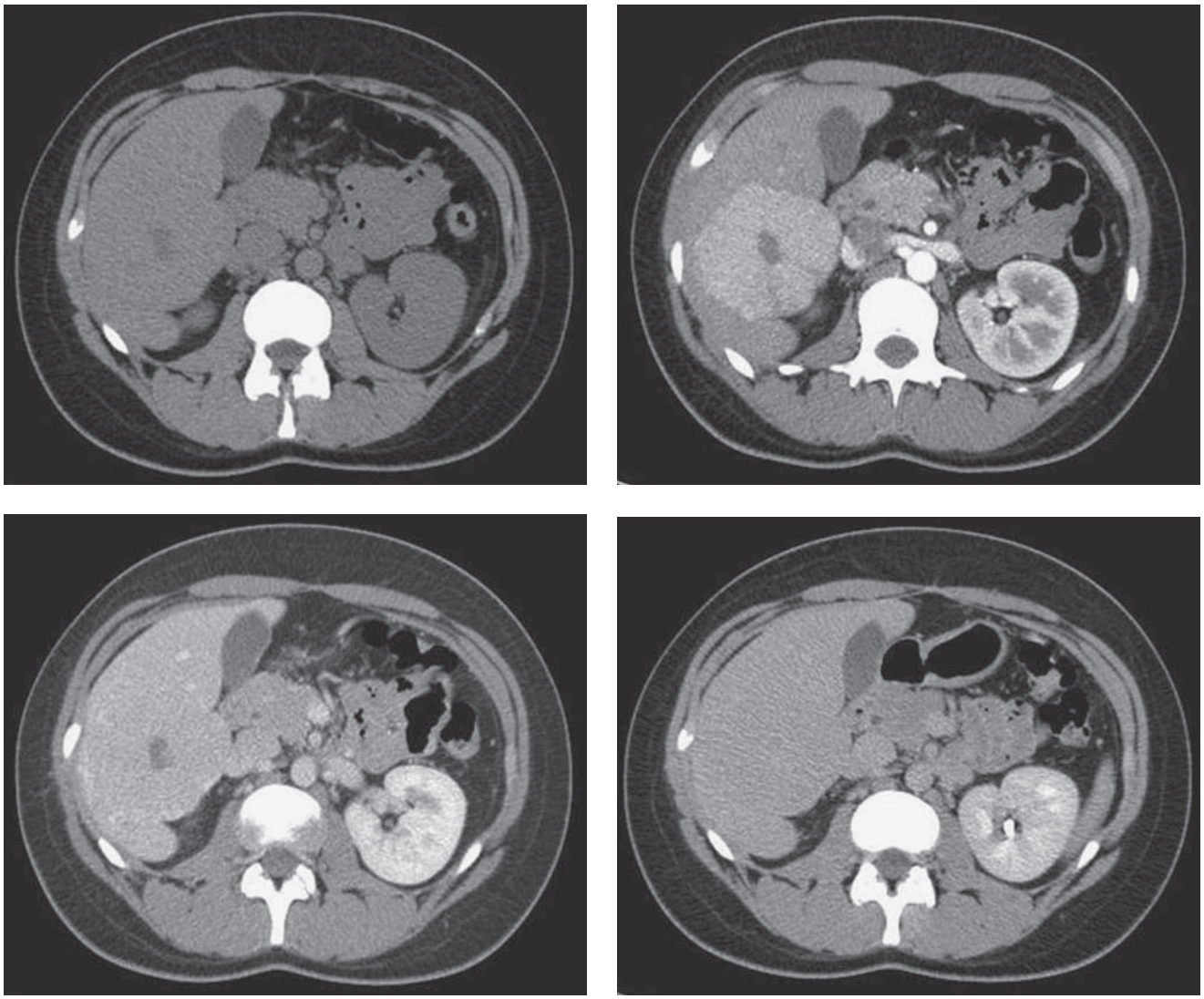


Fig. 48.1 **(A)** Unenhanced axial CT image demonstrates an isodense mass within the right hepatic lobe with a central region of low density. **(B)** The mass demonstrates homogeneous increased enhancement on arterial phase imaging with a central hypodense scar. **(C)** On venous phase imaging, the mass is isodense to surrounding hepatic parenchyma with maintenance of the central hypodense scar. **(D)** On delayed imaging, the central scar fills in, with the entire lesion now isodense to surrounding hepatic parenchyma.

Clinical Presentation

A 19-year-old woman presents with vague abdominal discomfort (**Fig. 48.1**).

Key Imaging Finding

Hypervascular liver mass

Top 3 Differential Diagnoses

- **Hemangioma.** Hemangiomas are the most common neoplastic hepatic lesion and second most common benign lesion following simple cysts. The classic imaging findings are initial discontinuous nodular peripheral enhancement in the arterial phase with delayed central filling. Smaller hemangiomas may demonstrate flash-filling during the arterial phase, and larger lesions may have central regions of fibrosis or cystic changes. On magnetic resonance imaging (MRI), hemangiomas are hyperintense on T2- and hypointense on T1-weighted imaging with similar enhancement patterns as seen with computed tomography. On ultrasound, most hemangiomas are well-circumscribed hyperechoic lesions.
- **Focal nodular hyperplasia (FNH).** FNH is an uncommon hepatic lesion that typically presents in young women (75%). The lesion is composed of hepatocytes and classically contains a central low-density scar. On arterial phase imaging, there is homogeneous enhancement of the lesion with a low-density central scar, which fills in on delayed imaging. The central scar is hyperintense on T2-weighted MRI. Because FNH is composed of hepatocytes, it may demonstrate uptake of sulfur colloid (other hepatic lesions demonstrate cold defects) on scintigraphy.
- **Hepatocellular carcinoma (HCC).** HCC is the most common primary hepatic malignancy with an increased incidence in patients with chronic liver disease. Patients may present with a single lesion, multiple lesions, or diffuse hepatic involvement. The lesions are typically hypodense and demonstrate increased arterial phase enhancement due to increased blood supply from the hepatic artery. Portal or hepatic vein invasion is common. Diagnosis can be difficult in cirrhosis with regenerating nodules. MRI can be helpful in these instances because HCC typically displays increased T2 signal intensity. Clinically, HCC is associated with elevated alpha fetoprotein. Fibrolamellar HCC is a rare variant that presents in younger patients. The lesion demonstrates peripheral arterial phase enhancement with a central low-density scar that does not fill in on delayed imaging (in contrast to FNH). The central scar in fibrolamellar HCC is hypointense on T2-weighted imaging, whereas the central scar in FNH is hyperintense on T2-weighted imaging.

Additional Differential Diagnoses

- **Hepatic adenoma.** Hepatic adenomas are benign lesions predominantly seen in women (90%). Most often they are solitary, but they may occasionally be multiple, especially in patients with glycogen storage disease. Hepatic adenomas have an increased frequency and risk of rupture with the use of oral contraceptives. Adenomas are typically hypervascular; internal hemorrhage can lead to heterogeneity.
- **Hypervascular metastases.** Hypervascular metastases are usually multiple but may rarely present as a solitary mass. Tumors that classically result in hypervascular metastases are melanoma, renal cell carcinoma, thyroid carcinoma, choriocarcinoma, pheochromocytoma, islet cell tumors, and sarcomas.

Diagnosis

Focal nodular hyperplasia

✓ Pearls

- Hemangiomas demonstrate peripheral, nodular, discontinuous enhancement on arterial phase imaging.
- Central scars are most commonly seen with FNH and HCC (especially the fibrolamellar variant).
- Hepatic adenomas are associated with oral contraceptives and are prone to hemorrhage.

Suggested Readings

Blachar A, Federle MP, Ferris JV, et al. Radiologists' performance in the diagnosis of liver tumors with central scars by using specific CT criteria. Radiology 2002;223(2):532–539

Kamel IR, Lawler LP, Fishman EK. Comprehensive analysis of hypervascular liver lesions using 16-MDCT and advanced image processing. AJR Am J Roentgenol 2004;183(2):443–452

Case 49

Robert A. Jesinger

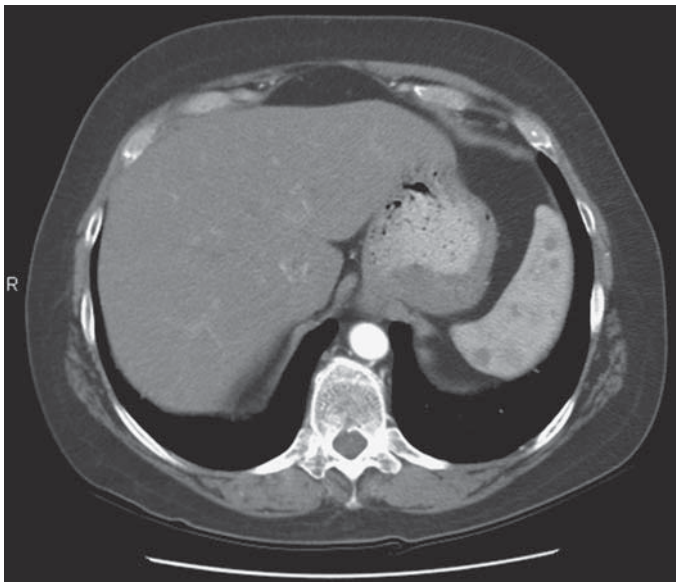


Fig. 49.1 Contrast-enhanced axial CT image through the liver and spleen demonstrates multiple small, hypodense splenic lesions.

Clinical Presentation

A 45-year-old man presents with fever of unknown origin (**Fig. 49.1**).

Key Imaging Finding

Multiple splenic nodules

Top 3 Differential Diagnoses

- **Metastases.** Any primary malignancy can metastasize to the spleen, but the more common primary malignancies include malignant melanoma and lung and breast carcinomas. Metastatic disease to the spleen is often asymptomatic and is usually found in later stage cancers. Imaging findings depend on the primary tumor type, but lesions are often hypoattenuating and multiple. An exceedingly rare complication of splenic metastases is spontaneous splenic rupture, with metastatic choriocarcinoma, melanoma, and lung cancer accounting for the majority of cases.
- **Lymphoma/leukemia.** Lymphomatous/leukemic involvement of the spleen is relatively common. Although splenomegaly is the most common manifestation, the presence of multiple hypoattenuating splenic masses is not unusual. Extrasplenic nodal enlargement supports the diagnosis of lymphoma.
- **Microabscesses.** Splenic abscesses are relatively rare, except in the setting of trauma with superimposed infection or in immunosuppressed patients. In the immunosuppressed patient population, candidiasis is a leading cause of splenic abscess formation. Characteristic imaging findings are nonenhancing, low-attenuation splenic lesions, usually round in shape. Ultrasound reveals multiple target lesions. Antimicrobial therapy is first-line treatment; percutaneous drainage is employed for larger organized collections.

Additional Differential Diagnoses

- **Granulomatous disease.** Granulomatous disease, including sarcoidosis, tuberculosis (TB), and fungal infection, may present as multiple hypoattenuating splenic nodules. Splenic granulomas commonly calcify and are usually found incidentally. Fungal disease (especially histoplasmosis) commonly involves the spleen, whereas TB involvement of the spleen is rare, except in the setting of human immunodeficiency virus (HIV). Sarcoid involvement of the spleen indicates more advanced disease, which may be difficult to treat.
- **Multiple splenic infarcts.** Splenic infarcts typically present as irregularly shaped, peripherally based hypoattenuating lesions. Hematologic disorders (e.g., sickle cell anemia) and embolization of arterial clots (e.g., left heart thrombi in the setting of myocardial infarction) are frequent etiologies. Splenic infarcts are clinically occult in ~30% of cases. Prognosis depends on the underlying cause, but most cases result in no significant long-term sequelae.

Diagnosis

Microabscesses

✓ Pearls

- Lymphoma, melanoma, lung cancer, and breast cancer account for the majority of splenic metastases.
- Candidiasis is a leading cause of splenic microabscesses in the immunosuppressed patients.
- Splenic infarcts can complicate myocardial infarction but usually result in no long-term sequelae.

Suggested Readings

Federle MP, Jeffrey RB, Desser TS, et al. Diagnostic Imaging: Abdomen. Salt Lake City, UT: Amirsys; 2004

Rabushka LS, Kawashima A, Fishman EK. Imaging of the spleen: CT with supplemental MR examination. Radiographics 1994;14(2):307–332

Webb WR, Brant WE, Major NM. Fundamentals of Body CT. 3rd ed. Philadelphia: Elsevier; 2006

Case 50

Shaun Loh

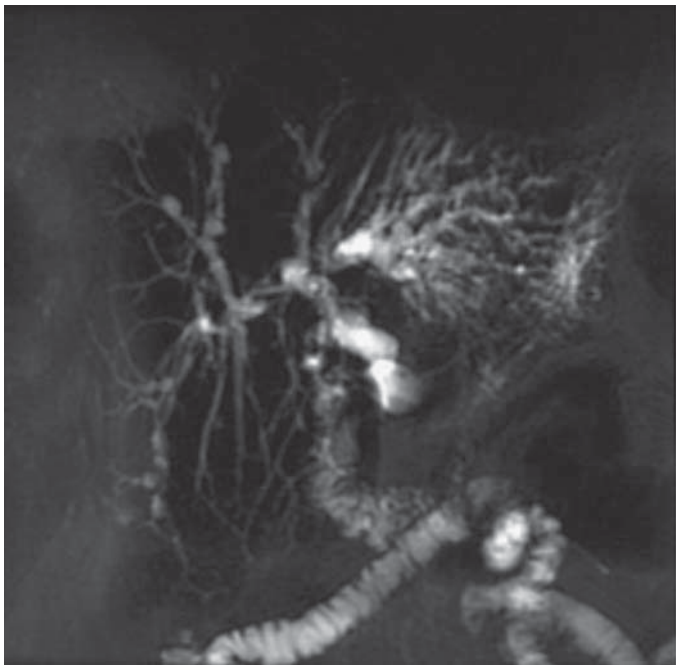


Fig. 50.1 Magnetic resonance cholangiopancreatography demonstrates a classic "string of beads" appearance, with an alternating pattern of dilated and strictured predominantly intrahepatic bile ducts.

Clinical Presentation

A 45-year-old woman presents with jaundice (**Fig. 50.1**).

Key Imaging Finding

Intrahepatic biliary ductal strictures

Top 3 Differential Diagnoses

- **Primary sclerosing cholangitis (PSC).** PSC is a chronic idiopathic inflammatory disease involving the bile ducts, which may progress to biliary ductal destruction, cholestasis, biliary cirrhosis, and cholangiocarcinoma. It is highly associated with ulcerative colitis. Classic findings include a "string of beads" appearance, with an alternating pattern of dilation and stenosis of the intrahepatic (IHBDs) and extrahepatic bile ducts (EHBDs). Diverticular outpouchings of the biliary tree on cholangiography are pathognomonic. Hypertrophy of the caudate lobe occurs in more advanced cases of PSC. Periportal fibrosis may occur and appears on magnetic resonance imaging as areas of decreased periportal signal on T1-weighted images, with increased signal on T2-weighted images.
- **Ascending cholangitis.** Ascending cholangitis is a bacterial infection of an obstructed biliary system. Patients may present with Charcot triad: pain, fever, and jaundice. Choledocholithiasis and strictures from prior surgery may result in biliary obstruction with biliary stasis and infection. The IHBDs and EHBDs are frequently dilated with high-density purulent bile and thickened walls. Left untreated, complications such as liver abscesses, sepsis, and even death may occur.
- **Acquired immunodeficiency syndrome (AIDS) cholangiopathy.** This cholangiopathy results from strictures caused by AIDS-related opportunistic infections, usually cytomegalovirus or *Cryptosporidium*. It is characterized by multiple intrahepatic biliary strictures, distal ampullary stenosis, or cholecystitis. The common bile duct is often involved with irregular areas of thickening and/or ulcerations. T1-weighted images with contrast will demonstrate IHBD and EHBD asymmetric ductal dilatation with pericholecystic inflammatory changes. On magnetic resonance cholangiopancreatography, an alternating pattern of high signal biliary ductal dilatation and intrahepatic and extrahepatic biliary strictures may be present. Prognosis is poor, as the cholangiopathy presents in late-stage AIDS.

Additional Differential Diagnoses

- **Neoplasm.** Neoplasms, such as cholangiocarcinoma and metastases, are another cause of intrahepatic biliary strictures. In cholangiocarcinoma, long strictures and prestenotic ductal dilatation with wall thickening may be the only findings. Malignant strictures may also result from pancreatic and ampullary carcinomas, as well as metastatic disease from colorectal, lung, and breast cancer and lymphoma.
- **Post-transplant arterial ischemia.** Intrahepatic biliary strictures may occur after liver transplantation and are thought to be secondary to hepatic artery occlusion and ischemia. The IHBDs are dilated with narrowed segments. Doppler ultrasound may show signs of hepatic artery occlusion or stenosis (e.g., a tardus/parvus waveform).

Diagnosis

Primary sclerosing cholangitis

✓ Pearls

- PSC is characterized by a "string of beads" appearance of the intrahepatic bile ducts.
- Biliary strictures may be seen as either the cause or the complication of ascending cholangitis.
- Care must be taken to assess for cholangiocarcinoma or metastases in the setting of a focal biliary stricture.
- Hepatic artery occlusion complicating liver transplantation leads to biliary necrosis and strictures.

Suggested Readings

Federle MP, Jeffrey RB, Desser TS, et al. Diagnostic Imaging: Abdomen. Salt Lake City, UT: Amirsys; 2004

Vitellas KM, Keogan MT, Freed KS, et al. Radiologic manifestations of sclerosing cholangitis with emphasis on MR cholangiopancreatography. Radiographics 2000;20(4):959–975, quiz 1108–1109, 1112

Webb WR, Brant WE, Major NM. Fundamentals of Body CT. 3rd ed. Philadelphia: Elsevier; 2006

Section III Genitourinary Imaging

Case 51

Todd M. Johnson

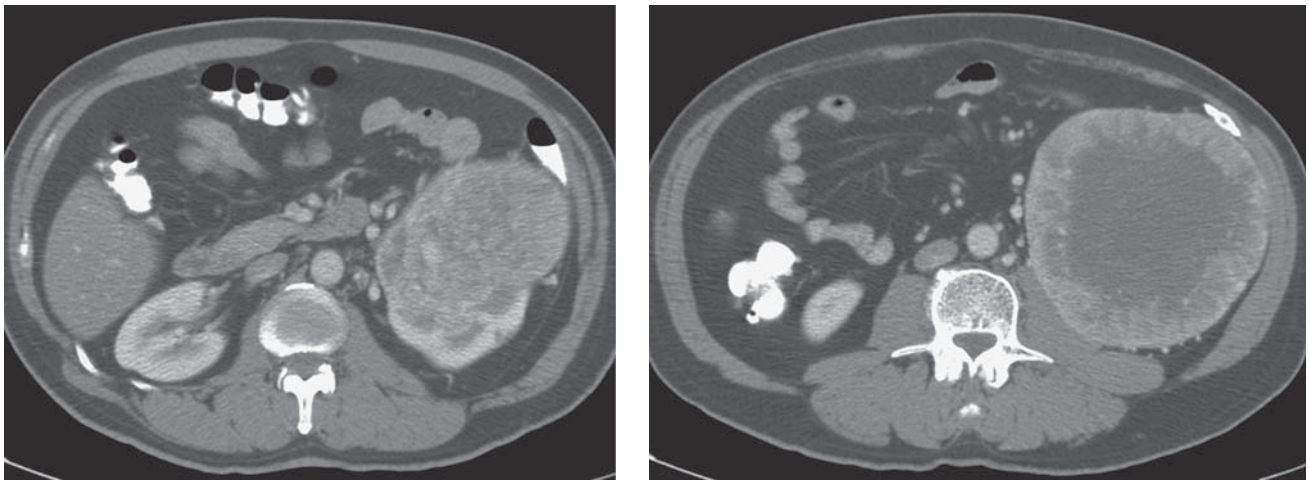


Fig. 51.1 **(A,B)** Contrast-enhanced axial CT images demonstrate a large enhancing mass with central necrosis arising from the lower pole of the left kidney.

Clinical Presentation

An older man presents with hematuria and left flank pain (**Fig. 51.1**).

Key Imaging Finding

Solid renal mass

Top 3 Differential Diagnoses

- **Renal cell carcinoma (RCC).** Renal cell carcinoma is a hypervascular malignant renal neoplasm that arises from tubular epithelium. Although RCC usually presents as a solid, exophytic cortical tumor, it may be cystic. Cystic forms typically have multiple thick septations; enhancing nodules in a cystic lesion are highly suspicious for RCC (Bosniak IV). Infiltrative RCC can invade the renal pelvis, simulating transitional cell carcinoma (TCC). If complicated by necrosis or hemorrhage, central low density may mimic the central scar of oncocytoma.
- **Oncocytoma.** Oncocytoma is a benign renal tumor that accounts for only ~7% of renal neoplasms. It occurs in older patients (7th decade), with a male predominance. On contrast-enhanced computed tomography, typically a large (average 7 cm), circumscribed, solid enhancing lesion is present that can have a central scar. This central scar can mimic the central necrosis seen in RCC. On angiography, oncocytomas demonstrate a spoke-wheel pattern of enhancement correlating to their arterial supply. Definitive differentiation from RCC can only be made by pathologic diagnosis.
- **Angiomyolipoma (AML).** Angiomyolipoma is a benign tumor of the kidney composed of variable amounts of vascular elements, smooth muscle, and adipose tissue. Gross fat and lack of calcifications in a renal lesion are virtually diagnostic of AML. Although there is no malignant potential, lesions composed predominantly of vascular elements and smooth muscle can show significant enhancement and are indistinguishable from RCC by imaging. Usually AML is sporadic and solitary; multiple AMLs are associated with tuberous sclerosis.

Additional Differential Diagnoses

- **Transitional cell carcinoma.** TCC is a uroepithelial neoplasm that usually arises from the bladder; a smaller portion (<10%) originates from the renal pelvis or infundibulocalyceal region. TCC that infiltrates the kidney causes enlargement with preservation of shape. It is relatively hypovascular and ill defined, demonstrating only mild enhancement.
- **Lymphoma.** Renal lymphoma most often presents as multiple bilateral hypodense renal masses; however, it can also present as a solitary hypodense mass that may simulate a cyst on ultrasound or present as diffuse infiltration of the renal parenchyma. The presence of associated lymphadenopathy is helpful in suggesting the diagnosis.

Diagnosis

Renal cell carcinoma

✓ Pearls

- RCCs are hypervascular tumors; smaller lesions are best visualized in the nephrographic phase.
- The central scar of oncocytoma is indistinguishable from central necrosis in RCC.
- AMLs are benign lesions composed of macroscopic fat, vascular elements, and smooth muscle.
- AMLs composed predominantly of vascular and smooth muscle elements can mimic RCC.

Suggested Readings

Federle MP. Diagnostic Imaging: Abdomen. Salt Lake City, UT: Amirsys; 2004

Silverman SG, Mortele KJ, Tuncali K, et al. Hyperattenuating renal masses: etiologies, pathogenesis, and imaging evaluation. Radiographics 2007;27:1131–1143

Zhang J, Lefkowitz RA, Ishill NM, et al. Solid renal cortical tumors: differentiation with CT. Radiology 2007;244:494–504

Case 52

James B. Odone

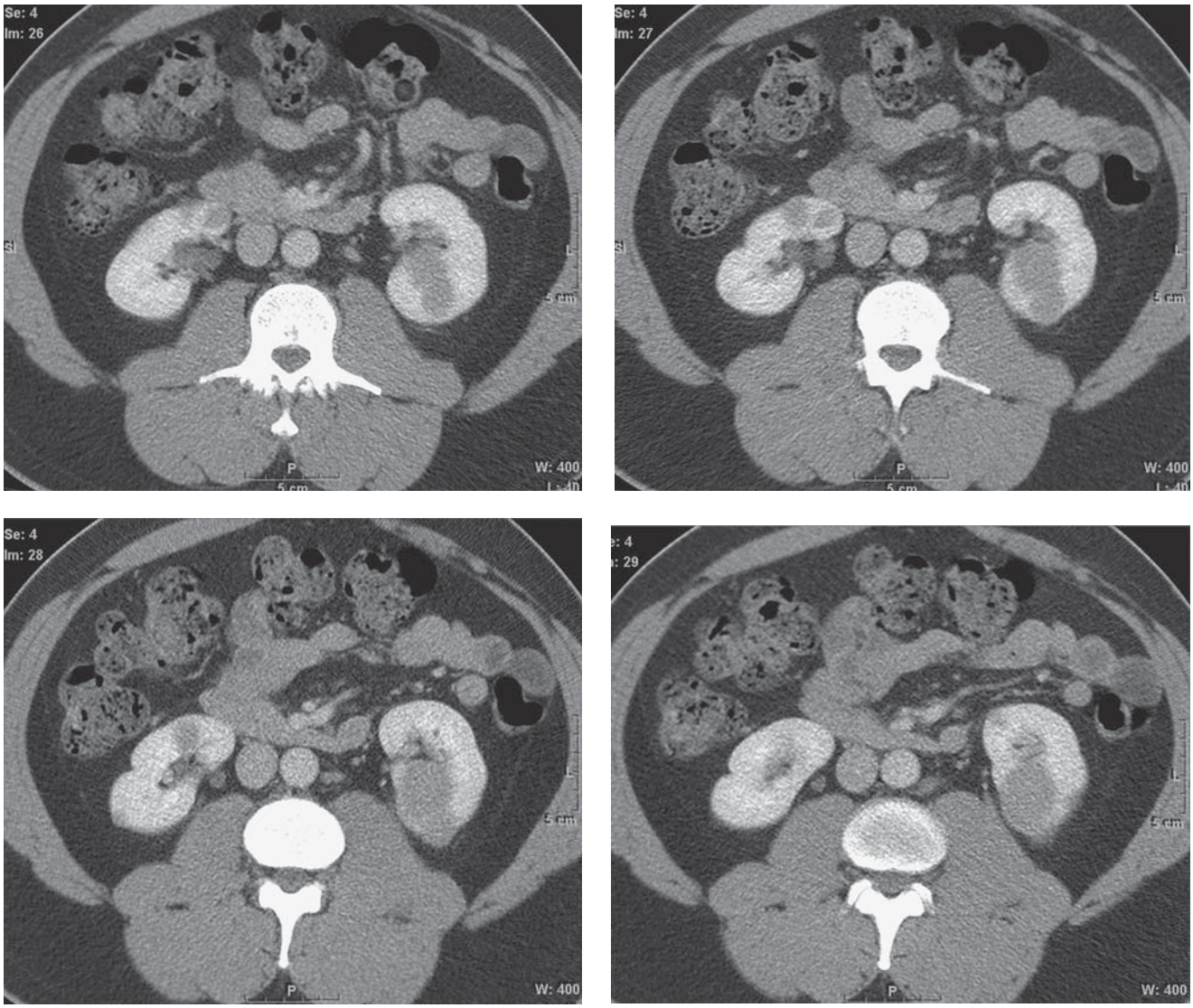


Fig. 52.1 **(A–D)** Sequential contrast-enhanced axial CT images through the kidneys demonstrate multiple hypodense solid renal masses.

Clinical Presentation

A 38-year-old man presents with weight loss and low-grade fever (**Fig. 52.1**).

Key Imaging Finding

Multiple bilateral renal lesions/masses

Top 3 Differential Diagnoses

- **Lymphoma.** Primary renal lymphoma is rare; however, secondary involvement is common in patients with a known history of lymphoma. The most common pattern of renal involvement is that of multiple bilateral homogeneous hypodense parenchymal masses. Accompanying perirenal lymphadenopathy is relatively common and may provide a diagnostic clue on initial imaging. Less common manifestations are a solitary renal mass and diffuse infiltration of the renal parenchyma, which leads to reniform enlargement.
- **Renal infection.** Pyelonephritis is most often a clinical diagnosis, with imaging typically performed to evaluate for complications. Early pyelonephritis may present as a striated nephrogram or focal area of decreased enhancement. Early abscess formation may mimic solid renal masses. The lesions are typically hypodense and cortically based. Perinephric stranding is a common secondary finding. Patients are febrile with leukocytosis on urinalysis. Immunosuppressed patients are at increased risk for multifocal renal involvement, especially in the setting of acquired immunodeficiency syndrome (AIDS) and intravenous drug abuse.
- **Renal cell carcinoma (RCC).** RCC most commonly presents as a solitary hypervascular renal mass; however, multifocal involvement may be seen in a small number of patients, especially those with von Hippel–Lindau (VHL) disease. There is an increased incidence of RCC in patients with acquired cystic renal disease of dialysis, as well as those with VHL disease. The papillary form of RCC may present with hypoenhancing masses. Local spread includes adjacent lymph nodes, as well as direct spread through the ipsilateral renal vein and inferior vena cava.

Additional Differential Diagnoses

- **Angiomyolipomas (AMLs).** AMLs are benign hamartomas composed of vessels, soft tissue, and gross fat. With a few rare exceptions, the presence of fat within a renal lesion is diagnostic of an AML. They are typically solitary and occur in young to middle-aged women; however, multiple lesions may be seen in the setting of tuberous sclerosis. Although usually found incidentally, lesions >4 cm are prone to hemorrhage, necessitating intervention.
- **Metastases.** Other than lymphoma, metastatic disease to the kidneys is uncommon. Neoplasms prone to renal metastases include melanoma, lung cancer, and breast cancer, as well as soft tissue and osseous sarcomas.

Diagnosis

Lymphoma

✓ Pearls

- Renal lymphoma often presents as bilateral hypodense renal masses; accompanying lymphadenopathy is a helpful clue.
- Pyelonephritis has a variety of imaging appearances; perinephric stranding is a common associated finding.
- Multifocal RCC typically is seen in association with syndromes, especially von Hippel–Lindau disease.
- Multiple bilateral AMLs are seen with tuberous sclerosis; larger lesions are prone to hemorrhage.

Suggested Readings

Dunnick NR. Textbook of Uroradiology. 3rd ed. Philadelphia: Lippincott Williams & Wilkins; 2001

Silverman SG, Mortele KJ, Tuncali K, et al. Hyperattenuating renal masses: etiologies, pathogenesis, and imaging evaluation. Radiographics 2007;27:1131–1143

Case 53

James B. Odone

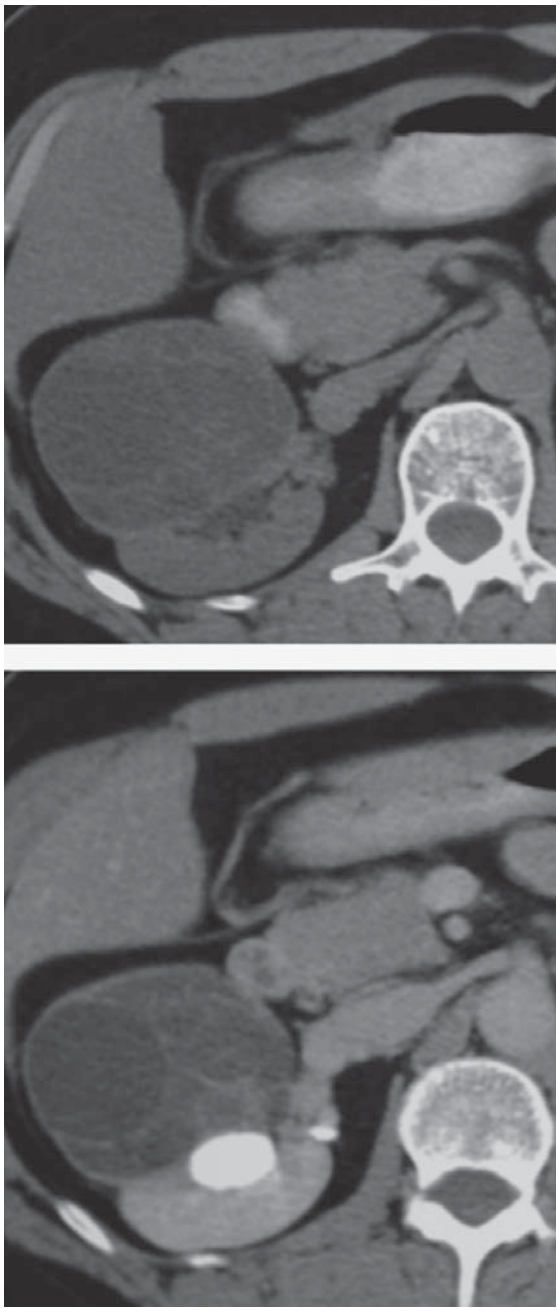


Fig. 53.1 Coned-down axial CT images of the right kidney **(A)** before and **(B)** after intravenous contrast administration demonstrate a complex cystic renal lesion with multiple thickened enhancing septations.

Clinical Presentation

A 49-year-old woman presents with flank pain (**Fig. 53.1**).

Key Imaging Finding

Cystic renal mass

Top 3 Differential Diagnoses

- **Complex renal cysts.** Simple renal cysts demonstrate simple fluid attenuation on computed tomography (CT) and do not contain septations, calcifications, or internal debris. Multiple cysts can be incidental or associated with various syndromes. Complicated or complex cysts are usually the result of hemorrhage or infection, which changes the imaging appearance. Complex cysts may have internal debris, clot, calcification, or septations. The Bosniak classification is used to determine whether these lesions can be managed medically or surgically.
- **Cystic neoplasm.** A malignant cystic neoplasm should be considered if a cystic lesion is expansile and/or exhibits suspicious imaging characteristics, such as wall calcification, thickened septations, or enhancement. In an adult, the most frequently encountered cystic malignancy is renal cell carcinoma (~20% of all RCCs), whereas in a child, Wilms tumor is the most common cystic malignancy. In either case, surgical resection is a necessity. Both RCC and Wilms tumor have a propensity for renal vein invasion and subsequent inferior vena cava propagation, which should be evaluated during presurgical staging.
- **Multilocular cystic nephroma (MLCN).** MLCN is a rare benign neoplasm that arises from the metanephric blastema. It is often difficult, if not impossible, to distinguish MLCN from malignant processes, such as cystic RCC or cystic Wilms tumors. The age distribution is bimodal, with half of the cases seen in young boys in the first decade of life and half arising in middle-aged women. The classic description is that of a complex cystic mass, with enhancing septations, that extends into the renal pelvis. It is typically classified as a Bosniak class III or IV lesion, which necessitates surgical resection. Hemorrhage or calcification is uncommon.

Additional Differential Diagnoses

- **Multicystic dysplastic kidney (MCDK) (focal).** MCDK results from failure of the ureteral bud to induce maturation of the metanephric blastema into nephrons. Most commonly, MCDK affects an entire kidney, which is replaced by a nonfunctioning cystic mass. Over time, the mass involutes and may eventually calcify. In the focal form, a portion of the kidney is dysplastic with a cystic mass, while the remainder of the kidney is relatively normal. On CT, there is a nonenhancing cystic mass with multiple septations.
- **Abscess.** Renal abscesses may present as heterogeneously enhancing cystic parenchymal masses. There is usually associated perinephric fat stranding, although this finding is nonspecific. Patients often have a history of fever, pyuria, and flank pain. Follow-up imaging should be performed to exclude an underlying lesion.

Diagnosis

Multilocular cystic nephroma

✓ Pearls

- Complex renal cysts are classified as surgical or medical lesions based on the Bosniak classification.
- Cystic renal tumors are classically RCC in adults and Wilms tumor in children.
- MLCN has a bimodal age distribution and characteristically herniates into the renal pelvis.

Suggested Readings

Federle MP. Diagnostic Imaging: Abdomen. Salt Lake City, UT: Amirsys; 2004

Hartman DS, Choyke PL, Hartman MS. From the RSNA refresher courses: a practical approach to the cystic renal mass. Radiographics 2004;24(Suppl 1):S101–S115

Case 54

William T. O'Brien Sr.

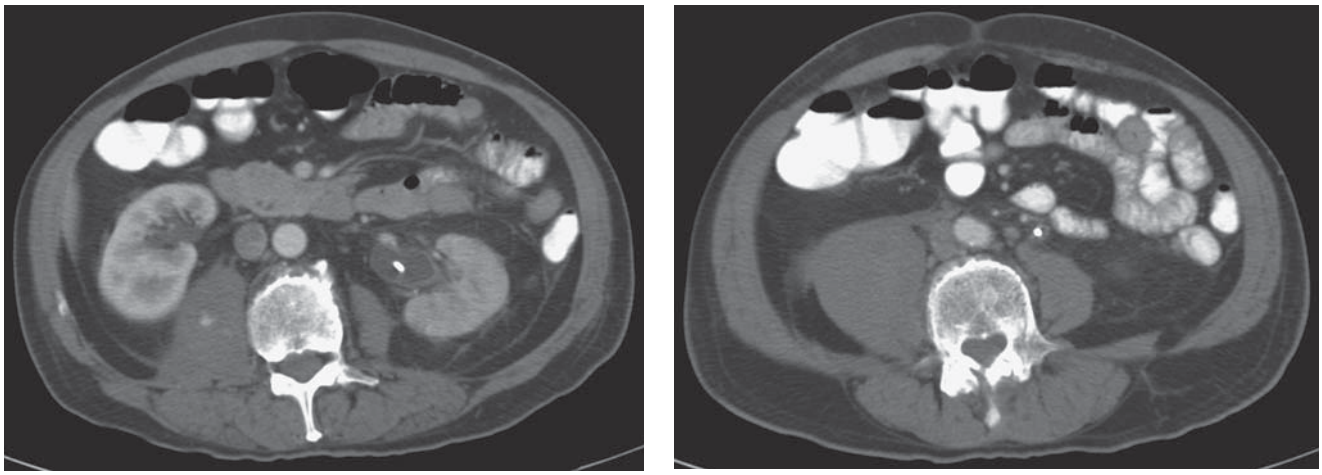


Fig. 54.1 **(A)** Contrast-enhanced axial CT image through the level of the kidneys demonstrates enlargement of the right psoas muscle with a focal region of contrast extravasation, consistent with active hemorrhage. **(B)** An axial image through the lower abdomen reveals inferior extension of the asymmetric right psoas muscle enlargement, as well as surrounding retroperitoneal fat stranding. Incidental note is made of a left nephroureteral stent on both CT images.

Clinical Presentation

A 58-year-old man with a prior left nephroureteral stent presents with new right-sided flank pain (**Fig. 54.1**).

Key Imaging Finding

Retroperitoneal mass

Top 3 Differential Diagnoses

- **Retroperitoneal hemorrhage.** Retroperitoneal hemorrhage may result from a variety of causes, including trauma, coagulopathy, aortic aneurysm rupture, and hemorrhage from an underlying mass. Acute hemorrhage will be mildly hyperdense on unenhanced computed tomography. Contrast is routinely given to evaluate for active extravasation. Traumatic hemorrhage usually involves the aorta or renal vessels, and abdominal aortic aneurysms may rupture spontaneously. Hemorrhage from coagulopathy is typically intramuscular with muscle enlargement, heterogeneous density, and fat stranding. Retroperitoneal neoplasms prone to hemorrhage include renal cell carcinoma (most common), angiomyolipoma, and adrenal neoplasms.
- **Lymphadenopathy.** Retroperitoneal lymphadenopathy is usually the result of lymphoma, but it may also be due to metastatic disease (especially testicular neoplasms) or an infectious process. Non-Hodgkin lymphoma affects the abdomen and retroperitoneum more frequently than Hodgkin lymphoma. Both varieties present as large soft tissue masses that displace the aorta anteriorly from the spine, a useful discriminator from other retroperitoneal processes. Following treatment, lymph nodes may calcify.
- **Retroperitoneal abscess.** Retroperitoneal abscesses result from either hematogenous spread of an occult bacteremia to paraspinal musculature or direct extension from disk osteomyelitis. *Staphylococcus aureus* is the most common organism, followed by *Mycobacterium tuberculosis*. Imaging features consist of rim-enhancing fluid collections with surrounding edema. Magnetic resonance imaging is helpful in evaluating for spinal involvement. Treatment includes percutaneous or surgical drainage of fluid collections, as well as intravenous antibiotics.

Additional Differential Diagnoses

- **Retroperitoneal fibrosis.** Retroperitoneal fibrosis is a rare disorder that is most commonly idiopathic but may be secondary to drugs or processes that result in a desmoplastic response. On imaging, retroperitoneal fibrosis demonstrates a soft tissue mass around retroperitoneal structures with medial displacement of the ureters. The process may extend superiorly into the mediastinum. Ureter or vascular compression is common. Associated conditions include primary sclerosing cholangitis, orbital pseudotumor, and thyroiditis.
- **Retroperitoneal sarcoma.** Retroperitoneal sarcomas are classified by tissue type, with liposarcoma being the most common. They are malignant neoplasms that are often large (>10 cm) at the time of presentation. On imaging, retroperitoneal liposarcomas are composed of fat, soft tissue, and occasionally calcification. Soft tissue components demonstrate mild enhancement. When large, retroperitoneal sarcomas displace bowel and the renal collecting system, and they are prone to hemorrhage.

Diagnosis

Retroperitoneal hemorrhage (intramuscular hematoma with active extravasation)

✓ Pearls

- Retroperitoneal hemorrhage and abscesses commonly present with paraspinal muscle involvement.
- Non-Hodgkin lymphoma is the most common cause of retroperitoneal lymphadenopathy.
- Retroperitoneal fibrosis presents as a soft tissue mass with medial displacement of the ureters.
- Liposarcoma is the most common retroperitoneal sarcoma; it is prone to hemorrhage.

Suggested Readings

Federle MP. Diagnostic Imaging: Abdomen. Salt Lake City, UT: Amirsys; 2004

Nishino M, Hayakawa K, Minami M, et al. Primary retroperitoneal neoplasms: CT and MR imaging findings with anatomic and pathologic diagnostic clues. Radiographics 2003;23:45–57

Case 55

Paul B. DiDomenico



Fig. 55.1 Unenhanced axial CT image through the kidneys demonstrates dense calcification of the entire renal cortex bilaterally.

Clinical Presentation

A patient presents with renal insufficiency and a history of bowel surgery (**Fig. 55.1**).

Key Imaging Finding

Cortical nephrocalcinosis

Top 3 Differential Diagnoses

- **Acute renal cortical necrosis.** Acute cortical necrosis is the most common cause of cortical nephrocalcinosis and may result from severe acute hypotension (due to shock, sepsis, or hemorrhage). Nephrotoxic drugs such as amphotericin B or ingested toxins such as ethylene glycol can also damage the cortex, resulting in cortical nephrocalcinosis.
- **Chronic glomerulonephritis.** Chronic glomerulonephritis is the second most common cause of cortical nephrocalcinosis. The pathophysiology is chronic inflammatory destruction of glomeruli within the renal cortex with resultant dystrophic calcification. There will often be marked renal atrophy with a smooth renal contour. Biopsy is required to determine the underlying cause, such as diabetic nephropathy, lupus nephritis, or membranous glomerulonephritis.
- **Oxalosis.** Hyperoxaluria can occur in both primary and secondary forms. The primary (inherited autosomal recessive) form is rare and usually fatal early in life. The secondary (enteric) form is more common and is related to altered bile acid metabolism from resection or chronic disease of the small bowel, as in Crohn disease. The resulting increased urinary secretion of oxalates may cause calcium oxalate renal stones, medullary nephrocalcinosis, or, less commonly, cortical nephrocalcinosis.

Additional Differential Diagnoses

- **Chronic transplant rejection.** A patient with a renal transplant may have some degree of chronic rejection, causing cortical necrosis and dystrophic calcification. This diagnosis would be supported by the presence of a kidney in the right lower quadrant, the most common location for a transplant.
- **Alport syndrome.** Alport syndrome is a rare syndrome of hereditary nerve deafness and nephritis. There are case reports of cortical nephrocalcinosis from the associated chronic renal disease.

Diagnosis

Oxalosis

✓ Pearls

- Acute cortical necrosis may be caused by severe acute hypotension or drug toxicity.
- Chronic glomerulonephritis may result in smooth renal atrophy and cortical nephrocalcinosis.
- Oxalosis (primary or more commonly secondary) may result in cortical or medullary nephrocalcinosis.
- Chronic transplant rejection may result in cortical nephrocalcinosis; look for a transplant kidney in the right lower quadrant.

Suggested Readings

Dunnick NR. Textbook of Uroradiology. 3rd ed. Philadelphia: Lippincott Williams & Wilkins; 2001

Dyer RB, Chen MY, Zagoria RJ. Abnormal calcifications in the urinary tract. Radiographics 1998;18:1405–1424

Case 56

William T. O'Brien Sr.

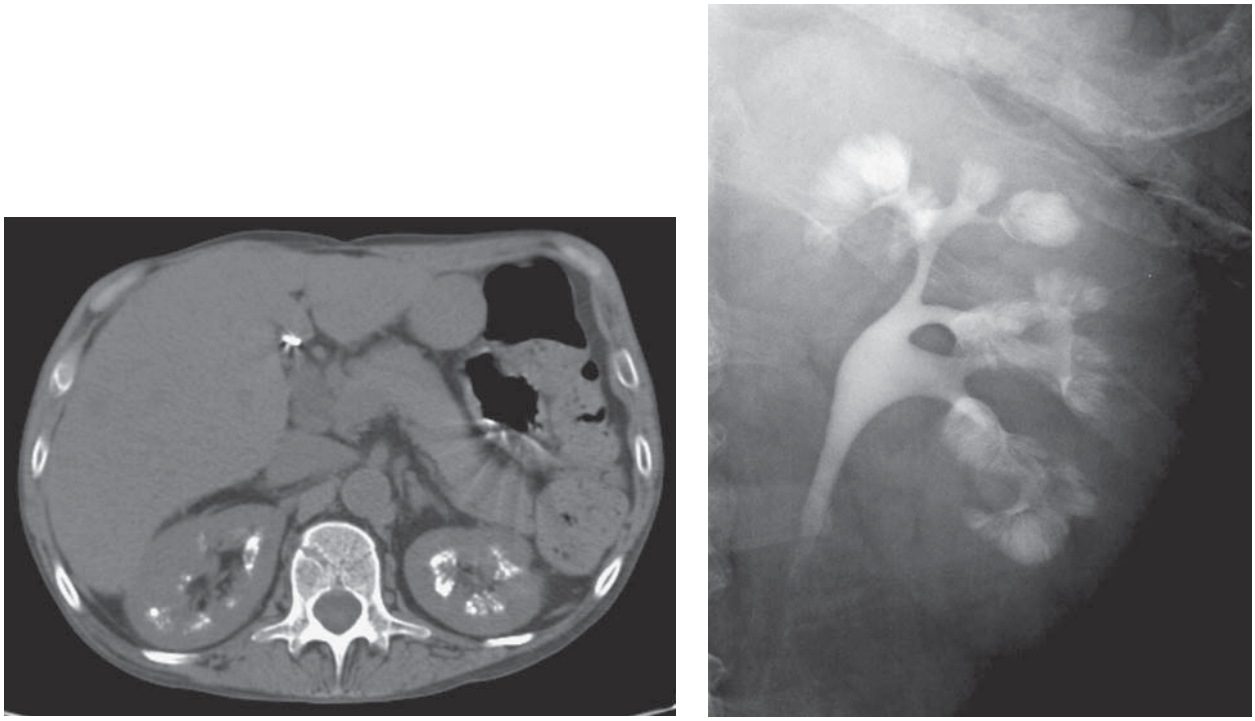


Fig. 56.1 **(A)** Unenhanced axial CT image through the kidneys demonstrates symmetric bilateral medullary calcifications. **(B)** Frontal coned-down view of the left kidney from an intravenous pyelogram reveals contrast within the collecting and the striated "paintbrush" appearance of the medullary pyramids.

Clinical Presentation

A 38-year-old man presents with mild renal insufficiency (**Fig. 56.1**).

Key Imaging Finding

Medullary nephrocalcinosis

Top 3 Differential Diagnoses

- **Hypercalcemia.** Hypercalcemia from a variety of etiologies, including hyperparathyroidism, paraneoplastic syndromes, and sarcoidosis, is a common cause of bilateral symmetric medullary nephrocalcinosis. The abundance of serum calcium that must be filtered by the kidneys results in precipitation of calcium deposits within the renal pyramids. Chronic hypercalcemia results in chronic renal failure, so the kidneys are usually smaller in size. Imaging studies demonstrate bilateral symmetric calcifications within the renal pyramids.
- **Medullary sponge kidney (MSK).** MSK is a common cause of medullary nephrocalcinosis. The disorder is characterized by idiopathic ectasia of the renal tubules, resulting in urinary stasis and stone formation. Most cases are noted incidentally, but patients may suffer from recurrent urolithiasis or pyelonephritis. MSK is usually bilateral and segmental with sparing of a portion of the renal pyramids. On plain radiographs or computed tomography, macroscopic chunky calcifications will be noted along the renal pyramids. Classic findings on intravenous pyelogram (IVP) include the "growing calculus" sign secondary to contrast filling the dilated tubules around the stones, and the striated, "paintbrush" appearance of the renal pyramids. Although usually an isolated finding, MSK may be associated with hemihypertrophy syndromes.
- **Renal tubular acidosis.** Type 1 or distal renal tubular acidosis (RTA) results in both medullary nephrocalcinosis and urolithiasis secondary to hypercalciuria. In this disorder, there is a citrate deficiency that results in an inability to adequately acidify the urine at the distal tubule. The body responds by releasing a large amount of calcium into the urine, causing hypercalciuria. Over a period of time chronic renal insufficiency ensues; therefore, the kidneys may be symmetrically decreased in size.

Additional Differential Diagnoses

- **Papillary necrosis.** Papillary necrosis may rarely result in medullary nephrocalcinosis, most commonly when associated with analgesic nephropathy from overuse of nonsteroidal antiinflammatory drugs. Analgesic nephropathy also causes chronic renal insufficiency, so the kidneys are typically small with irregular margins. Radiographic findings include those associated with papillary necrosis, such as ureteral filling defects and the "lobster claw" and "ball on a tee" configuration of the renal pyramids on IVP, as well as findings associated with medullary sponge kidney (calcifications along the renal pyramids).
- **Furosemide.** Chronic use of diuretics, specifically furosemide, in newborns may result in medullary nephrocalcinosis that appears radiographically as calcifications in the region of the renal pyramids. The radiographic findings often resolve over a period of time once the medication is discontinued.
- **Tuberculosis.** Renal tuberculosis may rarely result in medullary nephrocalcinosis. Unlike other causes of nephrocalcinosis, tuberculosis is usually focal and unilateral at sites of previous pyelonephritis. Inflammation of the urothelium results in infundibular stenosis, urinary stasis, and scarring of the overlying parenchyma. Bilateral involvement is unusual.

Diagnosis

Medullary sponge kidney

✓ Pearls

- Adult medullary nephrocalcinosis results from hypercalcemia, medullary sponge kidney, or RTA type 1.
- In medullary sponge kidney, the renal pyramids classically have a "paintbrush" appearance on IVP.
- Chronic furosemide therapy in newborns may result in medullary nephrocalcinosis.

Suggested Readings

Zagoria RJ. Genitourinary Radiology: The Requisites. 2nd ed. Philadelphia: Mosby; 2004

Case 57

Chirag V. Patel

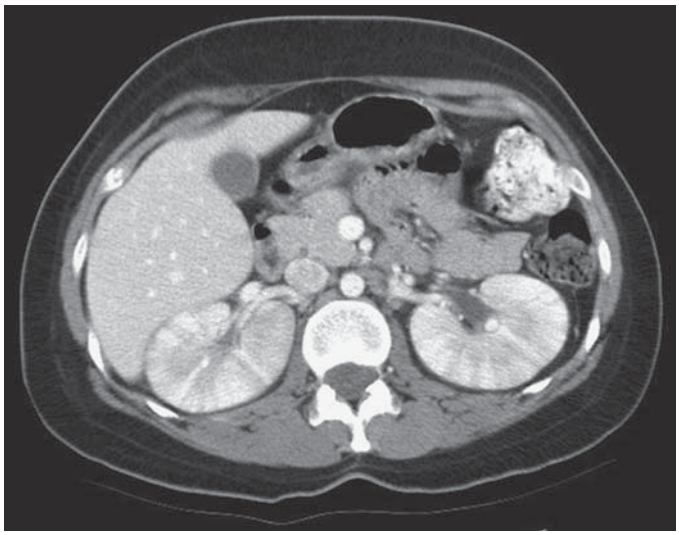


Fig. 57.1 Contrast-enhanced axial CT image demonstrates a bilateral striated nephrogram and mild diffuse renal enlargement.

Clinical Presentation

A 41-year-old man presents with urosepsis (**Fig. 57.1**).

Key Imaging Finding

Striated nephrogram

Top 3 Differential Diagnoses

- **Pyelonephritis.** Acute pyelonephritis results from bacterial invasion of the renal parenchyma. Most cases are diagnosed by typical clinical presentation and laboratory studies. Imaging is warranted in cases of atypical presentations and in the setting of worsening or refractory symptoms despite adequate medical therapy to evaluate for obstruction or abscess formation. Computed tomography (CT) is the imaging modality of choice and may reveal a striated nephrogram, with multiple linear or wedge-shaped regions of hypoperfusion. The focal areas of low attenuation result from edema and microvascular occlusion. Although commonly unilateral, a bilateral striated nephrogram may be seen in the setting of pyelonephritis if both kidneys are involved.
- **Urinary obstruction.** Acute urinary obstruction is most commonly due to ureteral calculi. Patients present with colicky abdominal pain, dysuria, and hematuria. Ultrasound or unenhanced CT is the preferred imaging modality. Contrast-enhanced CT (CT urogram) can be used in cases of obstruction demonstrated on noncontrast studies without an identifiable radiopaque calculus within the ureter and may be helpful in identifying neoplastic causes of ureteral or renal obstruction. The classic finding in acute urinary obstruction is delayed onset of a progressively dense nephrogram, which may be associated with hydronephrosis, hydroureter, and diffuse enlargement of the affected kidney. A striated nephrogram may occasionally be encountered.
- **Renal vein thrombosis (RVT).** The most common cause of RVT is nephrotic syndrome; in children, dehydration and sepsis are common etiologies. Other less common causes are renal neoplasms, trauma, and other acquired or inheritable hypercoagulable states. Imaging studies will show diffuse enlargement of the affected kidney with thrombus in the renal vein and possibly extension into the inferior vena cava. Common features on CT include prolonged corticomedullary differentiation, delayed or prolonged parenchymal opacification, and delayed or absent pyelocalyceal visualization. Occasionally a striated nephrogram is encountered.

Additional Differential Diagnoses

- **Renal contusion.** Interstitial edema resulting from renal contusion can produce a focal striated appearance in the nephrographic phase. The imaging appearance can mimic other etiologies of a striated nephrogram, especially focal pyelonephritis. A history of trauma or appreciation of injuries to adjacent organs can aid in establishing the correct diagnosis.
- **Hypotension.** Hypotension and subsequent hypoperfusion of the kidneys (as well as other organs) can be seen in the setting of trauma, aortic dissection, placental abruption, and other etiologies of shock. The most common imaging finding is bilateral persistent nephrograms. A striated nephrogram is a less frequent manifestation of hypotension.

Diagnosis

Bilateral acute pyelonephritis

✓ Pearls

- Pyelonephritis, urinary obstruction, RVT, and contusions usually result in unilateral striated nephrograms.
- Although pyelonephritis may demonstrate a striated nephrogram on contrast-enhanced CT, the diagnosis is a clinical one.
- Urinary obstruction may present as a persistent or a striated nephrogram.
- RVT most often results from nephritic syndrome; trauma and hypercoagulable states are less common.

Suggested Readings

Federle MP. Diagnostic Imaging: Abdomen. Salt Lake City, UT: Amirsys; 2004

Zagoria RJ. Genitourinary Radiology: The Requisites. 2nd ed. Philadelphia: Mosby; 2004

Case 58

Charles A. Tujo

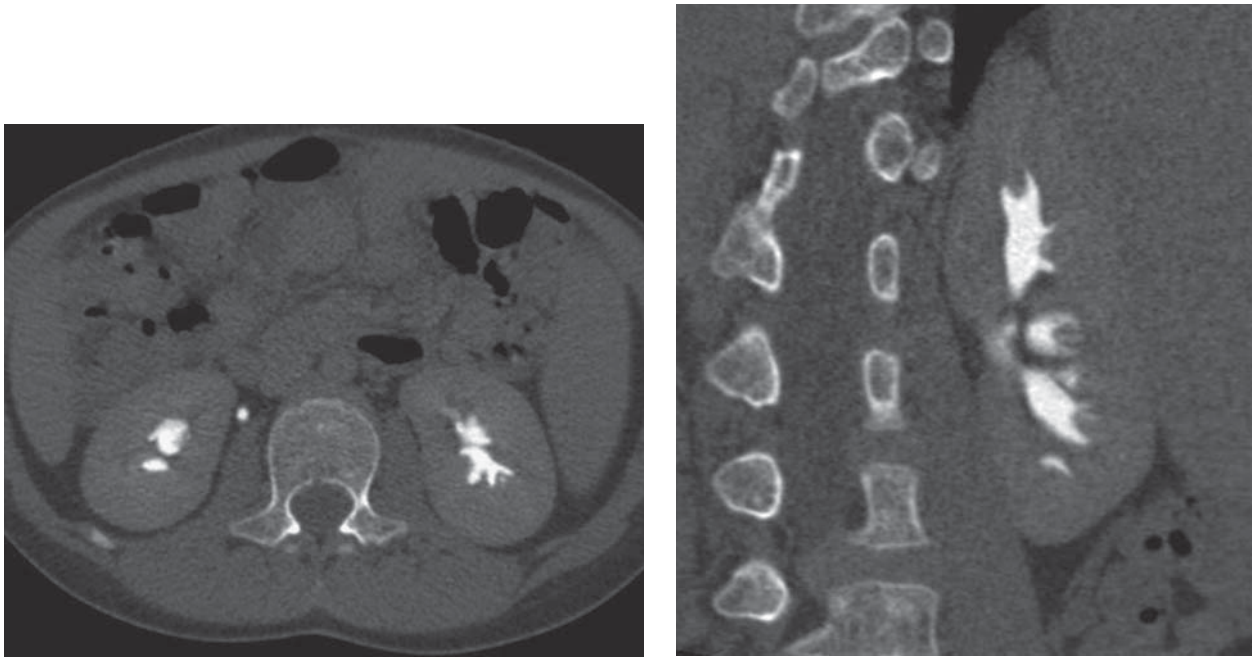


Fig. 58.1 **(A)** Axial and **(B)** reformatted coned-down coronal delayed images from a contrast-enhanced CT image of the abdomen demonstrate abnormal collections of contrast within the renal papillae, consistent with papillary necrosis. (Courtesy of Children's Hospital and Research Center, Oakland, California.)

Clinical Presentation

An 8-year-old boy presents with chronic renal insufficiency (**Fig. 58.1**).

Key Imaging Finding

Papillary necrosis

Top 3 Differential Diagnoses

- **Diabetes.** Diabetes is the most common cause of papillary necrosis. It is often associated with urinary tract infection and renal insufficiency or impairment. Diabetes results in small vessel ischemic disease, which affects the renal papillae. Papillary necrosis presents as abnormal contrast patterns involving the renal pyramids, including the "lobster claw" and "ball on tee" appearances. Ureteral filling defects may be seen with sloughed papillae. The findings are usually bilateral and may be asymmetric.
- **Analgesic nephropathy.** Caused by excessive intake of analgesics, analgesic nephropathy occurs most commonly in middle-aged women. The analgesics reach high concentrations in the renal medulla and lead to necrosis of the renal papillae. Findings are usually bilateral and may be asymmetric.
- **Pyelonephritis.** Renal infection, especially tuberculosis (TB), can result in papillary necrosis. The exact mechanism is difficult to determine, as associated diabetes and/or obstruction may contribute to the development of pyelonephritis. The most common organism to cause pyelonephritis is *Escherichia coli*; however, *E. coli* infrequently causes papillary necrosis. Infection with TB leads to vasculitis and ultimately vascular insufficiency, which results in papillary necrosis. Findings are typically unilateral.

Additional Differential Diagnoses

- **Sickle cell anemia.** The deformation of red blood cells that sludge through small arteries results in medullary ischemia and ultimately papillary necrosis. This process is exacerbated by the hypertonic and hypoxic environment of the renal medulla. Findings are usually bilateral and may be asymmetric.
- **Urinary obstruction.** Obstruction of the urinary tract leads to increased pressure in the renal papillae and decreased perfusion, which ultimately results in papillary necrosis. Depending on the etiology of the obstruction, the process may be unilateral or bilateral. Treatment is focused on relieving the source of obstruction.
- **Renal vein thrombosis (RVT).** RVT is typically the result of a hypercoagulable state, especially in the setting of nephritic syndrome. Venous obstruction leads to renal edema and resultant ischemia. Eventually, papillary necrosis may occur. Treatment is focused on preserving renal perfusion using thrombolysis and treatment of the underlying disorder. Findings are typically unilateral.

Diagnosis

Pyelonephritis (TB)

✓ Pearls

- Diabetes is the most common cause of papillary necrosis and is typically bilateral.
- Analgesic nephropathy occurs most often in middle-aged women; findings are usually bilateral.
- Pyelonephritis, especially TB, can result in papillary necrosis; findings are most commonly unilateral.
- Sickle cell anemia results in medullary ischemia with resultant papillary necrosis; it is typically bilateral.

Suggested Readings

Dunnick NR. Textbook of Uroradiology. 3rd ed. Philadelphia: Lippincott Williams & Wilkins; 2001

Jung DC, Kim SH, Jung SI, et al. Renal papillary necrosis: review and comparison of findings at multi-detector row CT and intravenous urography. Radiographics 2006;26:1827–1836

Sheth S, Fishman EK. Multidetector row CT of the kidneys and urinary tract: techniques and applications of the benign diseases. Radiographics 2004;24:E20

Case 59

Michael C. Kuo

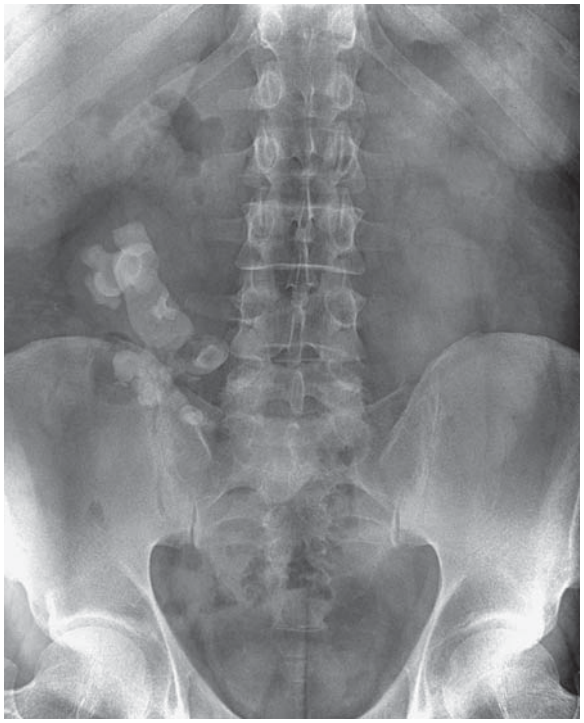


Fig. 59.1 Frontal view of the abdomen demonstrates a large branching calculus within the right renal pelvis. Both renal silhouettes are inferiorly located with lower poles oriented medially, consistent with a horseshoe kidney.

Clinical Presentation

A 45-year-old man with history of urolithiasis and renal insufficiency presents with increasing vague back pain (**Fig. 59.1**).

Key Imaging Finding

Staghorn calculus

Top 3 Differential Diagnoses

- **Xanthogranulomatous pyelonephritis (XGP).** XGP is a chronic renal infection characterized by parenchymal destruction and replacement by lipid-laden macrophages. It most commonly occurs in older women. The most common offending organisms are *Escherichia coli* and *Proteus mirabilis*. The entity presents with a centrally obstructing calculus in the majority of patients. The affected kidney is usually nonfunctional. Perirenal fibrofatty proliferation, poor excretion of contrast, and perinephric extension are secondary findings that suggest the diagnosis of XGP, which is best seen on computed tomography. Treatment usually requires nephrectomy.
- **Pyonephrosis with obstructing stone.** Patients with a large obstructing calculus and pyonephrosis are acutely ill with flank pain and fever. The dilated collecting system is filled with purulent material. This is best seen with ultrasound with mobile debris and layering of low-amplitude echoes in a hydronephrotic kidney. The most common organism is *E. coli.* Complications include abscess formation and progression to septic shock. Urgent percutaneous decompression of the infected collecting system is necessary, as this entity has a 25 to 50% mortality rate.
- **Calcified neoplasm.** Transitional cell carcinoma (TCC) and renal cell carcinoma (RCC) are far less common causes of calcified renal lesions. Only ~2% of TCCs calcify, whereas up to 10% of RCCs may contain calcifications. RCC presents as an intraparenchymal mass; TCC presents within the collecting system/renal pelvis. Calcifications are most commonly amorphous but may also appear in a curvilinear, dense, or diffuse pattern. An associated prominent soft tissue or cystic mass is commonly identified on cross-sectional imaging.

Diagnosis

XGP in a horseshoe kidney

✓ Pearls

- XGP presents with a staghorn calculus in most cases (>90%), along with a large nonfunctioning kidney.
- An obstructed urinary collecting system with secondary infection is a urologic emergency.
- TCC and RCC may present with calcifications that are typically amorphous.

Suggested Readings

Ahuja AT. Diagnostic Imaging: Ultrasound. Salt Lake City, UT: Amirsys; 2007

Federle MP. Diagnostic Imaging: Abdomen. Salt Lake City, UT: Amirsys; 2004

Case 60

Todd M. Johnson

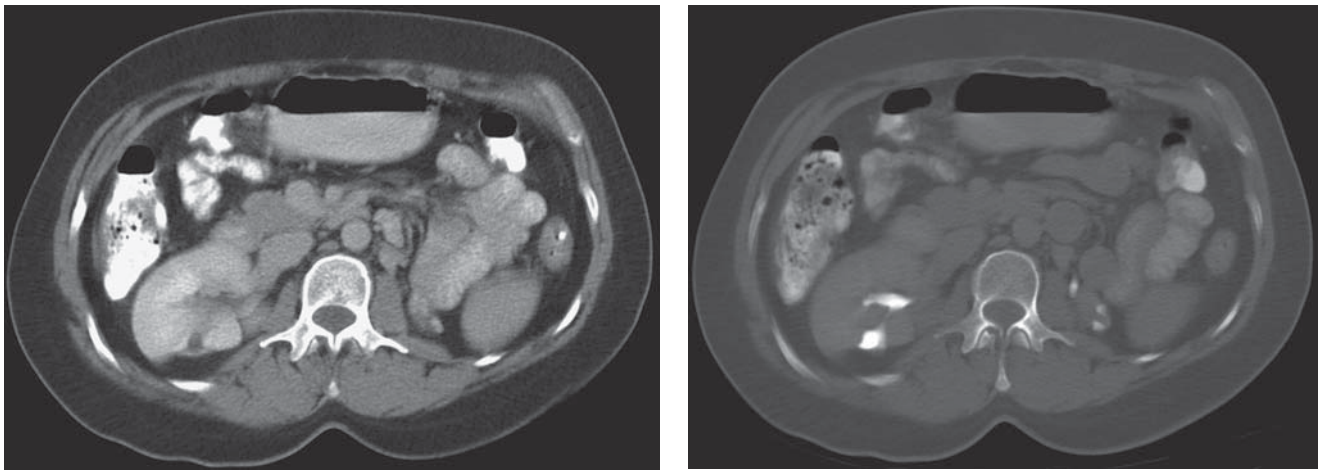


Fig. 60.1 Axial contrast-enhanced CT images **(A)** in the nephrographic phase and **(B)** in the delayed collecting system phase demonstrate focal right upper pole cortical thinning with underlying caliectasis, as well as a small left kidney.

Clinical Presentation

A 32-year-old woman presents with a history of pyelonephritis (**Fig. 60.1**).

Key Imaging Finding

Renal cortical defect

Top 3 Differential Diagnoses

- **Reflux nephropathy.** Although sterile reflux can result in renal scarring, scarring is usually secondary to underlying infection, with *Escherichia coli* representing the most common organism. Up to half of all patients with reflux nephropathy will have evidence of renal scarring; patients with more severe reflux have a higher prevalence of developing renal scarring. Scarring tends to favor the upper and lower renal poles. Calyceal dilatation and distortion can be seen underlying the renal scar.
- **Chronic pyelonephritis.** Pyelonephritis most commonly occurs in adult women. Patients typically present with fever, urinary urgency and frequency, and flank pain. Chronic pyelonephritis occurs more frequently in diabetic patients and results in cortical scarring with underlying dilated calices. *E. coli* is the most common organism. Renal size is decreased, which may mimic chronic global renal infarction. The contralateral kidney may demonstrate compensatory hypertrophy.
- **Renal infarct.** Renal infarction may be global or focal. With global infarction, there is decreased renal size and usually compensatory hypertrophy of the contralateral kidney. Embolic infarction typically results in multiple bilateral defects. Thrombotic or traumatic infarction is usually unilateral with a segmental or subsegmental defect. In the acute setting, a wedge-shaped region of nonenhancing renal parenchyma is seen. The cortical rim sign, in the subacute phase, can be seen in up to 50% of patients due to intact collateral circulation, which results from preserved capsular or subcapsular perfusion.

Additional Differential Diagnoses

- **Vasculitis.** Vasculitis results in multiple bilateral wedge-shaped regions of decreased perfusion. Parenchymal scarring with capsular retraction may occur, in addition to microaneurysm formation. Etiologies include polyarteritis nodosa, lupus, and drug abuse.
- **Partial nephrectomy.** Nephron-sparing surgery for renal cell carcinoma can be performed to preserve renal function in select patients with limited disease or in those for which complete nephrectomy would be contraindicated. Appropriate clinical history or secondary postoperative findings would be helpful to establish this diagnosis.

Diagnosis

Chronic pyelonephritis

✓ Pearls

- Reflux nephropathy scarring favors the upper and lower renal poles.
- Chronic pyelonephritis and renal infarction can both result in decreased renal size.
- Renal infarct may demonstrate the cortical rim sign due to preserved capsular perfusion.

Suggested Readings

Federle MP. Diagnostic Imaging: Abdomen. Salt Lake City, UT: Amirsys; 2004

Kawashima A, Sandler CM, Corl FM, et al. Imaging of renal trauma: a comprehensive review. Radiographics 2001;21:557–574

Case 61

Michael C. Kuo

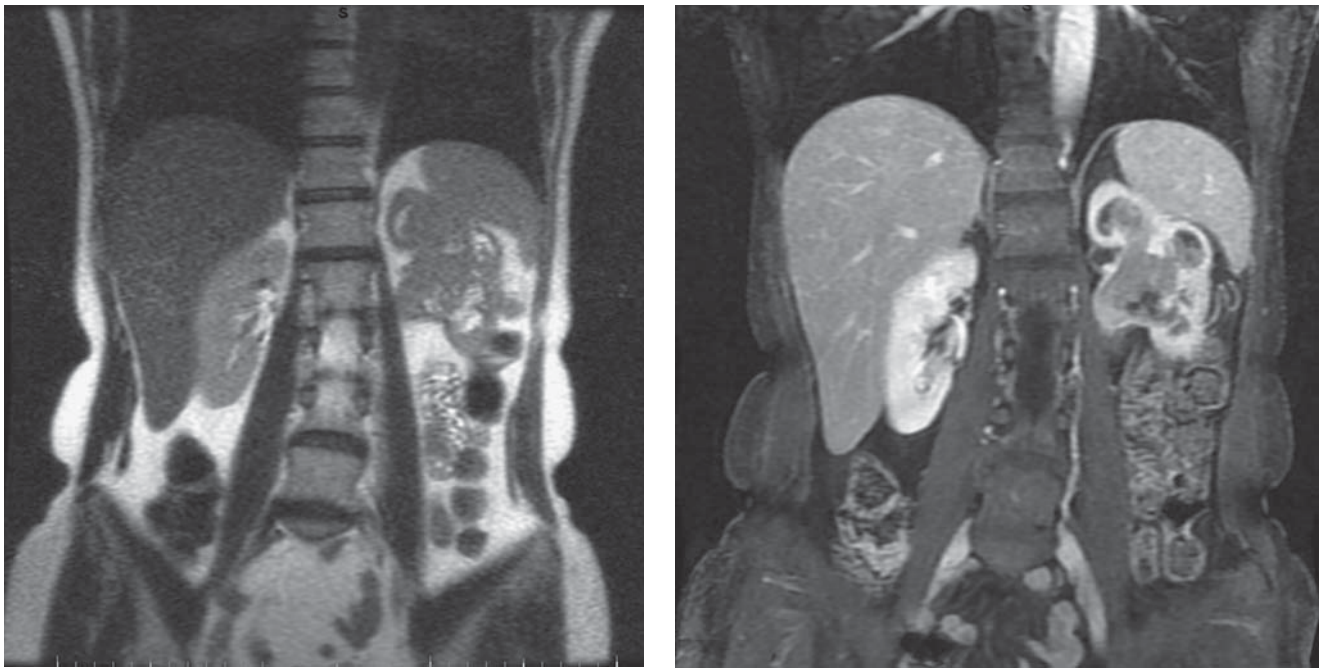


Fig. 61.1 **(A)** T2-weighted coronal magnetic resonance (MR) image shows a hypointense left renal pelvic mass with associated caliectasis. **(B)** Coronal T1-weighted delayed postcontrast MR image shows an enhancing (precontrast T1-weighted image not shown) soft tissue mass within the left renal pelvis that extends into the proximal ureter and calices. (Courtesy of John P. McGahan, MD, University of California, Davis, School of Medicine.)

Clinical Presentation

A 55-year-old woman presents with hematuria (**Fig. 61.1**).

Key Imaging Finding

Renal pelvic mass

Top 3 Differential Diagnoses

- **Transitional cell carcinoma (TCC).** TCC makes up 90% of renal pelvic uroepithelial cancers. It most commonly occurs within the bladder (90%), followed by the renal pelvis and proximal ureter. Single or multiple soft tissue filling defects can be seen with stippled, serrated, or frondlike surface irregularities. Once a mass is seen within the urinary collecting system, the remainder of the urothelium must be examined to evaluate for synchronous disease. When located within the ureter, the classic sign on intravenous pyelogram is the goblet sign, a cup-shaped contrast collection distal to an intraluminal filling defect of the ureter. TCC within the renal pelvis may obstruct the infundibulum, resulting in the "amputated calyx" sign. Treatment of renal and ureteral TCC includes total nephroureterectomy and bladder cuff excision.
- **Multilocular cystic nephroma (MLCN).** MLCN is a benign renal neoplasm originating from the metanephric blastema. It appears as a multilocular cystic mass that characteristically herniates into the renal pelvis. The cystic mass exhibits a capsule with thin internal septa, both of which may enhance. MLCN occurs most commonly in boys younger than 5 years of age and older women in their 5th and 6th decades. Surgical excision is the standard treatment, as MLCN is characterized as a Bosniak class III or IV complex cystic mass and is difficult to distinguish from multilocular cystic renal cell carcinoma (RCC).
- **Medullary carcinoma.** Renal medullary carcinoma is a rare renal tumor arising in the calyceal transitional epithelium. This highly aggressive tumor is seen in young African American patients with sickle cell trait. The mass is centrally located and infiltrative, while preserving the renal shape. The prognosis is very poor, with a mean survival rate of 15 weeks. If there is no metastasis, nephrectomy is the treatment.

Additional Differential Diagnoses

- **Renal cell carcinoma.** RCC is a malignant tumor arising from the tubular epithelium. RCCs are usually hypervascular solid cortical renal masses; however, they can occasionally be cystic masses that have enhancing septa, calcification of septa, or tumor capsule. Rarely, they may involve the renal pelvis, especially when large. Papillary RCC, which makes up to 10 to 15% of RCCs, is hypovascular and can easily be mistaken for a cyst on all imaging modalities. Evaluation requires particular attention for renal vein and inferior vena cava tumor extension. Radical nephrectomy is the standard treatment.

Diagnosis

Transitional cell carcinoma

✓ Pearls

- Upper tract TCC has a high association (up to 40%) with the development of bladder TCC.
- TCC most commonly affects the urinary bladder, followed by the renal pelvis and ureter.
- MLCN has a bimodal age distribution and classically herniates into the renal pelvis.
- Medullary carcinoma arises from the collecting system epithelium in patients with sickle cell trait.

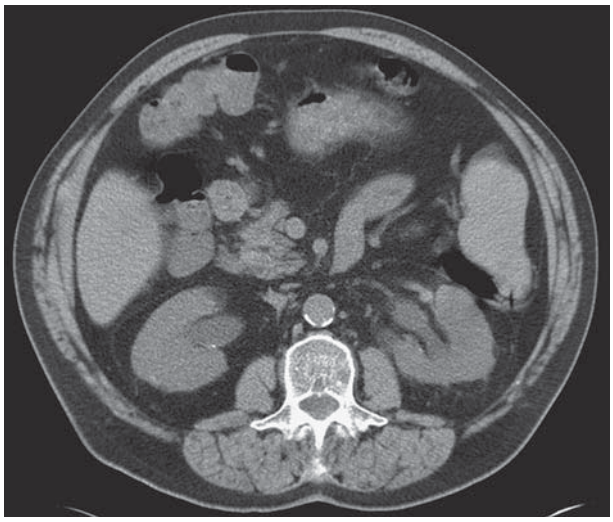
Suggested Readings

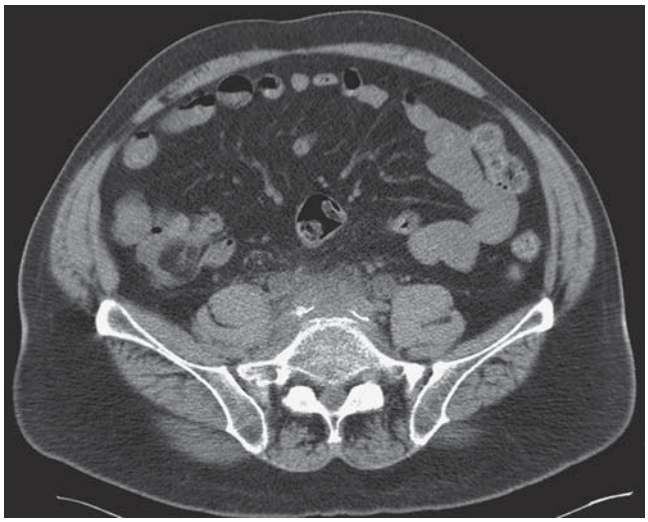
Federle MP. Diagnostic Imaging: Abdomen. Salt Lake City, UT: Amirsys; 2004

Wong-You-Cheong JJ, Wagner BJ, Davis CJ Jr. Transitional cell carcinoma of the urinary tract: radiologic-pathologic correlation. Radiographics 1998;18:123–142

Case 62

Todd M. Johnson





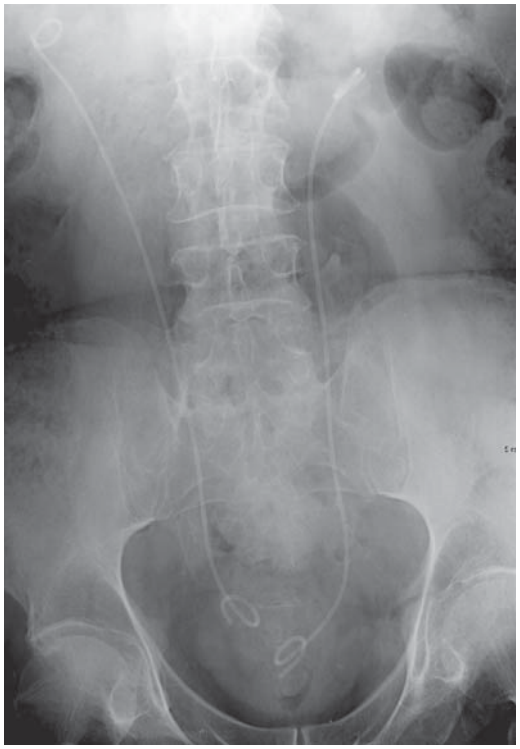


Fig. 62.1 Unenhanced axial CT images through the level of **(A)** the kidneys and **(B)** the pelvis demonstrate dilatation of the proximal renal collecting system to the level of the sacral promontory, where the ureters and common iliac vessels are surrounded by soft tissue density. The ureters are deviated medially. **(C)** Kidney, ureter, and bladder radiographic study following placement of bilateral ureteral stents shows medial deviation of the ureters most pronounced over the pelvis.

Clinical Presentation

A 55-year-old man presents with flank pain (**Fig. 62.1**).

Key Imaging Finding

Medial deviation of the ureters

Top 3 Differential Diagnoses

- **Retroperitoneal fibrosis.** Retroperitoneal fibrosis is an inflammatory process that typically affects older patients (50–60 years old), with a male predilection. It is most commonly idiopathic (Ormond disease) but may also be secondary to medications (especially migraine therapy), abdominal aortic aneurysms, neoplasms, and radiation therapy. It has associations with other systemic manifestations, such as mediastinitis, sclerosing cholangitis, and thyroiditis, which has led to a proposed autoimmune basis. Retroperitoneal fibrosis typically presents with an irregular, ill-defined mass centered at the aortic bifurcation. The fibrotic component compresses and medially deviates the ureters. In severe cases, ureteral obstruction may occur. Variable enhancement can be present on computed tomography (CT), depending on the degree of edema and active inflammation. In the chronic setting, fibrosis predominates, which will have low signal intensity on T1- and T2-weighted images.
- **Psoas muscle hypertrophy.** In athletic individuals, psoas muscle hypertrophy may result in medial deviation of the ureters due to the normally close anatomical relationship. Cross-sectional imaging can readily differentiate psoas muscle hypertrophy from other causes of medial deviation of the ureters.
- **Pelvic lipomatosis.** Pelvic lipomatosis is an idiopathic condition of increased unencapsulated fat within the pelvis. It occurs more commonly in middle-aged African American men. Compression of the pelvic hollow viscus, including the bladder and rectum, can occur. The distal ureters are medially deviated due to compression of the urinary bladder. In severe cases, ureteral obstruction may occur. Pelvic lipomatosis can be associated with cystitis glandularis.

Additional Differential Diagnoses

- **Postoperative changes.** Several surgical procedures may lead to postoperative medial deviation of the ureters. Common surgical procedures are retroperitoneal lymph node dissection (such as part of the treatment plan for testicular cancer), anterior abdominopelvic resections, and pelvic floor reconstructions. The distal ureters are most often affected.
- **Retrocaval ureter.** A retrocaval ureter occurs secondary to abnormal persistence of the right subcardinal vein. As a result of this anomaly, the right ureter deviates medially and passes posterior to the inferior vena cava (IVC) at approximately the L3–L4 level. Compression may result in proximal ureteral obstruction. Cross-sectional imaging such as CT urography can readily discern the variant location of the right ureter relative to the IVC.

Diagnosis

Retroperitoneal fibrosis

✓ Pearls

- Retroperitoneal fibrosis may be idiopathic or secondary to medications, abdominal aortic aneurysm, neoplasms, or radiation.
- Pelvic lipomatosis is most common in African American men and is associated with cystitis glandularis.
- Retrocaval ureter results in medial deviation of the right ureter and may result in proximal obstruction.

Suggested Readings

Cronin CG, Lohan DG, Blake MA, et al. Retroperitoneal fibrosis: a review of clinical features and imaging findings. AJR Am J Roentgenol 2008;191:423–431

Dunnick NR. Textbook of Uroradiology. Philadelphia: Lippincott Williams & Wilkins; 2001

Case 63

Todd M. Johnson

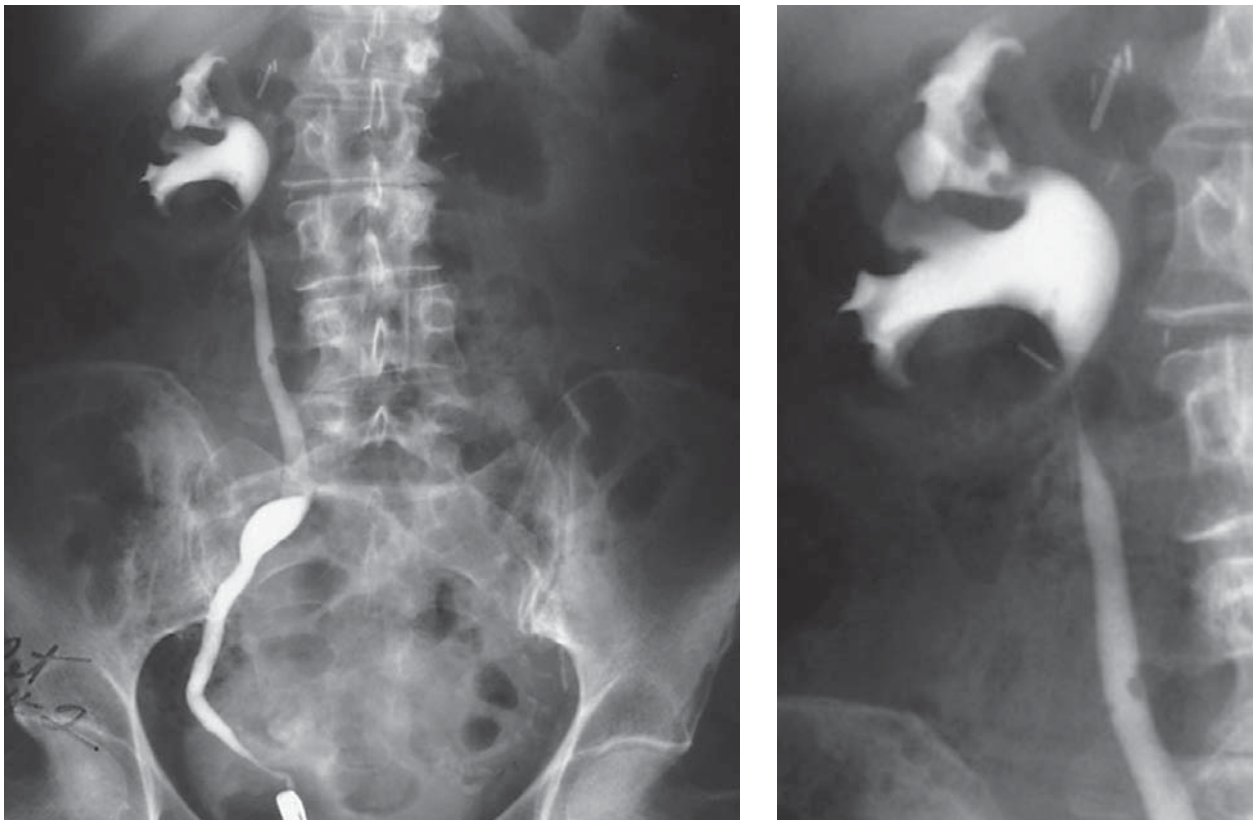


Fig. 63.1 **(A)** Retrograde pyelogram of the right ureter and **(B)** coned-down view of the right renal pelvis demonstrate multiple subcentimeter circumscribed filling defects. (Courtesy of Scot Campbell, MD.)

Clinical Presentation

A 53-year-old woman presents with a history of chronic urinary tract infections (**Fig. 63.1**).

Key Imaging Finding

Ureteral filling defects

Top 3 Differential Diagnoses

- **Transitional cell carcinoma (TCC).** TCC is the most common of the urothelial tumors (90–95%), and the urinary bladder is most commonly affected. If TCC is discovered in the upper urinary tract, the risk of TCC developing in the urinary bladder is ~20 to 40%. Conversely, bladder TCC is associated with upper tract disease developing in ~2 to 4% of patients. TCC is associated with exposure to carcinogens, including aromatic amines (smoking and rubber/dye industry) and cyclophosphamide. Multifocal papillary TCC may mimic other disorders, including ureteritis cystica and malacoplakia.
- **Radiolucent calculi.** Radiolucent stones can cause filling defects in the collecting system. Uric acid and xanthine stones occur in patients with malignancy on chemotherapy (marked cytolysis) and with gout. Other radiolucent stones are matrix (protein) and indinavir. Cystine stones may be faintly radiopaque.
- **Pyeloureteritis cystica.** Pyeloureteritis cystica is a benign condition associated with chronic urinary tract infection/mucosal irritation, resulting in urothelial metaplasia. It may affect the renal pelvis, ureter, or bladder. Multiple small, round, or oval filling defects are seen projecting into the collecting system lumen. The lesions can have a scalloped appearance when viewed in profile. No known malignant potential exists.

Additional Differential Diagnoses

- **Blood clot.** Blood clots may occur within the renal collecting system secondary to trauma, renal calculi, or underlying mass, such as renal cell carcinoma or TCC. The blood clots may form round, oval, or irregular mobile filling defects, or they may form a cast of the collecting system/ureter. When large, obstruction may occur.
- **Fungus ball.** *Candida* is the most common fungus to involve the urinary tract. Infection typically occurs in immunosuppressed patients (diabetes, transplant, chemotherapy, steroids, etc.) and in patients with indwelling catheters or stents. Radiologic manifestations include multiple mobile radiolucent filling defects.
- **Metastases.** Metastasis to the upper tract most commonly arise from a breast primary or melanoma. True metastatic involvement may be intramural or lymphatic (periureteral). Manifestations on pyelography include multiple filling defects and strictures.

Diagnosis

Pyeloureteritis cystica

✓ Pearls

- TCC is the most common urothelial tumor and may be multifocal; it is important to evaluate the bladder.
- Radiolucent stones include those composed of uric acid, xanthine, and indinavir.
- Pyeloureteritis cystica is associated with chronic inflammation and has no known malignant potential.
- Fungus balls typically occur in immunocompromised patients; *Candida* is the most common organism.

Suggested Readings

Dyer RB, Chen MY, Zagoria RJ. Intravenous urography: technique and interpretation. Radiographics 2001;21:799–821

Pollack HM, McClennan BL. Clinical Urography. 2nd ed. Philadelphia: WB Saunders; 2000

Zagoria RJ. Genitourinary Radiology: The Requisites. 2nd ed. Philadelphia: Mosby; 2004

Case 64

James B. Odone

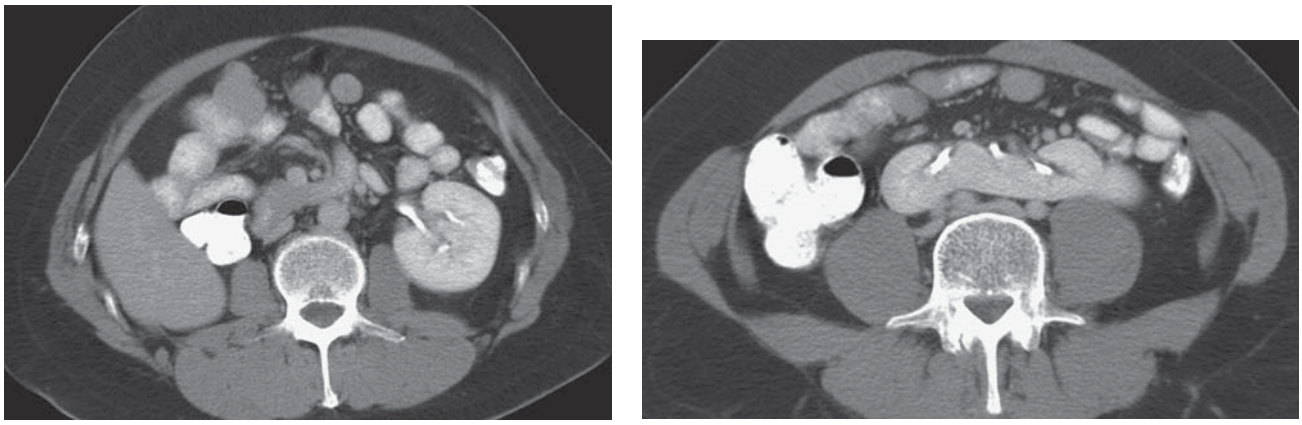


Fig. 64.1 **(A)** Contrast-enhanced axial CT image through the upper abdomen demonstrates an empty renal fossa on the right. **(B)** Enhanced axial CT image through the midabdomen reveals medial deviation of the inferior pole of the left kidney and renal parenchyma extending across the midline.

Clinical Presentation

A 24-year-old man presents with hematuria after minor blunt abdominal trauma (**Fig. 64.1**).

Key Imaging Finding

Renal migration anomaly

Top 3 Differential Diagnoses

- **Horseshoe kidney.** Horseshoe kidney is the most common congenital renal anomaly, with an incidence of 1 in every 400 live births. There is increased risk of a horseshoe kidney in Turner and Ellis–van Creveld syndromes. Fusion typically occurs at the lower poles, with subsequent arrest of cranial migration, due to restriction at the inferior mesenteric artery. As a result, the kidneys are lower within the abdomen, and the inferior renal poles appear more medial than expected on plain film radiography. The interconnecting isthmus may be fibrotic or composed of functioning renal parenchyma. Associated renal anomalies are ureteropelvic junction (UPJ) obstruction and duplication anomalies. Patients are more susceptible to trauma, obstruction, reflux, urinary tract infections, and stone formation. Wilms tumor is 2 to 8 times more common in children with a horseshoe kidney.
- **Cross-fused ectopia.** Cross-fused ectopia is an uncommon congenital anomaly. Usually, the left kidney crosses midline and fuses with the inferior pole of the right kidney. The anomaly is thought to be related to an abnormally situated umbilical artery. Intravenous urogram (IVU) will reveal an absent nephrogram in the expected renal fossa and fused renal parenchyma on the contralateral side. The ureters usually insert normally on the bladder; however, vascular supply to the ectopic kidney is typically anomalous. As with horseshoe kidney, patients are more susceptible to trauma, obstruction, reflux, urinary tract infections, and stone formation.
- **Ectopic kidney.** Isolated renal ectopia, typically resulting in a pelvic kidney, has a prevalence of ~1 in 1000 live births. On imaging with IVU, the pelvic kidney may be difficult to identify if it is overlying the sacrum, with the main clue being an empty renal fossa. The ectopic kidney usually has an anomalous blood supply, with the renal artery originating from the ipsilateral iliac artery. Complications include UPJ obstruction, vesicoureteral reflux (VUR), and urinary stasis with stone formation. Associated contralateral renal anomalies are agenesis and ectopia.

Additional Differential Diagnoses

- **Renal duplication.** Although supernumerary kidneys are extremely rare, a duplex kidney is a common congenital anomaly and occurs along a spectrum from partial to complete duplication. In most cases, the affected kidney will have two ureters—one for the upper pole moiety and one for the lower pole moiety. The lower pole ureter inserts into the bladder normally, whereas the ectopic upper pole ureter inserts inferomedially (Weigert–Meyer rule). The upper pole moiety is prone to obstruction (commonly due to a ureterocele at the ectopic insertion site), and the lower pole moiety is prone to reflux.

Diagnosis

Cross-fused ectopia

✓ Pearls

- Horseshoe kidney and renal ectopia are susceptible to injury in blunt abdominal trauma.
- In cross-fused renal ectopia, the ureters insert normally on the bladder.
- Ectopic kidney may be associated with UPJ obstruction, VUR, and urinary stasis with stone formation.
- A duplex kidney is prone to obstruction (upper pole) and reflux (lower pole).

Suggested Readings

Cohen HL, Kravets F, Zucconi W, et al. Congenital abnormalities of the genitourinary system. Semin Roentgenol 2004;39:282–303

Dunnick NR. Textbook of Uroradiology. 3rd ed. Philadelphia: Lippincott Williams & Wilkins; 2001

Case 65

Todd M. Johnson



Fig. 65.1 Coned-down view of the pelvis from an intravenous urogram demonstrates an irregular filling defect within the right lateral bladder.

Clinical Presentation

A 60-year-old man presents with gross hematuria (**Fig. 65.1**).

Key Imaging Finding

Bladder filling defect

Top 3 Differential Diagnoses

- **Transitional cell carcinoma (TCC).** TCC is the most common of urothelial tumors (90–95%), and the urinary bladder is the most common site of involvement. Carcinogen exposures associated with TCC include aromatic amines (smoking and rubber/dye industry) and cylophosphamide. Other less common malignant bladder tumors are squamous cell carcinoma (SCC) and adenocarcinoma. SCC is associated with chronic infection or inflammation; adenocarcinoma is the most common malignant tumor within urachal remnants.
- **Fungus ball.** *Candida* is the most common fungus to involve the urinary tract. Infection typically occurs in immunosuppressed patients (diabetes, transplant, chemotherapy, steroids, etc.) and in patients with indwelling catheters or stents. Radiographic manifestations include mobile radiolucent filling defects within the collecting system.
- **Blood clot.** Blood clots may occur within the renal collecting system secondary to trauma, renal calculi, or hemorrhage from an underlying mass, such as renal cell or TCC. Blood clots may form round, irregular, mobile filling defects, or they may form a cast of the collecting system.

Additional Differential Diagnoses

- **Radiolucent calculi.** Radiolucent stones can cause filling defects in the collecting system. Uric acid and xanthine stones occur in patients with malignancy on chemotherapy (marked cytolysis) and with gout. Other radiolucent stones are matrix (protein) and indinavir. Cystine stones may be faintly radiopaque.
- **Extrinsic compression.** Pelvic masses may cause extrinsic impression on the bladder, which can simulate an intraluminal filling defect on intravenous urogram. Common causes are retroperitoneal adenopathy, metastatic disease, and direct extension of a pelvic neoplasm (cervical, prostate, colon, or uterine). More benign pelvic masses such as ovarian cysts and abscesses may produce similar findings. Cross-sectional imaging can usually distinguish a primary bladder mass from extrinsic compression.

Diagnosis

Transitional cell carcinoma

✓ Pearls

- TCC is the most common of urothelial tumors; the bladder is the most common site involved.
- Adenocarcinoma occurs within urachal remnants; SCC occurs with chronic inflammation.
- Mobile filling defects within the bladder may be due to fungal infection, blood clot, or stones.
- *Candida* is the most common fungus to involve the renal collecting system.

Suggested Readings

Dyer RB, Chen MY, Zagoria RJ. Intravenous urography: technique and interpretation. Radiographics 2001;21:799–821

Wong-You-Cheong JJ, Woodward PJ, Manning MA, et al. From the *Archives of the AFIP:* neoplasms of the urinary bladder—radiologic-pathologic correlation. Radiographics 2006;26:553–580

Case 66

Paul B. DiDomenico

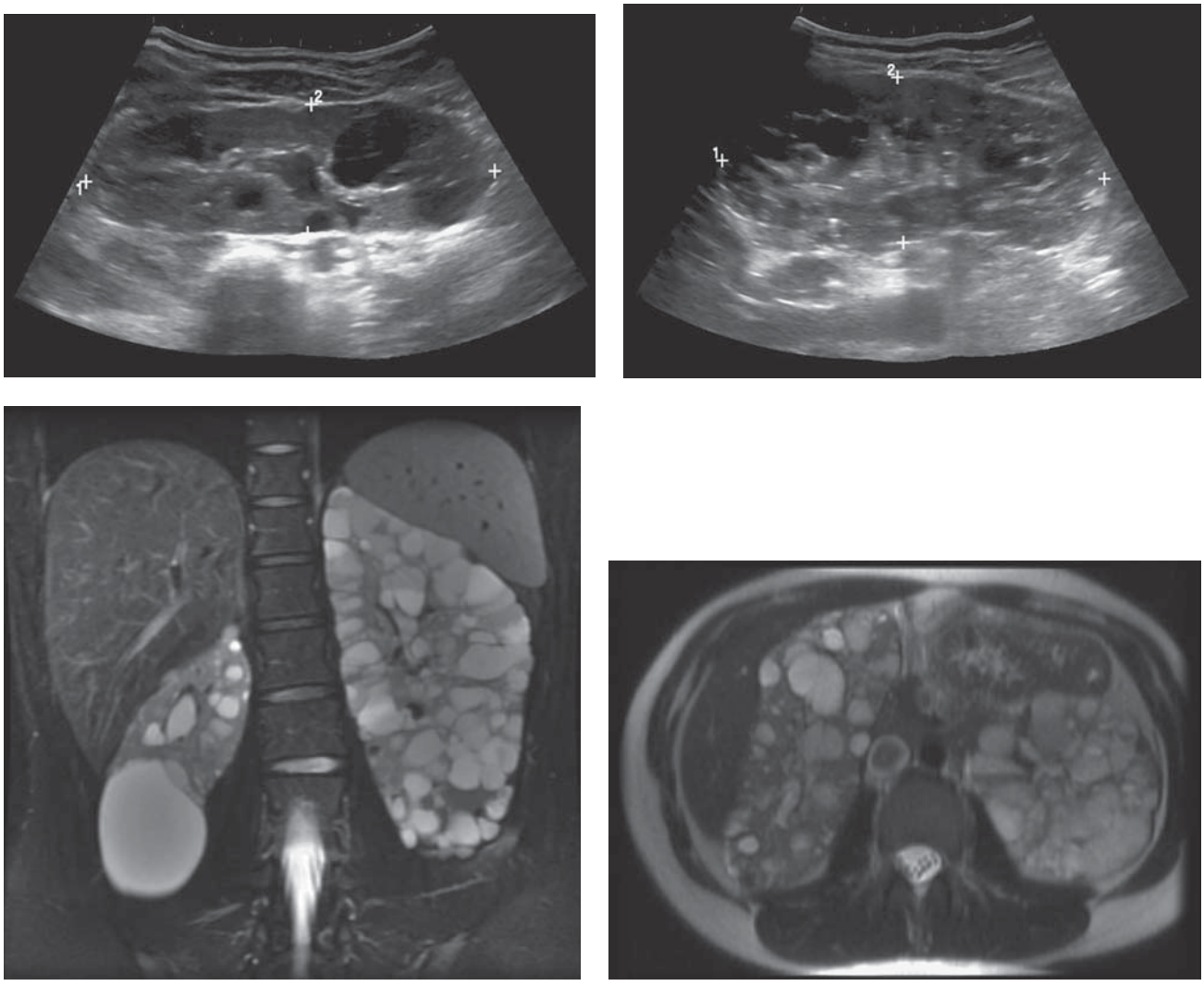


Fig. 66.1 Longitudinal sonographic images through **(A)** the right and **(B)** the left kidneys demonstrate marked enlargement of the kidneys with innumerable cysts of varying sizes. **(C)** Coronal and **(D)** axial T2-weighted fast spin echo magnetic resonance images (fat suppression on the coronal image) confirm the ultrasound findings and demonstrate the variable signal intensities within the cysts due to variable proteinaceous content, typically from prior hemorrhage.

Clinical Presentation

An adolescent presents with flank pain and hematuria (**Fig. 66.1**).

Key Imaging Finding

Bilateral renal cysts

Top 3 Differential Diagnoses

- **Autosomal dominant polycystic kidney disease (ADPKD).** The presence of multiple bilateral renal cysts (two or more cysts in each kidney in a patient younger than 60 years of age) of varying size suggests the diagnosis of ADPKD. The kidneys are usually massively enlarged in later stages of the disease, and patients may present with flank pain from mass effect. Cysts of other abdominal organs often coexist, with up to 75% of patients having simple cysts in the liver as well. Less commonly, there may be cysts in the pancreas, spleen, adnexa, or lung, and up to 15% of patients will have berry aneurysms of the cerebral arteries. ADPKD does not confer an increased risk of malignancy.
- **End-stage renal disease (hemodialysis).** Patients with chronic renal failure may develop multiple bilateral renal cysts in the setting of hemodialysis. Usually, the kidneys will be relatively atrophic; extrarenal cysts do not occur as a consequence of this disease, but they may be present due to other causes. It is important to be aware that up to 7% of patients on hemodialysis will develop renal cell carcinoma (RCC), although these cancers have low metastatic potential.
- **Von Hippel–Lindau (VHL) disease.** VHL disease causes cysts in multiple abdominal organs, including bilateral renal cysts in 75% of cases; however, there is a higher propensity (50%) for coexisting pancreatic cysts as compared with ADPKD. Additionally, up to 40% of patients with VHL develop RCCs, and 15% develop pheochromocytomas. Many other neoplasms may be present as well, including cerebellar hemangioblastomas, retinal angiomas, hepatic adenomas, pancreatic islet cell tumors, and cystadenomas of the epididymis.

Additional Differential Diagnoses

- **Tuberous sclerosis.** Renal involvement of tuberous sclerosis is classically described as bilateral angiomyolipomas (AMLs); however, bilateral renal cysts without AMLs have been described in children with this disease. The well-known "clinical triad" presentation includes adenoma sebaceum, seizures, and mental retardation. Imaging findings include subcortical and periventricular calcified hamartomas, subependymal giant cell astrocytomas at the foramen of Monro, pulmonary lymphangiomyomatosis with chylous effusions, cardiac rhabdomyomas, and skeletal osteomas.

Diagnosis

ADPKD

✓ Pearls

- ADPKD patients are at increased risk for RCC after initiation of dialysis.
- Acquired cystic renal disease in chronic renal failure results in small kidneys.
- Renal lesions associated with VHL disease include renal cysts and RCC.
- Tuberous sclerosis may present with multiple renal cysts or AMLs.

Suggested Readings

Dunnick NR. Textbook of Uroradiology. 3rd ed. Philadelphia: Lippincott Williams & Wilkins; 2001

Federle MP. Diagnostic Imaging: Abdomen. Salt Lake City, UT: Amirsys; 2004

Zagoria RJ. Genitourinary Radiology: The Requisites. 2nd ed. Philadelphia: Mosby; 2004

Case 67

Todd M. Johnson

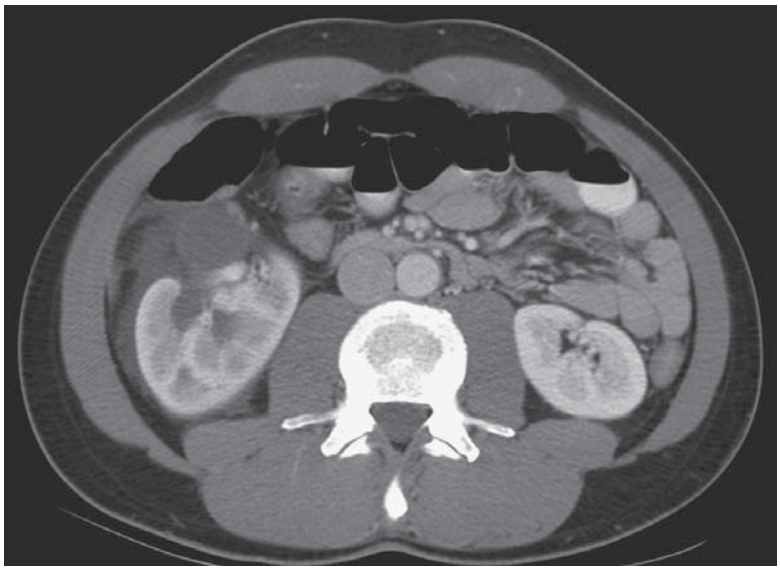


Fig. 67.1 Contrast-enhanced axial CT image through the level of the kidneys demonstrates fluid and fat stranding within the right perinephric space. There is asymmetric enlargement of the right kidney.

Clinical Presentation

A 37-year-old man presents with right flank pain (**Fig. 67.1**).

Key Imaging Finding

Perinephric fluid collection

Top 3 Differential Diagnoses

- **Perinephric hemorrhage.** Blunt or penetrating abdominal trauma may result in renal laceration, which may be associated with perinephric hemorrhage. Iatrogenic perinephric hemorrhage may occur in the setting of biopsy or following extracorporeal shock wave lithiotripsy for nephrolithiasis. Lacerations are graded based on the portion of the renal parenchyma involved and whether or not there is extension into the renal pelvis and/or vascular injury. In the absence of known trauma, initial and follow-up imaging will be required to evaluate for underlying malignancy, including renal cell carcinoma (RCC) and angiomyolipoma (AML). RCC is the most common primary renal malignancy, is hypervascular, and is prone to hemorrhage. AMLs have abnormal networks of vasculature and associated aneurysms, which may hemorrhage, especially when large (>4 cm).
- **Urine leak/urinary extravasation.** A urine leak or urinary extravasation may occur in the setting of trauma or obstruction. Trauma can result in lacerations that extend into the renal collecting system or avulsion of the ureteropelvic junction (UPJ). In either case, urine will collect in the perinephric space, as well as in other retroperitoneal compartments. To differentiate from hemorrhage, delayed imaging should be performed in the excretory phase. Percutaneous nephrostomy or ureteral stent placement may be necessary to divert urine and prevent urinoma formation. Obstruction from a ureteral or UPJ stone may result in significantly increased intraluminal pressures within the collecting system. Secondary findings include an identifiable cause of obstruction (stone or mass), renal enlargement, and a striated nephrogram. The weakest portion of the collecting system, which is prone to rupture, is the forniceal region of the calyx. Rapid decompression of the collecting system with forniceal rupture may result in reduction or alleviation of the patient's flank pain.
- **Pyelonephritis/perinephric infection.** Perinephric infection and inflammatory changes are most commonly the result of pyelonephritis. Secondary findings suggesting pyelonephritis are renal enlargement and a striated nephrogram. Complications of pyelonephritis such as renal abscess may extend into the perinephric space or into the ipsilateral psoas muscle. The presence of urinary obstruction and secondary infection is a urologic emergency and is often treated with percutaneous nephrostomy. Additionally, infectious processes of adjacent structures, such as the colon or pancreas, can extend into the fat of the perinephric and pararenal spaces.

Diagnosis

Urinary leak (forniceal rupture from an obstructed ureter)

✓ Pearls

- A renal laceration extending into the collecting system is best evaluated with delayed imaging.
- Perinephric hemorrhage without trauma requires follow-up imaging to exclude underlying malignancy.
- Urine extravasation may result from trauma or forniceal rupture from urinary obstruction.
- Perinephric infectious or inflammatory fat stranding is most often due to pyelonephritis.

Suggested Readings

Dunnick NR. Textbook of Uroradiology. 3rd ed. Philadelphia: Lippincott Williams & Wilkins; 2001

Federle MP. Diagnostic Imaging: Abdomen. Salt Lake City, UT: Amirsys; 2004

Case 68

Charles A. Tujo

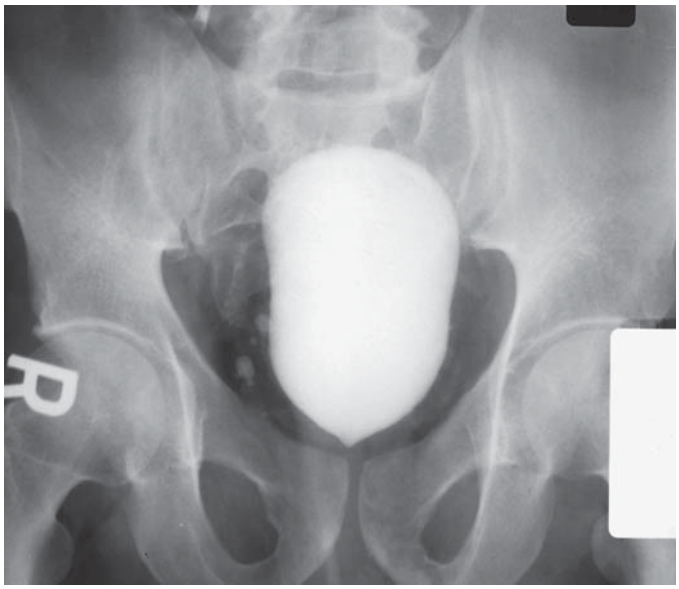


Fig. 68.1 Frontal view of the pelvis from an intravenous pyelogram demonstrates elongation of the bladder with a pear-shaped configuration. (Courtesy of the Department of Radiology, University of Cincinnati.)

Clinical Presentation

A 45-year-old man presents with abdominal and pelvic fullness (**Fig. 68.1**).

Key Imaging Finding

Pear-shaped bladder

Top 3 Differential Diagnoses

- **Pelvic hematoma.** Bladder wall compression from hemorrhage within the pelvis usually results from blunt trauma, laceration of the internal iliac artery, or following prostatectomy. Mass effect usually is a bilateral, symmetric process on the bladder walls; the bladder base may be elevated. There may also be medial deviation of the ureters. In the setting of trauma, pelvic fracture and pubic diastasis are commonly associated findings.
- **Lymphadenopathy.** If massive, pelvic lymphadenopathy could compress the bladder and result in a pear shape. The most common consideration in this setting would be lymphoma, but other etiologies would include metastatic disease from a local primary neoplasm, such as uterine or cervical carcinoma in a woman or prostate cancer in a man.
- **Pelvic lipomatosis.** A rare process primarily seen in overweight African American men, pelvic lipomatosis is a proliferation of nonencapsulated fat in the perivesical and perirectal space of the pelvis. Mass effect on the urinary bladder may result in an inverted pear-shaped bladder. The ureters may be symmetrically displaced medially, with up to 40% of patients developing urinary obstruction. Compression of the rectum occurs with elevation of the rectosigmoid junction on barium enema and can result in symptoms of constipation. Pelvic lipomatosis is associated with cystitis glandularis.

Additional Differential Diagnoses

- **Psoas muscle hypertrophy.** Psoas muscle hypertrophy is a rare cause of symmetric bladder narrowing that could result in a pear-shaped bladder. It occurs more commonly in high-performance athletes and weight lifters with a narrow bony pelvis. Bilateral medial deviation of the ureters may also be seen. Enlarged psoas muscles are best appreciated on cross-sectional imaging, such as computed tomography or magnetic resonance imaging. The renal axis may also be altered, and the midureter may demonstrate an abrupt transition over the psoas muscle.
- **Iliac artery aneurysms.** Commonly found in patients with underlying atherosclerotic vascular disease and abdominal aortic aneurysms, large bilateral iliac artery aneurysms could result in a pear-shaped bladder. Ectasia and minimal aneurysmal dilation are fairly common; however, the size necessary to produce compression of the bladder walls makes this a relatively rare etiology.

Diagnosis

Pelvic lipomatosis

✓ Pearls

- Etiologies of pelvic hematoma include blunt trauma with pelvic fractures and surgical complications.
- Pelvic lymphadenopathy is most often due to non-Hodgkin lymphoma; metastatic disease is less common.
- Pelvic lipomatosis is a benign proliferation of fat in the pelvis that compresses the bladder and rectum.

Suggested Readings

Dyer RB, Chen MY, Zagoria RJ. Classic signs in uroradiology. Radiographics 2004;24:S247–S280

Dyer RB, Chen MY, Zagoria RJ. Intravenous urography: technique and interpretation. Radiographics 2001;21:799–824

Xu T, Zhao WH, Wang XF, et al. Analysis of pelvic lipomatosis and a case report of two brothers. Beijing Da Xue Xue Bao 2007;39:355–360

Zagoria RJ, Glenn AT. Genitourinary Radiology: The Requisites. St. Louis, MO: CV Mosby; 1997

Case 69

Todd M. Johnson

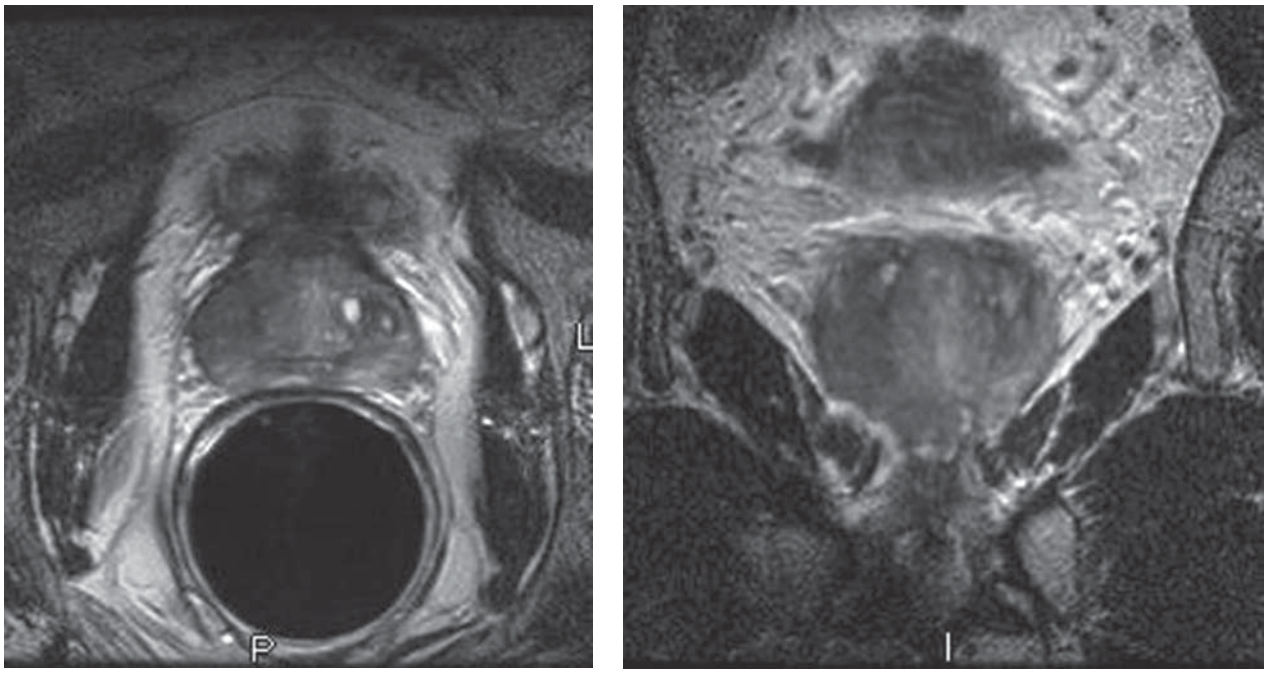


Fig. 69.1 **(A)** Axial and **(B)** coronal T2-weighted images through the prostate gland demonstrate a region of low signal intensity involving the peripheral zone within the midgland and extending to the base on the right. (Courtesy of Sadhna Verma, MD, University of Cincinnati.)

Clinical Presentation

A 60-year-old man presents with elevated prostate-specific antigen (**Fig. 69.1**).

Key Imaging Finding

Prostate enlargement

Top 3 Differential Diagnoses

- **Prostate adenocarcinoma.** Prostate adenocarcinoma is second only to lung cancer as a cause of cancer-related death in men. It most frequently occurs in the peripheral zone of the prostate. On T2-weighted imaging, prostate cancer is hypointense to the typically hyperintense peripheral zone. An important magnetic resonance imaging (MRI) finding is invasion of the neurovascular bundle or seminal vesicles. Computed tomography (CT) cannot differentiate prostate cancer from normal peripheral zone tissue, but it may detect gross extracapsular spread. Signs of extracapsular spread include obliteration of the periprostatic fat plane, lymphadenopathy, and invasion of adjacent structures, such as the urinary bladder or rectum. Microinvasion of the capsule is beyond the resolution of both MRI and CT. Mixed results have been reported on the benefits of MR spectroscopy to aid in the staging of prostate cancer; however, several centers have successfully implemented MR spectroscopy as a part of the workup for prostate adenocarcinoma. Hematogenous spread via the internal iliac veins and vertebral venous plexus results in osteoblastic metastases, readily detectable by bone scan.
- **Benign prostatic hypertrophy (BPH).** BPH is benign hypertrophy of the transitional zone of the prostate gland. Beyond the age of 50 years, nearly half of all men will be affected by some degree of hypertrophy. Cross-sectional imaging such as CT and MRI can demonstrate prostate size. On intravenous urogram, the effects of prostate enlargement on the bladder can be demonstrated. Bladder base elevation and a characteristic J-shaped appearance of the distal ureters may occur. With increasing outlet obstruction, poor bladder emptying with increased postvoid residual volume and bladder wall trabeculation with or without diverticula may be evident.
- **Prostatitis.** Prostatitis is an inflammatory condition of the prostate, which in the acute setting is most commonly a retrograde bacterial infection due to *Escherichia coli.* Enlargement of the prostate can occur, although this is not a specific finding. Chronic prostatitis also has nonspecific findings that may be indistinguishable from BPH and prostate carcinoma. Contrast-enhanced CT can be useful in the detection of prostatic abscess. Transrectal ultrasonography–guided aspiration of a suspected prostatic abscess can help confirm the diagnosis.

Diagnosis

Prostate adenocarcinoma

✓ Pearls

- Prostate adenocarcinoma occurs in the peripheral zone and is hypointense on T2-weighted sequences.
- An important prognostic factor in prostate adenocarcinoma is the presence of extracapsular spread.
- BPH is very common in older men and involves the transitional zone.
- Prostatitis is often secondary to a retrograde bacterial infection, most commonly *E. coli*.

Suggested Readings

Dunnick NR. Textbook of Uroradiology. Philadelphia: Lippincott Williams & Wilkins; 2001

Federle MP. Diagnostic Imaging: Abdomen. Salt Lake City, UT: Amirsys; 2004

Hricak H, Choyke PL, Eberhardt SA, et al. Imaging prostate cancer: a multidisciplinary perspective. Radiology 2007;243:28–53

Case 70

Charles A. Tujo

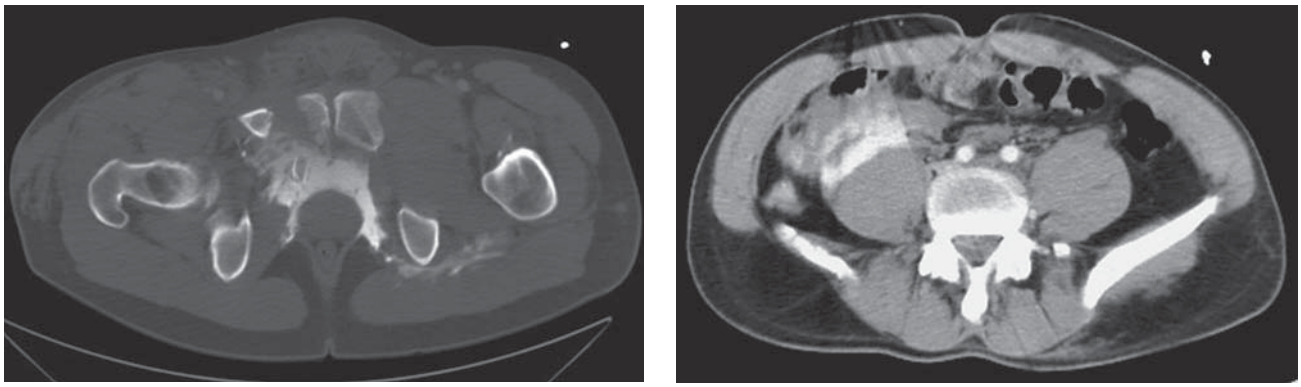


Fig. 70.1 **(A)** Axial CT image through the pelvis in the bone window after retrograde filling of the bladder with contrast reveals extraperitoneal contrast within the prevesical space and tracking along the left posterior soft tissues. There are multiple associated pelvic fractures. **(B)** Contrast-enhanced axial CT image through the upper pelvis in the soft tissue window on the same patient demonstrates intraperitoneal contrast interposed between bowel loops in the right lower quadrant and layering along the paracolic gutter.

Clinical Presentation

A patient presents after a motor vehicle accident (**Fig. 70.1**).

Key Imaging Finding

Bladder rupture

Top 3 Differential Diagnoses

- **Extraperitoneal bladder rupture.** Extraperitoneal bladder rupture is more common than intraperitoneal (80–90% of cases) and is usually associated with pelvic fractures. Contrast from retrograde bladder filling (cystography) will accumulate in the perivesical, prevesical, or retrorectal space. A "Christmas tree" or "molar tooth" appearance of contrast can be seen with sharp and often irregular margins. Management is typically nonsurgical, with catheter placement and bladder decompression.
- **Intraperitoneal bladder rupture.** Intraperitoneal bladder rupture is commonly associated with blunt trauma, typically with a full bladder. It can also occur spontaneously, which is more common with an underlying bladder process such as tumor, cystitis, or neurogenic bladder. Cystography may demonstrate contrast outlining bowel loops with smooth margins. This is readily seen on a computed tomography (CT) cystogram, where bowel loops are surrounded with dense contrast. Other places in which contrast may accumulate are the lateral pelvic recesses superior to the bladder, pericolic space, and perihepatic space. It is important to make the distinction between intraperitoneal and extraperitoneal bladder rupture, as intraperitoneal rupture is typically managed surgically.
- **Intra- and extraperitoneal bladder rupture.** Combined intraperitoneal and extraperitoneal bladder rupture occurs in 5 to 12% of cases of bladder injuries. Both patterns of injury listed above may be seen.

Additional Differential Diagnoses

- **Urethral injury.** More commonly seen in men, urethral injuries are classified by anatomical location, posterior versus anterior. Posterior urethral injuries can result in extravasation of contrast in the retropubic extraperitoneal space or perineum, which may mimic bladder rupture. If the bladder cannot be filled retrograde, the injury to the urethra is complete. Anterior urethral injuries should not be confused with extraperitoneal bladder rupture, as extravasation during retrograde filling collects in the corpora spongiosa.

Diagnosis

Intra- and extraperitoneal bladder rupture

✓ Pearls

- Extraperitoneal bladder rupture is the most common type and is associated with pelvic fractures.
- Intraperitoneal bladder rupture is usually due to blunt trauma with a full bladder.
- Intraperitoneal bladder rupture is surgically managed.
- Image the entire abdomen with a CT cystogram to fully evaluate for extravesical contrast collections.

Suggested Readings

Dahnert W. Radiology Review Manual. 4th ed. Philadelphia: Lippincott Williams & Wilkins; 2000

Morgan DE, Nallamala LK, Kenney PJ, et al. CT cystography: radiographic and clinical predictors of bladder rupture. AJR Am J Roentgenol 2000;174:89–95

Vaccaro JP, Brody JM. CT cystography in the evaluation of major bladder trauma. Radiographics 2000;20:1373–1381

Zagoria RJ, Glenn AT. Genitourinary Radiology: The Requisites. St. Louis, MO: Mosby; 1997

Case 71

Michael C. Kuo

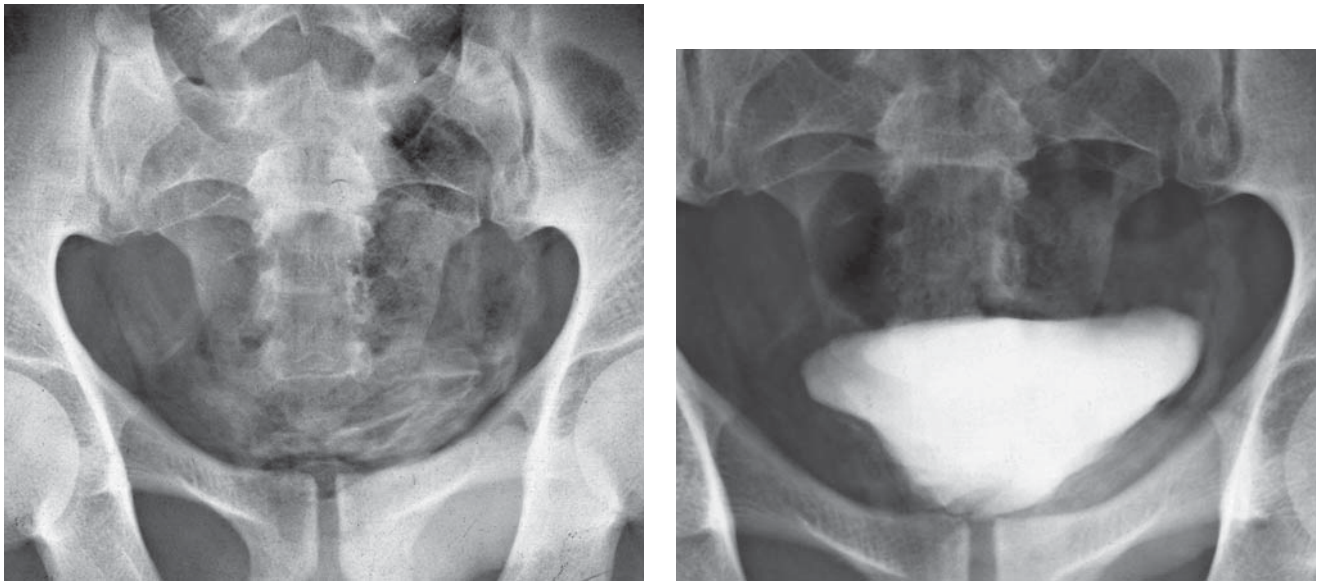


Fig. 71.1 **(A)** Kidney, ureter, and bladder study shows curvilinear calcifications within the pelvis. **(B)** Delayed intravenous urogram centered over the pelvis shows the calcification just superficial to the contrast-filled urinary bladder lumen. (Courtesy of Richard W. Katzberg, MD, University of California, Davis, School of Medicine.)

Clinical Presentation

A 21-one year-old man presents with a history of dysuria (**Fig. 71.1**).

Key Imaging Finding

Bladder wall calcifications

Top 3 Differential Diagnoses

- **Transitional cell carcinoma (TCC).** TCC comprises 90 to 95% of epithelial bladder carcinomas and may show punctate, linear, or central calcifications. The most common presenting sign is painless hematuria, typically occurring in patients 50 to 60 years of age, with a 4:1 male predominance. The bladder is the most common site, involved in 90% of cases of TCC. The renal pelvis, ureters, and proximal two thirds of the urethra make up the remaining cases. The entire urothelium must be examined with follow-up imaging due to increased risk for synchronous and metachronous TCC.
- **Schistosomiasis.** Schistosomiasis is an infectious etiology of cystitis and is the most common cause of bladder wall calcification worldwide. The parasite deposits ova within the bladder submucosa, which causes an inflammatory response. Mural calcifications may develop afterward. Complications of schistosomiasis include bladder carcinoma, especially squamous cell carcinoma.
- **Cystitis.** Noninfectious causes of cystitis include cyclophosphamide-induced hemorrhagic cystitis and radiation-induced cystitis, both of which may also cause bladder wall calcification. Complications of chronic cystitis are hyperplastic uroepithelial cell clusters, which may lead to cystitis cystica and cystitis glandularis.

Additional Differential Diagnoses

- **Tuberculosis (TB).** TB of the urinary bladder is almost always secondary to TB infection of the kidney. End-stage disease causes bladder fibrosis, diminishing the capacity of the urinary bladder. Bladder wall calcifications are relatively uncommon. Complications such as fistulas and sinus tract formation are rare.
- **Urachal carcinoma.** Urachal carcinomas are adenocarcinomas (90%), which commonly calcify (70%). Fine punctuate calcifications within tumor on computed tomography may suggest mucinous adenocarcinoma. These arise from urachal remnants and are clinically silent until the bladder dome is invaded. Patients are typically between 40 and 70 years of age, with a 3:1 male predominance, presenting with hematuria and/or mucoid discharge. Five-year survival is poor.

Diagnosis

Schistosomiasis

✓ Pearls

- TCC most often involves the bladder (90% of cases) and may have calcifications.
- Schistosomiasis is the most common cause of bladder wall calcification worldwide.
- Cystitis from infectious etiologies (TB), chemotherapy, or radiation may cause bladder wall calcifications.
- Urachal carcinomas are usually adenocarcinomas, which commonly calcify.

Suggested Readings

Dyer RB, Chen MYM, Zagoria RJ. Abnormal calcification in the urinary tract. Radiographics 1998;18:1405–1424

Federle MP. Diagnostic Imaging: Abdomen. Salt Lake City, UT: Amirsys; 2004

Case 72

Todd M. Johnson

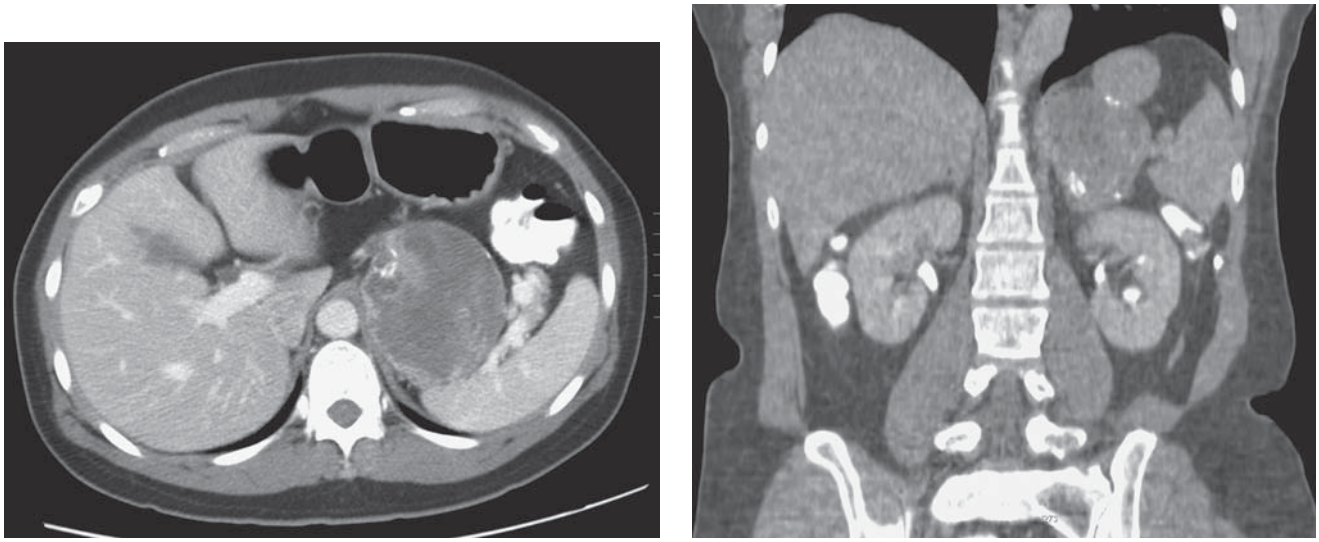


Fig. 72.1 Contrast-enhanced **(A)** axial and **(B)** coronal CT images demonstrate a large heterogeneously enhancing left adrenal mass with central cystic regions and irregular eccentric calcifications.

Clinical Presentation

History withheld (**Fig. 72.1**).

Key Imaging Finding

Adrenal mass

Top 3 Differential Diagnoses

- **Adrenal adenoma.** Adrenal adenomas are the most common adrenal cortex tumors, occurring in nearly 10% of the population. The majority are small (<2 cm), circumscribed, and have low attenuation (<15 HU). Up to one third can be lipid poor, requiring additional imaging, such as enhancement washout (>40% relative or >60% absolute) or magnetic resonance imaging (MRI) in/opposed phase sequences (signal loss on opposed phase).
- **Metastases.** The adrenal glands are a common site for metastatic disease. They may present as unilateral or bilateral, small or large, adrenal masses of soft tissue density. The appearance on MRI is usually hypointense on T1 and relatively hyperintense on T2. If complicated by hemorrhage and necrosis, they may have a heterogeneous appearance and irregular enhancement.
- **Hemorrhage.** Adrenal hemorrhage may be traumatic or nontraumatic. Nontraumatic etiologies include coagulopathy, stress (neonatal, surgery, sepsis, or hypotension), and underlying mass. Hemorrhage may be unilateral or bilateral. Enlargement of the gland occurs initially, with increased density in the acute to subacute phase; over time, the lesions decrease in size and attenuation and may develop calcifications.

Additional Differential Diagnoses

- **Pheochromocytoma.** Pheochromocytomas are rare tumors derived from chromaffin cells in the adrenal medulla. Patients can present with hypertension due to excess catecholamine secretion. Lesions can have variable imaging features depending on the degree of hemorrhage and necrosis. Classic imaging findings include avid contrast enhancement and marked hyperintensity on T2-weighted imaging. Pheochromocytomas typically demonstrate increased activity on iodine 131 meta-iodobenzylguanidine or indium 111 Pentetreotide nuclear scintigraphy.
- **Adrenal myelolipoma.** Myelolipomas are uncommon benign neoplasms that contain both hematopoietic and fat tissue. The fatty component is low density on computed tomography (CT) (−30 to −90 HU), and hyperintense on T1-weighted imaging that demonstrates signal loss with fat saturation. Larger lesions may hemorrhage spontaneously.
- **Adrenocortical carcinoma.** Adrenocortical carcinoma is a rare tumor that is usually unilateral, nonfunctioning, and large at presentation (5–20 cm). Imaging features can be heterogeneous due to hemorrhage and necrosis, with variable degrees of enhancement. Calcifications are seen in up to 30% of cases. Metastatic disease is found in 20% of patients at presentation.

Diagnosis

Adrenocortical carcinoma

✓ Pearls

- Adrenal adenomas are the most common adrenal masses; they can be confirmed on CT or MRI.
- Metastases commonly involve the adrenal glands; they present as unilateral or bilateral soft tissue masses.
- Adrenal hemorrhage is most common in children and evolves over time.
- Pheochromocytomas are classically “lightbulb” bright on T2-weighted MRI sequences.

Suggested Readings

Caoili EM, Korobkin M, FrancisI R, et al. Adrenal masses: characterization with combined unenhanced and delayed enhanced CT. Radiology 2002;222:629–633

Elsayes KM, Mukundan G, Narra VR, et al. Adrenal masses: MR imaging features with pathologic correlation. Radiographics 2004;24:S73–S86

Federle MP. Diagnostic Imaging: Abdomen. Salt Lake City, UT: Amirsys; 2004

Case 73

Todd M. Johnson

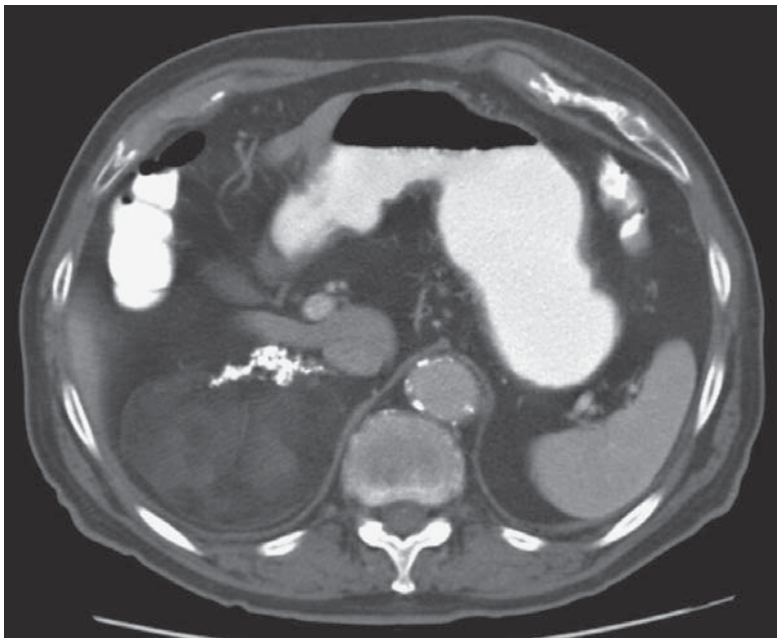


Fig. 73.1 Contrast-enhanced axial CT image through the upper abdomen demonstrates a large fat-containing retroperitoneal mass with soft tissue elements and calcifications anteriorly.

Clinical Presentation

A 42-year-old man presents with vague right upper quadrant pain (**Fig. 73.1**).

Key Imaging Finding

Fatty retroperitoneal mass

Top 3 Differential Diagnoses

- **Angiomyolipoma (AML).** Angiomyolipoma is a benign tumor of the kidney composed of vascular elements, smooth muscle, and adipose tissue. Gross fat (−30 to −90 HU) in a renal lesion is virtually diagnostic of AML, especially in the absence of calcification. Although there is no malignant potential, lesions composed predominantly of vascular elements and smooth muscle can show significant enhancement and are indistinguishable from RCC by imaging. This slow-growing tumor is at risk for hemorrhage, especially when the size is >4 cm, which is due to abnormal vessels and aneurysm formation.
- **Adrenal myelolipoma.** Adrenal myelolipomas are rare benign tumors composed of variable amounts of adipose tissue and hematopoietic elements. On computed tomography (CT) imaging, a circumscribed heterogeneous lesion with fat density is characteristic. A small portion will have calcifications, especially if complicated by hemorrhage. Although patients are usually asymptomatic, spontaneous hemorrhage may occur in large lesions. When large, they may be difficult to distinguish from retroperitoneal liposarcomas.
- **Retroperitoneal liposarcoma.** Liposarcomas are the most common primary malignant lesions of the retroperitoneum. They originate from adipose tissue, usually located in the peri/paranephric space. CT imaging will reveal a fat and soft tissue attenuation lesion with heterogeneous enhancement. Lesions are usually large at the time of diagnosis, with displacement of adjacent structures.

Additional Differential Diagnoses

- **Renal cell carcinoma (RCC).** RCC has rarely been reported to contain macroscopic fat, which can represent engulfed fat. A dedifferentiated RCC can create both bone and fat. There should be a high suspicion for RCC if a fat density renal lesion contains calcifications.

Diagnosis

Adrenal myelolipoma (complicated by prior hemorrhage)

✓ Pearls

- Gross fat in a renal lesion is virtually diagnostic of AML, especially in the absence of calcification.
- Adrenal myelolipomas consist of gross fat and hematopoietic elements; calcifications may be present.
- Liposarcoma is the most common retroperitoneal sarcoma; it contains gross fat and is typically large.
- Calcification within a fat-containing renal lesion should raise the suspicion for dedifferentiated RCC.

Suggested Readings

Behranwala KA, Chettiar K, El-Bahrawy M, et al. Retroperitoneal myolipoma. World J Surg Oncol 2005;3:72

Federle MP. Diagnostic Imaging: Abdomen. Salt Lake City, UT: Amirsys; 2004

Liang EY, Cooper JE, Lam WW, et al. Case report: myolipoma or liposarcoma—a mistaken identity in the retroperitoneum. Clin Radiol 1996;51:295–297

Case 74

Todd M. Johnson



Fig. 74.1 Selected image from an intravenous urogram demonstrates isolated dilatation of the distal left ureter with a normal-caliber proximal ureter, renal pelvis, and calyces.

Clinical Presentation

History withheld (**Fig. 74.1**).

Key Imaging Finding

Dilated ureter

Top 3 Differential Diagnoses

- **Ureteral obstruction.** Ureteral obstruction can result from stones, strictures, neoplasm, or extrinsic compression. Ureteral calculi may be radiopaque (most commonly calcium oxalate) or nonradiopaque (uric acid, xanthine, matrix, or protease inhibitor). Strictures can result from prior infection/inflammation, instrumentation, or surgery. Transitional cell carcinoma, the most common primary neoplasm of the ureter, can present as a stricture on intravenous urogram. Pelvic neoplasms (ovarian, uterine, cervical, or colonic) can cause obstruction from mass effect and extrinsic compression or from direct extension.
- **Reflux.** Vesicoureteral reflux is the abnormal flow of urine from the bladder into the upper urinary collecting system. Typically it is the result of a short distal ureteral submucosal tunnel within the bladder wall, which normally serves as a valve mechanism. Reflux can be graded according to severity on voiding cystourethrogram (VCUG) (grade I: ureter only; grade II: ureter, renal pelvis, and calyces; grade III: ureter and renal pelvis mildly dilated and calyces mildly blunted; grade IV: ureter and renal pelvis moderately dilated and calyces moderately blunted; and grade V: gross dilatation and tortuosity of the ureter, severely dilated renal pelvis, and severely blunted calyces with loss of papillary impression). Nuclear cystography can be used for initial screening in female patients and as a follow-up study in both male and female patients, with the benefit of lower patient radiation. VCUG is the initial study in male patients to evaluate the posterior urethra and exclude posterior urethral valves.
- **Primary megaureter.** Megaureter describes an enlarged ureter that may or may not have associated dilatation of the upper collecting system (megacalycosis). Primary megaureter can be classified into one of three categories: nonrefluxing and unobstructed (most common), obstructing, and refluxing. Nonrefluxing, unobstructed megaureter is idiopathic and has neither reflux nor stenosis at the ureterovesical junction. The obstructing variant of primary megaureter has ureteral dilatation above a focal segment of normal caliber but an aperistaltic juxtavesical ureter. It is thought that abnormal collagen deposition between muscle cells is a contributing cause of the aperistaltic segment. The refluxing variant of primary megaureter is a result of a short or absent intravesical ureter.

Additional Differential Diagnoses

- **Prune-belly syndrome.** Prune-belly syndrome is named after the appearance of the abdomen, which is wrinkled due to the lack of rectus muscles. It occurs almost exclusively in men and boys. Urinary tract abnormalities include dilated tortuous ureters (with renal dysmorphism) and a megalocystic, dilated prostatic urethra. The bladder is usually enlarged, and a majority of patients have vesicoureteral reflux. Additionally, the testicles are undescended and nonpalpable. Other abnormalities of the pulmonary, gastrointestinal, skeletal, and cardiac system may be present.

Diagnosis

Primary megaureter

✓ Pearls

- Ureteral obstruction is most commonly due to renal calculi but may also be due to stricture or neoplasm.
- Fluoroscopic VCUG is used as the initial study to evaluate for reflux in males.
- Nuclear cystography minimizes patient dose for reflux studies in female patients or follow-up studies in male patients.
- Most cases of primary megaureter are of the nonrefluxing, unobstructed type.

Suggested Readings

Berroca lT, López-Pereira P, Arjonilla A, Gutiérrez J. Anomalies of the distal ureter, bladder, and urethra in children: embryologic, radiologic, and pathologic features. Radiographics 2002;22:1139–1164

Lebowitz RL, Olbing H, Parkkulainen KV, Smellie JM, Tamminen-Moebius TE. International system of radiographic grading of vesicoureteric reflux. Pediatr Radiol 1985;15:105–109

Zagoria RJ. Genitourinary Radiology: The Requisites. 2nd ed. Philadelphia: Mosby; 2004

Case 75

Todd M. Johnson

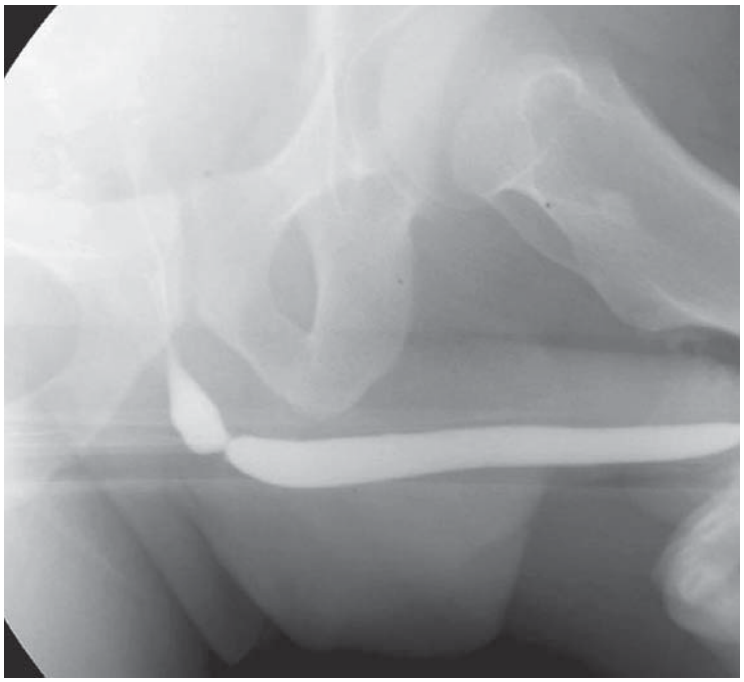


Fig. 75.1 Retrograde urethrogram demonstrates a focal stricture within the bulbous urethra.

Clinical Presentation

A 45-year-old man presents with a history of urethritis (**Fig. 75.1**).

Key Imaging Finding

Urethral stricture

Top 3 Differential Diagnoses

- **Urethral trauma.** Straddle injury is one of the most common external causes of posttraumatic urethral stricture, usually involving the bulbous portion. Instrument-related iatrogenic strictures typically occur at the bulbomembranous urethra and penoscrotal junction. Posterior urethral strictures are usually a result of disruption from trauma (high-speed motor vehicle accident with pelvic fractures) or surgery (transurethral prostate resection or radical prostatectomy). Retrograde urethrography is primarily used to diagnose anterior strictures, and simultaneous retrograde urethrography and antegrade cystourethrography help depict the length of posterior urethral strictures.
- **Postinfectious/postinflammatory stricture.** Gonococcal urethritis is one of the leading reportable sexually transmittable diseases in the United States. Nongonococcal urethritis is attributable to *Chlamydia trachomatis* in 30 to 50% of cases. Up to 15% of men with gonococcal urethritis will develop a stricture, typically in the distal bulbous urethra. It is thought that scars in this region occur due to the preponderance of Littre glands; dilation of Littre glands may also be seen at urethrography. If urethrography demonstrates a narrowed, elongated, irregular, or asymmetric proximal bulbous urethra, there is a high association with stricture extension into the membranous urethra. Involvement of the membranous urethra is important for the urologist due to the location of the distal urethral sphincter; transection of this sphincter can result in iatrogenic urinary incontinence.
- **Urethral carcinoma.** Malignant tumors of the urethra are uncommon and usually occur in older individuals (> age 50). Squamous cell carcinoma comprises the majority (>80%) of malignant tumors, involving the bulbomembranous urethra in 60% and the penile urethra in 30%. Strictures from urethral carcinoma can be demonstrated on urethrography as a focal irregular narrowing; urethral fistulas and periurethral abscess may also develop. On magnetic resonance imaging, urethral carcinomas are typically low signal intensity masses relative to the normal corporal tissue on T1- and T2-weighted sequences.

Diagnosis

Postinfectious stricture (gonococcal urethritis)

✓ Pearls

- Posttraumatic strictures commonly occur at the bulbomembranous urethra or penoscrotal junction.
- Postinfectious/postinflammatory urethral strictures typically involve the bulbous urethra.
- Strictures of the membranous urethra have surgical implications due to the location of the distal sphincter.
- Squamous cell carcinoma is the most common urethral neoplasm; it typically occurs in older men.

Suggested Readings

Federle MP. Diagnostic Imaging: Abdomen. Salt Lake City, UT: Amirsys; 2004

Kawashima A, Sandler CM, Wasserman NF, LeRoy AJ, King BFJr, Goldman SM. Imaging of urethral disease: a pictorial review. Radiographics 2004;24(Suppl 1):S195–S216

Section IV Musculoskeletal Imaging

Case 76

Eva Escobedo



Fig. 76.1 **(A)** Anteroposterior (AP) view of the right humerus demonstrates punched out lytic lesions of the shaft and endosteal scalloping. **(B)** Lateral view of the skull reveals similar multiple lytic lesions. **(C)** AP view of the left proximal femur shows punched out lesions and focal erosion of the endosteal surface, which is typical of an intramedullary process. **(D)** Lateral view of the thoracolumbar spine shows generalized osteopenia, vertical striations, and focal compressions of T11 and T12.

Clinical Presentation

A 42-year-old man presents with diffuse bone pain (**Fig. 76.1**).

Key Imaging Finding

Multiple lytic foci

Top 3 Differential Diagnoses

- **Metastases.** Bone metastases can be either well or poorly defined and may be difficult to distinguish from multiple myeloma. Purely osteolytic lesions originate from primary thyroid, renal, and uterine carcinomas. Mixed osteolytic/osteosclerotic lesions may arise from lung, breast, cervix, ovarian, and testicular malignancies. The osteolytic lesions arising from thyroid and renal primaries may produce bone expansion.
- **Multiple myeloma.** Multiple myeloma is the most common primary bone malignancy in adults. Plasma cell myeloma is a malignancy resulting in excessive proliferation of abnormal plasma cells. The predominant pattern is osteolysis and most commonly occurs at multiple sites, but it can be solitary (plasmacytoma). The axial skeleton is the typical site of involvement, but extensive disease will affect the extremities as well. The classic pattern of bone involvement is multiple discrete "punched out" lesions. Subcortical erosions of the endosteum may cause a characteristic "scalloped" appearance.
- **Lymphoma.** Skeletal involvement is common in both Hodgkin and non-Hodgkin lymphoma. The most common manifestation of non-Hodgkin lymphoma is multiple osteolytic lesions with a moth-eaten or permeative pattern of bone destruction, sometimes with endosteal scalloping and cortical destruction. Osteosclerosis is more commonly seen in Hodgkin lymphoma. Soft tissue masses are common and may be seen in the absence of significant cortical disruption.

Additional Differential Diagnoses

- **Langerhans cell histiocytosis (LCH).** Bone lesions may be seen in any of the LCHs, but eosinophilic granuloma is the most common subtype and manifests as single or multiple bone lesions in children and young adults. In the tubular bones, eosinophilic granuloma usually presents as a well-defined lucent lesion. As it enlarges, there may be associated periosteal reaction and cortical erosion. Characteristic radiographic appearances include "beveled edges" and "button sequestrum" in the skull and vertebra plana of the spine.
- **Fibrous dysplasia.** Fibrous dysplasia is a sporadic disease of bone-forming mesenchyme with abnormal osteoblastic differentiation. The normal bone is replaced by immature woven bone and fibrous stroma. Lesions may be solitary or multiple, are typically well defined, and may have a lucent or hazy ("ground-glass") matrix with sclerotic borders. They may be expansile or contain internal calcifications. Deformities may occur due to abnormal weakened bone or fractures. There is no associated periosteal reaction.
- **Chronic recurrent multifocal osteomyelitis (CRMO).** CRMO is a self-limiting inflammatory disorder of children of unknown etiology. It affects predominantly long bone metaphyses but can occur at any skeletal site. Although initially osteolytic, the hallmark is reactive sclerosis.

Diagnosis

Multiple myeloma

✓ Pearls

- Purely osteolytic osseous lesions may originate from thyroid, renal, and uterine primary malignancies.
- The classic appearance of multiple myeloma is multiple discrete "punched out" lytic lesions.
- Non-Hodgkin lymphoma commonly demonstrates a moth-eaten or permeative pattern of bone destruction.
- LCH results in calvarial lesions with "beveled edges" and "button sequestrum," as well as vertebra plana.

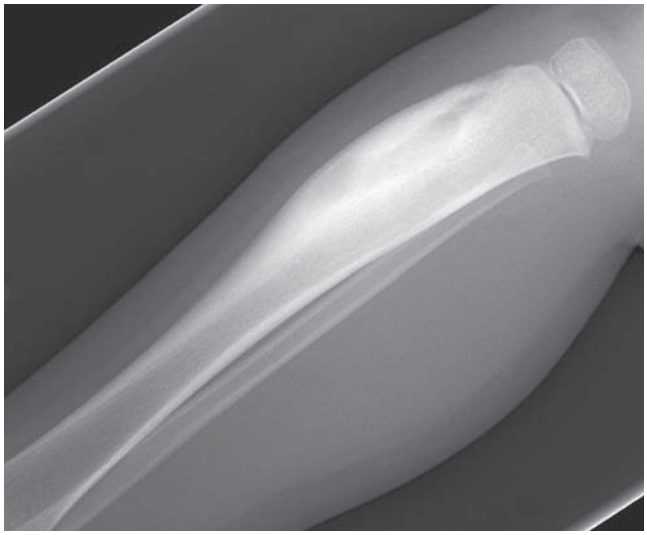
Suggested Readings

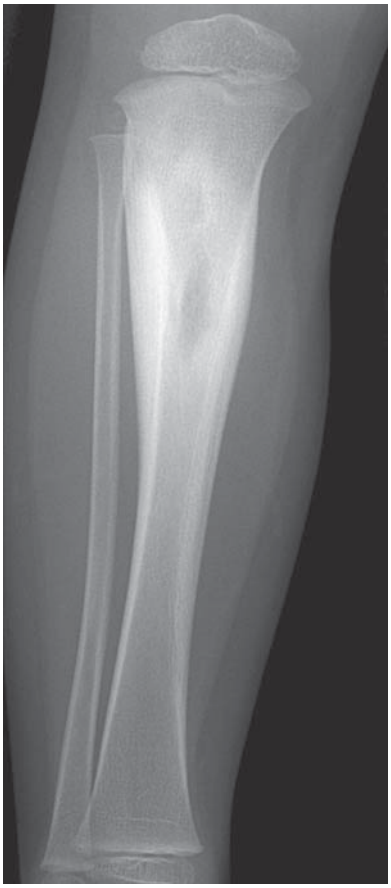
Resnick D, Kransdorf MJ. Bone and Joint Imaging. 3rd ed. Philadelphia: Elsevier Saunders; 2005

Stoller DW, Tirman PF, Bredella MA. Diagnostic Imaging: Orthopaedics. Salt Lake City, UT: Amirsys; 2004

Case 77

Michael A. Tall





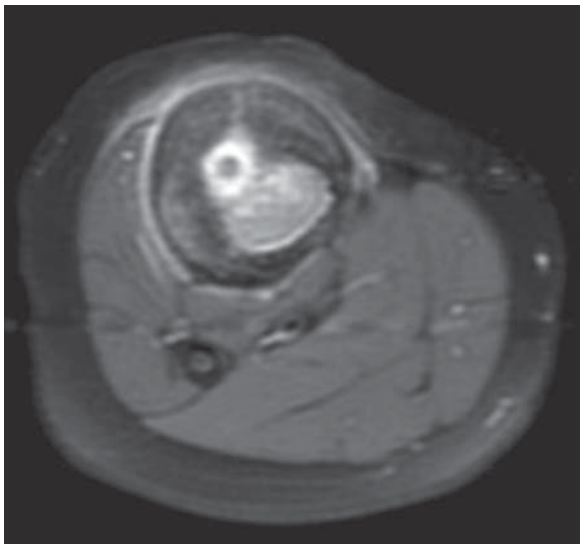


Fig. 77.1 **(A)** Lateral and **(B)** frontal radiographs of the tibia demonstrate a large region of sclerosis in the proximal tibia with a central lucent region that extends to the anterior cortex. **(C)** T1-weighted postgadolinium image with fat suppression through the proximal tibia demonstrates a centrally located, nonenhancing bony sequestrum in the medullary cavity. This is surrounded by enhancing granulation tissue (involucrum). A cloaca is present, extending from the involucrum to the overlying cortex.

Clinical Presentation

A 9-year-old girl presents with leg pain, swelling, and fevers (**Fig. 77.1**).

Key Imaging Finding

Sequestrum

Top 3 Differential Diagnoses

- **Osteomyelitis.** A sequestrum in the setting of osteomyelitis refers to a segment of dead, sclerotic bone that is separated from living bone by granulation tissue. The sequestrum may reside within the marrow and become a source of focal infection that can cause repeated flare-ups of acute osteomyelitis. A rim of living bone that surrounds the sequestrum is referred to as an involucrum. The involucrum may be permeated by a cloaca through which pus and the sequestrum itself may be expelled to the skin surface through a draining sinus tract.
- **Langerhans cell histiocytosis (LCH).** Eosinophilic granuloma is a subset of LCH that is characterized by multiple, predominantly lytic lesions throughout the axial and appendicular skeleton of children and young adults (<30 years of age). It accounts for ~70% of cases of LCH. Lesions within the long bones are characterized as lytic lesions with endosteal scalloping and occasionally periosteal reaction. A radiodense focus within a lytic lesion is referred to as a "button" sequestrum. Cranial involvement classically consists of a lytic lesion with beveled edges due to asymmetric involvement of the inner and outer tables.
- **Osteoid osteoma.** The classic radiographic findings in an osteoid osteoma are a centrally located oval or round radiolucent area surrounded by a uniform region of sclerotic bone. The central lucency is highly vascularized and is the target of surgical débridement or radiofrequency ablation. Patients typically have nighttime pain relieved by aspirin. Common sites are the long bones of the lower extremities and spine.

Additional Differential Diagnoses

- **Lymphoma.** Both Hodgkin and non-Hodgkin lymphoma can affect the bones in both primary and widespread disease. Primary non-Hodgkin lymphoma most commonly presents in the appendicular skeleton as an aggressive osteolytic lesion with poorly defined margins. Osteosclerosis, when evident, is more commonly found in Hodgkin disease, which can present with osteolytic lesions, osteosclerotic lesions, or a mixture of both. Sequestrum is more commonly seen in the Hodgkin variant.
- **Fibrosarcoma.** Fibrosarcomas are characterized by osteolytic foci with a geographic, moth-eaten, or permeative pattern of bone destruction. There is little osteosclerosis and a striking absence of a significant osseous reaction despite the bone destruction. Occasionally, a sequestrum may be evident.

Diagnosis

Osteomyelitis

✓ Pearls

- Osteomyelitis may demonstrate a sequestrum surrounded by an involucrum and permeated by a cloaca.
- LCH results in lytic calvarial lesions with beveled edges and button sequestrum.
- Osteoid osteomas typically demonstrate a round or oval radiolucent nidus surrounded by sclerotic bone.
- The central nidus in osteoid osteoma is highly vascularized and is the target of radiofrequency ablation.

Suggested Readings

Helms CA. Fundamentals of Skeletal Radiology. 3rd ed. Philadelphia: Elsevier Saunders; 2005

Krasnokutsky MV. The button sequestrum sign. Radiology 2005;236:1026–1027

Resnick D. Bone and Joint Imaging. 2nd ed. Philadelphia: WB Saunders; 1996

Case 78

Philip Granchi

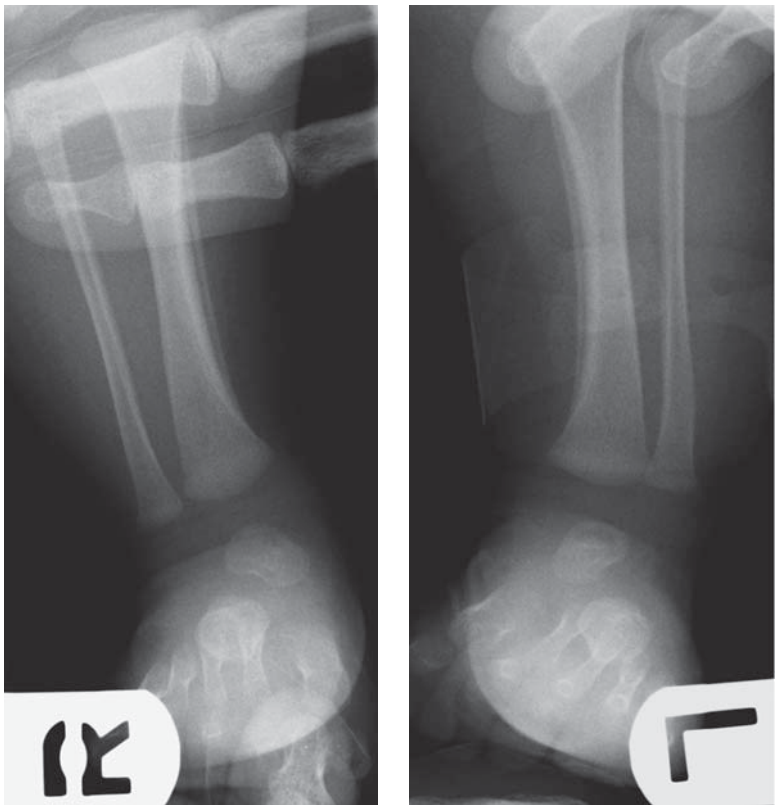


Fig. 78.1 **(A,B)** Frontal views of the lower legs demonstrate symmetric, smooth, continuous periosteal reaction along the medial aspect of the tibial diaphyses bilaterally.

Clinical Presentation

A 4-week-old male infant presents with unexplainable irritability (**Fig. 78.1**).

Key Imaging Finding

Periosteal reaction in a newborn/infant

Top 3 Differential Diagnoses

- **Physiologic periosteal reaction.** Between 1 and 6 months of age, periosteal new bone formation occurs as thin lines parallel to the cortices of long bones in about one third of all infants. Key to recognizing this process as benign is its symmetry. It commonly affects the humerus, femur, and tibia bilaterally. Follow-up films will show confluence of the periosteal reaction with the existing cortex. Physiologic periosteal bone formation will not involve the metaphyses. One to 6 months is the only period in which periosteal bone formation is considered physiologic.
- **Trauma.** Periosteal reaction occurs at sites of fracture from both accidental and nonaccidental trauma. In particular, nonaccidental trauma must be considered whenever periosteal reaction is identified in pediatric patients. Factors favoring a diagnosis of periosteal reaction secondary to nonaccidental trauma include multiple fractures of differing ages, as well as fractures with a high specificity for child abuse. High-specificity fractures include posterior rib and metaphyseal corner fractures.
- **Infection.** Skeletal findings secondary to infection are diverse, but a unifying element of these etiologies is the presence of lucency, either as vertical or longitudinal bands in the case of the TORCH (toxoplasmosis, other agents, rubella, cytomegalovirus, herpes simplex) infections, or as more poorly defined areas in osteomyelitis. The metaphyses are most commonly involved, which is a differentiating feature from normal physiologic periosteal bone formation.

Additional Differential Diagnoses

- **Prostaglandin therapy.** Patients with congenital heart disease may require patency of the ductus arteriosus to provide oxygenated blood to the systemic circulation. Prostaglandin therapy is used to keep the ductus open prior to corrective surgery. Although the periosteal reaction in these patients is diffuse, the patient will have clear history of cardiac anomaly and long-term treatment (4–6 weeks) with prostaglandins.
- **Infantile cortical hyperostosis (Caffey disease).** Occurring in the first few months of life, Caffey disease presents with fever, irritability, and periosteal reaction primarily involving the mandible, long bones, ribs, and scapulae. Key features that allow differentiation of Caffey disease are its coarse, irregular, asymmetric periosteal reaction, as well as the presence of soft tissue swelling over the affected areas.

Diagnosis

Physiologic periosteal reaction

✓ Pearls

- Physiologic periosteal reaction occurs between 1 and 6 months of age and does not involve the metaphyses.
- Trauma (accidental and nonaccidental) and infection result in localized periosteal reaction.
- Prostaglandin therapy may result in a diffuse periosteal reaction with long-term (4–6 weeks) treatment.
- Caffey disease results in a coarse, irregular, asymmetric periosteal reaction with soft tissue swelling.

Suggested Readings

Kirks D, Griscom NT. Practical Pediatric Imaging: Diagnostic Radiology of Infants and Children. 3rd ed. Philadelphia: Lippincott-Raven; 1998:335–336

Shannon FJ, Murphy M, Atchial, et al. Caffey's disease: an unusual cause for concern. Ir J Med Sci 2007;176:133–136

Swischuk LE, ed. Imaging of the Newborn, Infant and Young Child. 5th ed. Philadelphia: Lippincott Williams & Wilkins; 2004:733

Velaphi S, Cilliers A, Beckh-Arnold E, et al. Cortical hyperostosis in an infant on prolonged prostaglandin infusion: case report and literature review. J Perinatol 2004;24:263–265

Case 79

M. Jason Akers



Fig. 79.1 Coned-down lateral radiograph of the lumbar spine shows superior and inferior end-plate sclerosis at all levels. There is relative lucency within the central vertebral bodies between the areas of end-plate sclerosis with an indistinct transition between the areas of sclerosis and the central areas of lucency.

Clinical Presentation

A young adult patient presents with back pain (**Fig. 79.1**).

Key Imaging Finding

"Rugger jersey" appearance of the spine

Top 3 Differential Diagnoses

- **Renal osteodystrophy.** Renal osteodystrophy represents a constellation of musculoskeletal abnormalities that occur in chronic renal failure, including osteomalacia, secondary hyperparathyroidism, and osteosclerosis. Osteosclerosis is common and results from an increased amount of abnormal osteoid. A classic site for osteosclerosis is the vertebral body end plates. The "rugger jersey" appearance of the spine is created by the relative lucency of the central aspect of the vertebral bodies between the sclerotic end plates. The margins between the sclerotic and lucent portions of the vertebral body are smudgy rather than sharp. Look for extraskeletal evidence of chronic renal failure to include surgical clips in the abdomen from nephrectomy or renal transplant and dialysis catheters in the chest.
- **Osteopetrosis.** Osteopetrosis represents a group of hereditary disorders characterized by abnormal osteoclastic activity, resulting in dense bones. The "sandwich" appearance of the vertebral bodies is classic for osteopetrosis. The appearance is similar to the "rugger jersey" spine of renal osteodystrophy, with the difference being a sharp margin between the sclerotic end plates and more lucent bone centrally. The classic "bone in bone" appearance occurs within the pelvis and long bones.
- **Paget disease.** Paget disease occurs in middle-aged and elderly patients and is characterized by excessive and abnormal bone remodeling. Most cases are polyostotic, and the majority of cases involve the pelvis, spine, skull, femur, or tibia. The more common appearance of Paget disease in the spine is the "picture frame" vertebral body caused by overall increased density, with sclerosis most marked at the periphery and a relatively lucent center. As in other bones, the classic features of Paget disease in the spine are bony (vertebral) enlargement, coarsened trabeculae, and overall increased bone density.

Additional Differential Diagnoses

- **Metastatic disease.** Classic primary tumors that cause sclerotic bone metastases include prostate, breast, lymphoma, carcinoid, bladder, and medulloblastoma. Tumor cells most often spread to the vertebral body hematogenously. Metastatic deposits may occur as discrete or ill-defined lesions or involve the marrow diffusely. Magnetic resonance imaging shows solitary or multiple low T1 and T2 lesions. Diffuse involvement of the vertebral bodies causes diffusely low vertebral body signal as the metastases replace normal fatty marrow.
- **Myelofibrosis.** Myelofibrosis is bone marrow fibrosis that is most commonly secondary to leukemia, lymphoma, or metastatic disease. The disease initially involves primary sites of active hematopoiesis, including the vertebrae, ribs, and pelvis, and later secondary sites in the proximal and distal aspects of long bones. Myelofibrosis manifests as very low signal intensity marrow on all sequences. Radiographs may be normal, but when abnormal, they will show diffuse marrow sclerosis.

Diagnosis

Renal osteodystrophy

✓ Pearls

- The "rugger jersey" appearance of the vertebral bodies in renal osteodystrophy has smudgy margins.
- The "sandwich" vertebrae in osteopetrosis have sharp interfaces between sclerotic and lucent bone.
- Paget disease is characterized by bony enlargement, coarsened trabeculae, and increased bone density.
- With diffuse spine metastases, there is decreased marrow signal due to replacement of normal fatty marrow.

Suggested Readings

Chew F. Musculoskeletal Imaging A Teaching File. 3rd ed. Philadelphia: Elsevier Saunders; 2005
Graham TS. The ivory vertebra sign. Radiology 2005;235:614–615
Ross J, Brant-Zawadzki M, Chen M, et al. Diagnostic Imaging: Spine. Salt Lake City, UT: Amirsys; 2004
Wittenberg A. The rugger jersey spine. Radiology 2004;230:491–492

Case 80

Michael A. Tall

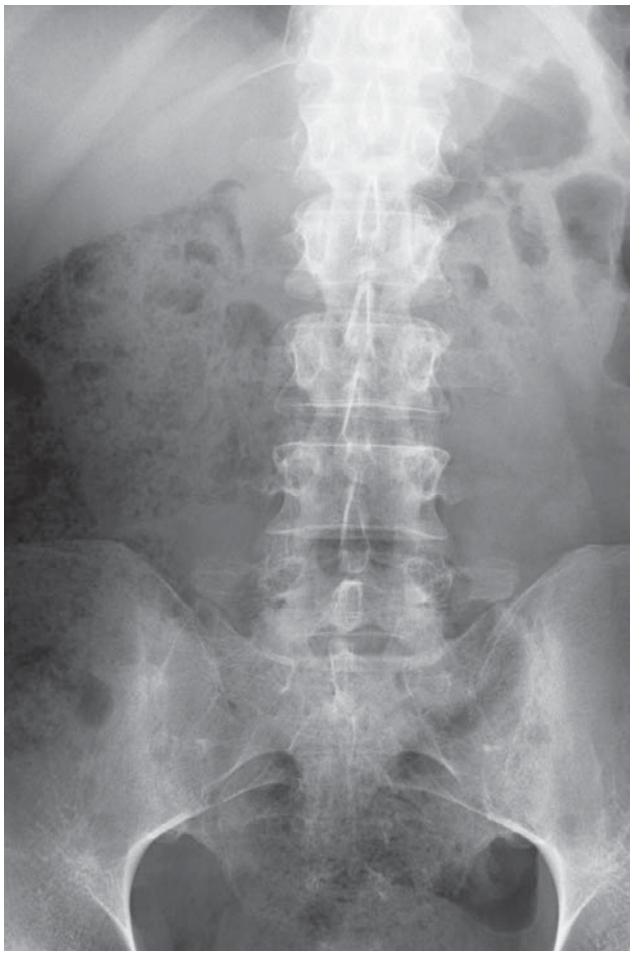


Fig. 80.1 Anteroposterior radiograph of the pelvis demonstrates symmetric bilateral sclerosis and erosions involving the sacral and iliac portions of the sacroiliac joints with areas of ankylosis across the joints.

Clinical Presentation

A 29-year-old man with a 3-year history of worsening back and hip pain presents with morning stiffness (**Fig. 80.1**).

Key Imaging Finding

Sacroiliitis

Top 3 Differential Diagnoses If Bilaterally Symmetric

- **Ankylosing spondylitis.** Ankylosing spondylitis is a seronegative spondyloarthropathy. The earliest radiographic manifestations of ankylosing spondylitis involve the sacroiliac joints. The sacroiliac joints are typically involved in a bilateral symmetric fashion with sclerosis on both sides of the joint, along with small erosions. Eventually, ankylosis or fusion across the joint occurs. Characteristic findings in the spine are erosions along the corners of the vertebral bodies (shiny corners), squaring of vertebral bodies, ossification and ankylosis along the anulus (bamboo spine), and interspinous ligament ossification (dagger sign).
- **Inflammatory bowel disease.** Between 5 and 15% of patients with Crohn disease develop sacroiliac and spinal changes. The radiographic manifestations of Crohn disease are identical to ankylosing spondylitis, including bilaterally symmetric sacroiliac sclerosis on both sides of the joint, small erosions, and ankylosis.
- **Rheumatoid arthritis.** Rheumatoid arthritis may result in bilateral, symmetric narrowing of the sacroiliac joints. Erosive changes occur but usually to a lesser extent than what is seen with the spondyloarthropathies. Ankylosis, when present, involves the synovial portion of the joint.

Top 3 Differential Diagnoses If Unilateral or Bilaterally Asymmetric

- **Psoriatic or reactive arthropathy.** Both psoriatic and reactive arthritis are categorized as seronegative spondyloarthropathies. Both processes involve the sacroiliac joints in a bilateral but asymmetric fashion. Radiographic manifestations include erosions that are more prominent than ankylosing spondylitis or rheumatoid arthritis, along with sclerosis. Ankylosis, when present, occurs later in the disease process.
- **Osteoarthritis.** Osteoarthritis of the sacroiliac joints may be unilateral or bilateral but asymmetric. The hallmark of osteoarthritis is irregular joint space narrowing with subchondral sclerosis. Osteoarthritis primarily involves the superior and inferior aspects of the synovial portion of the joint. Erosions and ankylosis are not features of osteoarthritis. Large bridging osteophytes may develop along the anterior margin of the joint, which should not be confused with true ankylosis.
- **Septic arthritis.** Septic arthritis is almost always a unilateral process. Early in the disease process, abnormal widening, erosions, and bone destruction are present. This typically extends beyond the synovial portion of the joint. Bony ankylosis may eventually occur. Septic arthritis should be suspected in any case of unilateral sacroiliitis. Failure to properly diagnosis and treat this condition will result in significant joint destruction.

Diagnosis

Ankylosing spondylitis

✓ Pearls

- The earliest radiographic manifestation of ankylosing spondylitis involves the sacroiliac joints.
- The radiographic manifestations of Crohn disease are identical to ankylosing spondylitis.
- Psoriatic and reactive arthropathies involve the sacroiliac joints in a bilateral, asymmetric process.
- Septic arthritis should be suspected in any case of unilateral sacroiliitis.

Suggested Readings

Bennett DL, Ohashi K, El-Khoury GY. Spondyloarthropathies: ankylosing spondylitis and psoriatic arthritis. Radiol Clin North Am 2004;42:121–134

Brower AC, Flemming DJ. Arthritis: in Black and White. 2nd ed. Philadelphia: WB Saunders; 1997

Case 81

Michael A. Tall

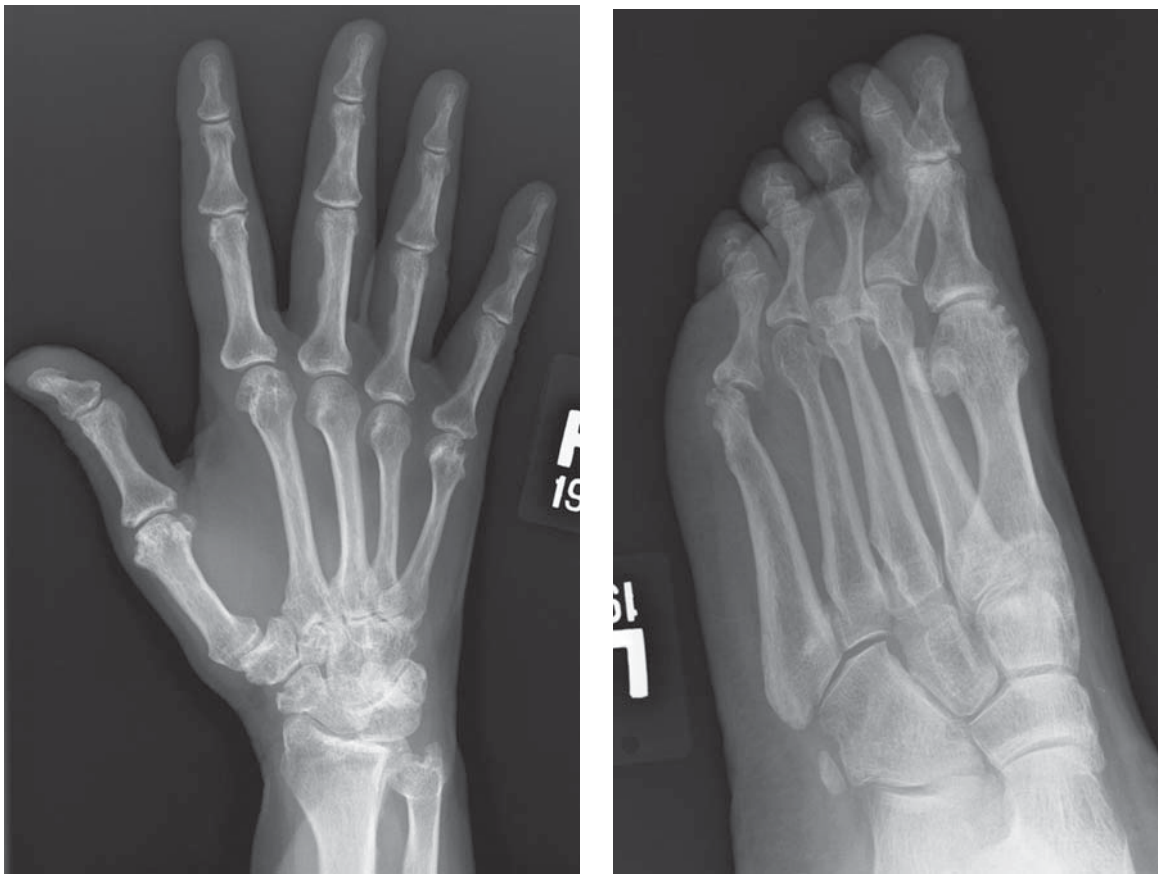


Fig. 81.1 **(A)** Oblique radiograph of the right hand demonstrates first and fifth metacarpophalangeal joint degenerative changes and periarticular osteopenia. Additionally, there are erosions of the first, second, and fifth metacarpal heads, ulnar styloid, and carpal bones. **(B)** Oblique radiograph of the left foot reveals metatarsophalangeal (MTP) joint degenerative changes (most pronounced along the fifth digit), mild interphalangeal joint degenerative changes, erosions of the first and fifth metatarsal heads, and subluxation of the third proximal phalanx at the third MTP joint.

Clinical Presentation

A 54-year-old woman presents with stiffness and pain in her hands and feet (**Fig. 81.1**).

Key Imaging Finding

Proximal arthropathy affecting primarily the metacarpophalangeal (MCP) joints

Top 3 Differential Diagnoses

- **Rheumatoid arthritis (RA).** The common radiographic manifestations of RA consist of periarticular osteopenia, uniform joint space loss with marginal erosions, subchondral cyst formation, and subluxations. Unlike psoriatic and reactive arthritis, there is a lack of bone formation. In the hand, the distribution primarily involves the MCPs, proximal interphalangeals, and carpal bones in a bilateral symmetric fashion. In the feet, the earliest erosive changes are seen along the lateral aspect of the fifth metatarsal heads. The other metatarsal heads demonstrate medial then lateral erosions. As the disease progresses, joint subluxations occur predominantly at the MCPs. Hand involvement precedes involvement of the feet in the vast majority of patients.
- **Crystalline arthropathy.** Calcium pyrophosphate dehydrate (CPPD) arthropathy is the most common crystalline arthropathy. The radiographic appearance resembles osteoarthropathy. Symmetric joint space narrowing, subchondral cysts, and osteophytes may be present, but unlike RA, erosions are absent. In the hand, the arthropathy is usually confined to the MCP joints. Chondrocalcinosis is often present, most frequently in the triangular fibrocartilage of the wrist. Gout is a crystalline arthropathy that involves primarily the hands and feet. The distribution is sporadic, and bilateral involvement, when present, is asymmetric. Unlike RA, the erosions in gout demonstrate sclerotic borders with characteristic overhanging edges. Soft tissue tophi occur in chronic disease. Bony mineralization is usually normal.
- **Collagen vascular disease (systemic lupus erythematosus [SLE]).** Radiographic findings of SLE include juxta-articular osteopenia, joint space narrowing, and joint subluxations. Unlike RA, erosions are typically not present.

Additional Differential Diagnoses

- **Hemochromatosis.** In hemochromatosis, there is a predilection for the second and third MCP joints in the hands with subchondral cysts and hooked osteophytes. Bony mineralization is preserved, and there are no erosions. As in CPPD arthropathy, chondrocalcinosis may be present.
- **Osteoarthritis.** Osteoarthritis is classically a distal arthropathy, affecting primarily the interphalangeal joints. Proximal involvement is seen at the first carpometacarpal joint. Radiographic findings include nonuniform joint space loss with subchondral sclerosis and osteophyte formation.

Diagnosis

Rheumatoid arthritis

✓ Pearls

- RA demonstrates uniform joint space loss, marginal erosions, and subchondral cysts.
- Erosions in gout demonstrate sclerotic borders, often with overhanging edges; tophi may also be present.
- SLE demonstrates periarticular osteopenia, joint space narrowing, and subluxations without erosions.
- Hemochromatosis results in joint space narrowing, hooked osteophytes, and chondrocalcinosis.

Suggested Readings

Brower AC, Flemming DJ. Arthritis: in Black and White. 2nd ed. Philadelphia: WB Saunders; 1997

Gupta KB, Duryea J, Weissman B. Radiographic evaluation of osteoarthritis. Radiol Clin North Am 2004;42:11–41

Case 82

Michael A. Tall

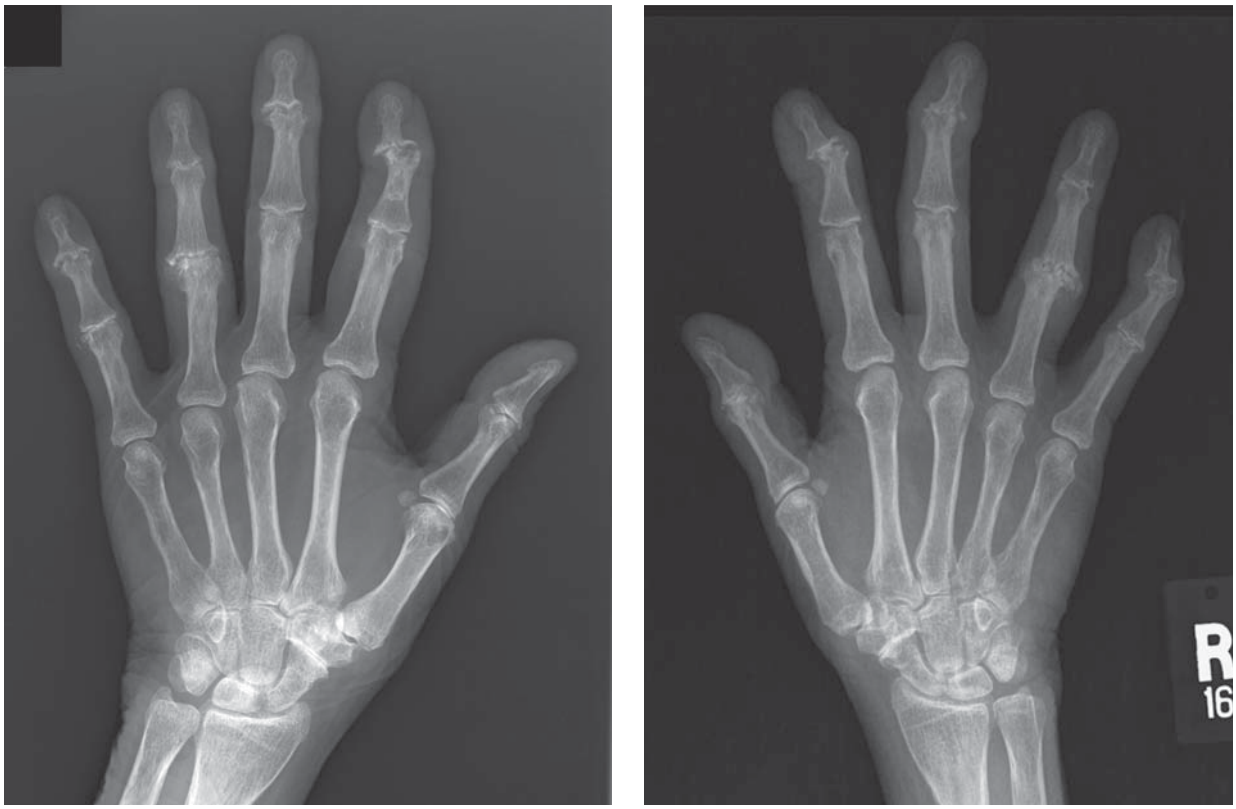


Fig. 82.1 **(A,B)** Frontal radiographs of the hands demonstrate bilateral symmetric joint space narrowing, irregularity, subchondral sclerosis, osteophytosis, and central erosions involving the proximal and distal interphalangeal joints. Bony mineralization is preserved.

Clinical Presentation

A 71-year-old woman presents with a history of long-standing bilateral hand and finger pain (**Fig. 82.1**).

Key Imaging Finding

Distal arthropathy affecting primarily the interphalangeal joints

Top 3 Differential Diagnoses

- **Osteoarthritis.** Multiple joint involvement of the distal and proximal interphalangeal (DIP and PIP) joints is characteristic of osteoarthritis. There is nonuniform joint space loss with subchondral sclerosis and osteophyte development in the areas of greatest cartilage loss. The soft tissue swelling around the DIP joint associated with osteophyte formation is called a Heberdon's node, and that around the PIP joint is called a Bouchard node. Erosion and anklylosis, manifestations of inflammatory disease, are not present.
- **Erosive osteoarthritis.** Erosive (inflammatory) arthritis most commonly affects the hands of postmenopausal women, particularly the DIP and PIP joints. The metacarpophalangeal (MCP) joints and large joints such as the shoulder hips and knees are rarely reported. The distribution is nearly identical to noninflammatory osteoarthropathy. The central erosions that are most commonly seen in the interphalangeal joints are characteristic of erosive osteoarthritis. Ankylosis of the joints may also occur. The exact relationship between erosive osteoarthritis and other arthropathies is controversial. Various investigators consider erosive osteoarthritis as an extension of noninflammatory osteoarthropathy, some consider it a separate disease entity, and others believe that it is an interface between noninflammatory osteoarthropathy and rheumatoid arthritis. Clinically, erosive osteoarthritis is characterized by acute inflammatory episodes, including swelling, erythema, pain, and loss of function.
- **Psoriatic arthritis.** The hands are most commonly involved in psoriatic arthritis. Erosions occur initially at the margins of the joint but eventually progress to involve the entire joint. The ends of the bones may become pointed and saucerized and give the classic "pencil in cup" appearance. Bony mineralization is usually preserved even with severe erosive disease. Bone proliferation is one of the most important features of psoriatic arthritis and is almost always present in some form.

Additional Differential Diagnoses

- **Reactive arthritis.** Lower extremity involvement is more common. Upper extremity involvement, when present, typically occurs in the hands. The specific radiographic changes are essentially identical to psoriatic arthritis, with erosive changes and new bone formation. This is often limited to just one joint. The PIP joints are more frequently involved than the DIPs or MCPs.
- **Rheumatoid arthritis.** The common radiographic manifestations consist of periarticular osteopenia progressing to generalized osteoporosis, uniform joint space loss with marginal erosions, subchondral cyst formation, and subluxations. Unlike psoriatic and reactive arthritis, there is a lack of bone formation. The distribution primarily involves the PIPs, MCPs, and carpal bones in a primarily symmetric fashion.

Diagnosis

Erosive osteoarthritis

✓ Pearls

- The hallmarks of osteoarthritis are joint space narrowing, sclerosis, and osteophyte formation.
- Central erosions ("gull wing" appearance) in the interphalangeal joints are characteristic of erosive osteoarthropathy.
- Marginal erosions and new bone formation are characteristic of reactive and psoriatic arthropathy.
- Advanced psoriatic arthritis may result in the classic "pencil in cup" deformity in the phalanges.

Suggested Readings

Brower AC, Flemming DJ. Arthritis: in Black and White; 2nd ed. Philadelphia: WB Saunders; 1997

Gupta KB, Duryea J, Weissman B. Radiographic evaluation of osteoarthritis. Radiol Clin North Am 2004;42:11–41

Case 83

Michael A. Tall



Fig. 83.1 Frontal radiograph of the right foot demonstrates multiple erosions at the first through fourth metatarsophalangeal (MTP) joints. The more prominent erosions have sclerotic borders and overhanging edges. There is soft tissue prominence consistent with a tophus along the medial aspect of the first MTP joint.

Clinical Presentation

A 72-year-old man presents with a several-year history of foot pain that is most pronounced at the hallux or big toe (**Fig. 83.1**).

Key Imaging Finding

Erosive arthropathy involving the foot

Top 3 Differential Diagnoses

- **Rheumatoid arthritis (RA).** RA is characterized by bilateral symmetric distribution, uniform proximal joint space narrowing, periarticular osteopenia, marginal erosions, and joint subluxation. The feet are involved in 80 to 90% of cases and usually lag behind the findings in the hands. The lateral aspect of the fifth metatarsal heads is often the earliest site of involvement, with subsequent involvement of nearly all metatarsophalangeal (MTP) joints. Retrocalcaneus bursitis with erosions and Achilles tendinitis are also common findings.
- **Gout.** Gouty arthritis is caused by the accumulation of sodium monourate crystals. It most commonly affects older men. Characteristic radiographic findings include well-defined, punched out erosions often with a sclerotic border and overhanging edges, along with soft tissue tophi. Bone mineralization is usually normal, and joint spaces are preserved until late in the disease. The distribution is typically polyarticular and asymmetric. The first MTP is the most common joint involved, and gout located here is referred to as podagra.
- **Reactive arthritis.** Early in the disease process, juxta-articular osteoporosis predominates. This may affect only a single joint. Normal bony mineralization may return. As the disease progresses, multiple joints are affected, with uniform joint space narrowing, marginal erosions, and adjacent bone proliferation. Eventually, ankylosis may occur; however, it does not occur as frequently as in psoriatic arthritis. Fluffy periostitis and erosions are also commonly seen along the posterosuperior aspect of the calcaneus.

Additional Differential Diagnoses

- **Infection.** Septic arthritis may be secondary to direct inoculation or hematogenous spread. Early in the disease process, the periarticular bone becomes osteopenic. As the infection progresses, uniform joint space narrowing occurs, with periarticular osseous destruction, subluxation, and soft tissue swelling. Patients often present with clinical signs and symptoms of infection; diagnosis is confirmed with joint aspiration. With delay in treatment, significant joint destruction may occur. Osteomyelitis is a known complication.
- **Psoriatic arthritis.** The hands are most commonly involved in psoriatic arthritis, but occasionally the feet may be involved as well. Marginal erosions coupled with bony proliferation are the hallmarks of the disease. Erosive changes may become so severe that they result in tapering of the distal aspects of the phalanges with sauceriza-tion of the articulating bone, referred to as the "pencil in cup" deformity. Diffuse soft tissue swelling of an entire digit may also occur, which is referred to as a "sausage digit" deformity. Ankylosis occurs relatively frequently. In addition to the proximal interphalangeal joints and, less commonly, the MTP joints, psoriatic arthritis may involve the posterosuperior aspect of the calcaneus with fluffy periostitis and erosions.

Diagnosis

Gout

✓ Pearls

- The first MTP is the most commonly affected joint, and gout located here is referred to as podagra.
- Bony mineralization is normal, and the joint spaces are generally preserved until late in the course of gout.
- RA has symmetric joint space narrowing, marginal erosions, and periarticular osteopenia.
- Reactive arthritis involves the feet, with joint space narrowing, marginal erosions, and bony proliferation.

Suggested Readings

Brower AC, Flemming DJ. Arthritis: in Black and White. 2nd ed. Philadelphia: WB Saunders; 1997

Monu JU, Pope TL Jr. Gout: a clinical and radiologic review. Radiol Clin North Am 2004;42:169–184

Case 84

Adrianne K. Thompson



Fig. 84.1 Frontal radiograph of the knee demonstrates linear calcifications projecting over the medial and lateral compartments, consistent with chondrocalcinosis.

Clinical Presentation

A 45-year-old man presents with chronic knee pain (**Fig. 84.1**).

Key Imaging Finding

Chondrocalcinosis

Top 3 Differential Diagnoses

- **Calcium pyrophosphate dehydrate (CPPD) arthropathy.** Chondrocalcinosis refers to abnormal calcification within cartilage. One of the most common conditions to cause chondrocalcinosis is CPPD arthropathy, in which calcium pyrophosphate crystals are deposited in and around joints. CPPD crystal deposition can occur within the cartilage, synovium, and joint capsule, as well as ligaments, tendons, and bursae. It most commonly affects the knees, wrists, and pubic symphysis, but it also may affect intervertebral disks, hips, and shoulders. It differs from osteoarthropathy in that it affects atypical joints and occurs in atypical distributions. Isolated or disproportionate patellofemoral involvement is highly suggestive of CPPD. When seen in the wrist, it displays a predilection for the radiocarpal joint space and can lead to development of scapholunate advanced collapse (SLAC) wrist. Calcification of the triangular fibrocartilage is characteristic.
- **Hyperparathyroidism.** Hyperparathyroidism refers to an underlying metabolic condition with abnormally high parathyroid hormone. Primary hyperparathyroidism results from disease of the parathyroid glands themselves, such as an adenoma, hyperplasia, or, rarely, carcinoma. Secondary hyperparathyroidism is usually the result of ongoing hypocalcemia, most commonly due to chronic renal failure. Lastly, tertiary hyperparathyroidism occurs when the parathyroid glands develop autonomous function after long-standing secondary hyperparathyroidism. Primary hyperparathyroidism is most associated with chondrocalcinosis when calcium pyrophosphate crystals deposit in joints. Other bony findings seen with primary hyperparathyroidism are subperiosteal/subchondral/subligamentous bone resorption and brown tumors.
- **Hemochromatosis.** Primary hemochromatosis is a genetic disorder that leads to iron deposition and secondary organ and tissue damage. Both hemosiderin granules and CPPD crystals accumulate in the joints abnormally. Chondrocalcinosis is seen in up to 30% of patients in the usual sites—knees, wrists, pubic symphysis, and intervertebral disks. It also is seen in atypical joints, most commonly affecting the metacarpophalangeal (MCP) joints, midcarpal/radiocarpal joints of the wrists, elbow, and glenohumeral joints. "Beaklike" osteophytes of the metacarpal heads are a characteristic feature, but they can also be seen in CPPD arthropathy. Hemochromatosis tends to affect all MCP joints, whereas CPPD tends to spare the fourth and fifth joints.

Additional Differential Diagnoses

- **Wilson disease.** Wilson disease results in abnormal copper accumulation in the body, with end-organ clinical manifestations seen in the basal ganglia of the brain, liver (resulting in cirrhosis), and cornea (Kayser-Fleischer rings). It is more commonly seen in boys and men between the ages of 5 and 40. Hepatic disease is typically the first to manifest. Joint disease is seen in ~50% of adult patients. Common sites of involvement are the MCP joints of the hands, as well as the wrists, elbows, shoulders, hips, and knees. Wilson arthropathy resembles CPPD and hemochromatosis, with chondrocalcinosis as a prominent feature.

Diagnosis

CPPD arthropathy

✓ Pearls

- CPPD results in disproportionate patellofemoral degenerative changes and SLAC wrist deformity.
- Hyperparathyroidism may result in chondrocalcinosis, subperiosteal bone resorption, and brown tumors.
- "Beaklike" osteophytes in the metacarpal heads may indicate hemochromatosis.
- "Beaklike" osteophytes may also be present in CPPD arthropathy, but they often spare the fourth and fifth joints.

Suggested Readings

Resnick D. Bone and Joint Imaging. 2nd ed. Philadelphia: WB Saunders; 1996

Case 85

Eva Escobedo

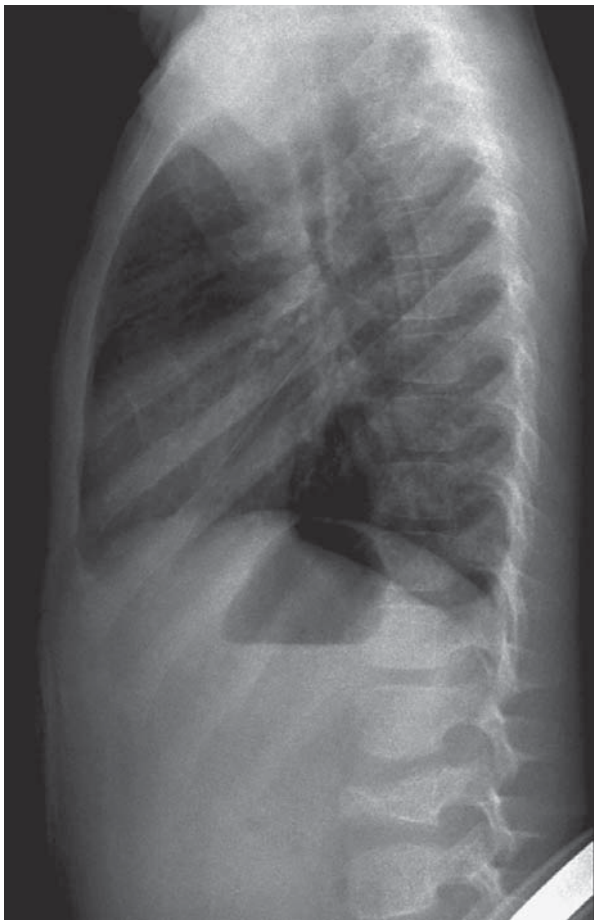


Fig. 85.1 Lateral radiograph of the chest shows marked flattening of the L3 vertebral body with preservation of the disk spaces and alignment, consistent with vertebra plana.

Clinical Presentation

Incidental finding on chest radiograph of a 12-year-old boy (**Fig. 85.1**).

Key Imaging Finding

Vertebra plana in a child

Top 3 Differential Diagnoses

- **Langerhans cell histiocytosis (LCH).** LCH is a group of idiopathic disorders characterized by the proliferation of Langerhans cells and mature eosinophils. It is by far the most common cause of vertebra plana in children. It most commonly occurs at a single site, but it can also occur at multiple levels. Compression may be progressive and rapid. More often, LCH manifests as a lytic lesion rather than vertebra plana. Bone lesions, especially with the eosinophilic granuloma form of LCH, may be asymptomatic.
- **Leukemia/lymphoma.** Leukemia is the most common pediatric primary malignancy. Loss of vertebral height and increased sclerosis are common findings in the vertebral body. Secondary lymphoma is much more common than primary lymphoma in the pediatric spine and presents in a similar manner. Constitutional symptoms and involvement of multiple levels is seen more commonly with these diseases, as opposed to LCH, which more commonly involves a single level.
- **Osteomyelitis.** Both bacterial and granulomatous (tuberculosis [TB]) infection can present as vertebra plana. It has also been reported with chronic recurrent multifocal osteomyelitis, which is more likely inflammatory rather than a true infection. Bacterial infection commonly involves the intervertebral disk, with disk destruction and vertebral body end-plate erosions. TB spondylitis, in contrast, more commonly results in predominant bone destruction with relative disk preservation, which can manifest as vertebra plana. However, some form of vertebral end-plate irregularity, sclerosis, or destruction is usually present.

Additional Differential Diagnoses

- **Metastases.** Neuroblastoma is the third most common primary malignancy in children and can metastasize to any bone. Peak age incidence for neuroblastoma is 2 to 3 years. Radiographic presentation of neuroblastoma metastases to the spine is similar to leukemia/lymphoma with multilevel involvement.

Diagnosis

Langerhans cell histiocytosis

✓ Pearls

- LCH is the most common cause of vertebra plana in children.
- The most common osseous manifestation of LCH is a lytic lesion.
- Leukemia or lymphoma may present with multiple levels of vertebral body collapse and sclerosis.
- TB may demonstrate predominant bone destruction with relative preservation of the disk space.

Suggested Readings

Chang MC, Wu HT, Lee CH, Liu CL, Chen TH. Tuberculous spondylitis and pyogenic spondylitis. Spine 2006;31(7):782–788

Greenlee JDW, Fenoy AJ, Donovan KA, Menezes AH. Eosinophilic granuloma in the pediatric spine. Pediatr Neurosurg 2007;43:285–292

Kilborn TN, The J, Goodman TR. Paediatric manifestations of Langerhans cell histiocytosis: a review of the clinical and radiological findings. Clin Radiol 2003;58:269–278

Kriss VM. My aching back: a serious complaint in children. Curr Probl Diagn Radiol 2001;30:23–30

Wei MA, Ruixue MA. Solitary spinal eosinophilic granuloma in children. J Pediatr Orthop B 2006;15:316–319

Case 86

Philip Granchi

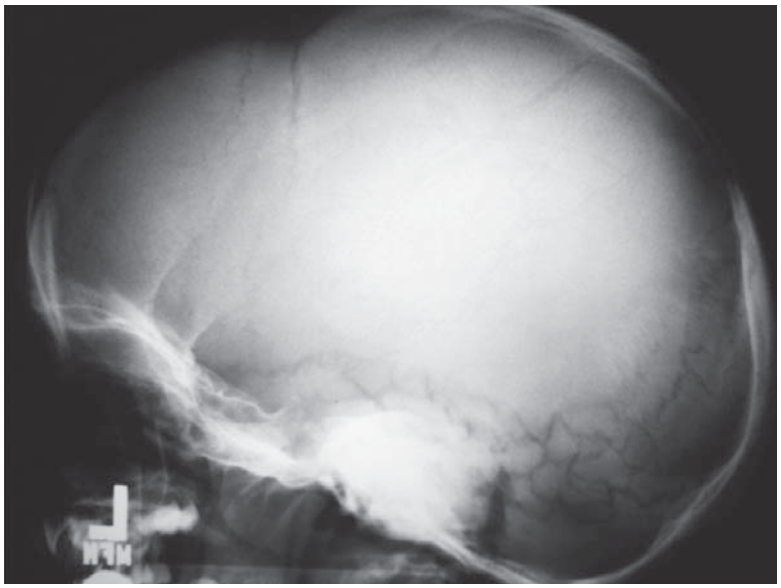


Fig. 86.1 Lateral skull radiograph reveals intrasutural ossification (wormian bones) involving the squamosal and lambdoid sutures.

Clinical Presentation

A child presents with facial abnormalities (**Fig. 86.1**).

Key Imaging Finding

Wormian bones

Top 3 Differential Diagnoses

- **Idiopathic.** The term *wormian bones* is a descriptive designation for irregular ossicles located within the calvarium. Idiopathic wormian bones are reported to be smaller and less numerous than those associated with an identifiable skeletal dysplasia, although no hard and fast criteria exist for this determination. Most commonly located within the lambdoid suture (50%), wormian bones may also occur in the coronal suture (25%) and have been identified in all cranial sutures and fontanelles. Unfortunately, arriving at a definitive diagnosis radiographically will often require multiple additional images to assess for the wide spectrum of entities that can encompass wormian bones.
- **Osteogenesis imperfecta (OI).** Wormian bones in OI may be numerous and demonstrate a mosaic ("crazy paving") pattern. Patients with OI will also have a history of multiple, repetitive fractures of varying ages that can cause deformity, such as thickening of the tubular bones.
- **Cleidocranial dysostosis.** A defect in the formation of membranous bones, cleidocranial dysostosis is a genetic disorder that leads to findings of a small face, enlarged head, and hypertelorism. Wormian bones are one part of a radiographic constellation of findings that include delayed closure of sutures and fontanelles, absence or hypoplasia of the clavicles, widened symphysis pubis, and coxa vara dysplasia of the femoral neck.

Additional Differential Diagnoses

- **Down syndrome.** Down syndrome (trisomy 21) is the most common genetic cause of mental impairment in children and has been associated with an increased incidence with advanced maternal age (>35 years of age). Several radiographic findings are associated with Down syndrome, including wormian bones. Additional classic findings are a hypoplastic arch of C1, atlantoaxial subluxation, absent 12th rib, short tubular bones of the hands (including clinodactyly of the middle phalanx of the little finger), wide iliac wings, hip dysplasia, and patellar dislocation.
- **Metabolic disease (hypothyroidism, rickets).** Wormian bones may be found in patients with multiple metabolic deficiencies. In rickets, wormian bones are associated with the healing phase of the deficiency. Early findings include frayed physes and flaring (cupping) of the metaphyses. Hypothyroidism is characterized by markedly delayed skeletal maturity, "bullet" vertebrae at the thoracolumbar junction, and fragmentation of the epiphyses. Hypophosphatasia, a rare genetic defect of alkaline phosphatase, leads to rickets in the absence of dietary deficiency.

Diagnosis

Cleidocranial dysostosis

✓ Pearls

- Wormian bones may be idiopathic in etiology, with the lambdoid suture most commonly involved.
- Wormian bones in OI may be numerous and demonstrate a mosaic pattern.
- Cleidocranial dysostosis presents with wormian bones and absence or hypoplasia of the clavicles.
- Wormian bones may be found in patients with multiple metabolic deficiencies.

Suggested Readings

Jeanty P, Silva SR, Turner C. Prenatal diagnosis of wormian bones. J Ultrasound Med 2000;19:863–869

Manaster BJ, May DA, Disler DG. Musculoskeletal Imaging: The Requisites. 3rd ed Philadelphia: Mosby Elsevier; 2007

Paterson CR. Radiological features of the brittle bone diseases. J Diagn Radiogr Imaging 2003;5:39–45

Case 87

Michael A. Tall



Fig. 87.1 Frontal radiograph of the wrist demonstrates a triangular configuration of the distal radius and ulna articulation with wedging of the proximal carpal bones between the distal radius and ulna, referred to as the Madelung deformity.

Clinical Presentation

A 15-year-old female patient presents with bilateral wrist pain and weakness (**Fig. 87.1**).

Key Imaging Finding

Madelung deformity

Top 3 Differential Diagnoses

- **Idiopathic Madelung deformity.** Idiopathic Madelung deformity often clinically manifests in young adulthood or adolescence and can present with visible deformity, pain, weakness, and limited range of motion. Radiographic findings consist of a widened distance between the distal radius and ulna, a decreased carpal angle, a triangular radial epiphysis, an ulna that is elongated relative to the radius, and wedging of the carpal bones between the distal radius and the ulna. The isolated form of Madelung deformity is typically bilateral, asymmetric, and more common in women.
- **Turner syndrome.** Turner syndrome occurs in females with a 45/XO chromosome complement. The most common radiographic manifestations of the wrists and hands are osteopenia, shortening of the metacarpal bones (particularly the fourth metacarpal bone), and decreased carpal angles, which resemble Madelung deformities. The abnormality is most commonly bilateral.
- **Skeletal dysplasia.** Dysplastic bone disorders associated with Madelung deformities include multiple enchondromatosis (Ollier disease), hereditary multiple exostoses, mucopolysaccharidoses, multiple epiphyseal dysplasia, and dyschondrosteosis. The deformities are usually bilateral, mimicking idiopathic Madelung deformity, and are the result of asymmetric growth along the distal radius and ulna growth plates.

Additional Differential Diagnoses

- **Trauma.** Severe trauma to the distal radius and ulna can result in osseous deformities and altered joint mechanics upon healing, especially in the setting of open physes. The Madelung deformity occurs when the medial joint space of the distal radius fuses after trauma while the lateral joint space continues to grow.
- **Infection.** Similar to trauma, a joint infection may result in abnormal fusion of a portion of the distal radius and ulna growth plates, resulting in osseous deformities and altered joint mechanics. The Madelung deformity occurs when the medial joint space of the distal radius fuses while the lateral joint space continues to grow.

Diagnosis

Idiopathic Madelung deformity

✓ Pearls

- The isolated form of Madelung deformity is typically bilateral, asymmetric, and more common in women.
- Osteopenia, short metacarpals, and decreased carpal angles are seen in Turner syndrome.
- Bilateral Madelung deformities may be present in several skeletal dysplasias.
- Trauma and infection are two common causes of a unilateral Madelung deformity.

Suggested Readings

Peh WC. Madelung's deformity. Am J Orthop 2001;30(6):512

Resnick D, Kransforf MJ. Bone and Joint Imaging. 3rd ed. Philadelphia: Elsevier Saunders; 2005

Schmidt-Rohlfing B, Schwöbel B, Pauschert R, Niethard FU. Madelung deformity: clinical features, therapy and results. J Pediatr Orthop B 2001;10(4):344–348

Case 88

Sonia Kaur Ghei



Fig. 88.1 Frontal radiograph of the left knee demonstrates metaphyseal lucent bands most prominent along the distal femur. Periosteal reaction is also seen along the distal femoral diaphysis/metadiaphysis.

Clinical Presentation

A 4-year-old boy presents with leg pain (**Fig. 88.1**).

Key Imaging Finding

Lucent metaphyseal bands

Top 3 Differential Diagnoses

- **Leukemia.** Leukemia is the most common malignancy of childhood, with a peak age of 2 to 5 years. Acute lymphoblastic leukemia (ALL) is the most common subtype. Skeletal findings include transverse lucent metaphyseal bands ("leukemic lines") and periosteal new bone formation secondary to subperiosteal infiltration of leukemic cells. This can also be demonstrated on T1 as low-intensity leukemic infiltrate replacing high-intensity marrow fat. Although several entities cause metaphyseal lucencies (see discussion below), leukemia more often presents over the age of 2.
- **Rickets.** Rickets occurs secondary to vitamin D deficiency, which prevents calcification of cartilage and osteoid. Radiographic findings include widening of the physis with cupping and fraying of the distal metaphysis. Looser zones are rarely seen today but describe linear lucencies perpendicular to the cortex. Rachitic rosary is caused by cartilage overgrowth and metaphyseal splaying at the costochondral junctions.
- **Osteomyelitis.** Acute osteomyelitis primarily affects the metaphysis due to slow-flowing venous sinusoids in this location. Although this can occur at any age, one third of cases present under the age of 2. Bone changes include subperiosteal absorption and scalloping, creating ill-defined asymmetric lucencies that may progress to destruction and periosteal new bone formation. Spread of the organism through the growth plate and joints may occur prior to 12 to 18 months of age.

Additional Differential Diagnoses

- **Neuroblastoma metastases.** Neuroblastoma is the third most common childhood malignancy, with at least two thirds of patients presenting with disseminated disease. Metastatic lesions to bone are asymmetric and are usually lytic and permeative, often located in the metaphysis.
- **Scurvy.** Scurvy is caused by vitamin C deficiency and usually occurs in children younger than 2 years of age. Findings include demineralization and lucent bands adjacent to a thickened zone of provisional calcification (ZPC), known as the scurvy line or "zone of Frankel." Subperiosteal hemorrhage and fractures result in periosteal new bone formation and metaphyseal spurs (corner sign, or "Perlkan spur"). The epiphysis is osteopenic with dense peripheral ZPC, which results in a prominent ring, known as the Wimberger ring.
- **Syphilis.** In syphilis, bilateral and symmetric metaphyseal lucent bands occur adjacent to a dense band in the subphyseal region. Focal lytic destructive lesions may occur, and bilateral upper medial tibial destruction is known as the (other) Wimberger sign, but this may also occur in other entities, such as osteomyelitis and hyperparathyroidism. Pathologic fractures and periosteal new bone formation occur, in both the metaphyses and the diaphyses. Saber shin deformity describes thickening of the anterior tibial cortex during healing.

Diagnosis

Leukemia (ALL)

✓ Pearls

- Transverse lucent metaphyseal bands and periosteal new bone formation may indicate acute leukemia.
- Rickets may demonstrate widening of the physes and "cupping" of the distal metaphyses.
- "Rachitic rosary" is cartilaginous overgrowth and metaphyseal splaying at the costochondral junctions.
- Acute osteomyelitis often initially affects the metaphyses due to slow-flowing venous sinusoids.

Suggested Readings

Blickman H. Pediatric Radiology: The Requisites. 2nd ed. St. Louis, MO: Mosby; 1998

Case 89

William T. O'Brien Sr.

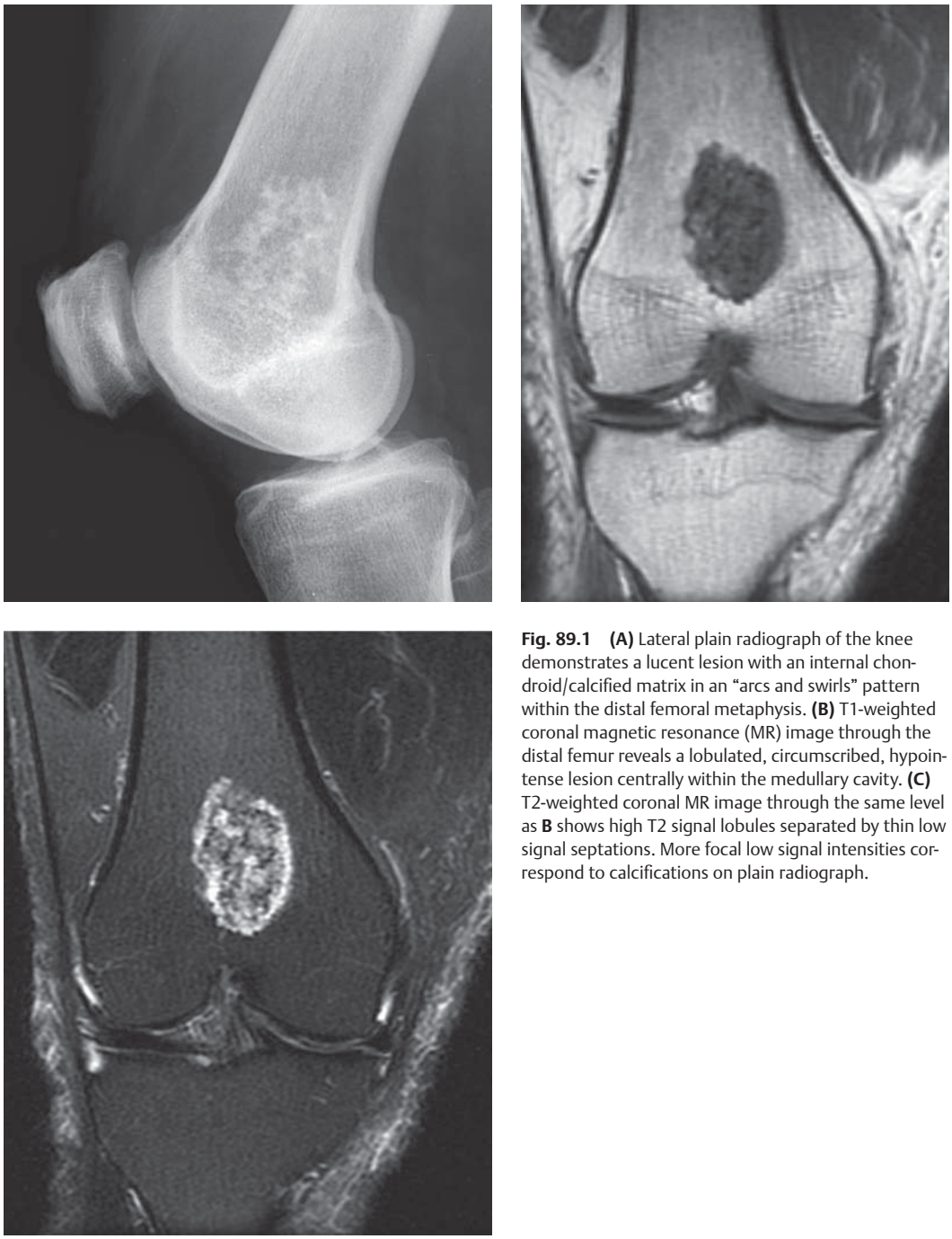


Fig. 89.1 **(A)** Lateral plain radiograph of the knee demonstrates a lucent lesion with an internal chondroid/calcified matrix in an "arcs and swirls" pattern within the distal femoral metaphysis. **(B)** T1-weighted coronal magnetic resonance (MR) image through the distal femur reveals a lobulated, circumscribed, hypointense lesion centrally within the medullary cavity. **(C)** T2-weighted coronal MR image through the same level as **B** shows high T2 signal lobules separated by thin low signal septations. More focal low signal intensities correspond to calcifications on plain radiograph.

Clinical Presentation

A 52-year-old man presents with chronic knee pain with activity (**Fig. 89.1**).

Key Imaging Finding

Medullary/chondroid lesion

Top 3 Differential Diagnoses

- **Enchondroma.** Enchondromas are benign chondroid lesions that contain a calcium matrix with a characteristic "arcs and swirls" pattern, except when they are located in the phalanges, in which they will appear purely lucent. They are typically located centrally within the medullary cavity but less commonly may be eccentric. The proximal humerus, distal femur, proximal tibia, and phalanges are among the most common sites of involvement. On magnetic resonance imaging (MRI), enchondromas are composed of high T2 signal intensity lobules with thin intervening low T2 signal intensity septations. Internal calcifications are typically low signal on T1- and T2-weighted sequences. On T1-weighted sequences, enchondromas are characteristically low in signal intensity. Postgadolinium, the lesions will internally enhance in an "arcs and swirls" pattern.
- **Bone infarct.** Although some bone infarcts are idiopathic, the vast majority of patients have an underlying risk factor, including trauma, sickle cell disease, corticosteroid use, glycogen storage disease, alcoholism, and dyslipidemia. On plain radiographs, bone infarcts may simulate enchondromas with ill-defined patchy regions of sclerosis and lucency. More characteristically, bone infarcts will consist of a serpentine rim of calcification or demonstrate a "bone within bone" appearance. On MRI, bone infarcts present as geographic medullary lesions with central fat (bright on T1) and a margin that is hypointense on both T1- and T2-weighted sequences. Mixed internal signal intensity is due to fibrosis and calcification.
- **Chondrosarcoma.** Chondrosarcomas (especially low grade) have a similar imaging appearance to that of enchondromas, and often it is impossible to distinguish between the two based on imaging alone. Findings that would suggest chondrosarcoma include size > 6 cm, rapid growth, cortical breakthrough, deep endosteal scalloping (more than two thirds of the overlying cortex), and, most importantly, pain.

Additional Differential Diagnoses

- **Chronic osteomyelitis.** Chronic intramedullary infection typically presents on plain radiographs with sclerotic margins and endosteal thickening. A sclerotic sequestrum, which consists of isolated necrotic bone, is commonly seen. On MRI, these lesions will be internally hypointense on T1-weighted sequences and hyperintense on T2-weighted sequences. The sequestrum will be low signal on both T1- and T2-weighted sequences. Postcontrast images demonstrate rim enhancement, as well as regions of enhancing granulation tissue. Secondary findings that suggest infection are marrow edema, subperiosteal fluid, and a sinus tract.

Diagnosis

Enchondroma

✓ Pearls

- Enchondromas are benign chondroid lesions with calcifications in an "arcs and swirls" pattern.
- Bone infarcts are geometric medullary lesions with a serpentine rim of calcification and fat centrally.
- Chondrosarcoma should be expected in the setting of pain or when malignant features are seen on imaging.
- Secondary findings that suggest chronic osteomyelitis are a sequestrum, marrow edema, and a sinus tract.

Suggested Readings

Kaplan PA, Helms CA, Dussault R, et al. Musculoskeletal MRI. New York: WB Saunders; 2001

Murphey MD, Flemming DJ, Boyea SR, ET AL. Enchondroma versus chondrosarcoma in the appendicular skeleton: differentiating features. Radiographics 1998;18:1213–1237

Skaggs DL, Kim SK, Greene NW, ET AL. Differentiation between bone infarction and acute osteomyelitis in children with sickle-cell disease with use of sequential radionuclide bone-marrow and bone scans. J Bone Joint Surg Am 2001;83-A:1810–1813

Case 90

William T. O'Brien Sr.



Fig. 90.1 Frontal plain radiograph of the left hand demonstrates resorption of all terminal phalangeal tufts (acro-osteolysis).

Clinical Presentation

A 32-year-old woman presents with chronic bilateral hand pain and ulcerations (**Fig. 90.1**).

Key Imaging Finding

Acro-osteolysis

Top 3 Differential Diagnoses

- **Hyperparathyroidism.** Hyperparathyroidism is a systemic abnormality of calcium homeostasis that can be primary (overproduction by the parathyroid glands), secondary (caused by renal failure or malabsorption), or tertiary (autonomous production by the parathyroid glands due to chronic renal failure or malabsorption). Subperiosteal resorption of bone, especially along the radial aspect of the second and third middle phalanges of the hands, is virtually diagnostic of hyperparathyroidism. Additional osseous abnormalities are resorption of the distal clavicles, bandlike osteosclerosis of the vertebral bodies referred to as "rugger jersey" spine, brown tumors, and resorption of the terminal phalanges.
- **Scleroderma.** Scleroderma is a systemic connective tissue disorder that results in characteristic musculoskeletal abnormalities that are most prominent in the hands. The most common manifestations are bony erosions and soft tissue resorption along the distal phalanges. Severe cases result in tapering or complete destruction of the distal phalanges (acro-osteolysis). Soft tissue calcifications are evident in ~10 to 30% of patients. CREST syndrome is a variant of scleroderma consisting of calcinosis, Raynaud phenomenon, esophageal dysmotility, sclerodactyly, and telangiectasia. Scleroderma also may produce pulmonary findings characterized by lower lobe interstitial fibrosis.
- **Trauma.** Thermal injury refers to either cold injury (frostbite) or burn injury. Both processes cause vascular occlusion and ischemia, resulting in soft tissue and osseous abnormalities. Osseous manifestations include osteoporosis, periostitis, and resorption of the distal phalanges. In the setting of frostbite, the findings are typically bilateral with sparing of the thumbs secondary to clenched fists, with the digits protecting the thumbs. Premature growth plate fusion is a complication in children.

Additional Differential Diagnoses

- **Psoriasis.** Psoriatic arthritis is a polyarticular arthritis with multiple variants. Although the distribution is variable, psoriasis has a predilection for the distal interphalangeal joints of the hands. Musculoskeletal involvement of the hand includes soft tissue swelling, periarticular erosions, "fluffy" periostitis, and resorption of the distal phalanges. Bone mineralization is usually normal. Classic radiographic findings are the "sausage digit" (diffuse soft tissue swelling) and the "pencil in cup" deformity from resorption and tapering of the distal aspect of the phalanges. Psoriasis may also involve the feet and sacroiliac joints.
- **Hajdu-Cheney syndrome.** Hajdu-Cheney is a rare syndrome that may occur sporadically or with an autosomal dominant familial inheritance. Patients have dysmorphic facies and cranial abnormalities, including an enlarged sella turcica, wormian bones, and basilar invagination. Hearing deficits and speech impediments are common. Osteolysis occurs within the distal phalanges of the hands and feet, with classic bandlike lucencies that isolate proximal and distal osseous fragments in the terminal tufts.

Diagnosis

Scleroderma

✓ Pearls

- Hyperparathyroidism results in radial-sided subperiosteal resorption of the second and third middle phalanges.
- Scleroderma may result in soft tissue resorption and calcifications with distal phalangeal acro-osteolysis.
- Thermal (burn and frostbite) injuries may manifest as osteoporosis, periostitis, and acro-osteolysis.
- Hajdu-Cheney is a rare syndrome with dysmorphic facies and bandlike acro-osteolysis.

Suggested Readings

Resnick D, Kransdorf MJ. Bone and Joint Imaging. 3rd ed. Philadelphia: Elsevier Saunders; 2005

Case 91

Philip Granchi



Fig. 91.1 Lateral view of the knee reveals a large, dense suprapatellar joint effusion. An ossific density along the posterior aspect of the tibial plateau represents a fracture fragment.

Clinical Presentation

A young male patient presents with knee pain (**Fig. 91.1**).

Key Imaging Finding

Dense joint effusion

Top 3 Differential Diagnoses

- **Hemarthrosis (hemophilia, posttraumatic).** A dense joint effusion is most commonly the result of traumatic hemarthrosis. When present, it is important to search for an underlying fracture or signs of internal derangement. Patients with hemophilia can suffer from hemarthrosis even after minor trauma. Long-term sequelae of multiple bouts of hemarthrosis include cartilage damage, subarticular cysts, osteopenia, and enlarged epiphyses. A widened intercondylar notch may be seen on plain radiographs, suggesting underlying hemophilia or chronic inflammatory process.
- **Juvenile chronic arthritis (JCA).** The radiographic appearance of JCA may be identical to that of hemophilia, because both entities cause inflammatory synovitis in skeletally immature patients. JCA, however, often has numerous other findings in multiple joints that allows for differentiation. Plain radiographs of the knee will show a joint effusion, periarticular erosions, osteopenia, enlarged epiphyses, and a widened intercondylar notch. Additional findings of JCA are erosions and ankylosis in the hands and wrists, erosions of the odontoid process, atlantoaxial subluxation, and erosions and ankylosis of the facet joints of the spine.
- **Pigmented villonodular synovitis (PVNS).** Occurring most commonly in the knee (80% of cases), PVNS is unchecked proliferation of synovium that may be accompanied by hemorrhagic effusions. Large subchondral cysts and erosions with preservation of joint space are characteristic. Treatment is surgical synovectomy. When found in tendon sheaths, the disease is termed giant cell tumor of the tendon sheath.

Additional Differential Diagnoses

- **Septic arthritis.** Septic arthritis most commonly occurs in the pediatric and young adult population and typically presents with a joint effusion, pain, and fever. Common organisms include *Staphylococcus aureus* and *Neisseria gonorrhea.* Erosion of adjacent bones, along with a joint effusion, may provide a hint for septic arthritis, especially in later stages. If suspicion exists of a septic hip in a child, ultrasound is the study of choice. Urgent orthopedic consultation is mandated due to the risk of joint destruction.
- **Crystalline arthropathy (gout, calcium pyrophosphate dehydrate [CPPD]).** Crystalline arthropathies such as gout and CPPD occur most commonly in older men and can affect one or multiple joints. When large joints are affected, patients commonly present with a joint effusion. Tophi and erosions with sclerotic overhanging margins are hallmarks of gout but may not always be present. CPPD is associated with hemochromatosis and hyperparathyroidism. Chondrocalcinosis is a common finding, especially in the knees and wrists.

Diagnosis

Hemarthrosis secondary to trauma

✓ Pearls

- Hemarthrosis secondary to trauma should elicit a search for intra-articular extension of a fracture.
- A widened intercondylar notch with a dense effusion may be present in both hemophilia and JCA.
- Hallmarks of PVNS are a joint effusion with subchondral cysts, erosions, and preservation of the joint.
- Septic arthritis typically presents with a joint effusion, pain, and fever; urgent management is indicated.

Suggested Readings

Brower AC, Flemming DJ. Arthritis: in Black and White. 2nd ed. Philadelphia: WB Saunders; 1997

Durr HR, Stabler A, Maier M, .et al Pigmented villonodular synovitis: review of 20 cases. J Rheumatol 2001;28:1620–1630

Manaster BJ, May DA, Disler DG. Musculoskeletal Imaging, The Requisites. 3rd ed. Philadelphia: Mosby Elsevier; 2007

Case 92

M. Jason Akers





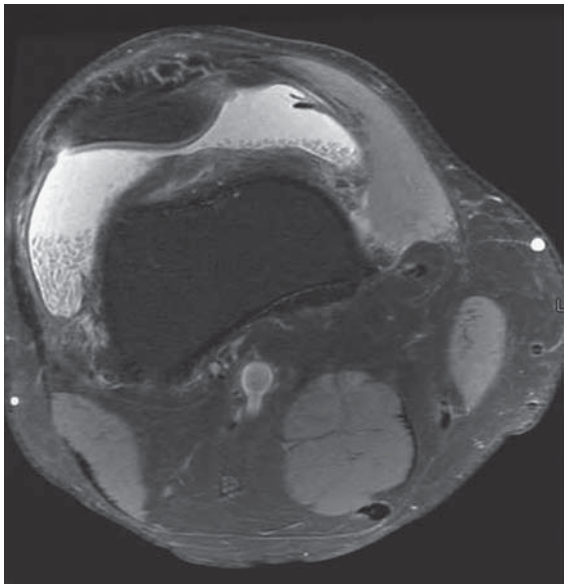


Fig. 92.1 **(A)** Sagittal T2 fat-suppressed, **(B)** sagittal T1, and **(C)** axial T2 fat-suppressed images through the knee show multiple tiny intermediate signal lesions within the suprapatellar bursa and lateral joint recess.

Clinical Presentation

A 54-year-old man presents with knee pain and swelling (**Fig. 92.1**).

Key Imaging Finding

Loose bodies with erosions

Top 3 Differential Diagnoses

- **Synovial (osteo)chondromatosis.** Synovial (osteo)chondromatosis is a disease of the synovium resulting from synovial metaplasia, the cause of which is unknown. It is seen in men between the ages of 20 and 50 and is most commonly intra-articular, but it may also occur in tendon sheaths and bursae. Occasionally, conglomerate masses may extend into the extracapsular soft tissues. The disease is typically monoarticular, with the knee, elbow, shoulder, and hip joints most commonly involved. Synovial metaplasia results in the formation of synovial villonodular projections that grow to form nodules. If the nodules remain attached to the synovium, they develop a blood supply and may become ossified. If the nodules break off, they are nourished by synovial fluid and become cartilaginous. Eighty-five percent of cases have sufficient calcification to be detected on radiographs, appearing as multiple, round, similar-sized calcified bodies. The bodies are of variable magnetic resonance (MR) signal depending on the proportion of calcium, chondroid, and mature ossific tissue, ranging from low signal on all sequences to marrow signal on all sequences. Mechanical articular cartilage destruction results in well-marginated erosions. The nodules may continue to grow but typically do not exceed 3 cm in size. Malignant degeneration is rare. Treatment is resection of the bodies along with synovectomy. Recurrences after surgical débridement can occur.
- **Pigmented villonodular synovitis (PVNS).** PVNS is a benign neoplastic process of the synovium. It can occur intra-articularly and involve the joint diffusely or focally. It may also occur extra-articularly in a bursa or tendon sheath (giant cell tumor of the tendon sheath). The intra-articular form is characterized by villonodular proliferation of the synovium with associated hemorrhage. It is monoarticular with common locations including the knee and hip joints. On radiographs, PVNS manifests as a large joint effusion with or without associated erosions and subchondral cysts. Joint spaces are usually preserved. Magnetic resonance imaging (MRI) shows a joint effusion and focal or diffuse synovial thickening that is low signal on T1 and T2 due to hemosiderin deposition. The hemosiderin causes susceptibility artifact and subsequent blooming on gradient echo sequences. Treatment is synovectomy; incomplete resection is associated with high recurrence rates.
- **Rheumatoid arthritis (RA).** Multiple small, loose bodies can occur within joints affected by RA and are termed "rice bodies" due to their resemblance to polished grains of rice. Rice bodies are small fragments of fibrous tissue that occur as a nonspecific response to synovial inflammation. The exact cause is unknown, but one theory postulates that rice bodies represent detached fragments of infarcted synovium. First described in association with tuberculous arthritis, rice bodies are now more frequently associated with RA. Previous MRI reports have shown involvement of only the shoulder and knee joints. On MRI, rice bodies are hypointense on T2 due to their fibrous nature and are associated with a joint effusion, synovial hypertrophy, and synovial enhancement after gadolinium administration.

Diagnosis

Synovial (osteo)chondromatosis

✓ Pearls

- Synovial (osteo)chondromatosis is a synovial metaplasia that results in loose bodies; 85% are calcified.
- PVNS shows low signal synovial thickening on T1 and T2 with blooming on gradient due to hemosiderin.
- "Rice bodies" are small, loose bodies that are most frequently associated with RA.

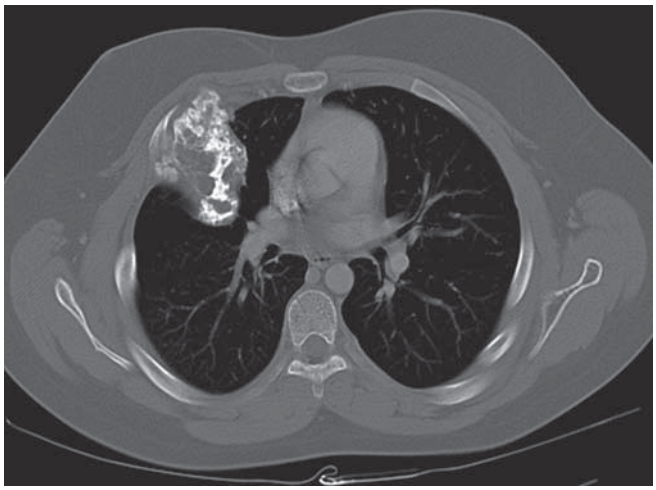
Suggested Readings

Cheung HS, Ryan L, Kozin F, McCarty D. Synovial origins of rice bodies in fluid. Arthritis Rheum 1980;23:72–76
Chew F. Musculoskeletal Imaging: A Teaching File. 3rd ed. Philadelphia: Elsevier Saunders; 2005
Chung C, Coley BD, Martin LC. Rice bodies in juvenile rheumatoid arthritis. AJR Am J Roentgenol 1998;170:698–700
Durr HR, Stabler A, Maier M, et al. Pigmented villonodular synovitis: review of 20 cases. J Rheumatol 2001;28:1620–1630
Stoller D, Tirman P, Bredella M, et al. Diagnostic Imaging: Orthopaedics. Salt Lake City, UT: Amirsys; 2004

Case 93

Philip Yen





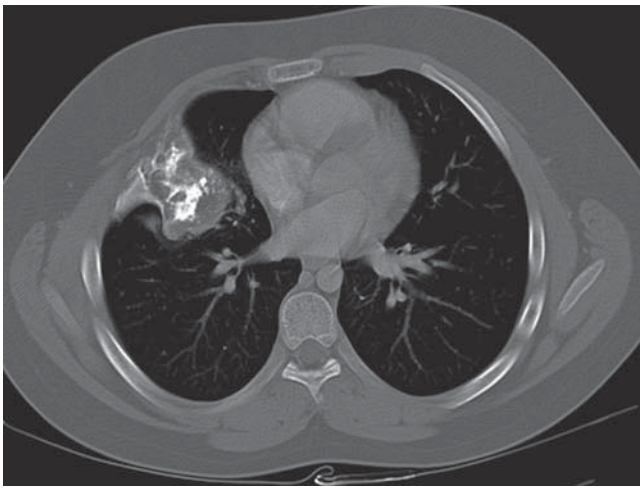


Fig. 93.1 **(A)** Frontal chest radiograph demonstrates an expansile rib lesion with calcifications involving the anterior aspect of the right fourth rib. **(B,C)** Axial computed tomography images through the chest in the bone window show a large, expansile, exophytic rib lesion with soft tissue attenuation and calcifications extending into the thoracic cavity. (Courtesy of Sandra Wootton-Gorges, MD, University of California, Davis.)

Clinical Presentation

A 14-year-old male patient presents with a chest wall mass (**Fig. 93.1**).

Key Imaging Finding

Expansile rib lesion in a child

Top 3 Differential Diagnoses

- **Fibrous dysplasia.** Fibrous dysplasia is a benign skeletal disorder characterized by replacement of medullary bone with fibrous tissue. The ribs are the most common site of involvement with monostotic disease. Polyostotic disease is termed McCune–Albright syndrome and is associated with endocrine dysfunction (most often precocious puberty) and café au lait spots. Bony lesions are expansile with variable internal matrix; the classic lesion has a characteristic ground-glass matrix. They are asymptomatic unless complicated by fracture.
- **Bone cyst.** Bone cysts are fluid-filled lesions that may be unicameral (UBC) or aneurysmal (ABC). They are expansile, lytic, and central in location. A pathognomonic finding in a UBC is the "fallen fragment" sign, which represents a bony fragment within the gravity-dependent area of the cyst. ABCs are multiloculated, with fluid–fluid levels secondary to hemorrhage. Patients are typically younger than 30 years and asymptomatic unless complicated by fracture.
- **Enchondroma.** An enchondroma is a common benign cartilaginous bone tumor. When located in the phalanges, the lesion is expansile and purely lytic. In other locations, enchondromas are expansile, with characteristic chondroid matrix and internal calcifications in an "arcs and swirls" pattern. Multiple lesions are associated with Ollier and Maffucci (multiple enchondromas and soft tissue hemangiomas) syndromes.

Additional Differential Diagnoses

- **Langerhans cell histiocytosis (LCH).** Eosinophilic granuloma is the most benign form of LCH and is characterized by isolated osseous involvement. Average age of onset is the second decade. Flat bones, including ribs, are involved more frequently than long bones. Although the imaging appearance is variable, LCH commonly presents as expansile lytic lesions. Periosteal reaction may be seen.
- **Ewing sarcoma.** Ewing sarcoma is a malignant primary bone neoplasm that frequently affects the diaphysis or metaphysis of long bones in the first and second decades of life. Less commonly, it can involve flat bones and ribs. Radiographic findings include a permeative intramedullary destructive lesion with a "moth-eaten" appearance and aggressive periosteal reaction ("onion skin" or "sunburst" pattern). Computed tomography and magnetic resonance imaging can better delineate associated soft tissue components. Metastases are common.
- **Metastases.** Rib lesions may arise from any primary malignancy that metastasizes to bone, including Ewing sarcoma, osteosarcoma, lymphoma, rhabdomyosarcoma, neuroblastoma, and Wilms tumor. Radiographic findings vary based on the primary neoplasm; lesions are often multifocal.

Diagnosis

Enchondroma

✓ Pearls

- Fibrous dysplasia classically has a "ground-glass" appearance to its matrix, which is pathognomonic.
- A "fallen fragment" sign is virtually pathognomonic for a pathologic fracture through a bone cyst.
- "Fluid–fluid levels" can be seen in ABCs but are not pathognomonic.
- Enchondromas are benign cartilaginous tumors that often have an "arcs and swirls" pattern of calcification.

Suggested Readings

Glass RB, Norton KI, Mitre SA, Kang E. Pediatric ribs: a spectrum of abnormalities. Radiographics 2002;22:87–104

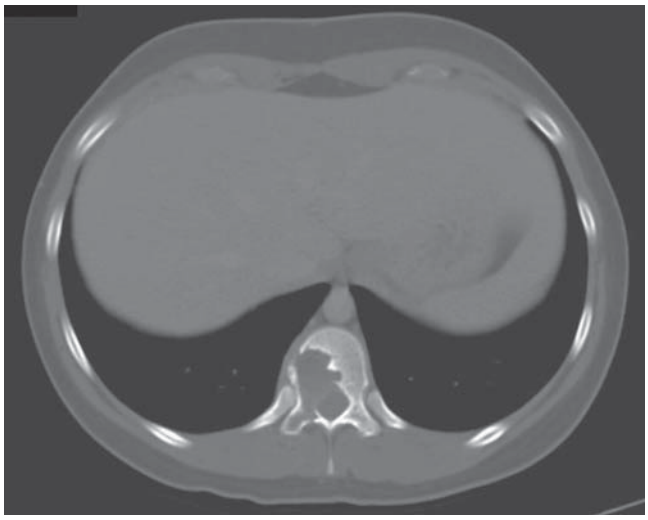
Helms CA. Fundamentals of Skeletal Radiology. 3rd ed. Philadelphia: Elsevier Saunders; 2005

Schulman H, Newman-Heinman N, Kurtzbart E, et al. Thoracoabdominal peripheral primitive neuroectodermal tumors in childhood: radiological features. Eur Radiol 2000;10:1649–1652

Case 94

M. Jason Akers





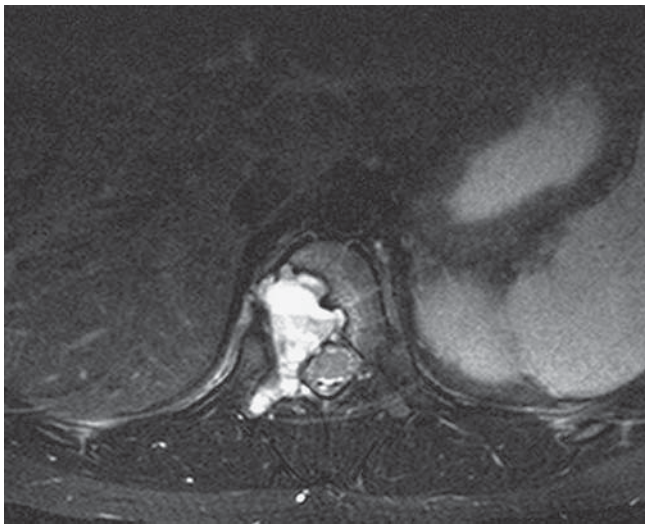


Fig. 94.1 **(A)** Frontal radiograph of the thoracic spine shows lucent expansion/absence of the right T11 pedicle. **(B)** Corresponding axial computed tomography image shows an expansile lytic lesion involving the right posterior T11 body and pedicle. There is cortical thinning of the lateral vertebral body and pedicle, as well as a small area of cortical breakthrough of the lateral vertebral body with extension of the lesion into the adjacent paravertebral soft tissues. There is mass effect on the spinal canal. **(C)** T2-weighted magnetic resonance image shows fluid–fluid levels within the lesion and slight epidural extension.

Clinical Presentation

A young adult patient presents with chronic back pain (**Fig. 94.1**).

Key Imaging Finding

Posterior element lytic lesion

Top 3 Differential Diagnoses

- **Aneurysmal bone cyst (ABC).** ABC is a benign expansile neoplasm containing thin-walled, blood-filled cavities thought to occur as a result of trauma. It can be isolated or associated with other tumors. ABCs are usually seen in children and young adults and commonly occur in long bone metaphyses and the posterior elements of the spine. In the spine, ABCs are classically centered in the pedicle and extend into the vertebral body. The pedicle appears absent on anteroposterior radiographs of the spine. Cortical thinning and focal cortical destruction are common. There may also be extension into the epidural space causing canal stenosis. Fluid–fluid levels result from hemorrhage within the lesion.
- **Osteoblastoma.** Osteoblastoma is a benign osteoid-forming tumor thought to be a larger version (>1.5 cm) of osteoid osteoma. Forty percent of these tumors occur in the spine and originate in the posterior elements, often extending into the vertebral body. They present as expansile lesions with narrow zones of transition and variable mineralization. The matrix is better visualized on computed tomography than radiographs. There may be an ABC component with fluid–fluid levels. Tumors can incite an inflammatory response with associated peritumoral edema that extends beyond the margins of the lesion.
- **Infection (tuberculosis [TB]).** TB causes granulomatous infection of the spine and adjacent soft tissues. Isolated posterior element involvement can occur, particularly in the thoracic spine. Patients usually have prominent epidural and paraspinal disease with large paraspinal abscesses dissecting over multiple levels. Tuberculous spondylitis is more likely to spare intervertebral disks while causing prominent bony destruction.

Additional Differential Diagnoses

- **Metastases.** Metastases usually occur in older patients and involve the posterior vertebral body first with extension into the posterior elements. Metastases most commonly spread to the spine hematogenously. Lytic metastases tend to be less expansile and more permeative in appearance, occurring as a destructive lesion with an associated soft tissue mass. Multiple vertebral levels are commonly involved.
- **Langerhans cell histiocytosis (LCH).** LCH is a disease occurring in children that is characterized by abnormal histiocyte proliferation producing granulomatous skeletal lesions. The classic presentation in the spine is vertebra plana with preservation of the disk space. LCH can also present as an aggressive lytic lesion with soft tissue mass and extension into the spinal canal. Other sites of involvement are the skull with a beveled edge appearance, mandible, long bones, ribs, and pelvis.

Diagnosis

Aneurysmal bone cyst

✓ Pearls

- ABCs are benign expansile lytic lesions that contain fluid–fluid levels due to internal hemorrhage.
- Osteoblastoma has an osteoid matrix and typically has peritumoral edema that extends beyond the lesion.
- Posterior element involvement of the thoracic spine with paraspinal abscesses suggests TB spondylitis.
- Lytic metastases typically occur in older patients, appear permeative/destructive, and affect multiple levels.

Suggested Readings

Chew F. Musculoskeletal Imaging: A Teaching File. 3rd ed. Philadelphia: Elsevier Saunders; 2005

DiCaprio MR, Murphy MJ, Camp RL. Aneurysmal bone cyst of the spine with familial incidence. Spine 2000;25:1589–1592

Shaikh MI, Saifuddin A, Pringle J, et al. Spinal osteoblastoma: CT and MR imaging with pathological correlation. Skeletal Radiol 1999;28:33–40

Stoller DW, Tirman P, Bredella M, et al. Diagnostic Imaging: Orthopaedics. Salt Lake City, UT: Amirsys; 2004

Case 95

Eva Escobedo

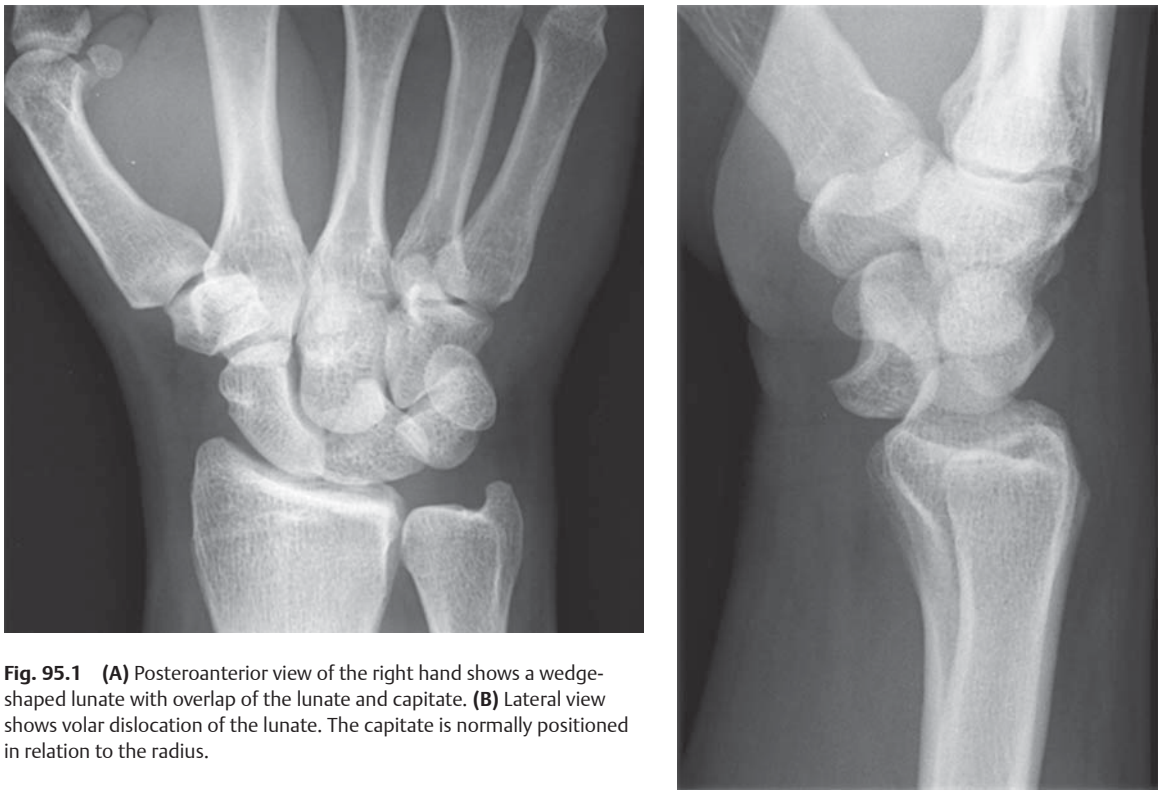


Fig. 95.1 **(A)** Posteroanterior view of the right hand shows a wedge-shaped lunate with overlap of the lunate and capitate. **(B)** Lateral view shows volar dislocation of the lunate. The capitate is normally positioned in relation to the radius.

Clinical Presentation

A patient presents after a fall on an outstretched hand (**Fig. 95.1**).

Key Imaging Finding

Carpal dislocation

Top 3 Differential Diagnoses

- **Perilunate dislocation.** Perilunate dislocation represents the second of the four stages of ligamentous injury around the lunate bone resulting from forced hyperextension. These are referred to as "lesser arc" injuries. The four stages of injury are scapholunate dissociation (stage I), perilunate dislocation (stage II), midcarpal dislocation (stage III), and lunate dislocation (stage IV). In perilunate dislocation, the lunate will appear to be triangular in shape on the posteroanterior (PA) radiograph of the wrist, and a normal articulation with the capitate will not be visible. On the lateral radiograph, the lunate articulates normally with the distal radius, and the capitate and the remaining carpal bones are dislocated dorsally. Fractures involving the radial styloid, scaphoid, capitate, hamate, triquetrum, and ulnar styloid ("greater arc" injuries) may accompany these injuries, the most common being the transcaphoid perilunate fracture-dislocation.
- **Lunate dislocation.** Lunate dislocation is stage IV of the lesser arc injuries. With increasing hyperextension force, a perilunate dislocation may become a lunate dislocation as the capitate forces the lunate ventrally, disrupting its ligamentous attachment to the radius. Thus, the capitate becomes realigned with the distal radius, and the lunate is dislocated palmarly. As with the perilunate dislocation, the PA view of the wrist will show an abnormal triangular shape of the lunate, without a normal articulation between the lunate and capitate.
- **Midcarpal dislocation.** Stage III of the lesser arc injuries, or the intermediate stage between perilunate and lunate dislocation, the midcarpal dislocation is a result of ligamentous injury at the lunotriquetral joint. The PA view of the wrist will appear similar to that of the perilunate and lunate dislocations. Appearance of a midcarpal dislocation may be variable and have features of either a perilunate or a lunate dislocation. However, the lateral view of the wrist typically shows dorsal dislocation of the capitate and volar tilt and subluxation of the lunate. Thus, neither the lunate nor the capitate is normally positioned in relation to the distal radius.

Diagnosis

Lunate dislocation

✓ Pearls

- The lateral radiograph is essential to differentiate between a lunate and a perilunate dislocation.
- With perilunate dislocation (more common), the lunate articulates normally with the radius.
- With lunate dislocation (more severe), the captitate is normally aligned with the radius.
- If the lunate and the capitate are malpositioned in relation to the radius, suspect a midcarpal dislocation.

Suggested Readings

Grabow RJ, Catalano L. Carpal dislocations. Hand Clin 2006;22:485–500

Helms CA. Fundamentals of Skeletal Radiology. 3rd ed. Philadelphia: Elsevier Saunders; 2005

Manaster BJ. Musculoskeletal Imaging: The Requisites. 2nd ed. St. Louis, MO: Mosby; 2002

Resnick D. Bone and Joint Imaging. 3rd ed. Philadelphia: Elsevier Saunders; 2005

Case 96

Sonia Kaur Ghei

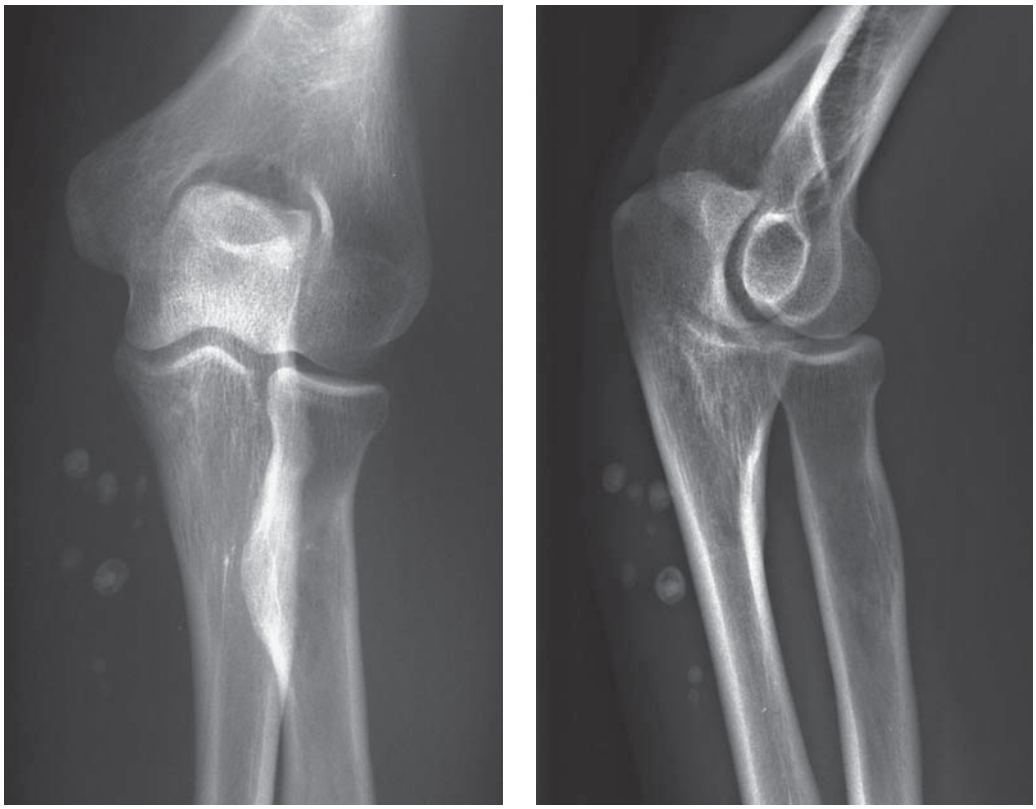


Fig. 96.1 **(A)** Anteroposterior and **(B)** oblique radiographs of the elbow demonstrate a soft tissue mass in the dorsomedial forearm with numerous round calcifications with central lucencies, consistent with phleboliths. (Courtesy of John C. Hunter, MD.)

Clinical Presentation

A 22-year-old patient presents with a palpable mass with intermittent enlargement and pain (**Fig. 96.1**).

Key Imaging Finding

Periarticular soft tissue calcifications

Top 3 Differential Diagnoses

- **Hemangioma.** Soft tissue hemangiomas are common benign vascular tumors, occurring most often in children and young adults. Patients can present with a soft tissue mass that varies in size and causes pain during activity. On radiographs, a soft tissue mass is seen with phleboliths, which is nearly pathognomonic if present. Reactive bony changes and smooth periosteal reaction can also be seen. On computed tomography, these masses are often intramuscular with reactive overgrowth of fat. On magnetic resonance imaging, hemangiomas contain flow voids, avidly enhance, and are often hyperintense to muscle on T1 and T2. Hemangiomas are also seen in association with Mafucci syndrome (multiple enchondromas and soft tissue hemangiomas).
- **Scleroderma.** Scleroderma demonstrates characteristic findings in the hands with acro-osteolysis (resorption of the distal phalanges) and atrophy of the soft tissues at the distal fingers. Sharply marginated calcifications are seen in a subcutaneous and periarticular distribution. The calcifications associated with scleroderma are described as calcinosis circumscripta because of their well-defined margins.
- **Myositis ossificans.** Also known as heterotopic ossification, myositis ossificans occurs secondary to trauma or immobility and can present as an enlarging painful mass. Cloudlike calcification is seen 4 to 6 weeks after trauma with peripheral maturation to cortical bone. On radiographs, this so-called zonal phenomenon is seen with central lucency and dense zone of mature ossification at the periphery, differentiating this entity from juxtacortical or extraskeletal osteosarcomas, which mature centrally.

Additional Differential Diagnoses

- **Arthropathy with calcified soft tissue nodule.** If a soft tissue mass with calcification occurs near a joint, underlying arthropathy should be considered. For example, synovial osteochondromatosis can present as multiple calcified masses in a large joint, such as the knee, hip, or shoulder, and occurs secondary to metaplasia of synovial connective tissue. Gouty tophi can also calcify in the setting of renal failure.
- **Soft tissue sarcoma.** Soft tissue sarcomas include entities such as synovial sarcoma, extraskeletal osteosarcoma and chondrosarcoma. Synovial sarcoma presents as a mass with amorphous calcifications in close proximity to a joint, particularly in the lower extremities and hands. On T2, "triple signal intensity" is seen due to hemorrhage, fibrous tissue, and cystic components often containing fluid–fluid levels. Extraskeletal osteosarcomas demonstrate central ossification, which is referred to as "reverse zoning." Chondrosarcomas usually arise from underlying bone and contain annular or comma-shaped calcifications.
- **Tumoral calcinosis.** Tumoral calcinosis is a rare idiopathic inherited disorder that occurs predominantly in African Americans. It most often presents in the 1st or 2nd decade with painless, enlarging periarticular calcifications. The hips, elbows, and shoulders are the most common sites of involvement.

Diagnosis

Hemangioma

✓ Pearls

- A soft tissue mass with phleboliths is nearly pathognomonic for a hemangioma.
- Myositis ossificans should eventually demonstrate a dense zone of mature ossification peripherally.
- Masses demonstrating central ossification or amorphous calcification may suggest a soft tissue sarcoma.

Suggested Readings

Fayad L, Hazirolan T, Bluemke D, et al. Vascular malformations in the extremities: emphasis on MR imaging features that guide treatment options. Skeletal Radiol 2006;35:127–137

Greenspan A. Orthopedic Imaging: A Practical Approach. 4th ed. Philadelphia: Lippincott Williams & Wilkins; 2004

Case 97

Chirag V. Patel





Fig. 97.1 **(A)** Frontal radiograph of the left ankle demonstrates an expansile lytic lesion with a thin sclerotic margin located centrally in the metadiaphysis of distal left tibia and extending to the physis. There are subtle internal septations and adjacent soft tissue swelling. **(B)** Coronal T2 fast spin echo magnetic resonance image shows multiloculated cystic osseous lesions with thin septations and differing signal intensities secondary to regions of hemorrhage. (Courtesy of Children's Hospital and Research Center, Oakland, California.)

Clinical Presentation

A 5-year-old boy presents with pain and swelling of the left leg (**Fig. 97.1**).

Key Imaging Finding

Benign expansile lytic lesion

Top 3 Differential Diagnoses

- **Fibrous dysplasia.** Fibrous dysplasia is a benign intramedullary fibro-osseous lesion with monostotic or less commonly polyostotic involvement. Common sites are long bones, ribs, craniofacial bones, and pelvis. Radiographically, it manifests as an intramedullary expansile lytic lesion, with metadiaphyseal localization. Unlike other benign lytic bone lesions, it demonstrates a thick "rind" of reactive bone. The tumor matrix has a characteristic ground-glass appearance and may show internal calcification.
- **Unicameral bone cyst.** Also known as simple bone cyst, unicameral bone cyst is a common bone lesion, following only nonossifying fibroma and osteochondroma in prevalence. It occurs in the 5-to-20-year age group, involving the metadiaphyses of long bones. Eighty percent of childhood cysts are located in the proximal humerus and proximal femur; in patients older than 17 years, about half of the lesions are located in the pelvis or calcaneus. Radiographic characteristics are a central location and cortical expansion, with a thin sclerotic rim.
- **Aneurysmal bone cyst (ABC).** ABC is a benign bone lesion of unknown etiology, occurring in the 5-to -20-year age group. It most commonly occurs in the metadiaphyseal region of long bones and posterior elements of the spine. Radiographically, it presents as an expansile lytic lesion with thin septations, more commonly eccentric in location, giving a characteristic "soap bubble" appearance. Computed tomography and magnetic resonance imaging demonstrate fluid–fluid levels within multiple cysts, separated by thin enhancing septations. The absence of ossification or calcification within the lesion and the absence of epiphyseal extension are other helpful features. Differing signal intensities are commonly seen within the lesion secondary to hemorrhage.

Additional Differential Diagnoses

- **Giant cell tumor.** Giant cell tumor rarely occurs before closure of growth plates and is seen commonly between 20 and 50 years of age. Epiphyseal extension is characteristic, and thin septations may be seen. The distal femur and proximal tibia account for >50% of giant cell tumors. Imaging characteristics include an eccentric location, extension to subcortical bone, and lack of a sclerotic rim. Approximately 5 to 10% of lesions may be malignant. Local recurrence after resection may occur in up to 25% of cases.
- **Eosinophilic granuloma.** Eosinophilic granuloma is the localized osseous form of Langerhans cell histiocytosis. The average age of onset is 10 to 14 years. Depending on the site of involvement and the stage of the disease, common manifestations are well-defined areas of cortical or medullary rarefaction; in the later stage there may be a sclerotic margin, periosteal reaction, and bone expansion. Long bones are involved less commonly as compared with flat bones. The femur is the most favored location; it may extend to the epiphysis.

Diagnosis

Aneurysmal bone cyst

✓ Pearls

- Fibrous dysplasia classically has a ground-glass matrix with calcification and a thick rind of reactive bone.
- Approximately 80% of unicameral bones cysts in childhood are in the proximal humerus or femur.
- Fluid–fluid levels suggest an ABC but may also be present in other lesions.
- Giant cell tumors occur after growth plate closure, extend to the subcortical bone, and lack a sclerotic rim.

Suggested Readings

Fitzpatrick KA, Taljanovic MS, Speer DP, et al. Imaging findings of fibrous dysplasia with histopathologic and intraoperative correlation. AJR Am J Roentgenol 2004;182:1389–1398

Mahnken AH, Nolte-Ernsting C, Wildberger J, et al. Aneurysmal bone cyst: value of MR imaging and conventional radiography. Eur Radiol 2003;13:1118–1124

Case 98

Adrianne K. Thompson



Fig. 98.1 Anteroposterior radiograph of the pelvis demonstrates multiple sclerotic lesions with symmetric distribution within the pelvis and proximal femurs.

Clinical Presentation

A young female patient presents with hip pain (**Fig. 98.1**).

Key Imaging Finding

Multiple sclerotic foci in the pelvis

Top 3 Differential Diagnoses

- **Osteopoikilosis.** Osteopoikilosis is an asymptomatic form of skeletal sclerotic dysplasia that occurs in both men and women. Cutaneous manifestations may be seen, such as keloids and fibrocollagenous infiltration of the skin. Imaging shows ovoid, well-defined sclerotic foci, which are usually small and symmetrically distributed. Osteopoikilosis shows a predilection for long and short tubular bones, carpal and tarsal bones, the pelvis, and scapulae. Usually, there is normal activity on bone scan. There may be an association with other osteosclerotic dysplasias, such as osteopathia striata (Voorhoeve syndrome) and melorrheostosis.
- **Metastatic disease.** Metastatic disease is a common cause of sclerotic foci within the pelvis, most commonly caused by prostate cancer in men and breast cancer in women. When presented with sclerotic foci within the pelvis, helpful features to suggest malignant disease include (1) lesion borders, which tend to be indistinct with a wide zone of transition; (2) the presence of periosteal reaction; (3) soft tissue extension; (4) size, as metastatic lesions would be larger and less uniform than those seen in benign conditions; and (5) multiplicity, particularly when lesions are seen in bones outside the pelvis.
- **Paget disease.** Paget disease is a disorder of bone metabolism seen in older patients, with a slight male predilection and onset in the 5th and 6th decades. Numerous etiologies have been proposed, but the cause remains elusive. The disease shows increased bone remodeling, leading to an abnormal balance between bone resorption and replacement. Osteoblastic activity results in increased alkaline phosphatase, and increased osteoclastic activity leads to high levels of hydroxyproline in urine. Most commonly affected bones are the pelvis, femurs, skull, tibiae, and spine. Radiographic findings reflect the cellular activity taking place at that phase. There are three main phases: osteolytic, mixed, and osteoblastic. In the osteolytic phase, bone resorption occurs, causing radiolucent changes in bone. In the calvarium, this results in bone destruction termed osteoporosis circumscripta; in the tibia, this results in a "blade of grass" appearance. The mixed phase shows both bone resorption and formation with prominent bony trabeculae and a "cotton wool" appearance. In the osteoblastic phase, there is a drastic increase in bone density with cortical thickening and bony deformity. Specific changes within the pelvis are trabecular thickening of the iliopectineal/ilioischial lines, hemipelvic asymmetry, and enlargement. Complications include pathologic fractures, early degenerative joint disease, neurologic impingement, and malignant transformation.

Diagnosis

Osteopoikilosis

✓ Pearls

- Osteopoikilosis is asymptomatic and usually demonstrates normal activity on a bone scan.
- Sclerotic metastatic disease to the pelvis most commonly originates from prostate and breast carcinoma.
- Paget disease in the pelvis may demonstrate thickening of the iliopectineal and ilioischial lines.

Suggested Readings

Greenspan A. Orthopedic Radiology: A Practical Approach. 2nd ed. Philadelphia: Lippincott-Raven; 1997

Resnick D. Bone and Joint Imaging. 2nd ed. Philadelphia: WB Saunders; 1996

Case 99

Sonia Kaur Ghei



Fig. 99.1 **(A)** Sagittal computed tomography image demonstrates an anterior wedge–compression deformity of L1 in an elderly patient. There is sclerosis of the posterior vertebral body. **(B)** Sagittal T2-weighted magnetic resonance image shows the L1 compression fracture with focal edema anteriorly and decreased signal intensity within the remainder of the vertebral body. **(C)** Sagittal short inversion time inversion recovery (STIR) image paramidline extending through the pedicle demonstrates extension of abnormal signal and marrow edema into the vertebral body pedicle with normal pedicle signal at other levels.

Clinical Presentation

A 72-year-old woman presents with acute back pain (**Fig. 99.1**).

Key Imaging Finding

Vertebral body wedge fracture

Top 3 Differential Diagnoses

- **Traumatic fracture.** Traumatic vertebral fractures tend to occur in the upper lumbar spine, and a history of fall or significant trauma is usually present. These most often involve the superior end plate, and surrounding paravertebral soft tissue swelling or hematoma can often be seen. This soft tissue should be smooth and rim-shaped, rather than irregular or nodular. If the fracture extends into the posterior elements, abnormal signal intensity may be seen in these regions.
- **Insufficiency fracture.** Insufficiency fractures of the spine tend to occur in older osteoporotic patients. Such fractures tend to have similar imaging characteristics as traumatic fractures, but they can occur at any level. In an older patient, the images should be carefully examined for signs of underlying malignancy because the spine is a common site of metastatic disease, and a fracture may be the presenting abnormality. Marrow edema in insufficiency fractures is limited to the vertebral body; extension of abnormal signal into the pedicles suggests an underlying lesion. In addition, the soft tissue component should be smooth and rim-shaped.
- **Pathologic fracture.** A pathologic fracture can occur anywhere in the spine where there is an underlying lesion. There are four features on magnetic resonance imaging that suggest an underlying malignant etiology: (1) abnormal marrow signal with ill-defined margins (all fractures will demonstrate increased T2 and inversion recovery signal secondary to marrow edema and hemorrhage, but it should be well defined if benign), (2) abnormal marrow signal extending into the pedicles, (3) associated soft tissue lesion with irregular or nodular borders (smooth paravertebral soft tissue swelling is normally seen surrounding a fracture), and (4) marked enhancement (mild enhancement can normally be seen with benign fractures). Also, because traumatic fractures tend to occur in the upper lumbar spine, an underlying lesion should be considered in a younger patient with a lower lumbar spine fracture, particularly if there is no history of significant antecedent trauma.

Diagnosis

Pathologic fracture (metastatic disease)

✓ Pearls

- Traumatic fractures commonly involve the superior end plates within the upper lumbar spine.
- Insufficiency fractures tend to occur in older, osteoporotic patients and spare the posterior elements.
- Marrow edema extending into the pedicles or marked enhancement is concerning for a pathologic fracture.
- Pathologic fractures should be considered in a younger patient with a lower lumbar spine fracture.

Suggested Readings

Haba H, Taneichi H, Kotani Y, et al. Diagnostic accuracy of magnetic resonance imaging for detecting posterior ligamentous complex injury associated with thoracic and lumbar fractures. J Neurosurg 2003;99:20–26

Shih TT, Huang KM, Li YW, et al. Solitary vertebral collapse: distinction between benign and malignant causes using MR patterns. J Magn Reson Imaging 1999;9:635–642

Wintermark M, Mouhsine E, Theumann N, et al. Thoracolumbar spine fractures in patients who have sustained severe trauma: depiction with multi-detector row CT. Radiology 2003;227:681–689

Case 100

Adrianne K. Thompson

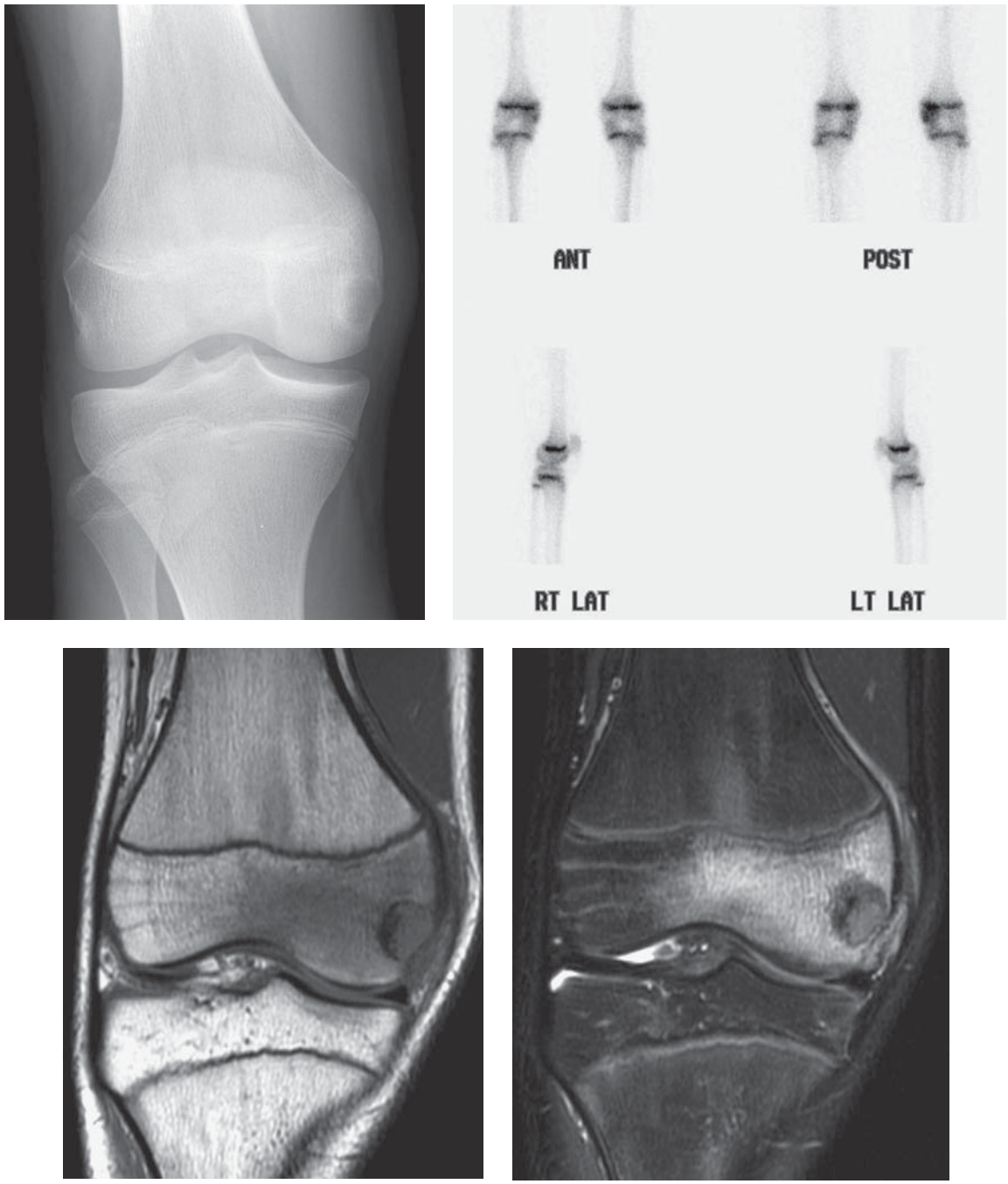


Fig. 100.1 **(A)** Frontal radiograph of the right knee demonstrates a circumscribed eccentric lucent lesion with thin sclerotic margins and a narrow zone of transition within the epiphysis of the medial femoral condyle. **(B)** The lesion demonstrates increased activity on bone scan. **(C)** Coronal T1- and **(D)** fat-suppressed T2-weighted images reveal a benign-appearing circumscribed T1 dark and T2 intermediate epiphyseal lesion with surrounding marrow edema. The thin curvilinear T1 and T2 dark region along the lateral aspect of the lesion represented calcification on computed tomography (not shown).

Clinical Presentation

An adolescent male patient presents with knee pain (**Fig. 100.1**).

Key Imaging Finding

Epiphyseal equivalent lucent lesion

Top 3 Differential Diagnoses

- **Chondroblastoma.** Chondroblastomas are rare lesions that occur in the epiphyses of long bones and are usually seen before skeletal maturity. Most common locations are the humerus, tibia, and femur, as well as within epiphyseal equivalents such as the patella. On radiographs, chondroblastomas tend to be well-defined lucent lesions with a thin rim of sclerosis; calcifications can be seen in ~50% of cases. Periosteal reaction can occasionally be seen quite a distance away from the primary lesion. On magnetic resonance imaging, they tend to show decreased signal intensity on T1-weighted and variable signal intensity on T2-weighted sequences, depending on the amount of chondroid matrix and calcification. However, chondroblastomas are associated with significant surrounding marrow edema that may extend into the soft tissues. They demonstrate increased uptake on nuclear medicine bone scans. The radiographic appearance of chondroblastoma is, unfortunately, nearly identical to that of a clear cell chondrosarcoma.
- **Giant cell tumor.** Giant cell tumors are locally aggressive bone tumors composed of giant cells, connective tissue, and stromal cells. They are most common in the 3rd and 4th decades and more so in women than men. The fundamental feature of a giant cell tumor is extensive epiphyseal involvement after growth plate closure; when uncommonly seen in adolescents or children, it has a metaphyseal location. Giant cell tumor favors long tubular bones but can also be seen in the spine and flat bones, such as the clavicles, ribs, and sternum. Radiographic evaluation shows a lucent, expansile, eccentric lesion producing overlying cortical thinning. Margins can be well or poorly defined. Unfortunately, giant cell tumors are prone to local extension and malignant transformation with metastases (5–10%). They also have a high rate of recurrence after treatment (40–60%).
- **Langerhans cell histiocytosis (LCH).** LCH typically occurs in children, adolescents, and young adults and has a 2:1 male predominance. Although LCH can be multiple, solitary lytic bone lesions predominate with a punched out appearance; it commonly involves the skull ("punched out" lesion with beveled edges) mandible ("floating tooth"), spine (flattened vertebral body or vertebra plana), ribs, and long bones. These lesions occur in the epiphyses and can cross an open growth plate. LCH can mimic more aggressive processes, such as infection and Ewing sarcoma, both clinically and radiographically.

Additional Differential Diagnoses

- **Intraosseous ganglion cyst.** These lesions tend to occur within the subchondral/subarticular regions of the shoulder, knee, ankle, hip, and carpal joints after skeletal maturation. On radiographs, they are well-defined lucent lesions with surrounding sclerotic margins. They demonstrate low T1 and high T2 signal intensity.

Diagnosis

Chondroblastoma

✓ Pearls

- Chondroblastomas usually occur in epiphyses or epiphyseal equivalents before skeletal maturity.
- Chondroblastomas tend to be associated with a significant amount of marrow and soft tissue edema.
- Giant cell tumors typically involve the epiphysis or epiphyseal equivalent only after skeletal maturity.
- LCH can occur in the epiphysis and can cross the growth plate.

Suggested Readings

Brower AC, Moser RP, Kransdorf MJ. The frequency and diagnostic significance of periostitis in chondroblastoma. AJR Am J Roentgenol 1990;154:309–314

Greenspan A, Remagen W. Differential Diagnosis or Tumors and Tumor-like Lesions of Bones and Joints. Philadelphia: Lipincott-Raven; 1998

Resnick D. Bone and Joint Imaging. 2nd ed. Philadelphia: WB Saunders; 1996

Section V Head and Neck Imaging

Case 101

William T. O'Brien Sr.

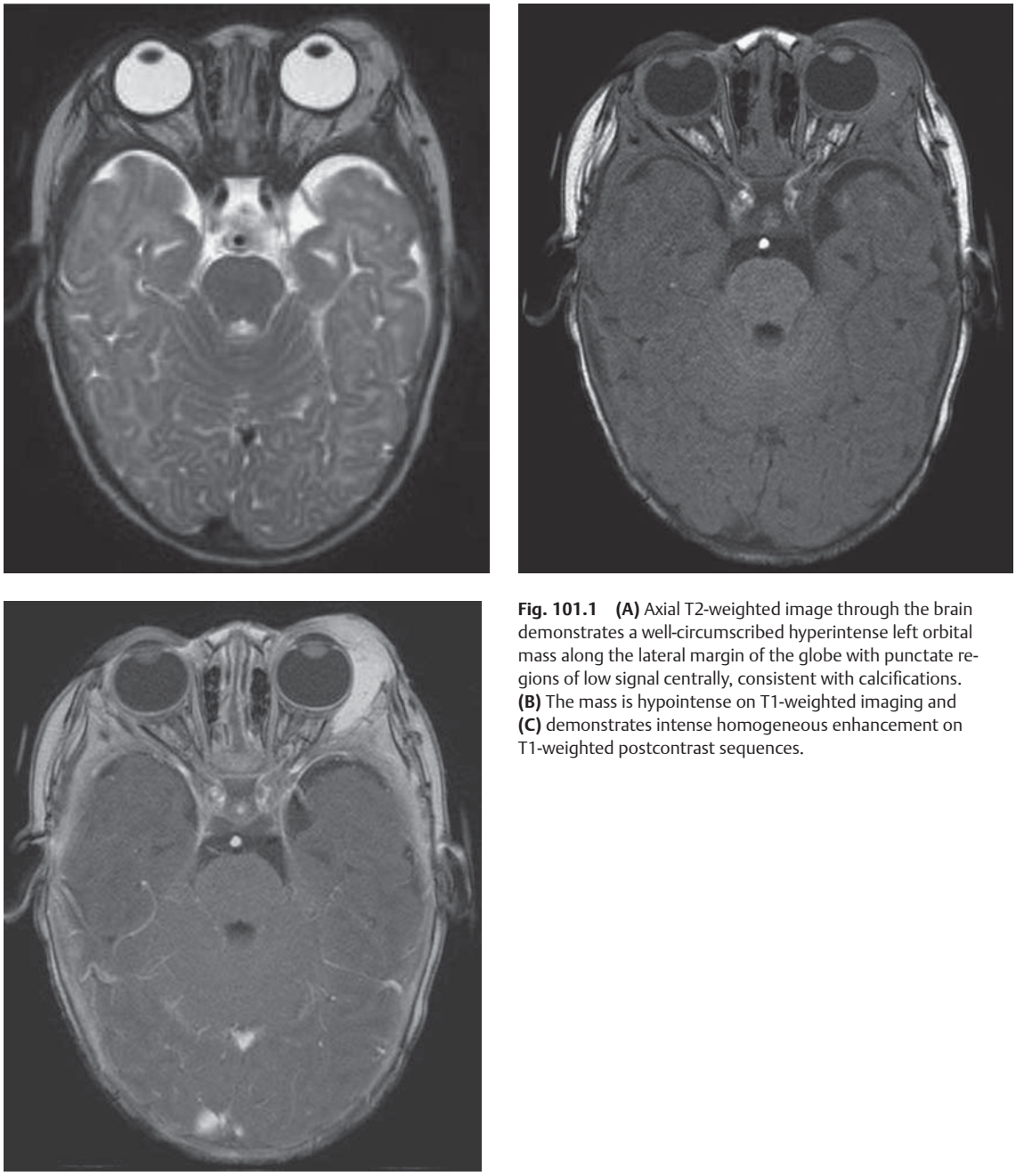


Fig. 101.1 **(A)** Axial T2-weighted image through the brain demonstrates a well-circumscribed hyperintense left orbital mass along the lateral margin of the globe with punctate regions of low signal centrally, consistent with calcifications. **(B)** The mass is hypointense on T1-weighted imaging and **(C)** demonstrates intense homogeneous enhancement on T1-weighted postcontrast sequences.

Clinical Presentation

A patient presents with orbital pain and swelling (**Fig. 101.1**).

Key Imaging Finding

Enhancing orbital mass

Top 3 Differential Diagnoses

- **Hemangioma.** Orbital cavernous hemangiomas are the most common intraorbital tumors. They are benign and often present with proptosis or pain. Hemangiomas are well circumscribed, with a round, oval, or lobulated configuration. Most commonly, they are intraconal and retrobulbar in location, although they may occur anywhere within the orbit. The lesions are typically hyperdense on computed tomography (CT), hypointense on T1-weighted sequences, and hyperintense on T2-weighted sequences. Intense enhancement is the rule. Calcifications are occasionally seen. As hemangiomas enlarge, they may remodel adjacent bony structures.
- **Lymphangioma.** Lymphangiomas are benign hamartomatous malformations that occur in children and young adults. Patients typically present with proptosis as the lesion enlarges. Although they most commonly involve the extraconal compartment, orbital lymphangiomas can involve any and multiple compartments. The lesions are multilocular, cystic, and prone to hemorrhage. Fluid–fluid levels are common after episodes of hemorrhage. Enhancement of septations is typical.
- **Meningioma.** Orbital meningiomas most commonly occur in middle-aged women; they occasionally can occur in children with neurofibromatosis 2. Extraconal involvement is typically due to intraorbital spread from a sphenoid wing meningioma. Cavernous sinus meningiomas can also spread directly into the orbit. Optic nerve sheath meningiomas are true intraconal lesions that typically do not extend intracranially, a differentiating feature from an optic nerve glioma. Meningiomas enhance avidly and may have calcifications. Optic nerve sheath meningiomas enhance in a "tram track" configuration on axial images (bright nerve sheath/meningioma enhancement peripherally and hypodense [CT] or hypointense [T1 magnetic resonance imaging] optic nerve centrally). Meningiomas commonly are associated with hyperostosis.

Additional Differential Diagnoses

- **Metastases.** Metastases account for ~10% of orbital tumors and can affect the bony orbit, globe, intraconal, and extraconal spaces. Breast and lung cancer are the most common primary tumors, followed by gastrointestinal, genitourinary, and soft tissue sarcomas. In children, neuroblastoma, leukemia, Wilms tumor, and Ewing sarcoma represent the most common primary neoplasms with orbital involvement.
- **Lymphoma.** Lymphoma usually involves the orbit secondarily and is of the non-Hodgkin variant. Patients present with proptosis or painless swelling. Lymphomatous infiltrates are commonly well circumscribed and may be bilateral, a helpful distinguishing feature. CT may show increased density with enhancement. The lesions are typically low to intermediate in signal intensity on T1- and hyperintense on T2-weighted images. Common locations are the lacrimal gland and the superior aspect of the orbit.

Diagnosis

Orbital hemangioma

✓ Pearls

- Hemangiomas are the most common orbital tumor, intensely enhance, and may have calcifications.
- Extraconal meningiomas involve the orbit secondarily; intraconal meningiomas occur along the optic nerve.
- Metastases and lymphoma involve the orbit secondarily and may be bilateral.

Suggested Readings

Harnsberger HR. Diagnostic Imaging: Head and Neck. Salt Lake City, UT: Amirsys; 2004

Mafee MF, Valvassori GE, Becker M. Valvassori's Head and Neck Imaging. 2nd ed. New York: Thieme; 2005

Tanaka A, Mihara F, Yoshiura T, et al. Differentiation of cavernous hemangioma from schwannoma of the orbit. AJR Am J Roentgenol 2004;183:1799–1804

Case 102

William T. O'Brien Sr.

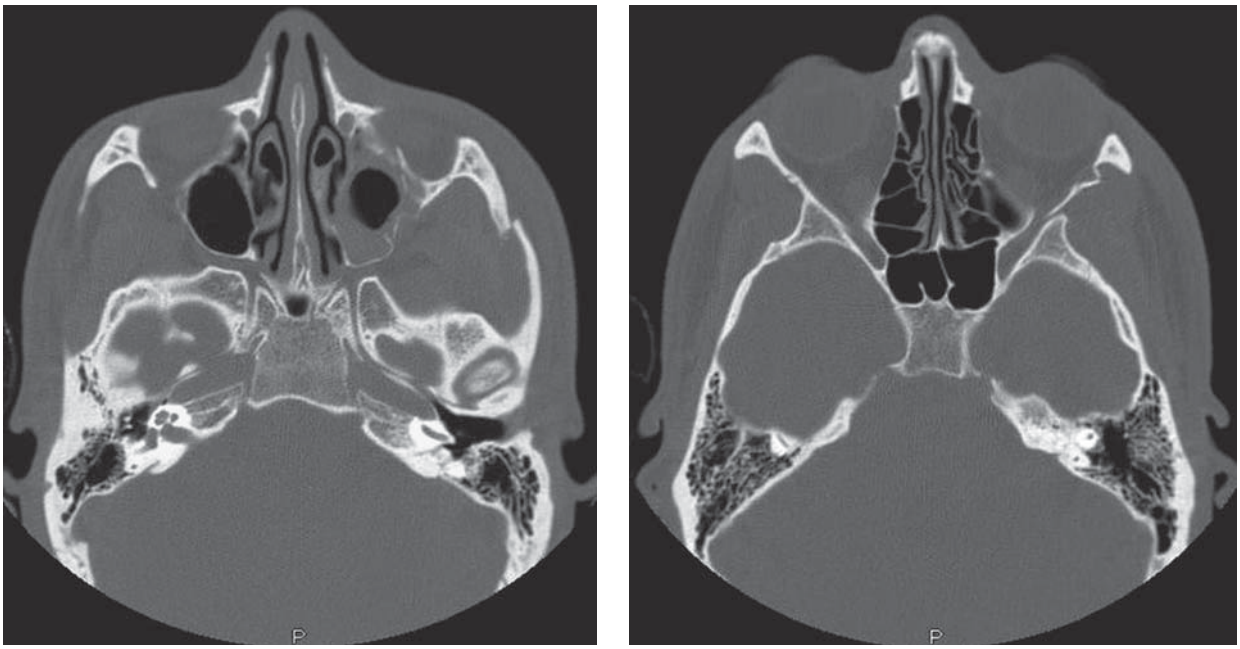




Fig. 102.1 **(A)** Axial computed tomography image through the facial bones demonstrates a fracture of the left lateral maxillary sinus wall that extends into the inferior orbital wall. There is also a displaced fracture of the zygomatic arch. **(B)** An axial image more superiorly reveals a fracture of the left lateral orbital wall. **(C)** Coronal image depicts fractures of the left inferior and lateral orbital walls, as well as the lateral maxillary sinus wall. Sinus opacification is seen in images **A** and **C**.

Clinical Presentation

A patient presents after a motor vehicle accident (**Fig. 102.1**).

Key Imaging Finding

Orbital rim fracture

Top 3 Differential Diagnoses

- **Orbital wall blowout fracture.** An orbital wall blowout fracture is the result of a direct blow to the globe. Increased intraorbital pressure is transmitted to the thin orbital floor, resulting in a characteristic fracture pattern. A fracture fragment may protrude inferiorly into the maxillary sinus with a "trapdoor" appearance. Intraorbital fat is usually displaced inferiorly into the maxillary sinus, and there may be an air–fluid level within the sinus due to hemorrhage. The inferior rectus muscle may also be displaced inferiorly, resulting in muscle entrapment. It is important to evaluate for globe injury, as well as additional orbital and facial fractures.
- **Tripod fracture.** A tripod fracture (also referred to as a zygomaticomaxillary complex fracture) is a common facial fracture that is caused by a direct blow to the zygomatic bone. The fracture involves the zygomatic arch and inferior and lateral orbital walls, resulting in disassociation of the anterior zygoma from the remainder of the facial bones. Patients commonly present with facial swelling, a localized deformity, and occasionally the inability to open the jaw due to impingement upon the mandibular coronoid process from the fracture fragment.
- **Le Fort fracture.** Le Fort fractures are characterized by some form of facial disassociation as a result of bilateral fractures and are grouped into three major subtypes. All subtypes involve fractures of the pterygoid plates. Le Fort I fractures occur through the maxillary bone below the orbital floor. There may be extension into one or both maxillary sinuses. The inferior portion of the maxilla below the fracture site is disassociated from the remainder of the facial bones. In Le Fort II fractures, the fracture is pyramidal in shape, involving the bilateral maxilla, and converging superiorly and medially through the inferior and medial orbital walls and nasal bridge. The nasal bridge and maxilla below the fracture are disassociated from the remainder of the facial bones. Le Fort III fractures are the most severe and are characterized by complete craniofacial disassociation. These fractures involve the bilateral zygomaticofrontal sutures, the nasofrontal suture, and the lateral, medial, and inferior orbital walls. Pure Le Fort-type fractures as described are unusual; most fractures are complex, with components of different subtypes.

Diagnosis

Tripod fracture

✓ Pearls

- Orbital wall blowout fractures are due to a direct blow to the globe; muscle entrapment may be seen.
- A tripod fracture involves the zygoma, inferior orbital wall, and lateral orbital wall.
- Le Fort fractures are characterized by varying degrees of facial disassociation; type III is the most severe.

Suggested Readings

Dolan KD, Jacoby CG, Smoker WR. The radiology of facial fractures. Radiographics 1984;4:577–663

Case 103

Adam J. Zuckerman

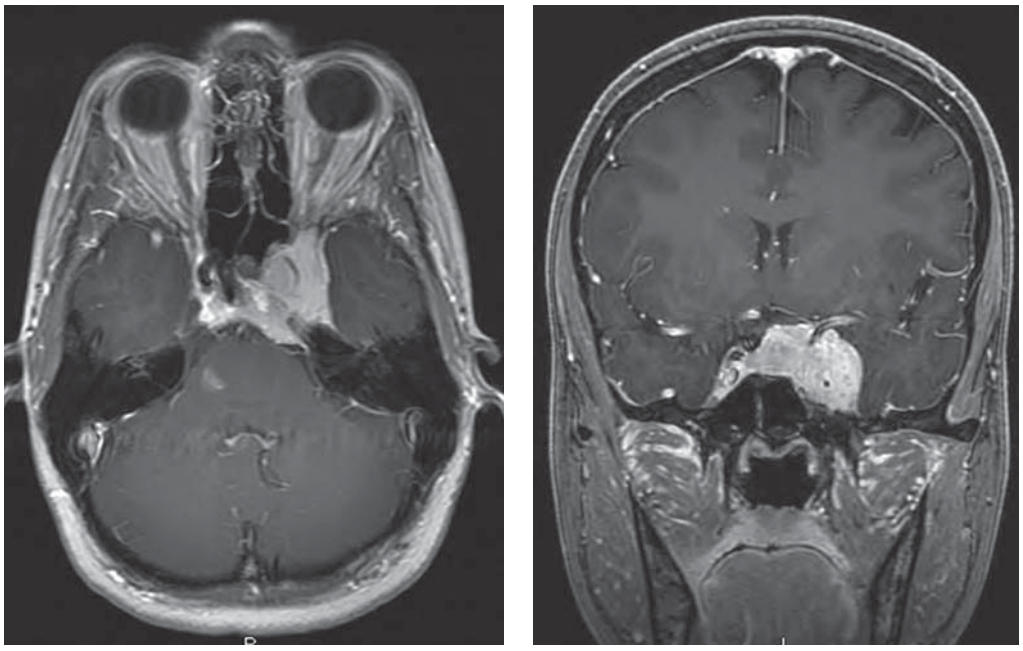


Fig. 103.1 **(A)** Axial and **(B)** coronal T1-weighted images postcontrast administration demonstrate a markedly enhancing left cavernous sinus mass with encasement and marked narrowing of the cavernous segment of the left internal carotid artery.

Clinical Presentation

A 31-year-old postpartum woman complains of facial numbness (**Fig. 103.1**).

Key Imaging Finding

Cavernous sinus mass/enhancement

Top 3 Differential Diagnoses

- **Meningioma.** Cavernous sinus meningiomas most commonly present with oculomotor symptoms (ophthalmoplegia, ptosis, and anisocoria) related to compressive effects. Stenosis of the ipsilateral cavernous internal carotid artery is another common complication. The lesions are typically isointense to gray matter on T1 and T2 sequences with intense homogeneous enhancement and a dural tail. Meningiomas may be hyperdense on computed tomography (CT) with calcification and hyperostosis of the adjacent skull base.
- **Schwannoma.** Schwannomas occur along the course of the cranial nerves within the cavernous sinus, most often involving the trigeminal nerve. Trigeminal schwannomas may extend into Meckel cave, the cerebellopontine angle, or the middle cranial fossa. CT may demonstrate erosion of the neural foramen and asymmetry of the cavernous regions. Lesions are typically well defined and lobulated with smooth margins. They are iso- to hypointense on T1 and hyperintense on T2 with heterogeneous enhancement.
- **Carotid-cavernous fistula (CCF).** CCFs are communications between the cavernous segment of the internal carotid artery and the venous spaces. They are most often direct fistulas related to trauma, followed by aneurysm rupture. Patients present with headaches, exophthalmos, ophthalmoplegia, and bruit. Angiographically, a CCF will demonstrate early venous drainage via the superior ophthalmic vein and inferior petrosal sinuses. On CT or magnetic resonance imaging (MRI), there is prominence and enhancement of the cavernous sinus. CCFs may be complicated by venous hypertension, which may lead to venous infarction.

Additional Differential Diagnoses

- **Tolosa–Hunt syndrome.** Tolosa–Hunt syndrome is an idiopathic, inflammatory process of the cavernous sinus that is pathologically related to orbital pseudotumor. The syndrome is characterized by recurrent, painful ophthalmoplegia with involvement of the oculomotor nerve from the superior orbital fissure to the cavernous sinus. MRI features are consistent with inflammatory pseudotumor, with an iso- to hypointense T1 and T2 appearance, enhancing following gadolinium administration.
- **Sarcoidosis.** Neurosarcoidosis results in granulomatous infiltration of perineural tissues with compressive effects. Smooth or nodular enhancement is seen along the course of the cranial nerves, along with dural or leptomeningeal enhancement. Patients will typically have pulmonary involvement on chest radiography.
- **Perineural spread of tumor.** Infiltrating sinonasal or head and neck carcinomas may extend into the cavernous sinus via entry through the skull base foramen. Postcontrast fat-saturated MRI is most helpful in demonstrating intracranial extension. The primary mass can typically be identified.

Diagnosis

Cavernous sinus meningioma

✓ Pearls

- Cavernous sinus meningiomas avidly enhance with a dural tail; they may encase and narrow the internal carotid artery.
- Cavernous sinus schwannomas most commonly involve the fifth cranial nerve; skull base erosion may be seen.
- Carotid-cavernous fistulas are most often direct and result from trauma or aneurysm rupture.
- Tolosa–Hunt syndrome is an inflammatory process of the cavernous sinus that is related to orbital pseudotumor.

Suggested Readings

Kamel HA, Toland J. Trigeminal nerve anatomy: illustrated using examples of abnormalities. AJR Am J Roentgenol 2001;176:247–251

Lee JH, Lee HK, Park JK, Choi CG, Suh DC. Cavernous sinus syndrome: clinical features and differential diagnosis with MR imaging. AJR Am J Roentgenol 2003;181:583–590

Morris P. Practical Neuroangiography. 2nd ed. Philadelphia: Lippincott Williams & Wilkins; 2007

Case 104

William T. O'Brien Sr.

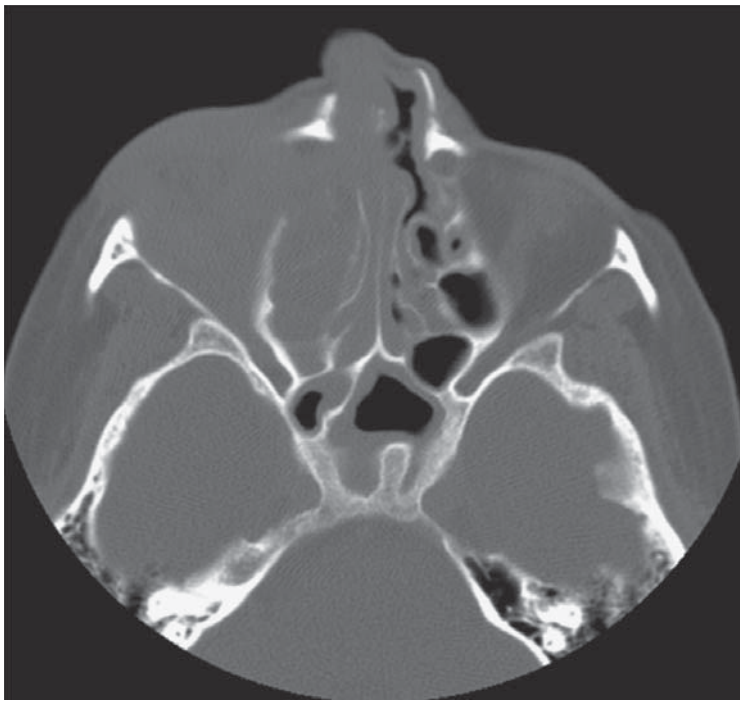


Fig. 104.1 Axial computed tomography image through the paranasal sinuses in the bone window reveals complete opacification of the right ethmoid sinus with bony erosion and overlying cartilage deformity. There is mucosal thickening involving the left ethmoid and sphenoid sinuses.

Clinical Presentation

A 32-year-old woman presents with chronic, progressive nasal congestion and cough (**Fig. 104.1**).

Key Imaging Finding

Aggressive sinus disease with bony destruction

Top 3 Differential Diagnoses

- **Invasive fungal sinusitis.** Fungal sinusitis most commonly occurs in immunosuppressed patients, especially elderly diabetics. *Mucormycosis* and *Aspergillus* are the most common causative agents, with aspergillosis also occurring in otherwise healthy individuals. *Mucormycosis* has a tendency to spread through the cavernous sinus and orbits, resulting in a life-threatening infection. *Aspergillus* invades vasculature, which results in mycotic aneurysm formation and vessel spasm or thrombosis. Fungal secretions are hyperdense on computed tomography (CT) scans; calcifications are common. Hypointensity on both T1 and T2 (more so on T2) is characteristic of fungal infection. Bony erosion is suggestive of an aggressive infection.
- **Wegener granulomatosis.** Wegner granulomatosis is a systemic vasculitis that primarily affects the kidneys and respiratory tract. Patients commonly present with recurrent sinonasal "infections," respiratory symptoms, and renal insufficiency. The necrotizing vasculitis of small and medium-sized vessels results in sinus disease (usually within the maxillary sinus) with locally erosive features. Early in the disease, the nasal septum is most involved. As the disease progresses, there is formation of a sinus mass with extensive bony erosion. The soft tissue mass is hypointense on T1- and T2-weighted sequences and enhances.
- **Sinonasal carcinoma.** Squamous cell carcinoma (SCC) accounts for ~90% of sinus malignancies. The maxillary sinus is most commonly involved, followed by the ethmoid sinus. Patients present relatively late in the disease process with obstructive sinus symptoms. Involvement of the pterygopalatine fossa allows for communication with the orbit and middle cranial fossa, most commonly through perineural spread of tumor. The tumor is hypointense on T1-weighted and intermediate to hypointense on T2-weighted sequences.

Additional Differential Diagnoses

- **Lymphoma.** Lymphoma of the paranasal sinuses is of the non-Hodgkin variant. The imaging appearance is nearly identical to that of SCC with a typically unilateral sinus mass that invades bone and is intermediate to hypointense on T2-weighted sequences. Key distinguishing features are the presence of significant lymphadenopathy within the neck and involvement of the Waldeyer tonsillar ring (a pharyngeal ring of lymphoid tissue composed of the adenoids, tubal tonsils, palatine tonsils, and lingual tonsils).
- **Cocaine nose.** Chronic use of cocaine results in a granulomatous response with a soft tissue mass and cartilaginous erosion. The local granulomatous response, combined with the vasoconstrictive properties of cocaine, results in necrosis of the nasal septum. Continued insults lead to expansion of the septal perforation.

Diagnosis

Wegener granulomatosis

✓ Pearls

- Fungal sinusitis typically occurs in immunosuppressed patients and may be hyperdense on CT and hypointense on magnetic resonance imaging.
- Wegner granulomatosis results in aggressive sinus disease, pulmonary symptoms, and renal insufficiency.
- SCC (by far the most common carcinoma) and lymphoma commonly involve the sinuses.
- Chronic cocaine abuse can lead to ischemic necrosis with bony and cartilaginous destruction.

Suggested Readings

Allbery SM, Chaljub G, Cho NL, et al. MR imaging of nasal masses. Radiographics 1995;15:1311–1327

Harnsberger HR. Diagnostic Imaging: Head and Neck. Salt Lake City, UT: Amirsys; 2004

Case 105

William T. O'Brien Sr.

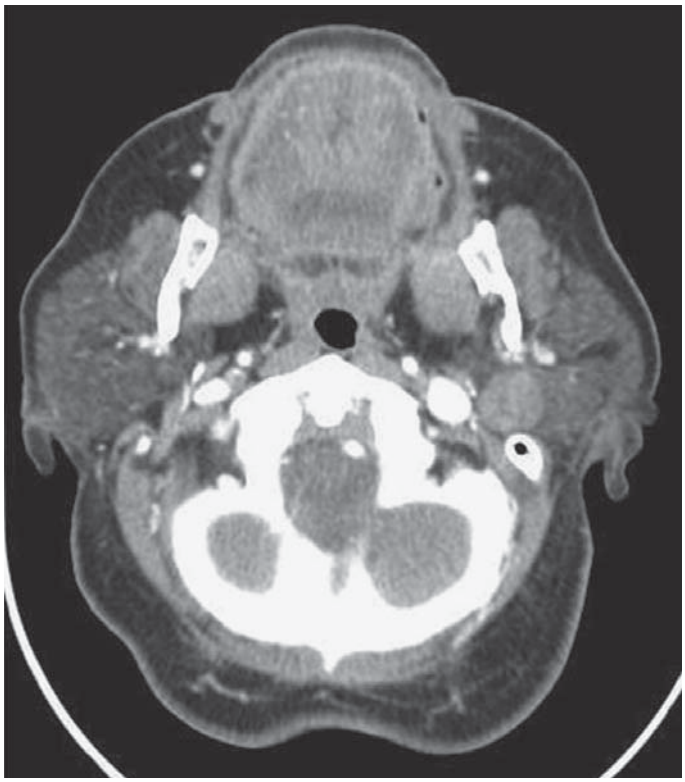


Fig. 105.1 Contrast-enhanced axial computed tomography image through the level of the skull base demonstrates a well-circumscribed, round, hyperdense mass within the deep lobe of the left parotid gland.

Clinical Presentation

A 43-year-old man presents with a palpable abnormality (**Fig. 105.1**).

Key Imaging Finding

Unilateral parotid mass

Top 3 Differential Diagnoses

- **Pleomorphic adenoma.** Benign parotid neoplasms are far more common (80%) than malignant primary neoplasms. Of all benign parotid neoplasms, pleomorphic adenoma is the most common (80%). Patients are often middle-aged and present with nonspecific symptoms or an asymptomatic palpable mass. On computed tomography (CT), pleomorphic adenomas appear as well-circumscribed, heterogeneous, round, oval, or lobulated masses. They may be located within either the superficial or deep parotid lobe, an important distinction for surgical planning. On magnetic resonance imaging (MRI), the lesions are iso- to hypointense on T1- and characteristically hyperintense on T2-weighted sequences. Delayed enhancement is typical.
- **Warthin tumor.** Warthin tumor, also known as papillary cystadenoma lyphomatosum, is the second most common benign parotid neoplasm and most commonly occurs in middle-aged men. It may be multifocal and bilateral. On imaging, the lesions are well circumscribed, with mixed cystic and solid components. CT findings include a slightly heterogeneous enhancing mass. On MRI, the solid portions are generally hypointense on T1- and intermediate in signal on T2-weighted sequences; the cystic components are hypointense on T1 and hyperintense on T2 sequences.
- **Parotid carcinoma.** Malignant neoplasms are more common in salivary glands other than the parotid gland. Of the malignant subtypes, mucoepidermoid is the most common in the parotid gland. Imaging appearance and clinical presentation vary based on the aggressiveness of the lesion. A well-circumscribed cystic lesion is more characteristic of a low-grade neoplasm, whereas an ill-defined infiltrative appearance with intermediate density and T1/T2 signal intensity suggests a more aggressive lesion. Adenoid cystic carcinoma is the second most common parotid malignancy and is typically an aggressive, infiltrative mass. Perineural spread is common, which leads to neuropathy involving the facial nerve, especially when located within the deep parotid lobe.

Additional Differential Diagnoses

- **Lymphadenopathy.** Lymphadenopathy may occur within the parotid gland from inflammatory, infectious, or neoplastic processes. Lymphoma may involve intraparotid lymph nodes and present as solitary, multiple, or bilateral masses. Lymphoma may also involve the parotid parenchyma in a diffuse, infiltrative pattern. Metastases from head and neck cancer (squamous cell carcinoma [SCC]) or skin cancer (SCC or melanoma) may also involve intraparotid lymph nodes.
- **Branchial cleft cyst.** A developmental defect of the first branchial cleft may result in an intraparotid branchial cleft cyst (type 1). The lesion is typically asymptomatic unless superinfected. Patients commonly present in adulthood with inflammation and/or a palpable mass. CT and MRI reveal a cystic mass with varying degrees of peripheral enhancement.

Diagnosis

Pleomorphic adenoma

✓ Pearls

- Pleomorphic adenomas are benign, represent the most common parotid masses, and are bright on T2-weighted images.
- Warthin tumors are typically mixed cystic and solid, occur in middle-aged men, and may be bilateral.
- Mucoepidermoid and adenoid cystic carcinomas are malignant parotid neoplasms.

Suggested Readings

Harnsberger HR. Diagnostic Imaging: Head and Neck. Salt Lake City, UT: Amirsys; 2004

Kinoshita T, Ishii K, Naganuma H, et al. MR imaging findings of parotid tumors with pathologic diagnostic clues: a pictorial essay. Clin Imaging 2004;28:93–101

Mafee MF, Valvassori GE, Becker M. Valvassori's Head and Neck Imaging. 2nd ed. New York: Thieme; 2005

Case 106

William T. O'Brien Sr.

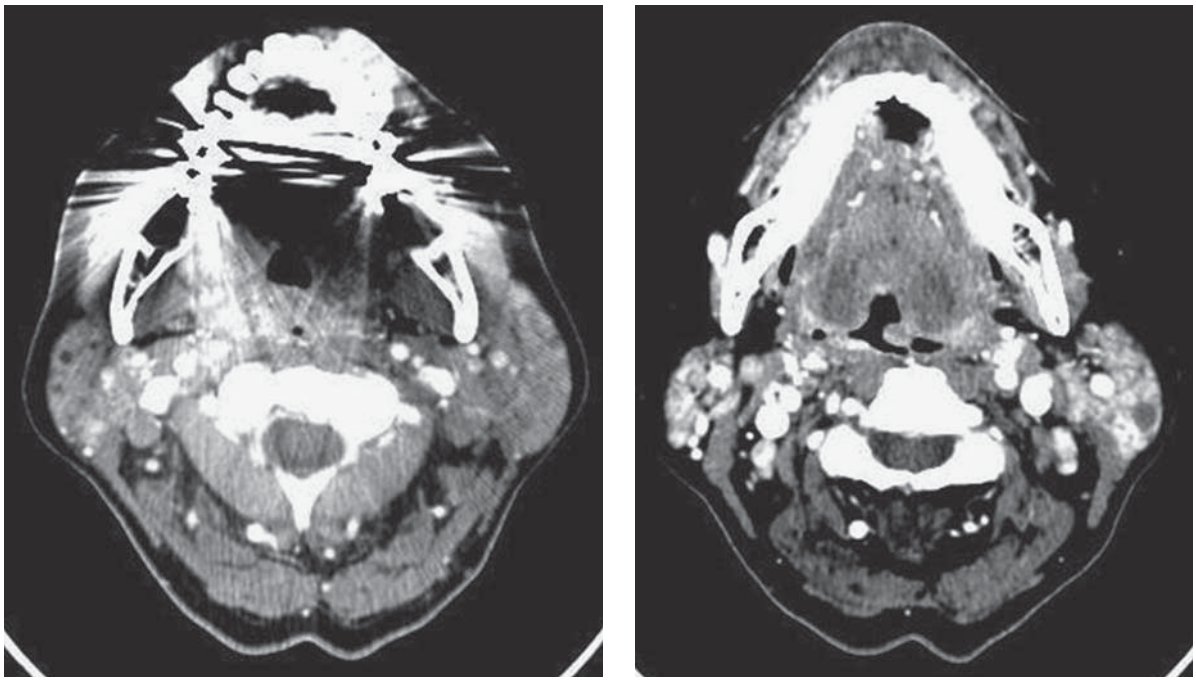


Fig. 106.1 **(A,B)** Axial computed tomography images through the neck demonstrate multiple bilateral hypodense masses within the parotid glands. (Courtesy of Rebecca Cornelius, MD, University of Cincinnati.)

Clinical Presentation

A 43-year-old woman presents with facial "swelling" (**Fig. 106.1**).

Key Imaging Finding

Bilateral parotid masses

Top 3 Differential Diagnoses

- **Lymphoepithelial lesions.** Benign lymphoepithelial lesions occur in patients with acquired immunodeficiency syndrome (AIDS) and present as bilateral parotid gland enlargement. Pathologically, there is lymphocytic infiltration of the gland (similar to Sjögren syndrome) with lymphoepithelial cyst formation. Computed tomography (CT) and magnetic resonance imaging (MRI) reveal bilateral cystic and solid parotid lesions with diffuse gland enlargement. Associated lymphadenopathy within the neck is common.
- **Sjögren syndrome.** Sjögren syndrome is an autoimmune disease that most commonly occurs in middle-aged to elderly women and results in lymphocytic infiltration of glandular tissue. The classic triad is parotid gland enlargement with keratoconjunctivitis sicca (dry eyes) and xerostomia (dry mouth). On CT and MRI, Sjögren syndrome presents as heterogeneous glandular enlargement with scattered enhancing nodules and fluid pockets. The appearance can mimic lymphoma.
- **Warthin tumors.** Warthin tumors, also known as papillary cystadenoma lymphomatosum, are the second most common benign parotid neoplasms and most commonly occur in middle-aged men. The may be both multifocal and bilateral. On imaging, the lesions are well circumscribed with mixed cystic and solid components. CT findings include a slightly heterogeneous enhancing mass. On MRI, the solid portions are generally hypointense on T1-weighted and intermediate in signal on T2-weighted sequences; the cystic components are hypointense on T1 and hyperintense on T2 sequences.

Additional Differential Diagnoses

- **Lymphadenopathy.** Lymphadenopathy may occur within the parotid gland from inflammatory, infectious, or neoplastic processes. Lymphoma may involve intraparotid lymph nodes and present as solitary, multiple, or bilateral masses. Lymphoma may also involve the parotid parenchyma in a diffuse, infiltrative pattern, similar in appearance to Sjögren syndrome. Metastases from head and neck cancer (squamous cell carcinoma [SCC]) or skin cancer (SCC or melanoma) may also involve intraparotid lymph nodes.
- **Sarcoidosis.** Sarcoidosis is a multisystem granulomatous disorder that most commonly occurs in adult African Americans. Diffuse sarcoidosis can lead to granulomatous infiltration of glandular tissue, including the parotid and lacrimal glands. Patients typically have elevated angiotensin-converting enzyme levels and may also present with uveitis and cranial nerve deficits. On imaging, there is heterogeneous glandular enlargement that is usually bilateral and symmetric. Gallium scan will reveal the classic "panda" sign with increased uptake in the parotid and lacrimal glands.

Diagnosis

Sjögren syndrome

✓ Pearls

- Lymphoepithelial lesions occur in patients with AIDS and present with bilateral cystic and solid parotid lesions.
- Sjögren syndrome is characterized by parotid enlargement/lesions, dry eyes, and dry mouth.
- Warthin tumors are typically mixed cystic and solid, occur in middle-aged men, and may be bilateral.
- Sarcoidosis results in bilateral heterogeneous parotid enlargement; the "panda" sign is seen on gallium 67 scans.

Suggested Readings

Harnsberger HR. Diagnostic Imaging: Head and Neck. Salt Lake City, UT: Amirsys; 2004

Kinoshita T, Ishii K, Naganuma H, et al. MR imaging findings of parotid tumors with pathologic diagnostic clues: a pictorial essay. Clin Imaging 2004;28:93–101

Mafee MF, Valvassori GE, Becker M. Valvassori's Head and Neck Imaging. 2nd ed. New York: Thieme; 2005

Case 107

Matthew J. Moore



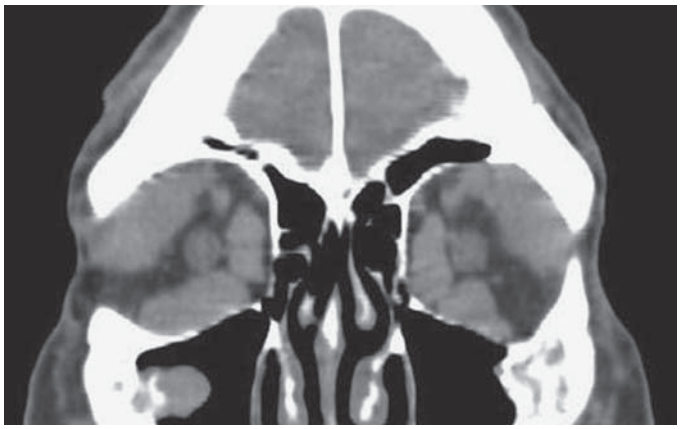


Fig. 107.1 **(A)** Axial and **(B)** coronal computed tomography images demonstrate bilateral enlargement of the extraocular muscles, primarily involving the medial, inferior, and lateral rectus muscles. Notice the bilateral proptosis and sparing of the myotendinous junctions, best appreciated at the medial rectus muscles on **A**. In addition, there is bilateral enlargement of the lacrimal glands adjacent to the superior aspect of the enlarged lateral rectus muscles.

Clinical Presentation

A 35-year-old woman complains of 3 months of "eye bulging" (**Fig. 107.1**).

Key Imaging Finding

Orbital muscle enlargement

Top 3 Differential Diagnoses

- **Thyroid-associated orbitopathy (TAO).** TAO, also known as Graves ophthalmopathy, is the most common cause of proptosis in adults. TAO is an autoimmune inflammatory condition characterized by enlargement of multiple extraocular muscle bellies with typical sparing of the myotendinous junctions. It is most commonly bilateral and preferentially affects the inferior > medial > superior > lateral > superior oblique muscles ("*I'M SLO*W" mnemonic). Increased orbital fat and lacrimal gland enlargement can also be seen. Look for stretching or compression of the optic nerve. TAO tends to affect young and middle-aged adults, particularly women. Corticosteroid treatment is effective, but some patients will require surgical therapy for uncontrolled mass effect.
- **Orbital pseudotumor.** Orbital pseudotumor, the most common cause of a painful orbital mass in adults, is an idiopathic inflammatory disease, causing infiltrative or masslike soft tissue enhancement involving any part of the orbit. Extraocular muscle (EOM) involvement, including the myotendinous junction, is the most common pattern. There may be involvement of multiple EOMs, but the findings are most commonly unilateral. When isolated lateral rectus muscle enlargement is seen, it is most likely due to orbital pseudotumor and essentially never due to thyroid orbitopathy. Other presentations are enlargement of the lacrimal gland and involvement of retrobulbar fat. Intracranial extension of pseudotumor into the cavernous sinus is known as Tolosa–Hunt syndrome.
- **Lymphoma.** Lymphoma involvement of the orbit has a broad range of imaging manifestations and should be considered in the differential for any inflammatory or infiltrative mass. Most commonly, it presents as a homogeneously enhancing solid tumor within the orbit. Lymphoma has a predilection for the lacrimal gland. Orbital lymphoma is pliable and encases normal orbital structures. It may occasionally present with primary extraocular muscle involvement, simulating thyroid orbitopathy. An indolent, painless orbital mass in an elderly patient (>60 years) is the most common clinical presentation.

Additional Differential Diagnoses

- **Sarcoidosis.** Approximately 25% of patients with sarcoidosis have associated ophthalmic disease. The most common imaging findings are the following: masslike lacrimal gland with enhancement and extraocular muscle enlargement, optic nerve thickening and enhancement, and orbital pseudotumor-like intraorbital masses. The most common presenting signs/symptoms are acute uveitis, chronic dacroadenitis, and lacrimal gland enlargement.
- **Infectious myositis.** Infectious cellulitis-myositis can be a complication of sinonasal infection, especially of the ethmoids. The most common finding is enlargement of the medial rectus muscle with associated ethmoid sinus disease. Secondary findings, in addition to adjacent sinus opacification, are subperiosteal abscess formation, osseous erosion or osteitis, and inflammatory intraorbital fat stranding.

Diagnosis

Thyroid-associated orbitopathy

✓ Pearls

- TAO is the most common cause of EOM enlargement; it is most often bilateral.
- Pseudotumor presents as a painful orbital mass; myotendinous junction involvement is characteristic.
- Infectious myositis is most commonly secondary to intraorbital extension from ethmoid sinus disease.
- Orbital lymphoma most commonly presents as an indolent painless mass in an elderly patient.

Suggested Readings

Harnsberger HR. Diagnostic Imaging: Head and Neck. Salt Lake City, UT: Amirsys; 2004

Case 108

William T. O'Brien Sr.

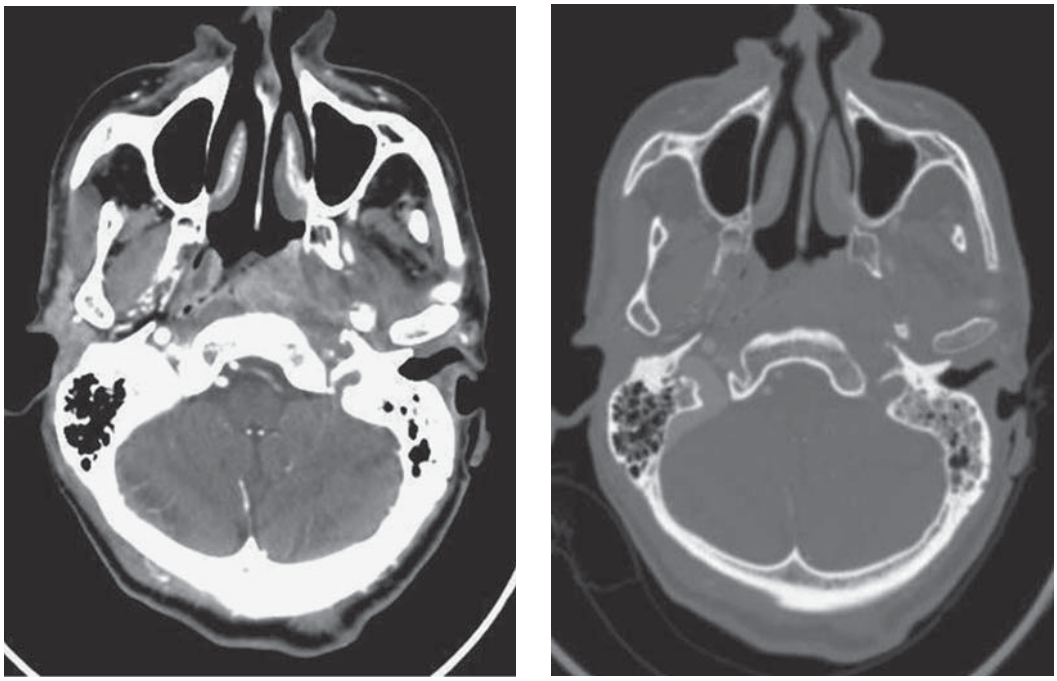


Fig. 108.1 **(A)** Axial CT image through the nasopharynx and posterior fossa in the soft tissue window reveals a heterogeneous mass in the fossa of Rosenmüller on the left with mass effect on the eustachian tube and nasopharyngeal airway. **(B)** Corresponding axial CT image in the bone window demonstrates fluid within the left mastoid air cells as a result of eustachian tube obstruction.

Clinical Presentation

A 58-year-old man presents with progressive nasal fullness and chronic ear "infections" (**Fig. 108.1**).

Key Imaging Finding

Pharyngeal mucosal mass

Top 3 Differential Diagnoses

- **Squamous cell carcinoma (SCC).** SCC is the most common primary malignancy of the head and neck. It commonly originates in the nasopharynx or oropharynx. The lesions are clinically occult until late in the disease process. Nasopharyngeal carcinoma arises from the fossa of Rosenmüller. Patients may be asymptomatic or present with nasal obstruction or hearing deficits due to obstruction of the eustachian tube and subsequent accumulation of fluid within the middle ear and mastoid air cells. Oropharyngeal SCC commonly extends laterally to involve the parapharyngeal space. The imaging appearance is that of an ill-defined heterogeneously enhancing mass. There may be local spread and lymphatic spread to cervical lymph nodes, which are commonly necrotic. Treatment depends on staging.
- **Lymphoma.** Non-Hodgkin lymphoma may involve the pharyngeal mucosa and appear similar to SCC. Patients with systemic lymphoma commonly have constitutional symptoms, along with abdominal lymphadenopathy, which are helpful discriminators. In the absence of constitutional symptoms or widespread disease, the presence of multiple enlarged cervical lymph nodes without necrosis is also suggestive of lymphoma. In some cases biopsy may ultimately be necessary to establish the diagnosis.
- **Infection/abscess.** Pharyngeal mucosal infections/abscesses result from adenoidal/tonsillar infections. Patients often present with fever and sore throat. Tonsillitis often demonstrates striated enhancement in a "tigroid" pattern without focal fluid collection. As the infection progresses and organizes, a rim-enhancing abscess may be seen. Prompt treatment is necessary to prevent retropharyngeal spread, which may allow for further spread to the mediastinum.

Additional Differential Diagnoses

- **Minor salivary gland tumor.** Benign (e.g., pleomorphic adenoma) and malignant (e.g., mucoepidermoid) minor salivary gland tumors may rarely involve the pharyngeal mucosal space. Imaging appearance is determined by the histology of the lesion, but most are ill-defined and heterogeneous, with an imaging appearance that mimics SSC and lymphoma. Metastases and associated lymphadenopathy are uncommon.
- **Thornwaldt cyst.** Thornwaldt cysts are benign developmental notochord remnants within the nasopharynx. They are cystic and midline, situated between the longissimus colli muscles. The amount of proteinaceous material determines the imaging appearances. Typically, they are hyperintense on T1- and T2-weighted sequences. Although usually incidental findings, they may be associated with halitosis and may become superinfected.

Diagnosis

Nasopharyngeal squamous cell carcinoma

✓ Pearls

- Nasopharyngeal SCC arises at the fossa of Rosenmüller and may obstruct the eustachian tube.
- The presence of constitutional symptoms or lymphadenopathy without necrosis suggests lymphoma.
- Striated tonsillar enhancement is seen with tonsillitis; abscesses show rim enhancement.
- Thornwaldt cysts are midline notochord remnants and are hyperintense on both T1- and T2-weighted sequences.

Suggested Readings

Harnsberger HR. Diagnostic Imaging: Head and Neck. Salt Lake City, UT: Amirsys; 2004

Harnsberger HR. Handbook of Head and Neck Imaging. 2nd ed. St. Louis, MO: Mosby; 1995

Shin JH, Lee HK, Kim SY, et al. Imaging of parapharyngeal space lesions: focus on the prestyloid compartment. AJR Am J Roentgenol 2001;177:1465–1470

Case 109

William T. O'Brien Sr.

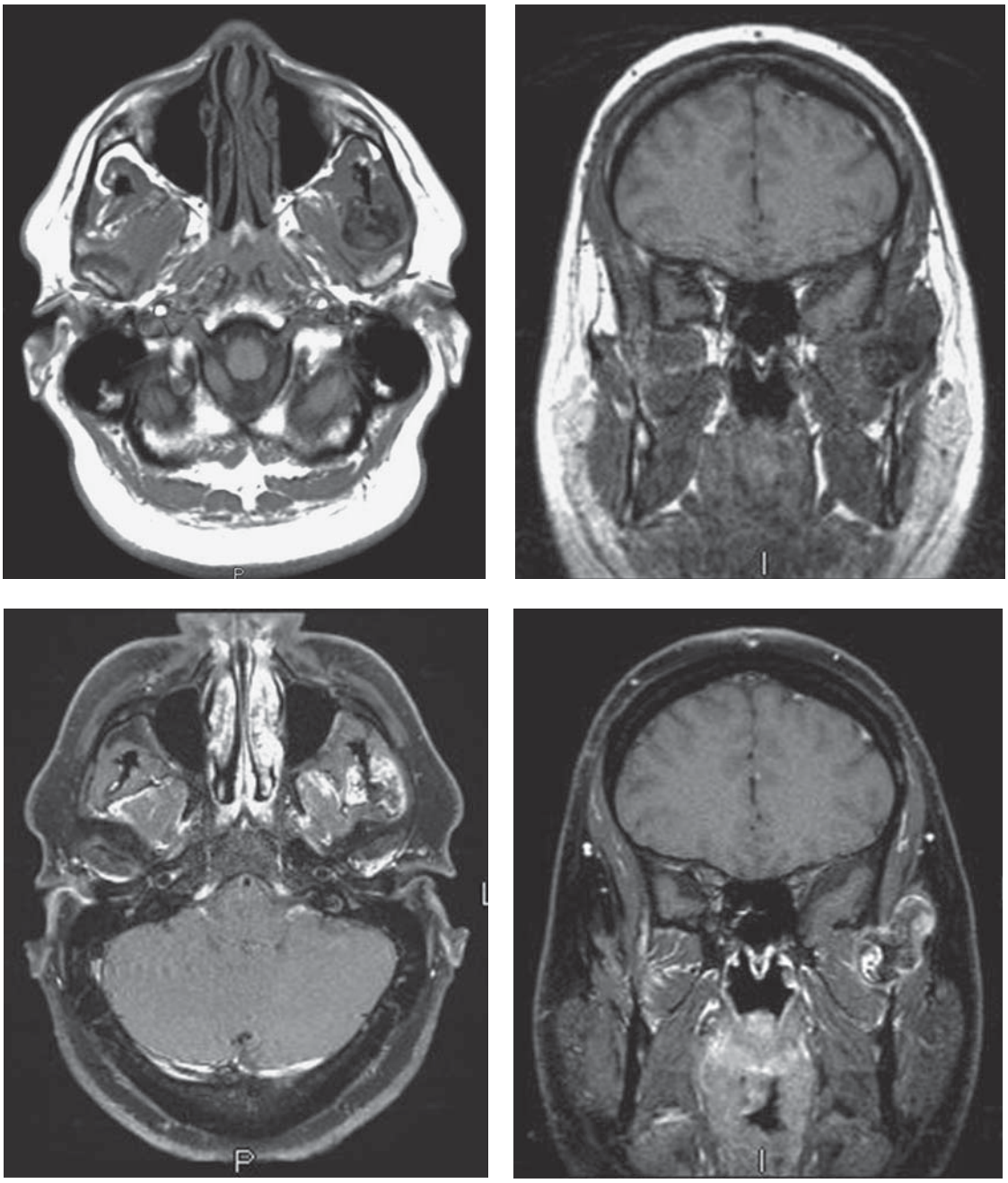


Fig. 109.1 **(A)** Axial and **(B)** coronal unenhanced T1-weighted images through the middle cranial fossa demonstrate a hypointense mass within the left masticator space centered over the mandibular condyle. **(C)** Axial and **(D)** coronal T1 postcontrast images with fat suppression reveal heterogeneous enhancement peripherally. (Courtesy of Rebecca Cornelius, MD, University of Cincinnati.)

Clinical Presentation

A young adult man presents with a palpable mass and difficulty chewing solid food (**Fig. 109.1**).

Key Imaging Finding

Masticator space mass

Top 3 Differential Diagnoses

- **Infection/abscess.** Most infections of the masticator space evolve from a dental origin. Infections may present as osteomyelitis, cellulitis, or an organized abscess. Care should be taken to evaluate the full extent of the infection, because spread to other spaces and even the intracranial compartment can occur along nerve roots and fascial planes. Bony erosion and marrow infiltration are important findings, as are drainable fluid collections, because these may alter clinical management.
- **Sarcoma.** Sarcomas within the masticator space most often arise from bone (chondrosarcoma, osteosarcoma, or Ewing sarcoma) or muscle (rhabdomyosarcoma). Occasionally, squamous cell carcinoma from a head and neck primary can secondarily involve the masticator space. Chondrosarcomas arise near the temporomandibular joint. There is typically a soft tissue mass; the presence of a chondroid matrix is a helpful distinguishing characteristic. Osteosarcoma occurs anywhere in the mandible and is an aggressive lesion with bone formation and periosteal reaction. Ewing sarcoma typically presents within the first 2 decades of life with permeative bone destruction and a soft tissue mass. The degree of periosteal reaction is variable. Rhabdomyosarcoma arises from the muscles of mastication and typically occurs in children. On magnetic resonance imaging (MRI), it may be difficult to distinguish between the types of sarcomas of the masticator space, as they all can be intermediate on T1- and hyperintense on T2-weighted sequences and demonstrate avid enhancement.
- **Venolymphatic malformation.** Hemangiomas and lymphangiomas are developmental lesions that occur within the masticator space and may expand to involve other spaces as well. Capillary hemangiomas are common in infancy but naturally regress. Cavernous hemangiomas and lymphangiomas enlarge and can cause symptoms from compression. Cavernous hemangiomas are well-circumscribed mass lesions composed of vascular channels; the presence of phleboliths is highly characteristic. Intense enhancement is seen on both computed tomography (CT) and MRI. Lymphangiomas are multiloculated (usually) cystic lesions that may cross fascial planes and involve multiple spaces. They are hypodense on CT and follow fluid signal on MRI.

Additional Differential Diagnoses

- **Nerve sheath tumor.** Both schwannomas and neurofibromas may occur within the masticator space, typically involving the mandibular division of the trigeminal nerve (V3). Schwannomas are usually more heterogeneous with cystic and solid components. They are often intermediate in signal intensity on T1- and hyperintense on T2-weighted sequences. Enhancement of the solid components is commonly seen. Neurofibromas are generally more homogeneous and typically occur in the setting of neurofibromatosis 1. They can be multiple and bilateral. On CT, the lesions are hypodense. MRI reveals an intermediate signal intensity mass on T1- and a heterogeneous mass on T2-weighted sequences. Enhancement is typical.

Diagnosis

Sarcoma (osteosarcoma)

✓ Pearls

- Most infections within the masticator space arise from a dental origin.
- Masticator space sarcomas most often arise from bone or muscle; imaging findings may overlap.
- Venolymphatic malformations occur within the masticator space and may involve multiple compartments.
- Nerve sheath tumors (neurofibromas and schwannomas) occur along the mandibular division of cranial nerve V.

Suggested Readings

Harnsberger HR. Diagnostic Imaging: Head and Neck. Salt Lake City, UT: Amirsys; 2004

Mafee MF, Valvassori GE, Becker M. Valvassori's Head and Neck Imaging. 2nd ed. New York: Thieme; 2005

Shin JH, Lee HK, Kim SY, et al. Imaging of parapharyngeal space lesions: focus on the prestyloid compartment. AJR Am J Roentgenol 2001;177:1465–1470

Case 110

William T. O'Brien Sr.

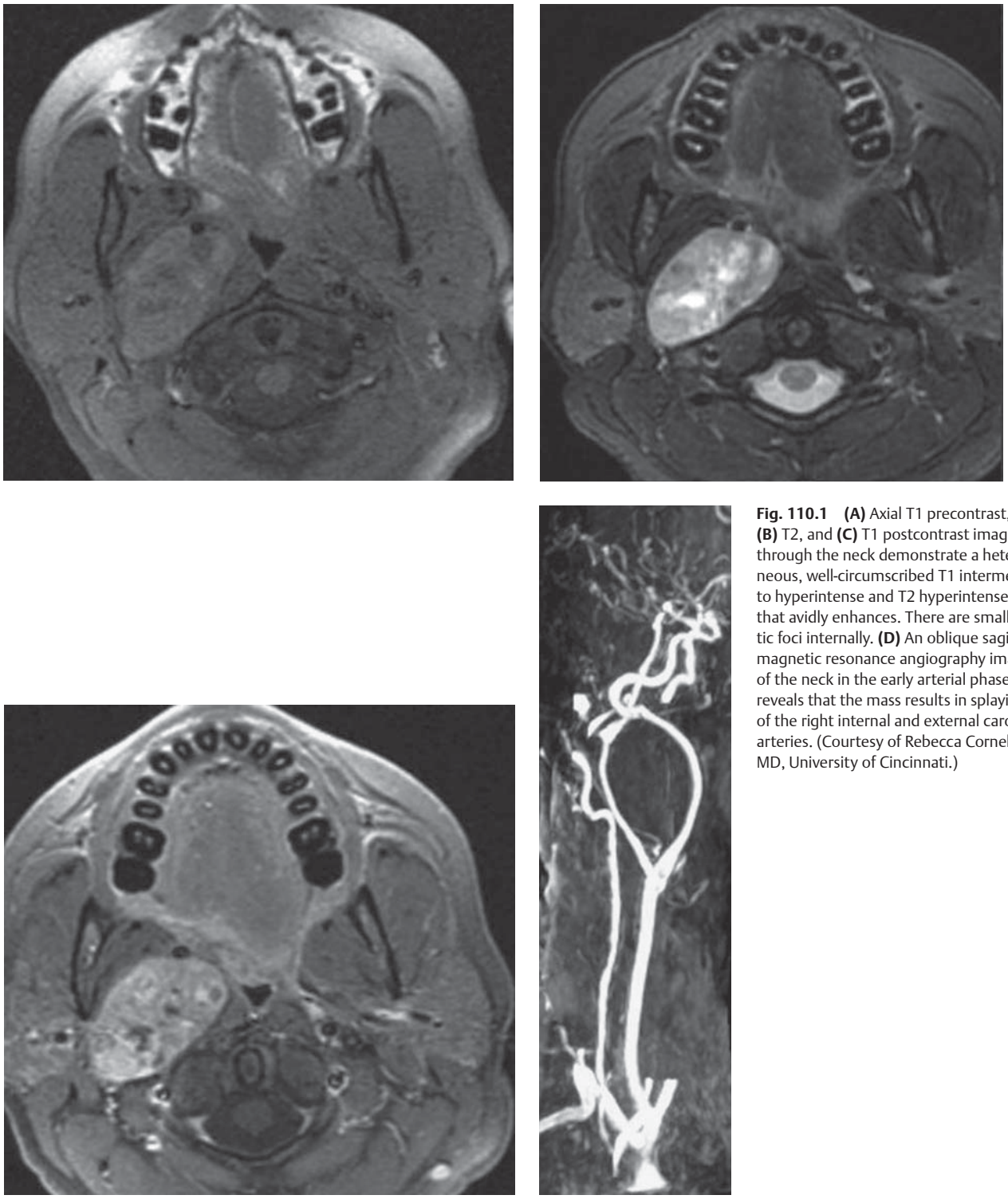


Fig. 110.1 **(A)** Axial T1 precontrast, **(B)** T2, and **(C)** T1 postcontrast images through the neck demonstrate a heterogeneous, well-circumscribed T1 intermediate to hyperintense and T2 hyperintense mass that avidly enhances. There are small cystic foci internally. **(D)** An oblique sagittal magnetic resonance angiography image of the neck in the early arterial phase reveals that the mass results in splaying of the right internal and external carotid arteries. (Courtesy of Rebecca Cornelius, MD, University of Cincinnati.)

Clinical Presentation

A 48-year-old woman presents with "fullness in the throat" (**Fig. 110.1**).

Key Imaging Finding

Carotid space mass

Top 3 Differential Diagnoses

- **Paraganglioma.** Paragangliomas arise from neural crest cells and are most common in middle-aged women. Ten percent are malignant, and 10% may be bilateral. The two most common to present as carotid space masses are the carotid body tumor, which occurs at the carotid bifurcation, and the glomus vagale, which occurs more superiorly along the course of the vagus nerve. The carotid body tumor splays the internal and external carotid arteries, which is characteristic but not pathognomonic, as other lesions may also splay the carotid arteries, including the glomus vagale. The glomus vagale displaces the internal carotid artery anteriorly. Paragangliomas are highly vascular and commonly contain calcifications and flow voids, resulting in a "salt and pepper" appearance on magnetic resonance imaging (MRI). They are associated with multiple endocrine neoplasia syndromes but are typically hormonally inactive.
- **Nerve sheath tumor.** Both schwannomas and neurofibromas may occur within the carotid space, typically involving the vagus nerve. When located more superiorly within the carotid space near the nasopharynx, cranial nerves IX, XI, and XII may occasionally be involved. Schwannomas are usually more heterogeneous with cystic and solid components. They are often intermediate in signal intensity on T1- and hyperintense on T2-weighted sequences. Enhancement of the solid components is commonly seen. Neurofibromas are generally more homogeneous and typically occur in the setting of neurofibromatosis 1. They can be multiple and bilateral. On computed tomography, the lesions are hypodense. MRI reveals an intermediate signal intensity mass on T1- and a heterogeneous mass on T2-weighted sequences. Enhancement is typical.
- **Vascular abnormality.** Vascular abnormalities and asymmetries are common causes of palpable abnormalities. The most important role for the radiologist is to identify the vascular origin of the abnormality, so that inadvertent biopsy is avoided. Normal variants, such as a dominant jugular vein, are commonly seen. In the setting of hypertension or trauma, aneurysms and pseudoaneurysms can present as carotid space masses. Venous thrombosis as a result of recent line placement, surrounding inflammation or neoplasm, or hypercoagulable state can present a diagnostic dilemma; often the wall and surrounding soft tissues enhance, mimicking a mass. The key is to identify the vascular origin of the abnormality.

Additional Differential Diagnoses

- **Lymphadenopathy.** Lymph node enlargement may be reactive, inflammatory, or neoplastic in nature. Squamous cell carcinoma from a head and neck origin is the most common cause of nodal metastases. There are typically multiple enlarged lymph nodes with abnormal architecture and possibly central necrosis. Non-Hodgkin lymphoma may also present as lymphadenopathy within the neck. Commonly, abdominal lymphadenopathy is also seen. Central necrosis may occur with treatment.

Diagnosis

Nerve sheath tumor (vagus schwannoma)

✓ Pearls

- Paragangliomas arise from neural crest cells, may have a "salt and pepper" appearance, and avidly enhance.
- Schwannomas and neurofibromas may occur along the course of the vagus nerve within the carotid space.
- Vascular abnormalities and asymmetries within the carotid space may mimic enhancing masses.
- Neoplastic lymphadenopathy is most commonly due to squamous cell carcinoma, followed by lymphoma.

Suggested Readings

Fruin ME, Smoker WR, Harnsberger HR. The carotid space in the suprahyoid neck. Semin Ultrasound CT MR 1990;11:504–519

Harnsberger HR. Handbook of Head and Neck Imaging. 2nd ed. St. Louis, MO: Mosby; 1995

Case 111

William T. O'Brien Sr.

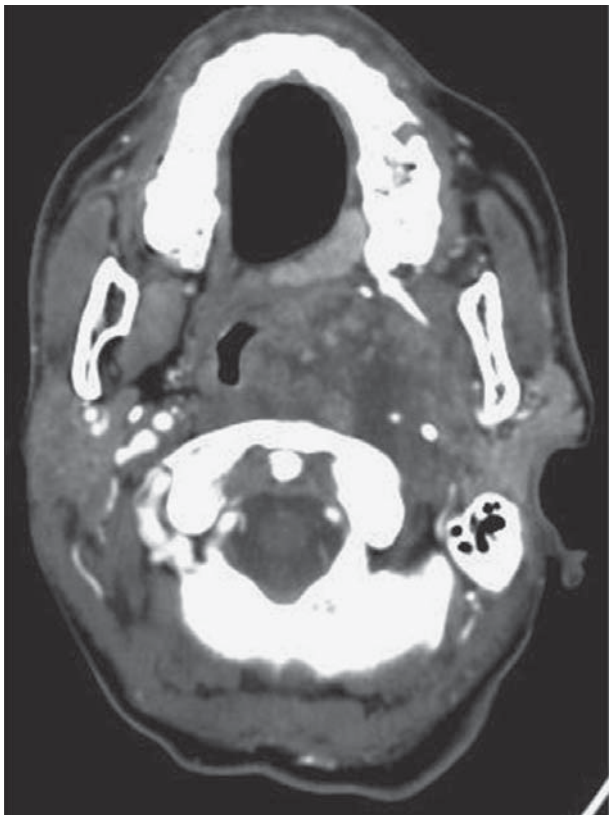


Fig. 111.1 Contrast-enhanced axial computed tomography image through the suprahyoid neck demonstrates a heterogeneous hypodense mass centered within the left retropharyngeal space with irregular peripheral enhancement and mass effect on the aerodigestive tract. The hypodensity extends into the carotid space.

Clinical Presentation

An adult man presents with a sore throat (**Fig. 111.1**).

Key Imaging Finding

Retropharyngeal mass

Top 3 Differential Diagnoses

- **Infection/abscess.** Patients with a retropharyngeal infection or abscess commonly present with fever, sore throat, and elevated white blood cell count. Involvement of the retropharyngeal space occurs from spread of infection from tonsillar tissue. Lateral radiographs will show prevertebral soft tissue swelling, prompting cross-sectional imaging. Contrast-enhanced computed tomography (CT) will show soft tissue swelling within the retropharyngeal space with inflammatory changes. An abscess will show central fluid density with peripheral enhancement. Prompt treatment is necessary, as the retropharyngeal space allows for contiguous spread of infection to the mediastinum.
- **Nodal metastases.** The vast majority of nodal metastases within the retropharyngeal space result from spread of squamous cell carcinoma (SCC), the most common neoplasm of the pharyngeal mucosa. Involvement of the lateral retropharyngeal nodes of Rouvière is characteristic, and central necrosis is common. Thyroid carcinoma (papillary variant) also metastasizes to the retropharyngeal lymph nodes, commonly resulting in central necrosis. Imaging of the remainder of the head and neck will help identify the primary lesion as originating from the pharyngeal mucosa (SCC) or thyroid gland.
- **Lymphoma.** Non-Hodgkin lymphoma may present as lymphadenopathy within the neck. Unlike other nodal chains within the neck, isolated retropharyngeal lymph node enlargement may be the initial presentation. Central necrosis may occur with treatment but is rare in the absence of treatment.

Additional Differential Diagnoses

- **Venolymphatic malformation.** Hemangiomas and lymphangiomas are developmental lesions that may occur within the suprahyoid neck. Involvement of the retropharyngeal space is usually secondary from involvement of adjacent compartments. Cavernous hemangiomas are well-circumscribed mass lesions composed of vascular channels; the presence of phleboliths is highly characteristic. Intense enhancement is seen on both CT and magnetic resonance imaging (MRI). Lymphangiomas are multiloculated (usually) cystic lesions that may cross fascial planes and involve multiple spaces. They are hypodense on CT and follow fluid signal on MRI.
- **Tortuous internal carotid artery.** Although not truly within the retropharyngeal space, tortuosity of the internal carotid artery may result in significant medial deviation, mimicking a pharyngeal/retropharyngeal mass clinically. When bilateral, they are referred to as "kissing" carotid arteries due to their close approximation. Cross-sectional imaging easily identifies the abnormality as carotid in origin, preventing inadvertent biopsy.

Diagnosis

Nodal metastases (SCC involving the lateral retropharyngeal node of Rouvière)

✓ Pearls

- Retropharyngeal infection/abscess must be treated promptly to prevent spread to the mediastinum.
- SCC is the most common cause of retropharyngeal nodal metastases, followed by papillary thyroid cancer.
- Lymphoma may initially present as isolated retropharyngeal lymphadenopathy.
- Venolymphatic malformations secondarily involve the retropharyngeal space from other compartments.

Suggested Readings

Harnsberger HR. Handbook of Head and Neck Imaging. 2nd ed. St. Louis, MO: Mosby; 1995

Shin JH, Lee HK, Kim SY, et al. Imaging of parapharyngeal space lesions: focus on the prestyloid compartment. AJR Am J Roentgenol 2001;177:1465–1470

Case 112

William T. O'Brien Sr.

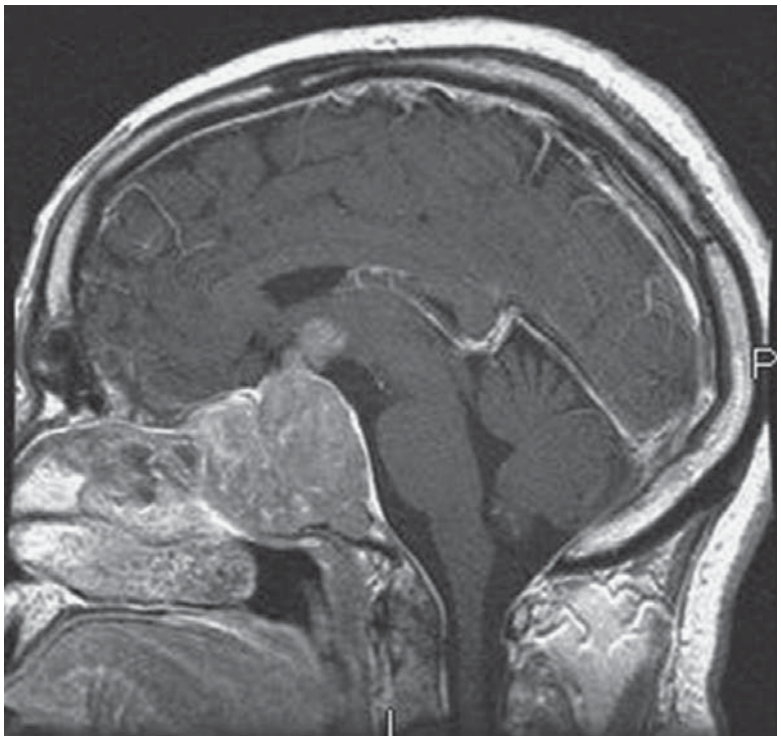


Fig. 112.1 Contrast-enhanced sagittal T1-weighted midline image through the brain demonstrates a large, expansile, enhancing soft tissue mass centered over the clivus. There is intracranial extension with involvement of the sella/suprasellar region. A pituitary gland was not identified separate from the mass.

Clinical Presentation

A 53-year-old man presents with visual disturbances (**Fig. 112.1**).

Key Imaging Finding

Clival mass

Top 3 Differential Diagnoses

- **Metastases.** Metastatic disease commonly involves the skull base. Common primary neoplasms are breast, lung, and prostate carcinoma. Breast and lung carcinoma are most often lytic, along with renal and thyroid carcinomas. Prostate (and occasionally breast) carcinoma produces sclerotic metastases. Computed tomography (CT) demonstrates bony involvement in better detail than magnetic resonance imaging (MRI), especially along the skull base. MRI is superior in evaluating the soft tissue component, as well as intracranial involvement. Metastases are hypointense on T1 and hyperintense on T2 sequences with avid enhancement. Multiple lesions are typical.
- **Chordoma.** Chordoma is a malignant tumor that arises from notochordal remnants. It most commonly occurs within the skull base and sacrum. Patients often present with headache and ophthalmoplegia due to cranial nerve involvement. It occurs most commonly in young to middle-aged adults, more often in men. CT reveals a midline, expansile lesion with hyperdense foci centrally. Chordomas are classically hyperintense on T2- and typically hypointense on T1-weighted sequences. Intratumoral hemorrhage is common. The lesions heterogeneously enhance.
- **Chondrosarcoma.** Chondrosarcomas are malignant primary bone lesions that may involve the skull base. They may occur at any age but are most common in middle-aged patients who present with cranial nerve deficits. CT demonstrates an expansile lesion with internal chondroid matrix in an "arcs and swirls" pattern. The soft tissue component is commonly hyperdense. On MRI, the chondroid matrix is hyperintense on T2 sequences; internal calcifications are hypointense. Heterogeneous enhancement is typical.

Additional Differential Diagnoses

- **Invasive pituitary macroadenoma.** Pituitary adenomas are common benign neoplasms of the pituitary gland. They are characterized as microadenomas (<10 mm) or macroadenomas (>10 mm). As a general rule, microadenomas are hormonally active, whereas macroadenomas are inactive but exert local mass effect. Occasionally, a macroadenoma can display infiltrative characteristics, invading the cavernous sinus, paranasal sinuses, clivus/skull base, and brain parenchyma. Imaging findings include a large, expansile soft tissue mass with decreased T1 and increased T2 signal; avid enhancement is typical. The normal pituitary gland is obliterated by the mass.
- **Plasmacytoma.** Plasmacytoma is the result of abnormal proliferation of plasma cells. It is the solitary form of multiple myeloma with involvement of a single bone. Patients are often older than 40 years of age. Presentation depends on the location of the mass; pain, headache, and cranial neuropathies are common. CT demonstrates a poorly marginated, expansile lytic lesion. On MRI, the lesions are typically isointense to gray matter on both T1 and T2 sequences; homogeneous enhancement is typical. Flow voids may also be present. Patients must be followed to exclude multiple myeloma.

Diagnosis

Invasive pituitary macroadenoma

✓ Pearls

- Metastases commonly involve the clivus; breast, lung, and prostate carcinomas are the most common.
- Chordomas arise from notochordal remnants; they are midline and characteristically bright on T2 sequences.
- Chondrosarcoma demonstrates a chondroid matrix with "arcs and swirls" calcifications and bright T2 signal.
- Invasive macroadenomas may involve the clivus, cavernous and paranasal sinuses, and brain parenchyma.

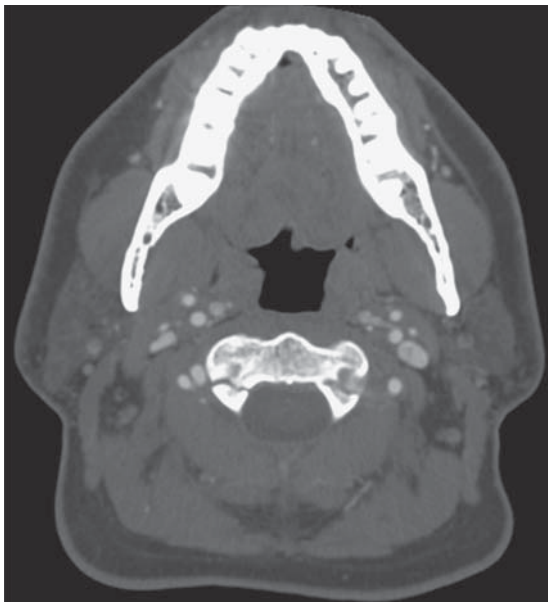
Suggested Readings

Harnsberger HR. Diagnostic Imaging: Head and Neck. Salt Lake City, UT: Amirsys; 2004

Mafee MF, Valvassori GE, Becker M. Valvassori's Head and Neck Imaging. 2nd ed. New York: Thieme; 2005

Case 113

Adam J. Zuckerman





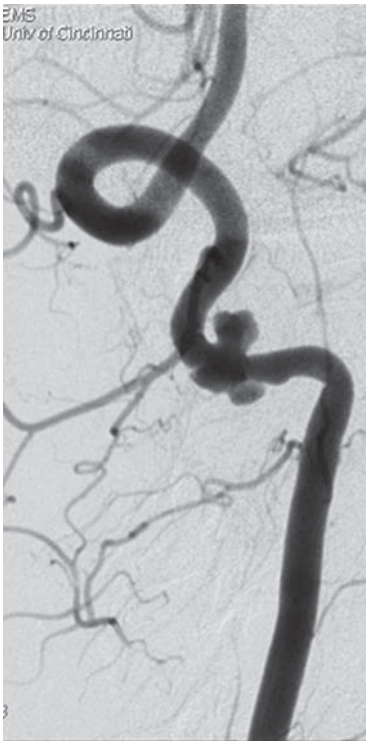




Fig. 113.1 **(A)** Contrast-enhanced axial computed tomography angiography (CTA) demonstrates a vertebral fracture of the neck through the foramen transversarium with an ovoid area of opacification adjacent to the right vertebral artery. **(B)** CTA, **(C)** conventional angiographic, and **(D)** three-dimensional rotational angiographic images depict a multilobular outpouching along the distal cervical right vertebral artery.

Clinical Presentation

A 36-year-old cyclist presents with neck pain following a collision (**Fig. 113.1**).

Key Imaging Finding

Vascular injury to the neck

Top 3 Differential Diagnoses

- **Dissection.** Arterial dissections are the result of intimal injury. They most commonly involve the cervical internal carotid and vertebral arteries; vertebral injury is most common in the V3 segment, where the vessel is most mobile. Early dissection can often present with complete occlusion of the vessel lumen preceded by a segment of tapered narrowing. Classic angiographic findings include the presence of an intimal flap or irregular segmental luminal narrowing. Computed tomography angiography (CTA) reveals eccentric luminal narrowing with relative enlargement of the cross-sectional area of the affected artery compared with the contralateral side secondary to thickening from mural hematoma. Axial fat-suppressed magnetic resonance imaging (MRI) demonstrates an eccentric, crescentic periarterial rim of signal abnormality along the margin of a flow void. Dissections can be complicated by pseudoaneurysm, thromboembolic, or occlusive phenomena. First-line treatment involves anticoagulation, with refractory cases necessitating endovascular or surgical intervention.
- **Pseudoaneurysm.** Pseudoaneurysms are more common in penetrating neck injuries than blunt neck trauma and are frequently associated with arterial dissection. They can also be due to infectious or iatrogenic causes. Pseudoaneurysms are commonly ovoid in appearance and located at the distal aspect of a stenotic segment. Doppler ultrasound of a pseudoaneurysm may demonstrate the classic "to and fro" pattern. Management is dependent upon size, location, and etiology of the pseudoaneurysm. Patients are at risk for expansion of the lesion with compression of adjacent structures and possible rupture. Treatment options are surgical resection/reconstruction or endovascular stent placement with or without coil embolization of the pseudoaneurysm.
- **Arteriovenous fistula (AVF).** AVFs are usually the result of a penetrating neck injury associated with partial transection of an artery and adjacent vein. Patients may present with a neck bruit or ischemic symptoms. AVFs may also occur spontaneously or be the result of blunt trauma with cervical spine fracture, infection, or iatrogenia. Up to 30% of patients may be asymptomatic. Posttraumatic AVFs can be diagnosed angiographically with early venous filling. CT and MRI provide additional detail on the relationship of an AVF to surrounding structures. Endovascular treatment aims to close the fistula while preserving flow in the parent artery.

Additional Differential Diagnoses

- **Thrombosis.** Complete or partial vascular occlusion is a common result of both blunt and penetrating neck injuries. A common sequela of dissection, thrombosis appears as vessel irregularity or narrowing with partial opacification or nonopacification on CTA or conventional angiography.

Diagnosis

Pseudoaneurysm

✓ Pearls

- Dissections result from intimal injury; common findings are an intramural hematoma and intimal flap.
- Pseudoaneurysms commonly result from penetrating injuries; they are at risk of expansion and rupture.
- AVFs are direct communications between an artery and vein, typically due to penetrating injuries.
- Vascular thrombosis is a common complication of both penetrating and blunt neck injuries.

Suggested Readings

Herrera DA, Vargas SA, Dublin AB. Endovascular treatment of traumatic injuries of the vertebral artery. AJNR Am J Neuroradiol 2008;29:1585–1589

Morris P. Practical Neuroangiography. 2nd ed. Philadelphia: Lippincott Williams & Wilkins; 2007

Nunez DB, Torres-Leon M, Munera F. Vascular injuries of the neck and thoracic inlet: helical CT-angiographic correlation. Radiographics 2004;24:1087–1098

Provenzale JM. Dissection of the internal carotid and vertebral arteries: imaging features. AJR Am J Roentgenol 1995;165:1099–1104

Case 114

William T. O'Brien Sr.



Fig. 114.1 Unenhanced axial computed tomography image of the orbits demonstrates soft tissue density and calcification along the posterior aspect of the right globe. The right globe is slightly larger than the left but otherwise normal in configuration. (Courtesy of Rebecca Cornelius, MD, University of Cincinnati.)

Clinical Presentation

A young child presents with an abnormal screening examination (**Fig. 114.1**).

Key Imaging Finding

Globe lesion in a child

Top 3 Differential Diagnoses

- **Retinoblastoma.** Retinoblastoma is a malignant neoplasm of the retina and represents the most common globe tumor in children. Nearly all cases present prior to 5 years of age, with leukocoria (white pupillary reflex) being the most common presenting sign. Approximately 75% of cases are unilateral, with the remainder bilateral. Trilateral (bilateral globe plus pineal gland involvement) and quadrilateral (trilateral plus suprasellar involvement) disease is seen in familial cases. Unenhanced computed tomography (CT) demonstrates a hyperdense globe mass with calcifications (95%). Globe size is normal. The mass is hyperintense on T1 and hypointense on T2 sequences with avid enhancement. Treatment options are chemotherapy, radiation, and enucleation. Distinguishing features include a normal globe size and the presence of calcification.
- **Persistent hyperplastic primary vitreous (PHPV).** PHPV results from persistence of the embryonic vascularity within the vitreous, which may result in vitreous hemorrhage, cataracts, and retinal detachment. In severe disease, phthisis bulbi may occur with globe deformity. Characteristic imaging findings are microphthalmia and increased density in the vitreous. The density may change location with repositioning of the patient. Magnetic resonance imaging (MRI) findings consist of increased T1 and T2 signal within the vitreous. Calcifications are not a feature of PHPV. This may be difficult to distinguish from other entities, especially noncalcified retinoblastoma. A key distinguishing feature is microphthalmia in a full-term infant.
- **Coats disease.** Coats disease occurs primarily in young male children and is characterized by subretinal exudates, retinal detachment, and vascular anomalies of the retina. The primary imaging findings are exudates in the region of the retina and retinal detachment. CT reveals increased density within the affected globe without calcification. Subretinal exudates are better visualized on MRI as regions of increased T1 and T2 signal. Distinguishing features are normal globe size and lack of calcification.

Additional Differential Diagnoses

- **Retinopathy of prematurity (ROP).** ROP, also referred to as retrolental fibroplasia, occurs as a sequela of prolonged oxygen therapy in premature infants, resulting in abnormal vascular development and hemorrhage. A key imaging feature is bilateral (usually) microphthalmia. Resultant hemorrhage leads to increased density within the globe and retinal detachment. Calcification may occur in advanced cases. Bilateral involvement and a history of prematurity help distinguish this entity from the other differentials.
- **Toxocariasis.** Ocular toxocariasis results from hypersensitivity to the larval form of *Toxocara*. The infection is transmitted through contact with dogs and cats. Patients present with unilateral visual disturbances. On CT, imaging findings include hyperdensity within the globe often without a focal mass. The lesion is isointense on T1- and hyperintense on T2-weighted sequences. Distinguishing features are normal globe size, lack of calcification, and a history of contact with dogs or cats.

Diagnosis

Retinoblastoma

✓ Pearls

- Retinoblastoma is the most common globe tumor in children and presents with leukocoria and calcification.
- PHPV is due to persistent embryonic vascularity and presents as microphthalmia in a full-term infant.
- Coats disease is characterized by retinal detachment and lack of calcification with a normal globe size.
- ROP is caused by prolonged oxygenation; bilateral microphthalmia without calcification is characteristic.

Suggested Readings

Chung EM, Specht CS, Schroeder JW. Pediatric orbit tumors and tumorlike lesions: neuroepithelial lesion of the ocular globe and optic nerve. Radiographics 2007;27:1159–1186

Harnsberger HR. Diagnostic Imaging: Head and Neck. Salt Lake City, UT: Amirsys; 2004

Case 115

William T. O'Brien Sr.

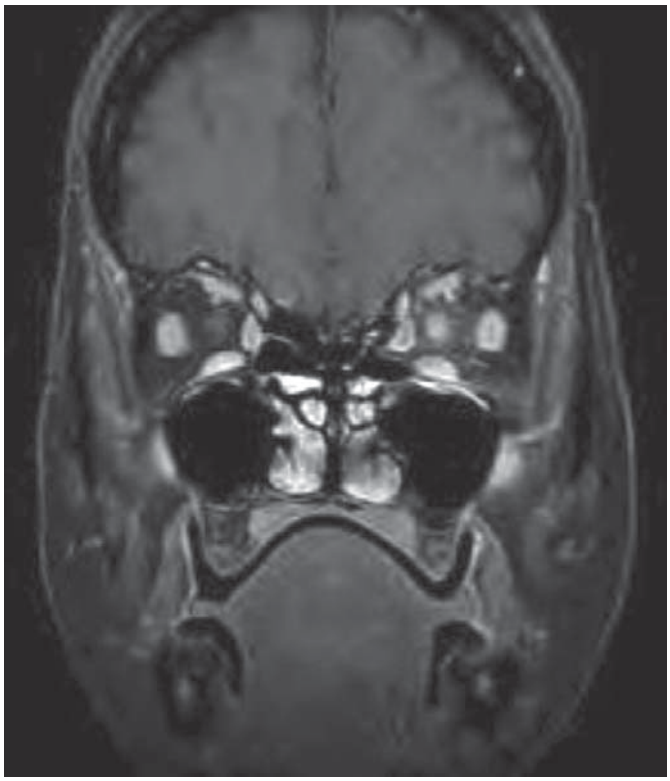


Fig. 115.1 Coronal T1 postgadolinium image with fat suppression demonstrates diffuse enlargement and abnormal enhancement involving the left optic nerve with some mild adjacent inflammatory changes. There is normal enhancement of the extraocular muscles.

Clinical Presentation

A young adult woman presents with visual changes (**Fig. 115.1**).

Key Imaging Finding

Optic nerve enlargement and enhancement

Top 3 Differential Diagnoses

- **Optic nerve glioma.** Optic nerve gliomas are low-grade neoplasms (juvenile pilocytic astrocytoma) that typically occur between 5 and 15 years of age. They are the most common cause of optic nerve enlargement. Patients present with vision loss with or without proptosis. Optic nerve gliomas may occur sporadically or be associated with neurofibromatosis 1 (NF1); bilateral optic nerve involvement is pathognomonic for NF1. Tumors cause enlargement, elongation, and "buckling" of the optic nerve, resulting in the "dotted *i*" sign. Enlargement of the optic canal may also be seen. Enhancement is variable. The tumor may extend along the optic pathway (chiasm, tracts, and optic radiations). NF1 predominantly involves the optic nerve with preservation of nerve morphology. Non-NF1 cases most often involve the optic chiasm/hypothalamus, are larger and masslike, commonly have cystic degeneration, and can extend beyond the optic pathways.
- **Optic neuritis.** Optic neuritis is most commonly due to demyelination secondary to an autoimmune or viral process. Multiple sclerosis (MS) involves the optic nerve in approximately one third of cases. Approximately one half to three fourths of patients will develop MS within 15 years of the first episode of optic neuritis. Other etiologies are ocular infection, toxic or metabolic degeneration, ischemia, and meningitis/encephalitis. Patients present with ipsilateral orbital pain with eye movement and vision loss over hours to days. Magnetic resonance imaging (MRI) best demonstrates an enlarged optic nerve with abnormal T2/fluid-attenuated inversion recovery (FLAIR) signal intensity, best visualized on coronal sequences. Axial and coronal T1-weighted postgadolinium images demonstrate enlargement and enhancement of the affected optic nerve.
- **Optic nerve sheath meningioma.** Meningiomas arise from arachnoid rests in the meninges covering the optic nerve. Eighty percent occur in female patients and typically present in the 4th decade with progressive loss of vision (optic nerve atrophy). They may occur as tubular (most common), fusiform, or eccentric masses associated with the optic nerve. The lesions may be hyperdense on computed tomography; calcification is common (20–25%). On MRI, they are typically isointense to gray matter on T1- and variable in signal on T2-weighted imaging. Enhancement is intense and relatively homogeneous. The "tram track" sign on postcontrast axial imaging represents linear bands of enhancement surrounding the central nonenhancing optic nerve. Sphenoid bone and/or optic canal hyperostosis may be seen, and there may be extension into the optic canal.

Additional Differential Diagnoses

- **Leukemia/lymphoma.** Leukemia and non-Hodgkin lymphoma may involve the orbit in a variety of presentations. Involvement of the optic nerve–sheath complex with regions of enhancement is the least common manifestation. The lesions may be bilateral.
- **Sarcoidosis.** Central nervous system involvement (neurosarcoidosis) occurs in ~5% of sarcoidosis patients. Isolated optic nerve involvement is rare but should be considered in the differential diagnosis of an optic nerve lesion. Varying degrees of enhancement (nodular) are commonly seen.

Diagnosis

Optic neuritis

✓ Pearls

- Optic nerve gliomas are the most common cause of optic nerve enlargement and are associated with NF1.
- Optic neuritis is commonly due to demyelination; the majority of patients will develop MS within 15 years.
- Optic nerve sheath meningiomas demonstrate "tram track" enhancement on axial imaging.

Suggested Readings

Kornreich L, Blaser S, Schwarz M, et al. Optic pathway glioma: correlation of imaging findings with the presence of neurofibromatosis. AJNR Am J Neuroradiol 2001;22:1963–1969

Osborn A, Blaser S, Salzman KL, et al. Diagnostic Imaging: Brain. Salt Lake City, UT: Amirsys; 2004

Case 116

Adam J. Zuckerman

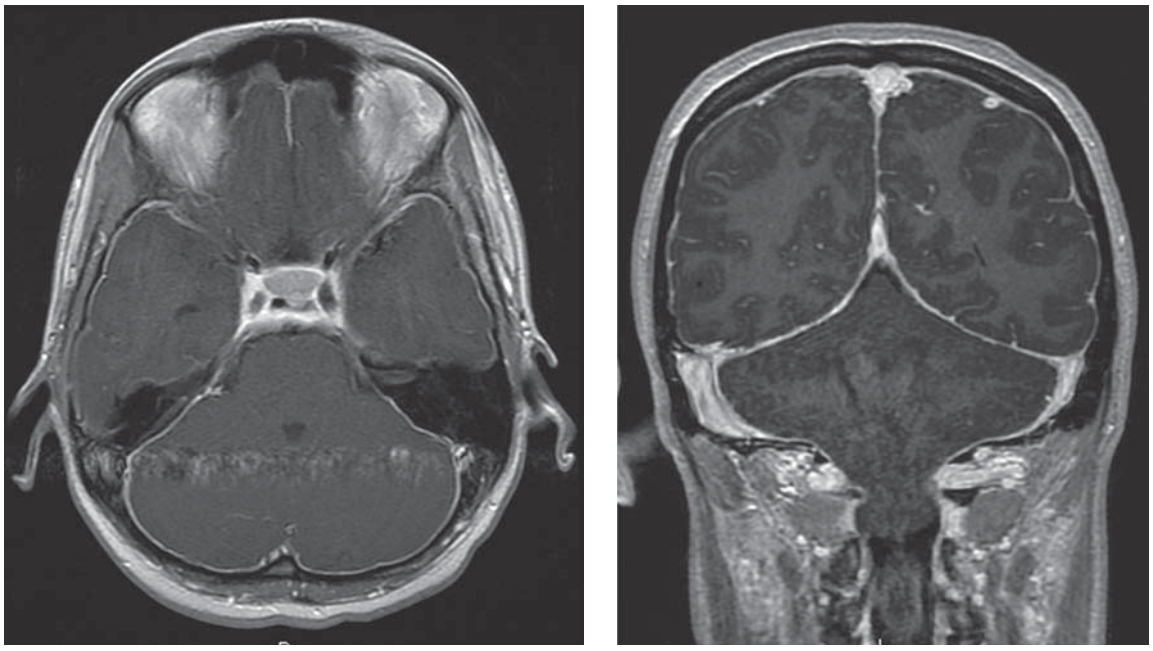


Fig. 116.1 **(A)** Postcontrast axial and **(B)** coronal T1-weighted images demonstrate diffuse abnormal pachymeningeal (dural) enhancement. The cerebellar tonsils are inferiorly displaced through the foramen magnum on the coronal view.

Clinical Presentation

A 26-year-old postpartum woman presents with orthostatic headaches (**Fig. 116.1**).

Key Imaging Finding

Pachymeningeal (dural) enhancement

Top 3 Differential Diagnoses

- **Intracranial hypotension.** Intracranial hypotension is caused by a cerebrospinal fluid (CSF) leak. Most cases are secondary to trauma or are iatrogenic in nature. Patients present with orthostatic headaches. Classic imaging findings include diffuse pachymeningeal (dural) enhancement and caudal displacement of the cerebellar tonsils ("sagging brain" appearance). Subdural fluid collections, venous engorgement/distention, and pituitary hyperemia are also found in patients with intracranial hypotension. If the site of the CSF leak is unknown, computed tomography, magnetic resonance imaging (MRI), or radionuclide cisternography may be useful in determining the origin of the leak. Epidural blood patching is the most common first-line treatment.
- **Metastases.** Metastatic disease commonly affects the pachymeninges/dura either from hematogenous spread or extension from skull-based lesions. Breast, lung, and prostate carcinomas are the most common primary neoplasms; hematologic malignancies, such as lymphoma and leukemia, may also demonstrate abnormal dural enhancement. The regions of abnormal enhancement may be smooth and diffuse or more focal and nodular. Although most lesions are asymptomatic, cranial neuropathies have been described.
- **Pachymeningitis.** Meningeal infection may be due to bacterial, viral, or fungal etiology. The diagnosis is made clinically with CSF sampling; imaging is used to evaluate for suspected complications. Meningeal enhancement is evident in only ~50% of patients with meningitis and commonly involves both the leptomeninges and pachymeninges. *Mycobacterium tuberculosis* classically results in meningeal disease involving the skull base, cerebritis, and intracranial abscess formation (tuberculoma); isolated tuberculosis pachymeningitis with associated enhancement has been described in immunocompromised patients.

Additional Differential Diagnoses

- **Subdural hemorrhage.** Subdural hemorrhage typically results from tearing of bridging veins and is most often due to trauma. In contrast to epidural hemorrhages, subdural collections may cross sutures but cannot cross the midline. The blood products within the hemorrhage are a source of meningeal irritation, which manifests as enhancement on MRI. Patients often have an antecedent history of trauma.
- **Sarcoidosis.** Approximately 5% of sarcoid patients develop symptoms of central nervous system involvement. Neurosarcoidosis commonly affects the meninges (leptomeningeal, pachymeningeal, or both) with granulomatous infiltration. This infiltration results in smooth or nodular (more common) meningeal enhancement. Perineural involvement along the skull base results in cranial neuropathies.

Diagnosis

Intracranial hypotension

✓ Pearls

- Intracranial hypotension results from a CSF leak; findings include dural enhancement and tonsillar ectopia.
- Dural-based metastases may result from hematogenous spread or direct spread from a skull-based lesion.
- Common imaging findings of meningitis are both leptomeningeal and pachymeningeal enhancement.
- Neurosarcoidosis often results in nodular meningeal enhancement; cranial neuropathies are common.

Suggested Readings

Castillo M. Imaging of meningitis. Semin Roentgenol 2004;39(4):458–464

Christoforidis GA, Spickler EM, Recio MV, Mehta BM. MR of CNS sarcoidosis: correlation of imaging features to clinical symptoms and response to treatment. AJNR Am J Neuroradiol 1999;20:655–669

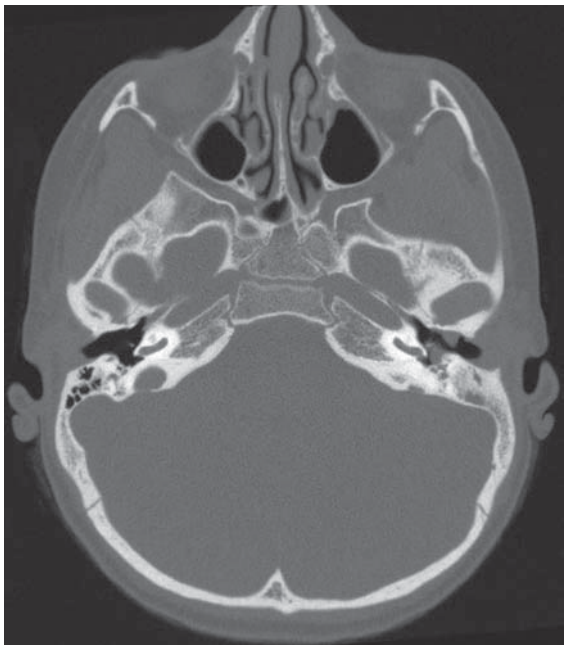
Goyal M, Sharma A, Mishra NK, Gaikwad SB, Sharma MC. Imaging appearance of pachymeningeal tuberculosis. AJR Am J Roentgenol 1997;169:1421–1424

Schievink WI, Maya MM, Louy C, Moser FG, Tourje J. Diagnostic criteria for spontaneous spinal CSF leaks and intracranial hypotension. AJNR Am J Neuroradiol 2008;29:853–856

Smirniotopoulos JG, Murphy FM, Rushing EJ, et al. From the *Archives of the AFIP:* patterns of contrast enhancement in the brain and meninges. Radiographics 2007;27:525–551

Case 117

William T. O'Brien Sr.



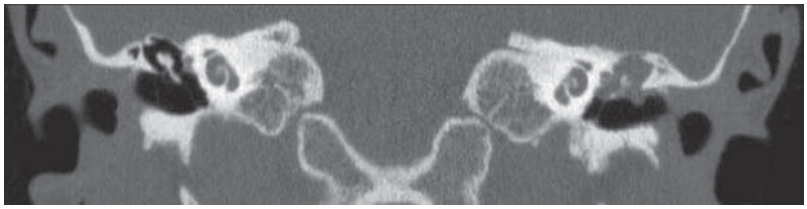


Fig. 117.1 **(A)** Axial image from a noncontrast head CT scan in the bone window demonstrates a lobulated soft tissue density within the left middle ear. There are sclerosis and opacification within the left mastoid air cells, suggestive of chronic inflammation. **(B)** Coronal reformatted CT image through the temporal bone in the bone window shows the mass within the epitympanum and lateral attic (Prussak space) with blunting of the scutum and erosion/demineralization of the ossicles.

Clinical Presentation

A young adult man presents with chronic ear pain and conductive hearing loss (**Fig. 117.1**).

Key Imaging Finding

Middle ear mass

Top 3 Differential Diagnoses

- **Acquired cholesteatoma.** Cholesteatomas are epidermoid cysts composed of keratinized squamous epithelium. Within the middle ear, the vast majority of cases result from chronic otitis media. Patients suffer from multiple ear infections with perforation of a retracted tympanic membrane and conductive hearing loss. On imaging, cholesteatomas appear as soft tissue masses within Prussak space in the lateral attic. There is often blunting of the scutum (lateral wall of the attic) and erosion of the ossicles. When large, cholesteatomas may extend into the mastoid air cells. It is important to identify the bony margin of the facial nerve for presurgical planning, as well as to define the full extent of the mass for the surgeon. Complications include coalescent mastoiditis, meningitis, epidural abscesses, and venous sinus thrombosis.
- **Facial nerve schwannoma.** Facial nerve schwannomas may occur anywhere along the course of the facial nerve. When they occur within the tympanic segment within the middle ear, there is often enlargement of the bony facial nerve canal. Postcontrast images will demonstrate enhancement of the mass, which may extend into the labyrinthine segment, a helpful finding to distinguish this entity from other middle ear masses. As these lesions can be subtle, it is important to look for asymmetry with the contralateral side.
- **Glomus tympanicum.** Glomus tympanicum is a paraganglioma that occurs within the middle ear along the cochlear promontory. It arises from neural crest origin and is highly vascular with avid enhancement. As the mass grows, it fills the middle ear and encroaches on the ossicles. Bony erosion may be seen. When large, these types of paragangliomas may contain calcifications and flow voids, resulting in a "salt and pepper" appearance on magnetic resonance imaging (MRI). Clinically, patients present with conductive hearing loss and pulsatile tinnitus.

Additional Differential Diagnoses

- **Normal variant vasculature.** An aberrant internal carotid artery (ICA) is a developmental abnormality that likely results from regression of the cervical and proximal petrous ICA and the development of alternate anastomoses. Imaging findings are medial deviation and narrowing of the ICA within the temporal bone (extending into the middle ear), along with absence of the cervical and proximal portion of the petrous ICA. A dehiscent jugular bulb occurs when the sigmoid plate of the jugular bulb is absent, allowing for extension of the jugular bulb into the middle ear cavity. Imaging findings are diagnostic.
- **Cholesterol granuloma.** Cholesterol granulomas occur secondary to nonspecific chronic inflammatory changes and are seen most commonly in the temporal bone (middle ear and petrous apex). Computed tomography reveals a soft tissue mass within the middle ear without osseous erosions. On physical examination, there is a bluish or purplish coloration of the tympanic membrane. The lesions are hyperintense on both T1- and T2-weighted MRI sequences due to hemorrhage within the lesions. There may be peripheral rim enhancement.

Diagnosis

Acquired cholesteatoma

✓ Pearls

- Acquired cholesteatomas occur in Prussak space and cause blunting of the scutum and ossicular erosion.
- Facial nerve schwannoma presents as an enhancing mass within an expanded facial nerve canal.
- Glomus tympanicum is a highly vascular paraganglioma and occurs along the cochlear promontory.
- Normal variant vasculature (aberrant ICA and dehiscent jugular bulb) may present as a middle ear mass.

Suggested Readings

Harnsberger HR. Diagnostic Imaging: Head and Neck. Salt Lake City, UT: Amirsys; 2004

Mafee MF, Valvassori GE, Becker M. Valvassori's Head and Neck Imaging. 2nd ed. New York: Thieme; 2005

Remley KB, Coit WE, Harnsberger HR, et al. Pulsatile tinnitus and the vascular retrotympanic membrane: CT, MR, and angiographic findings. Radiology 1990;174:383–389

Case 118

William T. O'Brien Sr.

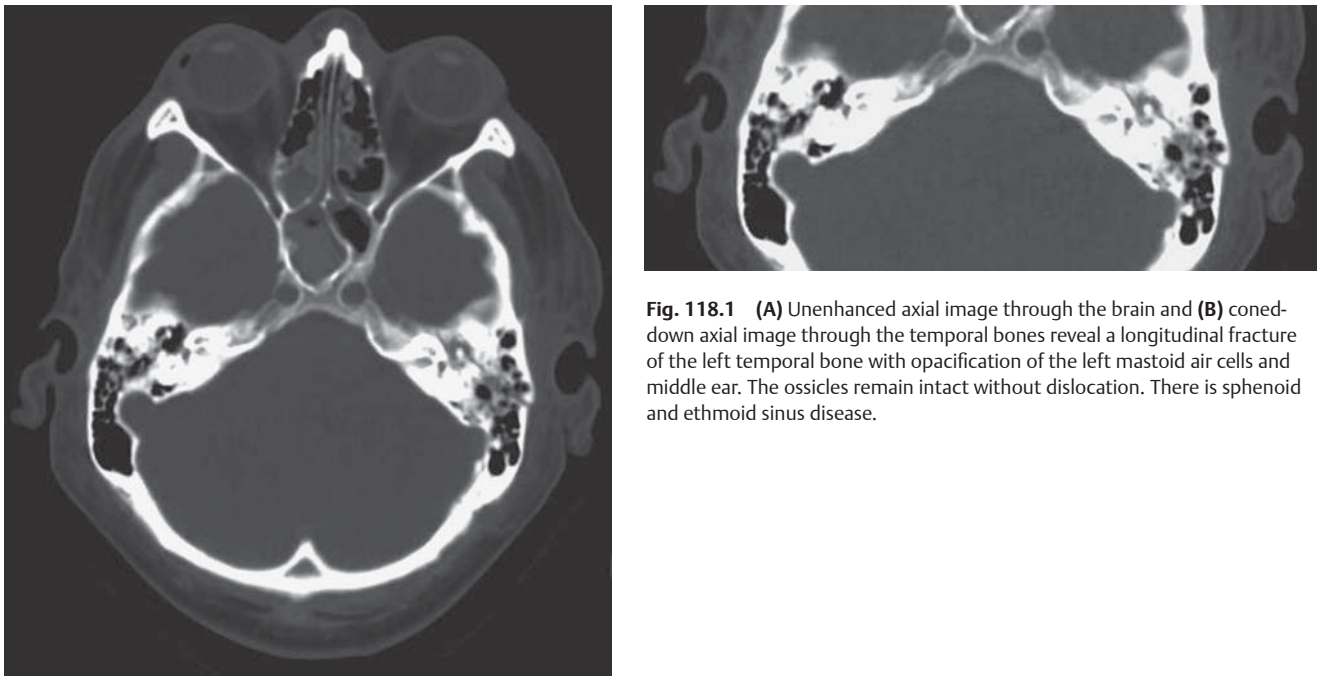


Fig. 118.1 **(A)** Unenhanced axial image through the brain and **(B)** coned-down axial image through the temporal bones reveal a longitudinal fracture of the left temporal bone with opacification of the left mastoid air cells and middle ear. The ossicles remain intact without dislocation. There is sphenoid and ethmoid sinus disease.

Clinical Presentation

A patient presents with difficulty hearing after a motor vehicle accident (**Fig. 118.1**).

Key Imaging Finding

Temporal bone trauma with mastoid fluid

Top 3 Differential Diagnoses

- **Longitudinal temporal bone fracture.** Temporal bone fractures typically occur in the setting of significant trauma. Patients may present with hearing loss (typically conductive), facial nerve deficits, or otorrhea. Longitudinal fractures are the most common subtype (75%) and are oriented along the long axis of the temporal bone, affecting the squamous portion of the temporal bone and extending into the mastoid portion. Unless there is significant displacement of the fracture, such fractures can be subtle on computed tomography examinations. Secondary findings are blood products within the mastoid air cells, middle ear, or external auditory canal. Complications of longitudinal fractures include ossicular dislocation (most common) and facial nerve injury (less common than with transverse fractures). Ossicular dislocation commonly presents as the "ice cream" (head of the malleus) falling off the "cone" (short process of the incus).
- **Transverse temporal bone fracture.** The clinical presentation of transverse temporal bone fractures is similar to that of longitudinal fractures. In addition, patients may present with an inner ear abnormality, such as sensorineural hearing loss or vertigo. The fractures are oriented perpendicular to the long axis of the temporal bone and commonly involve inner ear structures. Once identified, care should be taken to evaluate for involvement of the jugular fossa, inner ear structures, and facial nerve. Facial nerve injury is more common with transverse temporal bone fractures than longitudinal fractures; ~50% of all transverse fractures will involve the facial nerve.
- **Mixed temporal bone fracture.** In many instances, there will be variants of both longitudinal and transverse temporal bone fractures in the setting of trauma. When this occurs, it is important to evaluate all segments of the fracture, paying close attention to involvement of vascular channels (including the jugular canal and petrous segment of the internal carotid artery), inner ear structures, the facial nerve, and ossicles.

Diagnosis

Longitudinal temporal bone fracture

✓ Pearls

- Longitudinal temporal bone fractures commonly result in ossicular dislocation and conductive hearing loss.
- Transverse temporal bone fractures more commonly affect the facial nerve and inner ear structures.
- Vascular injury may occur when fractures extend into the jugular canal and petrous segments of the internal carotid artery.

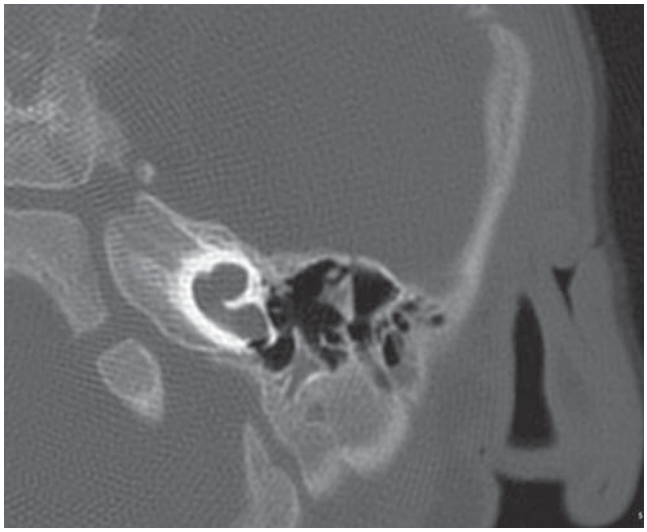
Suggested Readings

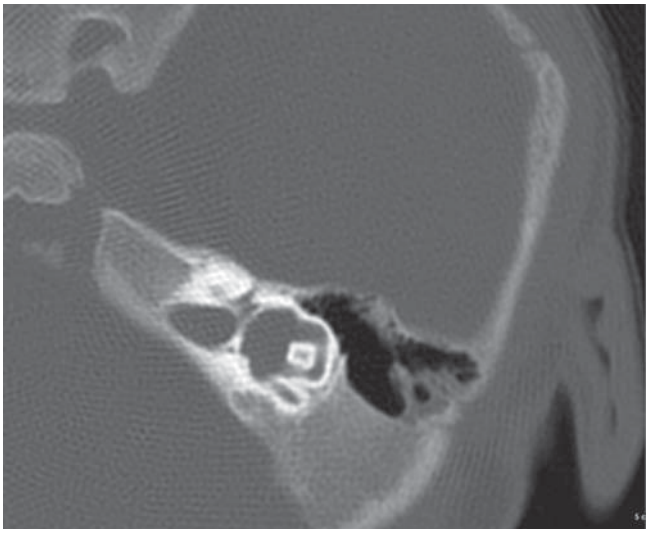
Fatterpekar GM, Doshi AH, Dugar M, et al. Role of 3D CT in the evaluation of the temporal bone. Radiographics 2006;26:S117–S132

Mafee MF, Valvassori GE, Becker M. Valvassori's Head and Neck Imaging. 2nd ed. New York: Thieme; 2005

Case 119

William T. O'Brien Sr.





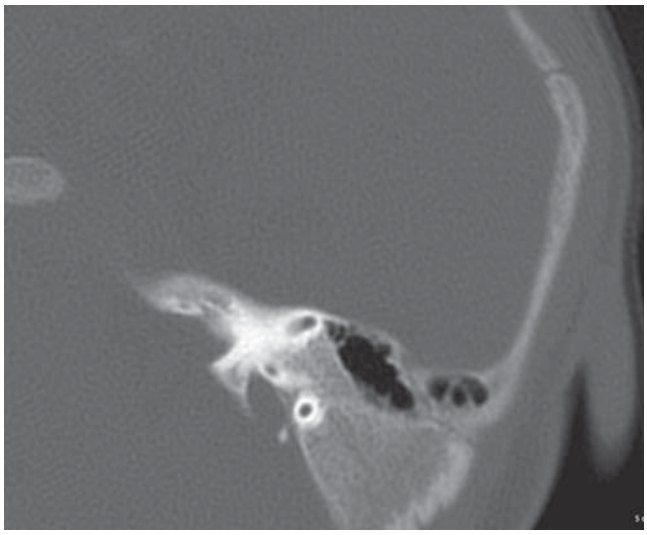


Fig. 119.1 **(A–C)** Coned-down axial computed tomography images in the bone window through the left inner ear demonstrate abnormal configuration of the cochlea with lack of visualization of **(A)** the normal two and a half turns, **(B)** an enlarged vestibule, and **(C)** enlargement of the vestibular aqueduct. The right side was similar in appearance. (Courtesy of Cincinnati Children's Hospital Medical Center.)

Clinical Presentation

A 6-year-old boy presents with hearing loss (**Fig. 119.1**).

Key Imaging Finding

Inner ear congenital malformation

Top 3 Differential Diagnoses

- **Large vestibular aqueduct syndrome (LVAS).** LVAS is a common cause of sensorineural deafness in early childhood. Affected patients hear normally at birth, with bilateral sensorineural hearing loss progressing over the first few months to years of life. Unenhanced computed tomography (CT) reveals bilateral enlargement of the vestibular aqueducts, measuring >1.5 mm in diameter. Associated abnormalities of the cochlea and vestibule are common but may be subtle.
- **Cystic cochleovestibular anomaly.** Cystic cochleovestibular anomaly is a result of arrested inner ear development, resulting in cystic dilatation of the cochlea and vestibule. No internal architecture or features can be identified. Patients have sensorineural hearing loss at birth. On unenhanced axial CT and T2 magnetic resonance imaging (MRI), the dilated cochlea and vestibule demonstrate a "figure 8" appearance. Semicircular canals are commonly dilated as well. The vestibular aqueduct is typically normal.
- **Cystic common cavity.** Cystic common cavity refers to the lack of development of the cochlea and vestibule. The semicircular canals are variably affected and may be normal, dysplastic, or absent (most common). As with cystic cochleovestibular anomaly, patients present with sensorineural hearing loss at birth. Imaging findings include a single cystic cavity in place of normal inner ear structures (cochlea, vestibule, and commonly semicircular canals). Middle ear structures and the vestibular aqueduct are typically normal.

Additional Differential Diagnoses

- **Cochlear aplasia.** Cochlear aplasia results from the arrest of normal development of the cochlea during embryogenesis. It is usually bilateral, and patients present with sensorineural hearing loss at birth. Imaging findings include an absent cochlea. The remainder of the inner ear structures, including the vestibule and semicircular canals, may be dysplastic or normal. The middle ear structures and vestibular aqueduct are typically normal.
- **Labyrinthine ossificans.** Labyrinthine ossificans refers to ossification of the membranous labyrinth due to some form of insult, typically infectious, inflammatory, or hemorrhagic. Patients commonly present with sensorineural hearing loss up to a year after an antecedent insult. Vertigo may also be seen and can be severe. Unenhanced CT demonstrates increased density within the labyrinth. On MRI, decreased signal replaces the normal fluid signal in the labyrinth on T2 sequences.

Diagnosis

Large vestibular aqueduct syndrome with associated cochlear and vestibule deformities

✓ Pearls

- LVAS presents with vestibular aqueducts >1.5 mm in diameter; hearing loss is bilateral and progressive.
- Cystic cochleovestibular anomaly has a characteristic "figure 8" appearance of the cochlea and vestibule.
- Cystic common cavity refers to a single cavity in place of normal inner ear structures.
- Labyrinthine ossificans results from a prior insult; patients present with hearing loss and possibly vertigo.

Suggested Readings

Harnsberger HR. Diagnostic Imaging: Head and Neck. Salt Lake City, UT: Amirsys; 2004

Case 120

William T. O'Brien Sr.

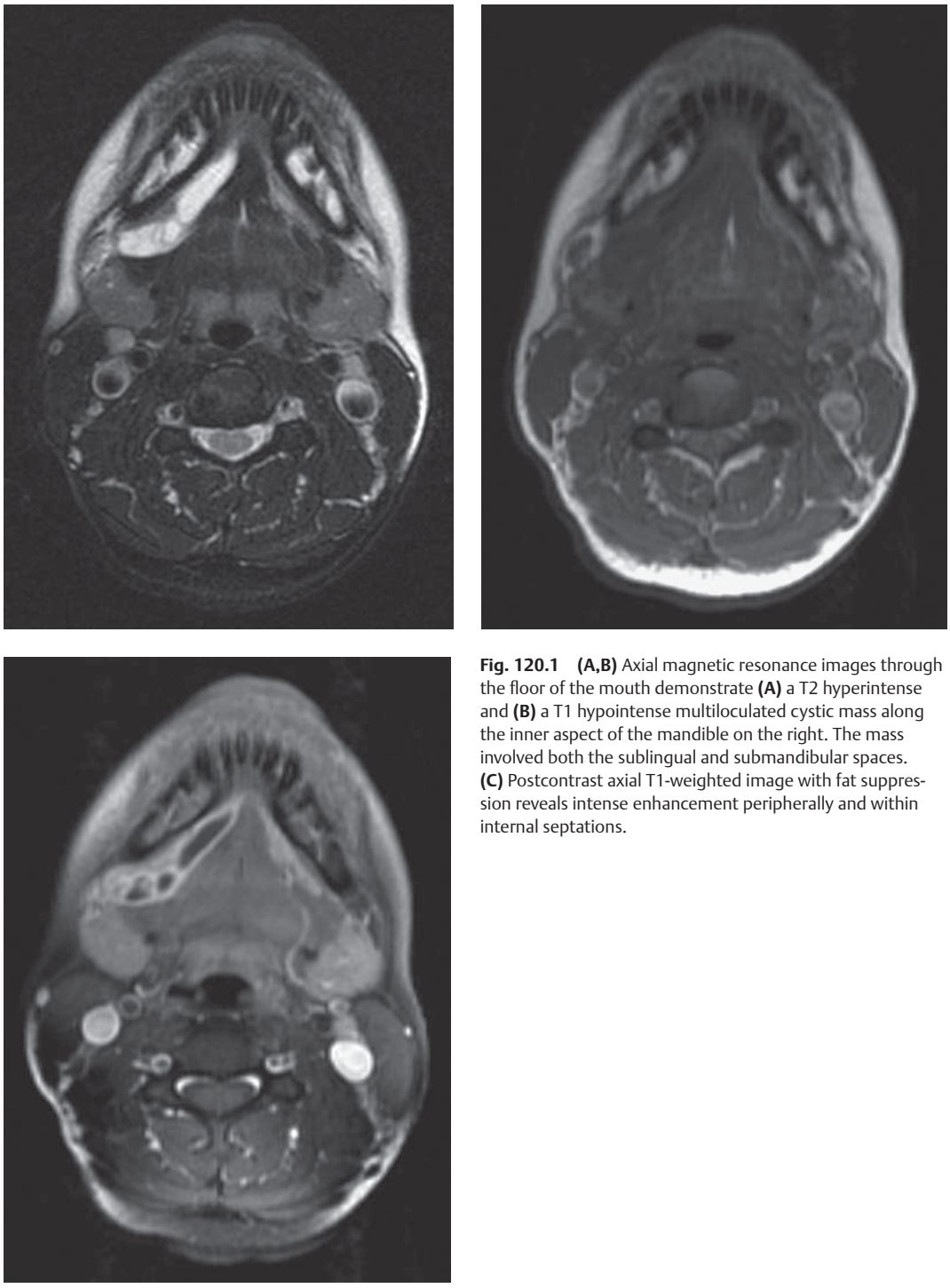


Fig. 120.1 **(A,B)** Axial magnetic resonance images through the floor of the mouth demonstrate **(A)** a T2 hyperintense and **(B)** a T1 hypointense multiloculated cystic mass along the inner aspect of the mandible on the right. The mass involved both the sublingual and submandibular spaces. **(C)** Postcontrast axial T1-weighted image with fat suppression reveals intense enhancement peripherally and within internal septations.

Clinical Presentation

A 29-year-old man presents with jaw pain (**Fig. 120.1**).

Key Imaging Finding

Floor of the mouth mass

Top 3 Differential Diagnoses

- **Squamous cell carcinoma (SCC).** SCCs are the most common neoplasms of the floor of the mouth and are highly associated with tobacco usage. They are often asymptomatic until late in the disease process. Common locations are the base of the tongue and the palate. The mylohyoid muscle divides floor of the mouth carcinomas into sublingual (above) and submandibular (below) compartments. SCC presents as an ill-defined enhancing mass. Lymphadenopathy, which may be necrotic, is commonly seen.
- **Infection/abscess.** Cellulitis and abscesses within the floor of the mouth are commonly due to dental procedures or infections. Cellulitis presents with inflammatory changes, and abscesses are organized fluid collections with rim enhancement. The term *Ludwig angina* refers to a severe, potentially life-threatening infection with abscess formation involving both the sublingual and submandibular spaces.
- **Ranula.** Ranulas are mucous retention cysts of the salivary glands in the floor of the mouth. When confined to the sublingual space, they are referred to as simple ranulas; when they extend below the mylohyoid muscle into the submandibular space, they are referred to as diving or plunging ranulas. The plunging ranulas lack true cyst walls. Ranulas typically follow fluid attenuation and signal intensity and are most often unilocular. Peripheral enhancement may be seen, especially when superinfected.

Additional Differential Diagnoses

- **Congenital thyroid lesion.** The thyroid gland descends from the base of the tongue (foramen cecum) to its normal anatomical position during fetal development. Failure to descend results in a lingual thyroid. In most cases, the lingual thyroid tissue is the only functioning thyroid tissue. Lingual thyroid tissue is hyperdense on computed tomography (CT) and avidly enhances on CT and magnetic resonance imaging (MRI). Thyroid carcinomas may occur within a lingual thyroid. Thyroglossal duct cysts are the most common congenital cysts of the head and neck. The vast majority (85%) are midline and infrahyoid. They are well circumscribed and typically unilocular with or without septations. Peripheral wall enhancement is common.
- **Venolymphatic malformation.** Hemangiomas and lymphangiomas are developmental lesions that may occur within the floor of the mouth and involve the tongue. Capillary hemangiomas are common in infancy but naturally regress. Cavernous hemangiomas are well-circumscribed lesions composed of vascular channels; the presence of phleboliths is highly characteristic. Intense enhancement is seen on both CT and MRI. Lymphangiomas are multiloculated (usually) cystic lesions that may cross fascial planes and involve multiple spaces. They are hypodense on CT and follow fluid signal on MRI.
- **Dermoid/epidermoid cyst.** Dermoid cysts are relatively uncommon malformations. They are typically cystic, well circumscribed, and fat containing. Epidermoid cysts appear as fluid-filled masses that may mimic ranulas. As with epidermoids in the brain, they demonstrate restricted diffusion on MRI.

Diagnosis

Ranula (plunging)

✓ Pearls

- SCC is the most common carcinoma of the tongue, is ill-defined, and is highly associated with tobacco.
- Cellulitis and abscesses are most often of dental origin; Ludwig angina is a severe form of infection.
- Ranulas are mucous retention cysts and characterized based on their relation to the mylohyoid muscle.
- Venolymphatic malformations, dermoids, and congenital thyroid lesions may involve the oral cavity.

Suggested Readings

Coit WE, Harnsberger H, Osborn A, et al. Ranulas and their mimics: CT evaluation. Radiology 1987;163:211–216

Harnsberger HR. Handbook of Head and Neck Imaging. 2nd ed. St. Louis, MO: Mosby; 1995

Case 121

William T. O'Brien Sr.

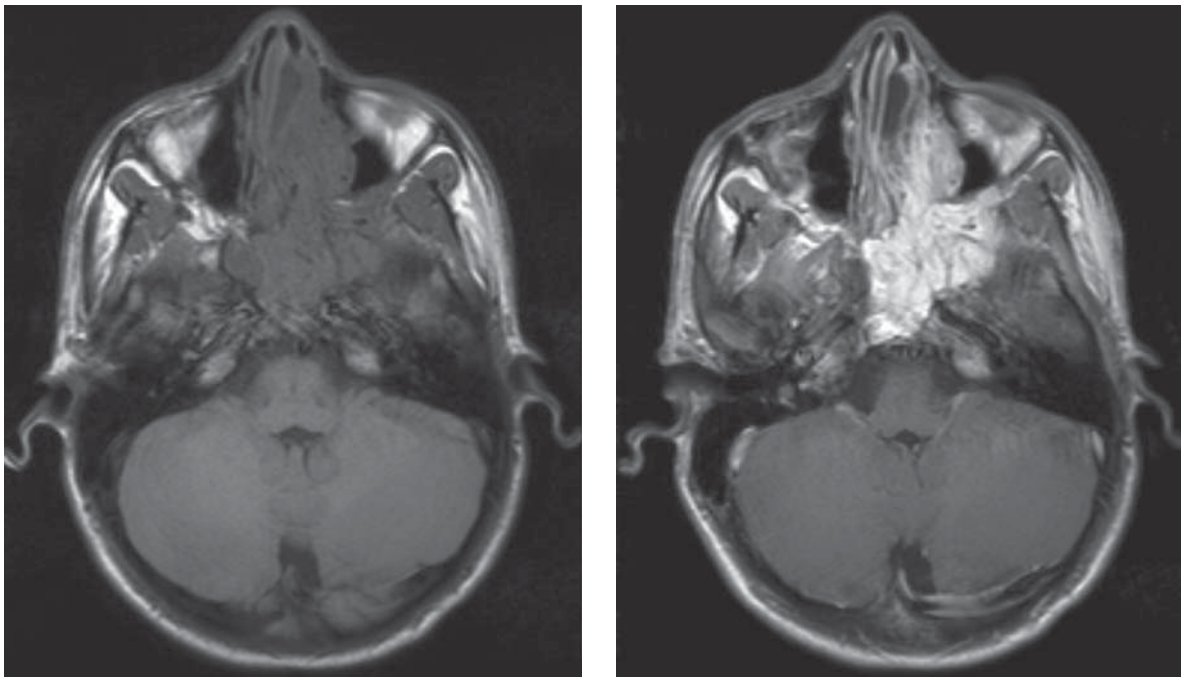


Fig. 121.1 **(A)** Precontrast and **(B)** postcontrast T1-weighted magnetic resonance images demonstrate a large T1 hypointense mass that demonstrates intense homogeneous enhancement. The mass involves the left nasopharynx, nasal cavity, and pterygopalatine fossa and extends laterally through the sphenopalatine foramen. The maxillary sinus is also involved. There was no intracranial or intraorbital extension (images not shown). (Courtesy of Children's Hospital and Research Center, Oakland, California.)

Clinical Presentation

A 17-year-old male patient presents with chronic "stuffy nose" and intermittent epistaxis (**Fig. 121.1**).

Key Imaging Finding

Aggressive nasal mass in an adolescent

Top 3 Differential Diagnoses

- **Juvenile angiofibroma (JAF).** JAFs are benign but locally aggressive lesions that occur in adolescent male patients. They originate in the nasopharynx adjacent to the sphenopalatine foramen and near the pterygopalatine fossa. The lesions commonly extend into multiple compartments, including the intracranial, intraorbital, infratemporal, and paranasal sinuses. Anterior bowing of the posterior maxillary sinus wall is commonly seen. Patients present with nasal obstruction and epistaxis. JAFs are hypointense to intermediate on T1 and intermediate to hyperintense on T2 sequences. They avidly enhance, and flow voids are commonly seen. The lesions are commonly resected with preoperative embolization.
- **Enthesioneuroblastoma (ENB).** ENB is a malignant neuroendocrine tumor that arises from olfactory endothelium within the superior nasal cavity. It most commonly occurs in adolescents and middle-aged patients who present with nasal obstruction and epistaxis. Imaging findings include an enhancing mass that is hypointense to intermediate on T1 and hyperintense on T2 sequences. Intracranial extension through the cribriform plate is common. The classic finding is a "dumbbell-shaped" mass in the nasal cavity/nasopharynx and anterior cranial fossa with a narrowed waist at the level of the cribriform plate.
- **Hemangioma.** Hemangiomas are benign tumors that may occur within the nasal cavity at any age but are most common in the pediatric population and during pregnancy. They may be capillary (more common) or cavernous and occur along the septum or turbinates. Presenting symptoms include nasal obstruction and epistaxis. A key imaging finding is a well-circumscribed, avidly enhancing nasal soft tissue mass that is intermediate on T1 and hyperintense on T2 sequences. Foci of hemorrhages may be seen.

Additional Differential Diagnoses

- **Rhabdomyosarcoma.** Rhabdomyosarcoma is the most common nasal sarcoma in adolescents. The mass may involve the sinuses, nasal cavity, and nasopharynx with bony destruction. The mass is homogeneous and avidly enhances. Squamous cell carcinoma and lymphoma are less common in younger patients.
- **Inverted papilloma (IP).** IPs are benign locally aggressive neoplasms that may occur in adolescents but are most common in adult male patients who present with nasal obstruction. They originate along the middle meatus and extend into the sinuses. Calcifications may be seen. They are isointense on T1 and hyperintense on T2 sequences with characteristic linear striations. There is heterogeneous enhancement.
- **Polyps.** Sinonasal polyp disease includes solitary polyps, sinonasal polyposis, and antrochoanal polyps. These entities most commonly arise from the maxillary sinus and may extend into the nasal cavity and nasopharynx. Their appearance on magnetic resonance imaging (MRI) varies based on protein content, but they are generally hypointense on T1- and hyperintense on T2-weighted imaging and demonstrate peripheral mucosal enhancement.

Diagnosis

Juvenile angiofibroma

✓ Pearls

- JAFs occur in adolescent male patients, avidly enhance, and commonly extend to involve multiple compartments.
- ENBs are malignant neuroendocrine tumors that may extend intracranially through the cribriform plate.
- Hemangiomas most commonly occur along the septum and turbinates in children and during pregnancy.
- IPs are locally aggressive, may have calcifications, and have a characteristic striated appearance on MRI.

Suggested Readings

Harnsberger HR. Diagnostic Imaging: Head and Neck. Salt Lake City, UT: Amirsys; 2004

Mafee MF, Valvassori GE, Becker M. Valvassori's Head and Neck Imaging. 2nd ed. New York: Thieme; 2005

Case 122

William T. O'Brien Sr.

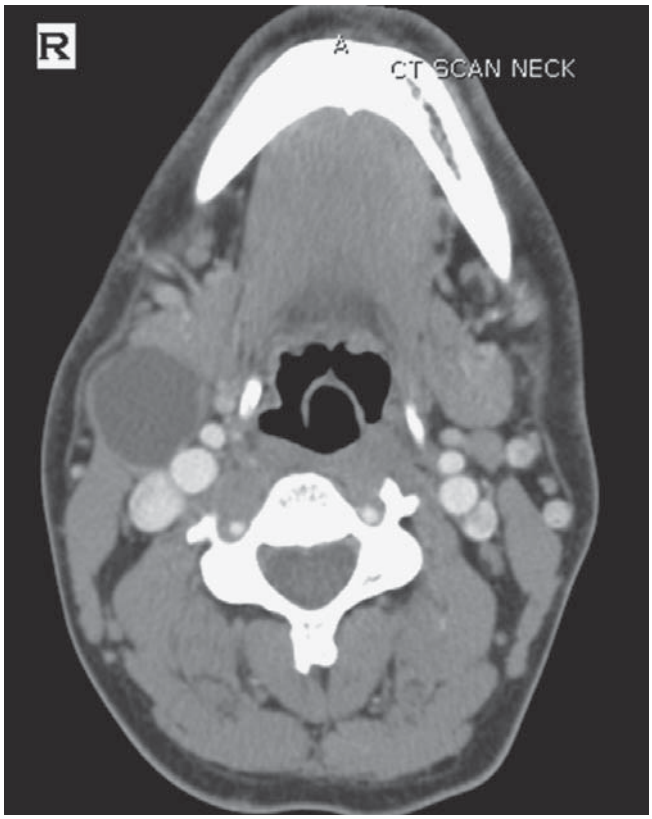


Fig. 122.1 Contrast-enhanced axial computed tomography image through the neck demonstrates a fluid collection with subtle peripheral enhancement between the carotid sheath and submandibular gland and anterior to the sternocleidomastoid muscle.

Clinical Presentation

A 17-year-old male patient presents with a painful right neck mass (**Fig. 122.1**).

Key Imaging Finding

Cystic neck mass

Top 3 Differential Diagnoses

- **Congenital cyst.** Thyroglossal duct cysts (TDCs) are the most common congenital cystic neck mass and are frequently asymptomatic unless they become infected. Eighty-five percent are midline, with the remainder paramedian; 75% are infrahyoid. Simple cysts demonstrate fluid attenuation on computed tomography (CT) without significant peripheral enhancement. Debris may be appreciated within the cyst with superimposed infection or hemorrhage. Rarely, thyroid cancer may occur within a thyroglossal duct cyst. Concerning imaging characteristics are soft tissue nodular components and calcification. Branchial cleft cysts are the result of developmental abnormalities of the branchial apparatus, and the location determines the type. There are four types of branchial cleft cysts, with the second being the most common, followed by the first. Type 1 branchial cleft cysts may occur anywhere from the external auditory canal to the angle of the mandible, including within the parotid gland. Type 2 branchial cleft cysts most commonly occur near the angle of the mandible anterior and medial to the sternocleidomastoid muscle. Types 3 and 4 are rare and frequently result in sinus formation. Type 3 branchial cleft cysts occur posteriorly, whereas type 4 branchial cleft cysts occur near the larynx or thyroid gland. Simple cysts demonstrate fluid attenuation on CT without significant peripheral enhancement. Debris may be appreciated within the cyst with superimposed infection or hemorrhage.
- **Abscess.** Abscesses can occur anywhere in the neck but are typically found within the peritonsillar or retropharyngeal regions. Clinical signs and symptoms are pain, fever, and elevated white blood cell count. Imaging characteristics include a rim-enhancing fluid collection with variable wall thickness and surrounding inflammatory changes. Drainage with subsequent antibiotic therapy is commonly warranted.
- **Cystic lymph node.** Cystic lymph nodes may result from local spread of infectious or malignant processes. Squamous cell carcinoma (SCC) and papillary thyroid cancer are the two most common primary neoplasms that demonstrate cystic metastases within cervical lymph nodes.

Additional Differential Diagnoses

- **Lymphatic malformation.** Lymphatic malformations are common in the neck and can occur in nearly any location. Cystic hygromas are the most common subtype and typically occur posteriorly. They are multiseptated and can be associated with chromosomal abnormalities, such as Turner and Down syndromes. Lymphangiomas are slightly less common, usually multiloculated, and can grow quite large, insinuating between and crossing tissue planes. Fluid–fluid levels may be seen with superimposed hemorrhage. When large, these lesions can exert local mass effect, particularly on the airway.
- **Cystic nerve sheath tumor.** Cystic nerve sheath tumors, such as schwannomas, typically occur within the carotid sheath and when large may mimic an infected branchial cleft cyst. Soft tissue components will usually demonstrate enhancement postcontrast.

Diagnosis

Branchial cleft cyst (type 2)

✓ Pearls

- TDCs are the most common congenital cystic neck mass; most are midline and infrahyoid.
- Type 2 branchial cleft cysts are the most common subtype and occur at the angle of the mandible.
- Abscesses commonly occur within the neck, are rim enhancing, and typically require drainage.
- Cystic lymphadenopathy may occur from infectious or neoplastic (SCC and papillary thyroid) processes.

Suggested Readings

Lev S, Lev MH. Imaging of cystic lesions. Radiol Clin North Am 2000;38:1013–1027

Case 123

Adam J. Zuckerman

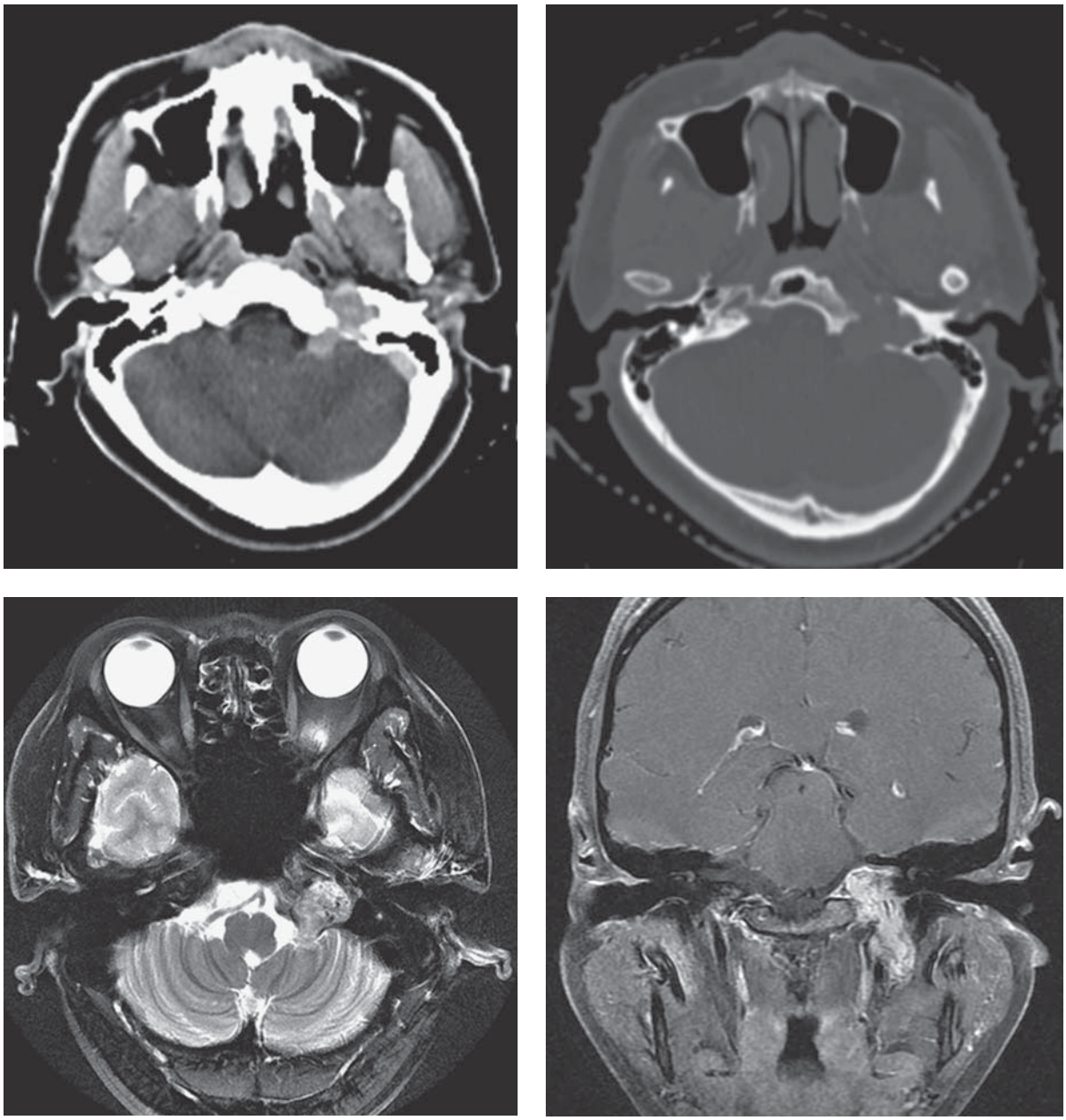


Fig. 123.1 Contrast-enhanced axial CT images in **(A)** soft tissue and **(B)** bone windows demonstrate an enhancing soft tissue mass with expansion and erosion of the jugular foramen. **(C)** T2-weighted axial image reveals the presence of multiple flow voids within an intermediate signal intensity left jugular foramen mass. **(D)** Coronal T1 postcontrast magnetic resonance image shows the extent of the avidly enhancing lesion originating from the jugular foramen.

Clinical Presentation

A 46-year-old woman presents with pulsatile tinnitus (**Fig. 123.1**).

Key Imaging Finding

Jugular foramen mass

Top 3 Differential Diagnoses

- **Meningioma.** The most common extra-axial tumors, meningiomas can arise within the jugular foramen. On computed tomography (CT), meningiomas typically appear isodense to slightly hyperdense relative to brain parenchyma. They are associated with hyperostosis of adjacent bone and may contain internal calcification. On magnetic resonance imaging (MRI), lesions appear relatively isointense with respect to gray matter on T1- and T2-weighted imaging with diffuse, homogeneous enhancement and a dural tail.
- **Schwannoma.** Schwannomas of the jugular foramen are relatively uncommon and most often arise from the glossopharyngeal nerve. Clinical symptoms are related to local mass effect, with unilateral hearing loss occurring most commonly, followed by dysphagia. Mass effect may also lead to smooth osseous expansion and erosion with compression of the ipsilateral jugular vein or sigmoid sinus. On MRI, schwannomas appear relatively hypointense on T1 and hyperintense on T2 with respect to brain parenchyma, demonstrating marked enhancement. Lesions tend to be isodense on noncontrast CT, with sharply demarcated erosive changes enlarging the jugular foramen.
- **Paraganglioma.** Jugular foramen paragangliomas (glomus jugulare) are highly vascular lesions that enlarge the jugular foramen with associated irregular, permeative bone destruction. These aggressive lesions are associated with jugular vein invasion and intraluminal growth. On MRI, glomus jugulare tumors may demonstrate the classic "salt and pepper" appearance, characterized by multiple flow voids. They are isointense on T1 and iso- to hyperintense on T2 sequences. The infiltrative osseous pattern is best appreciated on CT bone windows.

Additional Differential Diagnoses

- **Metastases.** Metastatic involvement of the jugular foramen may have a variety of imaging appearances, ranging from a nonaggressive pattern with osseous remodeling to an aggressive pattern with erosive, destructive osseous changes. Breast, lung, and prostate carcinomas are the most common primary tumors associated with skull base metastases. Metastatic foci are often multifocal, so it is important to search for additional lesions.
- **Dehiscent jugular bulb.** A dehiscent or high-riding jugular bulb has a prevalence of 7% in the general population and is a cause of pulsatile tinnitus. When the jugular bulb is seen above the inferior margin of the round window, it is considered high riding. High-resolution CT can evaluate for the presence of bony dehiscence of the petrous septum between the middle ear and the jugular bulb. CT venography may also be helpful in confirming the diagnosis.

Diagnosis

Paraganglioma (glomus jugulare)

✓ Pearls

- Jugular foramen meningiomas may be hyperdense on CT with calcification and avid enhancement.
- Jugular foramen schwannomas are sharply demarcated and result in smooth osseous expansion and erosion.
- Paragangliomas are highly vascular tumors that may demonstrate a "salt and pepper" appearance on MRI.
- Skull base metastases are most often from breast, lung, and prostate carcinomas; look for additional lesions.

Suggested Readings

Eldevik OP, Gabrielsen TO, Jacobsen EA. Imaging findings in schwannomas of the jugular foramen. AJNR Am J Neuroradiol 2000;21:1139–1144

Grossman RI, Yousem DM. Neuroradiology: The Requisites. 2nd ed. Philadelphia: Elsevier; 2003

Harnsberger HR. Diagnostic Imaging: Head and Neck. Salt Lake City, UT: Amirsys; 2004

Case 124

William T. O'Brien Sr.

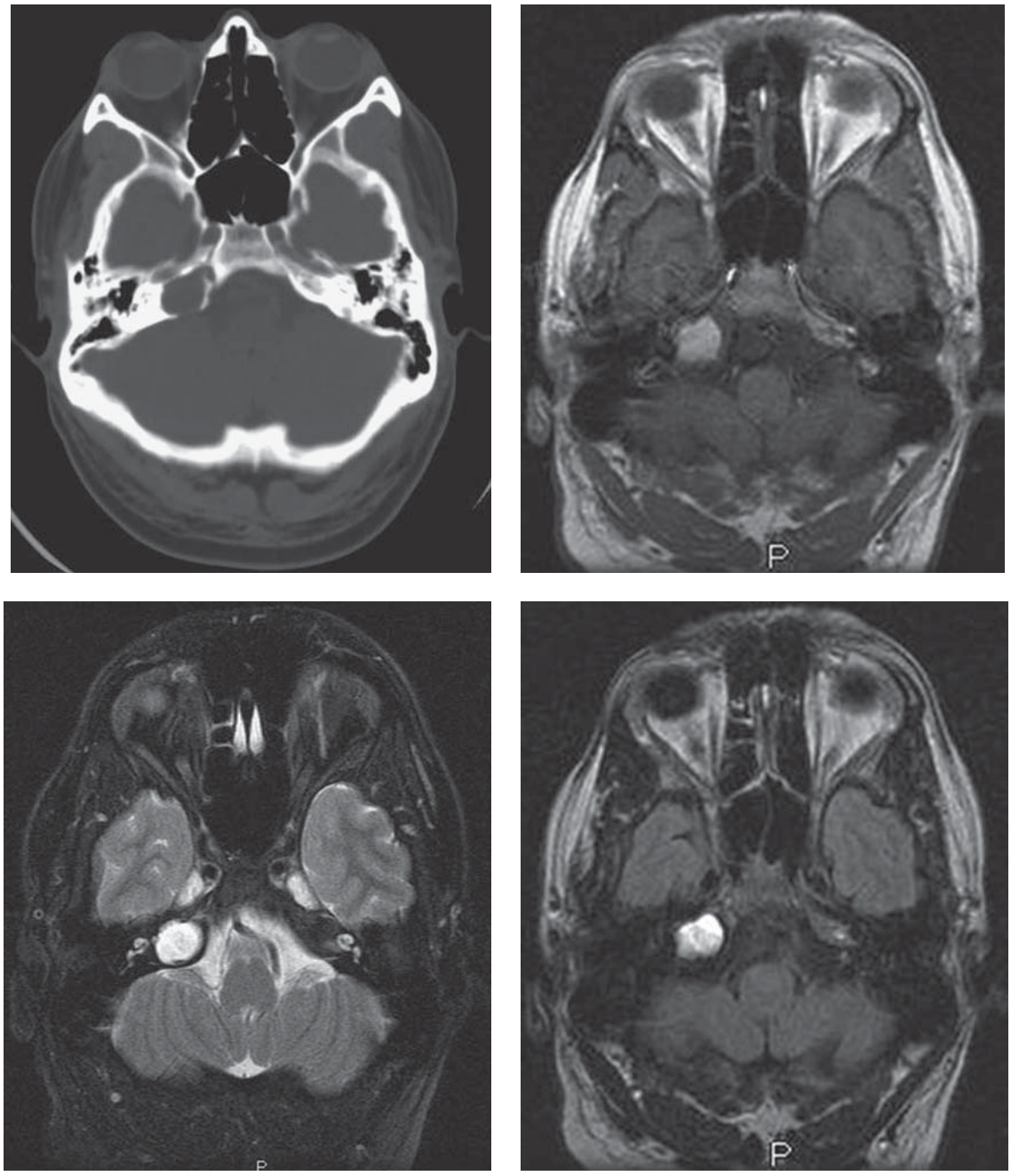


Fig. 124.1 **(A)** Axial CT image through the brain in the bone window demonstrates an expansile lesion within the right petrous apex. **(B)** The lesion is hyperintense on T1-, **(C)** T2- with fat suppression, and **(D)** fluid-attenuated inversion recovery–weighted images. The lesion did not enhance on postcontrast sequences (not shown). (Courtesy of Rebecca Cornelius, MD, University of Cincinnati.)

Clinical Presentation

A 37-year-old man presents with headaches and mild hearing loss (**Fig. 124.1**).

Key Imaging Finding

Petrous apex lesion

Top 3 Differential Diagnoses

- **Cholesterol granuloma.** Cholesterol granulomas occur secondary to nonspecific chronic inflammatory changes and are seen most commonly in the temporal bone (middle ear and petrous apex); they are the most common primary lesion that involves the petrous apex. Computed tomography (CT) reveals a hypodense mass that may expand and erode bone. On magnetic resonance imaging (MRI), the lesions are hyperintense on both T1- and T2-weighted sequences due to hemorrhage within the lesions. Occasionally, a hemosiderin ring is seen. There may be peripheral rim enhancement, but the lesions themselves will not enhance.
- **Mucocele.** Mucoceles are common in the paranasal sinuses and also occur within the petrous apex. They are thought to be secondary to entrapped secretions in an aerated petrous apex. They are hypodense and commonly expansile on CT. On MRI, mucoceles are typically hypointense on T1- and hyperintense on T2-weighted sequences. With increased mucus, they may be slightly hyperintense on T1, however, not to the same degree as cholesterol granulomas. They do not enhance.
- **Congenital cholesteatoma.** Congenital cholesteatomas are epidermoids that most commonly occur within the middle ear and petrous apex, similar to cholesterol granulomas. Patients commonly present with either sensorineural hearing loss or facial nerve deficits. On CT, the lesions are hypodense and expansile. MRI demonstrates increased T2 signal intensity secondary to internal cystic components. The lesions are commonly hypointense to slightly hyperintense on T1-weighted sequences but not to the same degree as cholesterol granulomas. As with other epidermoids, there may be restricted diffusion. There is typically thin peripheral enhancement, if any.

Additional Differential Diagnoses

- **Apical petrositis.** Serous or reactive fluid within a pneumatized petrous apex is a common finding in asymptomatic patients and is thus of little clinical significance. Apical petrositis, however, refers to infection of the pneumatized petrous apex, often secondary to otitis media. CT reveals fluid density within the petrous apex. The fluid is hypointense on T1- and hyperintense on T2-weighted sequences. Resultant inflammation results in enhancement. Gradenigo syndrome refers to retro-orbital pain and diplopia secondary to deficits of the sixth cranial nerve (CN VI) as a result of petrous apicitis. Prompt diagnosis and treatment are necessary to reduce morbidity associated with this entity.
- **Neoplasm.** Metastases commonly involve the skull base secondary to direct or hematogenous spread. Direct spread may result from nasopharyngeal or sinonasal primary neoplasms (squamous cell carcinoma). Lung, breast, and prostate cancers disseminate via hematogenous spread. Secondary involvement with lymphoma is not uncommon. Primary involvement can be seen with chondrosarcoma, multiple myeloma, or plasmacytoma. Chondrosarcomas are characteristically bright on T2-weighted sequences.

Diagnosis

Cholesterol granuloma

✓ Pearls

- Cholesterol granuloma is the most common primary petrous apex lesion and is bright on T1- and T2-weighted images.
- Mucoceles may appear similar to cholesterol granulomas but will not be as bright in signal intensity.
- Apical petrositis may lead to Gradenigo syndrome (apical petrositis, retro-orbital pain, and CN VI deficits).
- Chondrosarcomas may arise from the petrous bone and are characteristically bright on T2-weighted images.

Suggested Readings

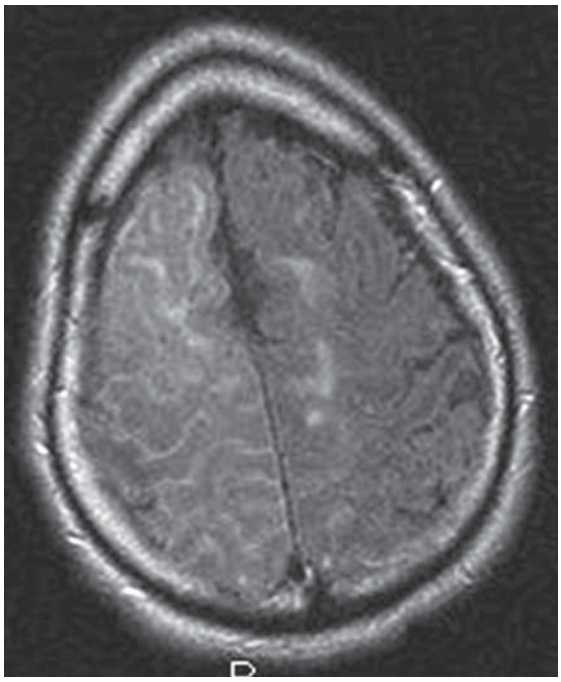
Harnsberger HR. Diagnostic Imaging: Head and Neck. Salt Lake City, UT: Amirsys; 2004

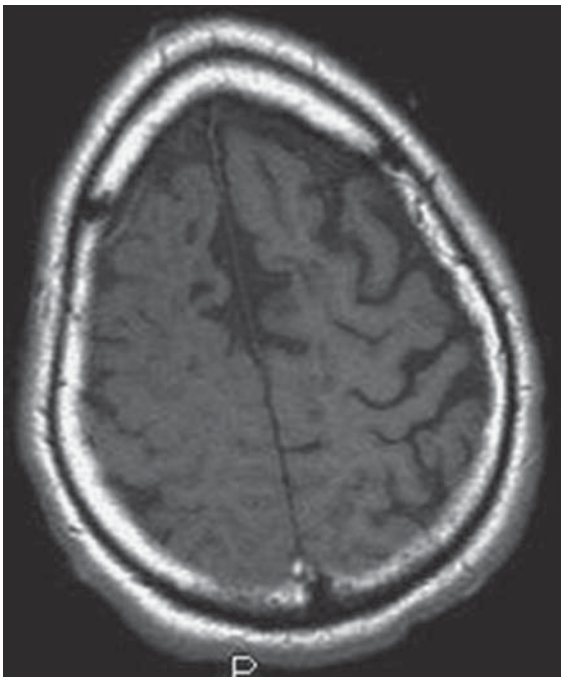
Harnsberger HR. Handbook of Head and Neck Imaging. 2nd ed. St. Louis, MO: Mosby; 1995

Mafee MF, Valvassori GE, Becker M. Valvassori's Head and Neck Imaging. 2nd ed. New York: Thieme; 2005

Case 125

Matthew J. Moore





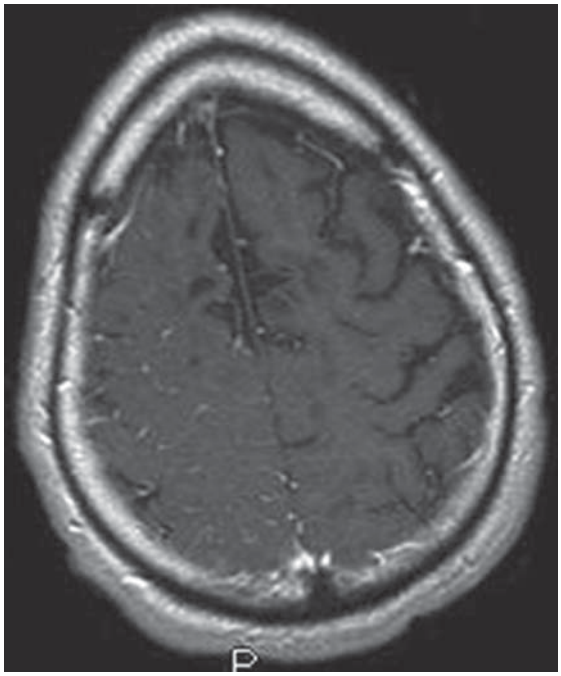


Fig. 125.1 **(A)** Axial fluid-attenuated inversion recovery image through the brain demonstrates abnormal increased signal involving the cortex, subcortical white matter, and sulci/subarachnoid space within the right frontal and parietal lobes and mild increased subcortical signal within predominantly the left frontal lobe. **(B)** Axial T1 precontrast and **(C)** postcontrast images reveal pronounced abnormal leptomeningeal enhancement involving the right frontal and parietal lobes.

Clinical Presentation

An adult patient presents with altered mental status (**Fig. 125.1**).

Key Imaging Finding

Leptomeningeal enhancement

Top 3 Differential Diagnoses

- **Leptomeningeal carcinomatosis.** Leptomeningeal carcinomatosis is most often caused by hematogenous spread of malignancy (most commonly lung and breast) or direct extension by a primary tumor of the central nervous system (CNS). Magnetic resonance imaging (MRI) is the best imaging tool, with a sensitivity of ~70% for extracranial solid tumor metastases and 55% for hematologic malignancies. Postcontrast MR sequences will show smooth or nodular leptomeningeal enhancement. The ependymal surfaces of the ventricles and cranial nerves may be coated. Hyperintense sulci on fluid-attenuated inversion recovery (FLAIR) can also be seen. Communicating hydrocephalus is a potential complication from involvement of the arachnoid villi, interfering with cerebrospinal fluid (CSF) absorption. Computed tomography (CT) is relatively insensitive for detection of leptomeningeal disease, but it will show hydrocephalus as an early sign.
- **Meningitis.** Meningitis is an inflammatory infiltration of the pia, arachnoid, and CSF most often due to hematogenous dissemination of a distant infection. Lumbar puncture is the most sensitive test, revealing increased white blood cells and protein with decreased glucose. The exact values vary based on the etiology of infection (most often viral or bacterial). MRI may show hyperintense FLAIR and enhancement of the subarachnoid space from the exudative inflammatory process. Potential complications include hydrocephalus, ventriculitis, cerebral abscesses, empyema, infarction, and venous thrombosis.
- **Neurosarcoidosis.** Sarcoidosis is a systemic inflammatory disease with an onset in the 3rd and 4th decades. It is characterized by noncaseating granulomas. Neurosarcoidosis is an uncommon complication that most often presents with smooth or nodular dural and/or leptomeningeal enhancement, especially along the basal cisterns. There is often involvement of the optic chiasm, hypothalamus, infundibulum, internal auditory canals, and cranial nerves at the skull base. Look for perivascular space and ependymal enhancement. Brain parenchyma can also be involved in one third of patients with the hypothalamus most commonly involved, followed by the brainstem, cerebral hemispheres, and cerebellar hemispheres. Approximately 5% will have a solitary extra-axial mass. Hydrocephalus is a potential complication. If not already obtained, look for lymphadenopathy with or without interstitial lung disease on chest radiography.

Additional Differential Diagnoses

- **Subacute infarction.** Contrast-enhanced CT or MRI of a subacute infarction can show gyriform parenchymal enhancement and swelling of the cerebral or cerebellar cortex within a vascular distribution. Remember the "2-2-2" rule: enhancement begins at 2 days, peaks at 2 weeks, and disappears by 2 months.
- **Subarachnoid hemorrhage (SAH).** SAH is hyperintense on FLAIR, which is nonspecific, and can also be seen with inflammatory or neoplastic processes. Look for hyperdense CSF on unenhanced CT. The most common cause of SAH is trauma. Eighty-five percent of nontraumatic SAHs are due to aneurysm rupture. The most common aneurysm locations are the anterior and posterior communicating arteries, middle cerebral artery bifurcations, and basilar terminus.

Diagnosis

Meningitis

✓ Pearls

- Leptomeningeal carcinomatosis is most often due to breast or lung metastases or a primary CNS tumor.
- Meningitis results from hematogenous spread of infection; leptomeningeal enhancement may be seen.
- Neurosarcoidosis presents with leptomeningeal enhancement most often along the basal cisterns.
- Subacute infarcts demonstrate gyriform enhancement that follows the "2-2-2" rule.

Suggested Readings

Osborn A, Blaser S, Salzman KL, et al. Diagnostic Imaging: Brain. Salt Lake City, UT: Amirsys; 2004

Phillips M, Ryals T, Kambhu S, Yuh W. Neoplastic vs. inflammatory meningeal enhancement with Gd-DTPA. J Comput Assist Tomogr 1990;14:536–541

Section VI Brain and Spine Imaging

Case 126

Paul M. Sherman

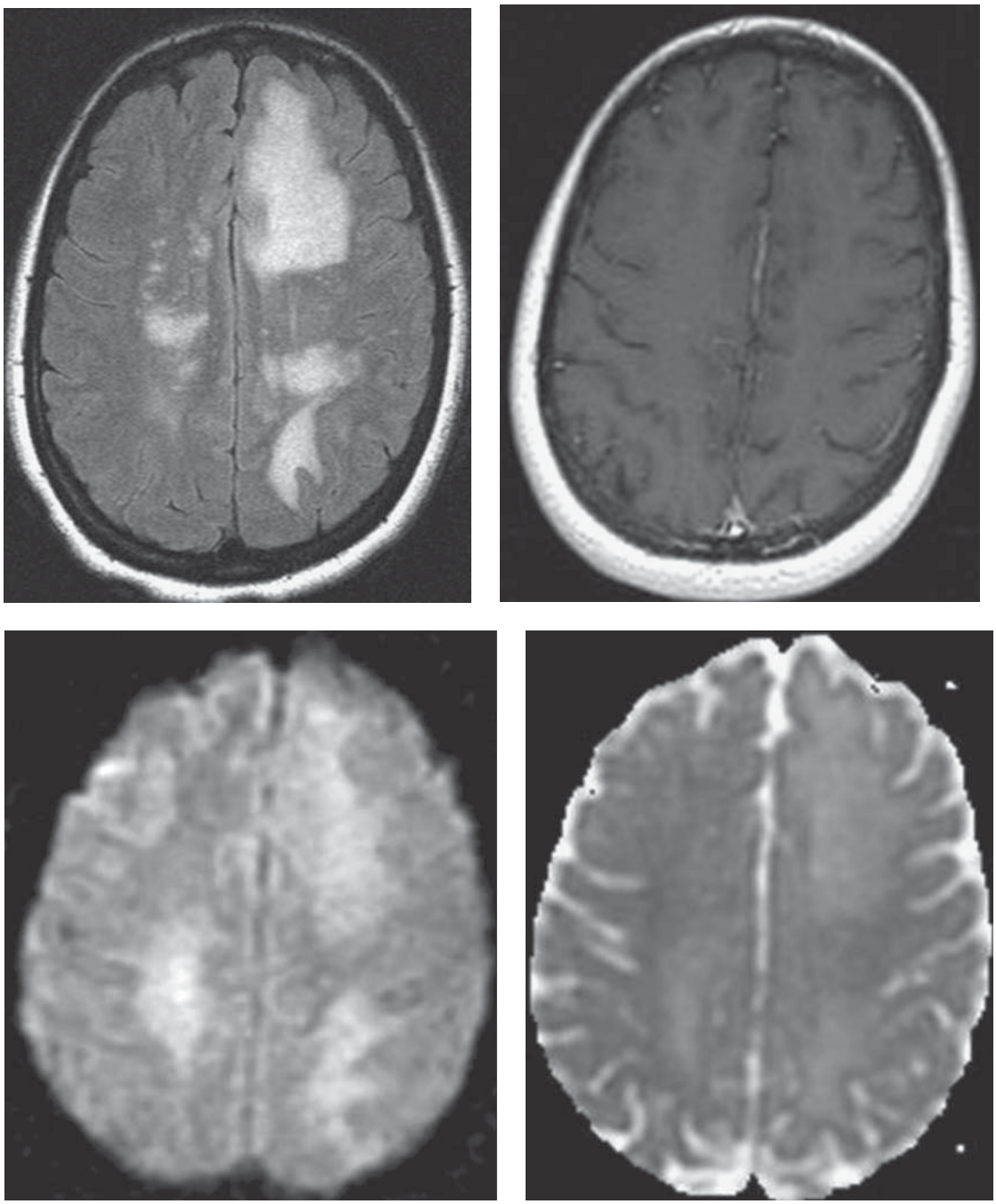


Fig. 126.1 **(A)** Axial fluid-attenuated inversion recovery (FLAIR), **(B)** T1 postgadolinium, and **(C)** diffusion-weighted images with **(D)** ADC map demonstrate extensive bilateral white matter FLAIR hyperintensity without significant mass effect. There is involvement of the subcortical U fibers, no restricted diffusion, and no enhancement.

Clinical Presentation

A 45-year-old woman presents with seizures (**Fig. 126.1**).

Key Imaging Finding

Confluent white matter lesions in an adult

Top 3 Differential Diagnoses

- **Demyelinating disease.** Multiple sclerosis (MS) demonstrates multiple perpendicular periventricular T2 hyperintensities with perivenular extension (Dawson fingers). The lesions are bilateral and asymmetric and often involve the cerebellum, corpus callosum, and cerebellar peduncles. There is transient enhancement during active demyelination. Plaques may be confluent or masslike ring-enhancing lesions (tumefactive). MS has a relapsing, remitting course, unlike acute disseminated encephalomyelitis, which is monophasic. Both processes may involve the spinal cord. Lyme disease is a tick-borne illness caused by the spirochete *Borrelia burgdorferi*. White matter lesions simulate MS, but there may be an associated viral-like illness or skin rash. Cranial nerve VII, leptomeningeal, and cauda equina involvement may be seen.
- **Neoplasm.** Gliomatosis cerebri is a densely infiltrating glial tumor involving two or more lobes and is frequently bilateral. There is hemispheric white matter involvement, but the cortex may also be involved. There is no or minimal enhancement and relative preservation of the underlying brain architecture. Anaplastic astrocytoma may be more discrete, with enhancement ranging from none to focal or patchy. Primary central nervous system lymphoma characteristically involves the deep gray matter or periventricular white matter and classically involves the corpus callosum. There is often T2 hypointensity (computed tomography [CT] hyperdensity), as it is a small, round, blue cell tumor. Enhancement is typically homogeneous unless steroids have been administered. Metastatic disease most commonly results in multiple lesions at the gray-white junction.
- **Progressive multifocal leukoencephalopathy (PML).** PML is caused by infection of the oligodendrocytes with a polyomavirus (JC virus). The virus remains latent until reactivation due to immunodeficiency (the vast majority of cases are seen in patients with acquired immunodeficiency syndrome). Magnetic resonance imaging (MRI) demonstrates periventricular and subcortical white matter T2 hyperintensities without mass effect and with characteristic involvement of the subcortical U fibers. There is typically no enhancement; if present, it is faint and peripheral.

Additional Differential Diagnoses

- **Microvascular ischemic disease.** Microvascular ischemic disease is common in the elderly population and can be advanced for age with comorbid conditions, such as hypertension, diabetes, and hyperlipidemia. Noncontrast CT reveals subcortical and periventricular white matter hypodensities; MRI demonstrates asymmetric white matter T2 hyperintense lesions without enhancement. White matter involvement may be confluent and extensive. Lacunar infarcts demonstrate signal intensity similar to cerebrospinal fluid and are commonly found in the basal ganglia, thalami, deep white matter tracts, and brainstem.
- **Autoimmune mediated vasculitis.** Vasculitis most commonly presents as multifocal gray and white matter lesions that are bilateral, usually cortical or subcortical, and often involve the basal ganglia and thalami. The lesions may mimic MS or infection if ring enhancing. Gradient echo MR sequences may demonstrate hemorrhage. Digital subtraction angiography (DSA) reveals alternating stenoses and dilatation involving the cerebral arterial vasculature.

Diagnosis

Progressive multifocal leukoencephalopathy (patient with human immunodeficiency virus)

✓ Pearls

- Microvascular ischemic disease is common in elderly patients and can be advanced with comorbidities.
- Demyelinating processes are a common cause of white matter lesions and may be confluent when severe.
- Gliomatosis cerebri and lymphoma may present as infiltrating masses involving white matter tracts.
- Vasculitis presents as multifocal lesions with hemorrhage; DSA shows alternating stenoses and dilatations.

Suggested Readings

Osborn A, Blaser S, Salzman K, et al. Diagnostic Imaging: Brain. Salt Lake City, UT: Amirsys; 2004

Case 127

William T. O'Brien Sr.

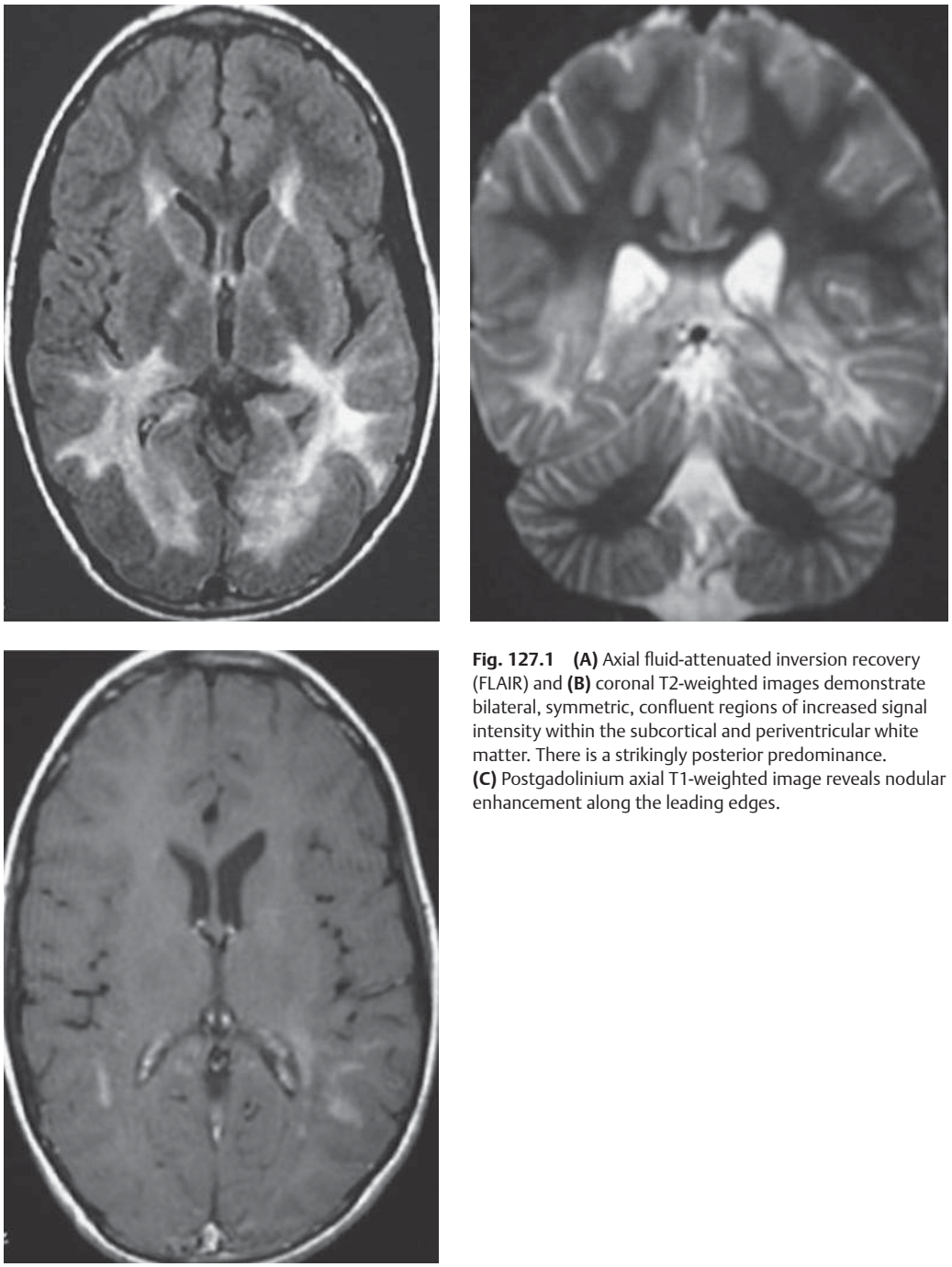


Fig. 127.1 **(A)** Axial fluid-attenuated inversion recovery (FLAIR) and **(B)** coronal T2-weighted images demonstrate bilateral, symmetric, confluent regions of increased signal intensity within the subcortical and periventricular white matter. There is a strikingly posterior predominance. **(C)** Postgadolinium axial T1-weighted image reveals nodular enhancement along the leading edges.

Clinical Presentation

A 4-year-old boy presents with new onset developmental delay (**Fig. 127.1**).

Key Imaging Finding

Confluent white matter lesions in a child

Top 3 Differential Diagnoses

- **Acute disseminating encephalomyelitis (ADEM).** ADEM is a monophasic demyelinating disease that occurs in children following an antecedent viral infection or vaccination. The demyelination is thought to be secondary to an autoimmune response against myelin due to cross-reaction with a viral protein. Patients present with neurologic deficits that mimic multiple sclerosis (MS). Disease course varies from self-limiting to fulminant, hemorrhagic encephalitis. Computed tomography and magnetic resonance imaging (MRI) reveal large, usually bilateral white matter lesions that are high signal on T2-weighted imaging. Postgadolinium images may demonstrate ring or nodular enhancement.
- **Multiple sclerosis.** MS is the most common demyelinating process encountered in clinical practice. It occurs predominantly in young to middle-aged women, but it may also affect children. Patients present with optic neuritis, cranial neuropathies, or vague sensorimotor deficits, which typically resolve prior to subsequent episodes. Most patients have a relapsing and remitting course. MRI findings include increased T2-weighted signal intensity within the periventricular white matter, corpus callosum, optic pathways, and cerebellar peduncles. Periventricular white matter lesions orient perpendicular to the ventricles, resulting in characteristic lesions referred to as Dawson fingers. Active regions of demyelination may enhance in a nodular or ring pattern. The Marburg variant of MS is a fulminant, aggressive form that leads to rapid death. Devic disease (neuromyelitis optica) is a variant that affects the optic nerves and spinal cord. Schilder disease is a rare progressive form of MS that begins in childhood.
- **Dysmyelinating disease (leukodystrophy).** Leukodystrophies are a group of rare metabolic disorders characterized by dysmyelination secondary to accumulation of toxic metabolites as a result of enzyme deficiencies. Patients present most commonly at an early age with visual or behavioral disturbances. MRI demonstrates bilateral symmetric increased T2-weighted signal intensity along white matter tracts. Metachromatic leukodystrophy is the most common form and has a predilection for the occipital lobes and splenium of the corpus callosum. Adrenoleukodystrophy has a similar pattern, commonly affects males (x-linked), and also affects the adrenal glands. Alexander disease has frontal lobe predominance, and Canavan disease is associated with increased levels of n-acetyl-aspartate on spectroscopy. Both Alexander and Canavan diseases often result in macrocephaly in addition to the white matter manifestations.

Additional Differential Diagnoses

- **Atypical infection (progressive multifocal leukoencephalopathy [PML]).** PML is an atypical viral (JC virus) infection that occurs in immunosuppressed patients (most commonly in patients with acquired immunodeficiency syndrome [AIDS]). The infection affects oligodendrocytes, resulting in confluent regions of increased T2-weighted signal intensity within the periventricular and subcortical white matter. Enhancement is unusual. White matter involvement may be bilateral but is typically asymmetric.

Diagnosis

Dysmyelinating disease (adrenoleukodystrophy)

✓ Pearls

- ADEM is a monophasic demyelinating process that follows an antecedent viral infection or vaccination.
- MS is the most common demyelinating process; multiple forms exist with varying presentations.
- Leukodystrophies are rare metabolic disorders that result in diffuse dysmyelination.
- PML is an aggressive infection that occurs in immunosuppressed patients (most commonly in patients with AIDS).

Suggested Readings

Barkovich AJ, Moore KR, Grant E, et al. Diagnostic Imaging: Pediatric Neuroradiology. Salt Lake City, UT: Amirsys; 2007

O'Brien WT, Palka PS, et al. Pediatric neuroimaging. In: Quattromani F, Handal GA, Lampe R, eds. Pediatric Imaging: Rapid-fire Questions and Answers. New York: Thieme; 2007:338–391

Osborn A, Blaser S, Salzman K, et al. Diagnostic Imaging: Brain. Salt Lake City, UT: Amirsys; 2004

Case 128

Paul M. Sherman

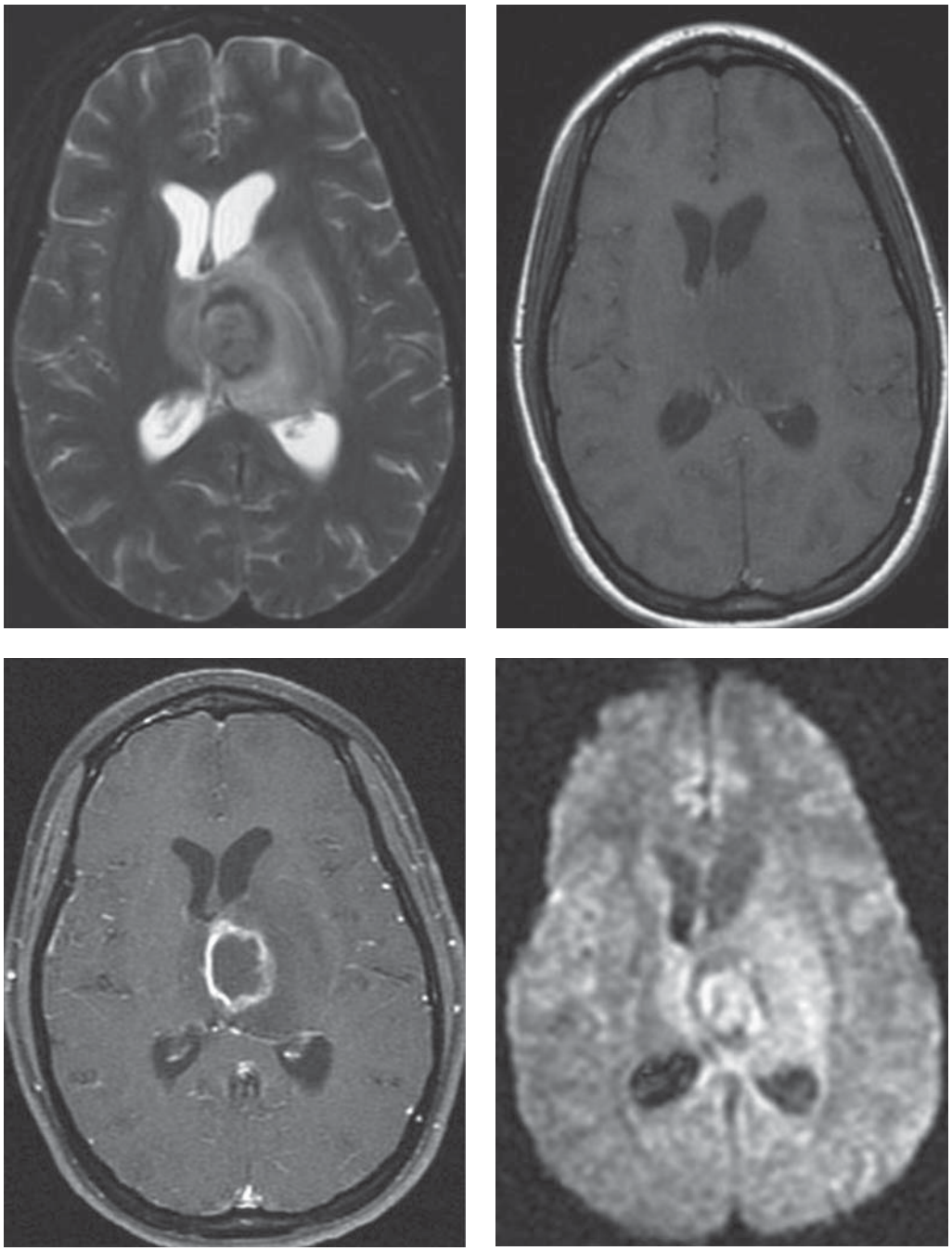


Fig. 128.1 **(A)** Axial T2 fast spin echo, **(B)** axial T1 pregadolinium, **(C)** postgadolinium, and **(D)** diffusion-weighted (apparent diffusion coefficient [ADC] not shown) images demonstrate a T2 hyperintense and T1 hypointense mass in the left thalamus, with a rim of T2 hypointensity that enhances. Enhancement is thinnest adjacent to the third ventricle. There is mass effect, surrounding edema, and restricted diffusion (ADC map is dark) within the mass.

Clinical Presentation

A patient presents with mental status changes (**Fig. 128.1**).

Key Imaging Finding

Ring-enhancing lesion

Top 3 Differential Diagnoses

- **Neoplasm**. Gliobastoma multiforme (GBM), a World Health Organization grade IV astrocytoma, is the most common primary intracranial neoplasm in adults and is extremely aggressive. Rapid growth leads to central necrosis and neovascularity (flow voids). There is marked mass effect; a thick irregular rind of peripheral enhancement; and adjacent T2/fluid-attenuated inversion recovery (FLAIR) hyperintensity, representing vasogenic edema and tumor invasion. The tumor itself is heterogeneous but is primarily T2 hyperintense and T1 iso- to hypointense with associated cystic changes, hemorrhage, and fluid–debris levels. There may be foci of diffusion-weighted imaging restriction. Involvement of the corpus callosum is common. Primary central nervous system lymphoma is characteristically located in the deep gray matter and periventricular white matter. Involvement of the corpus callosum is classic. Due to the high nuclear/cytoplasmic ratio, lymphoma is iso- to hypointense on T2-weighted images. There is less vasogenic edema than expected for GBM or metastatic foci. Ring enhancement, necrosis, and hemorrhage occur after therapy or in immunocompromised patients (e.g., those with acquired immunodeficiency syndrome). Positron emission tomography or thallium 201 single-photon emission computed tomography hypermetabolic activity is helpful in differentiating the neoplasm from toxoplasmosis. Metastatic lesions are often multiple, involving the gray-white matter junction or the posterior fossa. They are more often solid than cystic. Cystic/necrotic lesions characteristically ring enhance. There is significant associated vasogenic edema.
- **Demyelinating disease.** Multiple sclerosis (MS) plaques may show "horseshoe-shaped" or open-ring enhancement during periods of active demyelination. Typically, the open ring is toward the cortex. Lesions are usually located in a characteristic pattern (callososeptal interface). There is little or no mass effect, even in tumefactive lesions. Patients are younger than those with GBM or metastatic disease.
- **Abscess.** Brain abscesses are most commonly pyogenic, followed by fungal and parasitic. In the early capsule stage of abscess development, there is a well-defined, thin-walled enhancing rim (thinner toward the ventricle) that is T2 hypointense, restricted diffusion, and surrounding edema. The abscesses may be multiple.

Additional Differential Diagnoses

- **Subacute infarct**. Subacute infarcts are located in an expected vascular distribution. Edema, mass effect, potential hemorrhagic transformation, and gyral enhancement may mimic a mass lesion. Restricted diffusion may help distinguish ischemia from other etiologies, although abscesses and some neoplasms may demonstrate restricted diffusion as well.
- **Resolving contusion.** A history of trauma is important in differentiating a contusion from other ring-enhancing lesions. Blood products are present in varying stages, depending on the age of the hematoma. Rim enhancement occurs within a few days in a vascularized capsule. Acute blood products are isointense on T1- and hypointense on T2-weighted imaging. Subacute blood products (intra- or extracellular methemoglobin) are T1 hyperintense. Intracellular methemoglobin is T2 hypointense, and extracelluar methemoglobin is T2 hyperintense.

Diagnosis

Toxoplasmosis abscess

✓ Pearls

- Glioblastoma multiforme, lymphoma, and metastases may demonstrate ring enhancement.
- Glioblastoma multiforme and lymphoma characteristically involve the corpus callosum.
- Abscesses characteristically will have a T2 hypointense capsule and demonstrate restricted diffusion.
- Ring enhancement in demyelinating disease is typically incomplete toward the cortex.

Suggested Readings

Chepuri NB. Ring enhancing cerebral lesions. In: York DH, ed. Magnetic Resonance Imaging of CNS Disease. Philadelphia: Mosby; 2002

Osborn A, Blaser S, Salzman KL, et al. Diagnostic Imaging: Brain. Salt Lake City, UT: Amirsys; 2004

Case 129

William T. O'Brien Sr.

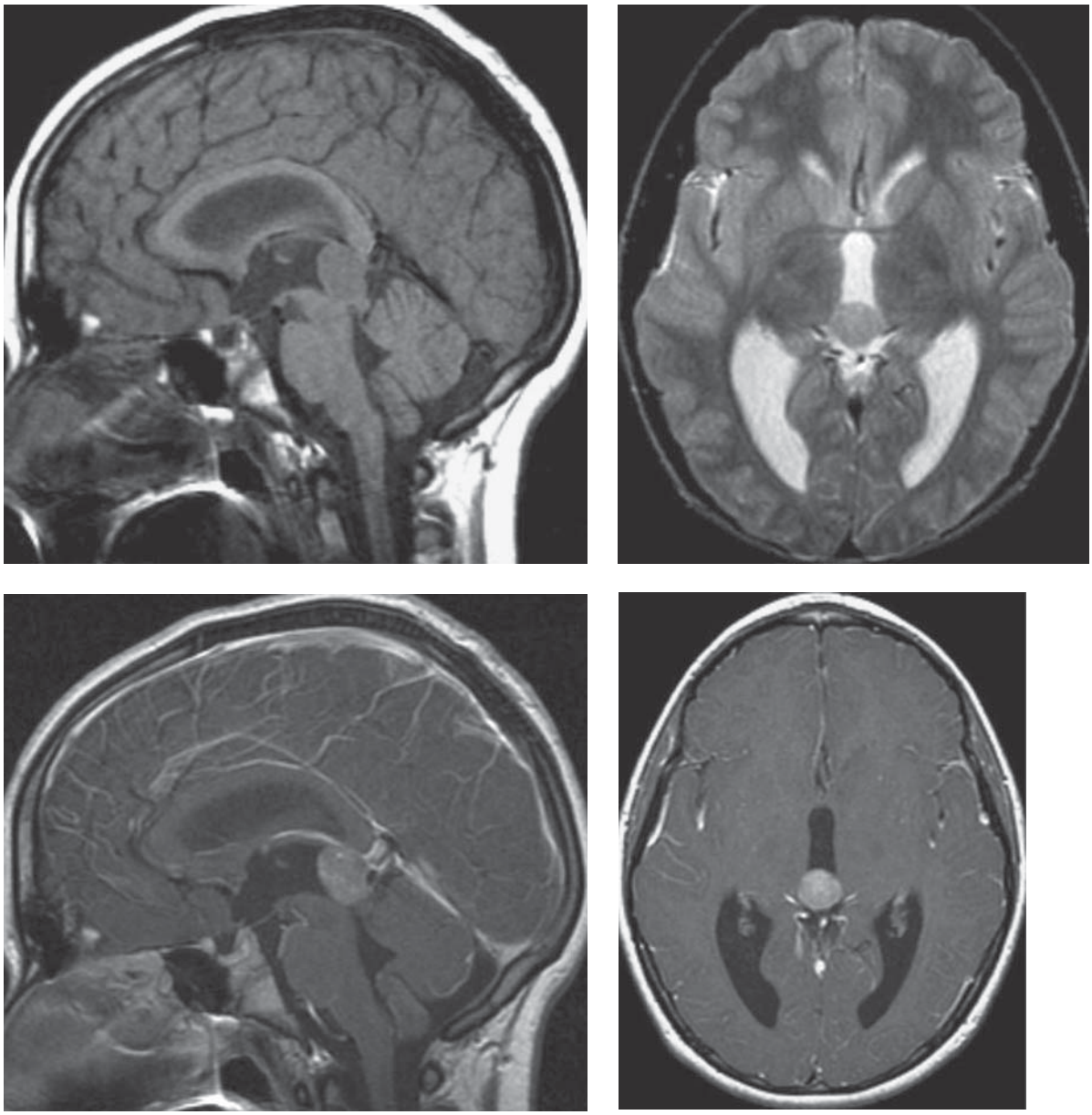


Fig. 129.1 **(A)** Sagittal T1, **(B)** axial T2 fast spin echo, and **(C)** sagittal and **(D)** axial T1 postgadolinium images demonstrate a pineal region mass that is intermediate in signal intensity on both T1- and T2-weighted sequences with homogeneous enhancement. There is mass effect on the tectal plate with obstructive hydrocephalus at the level of the cerebral aqueduct.

Clinical Presentation

A 56-year-old man presents with occasional headaches (**Fig. 129.1**).

Key Imaging Finding

Pineal region mass

Top 3 Differential Diagnoses

- **Pineal cyst.** Pineal cysts are common and usually discovered incidentally. Simple cysts follow fluid signal intensity on magnetic resonance imaging (MRI) and lack enhancement. The cysts may demonstrate increased signal intensity on T1-weighted sequences due to high protein content or hemorrhage. The internal cerebral veins should be closely inspected, as large cysts may result in occlusion of these vessels. Although peripheral calcifications and mild enhancement may occur with simple cysts, these findings should raise suspicion for a more malignant process. Cysts may be followed with serial imaging to ensure stability.
- **Germ cell tumor (GCT).** GCTs are the most common malignant neoplasms of the pineal gland, with germinomas (also referred to as seminomas) representing >60% of cases. Most cases occur in adolescent and young adult male patients. Presenting symptoms are usually secondary to mass effect, resulting in obstructive hydrocephalus, Parinaud syndrome (paralysis of upward gaze), or endocrine dysfunction. Germinomas are hyperdense on unenhanced computed tomography (CT) scans due to the high nuclear-to-cytoplasmic ratio and may contain calcifications centrally. On MRI, germinomas are usually intermediate in signal intensity on T1- and T2-weighted sequences with avid enhancement following gadolinium administration. On occasion, germinomas may appear cystic. Because cerebrospinal fluid (CSF) dissemination is common, the entire spine must be imaged to evaluate for drop metastases. Other GCTs are teratomas, yolk sac tumors, and choriocarcinomas. Teratomas will typically have macroscopic fat. Yolk sac tumors may be cystic and are associated with elevated levels of alpha fetoprotein. Choriocarcinomas have a propensity to bleed and are associated with elevated levels of human chorionic gonadotropin.
- **Pineal cell tumor.** Tumors of pineal cell origin are pineoblastomas and pineocytomas. Pineoblastomas are more malignant and occur in a younger patient population, with a peak incidence within the first 10 years of life. Seeding of the CSF is common. Pineocytomas have a peak incidence in the 3rd and 4th decades of life and are generally less aggressive. Presenting symptoms are usually due to mass effect resulting in obstructive hydrocephalus, Parinaud syndrome, or endocrine dysfunction. On imaging, the tumors closely resemble one another. On average, pineoblastomas are larger at the time of presentation. Both are hyperdense on unenhanced CT due to the high nuclear-to-cytoplasmic ratio. When calcifications occur in pineal cell tumors, they are along the periphery in an "exploded" pattern. On MRI, pineal cell tumors are of intermediate signal intensity on T1- and T2-weighted sequences, with avid enhancement following gadolinium administration. As with GCTs, the spine must be imaged to evaluate for drop metastases.

Additional Differential Diagnoses

- **Meningioma.** Meningiomas are the most common extra-axial intracranial tumors. They may occur along the margin of the tentorium, mimicking a pineal gland mass. The pineal gland and internal cerebral veins are often displaced superiorly. On noncontrast CT, meningiomas may be hyperdense; calcification is common. Enhancement pattern is typically homogeneous with a dural tail.
- **Tectal plate glioma.** Tectal plate gliomas are low-grade neoplasms which may cause aqueductal stenosis with associated hydrocephalus. When large, they may compress the pineal gland and mimic a pineal origin mass. They often present in childhood. The lesions are typically hyperintense on T2 sequences and rarely enhance. Treatment is geared toward CSF diversion in cases of obstructive hydrocephalus.

Diagnosis

Pineal germinoma

✓ Pearls

- Pineal cysts are often asymptomatic and incidentally found; no internal enhancement should be seen.
- GCTs are the most common pineal gland neoplasms and commonly result in CSF dissemination.
- Pineal cell tumors are the second most common neoplasms and may also result in CSF dissemination.
- Large tentorial meningiomas and tectal plate gliomas may mimic pineal origin masses.

Suggested Readings

Barkovich AJ. Pediatric Neuroimaging. 4th ed. Philadelphia: Lippincott Williams & Wilkins; 2005

Grossman RI, Yousem DM. Neuroradiology: The Requisites. Philadelphia: Elsevier; 2003

Case 130

William T. O'Brien Sr.

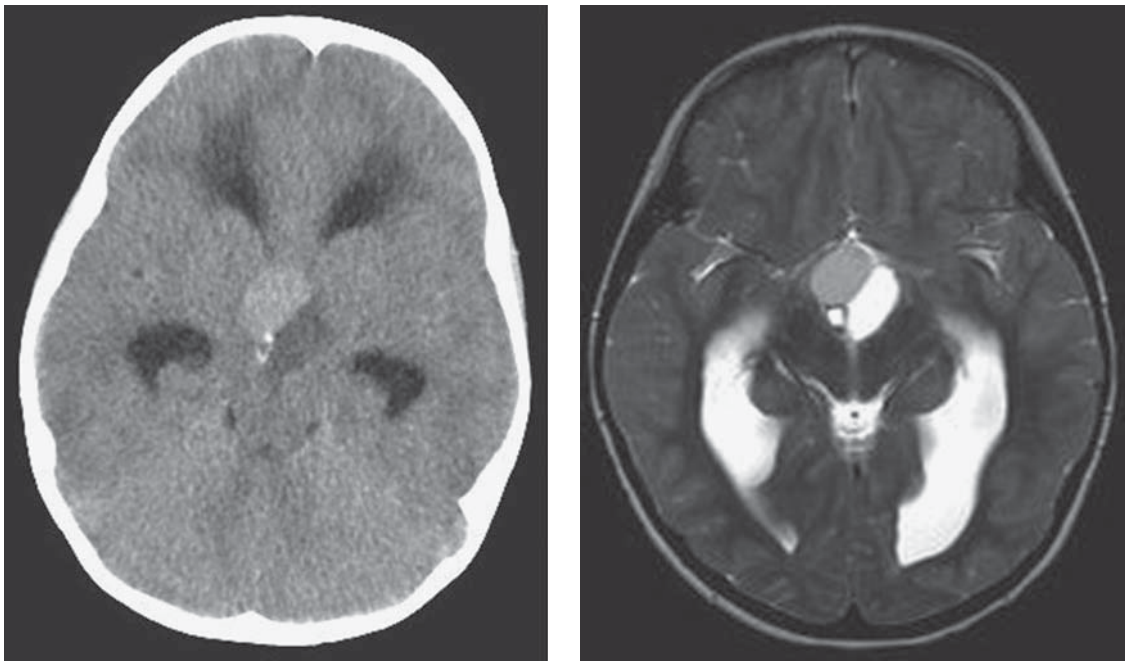


Fig. 130.1 **(A)** Axial unenhanced computed tomography and axial T2 fast spin echo images demonstrate a heterogeneous suprasellar mass with solid and cystic components and calcification. **(B)** The mass results in hydrocephalus due to mass effect on the third ventricle.

Clinical Presentation

A 5-year-old boy presents with a headache (**Fig. 130.1**).

Key Imaging Finding

Sellar/suprasellar mass in a child

Top 3 Differential Diagnoses

- **Craniopharyngioma.** Craniopharyngiomas are the most common suprasellar masses in children. They are benign tumors that arise from the Rathke pouch epithelium. There are adamantinomatous (peak age 5–15 years) and papillary (age >50 years) variants. Pediatric craniopharyngiomas present as multicystic suprasellar masses that may extend into the sella, anterior and middle cranial fossae, or retroclival regions. Computed tomography (CT) or skull films demonstrate amorphous calcifications (90% of pediatric lesions have calcifications), sellar expansion, and clival erosion. CT and magnetic resonance imaging (MRI) reveal a mixed cystic and solid mass with enhancement of the solid components and cyst wall. The lesions may be hyperdense on CT. Cystic contents may be T1 hyperintense (proteinaceous) and are predominantly T2 hyperintense. In contrast, the adult variant (papillary) most commonly presents as a solid enhancing suprasellar mass without calcifications.
- **Germ cell tumor (GCT).** GCTs are most common in the pediatric population. They occur most frequently in the pineal region, followed by the suprasellar region, and are often midline. Germinomas are the most common GCT and present as infiltrating, homogeneously enhancing masses that follow gray matter signal on MRI. Teratomas are more heterogeneous and have regions of fat. Dermoid cysts may have fat-fluid levels. GCTs may seed the CSF due to direct extension or rupture.
- **Rathke cleft cyst.** Rathke cleft cysts are nonneoplastic lesions that arise from remnants of the Rathke cleft. The lesions are intrasellar; however, many will have suprasellar extension. Approximately 10 to 15% of the cysts will have curvilinear wall calcification. On MRI, the cystic fluid may have variable signal intensity based on mucinous content. Lesions with high mucin content will be hyperintense on T1-weighted sequences. An intracystic nodule is commonly seen. There is no internal enhancement, but a rim of enhancing pituitary gland may be seen.

Additional Differential Diagnoses

- **Optic nerve/hypothalamic glioma.** Optic nerve gliomas are low-grade neoplasms (juvenile pilocytic astrocytomas) that typically occur between 5 and 15 years of age. They may occur sporadically or be associated with neurofibromatosis 1 (NF1); bilateral optic nerve involvement is pathognomonic for NF1. Tumors cause enlargement, elongation, and "buckling" of the optic nerve. Enhancement is variable. The tumor may extend along the optic pathway. Non-NF1 cases most often involve the optic chiasm/hypothalamus, are typically larger and more masslike, commonly have cystic degeneration, and often extend beyond the optic pathways.
- **Hypothalamic hamartoma.** Hypothalamic hamartomas are rare, benign neoplasms that occur in children who present with gelastic seizures and precocious puberty. The hamartomas are isointense to gray matter on T1- and iso- to hyperintense on T2-weighted sequences. No enhancement should be seen; the presence of enhancement suggests hypothalamic glioma rather than hamartoma.

Diagnosis

Craniopharyngioma

✓ Pearls

- Pediatric craniopharyngiomas present as multilobulated, multicystic masses with regions of calcification.
- GCTs occur midline and may seed the CSF; germinoma is the most common subtype.
- Optic nerve and hypothalamic gliomas may occur sporadically or be associated with NF1.
- Patients with hypothalamic hamartomas may present with precocious puberty and gelastic seizures.

Suggested Readings

Grossman RI, Yousem DM. Neuroradiology: The Requisites. 2nd ed. Philadelphia: Mosby; 2003

Osborn A, Blaser S, Salzman KL, et al. Diagnostic Imaging: Brain. Salt Lake City, UT: Amirsys; 2004

Case 131

Paul M. Sherman

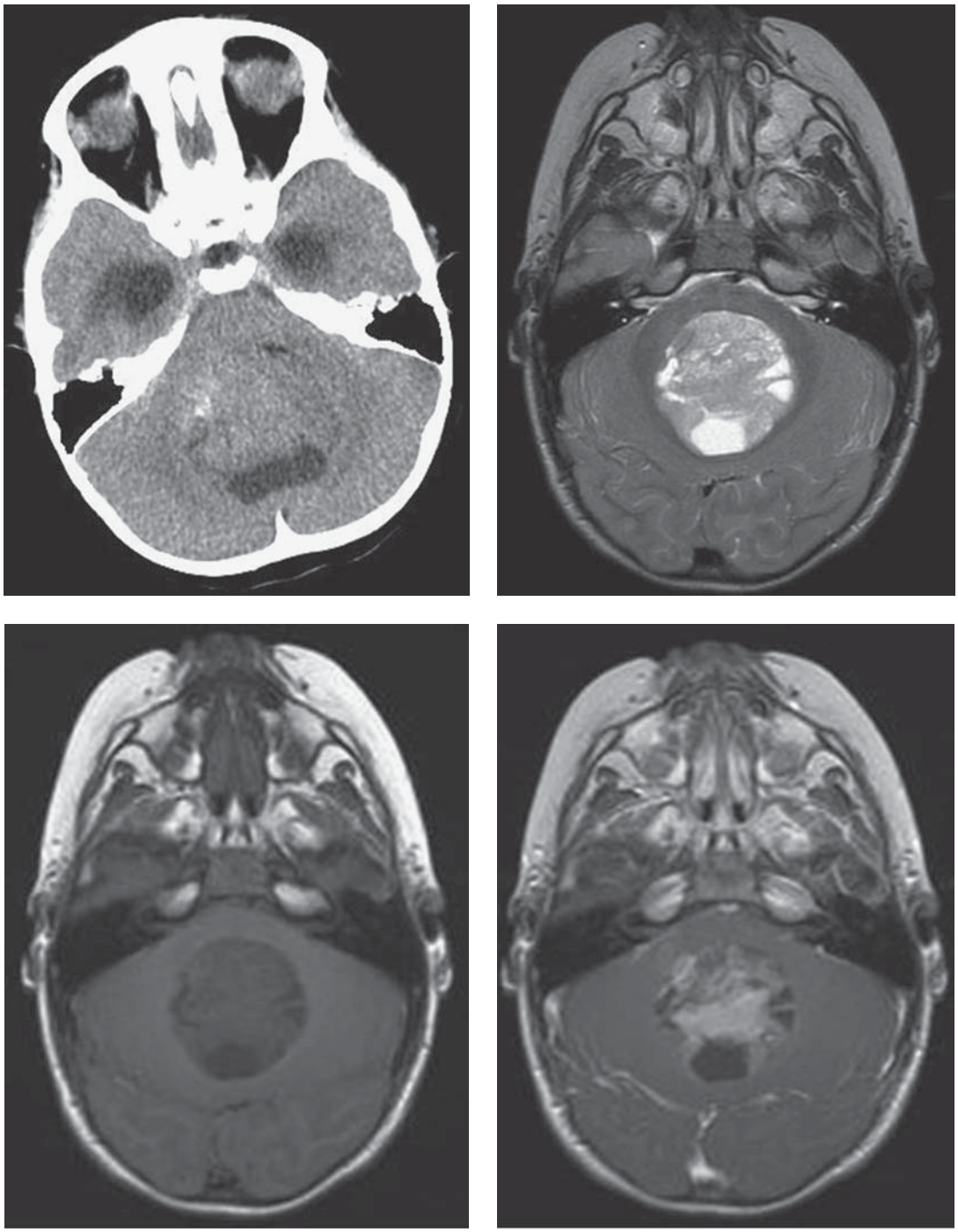


Fig. 131.1 **(A)** Axial computed tomography image demonstrates a hyperdense midline posterior fossa mass in the region of the fourth ventricle with obstructive hydrocephalus. **(B)** Axial T2 and **(C)** T1 precontrast and **(D)** postcontrast images demonstrate a heterogeneous fourth ventricular mass with cystic and enhancing solid components.

Clinical Presentation

A 6-year-old boy presents with headaches and loss of balance (**Fig. 131.1**).

Key Imaging Finding

Posterior fossa mass in a child

Top 3 Differential Diagnoses

- **Medulloblastoma.** Medulloblastoma is a World Health Organization (WHO) grade IV posterior fossa primitive neuroectodermal tumor and is the most common posterior fossa tumor in children. The tumor arises from the superior medullary velum (roof of the fourth ventricle), whereas ependymomas arise from the floor of the fourth ventricle. The peak incidence is within the 1st decade of life. Although characteristically a midline lesion, lateral (cerebellar hemisphere) origin may be seen in children and older adults. Medulloblastomas are hyperdense on computed tomography (CT; 90%) due to high cellular content. They are T1 hypointense, T2 iso- to hyperintense, and fluid-attenuated inversion recovery (FLAIR) hyperintense with restricted diffusion. Calcification is seen in up to 20% of cases. Enhancement is mildly heterogeneous. Up to one third of cases will have subarachnoid seeding (metastases) at presentation; therefore, evaluation of the entire neuroaxis prior to surgical intervention is required for any posterior fossa lesion in a child. Linear "icing-like" enhancement of the brain surface is referred to as "Zuckerguss."
- **Juvenile pilocytic astrocytoma (JPA).** JPA (WHO grade I astrocytoma) is the second most common primary posterior fossa brain tumor in children, with an incidence slightly below that of medulloblastoma. The tumor arises from the cerebellar hemisphere; as a result, it is most often located off-midline. Peak incidence is 5 to 15 years of age. The most common presentation is a cystic mass with an enhancing mural nodule. The cystic component is T1 iso- to hypointense and T2/FLAIR hyperintense. The solid component is T2 and FLAIR hyperintense. Less common imaging appearances include a solid mass with a necrotic center and heterogeneous enhancement or a solid homogeneously enhancing mass. It is important to closely interrogate the entire brain, especially the optic pathways, as lesions may be multiple in the setting of neurofibromatosis 1.
- **Ependymoma.** Ependymoma is a slow-growing midline posterior fossa tumor of ependymal cells that characteristically squeezes through the fourth ventricle foramina (plastic or toothpaste tumor) into the cerebellopontine angle, foramen magnum, or cisterna magna. Age of presentation is 1 to 5 years. On CT, calcification is seen in ~50% of cases. Cystic change and foci of hemorrhage are less common. Hydrocephalus is common. Two thirds arise from the fourth ventricle (infratentorial), and approximately one third of such tumors are supratentorial (the majority in the periventricular white matter). The tumor is typically heterogeneous and iso- to hypointense on T1- and T2-weighted images. Tumor cysts are hyperintense to cerebrospinal fluid (CSF) on T1 and FLAIR images. There is mild to moderate heterogeneous enhancement.

Additional Differential Diagnoses

- **Brainstem glioma.** Brainstem glioma represents ~10 to 20% of pediatric brain tumors and commonly presents within the 1st and 2nd decades of life. It typically presents as a diffuse, infiltrating pontine mass (WHO grade II–IV) that engulfs the basilar artery and may project into the fourth ventricle, causing obstruction and hydrocephalus. It is typically homogeneously low T1 and high T2 signal intensity with variable enhancement. Enhancement and necrosis may occur over time. Prognosis is poor.

Diagnosis

Medulloblastoma

✓ Pearls

- Medulloblastoma is the most common posterior fossa mass in a child, is midline, and seeds the CSF.
- JPA most commonly presents as an off-midline cystic mass with enhancing mural nodule.
- Ependymoma is a midline tumor that extends through the ventricular foramina.
- Brainstem glioma most commonly occurs within the pons; the prognosis is poor due to the location in the brainstem.

Suggested Readings

Barkovich AJ, Moore KR, Grant E, et al. Diagnostic Imaging: Pediatric Neuroradiology. Salt Lake City, UT: Amirsys; 2007

Osborn A, Blaser S, Salzman KL, et al. Diagnostic Imaging: Brain. Salt Lake City, UT: Amirsys; 2004

Case 132

Paul M. Sherman

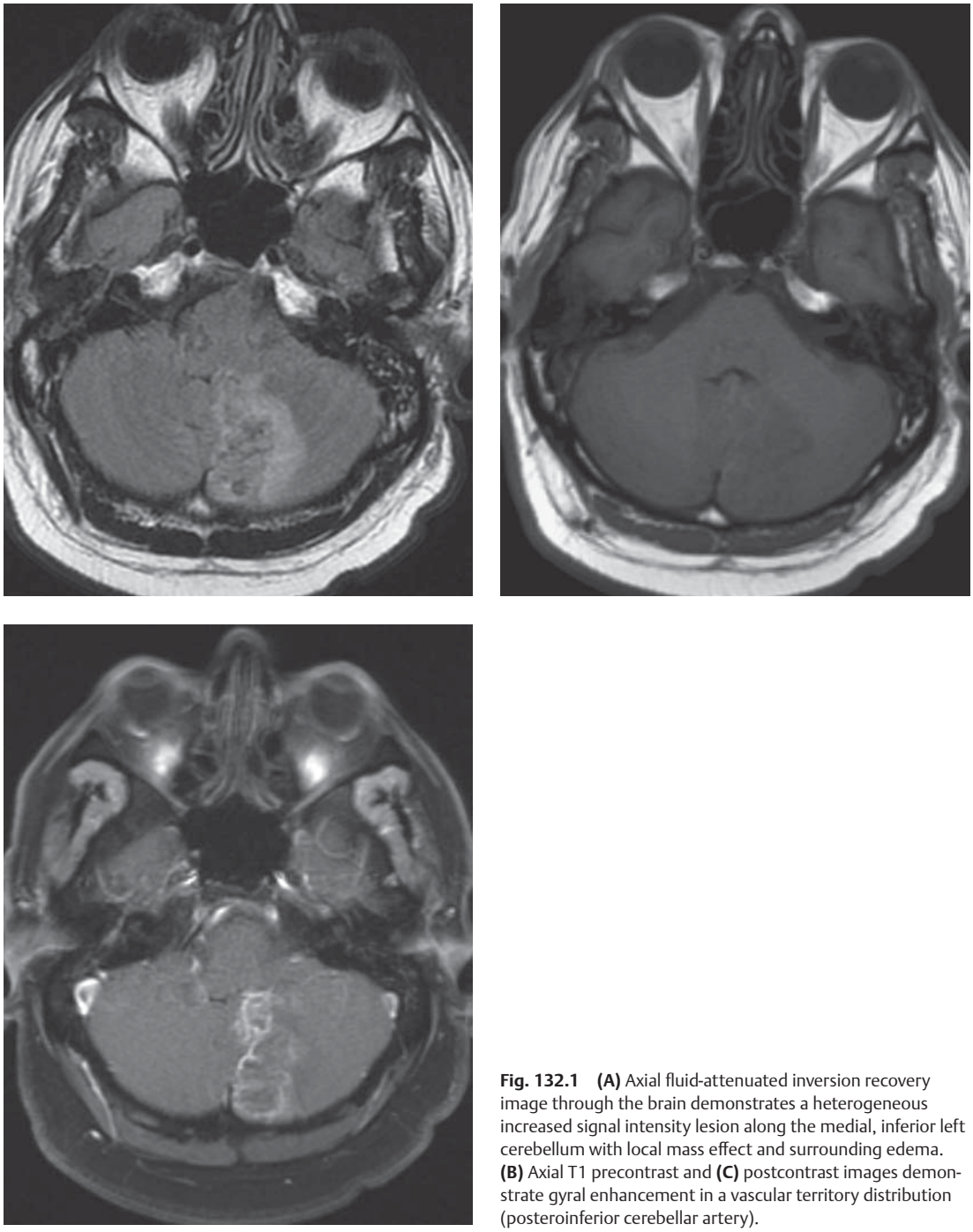


Fig. 132.1 **(A)** Axial fluid-attenuated inversion recovery image through the brain demonstrates a heterogeneous increased signal intensity lesion along the medial, inferior left cerebellum with local mass effect and surrounding edema. **(B)** Axial T1 precontrast and **(C)** postcontrast images demonstrate gyral enhancement in a vascular territory distribution (posteroinferior cerebellar artery).

Clinical Presentation

A 52-year-old man presents with a headache and gait disturbances (**Fig. 132.1**).

Key Imaging Finding

Posterior fossa mass in an adult

Top 3 Differential Diagnoses

- **Infarction.** Ischemic changes commonly affect the posterior fossa and may have a masslike appearance. The morphology of an infarct generally corresponds to the vascular territory of the involved vessel (posteroinferior [PICA], anteroinferior, and superior cerebellar arteries). Other differentiating features are restricted diffusion and vascular occlusion demonstrated on computed tomography (CT) or magnetic resonance (MR) angiography. Edema, mass effect, potential hemorrhagic transformation, and subacute enhancement may mimic a mass lesion.
- **Metastatic disease.** Metastatic disease is the most common cause of a posterior fossa intra-axial mass in middle-aged and older adults. Lung, breast, and gastrointestinal types are among the most common primary neoplasms. They are more often multiple and solid, although they may occasionally be solitary and cystic. Hemorrhagic metastases tend to have strong enhancement and an incomplete hemosiderin rim. Renal cell carcinoma (RCC) metastases may mimic hemangioblastoma, as they very vascular lesions.
- **Hemangioblastoma.** Hemangioblastomas are classified as meningeal neoplasms of uncertain histiogenesis. Ninety to 95% occur within the posterior fossa, typically within the cerebellar hemispheres, and 5 to 10% are supratentorial. The supratentorial lesions commonly involve the optic pathways and cerebral hemispheres and are more often associated with von Hippel–Lindau (VHL) disease. Larger lesions present as cystic masses with enhancing mural nodules (similar to juvenile pilocytic astrocytoma); smaller lesions commonly present as solid enhancing masses. The cystic components may be slightly hyperintense to cerebrospinal fluid on T1-weighted images. The cyst and nodule are hyperintense on T2/ fluid-attenuated inversion recovery images. Lesions abut the pial surface and may demonstrate flow voids. When identified, the entire neuroaxis should be imaged to look for additional lesions, especially within the spinal cord. Approximately one fourth to one half of patients with posterior fossa hemangioblastomas will have VHL. VHL commonly has multiple hemangioblastomas, as well visceral cysts and additional neoplastic lesions, including RCC, pheochromocytoma, and ocular angiomas.

Additional Differential Diagnoses

- **Vascular malformation.** Multiple arteriovenous malformations in vascular neurocutaneous syndromes (e.g., hereditary hemorrhagic telangiectasia) may mimic metastases or multiple hemangioblastomas. Cavernous malformations may also be seen in the posterior fossa. These may be distinguished from other lesions by a complete hemosiderin rim. They have a characteristic “popcorn” appearance secondary to intralesional blood products at different stages.
- **Hypertensive hemorrhage.** Hypertensive hemorrhage commonly involves the posterior fossa (pons and cerebellum). The lesions are typically round or oval. Acute hemorrhage is hyperdense on CT with mass effect and surrounding edema, mimicking a hemorrhagic metastatic lesion. MR findings vary based on the age of blood products, as in other intracranial hemorrhage. T2* gradient echo imaging may identify additional foci of prior hypertensive bleeds (lentiform nuclei and thalami).

Diagnosis

Subacute PICA territory infarct

✓ Pearls

- Ischemia commonly affects the posterior fossa, follows a vascular distribution, and has restricted diffusion.
- Metastases are the most common posterior fossa intra-axial masses in adults and are commonly multiple.
- Hemangioblastomas present as cystic masses with mural nodules and may be associated with VHL.
- Hypertensive hemorrhages commonly involve the lentiform nuclei, thalami, and posterior fossa.

Suggested Readings

Fischbein NJ, Dillon WP, Barkovich AJ. Teaching Atlas of Brain Imaging. New York: Thieme; 1999

Osborn A, Blaser S, Salzman KL, et al. Diagnostic Imaging: Brain. Salt Lake City, UT: Amirsys; 2004

Case 133

William T. O'Brien Sr.

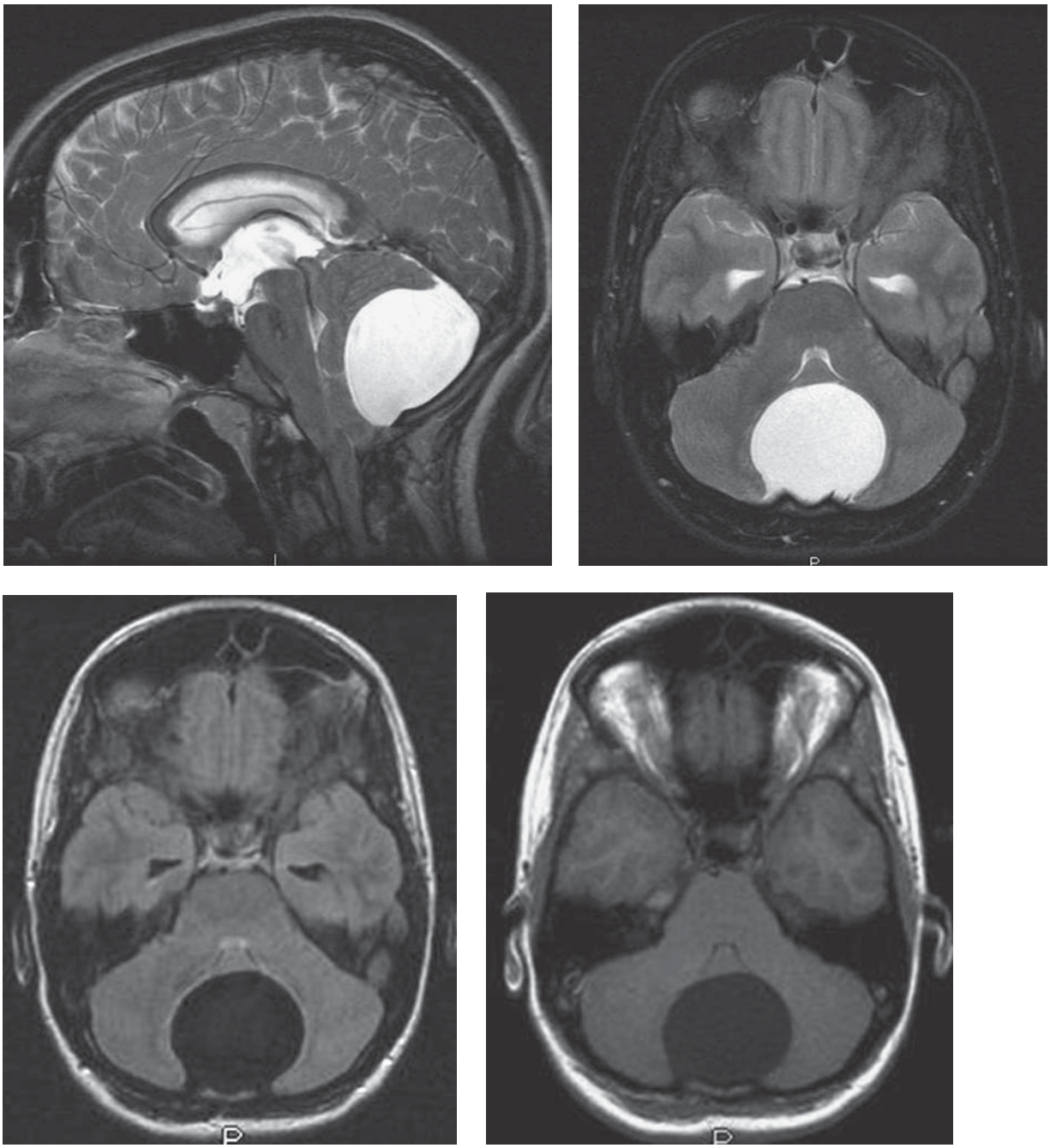


Fig. 133.1 **(A)** Sagittal T2-weighted sequence through the brain demonstrates a large cerebrospinal fluid (CSF) signal intensity mass within the posterior fossa with anterior and superior displacement of the cerebellum. There is also compression of the fourth ventricle, as well as associated enlargement of the third ventricle. **(B)** Axial T2, **(C)** fluid-attenuated inversion recovery, and **(D)** T1-weighted images reveal that the mass follows CSF signal intensity on all sequences. There is no direct communication with the fourth ventricle. Enlargement of the bilateral temporal horns of the lateral ventricles is also seen.

Clinical Presentation

An adolescent presents with headaches (**Fig. 133.1**).

Key Imaging Finding

Posterior fossa cyst

Top 3 Differential Diagnoses

- **Mega cisterna magna.** A mega cisterna magna is a common normal variant in which the cerebrospinal fluid (CSF)–filled cisterna magna is prominent. This entity can usually be differentiated from an arachnoid cyst or Dandy–Walker malformation by the normal appearance and size of the posterior fossa, a normal cerebellar vermis and fourth ventricle, the lack of mass effect, and the presence of internal vessels.
- **Arachnoid cyst.** Arachnoid cysts are developmental CSF-filled spaces within the arachnoid. Although typically asymptomatic and discovered incidentally, they may exert local mass effect. The majority are supratentorial along the middle cranial fossa or convexities. Common infratentorial locations are the cerebellopontine angle and the cisterna magna. When located within the posterior fossa, they may be large enough to compress the fourth ventricle or cerebral aqueduct, resulting in obstructive hydrocephalus. Arachnoid cysts follow CSF signal on all magnetic resonance imaging pulse sequences; occasionally, however, they may have slight increased signal intensity on proton density due to the stasis of CSF. Mass effect is evident by displacement of vessels around the arachnoid cyst and scalloping of the overlying cortex.
- **Dandy–Walker malformation.** Dandy–Walker malformation is a developmental abnormality that results from a defect in the cerebellar vermis and fourth ventricle during embryogenesis. The malformation consists of an enlarged posterior fossa, partial or complete absence of the cerebellar vermis, hypoplasia of the cerebellar hemispheres, and a dilated fourth ventricle that is in direct communication with a posterior CSF-filled fluid collection. The enlarged posterior fossa results in superior displacement of the torcula above the lambdoid sutures (lambdoid-torcular inversion). Dandy–Walker malformation is associated with other anomalies, including corpus colossal agenesis or hypogenesis and neuronal migration abnormalities.

Additional Differential Diagnoses

- **Joubert syndrome (vermian hypoplasia).** Joubert syndrome is an uncommon posterior fossa malformation characterized by a dysplastic and hypoplastic cerebellar vermis, as well as malformations of various nuclei and tracts. Patients present with neonatal hyperpnea, apnea, and mental retardation. Imaging findings include a dysplastic and hypoplastic cerebellar vermis, a bulbous fourth ventricle that has a characteristic "bat wing" configuration, and a "molar tooth" appearance of the midbrain secondary to a narrow, deep interpeduncular cistern and elongated superior cerebellar peduncles that are parallel with each other.

Diagnosis

Arachnoid cyst

✓ Pearls

- Mega cisterna magna is a normal variant with a normal-sized posterior fossa and normal cerebellar vermis.
- Arachnoid cysts follow CSF signal on all pulse sequences and exert local mass effect.
- Dandy–Walker malformation results from vermian aplasia or hypoplasia (Dandy–Walker variant).
- Joubert syndrome results in a "bat wing" configuration of the fourth ventricle and "molar tooth" midbrain.

Suggested Readings

Barkovich AJ, Kjos BO, Norman D, et al. Revised classification of posterior fossa cysts and cyst-like malformations based on the results of multiplanar MR imaging. AJR Am J Roentgenol 1989;153:1289–1300

Barkovich AJ, Moore KR, Grant E, et al. Diagnostic Imaging: Pediatric Neuroradiology. Salt Lake City, UT: Amirsys; 2007

O'Brien WT, Palka PS, et al. Pediatric neuroimaging. In: Quattromani F, Handal GA, Lampe R, eds. Pediatric Imaging: Rapid-fire Questions and Answers. New York: Thieme; 2007:338–391

Case 134

Jeffrey P. Tan

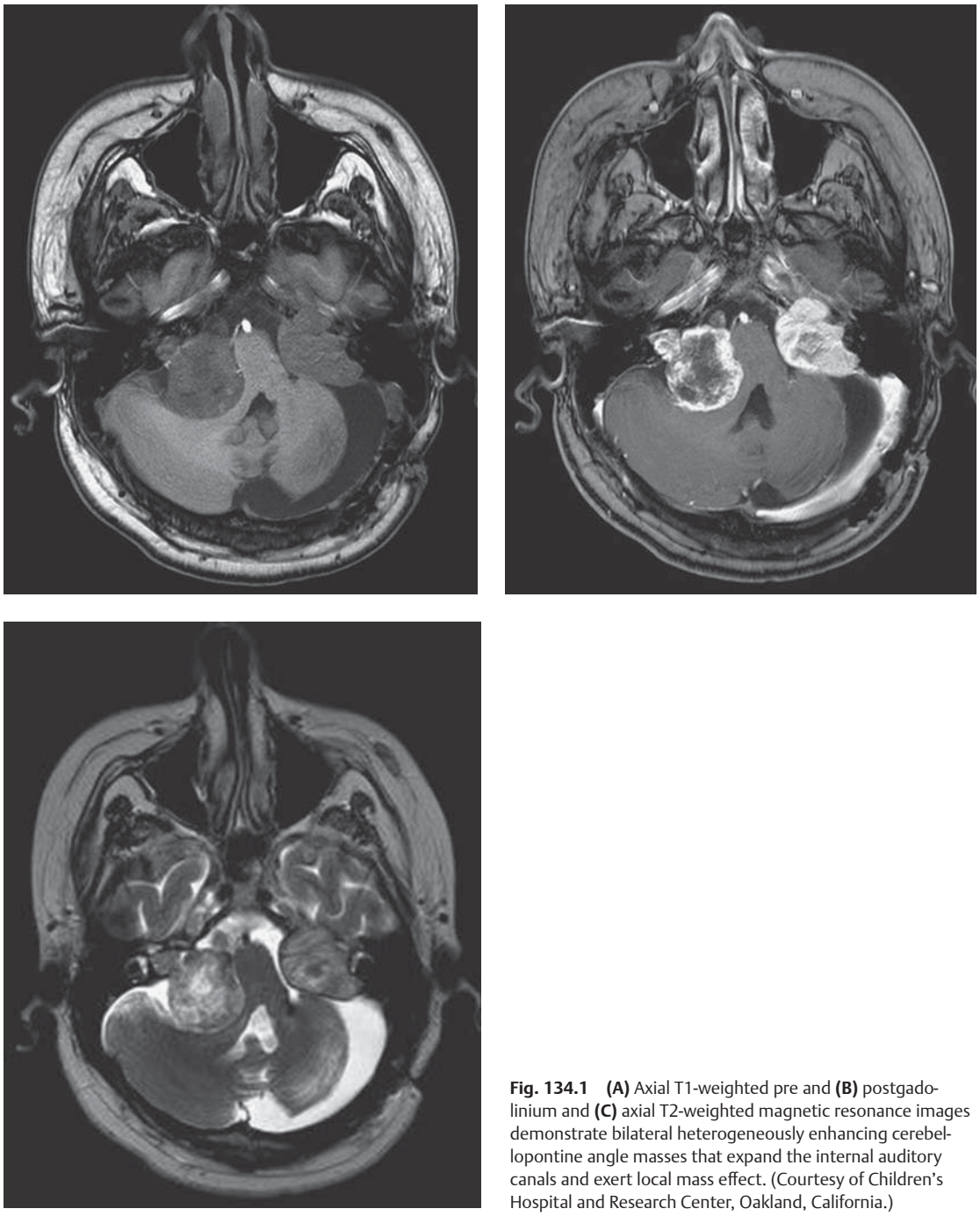


Fig. 134.1 **(A)** Axial T1-weighted pre and **(B)** postgadolinium and **(C)** axial T2-weighted magnetic resonance images demonstrate bilateral heterogeneously enhancing cerebellopontine angle masses that expand the internal auditory canals and exert local mass effect. (Courtesy of Children's Hospital and Research Center, Oakland, California.)

Clinical Presentation

A 28-year-old man presents with bilateral sensorineural hearing loss (**Fig. 134.1**).

Key Imaging Finding

Cerebellopontine angle (CPA) mass

Top 3 Differential Diagnoses

- **Vestibular schwannoma.** Vestibular schwannomas arise from the perineural Schwann cells and may be composed of two tissue types, Antoni A and B. Antoni A tissue is densely packed, which results in a darker signal on T2-weighted images; Antoni B tissue is loosely packed, which results in a brighter signal on T2. The border of a schwannoma usually makes an acute angle with the petrous bone. There is typically expansion of the internal auditory canal and flaring of the porus acusticus. Schwannomas most commonly involve the superior division of the eighth cranial nerve (vestibular schwannoma) and demonstrate homogeneous enhancement. Less commonly, schwannomas may have calcification, cystic change, and hemorrhage. Bilateral vestibular schwannomas are diagnostic of neurofibromatosis 2 (NF2).
- **Meningioma.** Meningiomas arise from meningothelial arachnoid cells and are the most common extra-axial intracranial tumors. An intracanalicular meningioma, however, is rare. Meningiomas commonly have a dural tail secondary to broad-based dural attachment along the petrous bone. On noncontrast computed tomography (CT), meningiomas may be hyperdense, and there may be hyperostosis along the adjacent bone. Calcification is common. In addition, meningiomas typically have a ragged border in contrast to a smooth, round border with schwannomas. Enhancement pattern is typically homogeneous.
- **Arachnoid cyst.** Arachnoid cysts are cerebrospinal fluid (CSF) collections contained within arachnoid as a result of embryonic failure of meningeal fusion. The lesions follow CSF fluid signal intensity on all magnetic resonance sequences. The most common sites are the middle cranial fossa and the posterior fossa. Proton density and T2-weighted images may occasionally show slightly increased signal intensity in relation to CSF due to the lack of normal CSF pulsations. There is no restricted diffusion on diffusion-weighted imaging. When large, arachnoid cysts demonstrate mass effect on the adjacent cerebellum and pons. There is no enhancement.

Additional Differential Diagnoses

- **Epidermoid cyst.** Epidermoid cysts are tumors of ectodermal origin composed of keratinaceous debris lined by stratified squamous epithelium. The most common intracranial location is the cerebellopontine angle. Epidermoid cysts are hypointense on T1- and hyperintense on T2-weighted imaging without enhancement. There may be heterogeneous loss of signal intensity on fluid-attenuated inversion recovery imaging. The key distinction from an arachnoid cyst is the presence of restricted diffusion on diffusion-weighted imaging. In addition, epidermoid cysts have irregular margins and engulf vessels and nerves, as opposed to arachnoid cysts, which displace them.

Diagnosis

Bilateral vestibular schwannomas (NF2)

✓ Pearls

- Vestibular schwannomas are the most common cerebellopontine masses; bilateral lesions are diagnostic of NF2.
- Meningiomas are hyperdense on CT, may have calcification, intensely enhance, and have a dural tail.
- Arachnoid cysts follow CSF signal on all pulse sequences and may exert local mass effect.
- Epidermoids mimic arachnoid cysts except that they demonstrate restricted diffusion.

Suggested Readings

Asaoka K, Bears DM, Sampson JH, et al. Intracanalicular meningioma mimicking vestibular schwannoma. AJNR Am J Neuroradiol 2002;23:1493–1496

Nakamura M, Roser F, Mirzai S, et al. Meningiomas of the internal auditory canal. Neurosurgery 2004;55:119–128

Osborn A, Blaser S, Salzman KL, et al. Diagnostic Imaging: Brain. Salt Lake City, UT: Amirsys; 2004

Case 135

Paul M. Sherman

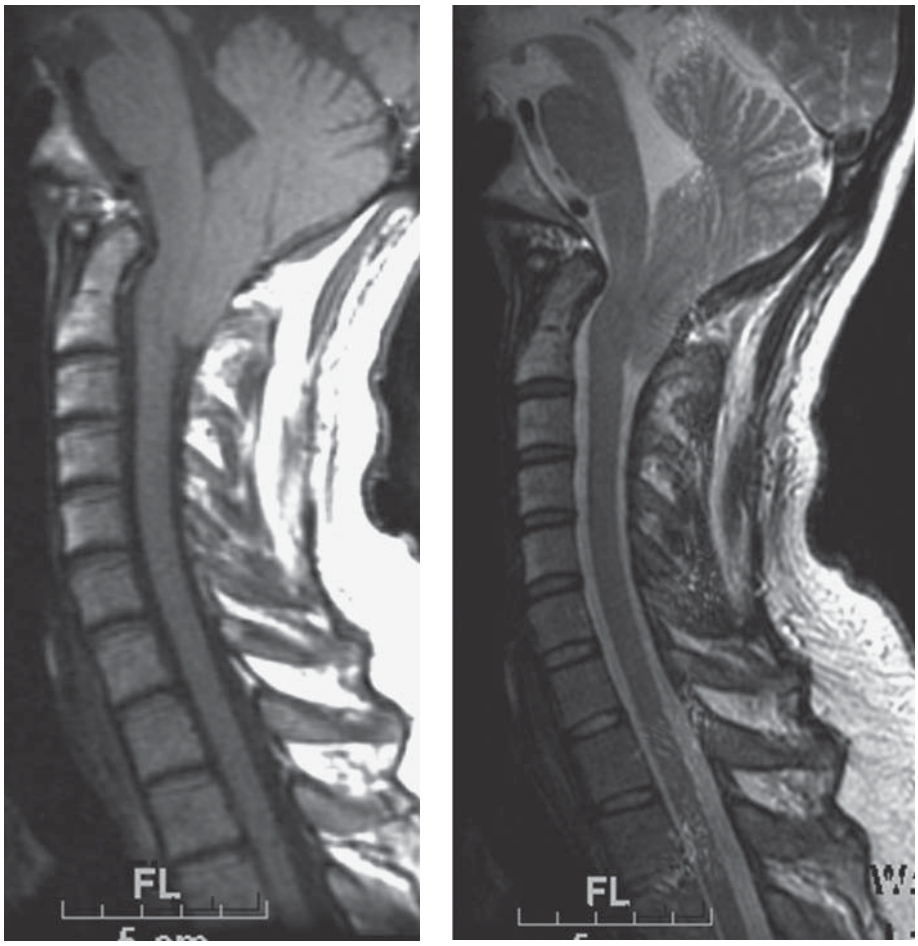


Fig. 135.1 **(A)** Sagittal T1 and **(B)** T2 fast spin echo images of the cervical spine demonstrate significant cerebellar tonsillar herniation below the foramen magnum with "peglike" tonsils. The posterior fossa is small, and there is mass effect on the brainstem. No significant syringohydromyelia is identified.

Clinical Presentation

A 34-year-old man presents with headaches and vertigo (**Fig. 135.1**).

Key Imaging Finding

Cerebellar tonsillar herniation

Top 3 Differential Diagnoses

- **Arnold–Chiari malformation.** Type I and II Arnold–Chiari malformations, although separate entities, both demonstrate caudal protrusion of "peg-shaped" cerebellar tonsils below the foramen magnum (basion–opisthion line) ≥5 mm. In both malformations, the posterior fossa is small. The tonsils may wrap anteriorly around the medulla in Chiari II. Chiari I malformations are associated with osseous abnormalities of the skull base and cervical spine. Approximately half of Chiari I patients are asymptomatic; the remaining may have symptoms associated with brainstem compression or hydrosyringomyelia. Chiari II malformations are associated with neural tube closure defects and a lumbar myelomeningocele. Intracranial imaging findings include a beaked tectum, cervicomedullary kinking, an enlarged massa intermedia, a low-lying torcula, a "towering" cerebellum protruding cranially through the incisura, a compressed and elongated fourth ventricle, and a Lückenschädel (lacunar) skull (to 6 months of age). There is dysgenesis of the corpus callosum in 90% and posterior C1 arch anomalies in approximately two thirds of cases. Hydrocephalus is common.
- **Ependymoma.** Ependymoma is the third most common posterior fossa tumor in children and arises from the ependymal cells of the fourth ventricle. It is a "plastic" tumor that may extend into the cerebellopontine angle, foramen magnum, or cisterna magna. Extension into the foramen magnum may mimic cerebellar tonsillar ectopia. Calcification is seen in ~50% of cases; cysts and hemorrhage are less common. The mass is heterogeneous in nature, typically iso- or hyperintense on T2-weighted imaging, with heterogeneous enhancement. Tumoral cysts are hyperintense to cerebrospinal fluid (CSF) on fluid-attenuated inversion recovery (FLAIR) imaging. Patients typically present with headache and vomiting between 1 and 5 years of age.
- **Posterior fossa mass.** Any primary or secondary posterior fossa mass may cause tonsillar herniation secondary to local mass effect. Common causes in children are medulloblastoma and juvenile pilocytic astrocytoma; common lesions in adults are infarction, metastases, hemangioblastoma, vascular malformations, and hypertensive hemorrhage.

Additional Differential Diagnoses

- **Intracranial hypotension.** Intracranial hypotension results in "sagging" of the brain and subsequent inferior tonsillar displacement. Etiologies include iatrogenic (postsurgical or procedural, e.g., lumbar puncture), trauma, violent coughing or strenuous exercise, spontaneous dural tear or ruptured arachnoid diverticulum, severe dehydration, and, rarely, disk protrusion with dural injury. Reduced intracranial pressure results in brain descent. Tonsillar ectopia is seen in up to 75% of cases. Additional imaging findings include diffuse thickened, FLAIR hyperintense, enhancing dura and subdural fluid collections, typically hygromas. There is a "sagging" midbrain (below the dorsum sella) and a "fat midbrain" sign (elongated appearance of the midbrain and pons). Radionuclide cisternography can be used to search for the site of CSF leak if blood patch therapy fails.

Diagnosis

Chiari I malformation

✓ Pearls

- Chiari I is characterized by tonsillar ectopia, skull base/cervical spine malformations, and syrinx.
- Chiari II is characterized by tonsillar ectopia, myelomeningocele, and multiple intracranial abnormalities.
- Ependymoma extension into the foramen magnum may mimic tonsillar ectopia.
- A posterior fossa mass or "sagging" from intracranial hypotension may result in tonsillar ectopia.

Suggested Readings

Fischbein NJ, Dillon WP, Barkovich AJ. Teaching Atlas of Brain Imaging. New York: Thieme; 1999

Osborn A, Blaser S, Salzman KL, et al. Diagnostic Imaging: Brain. Salt Lake City, UT: Amirsys; 2004

Case 136

Paul M. Sherman



Fig. 136.1 Contrast-enhanced axial computed tomography image through the lateral ventricles demonstrates a gray matter–lined cerebrospinal cleft that communicates with the frontal horn of the right lateral ventricle. There is also absence of the septum pellucidum.

Clinical Presentation

A patient presents with seizures (**Fig. 136.1**).

Key Imaging Finding

Cerebrospinal fluid (CSF)–lined cortical cleft

Top 3 Differential Diagnoses

- **Prior infarct with encephalomalacia.** Chronic cerebral infarction results in parenchymal volume loss and associated ventricular enlargement. Encephalomalacia may occur secondary to an arterial thromboembolic event, primary intracranial hemorrhage, hemorrhagic venous infarct, or even subarachnoid hemorrhage. Like porencephalic cysts, the CSF cavity is lined by gliotic white matter. Morphology depends on the location, size, and type of vascular insult, but it is classically wedge-shaped. CT and MRI demonstrate prominence of the adjacent sulci and enlargement of the ipsilateral ventricle in addition to the CSF signal intensity region. Gliotic parenchyma along the border of the infarction will show characteristic increased T2 signal. T2* gradient echo may show hemosiderin staining in the gliotic areas. CT or MR angiography usually shows the absence of flow within the affected vessel.
- **Schizencephaly.** Schizencephaly is a congenital malformation that occurs in the early prenatal period and is characterized by gray matter–lined clefts extending from the pial surface to the ventricle. The clefts are typically parasylvian in location. Type I (closed lip) schizencephaly consists of a fused cleft. This fused pial-ependymal seam is lined by polymicrogyric gray matter. Type II (open lip) schizencephaly consists of a large defect, often holohemispheric, filled with CSF and lined by polymicrogyric gray matter. The abnormality may be bilateral and can be associated with septo-optic dysplasia. Clinical manifestations depend on the severity of the lesion. Patients with type I are often almost normal in terms of development, but they may have seizures and hemiparesis. Patients with type II usually demonstrate mental retardation, seizures, hypotonia, spasticity, an inability to walk or speak, and blindness. Bilateral defects are associated with severe disability. Computed tomography (CT) and magnetic resonance imaging (MRI) demonstrate the gray matter lining. Deformity of the ventricle at the site of the closed-lip variant (dimple) "points" to the cleft. Heterotopia and cortical dysplasia may be associated findings.
- **Porencephalic cyst.** Porencephalic cysts are CSF clefts that are lined by dysplastic white matter. The cysts communicate with the subarachnoid space or ventricle. They may be congenital, related to a cerebrovascular accident or perinatal infection, or acquired, following head trauma, vascular insult, or infection. Familial porencephaly has been described but is a rare condition. Amygdala-hippocampal atrophy coexists in up to 95% of patients. Patients may have severe neurologic deficits, with hemiplegic cerebral palsy representing the most common feature. Seizures and mental retardation are also common. The location of the cysts usually corresponds to a vascular territory. They may be unilateral or bilateral. The walls of the cavity are smooth, and the abnormal white matter lining typically demonstrates fluid-attenuated inversion recovery hyperintensity. There is an absence of vessels at the site of porencephaly. The adjacent ventricle is typically enlarged.

Diagnosis

Schizencephaly (type II, open lip)

✓ Pearls

- Schizencephaly results in a CSF cleft lined by dysplastic gray matter; it is due to an intrauterine insult.
- Schizencephaly is associated with neural migration abnormalities and septo-optic dysplasia.
- Porencephalic cysts are caused by a perinatal insult and are lined by dysplastic white matter.
- Encephalomalacia results from prior brain parenchymal injury and is typically wedge-shaped.

Suggested Readings

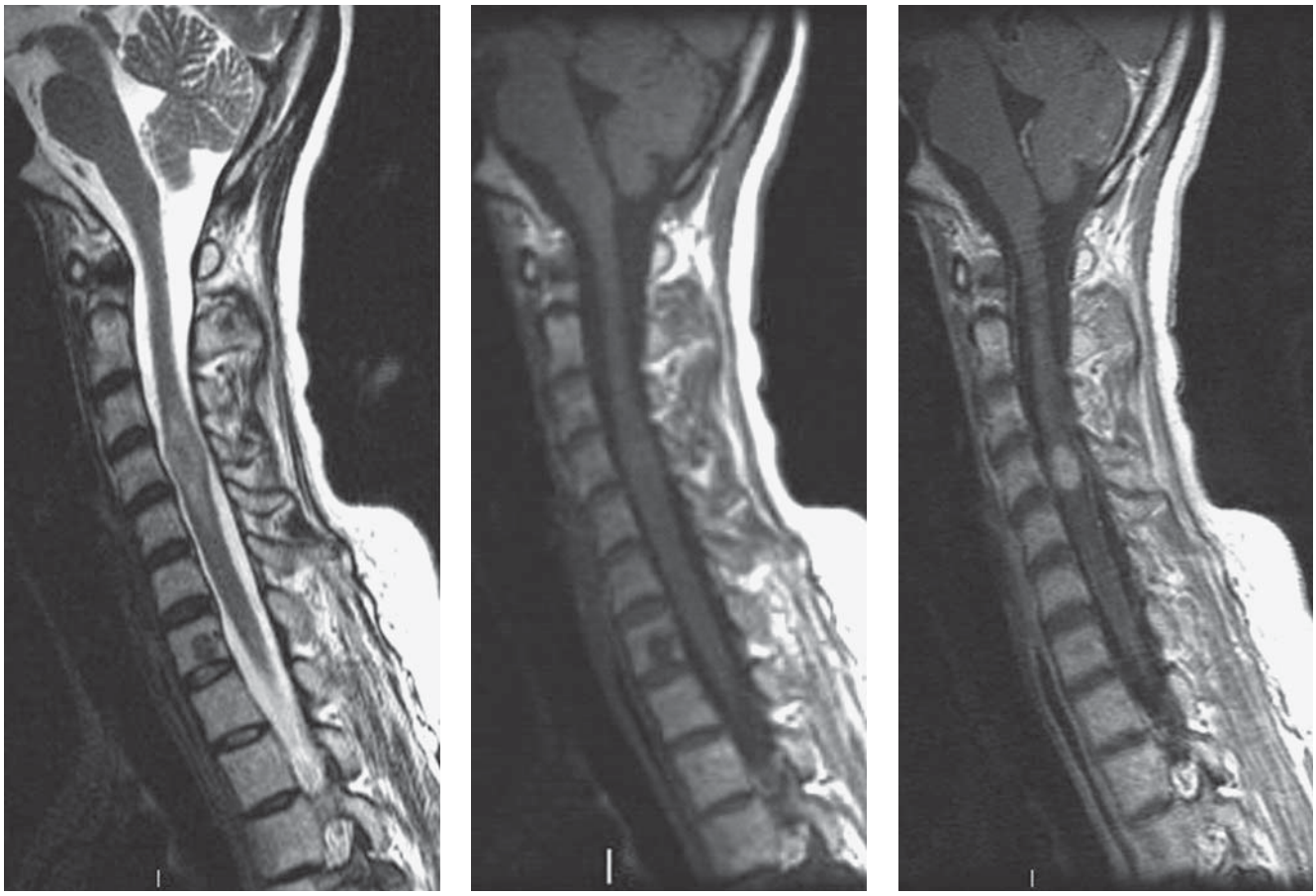
Barkovich AJ, Moore KR, Grant E, et al. Diagnostic Imaging: Pediatric Neuroradiology. Salt Lake City, UT: Amirsys; 2007

Hayashi N, Tsutsumi Y, Barkovich AJ. Morphological features and associated anomalies of schizencephaly in the clinical population: detailed analysis of MR images. Neuroradiology 2002;44:418–427

Osborn A, Blaser S, Salzman KL, et al. Diagnostic Imaging: Brain. Salt Lake City, UT: Amirsys; 2004

Case 137

Paul M. Sherman



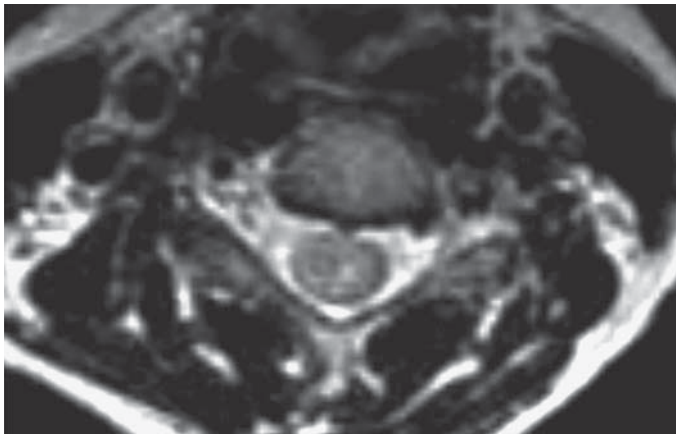


Fig. 137.1 **(A)** Sagittal T2, **(B)** T1 pregadolinium, and **(C)** T1 postgadolinium images demonstrate an ill-defined hyperintense T2 and isointense T1 expansile intramedullary mass within the cervical cord with a homogeneously enhancing nodular component. **(D)** Axial T2-weighted image confirms that the mass is intramedullary. Additional findings are an enhancing lesion within the C7 vertebral body and subtle leptomeningeal enhancement along the surface of the cord.

Clinical Presentation

An adult woman presents with neck pain and paresthesias (**Fig. 137.1**).

Key Imaging Finding

Enhancing intramedullary spinal mass

Top 3 Differential Diagnoses

- **Ependymoma.** Ependymoma is the most common spinal cord tumor and typically presents in the 4th and 5th decades of life (although they may occur at any age). The myxopapillary variant occurs in the conus medullaris, filum terminale, or cauda equina. It is a circumscribed ovoid or lobular mass, which commonly spans two to four vertebral segments. Mucin may cause T1-weighted hyperintensity. The lesion intensely enhances. The cellular variant originates from the ependymal lining of the central canal and most commonly occurs within the cervical followed by the thoracic spine. It is a circumscribed, central lesion with symmetric cord expansion, but it may have an exophytic component. It usually spans three or four vertebral segments. Intratumoral cysts are present in 50 to 90% of cases. Cord edema and syrinx are typically seen. Enhancement may be intense and homogeneous or nodular and heterogeneous. Both subtypes may cause widening of the interpediculate distance and scalloping of the vertebral bodies. The cellular variant may cause scoliosis, and the myxopapillary variant may extend through neural foramina. Hemorrhage is seen more commonly than with astrocytoma.
- **Astrocytoma.** Astrocytomas are the most common intramedullary spinal cord tumor in children and young adults. They are most common in the cervical followed by the thoracic spine but may also be holocord. Common presentation includes an infiltrating, expansile mass spanning up to four vertebral segments. Fusiform expansion of the cord is typical, with occasional asymmetric expansion or exophytic component. Syrinx and a cystic component are occasionally seen. The solid component is T1 hypo- or isointense and T2 hyperintense with heterogeneous enhancement. Astrocytomas are typically low grade, with an 80% 5-year survival.
- **Hemangioblastoma.** Hemangioblastomas are low-grade neoplasms of the cord and cerebellum. In the cord, 75% are sporadic, and 25% are associated with von Hippel–Lindau (VHL) syndrome. They are subpial and most often dorsal in location. Multiple lesions are common in VHL. Hemangioblastomas are typically isointense on T1 and hyperintense on T2 sequences with surrounding cord edema. Signal may be heterogeneous with hemorrhage. Smaller lesions homogeneously and larger lesions heterogeneously enhance. Flow voids may also be seen. The brain and entire spine must be imaged if VHL is suspected.

Additional Differential Diagnoses

- **Metastatic disease.** Intramedullary metastases are relatively uncommon. The most common primary neoplasms are lung carcinoma (especially small cell), breast carcinoma, melanoma, lymphoma, and renal cell carcinoma. There is typically a nidus of enhancement and extensive edema. Pial metastatic lesions can mimic hemangioblastomas.
- **Demyelinating disease.** Demyelinating disease (multiple sclerosis or acute disseminating encephalomyelitis) usually involves the posterolateral cervical cord but does not respect the gray-white boundary. The lesions are flame-shaped and T2 hyperintense with little cord swelling or edema. Enhancement may be seen during active demyelination. Concomitant brain lesions are usually present, although isolated cord disease is seen in 10 to 20% of cases. Lesions typically span fewer than two vertebral segments and involve less than half the cross-sectional area of the cord.

Diagnosis

Metastatic disease (breast cancer)

✓ Pearls

- Ependymomas are the most common spinal tumor and may be of the myxopapillary or cellular variants.
- Astrocytomas are the most common spinal tumors in children and present as infiltrating, expansile masses.
- Hemangiomas are highly vascular lesions that may be sporadic or associated with VHL syndrome.

Suggested Readings

Ross JS, Brant-Zawadzki M, Moore KR. Diagnostic Imaging: Spine. Salt Lake City, UT: Amirsys; 2005

Case 138

Paul M. Sherman

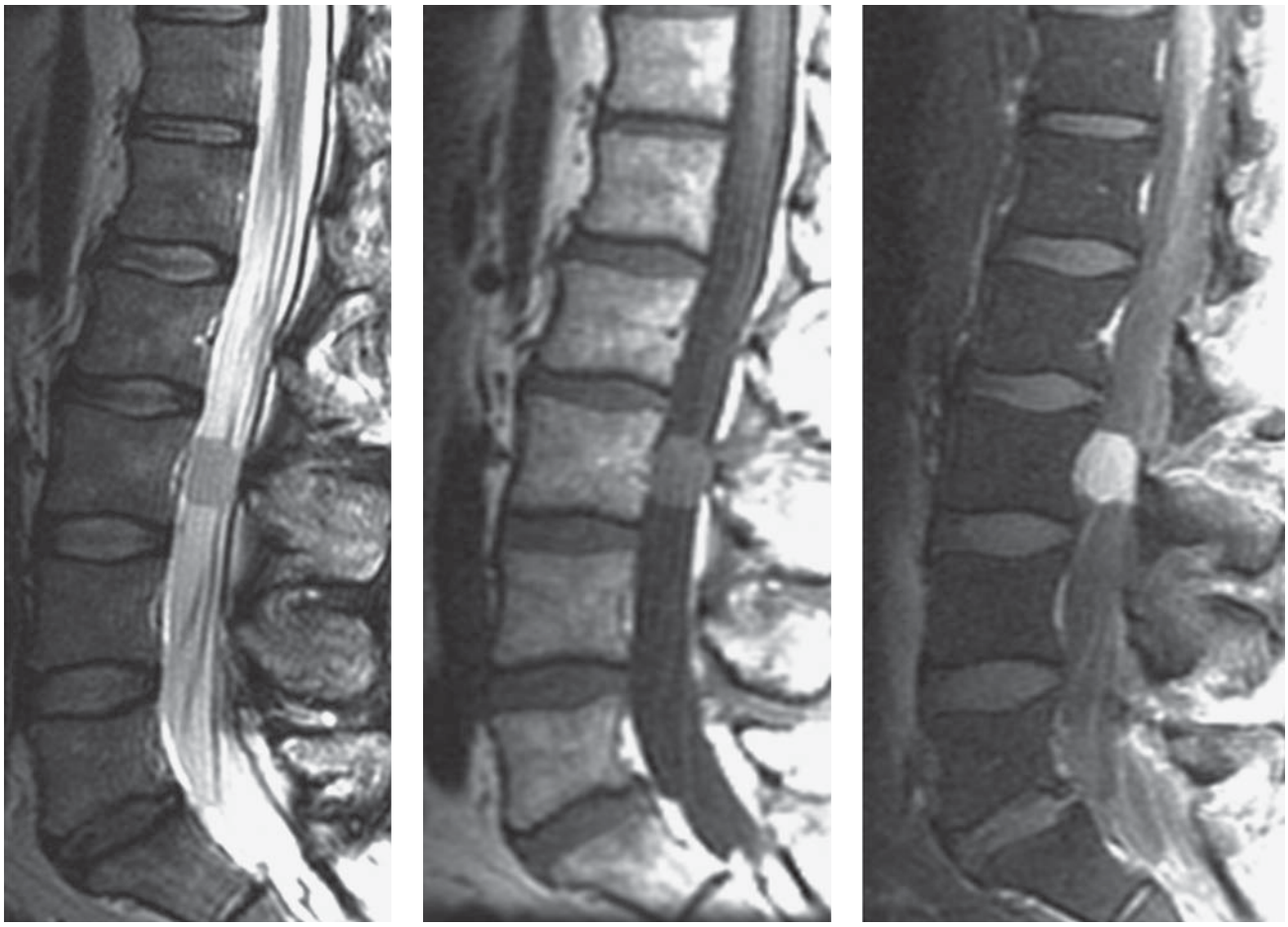


Fig. 138.1 **(A)** Sagittal T2 and **(B)** T1 images through the lumbar spine demonstrate a T2 hyperintense and T1 isointense intradural extramedullary mass at the level of the L3 vertebral body. **(C)** Sagittal T1 postcontrast image with fat suppression reveals intense homogeneous enhancement.

Clinical Presentation

A patient presents with radiculopathy (**Fig. 138.1**).

Key Imaging Finding

Intradural extramedullary spinal mass

Top 3 Differential Diagnoses

- **Nerve sheath tumor.** Schwannomas are the most common intradural extramedullary mass (75% present in this fashion). The remainder present as both intra- and extradural (classic dumbbell lesion) or isolated extradural lesions. They most commonly occur in the thoracic spine and may widen the interpediculate distance, enlarge the intervertebral foramen, and cause posterior vertebral scalloping. Cystic change and hemorrhage may be seen; calcification is rare. Schwannomas are well circumscribed and intensely enhance. Approximately 75% are hyperintense on T2, with an occasional "target" sign (high signal mass peripherally and central low signal); the target sign is more common with neurofibroma. Schwannomas are typically iso- or hypointense on T1-weighted sequences. Most cases are sporadic, but they may be associated with neurofibromatosis type 2 (NF2). The tumors are most often solitary unless part of an inherited syndrome. Malignant degeneration is rare. Neurofibromas may be indistinguishable in imaging appearance from schwannomas, especially when solitary (90% are sporadic and solitary). Unlike schwannomas, neurofibromas most often occur in the cervical spine. Up to 65% of patients with type 1 neurofibromatosis (NF1) will have spinal neurofibromas. Plexiform neurofibromas are a specific subtype that demonstrates T2-weighted hypointense septations. Five percent of plexiform neurofibromas will undergo malignant degeneration (rapid growth is suggestive). Additional spinal stigmata of NF1 are thoracic scoliosis/kyphosis, vertebral anomalies, meningocele, and dural ectasia.
- **Meningioma.** Meningiomas are the second most common intradural extramedullary mass and are more common in women (4:1) and patients with NF2 (chromosome 22q). The vast majority (90%) are intradural; the remainder present as both intra- and extradural (dumbbell lesion), extradural, or, rarely, paraspinous or intraosseous. They are most common in the thoracic spine (80%), followed by the cervical and lumbar spine. They are typically round with a broad dural base. Meningiomas are isointense to the cord on T1- and iso- to hyperintense on T2-weighted images. Up to 5% are calcified, which may be hypointense on T2-weighted images. Flow voids may also be present. The lesions intensely enhance; the presence of a dural tail is less common than in intracranial meningiomas.
- **Cerebrospinal fluid (CSF) metastases.** CSF metastases may present in one of several patterns, including a solitary mass on the cord surface or at the inferior portion of the thecal sac, multiple nodular enhancing masses along cord/nerve roots, "sugarcoating" of the cord/nerve roots, or thickening of the cauda equina. Rarely, metastases may present as an intramedullary mass. Focal metastases are usually isointense to the cord on T1- and T2-weighted images and intensely enhance. There is sheetlike leptomeningeal enhancement along the cord and nerve roots with a "sugarcoating" pattern. Fat-saturated T1 postcontrast sequences are the most sensitive. Extensive disease may fill the thecal sac, resulting in slightly increased precontrast T1-weighted signal of the CSF (dirty or ground-glass appearance of the CSF). It is critical to image the entire neuroaxis to determine the extent of disease. Short tau inversion recovery sequences are the most sensitive for bone metastases. Hematogenous dissemination is most often from lung and breast carcinoma, as well as lymphoma. Drop metastases are most common with anaplastic astrocytoma, glioblastoma multiforme, medulloblastoma, ependymoma, choroid plexus tumor, and germinoma. Patients may present with pain and radiculopathy.

Diagnosis

Drop metastasis (astrocytoma)

✓ Pearls

- Nerve sheath tumor (specifically schwannoma) is the most common intradural extramedullary mass.
- Meningiomas are more common in women and patients with NF2; they intensely enhance.
- CSF metastases result from hematogenous spread or drop metastases; the entire neuroaxis should be evaluated.

Suggested Readings

De Verdelhan O, Haeglen C, Carsin-Nicol B, et al. MR imaging of spinal schwannomas and meningiomas. J Neuroradiol 2005;32:42–49

Ross JS, Brant-Zawadzki M, Moore KR. Diagnostic Imaging: Spine. Salt Lake City, UT: Amirsys; 2005

Case 139

Paul M. Sherman

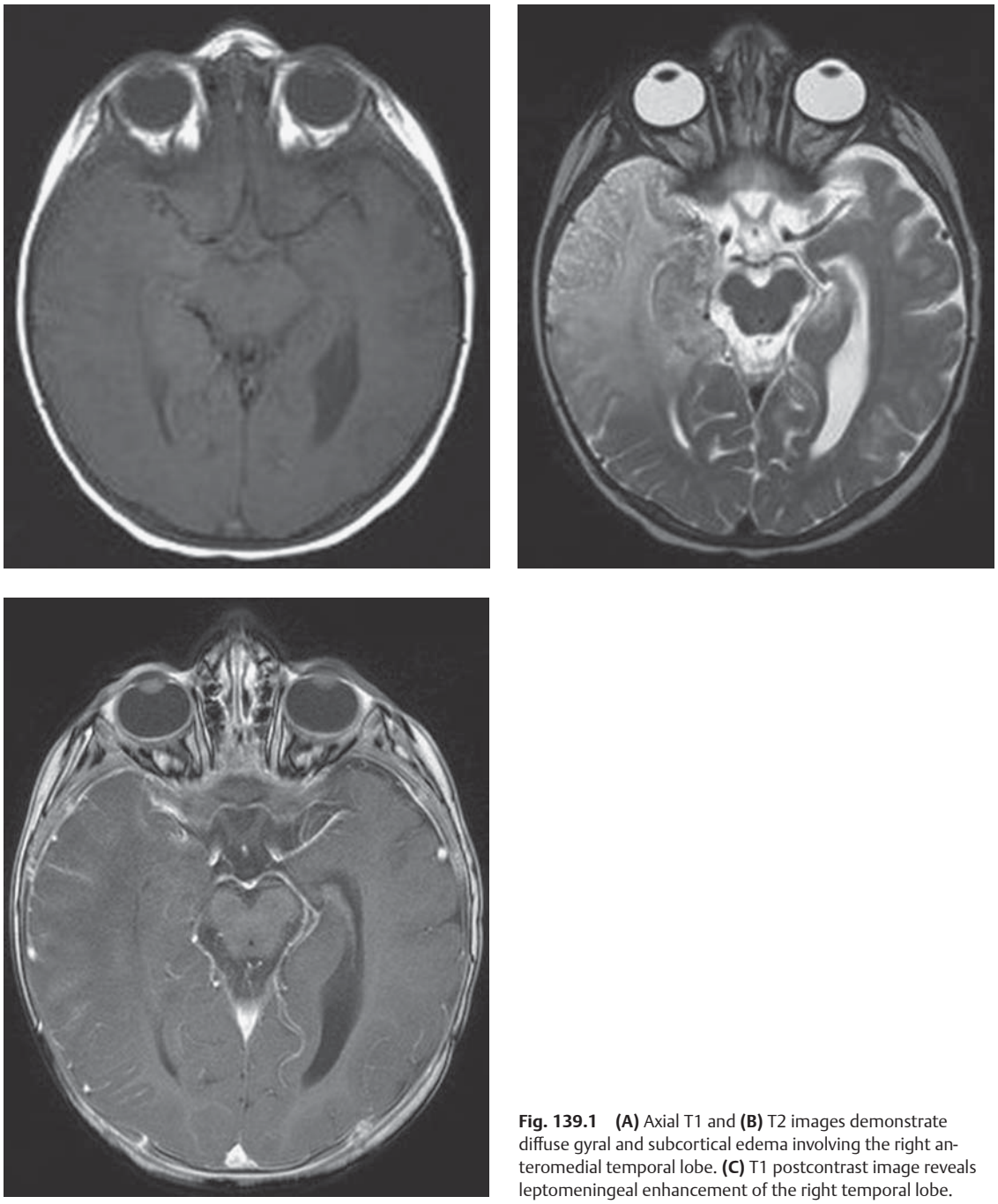


Fig. 139.1 **(A)** Axial T1 and **(B)** T2 images demonstrate diffuse gyral and subcortical edema involving the right anteromedial temporal lobe. **(C)** T1 postcontrast image reveals leptomeningeal enhancement of the right temporal lobe.

Clinical Presentation

A young adult patient presents with fever, headache, and seizures (**Fig. 139.1**).

Key Imaging Finding

Diffuse temporal lobe mass

Top 3 Differential Diagnoses

- **Herpes encephalitis.** Brain parenchymal infection secondary to herpes simplex virus (HSV 1 in adults and children and HSV 2 in neonates) characteristically involves the limbic system (temporal lobes, insula, subfrontal area, and cingulate gyri). Bilateral, asymmetric involvement is common, and the basal ganglia are spared. There is cortical and subcortical edema with loss of the gray-white junction and local mass effect. T2 hyperintense subacute hemorrhage and restricted diffusion may also be seen. Mild, patchy enhancement is commonly seen acutely, developing into gyriform enhancement usually within 1 week. Magnetic resonance imaging (MRI) findings may be seen within 2 days of onset of symptoms (fever, headache, and seizures). Mortality is 50 to 70%. Adult patients commonly present with fever, headache, and focal and nonlocalizing neurologic deficits.
- **Ischemia/infarction.** Cerebrovascular disease is the second most common cause of death worldwide. Etiologies include thromboembolic occlusion, dissection, vasculitis, and hypoperfusion. Patients present with focal neurologic deficits, altered mental status, and/or aphasia. Computed tomography (CT) and MRI demonstrate cytotoxic edema with local mass effect and effacement of sulci in a vascular territory distribution. Noncontrast CT may also show a characteristic "dense middle cerebral artery" sign and loss of the lentiform nucleus. Both CT and MR angiography may demonstrate the site of vascular occlusion. Acute and subacute infarcts show restricted diffusion. Gyral or patchy enhancement may be seen as early as 2 days after the infarct and peaks at approximately 2 weeks. CT/MRI perfusion evaluates the ischemic penumbra or potentially viable parenchyma. Hemorrhagic transformation occurs in 15 to 20% of cases.
- **Gliomatosis cerebri.** Gliomatosis cerebri is a World Health Organization grade III infiltrating astrocytoma that demonstrates T1 hypointensity, T2/fluid-attenuated inversion recovery (FLAIR) hyerintensity, mass effect, and occasionally minimal patchy enhancement. The neoplastic process typically involves two or more lobes and is frequently bilateral. The lesion may cross the corpus callosum or massa intermedia and may also involve the deep gray matter, cerebellum, brainstem, and spinal cord.

Additional Differential Diagnoses

- **Limbic encephalitis.** Limbic encephalitis is a paraneoplastic syndrome associated with a primary malignancy (typically lung or breast). Imaging findings may be indistinguishable from herpes encephalitis (predilection for limbic system and often bilateral), although hemorrhage does not occur. Onset of symptoms is usually more insidious (weeks to months). Treatment of the primary malignancy may result in stabilization or improvement of symptoms.
- **Status epilepticus.** Seizures result in disruption of the blood–brain barrier with hyperperfusion, which results in signal abnormalities and abnormal enhancement. MRI findings include hippocampal atrophy, as well as signal alteration (T1 hypointensity and T2/FLAIR hyperintensity) in the medial temporal lobe.

Diagnosis

Herpes encephalitis

✓ Pearls

- Herpes encephalitis is a life-threatening infection with abnormal signal in the limbic system.
- Ischemia results in cortical edema, sulcal effacement, and restricted diffusion in a vascular distribution.
- Gliomatosis cerebri is an infiltrating neoplasm involving two or more lobes.
- Limbic encephalitis is a paraneoplastic syndrome that mimics herpes encephalitis on imaging.

Suggested Readings

Fischbein NJ, Dillon WP, Barkovich AJ. Teaching Atlas of Brain Imaging. New York: Thieme; 1999

Osborn A, Blaser S, Salzman KL, et al. Diagnostic Imaging: Brain. Salt Lake City, UT: Amirsys; 2004

Case 140

Paul M. Sherman

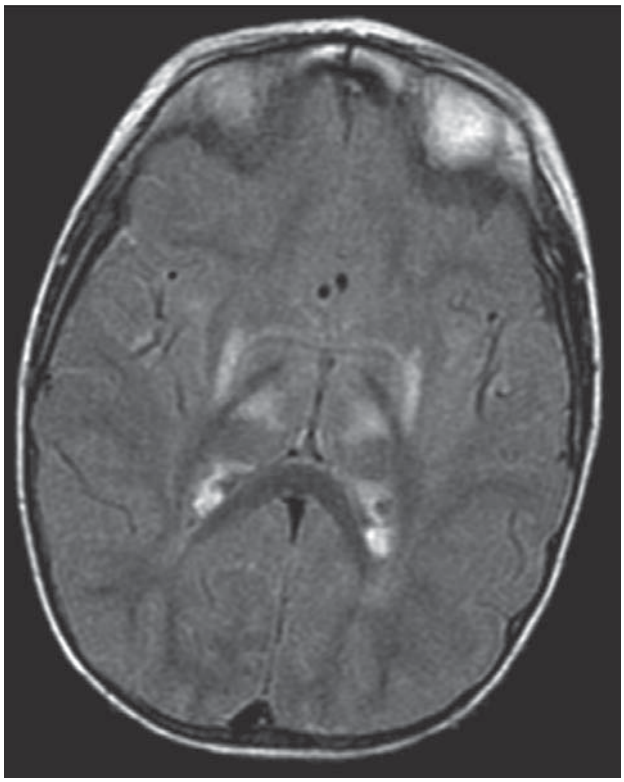


Fig. 140.1 Axial fluid-attenuated inversion recovery image demonstrates symmetric hyperintense signal in the posterior putamina and lateral thalami, representing atrophy and gliosis.

Clinical Presentation

The patient is an 8-year-old child; the history is otherwise withheld (**Fig. 140.1**).

Key Imaging Finding

Increased T2 signal intensity in basal ganglia/thalami in a child

Top 3 Differential Diagnoses

- **Ischemia.** Children (neonates in particular) are susceptible to hypoxic-ischemic encephalopathy secondary to profound hypoperfusion. Ischemic changes are most pronounced within the deep gray matter (basal ganglia and thalami), which is extremely vulnerable to hypoxia. The posterior putamina and ventrolateral thalamus are most commonly involved. There is loss of the gray-white junction, particularly at watershed areas. Affected areas demonstrate T2/fluid-attenuated inversion recovery (FLAIR) hyperintensity and restricted diffusion. Etiologies include trauma (must exclude nonaccidental), dehydration, and anoxic events.
- **Carbon monoxide poisoning.** Anoxic-ischemic encephalopathy due to inhalation of carbon monoxide results in symmetric hypodensity of the globus pallidi on computed tomography (CT). There is associated bilateral T2 hyperintensity (T1 hypointensity) of globus pallidi, often with a hypointense hemosiderin rim due to ischemia/infarct. The caudate and putamen may also be affected. Confluent periventricular white matter, centrum semiovale hyperintensity reflects diffuse demyelination. Restricted diffusion may be seen acutely.
- **Wilson disease.** Wilson disease (hepatolenticular degeneration) is an autosomal recessive disorder characterized by excessive copper accumulation in the brain (particularly the basal ganglia) and liver, resulting in chronic ischemia. There is increased T2/FLAIR signal in the lentiform nuclei, midbrain, thalami, and white matter tracts. The characteristic "face of the giant panda" sign on axial T2 images through the midbrain is due to hyperintense tegmentum and hypointense superior colliculi. Associated abnormalities include neuropsychiatric illnesses, Kayser–Fleischer corneal rings, and cirrhosis.

Additional Differential Diagnoses

- **Mitochondrial disorder.** Mitochondrial disorders result from damage to energy-producing mitochondria. MELAS (mitochondrial myopathy, encephalopathy, lactic acidosis, and strokelike episodes) is an uncommon but important cause of stroke in children that results from accumulation of pyruvate and lactate. There are ischemic findings in nonvascular distributions. Chronic atrophy of the basal ganglia and cortex occurs with T2 hyperintensity in the basal ganglia and deep white matter. Leigh syndrome (subacute necrotizing encephalomyelopathy) results in progressive impairment of cognitive and motor function typically by age 2. Findings include bilateral symmetric basal ganglia T2/FLAIR hyperintensities.
- **Kernicterus.** Kernicterus refers to encephalopathy due to deposition of unconjugated bilirubin. Acutely (within first 2–5 days of life), there is T1 hyperintensity in the bilateral globus pallidi, hippocampi, and substantia nigra with subtle T2 hyperintensity. Chronically, there is T2 hyperintensity in the posteromedial globus pallidi and the dentate nuclei with normal T1-weighted signal.
- **Osmotic demyelination.** Osmotic demyelination is classically due to rapid correction of hyponatremia. Fifty percent of cases involve the central pons, and 50% are extrapontine with involvement of the basal ganglia and cerebral white matter. Findings are typically bilateral and symmetric. Lesions are hypodense on CT, mildly T1 hypointense, and T2/FLAIR hyperintense.

Diagnosis

Hypoxic-ischemic insult (near-drowning episode)

✓ Pearls

- Deep gray matter is vulnerable to hypoxic-ischemic encephalopathy, particularly in at-risk neonates.
- Carbon monoxide poisoning results in characteristic symmetric increased T2/FLAIR signal in the globus pallidi.
- Deposition disorders (Wilson and kernicterus) involve the deep gray matter, particularly the basal ganglia.

Suggested Readings

Osborn A, Blaser S, Salzman KL, et al. Diagnostic Imaging: Brain. Salt Lake City, UT: Amirsys; 2004

Case 141

Paul M. Sherman

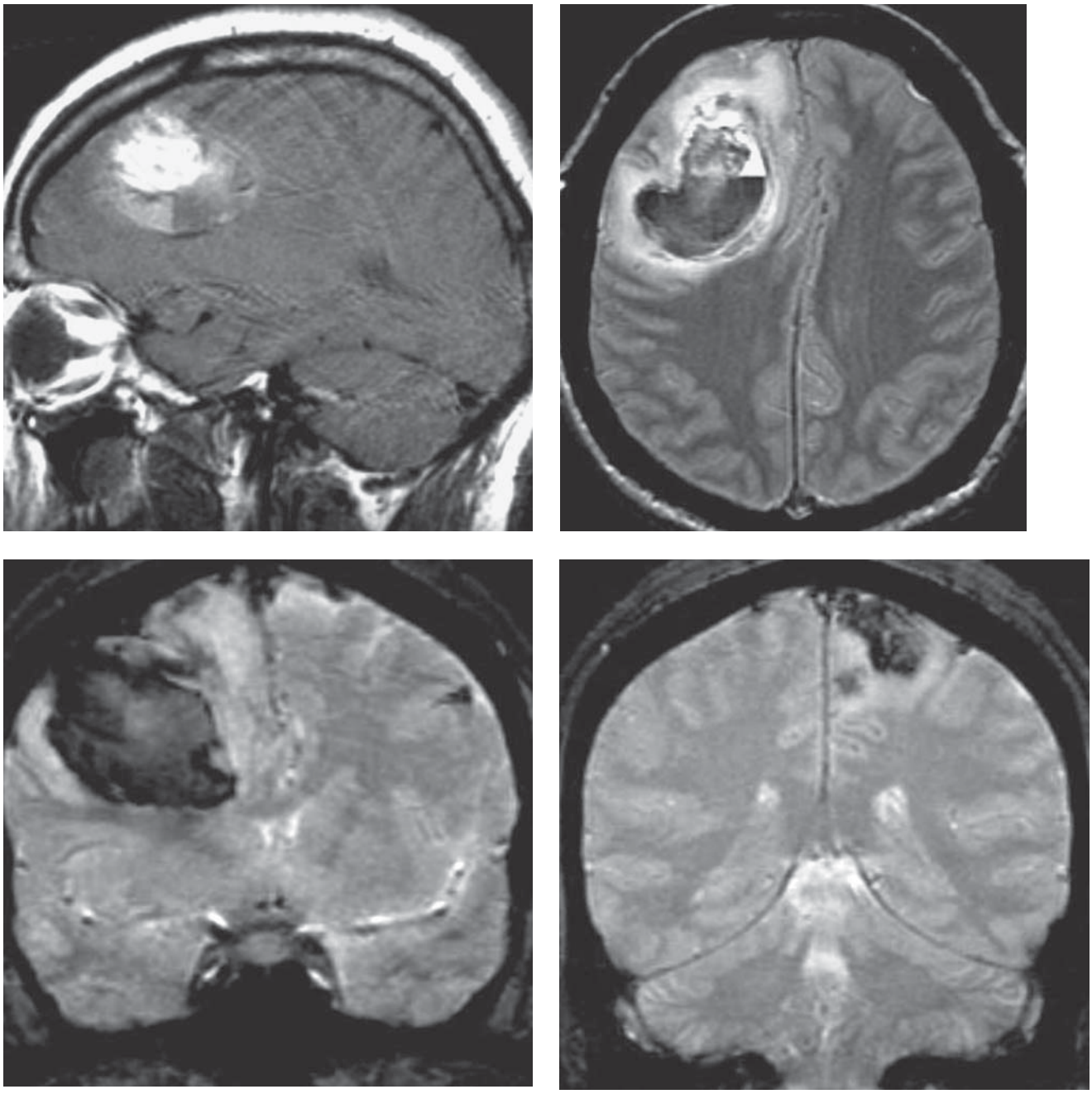


Fig. 141.1 **(A)** Sagittal T1 and **(B)** axial T2 images demonstrate a right frontal parenchymal hematoma with blood–blood levels (blood products of different ages) and surrounding edema (T2 hyperintensity). **(C,D)** Coronal T2* gradient echo images demonstrate blooming artifact in both frontal lobes, as well as in the superior sagittal sinus, consistent with hemorrhage. Magnetic resonance venography (not shown) revealed the absence of normal flow void within the superior sagittal sinus.

Clinical Presentation

A 46-year-old woman presents with a headache (**Fig. 141.1**).

Key Imaging Finding

Intraparenchymal hemorrhage

Top 3 Differential Diagnoses

- **Vascular malformation.** Arteriovenous malformations are abnormal networks of arteries and veins with no intervening capillary bed. The vast majority (>80%) are solitary and supratentorial. Unenhanced computed tomography (CT) may demonstrate iso- to hyperdense serpentine vessels and calcification. Magnetic resonance imaging (MRI) reveals flow voids in a "honeycomb" or "bag of worms" pattern with strong contrast enhancement. Associated aneurysms (arterial supply and intranidal) are common. They are classified based on size, location (eloquent or noneloquent brain), and venous drainage (superficial or deep). Cavernomas are benign masses of immature blood vessels with intralesional hemorrhages and a complete hemosiderin (T2 hypointense) rim. A "popcorn ball" appearance is secondary to mixed hyper- and hypointense blood products on T1- and T2-weighted imaging. The lesions "bloom" on T2* gradient echo and show little or no enhancement.
- **Hemorrhagic infarct.** Hypertensive infarcts most commonly occur in the basal ganglia/external capsule, thalamus, and posterior fossa. Hemorrhages are typically round or elliptical and may extend into the ventricles. They occur in older patients outside of drug abuse (cocaine). They typically do not enhance. Diffusion-weighted imaging results may be mixed with acute blood products. Hemorrhagic transformation of an arterial infarct usually occurs in the subacute phase when gyral enhancement is seen or after administration of thrombolytics. Characteristic vascular distribution and diffusion restriction are seen. T2* gradient echo is sensitive for hemosiderin. Hemorrhagic venous infarcts are secondary to dural venous sinus or cortical vein thrombosis. Hyperdense clot may be seen on unenhanced CT ("cord" sign for cortical veins), and the "empty delta" sign may be seen on contrast exam. CT and MR venography demonstrate venous thrombosis.
- **Hemorrhagic neoplasm.** Glioblastoma multiforme is the most common primary brain neoplasm in adults and may demonstrate intratumoral hemorrhage and arteriovenous shunting. Vasogenic edema, tumoral enhancement, and central necrosis help distinguish it. Hemorrhagic metastases (lung, renal cell, and thyroid carcinoma and melanoma) typically occur at the gray-white matter junction and often in the deep brain parenchyma.

Additional Differential Diagnoses

- **Contusion.** Contusions present as patchy, superficial hemorrhages with surrounding edema in characteristic locations where brain is adjacent to bone (temporal, inferior frontal, and parasagittal regions). Calvarial fractures and extra-axial hemorrhage are associated findings. Fluid-attenuated inversion recovery demonstrates hyperintense cortical edema and subarachnoid blood. T2* gradient echo blooming is sensitive for hemorrhage.
- **Cerebral amyloid disease.** Amyloid angiopathy presents as spontaneous, large parenchymal hemorrhages in elderly patients with white matter disease (70%), often with dementia. Hemorrhages are subcortical and most commonly involve the parietal and occipital lobes; frontal and temporal lobes are involved less frequently. Approximately one third of patients with acute bleeding will have old hemorrhages, either lobar or petechial. T2* gradient echo is the best sequence to detect chronic microbleeds.

Diagnosis

Hemorrhagic infarct (venous infarct secondary to sagittal sinus thrombosis)

✓ Pearls

- Arteriovenous malformations are most commonly solitary and supratentorial, have flow voids, and avidly enhance.
- Hemorrhagic infarcts include hypertensive hemorrhages, hemorrhagic conversion, and venous infarcts.
- Glioblastoma multiforme and hypervascular metastases may present as a hemorrhagic intraparenchymal mass.
- Contusions occur where brain abuts the calvarium—temporal, inferior frontal, and parasagittal regions.

Suggested Readings

Fischbein NJ, Dillon WP, Barkovich AJ. Teaching Atlas of Brain Imaging. New York: Thieme; 1999

Osborn A, Blaser S, Salzman KL, et al. Diagnostic Imaging: Brain. Salt Lake City, UT: Amirsys; 2004

Case 142

Paul M. Sherman

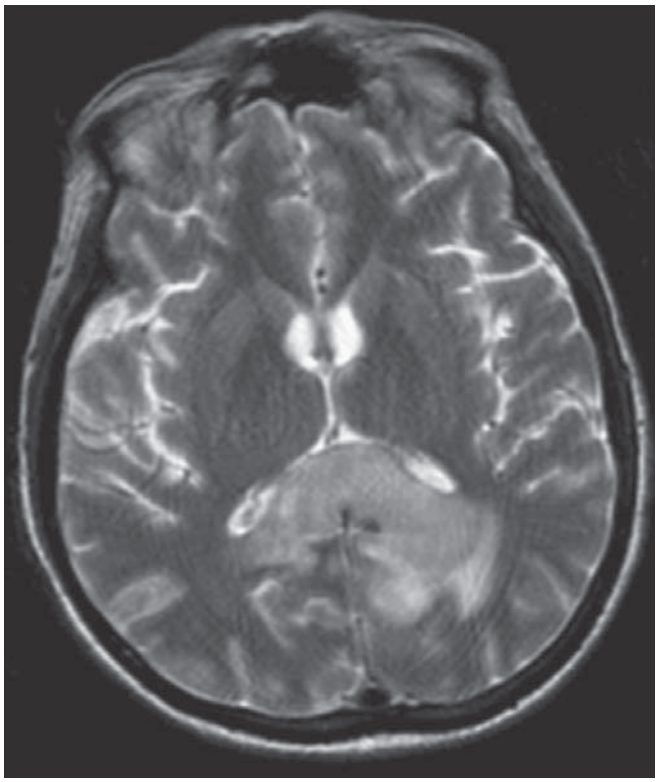


Fig. 142.1 Axial T2-weighted image through the brain demonstrates a large hyperintense lesion involving and expanding the splenium of the corpus callosum.

Clinical Presentation

A 53-year-old man presents with altered mental status (**Fig. 142.1**).

Key Imaging Finding

Corpus callosal lesion

Top 3 Differential Diagnoses

- **Glioblastoma multiforme (GBM).** GBM is a World Health Organization grade IV astrocytoma and is the most common primary intracranial neoplasm in adults. It crosses white matter tracts (corpus callosum) to involve the contralateral hemisphere; hence the term *butterfly glioma* of the corpus callosum. It is a rapidly enlarging tumor with central necrosis and neovascularity (flow voids). There is marked mass effect; a thick, irregular rind of enhancement; and adjacent T2/fluid-attenuated inversion recovery (FLAIR) hyperintensity representing edema and tumor invasion. Viable tumor extends beyond the abnormal signal intensity. The tumor itself is heterogeneous but primarily T2 hyperintense and T1 iso- to hypointense with associated cysts, hemorrhage, and fluid–debris. There may be foci of diffusion-weighted imaging restriction. GBM may occur at any age but peaks at 45 to 70 years.
- **Lymphoma.** Primary central nervous system (CNS) lymphoma is a relatively uncommon primary brain tumor that is almost exclusively of the non-Hodgkin variant. It typically occurs within the periventricular white matter and basal ganglia and commonly involves the corpus callosum and ependymal surfaces of the ventricles. Leptomeningeal and dural involvement occurs more often with secondary lymphoma. Lymphoma may present as a solitary mass or multiple lesions and can be circumscribed or infiltrative. The lesions are characteristically hyperdense on computed tomography (CT) and iso- to hypointense on both T1- and T2-weighted sequences due to increased nuclear-to-cytoplasmic ratio. Hemorrhage and necrosis are uncommon. There is only mild surrounding edema. Restricted diffusion may be seen. Enhancement is intense and homogeneous in immunocompetent patients and may be peripheral or ring enhancing in immunocompromised patients. Unlike toxoplasmosis, lymphoma is hypermetabolic on thallium single-photon emission computed tomography and positron emission tomography imaging.
- **Demyelinating disease.** Multiple sclerosis (MS) is the most common primary demyelinating disease and typically presents between 20 and 40 years of age. Characteristic imaging features are ovoid hyperintense T2/FLAIR white matter lesions in a periventricular location oriented perpendicular to the ventricles (Dawson fingers). High specificity locations include the corpus callosum, brainstem/brachium pontis, and temporal lobes. Transient enhancement of the lesions is seen during periods of active demyelination. Enhancement may be nodular, ring, or horseshoe-shaped, with the open area facing the cortex. Tumefactive MS (large masslike enhancing lesions) is rare but may mimic neoplasm.

Additional Differential Diagnoses

- **Diffuse axonal injury (DAI).** DAI results from shear injury and presents as multifocal punctate hemorrhages involving the gray-white matter junction (frontotemporal), corpus callosum, deep gray matter, and dorsolateral brainstem. T2* gradient echo is a sensitive sequence due to susceptibility artifact from blood products. Associated traumatic brain injury (contusions and extra-axial hemorrhage) is commonly seen.
- **Marchiafava–Bignami disease.** Chronic alcoholism (classically Italian red wine) and poor nutrition result in lesions involving predominantly the splenium of the corpus callosum. Findings of Wernicke encephalopathy (mammillary body and periaqueductal gray matter lesions) are typically absent.

Diagnosis

CNS lymphoma

✓ Pearls

- GBM is the most common primary brain neoplasm and commonly crosses the corpus callosum.
- Lymphoma is hyperdense on CT and low in signal intensity on magnetic resonance imaging.
- Characteristic MS lesions are Dawson fingers and involvement of the corpus callosum or brainstem.
- DAI is due to shear injury and may involve the corpus callosum; gradient echo imaging is most sensitive.

Suggested Readings

Osborn A, Blaser S, Salzman KL, et al. Diagnostic Imaging: Brain. Salt Lake City, UT: Amirsys; 2004

Case 143

Paul M. Sherman

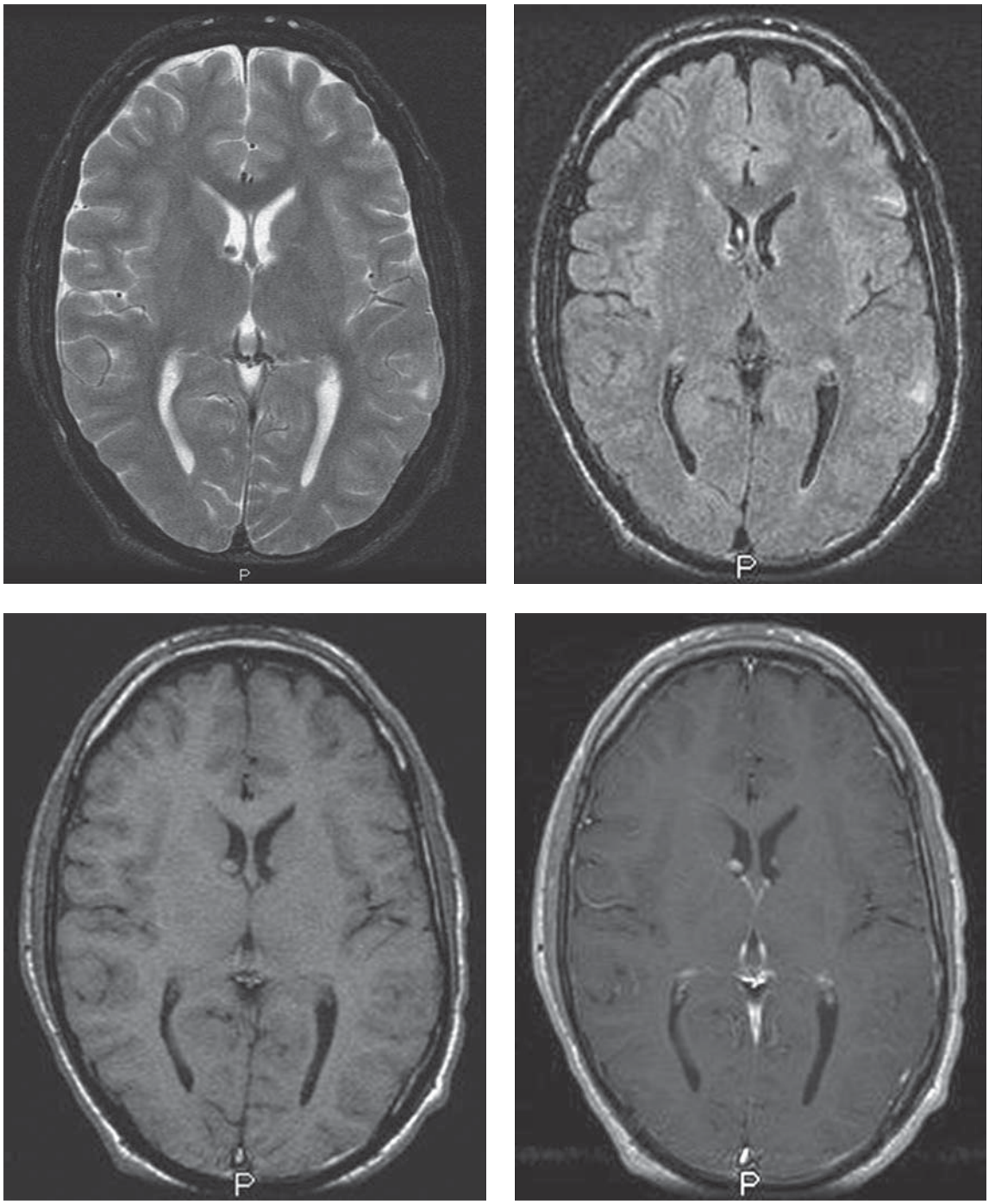


Fig. 143.1 **(A)** Axial T2 and **(B)** fluid-attenuated inversion recovery (FLAIR) images of the brain demonstrate a hypointense subependymal nodular lesion within the frontal horn of the right lateral ventricle. **(C)** The lesion is isointense to white matter on T1 sequences and **(D)** demonstrates homogeneous enhancement. Cortical tubers are also noted on T2/FLAIR sequences (left hemisphere).

Clinical Presentation

A patient presents with seizures (**Fig. 143.1**).

Key Imaging Finding

Subependymal nodules

Top 3 Differential Diagnoses

- **Tuberous sclerosis (TS).** Also known as Bourneville–Pringle syndrome, TS may occur sporadically or in an autosomal dominant fashion with variable penetrance. The classic clinical triad consists of facial angiofibromas, mental retardation, and seizures but is only seen in ~30% of cases. Central nervous system (CNS) manifestations include subependymal nodules (98% of cases), cortical tubers, and retinal hamartomas. Nearly all subependymal nodules calcify by age 20, and many demonstrate enhancement. Nodules have variable T1 and T2 signals but demonstrate T2* gradient echo susceptibility when calcified. Subependymal giant cell astrocytomas (World Health Organization grade I) are seen in ~15% of cases. They are located at the foramen of Monro, enlarge over time, and enhance homogeneously. Cortical tubers and white matter lesions occur in 70 to 95% of cases. Prior to myelination, tubers are T1 hyperintense. Tubers have variable T1 signal and are typically T2 hyperintense after myelination. Approximately 10% of tubers enhance. White matter lesions are linear or wedge-shaped T2/fluid-attenuated inversion recovery (FLAIR) hyperintensities along the radial migration lines from the ventricle to the cortex. Common associated abnormalities are cardiac rhabdomyomas, renal cysts and angiomyolipomas, pulmonary lymphangiomyomatosis, ash leaf spots and shagreen patches on the skin, subungual fibromas, and drusen.
- **Heterotopic gray matter.** Heterotopic gray matter is caused by arrest or disruption of neuronal migration from the subependymal germinal zones to the overlying cortex. It is commonly due to some form of fetal insult during development. Heterotopia may be nodular or bandlike. Subependymal heterotopic gray matter is isointense to gray matter on all magnetic resonance (MR) sequences, does not calcify, and does not enhance. Typical clinical presentation is developmental delay and seizures. However, mild cases may be asymptomatic.
- **(S)TORCH infection.** The (S)TORCH infections consist of group B streptococcus, toxoplasmosis, rubella, cytomegalovirus (CMV), and herpes simplex virus. CMV is the most likely to result in subependymal and periventricular calcifications, mimicking TS on computed tomography. Toxoplasmosis also causes intracranial calcifications but has less propensity for the periventricular region. Associated findings are microcephaly and neuronal migration abnormalities. Patients commonly suffer from mental retardation, seizures, and hearing loss.

Additional Differential Diagnoses

- **Metastatic disease.** Subependymal metastatic disease may result from primary CNS neoplasms or hematogenous spread from extracranial malignancies. Primary CNS neoplasms that spread along the ependymal surface include glioblastoma multiforme, medulloblastoma, ependymoma, primary CNS lymphoma, pineal neoplasms, and choroid plexus tumors. Extracranial metastases, particularly breast carcinoma, involve the subependymal surfaces and choroid plexus.

Diagnosis

Tuberous sclerosis

✓ Pearls

- TS results in subependymal nodules that calcify and may demonstrate enhancement.
- Heterotopic gray matter is due to an insult in utero and follows gray matter signal on all MR sequences.
- CMV is the most common (S)TORCH infection to cause subependymal/periventricular calcifications.
- Metastases from primary CNS or extracranial malignancies may present as subependymal nodules.

Suggested Readings

Barkovich AJ, Moore KR, Grant E, et al. Diagnostic Imaging: Pediatric Neuroradiology. Salt Lake City, UT: Amirsys; 2007

O'Brien WT, Palka PS, et al. Pediatric neuroimaging. In: Quattromani F, Handal GA, Lampe R, eds. Pediatric Imaging: Rapid-fire Questions and Answers. New York: Thieme; 2007:338–391

Osborn A, Blaser S, Salzman KL, et al. Diagnostic Imaging: Brain. Salt Lake City, UT: Amirsys; 2004

Case 144

Paul M. Sherman

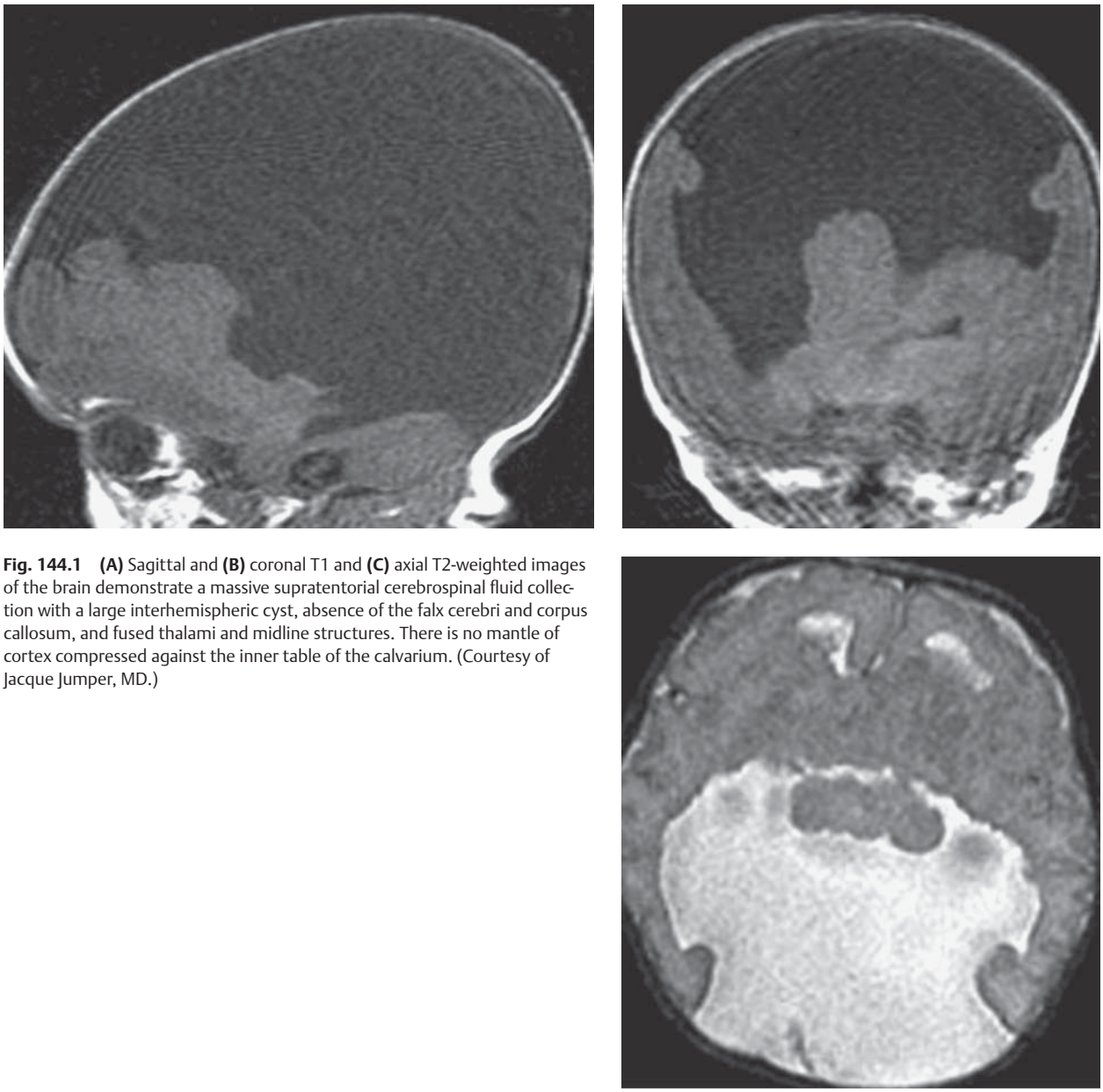


Fig. 144.1 **(A)** Sagittal and **(B)** coronal T1 and **(C)** axial T2-weighted images of the brain demonstrate a massive supratentorial cerebrospinal fluid collection with a large interhemispheric cyst, absence of the falx cerebri and corpus callosum, and fused thalami and midline structures. There is no mantle of cortex compressed against the inner table of the calvarium. (Courtesy of Jacque Jumper, MD.)

Clinical Presentation

A neonate presents with seizures (**Fig. 144.1**).

Key Imaging Finding

Massive supratentorial cerebrospinal fluid (CSF) collection in a newborn

Top 3 Differential Diagnoses

- **Massive hydrocephalus.** Hydrocephalus refers to increased volume of CSF due to obstruction, overproduction, or decreased absorption. In the newborn, this results in macrocephaly due to open sutures. Massive hydrocephalus displaces and compresses peripheral brain parenchyma, mimicking hydranencephaly or holoprosencephaly. Key distinguishing features are a thin mantle of cortex along the inner table of the calvarium and the presence of the falx. Aqueductal stenosis is a common cause; however, obstructing neoplasms (posterior fossa, pineal gland, tectal plate, intraventricular, etc.) should be excluded. T2-weighted sequences best evaluate for transependymal CSF flow, which may resolve in chronic obstruction. Causes of nonobstructive communicating hydrocephalus include meningitis/ventriculitis, prior subarachnoid hemorrhage, and idiopathic.
- **Hydranencephaly.** Hydranencephaly refers to liquefactive necrosis of the supratentorial brain parenchyma in the anterior circulation secondary to compromise of the supraclinoid internal carotid arteries (ICAs) between 20 and 27 weeks' gestation. There is sparing of the posterior circulation. Key findings include the presence of the falx cerebri and intact posterior fossa structures, as well as the absence of a cortical mantle around a large supratentorial CSF-filled cavity. Neonates commonly present with macrocranium and neurologic function limited to the brainstem; death typically occurs in infancy.
- **Alobar holoprosencephaly.** Holoprosencephaly is a spectrum of congenital forebrain malformations characterized as alobar, semilobar, and lobar variants. In the alobar form (most severe), there is a large dorsal interhemispheric cyst (monoventricle), and the remaining cerebral parenchyma is flattened anteriorly and fused. The thalami are also fused. The corpus callosum, anterior falx, interhemispheric fissure, and sylvian fissures are absent. Associated craniofacial abnormalities are hypotelorism, fused metopic suture, and cleft palate. Semilobar and lobar variants are less severe forms with varying degrees of defective separation of the anterior and central brain structures.

Additional Differential Diagnoses

- **Agenesis of the corpus callosum (ACC) with midline interhemispheric cyst.** ACC may be associated with midline interhemispheric cysts. The cysts may be a diverticulum of the lateral ventricle (type I) or multiple hyperintense interhemispheric cysts (type II). Ventriculomegaly is common. Distinguishing features from holoprosencephaly include shift of parenchyma laterally as opposed to anteriorly. One half to three fourths of cases of ACC have other CNS malformations.
- **Bilateral open-lip schizencephaly.** Type II (open-lip) schizencephaly consists of a large defect, often holohemispheric, filled with CSF and lined by polymicrogyric gray matter. The abnormality may be bilateral and can be associated with septo-optic dysplasia. Differentiating features include preservation of the falx and gray matter–lined CSF clefts. Heterotopia or cortical dysplasia may be an associated finding.

Diagnosis

Alobar holoprosencephaly

✓ Pearls

- Massive hydrocephalus in a neonate is commonly due to obstruction; a thin cortical mantle is seen.
- Hydranencephaly is due to bilateral ICA occlusions; the falx is present, but there is no cortical mantle.
- Alobar holoprosencephaly results in a large dorsal monoventricle with fused parenchyma anteriorly.

Suggested Readings

Barkovich AJ, Moore KR, Grant E, et al. Diagnostic Imaging: Pediatric Neuroradiology. Salt Lake City, UT: Amirsys; 2007

O'Brien WT, Palka PS, et al. Pediatric neuroimaging. In: Quattromani F, Handal GA, Lampe R, eds. Pediatric Imaging: Rapid-fire Questions and Answers. New York: Thieme; 2007:338–391

Case 145

Paul M. Sherman

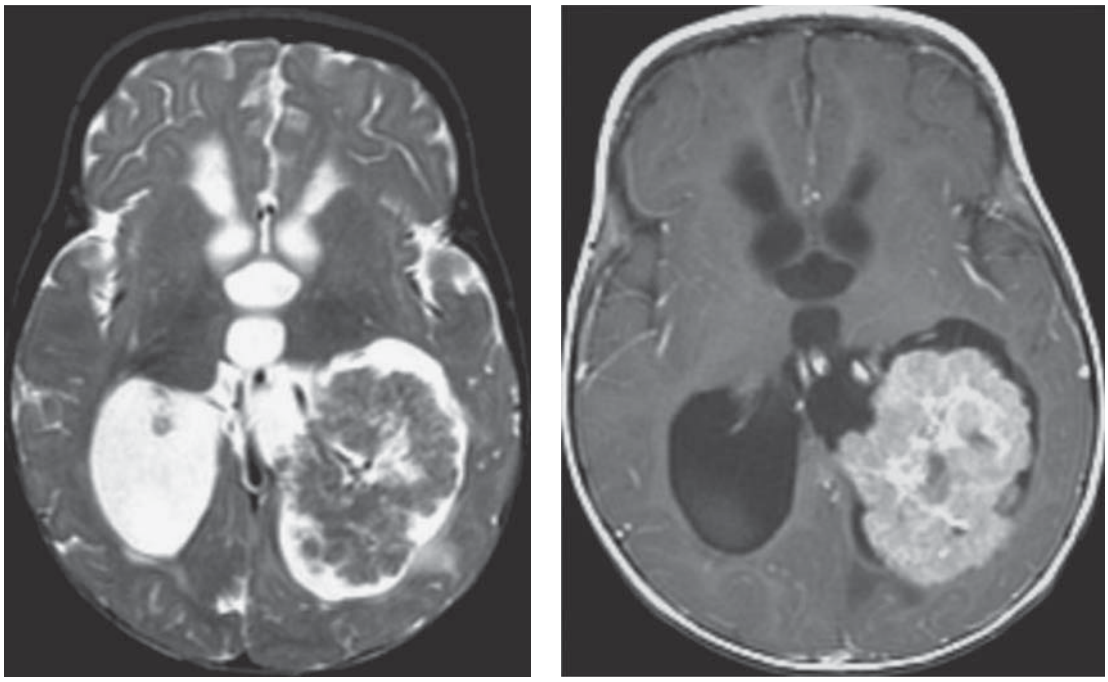


Fig. 145.1 **(A)** Axial T2-weighted sequence through the level of the lateral ventricles demonstrates a lobulated hypointense mass within the left lateral ventricle with frondlike margins. **(B)** Axial T1 postcontrast image through the same level reveals intense homogeneous enhancement (precontrast image not shown). There is associated hydrocephalus with transependymal interstitial edema. There is no brain parenchymal invasion.

Clinical Presentation

A young patient presents with persistent vomiting (**Fig. 145.1**).

Key Imaging Finding

Intraventricular mass

Top 3 Differential Diagnoses

- **Meningioma.** Meningiomas are the most common primary adult intracranial tumor. Approximately 10% are intraventricular and are most commonly seen in the trigone of the lateral ventricles in adults. They are circumscribed with intense homogeneous enhancement. Peritumoral vasogenic edema is commonly seen. Most meningiomas are hyperdense on computed tomography (CT); calcifications are present in ~20 to 25% of cases. T2-weighted sequences best demonstrate vascular flow voids and hyperintense cerebrospinal fluid (CSF) clefts. Angiography demonstrates "radial" enhancement with the "mother-in-law" sign (comes early and stays late).
- **Choroid plexus tumor.** Choroid plexus tumors comprise choroid plexus papilloma (CPP) and choroid plexus carcinoma (CPC). They occur most commonly in children within the atria of the lateral ventricles and less commonly in adults within the fourth ventricle. Infants and toddlers present with enlarging head size, vomiting, and ataxia. Hydrocephalus occurs due to overproduction of CSF. The tumors are well circumscribed with frondlike projections and a vascular pedicle. Calcifications are seen in 25% of cases. The lesions are hypointense on T1 and hyperintense on T2 sequences. They intensely and homogeneously enhance. Heterogeneous enhancement and brain parenchymal invasion suggest CPC.
- **Central neurocytoma.** Central neurocytomas most commonly occur in adults and are typically attached to the septum pellucidum. Patients present with obstructive hydrocephalus. Most occur within the lateral ventricles near the foramen of Monro; they may involve both lateral ventricles and extend into the third ventricle. They are well circumscribed and lobulated. Calcification and flow voids are common. Intratumoral cysts result in a characteristic "bubbly" appearance. Heterogeneous enhancement is typical.

Additional Differential Diagnoses

- **Ependymoma/subependymoma.** Ependymomas are common posterior fossa tumors in children and occur within the fourth ventricle. They may extend through the foramen magnum. Supratentorial ependymomas are rarely intraventricular. Subependymomas occur more frequently in the fourth ventricle in adults. When located in the lateral ventricles, they may be indistinguishable from central neurocytomas. Subependymomas commonly calcify. Magnetic resonance (MR) appearance is variable; faint or no enhancement is typical.
- **Colloid cyst.** Colloid cysts occur along the anterosuperior roof of the third ventricle near the foramen of Monro. Patients classically present with headaches in the 3rd and 4th decades due to intermittent, potentially life-threatening obstructive hydrocephalus. Two thirds are hyperdense on CT. MR appearance varies, but most are hyperintense on T1 and iso- to hypointense on T2 sequences. They do not enhance.
- **Subependymal giant cell astrocytoma.** Subependymal giant cell astrocytomas are World Health Organization grade I lesions that occur at the foramen of Monro in 15% of patients with tuberous sclerosis. They enlarge over time, enhance homogeneously, and may result in hydrocephalus. Treatment is usually geared toward CSF shunting when obstructed.

Diagnosis

Choroid plexus tumor (papilloma)

✓ Pearls

- Meningiomas are the most common intraventricular tumor in adults and occur within the trigone.
- CPPs occur in children, avidly enhance, and result in hydrocephalus due to overproduction of CSF.
- Central neurocytomas have a characteristic "bubbly" appearance and are attached to the septum.
- Colloid cysts are hyperdense on CT and may result in intermittent, life-threatening hydrocephalus.

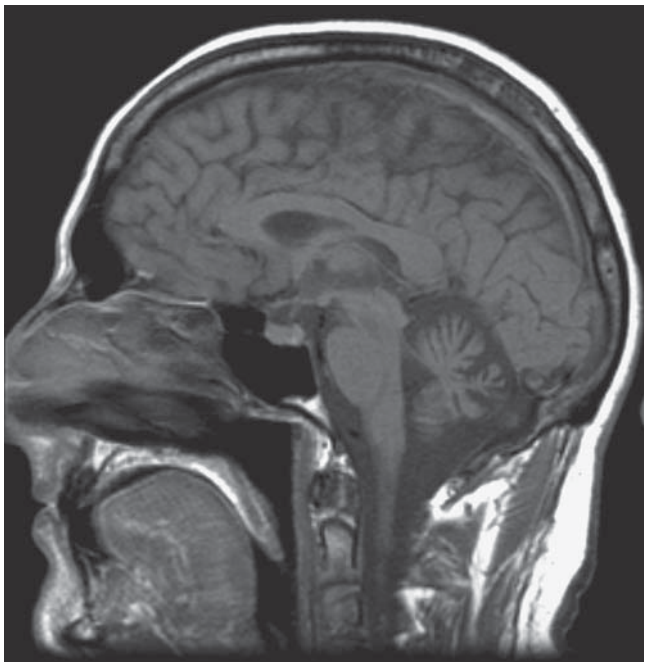
Suggested Readings

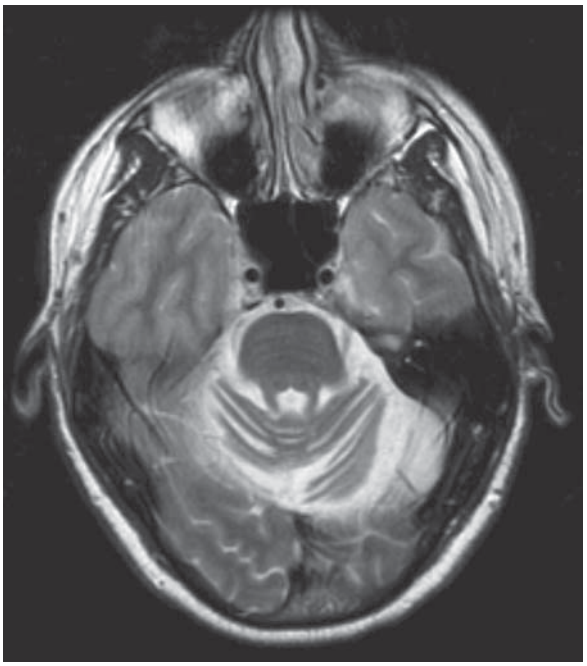
Fischbein NJ, Dillon WP, Barkovich AJ. Teaching Atlas of Brain Imaging. New York: Thieme; 1999

Osborn A, Blaser S, Salzman KL, et al. Diagnostic Imaging: Brain. Salt Lake City, UT: Amirsys; 2004

Case 146

Paul M. Sherman





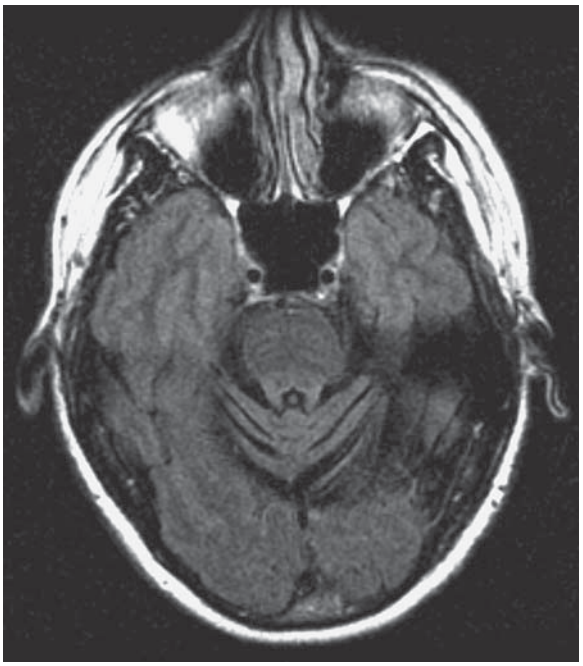


Fig. 146.1 **(A)** Sagittal T1-, **(B)** axial T2-, and **(C)** axial fluid-attenuated inversion recovery–weighted magnetic resonance sequences through the brain demonstrate diffuse cerebellar atrophy, which is markedly disproportionate to the supratentorial compartment.

Clinical Presentation

A 53-year-old man presents with a history of seizures (**Fig. 146.1**).

Key Imaging Finding

Cerebellar atrophy

Top 3 Differential Diagnoses

- **Alcohol abuse.** Alcohol abuse results in progressive cerebellar degeneration. Alcohol is neurotoxic, causing cortical (typically frontal lobe) and cerebellar degeneration, as well as peripheral polyneuropathy. There is disproportionate involvement of the superior vermis and cerebellum. Associated findings are Wernicke encephalopathy (T2 hyperintense periaqueductal gray matter, mammillary bodies, medial thalamus, and hypothalamus) and less commonly Marchiafava–Bignami disease (T2 hyperintense corpus callosum).
- **Anticonvulsant therapy.** Long-term anticonvulsant therapy may produce irreversible cerebellar degeneration. Patients present with nystagmus, ataxia, peripheral neuropathies, and slurred speech. Phenytoin may also cause calvarial thickening.
- **Paraneoplastic syndrome.** Cerebellar degeneration is a paraneoplastic syndrome associated with breast, lung, gastrointestinal, and genitourinary neoplasms, as well as Hodgkin lymphoma and neuroblastoma. It occurs as either an immune-mediated process secondary to autoantibodies to Purkinje fibers or a cytotoxic process with T cell–related mechanisms. It may precede the diagnosis of a primary tumor in the majority of cases.

Additional Differential Diagnoses

- **Sporadic olivopontocerebellar atrophy (OPCA).** Sporadic OPCA is a neurodegenerative disorder of unknown etiology with adult onset. There is atrophy of the ventral pons and midbrain with enlargement of the fourth ventricle and widening of the superior and middle cerebellar peduncles. There is hemispheric greater than vermian cerebellar atrophy, as well as cerebral atrophy, which most commonly involves the frontal and parietal lobes. Cruciform-like T2 hyperintensity in the base of the pons gives the characteristic "hot cross bun" sign. Abnormal signal intensity is also seen in the middle cerebellar peduncles and dorsolateral putamen. Patients present with parkinsonian features, ataxia, dysarthria, and autonomic dysfunction.
- **Cerebello-olivary degeneration.** Cerebello-olivary degeneration is a rare autosomal disorder that leads to progressive atrophy of the cerebellar cortex with resultant volume loss within the olivary nuclei of the medulla. The fourth ventricle may be significantly enlarged. Patients typically present in young adulthood with ataxia, tremors, and dysarthria. Selective atrophy of the lateral cerebellum results in a characteristic "fish mouth" deformity on parasagittal images.
- **Friedreich ataxia.** Also known as spinocerebellar ataxia, Friedreich ataxia presents in the 2nd decade of life and has autosomal dominant and recessive forms. Mild atrophy of the vermian and paravermian structures, small medulla oblongata, and significant atrophy of the spinal cord are seen. There is a flattened appearance of the dorsal cord. Lower extremity ataxia, kyphoscoliosis, and upper extremity tremors are the most common clinical presentation.

Diagnosis

Anticonvulsant therapy (long-term phenytoin use)

✓ Pearls

- Alcohol abuse leads to cerebellar atrophy and may be associated with Wernicke encephalopathy.
- Long-term phenytoin therapy may result in cerebellar atrophy and calvarial thickening.
- Cerebellar atrophy from a paraneoplastic syndrome typically precedes the diagnosis of a primary cancer.
- Sporadic OPCA, cerebello-olivary degeneration, and Friedreich ataxia are rare causes of cerebellar atrophy.

Suggested Readings

Fischbein NJ, Dillon WP, Barkovich AJ. Teaching Atlas of Brain Imaging. New York: Thieme; 1999

Grossman RI, Yousem DM. Neuroradiology: The Requisities. 2nd ed. Philadelphia: Mosby; 2003

Huang YP, Tuason MY, Wu T, Plaitakis A. MRI and CT features of cerebellar degeneration. J Formos Med Assoc 1993;92(6):494–508

Case 147

William T. O'Brien Sr.

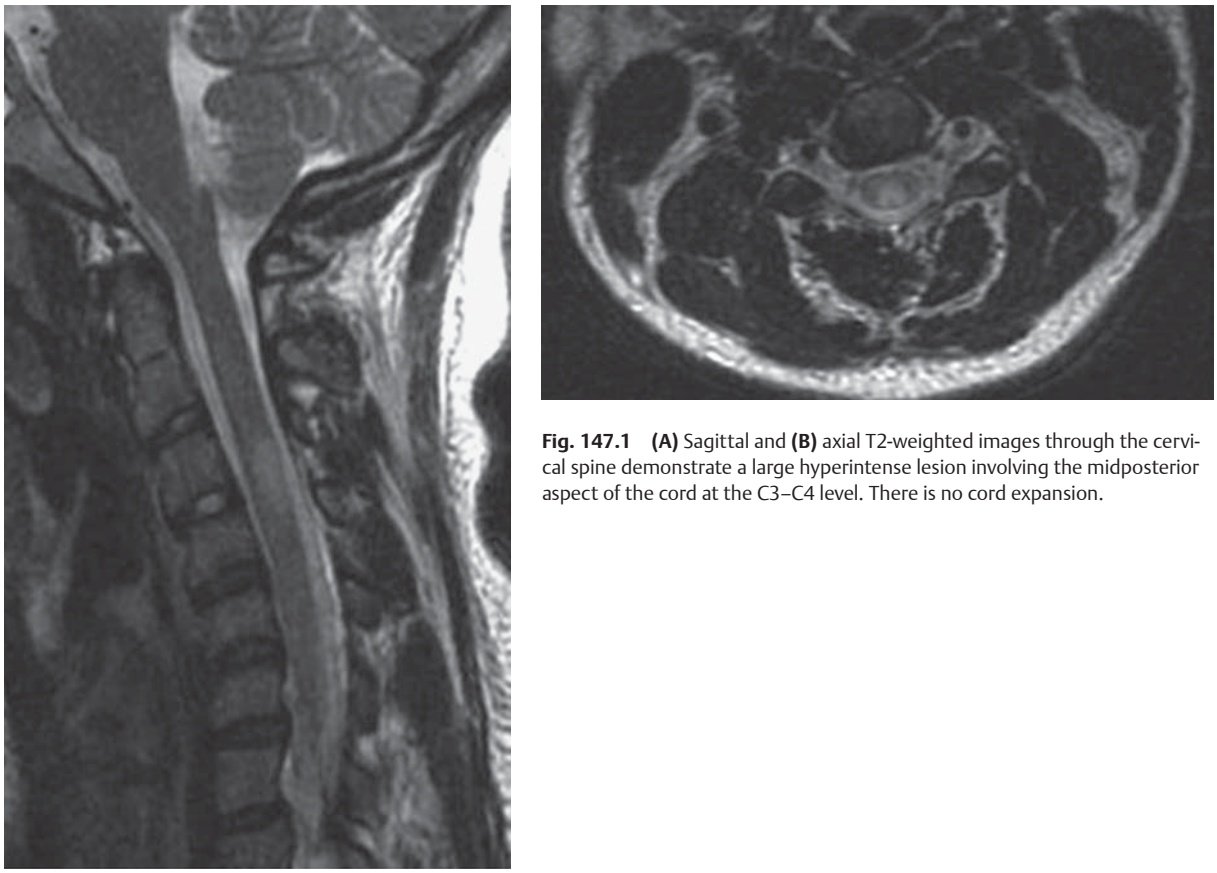


Fig. 147.1 **(A)** Sagittal and **(B)** axial T2-weighted images through the cervical spine demonstrate a large hyperintense lesion involving the midposterior aspect of the cord at the C3–C4 level. There is no cord expansion.

Clinical Presentation

A patient presents with cervical myelopathy (**Fig. 147.1**).

Key Imaging Finding

Spinal cord signal abnormality

Top 3 Differential Diagnoses

- **Demyelinating disease.** Demyelinating processes, such as multiple sclerosis (MS) and acute disseminating encephalomyelitis (ADEM), may affect the spinal cord, as well as the brain. Isolated cord disease is seen in ~10 to 20% of cases. The lesions are hyperintense on T2-weighted sequences and are most commonly located along the posterolateral aspect of the cord. There is little edema, if any; enhancement may be seen during periods of active demyelination. The plaques are typically small, usually spanning fewer than two vertebral bodies in length. Patients commonly present with neurologic deficits. MS demonstrates relapsing and remitting symptoms, whereas ADEM is characteristically monophasic after an antecedent viral infection or vaccination.
- **Cord contusion.** Cord contusions occur in the setting of trauma and often present with acute onset neurologic deficits. There is increased T2 signal intensity and edema within the involved segment(s) of the cord. Foci of hemorrhage and cord expansion may also be seen. Secondary findings to suggest contusion include spine fractures, marrow edema, ligamentous injury, and soft tissue injuries. The cervical spine is the most common portion of the spine involved.
- **Intramedullary neoplasm.** The most common intramedullary neoplasms are ependymomas, which are most common in adults, and astrocytomas, which are more common in children. Ependymomas may be either myxopapillary at the caudal end of the cord or cellular within the central portion of the cervical and thoracic cord. Both neoplasms may extend up to four vertebral bodies in length, although astrocytomas may rarely be holocord. In general, ependymomas are more circumscribed and heterogeneous; intratumoral cysts and cord edema are commonly seen. Astrocytomas are typically more ill-defined and diffuse, causing fusiform expansion of the cord.

Additional Differential Diagnoses

- **Transverse myelitis (TM).** TM refers to abnormalities involving both the ventral and dorsal cord at a particular level. Transverse myelitis may be caused by a variety of factors, including infectious, ischemic, autoimmune (collagen vascular diseases), demyelinating, and paraneoplastic processes. When no causative factor is identified, it is termed idiopathic TM. Patients with TM present with pain and sensorimotor deficits corresponding to the affected level. Imaging findings include the abnormal cord signal, which may affect the whole cord at that level; enhancement is variable.
- **Cord ischemia.** The spinal cord arterial supply consists of a single anterior spinal artery and paired posterior spinal arteries, as well as segmental radicular arteries, including the artery of Adamkiewicz. Cord infarcts are multifactorial and caused by arterial occlusion, usually the anterior spinal artery. Imaging findings include central increased T2 signal intensity involving the cord gray matter, as well as cord edema and swelling. Patients present with pain and acute onset neurologic deficits.

Diagnosis

Demyelinating disease (ADEM)

✓ Pearls

- Demyelinating disease commonly affects the posterolateral aspect of the spinal cord; acute lesions may enhance.
- Cord contusions occur in the setting of trauma; hemorrhage, edema, and cord expansion may be seen.
- The most common intramedullary neoplasms are ependymomas (adults) and astrocytomas (children).
- Cord ischemia is usually due to arterial occlusion; signal abnormality affects the central gray matter.

Suggested Readings

Ramsey RG. Teaching Atlas of Spine Imaging. New York: Thieme; 1999

Ross JS, Brant-Zawadski M, Moore KR, et al. Diagnostic Imaging: Spine. Salt Lake City, UT: Amirsys; 2005

Case 148

Paul M. Sherman

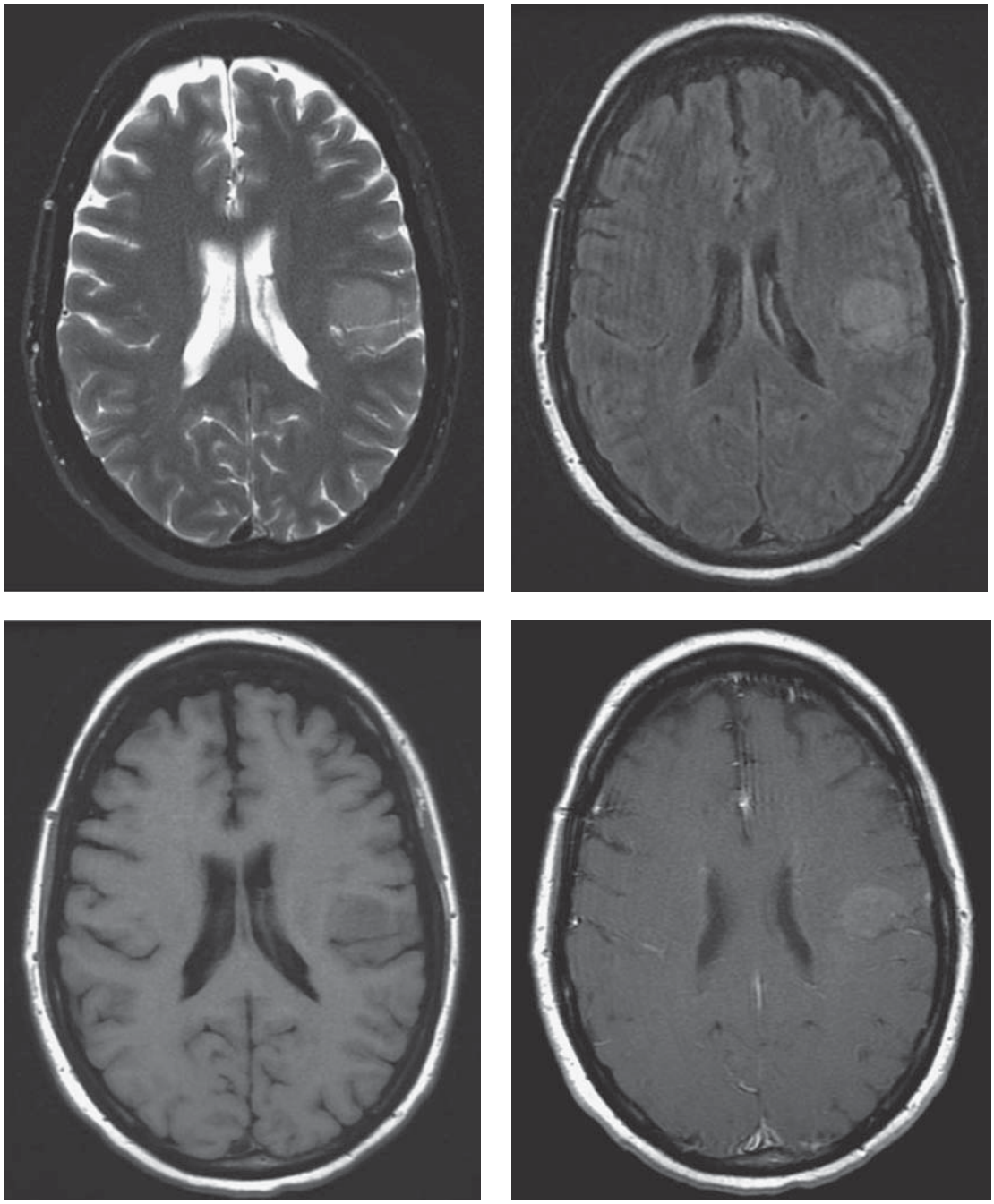


Fig. 148.1 **(A)** Axial T2 and **(B)** fluid-attenuated inversion recovery images of the brain demonstrate a cortically based hyperintense lesion within the left frontal lobe with no significant vasogenic edema. **(C)** The mass is hypointense on T1-weighted sequences and **(D)** demonstrates mild homogeneous enhancement after contrast administration.

Clinical Presentation

An adult female patient presents with a known primary central nervous system neoplasm (**Fig. 148.1**).

Key Imaging Finding

Cortically based enhancing neoplasm

Top 3 Differential Diagnoses

- **Oligodendroglioma.** Oligodendrogliomas are well-differentiated, slow-growing, diffusely infiltrating neoplasms involving the cortex and subcortical white matter. Patients typically present with headaches and/or seizures. Despite the infiltrating nature, the mass appears well circumscribed. There is cortical expansion without significant edema. Eighty-five percent of cases are supratentorial, most commonly within the frontal lobe. Calcifications are seen in up to 90% of cases (blooms on T2* gradient echo). Cystic degeneration occasionally occurs; hemorrhage is uncommon unless anaplastic. Heterogeneous enhancement is noted in half of all cases. There may be remodeling or erosion of the overlying calvarium.
- **Astrocytoma.** Low-grade diffuse astrocytomas involve the white matter but may extend to the cortex and be indistinguishable from other cortically based lesions. They may appear circumscribed with minimal or no edema or enhancement. Calcification, cysts, and hemorrhage are uncommon. Most cases occur between the ages of 20 and 50 years. Pleomorphic xanthoastrocytomas (PXAs) are supratentorial peripheral lesions that most often occur within the temporal lobe of adolescents and young adults. Most are cystic lesions with an enhancing mural nodule that abuts the meninges with a dural tail. They are usually well circumscribed without significant surrounding edema; however, an ill-defined mass may also be seen.
- **Ganglioglioma.** Gangliogliomas are the most common cause of temporal lobe epilepsy (90% of patients have chronic epilepsy) and occur predominantly in children and young adults. They are slow-growing, cortically based neuroepithelial tumors (neoplastic ganglion and glial cells) that are most frequently located within the temporal lobe, followed by the parietal and frontal lobes. The most common presentation is a well-circumscribed cystic mass with a mural nodule; however, it can also present as a solid tumor that expands the cortical gyri. Calcifications and enhancement may be seen in ~50% of cases. Attenuation is variable on computed tomography (CT). There is heterogeneous T2 hyperintensity.

Additional Differential Diagnoses

- **Dysembryoplastic neuroepithelial tumor (DNET).** DNETs are benign, cortically based masses with underlying cortical dysplasia. They occur in children and young adults who present with seizures. They most commonly occur in the temporal lobe, followed by the parietal lobe. Imaging appearance consists of a wedge-shaped, multinodular, pseudocystic cortical mass. There is no edema and little mass effect. Calcifications and nodular or rim enhancement are seen in ~20% of cases. There may be scalloping of the overlying calvarium. The masses are characteristically hyperintense on T2 sequences.
- **Desmoplastic infantile glioma (DIG).** DIGs are composed of dural-based desmoplastic stromal tissue and neoplastic astrocytes (World Health Organization grade I). Most patients present before 2 years of age with increasing head size, seizures, and/or paresis. Characteristic imaging appearance is a large cystic mass with a cortically based enhancing nodule with adjacent pial/dural enhancement. The nodule is iso- to hyperdense on CT and hypointense on T2 sequences. There is typically surrounding vasogenic edema.

Diagnosis

Astrocytoma

✓ Pearls

- Oligodendrogliomas are cortically based (usually frontal lobe) neoplasms that commonly calcify.
- Astrocytomas may be cortically based; PXAs are cystic with an enhancing mural nodule.
- Gangliogliomas are the most common cause of temporal lobe epilepsy; they are cystic with a mural nodule.
- DNET occurs with underlying cortical dysplasia and appears as a wedge-shaped pseudocystic cortical mass.

Suggested Readings

Osborn A, Blaser S, Salzman KL, et al. Diagnostic Imaging: Brain. Salt Lake City, UT: Amirsys; 2004

Case 149

Paul M. Sherman



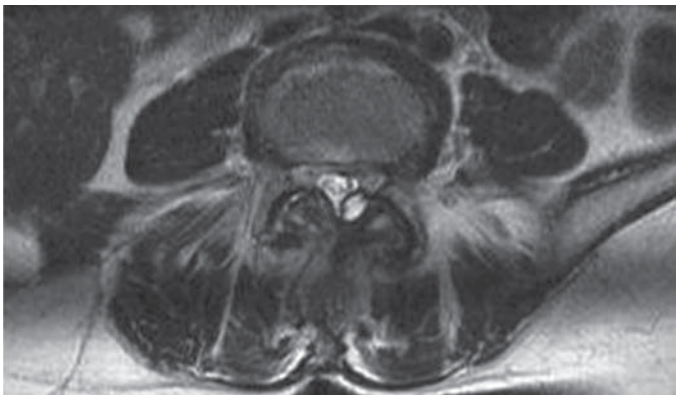


Fig. 149.1 **(A)** Sagittal and **(B)** axial T2-weighted sequences through the lumbar spine demonstrate a hyperintense epidural mass with a peripheral low signal margin along the left posterolateral aspect of the thecal sac at the L4–L5 level adjacent to the articular facet. There are degenerative changes involving the facets and intervertebral disk spaces.

Clinical Presentation

A middle-aged man presents with back pain and radiculopathy (**Fig. 149.1**).

Key Imaging Finding

Epidural spinal mass

Top 3 Differential Diagnoses

- **Disk extrusion.** Disk extrusion refers to herniations with migration of the disk fragment, usually within the anterior epidural space. There is often disk dessication and height loss with intact end plates. The extruded fragment is usually similar in signal to the parent disk; there may be peripheral enhancement. Epidural hematomas may be associated with disk extrusions; the extrusion is typically smaller and more focal.
- **Epidural hematoma.** Epidural hematomas may be spontaneous or result from trauma, transient venous hypertension (cough), iatrogenia, or coagulopathy. They are most often due to rupture of the epidural venous plexus. Most occur within the dorsal thoracolumbar spine in adults and cervicothoracic spine in children. They are generally biconvex and surrounded by epidural fat. Acute hemorrhage is T1 isointense, whereas subacute or chronic hemorrhage is most often T1 hyperintense. Blood products are heterogeneous on T2 imaging. On gradient echo imaging, deoxyhemoglobin is hypointense, with the remainder hyperintense. Peripheral enhancement is common; focal enhancement may represent extravasation.
- **Epidural abscess.** Epidural abscesses are associated with disk osteomyelitis. They most often occur anteriorly and are often associated with paraspinal phlegmon or abscess formation. They may result from hematogenous dissemination of a distant infection or direct inoculation from surgical procedures or epidural anesthesia. The latter types are less common and occur dorsally. *Staphylococcus aureus* (70–75%) is the most common organism; *Mycobacterium tuberculosis* most commonly occurs in immunocompromised patients. Epidural abscesses follow fluid signal with peripheral rim and adjacent dural enhancement.

Additional Differential Diagnoses

- **Metastatic disease.** Epidural foci from metastatic disease are often contiguous with a pedicle or posterior vertebral body lesion. A pathologic compression fracture may be present. The masses are typically T1 hypointense and T2 hyperintense with diffuse or heterogeneous enhancement depending on the presence of necrosis or hemorrhage. Common primary tumors are breast, lung, and prostate carcinomas. Non-Hodgkin lymphoma may also present as an extradural mass. Lymphoma is typically hyperdense on computed tomography, isointense on T1, and hyperintense on T2 with intense homogeneous enhancement.
- **Epidural lipomatosis.** Lipomatosis refers to abnormal proliferation of epidural fat. It is most commonly seen in the thoracolumbar spine. Lipomatosis is usually the result of excessive steroids (exogenous or endogenous), although it may also be idiopathic or associated with obesity. The lesions follow fat signal on all sequences and do not enhance. There may be compression of the spinal canal and neural structures.
- **Synovial cyst.** Synovial cysts result from degenerative facet disease and most commonly occur in the lumbar spine. They may extend into the posterolateral epidural space or through the neural foramen. The cyst follows fluid signal and has a T2 hypointense margin. Peripheral enhancement may be seen, as can hemorrhage or calcification. Patients commonly present with pain or radiculopathy.

Diagnosis

Synovial cyst

✓ Pearls

- Disk extrusions occur anterior to the thecal sac and commonly follow the signal intensity of the parent disk.
- Epidural hematomas are most often dorsal and may occur spontaneously or due to an inciting event.
- Epidural abscesses have rim enhancement and most commonly are associated with disk osteomyelitis.
- Synovial cysts result from degenerative facet disease and may compress the posterolateral thecal sac.

Suggested Readings

Ross JS, Brant-Zawadski M, Moore KR, et al. Diagnostic Imaging: Spine. Salt Lake City, UT: Amirsys; 2005

Case 150

Paul M. Sherman

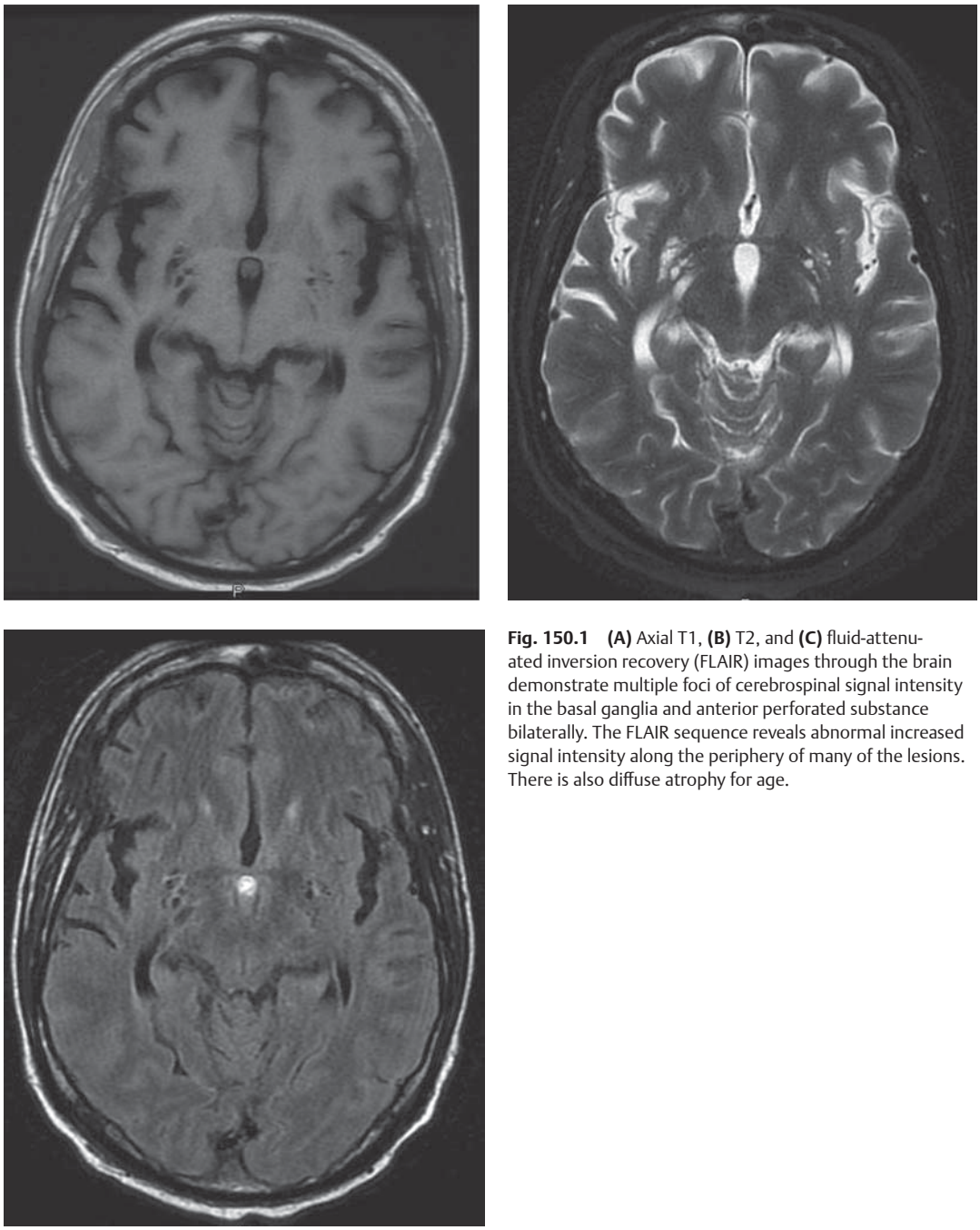


Fig. 150.1 **(A)** Axial T1, **(B)** T2, and **(C)** fluid-attenuated inversion recovery (FLAIR) images through the brain demonstrate multiple foci of cerebrospinal signal intensity in the basal ganglia and anterior perforated substance bilaterally. The FLAIR sequence reveals abnormal increased signal intensity along the periphery of many of the lesions. There is also diffuse atrophy for age.

Clinical Presentation

A 42-year-old African American man presents with progressive fatigue, somnolence, and decreased responsiveness (**Fig. 150.1**).

Key Imaging Finding

Prominent periventricular/basal ganglia cystic lesions

Top 3 Differential Diagnoses

- **Virchow–Robin (VR) spaces.** VR spaces are prominent pial–lined, fluid-filled structures that accompany penetrating arteries. They do not directly communicate with the subarachnoid space, but follow cerebrospinal fluid (CSF) signal intensity on all sequences and do not enhance. When present, they are commonly multiple and occur in clusters. The most common location is surrounding the anterior commissure/basal ganglia, but they are also frequently seen in the deep white matter, midbrain, and subinsular cortex/extreme capsule. Giant VR spaces most often occur in the midbrain and almost never involve the cortex. When large, they may cause local mass effect and rarely hydrocephalus (compression of the third ventricle or cerebral aqueduct).
- **Lacunar infarct.** Lacunar infarcts are small, well-circumscribed areas of encephalomalacia, typically located in basal ganglia, thalami, internal capsules, and the pons. Chronic lacunae simulate dilated VR spaces, as they follow CSF signal intensity without restricted diffusion, and do not enhance. There may be surrounding fluid-attenuated inversion recovery hyperintensity/gliosis. These are commonly seen in elderly patients with associated small vessel ischemic changes within the subcortical and periventricular white matter.
- **Infection.** Neurocysticercosis is a parasitic infection caused by the pork tapeworm (*Taenia solium*) and represents the most common cause of epilepsy in endemic regions. In the vesicular stage, the cystic lesion is isointense to CSF, mimicking a VR space. A hyperintense eccentric scolex may be seen (hyperdense by computed tomography). Enhancement is atypical. In the colloidal stage, the cyst is hyperintense to CSF with surrounding edema. There is incomplete enhancement of the cyst wall and nodular enhancement of the scolex. Ring enhancement is seen in the granular stage. Calcification occurs in the nodular stage. Lesions may be located within the subarachnoid space, parenchyma (gray-white junction), and the ventricles (often the fourth ventricle). Cryptococcosis is an opportunistic infection that occurs in the setting of acquired immunodeficiency syndrome (AIDS). The most common imaging finding is multiple T2 hyperintense regions in the basal ganglia. Four primary patterns of infection are granulomatous meningitis with nodular enhancement, dilated nonenhancing VR spaces representing cysts, "gelatinous pseudocysts" (which may or may not enhance) in the basal ganglia, and cryptococcomas with solid or ring-enhancing masses that often involve the choroid plexus.

Additional Differential Diagnoses

- **Cystic neoplasm.** Cystic astrocytomas are usually located in the posterior fossa (pons and cerebellum), thalamus, or hypothalamus. They are most often solitary and do not follow CSF signal intensity on all sequences. There is usually surrounding parenchymal signal abnormality, and there may be enhancement.
- **Neuroglial cyst.** Neuroglial cysts are nonenhancing parenchymal cysts with minimal or no surrounding signal abnormality. They most often occur within the frontal lobes. They are smooth, round, unilocular, and follow CSF signal intensity on all sequences. There is no communication with the ventricles.

Diagnosis

Infection (cryptococcosis in a patient with AIDS)

✓ Pearls

- Prominent VR spaces most commonly occur surrounding the basal ganglia and anterior commissure.
- Lacunar infarcts are most common in elderly individuals with microvascular ischemic disease.
- Neurocysticercosis is a parasitic infection and is the most common cause of epilepsy in endemic regions.
- Cryptococcosis occurs in the setting of AIDS and may simulate VR spaces or lacunar infarcts.

Suggested Readings

Fischbein NJ, Dillon WP, Barkovich AJ. Teaching Atlas of Brain Imaging. New York: Thieme; 1999

Salzman KL, Osborn AG, House P, et al. Giant tumefactive perivascular spaces. AJNR Am J Neuroradiol 2005;26:298–305

Section VII Pediatric Imaging

Case 151

Thomas Ray S. Sanchez

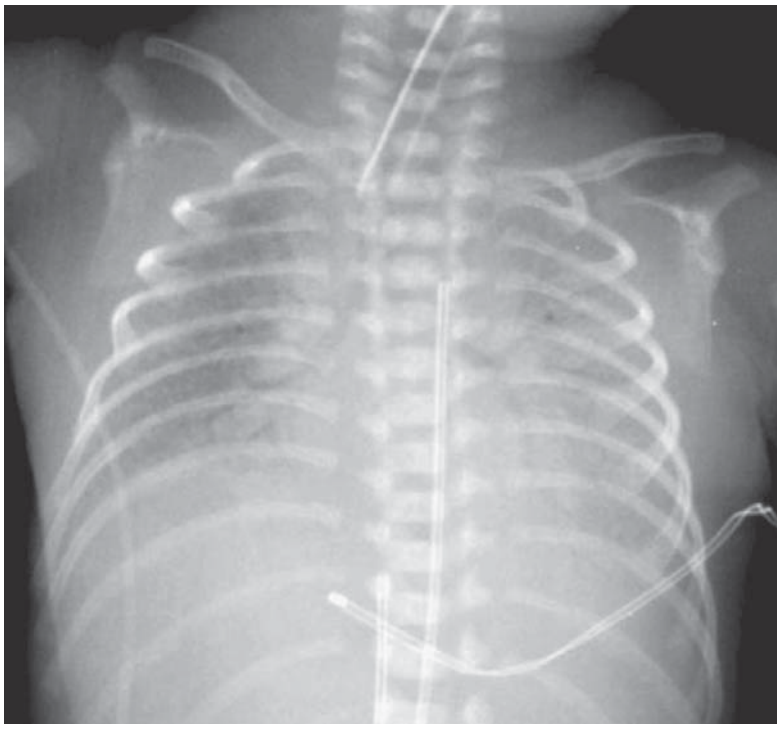


Fig. 151.1 Anteroposterior chest radiograph shows hypoaerated lungs that are diffusely hazy and granular with air bronchograms. Multiple lines and tubes are appropriately positioned. Humeral head ossification centers are not visualized, suggesting prematurity (confirmed by history).

Clinical Presentation

A newborn infant presents with respiratory distress (**Fig. 151.1**).

Key Imaging Finding

Neonatal lung disease with low lung volumes

Top 3 Differential Diagnoses

- **Surfactant deficiency.** Surfactant deficiency is the most common cause of respiratory distress in a preterm infant, especially in those born before 34 weeks of gestation and those who weigh <2500 g. It results from the immaturity of the lungs and their inability to produce enough surfactant to keep the alveoli open for effective air exchange. Clinically, respiratory distress (grunting, nasal flaring, subcostal retractions, tachypnea, and cyanosis) is manifested shortly after delivery. Most, if not all, cases will be apparent within 8 hours. A normal chest radiograph at or after 8 hours essentially excludes the diagnosis of surfactant deficiency. Radiographs typically show diffusely hazy and underaerated lungs with peripherally extending air bronchograms, indicative of atelectasis. The granularity and reticularity result from diffuse alveolar collapse. In severe cases (extreme prematurity and very low birth weight), assisted ventilation may be necessary, in addition to surfactant administration, to achieve acceptable gas exchange. This, however, comes with complications, such as pulmonary interstitial emphysema, pneumomediastinum, and pneumothorax, as well a bronchopulmonary dysplasia in the long term. Low lung volumes may not be a reliable finding in children who are intubated and receiving positive pressure ventilation.
- **Beta-hemolytic streptococcal pneumonia.** Bacterial pneumonias, especially those caused by group B *Streptococcus,* predominate in the neonatal period. The usual route of infection is after premature rupture of membranes. As with surfactant deficiency, clinical manifestations of respiratory distress will be apparent shortly after birth, usually within 6 to 8 hours. Radiographic findings of diffuse haziness and granularity can mimic surfactant deficiency. However, in patients with neonatal pneumonia, lung volumes are usually normal to slightly expanded, reflecting the underlying exudate-filled and distended alveoli. Because pleural effusions are rare in surfactant deficiency, their presence is suggestive of neonatal pneumonia. Complications after adequate antibiotic coverage are infrequent but may include empyema, pulmonary abscess, and pneumatocele formation.
- **Pulmonary hypoplasia.** Bilateral pulmonary hypoplasia is a result of a wide variety of factors, including pulmonary compression from oligohydramnios, thoracic dystrophies, and intrathoracic herniation of abdominal viscera. The best known cause of this disorder is Potter syndrome, which is pulmonary hypoplasia secondary to renal agenesis and resultant oligohydramnios. Again, clinical manifestations of respiratory distress become apparent shortly after birth. The lungs, however, are generally clear, and the only remarkable finding is the small size of the lungs. Complications such as pneumothorax and pneumomediastinum can be seen after ventilatory support due to barotrauma; these complications can also occur spontaneously as a result of the neonate's own effort to inflate the hypoplastic lungs.

Diagnosis

Surfactant deficiency

✓ Pearls

- Surfactant deficiency is the most common cause of respiratory distress in preterm infants.
- Surfactant deficiency presents with underaerated lungs and diffuse hazy opacities.
- Neonatal pneumonia presents with hazy opacities and normal lung volumes; there may be pleural effusions.

Suggested Readings

Agrons GA, Courtney SE, Stocker JT, Markowitz RI. From the *Archives of the AFIP:* lung disease in premature neonates—radiologic-pathologic correlation. Radiographics 2005;25(4):1047–1073

Donnelly LF. Fundamentals of Pediatric Radiology. Philadelphia: WB Saunders; 2001

Donnelly LF, Jones BV, O'Hara SM, et al. Diagnostic Imaging: Pediatrics. Salt Lake City, UT: Amirsys; 2005

Swischuk LE. Imaging of the Newborn, Infant and Young Child. 5th ed. Philadelphia: Lippincott Williams & Wilkins; 2004

Case 152

James B. Odone

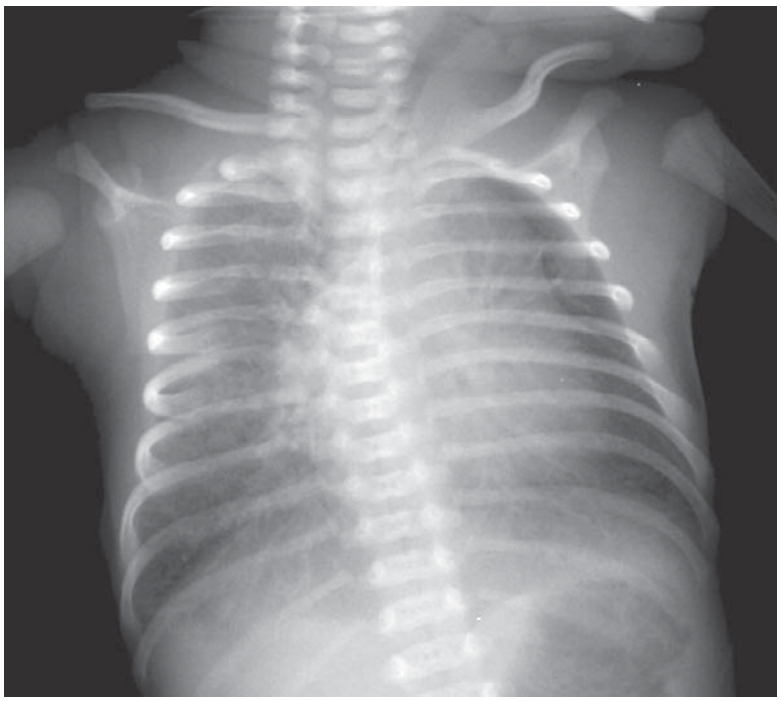


Fig. 152.1 Frontal radiograph of the chest demonstrates increased interstitial markings and vasculature congestion, along with expanded lung volumes.

Clinical Presentation

A term neonate born by cesarean section presents with respiratory distress (**Fig. 152.1**).

Key Imaging Finding

Neonatal lung disease with increased lung volumes

Top 3 Differential Diagnoses

- **Transient tachypnea of the newborn (TTN).** TTN most often manifests as acute respiratory distress in term neonates who have undergone a cesarean section or precipitous birth. The lack of vaginal squeeze results in retained fetal lung fluid that is slow to be cleared by the immature lymphatic system. Common radiographic features are hyperinflation with bilateral diffuse patchy air-space disease and a normal heart size. Other features are perihilar linear densities, pleural effusions, and fluid in the fissures. The air-space disease is similar in appearance to pulmonary edema and clears within 3 days of delivery. The typical course is mild; should these findings persist, an alternative diagnosis should be considered. Follow-up radiographs are generally not necessary in an otherwise healthy infant.
- **Meconium aspiration.** Meconium aspiration typically occurs in term to postterm neonates with in utero or peripartum fetal distress. The aspirated meconium causes a chemical pneumonitis that can result in moderate to severe respiratory distress. The diagnosis is suspected clinically when the amniotic fluid is stained with meconium. Radiographic appearance includes hyperinflation with patchy, asymmetric air-space disease. Pleural effusions may also be present, as well as areas of postobstructive atelectasis. Pneumothorax may be seen in up to 40% of cases.
- **Neonatal pneumonia.** Neonatal pneumonia may also result in respiratory distress combined with focal or diffuse air-space disease and hyperinflation. This entity is typically the result of an infection in utero or at birth. Causative organisms include *Listeria, Escherichia coli*, and *Klebsiella.* Beta-hemolytic streptoccci bacteria typically present with low lung volumes and are not included in this differential. Radiographic features include hyperinflation with patchy, asymmetric perihilar densities. The infection typically resolves over a short period of time with the correct antibiotic therapy.

Additional Differential Diagnoses

- **Congenital heart disease.** Congenital heart disease commonly presents with respiratory distress, parenchymal opacities, and hyperexpanded lungs. Radiographic features are abnormal cardiomediastinal contour such as cardiomegaly, pulmonary vascular congestion, and hyperinflation. Diagnostic considerations in an acyanotic infant include shunt lesions and congestive heart failure. Considerations in a cyanotic infant include transposition of the great arteries, truncus arteriosus, total anomalous pulmonary venous return, tricuspid atresia, and single ventricle.

Diagnosis

Transient tachypnea of the newborn

✓ Pearls

- Transient tachypnea of the newborn is a self-limiting process that should resolve within 3 days.
- Meconium aspiration typically presents with patchy asymmetric air-space disease in hyperinflated lungs.
- Air-block complications (e.g., pneumothorax) must be carefully searched for with meconium aspiration.
- Neonatal pneumonia can mimic most other disease processes on neonatal chest radiographs.

Suggested Readings

Donnelly LF. Fundamentals of Pediatric Radiology. Philadelphia: WB Saunders; 2001

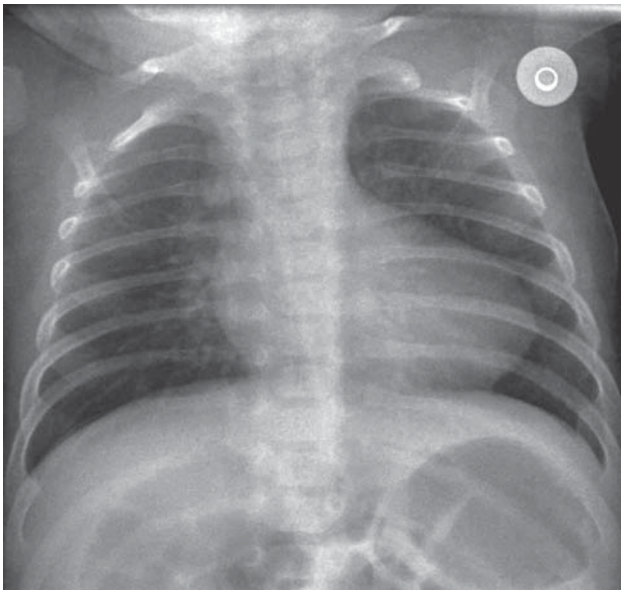
Donnelly LF, Jones BV, O'Hara SM, et al. Diagnostic Imaging: Pediatrics. Salt Lake City, UT: Amirsys; 2005

Kirks DR. Practical Pediatric Imaging: Diagnostic Radiology of Infants and Children. 3rd ed. Philadelphia: Lippincott Williams & Wilkins; 1998

Case 153

Karen M. Ayotte





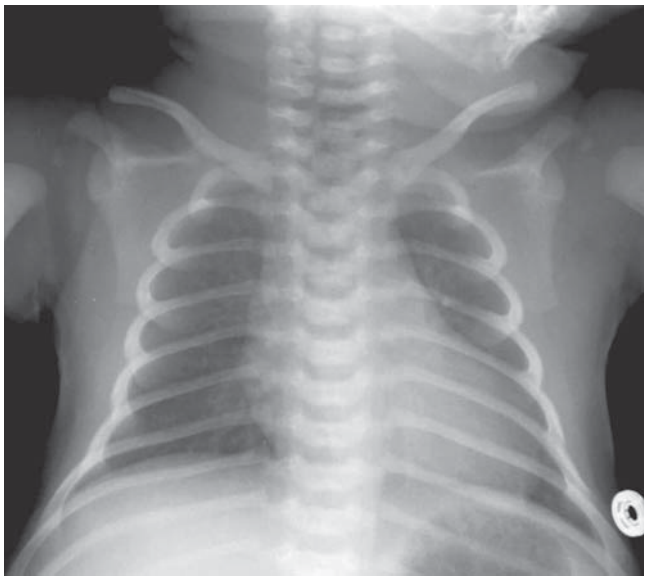


Fig. 153.1 **(A,B)** Frontal plain radiographs of the chest from different patients with the same disease process demonstrate a concave pulmonary artery shadow on the left with elevation of the cardiac apex, resulting in a boot-shaped heart. Relative pulmonary oligemia is present. A right-sided arch is seen in patient **A. (C)** A normal infant chest radiograph is given for comparison. (**[A]** courtesy of Children's Hospital and Research Center, Oakland, California.)

Clinical Presentation

Cyanotic infants (**Fig. 153.1A** and **B**). **Fig. 153.1C** is normal for comparison.

Key Imaging Finding

Cyanotic infant with decreased pulmonary flow

Top 3 Differential Diagnoses

- **Tetralogy of Fallot.** The four components that define this anomaly are right ventricular outflow tract obstruction (pulmonic stenosis), ventriculoseptal defect, overriding aorta, and right ventricular hypertrophy. Tetralogy of Fallot is the most common cyanotic heart condition in children. Deficiency of the main pulmonary artery segment and elevation of the cardiac apex as the result of right ventricular hypertrophy lead to the classic radiographic description of a boot-shaped heart. Pulmonary vascularity is classically decreased but is variable in its severity. A right-sided arch is present in 25% of patients.
- **Pulmonary atresia.** The primary anatomical defect is underdevelopment of the right ventricular outflow tract and pulmonary valve. When present with a ventricular septal defect, this anomaly is considered a severe variant of tetralogy of Fallot with similar radiographic findings. When the ventricular septum is intact, there is an obligatory right-to-left shunt at the atrial level. Although radiographic appearance is variable, severe cardiomegaly is common. Pulmonary vascularity is normal to decreased and dependent on a patent ductus arteriosus.
- **Tricuspid atresia.** In tricuspid atresia, there is no direct path for blood flow between the right atrium and right ventricle. As a result, there is a right-to-left shunt at the atrial level usually through a patent foramen ovale. Pulmonic blood flow is dependent on the presence of a ventricular septal defect and/or patent ductus arteriosus. Associated anomalies are seen in up to 30% of affected patients (most commonly transposition of the great arteries). In isolated tricuspid atresia with a small ventricular septal defect, chest radiographs demonstrate a normal or small heart with decreased pulmonary blood flow. However, when a large ventricular septal defect is present, there is usually cardiomegaly and increased pulmonary blood flow. A right-sided arch is present in up to 8% of patients.

Additional Differential Diagnoses

- **Double outlet right ventricle.** Double outlet right ventricle occurs when both the aorta and pulmonary outflow tracts arise from the right ventricle. With 16 described variants, plain film appearance is quite variable. Some forms mimic the tetralogy of Fallot with pulmonary oligemia and diminished left hilar shadow.
- **Ebstein anomaly.** Ebstein anomaly consists of apical displacement of the tricuspid valve resulting in atrialization of the right ventricle. Tricuspid regurgitation with stasis of blood flow within the right atrium leads to massive right-sided cardiomegaly with a “box-shaped” heart and pulmonary oligemia. A right-to-left shunt at the atrial level is common.

Diagnosis

Tetralogy of Fallot

✓ Pearls

- Tetralogy of Fallot is the most common cyanotic congenital heart disease.
- Tetralogy of Fallot is characterized by pulmonic stenosis, a ventricular septal defect, right ventricular hypertrophy, and an overriding aorta.
- Pulmonary atresia with a ventricular septal defect is considered a severe variant of tetralogy of Fallot.
- Ebstein anomaly leads to massive right-sided cardiomegaly with a “box-shaped” heart.

Suggested Readings

Donnelly LF. Fundamentals of Pediatric Radiology. Philadelphia: WB Saunders; 2001

Ferguson EC, Krishnamurthy R, Oldham SA. Classic imaging signs of congenital cardiovascular abnormalities. Radiographics 2007;27(5):1323–1334

Kirks DR. Practical Pediatric Imaging: Diagnostic Radiology of Infants and Children. 3rd ed. Philadelphia: Lippincott Williams & Wilkins; 1998

Case 154

Karen M. Ayotte

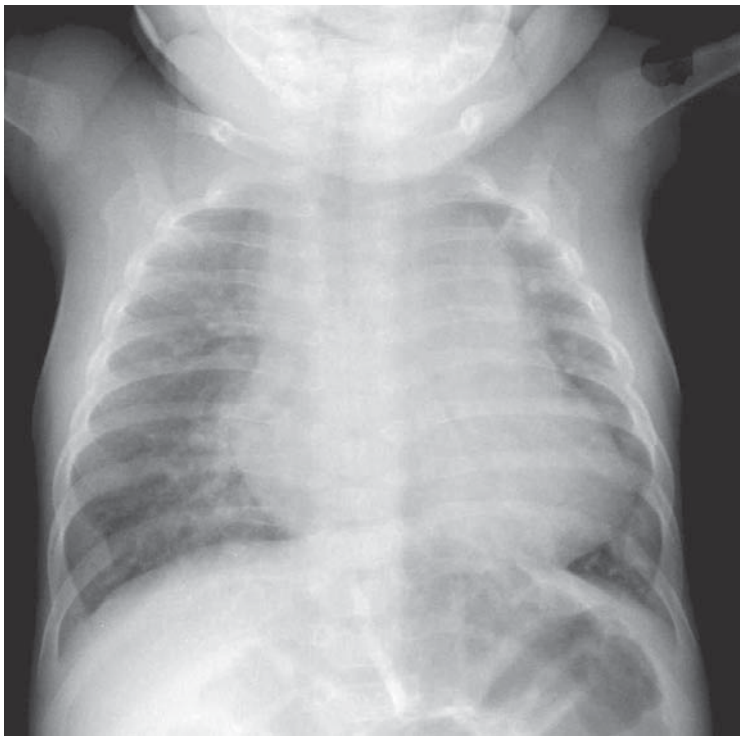


Fig. 154.1 Frontal chest radiograph demonstrates mild cardiomegaly and increased pulmonary vascularity. There is a probable left-sided aortic arch. The lungs are mildly hyperexpanded. (Courtesy of Children's Hospital and Research Center, Oakland, California.)

Clinical Presentation

Infant presents with cyanosis (**Fig. 154.1**).

Key Imaging Finding

Cyanotic infant with increased pulmonary vascularity

Top 3 Differential Diagnoses

- **Transposition of the great arteries.** In transposition of the great arteries, the aorta arises from the right ventricle, and the pulmonary artery arises from the left ventricle. Without a source for admixture (patent foramen ovale, ventricular septal defect, or patent ductus arteriosus), this anatomy is incompatible with life. The classic plain film appearance, which is rarely seen due to prompt treatment, is characterized by cardiomegaly, a narrowed mediastinum ("egg on a string" appearance), and increased pulmonary vascularity. A normal chest radiograph does not exclude the diagnosis.
- **Truncus arteriosus.** Truncus arteriosus results from failure of division of the primitive single truncal vessel into the aorta and main pulmonary artery. It is an uncommon lesion, constituting 1% of cases of congenital heart disease. There is always a large, high ventriculoseptal defect. Initially, the degree of pulmonary blood flow is variable depending on the pulmonary resistance. When this resistance drops, usually day 2 or 3 of life, pulmonary blood flow can increase dramatically. The combination of cardiomegaly, a right-sided arch (30% of cases), and increased pulmonary vascularity suggests the diagnosis.
- **Total anomalous pulmonary venous return (TAPVR).** In TAPVR, none of the pulmonary veins connect normally with the left atrium; instead, the pulmonary veins drain via other venous structures into the right heart. There are three types, which are classified according to the location of pulmonary venous drainage: supracardiac, cardiac, and infracardiac. Supracardiac type I is the most common and may result in the "snowman" configuration of the heart due to an enlarged superior vena cava and left vertical vein. In the cardiac type, pulmonary venous drainage is through the coronary sinus. With infracardiac TAPVR, the pulmonary veins drain below the diaphragm into the portal veins or inferior vena cava. This subtype is associated with heterotaxias. In all three types, intracardiac shunting occurs via a patent foramen ovale. Radiographic and clinical features are variable depending on the type of TAPVR.

Additional Differential Diagnoses

- **Tricuspid atresia.** In tricuspid atresia, there is no direct path for blood flow between the right atrium and right ventricle. As a result, there is a right-to-left shunt at the atrial level usually through a patent foramen ovale. Pulmonic blood flow is dependent on the presence of a ventricular septal defect and/or patent ductus arteriosus. When a large ventricular septal defect is present, there is usually cardiomegaly and increased pulmonary blood flow.
- **Single ventricle.** A single ventricle is a rare malformation in which the interventricular septum is absent. The nomenclature regarding this diagnosis can be confusing and relates to the fine detail of the underlying abnormal anatomy. Patients without pulmonic stenosis demonstrate cardiomegaly, an enlarged main pulmonary artery, and increased pulmonary blood flow.

Diagnosis

Total anomalous pulmonary venous return

✓ Pearls

- Transposition of the great arteries presents with parallel outflow tracts on prenatal ultrasound and "egg on a string" appearance on chest radiography.
- Severe pulmonary edema with a normal heart size is the classic description of infradiaphragmatic TAPVR.
- The dilated vessels of the "snowman" configuration in type 1 TAPVR are the superior vena cava and left vertical vein.

Suggested Readings

Donnelly LF. Fundamentals of Pediatric Radiology. Philadelphia: WB Saunders; 2001

Ferguson EC, Krishnamurthy R, Oldham SA. Classic imaging signs of congenital cardiovascular abnormalities. Radiographics 2007;27(5):1323–1334

Kirks DR. Practical Pediatric Imaging: Diagnostic Radiology of Infants and Children. 3rd ed. Philadelphia: Lippincott Williams & Wilkins; 1998

Case 155

Karen M. Ayotte

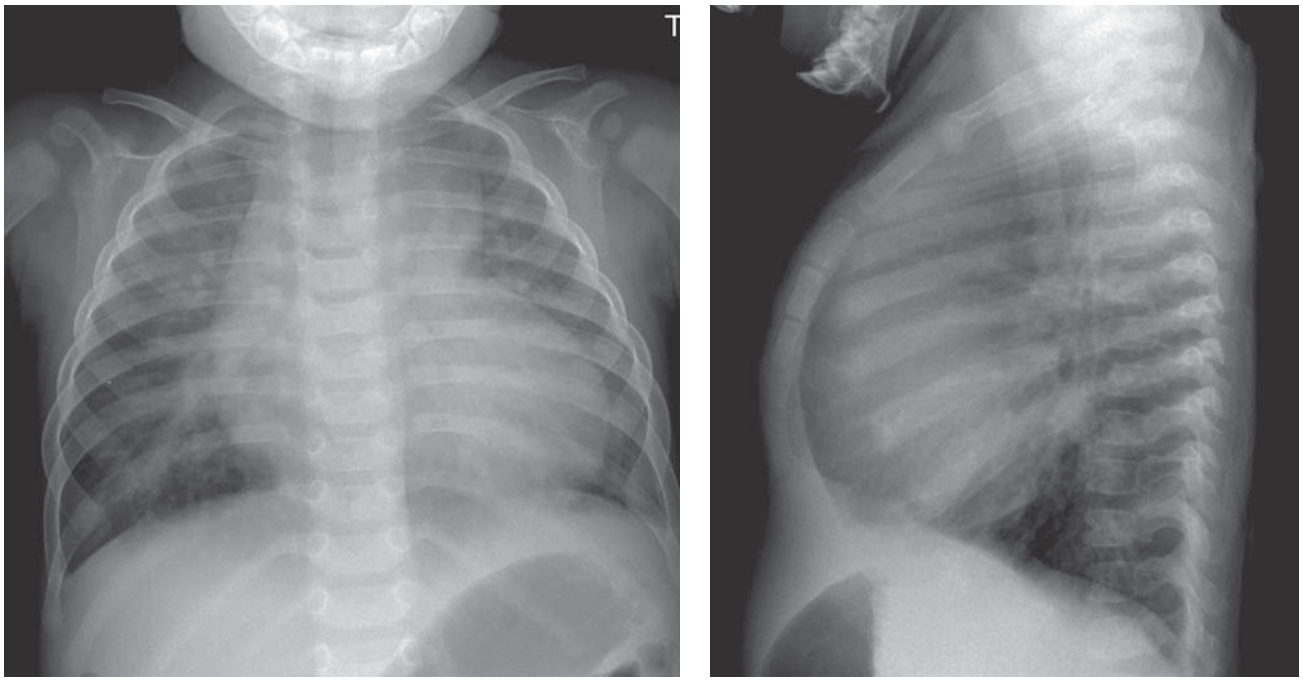


Fig. 155.1 **(A)** Frontal and **(B)** lateral chest radiographs demonstrate diffuse cardiomegaly, as well as increased and sharply defined pulmonary vascularity. The lungs are hyperexpanded, a common finding in patients with congenital heart disease.

Clinical Presentation

An acyanotic 6-month-old male infant presents with heart murmur (**Fig. 155.1**).

Key Imaging Finding

Shunt vascularity

Top 3 Differential Diagnoses

- **Ventricular septal defect (VSD).** VSD is the most common of the four differential considerations and the second most common congenital cardiac malformation after bicuspid aortic valve. Radiographic findings may be absent when the defect is small. Larger defects are associated with gross cardiomegaly; increased number and size of visualized, well-defined, "sharp" pulmonary vessels (i.e., shunt vascularity); an enlarged main pulmonary artery; and an enlarged left atrium. Pulmonary hyperinflation is a common associated finding. Patients typically present early in life with failure to thrive and a murmur on physical exam. As with any left-to-right shunt, if left undiagnosed or untreated, severe pulmonary hypertension may develop, with eventual reversal of flow across the shunt, referred to as Eisenmenger physiology.
- **Atrial septal defect (ASD).** As with VSD, radiographic findings may be absent with small atrial septal defects. Larger ASDs, in contrast, are associated with mild cardiomegaly, a normal to enlarged main pulmonary artery, and shunt vascularity. In contrast to an isolated VSD, the left atrium is not enlarged with an ASD. Patients with an ASD usually present at an older age than those with VSD due to the decreased flow across the shunt. Because ASDs are less evident clinically, they are also more likely to progress to more severe degrees of pulmonary hypertension at the time of presentation.
- **Patent ductus arteriosus (PDA).** The ductus arteriosus normally closes in the immediate perinatal period. Failure to close results in continued shunting of blood across the ductus. As an isolated lesion, PDA is commonly seen in premature infants. Radiographic findings include variable degrees of cardiomegaly and shunt vascularity. Over time, left atrial and left ventricular enlargement may develop. When associated with more complex congenital heart disease, patency of the ductus may be necessary for survival.

Additional Differential Diagnoses

- **Atrioventricular canal defect.** This defect is also commonly referred to as an endocardial cushion defect. The defect is characterized by failure of complete development of both the atrial and ventricular septa, as well as maldevelopment of the mitral and/or tricuspid valves. There is a strong association with trisomy 21 (nearly 50%). As with other left-to-right shunts, radiographic findings include cardiomegaly, pulmonary artery enlargement, and shunt vascularity.

Diagnosis

Atrioventricular canal defect

✓ Pearls

- VSD is the most common septal defect; larger lesions result in cardiomegaly and shunt vascularity.
- Patients with ASD typically present at a later age than those with VSD due to decreased flow across the shunt.
- PDA commonly occurs in premature infants, as well as in patients with complex congenital heart disease.
- Nearly half of all patients with an atrioventricular canal (endocardial cushion) defect have Down syndrome.

Suggested Readings

Donnelly LF. Fundamentals of Pediatric Radiology. Philadelphia: WB Saunders; 2001

Donnelly LF, Jones BV, O'Hara SM, et al. Diagnostic Imaging: Pediatrics. Salt Lake City, UT: Amirsys; 2005

Ferguson EC, Krishnamurthy R, Oldham SA. Classic imaging signs of congenital cardiovascular abnormalities. Radiographics 2007;27(5):1323–1334

Case 156

Rebecca Stein-Wexler

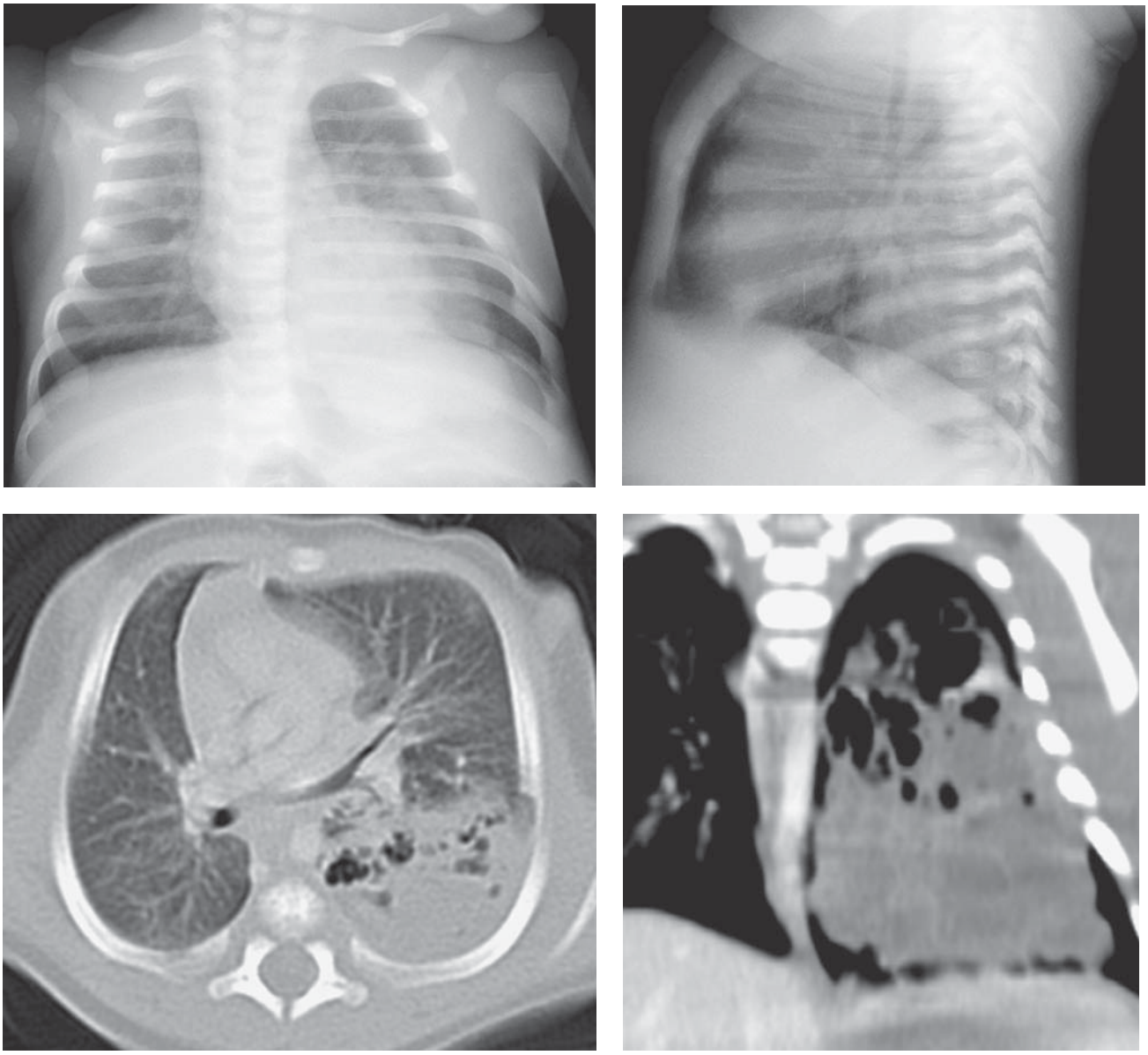


Fig. 156.1 **(A)** Frontal and **(B)** lateral radiographs of the chest demonstrate a large, solid-appearing mass in the left lower lobe. **(C)** Contrast-enhanced axial computed tomography image of the upper portion of the mass in the lung window reveals multiple small cysts (none >2 cm in diameter), as well as a large solid component. **(D)** The coronal reconstruction in the soft tissue window confirms the mixed solid/cystic nature of this lesion.

Clinical Presentation

A 4-week-old infant girl presents with respiratory distress (**Fig. 156.1**).

Key Imaging Finding

Solid pulmonary mass

Top 3 Differential Diagnoses

- **Round pneumonia.** Round pneumonia presents as a well-defined pulmonary opacity in children up to 8 years of age, most often in the superior segment of a lower lobe. Usually caused by *Streptococcus pneumoniae,* the inflammatory process is confined because collateral pathways of air flow are less developed. In the appropriate clinical setting, a follow-up chest radiograph is suggested to ensure resolution with antibiotic therapy.
- **Congenital cystic adenomatoid malformation (CCAM).** Part of the spectrum of bronchopulmonary foregut malformations, CCAM is often diagnosed in utero; older patients typically present with respiratory distress or recurrent pneumonia. CCAM consists of abnormal proliferation of respiratory elements that communicate with the tracheobronchial tree and is categorized as three types. In type I, the most common, cysts are ≥2 cm; type II features many smaller cysts and is associated with congenital anomalies; type III cysts are grossly solid but truly microcystic. In infants, the mass may appear solid or be unapparent; a solid or cystic mass is seen in older children. Computed tomography demonstrates air- or fluid-filled cysts or a solid lesion, depending on the type. Resection is generally recommended due to the increased risk of infection and malignancy.
- **Sequestration.** Sequestration is a congenital lesion consisting of dysplastic and nonfunctioning lung tissue with systemic arterial supply. The lesion connects with the tracheobronchial tree only when superinfected. It most often occurs in the left lower lobe. Frequently diagnosed in utero, sequestration can present with respiratory distress or pneumonia. Extralobar sequestration presents early in life, drains into the systemic venous system, and has its own pleural covering, whereas intralobar sequestration presents later in life with recurring infections, drains into the pulmonary venous system, and lacks a pleural covering. Both appear as a solid mass unless they contain areas of CCAM or have become superinfected, when tissue breakdown permits communication with the bronchial tree.

Additional Differential Diagnoses

- **Bronchogenic cyst.** This foregut duplication cyst typically presents as a solitary, discrete mediastinal mass, but it occasionally occurs in the medial aspect of the pulmonary parenchyma. It contains simple or complex fluid, and its wall is typically quite thin unless there has been superinfection. Mass effect on mediastinal structures causes dysphagia or respiratory distress; older children may complain of chest pain.
- **Plasma cell granuloma.** This rare, aggressive, primitive pleural-based or parenchymal neoplasm presents as a large soft tissue mass or as a lung cyst. It metastasizes to the central nervous system, bone, and liver. Associated pleural effusion is common, but chest wall invasion is rare. Childhood cancers are common in close relatives.

Diagnosis

Congenital cystic adenomatoid malformation, mixed types II and III

✓ Pearls

- Round pneumonia presents in children up to 8 years of age due to less developed collateral air flow.
- CCAMs communicate with the airway and are classified based on their cystic and/or solid makeup.
- Sequestrations have systemic arterial supply and are further classified according to venous drainage.
- Sequestrations occur most frequently in the lower lobes and are more common on the left.

Suggested Readings

Berrocal T, Madrid C, Novo S, Gutiérrez J, Arjonilla A, Gómez-León N. Congenital anomalies of the tracheobronchial tree, lung, and mediastinum: embryology, radiology, and pathology. Radiographics 2004;24(1):E17

Donnelly LF. Fundamentals of Pediatric Radiology. Philadelphia: WB Saunders; 2001

Donnelly LF, Jones BV, O'Hara SM, et al. Diagnostic Imaging: Pediatrics. Salt Lake City, UT: Amirsys; 2005

Case 157

William T. O'Brien Sr.

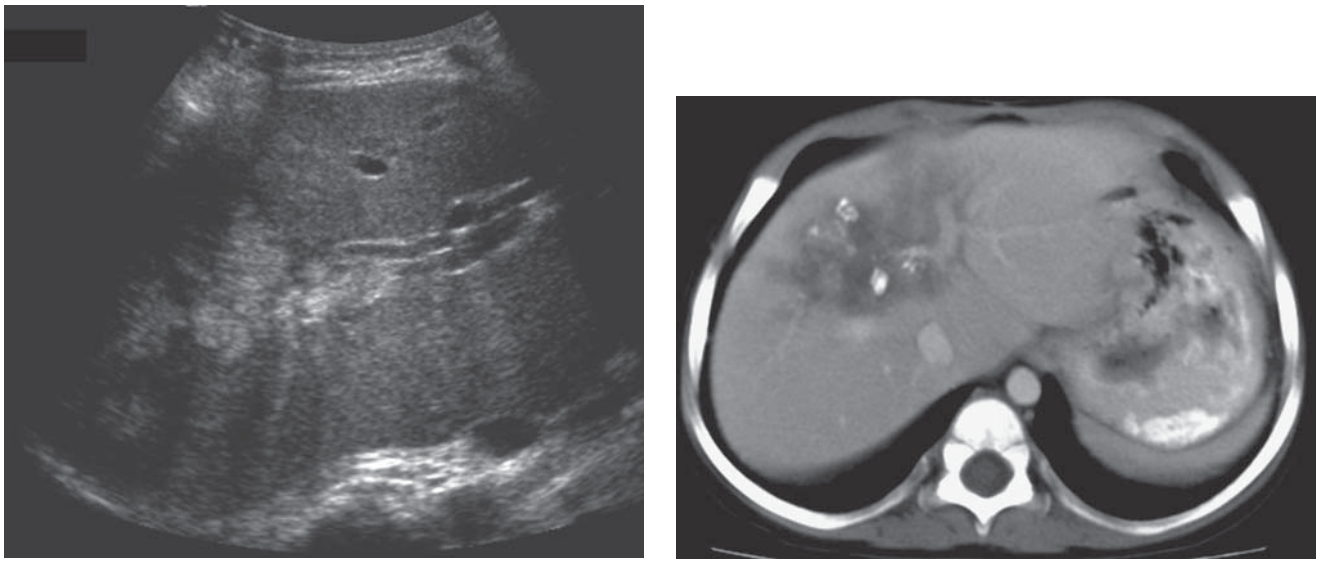


Fig. 157.1 **(A)** Sonographic image through the liver demonstrates a large, ill-defined hyperechoic mass within the right hepatic lobe with apparent extension into the right portal vein. **(B)** Contrast-enhanced axial computed tomography image reveals an ill-defined hypodense hepatic mass with regions of calcification and enhancement. (Courtesy of Children's Hospital and Research Center, Oakland, California.)

Clinical Presentation

A 14-month-old male infant presents with hepatomegaly on a physical exam (**Fig. 157.1**).

Key Imaging Finding

Liver mass in an infant

Top 3 Differential Diagnoses

- **Hepatoblastoma.** Hepatoblastoma is the most common primary hepatic neoplasm in infancy, with the vast majority of cases occurring within the first 3 years of life. Patients usually present with a painless abdominal mass. More than 90% of cases will have elevated levels of alpha fetoprotein, a useful discriminator. The lesions are typically large, solitary, heterogeneous, and well circumscribed, although they may also appear more ill-defined. Hepatoblastomas are hypodense on computed tomography (CT), with calcifications occurring in ~50% of cases. The calcifications are "chunky" in comparison to the fine or coarse calcifications of hemangioendothelioma. Solid components demonstrate slight enhancement. On ultrasound, hepatoblastomas demonstrate heterogeneous echotexture with regions of calcification.
- **Hemangioendothelioma.** Hemangioendothelioma is a vascular hepatic lesion that occurs in neonates, with ~90% of cases presenting within the first 6 months of life. When large, they can be associated with high-output cardiac failure from vascular shunting. The lesions are often large, heterogeneous, and hypodense to surrounding normal liver parenchyma on CT. Calcifications are common and are typically described as fine or coarse. Enhancement is the rule, although the pattern is variable, depending on the size and number of lesions. Vascular shunting may result in enlargement of the suprahepatic aorta and decreased caliber of the infrahepatic aorta.
- **Mesenchymal hamartoma.** Mesenchymal hamartomas are uncommon benign hepatic masses that typically present in infancy. The masses are typically large, well circumscribed, cystic, and multiloculated on imaging. Solid components, when present, result in an imaging appearance similar to hepatoblastoma or hemangioendothelioma.

Additional Differential Diagnoses

- **Metastases.** Neuroblastoma metastases typically arise from primary adrenal lesions, although they may also occur anywhere along the sympathetic chain. The metastatic foci are commonly heterogeneous secondary to hemorrhage and calcification. Metastatic foci from Wilms tumor are hypodense on CT.
- **Abscess.** Rarely, large abscesses may mimic primary hepatic lesions. As with abscesses in other regions, they are hypodense on CT and may demonstrate peripheral enhancement. The abscesses typically occur as a result of direct or hematogenous spread from the primary site of infection.
- **Hematoma.** Hepatic hematomas vary in size and appearance based on the mechanism and extent of trauma. They are hypodense to surrounding normal liver parenchyma on CT. Care should be taken to exclude areas of active extravasation of contrast. Follow-up imaging will show regression of the lesion.

Diagnosis

Hepatoblastoma

✓ Pearls

- Hepatoblastoma is the most common primary hepatic malignancy of infancy and has elevated alpha fetoprotein levels.
- Hemangioendotheliomas may be associated with vascular shunting and high-output cardiac failure.
- Mesenchymal hamartomas are multiloculated and cystic.
- Neuroblastoma and Wilms tumor are the most common malignancies to metastasize to the liver.

Suggested Readings

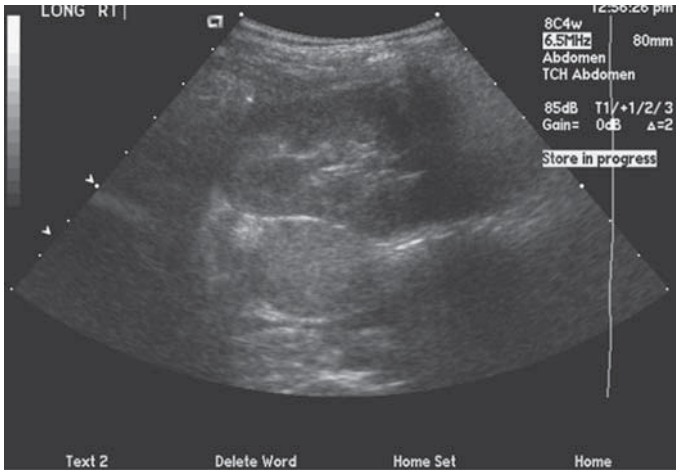
Donnelly LF. Fundamentals of Pediatric Radiology. Philadelphia: WB Saunders; 2001

Jabra AA, Fishman EK, Taylor GA. Hepatic masses in infants and children: CT evaluation. AJR Am J Roentgenol 1992;158(1):143–149

Woodward PJ, Sohaey R, Kennedy A, Koeller KK. From the *Archives of the AFIP:* a comprehensive review of fetal tumors with pathologic correlation. Radiographics 2005;25(1):215–242

Case 158

Karen M. Ayotte



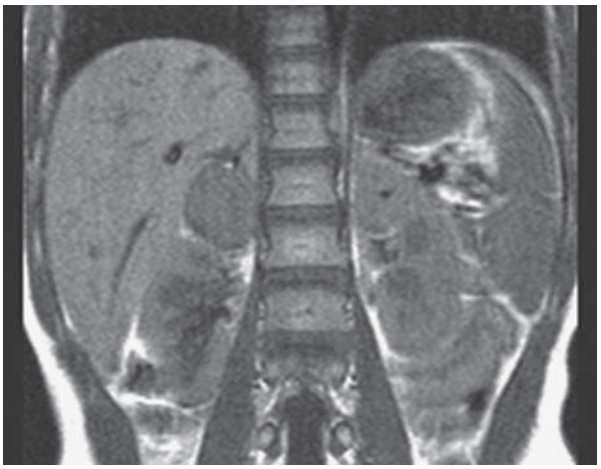




Fig. 158.1 **(A)** Longitudinal sonographic image through the right upper quadrant demonstrates a round, solid mass adjacent to the superior pole of the right kidney. **(B)** Coronal T1-weighted magnetic resonance (MR) image confirms a suprarenal location for the mass, which is slightly hypoechoic to normal renal parenchyma. **(C)** Axial T2-weighted MR image with fat suppression demonstrates that the lesion is heterogeneously hyperintense.

Clinical Presentation

A 9-year-old girl presents with hypertension (**Fig. 158.1**).

Key Imaging Finding

Suprarenal mass in a child

Top 3 Differential Diagnoses

- **Neuroblastoma.** Neuroblastoma is a malignant tumor of primitive neural crest cells. This tumor accounts for ~10% of all pediatric neoplasms. Average age at the time of diagnosis is ~2 years of age; nearly all cases are diagnosed by 10 years of age. This tumor can arise anywhere along the sympathetic chain, but it most commonly arises from the adrenal gland. Imaging features include an infiltrative soft tissue mass that commonly calcifies, engulfs rather than displaces vessels, and metastasizes to liver and bone.
- **Adrenal hemorrhage.** In the perinatal period, adrenal hemorrhage is a significantly more common etiology for a suprarenal mass than neuroblastoma. Classic imaging findings are a hypo- or anechoic, avascular suprarenal mass that decreases in volume on serial imaging studies. In the acute period, ultrasound features may be more complex but will resolve over time. Adrenal hemorrhage may be bilateral and is more common on the right than on the left. There should be no evidence of hepatic metastatic disease, as could be seen with perinatal neuroblastoma.
- **Pheochromocytoma.** Approximately 70% of pheochromocytomas arise from the adrenal gland. Although an unusual tumor in childhood, incidence is increased in patients with multiple endocrine neoplasia syndrome and von Hippel–Lindau syndrome. These tumors are usually meta-iodobenzylguanidine (MIBG) avid and are classically very bright on T2-weighted magnetic resonance images.

Additional Differential Diagnoses

- **Subdiaphragmatic sequestration.** Although far more common in the lower lobes, pulmonary sequestrations may rarely be subdiaphragmatic and suprarenal in location. Arterial supply is directly from the aorta, and venous drainage is typically systemic (extralobar variant).
- **Congenital adrenal hyperplasia (CAH).** CAH classically presents as bilateral adrenal enlargement, which may be diffuse or nodular. CAH is typically diagnosed clinically; laboratory evaluation is confirmatory.
- **Adrenocortical carcinoma.** Although rare tumors of childhood, adrenocortical carcinomas are more common than simple adenomas and are usually hormonally active. They are typically >5 cm in diameter at the time of presentation. Internal necrosis and calcification are common, yielding an irregular, heterogeneous mass.

Diagnosis

Pheochromocytoma

✓ Pearls

- Neuroblastoma is malignant, commonly calcifies, engulfs vessels, and metastasizes to liver and bone.
- Adrenal hemorrhages are common in the perinatal period and evolve (decrease in size) over time.
- Pediatric pheochromocytomas are most common in children with underlying syndromes.

Suggested Readings

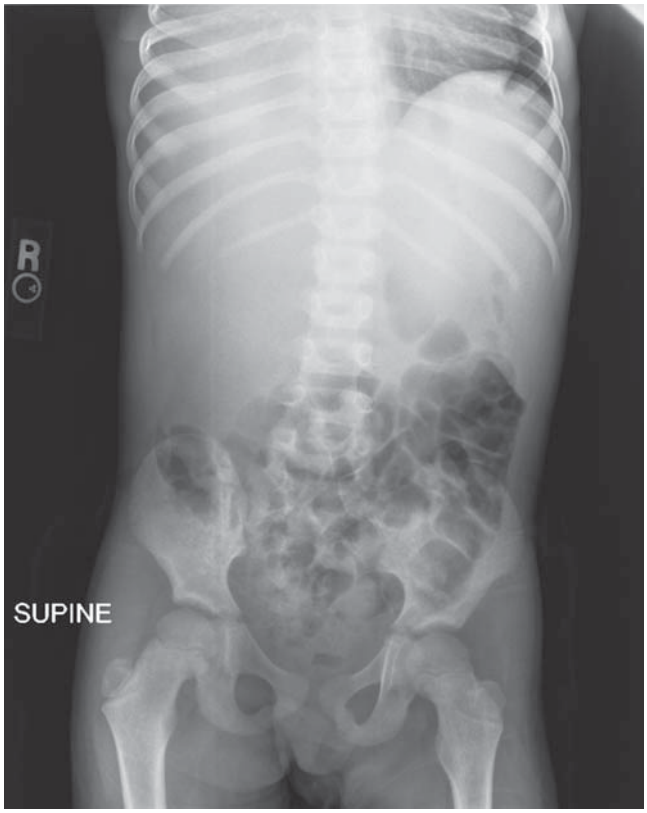
Donnelly LF, Jones BV, O'Hara SM, et al. Diagnostic Imaging: Pediatrics. Salt Lake City, UT: Amirsys; 2005

Kirks DR. Practical Pediatric Imaging: Diagnostic Radiology of Infants and Children. 3rd ed. Philadelphia: Lippincott Williams & Wilkins; 1998

Westra SJ, Zaninovic AC, Hall TR, Kangarloo H, Boechat MI. Imaging of the adrenal gland in children. Radiographics 1994;14(6):1323–1340

Case 159

John P. Lichtenberger III



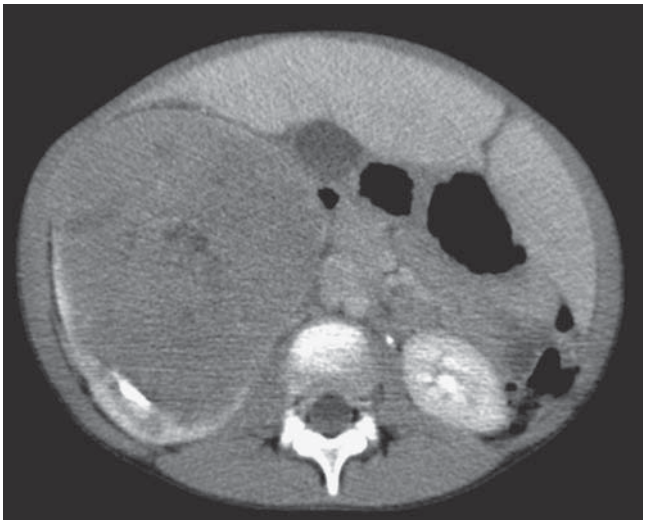


Fig. 159.1 **(A)** Frontal supine radiograph of the abdomen demonstrates a soft tissue mass within the right upper quadrant with inferior and leftward displacement of bowel loops. **(B)** Contrast-enhanced axial computed tomography image through the upper abdomen reveals a large, circumscribed solid mass originating from the right kidney. The "claw" sign confirms renal origin.

Clinical Presentation

A child presents with an asymptomatic abdominal mass on examination (**Fig. 159.1**).

Key Imaging Finding

Solid renal mass

Top 3 Differential Diagnoses

- **Wilms tumor.** Wilms tumor is the most common renal malignancy of childhood, with a peak incidence at 3 years of age. Patients often present with an abdominal mass revealed on physical examination. Wilms tumor is characteristically a well-defined, round mass arising from the renal cortex with local mass effect. The tumor generally enhances less than the surrounding renal parenchyma. Renal origin is confirmed on computed tomography by noting compressed renal parenchyma along the margin of the tumor, the "claw" sign. When large, these tumors may appear heterogeneous and partially cystic with internal necrosis and hemorrhage. Calcification is relatively uncommon. Intratumoral fat is extremely rare. Wilms tumor spreads locally through the ipsilateral renal vein, via lymphatics to local lymph nodes, and hematogenously to the liver, lungs, and bone. Associated syndromes include WAGR (Wilms tumor, aniridia, genital anomalies, and mental retardation) and Beckwith–Wiedemann syndrome. Staging is surgical.
- **Mesoblastic nephroma.** Mesoblastic nephroma is a hamartomatous solid tumor of the kidney and represents the most common solid renal mass in neonates. Mean age at the time of presentation is 2 months. Patients are typically asymptomatic other than an abdominal mass on exam. Hypercalcemia may occasionally be detected. Because mesoblastic nephroma is indistinguishable from Wilms tumor based on imaging, treatment is surgical.
- **Nephroblastomatosis.** Persistence of nephrogenic rests is termed nephroblastomatosis. These lesions typically present as bilateral, confluent, plaquelike, peripheral solid renal masses. Annual surveillance is required to exclude malignant degeneration to Wilms tumor.

Additional Differential Diagnoses

- **Lymphoma.** Although primary renal lymphoma is rare, secondary involvement is common. Patients may present with multiple bilateral homogeneous hypodense parenchymal masses (most common), a solitary renal mass, or diffuse infiltration of the renal parenchyma. Adjacent lymphadenopathy is a diagnostic clue.
- **Renal cell carcinoma (RCC).** RCC is rare in childhood, except in the setting of von Hippel–Lindau disease. Patients are typically older and often present with flank pain or hematuria. Imaging findings most commonly reveal a hypervascular renal mass. Calcification is seen in 25% of cases. RCC spreads locally through the ipsilateral renal vein, via lymphatics to local lymph nodes, and hematogenously to the liver, lungs, and bone.

Diagnosis

Wilms tumor

✓ Pearls

- Wilms tumor is the most common renal malignancy of childhood, with a peak incidence of 3 years of age.
- Wilms tumor may spread by direct extension (renal vein), lymphatic spread, or hematogenous spread.
- Mesoblastic nephroma is a benign hamartomatous lesion, with a peak incidence of 2 to 3 months of age.
- Nephroblastomatosis typically occurs bilaterally; patients are followed to exclude malignant degeneration.

Suggested Readings

Donnelly LF, Jones BV, O'Hara SM, et al. Diagnostic Imaging: Pediatrics. Salt Lake City, UT: Amirsys; 2005

Lonergan GJ, Martínez-León MI, Agrons GA, Montemarano H, Suarez ES. Nephrogenic rests, nephroblastomatosis, and associated lesions of the kidney. Radiographics 1998;18(4):947–968

Lowe LH, Isuani BH, Heller RM, et al. Pediatric renal masses: Wilms tumor and beyond. Radiographics 2000;20(6):1585–1603

Case 160

William T. O'Brien Sr.

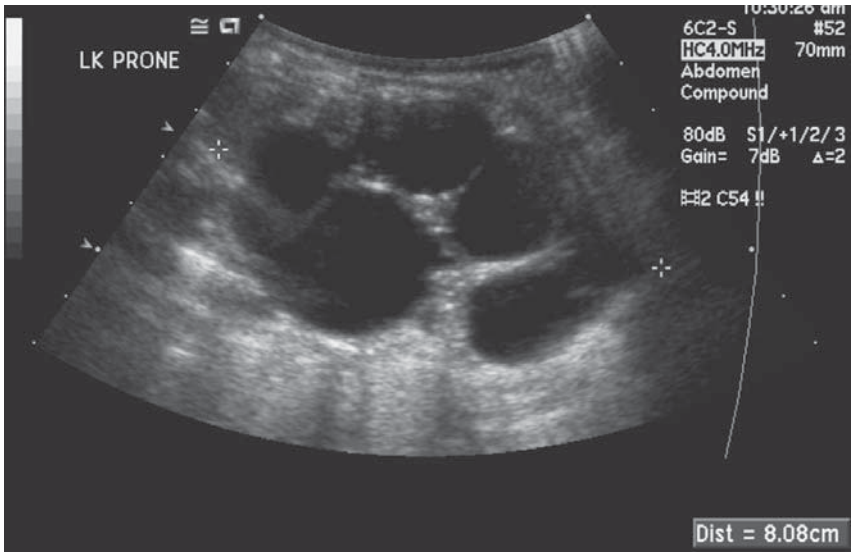


Fig. 160.1 Gray scale sonographic image through the left kidney demonstrates renal enlargement with multiple circumscribed anechoic lesions. The right kidney (not shown) was normal in imaging appearance. (Courtesy of Children's Hospital and Research Center, Oakland, California.)

Clinical Presentation

A 14-month-old boy presents with a left-sided palpable abdominal mass on a routine physical examination (**Fig. 160.1**).

Key Imaging Finding

Cystic renal lesion

Top 3 Differential Diagnoses

- **Hydronephrosis.** Hydronephrosis is the most common cause of a renal mass in a child. Unilateral disease is most commonly due to ureteropelvic junction (UPJ) obstruction or extrinsic compression on the ureter; bilateral hydronephrosis is usually due to bladder outlet obstruction (posterior urethral valves). On ultrasound, the cystic lesions will communicate centrally at the renal pelvis, a key distinguishing factor from other diagnostic entities.
- **Multicystic dysplastic kidney (MCDK).** MCDK is thought to result from an intrauterine obstruction of the fetal renal collecting system. Sonographic findings include multiple cysts of varying sizes that do not communicate with one another. The opposite kidney should be closely evaluated, as MCDK is associated with contralateral abnormalities, including UPJ obstruction.
- **Multilocular cystic nephroma (MLCN).** MLCN is a rare entity, with a bimodal age distribution that affects young boys and older women. Patients present with a multiloculated cystic renal mass that characteristically herniates into the renal pelvis/collecting system. The lesions are surgically resected.

Additional Differential Diagnoses

- **Cystic Wilms tumor.** Wilms tumor represents the most common childhood renal malignancy, with a peak incidence of 3 years of age. Patients typically present with a large, heterogeneous solid abdominal mass, but they may occasionally be cystic. Local spread includes the renal veins, inferior vena cava, and lymph nodes; distant metastases include the lungs and liver. Rarely, both kidneys may be involved. Unlike neuroblastoma, Wilms tumor displaces vessels rather than encasing them. Wilms tumor is typically sporadic but may be associated with hemihypertrophy syndromes.
- **Autosomal dominant polycystic kidney disease (ADPCKD).** ADPCKD usually presents in late adolescence or early adulthood with hypertension or hematuria. On imaging, the kidneys are enlarged with multiple bilateral cortical and medullary cysts of varying sizes. Cysts are also found in the liver and pancreas. Approximately 10% of patients will have associated intracranial berry aneurysms, which are prone to rupture.
- **Renal abscess.** Renal abscesses are rare but serious complications of urinary tract infections. They usually occur in children with chronic infections from persistent vesicoureteral reflux. Sonographic findings consist of an ill-defined region of decreased echotexture, usually at the corticomedullary junction.

Diagnosis

Multicystic dysplastic kidney

✓ Pearls

- Hydronephrosis is the most common cause of a renal mass in childhood.
- MCDK is thought to result from intrauterine obstruction; multiple noncommunicating cysts are seen.
- MLCN has a bimodal age distribution and characteristically herniates into the renal pelvis.
- Wilms tumor is the most common renal malignancy of childhood; it displaces rather than encases vessels.

Suggested Readings

Donnelly LF. Fundamentals of Pediatric Radiology. Philadelphia: WB Saunders; 2001

Donnelly LF, Jones BV, O'Hara SM, et al. Diagnostic Imaging: Pediatrics. Salt Lake City, UT: Amirsys; 2005

Lowe LH, Isuani BH, Heller RM, et al. Pediatric renal masses: Wilms tumor and beyond. Radiographics 2000;20(6):1585–1603

Case 161

Karen M. Ayotte

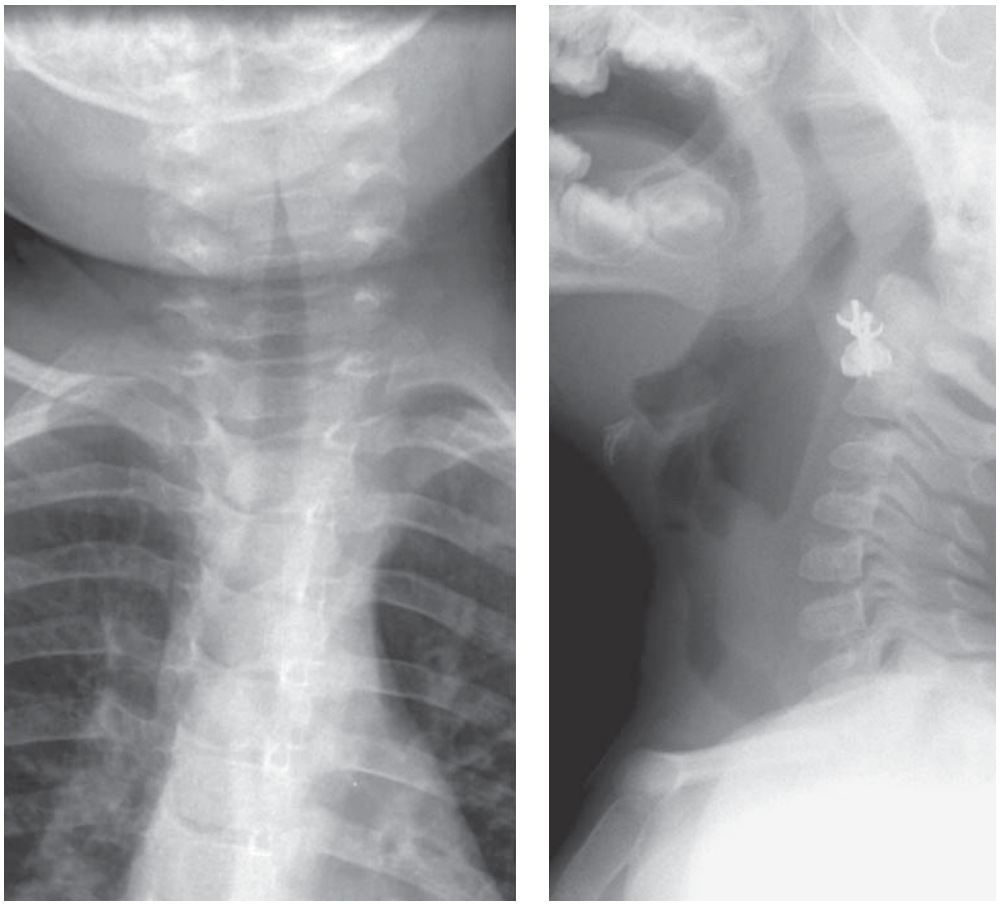


Fig. 161.1 **(A)** Frontal and **(B)** lateral radiographic views of the neck reveal subglottic airway narrowing with loss of the normal shouldering of the airway on the anteroposterior film, referred to as the "steeple" sign. The lateral view also demonstrates mild overdistention of the hypopharynx. The aryepiglottic folds and prevertebral soft tissue contours are normal. A metallic foreign body on the lateral view corresponds to an external earring.

Clinical Presentation

Toddler presents with stridor (**Fig. 161.1**).

Key Imaging Finding

Subglottic airway narrowing

Top 3 Differential Diagnoses

- **Laryngotracheobronchitis (croup).** Croup is the most common cause of upper airway obstruction in children between 6 months and 3 years of age, with a peak incidence around 1 year. The radiographic hallmark is subglottic airway narrowing manifested by loss of the normal shouldering of the upper airway on the frontal projection, referred to as the "steeple" sign. A lateral view will commonly demonstrate overdistention of the hypopharynx, as well as anteroposterior (AP) narrowing of the subglottic airway.
- **Epiglottitis.** Epiglottitis is potentially life-threatening. When the diagnosis is suspected, a provider capable of managing the child's airway should be immediately available during imaging. Visual inspection of the airway should be avoided, as it may precipitate airway compromise. On the lateral film, the radiographic hallmark is epiglottic enlargement (the "thumb" sign), as well as thickening of the aryepiglottic folds. The imaging appearance can mimic croup on an AP view. Croup and epiglottitis often coexist.
- **Retropharyngeal abscess.** Space-occupying processes in the prevertebral and retropharyngeal soft tissues may have mass effect on the airway, causing dyspnea and stridor. The differential diagnosis of widened prevertebral soft tissues includes abscess, hemorrhage, lymphadenopathy, and pseudothickening. If physiologic pseudothickening is suspected, a repeat inspiratory exam with the neck fully extended may resolve the dilemma. Airway fluoroscopy can also be used as a problem-solving tool in difficult cases.

Additional Differential Diagnoses

- **Bacterial tracheitis**. Bacterial tracheitis is characterized by exudative plaques that adhere to the tracheal walls. Because of their flat, longitudinal configuration, they may only be seen on one view. Associated subglottic airway narrowing may be similar to the radiographic appearance of croup. However, patients with bacterial tracheitis are typically older (6–10 years old). Adherent mucus in the airway is a common pitfall that mimics the plaques of bacterial tracheitis but should clear on repeat exam after coughing.
- **Aspirated foreign body.** Both aspirated and ingested foreign bodies may cause abnormal airway contours on radiographs, as well as present with dyspnea and stridor. Radiopaque foreign bodies are readily identified, whereas nonopaque foreign bodies are more problematic. Direct visualization may be necessary.
- **Hemangioma.** Hemangiomas tend to cause variably asymmetric airway narrowing and are commonly detected within the 1st year of age. When subglottic, the patient's symptoms may mimic other more common etiologies of stridor. On radiographs, asymmetric mass effect is noted narrowing the airway.

Diagnosis

Croup

✓ Pearls

- Croup is most common in children under 3 years of age; the "steeple" sign is seen on frontal radiographs.
- Epiglottitis is potentially life-threatening; lateral radiographs will show epiglottic thickening (the "thumb" sign).
- Retropharyngeal abscesses present with prevertebral soft tissue swelling.
- Foreign body aspiration must always be considered in a child with stridor.

Suggested Readings

Donnelly LF, Jones BV, O'Hara SM, et al. Diagnostic Imaging: Pediatrics. Salt Lake City, UT: Amirsys; 2005

Kirks DR. Practical Pediatric Imaging: Diagnostic Radiology of Infants and Children. 3rd ed. Philadelphia: Lippincott Williams & Wilkins; 1998

Case 162

Sandra L. Wootton-Gorges

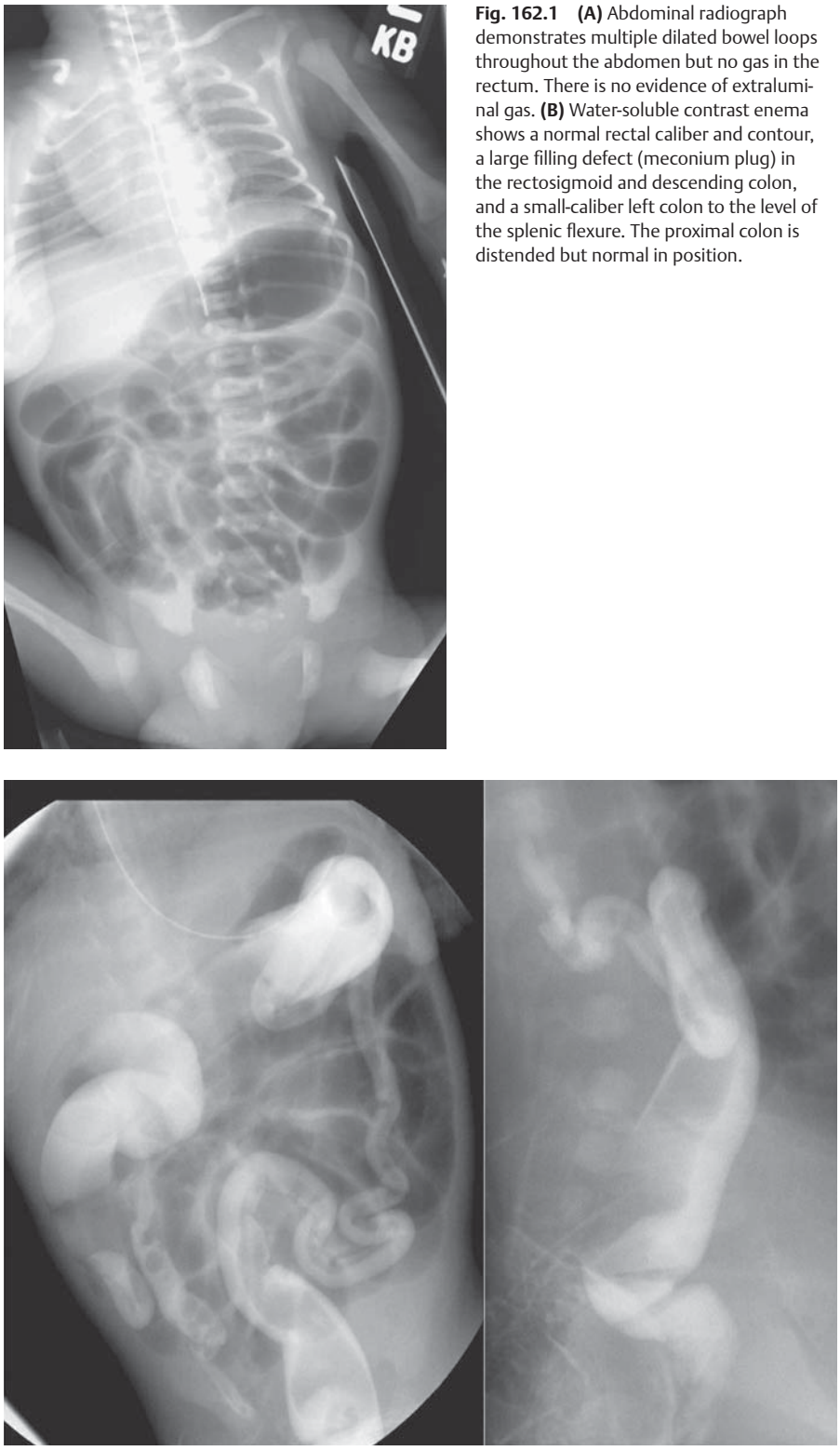


Fig. 162.1 **(A)** Abdominal radiograph demonstrates multiple dilated bowel loops throughout the abdomen but no gas in the rectum. There is no evidence of extraluminal gas. **(B)** Water-soluble contrast enema shows a normal rectal caliber and contour, a large filling defect (meconium plug) in the rectosigmoid and descending colon, and a small-caliber left colon to the level of the splenic flexure. The proximal colon is distended but normal in position.

Clinical Presentation

A 35-week gestational-age newborn boy presents with bilious residuals after feeding and abdominal distention. He has not passed meconium at 30 hours of age (**Fig. 162.1**).

Key Imaging Finding

Distal bowel obstruction pattern in a neonate

Top 3 Differential Diagnoses

- **Functional immaturity of the colon.** Functional immaturity includes small left colon and meconium plug syndrome. This common cause of low bowel obstruction is associated with prematurity, infants whose mothers received magnesium sulfate or opiates during labor, and infants of diabetic mothers. These infants present with failure to pass meconium, abdominal distention, and/or vomiting. Abdominal radiographs show diffuse bowel distention. Contrast enema defines a normal rectum and a meconium plug in the rectosigmoid colon. The left colon may be small in caliber to the splenic flexure. No organic obstruction is seen. The stooling pattern becomes normal after the contrast enema and passage of meconium.
- **Hirschsprung disease.** Hirschsprung disease results from failure of complete craniocaudal migration of intramural ganglion cells. The aganglionic segment cannot relax, resulting in a distal bowel obstruction. Symptoms may include constipation, abdominal distention, and/or bilious vomiting. About 2% of patients with Down syndrome have Hirschsprung disease. Kidney, ureter, and bladder (KUB) radiography shows a distal bowel obstruction pattern. A transition zone between the spastic and narrow distal colon and the dilated, more proximal colon is defined at contrast enema, usually in the rectosigmoid region. A rarer form of Hirschsprung disease affects the entire colon. Suction biopsy confirms the lack of ganglion cells below the transition zone.
- **Ileal atresia/stenosis.** Ileal atresia/stenosis probably results from a focal intrauterine ischemic injury. Neonates present with a low bowel obstruction pattern. Contrast enema is very helpful in defining the normally positioned microcolon, which results from colonic nonuse.

Additional Differential Diagnoses

- **Meconium ileus.** Meconium ileus may be the initial presenting symptom of cystic fibrosis. The tenacious meconium blocks the terminal ileum and right colon, resulting in a low bowel obstruction. KUB features may include a lack of air–fluid levels, as well as a bubbly stool pattern in the right lower quadrant. A contrast enema will define meconium pellets in the distal ileum and right colon, as well as a microcolon more distally. The water-soluble enema may be therapeutic (allowing meconium pellets to pass) as well as diagnostic.
- **Anal atresia/anorectal malformations.** Anal atresia is an important cause of low bowel obstruction in infants, but it is usually clinically evident. It is important to evaluate for associated renal and spinal cord anomalies in these babies.

Diagnosis

Functional immaturity of the colon

✓ Pearls

- Functional immaturity of the colon is associated with prematurity and infants of diabetic mothers.
- Hirschsprung disease is due to aganglionosis; the transition point is usually in the rectosigmoid region.
- Ileal atresia is thought to occur due to intrauterine ischemia; there is a microcolon as a result of nonuse.
- Meconium ileus occurs in cystic fibrosis; there are meconium pellets and a microcolon more distally.

Suggested Readings

Berrocal T, Lamas M, Gutiérrez J, Torres I, Prieto C, del Hoyo ML. Congenital anomalies of the small intestine, colon, and rectum. Radiographics 1999;19(5):1219–1236

Donnelly LF. Fundamentals of Pediatric Radiology. Philadelphia: WB Saunders; 2001

Donnelly LF, Jones BV, O'Hara SM, et al. Diagnostic Imaging: Pediatrics. Salt Lake City, UT: Amirsys; 2005

Case 163

Rebecca Stein-Wexler

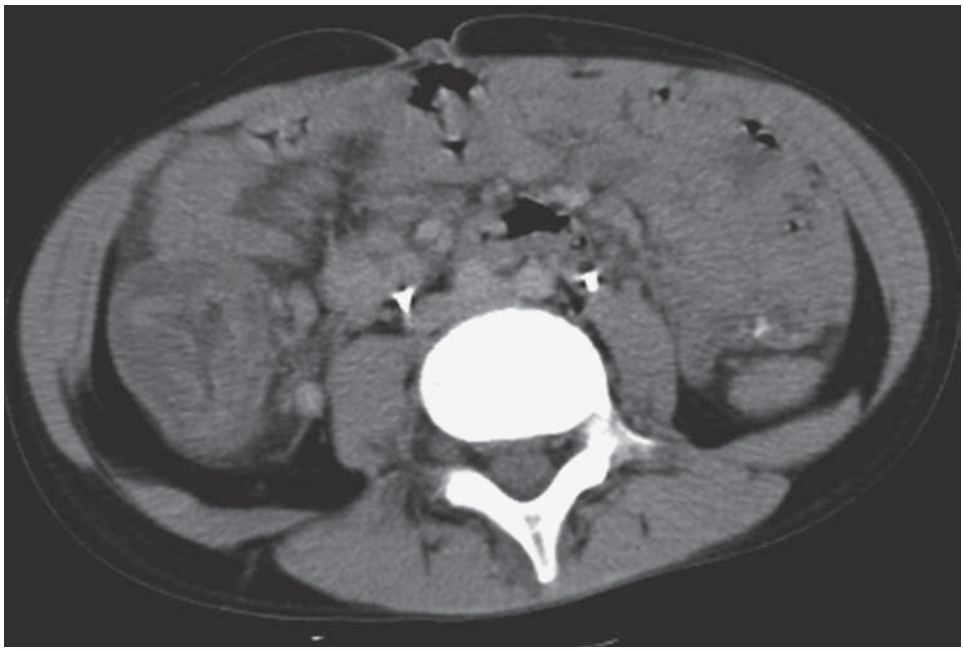


Fig. 163.1 Contrast-enhanced axial computed tomography image of the lower abdomen demonstrates circumferential, symmetric, marked thickening of the wall of the ascending colon. There is mild heterogeneous enhancement, as well as surrounding inflammation.

Clinical Presentation

A 12-year-old girl with a history of acute myelogenous leukemia, status post–bone marrow transplant, presents with fever and severe diarrhea (**Fig. 163.1**).

Key Imaging Finding

Bowel wall thickening in an immunocompromised child

Top 3 Differential Diagnoses

- **Pseudomembranous colitis.** Pseudomembranous colitis results from overgrowth of *Clostridium difficile* and usually occurs in patients receiving antibiotics. The wall of the entire colon is markedly thickened secondary to mucosal and submucosal edema that creates central hypodensity. Occasionally only the right colon is involved. The "accordion" sign results from oral contrast extending between pseudomembranes and edematous haustra. Pericolonic fat is relatively spared.
- **Neutropenic colitis/typhlitis.** This inflammatory and necrotizing colitis occurs in neutropenic children after chemotherapy and typically involves the entire right colon, although it can be limited to the cecum or include the terminal ileum. It is most common in those with acute leukemia and presents with fever, diarrhea, and tenderness. The classic appearance is circumferential, symmetric, massive mural thickening that is hypodense on unenhanced computed tomography (CT) and enhances heterogeneously. Pericolonic inflammatory stranding is common, and intramural pneumatosis can occur. Contrast enema is contraindicated due to the risk of perforation. Perforation and sepsis result in a high mortality rate of 40 to 50% in patients treated medically.
- **Graft-versus-host disease (GVHD).** GVHD occurs when marrow T lymphocytes damage recipient epithelial cells. Older children are at increased risk and typically present with diarrhea, hepatomegaly, ascites, and resultant abdominal distention. Mucosal ulceration and destruction occur, followed by replacement of mucosa with vascular granulation tissue. This results in the typical CT appearance of intense mucosal enhancement, along with dilatation affecting the entire small and large bowel. On small bowel follow-through (SBFT), the contrast-filled bowel has a "ribbonlike" appearance. Treatment consists of increased immunosuppression, and outcomes are usually good.

Additional Differential Diagnoses

- **Post-transplant lymphoproliferative disorder.** This disorder ranges from lymphoid hyperplasia to malignant proliferation and is associated with reactivation of Epstein–Barr virus in the setting of chronic immunosuppression. It typically occurs in recipients of organ transplants and results in circumferential bowel wall thickening, sometimes accompanied with aneurysmal dilatation. Lymphadenopathy, solid masses, and hepatosplenomegaly also occur. Early diagnosis and treatment are essential.
- **Shock bowel.** Shock bowel or hypoperfusion complex causes diffuse bowel wall enhancement and thickening, along with abnormally intense enhancement of solid organs. The bowel enhancement pattern is similar to GVHD, but shock bowel occurs with major trauma and usually spares the colon.

Diagnosis

Neutropenic colitis

✓ Pearls

- In the setting of severe colitis, contrast enema is contraindicated due to the risk of perforation.
- Pseudomembranous colitis is due to *C. difficile* overgrowth; the "accordion" sign may be seen on imaging.
- Neutropenic colitis occurs in immunosuppressed patients and most often involves the cecum/right colon.
- GVHD presents with intense mucosal enhancement on CT and a "ribbonlike" appearance on SBFT.

Suggested Readings

Donnelly LF. CT imaging of immunocompromised children with acute abdominal symptoms. AJR Am J Roentgenol 1996;167(4):909–913

Donnelly LF, Jones BV, O'Hara SM, et al. Diagnostic Imaging: Pediatrics. Salt Lake City, UT: Amirsys; 2005

Case 164

John P. Lichtenberger III

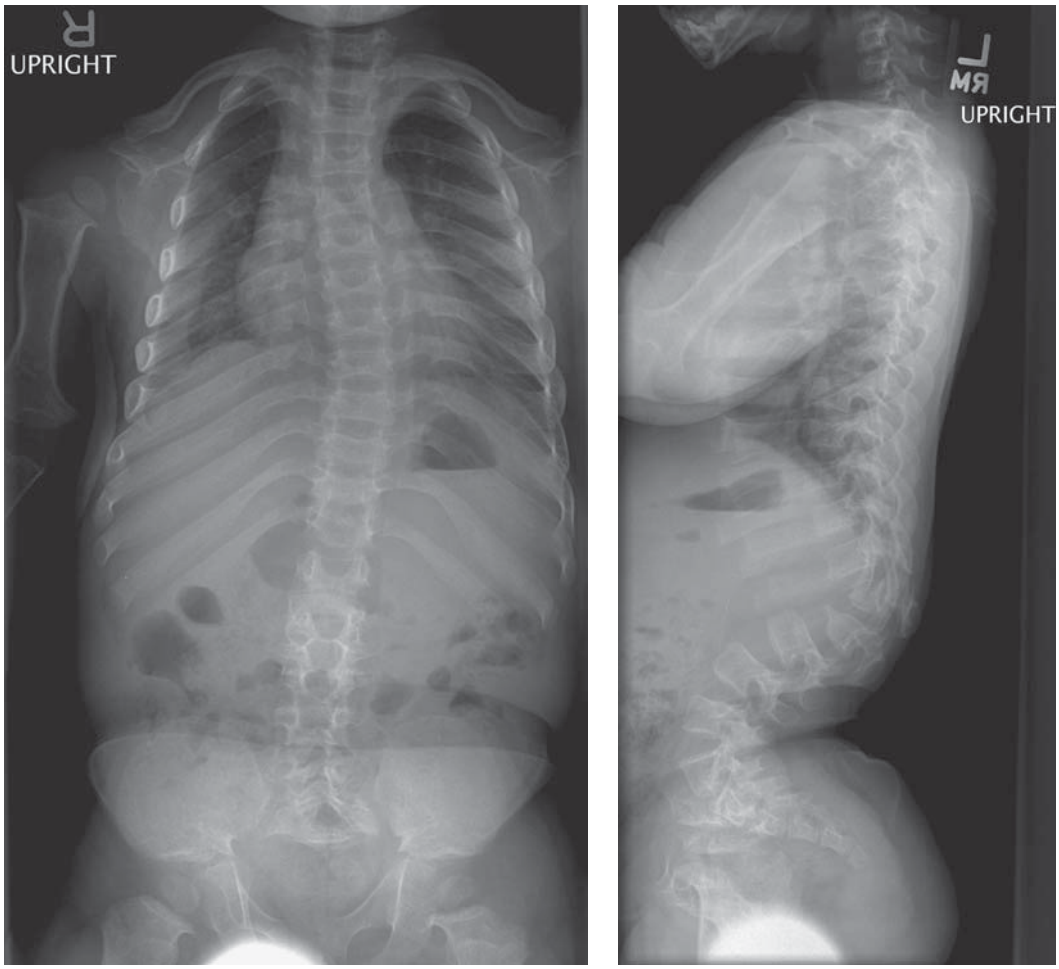


Fig. 164.1 **(A)** Frontal radiograph of the chest and abdomen demonstrates rhizomelic limb shortening (right humerus), thickened and shortened ribs, abnormal pelvic configuration with "tombstone" iliac bones secondary to decreased acetabular angles and a "champagne glass" pelvic inlet, and decreased interpediculate distances involving the lower lumbar spine. **(B)** Lateral radiograph of the thoracolumbar spine reveals posterior vertebral body scalloping, anterior beaking, and gibbus deformities.

Clinical Presentation

Patient presents with growth and skeletal abnormalities (**Fig. 164.1**).

Key Imaging Finding

Skeletal dysplasia

Top 3 Differential Diagnoses

- **Achondroplasia.** The most common nonlethal skeletal dysplasia, achondroplasia is an autosomal dominant disease characterized by skeletal abnormalities attributable to decreased cartilage matrix production and endochondral ossification. Rhizomelic (proximal) limb shortening, metaphyseal flaring, and decreased interpediculate distance within the lower lumbar spine are common findings. Shortened iliac bones with decreased acetabular angles have been described as having a "tombstone" appearance, and the inner pelvic contour has a "champagne glass" configuration. The small skull base and foramen magnum may result in brainstem compression. Spine anomalies result in varying degrees of spinal stenosis. Hypochondroplasia is a less severe form of achondroplasia in which findings may be mild and limited to the spine.
- **Thanatophoric dysplasia.** Thanatophoric dysplasia is a skeletal dysplasia characterized by rhizomelic (proximal) limb shortening and represents the most common lethal dysplasia. Distinguishing radiographic features include shortened ribs resulting in a narrow thorax and poor ventilation, platyspondyly, and small iliac bones. Abnormal bowing and shortening of the femora result in a characteristic "telephone receiver" appearance. This entity is uniformly fatal in the neonatal period.
- **Jeune syndrome.** In Jeune syndrome, also known as asphyxiating thoracic dysplasia, the thorax is long and bell-shaped with short horizontal ribs and flared anterior ends. This configuration results in early respiratory compromise. Although not always present, dysplastic acetabula resembling an upside down trident are characteristic of this syndrome. There is associated acromelic (distal) limb shortening.

Additional Differential Diagnoses

- **Ellis–van Creveld syndrome.** Although hair, nail, and teeth abnormalities are clinical hallmarks of this syndrome (also known as chondroectodermal dysplasia), radiographic features include acromelic (distal) limb shortening, shortened ribs, cone-shaped epiphyses, and postaxial polydactyly. Congenital heart disease is the major cause of morbidity.
- **Chondrodysplasia punctata.** Chondrodysplasia punctata is a skeletal dysplasia that is characterized by rhizomelic (proximal) limb shortening and multifocal epiphyseal stippling.

Diagnosis

Achondroplasia

✓ Pearls

- Achondroplasia is the most common nonlethal skeletal dysplasia; it is autosomal dominant and rhizomelic.
- Achondroplasia has decreased interpediculate distance, "champagne glass" pelvis, and "tombstone" iliacs.
- Thanatophoric dysplasia is uniformly fatal and reveals platyspondyly and "telephone receiver" femora.
- Jeune syndrome (asphyxiating thoracic dysplasia) presents with a bell-shaped thorax and trident acetabula.

Suggested Readings

Donnelly LF. Fundamentals of Pediatric Radiology. Philadelphia: WB Saunders; 2001

Donnelly LF, Jones BV, O'Hara SM, et al. Diagnostic Imaging: Pediatrics. Salt Lake City, UT: Amirsys; 2005

Glass RBJ, Norton KI, Mitre SA, Kang E. Pediatric ribs: a spectrum of abnormalities. Radiographics 2002;22(1):87–104

Case 165

Karen M. Ayotte

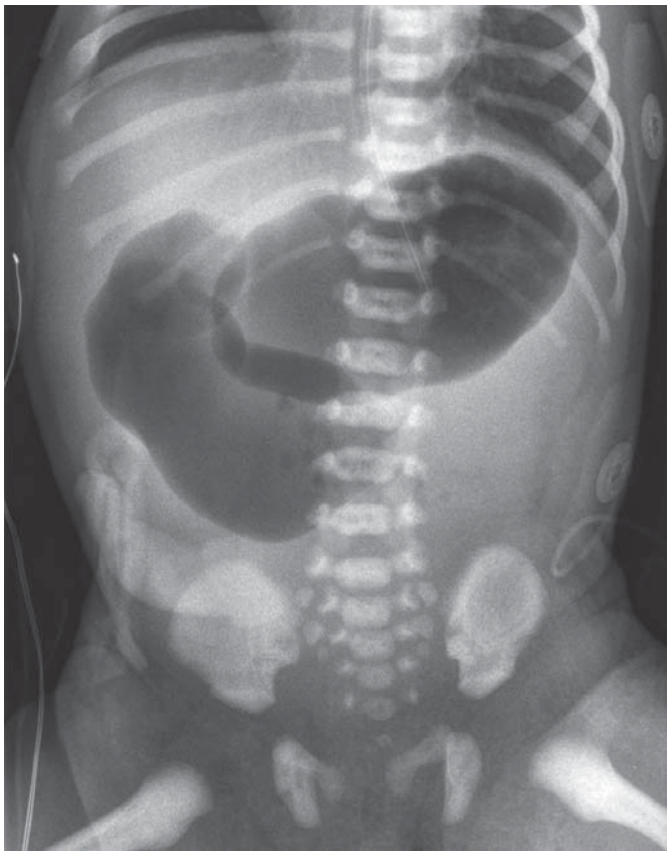


Fig. 165.1 Frontal radiograph of the abdomen demonstrates high-grade obstruction of the duodenum with a "double bubble" configuration of the proximal duodenum and stomach. No definite bowel gas is seen distal to the level of the obstruction. An enteric tube tip is noted within the stomach. (Courtesy of Children's Hospital and Research Center, Oakland, California.)

Clinical Presentation

A newborn presents with bilious emesis (**Fig. 165.1**).

Key Imaging Finding

"Double bubble" sign

Top 3 Differential Diagnoses

- **Malrotation with midgut volvulus.** A patient with midgut volvulus has a surgical emergency. When the diagnosis is suggested, expedited work-up is mandatory to minimize morbidity and mortality. The classic plain film appearance is partial, high-grade duodenal obstruction. The classic clinical scenario is an infant in the 1st week or month of life with bilious emesis. The spectrum of radiographic and clinical findings in this diagnosis, however, is variable. Patients with malrotation with midgut volvulus may have abdominal film findings ranging from normal to complete duodenal obstruction, mimicking duodenal atresia. An upper gastrointestinal (GI) examination is needed to confirm the course of the duodenum and positioning of the ligament of Treitz.
- **Duodenal atresia/stenosis.** Both duodenal atresia and duodenal stenosis result from a failure of recanalization of the duodenum, either partial (stenosis) or complete (atresia). The classic radiographic presentation is the "double bubble" sign. In patients with complete atresia, there will be no gas distal to the dilated duodenum. Clinical presentation is vomiting in the first hours of life. Eighty percent of patients will have bilious emesis, although obstruction proximal to the ampulla of Vater will present with nonbilious emesis. The degree of duodenal dilation is usually marked, implying long-standing obstruction of the duodenum. There is an increased incidence of associated abnormalities, including a 30% incidence of Down syndrome in infants with duodenal atresia.
- **Annular pancreas.** Annular pancreas usually coexists with duodenal atresia or stenosis. Annular pancreas may present in infancy with duodenal obstruction or be more occult and present in adulthood with chronic nausea and vomiting. Cross-sectional imaging shows a soft tissue mass contiguous with the pancreas, encircling the duodenum. An upper GI examination typically shows circumferential narrowing of the second portion of the duodenum.

Additional Differential Diagnoses

- **Duodenal web.** The severity of obstruction from intraluminal duodenal webs is variable, and the clinical presentation may occur well into adulthood. When there is severe obstruction, however, radiographic differentiation from other causes of duodenal obstruction in an infant may be difficult. Upper GI examination may show circumferential narrowing of the duodenum or a variable-sized aperture, allowing a restricted amount of contrast material to pass distally. Over time, the web may be stretched, leading to a "windsock" appearance.
- **Preduodenal portal vein.** A preduodenal portal vein may cause obstruction of the duodenum, but it is usually not the sole contributor. When found, a search for associated anomalies, including malrotation, should continue.

Diagnosis

Duodenal atresia

✓ Pearls

- Malrotation with midgut volvulus is a surgical emergency requiring immediate diagnosis and intervention.
- An upper GI exam is performed to confirm the course of the duodenum and the position of the ligament of Treitz.
- Duodenal atresia classically presents with the "double bubble" sign; 30% of patients have Down syndrome.
- Annular pancreas results in circumferential narrowing of the second portion of the duodenum.

Suggested Readings

Berrocal T, Torres I, Gutiérrez J, Prieto C, del Hoyo ML, Lamas M. Congenital anomalies of the upper gastrointestinal tract. Radiographics 1999;19(4):855–872

Donnelly LF, Jones BV, O'Hara SM, et al. Diagnostic Imaging: Pediatrics. Salt Lake City, UT: Amirsys; 2005

Kirks DR. Practical Pediatric Imaging: Diagnostic Radiology of Infants and Children. 3rd ed. Philadelphia: Lippincott Williams & Wilkins; 1998

Case 166

Karen M. Ayotte

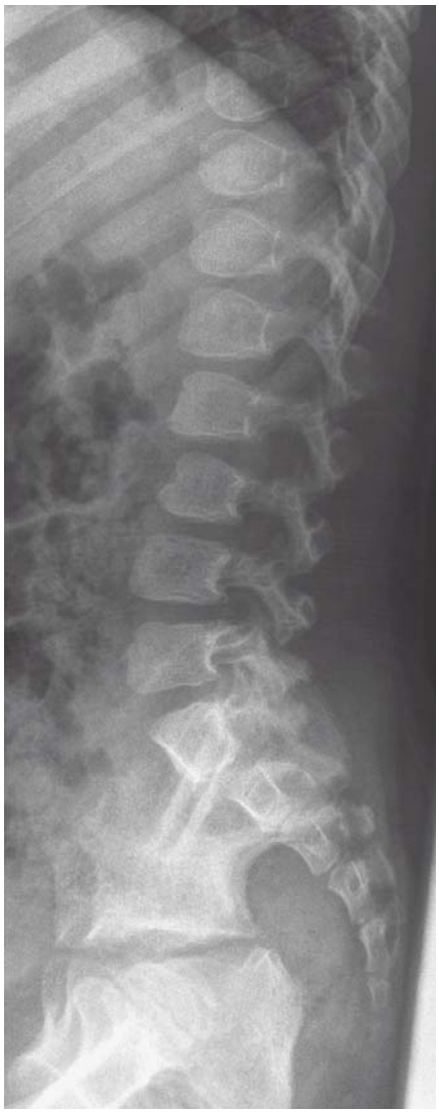


Fig. 166.1 Lateral lumbar spine plain film demonstrates exaggerated concavity of the posterior vertebral bodies (vertebral scalloping), most pronounced from L3 to L5. There is also vertebral beaking of the inferior end plate of L3.

Clinical Presentation

A child presents with hepatosplenomegaly and coarse facial features (**Fig. 166.1**).

Key Imaging Finding

Posterior vertebral body scalloping

Top 3 Differential Diagnoses

- **Dural ectasia.** Dural ectasia refers to enlargement or widening of the dural sac. Common causes are connective tissue disorders, such as Marfan and Ehlers–Danlos syndromes, and neurofibromatosis (NF). The widened dura results in increased pressure along the posterior aspect of the vertebral bodies with resultant posterior vertebral body scalloping. In patients with NF, masses such as neurofibromas and thoracic meningoceles may also cause posterior vertebral body scalloping. Marfan and Ehlers–Danlos patients are prone to additional abnormalities with connective tissues, such as aneurysm formation. Patients with NF will have cutaneous and neurologic manifestations of the disease.
- **Mucopolysaccharidosis.** Mucopolysaccharidoses are inherited disorders due to deficiencies in lysosomal enzymes necessary to break down certain complex carbohydrates. This results in excessive accumulation and deposition of mucopolysaccharides. Patients often present with short stature, craniofacial abnormalities, and mental retardation. There are multiple variants of mucopolysaccharidosis, with Hurler and Morquio syndromes representing common subtypes. Both Hurler and Morquio syndromes are associated with diffuse posterior vertebral scalloping, although the pathologic mechanism of this finding is not known. Hurler syndrome also demonstrates anterior beaking of the inferior aspect of the vertebral body, and Morquio syndrome demonstrates anterior beaking within the midportion of the vertebral body. An enlarged, J-shaped sella is classically seen with Hurler syndrome.
- **Dwarfism/achondroplasia.** Achondroplasia is a common form of dwarfism that is transmitted in an autosomal dominant fashion. Radiographic findings include a large skull with narrow foramen magnum, spinal stenosis, posterior vertebral body scalloping, squared iliac wings, decreased interpedicular distance as one moves caudally in the lumbar spine, flattened acetabula, short metacarpals, and short ribs. Posterior vertebral body scalloping is a common feature and is believed to be an adaptive response to congenital spinal stenosis. The identification of additional findings as above (especially narrowing of the interpedicular distance) and clinical correlation allow for correct diagnosis. Posterior scalloping is also associated with metatropic dwarfism and osteogenesis imperfecta.

Additional Differential Diagnoses

- **Spinal cord tumor.** Spinal cord tumors may cause increased pressure within the spinal canal, resulting in compensatory posterior vertebral body scalloping. The level of the vertebral scalloping typically corresponds to the location of the tumor. Common primary spinal cord tumors are ependymomas (most common primary cord tumors in adults), astrocytomas (most common spinal cord tumors in children), lipomas, dermoids, and epidermoid cysts.
- **Normal variant.** When mild and not associated with other skeletal abnormalities, posterior vertebral body scalloping may be a normal variant. Patients typically are followed after other causes are excluded.

Diagnosis

Mucopolysaccharidosis (Hurler syndrome)

✓ Pearls

- Dural ectasia with posterior vertebral body scalloping may be seen with connective tissue disorders and NF.
- Mucopolysaccharidosis (Hurler and Morquio syndromes) presents with posterior scalloping and anterior beaking of the vertebral body.
- Achondroplasia demonstrates squared iliac bones, flat acetabula, and decreased interpedicular distance.
- Mild posterior vertebral body scalloping may be a normal developmental variant.

Suggested Readings

Kirks DR. Practical Pediatric Imaging: Diagnostic Radiology of Infants and Children. 3rd ed. Philadelphia: Lippincott Williams & Wilkins; 1998

Wakely SL. The posterior vertebral scalloping sign. Radiology 2006;239:607–609

Case 167

Sandra L. Wootton-Gorges

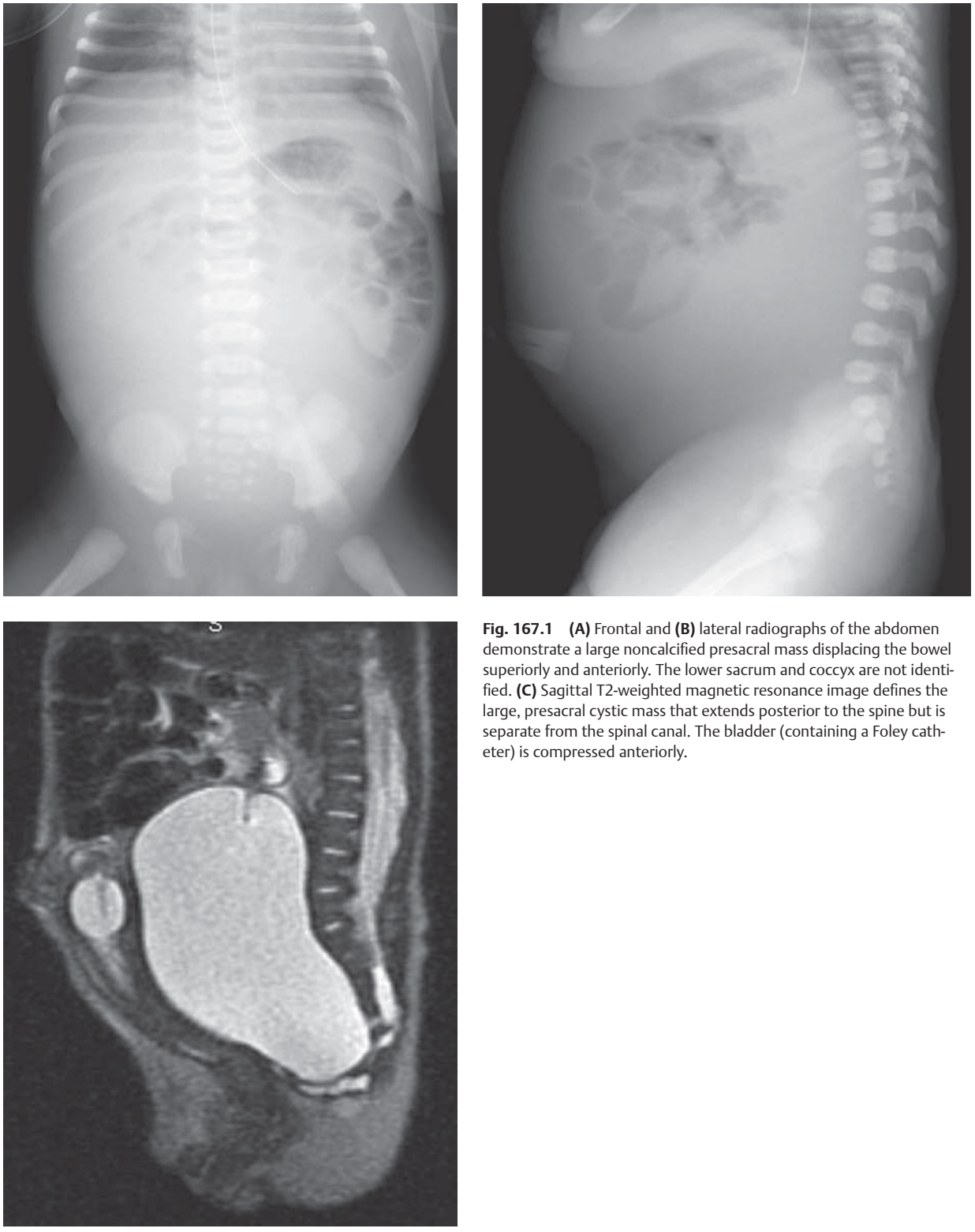


Fig. 167.1 **(A)** Frontal and **(B)** lateral radiographs of the abdomen demonstrate a large noncalcified presacral mass displacing the bowel superiorly and anteriorly. The lower sacrum and coccyx are not identified. **(C)** Sagittal T2-weighted magnetic resonance image defines the large, presacral cystic mass that extends posterior to the spine but is separate from the spinal canal. The bladder (containing a Foley catheter) is compressed anteriorly.

Clinical Presentation

A term female infant presents with a distended abdomen (**Fig. 167.1**).

Key Imaging Finding

Presacral mass

Top 3 Differential Diagnoses

- **Sacrococcygeal teratoma.** Sacrococcygeal teratomas (SCTs) are rare tumors that arise from multipotential cells and contain all three germ layers. SCTs are the most common tumors of the caudal region in infants. They may be extrapelvic, intrapelvic, or both. Most are benign at birth, but beyond the neonatal period the risk of malignancy increases. Cystic lesions are more often benign. Radiographs show the soft tissue mass. Calcifications are seen in 60% and vary in their appearance. The sonographic, computed tomography (CT), and magnetic resonance imaging (MRI) appearance is typically heterogeneous and varies based on the tumor composition—solid versus cystic, fatty or calcified components, and so on. MRI demonstrates the extent of the lesions, as well as intraspinal extension.
- **Anterior meningocele.** Anterior sacral meningoceles (ASMs) are rare herniations of cerebrospinal fluid (CSF)–distended meninges through a sacral foramen or defect. MRI is the best modality to define the lesion, but CT may be useful to demonstrate the bony defect. ASMs may be associated with genitourinary and/or anorectal malformations, as well as neurofibromatosis type 1. They may also occur as part of the Currarino triad: anorectal malformation, sacral osseous defect (scimitar sacrum), and presacral mass.
- **Rectal duplication cyst.** Rectal duplication cysts account for 5% of enteric duplication cysts. They are spherical, thin-walled, uni- or multilocular cystic lesions that may communicate with the rectal lumen. Pathologically, they contain smooth muscle in the wall and have a rectal mucosal lining.

Additional Differential Diagnoses

- **Lymphangioma.** Macrocystic lymphangiomas are fluid-filled lymphatic spaces resulting from malconnection of lymphatic vessels with the central lymphatic system. They appear as thin-walled, uni-or multilocular cystic masses with enhancing walls and septa.
- **Germ cell tumor.** Dermoid cysts are developmental lesions that may rarely occur in the presacral region. They are cystic masses containing mucoid fluid, calcification, and fatty tissue. Associated malformations include anorectal and osseous defects as part of the Currarino triad.
- **Adnexal mass.** Ovarian cysts are common in neonatal girls and can be very large. They result from maternal hormonal stimulation of the ovarian follicles. Ultrasound confirms the ovarian location of the cyst. Cysts >6 cm are at risk of torsion.

Diagnosis

Sacrococcygeal teratoma

✓ Pearls

- SCTs are the most common caudal region tumor in infants; appearance varies based on composition.
- SCTs may be intrapelvic, extrapelvic, or both; they may also demonstrate intraspinal extension.
- ASMs are CSF herniations through neural foramina or bony defects; they may have associated anomalies.
- Ovarian cysts are relatively common in neonatal girls; larger lesions are at risk of ovarian torsion.

Suggested Readings

Donnelly LF, Jones BV, O'Hara SM, et al. Diagnostic Imaging: Pediatrics. Salt Lake City, UT: Amirsys; 2005

Kocaoglu M, Frush DP. Pediatric presacral masses. Radiographics 2006;26(3):833–857

Case 168

Karen M. Ayotte

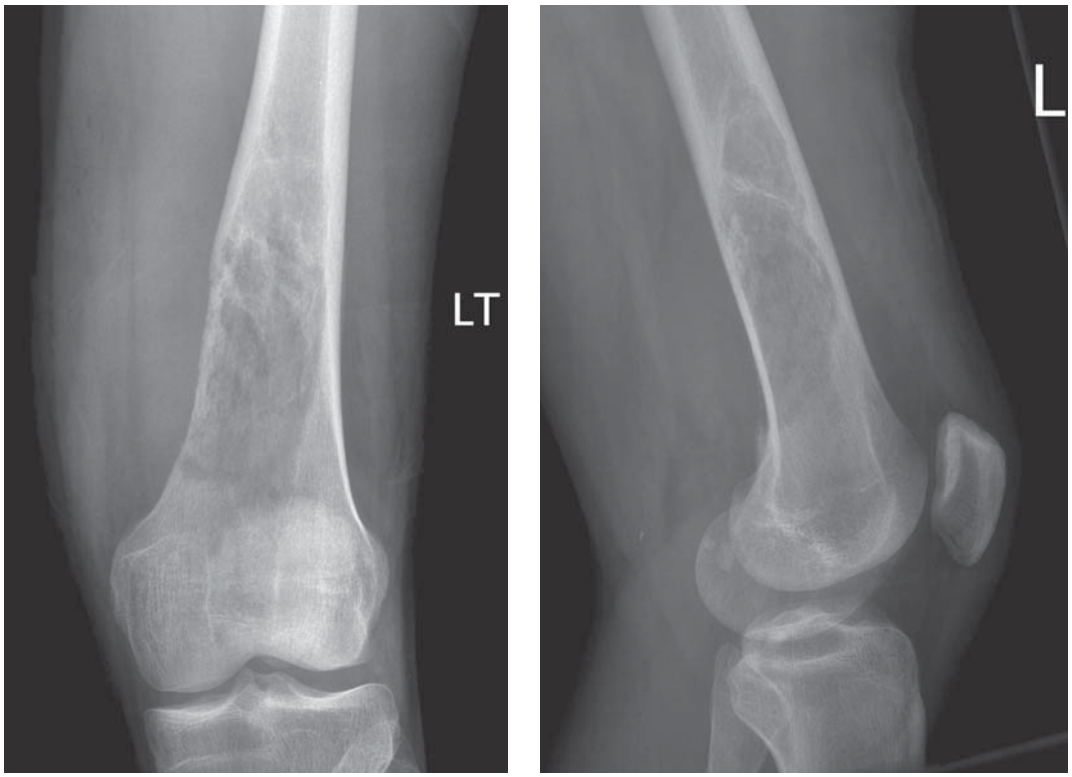


Fig. 168.1 **(A)** Frontal and **(B)** lateral radiographs of the knee demonstrate a mixed, predominantly lytic expansile lesion centered in the metadiaphysis of the distal femur. The superior and inferior margins, in particular, are not well defined, resulting in a wide zone of transition. There is cortical irregularity medially, as well as endosteal scalloping anteriorly. Subtle areas of calcification are seen outside the normal confines of the distal femur. There is also a suggestion of a soft tissue mass posteriorly.

Clinical Presentation

A college athlete presents with increasing knee pain (**Fig. 168.1**).

Key Imaging Finding

Long bone aggressive lesion

Top 3 Differential Diagnoses

- **Osteosarcoma.** Osteosarcoma is the most common primary bone malignancy of childhood, with a peak incidence between 10 and 20 years of age. The classic description is an aggressive lesion in the metaphysis of a long bone demonstrating abnormal new bone proliferation. In highly aggressive lesions, however, the appearance can be predominantly lytic. Magnetic resonance imaging (MRI) is useful for detection of "skip" lesions locally. Nuclear medicine bone scan (or positron emission tomography/computed tomography [CT]) is best suited during the initial work-up for detection of metastatic foci.
- **Ewing sarcoma.** Ewing sarcoma is the second most common primary bone malignancy of childhood, with a peak incidence between 10 and 15 years of age. The classic description is that of a lytic, medullary based metadiaphyseal lesion in a long bone with aggressive periosteal reaction. Associated large soft tissue masses are common. Despite this classic description, Ewing sarcomas range from purely lytic to predominantly sclerotic. Long bone lesions are more common in younger patients, and flat bone origin is seen more commonly in adolescents and young adults. Patients often present with pain, and constitutional symptoms such as fever are common. MRI is critical for local staging.
- **Osteomyelitis.** Osteomyelitis has such a wide spectrum of plain film appearances (including normal) that it is difficult if not impossible to conclusively exclude osteomyelitis. As such, the clinical history of fever or recent infection is helpful but not specific. Common radiologic findings of osteomyelitis, when present, include lytic lesions with varying degrees of aggressive features, resorption of bone, subcutaneous gas, and/or visualization of a sclerotic nidus. The degree of sclerosis within and about the lesion is variable depending on the age and overall health of the patient, organism, and duration of infection. CT and MRI examinations may add specificity when the clinical diagnosis is in doubt.

Additional Differential Diagnoses

- **Langerhans cell histiocytosis (LCH).** LCH may present as solitary or multifocal lytic bone lesions. The radiographic appearance is notoriously variable; therefore, LCH is a reasonable diagnostic consideration for nearly any bone lesion, benign or aggressive, in a patient under the age of 30.
- **Metastases.** Secondary malignancies commonly affect bones as a result of hematogenous dissemination. Leukemia is the most common entity to affect long bones in pediatric patients. Other common neoplasms that metastasize to bone are neuroblastoma and lymphoma. Metastatic foci typically present as lytic foci with a permeative or "moth-eaten" appearance.

Diagnosis

Osteosarcoma

✓ Pearls

- Osteosarcoma most often presents as an aggressive metaphyseal long bone lesion with bone proliferation.
- Ewing sarcoma presents as a lytic medullary lesion with aggressive periosteal reaction.
- Osteomyelitis has a wide variety of imaging appearances; a history of fever is helpful but not specific.
- Bone scan is useful to evaluate for metastases, multifocal lesions, or skip lesions as seen in osteosarcoma.

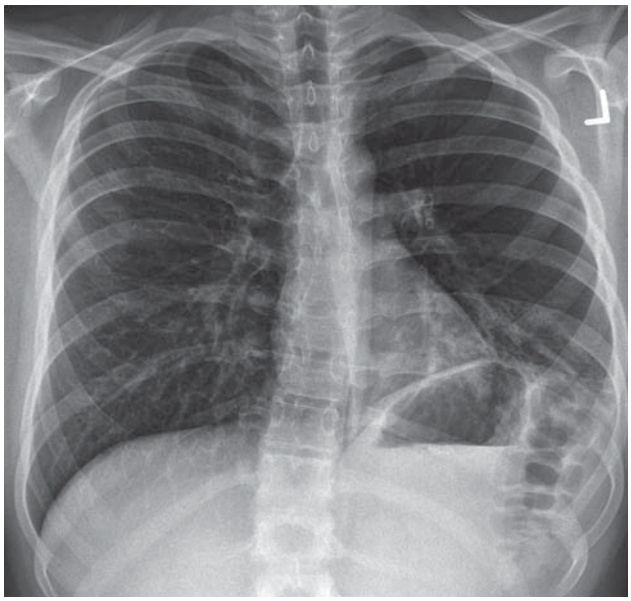
Suggested Readings

Donnelly LF, Jones BV, O'Hara SM, et al. Diagnostic Imaging: Pediatrics. Salt Lake City, UT: Amirsys; 2005

Kirks DR. Practical Pediatric Imaging: Diagnostic Radiology of Infants and Children. 3rd ed. Philadelphia: Lippincott Williams & Wilkins; 1998

Case 169

Arvind Sonik



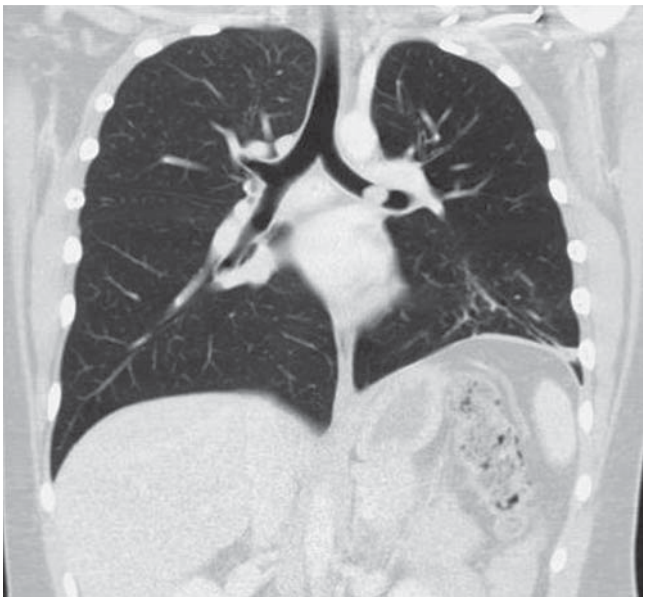




Fig. 169.1 **(A)** Frontal chest radiograph demonstrates atelectasis at the left lung base with associated volume loss within the left lung. **(B)** Coronal computed tomography images in the lung window and **(C)** volume rendering reveal an endobronchial lesion within the left mainstem bronchus. (Courtesy of Children's Hospital and Research Center, Oakland, California.)

Clinical Presentation

An 8-year-old boy presents with a chronic cough and wheezing (**Fig. 169.1**).

Key Imaging Finding

Endobronchial lesion in a child

Top 3 Differential Diagnoses

- **Foreign body.** Foreign body aspiration typically occurs in children 1 to 3 years of age. One should maintain a high index of suspicion for foreign body aspiration because it is often unwitnessed, and symptoms can mimic asthma and infection. Radiopaque foreign bodies are readily identified with plain radiographs. However, the majority of foreign bodies are not radiopaque, and food products such as nuts are the most common. Decubitus views, forced expiratory radiographs, and fluoroscopy may be useful to demonstrate air trapping secondary to a ball-valve mechanism. In equivocal cases, computed tomography (CT) may be useful.
- **Papilloma.** Benign tumors of the tracheobronchial tree are relatively uncommon. Squamous cell papillomas are the most common benign neoplasm of the tracheobronchial tree and can be solitary or multiple. The multiple form is known as juvenile laryngotracheal papillomatosis and is associated with infection with human papilloma virus types 6 and 11. Solitary lesions occur more commonly in adults and are associated with smoking. Lesions in the distal airways may cavitate.
- **Carcinoid tumor.** Approximately 80% of endobronchial neoplasms in children and adolescents are carcinoid tumors. Carcinoid tumors typically occur in the mainstem and lobar bronchi. They avidly enhance on CT and may have endobronchial, mural, and extrabronchial components. They are usually ovoid with a long axis that parallels the bronchovascular bundle.

Additional Differential Diagnoses

- **Inflammatory polyp.** Fibroepithelial polyps usually occur in the larger airways. They may be secondary to an irritant or inflammatory process, such as a foreign body, infection, or inhaled toxin. They often will regress when the causative factor is removed.
- **Salivary gland neoplasm.** Salivary gland tumors are rare endobronchial lesions. These tumors, such as adenoid cystic carcinoma and mucoepidermoid carcinoma, are usually malignant when they occur in the lung. Although pleomorphic adenoma is the most common subtype to occur within the salivary glands, it is an extremely rare, benign endobronchial neoplasm that occurs more often in adults.

Diagnosis

Carcinoid tumor

✓ Pearls

- Endobronchial lesions may present acutely or insidiously, mimicking asthma or persistent pneumonia.
- Decubitus views, expiratory views, and fluoroscopy may aid in detecting nonradiopaque foreign bodies.
- Papillomas are the most common benign neoplasms of the tracheobronchial tree; they may be multiple.
- Carcinoid tumors avidly enhance; they may have endobronchial, mural, and extrabronchial components.

Suggested Readings

Koj M, Jung JI, Park SH, et al. Benign tumors of the tracheobronchial tree: CT-pathologic correlation. AJR Am J Roentgenol 2006;186(5):1304–1313

Yedururi S, Guillerman RP, Chung T, et al. Multimodality imaging of tracheobronchial disorders in children. Radiographics 2008;28(3):E29

Case 170

Arvind Sonik



Fig. 170.1 Frontal radiograph of the bilateral lower extremities demonstrates significant symmetric elongation and flaring of the femoral and tibia metaphyses, resulting in Erlenmeyer flask deformities. Intermedullary rods and screws are noted within both tibias.

Clinical Presentation

A 17-year-old girl presents with alignment abnormality of the lower extremities (**Fig. 170.1**).

Key Imaging Finding

Erlenmeyer flask deformity

Top 3 Differential Diagnoses

- **Osteopetrosis.** Osteopetrosis is an inherited disorder caused by a failure of osteoclast function; this results in an accumulation of primary spongiosa in the medullary spaces. In addition to an Erlenmeyer flask deformity, findings are increased bone density, bone-in-bone appearance, "rugger jersey" spine, and alternating dense and lucent metaphyseal bands. Complications include fractures and anemia.
- **Fibrous dysplasia.** Fibrous dysplasia may be monostotic or polyostotic. Lesions typically arise in the central part of the bone, are expansile, and rarely involve the epiphysis or articular ends. The density of lesions is variable due to different degrees of osseous and fibrous tissue, but the classic lesion has a "ground-glass" matrix. Pathologic fractures are the most common complication. The polyostotic form of the disorder is more aggressive and often affects one side of the body. Associated disorders are McCune–Albright (precocious puberty and café au lait spots) and Mazabraud syndromes (intramuscular myxomas).
- **Gaucher disease.** Gaucher disease is a rare, heritable metabolic disorder caused by a deficiency of a lysosomal enzyme. The deficiency leads to an accumulation of glucosylceramide in cells of the reticuloendothelial system that infiltrate marrow spaces. Plain radiographs demonstrate osteopenia, medullary expansion, and remodeling. Complications are bone infarcts, avascular necrosis, and pathologic fractures. Magnetic resonance imaging may be useful in determining the extent of marrow infiltration. Infiltrating cells have a signal similar to hematopoietic marrow.

Additional Differential Diagnoses

- **Hemoglobinopathy.** The most common hemoglobinopathies are sickle cell disease and the thalassemias. Bony changes in these conditions are due to hyperplasia of the marrow and vascular occlusion. Marrow hyperplasia results in osteopenia, "hair on end" appearance of the skull, and remodeling. Vascular occlusion results in avascular necrosis, bone infarcts, and dactylitis. Growth disturbance may result from involvement of the physis.
- **Multiple hereditary exostoses.** Osteochondromatosis is an autosomal dominant dysplasia. As with solitary lesions, the cortex of the lesions is continuous with the underlying bone. Lesions that cause the Erlenmeyer flask deformity tend to be sessile rather than pedunculated. Common complications are growth disturbances, pain due to compression or neurovascular bundles, and, rarely, malignant transformation.

Diagnosis

Diagnosis unknown; the patient was lost to follow-up.

✓ Pearls

- Osteopetrosis results from failure of osteoclast function, resulting in dense but fragile bones.
- Fibrous dysplasia may be monostotic or polyostotic; the classic lesion has a ground-glass matrix.
- Hemoglobinopathies (sickle cell disease and thalassemias) result in bony changes with marrow hyperplasia.
- Sessile lesions associated with multiple hereditary exostoses result in the Erlenmeyer flask deformity.

Suggested Readings

Greenspan A. Orthopedic Imaging. 4th ed. Philadelphia: Lippincott Williams & Wilkins; 2004

States LJ. Imaging of metabolic bone disease and marrow disorders in children. Radiol Clin North Am 2001;39(4):749–772

Weissleder R, Wittenberg J, Harisinghani MG. Primer of Diagnostic Imaging. 4th ed. Philadelphia: Mosby; 2007

Case 171

Karen M. Ayotte

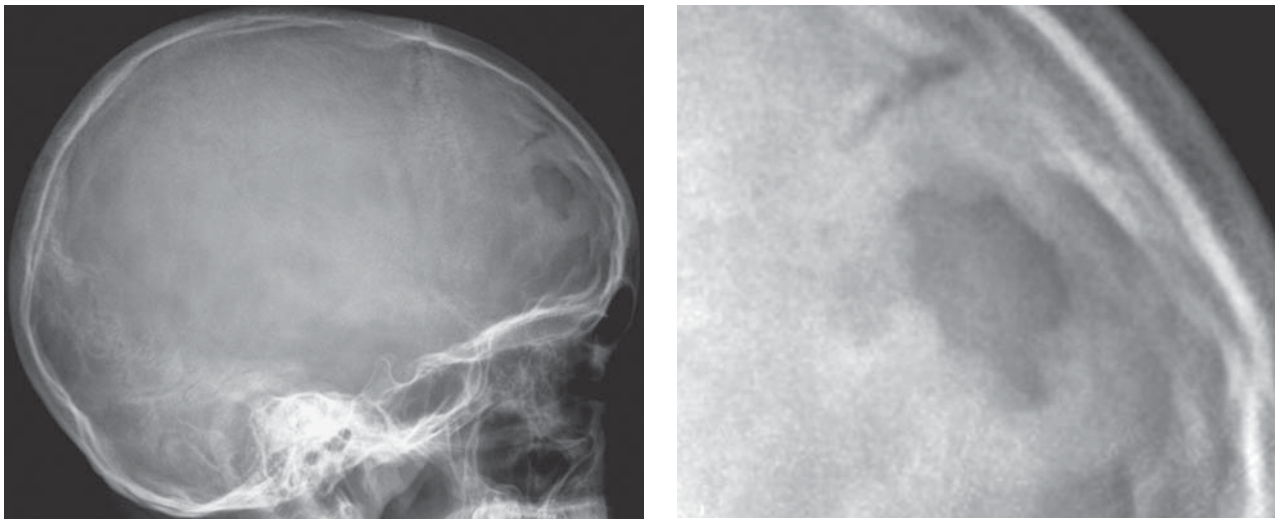


Fig. 171.1 **(A)** Lateral plain film of the skull with **(B)** coned-down image over the frontal bone demonstrates a solitary lytic lesion with well-defined borders but no sclerotic margins. There is no gross soft tissue component by plain film. The superior and posteroinferior margins demonstrate a "beveled edge" appearance.

Clinical Presentation

A 9-year-old boy presents with a headache (**Fig. 171.1**).

Key Imaging Finding

Lytic skull lesion in a child

Top 3 Differential Diagnoses

- **Langerhans cell histiocytosis (LCH).** The skull is the most common location for osseous involvement in LCH. The classic radiologic description is a well-defined lytic lesion without sclerotic borders. A "beveled edge" appearance can result from greater involvement of the inner than outer table of the skull. LCH may also present as a round, radiolucent skull defect with a central dense nidus or sequestrum of intact bone, referred to as a "button sequestrum." The most common clinical symptoms are pain, a palpable mass, and systemic symptoms.
- **Epidermoid cyst.** Epidermoid cysts result from abnormal deposition of epithelial rests within the diploic space during development. One pathologic survey reported epidermoid cysts as the second most common etiology for solitary skull lesions leading to biopsy in the pediatric population. When an epidermoid cyst involves the diploic space, plain film appearance may overlap that of LCH. Epidermoid cysts are generally well-defined expansile lesions without a central matrix. They may or may not have a sclerotic rim.
- **Neoplasm.** Leukemia, Ewing sarcoma, and metastatic neuroblastoma can each produce poorly defined osteolytic lucencies in all bones, including the skull. Metastatic deposits in the skull cause lytic destruction and expansion. Localized areas of bone destruction in leukemia are frequently surrounded by normal bone and likely represent tumor metastases. These lesions tend to have an aggressive appearance.

Additional Differential Diagnoses

- **Infection.** Osteomyelitis has a wide range of imaging manifestations, including a normal appearance to an appearance that mimics an aggressive neoplasm. Bone destruction from osteomyelitis can result in lytic skull lesions, often with poorly defined, infiltrating margins. There may be overlying soft tissue edema. Subacute and chronic infections may present radiographically as a round, radiolucent skull defect with a central dense nidus or sequestrum of intact bone, referred to as a "button sequestrum."
- **Leptomeningeal cyst.** The term *leptomeningeal cyst* (growing skull fracture) signifies a well-defined bone defect that arises when traumatic laceration of the dura exposes the bone to the pulsations of the cerebrospinal fluid (CSF) within the subarachnoid space. Pulsatile pressure erosion gradually widens the fracture line. Leptomeningeal cysts are an uncommon complication of skull fractures (0.6%) and are most common in children younger than 3 years of age.

Diagnosis

Langerhans cell histiocytosis

✓ Pearls

- LCH classically presents as a lytic skull lesion with nonsclerotic, beveled margins.
- LCH and osteomyelitis can have "button sequestra" and systemic symptoms.
- Common metastatic lesions to the skull in children are neuroblastoma and leukemia.
- A leptomeningeal cyst (growing skull fracture) is caused by CSF pulsations from disruption of the dura.

Suggested Readings

Gibson SE, Prayson RA. Primary skull lesions in the pediatric population: a 25-year experience. Arch Pathol Lab Med 2007;131(5):761–766

Glass RBJ, Fernbach SK, Norton KI, Choi PS, Naidich TP. The infant skull: a vault of information. Radiographics 2004;24(2):507–522

Kirks DR. Practical Pediatric Imaging: Diagnostic Radiology of Infants and Children. 3rd ed. Philadelphia: Lippincott Williams & Wilkins; 1998

Krasnokutsky MV. The button sequestrum sign. Radiology 2005;236(3):1026–1027

Case 172

Rebecca Stein-Wexler



Fig. 172.1 Frontal radiograph of the pelvis demonstrates flattening, sclerosis, and fragmentation of the left femoral head epiphysis with a linear subchondral lucency. There is also widening and shortening of the left femoral neck.

Clinical Presentation

A 9-year-old boy presents with a limp (**Fig. 172.1**).

Key Imaging Finding

Avascular necrosis (AVN) of the femoral head

Top 3 Differential Diagnoses

- **Legg–Calvé–Perthes (LCP) disease.** LCP disease occurs in children between 3 and 12 years of age and is more common in boys. About 20% of cases are bilateral. Patients typically present with a limp, no history of trauma, and decreased range of motion. Necrosis of the femoral head results from impaired epiphyseal blood supply across the physis, which is most vulnerable between the ages of 5 and 7. Magnetic resonance imaging (MRI) allows the earliest detection, demonstrating linear hypointensity on coronal T1-weighted images; in more advanced cases, T2-weighted sequences permit assessment of articular cartilage. Initial radiographs may show thinning of the subchondral plate, effusion, and a relatively dense epiphysis. The epiphysis then becomes more dense and inhomogeneous, demonstrating fragmentation and subchondral fractures; cystic change occurs in the metaphysis. In the reparative stage, normal bone replaces sclerotic bone, and the femoral head appears less heterogeneous. Finally, the femoral head contour becomes smoother. Femoral head contour and congruence between the femoral head and the acetabulum determine the long-term prognosis.
- **Traumatic injury.** Traumatic injury to the fragile blood vessels that traverse the physis can result in femoral head ischemia and subsequent AVN. This can result from a specific episode of trauma or from reduction of a dislocated hip. In the latter setting, the risk for AVN may be proportional to the degree of abduction.
- **Sickle cell disease.** Sickled erythrocytes occlude vessels, and subsequent hypoxemia further increases vascular distortion, exacerbating the resultant ischemia. The femoral and humeral heads are commonly involved, along with the diametaphyseal region of the long bones.

Additional Differential Diagnoses

- **Corticosteroid use.** Corticosteroid use predisposes to AVN due to a variety of mechanisms, including underlying demineralization and occlusion of small vessels by hepatic fat emboli. The risk is greatest with high doses and relatively short duration treatment. In the setting of corticosteroid usage, AVN is more likely to be bilateral.
- **Gaucher disease.** Gaucher disease manifests as an inability to clear glucocerebroside from the reticuloendothelial system. The resultant increased pressure occludes interosseous sinusoids, causing infarction. Additional radiographic findings are osteopenia, medullary expansion, and bony remodeling.
- **Meyer dysplasia.** Meyer dysplasia occurs in 2- to 4 year-old children, especially boys, and is painless and often bilateral. The dysplasia affects only the proximal femoral epiphyses, which appear small and irregular.

Diagnosis

Sickle cell disease

✓ Pearls

- MRI is more sensitive than plain films in detecting early changes associated with AVN.
- LCP disease results in AVN in the absence of trauma; it is more common in boys and may be bilateral.
- Trauma is a common cause of AVN due to disruption of blood supply to the femoral head.
- Sickle cell disease results in vascular occlusion and resultant AVN; corticosteroid use predisposes to bilateral AVN.

Suggested Readings

Donnelly LF, Jones BV, O'Hara SM, et al. Diagnostic Imaging: Pediatrics. Salt Lake City, UT: Amirsys; 2005

Mankin HJ. Nontraumatic necrosis of bone (osteonecrosis). N Engl J Med 1992;326(22):1473–1479

Case 173

Sandra L. Wootton-Gorges

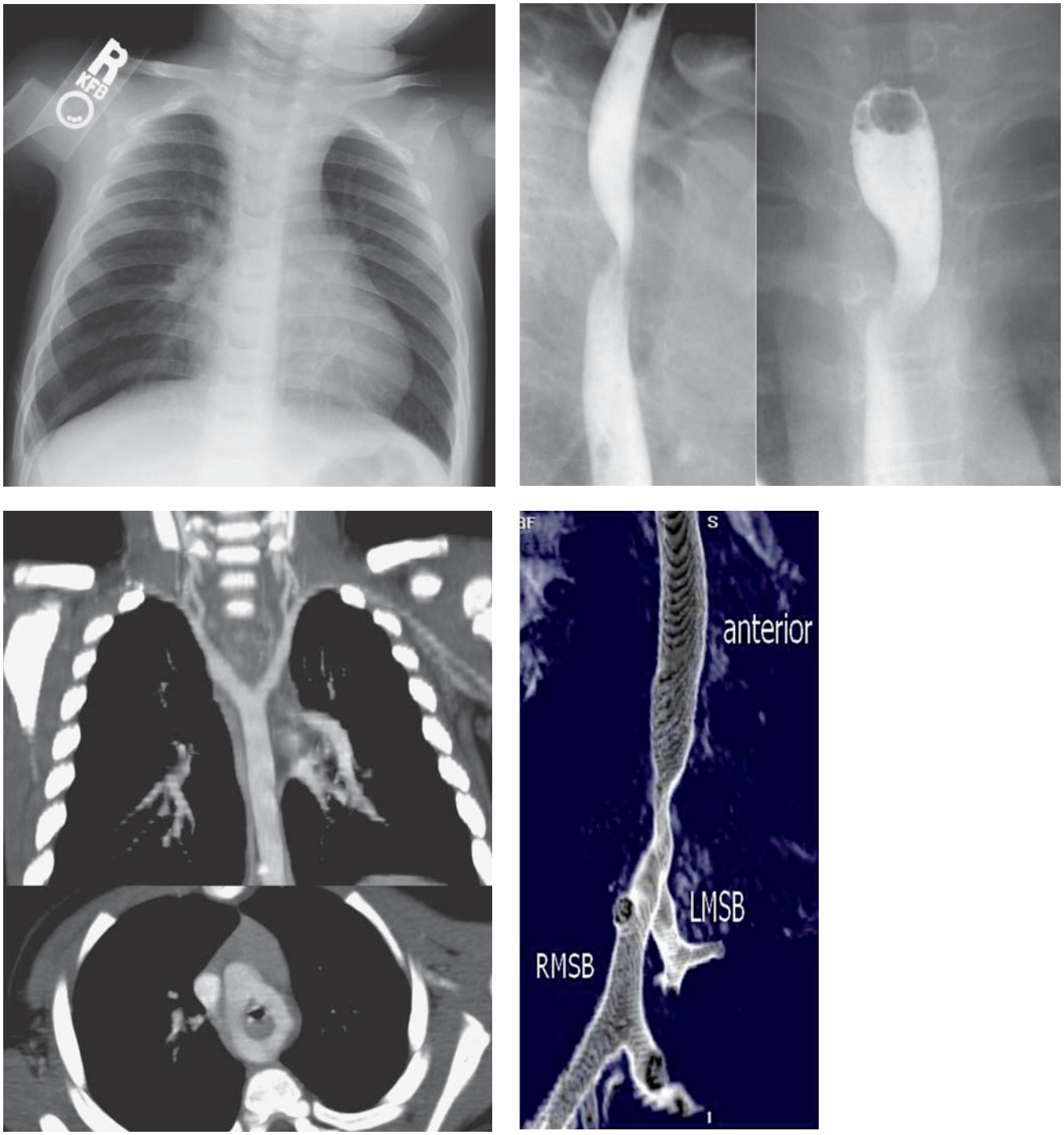


Fig. 173.1 **(A)** Frontal chest radiograph demonstrates a midline trachea. The side of the aortic arch cannot be determined. **(B)** Esophagram (from another patient with the same diagnosis) defines a posterior indentation on the esophagus on the lateral view. There is a higher, larger right-sided impression and a lower, smaller left-sided impression on the esophagus on the frontal view. **(C)** Coronal and axial contrast-enhanced computed tomography images from patient **A** shows a double aortic arch with a left descending aorta. **(D)** Distal tracheal compression is seen on the three-dimensional image.

Clinical Presentation

A 15-month-old boy presents with a long history of stridor (**Fig. 173.1**).

Key Imaging Finding

Vascular anomaly with esophageal and tracheal compression

Top 3 Differential Diagnoses

- **Aberrant right subclavian artery (RSCA).** Aberrant RSCA is a common isolated arch anomaly (1% of the population) that is rarely symptomatic. In this anomaly, the RSCA is the last branch of the left aortic arch and courses behind the esophagus toward the right upper chest, resulting in posterior indentation on the esophagus on an upper gastrointestinal (GI) examination. It is not considered a complete vascular ring.
- **Double aortic arch.** Double aortic arch is the most common symptomatic arch anomaly. It is an isolated anomaly in which two aortic arches are present; the right arch is higher and larger in 75% of cases. The two arches join posteriorly to form the (usually left-sided) descending aorta. The arches thus encircle and may compress the esophagus and trachea, resulting in respiratory or feeding symptoms. Because the trachea is fixed between the two smaller aortic arches, it is midline in position on a chest radiograph. The esophagram will show posterior and bilateral indentation on the esophagus, as well as narrowing of the trachea. Magnetic resonance imaging and contrast-enhanced computed tomography are excellent modalities to define this vascular anomaly and its effects on surrounding structures.
- **Right aortic arch with aberrant left subclavian artery (LSCA).** In this right aortic arch anomaly, the LSCA arises from the diverticulum of Kommerell and passes posterior to the esophagus to the left upper extremity. The ductal ligament extends from the LSCA to the left pulmonary artery, completing this often symptomatic vascular ring.

Additional Differential Diagnoses

- **Pulmonary sling.** In this anomaly, the left pulmonary artery arises from the right pulmonary artery and passes between the trachea and esophagus as it goes to the left lung. On an upper GI examination, there is an anterior indentation on the esophagus and posterior indentation on the trachea. Associated tracheobronchial anomalies, such as complete tracheal rings, are common and may significantly contribute to respiratory symptoms.
- **Innominate artery compression syndrome.** Compression of the trachea by the crossing innominate artery is a rare cause of respiratory compromise in infants. The innominate artery origin or course may be anomalous in these cases. The patients otherwise have a normal left aortic arch. Debate exists whether this is a real entity or whether symptoms are secondary to underlying tracheal maldevelopment. Surgical reimplantation or suspension may be helpful to relieve tracheal narrowing.

Diagnosis

Double aortic arch

✓ Pearls

- Aberrant RSCA is a common anomaly that is rarely symptomatic and is not considered a complete ring.
- Double aortic arch and right arch with aberrant LSCA are the most common symptomatic vascular rings.
- An aberrant LSCA (from a right aortic arch) arises from the diverticulum of Kommerell.
- Pulmonary sling (aberrant origin of the left pulmonary artery) is associated with complete tracheal rings.

Suggested Readings

Castañer E, Gallardo X, Rimola J, et al. Congenital and acquired pulmonary artery anomalies in the adult: radiologic overview. Radiographics 2006;26(2):349–371

Donnelly LF, Jones BV, O'Hara SM, et al. Diagnostic Imaging: Pediatrics. Salt Lake City, UT: Amirsys; 2005

Hernanz-Schulman M. Vascular rings: a practical approach to imaging diagnosis. Pediatr Radiol 2005;35(10):961–979

Moller JH, Amplatz K. Radiology of Congenital Heart Disease. St. Louis, MO: Mosby Year Book; 1993

Case 174

Karen M. Ayotte

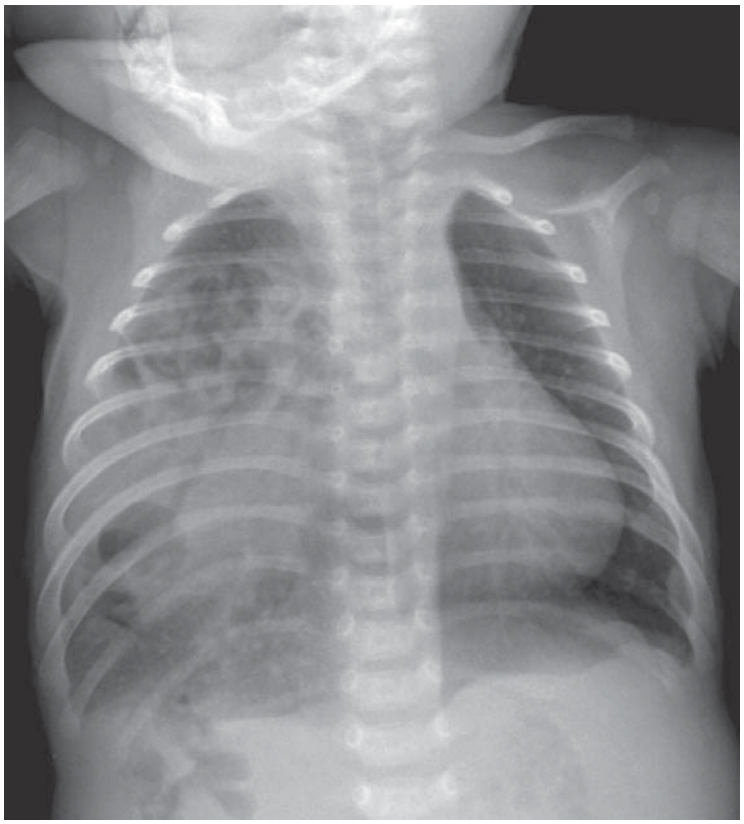


Fig. 174.1 Frontal radiograph of the chest demonstrates a multiloculated cystic and solid mass occupying the majority of the right thorax. The lungs are also hyperexpanded.

Clinical Presentation

A 5-week-old infant presents with a chronic cough (**Fig. 174.1**).

Key Imaging Finding

Cystic pulmonary mass

Top 3 Differential Diagnoses

- **Congenital lobar emphysema (CLE).** CLE is a progressive overexpansion of a pulmonary lobe secondary to obstruction of normal airflow, usually due to varying degrees of bronchial underdevelopment or obstruction. In prenatal life, the lung is filled with fluid. Perinatally, the radiographic appearance varies as the fluid within the affected lobe is gradually replaced with air. The most common location is the left upper lobe, followed by the right middle and right upper lobes. Patients often present in the neonatal period with respiratory distress. Definitive treatment consists of surgical resection of the affected lobe.
- **Congenital cystic adenomatoid malformation (CCAM).** CCAM is a hamartomatous proliferation of terminal bronchioles at the expense of alveolar development. There are both cystic and solid components to the majority of these masses, resulting in varying radiographic appearances. These lesions communicate with the tracheobronchial tree and tend to aerate early in life. Internal fluid–fluid levels may be seen in the absence of superimposed infection. CCAMs are classified into three types: type 1 consists of one or more cysts >2 cm in size, type 2 has cysts <2 cm in size, and type 3 is essentially solid. Conclusive management is surgical, although management of asymptomatic or incidentally discovered lesions is controversial.
- **Congenital diaphragmatic hernia.** Congenital defects in the diaphragm can lead to intrathoracic herniation of the solid and hollow viscous organs of the upper abdomen. Left-sided defects are significantly more common than those seen on the right. Radiographically, herniations may appear cystic or solid at birth. When the majority of the herniated contents are bowel, the fluid attenuation will resolve as the bowel aerates. Most children present as neonates secondary to respiratory distress. Prognosis depends on the degree of pulmonary hypoplasia, as well as the severity of any associated anomalies. Surgical consultation is required, regardless of the apparent size of the defect.

Additional Differential Diagnoses

- **Necrotizing pneumonia.** When areas of consolidation in the lung are complicated by necrosis and/or abscess formation, the radiographic appearance can mimic other cystic lesions of the lung. Necrotizing pneumonia more commonly occurs in the lower lobes. The cysts themselves may be solitary or multiple, may vary in size up to 10 cm in diameter, and may be filled with air, fluid, or both. Conservative management is often successful in otherwise healthy children.

Diagnosis

Congenital diaphragmatic hernia

✓ Pearls

- Prognosis for most chest masses is based primarily on the degree of pulmonary hypoplasia.
- CLE most commonly occurs within the left upper lobe, followed by the right middle and right upper lobes.
- CCAMs are categorized by the number and size of cystic components.
- Congenital diaphragmatic hernia can mimic cystic or solid primary thoracic masses and is more common on the left.

Suggested Readings

Berrocal T, Madrid C, Novo S, Gutiérrez J, Arjonilla A, Gómez-León N. Congenital anomalies of the tracheobronchial tree, lung, and mediastinum: embryology, radiology, and pathology. Radiographics 2004;24(1):E17

Donnelly LF, Jones BV, O'Hara SM, et al. Diagnostic Imaging: Pediatrics. Salt Lake City, UT: Amirsys; 2005

Kirks DR. Practical Pediatric Imaging: Diagnostic Radiology of Infants and Children. 3rd ed. Philadelphia: Lippincott Williams & Wilkins; 1998

Case 175

Arvind Sonik

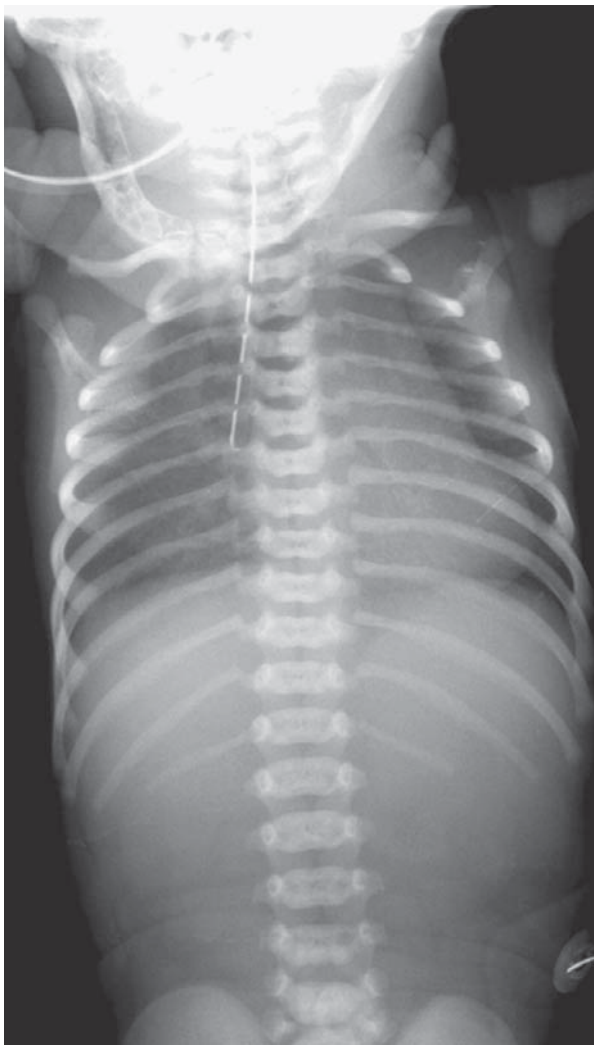


Fig. 175.1 Babygram demonstrates an esophageal catheter extending just below the level of the carina with a gasless abdomen.

Clinical Presentation

A 1-day-old infant does not tolerate oral feedings (**Fig. 175.1**).

Key Imaging Finding

Esophageal obstruction in a neonate

Top 3 Differential Diagnoses

- **Tracheoesophageal (TE) fistula/esophageal atresia.** Esophageal atresia is classified based on the presence and location, or absence, of a TE fistula. Proximal esophageal atresia with a fistula between the airway and the distal esophageal segment is the most common type. Esophageal atresia is often associated with additional anomalies of the gastrointestinal tract. Cardiac, renal, and vertebral anomalies (including the VACTERL [vertebral, anal, cardiac, tracheal, esophageal, renal, and limb] complex) are associated less frequently. Evaluation includes advancing a feeding tube to the level of the atresia and a radiograph of the abdomen (to evaluate for air in the stomach). If an H-type fistula is suspected, an upper gastrointestinal study is indicated, preferably with water-soluble contrast. Esophageal webs are considered a variant of esophageal atresia and may be associated with a TE fistula. On esophagograms, webs are thin, transverse, or oblique filling defects.
- **Foreign body.** Foreign bodies may become lodged in relatively narrow regions of the esophagus: the thoracic inlet, the level of the aortic arch, and, less commonly, at the gastroesophageal (GE) junction. Esophagograms may be useful when a nonopaque foreign body is suspected. Disk batteries constitute a medical emergency and should be considered in the differential diagnosis of a round foreign body.
- **Esophageal duplication cyst.** Esophageal duplications usually manifest as cysts (complete duplications are rare). These cysts are usually right sided, not in communication with the esophagus, and are in the posterior mediastinum. Duplication cysts are near water attenuation on computed tomography and do not enhance. On magnetic resonance imaging, they are bright on T2 and variable on T1 depending on the amount of proteinaceous material.

Additional Differential Diagnoses

- **Vascular ring.** The most frequent vascular anomalies to cause dysphagia are complete vascular rings: the double aortic arch and the right aortic arch with aberrant left subclavian artery and left ligament arising from the descending aorta. Esophagograms demonstrate posterior indentation of the esophagus on lateral and oblique views and bilateral compressions on the anteroposterior view. Double aortic arch is more common than the right arch with aberrant left subclavian artery. Although the most common anomaly of the aortic arch, a left aortic arch with an aberrant right subclavian artery is not a complete vascular ring and thus rarely causes symptoms.

Diagnosis

Esophageal atresia without fistula

✓ Pearls

- Esophageal atresia is classified based on the presence and location, or absence, of a TE fistula.
- Proximal esophageal atresia with a fistula between the airway and the distal esophagus is most common.
- Foreign bodies typically become lodged at the thoracic inlet, aortic arch, and GE junction (less common).
- Complete vascular rings may cause esophageal compression with dysphagia.

Suggested Readings

Berrocal T, Torres I, Gutiérrez J, Prieto C, del Hoyo ML, Lamas M. Congenital anomalies of the upper gastrointestinal tract. Radiographics 1999;19(4):855–872

Blickman H. Pediatric Radiology: The Requistes. 2nd ed. Philadelphia, PA: Mosby; 1998

Section VIII Ultrasound Imaging

Case 176

Sima Naderi

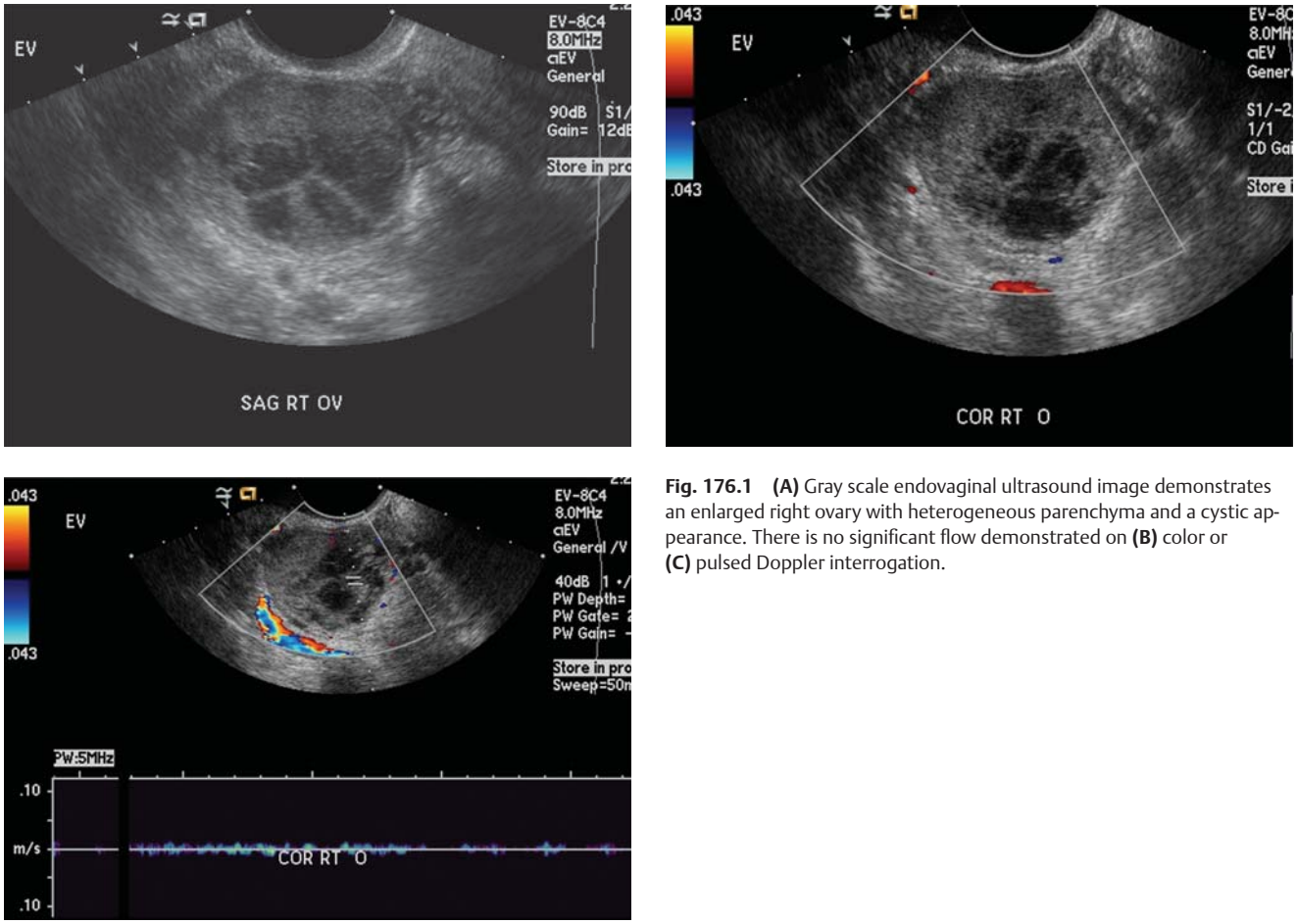


Fig. 176.1 **(A)** Gray scale endovaginal ultrasound image demonstrates an enlarged right ovary with heterogeneous parenchyma and a cystic appearance. There is no significant flow demonstrated on **(B)** color or **(C)** pulsed Doppler interrogation.

Clinical Presentation

An 18-year-old woman presents with severe acute onset right-sided pelvic pain (**Fig. 176.1**).

Key Imaging Finding

Enlarged ovary

Top 3 Differential Diagnoses

- **Ovarian torsion.** Torsion of the ovary is an acute gynecologic operative emergency. It is caused by partial or complete rotation of the ovarian pedicle on its axis. Torsion can occur at any time in life, but it is most common during the fertile years. Predisposing factors include an ipsilateral adnexal mass and pregnancy. Prepubertal patients can torse a normal ovary due to adnexal mobility. Sonographic findings are variable. The torsed ovary is commonly enlarged, with multiple cortical follicles. The parenchyma can be heterogeneous due to edema, hemorrhage, or necrosis. A lead mass may be appreciated. Free fluid in the pelvic cul-de-sac is also a common finding. Color and spectral Doppler examination may show absent flow in the affected ovary. However, the presence of blood flow does not exclude torsion, as torsion may be incomplete or intermittent, resulting in increased diastolic flow in the edematous ovary or decreased flow. Diagnosis also requires the appropriate clinical setting of severe acute onset of pelvic pain.
- **Ovarian neoplasm.** Ovarian tumors, both benign and malignant, can result in enlargement of the ovary due to a complex cystic mass. Differentiating features compared with ovarian torsion include the patient's age and clinical presentation. There is an increased risk of malignancy with increasing patient age and increasing size of the mass >10 cm. Also, malignant ovarian neoplasms have increased vascularity due to neovascularity.
- **Pelvic inflammatory disease (PID)/tubo-ovarian abscess.** The diagnosis of PID is made in the appropriate clinical setting of fevers, pelvic tenderness, and vaginal discharge. The dilated fallopian tube can best be differentiated from a cystic adnexal mass by transvaginal ultrasound. Tubo-ovarian abscess appears as a complex multiloculated mass with through transmission, scattered internal echogenicity, and increased vascularity. Ovarian enlargement may be seen in advanced presentations.

Additional Differential Diagnoses

- **Hemorrhagic cyst.** The sonographic appearance of a hemorrhagic cyst depends on the time of hemorrhage. Classically, the complex cyst forms a reticular-type pattern containing internal echoes. As the clot retracts, a fluid–fluid level can be seen, or the echogenic clot can settle at the dependent portion of the cyst. The key differentiating feature from malignancy is the lack of flow within the clot on color Doppler.

Diagnosis

Ovarian torsion

✓ Pearls

- Ovarian torsion most commonly presents as acute and severe adnexal tenderness with an enlarged ovary.
- Ovarian neoplasms are unlikely to cause acute pain and are more likely to be malignant with advanced age.
- PID is suggested in the appropriate clinical setting; hydrosalpinx may best be detected on transvaginal ultrasound.
- Hemorrhagic cysts classically present with a reticular-type pattern of internal echoes in a cystic mass.

Suggested Readings

Kaakaji Y, Nghiem HV, Nodell C, Winter TC. Sonography of obstetric and gynecologic emergencies: 2. Gynecologic emergencies. AJR Am J Roentgenol 2000;174(3):651–656

Middleton WD, Kurtz AB, Hertzberg BS. Ultrasound: The Requisites. St. Louis, MO: Mosby; 2004

Case 177

William T. O'Brien Sr.

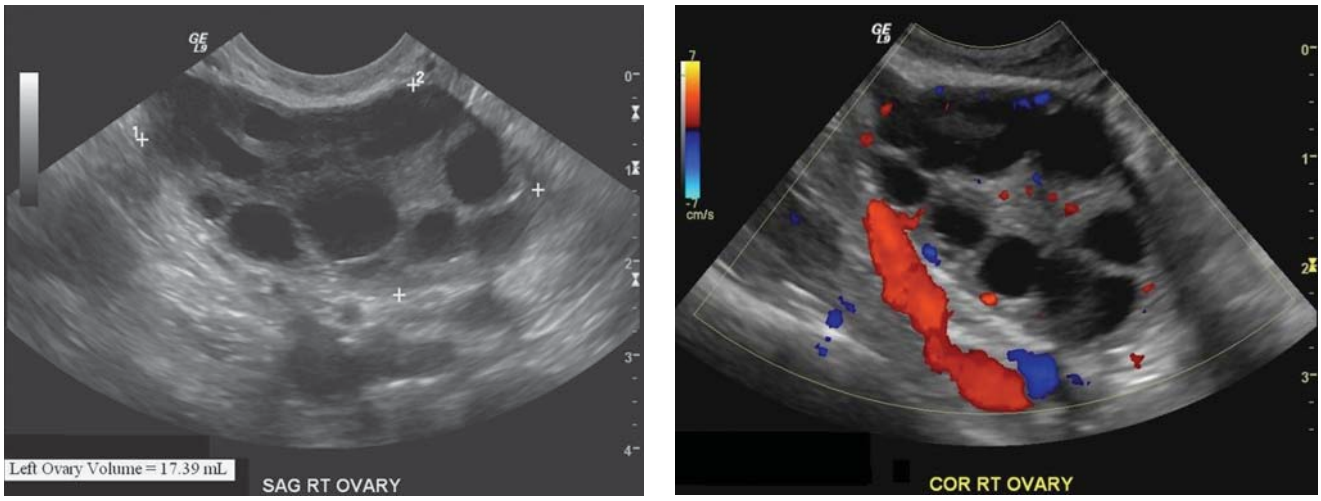


Fig. 177.1 **(A)** Sagittal gray scale and **(B)** color sonographic images through the left ovary demonstrate an enlarged ovary with multiple peripheral follicles. Flow is demonstrated within the ovary. Arterial and venous waveforms (not shown) were normal.

Clinical Presentation

Premenopausal patient; history otherwise withheld (**Fig. 177.1**).

Key Imaging Finding

Enlarged ovary with multiple peripheral follicles

Top 3 Differential Diagnoses

- **Ovarian torsion.** Ovarian torsion is the result of the ovary twisting about its vascular axis. Torsion is most common in premenopausal patients but may occur at any age when a pathologic lead point (e.g., an ovarian mass) is present. Patients typically present with severe pelvic pain. As the torsion occurs, venous outflow is first decreased, resulting in an enlarged ovary (>12 mL) with heterogeneous echotexture. As the edema progresses, arterial inflow is decreased. Hemorrhage, necrosis, and infarction may occur if left untreated. The presence of flow within the ovary is of limited diagnostic value, as the mere presence of flow does not exclude torsion. In cases of intermittent torsion, the ovary may actually be hyperemic. The absence of flow, however, is highly suggestive of torsion. Torsion may present sonographically as an enlarged edematous ovary with peripheral follicles.
- **Polycystic ovarian syndrome (PCOS).** PCOS, also referred to as Stein–Leventhal syndrome, is a clinical syndrome consisting of obesity, hirsutism, amenorrhea or irregular menses, and infertility. The syndrome is associated with a variety of endocrine disturbances, including increased androgen production. Classic sonographic findings consist of enlarged ovaries with multiple peripheral follicles (10 or more) of similar size (usually <5 mm) in a "string of pearls" configuration. The ovaries may have a thick echogenic capsule. Treatment is directed at restoring fertility through fertility medications.
- **Ovarian hyperstimulation syndrome (OHS).** Ovarian stimulation from fertility medications results in the maturation of multiple follicles during the menstrual cycle. Rarely, the ovaries may be overstimulated, resulting in enlarged ovaries with numerous enlarged peripheral follicles, ascites, and pleural effusions, referred to as OHS. When severe, the condition may be life-threatening due to fluid and electrolyte imbalances. The syndrome typically occurs when the dosage of medications is increased, and the ovaries may be massively enlarged (up to 15–20 cm). Treatment consists of correcting electrolyte imbalances and discontinuing fertility medications.

Diagnosis

Polycystic ovarian syndrome

✓ Pearls

- Ovarian torsion must be considered with enlarged ovaries and pain; flow does not exclude the diagnosis.
- PCOS presents clinically with obesity, hirsutism, irregular menses, and infertility.
- Ultrasound findings in PCOS include enlarged ovaries with peripheral follicles in a "string of pearls" configuration.
- OHS presents with enlarged ovaries with peripheral follicles, ascites, and pleural effusions.

Suggested Readings

Jeong YY, Outwater EK, Kang HK. Imaging evaluation of ovarian masses. Radiographics 2000;20(5):1445–1470

Middleton WD, Kurtz AB, Hertzberg BS. Ultrasound: The Requisites. St. Louis, MO: Mosby; 2004

Case 178

William T. O'Brien Sr.

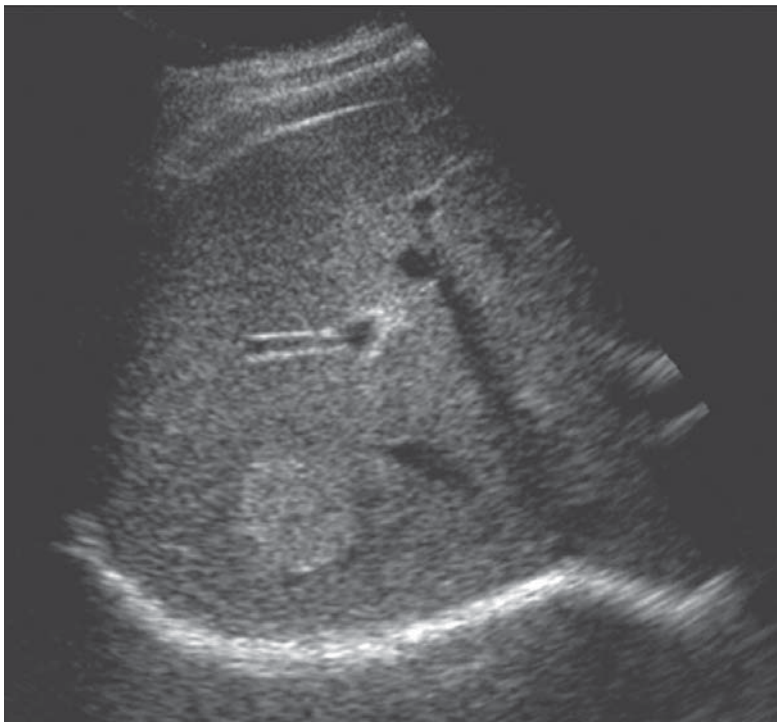


Fig. 178.1 Sonographic image through the right hepatic lobe demonstrates a well-circumscribed homogeneous hyperechoic mass.

Clinical Presentation

An adult female patient presents with an incidental finding on a study for right upper quadrant pain (**Fig. 178.1**).

Key Imaging Finding

Hyperechoic liver mass

Top 3 Differential Diagnoses

- **Hemangioma.** Hemangiomas are the most common neoplastic hepatic lesions and the second most common benign lesions following simple cysts. They are more common in women and typically are asymptomatic. The classic imaging findings on ultrasound are that of a sharply marginated homogeneously hyperechoic mass. Larger lesions may be more heterogeneous. A common atypical presentation is the "reverse target" sign, with a centrally hypoechoic mass with a peripheral hyperechoic rim. Multiphasic computed tomography or magnetic resonance imaging (MRI) may be helpful in confirming the diagnosis, especially in patients with risk factors for underlying malignancy.
- **Focal fatty infiltration.** Fatty infiltration of the liver is common and most often due to obesity. It usually results in diffuse increased echogenicity but may also occur focally. Focal fatty infiltration presents as geographic hyperechoic regions most commonly located along the falciform ligament and portal confluence. MRI is usually diagnostic in cases where the ultrasound findings are not characteristic.
- **Hepatocellular carcinoma (HCC).** HCC is the most common primary hepatic malignancy, with an increased incidence in patients with chronic liver disease. Patients may present with a single lesion, multiple lesions, or diffuse hepatic involvement. HCC has a variety of appearances on ultrasound; the most common manifestation is a dominant hypervascular lesion with smaller satellite foci. Portal or hepatic vein invasion is common. MRI can be helpful in difficult cases, as HCC typically displays increased T2 signal intensity. Clinically, HCC is associated with elevated levels of alpha fetoprotein.

Additional Differential Diagnoses

- **Metastases.** Metastases commonly involve the liver, with lung, breast, and gastrointestinal malignancies representing the most common primary tumors. The vast majority are multiple, involving both hepatic lobes. They may also be diffusely infiltrative. The most common sonographic appearance is a target lesion with a centrally hyperechoic mass with a peripheral hypoechoic rim. Colon cancer is the most common primary tumor to present with predominantly hyperechoic metastatic lesions.
- **Focal nodular hyperplasia (FNH).** FNH is an uncommon lesion that typically presents in young female patients. The lesion is composed of hepatocytes and classically contains a central scar. Classic ultrasound findings are an isoechoic mass with central scar and a "spoke-wheel" pattern of flow. Rarely, the lesions may be hyperechoic. Because FNH is composed of hepatocytes, it may demonstrate uptake on sulfur colloid scans.
- **Hepatic adenoma.** Hepatic adenomas are benign lesions predominantly seen in women (90%). Most often they are solitary but may occasionally be multiple, especially in patients with glycogen storage disease. Hepatic adenomas have an increased frequency and risk of rupture with the use of oral contraceptives. Adenomas have variable appearances on ultrasound but are most commonly isoechoic. Because they may contain fat, hyperechoic regions may be seen.

Diagnosis

Hemangioma

✓ Pearls

- Hemangiomas are the most common benign hepatic neoplasms; they are circumscribed and hyperechoic.
- Focal fatty infiltration appears as geographic regions of increased echogenicity in characteristic locations.
- HCC and metastases have a variety of imaging appearances on ultrasound and typically occur in at-risk patients.

Suggested Readings

Middleton WD, Kurtz AB, Hertzberg BS. Ultrasound: The Requisites. St. Louis, MO: Mosby; 2004

Prasad SR, Wang H, Rosas H, et al. Fat-containing lesions of the liver: radiologic-pathologic correlation. Radiographics 2005;25(2):321–331

Case 179

David J. Weitz

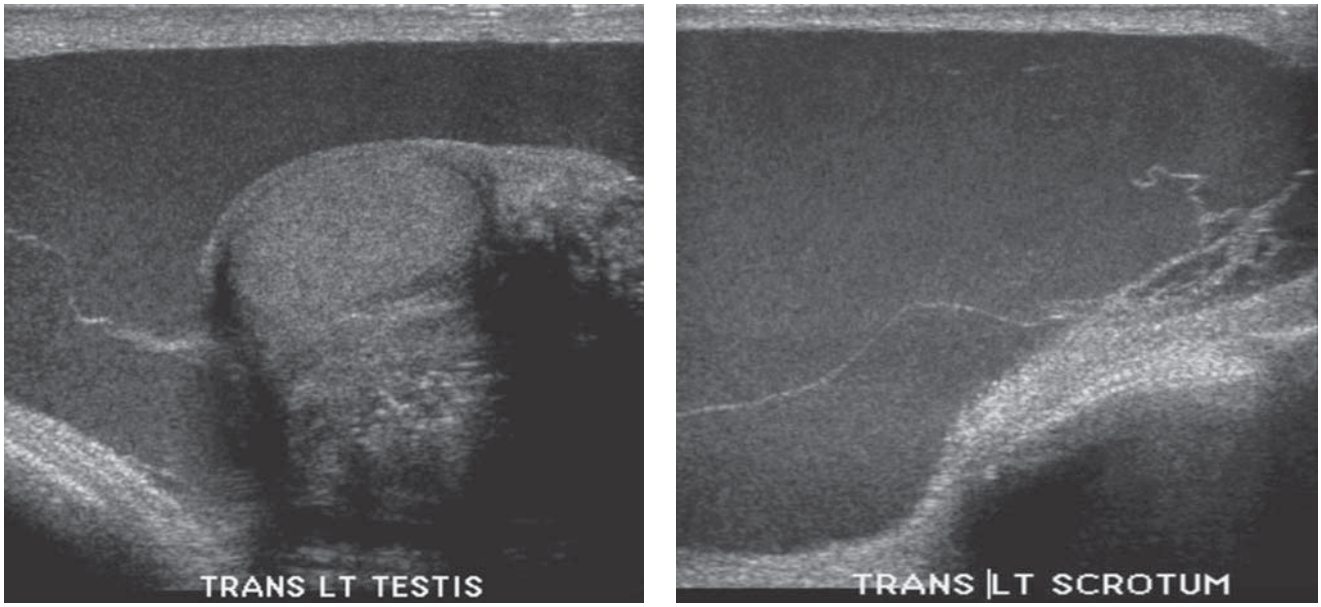


Fig. 179.1 **(A,B)** Transverse ultrasound images through the left scrotum reveal a large predominantly hypoechoic fluid collection with fine free-floating septations superimposed on a background of uniform low-level echoes.

Clinical Presentation

Enlarged painful scrotal mass in a young adult after vasectomy 1 month earlier (**Fig. 179.1**).

Key Imaging Finding

Complex extratesticular fluid collection

Top 3 Differential Diagnoses

- **Varicocele.** Abnormal dilatation of the spermatic cord veins (pampiniform plexus) is defined as a varicocele. Classically, patients will present with a palpable mass in the scrotum, which has the consistency of a "bag of worms." Larger varicoceles may be painful, but most do not produce discomfort and are generally discovered during a fertility evaluation where varicoceles are a well-established cause of male infertility. Seen in ~15% of men, varicoceles are the result of valvular incompetence. Most varicoceles (85%) are left-sided because of increased venous pressure from an asymmetrically longer left testicular vein, compression of the vein from the left testicular artery, or the gonadal vein's angled entrance into the left renal vein. An isolated right varicocele should prompt a search for a retroperitoneal mass. On ultrasound, testicular veins (usually in the superior lateral scrotum) dilated >2 mm are suspect, but demonstration of flow reversal during color Doppler interrogation is diagnostic. Other supporting findings on ultrasound are serpiginous tubular structures in the scrotum and a >1 mm change in caliber post Valsalva test (or supine to standing).
- **Hematocele.** A scrotal hematocele can be characterized as a type of complex hydrocele in which blood products collect within and separate the visceral and parietal layers of the tunica vaginalis. Hematoceles are most commonly a consequence of trauma (including iatrogenic), but they may occur in the setting of scrotal tumors or torsion. In the early stages, hematoceles are more uniformly echogenic or mildly heterogeneous, often with reactive hyperemia of the scrotum and epididymis. Skin thickening from edema is common. Over time, septations, fluid–fluid levels, or low-level echoes often develop on a background of hypoechoic fluid. Ultrasound is the initial study of choice in the evaluation of acute scrotal injury.
- **Pyocele.** Like a hematocele, a pyocele falls into the category of a complex hydrocele. A pyocele represents an infectious extratesticular fluid collection, most commonly a complication of epididymo-orchitis or retrograde spread of cystitis. Sonographic appearance may vary, but most pyoceles are complex fluid collections indistinguishable from hematoceles. Color Doppler may reveal reactive hyperemia of the scrotal wall, as well as vascular engorgement of the epididymis like a hematocele; however, ultrasound should always be correlated with clinical findings. Patients typically present with fever, leukocytosis, and acute onset of scrotal pain. On clinical exam, the scrotum is enlarged and tender, often with overlying skin erythema. The presence of hyperechoic foci producing ring-down artifact is highly suggestive of gas. This is seen in the setting of life-threatening necrotizing fasciitis, or Fournier gangrene, which is most common in diabetics.

Diagnosis

Hematocele (iatrogenic)

✓ Pearls

- Varicoceles are diagnosed by noting an increase in vein caliber during Valsalva test and reversal of flow.
- Hematoceles are usually the result of trauma, and ultrasound is the preferred initial study.
- Pyoceles are complex extratesticular fluid collections that are distinguished from hematoceles by history.

Suggested Readings

Deurdulian C, Mittelstaedt CA, Chong WK, Fielding JR. US of acute scrotal trauma: optimal technique, imaging findings, and management. Radiographics 2007;27(2):357–369

Dogra VS, Gottlieb RH, Oka M, Rubens DJ. Sonography of the scrotum. Radiology 2003;227(1):18–36

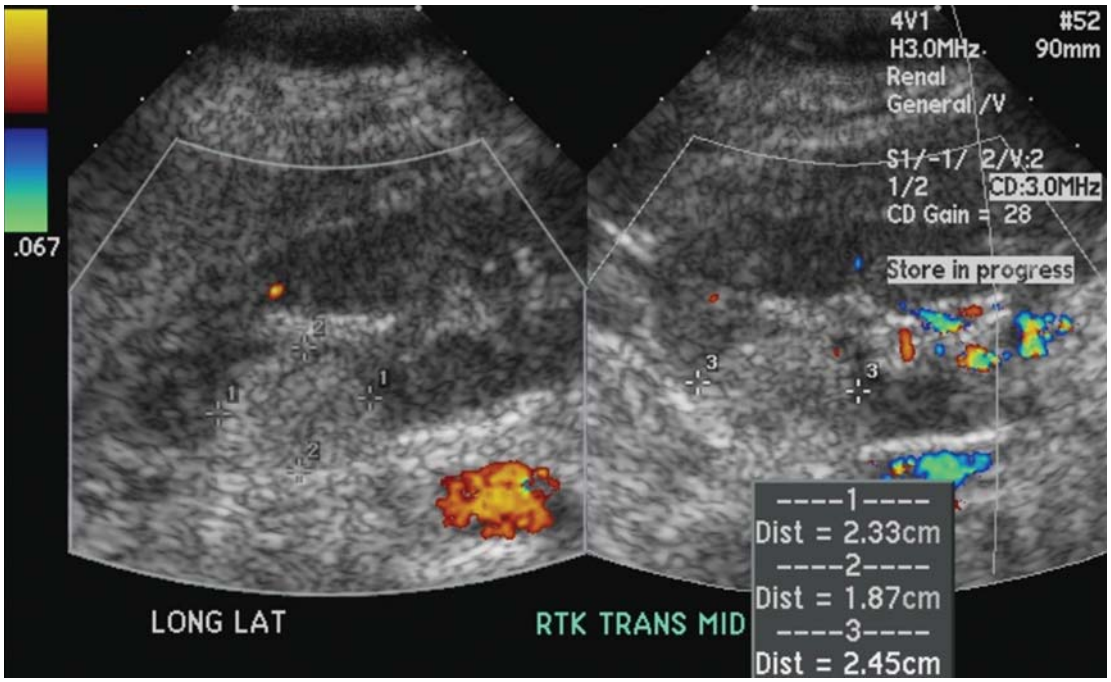
Kim W, Rosen MA, Langer JE, Banner MP, Siegelman ES, Ramchandani P. US MR imaging correlation in pathologic conditions of the scrotum. Radiographics 2007;27(5):1239–1253

Middleton WD, Kurtz AB, Hertzberg BS. Ultrasound: The Requisites. St. Louis, MO: Mosby; 2004

Woodward PJ, Schwab CM, Sesterhenn IA. From the *Archives of the AFIP:* extratesticular scrotal masses: radiologic-pathologic correlation. Radiographics 2003;23(1):215–240

Case 180

David J. Weitz



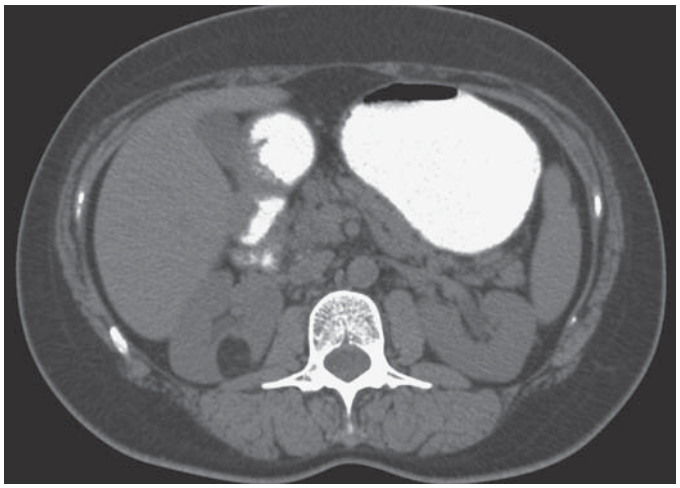


Fig. 180.1 **(A)** Longitudinal and transverse sonographic images of the right kidney reveal a cortically based hyperechoic lesion with echogenicity similar to peripelvic fat. **(B)** Axial computed tomography image through the upper abdomen with oral contrast demonstrates a sharply marginated fatty mass with scant internal soft tissue elements located within the upper pole of the right kidney.

Clinical Presentation

A middle-aged woman presents with generalized abdominal pain (**Fig. 180.1**).

Key Imaging Finding

Hyperechoic renal mass

Top 3 Differential Diagnoses

- **Angiomyolipoma (AML).** AMLs are benign renal hamartomas, aptly named given their composition of vessels, muscle, and fat. Small AMLs are usually incidental discoveries in the work-up of other conditions, as they rarely produce symptoms. In general, AMLs are soft, pliable tumors that may grow astoundingly large before symptoms prompt evaluation. Pain is usually from vessel rupture, as larger tumors (>4 cm) are prone to aneurysm formation. On ultrasound, these masses are usually found at the renal cortex and have a homogeneous hyperechoic appearance with posterior acoustic shadowing. Because of their overlapping ultrasound appearance with renal cell carcinoma (RCC), conclusive imaging with computed tomography (CT) or magnetic resonance imaging (MRI) is generally needed to demonstrate fat, which is considered pathognomonic for AML. Solitary AMLs are sporadic and found most frequently in women; multiple AMLs are known to occur in the setting of tuberous sclerosis.
- **Renal cell carcinoma.** All solid renal masses are suspect for RCC, because it is the most common renal mass, and its ultrasound appearance may mimic just about any other lesion. Patients present with hematuria, weight loss, anemia, and occasionally paraneoplastic syndromes. Risk factors are tobacco usage, long-term dialysis, and von Hippel–Lindau disease. Larger RCCs are most commonly hyperechoic; however, RCC can present as a hyper-, hypo-, or isoechoic mass. RCCs may appear as complex masses containing calcifications, cystic components, hemorrhage, or necrosis. Because these tumors are highly vascular, flow within a renal lesion lends support for RCC and can be particularly helpful in the detection of hard-to-identify isoechoic lesions. RCC spreads via lymphatics to local lymph nodes, direct spread to the ipsilateral renal vein and inferior vena cava, and hematogenously to distant sites.
- **Complex cyst.** Ultrasound is considered the modality of choice for confirming a simple renal cyst that requires no further imaging. Complex cysts, in contrast, may mimic a solid mass on ultrasound, prompting follow-up sonography, further imaging with CT or MRI, or intervention. These lesions are often the result of internal hemorrhage or protein and may demonstrate low-level echogenicity, fluid–debris levels, internal clot, calcification, or septations. The differential would include an infected cyst or abscess, a multiseptated cyst, and RCC, all of which may be sonographically indistinguishable. Thick septations (>1 mm), internal flow, nodularity, calcification, and demonstration of interval growth are highly suspicious findings for malignancy. The Bosniak classification using CT is a widely accepted standard for placing ultrasound indeterminate lesions into a medical or surgical category; however, MRI is gaining popularity and may be especially helpful for small lesions.

Diagnosis

Angiomyolipoma

✓ Pearls

- On ultrasound, AMLs typically have a homogeneous hyperechoic echotexture with posterior acoustic shadowing.
- Given the highly variable appearance of RCCs at ultrasound, all solid renal masses are suspect for RCC.
- Ultrasound is the preferred modality to confirm a simple cyst; complex cystic renal lesions are nonspecific.

Suggested Readings

Hartman DS, Choyke PL, Hartman MS. A practical approach to the cystic renal mass. Radiographics 2004;24(Suppl 1):S101–S115

Middleton WD, Kurtz AB, Hertzberg BS. Ultrasound: The Requisites. St. Louis, MO: Mosby; 2004

Siegel CL, Middleton WD, Teefey SA, McClennan BL. Angiomyolipoma and renal cell carcinoma: US differentiation. Radiology 1996;198(3):789–793

Zagoria RJ. Genitourinary Radiology: The Requisites. 2nd ed. Philadelphia: Mosby; 2004

Case 181

William T. O'Brien Sr.

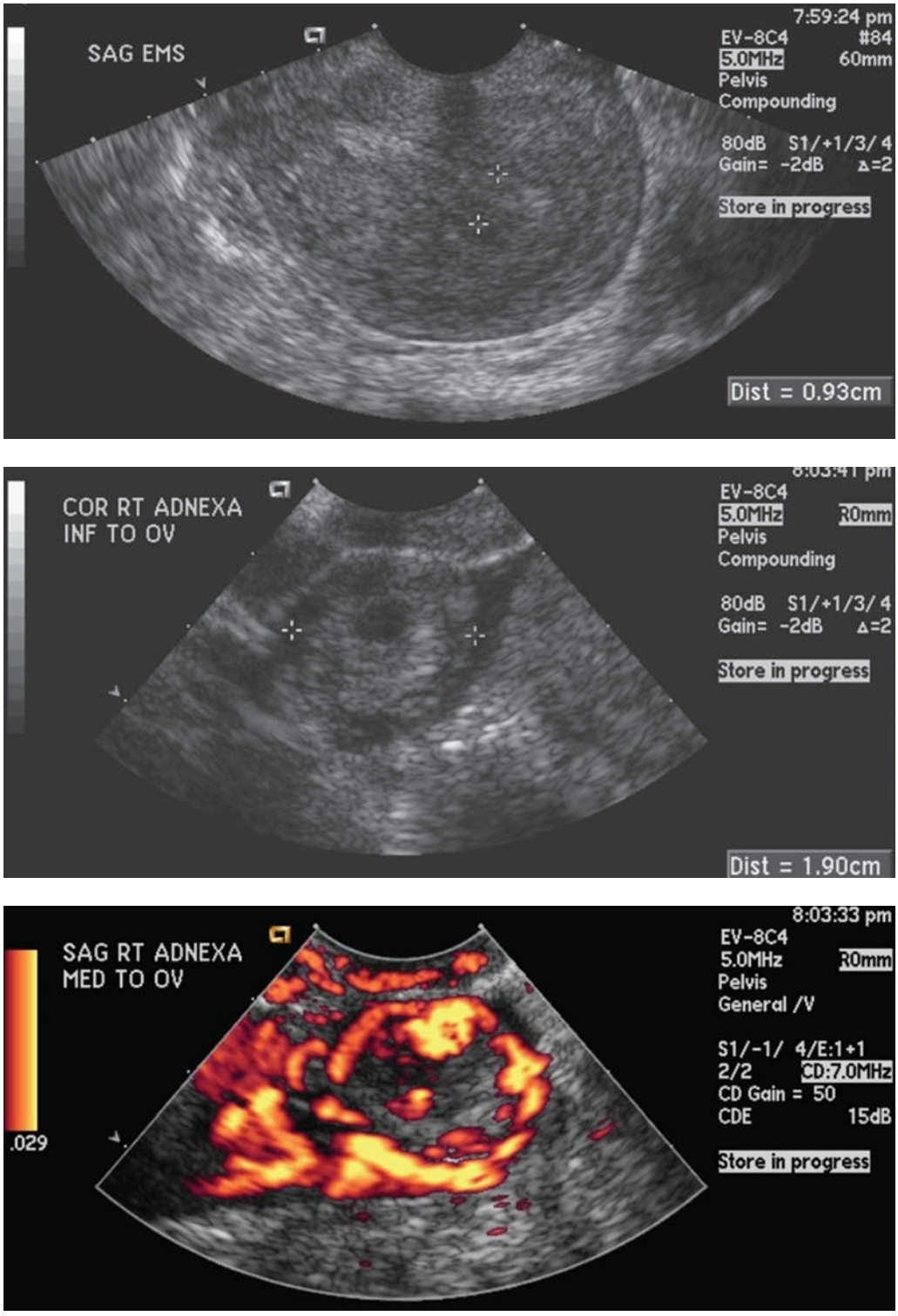


Fig. 181.1 **(A)** Sagittal sonographic image through the uterus demonstrates a normal endometrial echo complex without evidence of an intrauterine gestational sac. **(B)** Imaging through the right adnexa reveals a round adnexal mass with a thick hyperechoic rim and a small central hypoechoic region. **(C)** The mass demonstrates increased peripheral flow in a "ring of fire" pattern.

Clinical Presentation

A 24-year-old woman presents with severe right adnexal pain, vaginal spotting, and a positive human chorionic gonadotropin (HCG) test (**Fig. 181.1**).

Key Imaging Finding

Complex cystic adnexal mass with positive HCG

Top 3 Differential Diagnoses

- **Ectopic pregnancy.** Ectopic pregnancy is the result of implantation of the conceptus outside the endometrial canal, usually within the fallopian tube. It is currently the most common cause of pregnancy-related mortality in the first trimester. Risk factors include prior ectopic pregnancy, pelvic inflammatory disease, tubal ligation, and fertility medications or interventions. Patients present in the first trimester with pain and/or vaginal bleeding. Ultrasound is the diagnostic modality of choice. Intrauterine sonographic findings are the lack of an intrauterine pregnancy (except in the exceedingly rare case of heterotopic pregnancy) and the presence of a pseudogestational sac. Extrauterine sonographic findings are a complex cystic adnexal mass with increased vascularity and/or complex free fluid (hemorrhage). An ectopic pregnancy classically has a thick hyperechoic rim with a central hypoechoic region. The hyperechoic rim is more echogenic than ovarian or uterine tissue. Peripheral flow in a "ring of fire" pattern is characteristic with a low-resistance waveform. Sonographic findings must be correlated with HCG levels, especially when the levels are below the expected threshold for visualization of a gestational sac (1000–2000 IU).
- **Corpus luteal cyst.** The key differential diagnosis in the setting of a suspected ectopic pregnancy is a corpus luteal cyst. Although it may not always be possible to differentiate between the two, the corpus luteal cyst arises from (rather than is adjacent to) the ovary and has a thinner outer echogenic layer that is similar in echotexture to normal ovarian parenchyma. Additionally, the peripheral flow is not as avid; however, this observation is not always reliable. The presence of an anechoic, rather than hypoechoic, central fluid collection favors a corpus luteal cyst over ectopic pregnancy.
- **Hemorrhagic cyst.** Although hemorrhagic cysts typically present as cystic masses with lacelike internal echoes, they may occasionally mimic ectopic pregnancy both clinically and sonographically. Imaging findings that mimic ectopic pregnancy are a thick echogenic rim and the presence of hemoperitoneum. In the setting of a positive HCG, these characteristics would be highly suggestive of ectopic pregnancy.

Diagnosis

Ectopic pregnancy

✓ Pearls

- Ectopic pregnancy must be considered if no intrauterine gestation is seen in a patient with positive HCG.
- A corpus luteal cyst is commonly indistinguishable from an ectopic pregnancy.
- Shared features of a hemorrhagic cyst and ectopic gestation are a thick echogenic rim and hemoperitoneum.

Suggested Readings

Frates MC, Visweswaran A, Laing FC. Comparison of tubal ring and corpus luteum echogenicities: a useful differentiating characteristic. J Ultrasound Med 2001;20(1):27–31, quiz 33

Hertzberg BS, Kliewer MA, Bowie JD. Adnexal ring sign and hemoperitoneum caused by hemorrhagic ovarian cyst: pitfall in the sonographic diagnosis of ectopic pregnancy. AJR Am J Roentgenol 1999;173(5):1301–1302

Stein MW, Ricci ZJ, Novak L, Roberts JH, Koenigsberg M. Sonographic comparison of the tubal ring of ectopic pregnancy with the corpus luteum. J Ultrasound Med 2004;23(1):57–62

Case 182

David J. Weitz

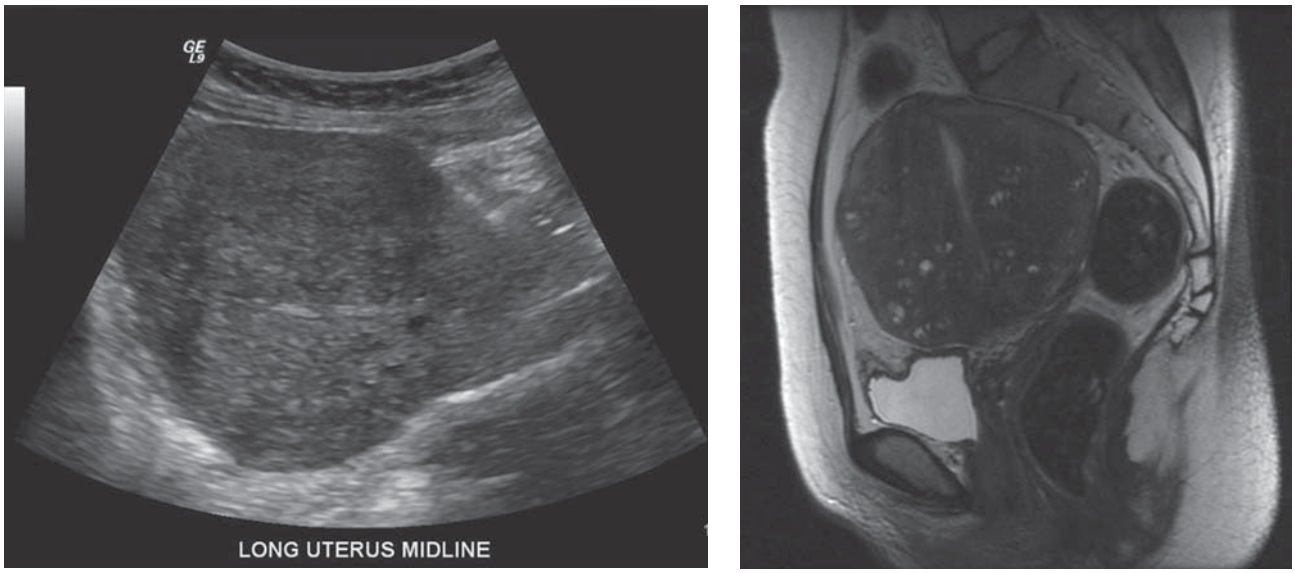


Fig. 182.1 **(A)** Longitudinal gray scale sonographic image demonstrates a heterogeneous enlarged globular uterus without discrete mass. **(B)** Sagittal T2-weighted magnetic resonance image reveals diffuse thickening of the junctional zone with high T2 cystic foci within the myometrium.

Clinical Presentation

A premenopausal patient presents with dysfunctional uterine bleeding and pain (**Fig. 182.1**).

Key Imaging Finding

Enlarged heterogeneous uterus

Top 3 Differential Diagnoses

- **Diffuse leiomyomas.** Fibroids are the most common uterine mass. They are benign tumors composed of estrogen-dependent smooth muscle and connective tissue. Fibroids most often present as discrete uterine masses but may also be infiltrative, resulting in an enlarged, heterogeneous uterus. When focal, ultrasound depicts a well-defined hypoechoic uterine mass with posterior acoustic shadowing. However, when these tumors outgrow their blood supply and degenerate, sonographic findings may include dense focal shadowing from calcific degeneration or cystic regions of central necrosis. Fibroids are often described as subserosal, submucosal, or intramural based on their location. They are usually asymptomatic, but patients may present with abnormal or dysfunctional uterine bleeding, pain, or, less commonly, infertility. Magnetic resonance imaging (MRI) may be helpful for treatment planning of symptomatic fibroids, as well as to differentiate a diffuse fibroid uterus from adenomyosis. On MRI, leiomyomas characteristically demonstrate low T2-weighted signal intensity.
- **Adenomyosis.** The finding of endometrial tissue displaced within the myometrium of the uterus characterizes adenomyosis, referred to as endometriosis of the uterus. Clinical manifestations are frequent and include dysmenorrhea, menorrhagia, and, in some cases, infertility. Adenomyosis can be overlooked by ultrasound because its appearance is often nonspecific; thus MRI is required for confirmation in most cases. The imaging appearance generally reflects its focal or diffuse pattern within the myometrium. An ill-defined focal echogenic mass suggests focal adenomyosis. Diffuse adenomyosis and myometrial fibroids are difficult to distinguish sonographically, as both are noted to cause increased uterine heterogeneity. One clue to identify diffuse adenomyosis on ultrasound is asymmetric uterine enlargement of the anterior and posterior walls. Myometrial cysts, when present, are very specific for adenomyosis. On MRI, adenomyosis results in focal or diffuse thickening of the junctional zone (>12 mm). Myometrial cysts, in contrast, display characteristic increased T2 signal intensity.
- **Endometrial carcinoma.** The most common gynecologic malignancy in North America, endometrial carcinoma is caused by factors that predispose women to unopposed estrogen stimulation. Postmenopausal uterine bleeding in an otherwise asymptomatic woman is considered a sentinel sign of malignancy until proven otherwise. On ultrasound, a thickened endometrium in a postmenopausal woman (>5 mm) is an early sign of endometrial carcinoma, and a biopsy is indicated. Ultrasound findings of more advanced disease include an enlarged heterogeneous uterus, irregular lobulated endometrial margins or loss of endometrial-myometrial borders, and a large endometrial fluid collection. When endometrial carcinoma invades the myometrium, the appearance can mimic other myometrial processes. Hysterosonography is superior to transvaginal ultrasound and is combined with computed tomography or MRI in staging endometrial carcinoma.

Diagnosis

Adenomyosis

✓ Pearls

- Fibroids are described on ultrasound as focal or diffuse in a subserosal, intramural, or submucosal location.
- Adenomyosis may be sonographically challenging, but it is suggested with asymmetric uterine enlargement.
- Biopsy is warranted in a woman with postmenopausal bleeding and a thickened endometrial stripe on ultrasound.

Suggested Readings

Fleischer AC. Transvaginal sonography of endometrial disorders: an overview. Radiographics 1998;18(4):923–930

Middleton WD, Kurtz AB, Hertzberg BS. Ultrasound: The Requisites. St. Louis, MO: Mosby; 2004

Mogavero G, Sheth S, Hamper UM. Endovaginal sonography of the nongravid uterus. Radiographics 1993;13(5):969–981

Case 183

David J. Weitz

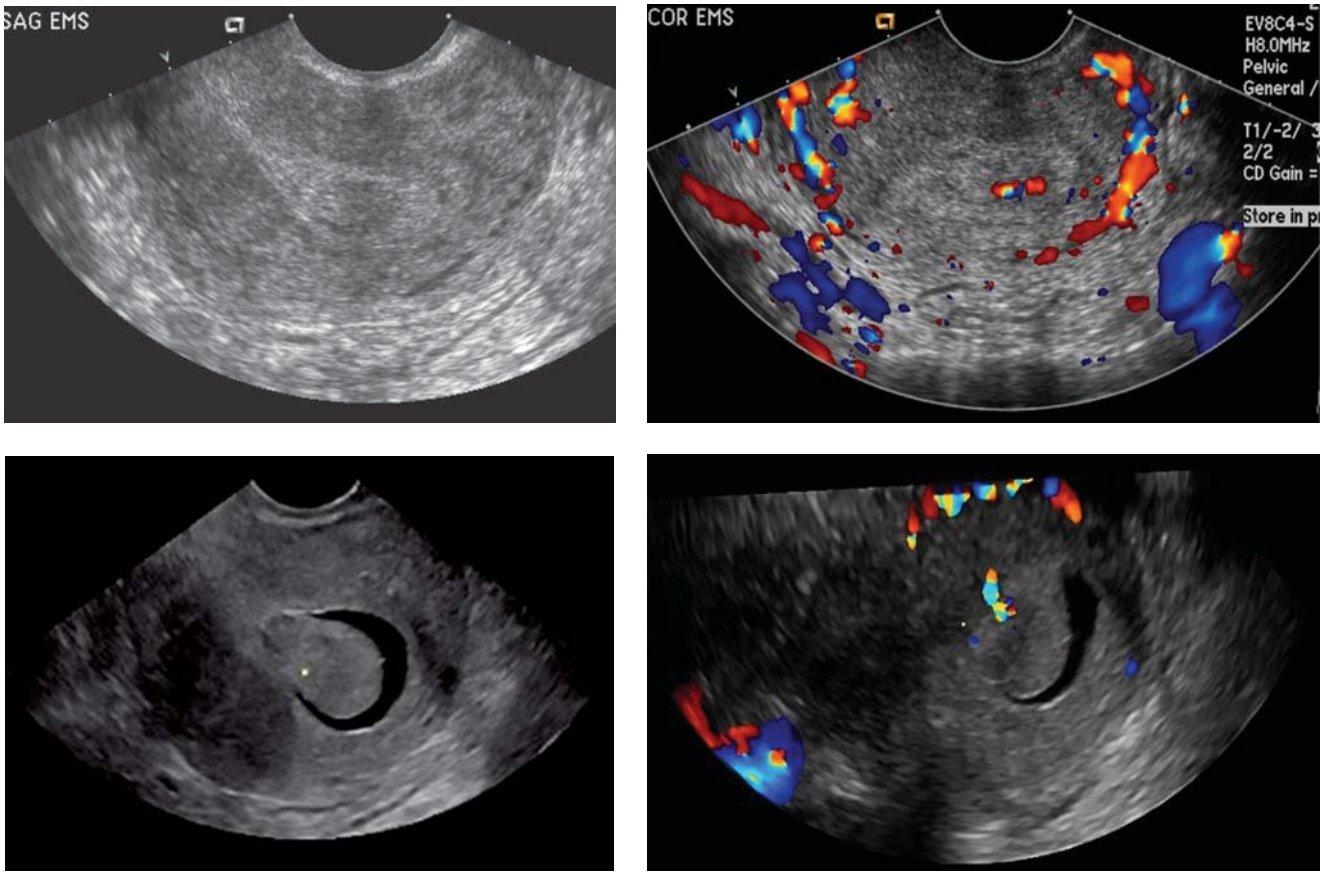


Fig. 183.1 **(A,B)** Images from a transvaginal ultrasound of the uterus reveal an abnormally thickened endometrial stripe with internal flow. **(C,D)** Further work-up with saline infusion sonohysterogram shows an echogenic predominately homogeneous endometrial polypoid mass with a vascular stalk captured on Doppler flow imaging.

Clinical Presentation

A 42-year-old woman presents with intermittent spotting between menstrual cycles (**Fig. 183.1**).

Key Imaging Finding

Thickened endometrial stripe

Top 3 Differential Diagnoses

- **Endometrial hyperplasia.** Endometrial hyperplasia is a common cause of abnormal uterine bleeding in both pre- and postmenopausal women. Hyperplasia is linked to unopposed estrogen stimulation (e.g., tamoxifen) and may progress to endometrial carcinoma. The most common appearance is a uniformly thickened hyperechoic endometrium with or without cysts; however, ultrasound is nonspecific, and confirmation with biopsy is required.
- **Endometrial polyps.** Endometrial polyps can occur in young adults, but they are a frequent source of uterine bleeding in postmenopausal women. Ultrasound may show echogenic endometrial thickening. The presence of a vascular stalk is helpful but not pathognomonic. Hysterosonography, the preferred imaging exam for endometrial masses, will confirm a polyp as a pedunculated echogenic mass outlined by fluid.
- **Endometrial carcinoma.** An endometrial stripe >5 mm (8 mm if the patient is on hormone replacement therapy) is abnormal in postmenopausal women and should prompt an investigation to exclude malignancy. Although the appearance is variable, suspicion for endometrial carcinoma should be raised when the endometrium is thickened, irregular, or poorly marginated or if there is disruption of the endometrial-myometrial border. Advanced endometrial carcinoma may obstruct the endometrial canal, resulting in hydrometra, or invade the myometrium, mimicking leiomyomas.

Additional Differential Diagnoses

- **Submucosal fibroids.** Submucosal fibroids are the least common but most symptomatic type of fibroid. They generally appear as hypoechoic shadowing subendometrial masses. Given their submucosal location, they may be outlined by a more echogenic endometrium. They can protrude deep into the endometrial canal, mimicking a polyp, which makes hysterosonography a useful tool to differentiate between these entities.
- **Retained products of conception (RPOC).** RPOC is an uncommon complication (1–2%) of pregnancy that should be suspected in recent postpartum women or recently terminated pregnancies with persistent vaginal bleeding and pelvic pain. Ultrasound commonly reveals an endometrial mass with or without Doppler flow. If flow is present, a high-velocity, low-resistance Doppler signature is suggestive of RPOC. Other findings are a round fluid collection or a gestational sac that may contain an embryo.
- **Gestational trophoblastic disease (GTD).** GTD ranges from a benign mole to choriocarcinoma. It is suspected in women with high beta HCG levels, abnormal bleeding, a uterine size greater than dates, and preeclampsia. Ultrasound features include an enlarged uterus, a thick echogenic endometrial canal, and through transmission; however, an additional finding of ovarian theca lutein cysts is highly suggestive of GTD.

Diagnosis

Endometrial polyp

✓ Pearls

- Endometrial hyperplasia commonly causes abnormal uterine bleeding and may progress to malignancy.
- Endometrial polyps can be confirmed by hysterosonography, a preferred exam for endometrial lesions.
- Findings for endometrial cancer include a thick irregular endometrium and disruption of the endometrial-myometrial border.
- GTD is suspected with elevated beta HCG, abnormal bleeding, a size greater than dates, and preeclampsia.

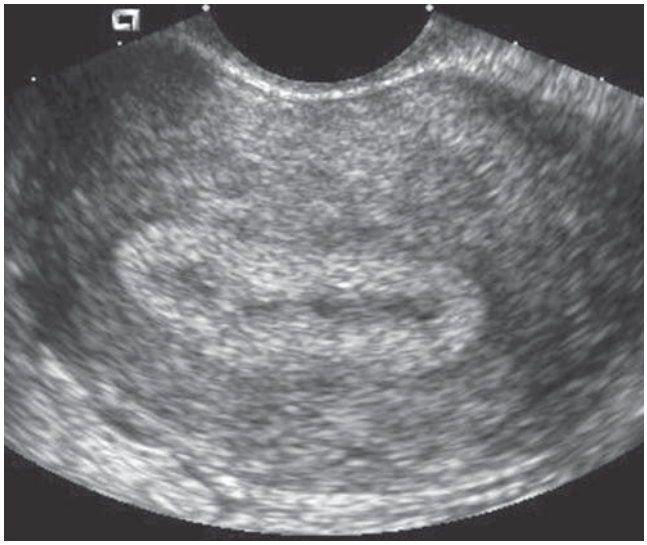
Suggested Readings

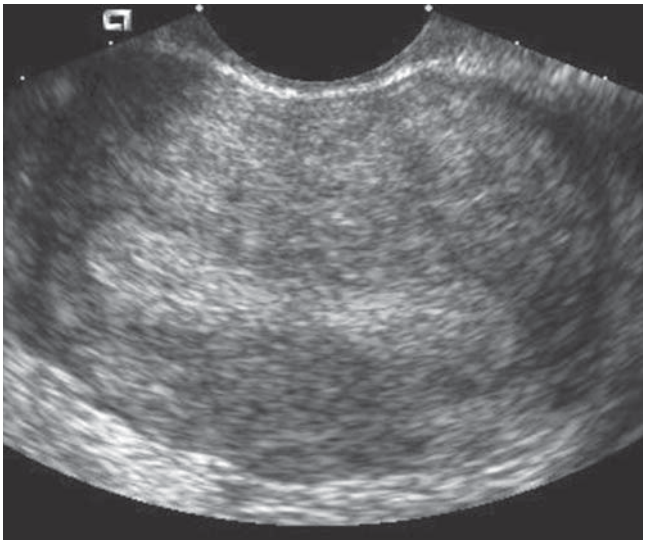
Davis PC, O'Neill MJ, Yoder IC, Lee SI, Mueller PR. Sonohysterographic findings of endometrial and subendometrial conditions. Radiographics 2002;22(4):803–816

Middleton WD, Kurtz AB, Hertzberg BS. Ultrasound: The Requisites. St. Louis, MO: Mosby; 2004

Case 184

David J. Weitz





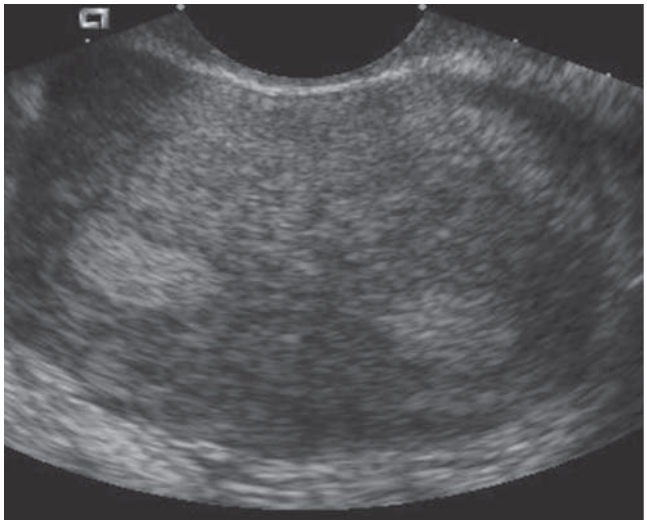


Fig. 184.1 **(A,B)** Ultrasound images demonstrate a thickened endometrial echo complex that begins to divide in the uterine body. **(C)** Two distinct and separated endometrial stripes are present in the uterine fundus.

Clinical Presentation

A premenopausal woman presents with dysfunctional uterine bleeding (**Fig. 184.1**).

Key Imaging Finding

Uterine anomaly

Top 3 Differential Diagnoses

- **Bicornuate uterus.** Uterine anomalies will be found in ~0.5% of the general population. Incomplete fusion of the müllerian ducts results in a bicornuate uterus and may manifest either as two uterine horns, two cervices, and one vagina (bicornuate bicollis), or as two uterine horns, one cervix, and one vagina (bicornuate unicollis). The uterine cornua in a bicornuate uterus can be hypoplastic, which may infrequently lead to fertility problems. If a rudimentary "functional" horn does not communicate with the other horn, symptomatic hydrometrocolpos may occur. On ultrasound, the endometrium is usually widely divided, and evaluation of the fundus reveals a midline uterine dimple at least 1 cm deep. Accuracy with newer three-dimensional coronal ultrasound approaches that of magnetic resonance imaging (MRI), the imaging gold standard. Treatment, if needed, is metroplasty. Any uterine anomaly should prompt a search for renal anomalies (commonly renal agenesis and ectopia), as uterine and renal anomalies frequently coexist because of their close relationship during fetal development.
- **Didelphus uterus.** Uterine didelphus results from the failure of paired embryonic müllerian (paramesonephric) ducts to fuse during fetal female development, resulting in two separate uteri, two cervices, and two vaginas. Ultrasound should be performed in the secretory phase because the endometrial stripe is thick and easily identified. Ultrasound will reveal two separate and distinct uteri, most often with widely separated uterine cornua. Fertility problems are unusual with this anomaly, which is usually discovered incidentally.
- **Septated uterus.** Failure of the median uterine septum to regress during development results in a septated uterus. Unlike uterine didelphus, which contains separate uterine cavities, a septated uterus is characterized by a thin septum that divides a single uterine cavity. Fertility problems occur frequently, as the fibrous septum generally will not support an embryo if implantation occurs on the relatively avascular septum. Though sometimes difficult, it is important to make the imaging distinction between septated and bicornuate anomalies, as treatment options differ. Although an involved metroplasty is required for a bicornuate uterus, a septated uterus is treated by a transvaginal hysteroscopic resection of the septum. On ultrasound, a narrowly divided endometrial echo complex is seen, but unlike a bicornuate anomaly, the fundal contour is normal, flat, or dimpled <1 cm.

Additional Differential Diagnoses

- **Arcuate uterus.** An arcuate uterus is generally considered a normal variant. This is an asymptomatic uterine variation with no observed complications. Sonographically, there may be a small indentation of the uterine fundus, but the uterine cavity is normal, leading to no fertility problems. As mentioned above, MRI is the imaging gold standard, but ultrasound may be preferred if findings are straightforward.

Diagnosis

Bicornuate uterus

✓ Pearls

- Ultrasound reveals a bicornuate uterus as a widely divided endometrial echo complex and midline dimple >1 cm.
- A didelphus uterus is usually an incidental finding, as complications with this anomaly are rare.
- A septated uterus is the most common uterine anomaly associated with infertility.
- An arcuate uterus causes no complications and is characterized as a small indentation of the uterine fundus.

Suggested Readings

Middleton WD, Kurtz AB, Hertzberg BS. Ultrasound: The Requisites. St. Louis, MO: Mosby; 2004

Trolano RN, McCarthy SM. Mullerian duct anomalies: imaging and clinical issues. Radiology 2004;233:19–34

Case 185

Anokh Pahwa

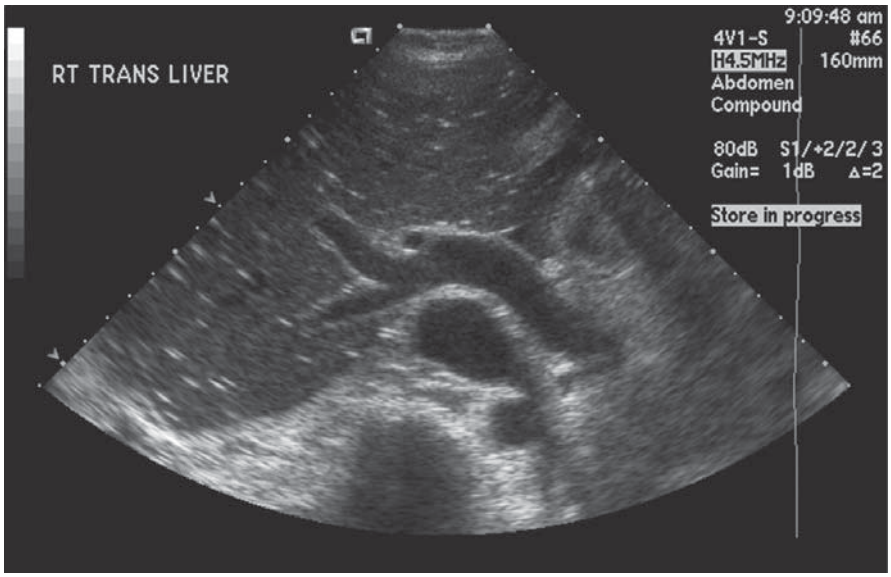


Fig. 185.1 Transverse sonographic image through the liver demonstrates increased echogenicity in the region of the portal triads, also referred to as a "starry sky" appearance.

Clinical Presentation

A 46-year-old woman presents with right upper quadrant pain (**Fig. 185.1**).

Key Imaging Finding

"Starry sky" liver

Top 3 Differential Diagnoses

- **Acute hepatitis.** Although usually sonographically undetectable, acute hepatitis is the most common cause of the "starry sky" appearance of the liver on ultrasound. Fibrosis of the portal venous walls leads to increased echogenicity of the portal triads. The "starry sky" appearance is secondary to this increased echogenicity of the portal triads in conjunction with decreased parenchymal echogenicity as a result of intralobular inflammatory edema. Of note, chronic hepatitis is more likely to present with opposite findings, including coarsened parenchymal echotexture and decreased visualization of the portal triads.
- **Hepatic congestion.** Hepatic congestion is typically secondary to right-sided heart failure or less commonly inferior vena cava (IVC) or hepatic vein occlusion (Budd–Chiari syndrome). The sonographic findings of passive hepatic congestion are hepatomegaly and enlargement of the IVC and hepatic veins. In right-sided heart failure, Doppler waveforms demonstrate increased pulsatility within the hepatic and portal veins as a result of transmittance of right heart pressures. Rarely, the liver demonstrates a "starry sky" appearance.
- **Infiltrating neoplasm.** Both metastatic disease to the liver and primary hepatocellular carcinoma (HCC) can present as diffuse/infiltrative masses. Occasionally, diffuse tumor infiltration results in decreased echogenicity of the hepatic parenchyma, mimicking the "starry sky" appearance on ultrasound. Secondary involvement of the liver may occur with breast or lung carcinoma, as well as leukemia/lymphoma, to name a few entities. Diffuse HCC and diffuse metastatic disease can both lead to a nonspecific, heterogeneous, and multinodular-appearing liver. The presence of advanced cirrhosis decreases the sensitivity of ultrasound in detecting hepatic masses by 50%, particularly when diffuse.

Additional Differential Diagnoses

- **Toxic shock syndrome (TSS).** TSS is a multisystem, toxin-mediated disease most commonly caused by *Staphylococcus aureus.* TSS presentation can be varied, but the hallmarks include rapid onset of fever, hypotension, rash, vomiting, and diarrhea. In the liver, TSS can cause inflammation of the portal venous tracts, leading to a "starry sky" liver on ultrasound.
- **Biliary or portal venous gas.** Gas within the biliary ducts or portal veins results in increased echogenicity of the portal triads, which may mimic the "starry sky" appearance on ultrasound. Key differentiating features are the mobility of echoes (gas) during real-time examination and the usually normal echotexture of the underlying hepatic parenchyma.

Diagnosis

Acute hepatitis

✓ Pearls

- Acute hepatitis is the most common cause of the "starry sky" appearance on ultrasound.
- Hepatic congestion presents with hepatomegaly, dilated IVC/hepatic veins, and, rarely, a "starry sky" liver.
- Infiltrating neoplasms may decrease the hepatic parenchymal echogenicity, mimicking a "starry sky" liver.
- Biliary or portal venous gas can be distinguished from a "starry sky" liver by mobility of the echoes.

Suggested Readings

Abu-Judeh HH. The "starry sky" liver with right-sided heart failure. AJR Am J Roentgenol 2002;178:78

Kurtz AB, Rubin CS, Cooper HS, et al. Ultrasound findings in hepatitis. Radiology 1980;136:717–723

Lieberman J, Bryan P, Cohen A. Toxic shock syndrome: ultrasonographic findings. AJR Am J Roentgenol 1981;137:606–607

Middleton WD, Kurtz AB, Hertzberg BS. Ultrasound: The Requisites. St. Louis, MO: Mosby; 2004

Case 186

David J. Weitz

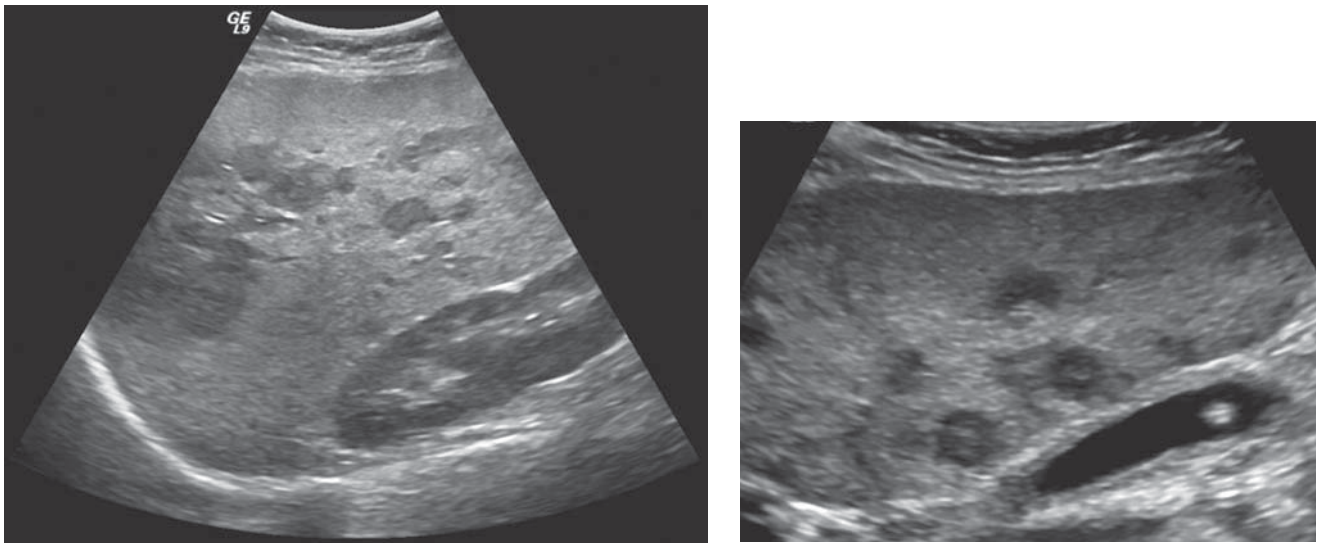


Fig. 186.1 **(A)** Ultrasound image of the right hepatic lobe reveals multiple heterogeneously hypoechoic lesions. **(B)** Focused gray scale image shows several discrete masses with an isoechoic central portion surrounded by a thick hypoechoic rim, referred to as "target" lesions. Multiple discrete and confluent targetlike lesions (not shown) were also present in the left hepatic lobe. An incidental gallstone is seen within the gallbladder lumen.

Clinical Presentation

A 60-year-old woman presents with generalized abdominal fullness (**Fig. 186.1**).

Key Imaging Finding

"Target" lesions in the liver

Top 3 Differential Diagnoses

- **Hepatocellular carcinoma (HCC).** In North America, HCC is the most common primary hepatic malignancy but is less common than metastases. It usually results from chronic liver disease and cirrhosis-causing conditions, including alcohol abuse, hepatitis B and C, aflatoxins, and other rarer entities. Ultrasound is used to screen patients with known risk factors. Commonly observed is a vascular mass surrounded by smaller lesions; however, HCC may present as a solitary lesion. A target lesion at sonography (iso- or echogenic center with a thick hypoechoic rim) is worrisome for HCC, as well as other malignancies. Portal vein invasion by HCC is common and can be accurately demonstrated on ultrasound. Any solid liver mass discovered in a patient with risk factors should be regarded as HCC until proven otherwise.
- **Metastatic disease.** The liver is a frequent site of metastatic involvement due to its rich blood supply from the hepatic artery and portal vein. Breast, lung, and gastrointestinal malignancies are among the most common metastases to the liver in adults. Although single lesions occasionally occur, metastases are nearly always multiple. The ultrasound appearance is quite variable, ranging from cystic to solid with variable echogenicity. Most often, liver metastases appear as multiple solid hypoechoic masses or target lesions. Computed tomography (CT) and magnetic resonance imaging (MRI) are usually obtained once a suspicious lesion is found. Ultrasound can be used to guide biopsies.
- **Lymphoma.** In the unusual case that lymphoma involves the liver, it is more likely to be the non-Hodgkin variant. Patterns on ultrasound include multiple nodules, large masses, and diffusely infiltrating disease without a discrete mass. Most commonly, ultrasound reveals small, diffuse, hypoechoic nodules or target lesions. A simple or complex "cystic" liver lesion in the setting of lymphoma should be considered suspicious. Other supportive findings are splenomegaly, hepatomegaly with or without discrete masses, and abdominal lymphadenopathy.

Additional Differential Diagnoses

- **Hepatic abscesses.** Liver abscesses have a variety of ultrasound appearances but may present as target lesions. Given that target lesions are most often associated with malignancy, abscess should be suspected in the appropriate clinical setting (fever or leukocytosis). Diagnosis is confirmed by percutaneous drainage.
- **Hepatic pseudotumor.** Hepatic pseudotumors are rare lesions that occur in the medial segment of the left lobe (segment 4) and are thought to arise from variations in hepatic blood flow leading to focal hepatic steatosis. Because benign target lesions are indistinguishable from malignancies, the diagnosis is suggested when a solitary target lesion is found in segment 4 of the liver. CT, MRI, and often biopsy are needed to exclude a more worrisome mass.

Diagnosis

Metastatic disease (breast cancer)

✓ Pearls

- HCC is the most common primary hepatic malignancy and frequently presents as a target lesion on ultrasound.
- Metastases are among the most common causes of target lesions in the liver.
- Ultrasound patterns of lymphoma are multiple nodules or masses and diffusely infiltrating tumor.
- Hepatic abscesses may be identified as target lesions and should be favored with clinical signs of infection.

Suggested Readings

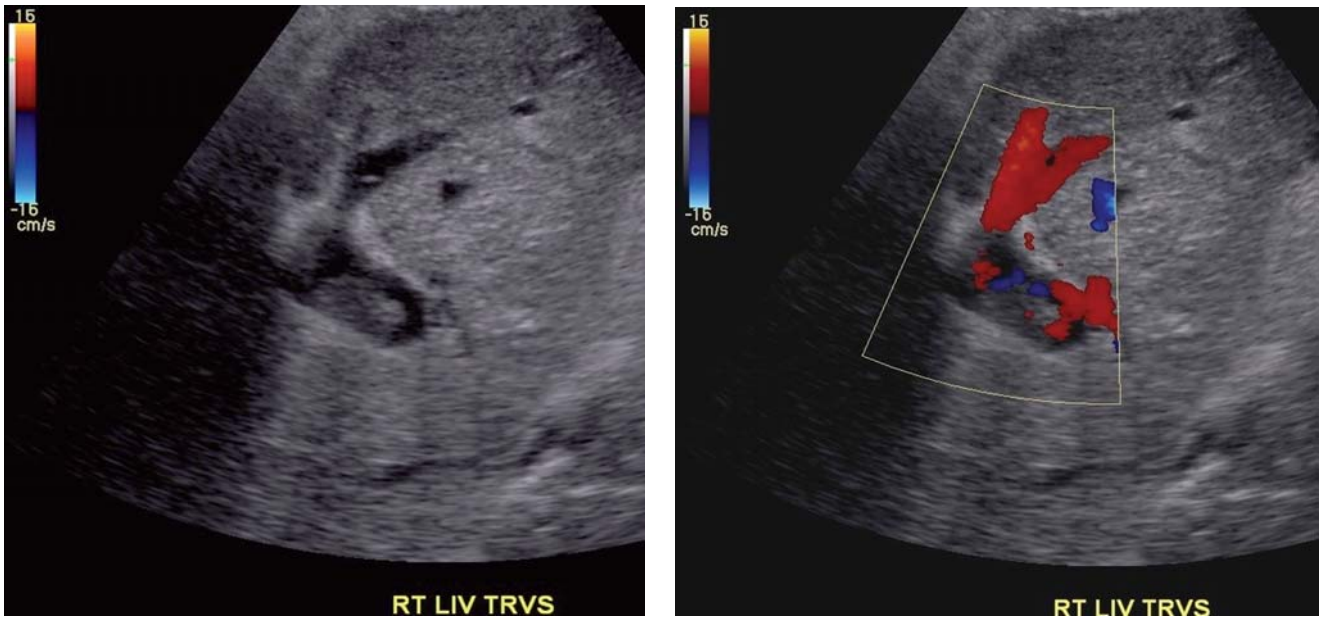
Castroagudin JF, Molina E, Abdulkader I, et al. Sonographic features of liver involvement by lymphoma. J Ultrasound Med 2007;26:791–796

Middleton WD, Kurtz AB, Hertzberg BS. Ultrasound: The Requisites. St. Louis, MO: Mosby; 2004

Rubaltelli L, Savastano S, Khadivi Y, et al. Targetlike appearance of pseudotumors in segment IV of the liver on sonography. AJR Am J Roentgenol 2002;178:75–77

Case 187

David J. Weitz



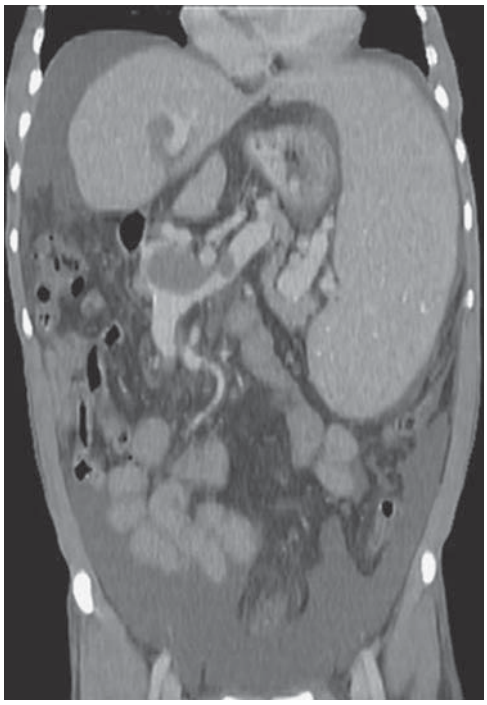


Fig. 187.1 **(A)** Transverse gray scale sonographic image through the liver demonstrates an isoechoic intraluminal filling defect (thrombus) within the main portal vein. **(B)** Color Doppler image delineates hepatopetal flow coursing around the thrombus, as well as vascularity within the thrombus itself. **(C)** Reformatted contrast-enhanced computed tomography (CT) image in the coronal plane reveals the extent of the thrombus that fills and expands the main portal vein and extends into the splenic vein. Additional CT findings are a nodular liver contour, massive splenomegaly, ascites, and varices, consistent with cirrhosis and portal hypertension. Additional imaging (not shown) revealed an infiltrating hepatic mass consistent with hepatocellular carcinoma in the setting of chronic liver disease.

Clinical Presentation

An adult male patient presents with increasing abdominal girth (**Fig. 187.1**).

Key Imaging Finding

Portal vein thrombosis

Top 3 Differential Diagnoses

- **Tumor thrombus.** Tumor invasion of the portal vein is most commonly caused by hepatocellular carcinoma; however, malignancies such as cholangiocarcinoma, gallbladder carcinoma, pancreatic carcinoma, gastric carcinoma, and metastases are well-established though less common offenders. Ultrasound can diagnose tumor invasion accurately by demonstrating flow within the thrombus. It is important to note that in some cases tumor thrombus may be hypovascular without detectable flow. Additional supportive findings are portal venous enlargement or expansion that favors a neoplastic process over a bland thrombus.
- **Hepatic cirrhosis with portal hypertension.** In the United States, alcohol abuse is the most common cause of cirrhosis; however, fibrosis of any etiology, if unchecked, will lead to portal hypertension with sluggish portal flow, stimulating thrombus formation. Ultrasound usually demonstrates an echogenic intraluminal clot in the portal vein; however, an acute thrombus may also be hypo- or anechoic. In chronic portal hypertension, collateral circulation may be seen as tortuous gastric, esophageal, and splenic varices. The development of collaterals within the porta hepatis is called cavernous transformation. Portal vein enlargement (>13 mm), ascites, and splenomegaly support the diagnosis of portal hypertension. Reversal of portal flow (hepatofugal) or a recanalized umbilical vein is virtually diagnostic of portal hypertension.
- **Periportal infection/inflammation.** Abundant literature supports the development of portal vein thrombosis in a variety of infectious and inflammatory conditions. The inflammatory process causes stasis of flow and subsequent clot formation. Common causes are sepsis, cholangitis, hepatitis, pancreatitis, and, occasionally, appendicitis.

Additional Differential Diagnoses

- **Hypercoagulable conditions.** Acquired hypercoagulable states include pregnancy, prolonged immobilization, medications (over-the-counter products), tobacco use, and underlying malignancy. Inherited conditions may summate with other risk factors, unmasking an underlying hypercoagulable state resulting in portal venous thrombosis. For example, factor V Leiden, protein C, or protein S deficiencies may become clinically evident when combined with external risk factors.
- **Trauma/iatrogenic.** Portal vein thrombosis may occur in the setting of trauma or as a complication of medical procedures. Common iatrogenic causes of portal vein thrombosis include umbilical catheter placement in neonates and patients undergoing orthotopic liver transplant.

Diagnosis

Tumor thrombus (hepatocellular carcinoma) in the portal vein

✓ Pearls

- Ultrasound can accurately demonstrate tumor invasion of the portal vein by revealing thrombus vascularity.
- Portal flow reversal and umbilical vein recanalization are diagnostic of portal hypertension.
- Sepsis, cholangitis, hepatitis, pancreatitis, and other inflammatory etiologies can cause venous thrombosis.
- Iatrogenic causes of portal vein thrombosis include umbilical catheter placement and liver transplant.

Suggested Readings

Middleton WD, Kurtz AB, Hertzberg BS. Ultrasound: The Requisites. St. Louis, MO: Mosby; 2004

Rumack CM, Wilson SR, Charboneau JW. Diagnostic Ultrasound. 3rd ed. St. Louis, MO: Mosby; 2005

Tessler FN, Gehring BJ, Gomes AS, et al. Diagnosis of portal vein thrombosis: value of color Doppler imaging. AJR Am J Roentgenol 1991;157(2):293–296

Case 188

Sima Naderi

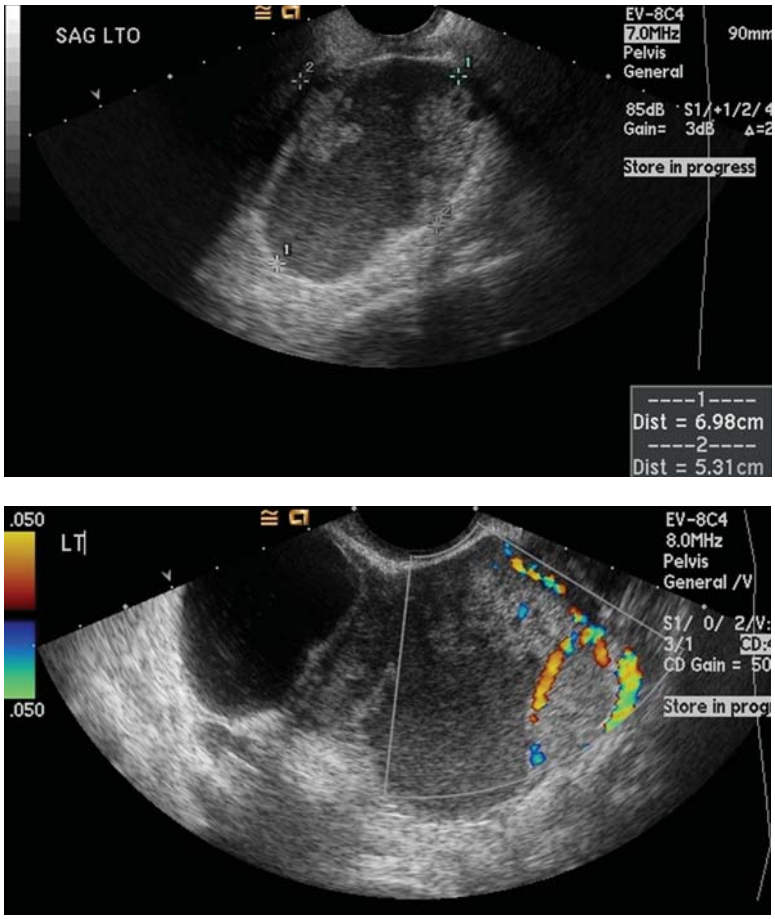


Fig. 188.1 **(A)** Gray scale endovaginal ultrasound image of the left ovary demonstrates a left ovarian cystic mass with low-level echoes and echogenic papillary projections. **(B)** Color flow interrogation shows flow within the solid portions of the mass.

Clinical Presentation

A 55-year-old woman presents with an adenexal mass on a pelvic exam. Human chorionic gonadotropin (HCG) is negative (**Fig. 188.1**).

Key Imaging Finding

Cystic adnexal mass with negative HCG

Top 3 Differential Diagnoses

- **Ovarian neoplasm.** Ninety percent of ovarian malignancies are epithelial neoplasms. The remaining are germ cell tumors, sex cord-stromal tumors, and metastatic tumors. Malignant masses are associated with advanced age, nulliparity, and a positive family history. Ultrasound is the initial study of choice for evaluating the adnexa. Ultrasound is not able to definitively differentiate benign ovarian neoplasms, such as serous cystadenoma and mucinous cystadenomas, from malignant. An ovarian mass has a higher incidence of being malignant if it is >10 cm or contains more complex ultrasound features, such as irregular walls, thick irregular septations with vascularity, papillary projections, and solid echogenic components. Peritoneal carcinomatosis and malignant ascites can also be present. Doppler findings may be helpful, but they should be interpreted in association with mass morphology. Malignant tumors are regularly staged with computed tomography. Magnetic resonance imaging (MRI) can be a valuable problem-solving tool for sonographically nondiagnostic masses.
- **Hemorrhagic cyst.** Functional cysts such as follicular or corpus luteal cysts can have internal hemorrhage. Clinically, patients may complain of acute onset of unilateral adnexal pain. Appearance is variable depending on the stage of the clot, but acute hemorrhage appears as a complex echogenic mass with through transmission. As the hemorrhage ages, the mass characteristically shows reticular-type internal echoes. As the clot retracts, fluid–fluid levels can be seen, or the echogenic clot can settle in the dependent portion of the cyst, which can mimic a papillary projection of malignancy. This is readily differentiated, however, by the lack of flow within the clot on color Doppler. Hemorrhagic cysts can reach an enormous size, but any adnexal mass larger than a follicle (>2.5 cm) in a premenopausal patient should warrant follow-up ultrasound to confirm diminishing size or resolution.
- **Tubo-ovarian abscess.** Tubo-ovarian abscess is usually suspected based on the clinical presentation of pelvic pain and localized adnexal tenderness in an ill-appearing patient. If significantly dilated and redundant, the fallopian tube can mimic a cystic adnexal mass. As the infection spreads, the ovaries enlarge, and the margins of pelvic structures become indistinct, such that inflammation may prevent the vaginal transducer from separating the ovary and tube. The distorted anatomy can make ultrasound challenging to interpret.

Additional Differential Diagnoses

- **Endometrioma.** Unlike the rapid onset of pain seen with hemorrhagic cysts, chronic pelvic pain is a frequent complaint with endometriosis. Endometriomas most commonly implant on the ovary. They are characteristically thick-walled cystic lesions with homogeneous low-level echoes and through transmission. Ultrasound may show a complex mass similar to a hemorrhagic cyst. Some endometriomas can appear solid or have thick septa mimicking an ovarian neoplasm. MRI can be helpful by demonstrating chronic blood products seen as T2 hypointensity (shading).

Diagnosis

Ovarian neoplasm (mucinous cystadenoma)

✓ Pearls

- Ultrasound findings for ovarian malignancy include papillary projections, thick septations, and a large-sized mass.
- The appearance of a hemorrhagic cyst changes over time and is associated with acute adnexal tenderness.
- A tubo-ovarian abscess is painful and should be suspected in ill-appearing patients with a history of pelvic inflammatory disease.
- Endometriomas are classically thick-walled, homogeneous adnexal lesions with through transmission.

Suggested Readings

Fried AM, Kenney CM III, Stigers KB, Kacki MH, Buckley SL. Benign pelvic masses: sonographic spectrum. Radiographics 1996;16(2):321–334

Jeong YY, Outwater EK, Kang HK. Imaging evaluation of ovarian masses. Radiographics 2000;20(5):1445–1470

Middleton WD, Kurtz AB, Hertzberg BS. Ultrasound: The Requisites. St. Louis, MO: Mosby; 2004

Case 189

Eleanor L. Ormsby

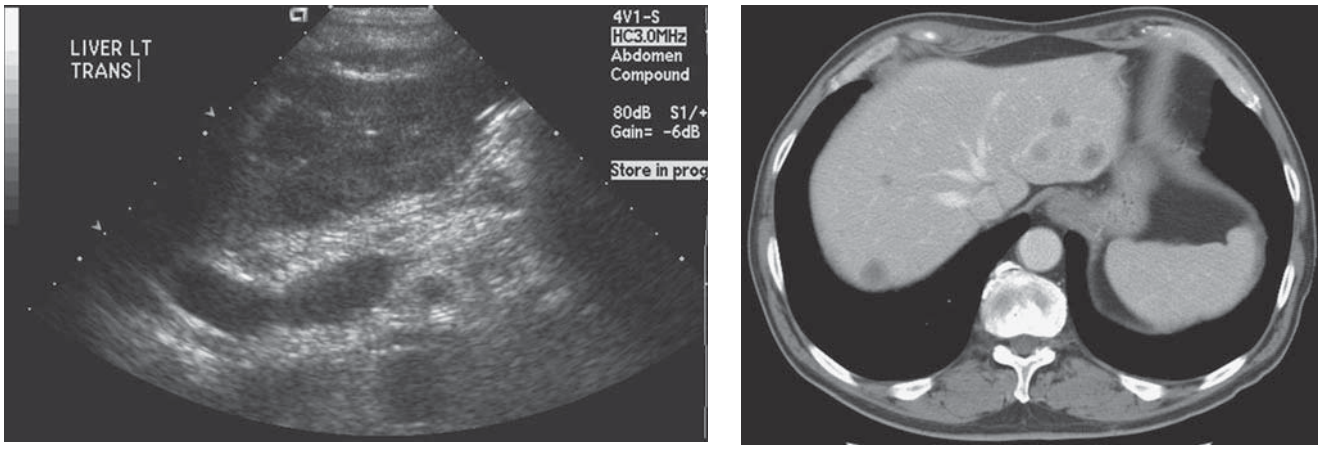


Fig. 189.1 **(A)** Transverse ultrasound image through the left hepatic lobe demonstrates multiple hypoechoic masses. **(B)** Contrast-enhanced axial computed tomography image through the liver in the soft tissue window shows multiple corresponding low-density masses in both lobes.

Clinical Presentation

A 67-year-old man presents with jaundice and a history of lymphoma (**Fig. 189.1**).

Key Imaging Finding

Multiple hypoechoic liver masses

Top 3 Differential Diagnoses

- **Neoplasm.** Metastatic disease is the most common malignancy to involve the liver and usually presents with multiple masses involving both hepatic lobes. Neoplasms can have a variety of sonographic appearances, including the classic "target" appearance, with an echogenic center and a hypoechoic halo, as well as multiple uniformly hypoechoic masses. Hepatocellular carcinoma (HCC) is the most common primary hepatic malignancy and may present as solitary, multifocal, or diffuse and infiltrating masses with variable echogenicity. HCC usually occurs in the setting of chronic liver disease or cirrhosis. Lymphoma is a homogeneous tumor that produces hypoechoic lesions in the liver. The sonographic appearance may mimic a cyst. Given the overlapping nature of these neoplasms, tissue diagnosis is often required.
- **Multifocal abscesses.** Multifocal abscesses in the liver commonly appear as complex fluid collections with mixed echogenicity and thick-walled cysts. They can also mimic solid hepatic masses with variable echogenicity, especially early in the disease process. Patients with multifocal abscesses are clinically symptomatic with fever, leukocytosis, and pain.
- **Candidiasis.** Fungal infections of the liver usually occur in immunocompromised patients; the most common organism is *Candida*. Although it usually causes very small lesions (microabscesses), larger lesions occasionally occur. These typically have a "target" appearance, with a central echogenicity and a peripheral hypoechoic halo, but they may also appear as hypoechoic masses. With healing, these become uniformly hyperechoic and ultimately may calcify.

Additional Differential Diagnoses

- **Hematoma.** Hepatic hematomas can be traumatic or iatrogenic. They can appear as complex cystic lesions or hypoechoic masses. Acute hematomas are often isoechoic to liver parenchyma and produce only subtle alterations in hepatic echogenicity. However, as they become progressively more liquefied, they appear more hypoechoic and cystic. There should be no blood flow on color Doppler imaging.
- **Diffuse fatty infiltration with focal fatty sparing.** With diffuse fatty infiltration of the liver, there is uniformly increased echogenicity of the liver. Under normal circumstances, liver parenchyma is only slightly more echogenic than the renal cortex. Fatty infiltration is recognized by seeing marked discrepancy between the hyperechoic liver and the less echogenic kidney. In many cases, there will be focal areas of spared normal liver parenchyma that appear hypoechoic with respect to the fatty infiltrated parenchyma. These can be mistaken for focal hypoechoic lesions. Knowledge of the usual location of focal sparing, such as adjacent to the gallbladder fossa, falciform ligament, and porta hepatis, helps differentiate this entity from other lesions.

Diagnosis

Neoplasm (lymphoma)

✓ Pearls

- Multiple hypoechoic masses are nonspecific and may be seen in primary or secondary hepatic neoplasms.
- In the clinical setting of infection, multiple masses within the liver are suggestive of pyogenic abscesses.
- Although candidiasis may produce multiple hypoechoic liver lesions, microabscesses are seen most often.

Suggested Readings

Middleton WD, Kurtz AB, Hertzberg BS. Ultrasound: The Requisites. St. Louis, MO: Mosby; 2004

Prasad SR, Wang H, Rosas H, et al. Fat-containing lesions of the liver: radiologic-pathologic correlation. Radiographics 2005;25(2):321–331

Case 190

David J. Weitz

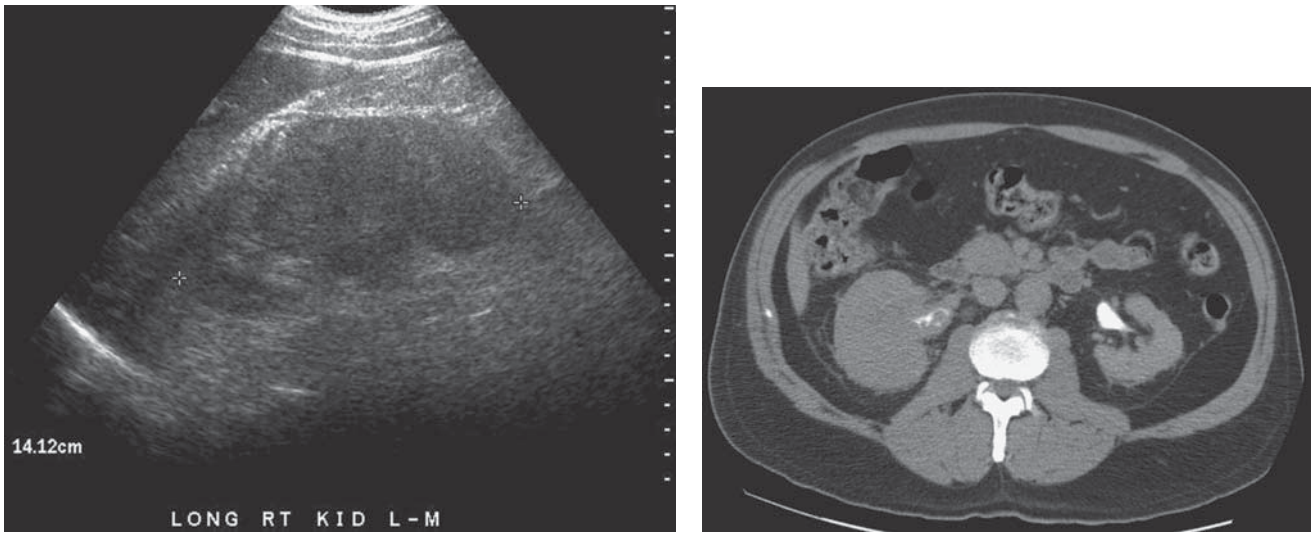


Fig. 190.1 **(A)** Sagittal ultrasound image shows enlargement of the right kidney and replacement of the normal echogenic renal sinus fat by a large hypoechoic mass involving the interpolar region and lower pole. **(B)** Axial computed tomography image from a delayed intravenous contrast examination reveals a large soft tissue mass invading the right kidney and collecting system.

Clinical Presentation

An elderly man presents with abnormal urinalysis (**Fig. 190.1**).

Key Imaging Finding

Hypoechoic renal mass

Top 3 Differential Diagnoses

- **Simple or complex renal cyst.** Cysts are overwhelmingly the most common renal mass. On ultrasound, simple cysts are circumscribed, anechoic, and have a sharp, well-defined back wall with through transmission. If the criteria for a simple cyst are satisfied, it is considered a benign lesion with no malignant potential. Complex cysts may have internal echoes, septations, fluid levels, calcification, or nodularity and are commonly seen in hemorrhagic or infected cysts; however, many of these features are shared by renal neoplasms. Internal vascularity and the absence of through transmission argue in favor of a solid mass rather than a complex cyst. Computed tomography (CT) and magnetic resonance imaging (MRI) are used to supplement ultrasound in characterizing cystic renal lesions.
- **Lymphoma.** Primary renal lymphoma is rare, as the kidneys are devoid of native lymph tissue. Thus the vast majority of renal lymphoma occurs in the setting of systemic disease or in an immunocompromised patient. Renal lymphoma is more frequently of the non-Hodgkin variant, and the majority of cases are bilateral. Most commonly, ultrasound will demonstrate bilateral hypoechoic masses. Lymphoma is a well-known mimicker of cysts and may appear homogeneously hypoechoic or anechoic, but a lack of through transmission is a helpful imaging clue in support of a solid mass. Because of the infiltrative nature of the tumor, enlarged kidneys without discrete masses should be considered suspicious in known cases of lymphoma. Retroperitoneal spread or transcapsular "perirenal growth" is another common ultrasound pattern that should not be confused for perinephric fluid.
- **Renal abscess.** Renal abscesses generally result from inadequately treated pyelonephritis. Although pyelonephritis usually does not warrant imaging, CT or ultrasound may be desired in patients who fail to improve after several days of antibiotics to assess for the possibility of an abscess. Ultrasound findings are indistinguishable from a complex cyst of any etiology, which underscores the importance of a relevant history of infection. CT is considered a superior modality for detecting small abscesses that may be sonographically occult.

Additional Differential Diagnoses

- **Renal cell carcinoma (RCC).** Although RCC typically manifests as a hyperechoic renal mass on ultrasound, it can also present as an iso- or hypoechoic mass. As they enlarge, RCCs often develop a heterogeneous echotexture, including development of cystic regions or septations. Because of the overlapping features of RCC with benign renal diseases, a suspicious renal mass on ultrasound warrants further work-up with CT or MRI.
- **Metastatic disease.** Renal metastases most commonly originate from melanoma, breast, lung, or gastrointestinal tract malignancies. Disease is most often bilateral, but solitary lesions do occur. When renal metastases are suspected, biopsy may be performed to distinguish metastatic disease from primary RCC. Ultrasound appearance is variable but should be suspected when a solid renal mass is discovered in the appropriate clinical setting.

Diagnosis

Renal lymphoma

✓ Pearls

- Simple renal cysts are benign and are the most common renal mass; complex cysts require further work-up.
- Non-Hodgkin lymphoma typically presents as bilateral hypoechoic renal masses; they may mimic cysts.
- Renal abscesses often result from inadequate treatment of pyelonephritis.
- Malignancies, such as atypical RCC and metastases, may present as hypoechoic renal masses.

Suggested Readings

Hartman DS, Choyke PL, Hartman MS. From the RSNA refresher courses: a practical approach to the cystic renal mass. Radiographics 2004;24(Suppl 1):S101–S115

Middleton WD, Kurtz AB, Hertzberg BS. Ultrasound: The Requisites. St. Louis, MO: Mosby; 2004

Case 191

David J. Weitz

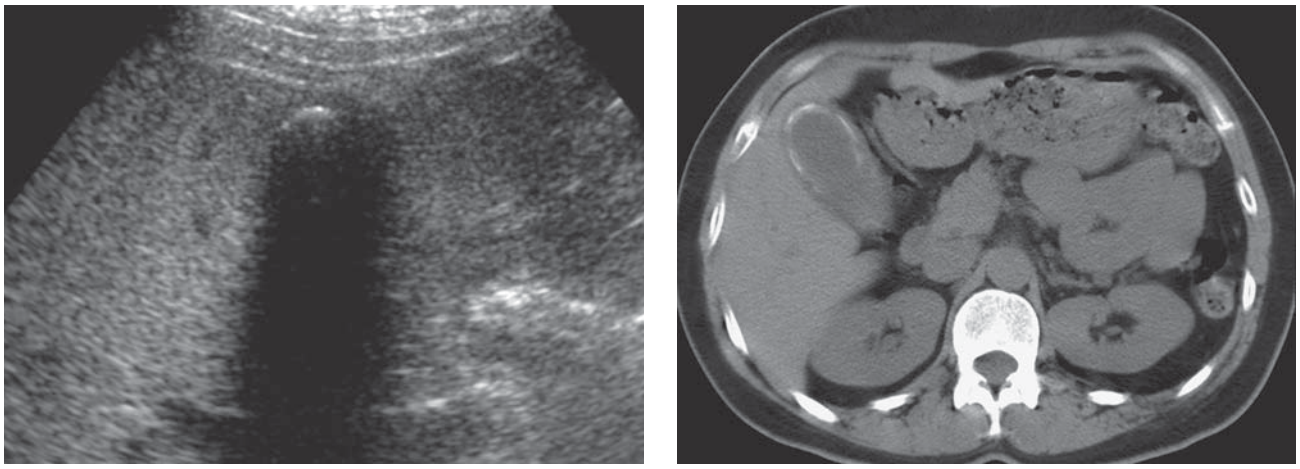


Fig. 191.1 **(A)** Right upper quadrant ultrasound image shows an echogenic curvilinear focus in the gallbladder fossa with extensive posterior shadowing. **(B)** Corresponding axial computed tomography image reveals a thin layer of calcification in the gallbladder wall.

Clinical Presentation

A 66-year-old woman presents with vague abdominal complaints (**Fig. 191.1**).

Key Imaging Finding

Hyperechoic foci in the gallbladder wall

Top 3 Differential Diagnoses

- **Porcelain gallbladder.** Porcelain gallbladder derives its name from the gross appearance at surgery, described as a brittle-appearing gallbladder with a bluish tint. A calcium-encrusted gallbladder wall occurs as a result of chronic inflammation, which, in large part, explains the very high association of gallstones and porcelain gallbladder. Porcelain gallbladder is considered to be an asymptomatic condition most often discovered incidentally. Once diagnosed, however, surgical removal is warranted due to an increased risk of gallbladder carcinoma. On ultrasound, the gallbladder wall appears as a highly reflective curvilinear interface with associated posterior shadowing and nonvisualization of the gallbladder lumen. If the sound beam is able to penetrate the calcification within the near wall, the posterior gallbladder wall will be visualized, distinguishing this entity from a stone-filled gallbladder where a back wall is absent. The diagnosis of porcelain gallbladder should prompt a search for a gallbladder mass, liver lesions, or lymphadenopathy. Confirmation of wall calcification is usually made by obtaining a plain film or computed tomography (CT) scan.
- **Emphysematous cholecystitis (EC).** EC is a rare complication of acute cholecystitis and is considered a surgical emergency. There is a high association of EC with older men with diabetes. The etiology is thought to be from vascular compromise, which leads to the production of gas in the gallbladder wall by bacteria such as *Escherichia coli.* Progression to gallbladder gangrene and perforation is much higher in EC than in uncomplicated acute cholecystitis. Early on, patients may complain of right upper quadrant tenderness. If gallbladder perforation occurs, temporary relief of symptoms is followed by generalized abdominal pain, usually from life-threatening peritonitis. Sonographically, the normal appearance of the gallbladder is replaced by a curvilinear hyperechoic line and dirty shadowing in the gallbladder fossa. Comet tail artifact, seen with gas and not calcification, is helpful to differentiate EC from a stone-filled gallbladder or porcelain gallbladder. Gas extending into the gallbladder lumen can appear as bright foci, which are mobile with patient positioning. Other findings are gallbladder calculi, wall thickening, and pericholecystic fluid. If ultrasound findings remain nonspecific, CT is exquisite for distinguishing between the entities above.
- **Adenomyomatosis.** Adenomyomatosis, a type of hyperplastic cholecystosis, is a relatively common benign finding affecting the gallbladder. Pathologically, there is muscular thickening of the gallbladder wall and deposition of cholesterol crystals into intramural diverticula, termed Rokitansky–Aschoff sinuses. Ultrasound typically shows a thickened gallbladder wall in asymptomatic patients. Punctate hyperechoic reflectors with comet tail artifact in the gallbladder wall are considered a very specific finding. Because gas will also produce comet tail artifact, care must be taken not to mistake this entity for EC. Therefore, it is important to note that adenomyomatosis is most often an incidental finding in contradistinction to the ill presentation noted in patients afflicted with EC.

Diagnosis

Porcelain gallbladder

✓ Pearls

- The diagnosis of porcelain gallbladder should prompt a cholecystectomy due to its association with malignancy.
- EC, seen in older men with diabetes, is a surgical emergency suggested by comet tail artifact in the gallbladder wall.
- Adenomyomatosis produces comet tail reflectors in the gallbladder wall but is found in asymptomatic patients.

Suggested Readings

Hanbidge AE, Buckler PM, O'Malley ME, Wilson SR. From the RSNA refresher courses: imaging evaluation for acute pain in the right upper quadrant. Radiographics 2004;24(4):1117–1135

Middleton WD, Kurtz AB, Hertzberg BS. Ultrasound: The Requisites. St. Louis, MO: Mosby; 2004

Rosenthal SJ, Cox GG, Wetzel LH, Batnitzky S. Pitfalls and differential diagnosis in biliary sonography. Radiographics 1990;10(2):285–311

Case 192

Sima Naderi

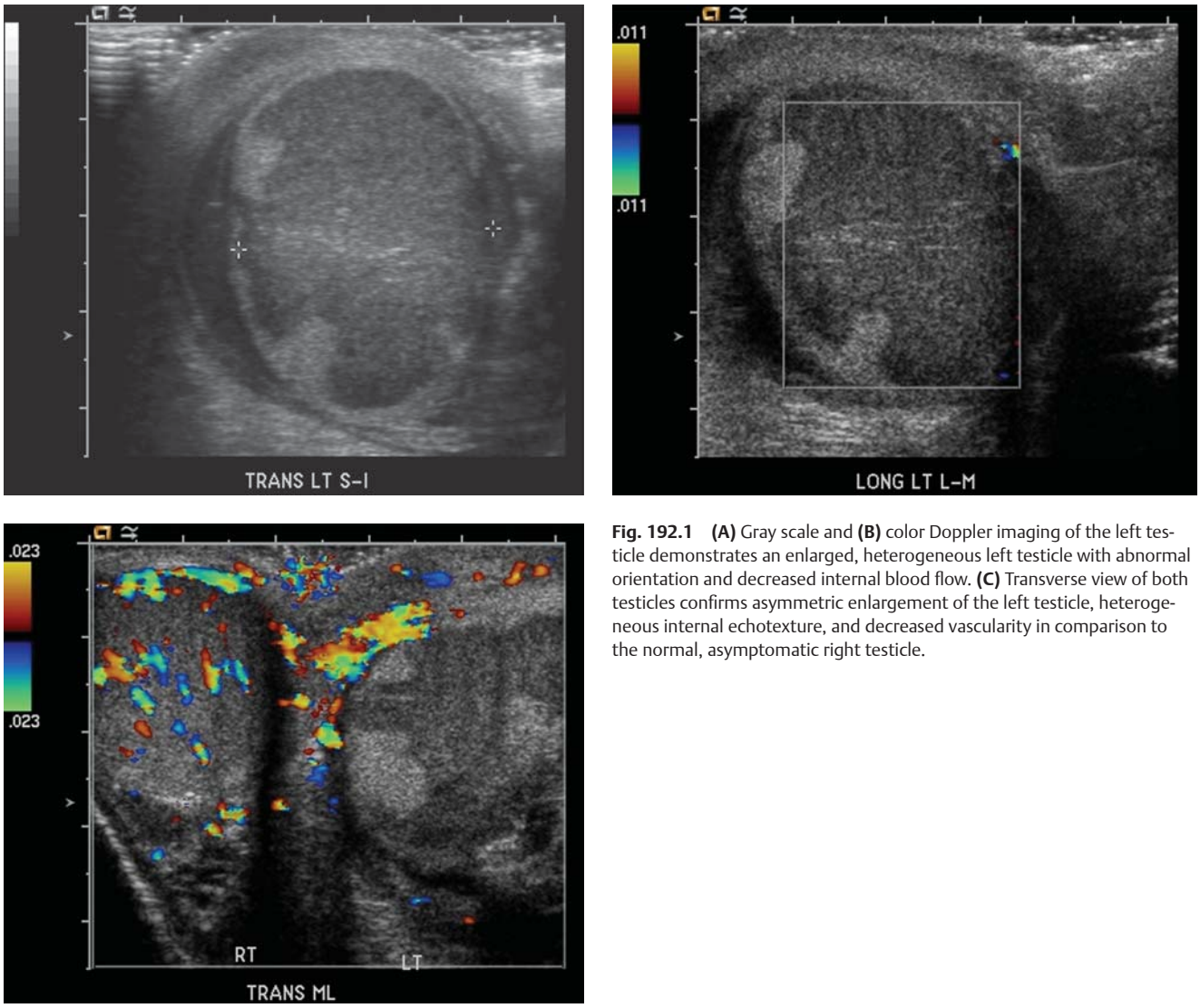


Fig. 192.1 **(A)** Gray scale and **(B)** color Doppler imaging of the left testicle demonstrates an enlarged, heterogeneous left testicle with abnormal orientation and decreased internal blood flow. **(C)** Transverse view of both testicles confirms asymmetric enlargement of the left testicle, heterogeneous internal echotexture, and decreased vascularity in comparison to the normal, asymptomatic right testicle.

Clinical Presentation

An 18-year-old patient presents with acute onset left testicular pain (**Fig. 192.1**).

Key Imaging Finding

Enlarged painful testicle

Top 3 Differential Diagnoses

- **Testicular torsion.** Torsion of the testicle occurs most commonly in the setting of the bell-clapper deformity. In this anomaly, the tunica vaginalis completely surrounds the testis, epididymis, and part of the spermatic cord, and there is no attachment of the testis to the posterior scrotal wall. Prompt diagnosis is needed. If surgery is performed within 6 hours of the onset of torsion/pain, there is improved chance of salvaging the testicle. Within the first 6 hours of torsion, gray scale imaging can show an enlarged testicle with normal echogenicity. As ischemia continues, the testicle becomes heterogeneous and hypoechoic. Color Doppler is a useful ultrasound function to diagnose torsion and demonstrates absent or significantly decreased blood flow in the affected testicle compared with the contralateral testicle. The number of twists of the spermatic cord determines testicular viability. Complete torsion, or >540 degrees of twisting, results in arterial occlusion. With partial torsion, or <360 degrees of twisting, the venous outflow is obstructed, resulting in arterial flow still visualized on Doppler examination, but with decreased diastolic flow. If spontaneous detorsion occurs, the resultant hyperemic testes may mimic orchitis.
- **Epididymo-orchitis.** Epididymo-orchitis is the key differential diagnosis in the adult patient with acute scrotal pain and swelling. The inflammatory disease usually involves the epididymis initially and spreads to the testis. The epididymis is enlarged, with decreased echogenicity and increased vascularity. Typical findings of orchitis are testicular enlargement and decreased echogenicity. In contrast to testicular torsion, the testicle has increased vascularity. If there is progression to testicular abscess, the complex fluid collections will have peripheral hyperemia. A potential pitfall is severe orchitis, which can cause global ischemia, mimicking testicular torsion.
- **Testicular hematoma/fracture.** Although testicular injury is in the differential of an enlarged painful testicle, there is typically a history of trauma. Sonographic findings include focal areas of increased and decreased testicular echogenicity due to areas of hemorrhage or infarction, as well as testicular contour irregularity. The testis may also appear distorted. If the surrounding tunica albuginea remains intact, surgery is not needed. However, if there is evidence of testicular rupture, surgery is required within 72 hours to salvage the testicle.

Diagnosis

Testicular torsion (left side)

✓ Pearls

- The testis is enlarged and hypoechoic in acute torsion; decreased or absent testicular flow is diagnostic.
- In contradistinction to torsion, epididymo-orchitis results in a hyperemic epididymis and testicle.
- Testicular injury is similar on ultrasound to torsion and epididymo-orchitis but is seen in the setting of trauma.

Suggested Readings

Middleton WD, Kurtz AB, Hertzberg BS. Ultrasound: The Requisites. St. Louis, MO: Mosby; 2004

Woodward PJ, Sohaey R, O'Donoghue MJ, Green DE. From the *Archives of the AFIP:* tumors and tumorlike lesions of the testis: radiologic-pathologic correlation. Radiographics 2002;22(1):189–216

Case 193

David J. Weitz

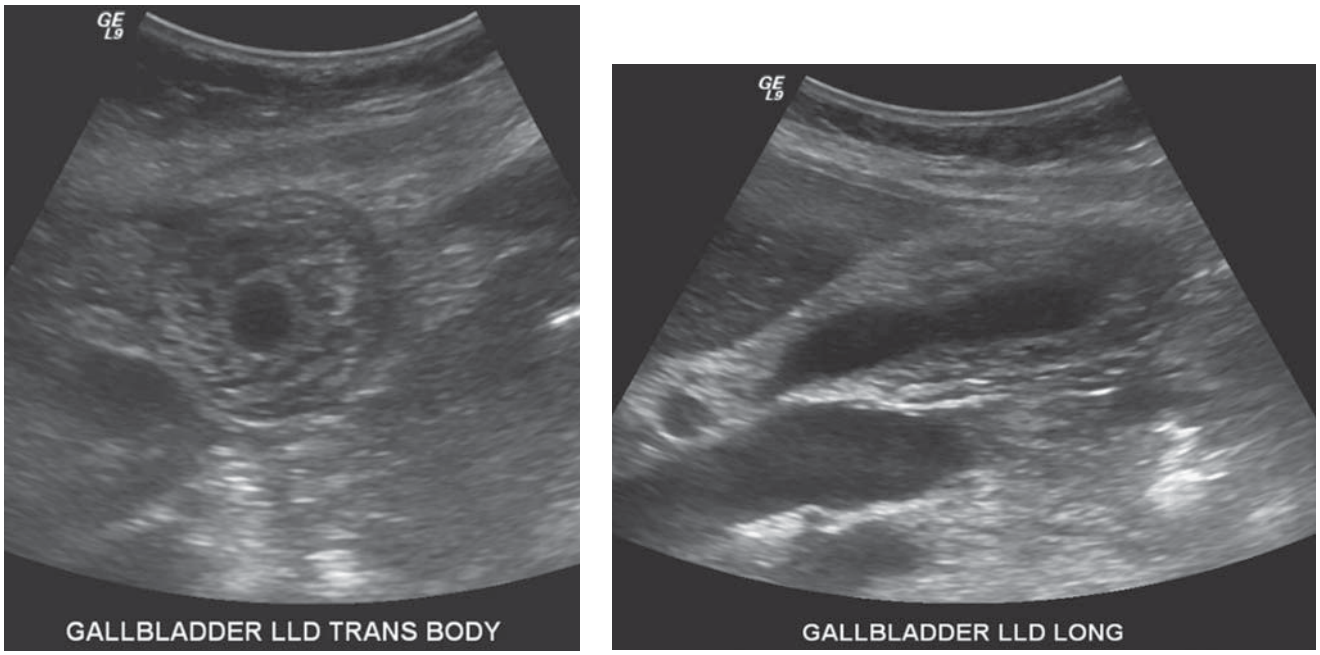


Fig. 193.1 Diffuse and marked thickening of the gallbladder wall is demonstrated in **(A)** transverse and **(B)** longitudinal ultrasound images of the gallbladder. Notice the absence of gallbladder calculi, the concentric striated appearance of an edematous gallbladder wall, and the increased caliber of the inferior vena cava.

Clinical Presentation

An elderly woman presents with vague abdominal pain (**Fig. 193.1**).

Key Imaging Finding

Gallbladder wall thickening

Top 3 Differential Diagnoses

- **Acute cholecystitis.** Acute cholecystitis is usually a consequence of cystic duct obstruction from an impacted calculus leading to gallbladder enlargement and pain. A hydropic gallbladder with intraluminal calculi and a sonographic Murphy sign allows a confident diagnosis of cholecystitis. Wall thickening (>3 mm) is often present but is not specific. Other supportive findings are pericholecystic fluid and gallbladder wall hyperemia. Acalculus cholecystitis typically occurs in critically ill patients who produce "hyperviscous" obstructive sludge. Hepatobiliary scanning, computed tomography, and magnetic resonance (MR) imaging/MR cholangiopancreatography are often used for complicated cases.
- **Gallbladder wall edema.** A striated sonographic appearance of the gallbladder wall containing pockets of fluid in the absence of a sonographic Murphy sign is more characteristic of gallbladder wall edema than acute cholecystitis. Gallbladder wall thickening in generalized edematous states includes congestive heart failure, hypoproteinemia, renal failure, advanced liver disease, and lymphatic obstruction secondary to portal lymphadenopathy or a mass.
- **Secondary inflammation.** Apart from primary gallbladder disease, there are focal and systemic inflammatory conditions that may evoke gallbladder wall inflammation. Pancreatitis, hepatitis, and pyelonephritis are common diseases that may secondarily inflame the gallbladder wall. In patients with acquired immunodeficiency syndrome, diffuse wall thickening may be a consequence of the primary human immunodeficiency virus or opportunistic infections (e.g., cytomegalovirus and cryptosporidiosis).

Additional Differential Diagnoses

- **Gallbladder carcinoma.** Asymmetric gallbladder wall thickening or a large mass in the gallbladder lumen or fossa is suspicious for malignancy. Doppler is useful in differentiating a neoplasm from nonvascular tumefactive sludge, as well as in assessing for vascular invasion or adenopathy in the setting of gallbladder carcinoma. Gallbladder carcinoma is closely associated with gallstones, and there is an increased risk in patients with porcelain gallbladder.
- **Gallbladder polyp.** Polyps are asymptomatic, nonshadowing, nonmobile masses growing from the gallbladder wall that may simulate focal wall thickening. Color or power Doppler is a useful tool to demonstrate a vascular pedicle. Though not considered true tumors, polyps with a diameter >1 cm warrant resection.
- **Adenomyomatosis.** This idiopathic condition results in diffuse or focal thickening of the muscular wall and overgrowth of gallbladder mucosa. Ring-down artifact arising from echogenic foci in the gallbladder wall on ultrasound is considered pathognomonic and reflects the deposition of cholesterol crystals into mucosal diverticula (Rokitansky–Aschoff sinuses). This is a benign finding and usually incidentally discovered.

Diagnosis

Gallbladder wall edema (congestive heart failure)

✓ Pearls

- The diagnosis of cholecystitis is made by demonstrating gallbladder calculi and a sonographic Murphy sign.
- A thickened striated appearance to the gallbladder wall without a sonographic Murphy sign suggests edema.
- Inflammatory conditions such as hepatitis and pancreatitis may secondarily thicken the gallbladder wall.
- Asymmetric gallbladder wall thickening should raise the suspicion of cancer.

Suggested Readings

Rumack CM, Wilson SR, Charboneau JW. Diagnostic Ultrasound. 3rd ed. St. Louis, MO: Mosby; 2005

van Breda Vriesman AC, Engelbrecht MR, Smithuis RH, Puylaert JB. Diffuse gallbladder wall thickening: differential diagnosis. AJR Am J Roentgenol 2007;188(2):495–501

Case 194

Eleanor L. Ormsby

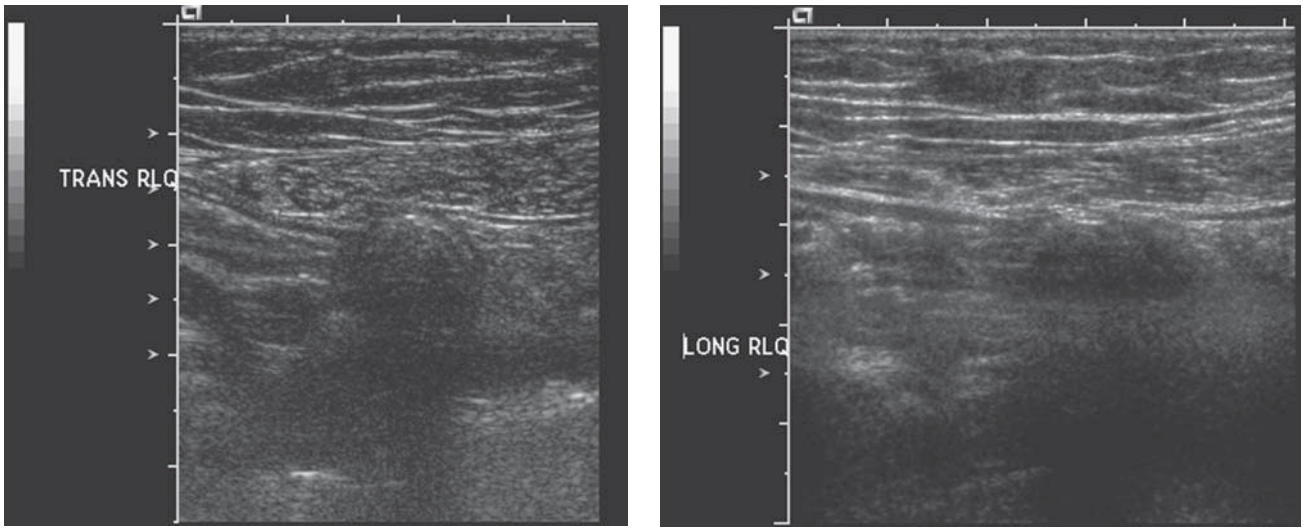


Fig. 194.1 **(A)** Transverse and **(B)** longitudinal sonographic images through the right lower quadrant demonstrate a thickened blind-ending tubular structure measuring 12 mm in diameter with adjacent inflamed fat. On the transverse view, there is a luminal filling defect with posterior acoustic shadowing.

Clinical Presentation

A 10-year-old boy presents with pain in the right lower quadrant (**Fig. 194.1**).

Key Imaging Finding

Right lower quadrant mass in a child

Top 3 Differential Diagnoses

- **Appendicitis.** The primary criterion for the diagnosis of appendicitis is an appendiceal diameter >6 mm on ultrasound with compression. The measurement is made from outer wall to outer wall. In some patients, an intraluminal appendicolith may be detected. Other associated findings are inflamed hyperechoic periappendiceal fat, loculated periappendiceal fluid collections, and hyperemia on color Doppler imaging.
- **Intussusception.** Intussusception can be idiopathic or secondary to a pathologic lead point. Possible lead points are a Meckel diverticulum, lymphoma, inspissated feces in cystic fibrosis, and bowel wall hemorrhage in Henoch–Schönlein purpura. On a transverse ultrasound image, the intussusception appears as a donut with multiple altering hyperechoic and hypoechoic layers due to the presence of overlapping mucosal and muscular layers of the intussuscipiens and the intussusceptum with interposed fat. On sagittal imaging, it can resemble a pseudokidney. Lack of blood flow in the intussusception increases the likelihood of necrosis, which would suggest the need for surgical intervention.
- **Enteric duplication cyst.** Duplication cysts typically present as a round, fluid-filled mass displacing the adjacent bowel. They may contain ectopic gastric mucosa, which can cause hemorrhage, focal bowel wall thickening, and/or inflammation. The ileum is the most common site of involvement.

Additional Differential Diagnoses

- **Adnexal mass in a woman.** In young women, right lower quadrant pain may be secondary to ovarian or adnexal pathology. Common etiologies are ovarian torsion with or without an associated mass, ruptured ovarian cyst, hemorrhagic cyst, endometrioma, infectious process (tubo-ovarian abscess), and ectopic pregnancy.
- **Meckel diverticulum.** Meckel diverticulum is an omphalomesenteric duct anomaly that can cause pain due to bleeding from ectopic gastric mucosa, focal inflammation, perforation, or intussusception. Meckel scan using technetium 99m pertechnetate is useful for detecting diverticula that contain ectopic gastric mucosa.
- **Mesenteric adenitis.** Mesenteric adenitis is a diagnosis of exclusion in which multiple enlarged and clustered lymph nodes are seen just anterior to the right psoas muscle without evidence of appendicitis. This entity can coexist with inflammation of the terminal ileum and cecum and generally has a self-limited clinical course.

Diagnosis

Acute appendicitis

✓ Pearls

- Appendicitis is diagnosed by observing a noncompressible tubular mass in the right lower quadrant >6 mm in diameter.
- Lead points for intussusception include Meckel diverticulum, lymphoma, inspissated feces, and hemorrhage.
- Enteric duplication cysts present as round, fluid-filled masses occurring most commonly in the ileum.
- Adnexal masses in women may mimic appendicitis, emphasizing the relevance of age and clinical history.

Suggested Readings

Middleton WD, Kurtz AB, Hertzberg BS. Ultrasound: The Requisites. St. Louis, MO: Mosby; 2004

Ripollés T, Martinez-Perez MJ, Morote V, Solaz J. Diseases that simulate acute appendicitis on ultrasound. Br J Radiol 1998;71(841):94–98

Case 195

David J. Weitz

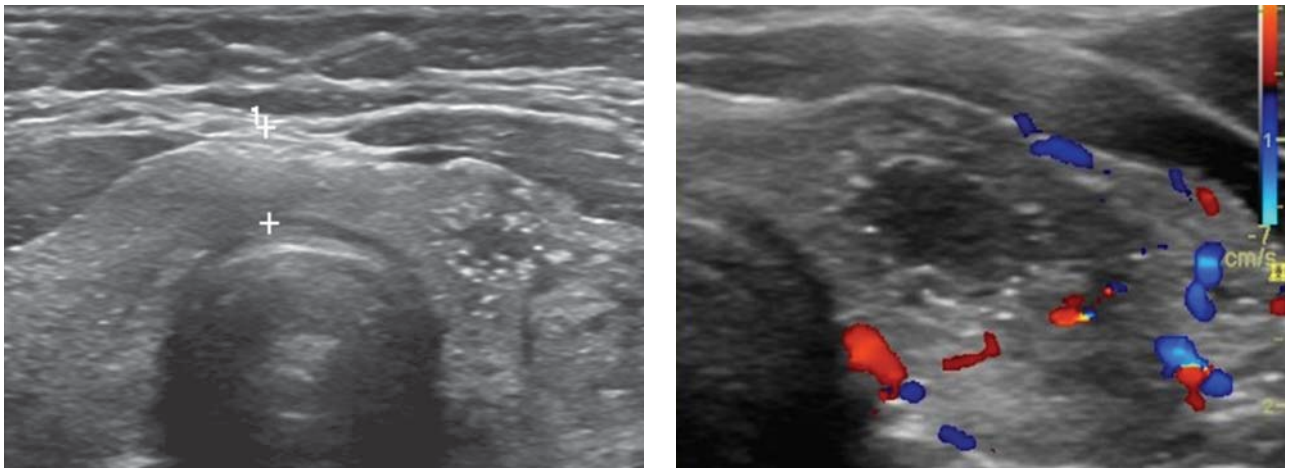


Fig. 195.1 **(A)** Transverse gray scale ultrasound image of thyroid gland demonstrates diffuse thickening and nodularity in a multinodular gland. Scattered echogenic foci are seen within a hypoechoic nodule in the medial anterior left lobe. **(B)** Coned-down color Doppler image of the same nodule reveals a predominantly hypoechoic echotexture with punctate nonshadowing hyperechoic foci, representing microcalcifications. Although flow is observed at the periphery of an ill-defined nodule border, no flow is demonstrated centrally.

Clinical Presentation

A middle-aged woman presents with palpable thyroid nodule (**Fig. 195.1**).

Key Imaging Finding

Thyroid mass

Top 3 Differential Diagnoses

- **Benign thyroid nodule.** Thyroid nodules are very common in the adult population, and their prevalence increases with age. The vast majority of nodules are benign and are categorized as hyperplastic (most common), colloid cysts, or adenomas. Common features shared by benign nodules include rim or eggshell calcification, cystic components, and a thin, regular, hypoechoic halo. Glandular hyperplasia can result in nonneoplastic nodules, whereas adenomas are true neoplasms. Both are sonographically indistinguishable from malignant nodules. Hyperplastic nodules and adenomas may be entirely solid or partially cystic. Echogenicity is variable and ranges from hyper- to hypoechoic. Coarse peripheral calcification may obscure the nodule secondary to extensive shadowing. Colloid nodules contain inspissated colloid (hyperechoic foci with comet tail artifact) that reliably differentiates them from microcalcifications (hyperechoic foci without comet tail artifact), which are suspect for thyroid malignancy.
- **Thyroid malignancy.** Risk factors for thyroid cancer include male gender, age younger than 20 or older than 60, a history of head/neck radiation, and a positive family history. Patients may present with pain or hoarseness. Common thyroid cancer types are papillary, follicular, medullary, anaplastic, Hürthle cell, lymphoma, mixed, and metastases. The differentiation of a benign nodule from thyroid cancer cannot reliably be made with ultrasound. However, microcalcifications in a hypoechoic solid nodule are very suspicious for thyroid malignancy, most commonly papillary cancer. Malignant nodules often have irregular borders. Enlarged cystic or calcified lymph nodes in the neck with a suspect thyroid nodule are suggestive of local extension of thyroid cancer. Flow patterns are generally nonspecific, but an avascular nodule is much more likely to be benign. Size, number of nodules, and interval growth are less helpful in nodule classification. Indeterminate and suspicious nodules require further evaluation with fine-needle aspiration, which may be accomplished using ultrasound guidance.
- **Parathyroid adenoma.** Normal parathyroid glands are rarely visualized on routine thyroid exams due to their small size, but ultrasound is useful for suspected parathyroid adenomas. Sonographically, they appear as solid, hypoechoic ovoid masses posterior to the thyroid gland. Ultrasound is also helpful in identifying ectopic adenomas. Because these tumors are highly vascular, Doppler technique is a useful search tool. Ultrasound may be combined with parathyroid scintigraphy, and sometimes computed tomography or magnetic resonance imaging to improve localization accuracy.

Additional Differential Diagnoses

- **Thyroglossal duct cyst (TDC).** The most common congenital neck mass, TDC occurs from failure of the epithelial tract of the developing thyroid to involute. Cysts may arise anywhere along the tract, which runs midline from the tongue base (foramen cecum) to the thyroid gland; the majority of cysts are found below the hyoid bone. Commonly, these lesions will have a homogeneously hypoechoic appearance in the midline neck with a smooth, circumscribed border. Below the hyoid bone, they are often in a paramidline location.

Diagnosis

Papillary thyroid carcinoma

✓ Pearls

- The presence of colloid crystals in a thyroid nodule is a reliable sign of benignity.
- A hypoechoic nodule containing microcalcifications raises suspicion of a thyroid malignancy.
- Ultrasound may be used to localize parathyroid adenomas and is commonly combined with other modalities.
- TDCs are usually midline, homogeneously hypoechoic, and defined by a smooth, circumscribed border.

Suggested Readings

Hoang JK, Lee WK, Lee M, Johnson D, Farrell S. US features of thyroid malignancy: pearls and pitfalls. Radiographics 2007;27(3):847–860, discussion 861–865

Middleton WD, Kurtz AB, Hertzberg BS. Ultrasound: The Requisites. St. Louis, MO: Mosby; 2004

Case 196

Anokh Pahwa

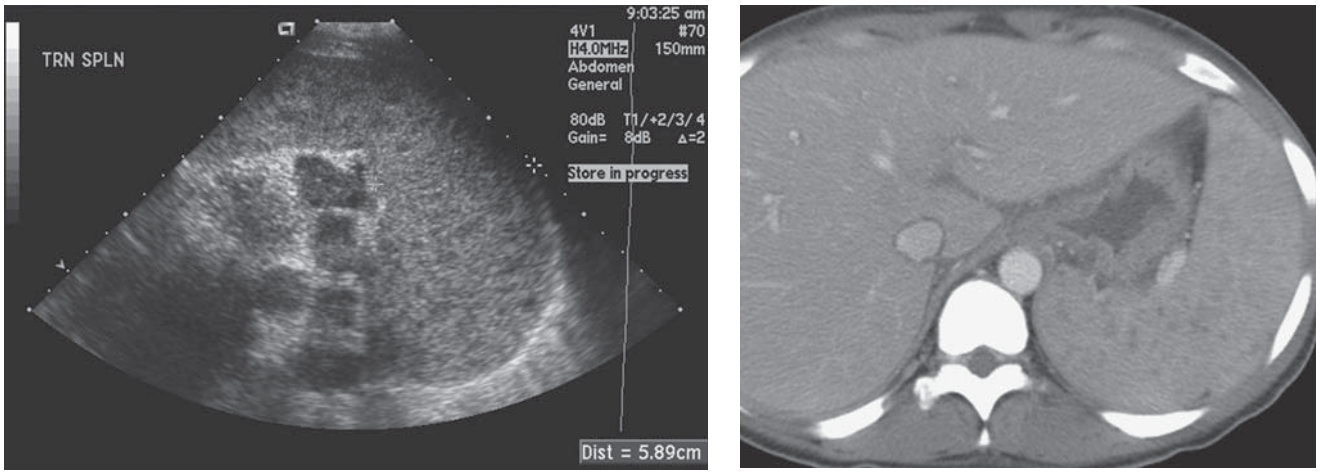


Fig. 196.1 **(A)** Transverse sonographic image through the left upper quadrant demonstrates innumerable small hypoechoic foci involving the spleen diffusely. **(B)** Contrast-enhanced axial computed tomography image in the same patient confirms the findings, showing multiple hypodense splenic lesions.

Clinical Presentation

A 26-year-old woman who has tested positive for human immunodeficiency virus presents with cough and fever (**Fig. 196.1**).

Key Imaging Finding

Multiple splenic hypoechoic foci

Top 3 Differential Diagnoses

- **Fungal abscess (candidiasis).** Most commonly occurring in immunocompromised patients, fungal abscesses are multifocal and can be caused by *Candida, Aspergillus,* or *Cryptococcus.* They are typically characterized by multiple "target" lesions on ultrasound, consisting of a hypoechoic central nidus of necrosis surrounded by a hyperechoic ring of viable fungal elements. When this lesion is surrounded by a peripheral hypoechoic zone of inflammatory change, it is referred to as a "wheel within a wheel" pattern.
- **Diffuse lymphoma.** Lymphoma is the most common malignant neoplasm of the spleen. It may manifest as unifocal, multifocal, or diffuse disease involvement. Splenomegaly is commonly, but not invariably, present. Although ultrasound is insensitive for diffuse splenic lymphoma, the finding of multiple hypoechoic foci with indistinct borders in a patient with known lymphoma is highly specific for splenic involvement.
- **Granulomatous disease.** Similar to fungal abscesses, active granulomatous disease can present as multiple hypoechoic splenic lesions that can calcify over time. The most frequent granulomatous disease to involve the spleen on ultrasound is histoplasmosis, but in immunocompromised patients, *Mycobacterium tuberculosis* or *Pneumocystis jiroveci* can have similar imaging characteristics. Discrete small, hypoechoic splenic nodules can also be seen with sarcoidosis.

Additional Differential Diagnoses

- **Metastatic disease.** Metastatic disease to the spleen is relatively rare and generally seen only in advanced disease with widespread metastatic involvement. Fifty percent of splenic metastases are secondary to malignant melanoma. Primary malignancies include carcinomas from the lung, breast, and colon. Ultrasonographic appearance can be quite variable, but the lesions are most typically hypoechoic with low-level internal echoes. These findings correlate to cystic masses with internal necrosis. A surrounding hypoechoic halo is thought to be a sign of aggressiveness.

Diagnosis

Granulomatous disease (miliary tuberculosis)

✓ Pearls

- Fungal abscesses are uncommon and nearly always occur in immunocompromised patients.
- Splenic lymphoma has a variable sonographic appearance and is suggested with appropriate history.
- Granulomatous disease of the spleen presents as hypoechoic nodules that often calcify over time.
- Metastatic disease to the spleen is most commonly from melanoma, lung, breast, and colon malignancies.

Suggested Readings

Chen MJ, Huang MJ, Chang WH, et al. Ultrasonography of splenic abnormalities. World J Gastroenterol 2005;11(26):4061–4066

Middleton WD, Kurtz AB, Hertzberg BS. Ultrasound: The Requisites. St. Louis, MO: Mosby; 2004

Urrutia M, Mergo PJ, Ros LH, Torres GM, Ros PR. Cystic masses of the spleen: radiologic-pathologic correlation. Radiographics 1996;16(1):107–129

Case 197

Anokh Pahwa

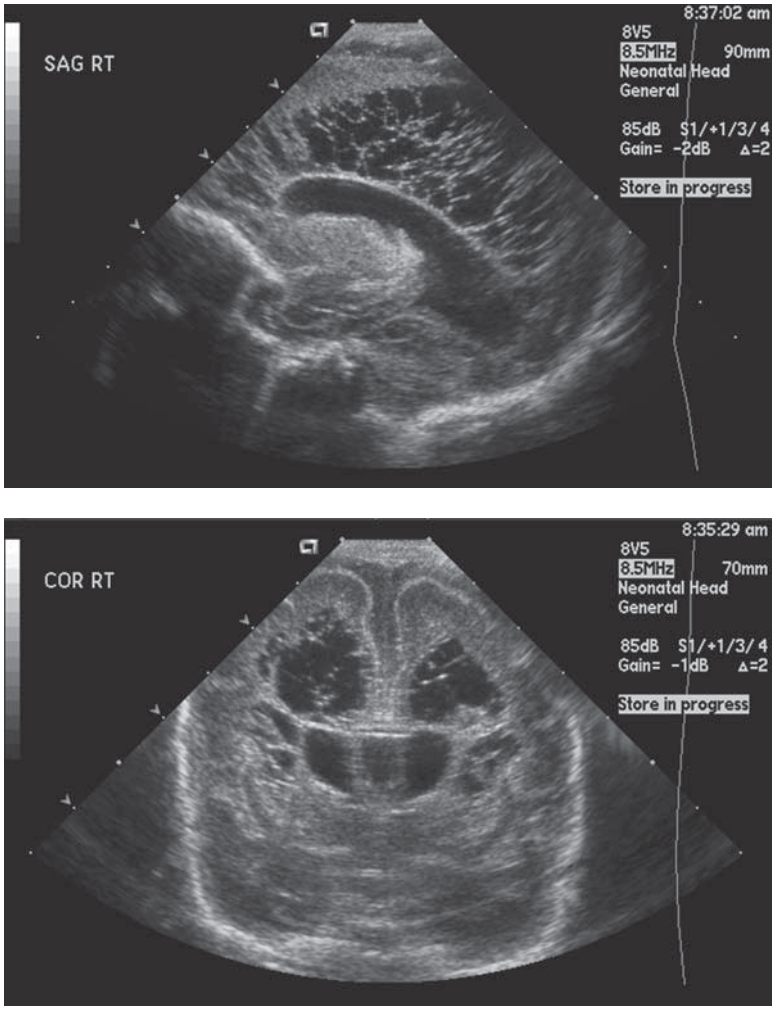


Fig. 197.1 **(A)** Sagittal and **(B)** coronal ultrasound images of the head demonstrate marked cystic changes in the posterior and lateral periventricular white matter with sparing of the cortex.

Clinical Presentation

A 1-month-old premature girl born at 29 weeks' gestation (**Fig. 197.1**).

Key Imaging Finding

Periventricular cysts

Top 3 Differential Diagnoses

- **Periventricular leukomalacia (PVL).** PVL is defined as ischemic injury to the periventricular white matter in the preterm infant. White matter in the preterm infant is poorly vascularized and sensitive to ischemic and infectious injury. In addition, the lack of autoregulation in preterm brains leaves these watershed areas at increased risk. The typical distribution includes the deep white matter dorsal and lateral to the lateral ventricles, particularly involving the optic and acoustic radiations with sparing of the cortex. Infants born at less than 32 weeks' gestation are at the highest risk. Immediate neonatal head ultrasound may be normal. The earliest findings are vague hyperechoic changes that may progress to multicystic involvement (cystic PVL) in serious cases. Prognosis is poor with cystic PVL, and large bilateral cysts (>10 mm) are highly predictive of development of cerebral palsy.
- **Subependymal cysts.** Subependymal cysts may be congenital or acquired. Acquired subependymal cysts are secondary to germinal matrix hemorrhage in the preterm infant. The germinal matrix is a highly vascular structure near the head of the caudate nucleus that regresses near term. Infants born at less than 32 weeks' gestation should be screened with a head ultrasound for germinal matrix hemorrhage at 4 and 7 days.
- **Infection.** With the exception of herpes simplex, which an infant acquires during passage through the birth canal, the other TORCH infections (toxoplasmosis, other agents, rubella, and cytomegalovirus [CMV]) affect a fetus by transplacental transmission. Head ultrasound can reveal a variety of findings, from microcephaly or hydranencephaly secondary to early gestational infection to porencephalic cysts and periventricular calcifications (CMV and toxoplasmosis) with infections later in gestation. Parasitic infection with cysticercosis leads to multiple cysts that are usually calcified.

Additional Differential Diagnoses

- **Choroid plexus cysts.** Choroid plexus cysts can vary in size and be solitary or multiple. They arise from the body of the choroid but may protrude into the ventricle. Although choroid plexus cysts can be seen in a small percentage (<5%) of normal pregnancies, there is a greater than expected association with aneuploidy, particularly trisomy 18. Their presence on prenatal ultrasound should trigger a search for associated anatomical defects.
- **Porencephaly.** Porencephaly describes a cerebrospinal fluid–filled cavity adjacent to and possibly communicating with the ventricles. It is secondary to encephalomalacia from any destructive process (e.g., hemorrhage or infection) occurring in the third trimester or postnatally. There may be discrete calcifications in the wall of the cavity.

Diagnosis

Periventricular leukomalacia

✓ Pearls

- Early signs of PVL include hyperechoic foci in the deep white matter, which may lead to cystic changes.
- Ultrasound is used to screen preterm infants (<32 weeks) for germinal matrix hemorrhage in the first week of life.
- TORCH infections are associated with a variety of sequelae, including cyst formation in the neonatal brain.
- Choroid plexus cysts are usually an isolated incidental finding, but there is an association with aneuploidy.

Suggested Readings

Blickman H. Pediatric Radiology: The Requisites. St. Louis, MO: Mosby; 1998

Epelman M, Daneman A, Blaser SI, et al. Differential diagnosis of intracranial cystic lesions at head US: correlation with CT and MR imaging. Radiographics 2006;26(1):173–196

Middleton WD, Kurtz AB, Hertzberg BS. Ultrasound: The Requisites. St. Louis, MO: Mosby; 2004

Case 198

Eleanor L. Ormsby

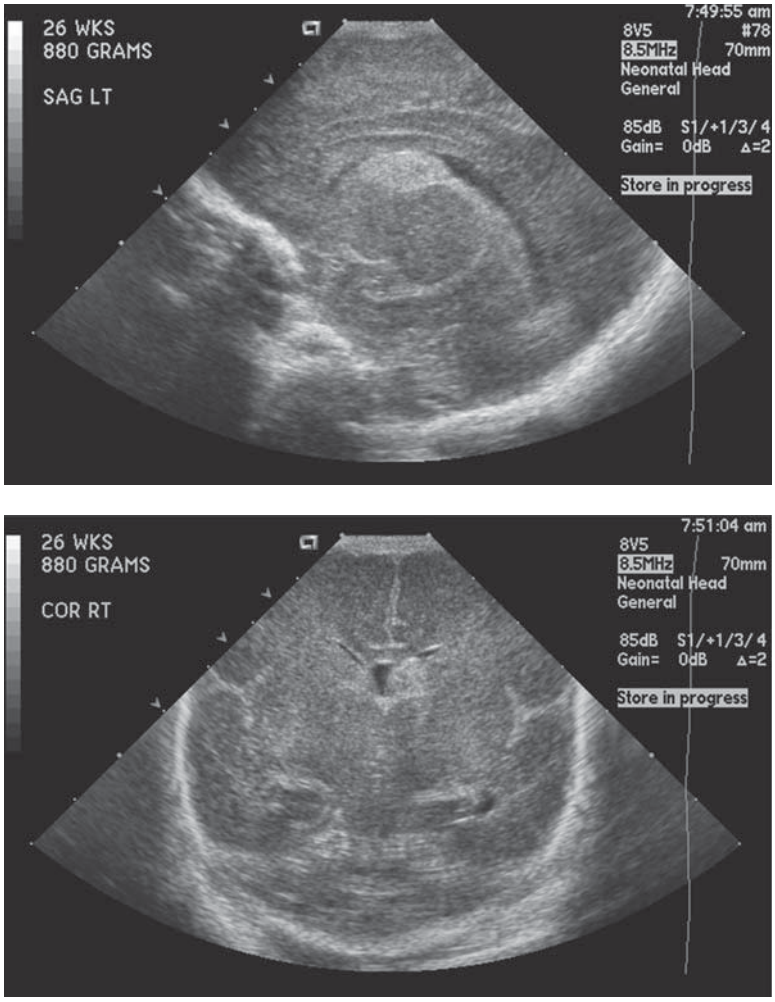


Fig. 198.1 **(A)** Coronal and **(B)** sagittal ultrasound images of the brain demonstrate homogeneous echogenic masses in the left caudothalamic groove.

Clinical Presentation

A preterm newborn presents with respiratory distress (**Fig. 198.1**).

Key Imaging Finding

Periventricular hyperechoic foci

Top 3 Differential Diagnoses

- **Germinal matrix hemorrhage (GMH).** GMH most commonly occurs in preterm neonates less than 32 weeks' gestation and weighing <1500 g. The germinal matrix lies within the caudothalamic groove and is highly vascular, predisposing it to hemorrhage with insult. GMH is categorized into four grades, as follows: grade 1: hemorrhage confined to the germinal matrix; grade 2: extension of hemorrhage into the lateral ventricles without ventricle dilatation; grade 3: intraventricular hemorrhage filling dilated ventricles; grade 4: intraparenchymal hemorrhage, which is considered venous hemorrhagic infarct rather than direct hemorrhagic extension. On ultrasound, acute GMH appears as a homogeneous hyperechoic mass in the caudothalamic region. Over time, GMH becomes smaller and less echogenic. Grade 3 and 4 GMHs have a poor prognosis associated with neurologic sequelae and increased mortality.
- **Intraventricular/intraparenchymal hemorrhage.** Trauma, coagulopathy, venous thrombosis, and heparin therapy during extracorporeal membrane oxygenation are a few conditions that may predispose term infants to intracranial hemorrhage. Unlike the hemorrhages associated with prematurity (GMHs), these hemorrhages occur most commonly within the subependymal region, rather than the germinal matrix. The hemorrhage may extend into the ventricles or surrounding periventricular parenchyma. Acutely on ultrasound, the hemorrhage is seen as a hyperechoic region that gradually becomes hypoechoic and cystic due to liquefaction of the hematoma. With complete clot retraction, the cystic area becomes filled with cerebrospinal fluid, resulting in porencephaly.
- **Early periventricular leukomalacia (PVL).** PVL represents perinatal partial ischemia in the periventricular white matter, the watershed zone of the premature infant. It results from diminished cerebral perfusion and hypotension. It usually affects the white matter adjacent to the atria and the frontal horns of the lateral ventricles. Ultrasound may initially demonstrate vague areas of increased echogenicity, which then progresses to cyst formation and eventual volume loss in the periventricular white matter.

Additional Differential Diagnoses

- **Hypoxic-ischemic brain injury.** Hypoxic-ischemic brain injury may occur in newborn infants complicated by intrauterine factors, trauma, pulmonary disease, or congenital heart disease (usually cyanotic). Although periventricular leukomalacia is the most common sequela in preterm infants, subcortical cerebral or basal ganglia injury is more common in term infants. Early ultrasound findings include subtle increased echogenicity within the periventricular white matter and/or deep gray matter.
- **Central nervous system (CNS) infection.** In utero infections, such as cytomegalovirus and toxoplasmosis, may present with periventricular calcifications that are hyperechoic on ultrasound. Additional abnormalities are commonly seen in these patients; the type and severity of associated findings depend on the stage of development/gestation at the time of insult. Neurocysticercosis results in multiple cystic lesions that may calcify.

Diagnosis

Germinal matrix hemorrhage (grade 1)

✓ Pearls

- GMH is classified into four grades depending on severity; grades 3 and 4 are predictive of a poor prognosis.
- Unlike GMH, intraventricular/intraparenchymal hemorrhage commonly occurs in a subependymal location.
- PVL represents damage to deep white matter in premature infants and occurs from cerebral hypoperfusion.
- Unlike PVL, hypoxic-ischemic brain injury more often affects the subcortical cerebrum or basal ganglia.

Suggested Readings

Blickman H. Pediatric Radiology: The Requisites. 2nd ed. St. Louis, MO: Mosby; 1998

Epelman M, Daneman A, Blaser SI, et al. Differential diagnosis of intracranial cystic lesions at head US: correlation with CT and MR imaging. Radiographics 2006;26(1):173–196

Case 199

David J. Weitz

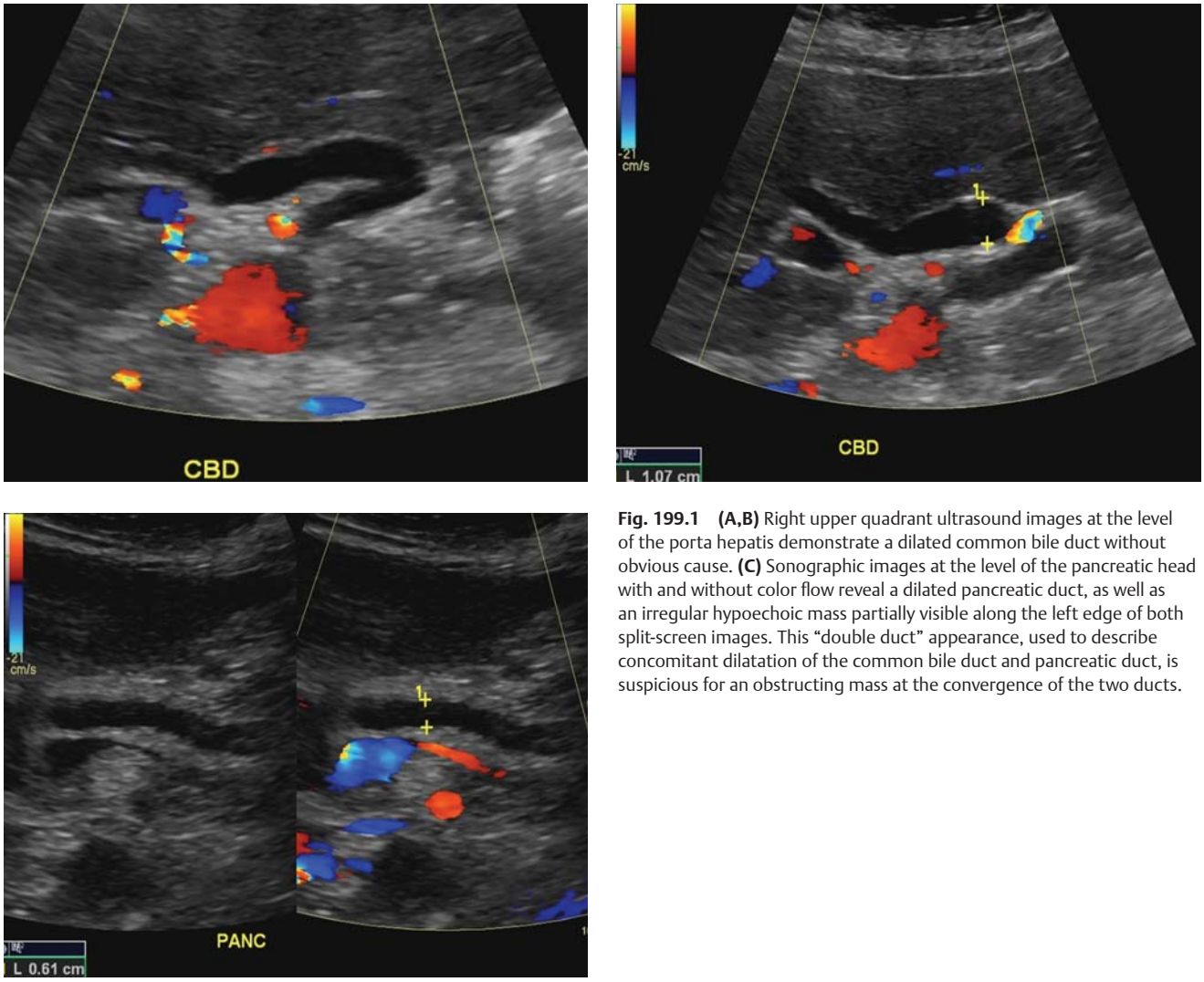


Fig. 199.1 **(A,B)** Right upper quadrant ultrasound images at the level of the porta hepatis demonstrate a dilated common bile duct without obvious cause. **(C)** Sonographic images at the level of the pancreatic head with and without color flow reveal a dilated pancreatic duct, as well as an irregular hypoechoic mass partially visible along the left edge of both split-screen images. This "double duct" appearance, used to describe concomitant dilatation of the common bile duct and pancreatic duct, is suspicious for an obstructing mass at the convergence of the two ducts.

Clinical Presentation

A middle-aged woman presents with painless jaundice (**Fig. 199.1**).

Key Imaging Finding

Common bile duct (CBD) dilatation

Top 3 Differential Diagnoses

- **Choledocholithiasis.** Biliary calculi are the most common cause of CBD dilatation. A dilated common bile duct is often the only finding on ultrasound and is considered dilated if the measurement exceeds 6 mm in patients younger than 70 years (a 1 mm dilatation is allowed per decade thereafter). Primary choledocholithiasis is the formation of stones in the CBD from stasis, whereas secondary choledocholithiasis is the result of stone passage from the gallbladder. Ultrasound may show a hyperechoic, rounded intraluminal lesion with posterior shadowing most commonly at the distal duct near the ampulla of Vater.
- **Malignancy.** Pancreatic adenocarcinoma is the leading cause of malignant biliary obstruction. Sonographically, adenocarcinoma appears as a hypoechoic avascular mass, and if located in the pancreatic head, CBD dilatation is common. Unfortunately, ultrasound cannot reliably distinguish neoplasm from pancreatitis. A "double duct" sign is seen when a pancreatic head mass obstructs and dilates both the CBD pancreatic duct. Cholangiocarcinoma is a rare biliary malignancy commonly seen in older men with painless jaundice and may be intrahepatic, hilar, or distal (common duct). A common appearance is proximal duct dilatation and abrupt tapering more distally with or without thickened duct walls. Less commonly seen is a hypoechoic polypoid mass expanding the CBD. Flow is usually absent.
- **Chronic pancreatitis.** Chronic pancreatitis causes fibrosis as a sequela of recurrent insult/inflammation. Imaging findings include pancreatic atrophy, ductal obstruction, and parenchymal calcification. Dilatation of the pancreatic duct in chronic pancreatitis may have a characteristic "chain of lakes" appearance. Pancreatic calcifications appear hyperechoic with posterior shadowing. Ultrasound findings may mimic malignancy with a heterogeneous pancreatic parenchyma or focal masslike lesions. Computed tomography, endoscopic retrograde cholangiopancreatography/magnetic resonance cholangiopancreatography, and/or endoscopic ultrasound with biopsy may be necessary to differentiate chronic pancreatitis from malignancy. Pancreatic pseudocysts and vascular injury/venous thrombosis are relatively common complications.

Additional Differential Diagnoses

- **Cholangitis.** Acute cholangitis results from biliary obstruction, usually as a result of intraductal calculi causing bile stasis with subsequent infection. Postoperative biliary strictures, tumors, sclerosing cholangitis, and iatrogenic seeding are also causes of cholangitis. Classic symptoms are fever, right upper quadrant pain, and jaundice. On ultrasound, dilated intra- and extrahepatic bile ducts are common, as are intraductal calculi. Biliary sludge, duct wall thickening, and hepatic abscesses are supporting ultrasound features.
- **Choledochal anomaly.** Nonobstructive cystic dilatation of the biliary tree can be seen in congenital choledochal anomalies. These anomalies are classified based on the level of biliary ductal dilatation, with saccular or fusiform dilatation of the common bile duct (type 1) representing the most common variant.

Diagnosis

Malignancy (pancreatic adenocarcinoma)

✓ Pearls

- On ultrasound, choledocholithiasis appears as a hyperechoic shadowing lesion most often in the distal CBD.
- Dilatation of the CBD and pancreatic duct (double duct sign) should raise suspicion for malignancy.
- Chronic pancreatitis may result in gland heterogeneity or focal masslike lesions mimicking malignancy.
- Classically described symptoms for acute cholangitis are fever, right upper quadrant pain, and jaundice.

Suggested Readings

Middleton WD, Kurtz AB, Hertzberg BS. Ultrasound: The Requisites. St. Louis, MO: Mosby; 2004

Rumack CM, Wilson SR, Charboneau JW. Diagnostic Ultrasound. 3rd ed. St. Louis, MO: Mosby; 2005

Case 200

David J. Weitz

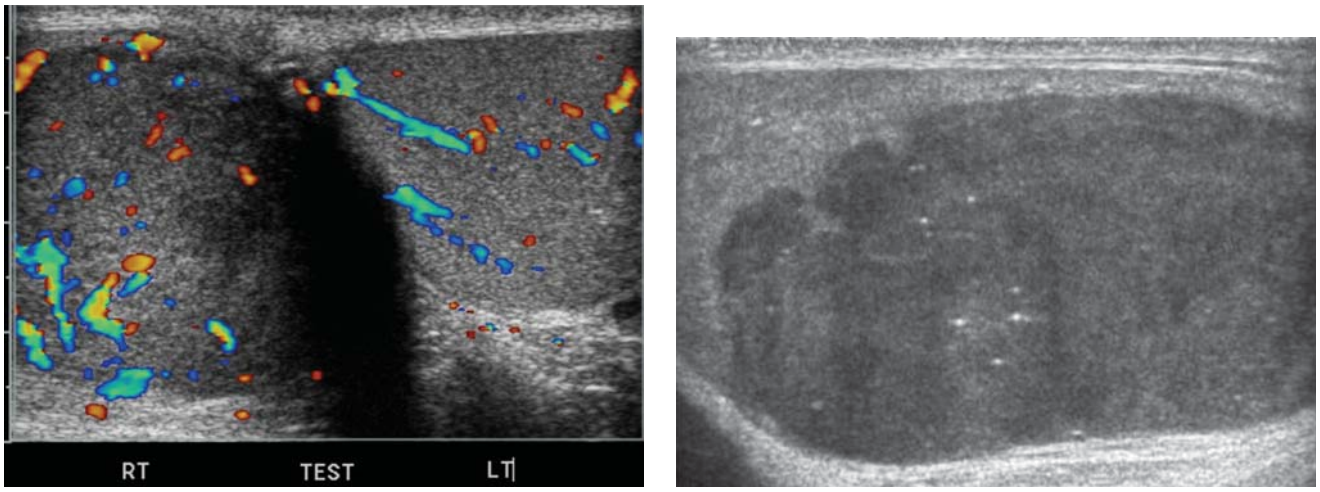


Fig. 200.1 **(A)** Transverse view of both testes shows an asymmetrically enlarged right testis. There is a heterogeneously hypoechoic parenchyma in the enlarged right testis compared with the left. Flow to the right testis is subtly increased. **(B)** Longitudinal image reveals a large lobulated hypoechoic mass replacing the majority of the right testis. Punctate hyperechoic foci scattered throughout the mass are consistent with microcalcifications (microlithiasis).

Clinical Presentation

A young man presents with a painless mass (**Fig. 200.1**).

Key Imaging Finding

Enlarged painless testicle

Top 3 Differential Diagnoses

- **Testicular neoplasm.** Testicular neoplasms are the most common malignancy in young men (ages 18–35). Thus any testicular mass must be considered malignant in the absence of known trauma or infection, prompting orchiectomy. The sentinel clinical symptom is painless testicular enlargement or a palpable testicular lump. A small number of patients experience pain from tumoral hemorrhage or infarction. Nearly all testicular neoplasms are germ cell tumors; the most common being mixed germ cell tumors and seminomas. Other neoplasms are sex chord stromal tumors, metastases, lymphoma, and epidermoid cysts. Epidermoid cysts are benign testicular neoplasms that may demonstrate characteristic alternating hyper- and hypoechoic rings. Treatment of these lesions is enucleation. Seminomas are classically homogeneously hypoechoic. Nonseminomatous tumors are more heterogeneous and may contain coarse calcifications or cystic regions. Although controversial, there appears to be an association between testicular malignancy and microlithiasis. Most tumors demonstrate vascularity, which may be normal or increased. It is important to scan the contralateral testis, as bilateral tumors may be found with metastases, lymphoma, and, rarely, seminomas. Retroperitoneal lymphadenopathy near the renal hila is highly suggestive of metastatic extension.
- **Lymphoma/leukemia.** Lymphoma of the testes is primarily a disease of older men, whereas leukemia is most often seen in children. Primary lymphoma/leukemia of the testes is rare, but because the blood–testes barrier hinders therapeutic concentrations of chemotherapeutic agents to the testes, it is a frequent site of recurrence. Worrisome ultrasound findings include diffuse hypoechoic unilateral or bilateral testicular enlargement. Occasionally, ultrasound may demonstrate a focal hypoechoic mass. In the absence of other findings, diffuse or focal hypervascularity of the testes may help identify tumor in subtle cases. Involvement of the epididymis is common, which is generally enlarged and hypoechoic, but epididymal vascularity is usually normal. Patients are generally asymptomatic, which helps distinguish tumor from epididymo-orchitis.
- **Testicular cysts.** Testicular cysts are found in 8 to 10% of men. They may be located within the testicular parenchyma or arise from the layer investing the testicle called the tunica albuginea. Given that intratesticular masses are nearly always malignant, the importance of confirming a simple cyst cannot be overstated. Tunica albuginea cysts are small (generally <5 mm) and peripherally located. Despite the small size, the majority of these cysts present as palpable abnormalities. Intratesticular cysts, in contrast, are not palpable, even when large. They are usually located near the mediastinum testis, but they may occur anywhere within the parenchyma. Because of their mediastinal location, they may originate from a dilated rete testis. An enlarged rete testis (tubular ectasia) is cystic transformation of the efferent ductules, located within the mediastinum testis. Ultrasound shows a network of dilated tubular structures, often bilateral, replacing the mediastinum in the presence of epididymal head cysts; the appearance is diagnostic of a benign entity.

Diagnosis

Testicular neoplasm (seminoma)

✓ Pearls

- Any intratesticular mass in the absence of a known cause should be considered suspicious for malignancy.
- The testes are often a site of lymphoma/leukemia recurrence due to a drug-inhibiting blood–testes barrier.
- Testicular cysts are common benign testicular lesions that must be differentiated from cystic neoplasms.

Suggested Readings

Dogra VS, Gottlieb RH, Reubens DJ, et al. Benign intratesticular cystic lesions: US features. Radiographics 2001;21:S273–S281

Mazzu D, Jeffrey RB Jr, Ralls PW. Lymphoma and leukemia involving the testicles: findings on gray-scale and color Doppler sonography. AJR Am J Roentgenol 1995;164(3):645–647

Middleton WD, Kurtz AB, Hertzberg BS. Ultrasound: The Requisites. St. Louis, MO: Mosby; 2004

Woodward PJ, Sohaey R, O'Donoghue MJ, Green DE. From the *Archives of the AFIP:* tumors and tumorlike lesions of the testis—radiologic-pathologic correlation. Radiographics 2002;22(1):189–216

Section IX Fetal Imaging

Case 201

Corinne D. Strickland

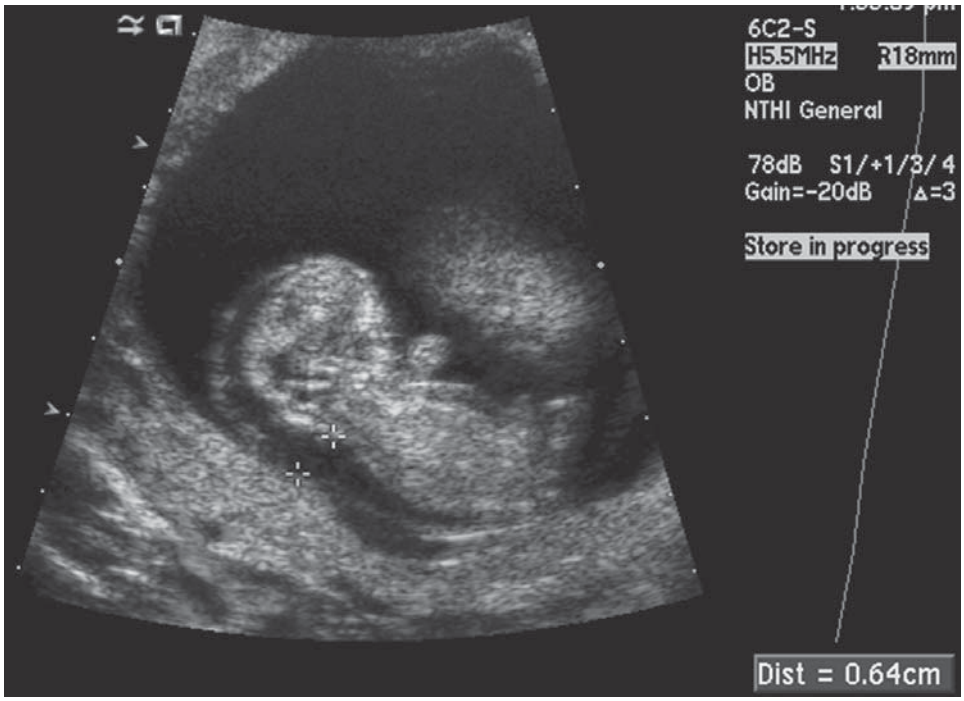


Fig. 201.1 Sagittal ultrasound image of a fetus reveals a nuchal translucency measuring >3 mm.

Clinical Presentation

Screening ultrasound of a 40-year-old woman (G2, P1) at 11 weeks' gestational age (**Fig. 201.1**).

Key Imaging Finding

Nuchal translucency

Top 3 Differential Diagnoses

- **Trisomy 21.** Trisomy 21 (Down syndrome) is the most common disorder caused by chromosomal nondisjunction and is a frequent cause of mental retardation. Like other nondisjunction syndromes, the incidence of Down syndrome is increased with advanced maternal age. Definitive prenatal diagnosis requires amniocentesis or chorionic villus sampling. Because these diagnostic procedures carry the risk of fetal loss, noninvasive screening methods are used to identify pregnancies at risk of Down syndrome. First-trimester screening uses sonographic measurement of the fluid layer in the posterior fetal neck, known as the nuchal translucency. Between 11 and 14 weeks' gestation, the nuchal translucency is normally <2. 8mm and is frequently increased in fetuses with chromosomal abnormalities and/or congenital heart defects. Nuchal translucency measurement is combined with maternal age and two maternal serum markers to yield an estimated risk of trisomy 21. Newer screening protocols combine these values with second-trimester maternal serum markers, elevating the trisomy 21 detection rate to ~85% with a false-positive rate of 5%. Patients with Down syndrome may have associated abnormalities, and findings on ultrasound may include cardiac defects, ventriculomegaly, duodenal atresia, pyelectasis, hyperechoic bowel, omphalocele, and short femora and humeri.
- **Turner syndrome.** Girls with Turner syndrome (monosomy XO) display short stature, ovarian dysgenesis, and variable learning difficulties. Congenital lymphedema is a common syndrome feature and may manifest as increased nuchal translucency (often >4.5 mm) on first-trimester ultrasound. Cystic hygroma, a form of nuchal fluid collection caused by abnormal lymphatic development, may be identified in the first or second trimester.
- **Trisomy 18.** Trisomy 18 (Edward syndrome) is the second most common chromosomal nondisjunction syndrome. Affected infants rarely survive beyond 1 year of age. Sonographic findings include increased nuchal translucency in the first trimester, cystic hygroma, growth restriction, abnormal extremities (clenched hands and overlapping digits), and choroid plexus cysts.

Additional Differential Diagnoses

- **Trisomy 13.** Trisomy 13 (Patau syndrome) is characterized by holoprosencephaly, cleft lip and palate, polydactyly, and renal and cardiac anomalies. Occasionally, nuchal translucency may be seen on first-trimester ultrasound. Survival beyond a few months of life is rare.

Diagnosis

Trisomy 21

✓ Pearls

- Down syndrome is the most common cause of increased nuchal translucency during first-trimester ultrasound.
- Down syndrome is characterized by mental retardation, as well as cardiac, central nervous system, gastrointestinal, and skeletal defects.
- Turner syndrome is characterized by short stature, ovarian dysgenesis, and cystic hygromas.
- Trisomy 18 presents with cystic hygromas, clenched fists with overlapping digits, and choroid plexus cysts.

Suggested Readings

Cuckle HS, Malone FD, Wright D, et al. Contingent screening for Down syndrome—results from the FaSTER trial. Prenat Diagn 2008;28(2):89–94

Fong KW, Toi A, Salem SW, et al. Detection of fetal structural abnormalities with US during early pregnancy. Radiographics 2004;24(1):157–174

Jones KL. Smith's Recognizable Patterns of Human Malformation. Philadelphia: WB Saunders; 1997

Tanriverdi HA, Hendrik HJ, Ertan AK, Axt R, Schmidt W. Hygroma colli cysticum: prenatal diagnosis and prognosis. Am J Perinatol 2001;18(8):415–420

Case 202

Corinne D. Strickland

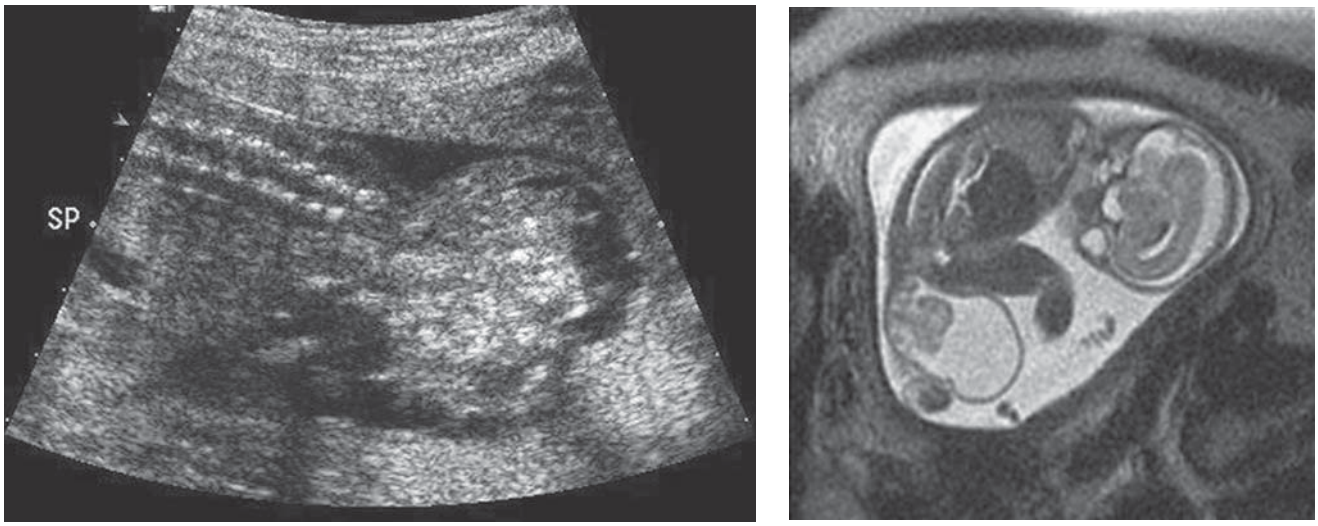


Fig. 202.1 **(A)** Longitudinal ultrasound image of the lower fetal spine in gray scale demonstrates a heterogeneous cystic and solid mass arising from the distal fetal spine. **(B)** Fetal magnetic resonance image better demonstrates the mass arising from the sacrum.

Clinical Presentation

Abnormal ultrasound findings in a woman (G1, P0) at 20 weeks' gestation (**Fig. 202.1**).

Key Imaging Finding

Sacral mass

Top 3 Differential Diagnoses

- **Sacrococcygeal teratoma.** Sacrococcygeal teratoma is the most common fetal neoplasm, with an incidence of 1 in 40,000. The neoplasm represents an extragonadal germ cell tumor resulting from aberrant migration of primordial germ cells. Ultrasound reveals a solid, cystic, or mixed sacrococcygeal mass. Type I lesions are entirely external, type IV are entirely intrapelvic, and types II and III have both internal and external components. Histologically, sacrococcygeal teratomas contain all three germ cell layers. Most tumors are benign; however, primarily internal tumors are more likely to contain malignant elements. Large, solid sacrococcygeal teratomas are associated with a worse prognosis than predominantly cystic masses, due to increased vascularity and arteriovenous shunting within the tumors that may lead to hydrops fetalis and maternal mirror syndrome (edema similar to hydrops but affecting the mother).
- **Myelomeningocele and variants.** Magnetic resonance imaging is the preferred modality for neural tube defects due to its superior demonstration of neural elements. On prenatal ultrasonography, both open and closed neural tube defects may appear as sacrococcygeal masses. Myelomeningocele and myelocele are open neural tube defects that occur most commonly at the lumbosacral level, and they are usually associated with a Chiari II malformation. Anterior meningocele is a presacral, closed neural tube defect involving herniation of a cerebrospinal fluid–filled dural sac through a bony sacral defect. Anterior meningoceles may be difficult to differentiate from a cystic sacrococcygeal teratoma.
- **Rhabdomyosarcoma.** Rhabdomyosarcoma is an aggressive, malignant soft tissue tumor that accounts for 4 to 8% of all pediatric neoplasms. Occurrence within the presacral space usually represents extension of a mass originating from the genitourinary tract.

Additional Differential Diagnoses

- **Duplication cyst.** Duplication cysts are congenital enteric cysts that may arise anywhere along the alimentary tract but are most common within the ileum. Duplication cysts of the rectum are rare but should be considered in the differential diagnosis of a cystic presacral mass.

Diagnosis

Sacrococcygeal teratoma

✓ Pearls

- Sacrococcygeal teratoma is the most common fetal neoplasm; it may be cystic, solid, or mixed.
- Myelomeningocele is usually associated with intracerebral findings of Chiari II malformation.
- Rhabdomyosarcoma within the presacral space is often due to extension from the genitourinary tract.

Suggested Readings

Kocaoglu M, Frush DP. Pediatric presacral masses. Radiographics 2006;26(3):833–857

Rossi A, Biancheri R, Cama A, Piatelli G, Ravegnani M, Tortori-Donati P. Imaging in spine and spinal cord malformations. Eur J Radiol 2004;50(2):177–200

Woodward PJ, Sohaey R, Kennedy A, Koeller KK. From the *Archives of the AFIP:* a comprehensive review of fetal tumors with pathologic correlation. Radiographics 2005;25(1):215–242

Case 203

Corinne D. Strickland

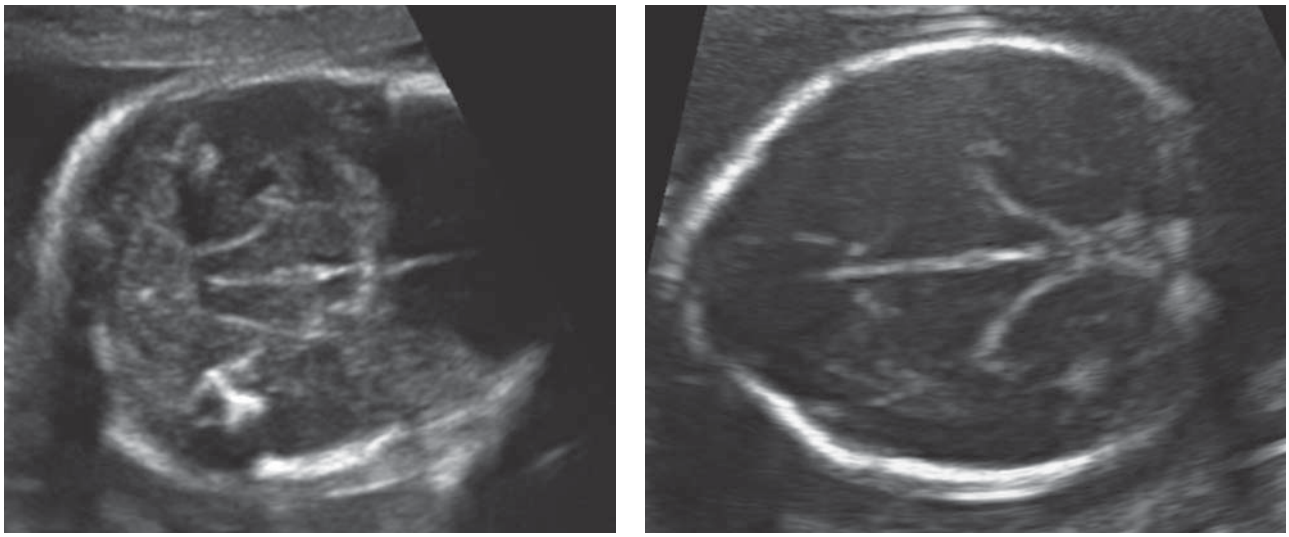


Fig. 203.1 **(A)** Axial ultrasound image of the fetal posterior fossa demonstrates a posterior fossa malformation with an abnormal "banana-shaped" configuration of the cerebellum. **(B)** An axial image more superiorly shows abnormal indentation of the frontal bones, referred to as a "lemon-shaped" head configuration. (Courtesy of Leann E. Linam, MD, Cincinnati Children's Hospital Medical Center.)

Clinical Presentation

A 28-year-old woman at 21 weeks' gestation (**Fig. 203.1**).

Key Imaging Finding

Posterior fossa malformation

Top 3 Differential Diagnoses

- **Chiari malformation.** The Chiari malformations are posterior fossa anomalies in which the cerebellar tonsils protrude through the foramen magnum. Chiari I, the mildest and most common malformation, may be asymptomatic or in adulthood produce headache and cerebellar signs. Chiari II, also known as Arnold–Chiari malformation, results from a primary defect of neural tube closure and is the most common cause of congenital hydrocephalus. The series of events resulting in Chiari II malformation include leakage of cerebrospinal fluid through a spinal defect that leads to collapse of the cerebral ventricles and underdevelopment of the posterior fossa. As the cerebellum develops within the small posterior fossa, the cerebellar tonsils herniate caudally, obstructing the outlets of the fourth ventricle and obliterating the cisterna magna. Associated signs on prenatal ultrasound include ventriculomegaly, a "banana-shaped" cerebellum, and indentation of the frontal bones, giving the skull a characteristic "lemon-shaped" appearance.
- **Dandy–Walker malformation.** A true Dandy–Walker malformation is defined by a triad of features: partial or complete agenesis of the cerebellar vermis, cystic dilatation of the fourth ventricle, and enlargement of the posterior fossa with upward displacement of the tentorium cerebelli and torcula. The term *Dandy–Walker variant* is often used to describe a hypoplastic or absent inferior vermis. Such variants include a spectrum of cerebellar hypoplasia malformations. Fetal magnetic resonance imaging (MRI) can be useful for clarification of the underlying malformation.
- **Joubert syndrome.** Joubert syndrome is a rare autosomal recessive disorder characterized by hypoplasia or absence of the cerebellar vermis. Elongation of the superior cerebellar peduncles and increased depth of the interpeduncular fossa may be observed on MRI. These findings comprise the "molar tooth" sign pathognomonic for this condition.

Diagnosis

Chiari malformation

✓ Pearls

- "Banana-shaped" cerebellum and "lemon-shaped" calvarium are ultrasound findings of Chiari II malformations.
- Chiari II malformations are the most common cause of congenital hydrocephalus.
- Dandy–Walker malformation is characterized by vermian agenesis with cystic fourth ventricular enlargement.
- Joubert syndrome presents with vermian aplasia/hypoplasia and a "molar tooth" brainstem configuration.

Suggested Readings

Fong KW, Toi A, Salem S, et al. Detection of fetal structural abnormalities with US during early pregnancy. Radiographics 2004;24(1):157–174

Niesen CE. Malformations of the posterior fossa: current perspectives. Semin Pediatr Neurol 2002;9(4):320–334

Oh KY, Rassner UA, Frias AE Jr, Kennedy AM. The fetal posterior fossa: clinical correlation of findings on prenatal ultrasound and fetal magnetic resonance imaging. Ultrasound Q 2007;23(3):203–210

Case 204

Daniel G. Church

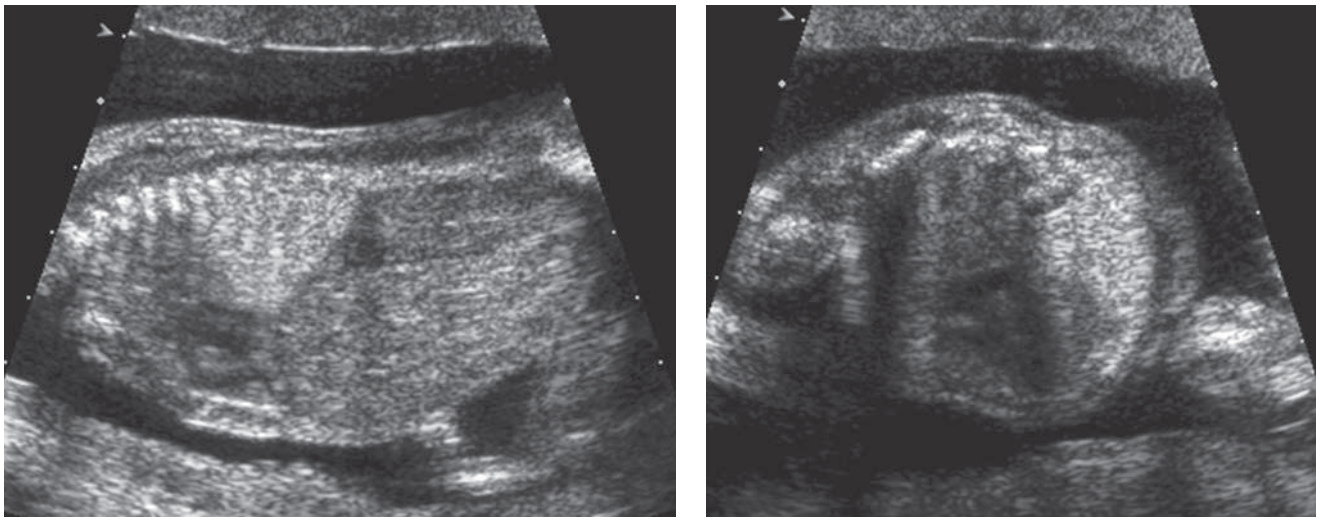


Fig. 204.1 **(A)** Longitudinal and **(B)** transverse ultrasound images of the fetus demonstrate the presence of an echogenic mass within the fetal chest.

Clinical Presentation

A 28-year-old woman (G3, P1) at 19 weeks' gestation (**Fig. 204.1**).

Key Imaging Finding

Hyperechoic thoracic mass

Top 3 Differential Diagnoses

- **Congenital pulmonary airway malformation (CPAM).** CPAM (also known as cystic adenomatoid malformation) constitutes >80% of lung masses detected by prenatal imaging. It is characterized by excessive growth of the terminal respiratory bronchioles. Prenatal ultrasonography demonstrates a hyperechoic pulmonary mass with or without cystic elements of varying sizes. On pathology, masses with large cysts are classified as type 1, masses with medium-sized cysts are classified as type 2, and predominantly solid masses with nonvisible (microscopic) cysts are classified as type 3. CPAM is limited to one lobe or segment of the lung in 95% of cases. Prognosis depends on the presence or absence of hydrops and polyhydramnios, which is likely to occur with large masses associated with mediastinal shift. CPAMs may increase in size, and many will decrease in size during the third trimester.
- **Pulmonary sequestration.** Pulmonary sequestration represents aberrantly developed lung tissue that is perfused (receiving its blood supply primarily from the systemic circulation) but not ventilated (typically, there is no communication with the tracheobronchial tree). Prenatal ultrasonography demonstrates a relatively homogeneous hyperechoic pulmonary mass, and Doppler studies may demonstrate a systemic feeding vessel. Pulmonary sequestrations are most commonly located in the medial lung base. Sequestrations are classified as intra- or extralobar. Extralobar sequestrations are more common than intralobar in the fetus and newborn. Intralobar sequestrations are contained within the pleura of the normal lung, have a systemic arterial blood supply, and have venous drainage into the pulmonary veins. Extralobar sequestrations are found above or below the diaphragm and have their own pleural lining, systemic arterial supply, and systemic venous drainage.
- **Congenital lobar emphysema (CLE).** CLE (also referred to as congenital lobar hyperinflation) represents a developmental anomaly of the bronchus resulting in a ball-valve phenomenon with subsequent lobar hyperinflation. Bronchial atresia is associated with CLE, and CLE usually occurs in the upper (left more common than right) or middle lobes. The masses may be opacified with fetal lung fluid at birth and gradually become more lucent as the fluid is cleared.

Additional Differential Diagnoses

- **Congenital diaphragmatic hernia (CDH).** CDH is the most common developmental abnormality of the diaphragm, with up to 90% of hernias occurring on the left side. The stomach, intestines, liver, and spleen may herniate into the chest. Prenatal ultrasonography demonstrates herniation of abdominal contents into the chest with a contralateral mediastinal shift. Prognosis depends on hernia volume and the extent of compression, as well as hypoplasia of the contralateral lung resulting from mediastinal shift.

Diagnosis

Congenital pulmonary airway malformation

✓ Pearls

- CPAM is the most common lung mass identified on prenatal ultrasound; it is classified by cystic/solid components.
- All sequestrations have systemic arterial supply; venous drainage pattern distinguishes the two types.
- CLE results from hyperinflation due to a ball-valve phenomenon; the left upper lobe is most commonly involved.
- Up to 90% of CDHs occur on the left side; prognosis depends on the extent of pulmonary hypoplasia.

Suggested Readings

Bromley B, Parad R, Estroff JA, Benacerraf BR. Fetal lung masses: prenatal course and outcome. J Ultrasound Med 1995;14(12):927–936, quiz p1378

Goldstein RB. Ultrasound evaluation of the fetal thorax. In: Callen PW. Ultrasonography in Obstetrics and Gynecology. 4th ed. Philadelphia: WB Saunders; 2000

Case 205

Joyce F. Sung



Fig. 205.1 Ultrasound image of the maternal uterus demonstrates a twin pregnancy with a thick membrane separating the two gestational sacs and a broad insertion into the maternal uterus, known as the "twin peak" sign.

Clinical Presentation

A 31-year-old woman (G1, P0) with twin pregnancy (**Fig. 205.1**).

Key Imaging Finding

Twin development (chorionicity)

Top 3 Differential Diagnoses

- **Dichorionic/diamnionic twin pregnancy.** Dichorionic/diamnionic pregnancies may be either dizygotic ("fraternal"), resulting from fertilization of two separate ova, or monozygotic ("identical"), resulting from division of a single zygote during the first 3 days following fertilization. Dizygotic pregnancies account for 80% of all twin pregnancies; thus most dichorionic/diamnionic twins are dizygotic. Monozygotic dichorionic/diamnionic twins account for ~6 to 7% of all twin pregnancies. The dividing membrane separating the twin fetuses appears relatively thick on ultrasound (usually ≥2 mm), because each twin is surrounded by its own amnion and chorion. A single fused placenta or two distinct placentas may be present. In the case of fused dichorionic placentas, a "twin peak" or "lambda" sign is visible on ultrasound, a result of placental tissue extending between the chorion layers of the dividing membrane. Risks associated with dichorionic/diamnionic twin pregnancy include growth restriction (25–30% risk), preterm (before 37 weeks) delivery (40%), and perinatal mortality (10–20%).
- **Monochorionic/diamnionic twin pregnancy.** Monochorionic/diamnionic twins are always monozygotic, resulting from division of the zygote between 4 and 8 days following fertilization, and account for 13 to 14% of all twin pregnancies. Two embryos develop with separate amniotic sacs but are covered by a common chorion and share a single placenta. On ultrasonography, the dividing membrane appears thin (usually <2 mm). Monochorionic/diamnionic twins risk fetal growth restriction (50% risk), preterm delivery (60%), and perinatal mortality (30–40%). The diagnosis of monochorionicity is critical given that monochorionic twins are at risk for developing twin-to-twin transfusion syndrome (TTTS). TTTS results from unequal shunting across vascular anastomoses within the monochorionic twin placenta and is associated with a risk of fetal demise.
- **Monochorionic/monoamnionic twin pregnancy.** Monochorionic/monoamnionic twin pregnancies are monozygotic twin pregnancies resulting from division of the zygote between 8 and 13 days following fertilization and account for <1% of all twin pregnancies. Two embryos share a single amniotic sac, as well as a single chorion and a single placenta. These twins are at particular risk for cord entanglement, which can result in fetal death. On ultrasound, no dividing membrane is seen. Additional risks associated with monoamnionic twins are fetal growth restriction (40%), preterm delivery (60–70%), and perinatal mortality (60%). Rarely, monochorionic/monoamnionic twin pregnancies may result in conjoined twins, resulting from division of the zygote after 13 days following fertilization.

Diagnosis

Dichorionic/diamnionic twin pregnancy

✓ Pearls

- Characteristic ultrasound findings associated with dichorionic twins include the "twin peak" or "lambda" sign.
- Monochorionic/diamnionic twins have a thin (<2 mm) separating membrane.
- Monoamnionic twins are at risk for cord entanglement, as well as increased perinatal morbidity/mortality.
- Division of the zygote after day 13 following fertilization results in conjoined twins.

Suggested Readings

Cunningham FG, Gant NF, Leveno KJ, et al. Multifetal pregnancy. In: Williams Obstetrics. 21st ed. New York: McGraw-Hill; 2001:765–810

Case 206

Laura J. Varich

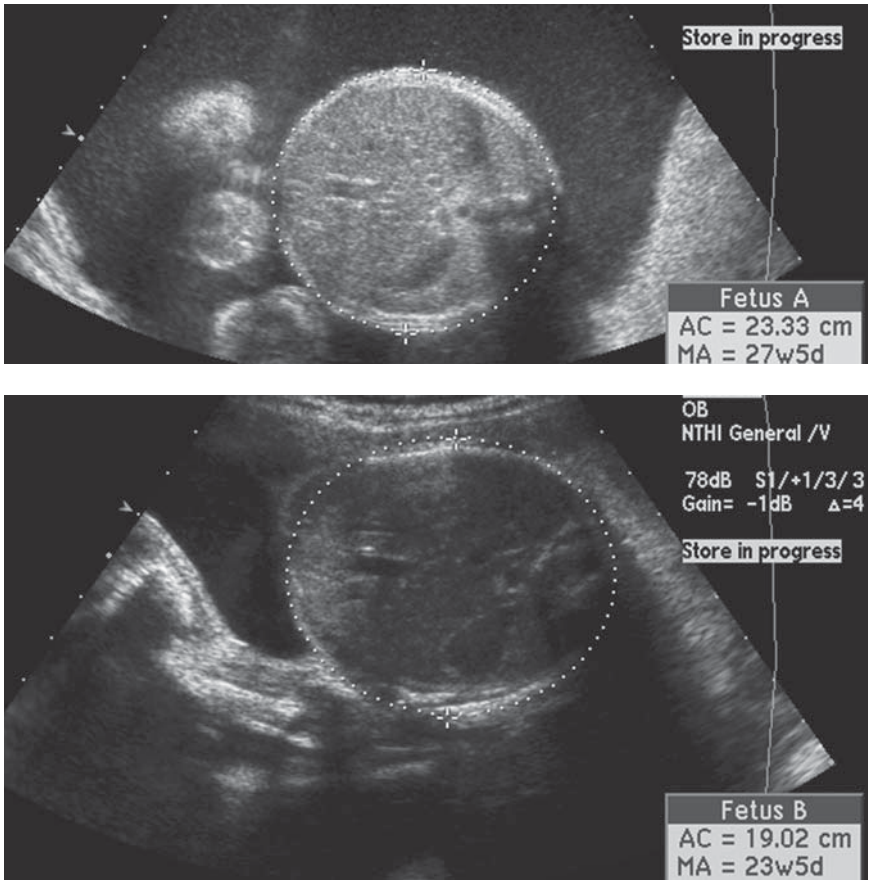


Fig. 206.1 Ultrasound images of the fetal abdominal circumference in a twin pregnancy demonstrate significant asymmetry in fetal size (difference of 4 weeks of gestational age) between **(A)** fetus A and **(B)** fetus B.

Clinical Presentation

A 24-year-old woman (G1, P0) with twin pregnancy at 26 weeks' gestation (**Fig. 206.1**).

Key Imaging Finding

Twin pregnancy with asymmetric fetal sizes

Top 3 Differential Diagnoses

- **Twin-to-twin transfusion syndrome (TTTS).** In monochorionic twins (in which the two fetuses share the same placenta), there are known placental vascular anastomoses. In 35% of monochorionic twins, an imbalance in blood flow to the fetuses produces asymmetry in fetal size and amniotic fluid volume. The underperfused twin will demonstrate evidence of oligohydramnios and restricted growth. When the fluid is so severely restricted that the fetus is immobilized within its gestational sac, the fetus will appear in a static position, referred to as a "stuck twin." The twin with increased perfusion will demonstrate increased growth and polyhydramnios. TTTS is diagnosed when there is more than a 20% discrepancy in estimated fetal weight (EFW) and a major difference in the volumes of amniotic fluid.
- **Fetal demise.** Twin pregnancies are associated with a four- to sixfold increase in mortality relative to singleton pregnancies. In up to 20% of twin gestations identified in the first trimester, there will be demise of one twin prior to delivery. Asymmetry in size of the fetuses may be the first clue to demise of a twin. Absolute signs of demise are absence of fetal cardiac activity and absence of fetal movement at the appropriate stage of fetal gestation (remember that it is important to always give the pregnancy the benefit of the doubt and obtain a repeat confirmatory scan). Other signs of fetal demise are overlapping cranial sutures, maceration and edema of the soft tissues, and decrease in size of the gestational sac.
- **Normal variation.** There can be some normal variation in the size of twin fetuses, especially in dizygotic twins (whose genetic makeup differs). However, discordance in EFW more than 20% is considered abnormal and should be monitored closely.

Diagnosis

Twin-to-twin transfusion syndrome

✓ Pearls

- TTTS occurs in monochorionic twins and results from blood flow imbalances.
- The underperfused twin in TTTS has oligohydramnios and restricted growth.
- The hyperperfused twin in TTTS has polyhydramnios and increased growth.
- Fetal demise results in asymmetric sizes; absolute signs are lack of cardiac activity and movement.

Suggested Readings

Callen P. Ultrasound in Obstetrics and Gynecology. 5th ed. Philadelphia: WB Saunders; 2008

Duncombe GJ, Dickinson JE, Evans SF. Perinatal characteristics and outcomes of pregnancies complicated by twin-twin transfusion syndrome. Obstet Gynecol 2003;101(6):1190–1196

Case 207

Hedieh K. Eslamy

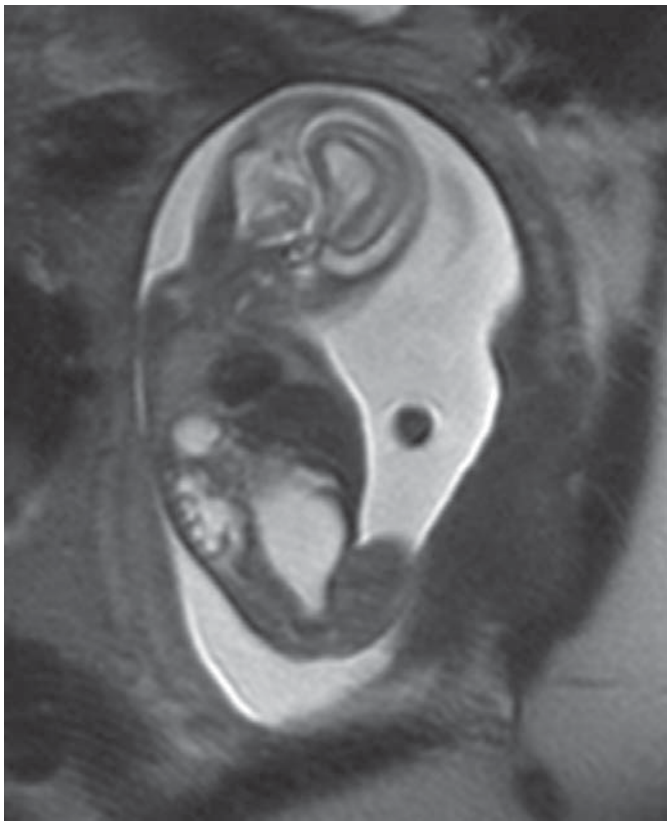


Fig. 207.1 T2-weighted sagittal magnetic resonance image of a fetus demonstrates an enlarged urinary bladder with a dilated bladder neck and hydronephrosis involving the left kidney.

Clinical Presentation

A 19-year-old woman (G1, P0) with a 19-week gestational age male fetus (**Fig. 207.1**).

Key Imaging Finding

Enlarged bladder (megacystis)

Top 3 Differential Diagnoses

- **Posterior urethral valves (PUVs).** The bladder is the first structure of the urinary tract visible in the pelvis, identifiable at ~9 to 10 weeks of embryonal life. Anomalies of the urinary tract may be suspected when the urinary bladder is enlarged or not visualized. Megacystis is defined as a urinary bladder >3 cm in length in the second trimester and >6 cm in length in the third trimester. The most common etiology of megacystis is bladder outlet obstruction. A male fetus with megacystis in the second or third trimester will almost invariably have PUVs as the cause of obstruction. Ultrasonographic findings of PUVs are megacystis, bladder wall thickening, hydroureter, variable degrees of hydronephrosis, renal dysplasia, urinary ascites, urinoma, oligohydramnios, and hypoplastic lungs secondary to mass effect.
- **Prune-belly syndrome.** Megacystis within a fetus (usually male) in the first and early second trimester may indicate prune-belly syndrome. In this condition, the abdominal musculature is deficient or absent, and genitourinary tract anomalies are present. Genitourinary findings are an enlarged thick-walled bladder, megaureter, hydronephrosis, and cryptorchidism. Complications include oligohydramnios and resultant pulmonary hypoplasia.
- **Megacystis-microcolon–intestinal hypoperistalsis (MMIH) syndrome.** MMIH syndrome is a rare anomaly most often seen in female fetuses and characterized by a massively distended bladder and a small colon. Although the exact cause of this abnormality is not completely understood, it is thought to represent a form of neuropathy or myopathy. Ultrasound findings consist of nonobstructive megacystis and varying degrees of hydroureter and hydronephrosis. Unlike causes of bladder outlet obstruction, amniotic fluid is typically normal or increased. A microcolon may or may not be detected on sonography.

Additional Differential Diagnoses

- **Marked vesicoureteral reflux.** Marked vesicoureteral reflux may result in nonobstructive megacystis secondary to persistent and increased postvoid residuals due to reflux. It is seen more often in female fetuses. Patients typically have associated hydroureter and hydronephrosis when severe.

Diagnosis

Posterior urethral valves

✓ Pearls

- Megacystis in male fetuses is most commonly due to bladder outlet obstruction from posterior urethral valves.
- Prune-belly syndrome consists of deficient abdominal musculature, urinary anomalies, and cryptorchidism.
- Nonobstructive causes of megacystis include MMIH syndrome and marked vesicoureteral reflux.

Suggested Readings

Callen PW. Ultrasonography in Obstetrics and Gynecology. 5th ed. Philadelphia: WB Saunders; 2008

Donnelly LF. Diagnostic Imaging Pediatrics. Salt Lake City, UT: Amirsys; 2005

Montemarano H, Bulas DI, Rushton HG, Selby D. Bladder distention and pyelectasis in the male fetus: causes, comparisons, and contrasts. J Ultrasound Med 1998;17(12):743–749

Swischuk LE. Imaging of the Newborn, Infant and Young Child. 5th ed. Philadelphia: Lippincott Williams & Wilkins; 2004

Case 208

Joyce F. Sung

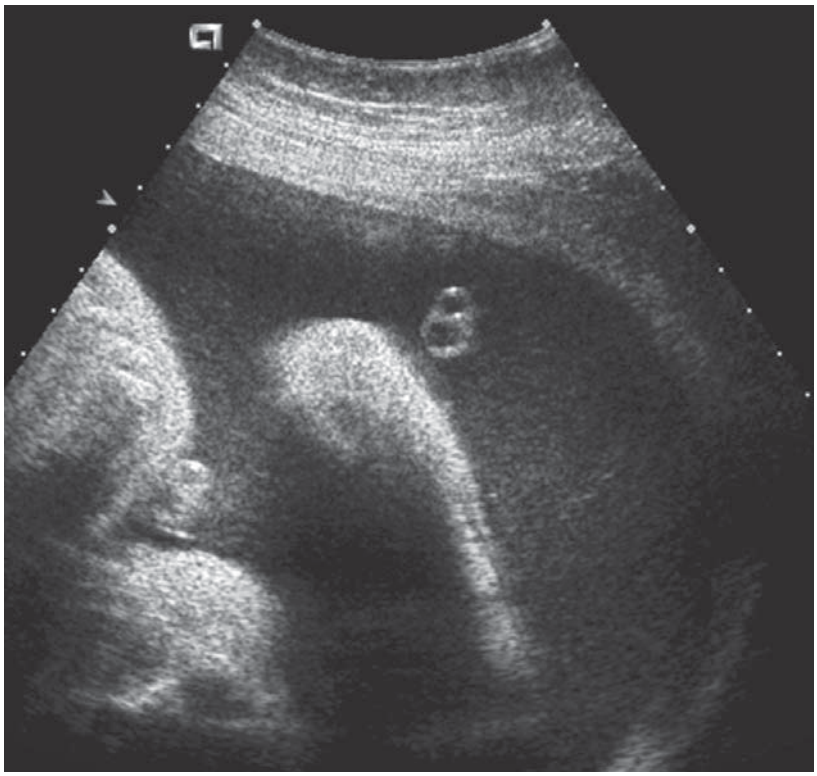


Fig. 208.1 Fetal ultrasound image demonstrates two round hypoechoic foci within the umbilical cord, consistent with a two-vessel cord.

Clinical Presentation

A 36-year-old woman (G2, P1) with a small fetus at 34 weeks' gestation (**Fig. 208.1**).

Key Imaging Finding

Umbilical cord vascular abnormality

Top 3 Differential Diagnoses

- **Two-vessel cord.** The normal umbilical cord contains three vessels (two arteries and one vein), which can be verified on color Doppler by visualizing the two arteries on each side of the fetal bladder or by visualizing a cross section of the umbilical cord demonstrating two arteries and one vein. A two-vessel cord (or single umbilical artery) occurs in 1% of pregnancies. It is important to evaluate the cord at the fetal end, as there may occasionally be only two vessels within the cord near the placental end, which is considered normal if three vessels are seen within the remainder of the cord. Although most often an incidental finding, an increase in fetal anomalies (especially cardiac and genitourinary) and chromosomal abnormalities has been reported in association with a two-vessel cord. Therefore, it is important to conduct a thorough anatomical survey when a two-vessel cord is found. Additionally, a two-vessel cord is associated with increased risk of growth restriction.
- **Cord hematoma.** Umbilical cord hematomas are usually iatrogenic in nature, resulting from invasive procedures such as amniocentesis and cordocentesis; they only rarely occur spontaneously. Because they are associated with a 50% risk of fetal demise, fetuses with a cord hematoma should be monitored closely with consideration for expectant delivery. On ultrasound, cord hematomas present as focal cord expansion with variable echogenicity ranging from hypo- to hyperechoic.
- **Cord hemangioma.** Cord hemangiomas are vascular tumors of endothelial cell origin that most commonly occur near the placental cord insertion. They appear as hyperechoic and/or multicystic masses. Associated findings include polyhydramnios. The lesions may exert local mass effect within the cord, jeopardizing fetal blood flow, and they may spontaneously hemorrhage.

Additional Differential Diagnoses

- **Wharton jelly cyst.** Wharton jelly is a substance that insulates and supports umbilical cord vessels, protecting them from injury. A Wharton jelly cyst represents a focal thickening of Wharton jelly, which typically occurs close to the fetal cord insertion. These lesions are often associated with omphaloceles.
- **Umbilical cord varix.** An umbilical cord varix is a relatively uncommon anomaly characterized by focal dilatation of the umbilical vein, likely caused by weakness of the umbilical vein wall. It may occur anywhere within the cord or within the intrahepatic segment of the umbilical vein. The lesions cause local turbulent flow (and possibly "vascular steal" phenomenon) and are prone to occlusion, which may result in fetal demise.

Diagnosis

Two-vessel cord

✓ Pearls

- Two-vessel cords are most often incidental but may be associated with growth restriction and anomalies.
- Umbilical cord hematomas are usually iatrogenic and are associated with a high risk of fetal demise.
- Umbilical cord hemangiomas are hyperechoic and/or multicystic; they may jeopardize fetal blood flow.
- An umbilical cord varix produces local turbulent flow and may thrombose, resulting in fetal demise.

Suggested Readings

Callen PW. Ultrasonography in Obstetrics and Gynecology. 5th ed. Philadelphia: Saunders Elsevier; 2008

Middleton WD, Kurtz AB, Hertzbery BS. Ultrasound: The Requisites. 2nd ed. St. Louis, MO: Mosby; 2004

Sherer DM, Anyaegbunam A. Prenatal ultrasonographic morphologic assessment of the umbilical cord: a review. Obstet Gynecol Surv 1997;52(8):506–514, 515–523

Case 209

Hedieh K. Eslamy

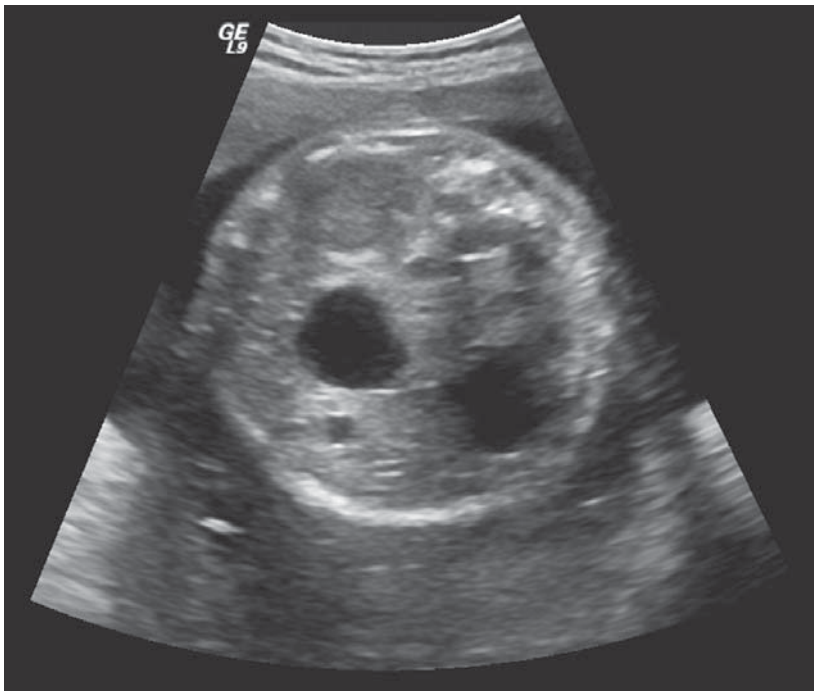


Fig. 209.1 Transverse ultrasound image of the fetal abdomen demonstrates two fluid-filled structures corresponding to a dilated stomach and duodenum.

Clinical Presentation

A 22-year-old woman (G4, P2) at 28 weeks' gestation (**Fig. 209.1**).

Key Imaging Finding

"Double bubble" sign

Top 3 Differential Diagnoses

- **Congenital duodenal obstruction (duodenal atresia or stenosis).** Congenital duodenal obstruction is the most common cause of fetal small bowel obstruction, with an incidence of 1:5000 to 10,000 live births. Duodenal atresia and stenosis are secondary to failure of recanalization of the bowel, whereas atresia of the jejunum and ileum is related to vascular insult. Duodenal obstruction occurs in the second or third portion of the duodenum. The two fluid-filled bubbles demonstrated on obstetric ultrasound represent the dilated stomach and proximal duodenum. Approximately 70% of cases are associated with other structural anomalies, mainly of the gastrointestinal tract (GI) or heart, and 40% of cases have associated polyhydramnios. In fetuses found to have duodenal obstruction, ~30% will have Down syndrome.
- **Annular pancreas.** Annular pancreas is the second most common condition to produce the characteristic "double bubble" sign. Annular pancreas is believed to result from failure of the embryonic pancreas to properly rotate around the duodenum, producing a ring of pancreatic tissue surrounding the second portion of the duodenum and causing varying degrees of duodenal obstruction. Polyhydramnios is present in obstructive cases; fetuses may also have restricted growth.
- **Intestinal malrotation with volvulus.** In the fetus, the GI tract is initially located outside the abdominal cavity. The bowel rotates as it is gradually withdrawn into the abdomen. In intestinal malrotation, the GI tract fails to completely rotate. In general, the cecum and terminal ileum are displaced medially and superiorly, and the normal small bowel mesenteric attachment is lost. In these cases, the mesenteric attachment is a very short pedicle, allowing the bowel to twist around the superior mesenteric artery. Volvulus may be intermittent or persistent, causing vascular compromise with potential complications of bowel ischemia, necrosis, perforation, and gangrene.

Diagnosis

Congenital duodenal obstruction (duodenal atresia)

✓ Pearls

- "Double bubble" sign on ultrasound corresponds to a dilated, fluid-filled stomach and proximal duodenum.
- Duodenal atresia is a failure of recanalization; it is associated with fetal anomalies and Down syndrome.
- Annular pancreas results in a ring of pancreatic tissue surrounding the second portion of the duodenum.
- Malrotation with volvulus can result in vascular compromise with resultant bowel ischemia and necrosis.

Suggested Readings

Callen PW. Ultrasonography in Obstetrics and Gynecology. 5th ed. Philadelphia: WB Saunders; 2008

Swischuk LE. Imaging of the Newborn, Infant and Young Child. 5th ed. Philadelphia: Lippincott Williams & Wilkins; 2004

Traubici J. The double bubble sign. Radiology 2001;220(2):463–464

Case 210

Erika Rubesova

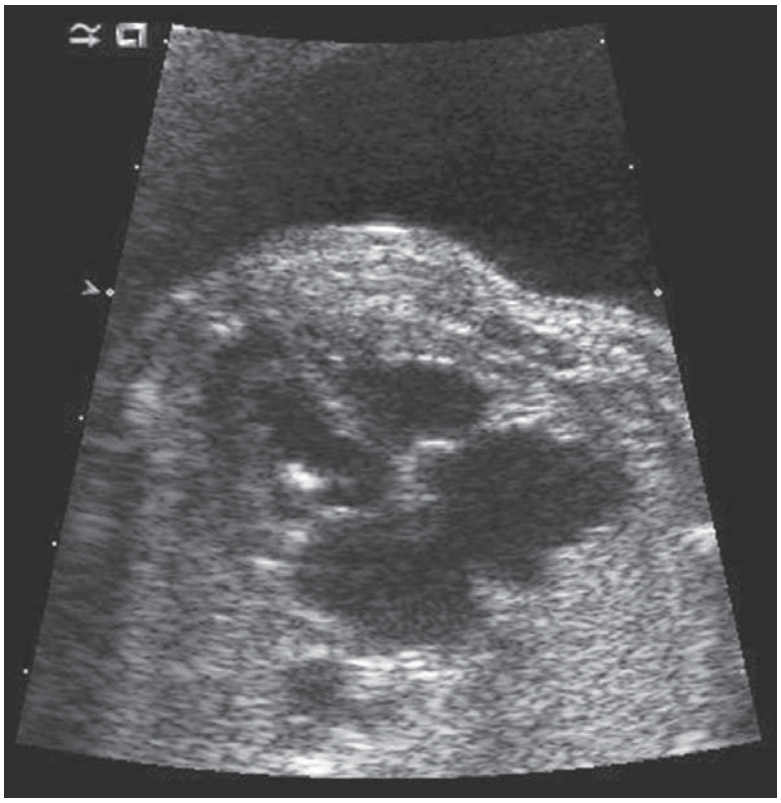


Fig. 210.1 Ultrasound image (four-chamber view) of the fetal heart demonstrates an echogenic focus in the left ventricle.

Clinical Presentation

A 34-year-old woman (G3, P2) at 21 weeks' gestation (**Fig. 210.1**).

Key Imaging Finding

Hyperechoic intracardiac focus

Top 3 Differential Diagnoses

- **Echogenic intracardiac focus (EIF)/papillary muscle calcification.** An EIF is commonly seen in the left ventricle and is considered a normal variant in the patient population at low risk for chromosomal abnormalities. The prevalence is 3 times higher in the Asian population. In the patient population at increased/high risk for chromosomal abnormalities (e.g., advanced maternal age), the presence of an EIF is a marker of increased risk of Down syndrome and trisomy 13. In and of itself, it is not associated with cardiac anomalies.
- **Rhabdomyoma.** Rhabdomyomas are benign neoplasms that are associated with tuberous sclerosis in 50 to 80% of cases. They are the most common benign cardiac tumors in infants and children. These tumors often appear as multiple hyperechoic round masses found during the second trimester. The masses can grow until the third trimester but are then seen to regress during the later stages of pregnancy and first years of life; therefore, they have a good prognosis. Very large tumors may cause outflow obstruction, alter valve function, and generate arrhythmias. Very small lesions may be difficult to detect, with their only manifestation being an alteration in myocardial echogenicity.
- **Fibroma.** Cardiac fibromas are rare lesions that usually appear on ultrasound as echogenic masses within the septal myocardium. They may undergo cystic transformation and do not usually regress. On magnetic resonance imaging (MRI), the lesions are characteristically hypointense on T2-weighted sequences due to the presence of fibrous tissue. They have been described in association with other abnormalities, including Beckwith–Wiedemann syndrome and cleft palate.

Additional Differential Diagnoses

- **Teratoma.** Cardiac teratomas are rare and most often located within the pericardium; myocardial teratomas are extremely rare. The masses are often heterogeneous and large, with marked mass effect and cardiac enlargement. They are composed of all three germ cell layers, often have cystic components, and may contain calcifications. They are associated with large pericardial effusions.
- **Hemangioma.** Cardiac hemangiomas are benign vascular lesions that may involve the heart and/or pericardium. They are most frequently located within the right atrium and are associated with pericardial effusions. Ultrasound findings include a hyperechoic mass with cystic components. Hemangiomas are typically treated surgically.

Diagnosis

Echogenic intracardiac focus/papillary muscle calcification

✓ Pearls

- An EIF is associated with increased risk of Down syndrome and trisomy 13 in high-risk populations.
- Rhabdomyomas are the most common intracardiac tumors in the fetus and may be associated with tuberous sclerosis.
- Cardiac fibromas typically occur along the septum and are characteristically hypointense on T2 MRI.
- Teratomas are large and heterogeneous; they often present with large pericardial effusions.

Suggested Readings

Callen P. Ultrasound in Obstetrics and Gynecology. 5th ed. Philadelphia: WB Saunders; 2008

Coco C, Jeanty P, Jeanty C. An isolated echogenic heart focus is not an indication for amniocentesis in 12,672 unselected patients. J Ultrasound Med 2004;23(4):489–496

Case 211

Bo Yoon Ha

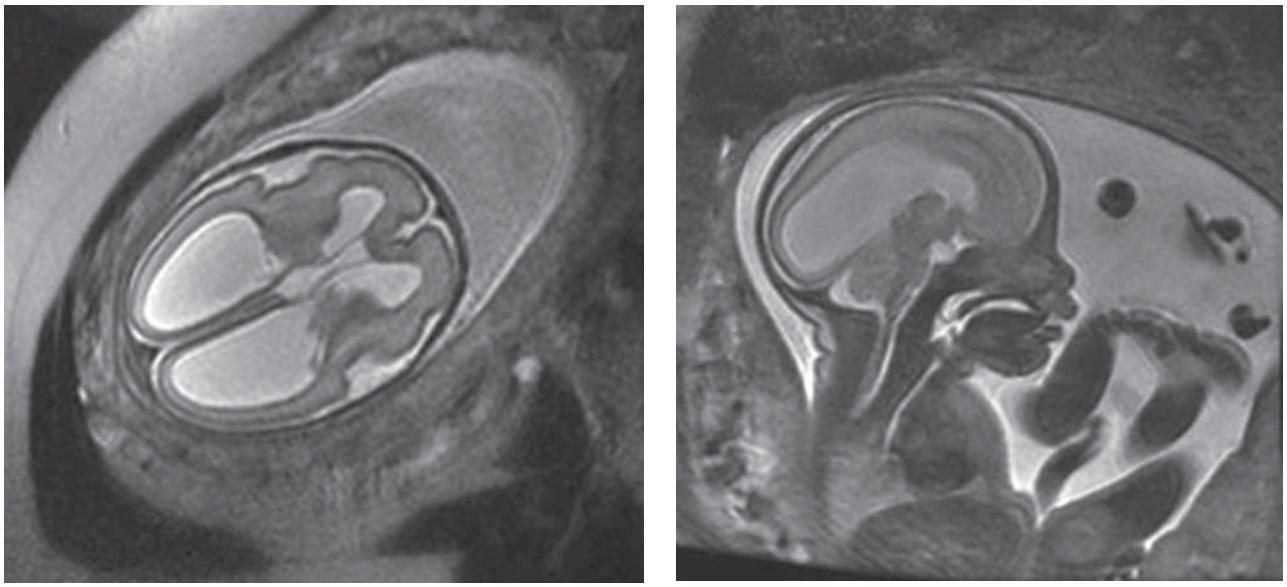


Fig. 211.1 **(A)** Axial and **(B)** sagittal T2-weighted magnetic resonance images of the fetal brain demonstrate dilated third and lateral ventricles with a normal-sized fourth ventricle.

Clinical Presentation

Follow-up of an abnormal ultrasound at 20 weeks' gestation in a 20-year-old woman (G1, P0) now at 28 weeks' gestation (**Fig. 211.1**).

Key Imaging Finding

Central nervous system (CNS) ventriculomegaly

Top 3 Differential Diagnoses

- **Ventriculomegaly.** Ventriculomegaly is defined as dilatation of the lateral ventricles >10 mm in width as measured in the transverse plane at the atrial level. Slight asymmetry between the lateral ventricles can be normal. Follow-up imaging is typically performed in the third trimester to document stability.
- **Congenital aqueductal stenosis.** Congenital aqueductal stenosis occurs at the aqueduct of Sylvius (between the third and fourth ventricles) and results in dilatation of the lateral and third ventricles with a normal-sized fourth ventricle. It may be caused by webs/septations or secondary to prior intraventricular bleeding or infection. Adjacent masses can also rarely result in aqueductal stenosis or obstruction.
- **Chiari malformation.** The Chiari malformations are posterior fossa anomalies in which the cerebellar tonsils protrude through the foramen magnum. Chiari I malformations are associated with cervical spine abnormalities and cord syrinx (usually cervical); hydrocephalus may occur but is not nearly as common as with Chiari II malformations. Chiari II malformations consist of inferior cerebellar tonsillar displacement with crowding at the foramen magnum, a small posterior fossa, and hydrocephalus—all of which are secondary to a lumbosacral myelomeningocele. Prenatal ultrasound findings are ventriculomegaly, a "banana-shaped" cerebellum, a "lemon–shaped" calvarium, and a lumbosacral myelomeningocele.

Additional Differential Diagnoses

- **Agenesis of the corpus callosum (ACC).** ACC is an anomaly that may be partial or complete. It is often associated with other CNS or systemic malformations, including disorders of neuronal migration, hydrocephalus, midline lipoma, Chiari malformation, Dandy–Walker malformation, and interhemispheric cysts. Findings include parallel lateral ventricles, colpocephaly, and a high-riding third ventricle.
- **Dandy–Walker malformation.** Dandy–Walker malformation is a rare congenital malformation that involves the cerebellum and fourth ventricle. It is characterized by agenesis or hypoplasia of the cerebellar vermis, cystic dilatation of the fourth ventricle, and enlargement of the posterior fossa. It is often associated with hydrocephalus, as well as other congenital CNS malformations, including ACC.
- **Holoprosencephaly.** The result of incomplete or absent cleavage of the primitive forebrain into two cerebral hemispheres, holoprosencephaly is categorized as three types depending on severity: alobar, semilobar, and lobar. The alobar type is most severe, with complete absence of division of the forebrain resulting in monoventricle and fused cerebral hemispheres. The lobar type is the least severe, with almost complete division of the hemispheres.

Diagnosis

Congenital aqueductal stenosis

✓ Pearls

- Mild ventriculomegaly may have a good outcome.
- Aqueductal stenosis may result from intrinsic webs or occur secondarily; the fourth ventricle is normal in size.
- Chiari II malformations (tonsillar displacement and myelomeningocele) commonly cause hydrocephalus.
- ACC results in a parallel configuration of the lateral ventricles, colpocephaly, and high-riding third ventricle.

Suggested Readings

Barkovich AJ. Pediatric Neuroimaging. 3rd ed. Philadelphia: Lippincott Williams & Wilkins; 2000

D'Addario V, Pinto V, Di Cagno L, Pintucci A. Sonographic diagnosis of fetal cerebral ventriculomegaly: an update. J Matern Fetal Neonatal Med 2007;20(1):7–14

Case 212

Hedieh K. Eslamy

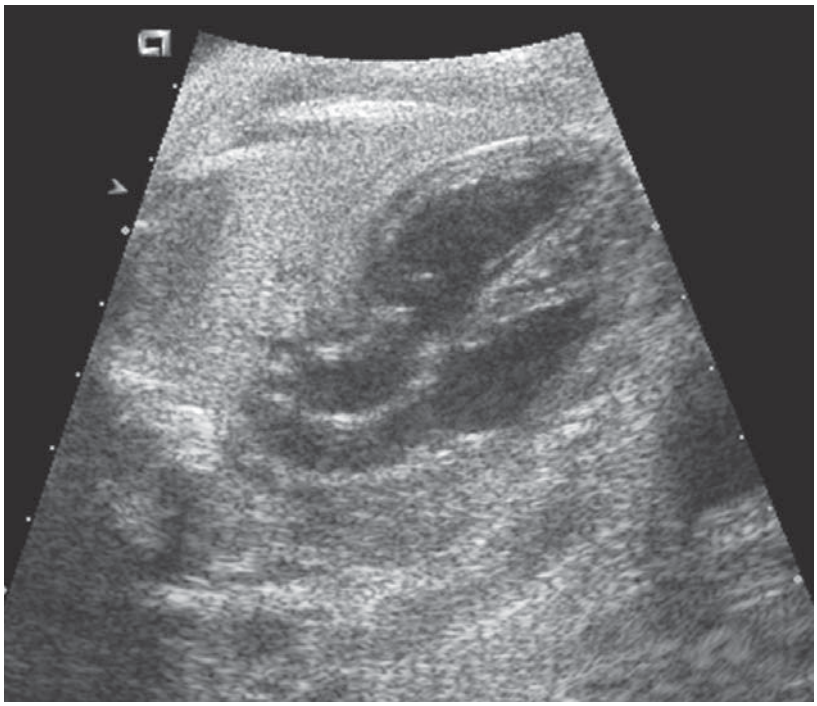


Fig. 212.1 Ultrasound image of the fetal heart demonstrates abnormal parallel configuration of the ventricular outflows tracts (they are not crossing as is normally expected).

Clinical Presentation

A 31-year-old woman (G1, P0) for a fetal anatomy scan (**Fig. 212.1**).

Key Imaging Finding

Abnormal ventriculoarterial configuration

Top 3 Differential Diagnoses

- **Tetralogy of Fallot.** The incidence of tetralogy of Fallot is 3 to 5 per 10,000 live births; it is the most common cyanotic congenital heart anomaly. Tetralogy of Fallot occurs secondary to underdevelopment of the right ventricular outflow tract. The four components of this anomaly are right ventricular outflow tract stenosis, right ventricular hypertrophy, ventricular septal defect (VSD), and an overriding aorta. Associated cardiac abnormalities are pulmonary artery branch stenosis or hypoplasia, absence of the pulmonary valve, right aortic arch, and anomalies of the origins of the coronary arteries.
- **Transposition of the great arteries (TGA).** TGA is divided into two subtypes: D-TGA and L-TGA. D-TGA is more common (5% of congenital heart disease) and consists of discordant ventriculoarterial connections (i.e., the right ventricle connected to the aorta, and the left ventricle connected to the pulmonary trunk) with concordant atrioventricular connections (i.e., the right atrium connected to the right ventricle, and the left atrium connected to the left ventricle). In most cases of TGA, the ventricular outflow tracts are parallel to each other. The aorta arises anterior and to the right of the left ventricular connection to the pulmonary artery. L-TGA is less common (1% of cases of congenital heart disease) and has discordant ventriculoarterial and atrioventricular connections.
- **Truncus arteriosus.** In truncus arteriosus, a common arterial trunk arises from the base of the ventricles and gives rise to the aorta and pulmonary arteries, as well as the coronary arteries. It constitutes ~2% of congenital cardiac anomalies and is associated with VSD (100%), right-sided aortic arch (30–40%), and DiGeorge syndrome (absent thymus and parathyroid glands).

Additional Differential Diagnoses

- **Double outlet right ventricle (DORV).** In DORV, both great arteries arise completely or predominantly from the morphologic right ventricle. DORV constitutes ~1.0 to 1.5% of congenital heart disease and is highly associated with a VSD. The relationship of the outflow tracts varies, with a side-by-side configuration being most common.
- **Hypoplastic left heart syndrome.** Hypoplastic left heart syndrome refers to severe underdevelopment of the left heart due to mitral and aortic valve atresia. The heart is enlarged, and the ascending aorta is hypoplastic with a threadlike configuration. Left-to-right shunting occurs at the atrial level. A patent ductus arteriosus is the only connection that allows for systemic circulation.

Diagnosis

Transposition of the great arteries

✓ Pearls

- Visualization of normal-crossing ventricular outflow tracts is essential during a fetal survey.
- Tetralogy of Fallot consists of pulmonic stenosis, right ventricular hypertrophy, VSD, and overriding aorta.
- TGA (D-TGA most common) results in a parallel configuration of the ventricular outflow tracts.
- Truncus arteriosus consists of a common trunk giving rise to the aorta, pulmonary arteries, and coronary arteries.

Suggested Readings

Callen PW. Ultrasonography in Obstetrics and Gynecology. 5th ed. Philadelphia: WB Saunders; 2008

Case 213

Bo Yoon Ha

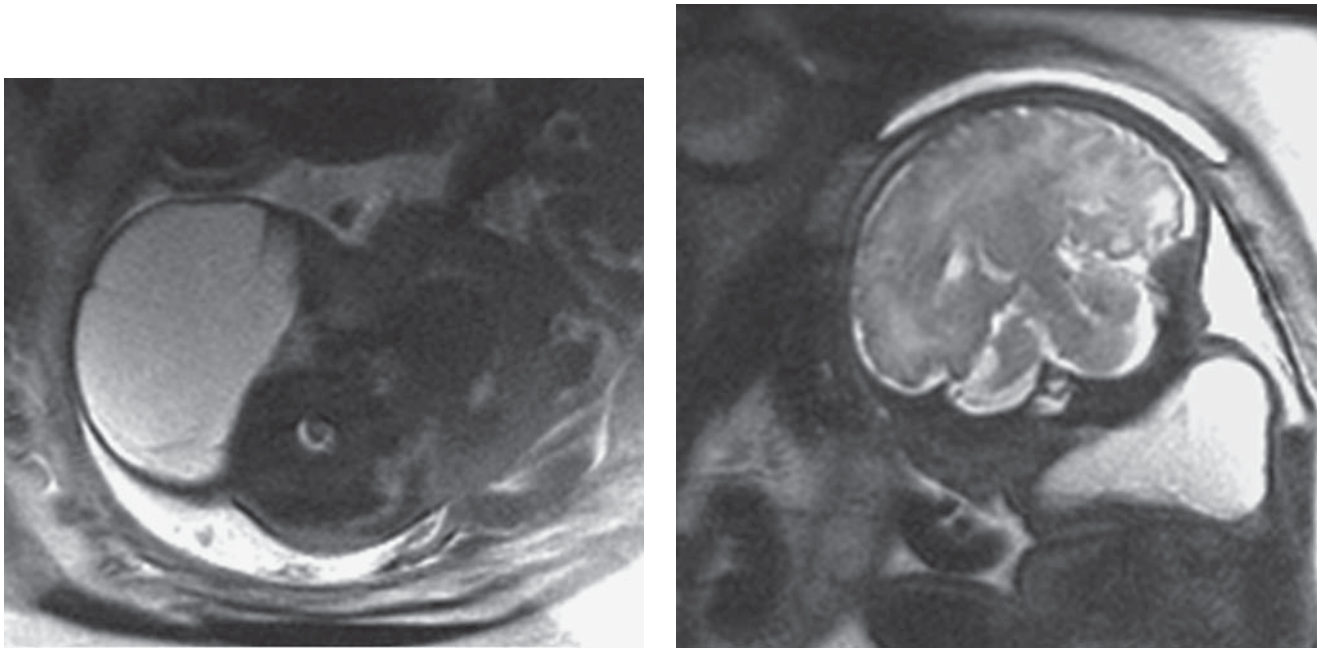


Fig. 213.1 **(A)** Axial and **(B)** sagittal T2-weighted magnetic resonance images of the fetal head demonstrate a large, hyperintense cystic mass with internal septations in the posterolateral neck.

Clinical Presentation

A 21-year-old woman (G2, P1) with an abnormal ultrasound at 19 weeks' gestation (**Fig. 213.1**).

Key Imaging Finding

Cystic posterior neck mass

Top 3 Differential Diagnoses

- **Cystic hygroma.** Cystic hygroma belongs to a group of diseases now recognized as lymphatic malformations. Almost 50% of cases of fetal cystic hygromas have an association with chromosomal disorders, such as Turner syndrome, although sporadic cases can occur. The ultrasound findings in fetal cystic hygroma can vary with gestational age. Increased nuchal translucency may be seen during the first trimester, with progression to a large, thin-walled, multiseptated cystic mass during the second trimester. Occasionally, cystic hygromas can become large and extend into the adjacent mediastinum, axillae, mouth, and chest. Cystic hygroma is most frequently diagnosed by fetal ultrasonography, with magnetic resonance imaging used to further characterize the extent of involvement. Cystic hygromas may be associated with either oligohydramnios or hydrops.
- **Occipital encephalocele and cervical myelomeningocele.** Encephaloceles and myelomeningoceles are the most serious types of neural tube defects. Both conditions involve herniation of central nervous tissue and meninges through an osseous defect. In the case of encephalocele, brain tissue is herniated through a calvarial defect that is usually occipital in location. Myelomeningoceles can occur anywhere along the spinal canal, including the cervical region. Evaluation for an underlying calvarial or spinal defect is helpful in suggesting the diagnosis.
- **Cystic teratoma.** Teratomas are tumors derived from more than one germ cell layer (usually all three layers). The most common site of origin is sacrococcygeal, and tumor location is typically midline or paraxial. These tumors can also originate from sequestered midline embryonic cell rests in the mediastinum, retroperitoneum, and neck. Ultrasound findings are those of a cystic mass that may contain septations, solid components, calcification, or fat.

Diagnosis

Cystic hygroma

✓ Pearls

- Cystic hygromas may be associated with chromosomal abnormalities, especially Turner syndrome.
- Encephaloceles and myelomeningoceles may present as neck masses with underlying osseous defects.
- Cystic teratoma is a cystic mass that may contain septations, solid components, calcification, or fat.

Suggested Readings

Mernagh JR, Mohide PT, Lappalainen RE, Fedoryshin JG. US assessment of the fetal head and neck: a state-of-the-art pictorial review. Radiographics 1999;19(Spec No):S229–S241

Tanriverdi HA, Hendrik HJ, Ertan AK, Axt R, Schmidt W. Hygroma colli cysticum: prenatal diagnosis and prognosis. Am J Perinatol 2001;18(8):415–420

Case 214

Daniel G. Church

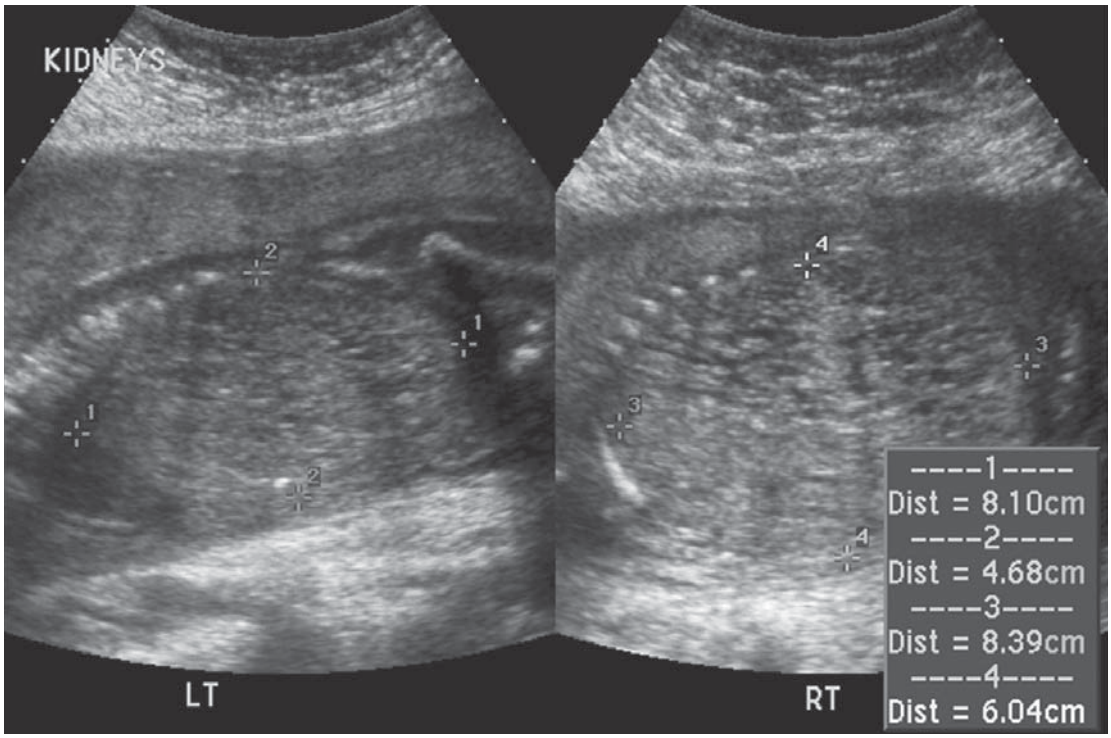


Fig. 214.1 Longitudinal sonographic images through the fetal abdomen demonstrate bilateral enlarged, hyperechoic kidneys with loss of corticomedullary differentiation.

Clinical Presentation

A 24-year-old woman (G1, P0) at 24 weeks' gestation (**Fig. 214.1**).

Key Imaging Finding

Enlarged hyperechoic kidneys

Top 3 Differential Diagnoses

- **Autosomal recessive polycystic kidney disease (ARPKD).** ARPKD is a rare disorder, occurring in ~1 in 40,000 pregnancies. There is association with congenital hepatic fibrosis, and the severity of the renal abnormalities varies inversely with hepatic disease. Prenatal ultrasound demonstrates bilateral, markedly enlarged echogenic kidneys. The medullary portion of the kidneys is affected, and hyperechogenicity is confined to the pyramids with a preserved hypoechoic "halo" of cortical tissue. The majority of renal cysts are below the size resolution for sonography. In severe cases, oligohydramnios will not be apparent until after 16 weeks' gestation, when fetal urination becomes the major source of amniotic fluid. Associated pulmonary hypoplasia is often seen.
- **Trisomy 13.** Thirty percent of trisomy 13 fetuses have enlarged echogenic kidneys, similar to ARPKD. The list of anomalies occurring with this trisomy include cardiac defects, cystic hygroma, echogenic intracardiac focus, facial clefts, holoprosencephaly, intrauterine growth retardation, microcephaly, neural tube defects, ocular anomalies, omphalocele, polydactyly, and ventriculomegaly.
- **Meckel–Gruber syndrome.** Meckel–Gruber is a rare and lethal syndrome consisting of an occipital encephalocele, postaxial polydactyly, and dysplastic cystic kidneys. The kidneys develop microscopic cysts that destroy the renal parenchyma and cause marked nephromegaly. Oligohydramnios is typical, and associated pulmonary hypoplasia is often seen. In the presence of a normal karyotype, two out of three of the classic features are diagnostic of the syndrome.

Additional Differential Diagnoses

- **Autosomal dominant polycystic kidney disease (ADPKD).** Although usually diagnosed in adult life, ADPKD may manifest in childhood or in the fetus. As this condition has an autosomal dominant inheritance pattern, one of the parents is likely to have the disease (although sporadic cases can occur). Therefore, the parental kidneys should be evaluated if the diagnosis is suspected in the fetus. Prenatal ultrasound will demonstrate enlarged echogenic kidneys. Cysts do not appear until late pregnancy and are not a dominant finding.

Diagnosis

Autosomal recessive polycystic kidney disease

✓ Pearls

- ARPKD results in markedly enlarged echogenic kidneys with a thin, hypoechoic "halo" of preserved cortex.
- Trisomy 13 presents with echogenic kidneys similar to ARPKD, as well as other structural defects.
- Meckel–Gruber is characterized by an occipital encephalocele, polydactyly, and dysplastic cystic kidneys.

Suggested Readings

Callen PW. Ultrasonography in Obstetrics and Gynecology. 4th ed. Philadelphia: WB Saunders; 2000

Fong KW, Toi A, Salem S, et al. Detection of fetal structural abnormalities with US during early pregnancy. Radiographics 2004;24(1):157–174

Case 215

Laura J. Varich

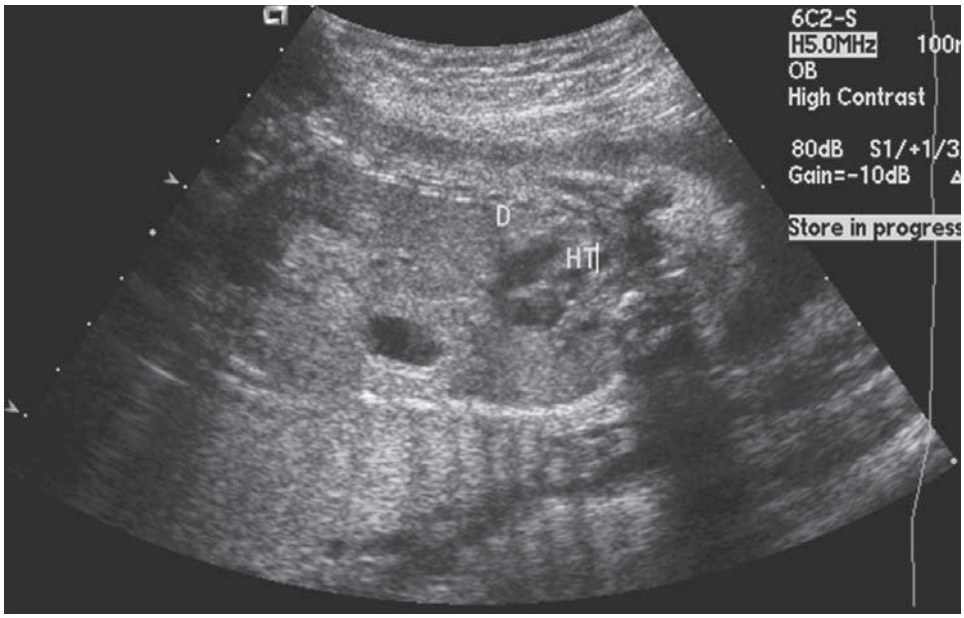


Fig. 215.1 Ultrasound image of the fetus in the coronal plane with absence of amniotic fluid around the fetus.

Clinical Presentation

A 29-year-old woman (G1, P0) at 20 weeks' gestation (**Fig. 215.1**).

Key Imaging Finding

Oligohydramnios. Oligohydramnios is the condition of decreased amniotic fluid volume relative to gestational age. This is defined subjectively by obvious lack of amniotic fluid, crowding of fetal parts, and poor fluid-fetal interface. Objectively, oligohydramnios is defined by an amniotic fluid index of <5 cm and a maximum vertical pocket of <1 to 2 cm. Amniotic fluid is necessary for normal lung development; therefore, fetuses with prolonged oligohydramnios will suffer from pulmonary hypoplasia at birth.

Top 3 Differential Diagnoses

- **Bilateral renal failure or outlet obstruction.** In the second and third trimesters, fetal urination is an important contributor to amniotic fluid volume. Therefore, lack of urine production or inability to excrete urine produces fetal oligohydramnios. Specific causes of oligohydramnios are renal failure involving both kidneys (renal agenesis, renal dysplasia, multicystic dysplastic kidneys, and autosomal recessive polycystic kidney disease) and severe urinary outflow tract obstruction (especially posterior urethral valves). It is important to remember that renal causes of oligohydramnios may not become evident until after 16 weeks' gestation, when fetal urination becomes a significant contributor to amniotic fluid volume.
- **Premature rupture of membranes (PROM).** PROM is defined as rupture of the fetal membranes prior to the onset of labor. In the 10% of pregnancies affected by PROM at term, obstetricians will choose to induce labor. In the 2% of preterm pregnancies affected by PROM, patients will be treated conservatively. In preterm cases, there may be a long latency period during which the fetus has decreased amniotic fluid (increasing the risk of pulmonary hypoplasia), as well as loss of the normal barrier to ascending infection (increasing the risk for chorioamnionitis).
- **Intrauterine growth restriction.** Decreased placental perfusion, which can result from various causes, will produce a hypoxic state within the fetus. When the fetus becomes hypoxic, there is redistribution of cardiac output, preserving blood flow to the brain. The remaining organs are consequently underperfused. The kidneys respond to this decreased vascular flow by decreasing urine output (prior to renal failure), resulting in oligohydramnios.

Additional Differential Diagnoses

- **Fetal demise.** Intrauterine demise of the fetus will result in decreased size of the gestational sac, as amniotic fluid is no longer produced and begins to resorb. Other signs of fetal demise are routinely visible, including absence of fetal cardiac activity, absence of fetal movement, overlapping cranial sutures, and maceration and edema of the fetal soft tissues.

Diagnosis

Premature rupture of membranes

✓ Pearls

- Prolonged oligohydramnios, regardless of the cause, will result in pulmonary hypoplasia.
- Renal causes of oligohydramnios may not be evident until the second trimester (typically after 16 weeks).
- Prolonged PROM (preterm) may result in pulmonary hypoplasia and increased risk of chorioamnionitis.
- Intrauterine growth restriction secondary to hypoxia results in redistribution of cardiac output and decreased urine output.

Suggested Readings

Callen P. Ultrasound in Obstetrics and Gynecology. 5th ed. Philadelphia: WB Saunders; 2008

Ott WJ. Reevaluation of the relationship between amniotic fluid volume and perinatal outcome. Am J Obstet Gynecol 2005;192(6):1803–1809, discussion 1809

Case 216

Hedieh K. Eslamy

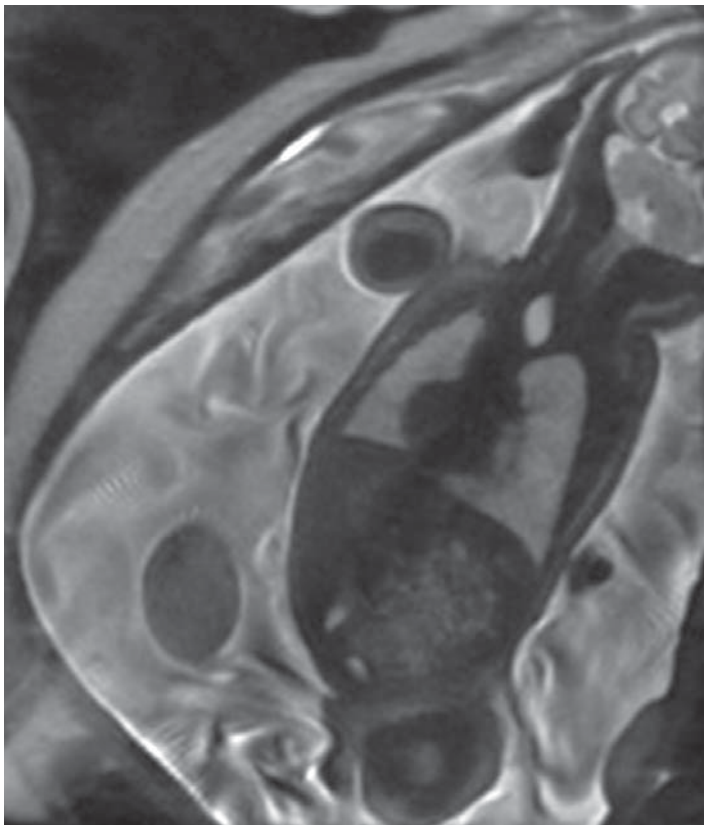


Fig. 216.1 Coronal T2-weighted magnetic resonance image of the fetus demonstrates increased amniotic fluid and a high signal intensity pouch within the fetal neck.

Clinical Presentation

A 33-year-old woman (G2, P1) with increased uterine height for the 33 weeks' gestational age (**Fig. 216.1**).

Key Imaging Finding

Polyhydramnios. Polyhydramnios is an excessive accumulation of amniotic fluid (>1500 cc). The balance of fluid flow into the amniotic sac (fetal urination and lung fluid production) and out of the amniotic sac (swallowing and intramembranous absorption) determines the volume of amniotic fluid. Polyhydramnios typically results from decreased fetal swallowing or increased fetal urination. On ultrasound, polyhydramnios can be diagnosed subjectively (the fetus in mid to late second or third trimester appears to float in the amniotic fluid, displaced away from the anterior uterine wall or placenta) or objectively (the deepest amniotic fluid volume pocket >8 cm or an amniotic fluid index >25 cm).

Top 3 Differential Diagnoses

- **Fetal gastrointestinal (GI) anomalies.** Fetal GI obstruction is the most common congenital anomaly that causes polyhydramnios. The abnormality is usually located proximal to the colon, where water absorption occurs. Primary considerations are esophageal atresia, duodenal atresia, and small bowel atresia
- **Fetal central nervous system (CNS) anomalies.** Fetal CNS and associated chromosomal abnormalities were once a large cause of third trimester polyhydramnios; however, with the advent of second trimester anatomical screening and the wide use of ultrasound, this is no longer the case. Major CNS structural defects associated with polyhydramnios are anencephaly, hydranencephaly, and encephalocele; however, any CNS anomaly that causes a lack of normal swallowing function can lead to polyhydramnios.
- **Maternal diabetes mellitus.** Fetal polyhydramnios is often seen in diabetic mothers with poorly controlled blood sugars. Polyhydramnios is likely related to fetal hyperglycemia, causing osmotic diuresis and polyuria. There is typically associated fetal macrosomia; therefore, accurate assessments of fetal weight should be performed.

Additional Differential Diagnoses

- **Idiopathic polyhydramnios.** Idiopathic polyhydramnios refers to the presence of ultrasound findings of polyhydramnios in a nondiabetic mother and the lack of a discernible fetal cause of excess amniotic fluid. The condition is most often considered benign in the absence of other abnormalities, but the pregnancy should be closely monitored, with follow-up imaging as necessary.
- **Fetal hydrops.** Fetal hydrops is characterized by abnormal fluid accumulation in at least two fetal cavities, including placental enlargement, body wall edema, ascites, pericardial effusions, and pleural effusions. Polyhydramnios is often present. Hydrops is most often due to nonimmune causes (e.g., cardiovascular anomalies, intrauterine infection, or chromosomal abnormality) and less commonly to circulating maternal antibodies against fetal red blood cells due to Rh incompatibility (immune hydrops).

Diagnosis

Fetal GI anomaly (esophageal atresia)

✓ Pearls

- Common fetal causes of polyhydramnios are GI and CNS anomalies, as well as fetal hydrops.
- Poorly controlled maternal diabetes results in polyhydramnios and fetal macrosomia.
- Idiopathic polyhydramnios is typically considered a benign condition once other causes are excluded.

Suggested Readings

Alexander ES, Spitz HB, Clark RA. Sonography of polyhydramnios. AJR Am J Roentgenol 1982;138(2):343–346

Callen PW. Ultrasonography in Obstetrics and Gynecology. 5th ed. Philadelphia: WB Saunders; 2008

Hill LM, Breckle R, Thomas ML, Fries JK. Polyhydramnios: ultrasonically detected prevalence and neonatal outcome. Obstet Gynecol 1987;69(1):21–25

Case 217

Joyce F. Sung

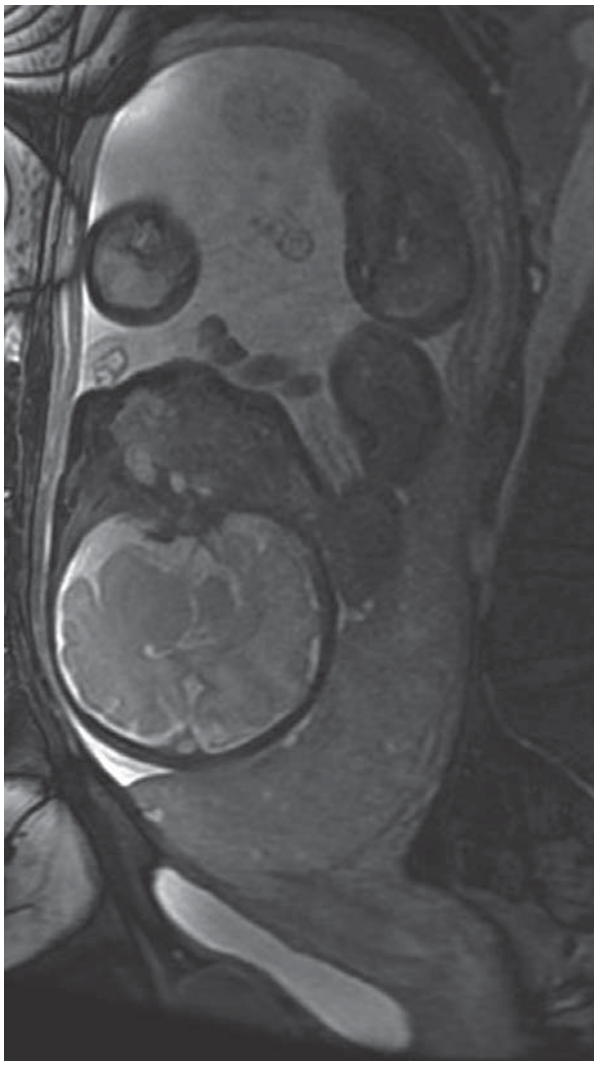


Fig. 217.1 Sagittal T2-weighted magnetic resonance image of the maternal uterus demonstrates complete coverage of the cervix by the placenta.

Clinical Presentation

A 38-year-old woman (G3, P2) with vaginal bleeding at 34 weeks' gestation (**Fig. 217.1**).

Key Imaging Finding

Placental location abnormality

Top 3 Differential Diagnoses

- **Placenta previa.** Placenta previa occurs when the placenta lies near or over the cervical internal os. There are four types of placenta previa: complete (the placenta completely covers the internal os), partial (the placenta partially covers the internal os), marginal (the placenta reaches the edge of but does not cover the internal os), and low-lying (the placenta lies close to but does not reach the edge of the internal os—usually defined as within 2 cm of the internal os on ultrasound). Risk factors include prior cesarean section, pregnancy termination, and uterine surgery, as well as multiparity, smoking, increased age, cocaine use, and multiple pregnancies. Pregnancy complications associated with placenta previa are painless antepartum bleeding, intrapartum and postpartum hemorrhage, placental implantation abnormalities, and increased preterm delivery. Transvaginal ultrasound is more accurate in cases where the diagnosis is in question.
- **Placenta accreta/increta/percreta.** In placenta accreta, the placenta is abnormally adherent to the uterine myometrium. The depth of invasion into the uterine wall defines the two variants: placenta increta describes invasion into the myometrium, and placenta percreta describes invasion through the entire thickness of the myometrium and uterine serosa (invasion can even involve adjacent organs such as the bladder and rectum). Risk factors for placenta accreta include prior cesarean delivery and other uterine surgery. When placenta previa is present and is associated with a history of prior cesarean delivery or uterine surgery, ultrasound and magnetic resonance imaging should be used to evaluate for placenta accreta. Suspicious ultrasonographic findings are irregularly shaped vascular spaces (lacunae) within the placenta, turbulent blood flow in the lacunae on Doppler imaging, thinning of the myometrium at the placental site, loss of retroplacental echolucency, protrusion of the placenta into the bladder, and increased vascularity between the uterine serosa and bladder. Clinically, it is important to make the diagnosis of accreta prior to delivery to plan for possible perinatal complications, including massive hemorrhage and disseminated intravascular coagulation.
- **Marginal insertion of the cord.** A marginal insertion is defined as insertion of the umbilical cord within 1 to 2 cm of the placental edge. Although some pathologic studies have suggested an association with growth restriction, a recent study of sonographically identified marginal placental cord insertions in singleton pregnancies failed to demonstrate any association with fetal growth restriction.

Additional Differential Diagnoses

- **Velamentous insertion of the cord.** A cord insertion is considered velamentous when the cord inserts into the fetal membranes rather than into the placenta (1% of pregnancies). In this condition, the fetal vessels run through a portion of the membranes before reaching the placenta. If the fetal vessels cross the cervix, the condition is known as vasa previa. In vasa previa, rupture of the fetal membranes may cause vessel rupture and catastrophic fetal hemorrhage; therefore, cesarean section should be anticipated.

Diagnosis

Placenta previa

✓ Pearls

- Placenta previa refers to the placenta lying near or over the cervical os and is associated with hemorrhage.
- Placenta accreta refers to placental invasion into the uterine myometrium; it is associated with hemorrhage.
- Marginal insertion of the cord is described as cord insertion within 2 cm of the placental edge.
- Velamentous cord insertion occurs when the placenta inserts into the fetal membranes rather than the placenta.

Suggested Readings

Callen PW. Ultrasonography in Obstetrics and Gynecology. 5th ed. Philadelphia: Saunders Elsevier; 2008

Wu S, Kocherginsky M, Hibbard JU. Abnormal placentation: twenty-year analysis. Am J Obstet Gynecol 2005;192(5):1458–1461

Case 218

Daniel G. Church



Fig. 218.1 Sagittal ultrasound image demonstrates a fetus with an anterior abdominal wall defect. The umbilical cord inserts at the inferior aspect of the defect. An anechoic fetal bladder is seen.

Clinical Presentation

A 28-year-old woman (G1, P0) at 34 weeks' gestation (**Fig. 218.1**).

Key Imaging Finding

Abdominal wall defect

Top 3 Differential Diagnoses

- **Omphalocele.** An omphalocele is an abdominal wall defect that results in herniation of the abdominal contents into the base of the umbilical cord. Two layers of intact membranes (the peritoneum and the amnion) form a sac that separates the eviscerated organs from the amniotic fluid. Prenatal ultrasound demonstrates a midline defect with the umbilical cord at its apex. The liver more commonly herniates than the small bowel. Associated anomalies are present in 67 to 88% of cases and include intestinal atresias, malrotation, cardiac anomalies, and chromosomal anomalies. The mortality rate of an isolated omphalocele is 10%; it is much higher with associated anomalies.
- **Gastroschisis.** In gastroschisis, bowel loops herniate through a paraumbilical full-thickness abdominal wall defect into the amniotic cavity. Unlike omphaloceles, there is no surrounding membrane with gastroschisis. The defect is usually right-sided, and the umbilical cord insertion is normal and separate from the defect. There is no association with chromosomal or other congenital anomalies. Gastroschisis mortality rates are lower than with omphaloceles (<10%).
- **Limb–body wall complex.** Limb–body wall complex is a universally fatal condition that has as one component a ventral wall anomaly (omphalocele) but can be differentiated from an isolated omphalocele and gastroschisis by its other features. Associated findings are craniofacial defects, limb reductions, and spinal defects.

Additional Differential Diagnoses

- **Pentalogy of Cantrell.** The pentalogy of Cantrell is a rare condition of unknown etiology. It consists of an omphalocele, ectopia cordis, diaphragmatic defect, pericardial defect, and cardiovascular malformation. It can be associated with other anomalies and chromosomal abnormalities. Prognosis depends on the severity of the multiple defects, especially cardiac.
- **Bladder and cloacal exstrophy.** Bladder exstrophy is a congenital malformation of unknown etiology that refers to exstrophy of the bladder through an abdominal wall (anteroinferior) defect, as well as musculoskeletal abnormalities. Findings include absence of a normal bladder, a protruding soft tissue mass, and pubic diastasis. Cloacal exstrophy is more severe and refers to defects involving the bladder and bowel.

Diagnosis

Omphalocele

✓ Pearls

- Omphalocele has a membrane covering the herniated bowel; the cord inserts at the apex of the defect.
- Gastroschisis occurs to the right of the midline and contains bowel loops without a membrane covering.
- Omphalocele has a high incidence of associated anomalies and a worse prognosis than gastroschisis.

Suggested Readings

Emanuel PG, Garcia GI, Angtuaco TL. Prenatal detection of anterior abdominal wall defects with US. Radiographics 1995;15(3):517–530

Case 219

Bo Yoon Ha

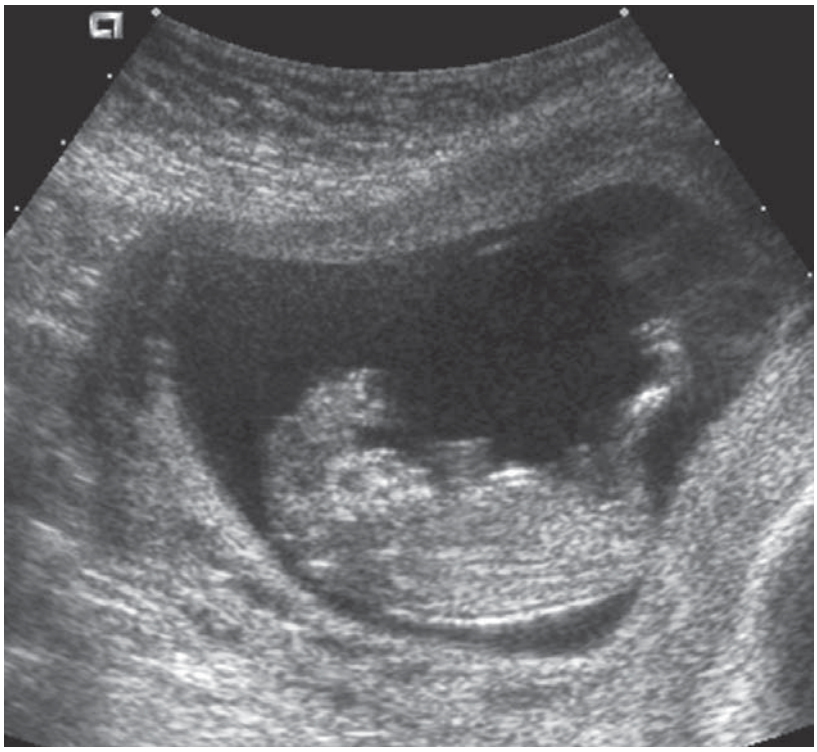


Fig. 219.1 Longitudinal ultrasound image of the fetus demonstrates absence of the fetal cranium and brain.

Clinical Presentation

A 38-year-old woman (G1, P0) at 12 weeks' gestation (**Fig. 219.1**).

Key Imaging Finding

Cranial/calvarial defect

Top 3 Differential Diagnoses

- **Anencephaly.** Anencephaly is a serious, lethal developmental anomaly of the central nervous system resulting from failure of closure of the rostral portion of the neural tube (neural tube defect). It may first be suspected due to elevated maternal serum alpha fetoprotein. Ultrasound findings include reduction or absence of the cerebrum and cerebellum with preservation of a portion of the hindbrain. Tissue located above the orbits on ultrasound is referred to as angiomatous stroma. The diagnostic feature is the absence of the cranial bones (skull base is present) after 11 weeks' gestation when normal cranial ossification should be visible. Anencephaly, like other forms of neural tube defects, is associated with chromosomal abnormalities, and the risk of recurrence is increased in fetuses with a previously affected sibling.
- **Acrania.** Acrania (also referred to as exencephaly) is characterized by the partial or complete absence of the cranium. It results from failure of membranous bone formation (as seen with ectodermal migrational abnormalities) and is universally fatal. Although the underlying brain typically forms to some degree, it is abnormal. The condition can be associated with anencephaly. Ultrasonography will demonstrate variable degrees of cranial absence, beginning in the first trimester.
- **Amniotic band syndrome.** Amniotic bands are thin, fibrous bands that may be found within the amniotic sac, which may be difficult to visualize on ultrasound. Amniotic band syndrome is a rare condition in which the bands cause associated anomalies, including regions of constriction and amputation. The cranium may be involved with asymmetric amputation or disruption of normal bone formation. Amniotic band syndrome may be distinguished from other calvarial defects by noting asymmetric calvarial defects, the presence of underlying brain parenchyma, and evaluation for other sequelae of amniotic band syndrome.

Additional Differential Diagnoses

- **Encephalocele or myelomeningocele.** Encephaloceles and myelomeningoceles are characterized by herniation of portions of the brain (encephalocele), spinal cord, nerves, cerebrospinal fluid, and meninges through a bony defect of the calvarium or spine, respectively. Encephaloceles are most common in the occipital region. They can be differentiated from anencephaly or acrania by the presence of a bony calvarium. Myelomeningoceles are the most serious form of spina bifida and can occur anywhere along the spinal cord. They most commonly occur within the lumbosacral spine, followed by the cervical spine. Associated findings may be identified within the fetal head, including ventriculomegaly, Chiari II malformation, and concavity of the frontal bones. Magnetic resonance imaging is useful in evaluating the level and extent of the myelomeningocele.

Diagnosis

Anencephaly

✓ Pearls

- Anencephaly is a defect with the absence of normal brain and calvarial development above the orbits.
- Acrania is characterized by partial or complete absence of the calvarium due to failed bone formation.
- Amniotic band syndrome may result in constriction and amputations with asymmetric calvarial defects.
- Encephaloceles consist of herniated brain parenchyma through a calvarial defect; most are occipital.

Suggested Readings

Mangels KJ, Tulipan N, Tsao LY, Alarcon J, Bruner JP. Fetal MRI in the evaluation of intrauterine myelomeningocele. Pediatr Neurosurg 2000;32(3):124–131

McComb JG. Spinal and cranial neural tube defects. Semin Pediatr Neurol 1997;4(3):156–166

Case 220

Daniel G. Church

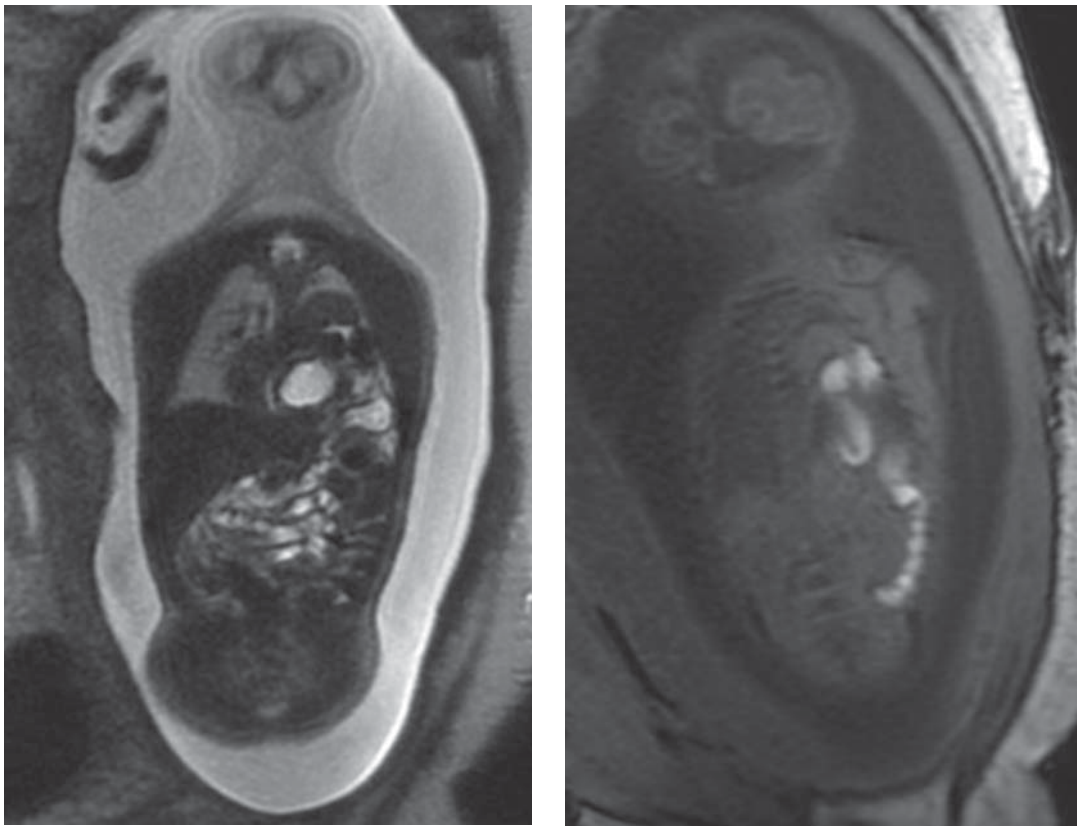


Fig. 220.1 **(A)** Coronal T2 and **(B)** T1 fetal magnetic resonance images demonstrate herniation of the abdominal contents (stomach and bowel) into the left chest with mass effect on the mediastinum. The T1-weighted image shows the presence of meconium (bright on T1) within the herniated bowel.

Clinical Presentation

A 31-year-old woman (G2, P1) at 24 weeks' gestation (**Fig. 220.1**).

Key Imaging Finding

Diaphragm abnormality

Top 3 Differential Diagnoses

- **Congenital diaphragmatic hernia (CDH).** CDH is the most common developmental abnormality of the diaphragm. Up to 90% occur on the left; Bochdalek (posterior) hernias far outnumber Morgagni (anterior) hernias. The stomach, intestines, liver, and spleen can all herniate into the chest. Prenatal ultrasound is highly accurate (>90% sensitivity) for the prenatal diagnosis of CDH, demonstrating herniation of abdominal contents into the chest with contralateral mediastinal shift. CDH is associated with other congenital malformations in up to half of all cases, with congenital heart disease being the most common. Prognosis depends on hernia volume and the degree of mediastinal shift, which causes compression and pulmonary hypoplasia, as well as pulmonary hypertension. Intrathoracic liver in a left-sided CDH carries a worse prognosis. Sonography can quantify the contralateral lung area on a four-chamber view of the heart. Fetal magnetic resonance imaging is a complementary method to ultrasound for evaluating CDH and fetal lung volume.
- **Congenital pulmonary airway malformation (CPAM).** CPAM (also known as cystic adenomatoid malformation) constitutes > 80% of lung masses detected by prenatal imaging. It is characterized by excessive growth of the terminal respiratory bronchioles. Prenatal ultrasonography demonstrates a hyperechoic pulmonary mass with or without cystic elements of varying sizes. Occasionally, CPAMs may approximate the diaphragm, simulating a mass associated with a diaphragmatic hernia.
- **Pulmonary sequestration.** Pulmonary sequestration represents aberrantly developed lung tissue that is perfused (receiving its blood supply primarily from the systemic circulation) but not ventilated (typically, there is no communication with the tracheobronchial tree). Prenatal ultrasonography demonstrates a relatively homogeneous hyperechoic pulmonary mass, and Doppler studies may demonstrate a systemic feeding vessel. Pulmonary sequestrations are most commonly located in the medial lung base and are classified as intra- or extralobar. Given their common location within the medial lung bases, they may simulate a mass associated with a diaphragmatic hernia.

Additional Differential Diagnoses

- **Diaphragmatic eventration.** Congenital eventration of the diaphragm is caused by hypoplasia of the diaphragmatic muscle and is usually right sided. With an eventrated diaphragm, the inferior abdominal components also shift superiorly. On axial imaging, the liver may be mistaken for a chest mass with an associated diaphragmatic defect. Sagittal imaging may help verify an intact but elevated diaphragm.

Diagnosis

Congenital diaphragmatic hernia

✓ Pearls

- CDH is the most common congenital diaphragmatic abnormality and is more common on the left.
- Prognosis of CDH depends on the severity of pulmonary compression and the presence of intrathoracic liver.
- CPAMs and sequestrations can simulate a mass associated with a diaphragmatic hernia.
- Diaphragmatic eventration is more common on the right; the liver may be mistaken for a thoracic mass.

Suggested Readings

Goldstein RB. Ultrasound evaluation of the fetal thorax. In: Callen PW, ed. Ultrasonography in Obstetrics and Gynecology. 4th ed. Philadelphia: WB Saunders; 2000

Guibaud L, Filiatrault D, Garel L, et al. Fetal congenital diaphragmatic hernia: accuracy of sonography in the diagnosis and prediction of the outcome after birth. AJR Am J Roentgenol 1996;166(5):1195–1202

Hedlund GL, Griscum NT, Cleveland RH, Kirks DR. Respiratory system. In Kirks DR, ed. Practical Pediatric Imaging. 3rd ed. Philadelphia: Lippincott-Raven; 1998

Case 221

William T. O'Brien Sr.

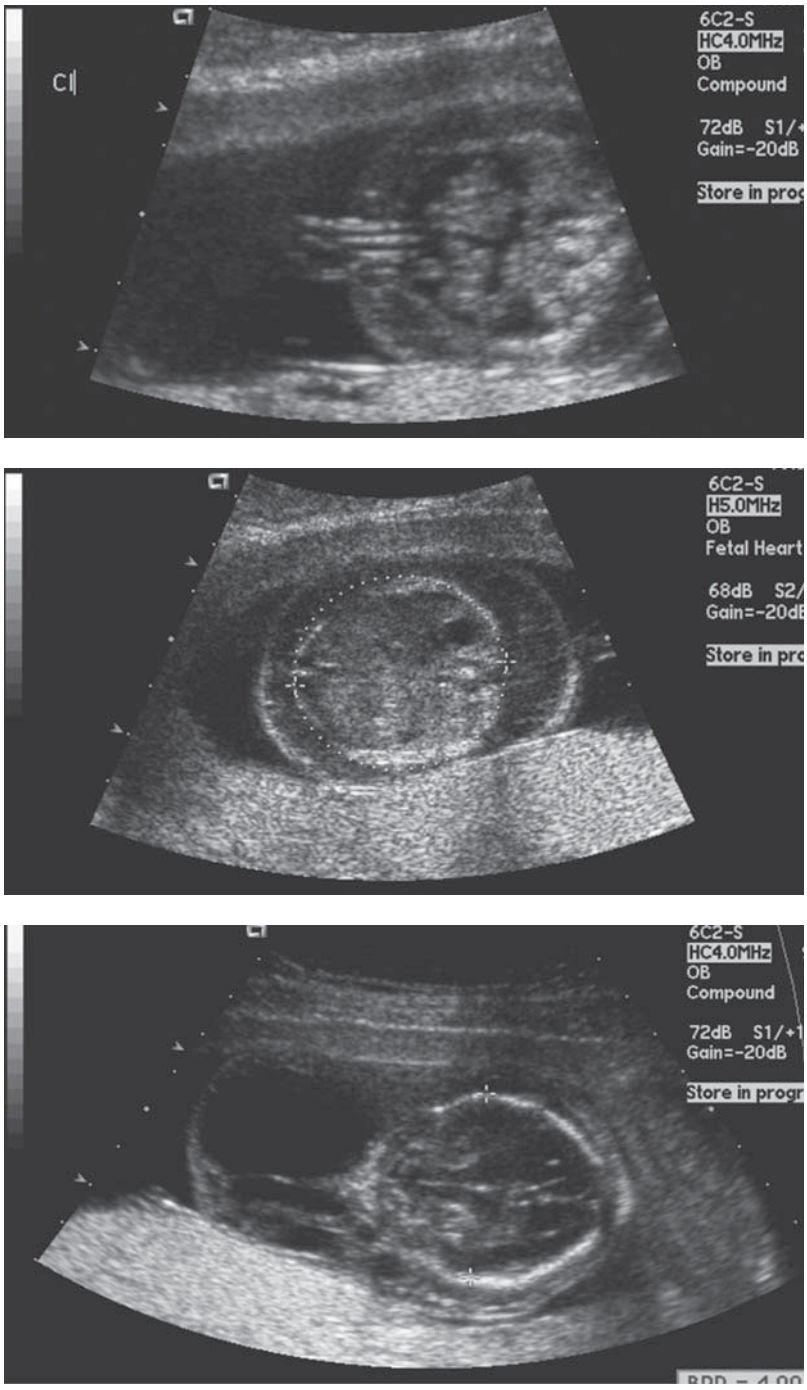


Fig. 221.1 **(A,B)** Transverse sonographic images through the fetal abdomen during a second-trimester anatomy scan demonstrate diffuse body wall edema, as well as ascites. **(C)** Transverse sonographic image through the fetal head reveals diffuse scalp edema with a complex cystic hygroma along the posterior aspect of the neck and base of the skull.

Clinical Presentation

A 34-year-old woman (G1, P0) with an abnormal triple screen (**Fig. 221.1**).

Key Imaging Finding

Fetal hydrops

Top 3 Differential Diagnoses

- **Cardiac anomalies.** Cardiovascular disease (including structural anomalies, cardiac arrhythmias, and high output failure) is the most common cause of fetal hydrops, accounting for ~25% of cases. Diagnostic findings on ultrasound include abnormal fluid accumulation in at least two fetal cavities, such as placental enlargement, body wall edema (anasarca), ascites, pericardial effusions, and pleural effusions. Abnormal fluid accumulation in a single cavity should not result in the diagnosis of fetal hydrops. Once hydrops is found, a thorough anatomy scan should be performed to identify potentially treatable causes.
- **Chromosomal abnormalities.** Chromosomal abnormalities, including Down syndrome, trisomy 18, trisomy 13, and Turner syndrome (XO), represent the most common genetic disorders that result in fetal hydrops. Often, secondary signs can be identified to suggest a genetic cause. In Down syndrome, secondary findings include a short or absent nasal bone, increased nuchal thickness, endocardial cushion defects, echogenic intracardiac focus, hyperechoic bowel, pyelectasis, and short limbs. The hallmark sonographic finding in trisomy 18 (Edward syndrome) is choroid plexus cysts. Other abnormalities are clenched fists with or without overlapping digits, club feet, rocker-bottom feet, nuchal translucency, two-vessel cord, and cardiac anomalies. Ultrasound findings in trisomy 13 (Patau syndrome) are holoprosencephaly, neural tube defects, cardiac anomalies, polydactyly, and enlarged hyperechoic kidneys. Turner syndrome is characterized by lymphatic malformations, including a cervical cystic hygroma, aortic coarctation, cardiac defects, and renal abnormalities.
- **Infection.** Infections represent a relatively rare cause of fetal hydrops. Numerous viral, bacterial, and parasitic infections may result in fetal hydrops, with the vast majority resulting from parvovirus B19, cytomegalovirus, toxoplasmosis, and syphilis.

Additional Differential Diagnoses

- **Immune hydrops.** Immune hydrops is the result of circulating maternal antibodies that destroy fetal red blood cells due to Rh incompatibility. Increased prenatal surveillance and application of the Rh immunoglobulin prophylaxis have drastically decreased the incidence of immune fetal hydrops. Today, immune hydrops is uncommon.

Diagnosis

Chromosomal abnormality (Turner syndrome)

✓ Pearls

- Fetal hydrops is characterized by abnormal fluid accumulation in at least two fetal cavities.
- Nonimmune causes of hydrops are more common than immune hydrops due to Rh prophylaxis.
- Cardiac anomalies most commonly cause hydrops, followed by infection and chromosomal abnormalities.

Suggested Readings

Tercanli S, Gembruch U, Holzgreve W. Nonimmune hydrops fetalis: diagnosis and management. In: Callen PW, ed. Ultrasonography in Obstetrics and Gynecology. 5th ed. Philadelphia: WB Saunders; 2008

Case 222

Erika Rubesova

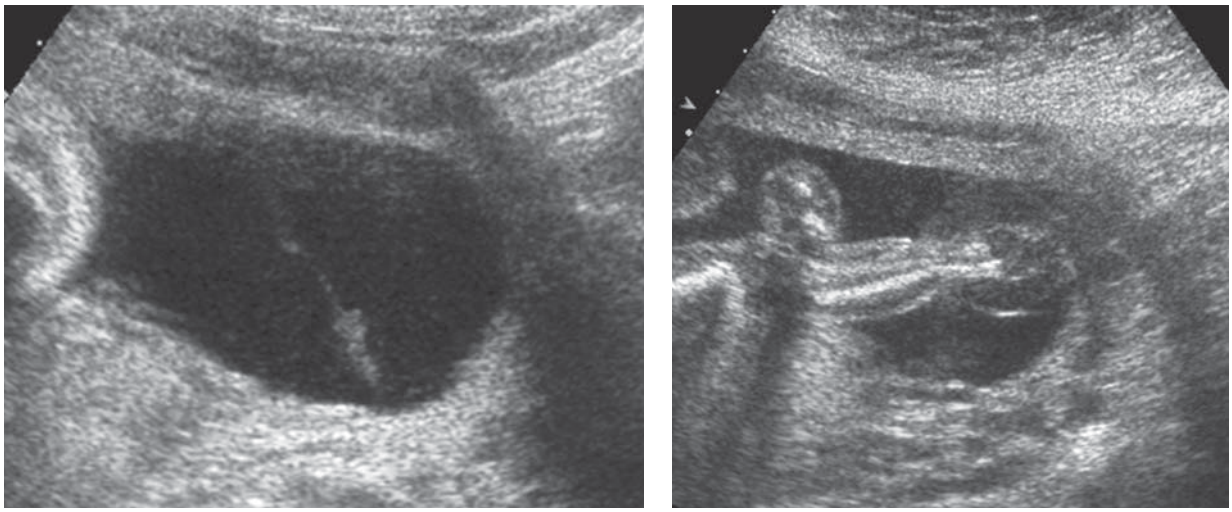


Fig. 222.1 **(A)** Fetal ultrasound image through the amniotic sac demonstrates an echogenic linear band within the amniotic fluid. **(B)** Ultrasound image of the fetal lower extremity reveals soft tissue constriction and distal soft tissue edema.

Clinical Presentation

Abnormal findings on fetal ultrasound at 20 weeks' gestation (**Fig. 222.1**).

Key Imaging Finding

Linear echoes within the amniotic fluid

Top 3 Differential Diagnoses

- **Amniotic band syndrome.** Amniotic bands typically crisscross the uterus, may be attached to the fetus, and entangle and disrupt fetal parts. Bands may be difficult to visualize by ultrasound. The term *amniotic band syndrome* should be used only if there is an association with congenital anomalies such as limb constriction, amputation, lymphedema, and other multiple, bizarre congenital anomalies. This syndrome is relatively rare, and the etiology is not clear. The prognosis for fetuses with amniotic band syndrome is poor; however, in some circumstances fetal surgery may be performed to free the fetus from some constrictive bands.
- **Synechiae (or amniotic shelves).** Synechiae are thick bands that do not attach to the fetus and have no impact on the development. Most women with synechiae have a history of uterine instrumentation or uterine infection, resulting in intrauterine scars and adhesions. However, synechiae have also been reported in women with no prior history of uterine surgery or infection.
- **Chorioamniotic separation.** Chorioamniotic separation is considered normal before 16 weeks' gestation. Abnormal chorioamniotic separation may occur during the second and third trimesters. Small separations are usually clinically insignificant, having no effect on the pregnancy.

Additional Differential Diagnoses

- **Hemorrhage.** Bands of fibrin may be present following any bleeding within the amniotic cavity (e.g., following traumatic amniocentesis). Fibrin strands appear irregular, allowing for differentiation from chorioamniotic separation. They resolve with time and usually do not interfere with fetal development.

Diagnosis

Amniotic band syndrome

✓ Pearls

- Amniotic bands attach to the fetus and may be associated with fetal anomalies.
- Uterine synechiae appear thick and are attributed to adhesions; they have no effect on fetal development.
- Chorioamniotic separation is abnormal after 16 weeks; prognosis depends on the degree of separation.
- Fibrin strands from hemorrhage are irregular and resolve with time; they have no effect on development.

Suggested Readings

Callen P. Ultrasound in Obstetrics and Gynecology. 5th ed. Philadelphia: WB Saunders; 2008

Middleton K, Hertzberg BS. Ultrasound: The Requisites. 2nd ed. St. Louis, MO: Mosby; 2004

Case 223

Erika Rubesova

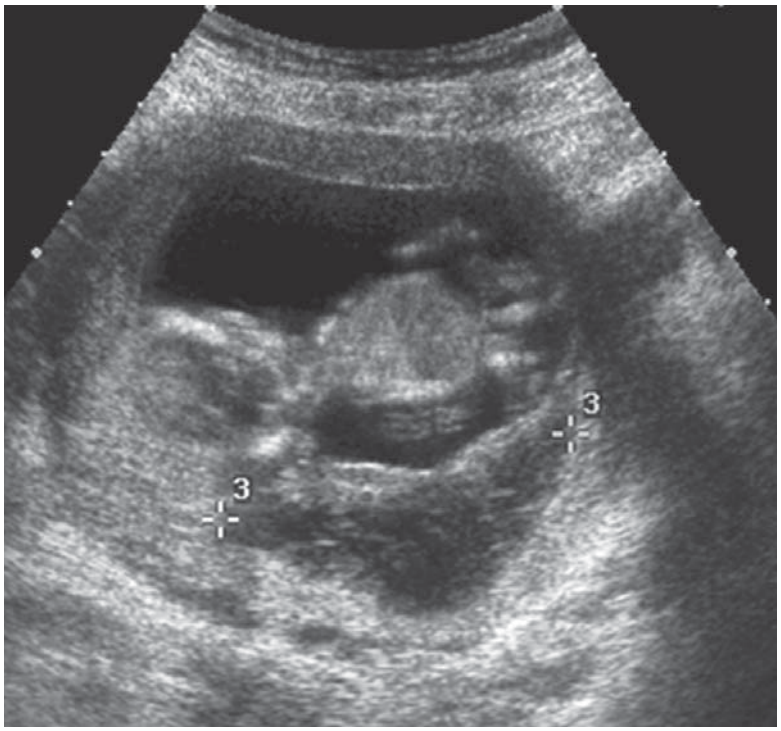


Fig. 223.1 Ultrasound image of the pelvis demonstrates a hypoechoic heterogeneous area between the maternal uterus and the chorion.

Clinical Presentation

A 30-year-old woman (G3, P2) at 13 weeks' gestation (**Fig. 223.1**).

Key Imaging Finding

Placental abnormality/mass

Top 3 Differential Diagnoses

- **Subchorionic/retroplacental hematoma.** The ultrasonographic features of retroplacental hematomas differ based on the age of the bleed. They appear hyperechoic in the acute phase and hypoechoic with no internal vascular flow at 1 to 2 weeks of age. The reported incidence is 5%, but many cases are not visualized on ultrasound. Retroplacental hematomas may cause placental abruption, a major cause of perinatal death. They are associated with maternal hypertension, preeclampsia, tobacco and cocaine use, blunt trauma, chorioamnionitis, obstruction of venous drainage, and cardiolipin antibodies.
- **Placental venous lakes.** Venous lakes result from perivillous fibrin deposition and appear as hypoechoic intraplacental lesions. They are usually visualized under the fetal surface of the placenta. Venous lakes occur in ~20% of pregnancies and are not associated with increased fetal morbidity or mortality.
- **Circumvallate placenta.** Circumvallate placenta is characterized by thickened chorioamniotic membranes at the periphery of the placenta. The placental edge has a rolled-up appearance on ultrasound. Complete circumvallation of the placenta is associated with increased risk for bleeding, intrauterine growth restriction, perinatal mortality, placental abruption, and preterm labor.

Additional Differential Diagnoses

- **Succenturiate lobe.** A succenturiate lobe appears as a mass of placental tissue separate from the main placental mass. It occurs in 5% of pregnancies and is associated with placental infarction and vellamentous insertion of the umbilical cord.

Diagnosis

Subchorionic hematoma

✓ Pearls

- The appearance of retroplacental hematomas varies based on age; hematomas may not always be visualized on ultrasound.
- Large retroplacental hematomas may result in placental abruption, the leading cause of perinatal mortality.
- Venous lakes occur along the fetal surface of the placenta and do not increase morbidity or mortality.
- Circumvallate placenta and succenturiate lobes are placental variants with potentially increased morbidity.

Suggested Readings

Callen P. Ultrasound in Obstetrics and Gynecology. 5th ed. Philadelphia: WB Saunders; 2008

Middleton K, Hertzberg BS. Ultrasound: The Requisites. 2nd ed. St. Louis, MO: Mosby; 2004

Case 224

Jeffrey P. Tan

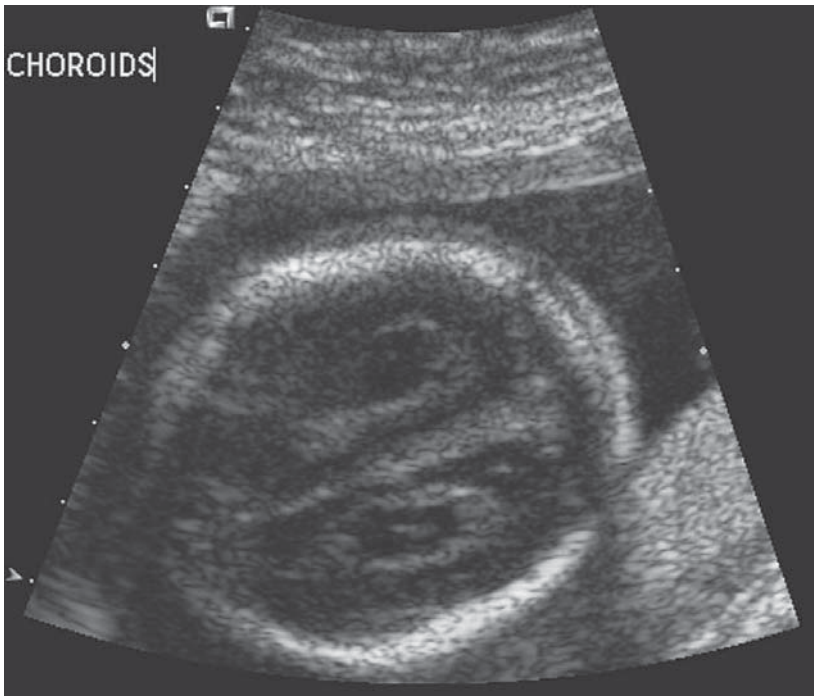


Fig. 224.1 Transverse sonographic image of the fetal head demonstrates bilateral choroid plexus cysts.

Clinical Presentation

A 37-year-old woman (G1, P0) with an abnormal triple screen (**Fig. 224.1**).

Key Imaging Finding

Choroid plexus cyst

Top 3 Differential Diagnoses

- **Incidental finding.** Choroid plexus cysts are found incidentally in ~1 to 2% of the population. The sonographic appearance of choroid plexus cysts should be made on axial images of the lateral ventricles. Oblique coronal images may falsely interpose hypoechoic structures into the choroid, simulating a cyst. Once identified, a detailed anatomy scan should be performed to evaluate for additional fetal abnormalities. An isolated choroid plexus cyst with otherwise normal fetal anatomy and a normal triple/quadruple screen is likely an incidental finding; the risk of amniocentesis in these cases may outweigh the potential benefit.
- **Trisomy 18 (Edward syndrome).** Trisomy 18, or Edward syndrome, is a relatively rare chromosomal abnormality, with an incidence of 3 in 10,000 live births. The mortality rate is ~90% within the first year of life. Choroid plexus cysts can be found in approximately one third of fetuses with trisomy 18. These fetuses usually present with intrauterine growth restriction. Other abnormalities associated with trisomy 18 are cardiac defects, club feet, clenched fists with overlapping digits, facial defects, neural tube defects, radial ray abnormalities, and a two-vessel cord. As with other chromosomal abnormalities, a thickened nuchal translucency can be seen during first-trimester imaging.
- **Trisomy 21 (Down syndrome).** Trisomy 21 is the most common chromosomal anomaly and occurs more frequently with advanced maternal age. Although once thought to be associated with choroid plexus cysts, recent studies show that the incidence of choroid plexus cysts in Down syndrome is similar to that of the general population. Other sonographic abnormalities associated with trisomy 21 are an increased first-trimester nuchal translucency (>3 mm) or second-trimester nuchal fold (>6 mm), ventriculomegaly, brachycephaly, flat facies, endocardial cushion defects, echogenic cardiac focus, hyperechoic bowel, duodenal atresia, pyelectasis, clinodactyly, hypoplasia of the fifth digit, short femur, and short humerus.

Diagnosis

Trisomy 18 (Edward syndrome)

✓ Pearls

- Choroid plexus cysts are typically incidental findings in the setting of otherwise normal fetal anatomy.
- Choroid plexus cysts do have an association with trisomy 18; associated anomalies are commonly seen.
- There is some debate as to whether choroid plexus cysts are associated with trisomy 21.

Suggested Readings

Benacerraf B. Ultrasound evaluation of chromosomal abnormalities. In: Callen PW, ed. Ultrasonography in Obstetrics and Gynecology. 5th ed. Philadelphia: WB Saunders; 2008

Dagklis T, Plasencia W, Maiz N, Duarte L, Nicolaides KH. Choroid plexus cyst, intracardiac echogenic focus, hyperechogenic bowel and hydronephrosis in screening for trisomy 21 at 11 + 0 to 13 + 6 weeks. Ultrasound Obstet Gynecol 2008;31(2):132–135

Middleton W, Kurtz A, Hertzberg B. Ultrasound: The Requisites. St. Louis, MO: Mosby; 2004

Pilu G, Falco P, Perolo A. Ultrasound evaluation of the fetal neural axis. In: Callen PW, ed. Ultrasonography in Obstetrics and Gynecology. 5th ed. Philadelphia: WB Saunders; 2008

Turner SR, Samei E, Hertzberg BS, et al. Sonography of fetal choroid plexus cysts: detection depends on cyst size and gestational age. J Ultrasound Med 2003;22(11):1219–1227

Case 225

Laura J. Varich

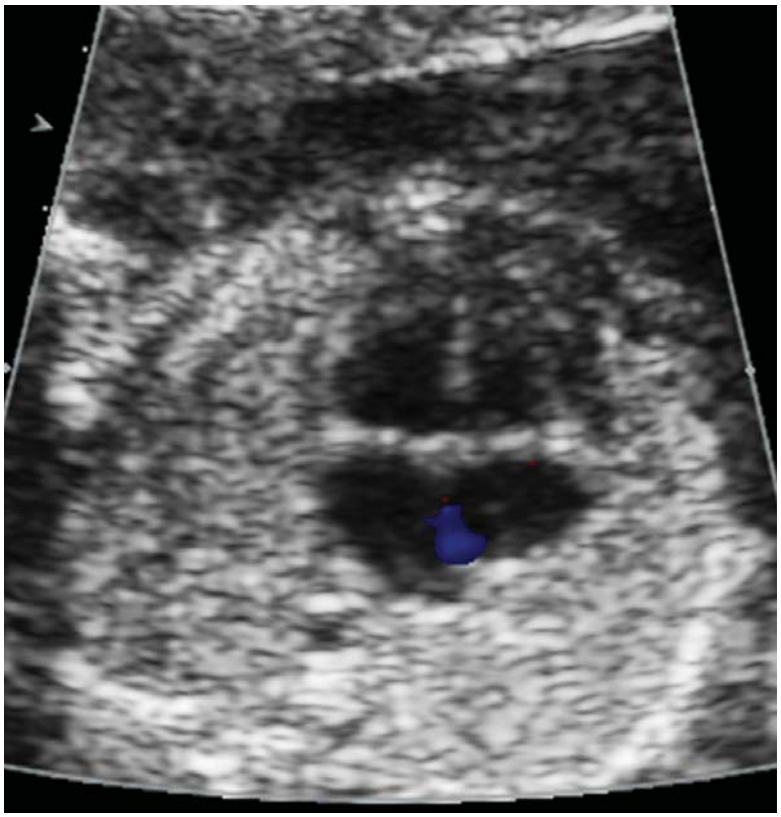


Fig. 225.1 Ultrasound four-chamber view of the fetal heart demonstrates a septal defect of the interventricular septum.

Clinical Presentation

A 30-year-old woman (G3, P2) at 18 weeks' gestation (**Fig. 225.1**).

Key Imaging Finding

Ventricular septal defect

Top 3 Differential Diagnoses

- **Ventricular septal defect (VSD).** The fetal heart is optimally scanned between 18 and 22 weeks' gestation. An adequate fetal cardiac examination should include a four-chamber view and ventricular outflow views, at minimum. The four-chamber view is used to evaluate chamber size, symmetry, situs, axis, valves, and integrity of the septum. Ventricular septal defects account for 20 to 40% of congenital cardiac defects. The abnormal communication between the ventricles results in a left-to-right shunt after birth. VSDs can typically be diagnosed on the four-chamber view; however, small, isolated VSDs are the most commonly missed congenital cardiac defects when using fetal ultrasonography. Color Doppler may be useful, increasing the sensitivity for detecting smaller abnormalities.
- **Endocardial cushion defect.** Endocardial cushion defects represent 2 to 7% of congenital heart defects. These defects involve both the lower atrial septum (ostium primum–type defect) and the ventricular septum; they result from the failure of the endocardial cushion to fuse. Ultrasound has a high sensitivity for detection of this abnormality. Of patients with endocardial cushion defects, 30 to 40% will have Down syndrome.
- **Normal foramen ovale.** The foramen ovale is a normal fetal connection between the atria. The anatomical communication shunts a portion of oxygenated blood (from the placenta via the umbilical vein) to the systemic side of the heart, bypassing the fetal lungs. This directs more highly oxygen-saturated blood to vital organs, including the developing fetal brain. The foramen ovale is normally visualized as a flap valve at the upper atrial septum opening into the left atrium.

Diagnosis

Ventricular septal defect

✓ Pearls

- A fetal cardiac examination should at least consist of a four-chamber view and ventricular outflow views.
- The four-chamber view should assess chamber size, symmetry, situs, axis, valves, and integrity of the septum.
- VSD is a common congenital cardiac defect that results in a left-to-right shunt after birth.
- Endocardial cushion defect affects the ventricular septum and lower atrial septum; it is associated with Down syndrome.

Suggested Readings

Callen P. Ultrasound in Obstetrics and Gynecology. 5th ed. Philadelphia: WB Saunders; 2008

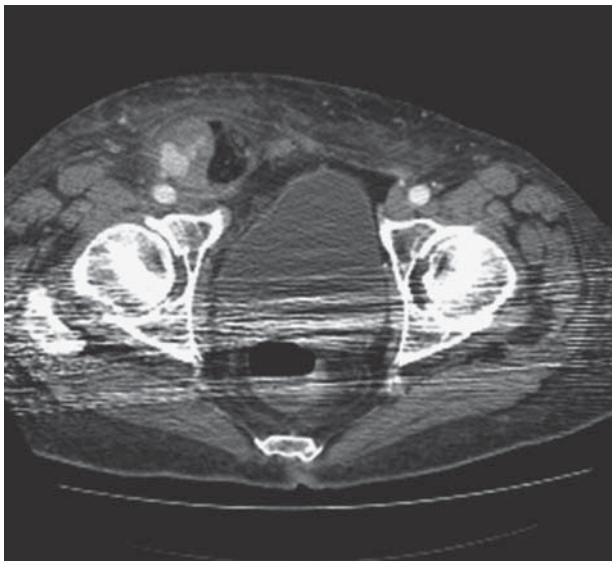
Kirk JS, Comstock CH, Lee W, Smith RS, Riggs TW, Weinhouse E. Sonographic screening to detect fetal cardiac anomalies: a 5-year experience with 111 abnormal cases. Obstet Gynecol 1997;89(2):227–232

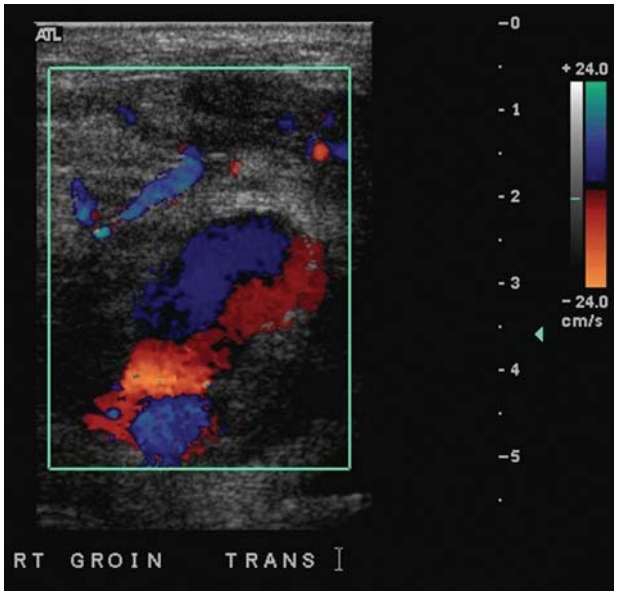
Lee W. Performance of the basic fetal cardiac ultrasound examination. J Ultrasound Med 1998;17(9):601–607

Section X Vascular and Interventional Radiology

Case 226

David D. Gover





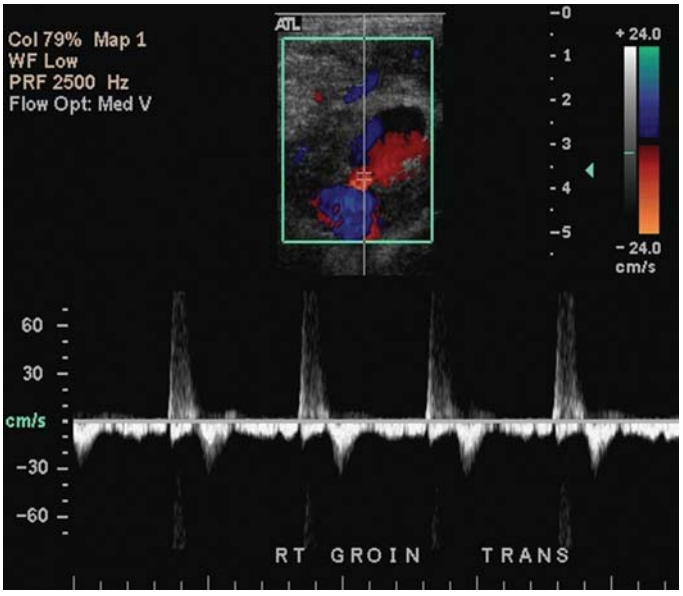


Fig. 226.1 **(A)** Contrast-enhanced axial computed tomography image of the pelvis shows an inflammatory mass in the right groin with areas of contrast enhancement equal to the adjacent artery. **(B,C)** Duplex ultrasound images of the right groin reveal a "yin-yang" color configuration within the right groin mass, as well as a "to-and-fro" waveform.

Clinical Presentation

A 53-year-old man presents with right leg and groin pain after cardiac catheterization (**Fig. 226.1**).

Key Imaging Finding

Postprocedure arterial abnormality

Top 3 Differential Diagnoses

- **Hematoma.** The most frequent complication of diagnostic angiography, minor hematomas occur in up to 10% of cases and typically are self-limited. Major hematomas, defined as those requiring transfusion, surgical evacuation, or delay in discharge, occur in 0.5% of femoral punctures. Differentiating hematoma from pseudoaneurysm can be done by physical examination; however, confirmation with ultrasound is the norm.
- **Pseudoaneurysm.** Also known as false aneurysms, these areas of dilated vessel lack all three arterial layers. Therefore, blood flows out of the vessel, is contained by juxtaarterial tissues (connective tissue and hematoma), and is returned to the original vessel. This creates the classic "yin-yang" or "to-and-fro" appearance on ultrasonography. Causative etiologies include infection, trauma (both penetrating and blunt), and iatrogenia. Iatrogenic lesions form at a rate of 0.1 to 0.2% in diagnostic angiography and up to 2% in interventional cases. Risk factors include a "high" or "low" puncture of the femoral artery, the use of anticoagulants or antiplatelet agents, thrombocytopenia, the use of thrombolytics, and large cannulas. On physical examination, the presence of a pulsatile mass is virtually diagnostic. The presence of a bruit is helpful but is not specific, as other complications may present with a bruit (e.g., dissection, stenosis, and arteriovenous fistula [AVF]). Pseudoaneurysms are painful and may lead to rupture, embolization, or overlying skin ischemia. Treatment options include ultrasound-guided compression, percutaneous thrombin (or collagen) injection under ultrasound guidance, endoluminal coils or stent–graft placement, and surgery. Percutaneous options are usually the first-line treatments. Surgery is required with rapid expansion, distal ischemia, neurologic deficit, failure of percutaneous interventions, infection, or compromised soft tissue viability.
- **Arteriovenous fistula.** This abnormal communication between an artery and an adjacent vein occurs secondary to access of ipsilateral vessels or unnoticed puncture of the vein when accessing the artery. Fistulas form rarely after diagnostic arteriography, at rates <0.2%. Clinically, patients complain of leg pain and swelling, and a bruit is audible on physical examination. Ultrasound interrogation will reveal arterialized flow in the adjacent vein extending centrally. The site of communication can usually be determined. Treatment options include stent–graft placement, coiling of the communication, and open surgery.

Diagnosis

Pseudoaneurysm

✓ Pearls

- Groin hematomas are the most common puncture site complication; the vast majority of hematomas are self-limiting.
- Pseudoaneurysms present as pulsatile masses with a classic "yin-yang" or "to-and-fro" appearance on ultrasound.
- Arteriovenous fistulas most often result from inadvertent venous puncture during arterial access.
- AVFs reveal arterialized flow in the adjacent vein; they can be treated endovascularly or with surgery.

Suggested Readings

Lenartova M, Tak T. Iatrogenic pseudoaneurysm of femoral artery: case report and literature review. Clin Med Res 2003;1(3):243–247

Singh H, Cardella JF, Cole PE, et al; Society of Interventional Radiology Standards of Practice Committee. Quality improvement guidelines for diagnostic arteriography. J Vasc Interv Radiol 2003;14(9, Pt 2):S283–S288

Case 227

William T. O'Brien Sr.

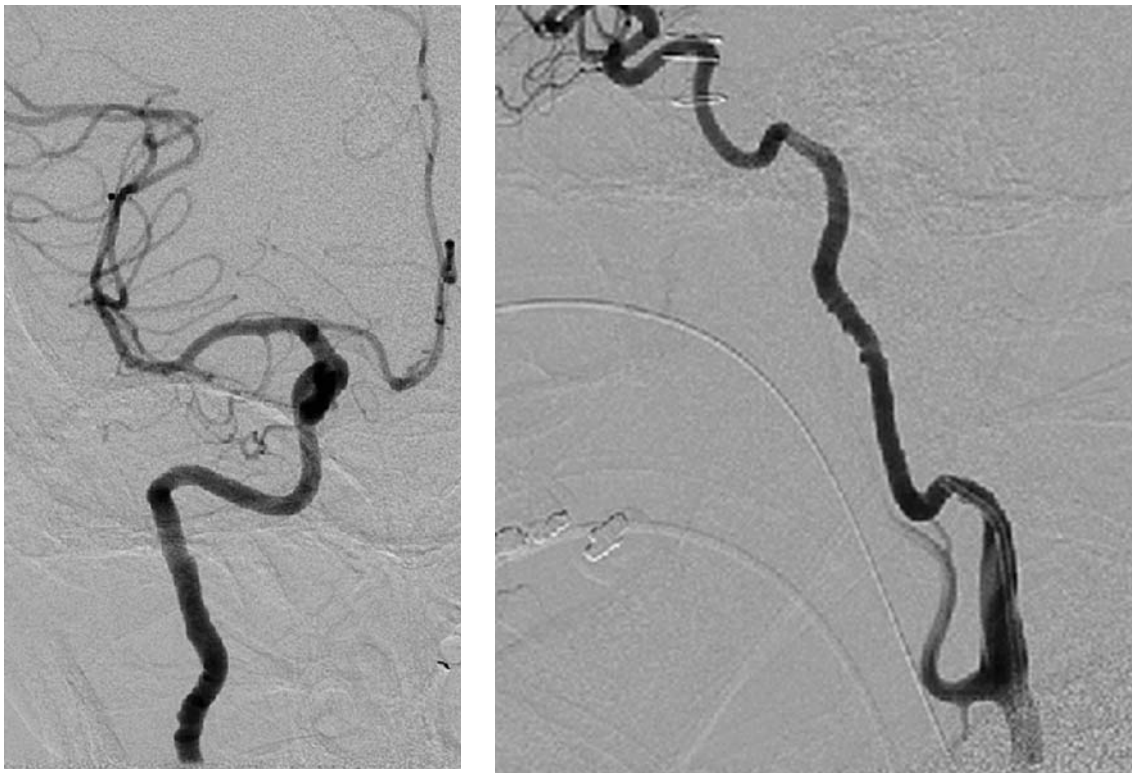


Fig. 227.1 **(A)** Frontal projection centered over the head and **(B)** lateral projection centered over the neck from a digital subtraction angiogram via selective catheterization of the right internal carotid artery reveals a segment of alternating regions of stenosis and dilatation involving the mid cervical internal carotid artery with a "string of beads" appearance. Support tubes and overlying surgical staples are also noted on the lateral view.

Clinical Presentation

A 51-year-old woman with a large middle cerebral artery territory infarct was referred for cerebral angiogram. Patient has a history of bilateral carotid bruits (**Fig. 227.1**).

Key Imaging Finding

Carotid artery stenosis

Top 3 Differential Diagnoses

- **Atherosclerosis.** Atherosclerosis is the most common cause of carotid artery stenosis. It most often occurs in older individuals and is more advanced with a history of smoking, hypertension, hyperlipidemia, and diabetes. The carotid bifurcation and proximal internal carotid artery are the most common sites involved, although atherosclerosis may involve any segment, including intracranially. Doppler ultrasound is the initial screening study. Typical findings on ultrasound are visualization of plaque with vessel stenosis, elevated velocities, and turbulent flow with aliasing. Magnetic resonance and computed tomography angiography (CTA) should be used as confirmatory studies. Carotid endarterectomy (CEA) remains the treatment of choice in low-risk surgical candidates. Current guidelines recommend CEA for symptomatic lesions with >50% stenosis (data from the North American Symptomatic Carotid Endarterectomy Trial) or asymptomatic lesions with >60% stenosis (data from the Asymptomatic Carotid Atherosclerosis Study). Although many recent trials have shown a benefit of endovascular carotid stent placement with distal embolic protection devices in many patient populations, current guidelines recommend this treatment only for high-risk surgical patients with symptomatic lesions of ≥70% stenosis. High-risk surgical patients are defined as follows: clinically significant cardiac disease, severe pulmonary disease (if general anesthesia will be used), recurrent stenosis after prior CEA, prior neck surgery or irradiation, contralateral recurrent laryngeal nerve paralysis, contralateral carotid artery occlusion, and surgically inaccessible lesions (high or low lesions).
- **Fibromuscular dysplasia (FMD).** FMD is a dysplastic vascular disease that primarily affects young women. The renal arteries are most commonly involved, followed by the carotid arteries. The disease results in vascular stenosis and resultant hypertension (renal artery) or stroke (internal carotid artery). Patients are at increased risk of aneurysms and dissections. The medial fibroplasia variant is the most common subtype and presents with the classic "string of beads" appearance due to alternating regions of stenosis and dilatation. Symptomatic lesions are treated with angioplasty.
- **Dissection.** Carotid artery dissection may be due to hypertension, trauma, iatrogenia, or even FMD. Most nontraumatic dissections can be managed medically with some form of anticoagulation and follow-up imaging (usually CTA) to ensure stability or resolution. Symptomatic lesions or lesions that progress despite medical management often require intervention, including stent placement.

Additional Differential Diagnoses

- **Iatrogenic.** The most common iatrogenic causes of carotid stenosis are clamp injury during surgical procedures and vasculitis secondary to radiation therapy for head and neck cancer. Treatment depends on symptoms and morphology of the lesions, with endovascular therapy favored over surgical intervention.

Diagnosis

Fibromuscular dysplasia

✓ Pearls

- Atherosclerosis is the most common cause of carotid artery stenosis; it typically occurs in older individuals.
- Carotid stents are indicated for symptomatic lesions of ≥70% stenosis in high-risk surgical patients.
- FMD affects primarily young women; angioplasty is the primary treatment option for symptomatic lesions.
- Most dissections are due to hypertension or trauma; treatment depends on morphology and symptoms.

Suggested Readings

Executive Committee for the Asymptomatic Carotid Atherosclerosis Study. Endarterectomy for asymptomatic carotid artery stenosis. JAMA 1995;273(18):1421–1428

Gurm HS, Yadav JS, Fayad P, et al; SAPPHIRE Investigators. Long-term results of carotid stenting versus endarterectomy in high-risk patients. N Engl J Med 2008;358(15):1572–1579

North American Symptomatic Carotid Endarterectomy Trial (NASCET) Collaborators. Beneficial effect of carotid endarterectomy in symptomatic patients with high-grade stenosis. N Engl J Med 1991;325:445–453

Roffi M, Yadav JS. Carotid stenting. Circulation 2006;114(1):E1–E4

Case 228

Glade E. Roper

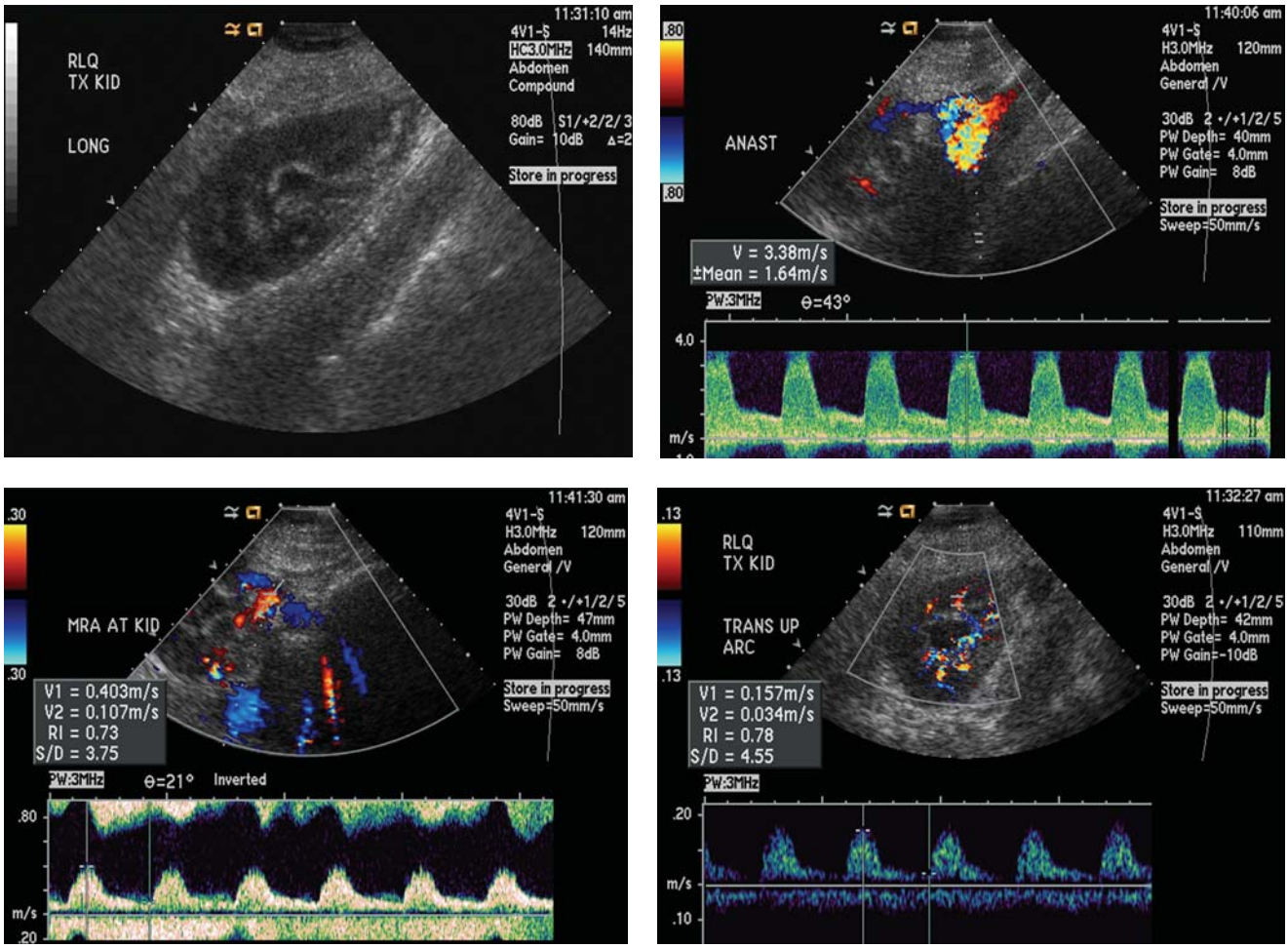


Fig. 228.1 **(A)** Gray scale ultrasound of a right lower quadrant transplant kidney reveals subtle loss of corticomedullary differentiation and no peritransplant fluid. **(B)** Doppler ultrasound of the renal artery reveals turbulent flow with aliasing at the anastomosis of a transplant renal artery and the host iliac artery, with maximum velocity >300 cm per second. **(C)** The more distal renal artery reveals parvus et tardus waveform. **(D)** Doppler ultrasound of intrarenal arcuate arteries reveals a normal resistive index and moderate hydronephrosis. There was also hydroureter, although the distal ureter could not be interrogated due to patient body habitus.

Clinical Presentation

A 60-year-old woman presents with rising creatinine levels following a renal transplant done 6 weeks earlier (**Fig. 228.1**).

Key Imaging Finding

Failing renal transplant with abnormal Doppler examination

Top 3 Differential Diagnoses

- **Acute tubular necrosis (ATN).** ATN is the most common cause of graft dysfunction within the 1st posttransplant week. Ultrasound reveals an enlarged, swollen kidney with poor corticomedullary differentiation, elevated resistive indices (RIs) within the kidney (0.8–0.9 equivocal; >0.9 requires further workup, often with biopsy), and a self-limited course with recovery of function in days to weeks. Imaging findings are nonspecific and overlap with transplant rejection.
- **Renal artery stenosis (RAS).** RAS is a potentially treatable cause of transplant failure due to stricture at the anastomotic site. It is the most common vascular complication of renal transplant. Ultrasound criteria include turbulent flow at the anastomotic site, peak systolic velocity >250 cm per second, and parvus et tardus waveform in the renal artery distal to the stenosis. The gold standard for diagnosis is angiography, though care must be taken to minimize contrast dose; carbon dioxide may be used as a contrast agent.
- **Urinary obstruction.** Urinary obstruction is a relatively common transplant complication, as ureteral strictures form due to disruption of ureteral blood supply when performing the ureterovesicular anastomosis. Ultrasound reveals hydronephrosis. Cystoscopy and retrograde ureterography with ureteral stent placement may be diagnostic and therapeutic options.

Additional Differential Diagnoses

- **Transplant rejection.** Rejection occurs in 20 to 30% of cadaveric allograft recipients. Acute rejection is usually found in the 1st week; chronic rejection occurs in months to years. Ultrasound findings overlap with ATN, although the RI may be normal in early acute rejection. Other possible findings are urothelial wall thickening, areas of hypoechogenicity due to infarction, and perinephric fluid if there is necrosis or hemorrhage. In chronic rejection, the graft becomes small and echogenic, classically with thinning of the cortices and sparing of the medullary pyramids. Biopsy is often required, as imaging findings are nonspecific. The prognosis with early acute rejection is typically good, whereas the prognosis with chronic rejection is poor.
- **Renal vein thrombosis (RVT).** RVT is a relatively uncommon complication of renal transplants, but it is important to recognize as it is a surgical emergency. It is most commonly due to mechanical obstruction. The transplanted kidney does not have venous collaterals; therefore, a delay in diagnosis may result in venous infarction. Ultrasound demonstrates reversal of diastolic flow in a "to-and-fro" pattern.
- **Cyclosporine toxicity.** Cyclosporine has a constrictive effect on renal arterioles, resulting in decreased perfusion. Ultrasound findings are nonspecific and essentially unremarkable, with no change in RI or renal size. Effective renal plasma flow is reduced, which can be evaluated with nuclear medicine imaging. With chronic or more long-standing toxicity, the RI may be elevated.

Diagnosis

Renal artery stenosis

✓ Pearls

- ATN is the most common graft dysfunction in the 1st week posttransplant and is usually self-limited.
- RAS is most often due to stricture at the anastomotic site; it is the most common vascular complication.
- Acute transplant rejection occurs in the 1st week; chronic rejection occurs in months to years.

Suggested Readings

Federle MP. Diagnostic Imaging: Abdomen. Salt Lake City, UT: Amirsys; 2004

Urban BA, Ratner LE, Fishman EK. Three-dimensional volume-rendered CT angiography of the renal arteries and veins: normal anatomy, variants, and clinical applications. Radiographics 2001;21(2):373–386, 549–555

Case 229

William T. O'Brien Sr.



Fig. 229.1 Digital subtraction angiogram of the right hand demonstrates multiple filling defects within the digital arteries, most pronounced within the third through fifth digits. There is underlying deformity of the third distal phalanx.

Clinical Presentation

A 38-year-old man presents with chronic unilateral hand pain and intermittent pallor (**Fig. 229.1**).

Key Imaging Finding

Digital artery occlusion/ischemia

Top 3 Differential Diagnoses

- **Raynaud disease.** Raynaud disease is a vasospastic disorder prompted by cold temperatures. It represents the most common cause of upper extremity ischemia. Imaging findings include stenosis or occlusion of digital artery branches that are relieved by warming of the affected extremity or administration of a vasodilator. Although Raynaud disease is associated with scleroderma, other connective tissue disorders can produce similar clinical symptoms and radiographic findings.
- **Vasculitis.** Vasculitis may result in upper extremity ischemia and has a variety of etiologies, including systemic lupus erythematosus, connective tissue disorders, and Buerger disease. Imaging findings typically include stenosis or occlusion of the arteries within the hand or wrist. Systemic steroids provide relief of acute episodes. Buerger disease (thromboangiitis obliterans) occurs predominantly in young male smokers and has a particular prevalence for the upper extremities. With chronic ischemia, "corkscrew collaterals" develop, which are classic for this entity. Symptoms are improved with smoking cessation.
- **Embolic disease.** Embolic disease may emanate either from the heart or within the vascular supply to the affected upper extremity. Cardiac emboli constitute the most common cause of acute upper extremity ischemia. Imaging findings include arterial occlusions, most commonly within the small vessels of the hand(s). A cardiac source usually involves both upper extremities, whereas a source from a more proximal artery results in unilateral disease. The entire extremity should be evaluated to find lesions amenable to percutaneous interventions, and thrombolysis may be beneficial in certain circumstances.

Additional Differential Diagnoses

- **Thoracic outlet syndrome.** Thoracic outlet syndrome results from chronic compression of the upper extremity neurovascular structures secondary to abnormal insertion of scalene musculature or the presence of a cervical rib. Imaging findings include stenosis or occlusion of the subclavian artery, arterial injury (aneurysm or pseudoaneurysm), and distal emboli. If the angiogram in the neutral position is normal, the angiogram should be repeated with the affected extremity abducted and externally rotated. Percutaneous treatment may be beneficial, but the definitive treatment is surgical correction of the compressive lesion.
- **Trauma.** Frostbite or repetitive injury commonly involves the hands. Frostbite results in ischemia/occlusion of the digital arteries with sparing of the thumbs secondary to clenched fists with the digits protecting the thumbs. Hypothenar hammer syndrome is due to repetitive trauma and results in pseudoaneurysm formation along the hypothenar eminence with distal emboli to the digital arteries.
- **Atherosclerosis.** Atherosclerotic disease constitutes the most common cause of chronic upper extremity ischemia. Although any artery may be involved, the digital arteries are affected in patients with chronic hypertension, diabetes, and/or renal failure. Imaging findings include stenosis or occlusion of the arteries of the wrist, hand, or digits. The vascular supply of the entire extremity should be interrogated to find lesions amenable to percutaneous interventions.

Diagnosis

Thoracic outlet syndrome

✓ Pearls

- Raynaud disease is vasospasm due to cold temperatures; it is relieved with warming or vasodilators.
- Many vasculitides may cause digital artery occlusion; Buerger disease results in "corkscrew collaterals."
- Embolic disease from a proximal source (cardiac or thoracic outlet) may cause digital artery occlusion.

Suggested Readings

Kaufman JA, Lee MJ. Vascular and Interventional Radiology: The Requisites. Philadelphia: Elsevier; 2004

Case 230

David D. Gover

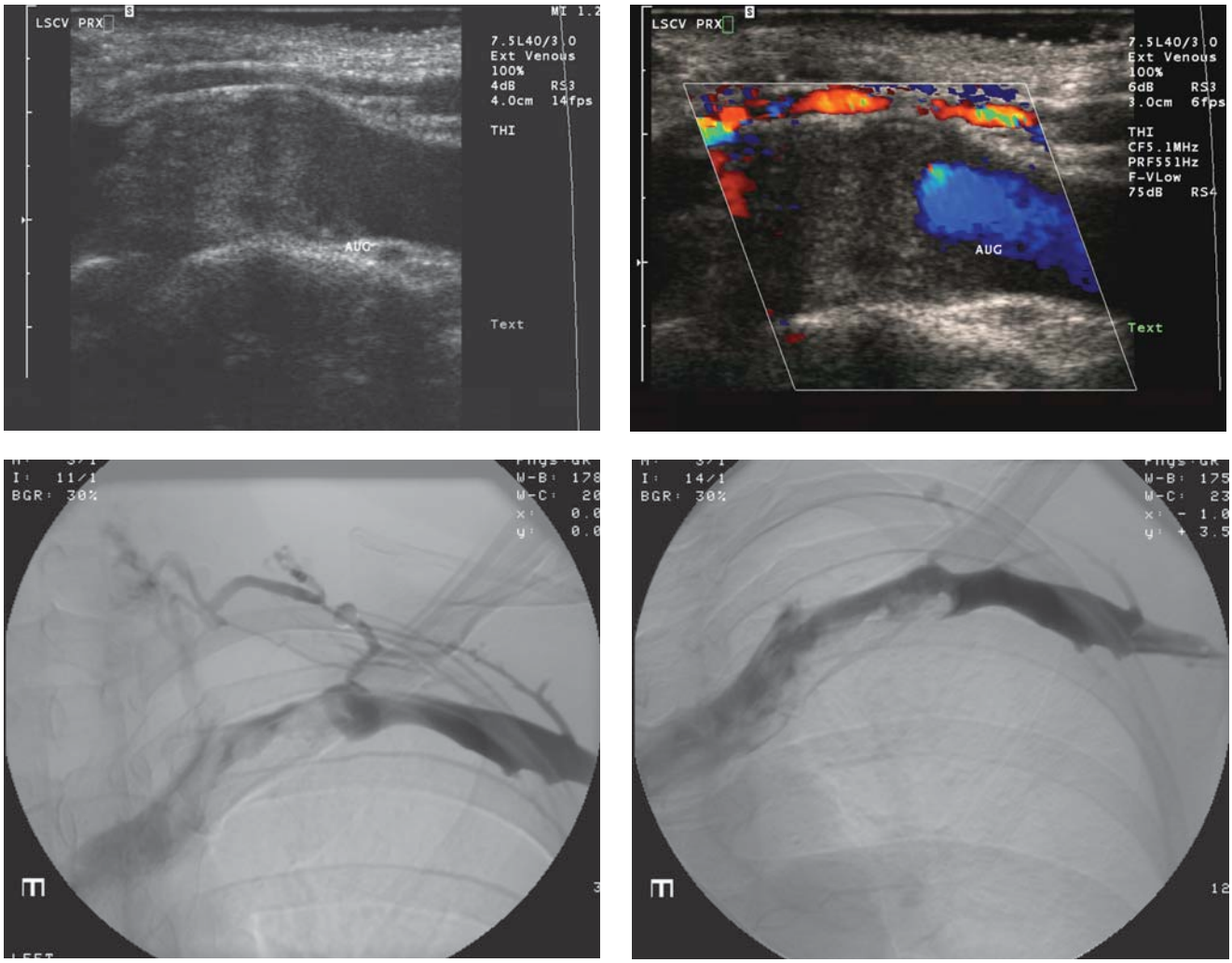


Fig. 230.1 **(A)** Gray scale and **(B)** color Doppler ultrasound images of the left subclavian vein reveal an echogenic focus within the vessel and expansion of the lumen without flow. **(C)** Conventional venography reveals a corresponding filling defect with minimal contrast flow around the abnormality, as well as the presence of collateral vessels. **(D)** Venogram at the same level after overnight pharmacological thrombolysis and angioplasty demonstrates improved contrast opacification of the vessel with resolution of the collateral venous pathways.

Clinical Presentation

A 33-year-old woman presents with acute left arm swelling that began after wearing a new backpack (**Fig. 230.1**).

Key Imaging Finding

Subclavian vein occlusion

Top 3 Differential Diagnoses

- **Prior instrumentation/catheter placement.** Upper extremity deep venous thrombosis (DVT) accounts for nearly 10% of all DVT cases; most attribute this change to the use of chronic indwelling catheters and cardiac devices. Ultrasound is the initial exam of choice, followed by computed tomography venography or conventional venography in equivocal cases. Contrast exam will reveal a filling defect or occlusion at areas of prior or current devices, along with collateral venous circulation. Management depends on symptoms, ability to receive anticoagulation, and clinical necessity of any medical devices weighted against the risk of thromboembolic disease. Treatment options range from conservative measures, anticoagulation, thrombolysis, or all of the previously mentioned plus removal of the catheter or cardiac device.
- **Hypercoagulability.** Virchow triad refers to a predisposition for venous thromboses secondary to trauma (intimal injury), stasis/immobility, and/or an underlying hypercoagulable state. Genetic conditions that result in a hypercoagulable state include factor V Leiden, antithrombin III, and protein S or C deficiencies; acquired conditions include oral contraceptives, tobacco usage, and underlying malignancy. In cases of an inherited hypercoagulable state or underlying malignancy, lifelong anticoagulation is the usual treatment. Endovascular therapy with catheter-directed thrombolysis or angioplasty may be beneficial in many instances.
- **Paget–von Schroetter syndrome/effort thrombosis.** Defined as primary thrombosis at the thoracic inlet, Paget–von Schroetter syndrome is usually found in young patients with cervical ribs, osseous deformity (e.g., tumor or trauma) of the clavicle or first rib, or myofascial narrowing. It may occasionally occur bilaterally. Definitive diagnosis is obtained through conventional venography with provocative maneuvers such as abduction with external rotation (caution, as possible false-positive results may occur). Management consists of thrombolysis followed by anticoagulation of symptomatic lesions until definitive surgical decompression can be performed. Follow-up venography may yield persistent irregular stenosis that may require percutaneous transluminal angioplasty.

Diagnosis

Paget–von Schroetter syndrome

✓ Pearls

- Chronic indwelling catheters are the most common cause of upper extremity DVT.
- Virchow triad refers to trauma (intimal injury), stasis/immobility, or underlying hypercoagulable state.
- Paget–von Schroetter syndrome results in venous thrombosis due to osseous or myofascial abnormalities.
- Definitive treatment of Paget–von Schroetter syndrome requires surgical intervention.

Suggested Readings

Demondion X, Herbinet P, Van Sint Jan S, Boutry N, Chantelot C, Cotten A. Imaging assessment of thoracic outlet syndrome. Radiographics 2006;26(6):1735–1750

Sheeran SR, Hallisey MJ, Murphy TP, Faberman RS, Sherman S. Local thrombolytic therapy as part of a multidisciplinary approach to acute axillosubclavian vein thrombosis (Paget–Schroetter syndrome). J Vasc Interv Radiol 1997;8(2):253–260

Case 231

David D. Gover

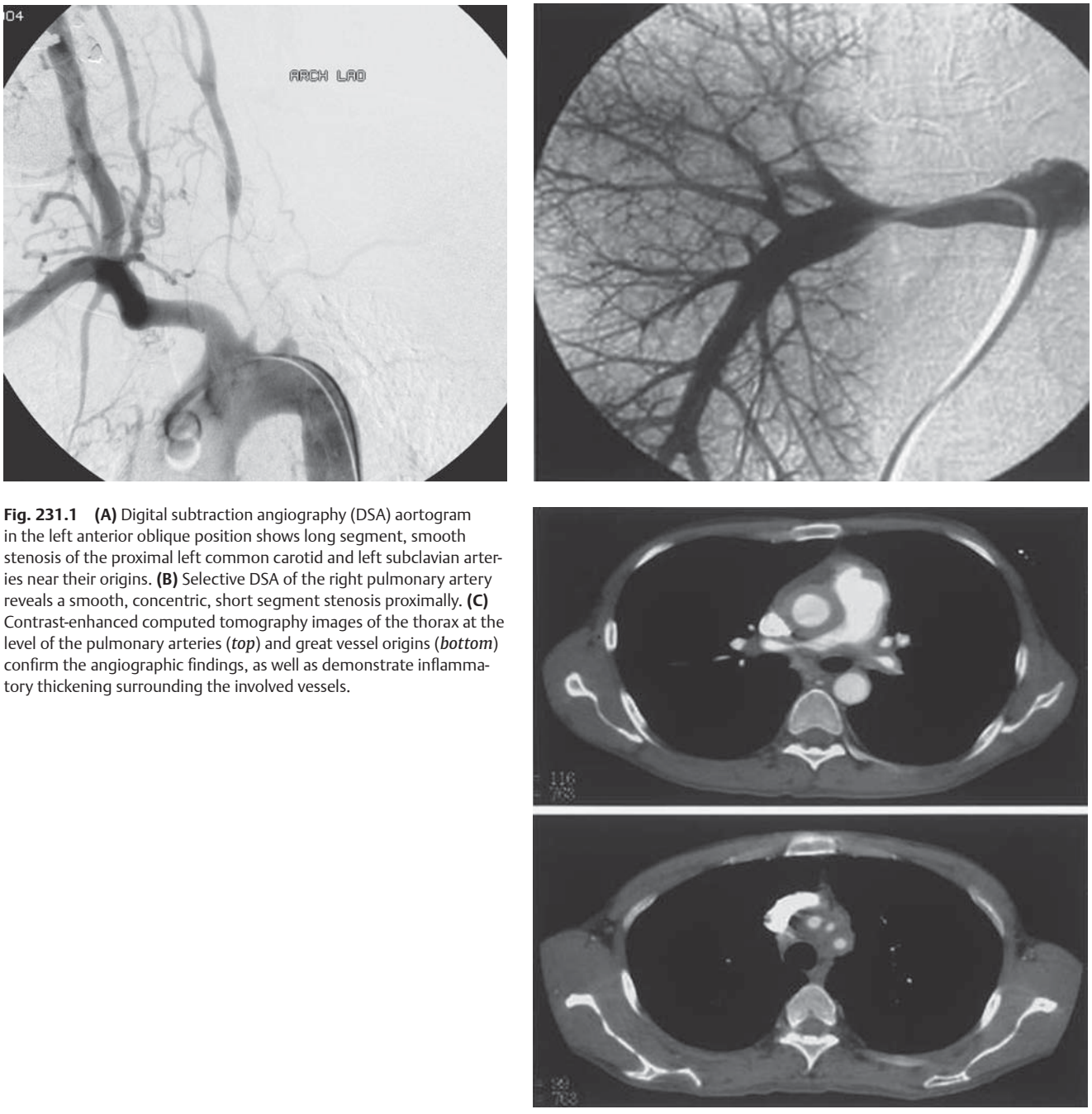


Fig. 231.1 **(A)** Digital subtraction angiography (DSA) aortogram in the left anterior oblique position shows long segment, smooth stenosis of the proximal left common carotid and left subclavian arteries near their origins. **(B)** Selective DSA of the right pulmonary artery reveals a smooth, concentric, short segment stenosis proximally. **(C)** Contrast-enhanced computed tomography images of the thorax at the level of the pulmonary arteries (*top*) and great vessel origins (*bottom*) confirm the angiographic findings, as well as demonstrate inflammatory thickening surrounding the involved vessels.

Clinical Presentation

A 27-year-old Asian woman presents with left arm pain (**Fig. 231.1**).

Key Imaging Finding

Great vessel stenosis

Top 3 Differential Diagnoses

- **Atherosclerosis.** Atherosclerosis is the most common cause of great vessel stenosis. Multiple vessels are usually involved. Patients are typically older and have risk factors such as hypertension, smoking, hyperlipidemia, and diabetes. Concomitant cardiovascular and peripheral vascular disease is common. Symptoms are related to the specific end-organ being underperfused, and therapy is geared toward relief of said symptoms. Catheter-directed therapies are attempted due to the decreased morbidity compared with open surgery. Technical success rates exceed 95%. Long-term clinical success of angioplasty for stenosis and stent placement for occlusion ranges from 70 to 90%.
- **Vasculitis.** Great vessel and aortic vasculitis is usually secondary to primary conditions such as Takayasu or giant cell arteritis (GCA). Takayasu arteritis tends to affect younger Asian women and manifests clinically with malaise, arthralgias, and gradual onset of extremity claudication. Clinical examination may reveal asymmetric pulses or blood pressure in the upper extremities. GCA typically is seen in older Caucasian women. Patients have fevers, polymyalgia rheumatica, facial or upper extremity claudication, visual disturbances, blindness, and generalized constitutional symptoms. The diagnosis of GCA is confirmed with temporal artery biopsy. Treatment of vasculitis consists of corticosteroid administration. Once acute flares have resolved, residual stenoses may be treated percutaneously should concordant symptoms persist.
- **Dissection.** Stanford A dissections may have false lumen extension into the origins of the great vessels. This can lead to end-organ hypoperfusion/stroke. Surgical management is the usual treatment. In nonsurgical patients, endoluminal options include stent or stent–graft placement at the leading intimal tear or fenestration of the intimal flap.

Additional Differential Diagnoses

- **Radiation.** Radiation therapy to the chest wall or neck may lead to multiple, smooth, long-segment strictures of affected vessels. History is the key to making this diagnosis. Treatments are centered on endoluminal options for arch vessel involvement given the high morbidity associated with surgical procedures, along with similar patency rates.

Diagnosis

Vasculitis (Takayasu arteritis)

✓ Pearls

- Atherosclerosis is the most common cause of great vessel stenosis and typically affects older individuals.
- GCA and Takayasu arteritis are common vasculitides affecting the great vessels; treatment is with steroids.
- Aortic dissections may involve the great vessels; Stanford A dissections are typically managed surgically.
- Radiation therapy to the neck results in long-segment strictures; endoluminal treatment is preferred.

Suggested Readings

Hadjipetrou P, Cox S, Piemonte T, Eisenhauer A. Percutaneous revascularization of atherosclerotic obstruction of aortic arch vessels. J Am Coll Cardiol 1999;33(5):1238–1245

Roane DW, Griger DR. An approach to diagnosis and initial management of systemic vasculitis. Am Fam Physician 1999;60(5):1421–1430

Zimpfer D, Czerny M, Kettenbach J, et al. Treatment of acute type a dissection by percutaneous endovascular stent-graft placement. Ann Thorac Surg 2006;82(2):747–749

Case 232

David D. Gover

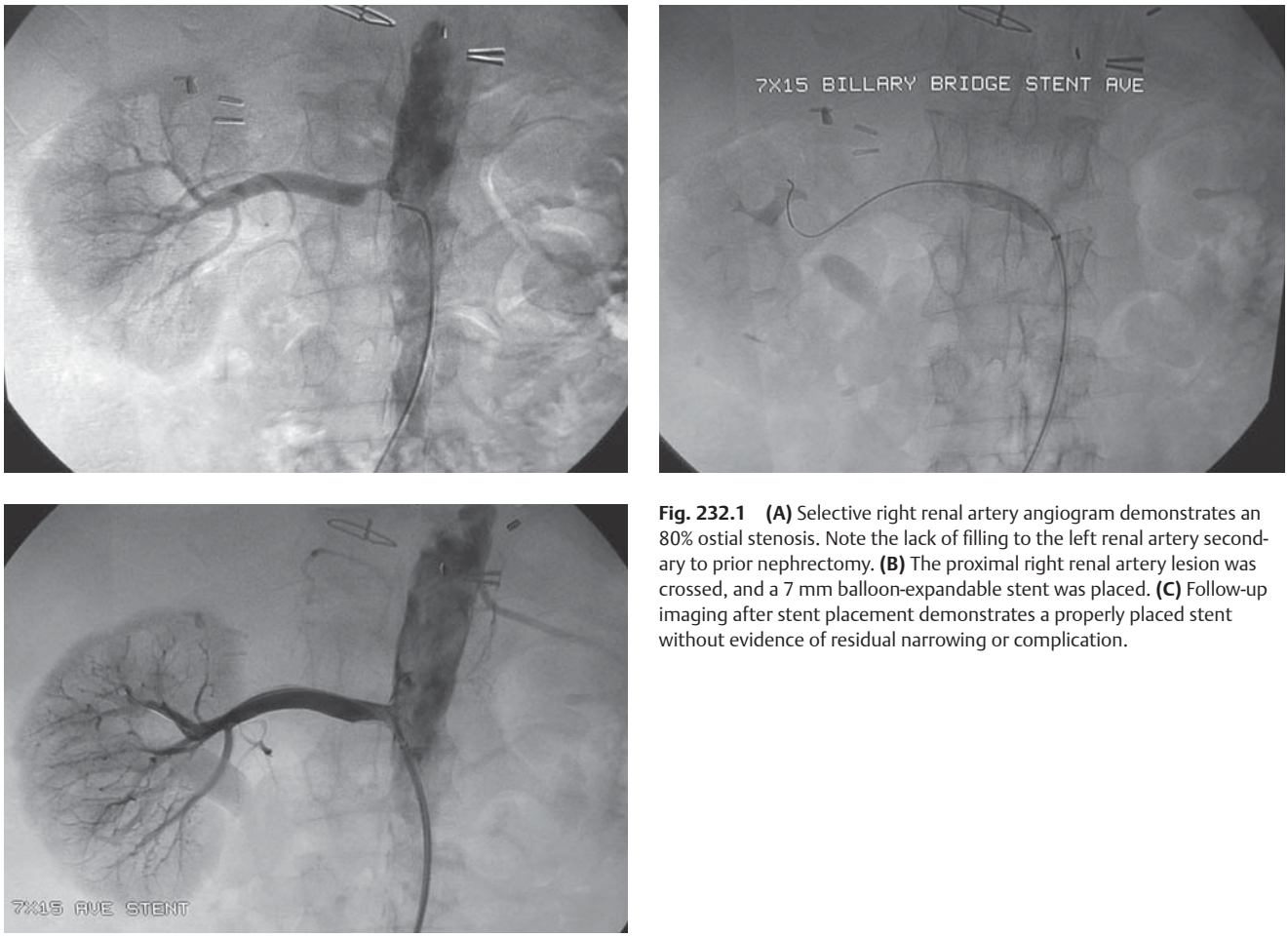


Fig. 232.1 **(A)** Selective right renal artery angiogram demonstrates an 80% ostial stenosis. Note the lack of filling to the left renal artery secondary to prior nephrectomy. **(B)** The proximal right renal artery lesion was crossed, and a 7 mm balloon-expandable stent was placed. **(C)** Follow-up imaging after stent placement demonstrates a properly placed stent without evidence of residual narrowing or complication.

Clinical Presentation

A 66-year-old man presents with prior left nephrectomy, worsening hypertension, and renal failure while on an angiotensin-converting enzyme (ACE) inhibitor. **Fig. 232.1A** and **B** are pretreatment; **Fig. 232.1C** is posttreatment.

Key Imaging Finding

Renal artery stenosis

Top 3 Differential Diagnoses

- **Atherosclerosis.** The most common cause of renal artery stenosis, atherosclerotic plaques usually form at the ostia (first centimeter) of the renal artery due to disease of the aorta. Patients may be asymptomatic or suffer from renovascular hypertension, chronic renal failure, or episodes of flash pulmonary edema. In the setting of symptoms, intervention is usually offered. The mainstay intervention has become percutaneous stent placement. Despite a high technical success rate (>98%), clinical responses are variable and difficult to predict. For example, in the setting of renovascular hypertension, approximately one third of patients have improvement in blood pressure, one third stabilize, and one third continue to deteriorate. Reasons for failure include contrast-induced nephropathy, progressive nephrosclerosis, diffuse distal renal artery atherosclerotic disease, and atheroembolism. The theory of atheroembolism has led to the development of low-profile systems for interventions and distal embolic protection devices. Embolic protection appears safe to incorporate into the procedure but is still not widely accepted as a proven benefit. Lastly, the decision to treat stenosis is somewhat controversial. Most current studies, although not definitive, show no benefit to stent placement over maximal medical management (especially with the use of statins for plaque stabilization or even regression). Although some experts espouse early treatment despite symptoms, most currently consider invasive intervention only in the setting of the symptoms mentioned previously.
- **Fibromuscular dysplasia (FMD).** Although relatively uncommon, FMD is the leading cause of curable hypertension and most often occurs in younger women. The most common form is that of medial fibroplasia (~90% of all FMD), which has the typical angiographic appearance of a "string of beads" with alternating regions of stenosis and dilatation. The other subtypes may present with stenosis similar to atherosclerosis. Patients usually present with renovascular hypertension but are younger than is typical for atherosclerosis. Angioplasty is highly effective, with 80% improvement in hypertension at 1 month and 93% at 2 years. Angioplasty can be repeated as needed with similar clinical results. Other medium-sized vessels may also be affected (e.g., internal carotid artery).
- **Dissection.** Dissections often begin in the aorta (ascending or descending) and affect the perfusion and origin caliber of the renal arteries. Additionally, iatrogenic dissection of the renal artery can occur with diagnostic angiography or endoluminal interventions. Treatment is based on the morphology of the dissection and clinical symptoms, with operative therapy, fenestration, or stenting all used.

Diagnosis

Atherosclerosis

✓ Pearls

- Atherosclerosis is the most common cause of renal artery stenosis and typically involves the renal ostia.
- Despite the technical success of renal artery stents for atherosclerotic lesions, clinical response is variable.
- FMD most often occurs in young women; lesions are treated with angioplasty, which is highly effective.
- Treatment of renal artery dissections is based on the morphology of the dissection and clinical symptoms.

Suggested Readings

Kim HJ, Do YS, Shin SW, et al. Percutaneous transluminal angioplasty of renal artery fibromuscular dysplasia: mid-term results. Korean J Radiol 2008;9(1):38–44

Misra S, Gomes MT, Mathew V, et al. Embolic protection devices in patients with renal artery stenosis with chronic renal insufficiency: a clinical study. J Vasc Interv Radiol 2008;19(11):1639–1645

van Bockel JH, Weibull H. Fibrodysplastic disease of the renal arteries. Eur J Vasc Surg 1994;8(6):655–657

Case 233

David D. Gover



Fig. 233.1 Selective digital subtraction angiography of the right renal artery shows numerous small intraparenchymal aneurysms.

Clinical Presentation

A 44-year-old woman presents with hematuria (**Fig. 233.1**).

Key Imaging Finding

Intraparenchymal renal artery aneurysms

Top 3 Differential Diagnoses

- **Vasculitis.** Vascular inflammatory conditions are the major cause of intraparenchymal renal aneurysms. The most common condition to affect the small to medium-sized renal arteries is polyarteritis nodosa (PAN). This is usually idiopathic, but it can be associated with cryoglobinemia, leukemia, rheumatoid arthritis, Sjögren syndrome, and hepatitis B (mnemonic CLASH). Patients are usually middle-aged and suffering from peripheral neuropathy, intestinal ischemia, and livedo reticularis. Patients with Wegener vasculitis present with recurrent sinusitis or epistaxis, mucosal ulcerations, hemoptysis, tracheal stenosis, and eye involvement. Other vasculitides affecting the renal arteries are Takayasu and Churg–Strauss syndromes. Treatment involves corticosteroid administration, sometimes with the addition of less proven immunosuppressive therapy.
- **Mycotic/septic emboli.** Sources of septic emboli include bacterial endocarditis (often associated with intravenous drug abuse), infected valves, infected atrial thrombus, and noncardiac sources. Emboli can lead to multiple renal pseudoaneurysms. Typical organisms are gram-positive bacteria (*Streptococcus* and *Staphylococcus* subspecies). Treatment is supportive, and antibiotic therapy is directed toward the offending organism accounting for susceptibility. If congestive heart failure occurs, valve replacement may be necessary.
- **Trauma.** Aneurysms are usually solitary with a history of recent blunt or penetrating trauma. Iatrogenic injury from endovascular procedures has led to an increase in this condition, with rupture being the most dreaded complication. Coils, stent-grafts, open surgical repair, or nephrectomy are effective treatment options depending on the anatomical location and clinical scenario.

Additional Differential Diagnoses

- **Ehlers–Danlos syndrome.** Ehlers-Danlos syndrome is a connective tissue disorder characterized by abnormal collagen synthesis, which results in skin hyperelasticity, joint hyperextensibility, and vascular fragility. Aneurysms can be seen in multiple vascular beds with mass effect or bleeding. Early diagnosis results in minimizing invasive vascular procedures, which can be catastrophic (especially in type IV Ehlers–Danlos syndrome).
- **Speed kidney.** Chronic oral amphetamine use (50 mg daily for 22 years to 200 mg daily for 2 years) may be an independent risk factor for multiple renal artery aneurysms. These patients have no other risk factors but present with multiple visceral artery aneurysms.

Diagnosis

Vasculitis (polyarteritis nodosa)

✓ Pearls

- PAN classically results in multiple aneurysms involving small and medium-sized renal arteries.
- Mycotic/septic emboli may result from cardiac or noncardiac sources; multiple pseudoaneurysms are seen.
- Blunt or penetrating trauma, along with iatrogenia, may cause renal artery aneurysms.
- Chronic amphetamine usage predisposes patients to multiple renal artery aneurysms (speed kidney).

Suggested Readings

Bloch R, Hoffer E, Borsa J, Fontaine A. Ehlers-Danlos syndrome mimicking mesenteric vasculitis: therapy, then diagnosis. J Vasc Interv Radiol 2001;12(4):527–529

Nosher JL, Chung J, Brevetti LS, Graham AM, Siegel RL. Visceral and renal artery aneurysms: a pictorial essay on endovascular therapy. Radiographics 2006;26(6):1687–1704, quiz 1687

Roane DW, Griger DR. An approach to diagnosis and initial management of systemic vasculitis. Am Fam Physician 1999;60(5):1421–1430

Welling TH, Williams DM, Stanley JC. Excessive oral amphetamine use as a possible cause of renal and splanchnic arterial aneurysms: a report of two cases. J Vasc Surg 1998;28(4):727–731

Case 234

Glade E. Roper

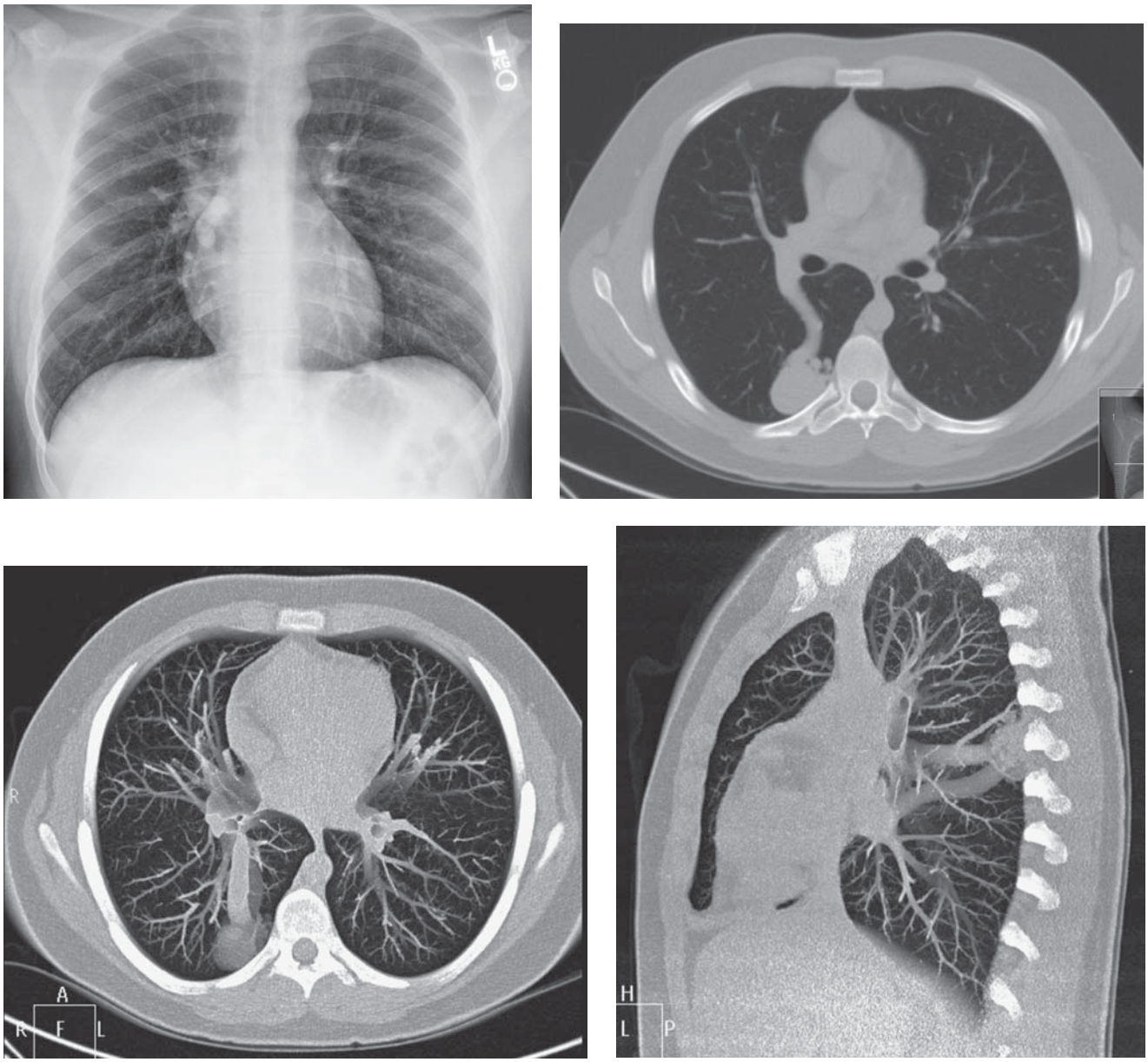


Fig. 234.1 **(A)** Frontal chest radiograph demonstrates rounded densities overlying the right hilum. **(B)** Axial computed tomography image in the lung window reveals a rounded peripheral mass within the superior segment of the right lower lobe with an enlarged feeding vessel. Contrast-enhanced maximum intensity projection images in the **(C)** axial and **(D)** sagittal planes following contrast confirm the peripheral mass with an enlarged feeding artery and draining vein. (Courtesy of Children's Hospital and Research Center, Oakland, California.)

Clinical Presentation

A patient presents with a cough (**Fig. 234.1**).

Key Imaging Finding

Hypervascular pulmonary mass

Top 3 Differential Diagnoses

- **Arteriovenous malformation (AVM).** AVMs are anomalous connections between the pulmonary arteries and veins that bypass the normal pulmonary capillary bed. Large AVMs can result in paradoxical emboli or high-output heart failure. AVMs may occur sporadically or be associated with Osler–Weber–Rendu disease, in which case they are multiple. Contrast-enhanced computed tomography (CT) reveals a noncalcified, homogeneously enhancing nodule with one or more feeding arteries and one or more draining veins. Angiography reveals opacification of the pulmonary veins on arterial injection of contrast. AVMs fed by an artery >3 mm and those contributing to paradoxical emboli or heart failure should be treated with coil embolization.
- **Bronchogenic carcinoma.** Lung cancer is the most common cause of cancer death in the United States. Adenocarcinoma is the most common subtype. Squamous and small cell subtypes are highly associated with tobacco usage. Nodules <5 mm in diameter on CT have <1% chance of being malignant. Nodules >7 mm can be interrogated for enhancement; nearly all of those with <15 HU of enhancement will be benign. Large, spiculated nodules and those with concurrent mediastinal lymphadenopathy are most concerning for cancer. Positron emission tomography imaging or biopsy can help establish a diagnosis and direct treatment in more difficult cases.
- **Hypervascular metastasis.** The lung is the most common site of metastatic disease; ~50% of cancer patients have lung metastases at autopsy. A solitary enhancing lung nodule may represent metastases from a hypervascular primary malignancy, such as malignant melanoma, sarcoma, carcinoid, or renal cell carcinoma. Thyroid carcinoma metastatic lesions are quite vascular and thus enhance avidly, but they usually present as multiple lesions.

Additional Differential Diagnoses

- **Pulmonary carcinoid.** Carcinoid is an uncommon malignant tumor of bronchial neuroendocrine cells. Patients present between 30 and 60 years of age with a chronic cough and often with hemoptysis. Radiography reveals a smooth mass, usually centrally located, with or without postobstructive pneumonia. CT reveals a centrally located mass with avid contrast enhancement. Thirty percent of carcinoid tumors demonstrate calcification. Often there is a small endobronchial component with a large extrabronchial component, referred to as the "tip of the iceberg" sign.
- **Pulmonary artery aneurysm.** Pulmonary artery aneurysms are relatively rare and are most commonly due to pulmonary hypertension, pulmonary infections (Rasmussen aneurysm with tuberculosis), or vasculitides. They may involve the main or more distal pulmonary artery branches, in which they may present as a hyperenhancing pulmonary nodule or mass.

Diagnosis

Arteriovenous malformation

✓ Pearls

- AVMs may occur sporadically or be multiple and associated with Osler–Weber–Rendu disease.
- Pulmonary neoplasms may appear as hypervascular masses, especially carcinoid.
- Rasmussen aneurysms occur secondary to pulmonary infection with tuberculosis; they are prone to hemorrhage.

Suggested Readings

Gossage JR, Kanj G. Pulmonary arteriovenous malformations: a state of the art review. Am J Respir Crit Care Med 1998;158(2):643–661

Gurney JW. Diagnostic imaging: Chest. Salt Lake City: Amirsys; 2006

Swensen SJ, Viggiano RW, Midthun DE, et al. Lung nodule enhancement at CT: multicenter study. Radiology 2000;214(1):73–80

Case 235

David D. Gover

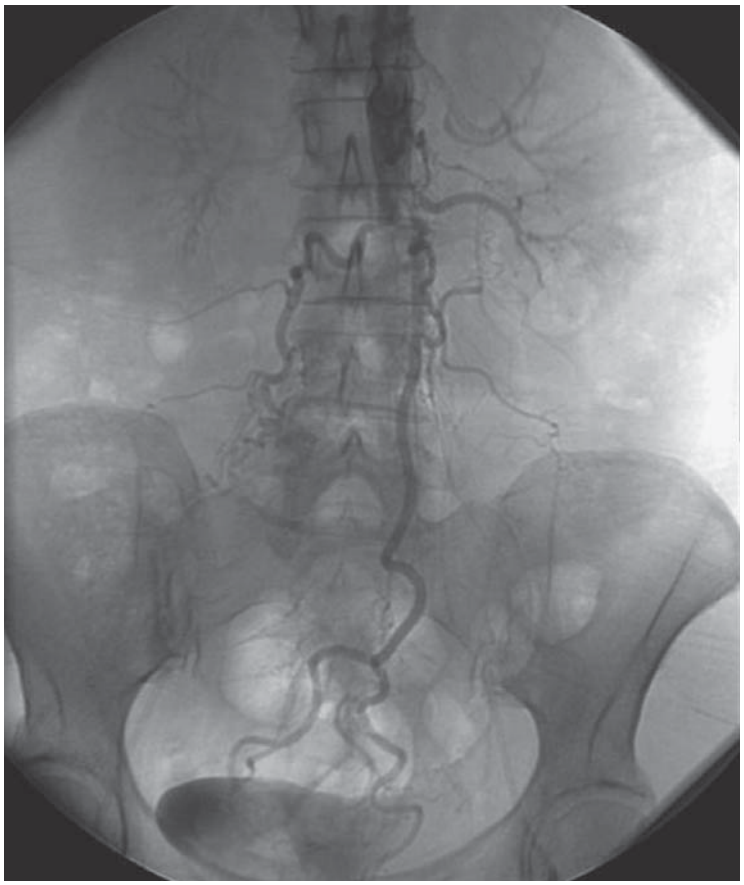


Fig. 235.1 Frontal angiogram of the abdominal aorta and pelvis from a left brachial artery access shows occlusion of the aorta below the level of the inferiormost left renal artery. Note the hypertrophied lumbar vessels that serve as collateral pathways reconstituting the external iliac vessels to supply the lower extremities.

Clinical Presentation

A 58-year-old woman presents with bilateral lower extremity claudication and diminished femoral pulses (**Fig. 235.1**).

Key Imaging Finding

Infrarenal aortic occlusion

Top 3 Differential Diagnoses

- **Atherosclerosis.** This distribution of occlusive disease is most often seen in smokers, presenting with claudication (80%), rest pain (25%), and tissue loss (15%). About 75% of men will be impotent. Add diminished or absent femoral pulses to complete the constellation of findings in Leriche syndrome. Preoperative computed tomography angiography (CTA) should be used to aid in management decisions. With long segment disease (TransAtlantic InterSociety Consensus [TASC] C and D), surgical management usually entails aortobifemoral bypass. Operative mortality is around 5%, with 67% 5-year survival rates. Medical options are reserved for nonoperative candidates. Short segment occlusive disease (TASC A and B), which is less common, can be managed with stent placement. Stent placement in the infrarenal aorta and iliac systems has a >95% technical and clinical success, with a mean 30-day mortality of 0.5%. Primary patency rates are >80% at 3 years. Patients are often placed on aspirin.
- **Thrombus/embolus.** Clot may be formed in situ or come from a proximal source (e.g., cardiac). The underlying pathology is extremely important for management purposes. In the setting of a previously placed aortobifemoral bypass graft, the patient may present acutely with recurrence of symptoms. Endoluminal management is preferred and entails thrombolysis with probable perianastomotic angioplasty and/or stent placement. Embolus lodging in a region of aortic tapering may present with acute ischemia, requiring endoluminal thrombolysis or embolectomy (depending on clinical status). Thrombosis of an aneurysm can also occur (usually in hypercoagulable states) and may merit anything from emergent operative intervention to conservative management with surveillance. History and CTA are important steps in initial management and determination of appropriate therapy.
- **Vasculitis (Takayasu arteritis).** Takayasu arteritis can involve the aorta and its branches. Patients tend to be younger than those with atherosclerosis and typically have systemic clinical findings (e.g., fevers, fatigue, and malaise). Management of the vascular lesions should be delayed until the more fibrotic phase of the disease. When the erythrocyte sedimentation rate has normalized, the lesions can be handled like atherosclerotic lesions with surgery or endovascular options. Appropriate treatment depends on the morphology of the lesions, as well as the clinical status of the patient (e.g., symptoms and comorbidities). Relapses can occur.

Additional Differential Diagnoses

- **Dissection.** Dissections may occur as a result of hypertension, trauma, or iatrogenia. Preoperative CTA helps to make the diagnosis and also aids in management decisions. Medical management, endoluminal stent placement or fenestration, and open surgical repair have all been used, depending on the patient's symptoms and comorbidities.

Diagnosis

Atherosclerosis

✓ Pearls

- Atherosclerosis is a common cause of infrarenal aortic occlusion; treatment depends on lesion morphology.
- Clot may form in situ (thrombus) or result from proximal embolic sources, such as cardiac thrombi.
- Vasculitis involves younger patients with systemic findings; lesions are treated in the fibrotic phase.
- Dissections often occur from hypertension or trauma; treatment depends on symptoms and comorbidities.

Suggested Readings

Kim SH, Jeong JY, Kim YI, Choi YH, Chung JW, Hyung Park J. SCVIR 2002 Film Panel case 3: aortic occlusion secondary to intimal sarcoma. J Vasc Interv Radiol 2002;13(5):537–541

Ligush J Jr., Criado E, Burnham SJ, Johnson G Jr., Keagy BA. Management and outcome of chronic atherosclerotic infrarenal aortic occlusion. Discussion J Vasc Surg 1996;24(3):394–404, discussion 404–405

Uberoi R, Tsetis D. Standards for the endovascular management of aortic occlusive disease. Cardiovasc Intervent Radiol 2007;30:814–819

Case 236

David D. Gover

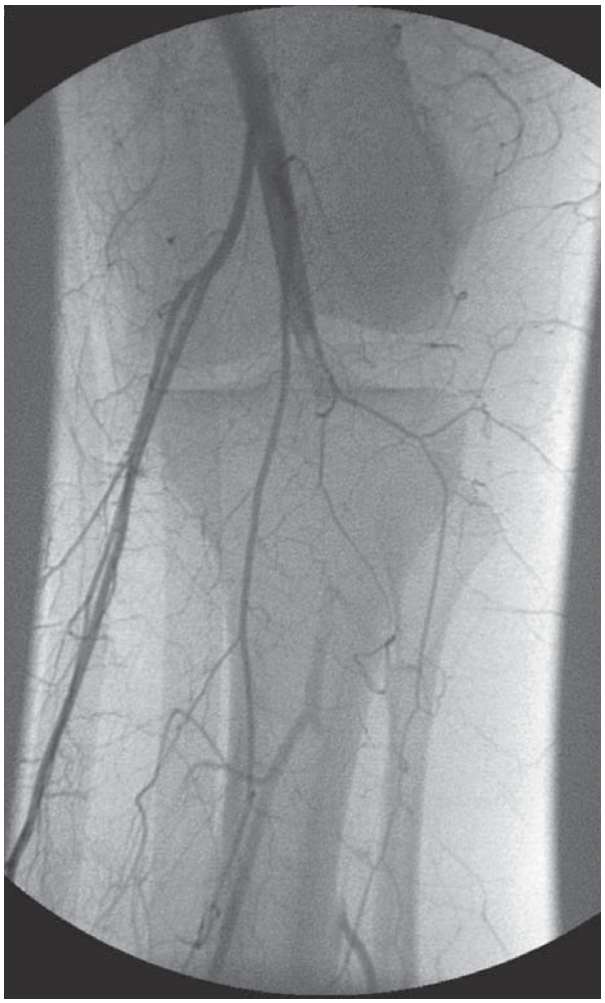


Fig. 236.1 Run-off angiogram of the left popliteal artery shows occlusion at the level of the knee with collateral vessels filling the tibial and peroneal vessels. Secondary findings include asymmetric widening of the medial joint compartment in comparison to the lateral compartment.

Clinical Presentation

A 38-year-old man presents with left leg pain (**Fig. 236.1**).

Key Imaging Finding

Popliteal artery occlusion

Top 3 Differential Diagnoses

- **Atherosclerosis.** Atherosclerosis is the most common cause of popliteal artery stenosis and occlusion. Risk factors include hypertension, diabetes, smoking, and hyperlipidemia. Endothelial injury leads to a fibrotic plaque that can rupture or calcify, ultimately leading to narrowing and occlusion. Patients may present with claudication, rest pain, or tissue loss. Treatment is geared toward the morphology of the lesion and the symptoms. Medical management focuses on risk factors (e.g., hyperlipidemia) or symptoms (e.g., claudication). Interventions include angioplasty, stents/stent grafts, patch angioplasty, and bypass surgery. Overall patient health plays an important role in the choice of intervention.
- **Embolism.** Emboli present acutely with pain or limb threat. Sources include the heart (e.g., arrhythmias) and proximal arterial lesions (abdominal aortic aneurysm). Thrombolysis rather than thrombectomy can be used if time allows.
- **Trauma.** Occlusion of the popliteal artery can be seen in blunt (e.g., motor vehicle accident) or penetrating trauma. A high index of suspicion is necessary, given the possible relocation of the knee joint prior to presentation, as well as preservation of the distal arterial pulse despite injury. Prompt and accurate diagnosis is required to limit morbidity, with angiography being the best exam tool. Surgical repair is almost always necessary.

Additional Differential Diagnoses

- **Thrombosed popliteal artery aneurysm.** Aneurysms are usually true (involving all layers) and degenerative (similar risk factors to atherosclerosis). Rarely, aneurysms form from connective tissue disorders, trauma, or vasculitis. Aneurysms are defined in the popliteal artery as focal areas of widening when compared with normal areas (≥8 mm in diameter). Popliteal artery aneurysms are bilateral 50 to 70% of the time and are associated with abdominal aortic aneurysms in 30 to 50% of cases. Patients may present with thrombosis, distal emboli ("blue toe" syndrome), or rupture (rare). Treatment is usually surgical, but stent grafts have been used in patients at high operative risk.
- **Popliteal artery entrapment syndrome.** Narrowing of the vessel occurs due to an abnormal relationship of the artery to the medial head of the gastrocnemius or popliteus, or sometimes due to muscle hypertrophy. Patients are usually young and athletic, presenting with claudication. In the proper setting, magnetic resonance imaging (MRI) or angiography with the foot neutral and in flexion can be diagnostic. Treatment consists of myomectomy. Left untreated, permanent arterial narrowing will usually result.
- **Cystic adventitial disease.** This rare disease consists of mucoid cysts in the adventitia, leading to compression of the artery. Patients are usually middle-aged men with claudication. MRI best characterizes the lesion, showing the narrowing of the vessel and the mucinous cyst. Treatment options include cyst aspiration (with risk of recurrence), surgical resection with preservation of the artery, and patch angioplasty.

Diagnosis

Trauma (posterior knee dislocation)

✓ Pearls

- Atherosclerotic and embolic disease encompasses the majority of cases of popliteal artery occlusion.
- Traumatic occlusion of the popliteal artery is evaluated with angiography and treated surgically.
- Popliteal artery aneurysms are often bilateral and are associated with abdominal aortic aneurysms.
- Popliteal artery entrapment syndrome is due to an abnormal relationship between the artery and musculature.

Suggested Readings

Wright LB, Matchett WJ, Cruz CP, et al. Popliteal artery disease: diagnosis and treatment. Radiographics 2004;24(2):467–479

Case 237

David D. Gover

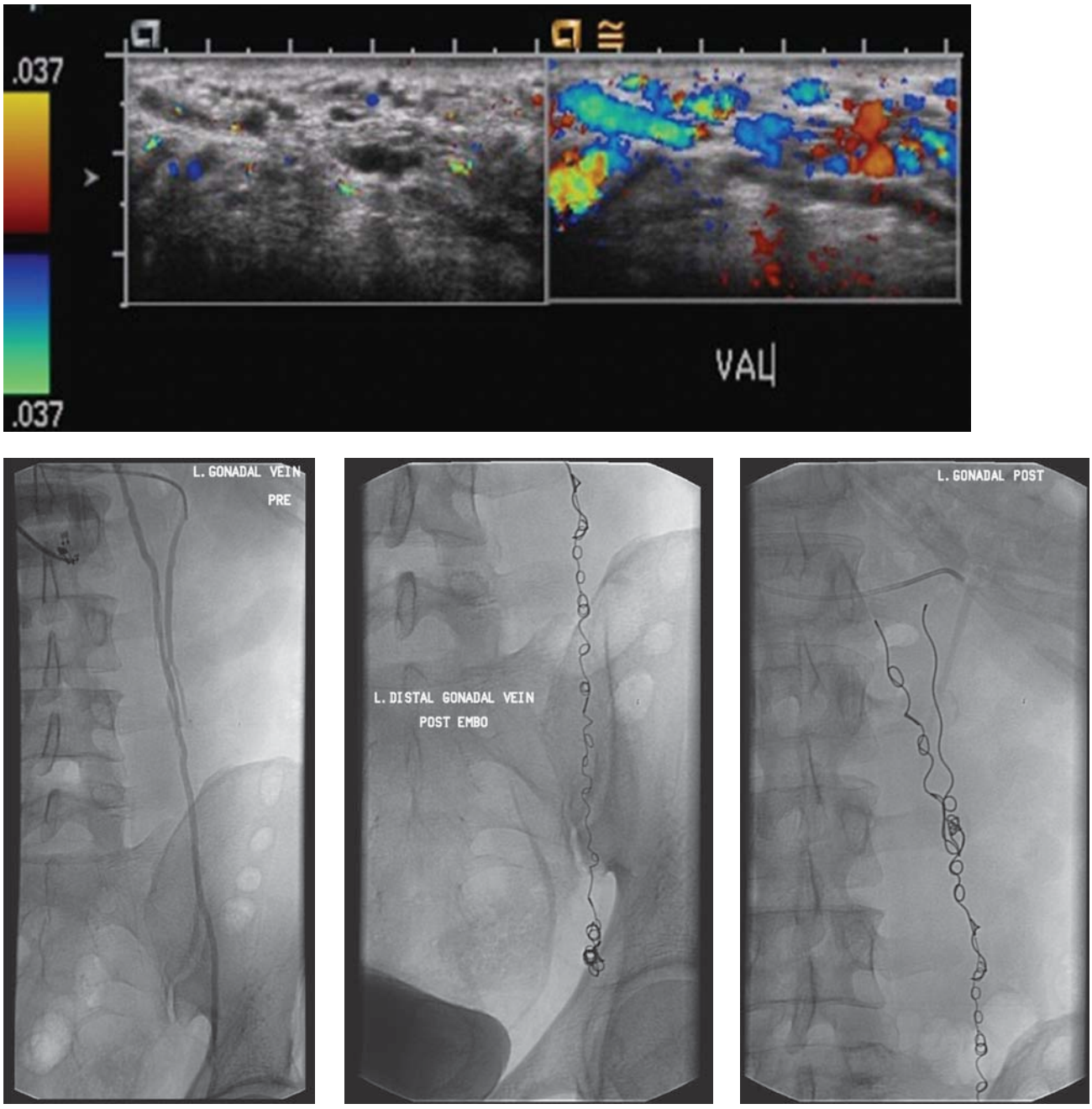


Fig. 237.1 **(A)** Color Doppler ultrasound of the left scrotum reveals a vascular, extratesticular mass with increased flow during Valsalva maneuver, consistent with a varicocele. **(B)** On selective left gonadal venography, there is reflux of contrast to the level of the inguinal canal. Note the partial duplication of the vessel at the renal vein end. **(C)** Coil embolization is performed, **(D)** inclusive of the area of duplication.

Clinical Presentation

A 28-year-old man presents with a painful left scrotal mass (**Fig. 237.1**).

Key Imaging Finding

Extratesticular mass

Top 3 Differential Diagnoses

- **Varicocele.** Varicoceles are usually caused by venous reflux of the ipsilateral gonadal vein and have been classically described as a "bag of worms" on scrotal physical examination. They enlarge or worsen with increased intra-abdominal pressure (e.g., Valsalva maneuver). Unlike lower extremity varicosities that are caused by valvular incompetence (due to prior inflammatory or thrombotic events), varicoceles are usually the result of congenital absence of valves. Varicoceles lead to any combination of male infertility, testicular atrophy, and pain. The vast majority of varicoceles occur on the left side. An isolated right varicocele should prompt a search for a retroperitoneal mass. Treatment options are open, microsurgical, or laparoscopic varicocelectomy versus endoluminal ablation with a variety of materials (e.g., coils, Gelfoam, detergent sclerosants, balloons, and glue). Surgical failure rates range from 1 to 10% at 2 years, with recurrence most likely due to anatomical variations and duplications that evade the surgeon (most in or near the inguinal canal). Endoluminal techniques may be employed as first-line or salvage procedures for symptomatic patients. Endoluminal measures carry the benefit of decreased complication rates, decreased morbidity, and quicker recovery times. Pregnancy rates are similar (~35%) for the partners of patients treated with surgical varicocele repair or embolization.
- **Pyocele/hematocele.** Pyoceles and hematoceles are abnormal collections of pus or blood in the scrotum, respectively. Both present on ultrasound as complex cystic lesions with internal septations and loculations without the blood flow and flow alterations seen with a varicocele. Hematoceles are usually secondary to trauma, surgery, or neoplasm. Pyoceles result from untreated epididymo-orchitis or rupture of an intratesticular abscess. Treatment is centered on the underlying cause.
- **Hydrocele.** A small amount of serous fluid collecting between the layers of the tunica vaginalis may be normal in an asymptomatic patient. Larger or symptomatic collections are abnormal. On ultrasound, these fluid collections are mostly anechoic with good through transmission. Abnormally large collections of fluid may be congenital (patent processus vaginalis), idiopathic, or the result of trauma, infection, torsion, or tumor; therefore, the presence of a hydrocele should prompt a search for underlying pathology.

Diagnosis

Varicocele

✓ Pearls

- Varicoceles result from reflux of the ipsilateral gonadal vein; they enlarge or worsen with Valsalva maneuver.
- An isolated right varicocele should prompt a search for a retroperitoneal mass.
- Pyoceles and hematoceles result in complex extratesticular fluid collections within the scrotum.
- Although often incidental, the presence of a hydrocele should prompt a search for the underlying pathology.

Suggested Readings

Dogra VS, Gottlieb RH, Oka M, Rubens DJ. Sonography of the scrotum. Radiology 2003;227(1):18–36

Shlansky-Goldberg RD, VanArsdalen KN, Rutter CM, et al. Percutaneous varicocele embolization versus surgical ligation for the treatment of infertility: changes in seminal parameters and pregnancy outcomes. J Vasc Interv Radiol 1997;8(5):759–767

Sze DY, Kao JS, Frisoli JK, McCallum SW, Kennedy WA II, Razavi MK. Persistent and recurrent postsurgical varicoceles: venographic anatomy and treatment with n-butyl cyanoacrylate embolization. J Vasc Interv Radiol 2008;19(4):539–545

Case 238

Wayne L. Monsky

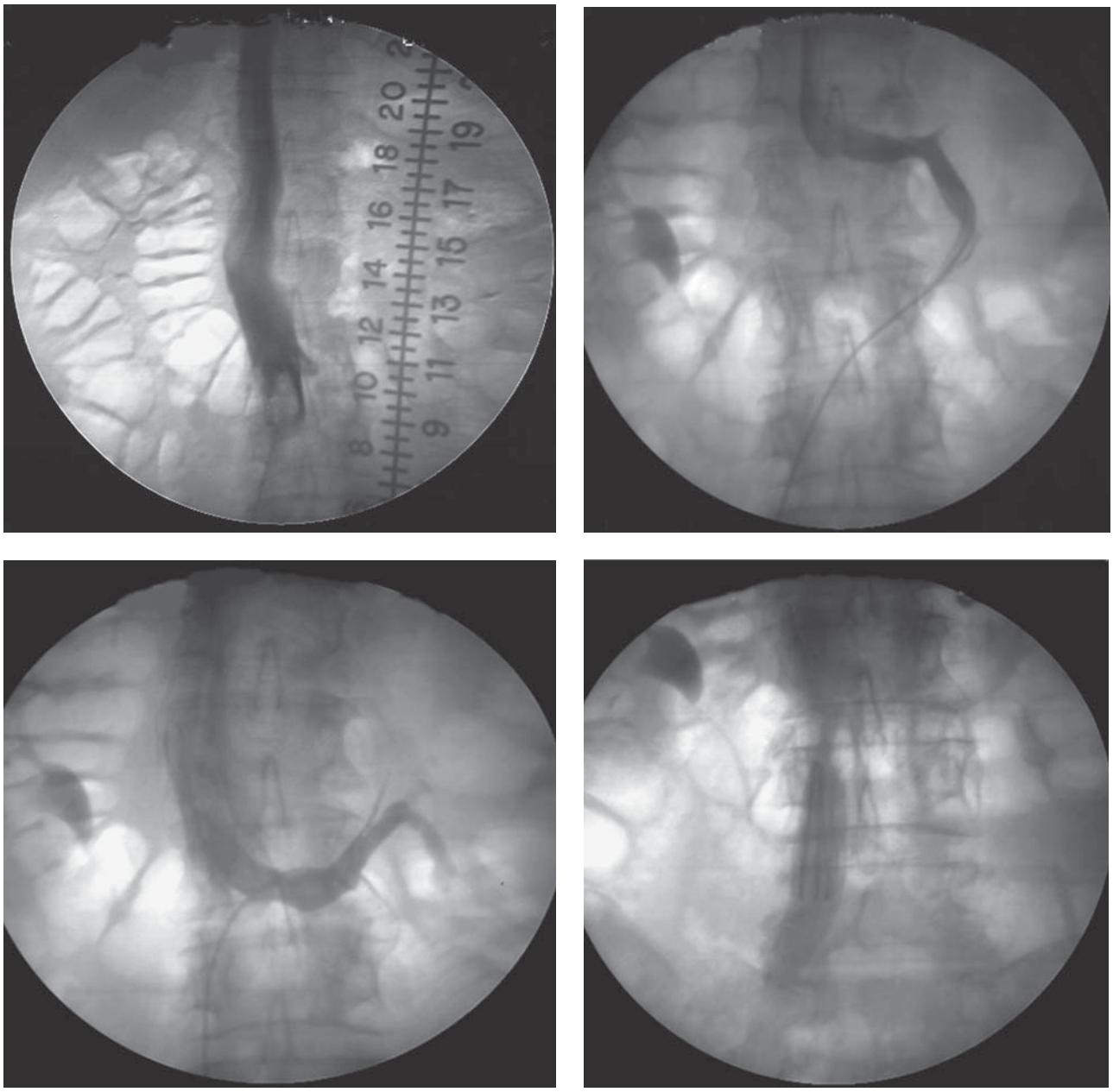


Fig. 238.1 **(A)** Inferior vena cavagram with ruler in place demonstrates contrast refluxing into a lower than expected left renal vein at the level of the third lumbar vertebra (11 cm mark), as well as mixing/inflow at the level of the expected left and right renal veins (14–15 cm marks). Venogram with selected catheterization of the **(B)** left inferior and **(C)** superior renal veins confirms two separate regions of venous drainage on the left. **(D)** Postprocedure venogram demonstrates an inferior vena cava (IVC) filter placed below the level where the most inferior portion of the left renal vein enters the IVC.

Clinical Presentation

A patient presents with lower extremity deep venous thrombosis and recent trauma (anticoagulation is contraindicated) (**Fig. 238.1**).

Key Imaging Finding

Inferior vena cava (IVC) vascular anomaly/abnormality

Top 3 Differential Diagnoses

- **Circumaortic/retroaortic left renal vein.** A circumaortic left renal vein occurs when both the left renal vein and the infrarenal segment of the left supracardinal vein persist; a retroaortic renal vein occurs when only the left supracardinal vein persists. The circumaortic left renal vein is seen in 1.5 to 8.7% of the population; retroaortic left renal veins are reported in 1.8 to 2.4%. In the circumaortic variant, a vena cavagram demonstrates the renal vein passing anterior to the aorta with a normal course, whereas the persistent left supracardinal vein courses posterior to the aorta and enters the IVC more inferiorly (typically the L2 or L3 level). In the retroaortic variant, the left renal vein (persistent left supracardinal vein) also enters the IVC at a lower than expected level. A review of any prior cross-sectional imaging is useful. It is helpful to position the catheter tip within the left renal vein to best demonstrate these anatomical variants. These anomalies require filter placement inferior to the lower left renal vein IVC insertion. If the filter is placed above the insertion of these variant left renal veins, they serve as a collateral pathway for emboli to circumvent the filter, resulting in pulmonary embolism.
- **Megacava.** Megacava is defined when the IVC measures ≥28 mm. The incidence may be as high as 3%. Placement of a bird's nest filter within the infrarenal IVC or the placement of a filter within each common iliac vein would be required. A bird's nest filter has been placed in a 42 mm IVC.
- **Duplicated inferior vena cava.** A duplicated IVC occurs when the embryonic right and left supracardinal veins persist. This is seen in 0.2 to 3.0% of the population. The right IVC is usually larger. The left common iliac vein drains into the left IVC, which in turn typically drains into the left renal vein. A catheter cannot be positioned within the left common iliac vein from a right femoral approach, as there is no direct communication between the IVCs. However, the catheter can be advanced into the left common iliac vein from the left renal vein to demonstrate a duplicated IVC. When present, IVC filters must be placed in both IVCs. Alternatively, but less commonly, a single suprarenal filter can be placed. Placement of only a single infrarenal filter in the "normal" right IVC will not prevent contralateral pelvic and lower extremity emboli from reaching the lungs.

Additional Differential Diagnoses

- **Inferior vena cava thrombosis.** Free-floating iliofemoral or IVC thrombus has been associated with a significant rate of pulmonary embolism and is considered an indication for IVC filter placement. In patients with nonocclusive IVC thrombus, the filter must be placed superior/cranial to the thrombus within the IVC. A suprarenal IVC filter may be placed if there is IVC thrombosis extending above the level of the renal veins, thrombus in the infrarenal IVC that does not leave enough room for the filter between the thrombus and renal veins, or in the setting of renal vein thrombosis.

Diagnosis

Circumaortic left renal vein

✓ Pearls

- Prior to filter placement, look for caval anomalies, thrombus, size of the IVC, and location of renal veins.
- With circumaortic or retroaortic left renal veins, a filter must be placed below the most inferior renal vein.
- Megacava is defined as ≥28 mm; either a bird's nest or bilateral iliac vein filter must be placed.
- With a duplicated IVC, either a filter must be placed in each IVC, or a suprarenal filter must be placed.

Suggested Readings

Mejia EA, Saroyan RM, Balkin PW, Kerstein MD. Analysis of inferior venacavography before Greenfield filter placement. Ann Vasc Surg 1989;3(3):232–235

Case 239

Charlyne Wu

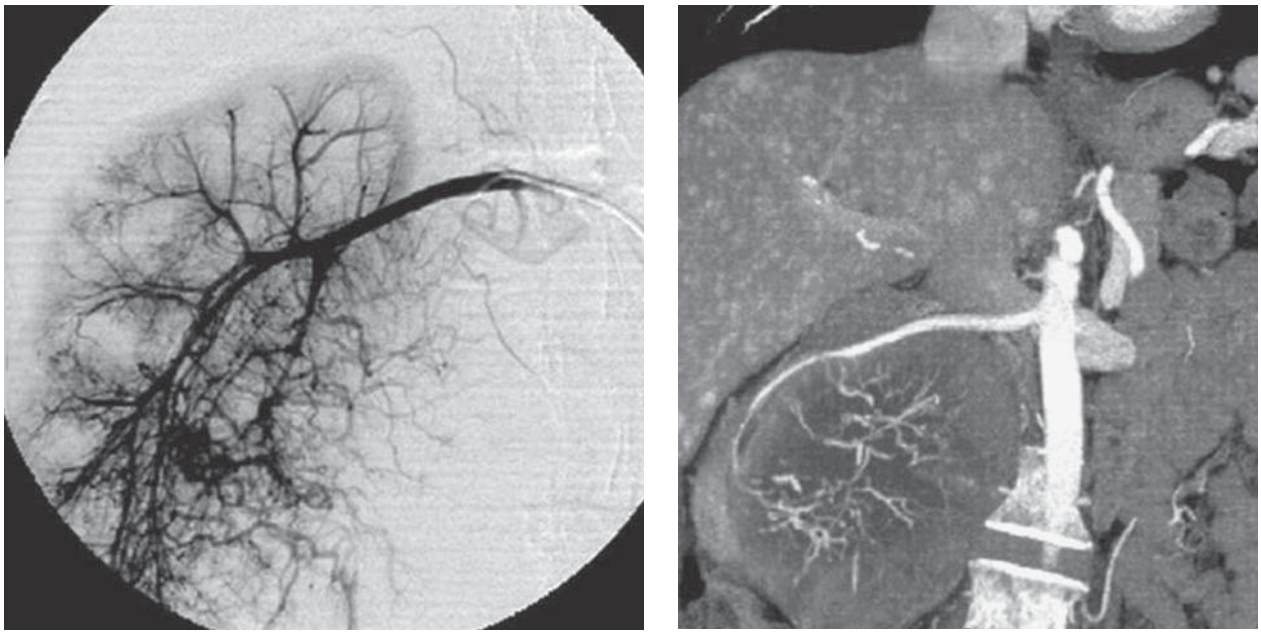


Fig. 239.1 **(A)** Digital subtraction angiography of the right kidney demonstrates a hypervascular mass with tumor neovascularity, particularly at the middle to lower pole. **(B)** Enhanced cortical phase, coronally reconstructed maximum intensity projection computed tomography image demonstrates a large right renal mass with central necrosis and neovascularity as reflected in **A**, along with multiple hypervascular hepatic metastatic lesions.

Clinical Presentation

A 50-year-old woman presents with hematuria (**Fig. 239.1**).

Key Imaging Finding

Hypervascular renal mass

Top 3 Differential Diagnoses

- **Renal cell carcinoma (RCC).** In adults, RCC comprises >80% of all malignant renal masses. It is more common in older men and may be multiple when associated with von Hippel–Lindau disease. Angiographically, RCC most often has prominent neovascularity (94%) and shunting with or without venous invasion. On computed tomography (CT), RCC presents as a hypervascular mass. When large, the masses may become centrally necrotic. The central hypodensity in these instances should not be confused with fat, as is seen in benign angiomyolipomas (AMLs). The typical indication for angiographic intervention is usually 24-hour preoperative embolization of the tumor or kidney to decrease intraoperative hemorrhage. Devascularization with smaller particles for peripheral embolization is preferred, provided no arteriovenous shunts are present. Otherwise, alcohol ablation with balloon occlusion catheter or coils may be used. Smaller RCCs can be treated with nephron-sparing surgery or radiofrequency/cryoablation. RCC commonly produces hypervascular hepatic metastases and lytic bone lesions.
- **Angiomyolipoma.** AMLs are benign hamartomatous lesions that contain fat, smooth muscle, and blood vessels. The typical patient is a woman between 30 and 60 years old. Multiple bilateral lesions are found in up to 80% of patients with tuberous sclerosis. Large lesions (>4 cm) are prone to acute spontaneous hemorrhage. On CT, a fat-containing mass originating from the kidney is virtually pathognomonic. Angiography demonstrates neovascularity and bizarre aneurysms without vascular shunting. Embolization with permanent particles or alcohol is an excellent alternative to resection.
- **Oncocytoma.** Oncocytomas are solid, benign renal neoplasms composed of oncocytes. They are usually asymptomatic, but they may present with hematuria, flank pain, and/or an abdominal mass, mimicking RCC. The lesions are typically large (>5 cm) at presentation and have a pseudocapsule. On CT, the lesions are hypervascular, and up to one third will have a central stellate scar. The classic angiographic finding is a "spoke-wheel" arrangement of tumor vascularity. Although the diagnosis may be suggested by imaging findings, there is significant overlap with the findings of RCC.

Additional Differential Diagnoses

- **Arteriovenous malformation/fistula (AVM/AVF).** AVMs are congenital and rare in the absence of Osler–Weber–Rendu disease. AVFs are almost always acquired from trauma or iatrogenic causes. Angiography demonstrates enlarged feeding arteries and early draining veins. Symptoms include hematuria, hypertension, flank pain, and, less commonly, spontaneous retroperitoneal hemorrhage. Treatment options include percutaneous embolization with coils, glue, or alcohol.

Diagnosis

Renal cell carcinoma

✓ Pearls

- RCC is the most common renal tumor in adults; it is hypervascular with neovascularity and shunting.
- Large AMLs (>4 cm) are prone to hemorrhage secondary to neovascularity and bizarre aneurysms.
- Oncocytomas are solid, benign renal neoplasms with a central scar and "spoke-wheel" pattern of vascularity.
- AVMs are rare congenital lesions; AVFs occur secondary to trauma, including iatrogenia.

Suggested Readings

Davidson AJ, Hartman DS, Choyke PL, Wagner BJ. Radiologic assessment of renal masses: implications for patient care. Radiology 1997;202(2):297–305

Federle MP. Diagnostic Imaging: Abdomen. Salt Lake City, UT: Amirsys; 2004

Israel GM, Bosniak MA. How I do it: evaluating renal masses. Radiology 2005;236(2):441–450

Kaufman JA, Lee MJ. Vascular and Interventional Radiology: The Requisites. Philadelphia: Elsevier; 2004:6–11, 337–346

Case 240

Matthew J. Moore

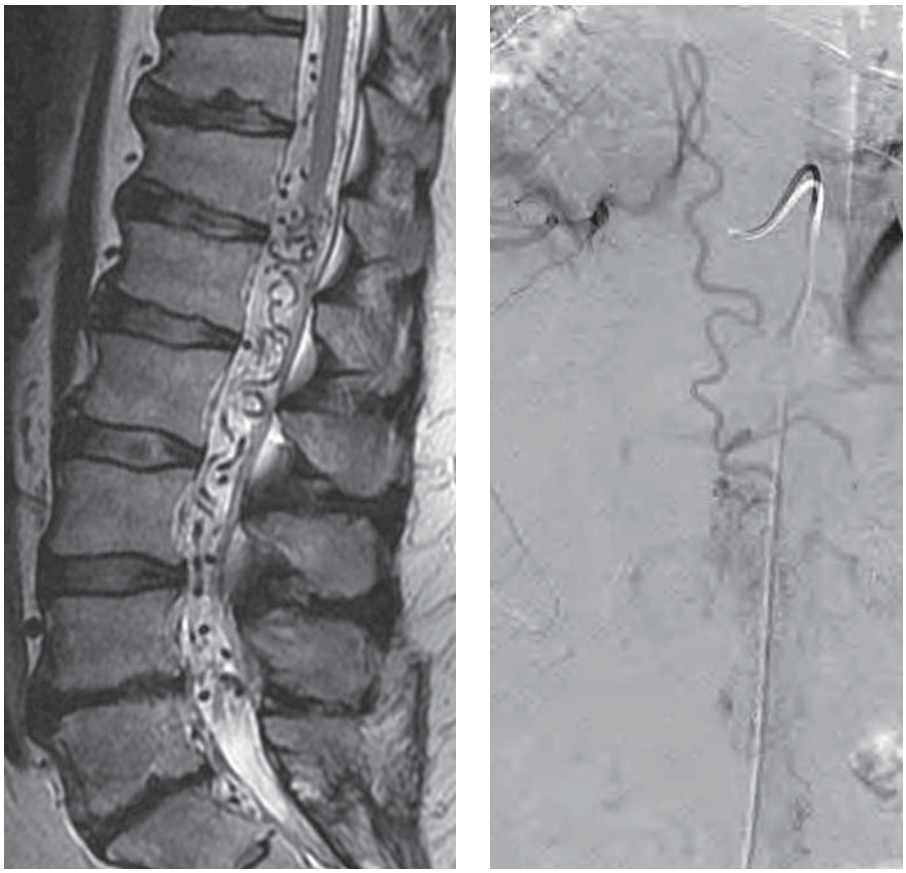


Fig. 240.1 **(A)** Sagittal T2-weighted magnetic resonance image demonstrates multiple serpentine extramedullary, intradural vascular flow voids in the lumbar spine. **(B)** Subsequent spinal digital subtraction angiogram image during the arterial phase of a right T10 intercostal artery injection reveals an enlarged anterior spinal artery with early filling of a plexus of intradural veins from arteriovenous shunting.

Clinical Presentation

A 55-year-old man presents with progressive lower extremity weakness (**Fig. 240.1**).

Key Imaging Finding

Prominent paraspinal flow voids

Top 3 Differential Diagnoses

- **Dural arteriovenous fistula (AVF).** There are four types of spinal arteriovenous shunt lesions. The most common (80%) is the type I dural AVF, which is a direct arteriovenous connection (no intervening nidus) within the spinal dura mater itself. The lesion drains into distended and enlarged pial veins, which are seen as extramedullary, intradural serpentine flow voids on sagittal T2-weighted magnetic resonance imaging (MRI) or multiple enhancing serpentine vessels on sagittal T1 contrast-enhanced MRI. There may also be "flame-shaped" cord edema with sparing of the periphery, best seen on T2-weighted MRI. The lesions cause intramedullary venous hypertension leading to chronic ischemia, which results in clinical symptoms. These lesions typically present in the 5th or 6th decade, more commonly in men, with progressive lower extremity weakness that is exacerbated by exercise. Spinal angiogram is the gold standard for accurate diagnosis and localization. Endovascular coiling is the treatment of choice. The type IV AVF or "perimedullary fistula" is the other true arteriovenous fistula, which may be indistinguishable from the type I dural AVF on MRI.
- **Spinal cord arteriovenous malformation (AVM).** The other two types of spinal arteriovenous shunting are the true AVMs with an intervening nidus. These type II and III AVMs will also present with vascular flow voids; however, you will see intramedullary in addition to extramedullary flow voids. Spinal type II AVMs are similar to brain AVMs. They commonly present with acute onset of symptoms due to subarachnoid hemorrhage. Type III, or juvenile AVMs, are rare lesions that occur in the 1st through 3rd decades. The AVM malformation has both intramedullary and extramedullary components.
- **Collateral venous flow from inferior vena cava (IVC) occlusion.** IVC occlusion may cause prominent collateral epidural or intradural veins. Look for a small or ill-defined IVC or metal artifact in the IVC region due to filter. Common etiologies of IVC occlusion are trauma, extrinsic compression, tumor invasion, and hypercoagulable states.

Additional Differential Diagnoses

- **Spinal cord neoplasm with increased vascular flow.** Spinal flow voids can be seen with several spinal cord neoplasms. Hemangioblastoma is classically an expansile intramedullary mass with serpentine flow voids, often associated with a syrinx or cystic component and an enhancing mural nodule. Ependymomas, paragangliomas, and schwannomas can also be seen with flow voids related to increased vascular flow.
- **Cerebrospinal fluid (CSF) pulsations.** Normal CSF pulsations are seen dorsal to the cord on T2-weighted MRI sequences. They have ill-defined margins that easily differentiate them from the well-defined vascular flow voids seen with spinal arteriovenous shunt lesions. The lack of corresponding abnormality on non-T2-weighted sequences allows for identification of this common artifact.

Diagnosis

Dural arteriovenous fistula (type I)

✓ Pearls

- Type I dural AVFs result in vascular shunting with chronic cord ischemia and progressive weakness.
- Spinal cord AVMs are similar to brain AVMs, with a vascular nidus and arteriovenous shunting.
- Collateral epidural and intradural veins may be seen with IVC occlusion, simulating an AVF or AVM.
- Hemangioblastomas, ependymomas, and neurogenic tumors may have prominent paraspinal flow voids.

Suggested Readings

Ross JS, Brant-Zawadski M, Moore KR, et al. Diagnostic Imaging: Spine. Salt Lake City, UT: Amirsys; 2005

Case 241

Matthew J. Moore

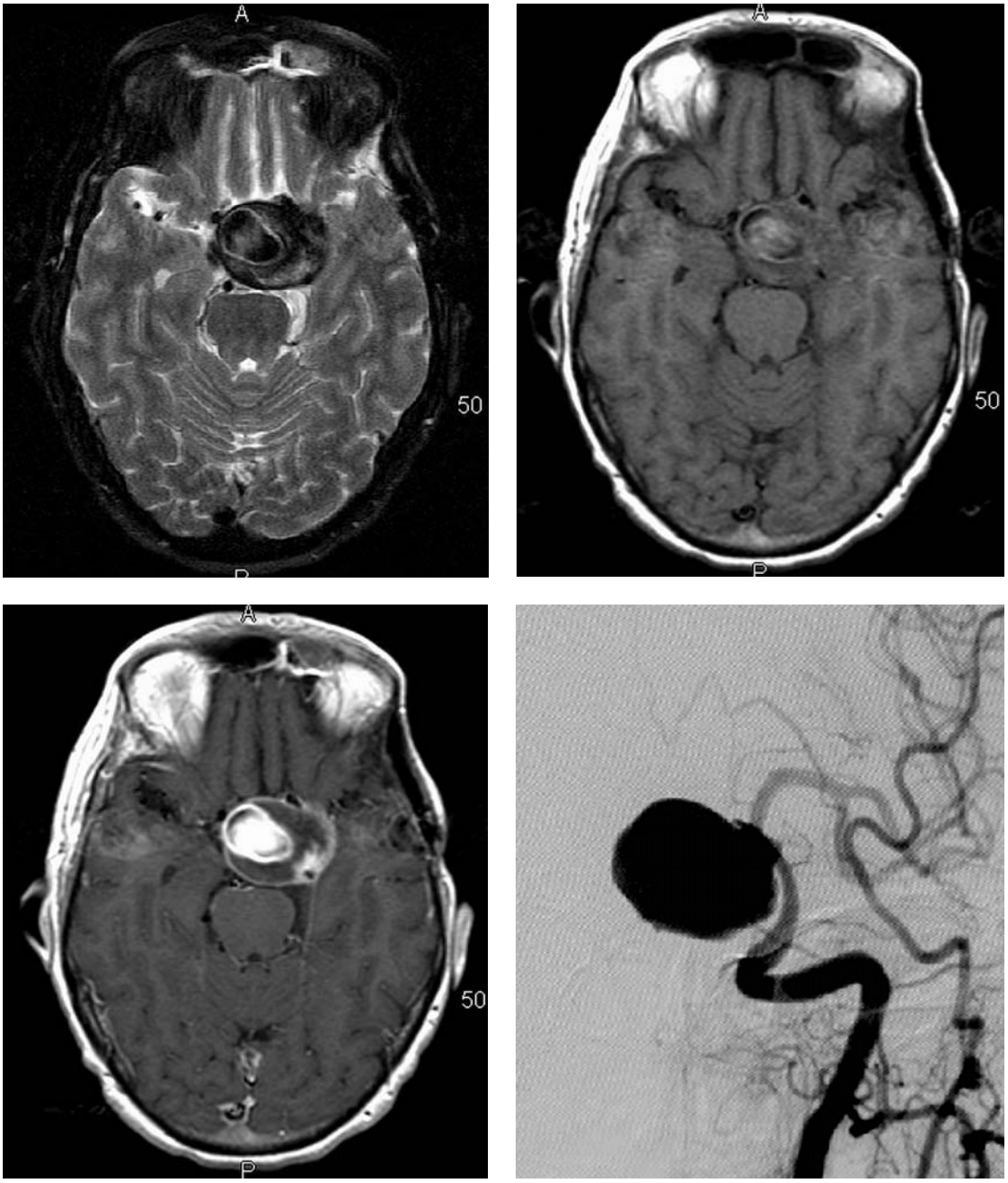


Fig. 241.1 **(A)** Axial T2-weighted image demonstrates a large, predominantly hypointense suprasellar mass eccentric to the left with regions of increased signal internally. **(B)** Axial T1 precontrast image reveals a predominantly iso- to hypointense suprasellar mass with a circumscribed region of increased T1 signal medially. **(C)** Axial T1 postcontrast image demonstrates intense enhancement along the medial aspect of the suprasellar mass, as well as peripheral enhancement. Both T1 images **(B,C)** show pulsation artifact in association with the mass. **(D)** Frontal projection from a left carotid angiogram reveals a large (giant) aneurysm involving the cavernous segment of the left internal carotid artery. (Courtesy of Thomas Tomsick, MD, University of Cincinnati.)

Clinical Presentation

A 57-year-old woman presents with headache and blurred vision (**Fig. 241.1**).

Key Imaging Finding

Suprasellar mass in an adult

Top 3 Differential Diagnoses

- **Pituitary macroadenoma.** Upward extension of a pituitary macroadenoma (>10 mm) from the sella is the most common cause of a suprasellar mass in adults. The best diagnostic clue is a sellar mass without a separate identifiable pituitary gland. The classic appearance is a "snowman" configuration due to impression on the mass by the diaphragma sella. The tumor is most commonly isodense to gray matter on computed tomography (CT) and isointense to gray matter on T1- and T2-weighted magnetic resonance imaging (MRI). Density or signal may be heterogeneous due to hemorrhage (10%), calcification (1–2%), or cystic change. Almost all macroadenomas enhance, usually heterogeneously. Look for internal carotid artery displacement. With cavernous sinus invasion, there can be carotid artery encasement (>180 degrees typically considered a sign of invasion). Malignant transformation is exceedingly rare, but macroadenomas can appear aggressive with skull base invasion. Peak age of onset is 20 to 40 years. Visual field defects or cranial nerve palsy may occur due to local mass effect. The treatment of choice is resection.
- **Craniopharyngioma.** Craniopharyngiomas are more common in children than adults. The classic pediatric case will present as a suprasellar mass with calcification and cystic change with rim or nodular enhancement. In adults older than 50 years, craniopharyngiomas are of the papillary subtype and present as a solid suprasellar mass without calcification.
- **Aneurysm.** Aneurysm of the parasellar internal carotid artery should always be considered when a suprasellar mass is identified. Aneurysms tend to be eccentric and not directly suprasellar in location. Look for a flow void and pulsation artifact on MRI. Calcification is more common than with pituitary adenomas. The pituitary gland will be seen separate from an aneurysm. CT, MR, or digital subtraction angiography can be used to characterize the aneurysm.

Additional Differential Diagnoses

- **Meningioma.** Meningiomas arising from the diaphragma sella can appear similar to a pituitary neoplasm; however, the pituitary gland will be identified separate from the mass. Look for the low MR signal line of the diaphragma sella between the mass (above) and the pituitary gland (below). Dural thickening due to meningioma is more extensive than with a pituitary macroadenoma. Meningiomas more commonly cause internal carotid artery narrowing with encasement than is seen with pituitary macroadenomas. Classically, there is avid, homogeneous enhancement with a dural tail. Calcification and adjacent hyperostosis may be seen. Meningiomas are usually hyperdense on CT with or without calcification.

Diagnosis

Aneurysm (partially thrombosed)

✓ Pearls

- Macroadenomas are the most common suprasellar masses in adults; a "snowman" configuration is classic.
- Craniopharyngiomas are solid in adults without calcification; in children, they are commonly calcified.
- Aneurysms must be considered with a suprasellar mass; look for flow voids and pulsation artifact.
- Meningiomas are commonly hyperdense and avidly enhance; calcification and hyperostosis may be seen.

Suggested Readings

Osborn AG, Salzman KL, Katzman G, et al. Diagnostic Imaging: Brain. Salt Lake City, UT: Amirsys; 2004

Case 242

Matthew J. Moore

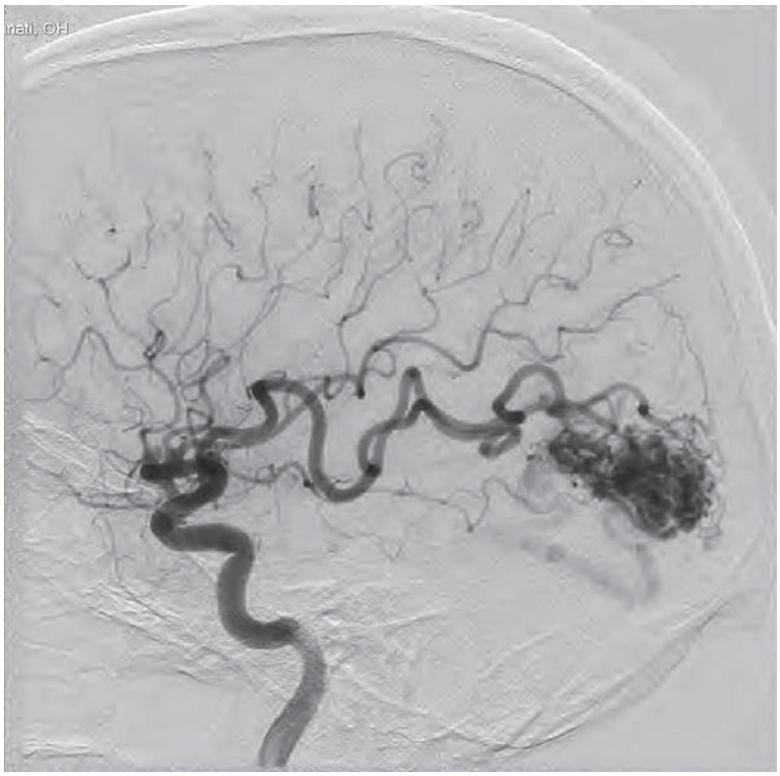


Fig. 242.1 Digital subtraction angiogram of an internal carotid artery injection during the late arterial phase demonstrates a large hypervascular mass in the occipital region supplied by enlarged arterial feeders. Notice the early venous opacification just below the mass due to arteriovenous shunting within the lesion.

Clinical Presentation

A 40-year-old man presents with headache lasting for 2 months (**Fig. 242.1**).

Key Imaging Finding

Hypervascular cerebral mass/abnormality

Top 3 Differential Diagnoses

- **Arteriovenous malformation (AVM).** AVM is a form of arteriovenous shunting with no intervening capillary network. The peak age of presentation is 20 to 40 years. The vast majority of AVMs become symptomatic during the patient's lifetime, with hemorrhage, seizures, and headaches representing the most common presentations. The vast majority are supratentorial and solitary. The best diagnostic clue is a cluster or tangle of flow voids on magnetic resonance imaging (MRI) with minimal or no mass effect. There is little or no intervening brain tissue. Fluid-attenuated inversion recovery imaging may show high signal due to gliosis. AVMs demonstrate avid enhancement. Complete characterization is obtained with digital subtraction angiography (DSA), which will define the arterial supply, the size of the nidus, and the location of venous drainage. The Spetzler–Martin classification system determines the operative risk and is based on the AVM's size, location, and venous drainage pattern. Treatment options include transarterial embolization, stereotaxic radiosurgery, and microvascular surgery.
- **Hypervascular tumor.** A hypervascular tumor, such as a glioblastoma multiforme (GBM) or a meningioma, will demonstrate avid enhancement. However, unlike an AVM, a hypervascular tumor will tend to have edema and mass effect. GBMs can have MRI flow voids from neovascularity, but they will tend to show some brain parenchyma between the flow voids. DSA of a hypervascular tumor will show a prominent tumor blush. Rarely, a GBM may mimic an AVM with early draining veins on DSA due to intralesional shunting. Meningioma on DSA will show a "sunburst" or radial appearance with a prolonged vascular stain. This is termed the "mother-in-law" sign, meaning the enhancement "comes early and stays late."
- **Aneurysm.** A patent intracranial aneurysm can be seen as a well-delineated round, extra-axial mass slightly hyperdense to the brain, particularly if partially thrombosed or calcified. Aneurysms show strong enhancement when patent. On MRI, 50% have a flow void, and 50% have heterogeneous signal. Computed tomography, magnetic resonance, and digital subtraction angiography can be used to identify an aneurysm. Ninety to 95% of aneurysms arise from the circle of Willis. The classic clinical profile is a middle-aged patient with the "worst headache of my life" related to aneurysm rupture with subarachnoid hemorrhage. Cranial neuropathy (especially cranial nerve III) and seizure are less common presentations. Treatment options include endovascular coiling and craniotomy with aneurysm clipping.

Additional Differential Diagnoses

- **Moyamoya disease.** Moyamoya refers to an idiopathic, progressive narrowing of the distal internal carotid artery and proximal circle of Willis with secondary formation of multiple collaterals. The moyamoya, or "puff of smoke" appearance, of cloudlike lenticulostriate and thalamostriate collaterals is seen on MRI and angiography. There is a bimodal age distribution, with peaks in the 1st and 4th decades of life.

Diagnosis

Arteriovenous malformation

✓ Pearls

- AVMs have an arterial supply, a nidus of vessels, and enlarged draining veins without a capillary network.
- AVMs present with headache or hemorrhage; they are classified by size, location, and venous drainage.
- GBMs and meningiomas may have flow voids from neovascularity, as well as arteriovenous shunting.
- Moyamoya disease refers to collateral vessel formation secondary to internal carotid artery occlusion.

Suggested Readings

Osborn AG, Salzman KL, Katzman G, et al. Diagnostic Imaging: Brain. Salt Lake City, UT: Amirsys; 2004

Yoon HK, Shin HJ, Chang YW. "Ivy sign" in childhood moyamoya disease: depiction on FLAIR and contrast-enhanced T1-weighted MR images. Radiology 2002;223(2):384–389

Case 243

Wayne L. Monsky

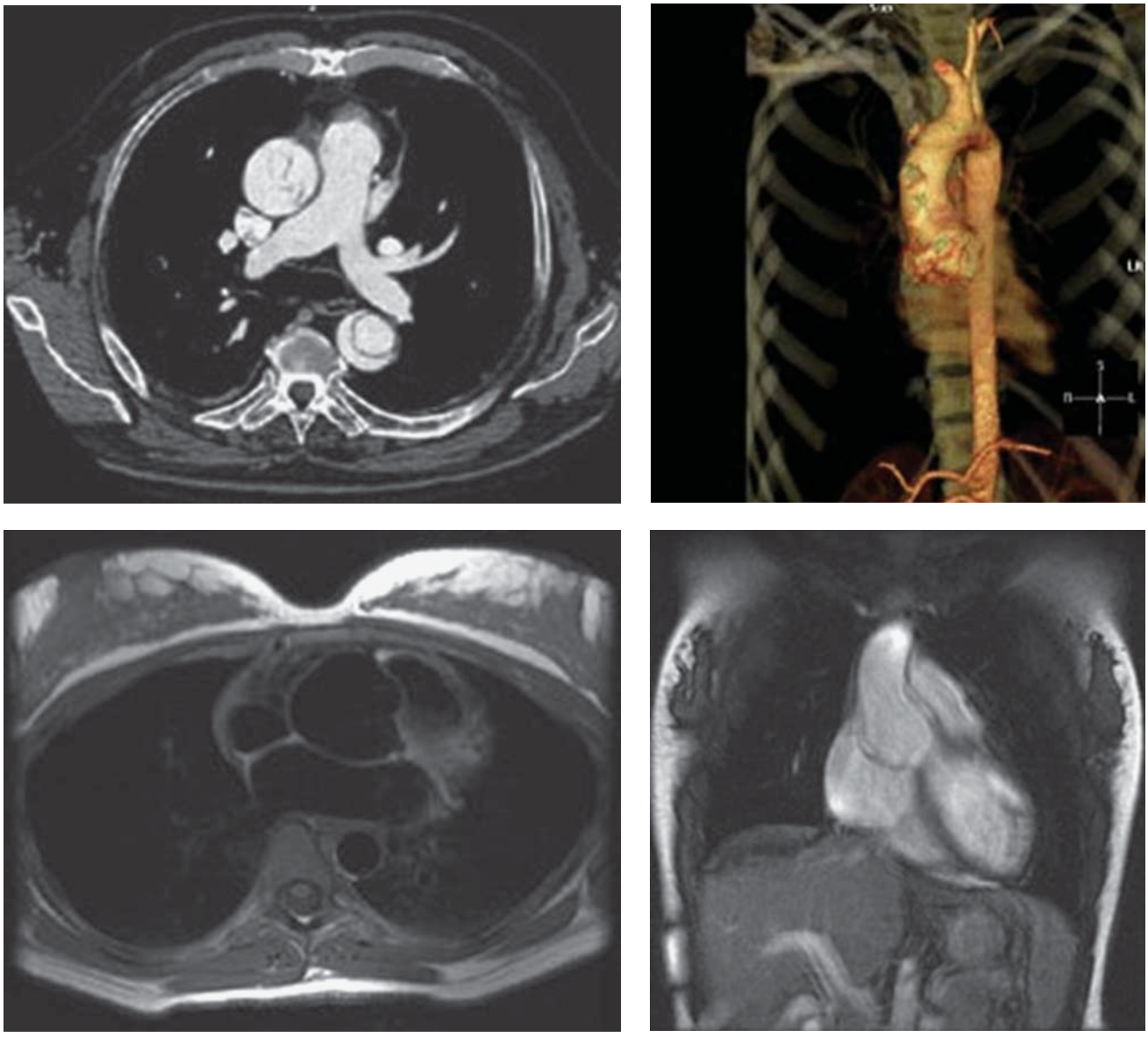


Fig. 243.1 **(A)** Contrast-enhanced axial image through the chest in the soft tissue window demonstrates an intimal flap within both the ascending and descending aorta. **(B)** Frontal surface-rendered computed tomography angiography image demonstrates enlargement of the aortic root/anulus and proximal ascending aorta. The thorax is elongated and narrowed. **(C)** Axial T1-weighted spin echo and **(D)** coronal spoiled gradient recalled images show dilation of the aortic anulus and root, measuring up to 47 mm. Slight aortic insufficiency may be seen.

Clinical Presentation

A pregnant woman presents with mild chest pain and early midsystolic blowing, decrescendo, and flow murmur auscultated over the right upper sternal border (**Fig. 243.1**).

Key Imaging Finding

Aortic dissection

Top 3 Differential Diagnoses

- **Hypertension.** Hypertension is the most common cause of aortic dissection and typically occurs in men between 50 and 70 years of age. Poorly controlled hypertension results in intimal tearing that may progress to dissection. Patients present acutely with chest pain that radiates to the back. Involvement of the ascending aorta (Stanford A) requires surgical or endovascular intervention; dissections involving only the descending aorta (Stanford B) are treated medically in the absence of end-organ ischemia.
- **Trauma.** Thoracic aortic injury from blunt chest trauma typically occurs at the aortic isthmus, just distal to the left subclavian artery, and at the level of the diaphragm. Aortic root injuries are usually fatal. Imaging findings include a widened mediastinum, blurring of the aortic shadow, left apical cap, right tracheal deviation, wide paraspinal lines and right paratracheal stripe, blood in the mediastinum, deformed aortic contour, intimal flaps and debris, and pseudoaneurysm. Frank extravasation is rare.
- **Connective tissue disease.** Connective tissue diseases, such as Ehlers–Danlos syndrome, affect the aortic media. Ehlers–Danlos syndrome may feature arterial, intestinal, and uterine fragility. Vascular rupture or dissections are common presenting signs in the majority of cases. Arterial rupture may be preceded by aneurysm, arteriovenous fistulas, or dissection, which may be seen with magnetic resonance (MRA), computed tomography (CTA), or conventional angiography.

Additional Differential Diagnoses

- **Annuloaortic ectasia (cystic medial necrosis).** Degeneration of the connective tissue of the aortic media results in cystic medial necrosis, leading to dilatation of the ascending aorta and aortic anulus with aortic insufficiency, as seen in Marfan syndrome. Congestive heart failure and aortic dissection are frequent complications. Dissection usually involves the entire length of the aorta, DeBakey type I/Stanford type A. Imaging findings of Marfan syndrome include an elongated narrow thorax; cardiomegaly; enlargement of the sinus of Valsalva, aortic root (>35 mm) and proximal ascending aorta; and aortic or mitral regurgitation.
- **Bicuspid aortic valve.** A bicuspid aortic valve is a common congenital anomaly that is more common in men. Abnormal valve leaflet morphology results in early degeneration, leading first to stenosis followed in some instances by valve incompetence. Patients with a bicuspid aortic valve are at higher risk of aortic aneurysms and dissection. MRA, CTA, and conventional angiography can demonstrate the bicuspid valve.
- **Coarctation of the aorta.** Aortic coarctation is a congenital anomaly that results in eccentric narrowing and infolding of the aorta adjacent to the left subclavian artery and stenosis to the left ventricular outflow. It may be associated with a bicuspid aortic valve, aortic aneurysms, dissection, and congenital heart disease. Imaging findings include inferior rib notching due to enlarged intercostal arteries providing collateral blood flow. A "figure 3" aortic appearance results from stenosis and dilatation of the aorta.

Diagnosis

Annuloaortic ectasia (Marfan syndrome)

✓ Pearls

- Hypertension and trauma are the most common causes of aortic dissection.
- Stanford A (ascending aorta involved) lesions are managed surgically; Stanford B lesions are managed medically.
- Annuloaortic ectasia, connective tissue disease, bicuspid aortic valve, and aortic coarctation have increased risk of aortic dissection.

Suggested Readings

Kuhlman JE, Pozniak MA, Collins J, Knisely BL. Radiographic and CT findings of blunt chest trauma: aortic injuries and looking beyond them. Radiographics 1998;18(5):1085–1106, discussion 1107–1108, quiz 1

Tatli S, Yucel EK, Lipton MJCT. CT and MR imaging of the thoracic aorta: current techniques and clinical applications. Radiol Clin North Am 2004;42(3):565–585

Case 244

Charlyne Wu

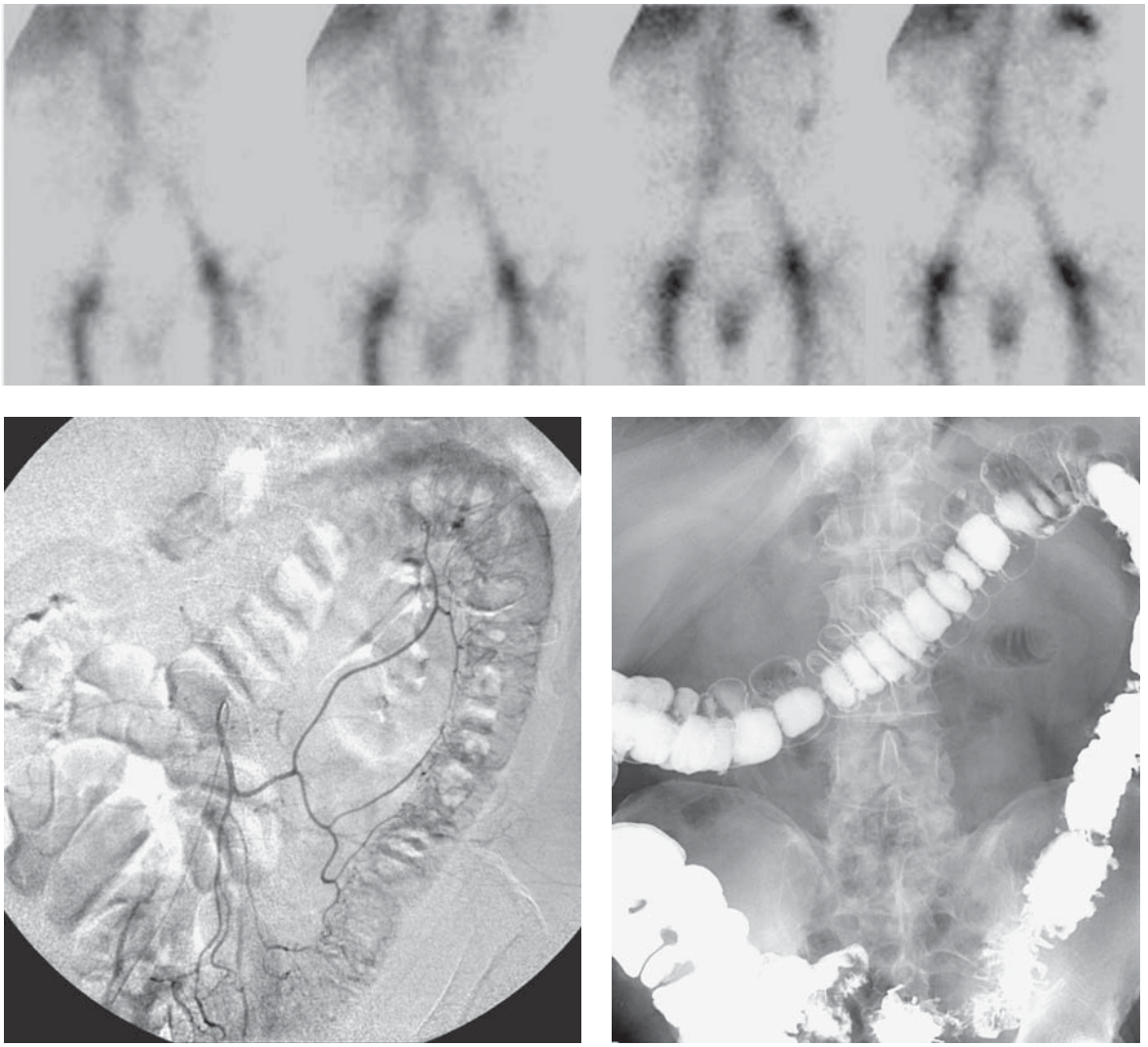


Fig. 244.1 **(A)** Sequential images from a technetium 99m–labeled red blood cell scan demonstrate extravasated activity within the left upper quadrant. Continued imaging demonstrates transit of intraluminal activity in a pattern consistent with active bleeding from the splenic flexure. **(B)** Digital subtraction angiography of the inferior mesenteric artery reveals extravasation of contrast at the splenic flexure. **(C)** Postevacuation barium enema shows en face diverticula with pooling barium (ring shadow) at the splenic flexure and additional diverticula pointing away from the bowel wall ("bowler hat" sign) at the sigmoid colon.

Clinical Presentation

A 57-year-old man with intermittent lower gastrointestinal (GI) bleeding over several years now presents with bright red blood per rectum and light-headedness (**Fig. 244.1**).

Key Imaging Finding

Lower GI bleeding

Top 3 Differential Diagnoses

- **Diverticulosis.** The most common cause of symptomatic lower GI bleeding is diverticulosis (30–50%), which usually presents with hematochezia. Most diverticula are in the left colon; however, most bleeding diverticula are in the right colon. Both scintigraphy (technetium 99m [Tc99m] red blood cell and Tc99m sulfur colloid) and angiography demonstrate extravasation of activity or contrast, respectively. On barium enema, a diverticulum may mimic a polyp. En face there is a round barium collection appearing as a ring shadow. The "bowler hat" sign refers to the dome of the hat pointing away from the bowel wall, as opposed to toward the lumen, as would be expected in a polyp. Because scintigraphy is more sensitive than angiography at identifying GI bleed (0.1 mL/min vs 1.0 mL/min), it is the initial diagnostic procedure of choice for hemodynamically stable patients. For hemodynamically unstable patients, angiography is best for diagnosis and possibly treatment. Treatment first involves fluid resuscitation and correction of any underlying coagulopathies. Most patients will stop bleeding after conservative management. Colonoscopy and angiography are therapeutic options for hemodynamically stable patients who fail conservative management. For hemodynamically unstable patients, embolization (typically Gelfoam, coils, or vasopressin infusion) or surgery is considered.
- **Neoplasm.** Both neoplasm, specifically colon carcinoma, and postpolypectomy bleeding account for ~20% of cases of lower GI bleeding. Once the patient is stabilized and the bleeding has been treated, proper colorectal cancer screening should be verified or performed.
- **Angiodysplasia.** Colonic angiodysplasias are reported to be responsible for ~5 to 10% of cases of acute lower GI bleeding. These are arteriovenous malformations of mucosa and submucosa, the majority at the cecum and ascending colon, as well as in the small bowel. An association with various systemic diseases has been described; these diseases include aortic stenosis, von Willebrand disease, chronic obstructive pulmonary disease, cirrhosis, chronic renal disease, and collagen vascular disease. On angiography, there is a cluster or tangle of small arteries in the arterial phase with early filling and delayed emptying of dilated veins.

Additional Differential Diagnoses

- **Focal colitis.** Focal colitis, typically from inflammatory, infectious, ischemic, or radiation insult, accounts for ~20% of cases of lower GI bleeding. Treatment is often medical and directed at the underlying cause of the bleeding. If severe, endoscopic, endovascular, or surgical treatment may be necessary.

Diagnosis

Diverticulosis

✓ Pearls

- Lower GI bleeds are first evaluated by scintigraphy, followed by angiography if positive for active bleed.
- Diverticulosis is the most common cause of lower GI bleed; most bleeding diverticula are on the right.
- Colon carcinoma may present with a lower GI bleed, or bleeding may occur due to polypectomy.
- Angiodysplasia involves the right colon and demonstrates early filling of dilated veins during the arterial phase.

Suggested Readings

Bunker SR, Lull RJ, Tanasescu DE, et al. Scintigraphy of gastrointestinal hemorrhage: superiority of 99mTc red blood cells over 99mTc sulfur colloid. AJR Am J Roentgenol 1984;143(3):543–548

Federle MP. Diagnostic Imaging: Abdomen. Salt Lake City, UT: Amirsys; 2004

Tew K, Davies RP, Jadun CK, Kew J. MDCT of acute lower gastrointestinal bleeding. AJR Am J Roentgenol 2004;182(2):427–430

Zuckerman GR, Prakash C. Acute lower intestinal bleeding: 2. Etiology, therapy, and outcomes. Gastrointest Endosc 1999;49(2):228–238

Case 245

Wayne L. Monsky

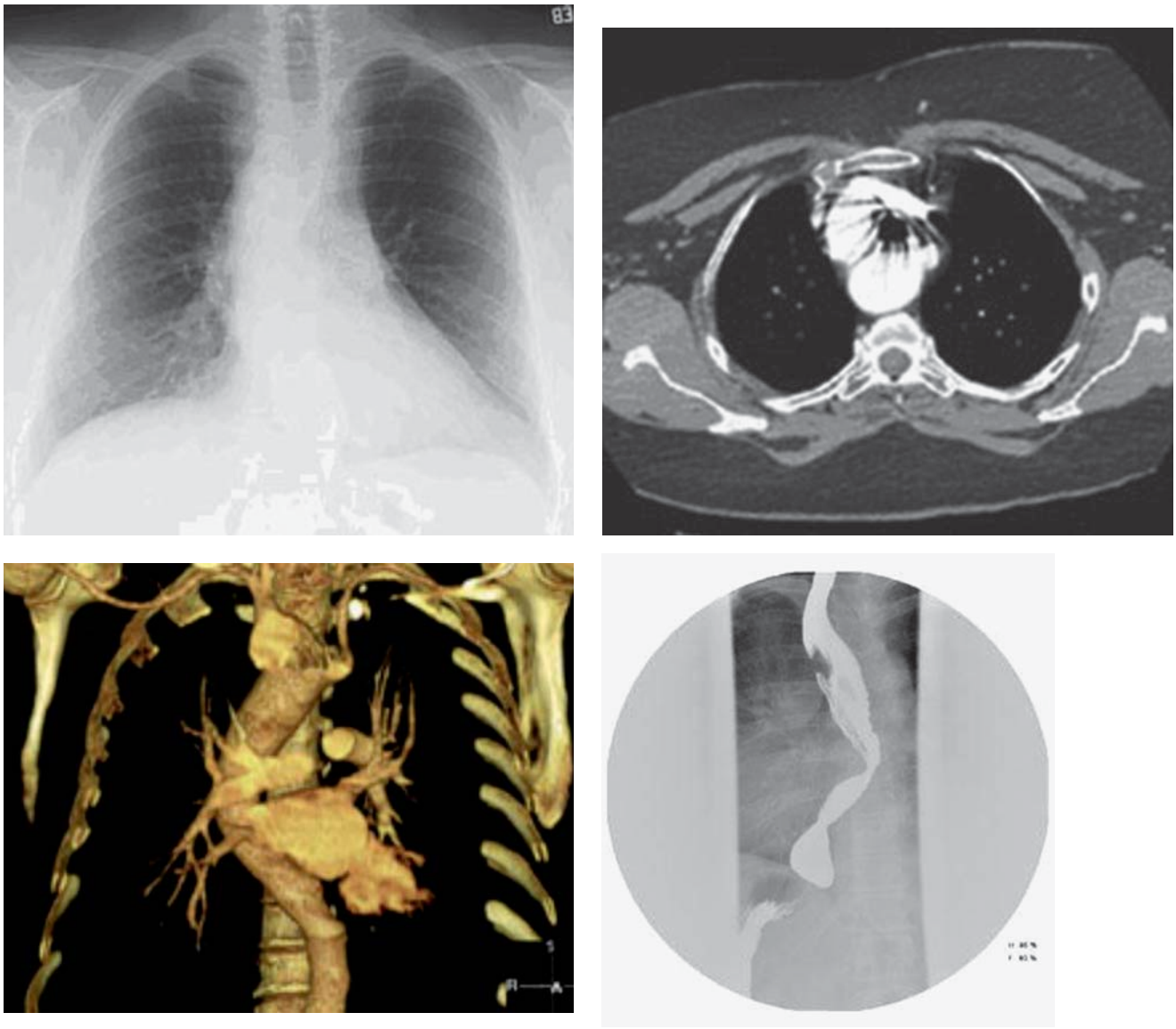


Fig. 245.1 **(A)** Frontal chest radiograph reveals a right-sided aortic arch with an ectatic tortuous thoracic aorta. **(B)** Axial enhanced computed tomography (CT) image demonstrates the right-sided aortic arch and depicts the origin of the left subclavian artery from a retroesophageal diverticulum (diverticulum of Kommerell). **(C)** Frontal three-dimensional surface-rendered CT angiographic image demonstrates a right-sided aortic arch and the left subclavian artery originating as the last branch of the aortic arch (distal to the right subclavian artery) and arising from the protuberant diverticulum of Kommerell. **(D)** Frontal esophagogram demonstrates the esophagus to be tortuous, with distortion and effacement produced by the patient's right-sided aortic arch.

Clinical Presentation

A patient presents with worsening dysphasia (**Fig. 245.1**).

Key Imaging Finding

Vascular ring/sling

Top 3 Differential Diagnoses

- **Aberrant right subclavian artery.** A left aortic arch with aberrant right subclavian artery occurs with a frequency of 0.4 to 2.0%. It results from involution of the embryonic aortic segment between the right subclavian and common carotid arteries. The right subclavian becomes the last aortic branch, reaching the right thorax by passing behind the trachea and esophagus in 85% and between them in 15% of cases. The majority of cases are asymptomatic, although dysphagia (dysphagia lusoria) may occur.
- **Double aortic arch.** A double aortic arch accounts for 40% of all thoracic vascular rings. It is caused by persistence of the right and left fourth branchial arches and is rarely associated with congenital heart disease. The aortic arches pass on both sides of trachea, joining posteriorly behind the esophagus and anteriorly in front of the trachea. The vascular ring produces tracheal and/or esophageal compression with possible airway compromise and dysphagia. Imaging findings include a right arch that is higher and larger than the left. An esophagogram shows the reverse S pattern, with bilateral esophageal impressions on frontal views and posterior impressions on lateral views. Angiography demonstrates the right arch supplying the right subclavian and right common carotid and the left arch supplying the left common carotid and subclavian arteries.
- **Right arch with aberrant left subclavian artery.** The most frequent branching pattern for a vascular ring with a right aortic arch is an aberrant left subclavian artery originating as the last branch of the aortic arch from a retroesophageal diverticulum of Kommerell. This occurs in 0.05 to 0.10% of the population. The ring is completed by a left-sided ligamentum arteriosum. A right aortic arch occurs when the right dorsal aorta remains patent, and the left dorsal aorta regresses abnormally. Vascular rings encircle the trachea and/or esophagus and may cause esophageal compression and dysphagia. Cardiac defects, such as tetralogy of Fallot, occur in 5 to 10%. Radiographic findings include the presence of a right aortic knob, slight leftward deviation of the lower trachea, and posterior indentation of the trachea. An esophagogram may show a right-sided indentation of the esophagus and posterior indentation of the esophagus. Cross-sectional imaging and angiography demonstrate the right arch and aberrant left subclavian artery arising from the protuberant diverticulum of Kommerell, which should not be mistaken for a pseudoaneurysm.

Additional Differential Diagnoses

- **Pulmonary sling.** Five percent of thoracic vascular rings are due to a pulmonary artery sling. The left pulmonary artery arises from the posterior aspect of the right pulmonary artery and passes between the trachea and the esophagus to reach the left hilum. The left pulmonary artery thus forms a sling around the distal trachea and the proximal right main bronchus. There may be associated malformations of the bronchotracheal tree, as well as cardiovascular abnormalities. This may mimic a mediastinal mass on chest radiographs. Computed tomography or magnetic resonance imaging may establish the diagnosis.

Diagnosis

Right aortic arch with aberrant left subclavian artery

✓ Pearls

- The majority of aberrant right subclavian arteries pass posterior to the esophagus and are asymptomatic.
- A double aortic arch joins posteriorly behind the esophagus and anteriorly in front of the trachea.
- Right arch with aberrant left subclavian artery is a complete ring, causing tracheal/esophageal compression.
- Pulmonary sling (left pulmonary artery arising from the right) passes between the trachea and the esophagus.

Suggested Readings

Castañer E, Gallardo X, Rimola J, et al. Congenital and acquired pulmonary artery anomalies in the adult: radiologic overview. Radiographics 2006;26(2):349–371

Case 246

William T. O'Brien Sr.

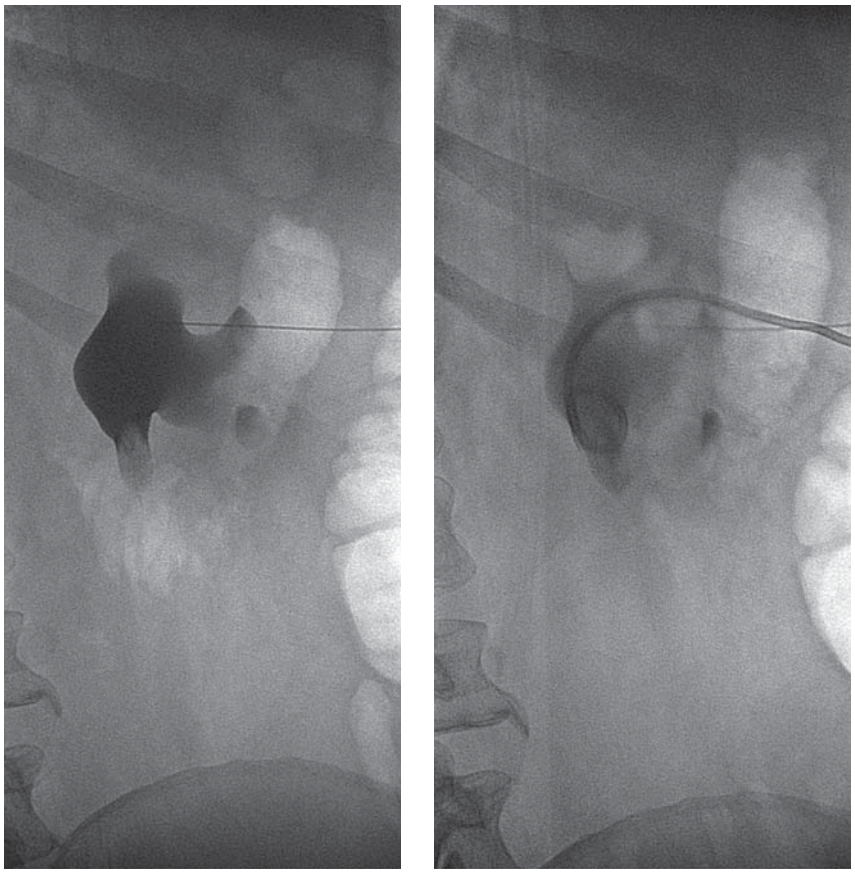


Fig. 246.1 **(A)** Percutaneous nephrogram demonstrates a large mass obstructing the proximal ureter with contrast within a dilated renal pelvis, consistent with obstruction. **(B)** Postprocedure image reveals placement of a percutaneous nephrostomy tube above the level of obstruction with decompression of the renal pelvis.

Clinical Presentation

A 48-year-old man presents with flank pain and fever (**Fig. 246.1**).

Key Imaging Finding

Urinary obstruction

Top 3 Differential Diagnoses

- **Nephrolithiasis.** Nephrolithiasis is the most common cause of urinary tract obstruction. Obstruction most often occurs at the ureterovesicular junction (UVJ) or ureteropelvic junction (UPJ). Computed tomography (CT) is useful at identifying the vast majority of stones, which are typically radiopaque. As a general rule, obstructing stones ≤4 mm in size should pass, whereas stones ≥8 mm are unlikely to pass. Stones between 4 and 8 mm may or may not pass without intervention. Percutaneous nephrostomy is used to alleviate obstruction in an infected system, which is a medical emergency, or used in conjunction with treatment of larger stones. The procedure is typically performed with ultrasound guidance. An inferior or middle posterior calyx is accessed via a posterolateral approach to minimize the risk of hemorrhage. A minimal amount of contrast is used to verify positioning, as excess manipulation of an infected system could lead to sepsis. The tract is then dilated, and a pigtail catheter (most common) is placed.
- **Neoplasm.** Transitional cell carcinoma (TCC) is the most common neoplasm to involve the renal collecting system; it arises from the urothelium. The urinary bladder is most commonly involved, followed by the renal pelvis and the ureters. When identified within the upper urinary tract, careful evaluation of the bladder should be performed to look for multifocal disease. Risk factors include smoking, exposure to aromatic amines, and cyclophosphamide. CT urography is useful for evaluation of the kidneys and the entire collecting system.
- **Blood clot.** Blood clots may occur within the collecting system due to trauma, stones, or tumors (TCC or renal cell carcinoma). Usually, they present as multiple ureteral filling defects that conform to the contour of the collection system. If large, they can cause obstruction. Treatment is directed at the cause of hemorrhage.

Additional Differential Diagnoses

- **Fungus ball.** Fungus balls tend to occur in immunocompromised patients or in those with indwelling urinary catheters. Most often, the findings consist of multiple filling defects within the ureter and/or bladder. Occasionally, obstruction may occur when the masses become coalescent. *Candida* is the most common organism.
- **Sloughed papillae.** Papillary necrosis may result from a variety of conditions, including diabetes, analgesic nephropathy, pyelonephritis (especially tuberculosis), sickle cell disease, urinary obstruction, and renal vein thrombosis. The necrotic papillae may become dislodged and result in obstruction of the collecting system. Identification of findings compatible with papillary necrosis in conjunction with filling defects within the collecting system helps suggest the diagnosis. Findings of papillary necrosis include the "lobster claw" and "ball on tee" signs secondary to abnormal contrast collections in the renal pyramids.

Diagnosis

Nephrolithiasis (with superimposed infection)

✓ Pearls

- Infection of an obstructed urinary system is a medical emergency requiring emergent decompression.
- Nephrolithiasis is the most common cause of urinary obstruction; the vast majority of cases are radiopaque.
- In general, stones ≤4 mm will pass without intervention, whereas those ≥8 mm will not.
- TCC is the most common urothelial neoplasm; be sure to evaluate the entire collecting system.

Suggested Readings

Barbaric ZL. Percutaneous nephrostomy for urinary tract obstruction. AJR Am J Roentgenol 1984;143(4):803–809

Zagoria RJ. Genitourinary Radiology: The Requisites. 2nd ed. Philadelphia: Mosby; 2004

Case 247

David D. Gover

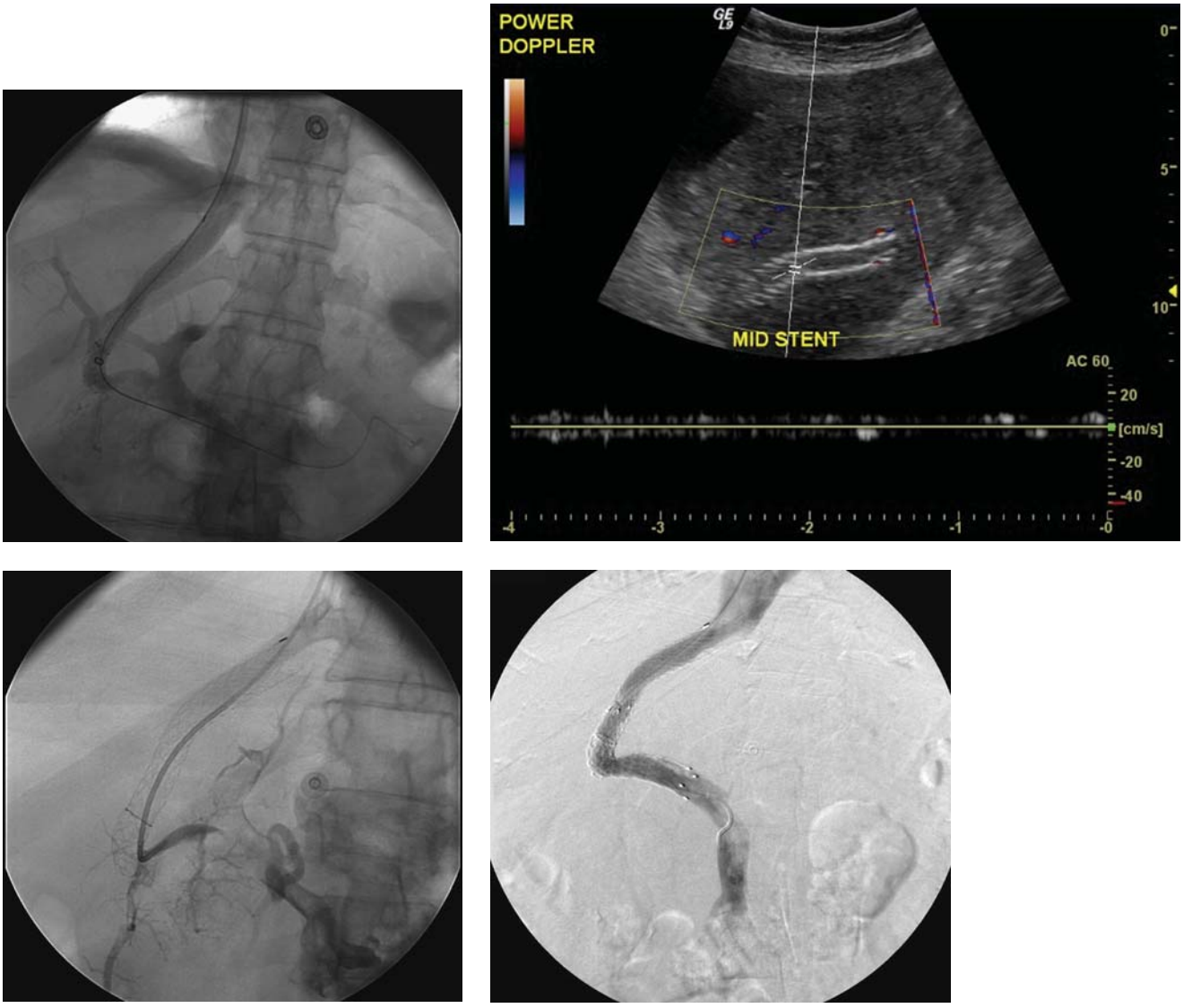


Fig. 247.1 **(A)** Angiogram of the right upper quadrant shows a transjugular intrahepatic portosystemic shunt (TIPS) using a stent graft. There are two "right" portal veins (to segments 5/6 and 7/8). The stent graft connects the segment 5/6 portal vein to the right hepatic vein. Note the irregular stenosis of the segment 5/6 portal vein immediately after bifurcation with the main portal vein. **(B)** The initial follow-up ultrasound, done on postprocedure day 5, shows no flow in the TIPS, which is confirmed **(C)** on angiography. Findings are consistent with acute thrombosis of the portal vein and TIPS. **(D)** Digital subtraction angiography after thrombolysis and extension of the stent into the portal system shows resumption of flow in the main portal vein and TIPS with resolution of the areas of stenoses.

Clinical Presentation

A 71-year-old woman presents with alcoholic end-stage liver disease and refractory hepatic hydrothorax despite a transjugular intrahepatic portosystemic shunt (TIPS) procedure. **Fig. 247.1A** is from the initial TIPS procedure; **Fig. 247.1B,C** are follow-up studies; **Fig. 247.1D** is postintervention.

Key Imaging Finding

TIPS dysfunction

Top 3 Differential Diagnoses

- **Neointimal hyperplasia.** Growth of the intima occurs due to the alterations in blood flow and the presence of a stent, slowly leading to luminal ingrowth and return of the portosystemic gradient (PSG). This effect is somewhat mitigated when stent grafts are used instead of bare metal stents. At follow-up, recurrence of symptoms (e.g., enlarged varices or recurrent ascites) is the best indicator of TIPS dysfunction. Ultrasonography traditionally has had a role in TIPS surveillance but is not sensitive. Most institutions will perform a baseline ultrasound, then at 1, 3, 6, and 12 months after the TIPS procedure, followed by annual examinations. Doppler interrogation should evaluate for stent patency and possible stenosis with velocity and waveform analysis (specific for each vascular laboratory). Proposed ultrasound findings that suggest TIPS dysfunction are filling defects in the stent, velocity gradients across the shunt (with associated turbulence), marked increase or decrease in shunt velocities (especially relative to baseline), and changes in portal venous flow direction (relative to baseline). Doppler velocity changes necessitating TIPS venography include main portal venous velocity <50 cm/second, shunt velocity <50 or >150 cm/second, or a change in velocity (increase or decrease) from baseline of >50 cm/second. The presence of new varices or ascites should be noted on these exams; these findings require follow-up TIPS venography. Angioplasty or stent placement may be indicated to lessen the PSG to ≤12 mm Hg for bleeding esophageal varices. The target PSG for refractory ascites is less certain; some experts suggest ≤8 mm Hg depending on the degree of hepatic encephalopathy.
- **Thrombosis.** Occlusion of the shunt with clot can occur early after TIPS creation or as a late finding. Early on, thrombosis is most likely attributed to bile leak; venous stasis in conjunction with neointimal hyperplasia is a later finding. Patients can present with recurrence of symptoms, similar to TIPS stenosis. Alternatively, TIPS ultrasonography may discover the occlusion. Occlusions are treated with catheter-directed or mechanical thrombolysis and stent/stent graft revision with angioplasty or stent.
- **Technical error.** Early shunt occlusion may occur due to malposition or migration of stents. Injury to the portal system may also lead to occlusion or thrombosis. Careful technique and scrutiny of angiograms during placement of the shunt help reduce the incidence of technical error. Technical expertise has been shown to be important in successful placement of a TIPS; fatal complications are reduced when >150 shunts have been placed by the interventionalist (3.0% vs 1.4%).

Diagnosis

Technical error (portal venous injury)

✓ Pearls

- Neointimal hyperplasia is a common cause of TIPS dysfunction; abnormalities on ultrasound require venography.
- Ultrasound evaluation of TIPS should include interrogation of stent patency with velocity and waveform analysis.
- Shunt occlusion may be an early or late finding; patients often present with recurrent symptoms.
- Technical error may be secondary to malposition or migration of stents or due to vessel injury.

Suggested Readings

Boyer TD, Haskal ZJ. American Association for the Study of Liver Diseases Practice Guidelines: the role of transjugular intrahepatic portosystemic shunt creation in the management of portal hypertension. J Vasc Interv Radiol 2005;16(5):615–629

Carr CE, Tuite CM, Soulen MC, et al. Role of ultrasound surveillance of transjugular intrahepatic portosystemic shunts in the covered stent era. J Vasc Interv Radiol 2006;17(8):1297–1305

Case 248

Charlyne Wu

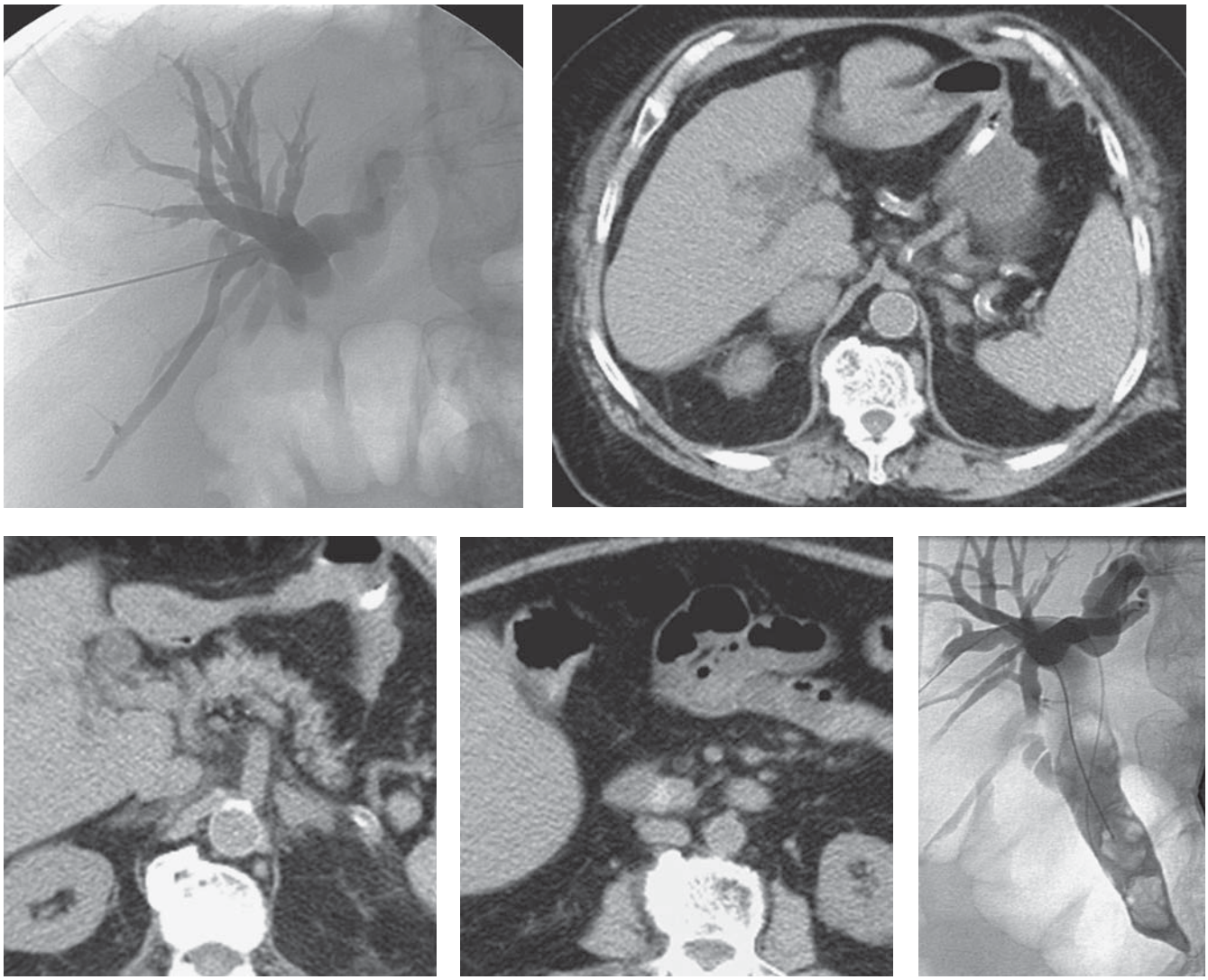


Fig. 248.1 **(A)** Percutaneous transhepatic cholangiogram (PTC) demonstrates diffusely dilated intrahepatic and extrahepatic biliary ducts with abrupt obstruction at the common bile duct. **(B)** Axial noncontrast computed tomography (CT) image reveals the "too many tubes" appearance of the dilated intrahepatic ducts. **(C)** Axial noncontrast CT image slightly more inferiorly demonstrates extrahepatic biliary ductal dilatation without pancreatic ductal dilatation. **(D)** Axial noncontrast CT image through the level of the distal common bile duct shows a hyperdense focus at the junction of the duodenum, *d*, and the pancreas, *p*, in the region of the ampulla of Vater. **(E)** PTC with the catheter advanced beyond the area of obstruction demonstrates multiple filling defects along the course of the common bile duct, consistent with choledocholithiasis. (Courtesy of Bijan Bijan, MD.)

Clinical Presentation

An 87-year-old woman presents with multiple episodes of nausea accompanied by vomiting of gastric contents and decreased oral intake for 4 days (**Fig. 248.1**).

Key Imaging Finding

Biliary duct obstruction

Top 3 Differential Diagnoses

- **Choledocholithiasis.** Choledocholithiasis is responsible for 20% of cases of adult obstructive jaundice. Fluoroscopy and magnetic resonance cholangiopancreatography demonstrate filling defects and/or obstruction with dilatation of the more proximal biliary ducts. Ultrasound will reveal ductal dilatation and possibly cholelithiasis or choledocholithiasis, although bowel gas may obscure complete evaluation of the common bile duct. Computed tomography (CT) may demonstrate intraluminal masses of varying attenuation. A "bull's-eye," "target," or "crescent" sign describes a rim of low-attenuation bile surrounding the stone within the bile duct.
- **Cholangiocarcinoma.** Cholangiocarcinoma is the second most common malignant primary hepatic tumor. These malignancies arise from the epithelium of the biliary duct system. There are three main areas in which cholangiocarcinomas occur: intrahepatic, perihilar (Klatskin tumor), and distal extrahepatic. Perihilar tumors are the most common and are seen at the bifurcation of the right and left hepatic ducts. Abrupt stricture and thickening of the duct wall may be the only findings. The prognosis is poor, with <20% of tumors being resectable.
- **Pancreatic adenocarcinoma.** Pancreatic and ampullary carcinomas are the cause of 20 to 25% of adult biliary obstructions. Tumors arise from pancreatic ducts. The diagnosis is rarely made at an early stage due to the late presentation of obstructive symptoms. The role of imaging is to demonstrate the tumor, its relationship to the surrounding vasculature, and the possibility of curative resection. Imaging demonstrates abrupt obstruction of the common bile and/or pancreatic ducts ("double duct" sign). On CT a hypovascular mass can be seen associated with the pancreatic head (60%), body (20%), diffusely (15%), or tail (5%).

Additional Differential Diagnoses

- **Chronic pancreatitis.** Chronic pancreatitis is responsible for ~8% of cases of adult biliary obstruction. Recurrent inflammation, fibrosis, and inflammatory masses cause narrowing and strictures of the bile ducts. Alternating regions of pancreatic ductal narrowing and dilatation lead to the "chain of lakes" appearance. Pancreatic calcifications and atrophy are associated findings.
- **Primary sclerosing cholangitis (PSC).** PSC is characterized by insidious onset of jaundice with progressive disease, affecting both intra- and extrahepatic biliary ducts. It is associated with a history of ulcerative colitis in 50 to 70% of cases. Imaging demonstrates a characteristic beaded pattern of the intrahepatic biliary ducts. On cholangiography, ductal diverticula are pathognomonic. Complications include biliary cirrhosis and cholangiocarcinoma.
- **Parasites.** *Ascaris* and liver fluke eggs from *Clonorchis* can lead to biliary obstruction. Also consider *Opisthorchis.* Pharmacological treatment is the mainstay. Endoscopic sphincterotomy and extraction of parasites may alleviate symptoms in complex cases with biliary obstruction.

Diagnosis

Choledocholithiasis

✓ Pearls

- Choledocholithiasis is a common cause of obstructive jaundice in adults; ultrasound and CT are used for diagnosis.
- Cholangiocarcinoma arises from biliary ductal epithelium; lesions at the hilum are termed Klatskin tumors.
- Pancreatic carcinoma results in the classic "double duct" sign (biliary and pancreatic ductal dilatation).
- PSC is associated with ulcerative colitis; imaging findings include a beaded appearance of biliary ducts.

Suggested Readings

Federle MP. Diagnostic Imaging: Abdomen. Salt Lake City, UT: Amirsys; 2004

Han JK, Choi BI, Kim AY, et al. Cholangiocarcinoma: pictorial essay of CT and cholangiographic findings. Radiographics 2002;22(1):173–187

Case 249

Glade E. Roper

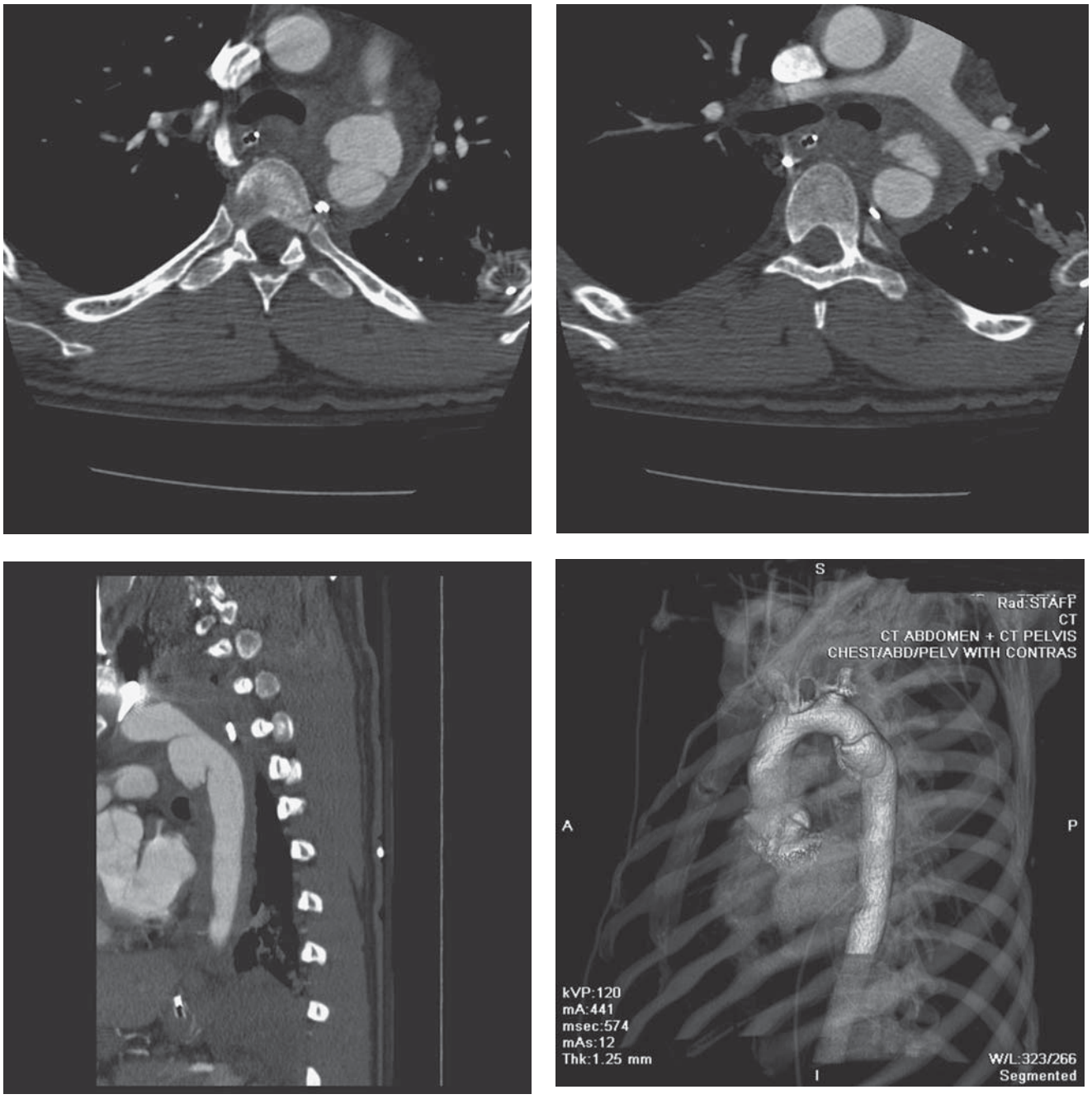


Fig. 249.1 Images from a computed tomography aortogram. **(A,B)** Coned-down axial images at the level of the aortic isthmus reveal focal irregularity of the aortic wall and a hypodense linear structure within the aortic lumen. Additional findings include a mediastinal hematoma and support tubes. **(C)** Sagittal maximum intensity projection image through the aorta and **(D)** three-dimensional reconstruction reveal a well-demarcated anterior bulge from the aortic isthmus. The bulge is 3 cm distal to the origin of the left subclavian artery.

Clinical Presentation

A 22-year-old restrained passenger in a high-speed automobile accident (**Fig. 249.1**).

Key Imaging Finding

Traumatic aortic injury

Top 3 Differential Diagnoses

- **Pseudoaneurysm.** The aortic wall is composed of three layers of tissue—the intima, composed of endothelium and basement membrane; the media, composed of elastic and muscular tissue; and the adventitia, composed of thin connective tissue. A tear of both the intima and the media results in a pseudoaneurysm, a bulge in the lumen of the aorta contained only by the adventitia or other mediastinal tissues. In patients who survive to receive medical attention, such a tear usually involves only a portion of the aortic circumference. Most aortic injuries occur near the ligamentum arteriosum. Radiographs may reveal an enlarged aortic contour and/or widened mediastinum. Contrast-enhanced computed tomography (CT) or angiography reveals focal irregularity or bulge of the aortic wall without an intimal flap. Often the injured aorta will be surrounded by hematoma on CT. The risk of pseudoaneurysm rupture is high, although delayed repair is an option in some patients. Management may include percutaneous stent graft placement in select patients. Surgical graft placement is often necessary due to the proximity of the great vessels.
- **Aortic dissection.** When an injury causes a defect in the intima, blood may enter the media of the artery at arterial pressure. The pressurized blood dissects through the tissue of the media, peeling the intima off the wall of the aorta. Radiographs may reveal enlarged aortic contour. Contrast-enhanced CT and angiography may reveal irregularity of the aortic lumen, an enlarged aorta, and an intimal flap. Aortic intimal calcifications may be displaced. Management depends on several factors, including the location of the dissection and its relationship to the great vessels. Some traumatic dissections are amenable to percutaneous stent graft placement, although dissections of the ascending aorta require urgent surgical management.
- **Intramural hematoma.** The aortic media layer contains vaso vasorum, blood vessels that supply the tissue of the aorta. Injury to these vessels causes bleeding into the wall of the aorta, resulting in an intramural hematoma. The intima is usually intact. Imaging findings include focal hyperdensity within the wall of the aorta on noncontrast CT and a focally thickened, nonenhancing aortic wall on contrast-enhanced CT. Transesophageal echocardiography and magnetic resonance imaging (MRI) are more accurate in making the diagnosis, revealing a curvilinear intramural mass with blood products. Angiography often fails to demonstrate the intramural hematoma. Current management is the same as that of aortic dissection, although there is a paucity of clinical trial data.

Additional Differential Diagnoses

- **Aortic transection.** When all three layers of the aortic wall are circumferentially torn, blood flows freely out of the aorta into the surrounding tissues. Such injuries are nearly always fatal. Eighty-five percent of patients with aortic injuries die before reaching the hospital. Emergent surgical repair is the only treatment option for patients who survive long enough to receive medical care.

Diagnosis

Aortic pseudoaneurysm

✓ Pearls

- Pseudoaneurysms are contained ruptures; prompt treatment (surgical or endovascular) is warranted.
- Dissections result from intimal injury with true and false lumens; treatment depends on the extent of injury.
- Intramural hematomas are hyperdense (CT) or hyperintense (MRI) collections within the vessel wall.
- Aortic transection results when all three layers of the aorta are torn; it is nearly always fatal.

Suggested Readings

Koenig TR, West OC. Diagnosing acute traumatic aortic injury with computed tomography angiography: signs and potential pitfalls. Curr Probl Diagn Radiol 2004;33(3):97–105

Rousseau H, Dambrin C, Marcheix B, et al. Acute traumatic aortic rupture: a comparison of surgical and stent-graft repair. J Thorac Cardiovasc Surg 2005;129(5):1050–1055

Case 250

David D. Gover

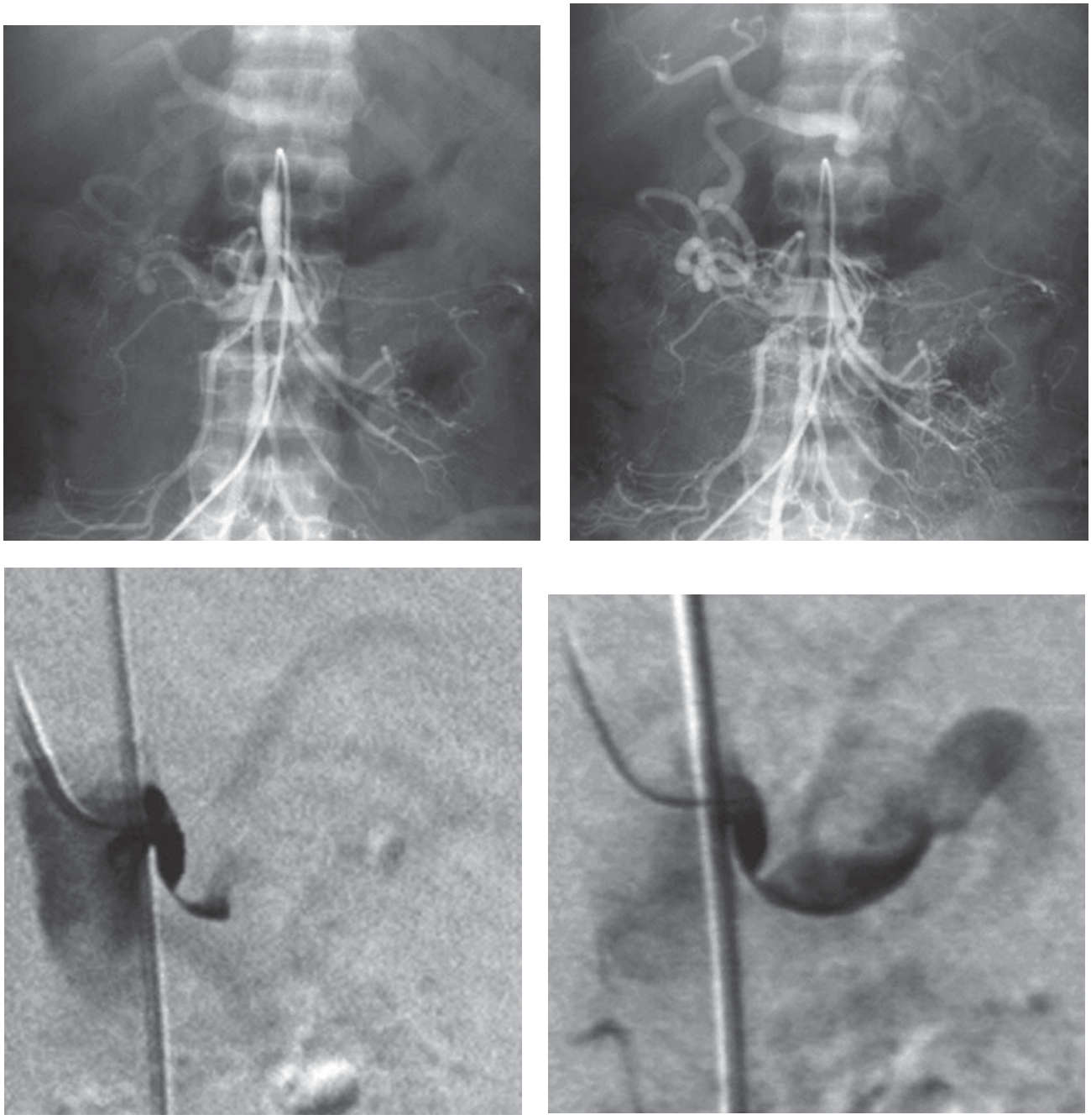


Fig. 250.1 Selective angiogram of the superior mesenteric artery both **(A)** early in the contrast run and **(B)** more delayed shows enlargement of the inferior pancreaticoduodenal and gastroduodenal arteries with retrograde filling of the celiac axis. **(C,D)** Two lateral views from a selective angiogram of the celiac axis confirm a severe origin stenosis with post-stenotic dilatation. The stenosis has an extrinsic bandlike appearance.

Clinical Presentation

A 33-year-old woman presents with vague, postprandial abdominal pain and weight loss (**Fig. 250.1**).

Key Imaging Finding

Celiac axis stenosis/occlusion

Top 3 Differential Diagnoses

- **Atherosclerosis.** Atherosclerosis is the most common cause of narrowing of the mesenteric vessel origins. Patients with atherosclerosis typically present at an older age, have irregularity of multiple vessels, and commonly have associated peripheral vascular disease and/or abdominal aortic aneurysm. Individuals with inadequate collateral circulation will usually present with intestinal ischemia (postprandial pain) and "food fear," leading to weight loss. Management usually involves angioplasty or stent placement over surgery.
- **Thromboembolism.** Thromboembolic disease is usually from a cardiac (atrial fibrillation) or proximal aortic source. The celiac axis is rarely affected in comparison to the superior mesenteric artery, cerebral circulation, or peripheral vessels. When intra-abdominal vessels are involved, patients usually present with acute mesenteric ischemia. Affected vessels may have a filling defect or be occluded. Treatment options are catheter-directed thrombolysis or open surgery in cases of bowel infraction.
- **Vasculitis.** Patients with vasculitis present with a multitude of clinical features, including constitutional symptoms. Vasculitis may be a primary syndrome (e.g., Takayasu arteritis) or secondary to underlying infection or malignancy. Treatment centers on corticosteroid administration for primary vasculitides. Catheter-directed treatments may be offered if end-organ involvement in the fibrotic phase of the disease is significant.

Additional Differential Diagnoses

- **Median arcuate ligament syndrome.** Median arcuate ligament syndrome typically affects thin women between 20 and 40 years of age who present with vague postprandial abdominal pain. A low insertion of the median arcuate ligament (a fibrous arch that unites the diaphragmatic crura on either side of the aortic hiatus) causes narrowing of the celiac axis. Angiography reveals an indentation along the superior aspect of the celiac axis, which is worse during expiration. Surgical decompression is the treatment of choice; however, there is controversy regarding treatment, as many patients have this abnormality without symptoms.
- **Fibromuscular dysplasia (FMD).** FMD most commonly occurs in younger, mostly female patients. Characteristic imaging findings include a beaded appearance secondary to alternating regions of stenosis and dilatation. Angioplasty is the primary treatment option.
- **Radiation.** Radiation changes usually lead to multiple, smooth, long-segment regions of vessel narrowing. Endoluminal treatments (e.g., stent placement) are the norm for symptomatic lesions.

Diagnosis

Median arcuate ligament syndrome

✓ Pearls

- Atherosclerotic and embolic disease constitutes most cases of mesenteric vessel stenosis or occlusion.
- Vasculitides (Takayasu arteritis) may cause narrowing of the aortic branch vessels; treatment is with steroids.
- Median arcuate ligament syndrome affects young, thin women who present with postprandial pain.

Suggested Readings

Horton KM, Talamini MA, Fishman EK. Median arcuate ligament syndrome: evaluation with CT angiography. Radiographics 2005;25(5):1177–1182

Kaufman JA, Lee MJ. Vascular and Interventional Radiology: The requisites. St. Louis: Mosby; 2003

Section XI Nuclear Medicine

Case 251

Kamal D. Singh

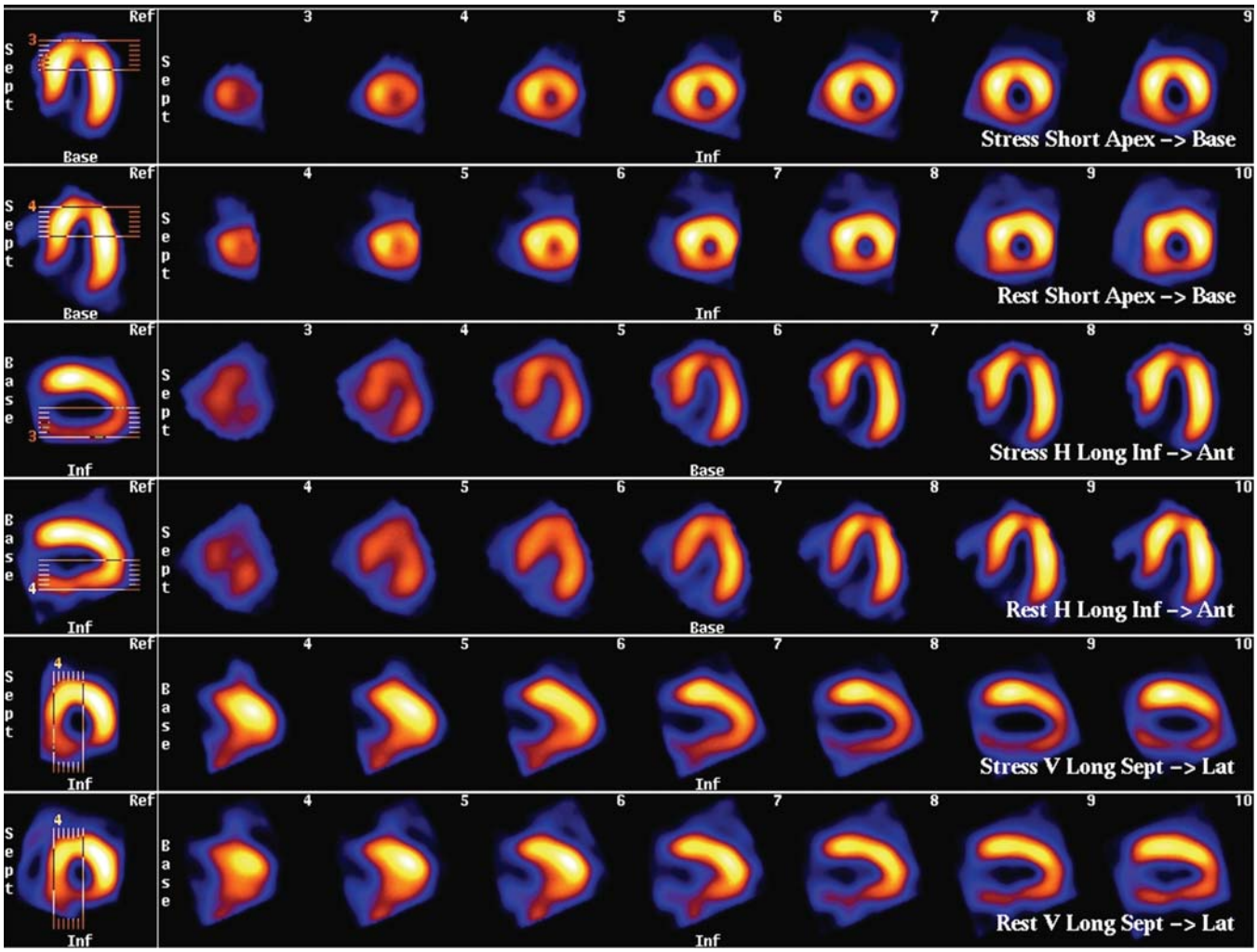


Fig. 251.1 Myocardial perfusion scan with technetium 99m sestamibi demonstrates transient ischemic dilatation of the left ventricle on stress imaging, as well as a small, mild reversible apical perfusion defect. There was mild global hypokinesis (not shown).

Clinical Presentation

A 52-year-old man presents with atypical angina (**Fig. 251.1**).

Key Imaging Finding

Transient ischemic dilatation (TID)

Top 3 Differential Diagnoses

- **Multivessel coronary artery disease.** Myocardial perfusion imaging is designed to detect a reversible defect or ischemia that may benefit from reperfusion. Ischemia is diagnosed by noting decreased activity in a portion of the myocardium on stress imaging (exercise or chemical stress) in comparison to rest. In the setting of multivessel balanced ischemia, however, focal regions of decreased activity may not be present. In these situations, abnormal dilatation of the left ventricular cavity on stress imaging may be the only sign of ischemia. This is an important finding to make, as it is associated with high-grade stenoses.
- **Subendocardial ischemia.** Apparent dilatation of the left ventricular cavity may be seen in the setting of global subendocardial (nontransmural) ischemia. In these situations, the subendocardial region has decreased perfusion on stress imaging and thus demonstrates decreased activity. This relative subendocardial photopenia creates apparent dilatation of the left ventricular cavity. As with multivessel ischemia, these patients may benefit from reperfusion.
- **Systolic dysfunction.** Systolic dysfunction from a variety of causes may result in myocardial stunning during stress imaging. The myocardial stunning leads to reduced ejection fraction and thus increased end-diastolic volume (ventricular cavity dilatation) during the stress portion of the test compared with the rest. This is especially true in patients with hypertrophic cardiomyopathy.

Additional Differential Diagnoses

- **Misaligned single-photon emission computed tomography (SPECT) images.** Misaligned stress and rest images from SPECT analysis may result in apparent transient ischemic dilatation of the left ventricular cavity. A careful inspection of overall SPECT image alignment at rest and stress should be made to avoid this common postprocessing pitfall.

Diagnosis

Multivessel coronary artery disease

✓ Pearls

- Transient ischemic dilatation on stress imaging suggests significant multivessel disease.
- In the setting of multivessel balanced ischemia, TID may be the only clue to the underlying pathology.
- Global subendocardial ischemia may result in apparent ventricular cavity dilatation.
- Be sure stress and rest SPECT images are appropriately aligned prior to interpretation.

Suggested Readings

Robinson VJB, Corley JH, Marks DS, et al. Causes of transient dilatation of the left ventricle during myocardial perfusion imaging. AJR Am J Roentgenol 2000;174(5):1349–1352

Ziessman HA, O'Malley JP, Thrall JH. Nuclear Medicine: The Requisites. 3rd ed. Philadelphia: Elsevier; 2006

Case 252

Kamal D. Singh



Fig. 252.1 Whole-body bone scans with technetium 99m hydroxymethylene diphosphonate demonstrate bilateral linear cortical uptake within femoral and tibial diaphyses and metaphyses in a "tram track" pattern. Additionally, there is diffuse increased uptake within the L2 vertebral body and degenerative-type uptake of multiple upper and lower extremity joints.

Clinical Presentation

A 60-year-old man presents with a chronic cough and bilateral lower extremity pain and tenderness (**Fig. 252.1**).

Key Imaging Finding

Symmetric "tram track" cortical uptake of the long bones

Top 3 Differential Diagnoses

- **Hypertrophic osteoarthropathy.** Secondary hypertrophic osteoarthropathy (HOA) is a clinical syndrome of symptomatic periostitis of the long bones due to various neoplastic and nonneoplastic pulmonary and extrapulmonary disorders. Common pulmonary causes are bronchogenic carcinoma, fibrous tumor of the pleura, mesothelioma, and chronic pulmonary infection/inflammation; as a result, a chest radiograph should be obtained in patients with scintigraphic evidence of HOA. Extrapulmonary etiologies include inflammatory bowel disease, cyanotic congenital heart disease, and thyroid acropachy. The exact pathophysiology of HOA remains unclear; however, vasoactive agents and hormones secreted by tumors and other inflammatory/infectious processes have been implicated. Scintigraphic findings of bilateral symmetric upper and lower extremity parallel cortical activity in a "tram track" configuration often precede plain film evidence of undulating periosteal proliferation. There may be associated increased activity within the scapula, mandible/maxilla, and periarticular regions. Patients usually report painful swelling of the affected limb and stiff joints and demonstrate digital clubbing on physical examination. The radiographic and scintigraphic findings usually resolve after treatment of the underlying disease.
- **Shin/quadriceps splints.** Severe bilateral shin and quadriceps splints may produce increased parallel cortical activity within the lower extremities of physically active patients with exertional or overuse lower leg pain. Shin splints (medial tibial stress syndrome) result in unilateral or bilateral posteromedial tibial cortical periostitis. These patients present with dull-aching leg pain. Unlike stress fracture, which appear as focal regions of increased uptake on all three phases of a bone scan, splints are generalized linear or longitudinal activity along the diaphyses and are detected only on delayed-phase imaging. Although stress fractures may coexist in a patient with shin or quadriceps splints, there has been no evidence to suggest a progression of splints to stress fracture.
- **Chronic venous stasis.** Chronic venous insufficiency can lead to soft tissue edema, associated skin changes (including stasis ulcers), and thick undulating or nodular periosteal proliferation of the affected extremity due to local hypoxia. Physical examination can help differentiate this entity from other causes of increased parallel long bone activity within an extremity by noting overlying skin changes. In the setting of cellulitis and chronic venous stasis, it may be difficult to exclude superimposed osteomyelitis.

Diagnosis

Hypertrophic osteoarthropathy (secondary to lung carcinoma)

✓ Pearls

- Benign and malignant etiologies can lead to HOA; obtain a chest radiograph to evaluate for underlying tumor.
- Shin and quadriceps splints are common in athletes and result in cortical periostitis with linear activity.
- Chronic venous stasis may lead to undulating periosteal proliferation due to hypoxia.

Suggested Readings

Ali A, Tetalman MR, Fordham EW, et al. Distribution of hypertrophic pulmonary osteoarthropathy. AJR Am J Roentgenol 1980;134(4):771–780

Love C, Din AS, Tomas MB, Kalapparambath TP, Palestro CJ. Radionuclide bone imaging: an illustrative review. Radiographics 2003;23(2):341–358

Mettler FA, Guiberteau MJ. Essentials of Nuclear Medicine Imaging. 5th ed. Philadelphia: Elsevier; 2006

Case 253

Kamal D. Singh

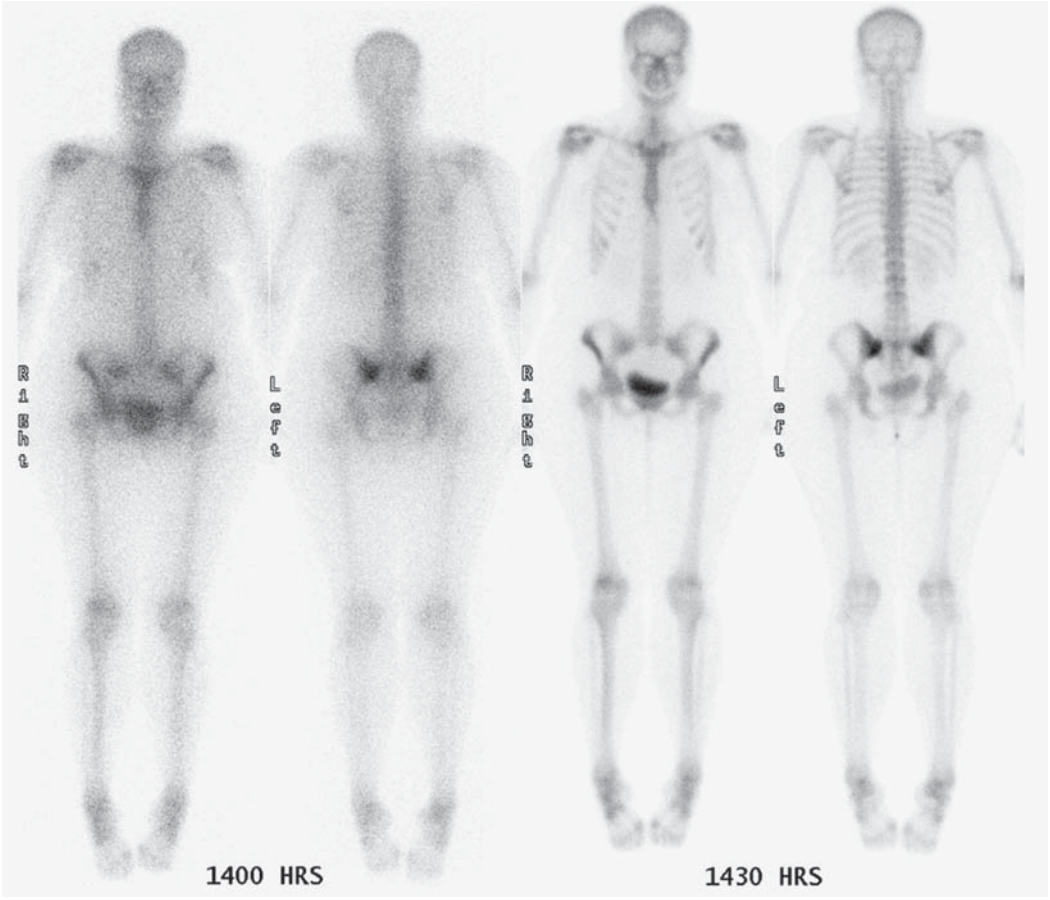


Fig. 253.1 Initial delayed whole-body bone scan (*left*) with technetium 99m (Tc99m) hydroxymethylene diphosphonate demonstrates poor spatial resolution. Repeat imaging (*right*) demonstrates improved spatial resolution. Incidentally, the patient had mild bilateral sacroiliitis, which was seen on prior computed tomography (not shown).

Clinical Presentation

A 24-year-old woman presents with chronic hip pain (**Fig. 253.1**). What is the difference between these two scans performed on the same day?

Key Imaging Finding

Poor-quality bone scan

Top 3 Differential Diagnoses

- **Off-peak gamma camera.** Gamma cameras employ an energy window centered about the photopeak of the desired radioisotope to reject scatter radiation. In the case of technetium 99m (Tc99m), a 20% energy window is centered about the 140 keV photopeak. Daily morning quality control involves extrinsic field uniformity testing using a cobalt 57 (Co57) sheet source prior to camera use for clinical studies. The extrinsic field uniformity test requires an energy window for Co57 (122 keV), which is lower than that for Tc99m. Failure to readjust the window setting for Tc99m prior to clinical use results in a poor resolution scan due to downscatter from 140 keV photons into the 122 keV window. This is referred to as "off-peak" imaging.
- **Incorrect radiopharmaceutical administration.** Administration of an incorrect radiopharmaceutical or incorrect dose (>20% difference from prescribed dose) and using an unprescribed route of administration are classified as "misadministration" and may account for unexpected imaging results. "Medical event" is a subset of misadministration in which the patient's whole-body dose exceeds 5 rem (0.05 Sv) or a single organ dose exceeds 50 rem (0.5 Sv), requiring verbal and written notification of the Nuclear Regulatory Commission (NRC).
- **Poor radiopharmaceutical preparation.** Technical errors in radiopharmaceutical preparation can lead to chemical or radionuclidic impurities and poor radiochemical labeling. These errors result in image degradation and, in some cases, increased dose to the patient. Regulations for radiopharmaceutical quality control have been established by the NRC and the U.S. Pharmacopeia (USP). Examples for Tc99m include <0.15 µCi of molybdenum 99 (Mo99) per 1 mCi of Tc99m (at the time of administration) and a maximum of 10 µg of aluminum break-through per 1 mL of Tc99m eluate.

Additional Differential Diagnoses

- **Infiltrated dose.** Quantum mottle (image noise) may result from inadequate radiotracer accumulation in the organ of interest due to infiltration of the dose at the injection site. This results in decreased counts during image acquisition, resulting in a poor target-to-background ratio. If not recognized during the time of injection, dose infiltration may be confirmed by including the injection site in the imaging field of view.

Diagnosis

Off-peak bone scan

✓ Pearls

- Off-peak imaging results in poor resolution imaging from improper radiotracer photopeak selection.
- Poor target-to-background ratio can also result from technical errors in radiotracer preparation or administration.
- Medical events include the misadministration of radiotracer, exceeding the allowable limits of the radiation dose.

Suggested Readings

Mettler FA, Guiberteau MJ. Essentials of Nuclear Medicine Imaging. 5th ed. Philadelphia: Elsevier; 2006

Case 254

Kamal D. Singh

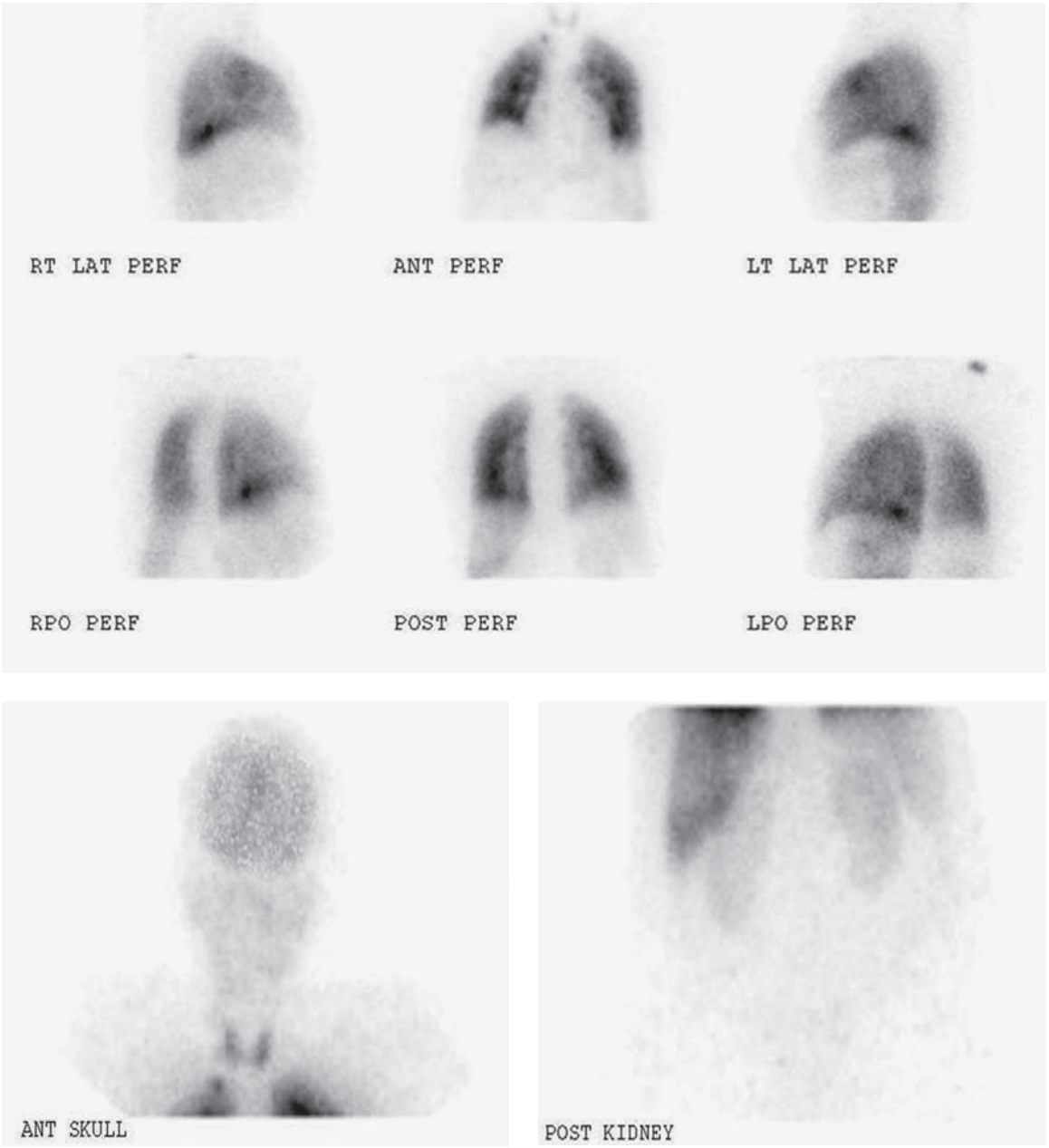


Fig. 254.1 **(A)** Perfusion scans with technetium 99m macroaggregated albumin demonstrate heterogeneous distribution without segmental defects and incidental note of extrapulmonary activity. **(B)** Spot imaging over the head reveals intracranial and thyroid radiopharmaceutical uptake. **(C)** Spot imaging over the abdomen confirms hepatic and renal parenchymal activity.

Clinical Presentation

A 51-year-old man presents with acute shortness of breath and tachycardia (**Fig. 254.1**).

Key Imaging Finding

Extrapulmonary activity on a lung perfusion scan

Top 3 Differential Diagnoses

- **Free technetium 99m (Tc99m).** Free Tc99m is the result of poor labeling of the radiopharmaceutical. The free Tc99m passes through the pulmonary capillary bed and into systemic circulation. Normal biodistribution of Tc99m pertechnetate includes the choroid plexus, salivary glands, thyroid, stomach/intestines, kidneys, urinary collecting system, and bladder. Determination of unbound or free Tc99m within a radiopharmaceutical preparation can be done by thin layer chromatography (TLC) with acetone solvent. Regulatory standards require at least 95% radiolabeling efficiency.
- **Right-to-left shunt.** Intrapulmonary or intracardiac shunting can be detected on perfusion imaging when Tc99m macroaggregated albumin (MAA) particles bypass the lungs and localize in systemic capillary beds. Cerebral cortical activity distinguishes shunting from other causes of extrapulmonary uptake, such as free Tc99m. Hence imaging over the brain improves specificity when shunting is suspected. Unlike free Tc99m, the renal uptake in shunting is primarily within the renal cortex; therefore, collecting system excretion and bladder activity are absent. Quantification of the shunt can be performed by whole-body imaging to determine the ratio of systemic counts to whole-body counts, which is proportional to the shunt size. Shunting >5 to 10% is generally considered significant. A lung perfusion scan is normally accomplished with 2 to 5 mCi of Tc99m MAA containing 200,000 to 500,000 particles. In cases of a known or suspected shunt, the number of particles should be reduced to 100,000. The reduced number of particles also applies for children, pregnant women, and patients with known pulmonary hypertension.
- **Retained activity from a different radiotracer study.** Knowledge of any recent nuclear medicine scans is helpful to avoid interfering activity, which may be an issue for radiotracers with long half-lives.

Diagnosis

Right-to-left shunt (intracardiac)

✓ Pearls

- Extrapulmonary activity on a perfusion scan should be assessed with brain imaging to exclude shunting.
- Right-to-left shunts can be detected and quantified on a lung perfusion scan with Tc99m MAA.
- A reduced number of particles is used for shunts, pulmonary hypertension, and pregnant/pediatric patients.

Suggested Readings

Mettler FA, Guiberteau MJ. Essentials of Nuclear Medicine Imaging. 5th ed. Philadelphia: Elsevier; 2006

Ziessman HA, O'Malley JP, Thrall JH. Nuclear Medicine: The Requisites. 3rd ed. Philadelphia: Elsevier; 2006

Case 255

John P. Lichtenberger III

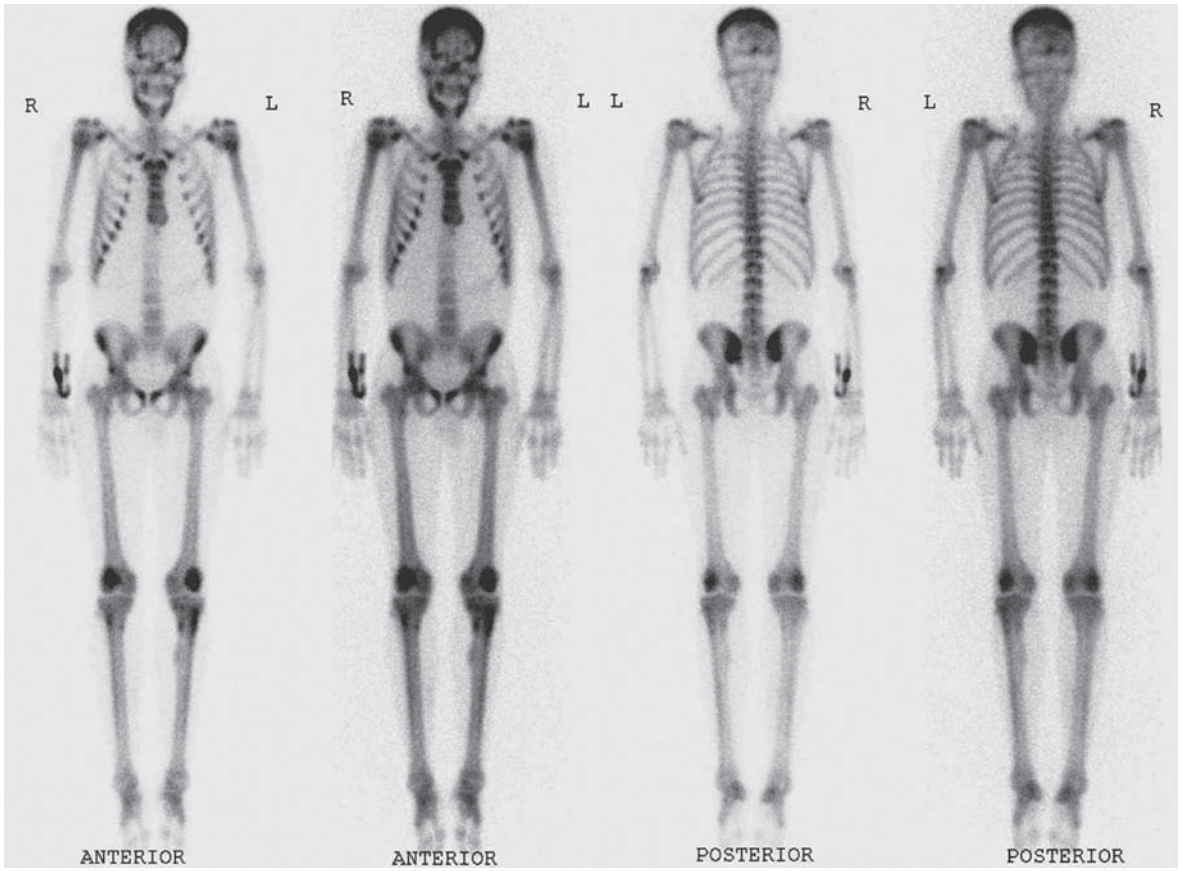


Fig. 255.1 Whole-body bone scans with technetium 99m hydroxymethylene diphosphonate show diffuse, symmetric uptake of the radiopharmaceutical in the skeletal system and no significant renal activity. The uptake is seen within both the axial and appendicular skeleton. Prominent increased activity is seen at the anterior costochondral junctions bilaterally.

Clinical Presentation

A 68-year-old man presents with a history of prostate cancer and chronic renal failure (**Fig. 255.1**).

Key Imaging Finding

Superscan

Top 3 Differential Diagnoses

- **Metastatic disease.** A superscan refers to increased skeletal uptake of technetium 99m hydroxymethylene diphosphonate (or methylene diphosphonate) with decreased or absent renal and soft tissue activity. The most common cause of a superscan is metastatic prostate cancer. Breast or lung cancer and lymphoma may cause a similar appearance on a bone scan. With metastatic disease, the skeletal activity is typically inhomogeneous and centered primarily within the axial skeleton. Distinct metastatic foci may be discernible.
- **Metabolic disease.** Although somewhat varied in scintigraphic appearance, metabolic diseases, such as renal osteodystrophy, hyperthyroidism, and osteomalacia, may result in generalized increased activity in the skeleton relative to the kidneys and soft tissues (superscan). Features that suggest metabolic disease include uniform distribution of activity, involvement of the appendicular skeleton, and disproportionate increased calvarial uptake. The osseous manifestations of renal osteodystrophy result from altered vitamin D metabolism and secondary hyperparathyroidism. This diagnosis is suggested on a bone scan by prominent activity along the costochondral junctions, involvement of distal long bones, "railroad tracking" and bowing of the femurs, and sternal activity. Pseudofractures may be seen in the setting of osteomalacia.
- **Paget disease.** Intense activity and expansion of bones are characteristic of Paget disease, most commonly involving the pelvis, femurs, spine, and skull. When multifocal or widespread, the concentration of the radiopharmaceutical in the skeletal lesions and an increased target-to-soft tissue ratio may result in an apparent superscan.

Additional Differential Diagnoses

- **Myeloproliferative/marrow infiltrative disorder.** A superscan from myeloproliferative diseases, such as lymphoma, leukemia, mastocytosis, and myelofibrosis, usually manifests as uniform and homogeneous radiotracer uptake within both the axial and appendicular skeleton, similar to metabolic disease. Appropriate history and laboratory values aid in distinguishing between myeloproliferative/marrow infiltrative disorders and metabolic disease.

Diagnosis

Renal osteodystrophy

✓ Pearls

- A superscan refers to increased skeletal uptake with decreased or absent renal activity.
- Metastatic disease is the most common cause of a superscan and typically involves the axial skeleton.
- Metabolic disease, such as renal osteodystrophy, involves both the axial and appendicular skeleton.
- Paget disease may result in a superscan when widespread.

Suggested Readings

Love C, Din AS, Tomas MB, Kalapparambath TP, Palestro CJ. Radionuclide bone imaging: an illustrative review. Radiographics 2003;23(2):341–358

Mettler FA, Guiberteau MJ. Essentials of Nuclear Medicine Imaging. 5th ed. Philadelphia: Elsevier; 2006

Case 256

William T. O'Brien Sr.

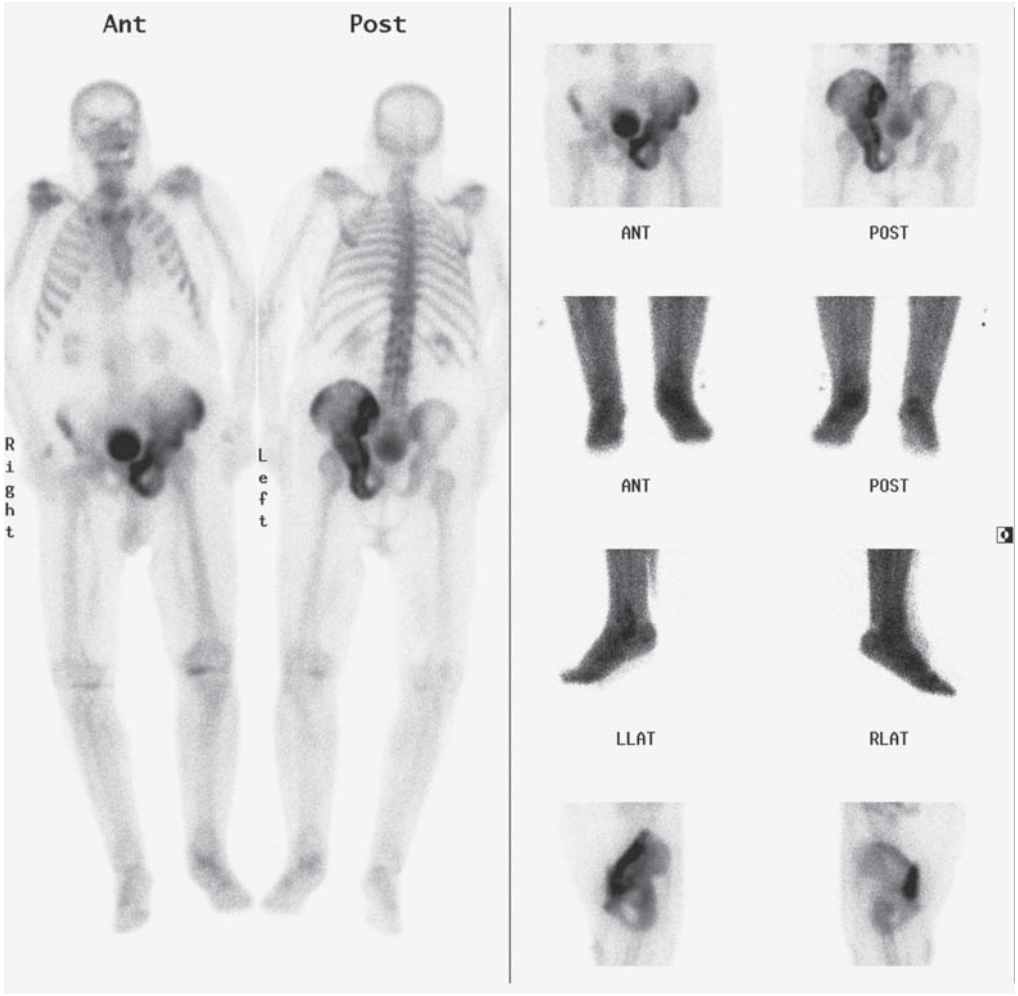


Fig. 256.1 Whole-body bone scans with technetium 99m hydroxymethylene diphosphonate demonstrate diffuse increased uptake and enlargement of the left hemipelvis.

Clinical Presentation

A 68-year-old man presents with prostate cancer and chronic hip pain (**Fig. 256.1**).

Key Imaging Finding

Increased activity and osseous expansion in the pelvis

Top 2 Differential Diagnoses in Adults

- **Paget disease**. Paget disease most commonly occurs in middle-aged to older men. The cause is unknown. On bone scans, Paget disease exhibits increased activity within involved bone(s), along with osseous expansion. The pelvis is the most common bone involved, followed by the femur. A classic large lytic lesion of the skull is termed osteoporosis circumscripta. When long bones are involved, Paget disease progresses from one end of the bone to the other with a sharp demarcation from the involved portion of the bone to the uninvolved portion, rendering the classic "blade of grass" appearance along the leading edge. The activity on bone scan is typically increased during all three phases of the disease (lytic, mixed, and sclerotic). Bone scans can be used to monitor treatment and to evaluate for sarcomatous degeneration, which would appear as a focal region of increasing activity on serial scans.
- **Metastases.** Bone scan is the most useful imaging modality to search for metastatic disease. Although usually multifocal, metastases may occasionally be monostotic. The axial skeleton is most commonly involved. Sclerotic metastases in a man are most likely due to prostate cancer, whereas sclerotic metastases in a woman are most likely due to breast carcinoma. On scintigraphy, metastatic disease typically presents as multifocal regions of increased activity. The involved bone may be enlarged secondary to tumor burden. Increased activity on a bone scan is thought to be due to the body's reaction to the tumor, rather than the tumor itself. Bone scans may be used to follow therapy; however, within the first 6 months after chemotherapy, bone scans may demonstrate increased activity within metastatic foci, referred to as the "flare phenomenon." This occurs as a result of a healing osteoblastic response to therapy. Any region of increasing activity 6 months or later posttreatment should be considered a progression of the disease.

Top 3 Differential Diagnoses in Children

- **Ewing sarcoma.** Ewing sarcoma is the second most common primary bone tumor in children (after osteosarcoma) and most commonly involves the pelvis or femur. Patients typically present with progressive pelvic or leg pain. Bone scans demonstrate increased activity within the involved osseous structures, and bone expansion may also be seen. Osseous metastases occur in approximately half of all patients; therefore, follow-up imaging is warranted to evaluate for disease progression.
- **Lymphoma.** Lymphoma is a small, round blue cell tumor that can mimic Ewing sarcoma clinically and radiographically; however, the prognosis for lymphoma is far more favorable. Bone scans demonstrate increased activity within the involved osseous structures, and bone expansion may also be seen. The pelvis is commonly involved in children. Biopsy is warranted to confirm the diagnosis but should be coordinated with the pediatric surgeon as the tract used for biopsy may alter the surgical approach.
- **Fibrous dysplasia.** Fibrous dysplasia may be monostotic or polyostotic (McCune–Albright syndrome). The lesions may be lucent, have a ground-glass matrix, or be sclerotic. Bony expansion is common. Increased uptake is noted in involved bones. Common locations are the long bones, pelvis, craniofacial bones, spine, and ribs.

Diagnosis

Paget disease

✓ Pearls

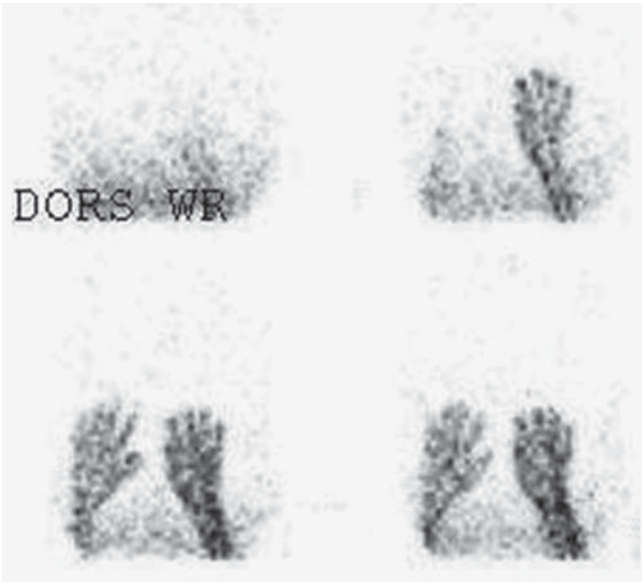
- Paget disease most commonly affects the pelvis; bone scans help evaluate for sarcomatous degeneration.
- Paget disease and fibrous dysplasia can be monostotic or polyostotic; metastases are usually multifocal and widespread.
- Correlation with anatomical imaging can be paramount in distinguishing benign from malignant disease.

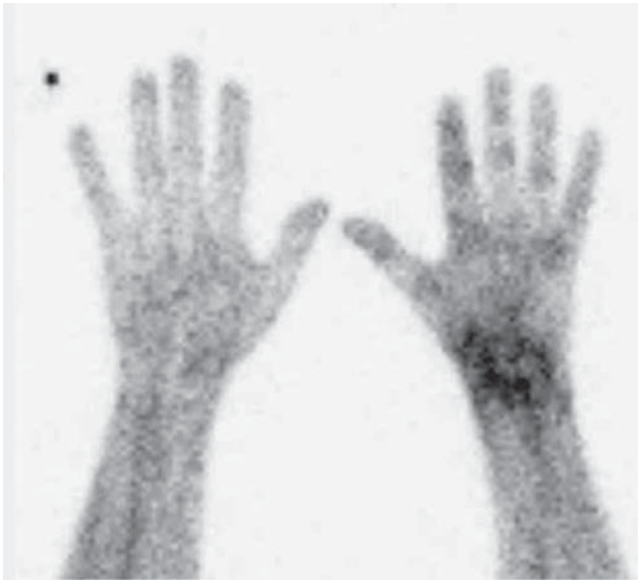
Suggested Readings

Mettler FA, Guiberteau MJ. Essentials of Nuclear Medicine Imaging. 5th ed. Philadelphia: Elsevier; 2006

Case 257

Kamal D. Singh





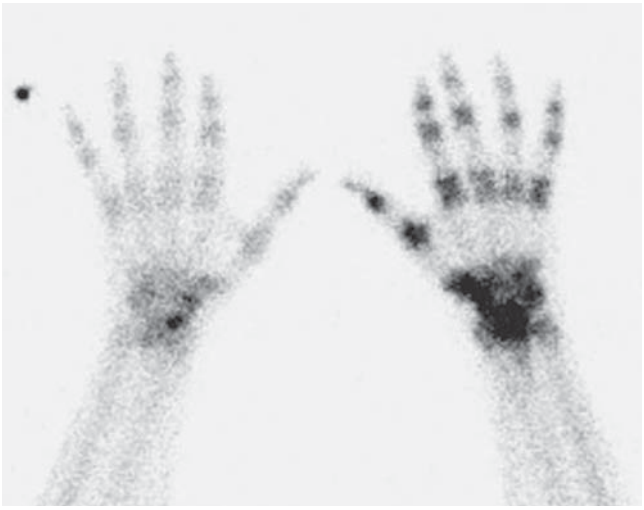


Fig. 257.1 Three-phase bone scans of bilateral hands with technetium 99m hydroxymethylene diphosphonate (by convention, the marker denotes the right side of the body). **(A)** Flow imaging reveals diffuse hyperemia of the left hand. **(B)** Similar findings are seen on the blood pool or tissue phase imaging. **(C)** Three-hour delayed imaging reveals periarticular increased activity within the left hand and wrist.

Clinical Presentation

A 37-year-old woman presents with persistent left hand swelling and pain after a minor fall 2 months ago (**Fig. 257.1**).

Key Imaging Finding

Three-phase positive bone scan

Top 3 Differential Diagnoses

- **Trauma.** A three-phase bone scan involves dynamic flow imaging for the first minute after radiopharmaceutical injection, static blood pool imaging for the next few minutes, and subsequent static delayed imaging at 2 to 4 hours. Although a three-phase bone scan is classically performed for determination of osseous infection, increased uptake on all three phases is a nonspecific finding and can be seen in the setting of acute fracture or recent surgery. Approximately 80% of fractures demonstrate increased activity within 24 hours, and over 95% of fractures demonstrate increased activity by day 3. A healed extremity fracture may have persistent focal increased activity on the delayed phase of the bone scan for over a year.
- **Osteomyelitis.** Three-phase bone scan not only has a high sensitivity and negative predictive value for acute osteomyelitis, but also may detect abnormalities 1 to 2 weeks earlier than radiographic manifestations. False-negative bone scans, however, are often seen in the setting of disrupted blood supply and abscess formation, especially in neonates and infants with hematogenously acquired osteomyelitis. Specificity is decreased in the setting of recent surgery, trauma, or orthopedic hardware. Dual-isotope imaging with indium 111 labeled white blood cell (WBC; for infection) and technetium 99m sulfur colloid (TcSC; for normal bone marrow mapping) can aid in the assessment of hardware-related osteomyelitis. Focal uptake on a In111 WBC scan, which is spatially discordant from a TcSC bone marrow scan, is suggestive of infected hardware.
- **Bone tumor.** Primary or secondary malignant bone tumors may demonstrate increased activity on all three phases. Although most benign osseous neoplasms will not demonstrate increased flow or blood pool activity, osteoid osteomas contain a three-phase positive nidus with a "target" sign on delayed imaging.

Additional Differential Diagnoses

- **Reflex sympathetic dystrophy (RSD).** RSD typically occurs after trauma or surgery and is characterized by pain, swelling, and vasomotor instability out of proportion to the degree of injury. Periarticular swelling and osteopenia may be seen on plain radiographs. Early or acute RSD classically demonstrates unilateral periarticular increased radiotracer activity on all three phases of a bone scan. This classic pattern is seen in two thirds of affected patients. The flow and blood pool activity may normalize in chronic or long-standing RSD. Interestingly, RSD in children commonly demonstrates normal or even decreased activity.

Diagnosis

Reflex sympathetic dystrophy

✓ Pearls

- Flow, blood pool, and delayed imaging at 2 to 4 hours make up a three-phase bone scan.
- Three-phase positive scans may be seen with acute fractures, osteomyelitis, osteoid osteomas, and RSD.
- In111 WBC scan in conjunction with Tc99m sulfur colloid scan is highly specific for hardware osteomyelitis.
- RSD presents with periarticular osteopenia and corresponding increased activity on a three-phase bone scan.

Suggested Readings

Kozin F, Soin JS, Ryan LM, Carrera GF, Wortmann RL. Bone scintigraphy in the reflex sympathetic dystrophy syndrome. Radiology 1981;138(2):437–443

Love C, Din AS, Tomas MB, Kalapparambath TP, Palestro CJ. Radionuclide bone imaging: an illustrative review. Radiographics 2003;23(2):341–358

Case 258

Kamal D. Singh

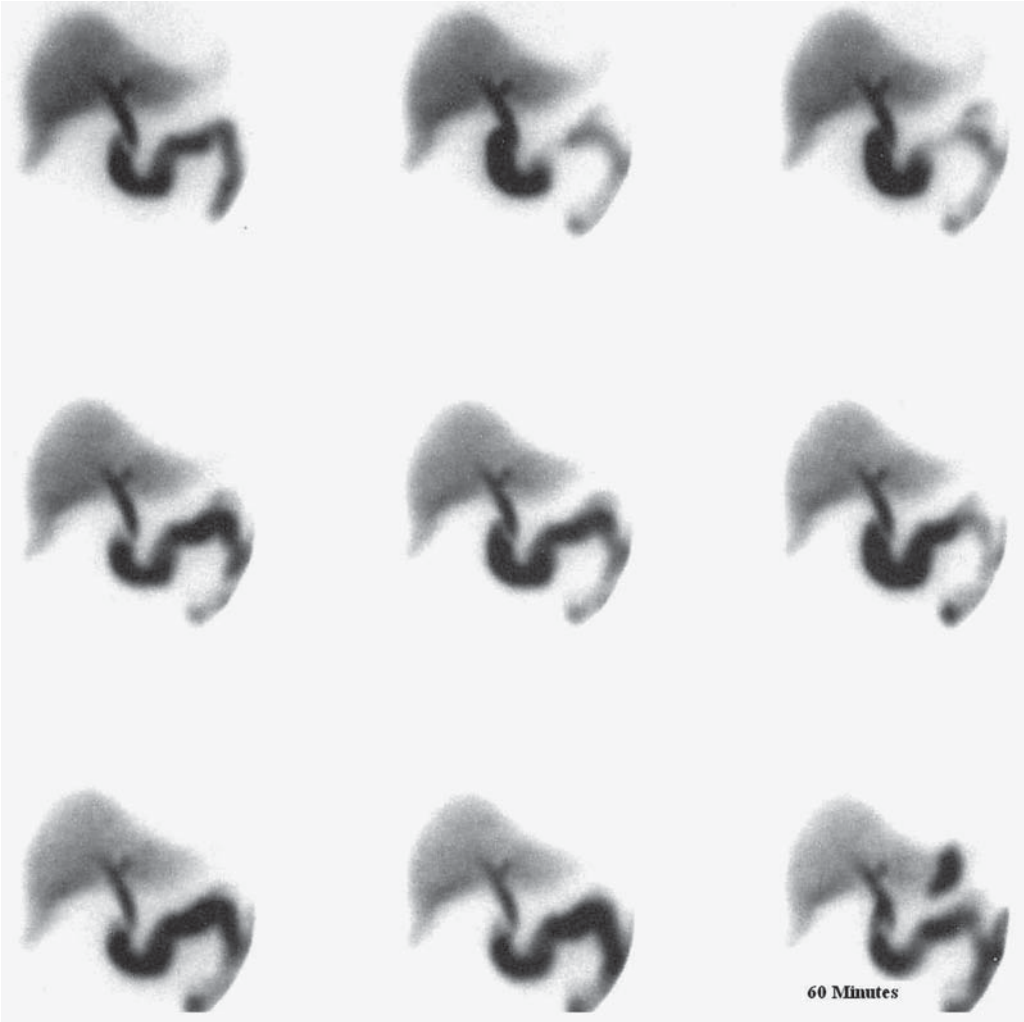


Fig. 258.1 Representative images from a hepatobiliary scan with technetium 99m Mebrofenin reveals no significant radiotracer uptake within the expected region of the gallbladder during the first hour of imaging. There is normal tracer transit through the common bile duct into the small bowel with incidental note of enterogastric reflux. Slight increased hepatic parenchymal activity ("rim" sign) is seen along the gallbladder fossa. No gallbladder activity was noted despite subsequent morphine administration (images not included).

Clinical Presentation

A 45-year-old woman presents with right upper quadrant pain and fever (**Fig. 258.1**).

Key Imaging Finding

Nonvisualization of the gallbladder on hepatobiliary imaging

Top 3 Differential Diagnoses

- **Acute cholecystitis.** Acute cystic duct obstruction by gallstones is the hallmark of acute cholecystitis. Hepatobiliary imaging has a high specificity (98%) and negative predictive value (99%) and is very useful in cases where ultrasound findings are equivocal. Under normal circumstances, the gallbladder is visualized within 1 hour of radiotracer administration. Nonvisualization of the gallbladder within 4 hours of radiotracer injection and in the setting of normal visualization of biliary and bowel activity is diagnostic of acute cholecystitis. Alternatively, morphine (0.04 mg/kg intravenous [IV]) may be administered after 1 hour of dynamic imaging in cases where normal biliary-to-bowel transit is present. Nonvisualization of the gallbladder within 30 minutes of morphine administration is also diagnostic of acute cholecystitis. The "cystic duct" or "nubbin" sign may be seen as focal activity within the cystic duct proximal to the site of obstruction. Increased pericholecystic hepatic parenchymal activity ("rim" sign) can be an ominous sign of complicated (gangrenous, necrotic, or perforated) cholecystitis, necessitating immediate surgical intervention.
- **Chronic cholecystitis.** Delayed visualization of the gallbladder (1–4 h postinjection) or delayed biliary-to-bowel transit (absence of bowel activity at 1 h despite visualization of the gallbladder) is suggestive of chronic cholecystitis. Chronic cholecystitis can be confirmed by demonstrating a gallbladder ejection fraction (EF) <35%. The EF is obtained during a 30-minute cholecystokinin (CCK) infusion (0.02 µg/kg slow IV).
- **Inadequate patient preparation.** False-positives can occur with prolonged fasting (>24 h), a recent meal (<4 hours), or prolonged hyperalimentation. Pretreatment with CCK 30 minutes prior to injection is usually recommended for prolonged fasting and hyperalimentation to allow the distended gallbladder to drain. Patients with a recent meal are imaged after fasting for a minimum of 4 hours.

Additional Differential Diagnoses

- **Severe hepatocellular disease.** Poor hepatocellular function can result in poor extraction and excretion of the radiotracer, resulting in delayed blood pool clearance (>10 min). False-positive studies occur due to delayed visualization or nonvisualization of the gallbladder. The key is to note the delayed blood pool clearance.
- **High-grade biliary obstruction.** Prompt hepatic uptake without biliary excretion of the radiotracer ("liver scan" sign) suggests a biliary duct obstruction. In the absence of bowel activity, morphine is contraindicated. Delayed 4- and 24-hour imaging is generally obtained to evaluate for bowel activity. The gallbladder may or may not fill depending on the location and duration of obstruction. Computed tomography or magnetic resonance cholangiopancreatography may be helpful not only in establishing the diagnosis but also in determining a possible cause of the obstruction.

Diagnosis

Acute gangrenous cholecystitis

✓ Pearls

- Hepatobiliary scan is highly sensitive and specific for acute calculus cholecystitis.
- False-positives may be seen with recent meal, extended fasting (>24 h), and hepatocellular dysfunction.
- Delayed visualization of bowel (>1 h) may be normal or associated with chronic cholecystitis.
- In the setting of a high-grade biliary obstruction with absent bowel activity, morphine is contraindicated.

Suggested Readings

Dorio PJ. The rim sign. Radiology 1998;209(3):801–802

Mettler FA, Guiberteau MJ. Essentials of Nuclear Medicine Imaging. 5th ed. Philadelphia: Elsevier; 2006

Case 259

Kamal D. Singh

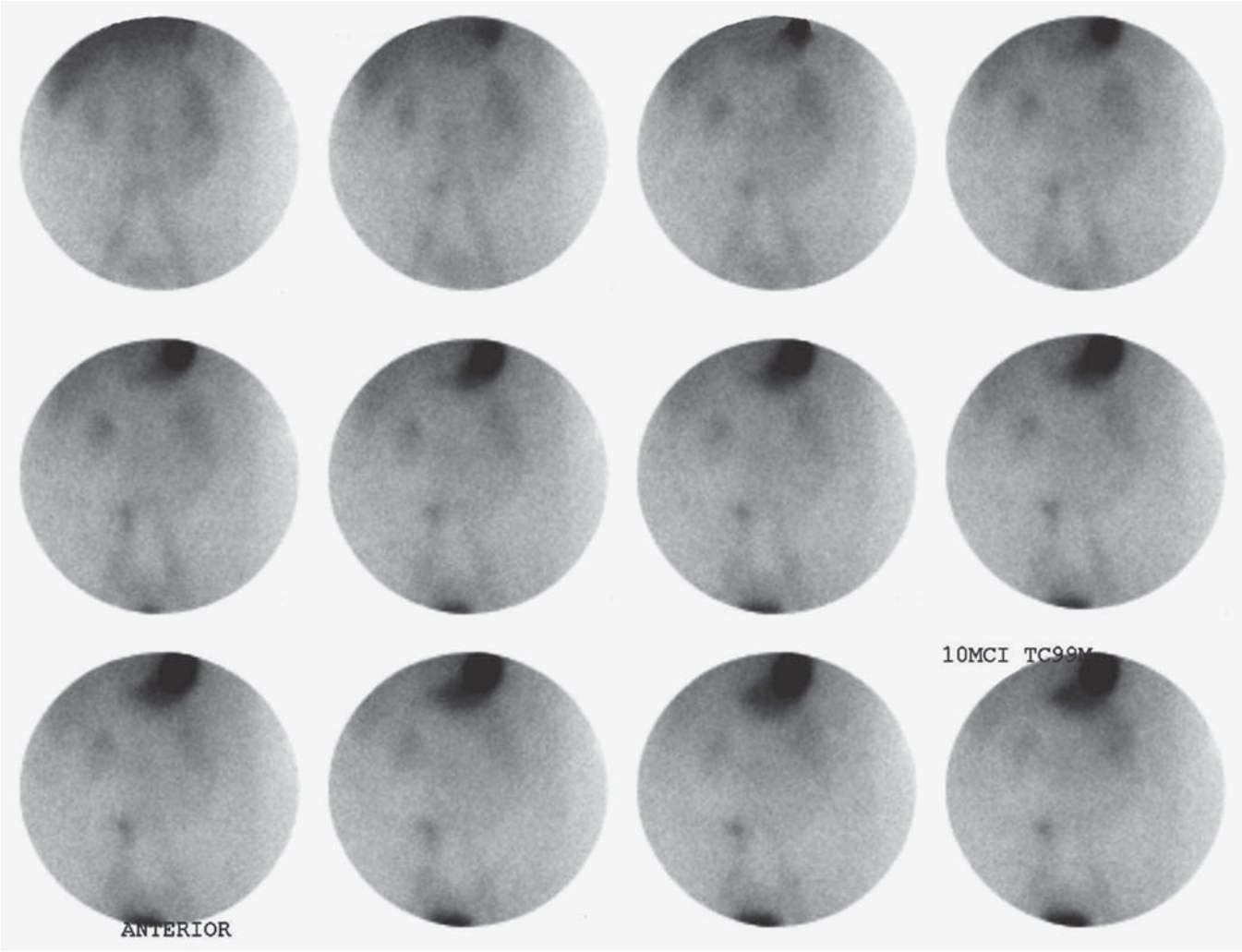


Fig. 259.1 Sequential images from a Meckel scan with technetium 99m pertechnetate demonstrate focal uptake in the right lower quadrant that appears at the same time as the physiologic gastric mucosal activity and intensifies over time without evidence of peristalsis. The anterior intra-abdominal location of this activity was confirmed on a static lateral projection (not included). Physiologic urinary excretion of the radiotracer is also noted.

Clinical Presentation

An 8-year-old boy presents with chronic abdominal discomfort and a history of intermittent lower gastrointestinal (GI) bleeding (**Fig. 259.1**).

Key Imaging Finding

Focal intra-abdominal activity on pertechnetate imaging

Top 3 Differential Diagnoses

- **Meckel diverticulum.** Meckel diverticulum is a congenital persistence of the omphalomesenteric (vitelline) duct. It occurs in 2% of the population, has a 2:1 male-to-female ratio, occurs 2 feet from the ileocecal valve, and generally presents within 2 years of age (rule of 2s). Although not all Meckel diverticula have gastric mucosa, the vast majority of symptomatic cases do. Patients may present with bleeding, obstruction, intussusception, or volvulus. Technetium 99m (Tc99m) pertechnetate is taken up by mucin-producing cells and can detect enteric diverticula with ectopic gastric mucosa. Proper patient preparation can improve the sensitivity of a Meckel scan, which includes nothing by mouth for at least 4 hours and pretreatment with cimetidine (blocks radiotracer release from ectopic mucosa), pentagastrin (enhances ectopic mucosal uptake), and glucagon (decreases small bowel peristalsis). Focal activity in the right lower quadrant that appears at the same time as physiologic gastric uptake, intensifies over time, and is nonperistaltic is diagnostic of a Meckel diverticulum. Uptake usually appears within 30 minutes but make take up to 60 minutes depending on the amount of gastric mucosa present. False-negative studies may be due to the absence of gastric mucosa (no radiotracer uptake mechanism) or secondary to diverticular ischemia/necrosis. If the patient is actively bleeding, a Tc-labeled red blood cell scan may be considered to localize the site of bleeding prior to a Tc-pertechnetate study to confirm the presence of a Meckel diverticulum.
- **Focal intra-abdominal infectious or inflammatory processes.** False-positive studies may occur in the setting of focal infectious or inflammatory intra-abdominal processes, such as GI duplication cyst with heterotopic gastric mucosa, inflammatory bowel disease, appendicitis, and focal enteritis/colitis. Hypervascular masses such as arteriovenous malformations and neoplasms may also be seen as focal regions of increased activity on a Meckel scan. With the exception of a duplication cyst with heterotopic gastric mucosa, the remainder of these entities demonstrate an increased blood pool that fades over time, rather than focal activity that mirrors physiologic gastric activity. Correlation with cross-sectional imaging may be necessary in some cases to differentiate these conditions from a true Meckel diverticulum.
- **Physiologic renal/urinary activity.** Additional static lateral views can confirm whether focal activity is intra-abdominal or retroperitoneal in location. Upright and post-void imaging can also help distinguish physiologic activity within a distended renal pelvis, ureter, ectopic kidney, or bladder diverticulum from a Meckel diverticulum.

Diagnosis

Meckel diverticulum

✓ Pearls

- Tc-pertechnetate scan detects a Meckel diverticulum with ectopic gastric mucosa.
- Focal intra-abdominal activity that intensifies over time without peristalsis suggests a Meckel diverticulum.
- False-positives include urinary tracer excretion and intra-abdominal inflammatory/infectious processes.

Suggested Readings

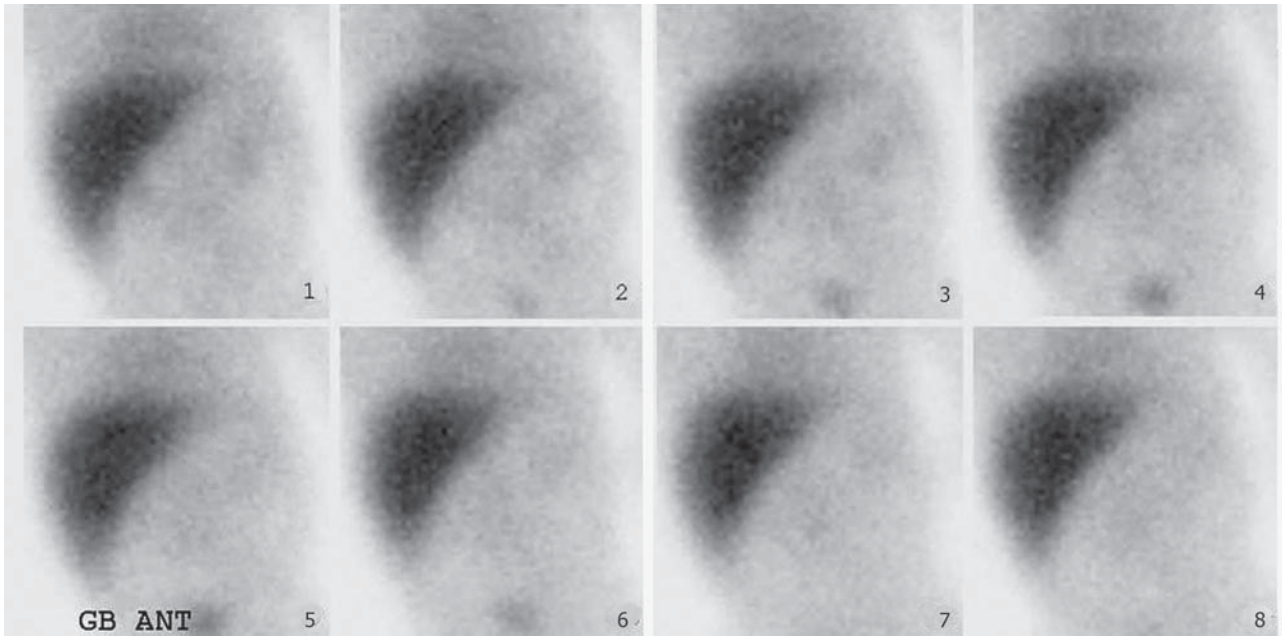
Emamian SA, Shalaby-Rana E, Majd M. The spectrum of heterotopic gastric mucosa in children detected by Tc-99m pertechnetate scintigraphy. Clin Nucl Med 2001;26(6):529–535

Treves ST, Grand RJ. Gastrointestinal bleeding. In: Treves ST, ed. Pediatric Nuclear Medicine. New York: Springer-Verlag; 2006:192–208

Ziessman HA, O'Malley JP, Thrall JH. Nuclear Medicine: The Requisites. 3rd ed. Philadelphia: Elsevier; 2006

Case 260

Kamal D. Singh



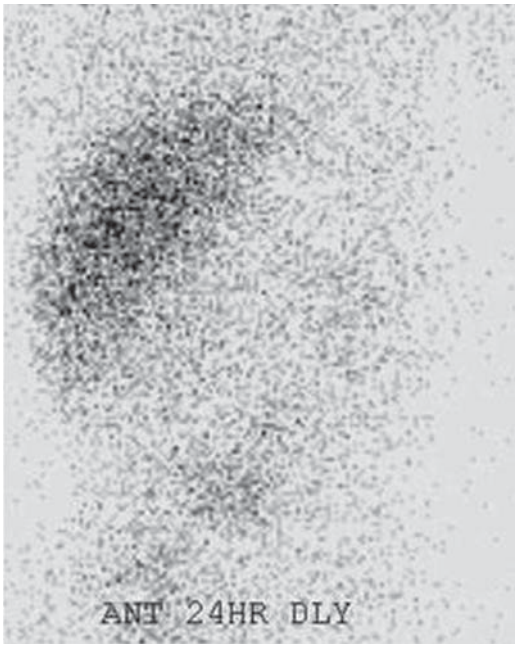


Fig. 260.1 Hepatobiliary scan with technetium 99m Mebrofenin. **(A)** Sequential imaging during the first hour demonstrates no biliary excretion of the radiotracer or bowel activity. There is mild persistence of cardiac blood pool activity. No significant change was noted on 4-hour delayed imaging (not included). **(B)** Twenty-four-hour delayed anterior static image reveals persistent hepatic parenchymal activity with vicarious genitourinary excretion of the radiotracer. There is no evidence of bowel activity.

Clinical Presentation

A 2-week-old neonate presents with jaundice (**Fig. 260.1**).

Key Imaging Finding

Persistent hepatogram on neonatal hepatobiliary imaging

Top 3 Differential Diagnoses

- **Biliary atresia.** Persistent neonatal conjugated hyperbilirubinemia may be due to biliary atresia or neonatal hepatitis. Biliary atresia involves malformation of extrahepatic ducts, leading to obstructive cholestasis and jaundice. Despite extrahepatic biliary ductal obstruction, intrahepatic biliary ducts are nondilated due to fibrosis. Prompt diagnosis of biliary atresia is essential, as success of the Kasai surgical procedure is greatest if performed within the first 2 months of life. Hepatobiliary imaging can exclude biliary atresia by demonstrating patency of the extrahepatic biliary system. Patients are pretreated with phenobarbital (5 mg/kg orally [PO] daily for 5 days) to optimize biliary excretion. Good hepatic uptake with poor hepatic clearance (persistent hepatogram) and nonvisualization of intestinal activity within 24 hours of radiotracer injection is essentially diagnostic of biliary atresia. Intraoperative cholangiogram, however, remains the gold standard for definitive diagnosis.
- **Neonatal hepatitis.** Neonatal hepatitis may be due to a variety of metabolic, congenital, or infectious causes, as well as idiopathic. Scintigraphic findings include poor hepatic uptake of radiotracer with delayed or decreased biliary excretion secondary to impaired hepatocyte function. On 24-hour delayed imaging, bowel activity is nearly always present, confirming patency of the biliary system. The lack of bowel activity may rarely be seen in severe hepatic dysfunction or inadequate patient preparation. Hepatic biopsy may further aid in definitive diagnosis prior to medical treatment.
- **Intrahepatic cholestasis from severe parenchymal disease.** Rarely, severe hepatocellular dysfunction or intrahepatic biliary malformation may result in cholestasis with no scintigraphically detectable excretion of the radiotracer, resulting in a false-positive study for biliary atresia. A repeat study could theoretically help exclude biliary atresia if the patient's hepatic function continues to improve. However, liver biopsy and/or intraoperative cholangiogram may be necessary for a definitive diagnosis.

Diagnosis

Biliary atresia

✓ Pearls

- Pretreatment with phenobarbital increases biliary secretion of tracer, improving the sensitivity of the scan.
- Prompt hepatic uptake without biliary excretion into the bowel over 24 hours suggests biliary atresia.
- Visualization of bowel activity essentially excludes biliary atresia.
- Neonatal hepatitis demonstrates poor hepatic uptake with delayed bowel activity.

Suggested Readings

Treves ST, Jones AG. Liver and spleen. In: Treves ST, ed. Pediatric Nuclear Medicine. New York: Springer-Verlag; 2006: 209–238

Ziessman HA, O'Malley JP, Thrall JH. Nuclear Medicine: The Requisites. 3rd ed. Philadelphia: Elsevier; 2006

Case 261

Kamal D. Singh

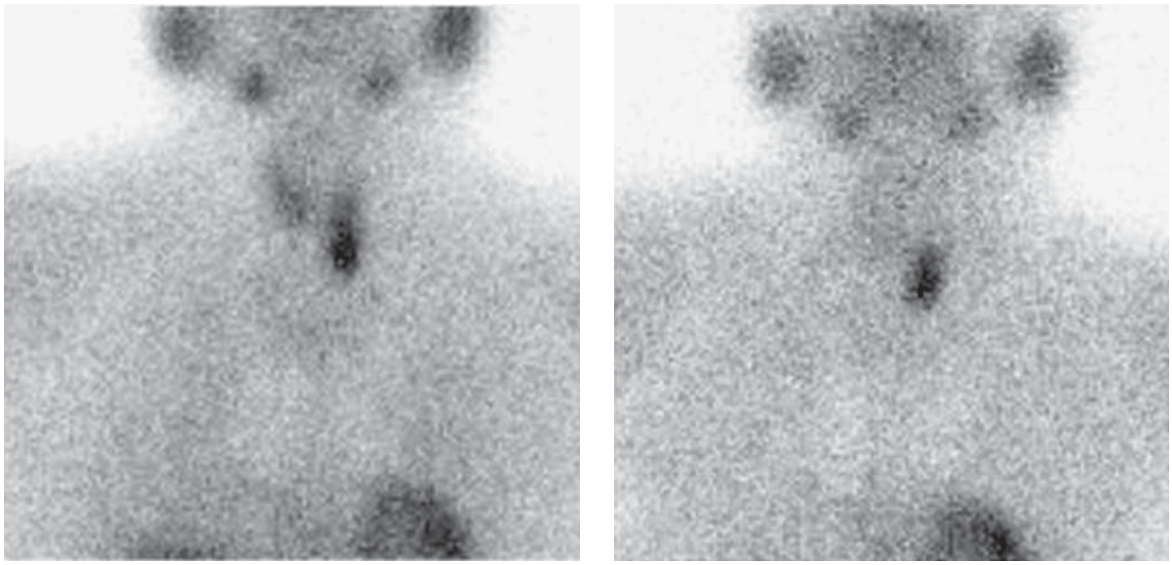


Fig. 261.1 Dual-phase parathyroid scan with technetium 99m sestamibi. **(A)** Early imaging 20 minutes postinjection demonstrates radiotracer uptake within the thyroid gland, along with a focus of moderately intense uptake adjacent to the left inferior thyroid pole. **(B)** Delayed imaging 2 hours postinjection reveals appropriate washout of thyroid activity with persistent focal uptake adjacent to the left inferior thyroid pole. Physiologic activity is seen within salivary glands and myocardium on both early and delayed imaging.

Clinical Presentation

A 44-year-old woman presents with hypercalcemia and elevated parathyroid hormone (PTH) (**Fig. 261.1**).

Key Imaging Finding

Persistent focal cervical uptake on delayed sestamibi imaging

Top 3 Differential Diagnoses

- **Parathyroid adenoma.** Etiologies of primary hyperparathyroidism include parathyroid adenoma (85%), hyperplasia (15%), and, much less commonly, parathyroid carcinoma. Clinically, patients have manifestations of serum hypercalcemia and hypophosphatasia due to elevated PTH. Technetium 99m (Tc99m) sestamibi initially localizes within the thyroid gland and hyperfunctioning parathyroid adenoma with normal washout of thyroid activity on a delayed scan. Dual-phase (early and delayed) parathyroid scan uses this differential washout between the thyroid gland and hyperfunctioning parathyroid tissue to localize an adenoma with high sensitivity (90%). Although the majority of parathyroid adenomas are solitary and located adjacent to the thyroid tissue, they can be multiple in number and/or ectopic in location (10–15%); hence the mediastinum is included in the field of view. Single-photon emission computed tomography imaging following delayed planar views can improve contrast resolution for detection and localization of adenomas. Frequently, parathyroid adenomas may demonstrate rapid washout of the radiotracer (similar to thyroid tissue), resulting in a false-negative study, as no discrete focus persists on delayed imaging. In such cases, either an iodine 123 (I 123; oral) or Tc99m pertechnetate (intravenous) scan can be performed to outline normal thyroid tissue; this image may be subtracted from an early Tc99m sestamibi image, making the parathyroid adenoma more conspicuous.
- **Thyroid adenoma or carcinoma.** Tc99m sestamibi demonstrates nonspecific localization in tumors via passive transport across cell membranes and active transport into mitochondria. False-positive studies include thyroid adenoma (most common), thyroid carcinoma, and parathyroid carcinoma. Dual isotope imaging (Tc-99m sestamibi plus either I123 or Tc99m pertechnetate) with or without subtraction can improve sensitivity and avoid some of these pitfalls. Also, correlation with ultrasound or any cross-sectional imaging can be helpful.
- **Metastatic lymphadenopathy.** Tc99m sestamibi is a nonspecific tumor-localization agent. Focal cervical activity may be seen within metastatic lymph nodes from any primary malignancy (including thyroid, head/neck, and breast cancers). Correlation with clinical history and any cross-sectional imaging is helpful in these cases.

Diagnosis

Parathyroid adenoma

✓ Pearls

- Parathyroid scan is performed as a "localizing" and not diagnostic procedure prior to surgical exploration.
- Parathyroid adenoma is seen as a focal persistent activity on a delayed Tc99m sestamibi scan.
- False-positives include thyroid adenoma and thyroid carcinoma, which may be confirmed on a thyroid scan.

Suggested Readings

Mettler FA, Guiberteau MJ. Essentials of Nuclear Medicine Imaging. 5th ed. Philadelphia: Elsevier; 2006

Ziessman HA, O'Malley JP, Thrall JH. Nuclear Medicine: The Requisites. 3rd ed. Philadelphia: Elsevier; 2006

Case 262

Kamal D. Singh

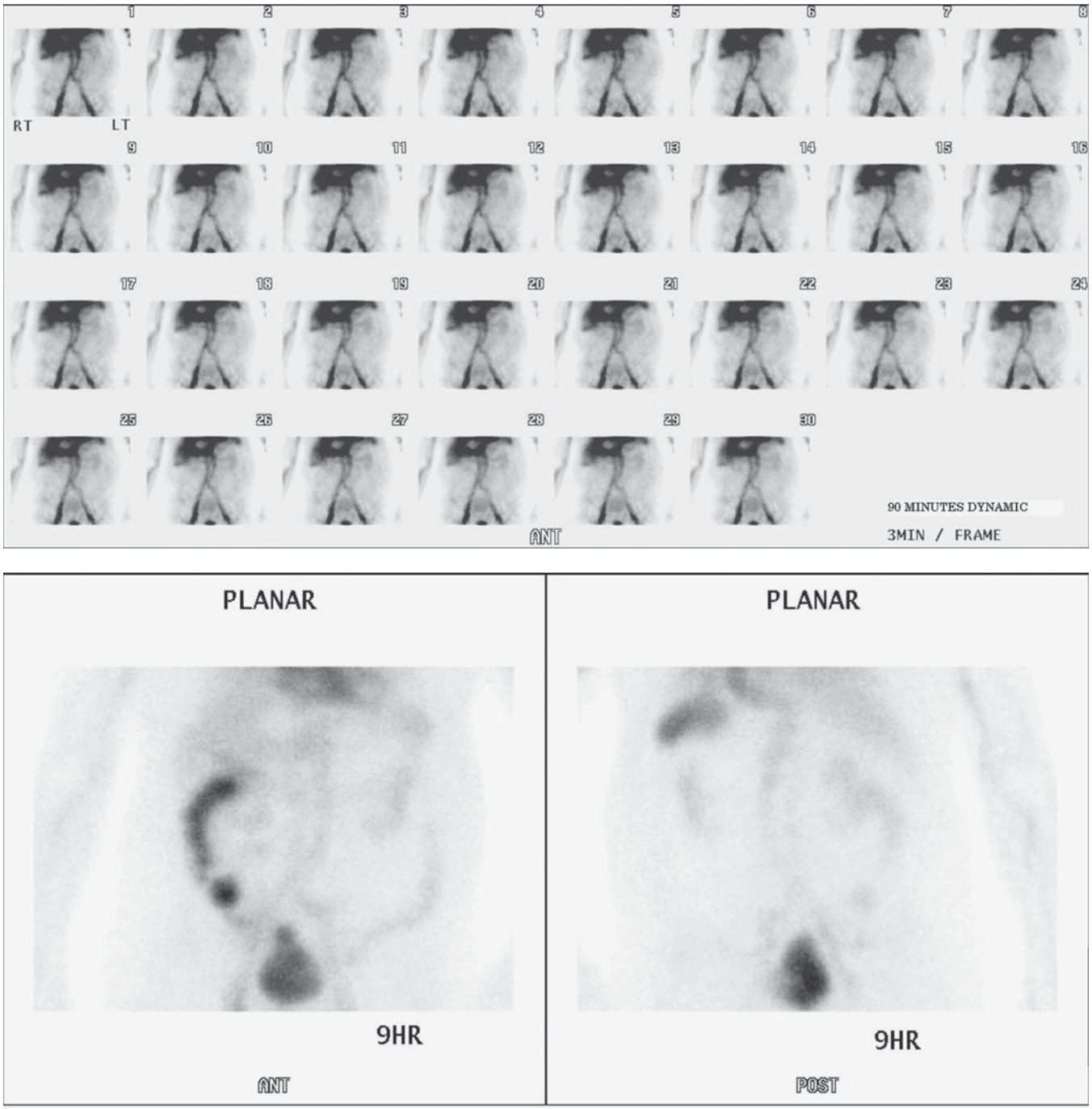


Fig. 262.1 **(A)** Images from a technetium 99m-labeled red blood cell scan demonstrate no active bleeding on initial dynamic imaging performed for 90 minutes. Incidental note is made of a photopenic hepatic lesion, consistent with a known simple cyst. **(B)** Delayed static images obtained 9 hours following radiotracer injection after another episode of gastrointestinal bleeding reveal tubular radiotracer activity along the right abdomen in the expected region of the ascending colon. Faint activity is also seen within the terminal ileum and distally within the transverse and descending colon. The patient was transferred to interventional radiology for angiography, which localized the bleeding site within the cecum.

Clinical Presentation

A 56-year-old man presents with acute intermittent bright red blood per rectum (BRBPR) (**Fig. 262.1**).

Key Imaging Finding

Intra-abdominal activity on technetium 99m (Tc99m) labeled red blood cell (RBC) scan

Top 3 Differential Diagnoses

- **Active gastrointestinal (GI) bleed.** Tc99m-labeled RBC scan is obtained for confirmation and localization of an active lower gastrointestinal (GI) bleed (hematochezia or BRBPR) prior to angiographic intervention. In contrast, patients with hematemesis from an upper GI bleed (proximal to the ligament of Treitz) typically undergo endoscopy for diagnosis and management. Common causes of lower GI bleeding are diverticulosis, angiodysplasia, inflammatory bowel disease, and neoplasm. After intravenous administration of the Tc99m-labeled RBC, dynamic imaging is performed for 60 to 90 minutes. Classic findings for active GI bleed include a focus of activity that appears "out of nowhere," increases in activity over time, and demonstrates peristalsis (intraluminal antegrade or retrograde transit). Scintigraphy is highly sensitive and can detect bleeding rates as low as 0.1 cc/minute compared with 1 cc/minute for angiography. Given the intermittent nature of most GI bleeds, Tc99m RBC allows for delayed imaging up to 24 hours from the time of initial injection. However, if bleeding is detected only on the delayed static imaging, precise localization is not possible.
- **Neoplasm or inflammatory bowel disease.** Hypervascular intestinal tumors or inflammatory bowel disease may be detected on a Tc99m-labeled RBC scan as focal or segmental static activity that does not change in position over time. Cross-sectional imaging or colonoscopy may aid in definitive diagnosis.
- **Genitourinary activity.** An area of activity that is fixed in location is not typical of an active GI bleed. Common causes of fixed activity include urinary tract activity, especially within the bladder, due to renal excretion of Tc99m RBC. Additionally, penile activity in a man and uterine activity in a menstruating woman can mimic rectosigmoid bleeding. Static lateral views are useful in distinguishing these entities from an active GI bleed.

Additional Differential Diagnoses

- **Free technetium.** The in vitro technique for Tc99m RBC allows for higher labeling efficiency (98%) compared with the modified in vivo (90%) or the in vivo (80%) methods. A higher labeling efficiency results in less free or unbound Tc99m in the bloodstream. Excess free Tc99m accumulates in the gastric mucosa and may enter the small bowel through peristalsis, simulating an active GI bleed. Imaging over the neck to detect thyroid activity can confirm the presence of free Tc99m.

Diagnosis

Active lower gastrointestinal (cecal) bleed

✓ Pearls

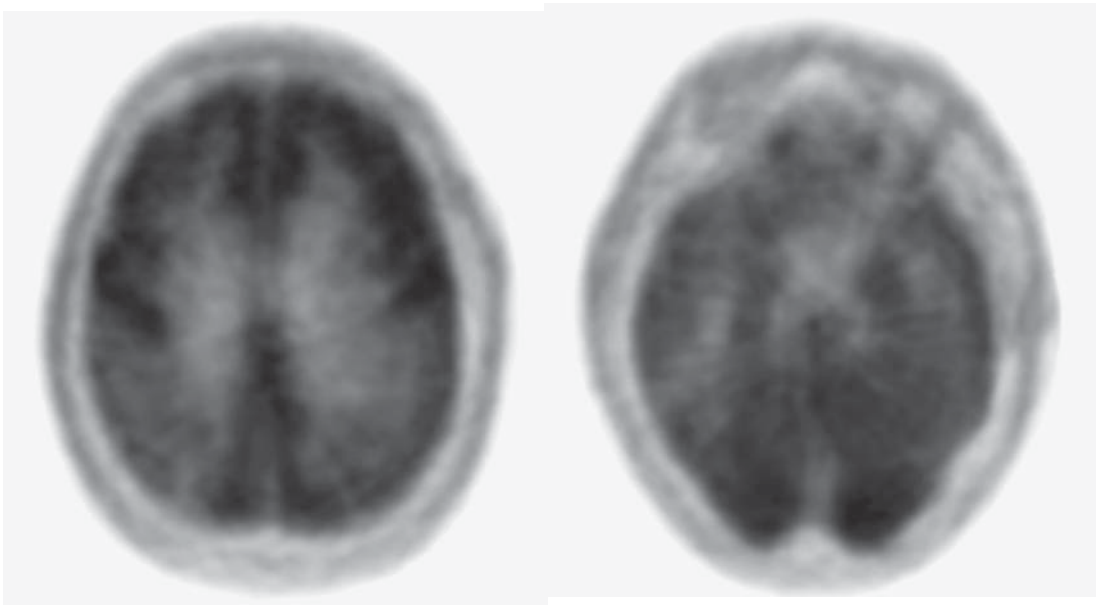
- In vitro labeling of RBC has high labeling efficiency and is the preferred method for a GI bleed scan.
- If bleeding is not detected on initial dynamic imaging, delayed images can be obtained up to 24 hours.
- Technetium sulfur colloid scan has a comparatively shorter preparation time but does not offer the flexibility of delayed imaging.
- Etiologies of false-positive scans usually present as focal activity without peristalsis.

Suggested Readings

Mettler FA, Guiberteau MJ. Essentials of Nuclear Medicine Imaging. 5th ed. Philadelphia: Elsevier; 2006

Case 263

Cameron C. Foster



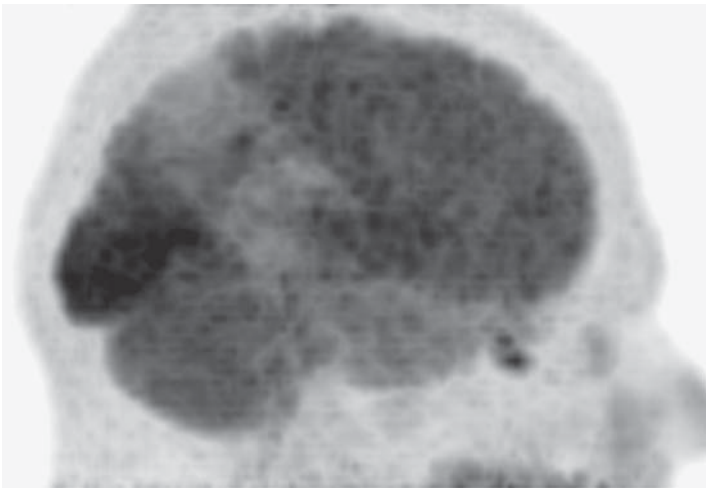


Fig. 263.1 Attenuation-corrected axial 18F-fluorodeoxyglucose positron emission tomography (FDG PET) images of the brain demonstrate decreased activity within **(A)** the bilateral parietal and **(B)** temporal lobes, with intact normal activity within the bilateral frontal and occipital lobes. **(C)** Attenuation-corrected FDG PET maximum intensity projection image, in sagittal projection, demonstrates decreased activity in both the parietal and temporal lobes with intact normal activity within the cerebellum and frontal and occipital lobes.

Clinical Presentation

A 62-year-old man presents with a 6-year history of cognitive decline (**Fig. 263.1**).

Key Imaging Finding

Decreased cortical 18F-fluorodeoxyglucose (FDG) activity in the setting of dementia

Top 3 Differential Diagnoses

- **Alzheimer disease (AD).** AD is the most common dementing disorder affecting adults. Presentation is usually after age 65, and prevalence increases with age. Initial imaging findings are of decreased metabolism (FDG positron emission tomography [PET]) and blood flow (single-photon emission computed tomography [SPECT]) in the bilateral temporoparietal areas with relative sparing of the primary motor, somatosensory, and visual cortices. One of the earliest findings is hypometabolic posterior cingulate gyri. Early-stage AD may show hemispheric asymmetry. Later-stage AD will also begin to show metabolic decline in the frontal lobes at a faster rate than normal aging dementia. In general, the amount of decreased metabolism directly correlates with the degree of symptoms. Studies have shown FDG PET to have 94% sensitivity and 73% specificity for AD.
- **Pick disease.** Pick disease is the classic though rare member of the frontotemporal dementia (FTD) family. It is characterized by decreased metabolism in the bilateral frontal lobes and anterior temporal lobes on FDG PET imaging. Differentiation from other disorders such as AD are based on symptoms, as Pick disease has memory impairment as a secondary or absent feature rather than a primary symptom as is seen in AD. Differential considerations for isolated decreased metabolism in the frontotemporal regions include such entities as depression, cocaine abuse, and amyotrophic lateral sclerosis. This distribution is rarely seen in AD.
- **Multi-infarct dementia (MID).** MID is the most common cause of vascular dementia and is the second most common cause of all dementias for adults older than age 65 (behind AD). Although MID is usually identified via computed tomography or magnetic resonance imaging, FDG PET and SPECT imaging show similar patterns of decreased activity in a diffuse or multifocal distribution that progress over time. Frontotemporal distribution can be seen in MID and can be difficult to differentiate from other FTDs; diffuse distribution of MID can also be difficult to differentiate from severe AD.

Additional Differential Diagnoses

- **Parkinson disease.** Parkinson disease is largely a clinical diagnosis that has a normal appearance on FDG PET in the early stages (striatum may be mildly increased). In later stages, decreased activity will be seen in the cortices and will progress along with the disease. Use of serial FDOPA-PET scans in patients with Parkinson disease will initially show decreased activity within the posterior putamen with sparing of the caudate that, over time, will involve more of the putamen and eventually include the posterior aspect of the caudate.

Diagnosis

Alzheimer disease

✓ Pearls

- AD shows bilateral temporoparietal hypometabolism with sparing of the occipital lobes (visual cortices).
- Frontal lobe hypometabolism can be seen in FTD (e.g., Pick disease), depression, and schizophrenia.
- MID presents as multifocal regions of decreased activity.
- Dementia with Lewy bodies has a similar appearance to AD with less sparing of the occipital lobe.

Suggested Readings

Herholz K, Herscovitch P, Heiss WD. NeuroPET. Berlin, Germany: Springer-Verlag; 2004

Hoffman JM, Welsh-Bohmer KA, Hanson M, et al. FDG PET imaging in patients with pathologically verified dementia. J Nucl Med 2000;41(11):1920–1928

Van Heertum RL, Tikofsky RS. Positron emission tomography and single-photon emission computed tomography brain imaging in the evaluation of dementia. Semin Nucl Med 2003;33(1):77–85

Ziessman HA, O'Malley JP, Thrall JH. Nuclear Medicine: The Requisites. 3rd ed. Philadelphia: Elsevier; 2006

Case 264

Cameron C. Foster

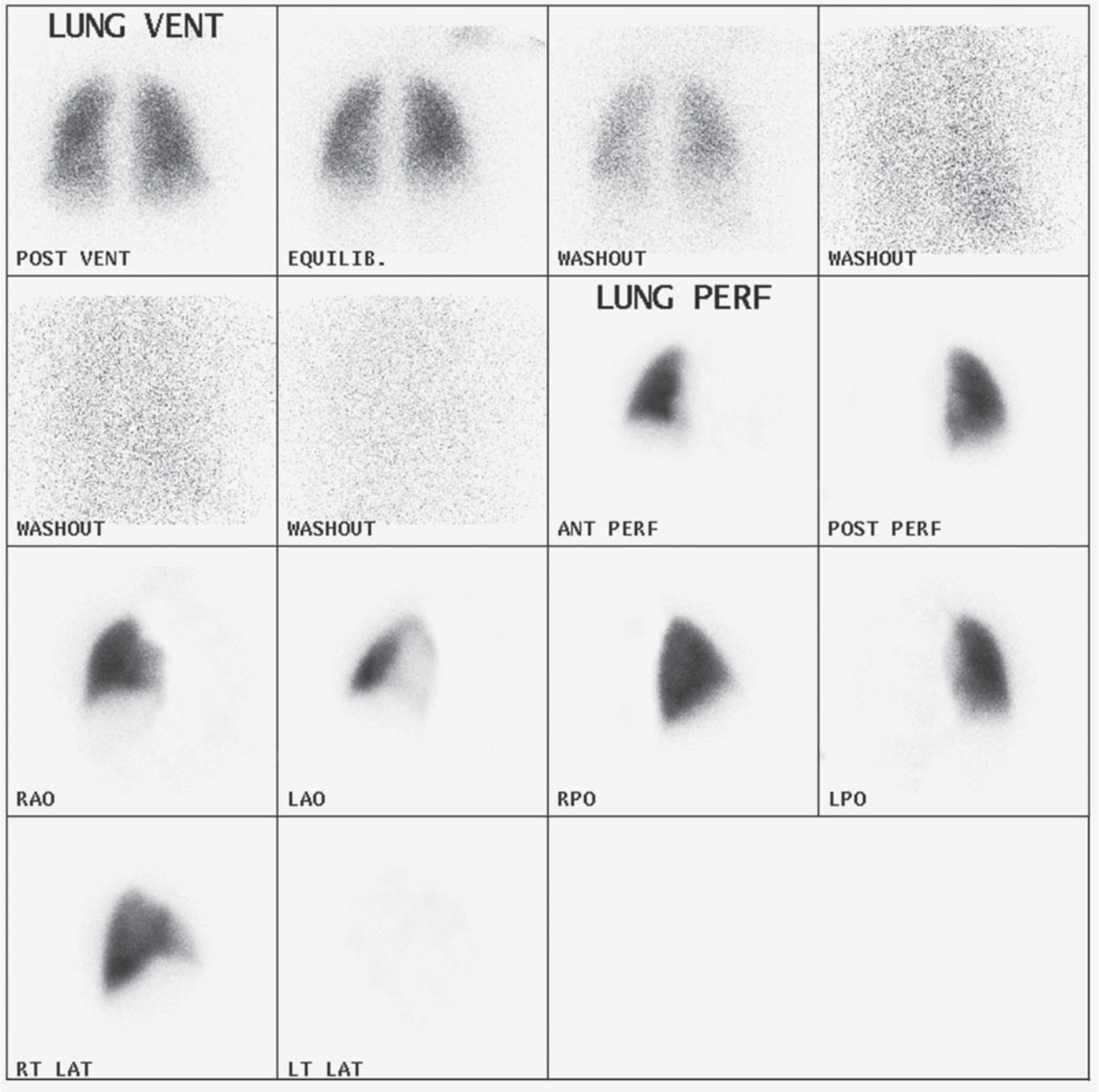


Fig. 264.1 Ventilation/perfusion scintigraphy (V/Q scan) demonstrates normal inspiratory and equilibrium ventilation images in posterior projection without evidence of tracer (xenon 133 gas) retention on washout images. Perfusion imaging in multiple obliquities demonstrates unilateral absence of tracer (technetium 99m macroaggregated albumin) in the left lung with normal distribution of tracer within the right lung.

Clinical Presentation

A 54-year-old man presents with shortness of breath (**Fig. 264.1**).

Key Imaging Finding

Unilateral absent lung perfusion

Top 3 Differential Diagnoses for Perfusion Worse Than Ventilation

- **External compression (tumor, fibrosing mediastinitis).** Unilateral absence of lung perfusion is a rare finding. A ventilation/perfusion (V/Q) scan cannot determine the cause on its own. However, in the setting of a perfusion defect that is worse than ventilation, extrinsic compression of the pulmonary artery is the most common cause. Typically it is from a central lung tumor. Fibrosing mediastinitis is another entity that could lead to pulmonary artery occlusion and absence of perfusion. Cross-sectional imaging is essential to determine the presence of external compression.
- **Pulmonary artery anomalies or corrected congenital heart disease.** Pulmonary artery atresia, severe pulmonary artery stenosis, or pulmonary webs may cause unilateral absence of perfusion with perfusion defect worse than ventilation. Additionally, corrected congenital heart disease may produce similar findings on V/Q scan. Dedicated contrast cross-sectional imaging via computed tomography or magnetic resonance imaging/angiography can greatly improve detection, as well as correlation for prior surgical history.
- **Massive unilateral pulmonary embolism.** Although massive unilateral pulmonary embolism and aortic dissection both can produce a similar appearance on V/Q scan (unilateral absent perfusion), they are less likely in comparison to other causes such as compression. Massive pulmonary emboli of this magnitude will often have more than one V/Q mismatch affecting both lungs.

Top 3 Differential Diagnoses for Ventilation Worse Than Perfusion

- **Mucous plug.** A mucous plug may obstruct ventilation with compensatory vasoconstriction of the pulmonary arteries. The degree of accompanying perfusion abnormality will increase with time with continued obstruction due to arteriolar constriction induced by local hypoxia. Because this is primarily an airway abnormality, the ventilation defect will be larger than the perfusion defect.
- **Unilateral diffuse parenchymal disease.** Diffuse air-space disease, atelectasis, or large pneumothorax involving an entire lung will result in decreased or absent ventilation with compensatory vasoconstriction of the pulmonary arteries. The degree of lung involvement will determine the degree of perfusion and ventilation defects.
- **Endobronchial lesion (mass or foreign body).** Endobronchial lesions can cause a ventilation defect that is larger than perfusion. Central lesions can cause diminished activity within an entire lung. The relative decrease in ventilation to perfusion is an indicator of the extent of luminal involvement.

Diagnosis

Extrinsic compression (left hilar malignancy)

✓ Pearls

- Ventilation scan may be performed with xenon 133 (Xe 133) gas or technetium 99m diethylenetriamine pentaacetic acid (DTPA) aerosol.
- Ventilation scan with Xe-133 requires a negative pressure room and charcoal traps for proper elimination.
- Wedge-shaped (peripheral), segmental mismatched perfusion defects are concerning for pulmonary emboli.
- Unilateral absent or decreased lung perfusion or ventilation is usually seen with nonembolic etiologies.

Suggested Readings

Mettler FA, Guiberteau MJ. Essentials of Nuclear Medicine Imaging. 5th ed. Philadelphia: Elsevier; 2006

White RI Jr, James AE Jr, Wagner HN Jr. The significance of unilateral absence of pulmonary artery perfusion by lung scanning. Am J Roentgenol Radium Ther Nucl Med 1971;111(3):501–509

Ziessman HA, O'Malley JP, Thrall JH. Nuclear Medicine: The Requisites. 3rd ed. Philadelphia: Elsevier; 2006

Case 265

Cameron C. Foster

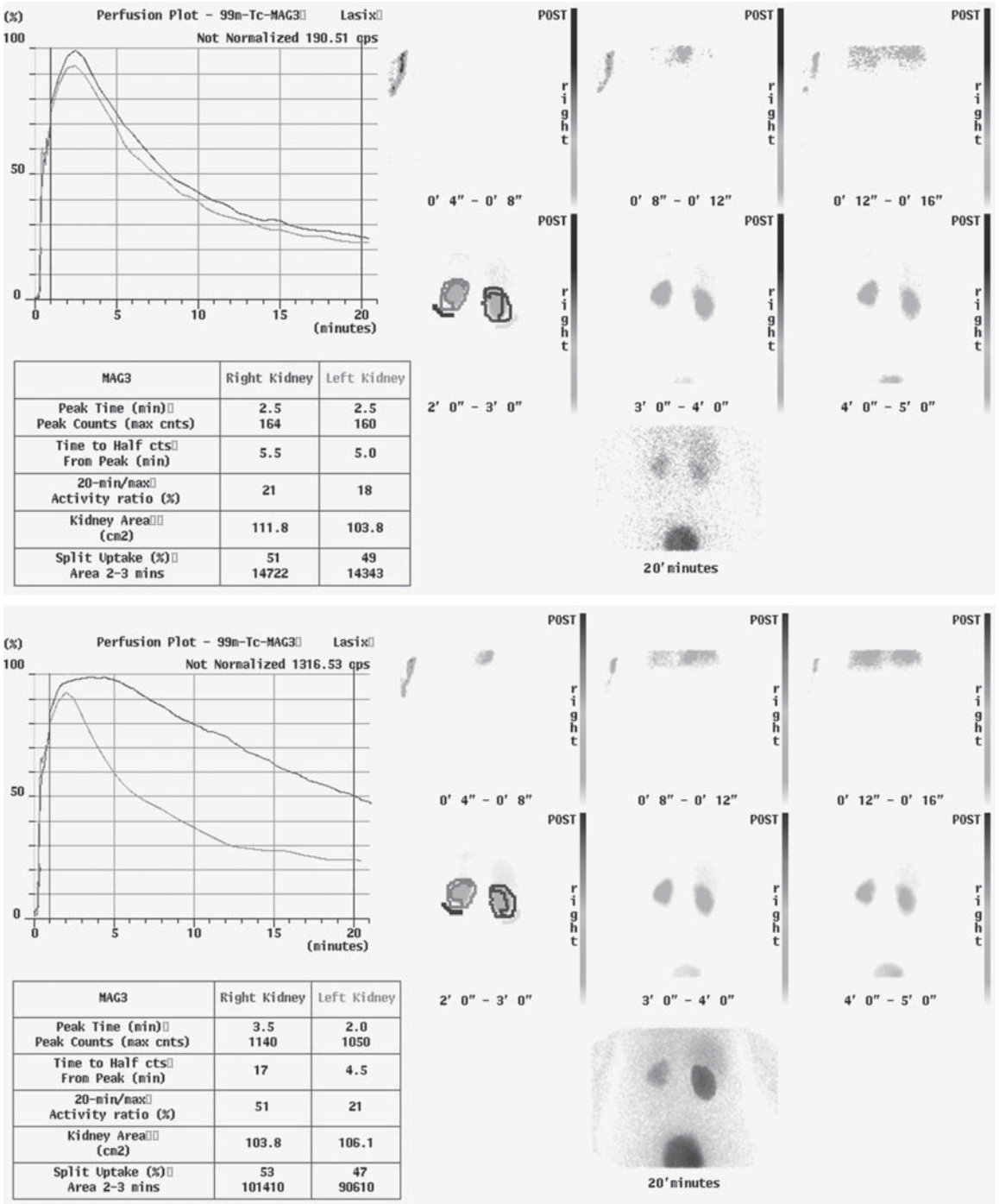


Fig. 265.1 **(A)** Baseline mercapto-acetyltriglycine 3 (MAG 3) renogram with angiotensin-converting enzyme inhibitor and angiotensin II receptor blocker medication held demonstrates normal bilateral renal function. Normal faint activity is seen in both kidneys on the final image at 20 minutes. **(B)** Captopril MAG 3 renogram demonstrates normal left renal function and marked increase in 20/max, T ½, peak time, and generalized rightward shift of the renal curve on the right. Asymmetrically increased right renal activity is seen on the final image at 20 minutes.

Clinical Presentation

A 61-year-old woman presents with hypertension (**Fig. 265.1**).

Key Imaging Finding

Worsening renal function on mercapto-acetyltriglycine 3 (MAG 3) renal scan following Captopril administration

Top 3 Differential Diagnoses

- **Renal artery stenosis (RAS).** Renovascular hypertension accounts for ~1 to 4% of all hypertension cases. It is most commonly due to atherosclerosis or fibromuscular dysplasia. Although other modalities such as magnetic resonance angiography may be better at detecting an actual stenosis, angiotensin-converting enzyme (ACE) inhibition renography is very specific for functional renovascular hypertension. Narrowing of the afferent renal artery >60% typically is the low-end cutoff for causing renovascular hypertension via the renin angiotensin cascade. ACE inhibitor is administered before radiotracer injection, and the patient is monitored hemodynamically during imaging. MAG 3 imaging is considered positive by curvilinear changes due to cortical retention (increase in time to peak cortical activity and 20/max, decreased split function, rightward shift of the curve, etc.) when compared with a baseline scan. When appropriately performed, the test approaches 90% sensitivity and 95% specificity. A positive study generally predicts improvement of hypertension upon revascularization.
- **Unilateral urinary obstruction.** Differentiating between unilateral urinary obstruction and RAS by MAG 3 renography is usually done by the appearance of an obstructive curve (poor/delayed excretion) on the baseline scan that does not improve with Lasix administration. If the affected kidney is already demonstrating significant renal impairment, the response to Lasix as well as the response to the ACE inhibitor challenge may be diminished, which results in reduced sensitivity and specificity for both entities.
- **False-positive scan in patients on calcium channel blocker.** False-positive renal impairment on a MAG 3 renogram with ACE inhibitor challenge study can be seen in patients who are on chronic calcium channel blockers. This effect would be bilateral and symmetric (except in cases of existing unilateral renal impairment or nephrectomy). In the setting of bilateral renal decline on a renogram in the presence of calcium channel blocking medication, the study should be repeated after discontinuance of these medications.

Diagnosis

Renal artery stenosis (right-sided)

✓ Pearls

- Adequate fluid hydration prior to and blood pressure monitoring during a Captopril scan is important.
- A positive scan suggests hemodynamically significant RAS and predicts benefit from revascularization.
- Baseline renal scan with MAG 3 is compared with a post-Captopril renal scan with MAG 3 for diagnosis.
- False-positives for bilateral RAS include dehydration, bilateral obstruction, and significant hypotension.

Suggested Readings

Fine EJ. Diuretic renography and angiotensin converting enzyme inhibitor renography. Radiol Clin North Am 2001;39(5):979–995

Mettler FA, Guiberteau MJ. Essentials of Nuclear Medicine Imaging. 5th ed. Philadelphia: Elsevier; 2006

Ziessman HA, O'Malley JP, Thrall JH. Nuclear Medicine: The Requisites. 3rd ed. Philadelphia: Elsevier; 2006

Case 266

Kamal D. Singh

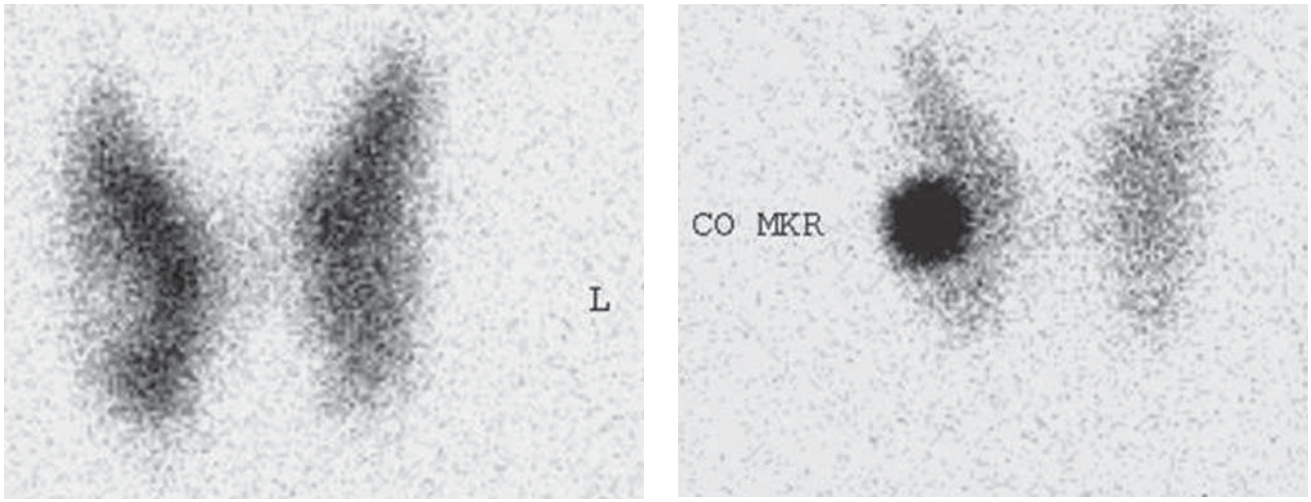


Fig. 266.1 **(A)** Planar pinhole imaging of the thyroid with iodine 123 performed at 24 hours after oral radioiodine administration demonstrates a round photopenic defect in the midaspect of the right thyroid lobe. **(B)** A cobalt marker was placed over the palpable abnormality, which corresponds to this cold nodule. Radioactive iodine uptake levels at 4 and 24 hours were within normal limits.

Clinical Presentation

A 48-year-old woman presents with a palpable right thyroid nodule and normal thyroid-stimulating hormone (TSH) (**Fig. 266.1**).

Key Imaging Finding

Cold nodule on an iodine 123 (I123) thyroid scan

Top 3 Differential Diagnoses

- **Thyroid carcinoma.** Ultrasound and fine-needle aspiration (FNA) are the primary diagnostic procedures for a thyroid nodule in a euthyroid patient. Nuclear medicine thyroid imaging is reserved for patients with hyperthyroidism (suppressed TSH). Cold or nonfunctioning nodules on I123 or technetium (Tc) pertechnetate thyroid scans are nonspecific findings and may represent colloid cyst (40%), nonfunctioning adenoma (40%), or thyroid carcinoma (15–20%). The incidence of cancer is lower (<5%) in the setting of multinodular goiter. Hot or hyperfunctioning nodules on I123 scans are essentially always benign. However, a hot nodule on a Tc pertechnetate scan requires further evaluation with an I123 scan to exclude a discordant nodule, which requires further evaluation with FNA to exclude thyroid carcinoma. Risk factors for thyroid malignancy include age <20 or >60 years, male patient, family history, prior radiation therapy to the head/neck, and a dominant nodule with concerning ultrasound features (solid, hypoechoic, hypervascular nodule with microcalcifications). Papillary carcinoma is the most common subtype, followed by follicular. Medullary and anaplastic carcinomas are less common and highly aggressive. Treatment of localized thyroid carcinoma typically consists of total thyroidectomy followed by I131 ablation therapy. Patients are followed with thyroglobulin levels, as well as whole-body I131 imaging, for at least 2 years after radioiodine ablation.
- **Colloid cyst.** Colloid cysts are benign localized follicles filled with gelatinous colloid. They usually originate from cystic degeneration of thyroid adenomas and are hyperintense on T1-weighted magnetic resonance imaging due to their high protein content. Ultrasound characteristics include a cystic lesion with inspissated colloid, which is hyperechoic and demonstrates ring-down or comet tail artifact.
- **Nonfunctioning adenoma.** Thyroid adenomas are benign lesions that may be functioning (hot nodule) or nonfunctioning (cold nodule). They can be multiple in the setting of a multinodular goiter. On ultrasound, benign adenomas are typically well encapsulated with a hypoechoic halo. Interval growth is not unusual. A dominant hyperfunctioning adenoma with suppression of the remainder of the gland in the setting of hyperthyroidism is called an autonomous nodule (produces thyroid hormones independent of TSH). Hyperthyroid patients with multinodular goiter or autonomous nodules are generally more resistant to ablation therapy than patients with Graves disease; hence these patients are treated with higher doses of I131 (~30 mCi).

Diagnosis

Thyroid cancer

✓ Pearls

- I123 thyroid scan is indicated in hyperthyroidism (low TSH) or to detect the functional status of a nodule.
- A cold nodule may represent a colloid cyst (40%), nonfunctioning adenoma (40%), or thyroid cancer (20%).
- A hot nodule on Tc pertechnetate (trapping without organification) may be cold or "discordant" on I123.
- Papillary and follicular cancers are amenable to I131 ablation, whereas medullary and anaplastic carcinomas are not.

Suggested Readings

Mettler FA, Guiberteau MJ. Essentials of Nuclear Medicine Imaging. 5th ed. Philadelphia: Elsevier; 2006

Ziessman HA, O'Malley JP, Thrall JH. Nuclear Medicine: The Requisites. 3rd ed. Philadelphia: Elsevier; 2006

Case 267

Vicki E. Nagano

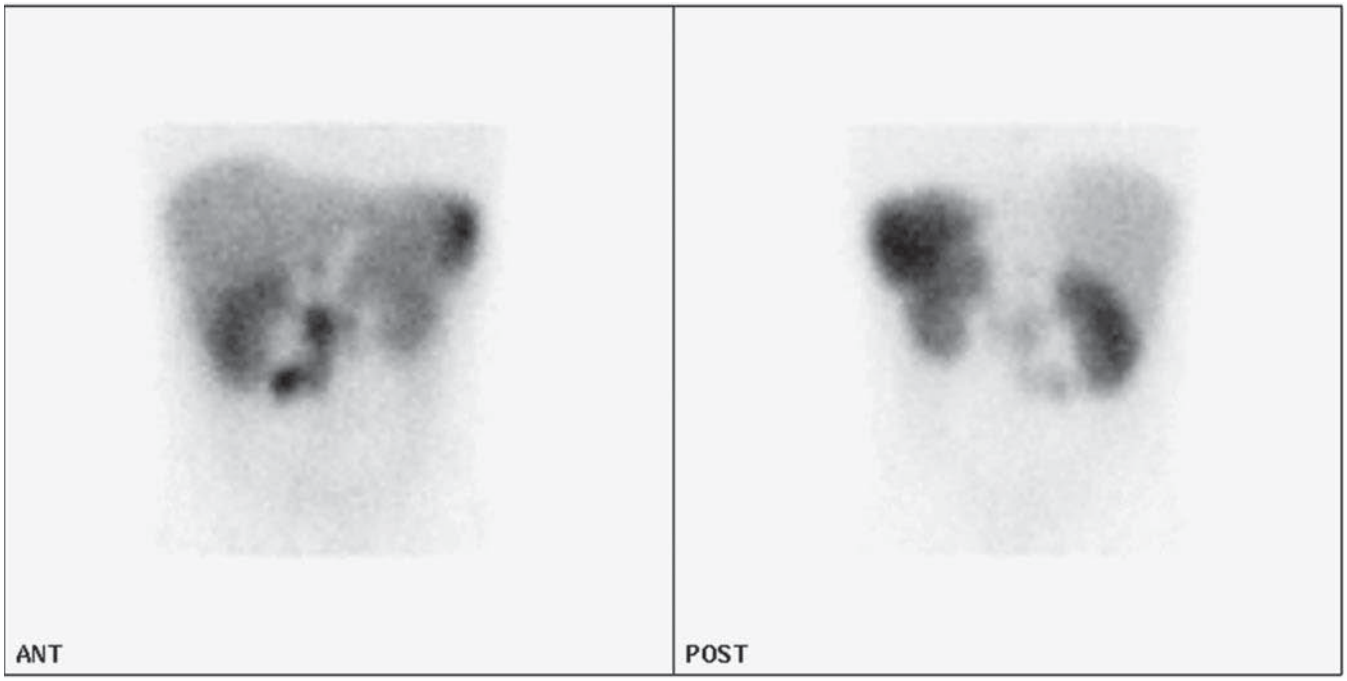




Fig. 267.1 **(A)** Forty-eight-hour delayed anterior and posterior abdominal indium 111 pentreotide images show uptake within a large mesenteric mass just to the right of the midline and a portacaval lymph node. **(B)** Contrast-enhanced coronal computed tomography image shows a 7 cm mesenteric mass encasing the distal superior mesenteric artery.

Clinical Presentation

A 43-year-old man presents with abdominal pain and weight loss for 2 years (**Fig. 267.1**).

Key Imaging Finding

Focal abdominal uptake on indium 111 (In111) pentreotide scan (Ostreoscan)

Top 3 Differential Diagnoses

- **Neuroendocrine tumor.** Somatostatin is a peptide that inhibits the release of anterior pituitary hormones and certain intestinal and pancreatic peptides, such as insulin, gastrin, glucagon, and cholecystokinin. Indium 111 (In111) pentreotide (Octreoscan) contains an amino acid analogue of somatostatin and is frequently used for the evaluation of neuroendocrine tumors. Normal radiopharmaceutical distribution includes intense splenic uptake with slightly less prominent uptake in the kidneys, followed by the liver. Physiologic uptake is also seen within the thyroid gland, gallbladder, bowel, and bladder. Planar imaging surveys the entire body; single-photon emission computed tomography imaging is essential in the chest and abdomen. Octreoscan is most commonly used for islet cell and carcinoid tumors. The sensitivity for islet cell tumors varies based on the subtype: insulinoma (50%), gastrinoma (75–93%), glucagonoma (73%), and VIPoma (88%). Sensitivity for various other neuroendocrine tumors is as follows: carcinoid (80–90%), neuroblastoma (over 85%), medullary thyroid carcinoma (54%), malignant pheochromocytoma (87%), paraganglioma (93%), and small cell carcinoma of the lung (100%). Neuroblastoma and pheochromocytoma are more commonly imaged with iodine 123 or 131 (I123 or I131) meta-iodobenzylguanidine (MIBG).
- **Metastatic disease.** Nonneuroendocrine tumors, which contain somatostatin receptors and can metastasize to the mesentery, include non–small cell lung cancer, breast cancer, and lymphoma (sensitivity of 70% each). Lymphoma is the most common malignant neoplasm affecting the mesentery. Approximately 30 to 50% of patients with non-Hodgkin lymphoma will have disease in the mesenteric lymph nodes.
- **Granulomatous disease.** Somatostatin receptors are also present in granulomatous diseases, such as sarcoidosis and tuberculosis (TB). Intra-abdominal TB lymphadenopathy has most commonly been reported in the lesser omental, mesenteric, and upper para-aortic regions. Contrast computed tomography (CT) typically demonstrates rim enhancement in the peripheral inflammatory reaction and a low-attenuation center in the central caseous necrosis. In contrast, malignant and reactive lymph nodes generally demonstrate homogeneous enhancement on contrast CT. Enlarged mesenteric nodes can also be seen in some noninfectious, inflammatory conditions such as sarcoidosis.

Diagnosis

Neuroendocrine tumor (carcinoid)

✓ Pearls

- In111 pentreotide (Octreoscan) is useful for imaging metastatic neuroendocrine tumors.
- Physiologic activity is seen within the spleen, liver, gallbladder, kidneys, bowel, bladder, and faint thyroid.
- Uptake is also seen in granulomatous disease, lymphoma, meningioma, astrocytoma, and breast cancer.
- Neuroblastoma and pheochromocytoma are more commonly imaged with MIBG.

Suggested Readings

Intenzo CM, Jabbour S, Lin HC, et al. Scintigraphic imaging of body neuroendocrine tumors. Radiographics 2007;27(5):1355–1369

Sheth S, Horton KM, Garland MR, Fishman EK. Mesenteric neoplasms: CT appearances of primary and secondary tumors and differential diagnosis. Radiographics 2003;23(2):457–473, quiz 535–536

Ziessman HA, O'Malley JP, Thrall JH. Nuclear Medicine: The Requisites. 3rd ed. Philadelphia: Elsevier; 2006

Case 268

Kamal D. Singh

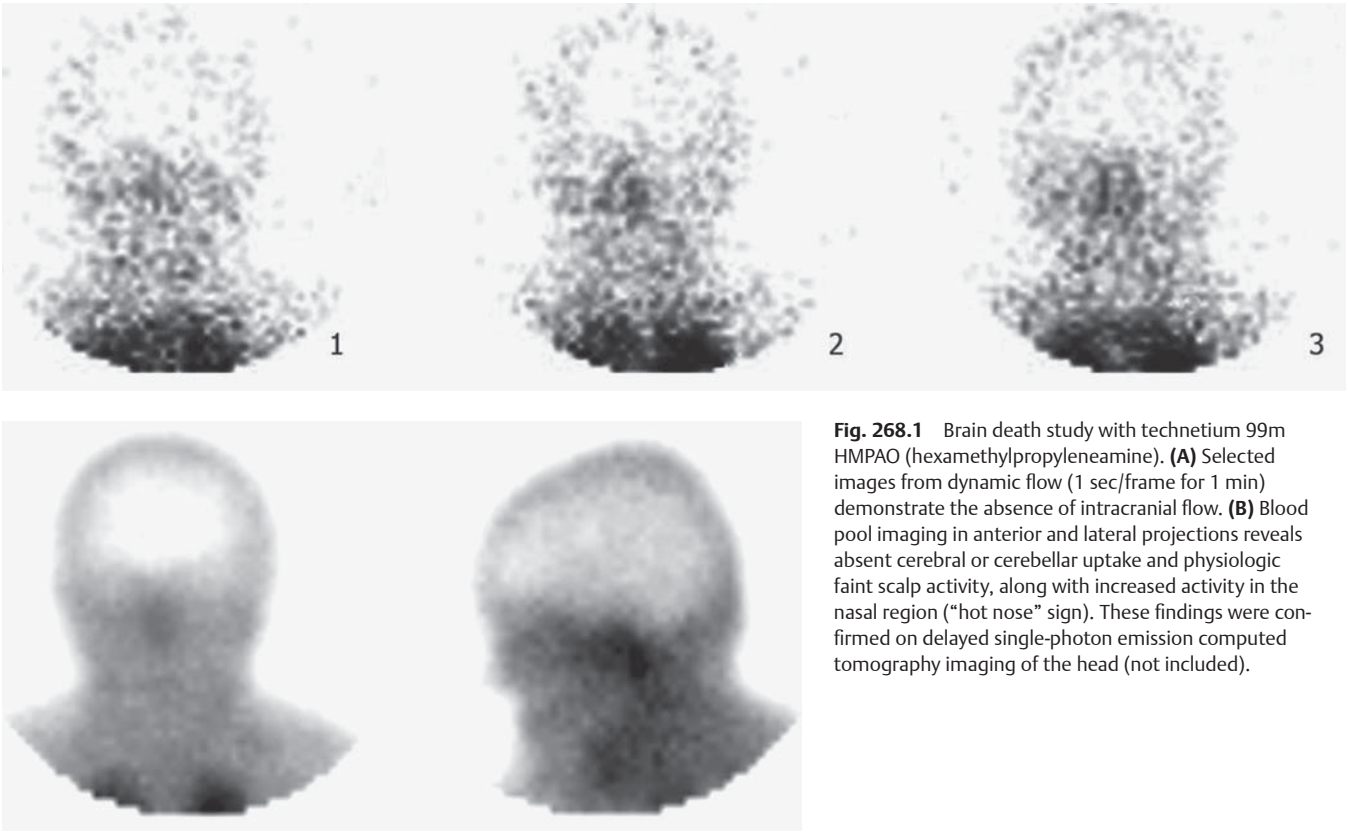


Fig. 268.1 Brain death study with technetium 99m HMPAO (hexamethylpropyleneamine). **(A)** Selected images from dynamic flow (1 sec/frame for 1 min) demonstrate the absence of intracranial flow. **(B)** Blood pool imaging in anterior and lateral projections reveals absent cerebral or cerebellar uptake and physiologic faint scalp activity, along with increased activity in the nasal region ("hot nose" sign). These findings were confirmed on delayed single-photon emission computed tomography imaging of the head (not included).

Clinical Presentation

A 57-year-old man is unresponsive after a motor vehicle accident (**Fig. 268.1**).

Key Imaging Finding

Absent intracranial activity on a technetium 99m (Tc99m) HMPAO (hexamethylpropyleneamine) scan

Top 2 Differential Diagnoses

- **Brain death.** Brain death is a clinical diagnosis using a combination of physical examination, electroencephalography, and imaging findings. A brain death scan has a high specificity as a confirmatory study for absent intracranial perfusion. Scintigraphic imaging can be performed at the patient's bedside with a portable gamma camera. Imaging may be performed with a nonspecific flow agent (Tc99m DTPA [diethylenetriamine pentaacetic acid]) or with lipophilic brain perfusion agents (Tc99m HMPAO or Tc99m ECD [ethyl cisteinate dimer]), which are extracted by viable brain tissue proportional to cerebral flow. A scalp band or tourniquet may be placed around the head to avoid interfering activity from extracranial vessels. The scalp band, however, is contraindicated in pediatric patients due to increased intracranial pressure. First-minute dynamic flow imaging is performed in an anterior projection, with subsequent static blood pool images in both anterior and lateral projections. Delayed single-photon emission computed tomography (SPECT) imaging may improve sensitivity in cases where brain perfusion agents are used. Normal imaging reveals symmetric flow within the anterior and middle cerebral arteries ("trident" sign) on the anterior view, with visualization of dural venous sinuses on blood pool imaging. In brain death, there is termination of carotid activity at the skull base due to increased intracranial pressure overcoming perfusion pressure, thereby shunting blood through the external carotid artery branches projecting over the nasal region ("hot nose" sign).
- **Quality control—poor radiopharmaceutical bolus.** Peripheral intravenous injection of the radiotracer is performed as a rapid/tight bolus. A proper bolus is confirmed by visualizing distinct activity within the proximal common carotid arteries. Dose infiltration, slow radiotracer injection, or missed bolus can result in false-positive studies, especially when flow agents (like Tc99m DTPA, which does not cross the blood–brain barrier) are used. Tc99m DTPA is rapidly cleared through renal excretion, which allows for reinjection and reimaging in the setting of equivocal or technically limited studies.

Diagnosis

Brain death

✓ Pearls

- Besides brain death, Tc99m HMPAO can image cerebral ischemia, seizure focus, and dementia.
- Absent intracranial flow and no cerebral/cerebellar uptake of Tc99m HMPOA confirm brain death.
- Brain parenchymal uptake of radiotracer is normally not seen with flow agents like Tc99m DTPA.
- Scintigraphic evaluation is unaffected by drug intoxication, hypothermia, or metabolic derangements.

Suggested Readings

Conrad GR, Sinha P. Scintigraphy as a confirmatory test of brain death. Semin Nucl Med 2003;33(4):312–323

Mettler FA, Guiberteau MJ. Essentials of Nuclear Medicine Imaging. 5th ed. Philadelphia: Elsevier; 2006

Ziessman HA, O'Malley JP, Thrall JH. Nuclear Medicine: The Requisites. 3rd ed. Philadelphia: Elsevier; 2006

Case 269

Kamal D. Singh

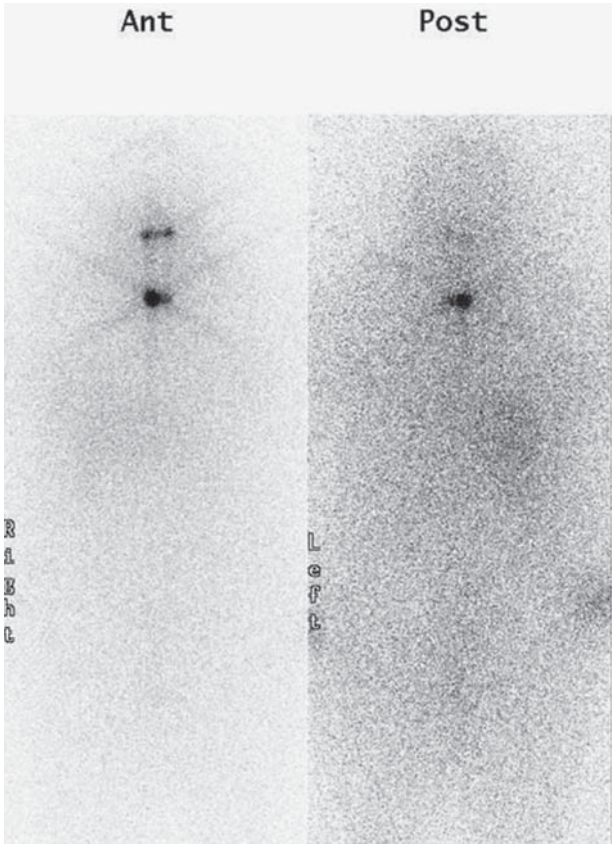
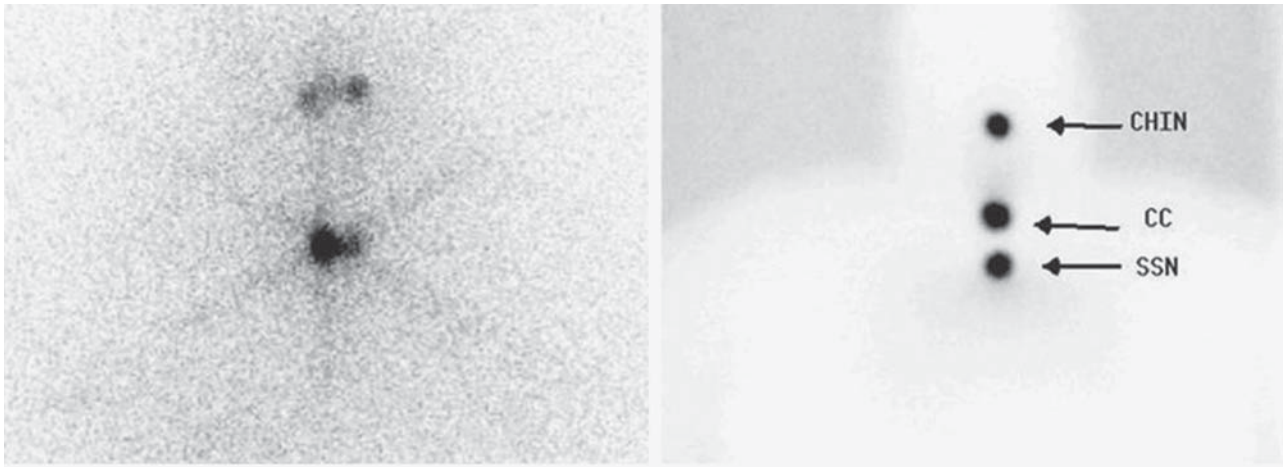


Fig. 269.1 Postablation iodine 131 whole-body scan. **(A)** Anterior and posterior whole-body images, along with spot views of the neck without and **(B)** with cobalt markers, demonstrate significant midline cervical uptake in the expected region of the thyroid bed with "star artifact." There is physiologic salivary gland or nasopharyngeal uptake as well as faint diffuse hepatic activity.



Clinical Presentation

A 45-year-old woman presents with a history of papillary thyroid carcinoma. The patient underwent a total thyroidectomy and recently had iodine 131 (I131) therapy (**Fig. 269.1**).

Key Imaging Finding

Focal neck uptake on an I131 postablation scan

Top 3 Differential Diagnoses

- **Residual thyroid tissue.** Patients with differentiated thyroid carcinoma are typically treated surgically with postoperative radioiodine (I131) ablation. In the postoperative but preablation period, whole-body thyroid imaging is typically performed with I131 (<5 mCi) or I123 (2 mCi) to evaluate for the amount of residual thyroid tissue, as well as the presence of local or distant metastases. The patient's thyroid supplementation is withheld for 4 weeks prior to imaging to allow the thyroid-stimulating hormone (TSH) level to rise (alternatively, recombinant TSH may be administered without withdrawal of thyroid hormone replacement), which improves the sensitivity of the study. I131 ablation is then performed; the dose depends on whether the patient is being treated for residual thyroid tissue (30–75 mCi), local metastases to cervical lymph nodes (75–150 mCi), or distant metastases from hematogenous spread (150–200 mCi). Imaging is performed 10 days after ablation therapy as a baseline for future surveillance scans. On any I131 imaging study, a high degree of functional thyroid tissue (residual thyroid tissue or metastatic disease) may result in septal penetration due to the high energy of the I131 photons (364 keV). This may result in the "star artifact."
- **Cervical nodal metastases.** Thyroid carcinoma may have local (cervical nodes) or distant (mediastinal, pulmonary, or osseous nodes) metastases, which require a larger I131 ablation dose than does ablation of a normal thyroid gland remnant. Papillary carcinoma typically spreads via lymphatics to local cervical lymph nodes, whereas follicular carcinoma spreads hematogenously to distant sites. The I131 dose varies based on the location and extent of disease (75–150 mCi to treat local disease; 150–200 mCi for distant metastases). After initial radioiodine therapy, yearly surveillance includes serum thyroglobulin levels and, if indicated, a diagnostic I131 whole-body metascan. I131 cancer treatment may be repeated in the event of recurrent disease, with generally 6 months to a year interval between ablation doses to avoid bone marrow suppression from a cumulated dose effect.
- **Physiologic pharyngeal/esophageal activity.** On all I131 or I123 scans, physiologic uptake is expected within the salivary glands, stomach, intestines, and urinary bladder. Nonfocal hepatic uptake is also seen in cases where there is residual functioning thyroid tissue (normal remnant or metastases), as thyroid hormone is metabolized by the liver. Focal increased activity, however, is more suggestive of metastases. In addition to primary renal excretion, radioiodine is excreted in saliva; hence transient swallowed activity within the pharynx or esophagus may mimic cervical or mediastinal metastases. Physiologic activity can be confirmed by administration of oral fluids to clear the proximal digestive tract with reimaging in anterior and lateral projections.

Diagnosis

Residual or remnant thyroid bed activity

✓ Pearls

- Pretherapy I123 or I131 diagnostic metascan can identify residual thyroid and detect metastases.
- If using I131 for diagnostic metascan, dose <5 mCi is recommended to avoid "stunning" prior to therapy.
- Postablation I131 whole-body scan establishes the baseline for future surveillance.
- In patients with elevated thyroglobulin and negative I131 whole-body scan, a positron emission tomography scan is recommended.

Suggested Readings

Maxon HR III, Smith HS. Radioiodine-131 in the diagnosis and treatment of metastatic well differentiated thyroid cancer. Endocrinol Metab Clin North Am 1990;19(3):685–718

Mettler FA, Guiberteau MJ. Essentials of Nuclear Medicine Imaging. 5th ed. Philadelphia: Elsevier; 2006

Case 270

Kamal D. Singh

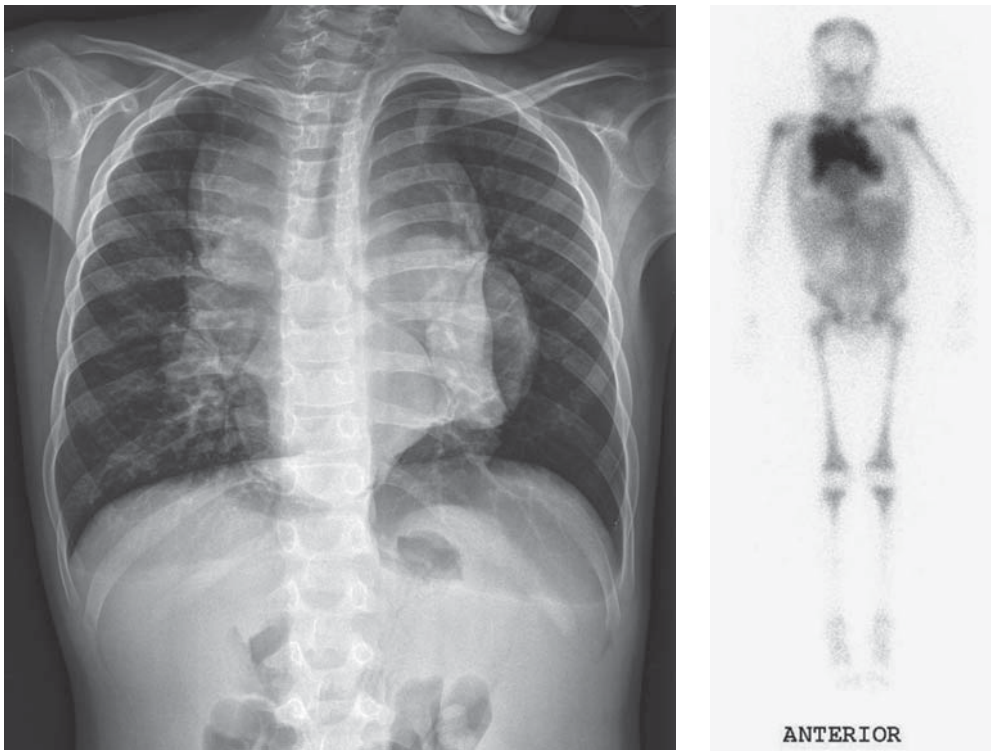


Fig. 270.1 **(A)** Frontal chest radiograph demonstrates mediastinal widening with bilateral hilar enlargement. **(B)** Anterior whole-body gallium 67 scan performed 48 hours postinjection demonstrates corresponding intense mediastinal and hilar uptake. Physiologic uptake is seen within the lacrimal glands, salivary glands, liver, spleen, intestines, bone, and bone marrow. (Courtesy of Children's Hospital and Research Center, Oakland, California.)

Clinical Presentation

A 10-year-old boy presents with a cough and weight loss (**Fig. 270.1**).

Key Imaging Finding

Increased mediastinal uptake on a gallium scan

Top 3 Differential Diagnoses

- **Malignancy.** Gallium-avid neoplasms are lymphoma, hepatoma, lung cancer, sarcoma (except Kaposi sarcoma, which is thallium avid but gallium negative), and melanoma. The typical dose for tumor imaging is 10 mCi with whole-body imaging performed at 48 to 72 hours postinjection. Physiologic activity includes the lacrimals, salivary glands, liver, spleen, breast, cortical bone, and bone marrow, with primarily renal excretion during the first 24 hours and gastrointestinal (GI) excretion thereafter. Gallium 67 (Ga67) has a physical half-life of 78 hours and multiple photopeaks (only 93, 184, and 296 keV are acquired for clinical imaging). Sensitivity for detection of lymphoma is based on the size of the lesion (higher if >1 cm) and tumor grade (lower detection rate for low grade). Ga67 is especially useful for defining the complete response and for early detection of viable tumor recurrence/relapse after chemoradiation therapy. A baseline Ga67 scan prior to therapy initiation is important for future disease follow-up. Evaluation of the abdomen is limited due to interfering physiologic intestinal activity. Positron emission tomography/computed tomography with its higher resolution has now largely replaced Ga67 for malignancy (lymphoma) work-up.
- **Granulomatous disease.** Active pulmonary or mediastinal sarcoidosis is gallium avid, and the degree of uptake typically corresponds to the severity of the disease. Right paratracheal and bilateral hilar lymphadenopathy uptake is seen as the "lambda" sign; prominent bilateral lacrimal and parotid activity represents the "panda" sign. Ga67 scan is positive only in the setting of active parenchymal disease and is negative while in remission. Gallium uptake is also seen with other pulmonary granulomatous processes, including tuberculosis and fungal disease.
- **Nonspecific inflammatory/infectious process.** Ga67 citrate accumulates within sites of inflammation or infection. Infection imaging is generally performed with 5 mCi, starting at 24 hours postinjection. Ga67 is especially useful for doing a workup of a fever of unknown origin, detecting opportunistic pulmonary infections in immunocompromised patients (particularly those with acquired immunodeficiency syndrome [AIDS]), and monitoring treated osteomyelitis (especially vertebral osteomyelitis). Ga67 may have nonspecific uptake within areas of inflammation, such as reactive lymphadenopathy in the setting of pneumonia, hyperplastic thymic tissue, postsurgical bed, or recent radiation therapy. Indium 111–labeled white blood cell is a more specific agent for acute pyogenic infections.

Diagnosis

Malignancy (Hodgkin lymphoma)

✓ Pearls

- Ga67 citrate's primary modes of localization are its resemblance to ferric ion and use as a calcium analogue.
- Focal uptake on a gallium scan is nonspecific and may represent inflammation, infection, or neoplasm.
- Diffuse lung activity can be seen with pneumocystis pneumonia in patients with AIDS.
- Physiologic renal excretion of radiotracer is seen during the first 24 hours, with primarily GI excretion thereafter.

Suggested Readings

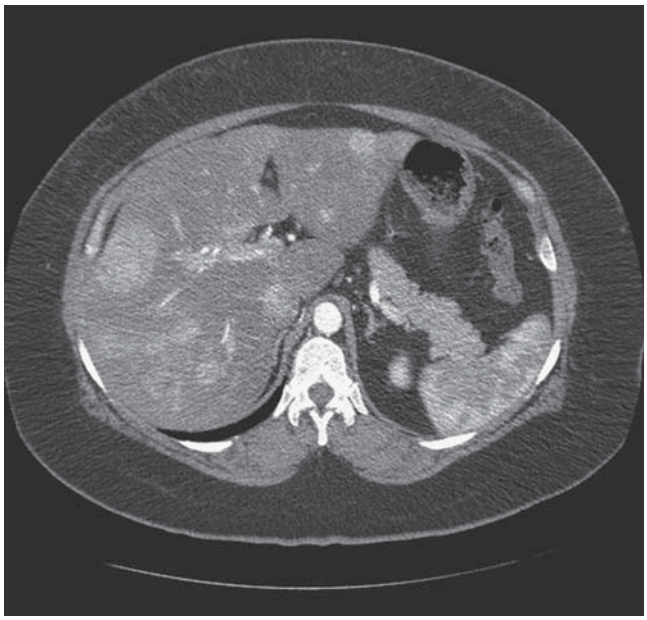
Hussain R, Christie DR, Gebski V, Barton MB, Gruenewald SM. The role of the gallium scan in primary extranodal lymphoma. J Nucl Med 1998;39(1):95–98

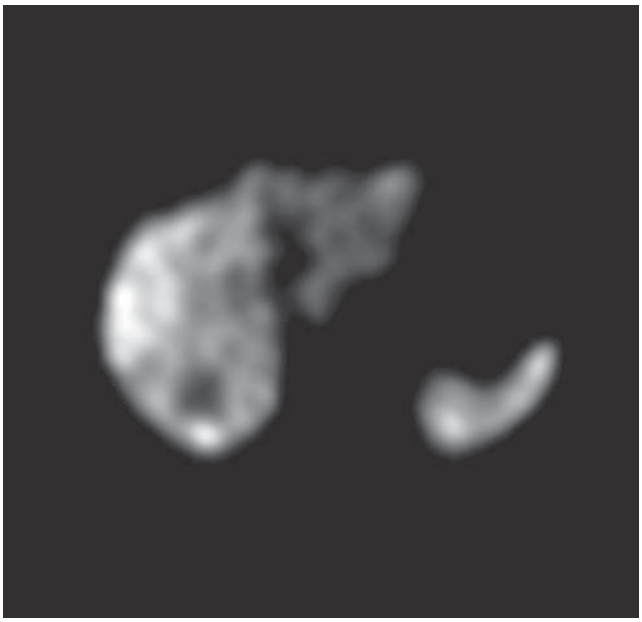
Liu FY, Shiau YC, Yen RF, Wang JJ, Ho ST, Kao CH. Comparison of gallium-67 citrate and technetium-99m tetrofosmin scan to detect Hodgkin's disease. Ann Nucl Med 2003;17(6):439–442

Ziessman HA, O'Malley JP, Thrall JH. Nuclear Medicine: The Requisites. 3rd ed. Philadelphia: Elsevier; 2006

Case 271

Vicki E. Nagano





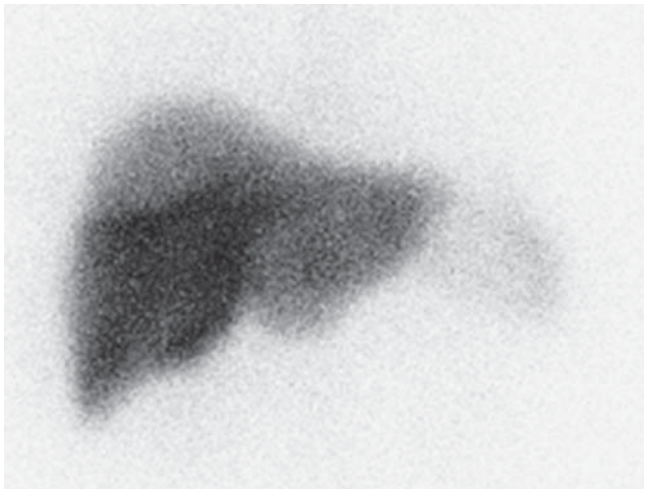


Fig. 271.1 **(A)** Contrast-enhanced axial computed tomography image through the liver shows multiple hyperdense enhancing lesions in both lobes of the liver. The heterogeneous appearance of the spleen is due to the phase of contrast. **(B)** Technetium 99m (Tc99m) sulfur colloid single-photon emission computed tomography image shows mildly increased uptake in the lateral right lobe and lateral left lobe, which is compatible with focal nodular hyperplasia. The large cold defect in the posterior right lobe was diagnosed as a hemangioma on subsequent Tc99m red blood cell scintigraphy (not shown). **(C)** Planar image demonstrating the normal radiopharmaceutical distribution of technetium sulfur colloid predominantly within the liver with faint activity within the spleen. Breast attenuation creates geographic decreased counts overlying the hepatic dome.

Clinical Presentation

A 35-year-old woman who is not on birth control pills (**Fig. 271.1**).

Key Imaging Finding

Focal increased hepatic uptake on a sulfur colloid scan

Top 3 Differential Diagnoses

- **Focal nodular hyperplasia (FNH).** FNH is a benign hepatic tumor that is found most commonly in women (80%). It typically appears as a solitary solid mass consisting of hepatocytes, bile ducts, and Kupffer cells. Most lesions are 2 to 5 cm in diameter, 20% are multiple, and they are more common in the right lobe of the liver (70%). Computed tomography often demonstrates a contrast-enhancing lesion with a central area of scarring. Due to the presence of Kupffer cells, two thirds of FNH nodules have normal or increased sulfur colloid uptake. One third have decreased uptake, which may be related to the existence of a large number of fibrotic cells. If the nodule does not accumulate sulfur colloid, FNH is not ruled out, and the remaining broad differential includes hepatic adenoma, hepatocellular carcinoma (including the fibrolamellar variant), and metastases. For radionuclide studies, the practical limits of resolution are 1 to 2 cm for single-photon emission computed tomography (SPECT) imaging and 2 to 3 cm for planar imaging.
- **Regenerating nodular cirrhosis.** Decreased hepatic uptake of sulfur colloid occurs in cirrhosis due to alteration of the liver's microcirculation. Regenerating nodules are composed primarily of hepatocytes that are surrounded by coarse fibrous septations. They have normal sulfur colloid uptake and can appear as a hot spot surrounded by a region of diminished uptake.
- **Budd–Chiari syndrome.** In Budd–Chiari syndrome, obstruction of the hepatic veins results in congestion, hemorrhage, and necrosis of the liver parenchyma. However, the caudate lobe retains its function due to direct venous drainage into the inferior vena cava. On sulfur colloid imaging, it appears as a hot spot in the caudate lobe of the liver, surrounded by an area of diminished uptake.

Additional Differential Diagnoses

- **Superior vena cava (SVC) syndrome.** In obstruction of the SVC, collateral vessels return blood via the left internal mammary and left umbilical veins into the quadrate lobe, resulting in a focal hot spot when sulfur colloid is injected into the upper extremity. Injection in the lower extremity results in a normal scan.

Diagnosis

Focal nodular hyperplasia

✓ Pearls

- Two thirds of FNH nodules demonstrate uptake on a technetium 99m sulfur colloid (Tc99m SC) scan; one third can be photopenic.
- Hepatic adenomas are photopenic on a Tc99m SC scan, as are hemangiomas, hepatocellular carcinomas, metastases, and abscesses.
- Hemangiomas are cold on Tc99m SC and hepatobiliary scans but have uptake on delayed Tc99m red blood cell scans.
- Regenerating nodules, Budd–Chiari syndrome, and SVC syndrome produce focal hepatic hot spots on Tc99m SC scans.

Suggested Readings

Boulahdour H, Cherqui D, Charlotte F, et al. The hot spot hepatobiliary scan in focal nodular hyperplasia. J Nucl Med 1993;34(12):2105–2110

Huynh LT, Kim SY, Murphy TF. The typical appearance of focal nodular hyperplasia in triple-phase CT scan, hepatobiliary scan, and Tc-99m sulfur colloid scan with SPECT. Clin Nucl Med 2005;30(11):736–739

Morton K, Clark P. Diagnostic Imaging: Nuclear Medicine. Salt Lake City, UT: Amirsys; 2007

Ziessman HA, O'Malley JP, Thrall JH. Nuclear Medicine: The Requisites. 3rd ed. Philadelphia: Elsevier; 2006

Case 272

Kamal D. Singh

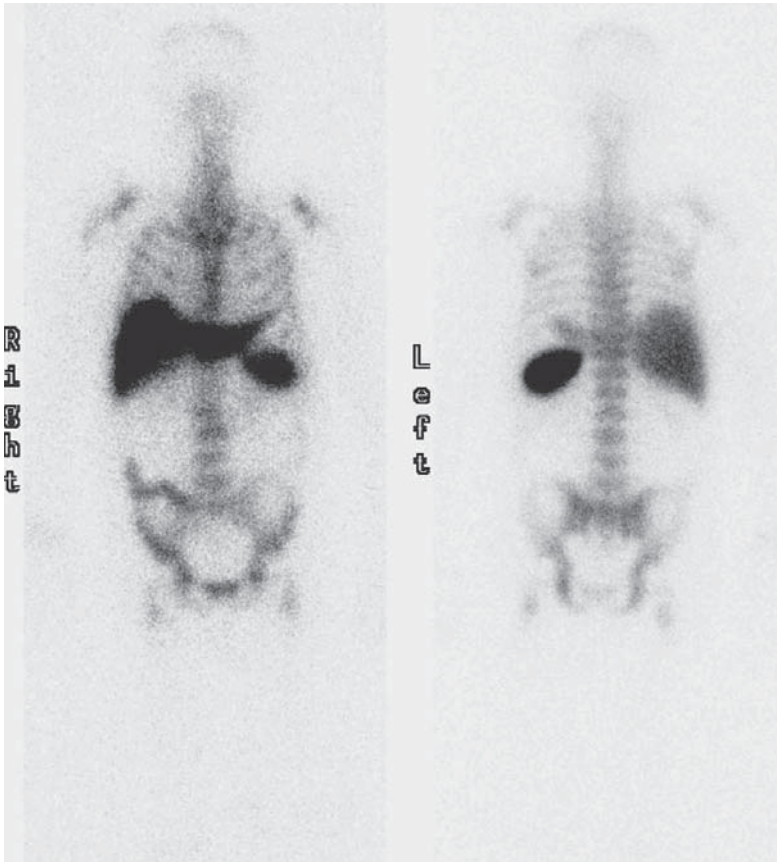


Fig. 272.1 Whole-body indium 111–labeled white blood cell scan 24 hours postinjection in anterior and posterior projections demonstrates segmental tubular uptake within the anterior right lower quadrant of the abdomen. Physiologic uptake is seen within the spleen greater than liver, as well as bone marrow.

Clinical Presentation

A 39-year-old man presents with vague abdominal pain, fever, and an elevated white blood cell (WBC) count (**Fig. 272.1**).

Key Imaging Finding

Focal bowel uptake on an indium 111 (In111)–labeled WBC scan

Top 3 Differential Diagnoses

- **Infectious enteritis/colitis.** Indications for an In111-labeled WBC scan include detection and localization of abdominopelvic abscesses, acute osteomyelitis (including orthopedic hardware), and infected vascular grafts, as well as for work-up of a fever of unknown origin. Approximately 50 cc of blood is drawn from the patient, and In111 oxine is labeled to leukocytes (predominantly neutrophils). Imaging is generally performed starting 24 hours after injection. In111-labeled WBCs localize to sites of infection by chemotaxis and increased vascular permeability. Donor WBCs (ABO matched) may be used in neutropenic patients with WBC<2000 cells/mL. Physiologic activity is seen within spleen, liver, and bone marrow. Early transient, nonfocal pulmonary activity is physiologic and normally decreases over time. The lack of significant gastrointestinal (GI) uptake or hepatobiliary/renal excretion makes In111-labeled WBCs preferable over gallium for abdominopelvic infectious processes, such as abscesses, enteritis/colitis, and appendicitis. There is lower sensitivity for detection of chronic nonpyogenic processes. False-positive studies may be secondary to an accessory spleen or abdominal wall inflammation from surgical wounds, percutaneous tubes, or catheters.
- **Inflammatory bowel disease (IBD).** Segmental bowel activity may be seen in active IBD due to WBCs within sloughed mucosa at the site of inflammation. Localization and the extent of active disease are best depicted on early imaging (1–6 hours postinjection) before migration of activity distal to the site of origin due to peristalsis. Technetium 99m (Tc99m) HMPAO (hexamethylpropyleneamine)–labeled WBCs are typically used in pediatric patients instead of indium to reduce the radiation dose to the spleen. When Tc99m HMPAO is used, early imaging (before 4 hours) is paramount to avoid interfering with physiologic colonic activity.
- **Gastrointestinal bleeding.** Active GI bleeding causes passage of WBC (along with red blood cells [RBCs] and platelets) into the bowel lumen, resulting in activity that may simulate active intestinal infection or inflammation. Careful patient history and correlation with Tc99m-labeled RBCs (more sensitive and specific for active GI bleeding) can aid in establishing the correct diagnosis. Acute hematomas can also accumulate labeled WBCs.

Additional Differential Diagnoses

- **Swallowed activity from sinusitis/pharyngitis.** Focal infection from a more proximal source, such as sinusitis, pharyngitis, or esophagitis, may have mucosal shedding of WBCs, resulting in poorly localized transient bowel activity. This can also be seen in the setting of inflammation around indwelling endotracheal or nasogastric tubes.

Diagnosis

Inflammatory bowel disease (Crohn disease)

✓ Pearls

- In111-labeled WBC scan is more specific than a three-phase bone scan and gallium 67 for acute pyogenic infection.
- Sensitivity of the In111 WBC scan is generally not affected by antibiotic therapy for acute infection.
- False-negative scans are seen in chronic nonpyogenic infections and vertebral osteomyelitis.
- False-positive scans are seen in operative wounds, GI bleeding, focal inflammation, and reactive marrow.

Suggested Readings

Mettler FA, Guiberteau MJ. Essentials of Nuclear Medicine Imaging. 5th ed. Philadelphia: Elsevier; 2006

Navab F, Boyd CM. Clinical utility of In-111 leukocyte imaging in Crohn's disease. Clin Nucl Med 1995;20(12):1065–1069

Ziessman HA, O'Malley JP, Thrall JH. Nuclear Medicine: The Requisites. 3rd ed. Philadelphia: Elsevier; 2006

Case 273

Vicki E. Nagano

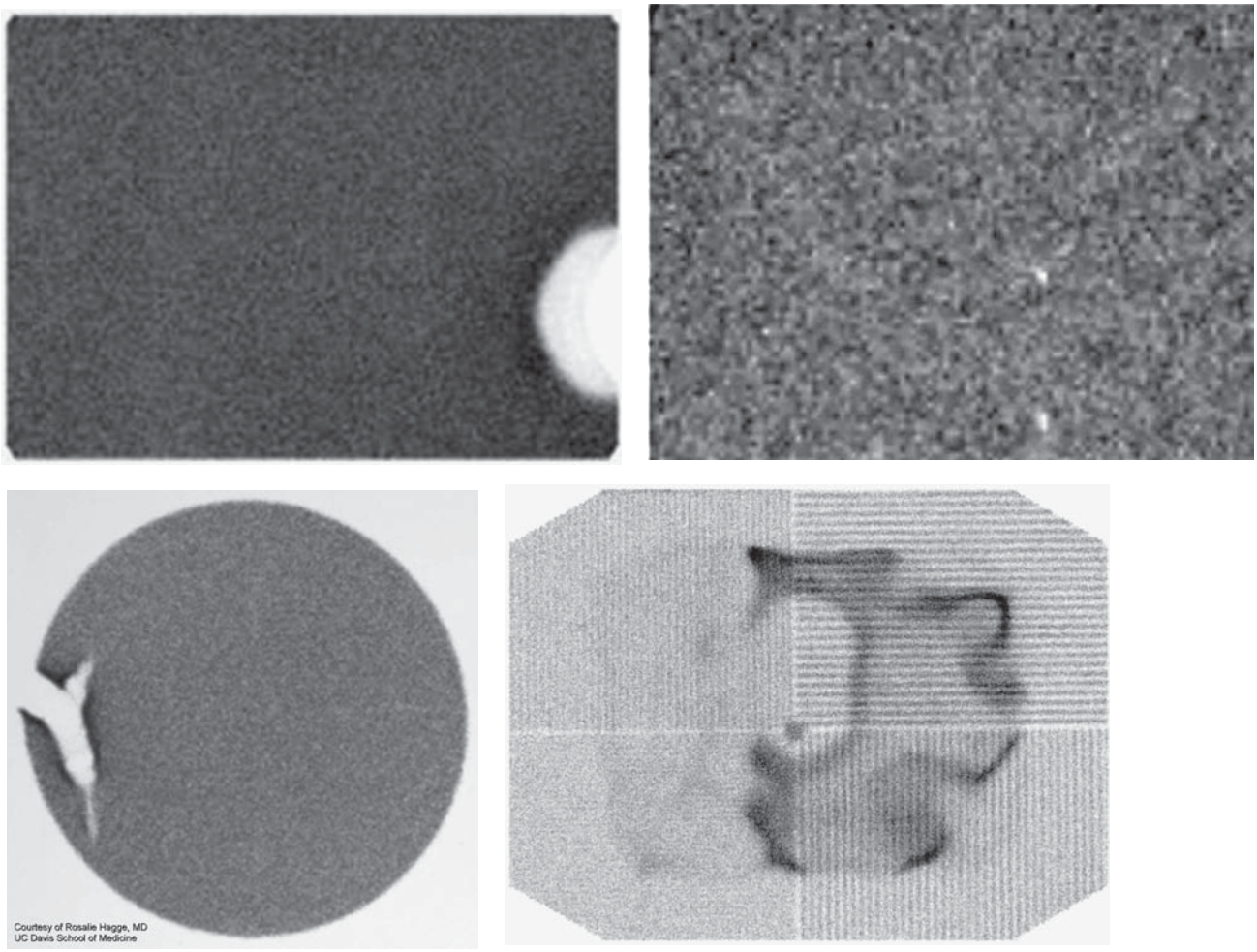


Fig. 273.1 Multiple field uniformity flood images show **(A)** a defective photomultiplier tube, **(B)** two subtle photopenic defects due to dented lead in the collimator, **(C)** a crack in the sodium iodide crystal, and **(D)** an electronic problem affecting the main circuitry behind the photomultiplier tubes.

Clinical Presentation

A technician presents flood field images for quality control (QC) (**Fig. 273.1**).

Key Imaging Finding

Focal defect on QC images

Top 3 Differential Diagnoses

- **Photomultiplier tube failure.** An array of photomultiplier tubes (PMTs) behind the sodium iodide crystal converts the light pulse from the scintillation event into an electrical signal. Malfunction of the PMTs can be caused by a damaged tube, decoupling of the gel between the crystal and a PMT, or a loose electrical connection. Scintillation events occurring under the defective PMT will not result in a measurable electrical signal. A round defect will be seen in the field uniformity image, corresponding to the position of the malfunctioning PMT. A similar focal defect can also be caused by an overlying attenuating structure on the camera head or by an air bubble in the liquid flood phantom.
- **Crystal defect.** Gamma ray photons produce a scintillation event within the sodium iodide crystal. A crack in the sodium iodide crystal on a flood field image results in a branching white pattern due to the lack of scintillations in this region. The surrounding dark edges are due to the edge-packing phenomenon.
- **Collimator defect.** The collimator helps to localize the radionuclide in the patient by allowing only those photons traveling in an appropriate direction to interact with the crystal. The soft lead in the collimators can be dented, resulting in bending and distorting of the septa. The defect appears as a focal area of decreased activity on the flood field image. Repeating the flood image with the collimator removed will show resolution of the defect.

Additional Differential Diagnoses

- **Electronic artifact.** Complex computer circuitry mounted along each PMT calculates the position and strength of the scintillation event. Electronic malfunctions can result in various artifacts, depending on which electronic system is involved. The findings on flood imaging are less characteristic than those seen with other flood field artifacts.

Diagnosis

PMT failure (**Fig. 273.1A**); dented collimator (**Fig. 273.1B**); cracked crystal (**Fig. 273.1C**); electronic artifact (**Fig. 273.1D**)

✓ Pearls

- Daily camera QC includes extrinsic flood with a cobalt 57 (Co57) sheet source placed on the camera with a collimator.
- Daily flood QC images should be reviewed if there is concern for external artifact on any diagnostic study.
- Weekly spatial resolution/linearity is tested with a bar phantom between the Co57 sheet source and the collimator.
- Monthly QC includes intrinsic floods (a technetium 99m point source with the collimator off) and SPECT (single-photon emission computed tomography) QC.

Suggested Readings

Mettler FA, Guiberteau MJ. Essentials of Nuclear Medicine Imaging. 5th ed. Philadelphia: Elsevier; 2006

Ziessman HA, O'Malley JP, Thrall JH. Nuclear Medicine: The Requisites. 3rd ed. Philadelphia: Elsevier; 2006

Case 274

Kamal D. Singh



Fig. 274.1 Whole-body bone scan with technetium 99m hydroxymethylene diphosphonate demonstrates focal intense uptake within the distal left tibia. This uptake corresponds to a cortical-based sclerotic lesion with subtle central lucency noted on plain film (not shown). Mild degenerative uptake is seen along with physiologic renal and bladder activity.

Clinical Presentation

A 36-year-old woman presents with chronic achy pain within the left lower extremity (**Fig. 274.1**).

Key Imaging Finding

Focal increased activity within an extremity on a bone scan

Top 3 Differential Diagnoses

- **Stress fracture.** Technetium 99m (Tc99m) hydroxymethylene diphosphonate (HDP) or methylene diphosphonate (MDP) localizes to areas of increased osteoblastic activity. Over 80% of fractures are detected within the first 24 hours and nearly 95% by 72 hours. Stress fractures are classified as fatigue and insufficiency fractures. Fatigue fractures develop in a normal bone exposed to abnormal stress; insufficiency fractures develop in an abnormal bone exposed to normal stress. Repetitive stress can lead to microfractures, which in turn may develop into overt fractures if unrecognized. Typical sites for fatigue-type stress fractures are the tibia, fibula, medial femoral neck, inferior pubic ramus, metatarsals, and calcaneus. Stress fractures are seen as intense focal, fusiform activity on a bone scan. In the acute setting, increased activity may be seen on all three phases of a bone scan. Stress fractures within the long bones can be graded based on their extent of corticomedullary involvement. Treatment includes rest and modification of activity.
- **Osteomyelitis.** Osteomyelitis may occur due to extension from adjacent soft tissue cellulitis, direct inoculation from an open wound, or hematogenous spread. A three-phase bone scan has a high negative predictive value for osteomyelitis. Cellulitis demonstrates hyperemia and soft tissue uptake on early phases (flow and blood pool only) but no abnormal bone activity on delayed imaging. Osteomyelitis, in contrast, is positive on all three phases. Specificity for osteomyelitis is lower in the setting of recent trauma, surgery, or orthopedic hardware, necessitating correlation with indium 111–labeled white blood cell and Tc99m sulfur colloid scans.
- **Neoplasm (benign and malignant).** Primary bone malignancies (e.g., osteosarcoma and Ewing sarcoma) and osteoblastic metastases generally demonstrate avid uptake on bone scans. Sensitivity is lower, however, for the predominantly lytic lesions (multiple myeloma, renal cell, or thyroid cancer). Benign bone tumors have a variable appearance on bone scans, and with the exception of osteoid osteoma, they generally do not demonstrate significant hyperemia. Osteoid osteoma, however, has focal intense uptake within a central vascular nidus with comparatively less uptake in the surrounding reactive sclerosis—classically described as the "double density" or "target" sign. Clinically, patients present with dull, achy night pain that is relieved by nonsteroidal antiinflammatory drugs. Solitary bone cysts are generally photopenic, whereas bone islands and osseous hemangiomas rarely are detectable on bone scans. Benign, uncomplicated exostoses and enchondromas are usually warm on bone scans.

Additional Differential Diagnoses

- **Fibrous dysplasia.** Fibrous dysplasia is a congenital, nonhereditary skeletal dysplasia that generally demonstrates intense uptake on bone scans. Common areas of involvement are the ribs, tibia, femur, and craniofacial bones. The skeletal lesions demonstrate the classic expanded, ground-glass matrix on plain film. A bone scan is helpful in detecting polyostotic involvement.

Diagnosis

Neoplasm (osteoid osteoma)

✓ Pearls

- Stress fractures (fatigue or insufficiency) present as focal uptake in characteristic locations.
- Osteoid osteoma is positive on all three phases of a bone scan with a characteristic "target" sign.
- Multifocal uptake may be seen with metastases, osteomyelitis, insufficiency fractures, fibrous dysplasia, and Paget disease.
- Osseous metastases are generally seen within the axial rather than the appendicular skeleton.

Suggested Readings

Mettler FA, Guiberteau MJ. Essentials of Nuclear Medicine Imaging. 5th ed. Philadelphia: Elsevier; 2006

Ziessman HA, O'Malley JP, Thrall JH. Nuclear Medicine: The Requisites. 3rd ed. Philadelphia: Elsevier; 2006

Case 275

Kamal D. Singh

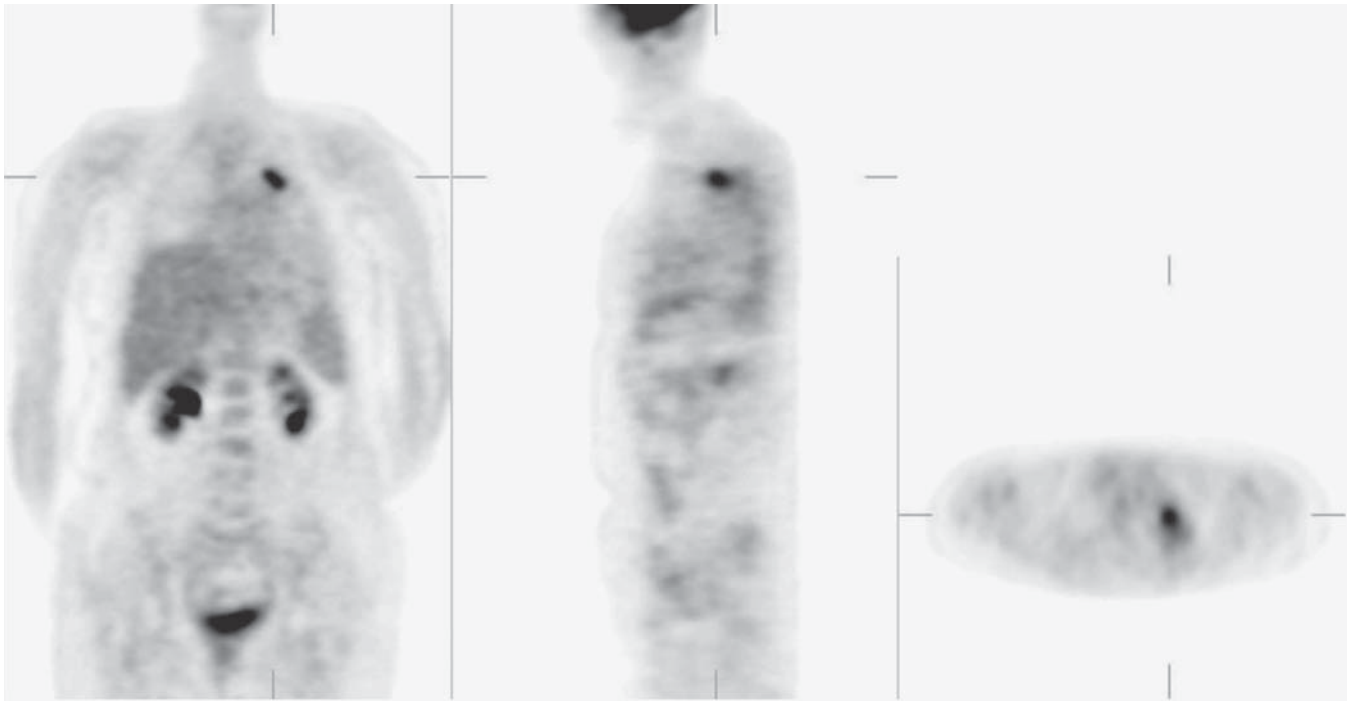


Fig. 275.1 Positron emission tomography scans with 18F-fluorodeoxyglucose demonstrate a hypermetabolic left upper lobe pulmonary nodule. No additional foci of abnormal uptake are seen. Physiologic uptake is seen within the brain, liver, spleen, kidneys, bladder, and bone marrow.

Clinical Presentation

A 51-year-old man presents with an incidental left lung nodule on a chest radiograph (**Fig. 275.1**).

Key Imaging Finding

Solitary hypermetabolic pulmonary lesion on a positron emission tomography (PET) scan

Top 3 Differential Diagnoses

- **Malignancy.** FDG (18F-fluorodeoxyglucose) is a glucose analogue that enters cells via glucose transporters and is phosphorylated. Unlike glucose, FDG is trapped in cells and does not undergo glycolysis. FDG is a cyclotron-produced positron emitter that simultaneously generates two 511 keV gamma photons at ~180 degrees through an annihilation reaction. Standard PET imaging is performed from the skull base to the proximal thighs 45 to 60 minutes after injection of 15 mCi of FDG. Corresponding low-dose computed tomography (CT) is performed for attenuation correction and anatomical localization. Malignant cells have increased metabolic activity. PET/CT is indicated for the detection and staging of malignancies, including the posttherapy response. PET/CT has a sensitivity of 95% and a specificity of 80% for determining whether a solitary pulmonary nodule (>1 cm in size) is benign or malignant. Standardized uptake value (SUV) is a semiquantitative index for tumor metabolism, and a maximum SUV of 2.5 is generally regarded as the cutoff for malignancy. However, any uptake within a pulmonary nodule greater than the mediastinal background activity is suspicious. False-negatives may occur due to the partial-volume effect in subcentimeter nodules and low-grade or well-differentiated malignancies.
- **Active granulomatous disease.** FDG uptake is nonspecific and can be seen within active nonneoplastic processes, including granulomatous diseases such as sarcoidosis, fungal infection, and tuberculosis. Increased glycolysis within activated macrophages is likely responsible for FDG uptake. SUV may be high (>2.5) within these benign lesions. A biopsy or close follow-up may be the next appropriate step for a definitive diagnosis. Dual-time point imaging in some instances may improve accuracy because nonneoplastic lesions generally do not demonstrate increasing FDG accumulation on delayed scans.
- **Pulmonary infection/inflammation.** Increased activity is also seen within the sites of active infection or inflammation, likely due to inflammatory cell metabolism and mediators. Focal pulmonary infection, abscesses, radiation pneumonitis, active fibrosis, and postsurgical changes can demonstrate high FDG uptake, simulating malignancy. Correlation with the patient's history and corresponding anatomical imaging (i.e., CT scan) can aid in making the appropriate diagnosis.

Diagnosis

Malignancy (bronchogenic carcinoma)

✓ Pearls

- Patient preparation prior to PET include 4-hour fasting, no recent regular insulin, and serum glucose <200.
- FDG uptake is nonspecific and is seen in the setting of neoplasm and active infection or inflammation.
- An SUV ≥2.5 is generally considered as the cutoff for malignancy.
- Bronchoalveolar carcinoma or mucinous metastases to the lung may be false-negative on PET scans.

Suggested Readings

Mettler FA, Guiberteau MJ. Essentials of Nuclear Medicine Imaging. 5th ed. Philadelphia: Elsevier; 2006

Ziessman HA, O'Malley JP, Thrall JH. Nuclear Medicine: The Requisites. 3rd ed. Philadelphia: Elsevier; 2006

Section XII Breast Imaging

Case 276

Chloe M. Chhor

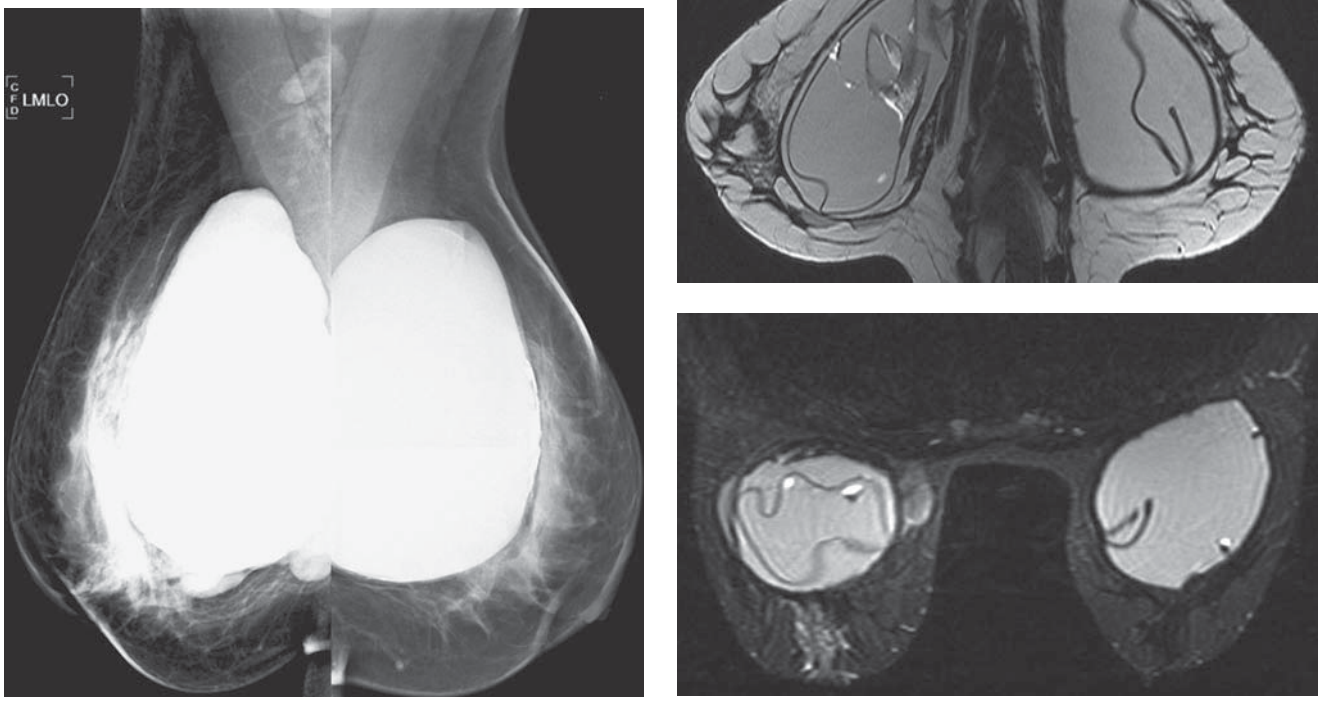


Fig. 276.1 **(A)** Mammograms in the medial-lateral oblique projection demonstrate bilateral prepectoral silicone implants. Extravasated silicone and implant discontinuity are present in the left breast. The right breast silicone implant appears intact. **(B)** Sagittal spin echo and **(C)** axial short tau inversion recovery magnetic resonance images show multiple curvilinear hypointense lines within high-signal silicone and free silicone within the breast parenchyma on the left. On the right, there are long hypointense curvilinear folds inferiorly, superiorly, and medially within the implant that end blindly within the silicone gel.

Clinical Presentation

A 54-year-old woman with a history of bilateral breast augmentation presents with a change in contour of the left implant (**Fig. 276.1**).

Key Imaging Finding

Implant defect

Top 3 Differential Diagnoses

- **Intracapsular rupture.** A silicone implant is a foreign body. The breast forms a fibrous capsule around the implant as a foreign body response, thus walling off the implant from the breast. Intracapsular rupture occurs when the shell of the implant ruptures, but the fibrous capsule formed by the breast remains intact. Silicone remains encapsulated and therefore does not freely extravasate. The contour of the implant remains largely intact; hence this diagnosis is difficult to make on clinical examination or mammography. Magnetic resonance imaging (MRI) is the best method to diagnose intracapsular rupture. When the implant shell collapses within the fibrous capsule, curvilinear hypointense lines within high-signal silicone are seen, giving rise to the "linguine" sign of intracapsular rupture. The high-signal silicone is seen on both sides of the collapsed shell.
- **Extracapsular rupture.** If the fibrous capsule ruptures in addition to the implant shell, then extracapsular rupture occurs, allowing free silicone to extrude into the breast parenchyma. By definition, intracapsular rupture is also present when there is extracapsular rupture. Extracapsular rupture can lead to a change in the implant contour and thus may be detected on clinical examination or mammography.
- **Radial fold.** Radial folds represent infolding of an intact implant shell and may be confused with subtle intracapsular rupture. They appear thicker than the lines associated with a collapsed implant shell, because the folds consist of two adjacent shell layers. On a single image, radial folds may be confused with intracapsular rupture. Careful and detailed evaluation of serial images can usually distinguish between radial folds and intracapsular rupture. Radial folds are characteristically blind-ending within the implant.

Additional Differential Diagnoses

- **Gel bleed.** A gel bleed can occur when silicone molecules diffuse through an intact implant shell. If enough silicone molecules diffuse through the shell, a "gross" gel bleed can be seen as a visible layer of silicone coating the outer surface of the implant. This may appear as if there is extracapsular rupture, even when the implant shell is intact. Separation of the intact shell from the fibrous capsule can also be seen when a gross gel bleed occurs, giving the appearance of intracapsular rupture. Ruptures are more common than gross gel bleeds and should be considered first.
- **Herniation.** Herniation refers to bulging of the implant with an intact shell. It can occur through a defect in the surrounding fibrous capsule before the defect envelops the entire implant shell. Herniation can be confused with rupture and capsular contraction. Unlike rupture or capsular contraction, the deformity from herniation remains stable with time, and no extravasated silicone is seen elsewhere.

Diagnosis

Left breast: intra- and extracapsular rupture; right breast: radial folds

✓ Pearls

- Intracapsular rupture is best detected at MRI; the "linguine" sign is characteristic.
- Extracapsular rupture implies intracapsular rupture as well; extravasated silicone may be seen in the breast.
- Radial folds are thicker than a collapsed implant shell; they are typically blind-ending within the implant.
- A gel bleed mimics extravasated silicone but occurs with an intact implant shell.

Suggested Readings

Everson LI, Parantainen H, Detlie T, et al. Diagnosis of breast implant rupture: imaging findings and relative efficacies of imaging techniques. AJR Am J Roentgenol 1994;163(1):57–60

Hölmich LR, Vejborg I, Conrad C, Sletting S, McLaughlin JK. The diagnosis of breast implant rupture: MRI findings compared with findings at explantation. Eur J Radiol 2005;53(2):213–225

Kopans DB. Breast Imaging. 3rd ed. Philadelphia: Lippincott Williams & Wilkins; 2007

Soo MS, Kornguth PJ, Walsh R, Elenberger CD, Georgiade GS. Complex radial folds versus subtle signs of intracapsular rupture of breast implants: MR findings with surgical correlation. AJR Am J Roentgenol 1996;166(6):1421–1427

Case 277

Jessica W. T. Leung

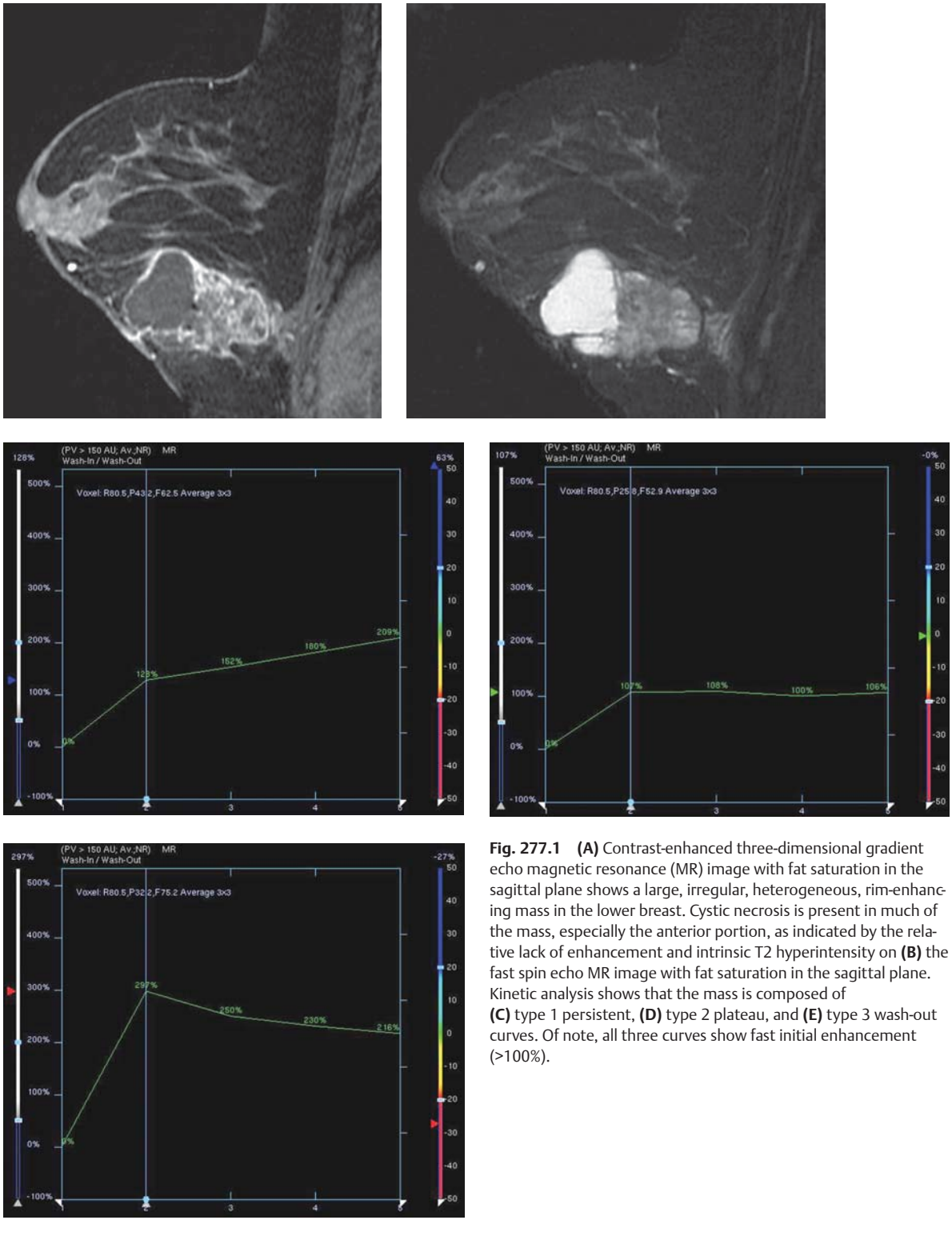


Fig. 277.1 **(A)** Contrast-enhanced three-dimensional gradient echo magnetic resonance (MR) image with fat saturation in the sagittal plane shows a large, irregular, heterogeneous, rim-enhancing mass in the lower breast. Cystic necrosis is present in much of the mass, especially the anterior portion, as indicated by the relative lack of enhancement and intrinsic T2 hyperintensity on **(B)** the fast spin echo MR image with fat saturation in the sagittal plane. Kinetic analysis shows that the mass is composed of **(C)** type 1 persistent, **(D)** type 2 plateau, and **(E)** type 3 wash-out curves. Of note, all three curves show fast initial enhancement (>100%).

Clinical Presentation

A 49-year-old woman presents with a large palpable lump in the lower breast of unknown duration (**Fig. 277.1**).

Key Imaging Finding

Magnetic resonance imaging (MRI) enhancement patterns

Top 3 Differential Diagnoses

- **Type 1 persistent kinetics.** In type 1 persistent kinetics, the degree of contrast enhancement continues to increase over the duration of the MRI in the delayed phase. Type 1 persistent kinetics is consistent with the biology of benign lesions such as fibrocystic change or fibroadenoma. However, many cancers may also display type 1 persistent kinetics. Kinetic analysis cannot be used alone to establish or exclude malignancy.
- **Type 2 plateau kinetics.** In type 2 plateau kinetics, the degree of contrast enhancement levels over the duration of the MRI in the delayed phase. Type 2 plateau kinetics are indeterminant and seen in both benign and malignant conditions. Kinetic analysis cannot be used alone to establish or exclude malignancy.
- **Type 3 wash-out kinetics.** In type 3 wash-out kinetics, the degree of contrast enhancement decreases over the duration of the MRI in the delayed phase. Type 3 wash-out kinetics are consistent with the principle of angiogenesis and the biology of malignancy. Neovessels form in cancers, which are characterized by increased vascular permeability. Therefore, cancers will enhance strongly and rapidly in the initial phase but demonstrate wash-out of contrast in the delayed phase. However, not all cancers demonstrate type 3 wash-out kinetics, and some benign entities display type 3 wash-out kinetics. Hence kinetic analysis cannot be used alone to establish or exclude malignancy.

Additional Differential Diagnoses

- **Initial phase.** The initial phase of contrast enhancement may be more predictive for malignancy than the delayed phase. There are three patterns of contrast enhancement in the initial phase: slow, medium, and fast. Cancers generally enhance fast in the initial phase.

Diagnosis

Poorly differentiated invasive ductal carcinoma with types 1, 2, and 3 kinetic curves

✓ Pearls

- Kinetic analysis of breast MRI consists of both initial and delayed phases.
- Proper interpretation of breast MRI requires consideration of both morphology and kinetic data.
- Classically, cancers show fast initial enhancement and wash-out of contrast in the delayed phase.

Suggested Readings

American College of Radiology. ACR Breast Imaging Reporting and Data System (BI-RADS). 4th ed. Reston, VA: Author; 2003

Ikeda DM. Breast Imaging: The Requisites. Philadelphia: Elsevier; 2004

Kopans DB. Breast Imaging. 3rd ed. Philadelphia: Lippincott Williams & Wilkins; 2007

Kuhl CK, Schild HH, Morakkabati N. Dynamic bilateral contrast-enhanced MR imaging of the breast: trade-off between spatial and temporal resolution. Radiology 2005;236(3):789–800

Case 278

Chloe M. Chhor

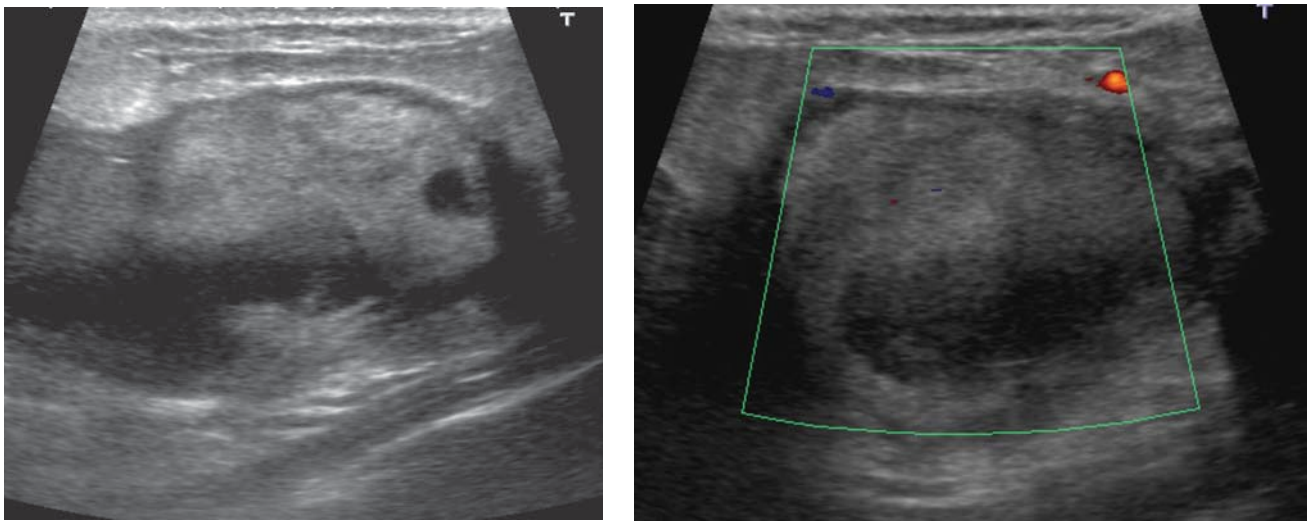


Fig. 278.1 **(A)** Gray scale ultrasound image in the transverse plane of the palpable lump demonstrates a 5 cm ovoid mass of mixed echogenicity that is oriented parallel to the chest wall. **(B)** Doppler ultrasound image reveals no vascular flow within the mass, supporting the diagnosis that it is a cystic lesion.

Clinical Presentation

A 29-year-old lactating woman presents with a large palpable breast lump of 3 weeks' duration (**Fig. 278.1**).

Key Imaging Finding

Complex cystic mass in a lactating woman

Top 3 Differential Diagnoses

- **Galactocele.** Galactocele is the most common of the several benign breast masses found in lactating women. It is a cystic mass that forms as a result of duct dilatation and contains fluid that resembles milk. Diagnosis and therapy can be achieved with percutaneous aspiration. Mammographic and sonographic appearances depend on the stage of development and on varying proportions of fat and proteinaceous material present, as well as the density and viscosity of the fluid.
- **Abscess.** Infection is relatively common during lactation due to disruption of the epithelial interface of the nipple–areola complex with retrograde dissemination of bacteria. On ultrasound, abscesses usually appear as irregular hypoechoic or anechoic masses, sometimes with fluid–debris levels and posterior acoustic enhancement. Treatment consists of antibiotic therapy, as well as surgical incision or percutaneous aspiration or drainage in some cases. If patients do not respond, biopsy is indicated to exclude malignancy.
- **Fibroadenoma.** Fibroadenoma is the most common benign solid mass in young women. It has a variable appearance on ultrasound but classically appears as a circumscribed or gently lobulated, mildly hypoechoic, thinly encapsulated, elliptically shaped mass that is oriented parallel to the chest wall. During pregnancy, a fibroadenoma may grow to a very large size because of hormonal influences and undergo infarction because it has outgrown its blood supply. It may also develop secretory hyperplasia. These changes may result in varying sonographic appearances, including a complex cystic appearance.

Additional Differential Diagnoses

- **Hematoma.** Hematoma is usually preceded by trauma or anticoagulation use. It may appear well defined or poorly defined on mammography. The ultrasound appearance varies based on the age of the hematoma. It is often anechoic in its hyperacute stage, mimicking a cyst. As it evolves, it may become hyperechoic and heterogeneous as the clotting process proceeds. Hematomas should be followed to resolution.
- **Lactating adenoma.** Lactating adenoma is a benign solid breast mass that occurs in response to the physiologic changes that characterize pregnancy and lactation. Its sonographic appearance closely resembles that of a fibroadenoma. Hyperechoic areas represent the fat content of milk due to lactational hyperplasia. Lactating adenoma occasionally displays suspicious features for malignancy, some of which may be attributed to infarction. It usually regresses spontaneously after pregnancy and lactation.
- **Fibrocystic change.** Fibrocystic change is a physiologic finding consisting of varying degrees of cystic dilatation and enlargement. The ultrasound features of fibrocystic change will vary depending on the predominating tissue component: cystic or solid proliferative.

Diagnosis

Galactocele

✓ Pearls

- Galactocele is the most common benign mass in lactating women; the fluid resembles milk.
- In patients with suspected breast abscesses unresponsive to treatment, malignancy needs to be excluded.
- Fibroadenoma can grow, undergo infarction, or develop secretory hyperplasia during pregnancy.
- Lactating adenoma is a benign solid mass that occurs with pregnancy/lactation; it spontaneously regresses.

Suggested Readings

Kopans DB. Breast Imaging. 3rd ed. Philadelphia: Lippincott Williams & Wilkins; 2007

Sabate JM, Clotet M, Torrubia S, et al. Radiologic evaluation of breast disorders related to pregnancy and lactation. Radiographics 2007;27(Suppl 1):S101–S124

Stavros AT. Breast Ultrasound. Philadelphia: Lippincott Williams & Wilkins; 2004

Case 279

Jessica W. T. Leung

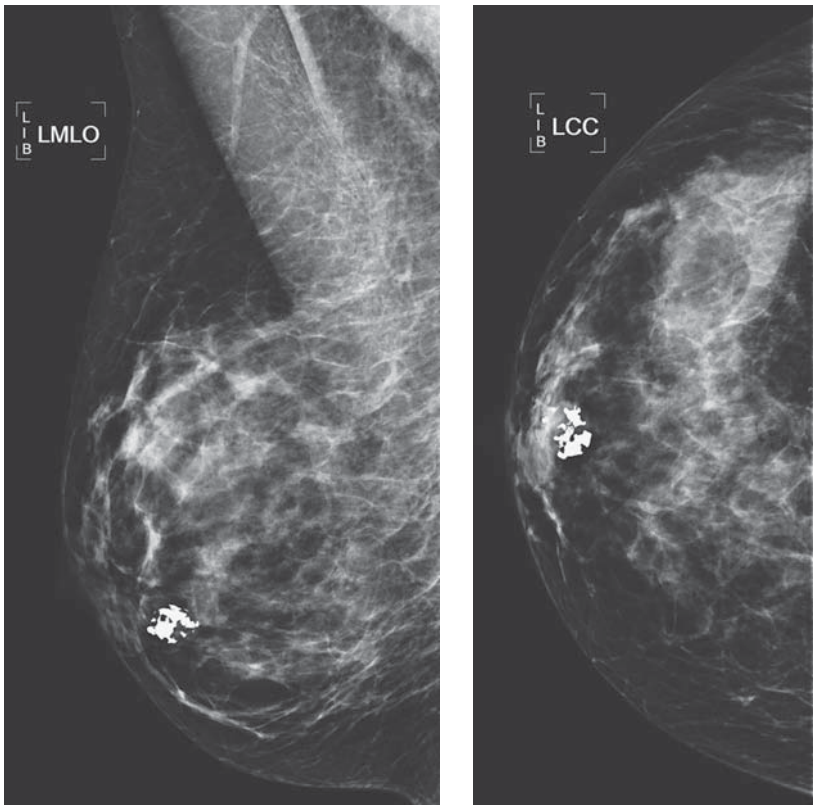


Fig. 279.1 Screening mammograms of the left breast in **(A)** the medial-lateral oblique and **(B)** Craniocaudal projections show a partially circumscribed mass containing coarse curvilinear calcifications in the retroareolar region.

Clinical Presentation

A 43-year-old woman presents for screening mammography (**Fig. 279.1**).

Key Imaging Finding

Coarse calcifications in a partially circumscribed mass

Top 3 Differential Diagnoses

- **Degenerating fibroadenoma.** Fibroadenoma is a benign solid mass. It is the most common mass in young women and the most common palpable mass in women in their 30s. It may be seen on a mammogram as a circumscribed or lobulated, round or oval mass. As a fibroadenoma involutes or degenerates with time, its stromal components become hyalinized. Coarse, curvilinear, "popcorn" calcifications may appear. Such characteristic calcifications are pathognomonic for a degenerating fibroadenoma. This is a benign mass that does not need to be biopsied.
- **Fat necrosis.** Trauma to the breast, including postsurgical changes and ischemia, results in fat necrosis and the formation of dystrophic calcifications. Such calcifications are dense and coarse and may be associated with a mass. Dystrophic calcifications may increase over time. They are benign and do not need to be biopsied.
- **Oil cyst.** Oil cyst formation is a dystrophic reaction of the breast. It appears as a round or oval lucent mass. Curvilinear rim calcifications are often present at the periphery of the lucent mass. This is a benign lesion that does not need to be biopsied.

Additional Differential Diagnoses

- **Hematoma.** Hematoma appears as a high-density mass on mammograms. It is usually preceded by a history of trauma or anticoagulation use. As a hematoma evolves and becomes organized, dense dystrophic calcifications may appear. Clinical history contributes to making this diagnosis. This is a benign mass that does not need to be biopsied.
- **Abscess.** Abscess appears as an irregular or circumscribed mass, often associated with signs of mastitis (e.g., skin thickening and edema). Over time, calcifications may form as part of a dystrophic reaction. These calcifications are usually dense and coarse. As with hematoma, the clinical history contributes to making this diagnosis. This is a benign mass that does not need to be biopsied; however, percutaneous drainage may be necessary for treatment, along with antibiotic therapy.

Diagnosis

Degenerating fibroadenoma

✓ Pearls

- Fibroadenomas are the most common benign solid masses in premenopausal women.
- "Popcorn" calcifications are pathognomonic for a degenerating fibroadenoma; biopsy is not necessary.
- A lucent mass with curvilinear rim calcifications is a benign oil cyst.
- Diagnoses of hematoma and abscess are primarily based on clinical findings.

Suggested Readings

Ikeda DM. Breast Imaging: The Requisites. Philadelphia: Elsevier; 2004

Kopans DB. Breast Imaging. 3rd ed. Philadelphia: Lippincott Williams & Wilkins; 2007

Tse GM, Tan PH, Pang AL, Tang AP, Cheung HS. Calcification in breast lesions: pathologists' perspective. J Clin Pathol 2008;61(2):145–151

Case 280

Matthew R. Denny and Jessica W. T. Leung

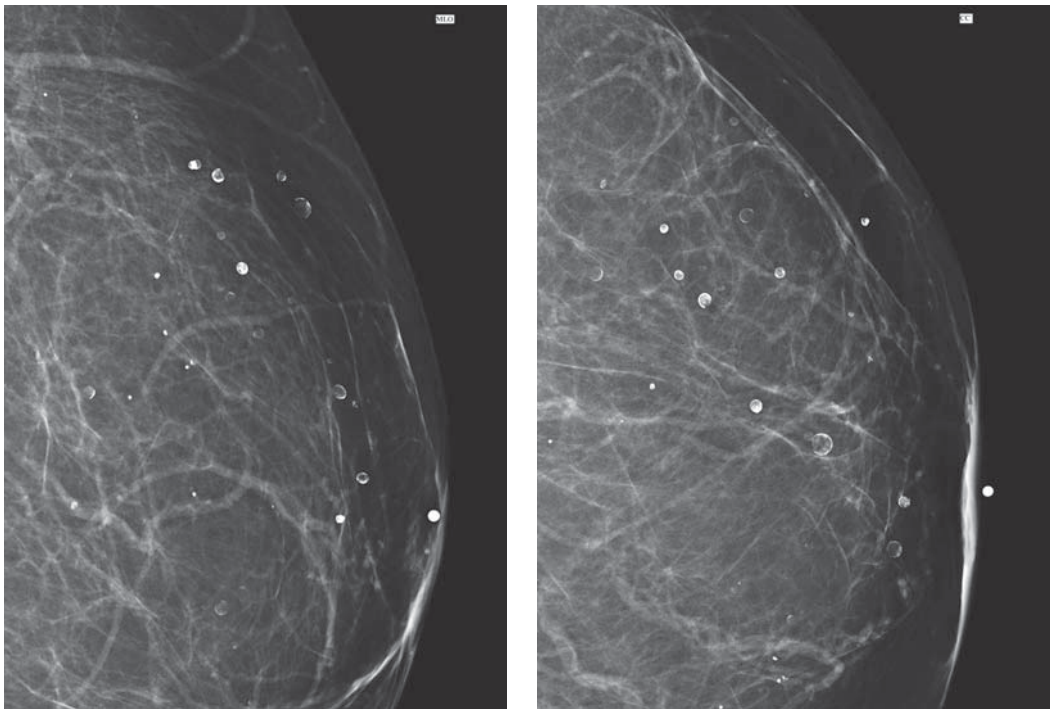


Fig. 280.1 Anterior aspects of screening mammograms in **(A)** the medial-lateral oblique and **(B)** craniocaudal projections show calcifications with diffuse distribution and rim, punctate, and round forms.

Clinical Presentation

A 62-year-old woman presents for screening mammography (**Fig. 280.1**).

Key Imaging Finding

Benign-appearing calcifications: rim, punctate, and round forms

Top 3 Differential Diagnoses

- **Calcified oil cyst.** Oil cysts form as a result of fat necrosis in the breast. Various etiologies may result in fat necrosis and oil cyst formation, including surgery, trauma, and ischemia. Oil cysts are round or oval radiolucent structures that calcify over time. Most commonly, the calcifications occur along the periphery; occasionally, the entire oil cyst may become calcified, so that the calcifications appear round or punctate. Rim, punctate, and round calcifications are benign and do not need to be biopsied.
- **Dystrophic calcifications.** Dystrophic calcifications form in the breast as part of fat necrosis, which may result from various etiologies, including surgery, trauma, and ischemia. Such calcifications are dense and coarse. Dystrophic calcifications may increase over time. They are benign and do not need to be biopsied.
- **Dermal calcifications.** Dermal calcifications are of geometric or polygonal shape, often with lucent centers. They are most commonly found in the upper inner breast in a regional distribution, but they may be diffuse. Dermal calcifications are diagnosed when they display the classic morphology or when they project over the skin. When there is uncertainty regarding the diagnosis of dermal calcifications, tangential mammographic views may be performed for confirmation or exclusion of dermal calcifications. Dermal calcifications are benign and do not need to be biopsied.

Additional Differential Diagnoses

- **Fibrocystic change.** Fibrocystic change is a normal spectrum of breast physiology, likely related to hormonal influences. It most commonly occurs in premenopausal women and may give rise to calcifications with various appearances. Some calcifications of fibrocystic change are characteristically benign in morphology (e.g., round or punctate) or distribution (e.g., bilateral and diffuse), whereas others are indeterminant (e.g., clustered or amorphous) and require biopsy to exclude malignancy.
- **Hyalinized fibroadenoma calcifications.** As a fibroadenoma involutes or degenerates with time, its stromal components become hyalinized. Coarse, curvilinear, "popcorn" calcifications may appear. Such characteristic calcifications are pathognomonic for a degenerating fibroadenoma. Calcifications associated with a hyalinized fibroadenoma are benign and do not need to be biopsied.

Diagnosis

Calcified oil cysts

✓ Pearls

- Benign oil cyst calcifications may be rim, punctate, or round; they should not be biopsied.
- Dystrophic calcifications may result from surgery, trauma, or ischemia; they should not be biopsied.
- Tangential views are useful in confirming dermal origin of calcifications on mammography.
- Calcifications associated with fibrocystic change vary from classically benign to indeterminant.

Suggested Readings

American College of Radiology. ACR Breast Imaging Reporting and Data System (BI-RADS). 4th ed. Reston, VA: Author; 2003

Berg WA, Arnoldus CL, Teferra E, Bhargavan M. Biopsy of amorphous breast calcifications: pathologic outcome and yield at stereotactic biopsy. Radiology 2001;221(2):495–503

Ikeda DM. Breast Imaging: The Requisites. Philadelphia: Elsevier; 2004

Kopans DB. Breast Imaging. 3rd ed. Philadelphia: Lippincott Williams & Wilkins; 2007

Sickles EA. Breast calcifications: mammographic evaluation. Radiology 1986;160(2):289–293

Case 281

Jessica W. T. Leung

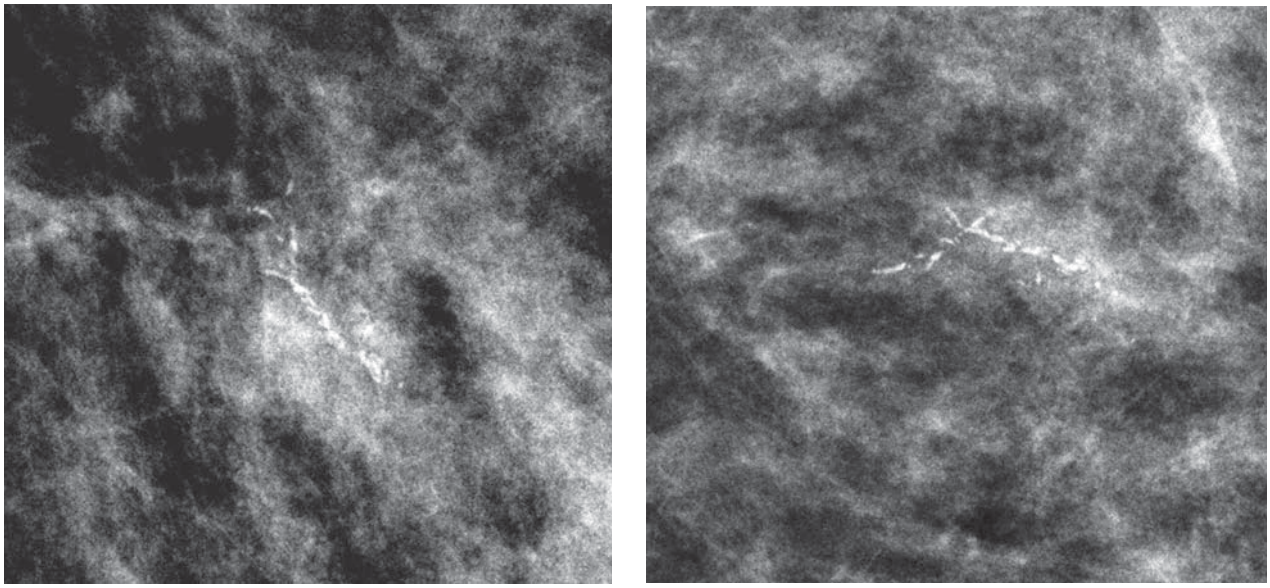


Fig. 281.1 Spot compression magnification mammograms in **(A)** the lateral-medial and **(B)** craniocaudal projections show calcifications with linear distribution and linear and branching forms.

Clinical Presentation

A 77-year-old woman is recalled from screening mammography for new breast calcifications (**Fig. 281.1**).

Key Imaging Finding

Malignant-appearing calcifications; linear, branching forms

Top 3 Differential Diagnoses

- **Ductal carcinoma in situ (DCIS)/invasive ductal carcinoma.** DCIS is most commonly diagnosed as calcifications at screening mammography. The calcifications result from ischemic necrosis as the tumor outgrows its blood supply. Malignant calcifications display a variety of appearances: some are classic for cancer, whereas others are indeterminant and cannot be distinguished from benign calcifications without biopsy. When analyzing calcifications, consider both the morphology (shape or form) and distribution (how the calcifications are arranged in space). Linear distribution and linear, branching morphology are highly suggestive of malignancy. Spot compression magnification views better portray the morphology and distribution of calcifications. Malignant calcifications may represent DCIS with invasive carcinoma.
- **Vascular calcifications.** Calcifications deposit in arterial walls as a result of aging, atherosclerosis, or hypercalcemic state. When the vessel is seen in cross section, vascular calcifications may appear curvilinear or rimlike. "Tram track" calcifications are seen in profile when both walls of the vessel are calcified. Vascular calcifications may increase over time. They may be identified with confidence by recognizing their typical morphology and distribution; biopsy should not be performed.
- **Secretory calcifications.** Also known as plasma cell mastitis, secretory calcifications form in large or intermediate-sized ducts and are benign. They are more common in elderly women and appear as coarse linear (sometimes branching) calcifications, located in the retroareolar breast, radiating to the nipple. They are usually unilateral or asymmetric if bilateral. Secretory calcifications may increase over time. Classic imaging features are diagnostic; when present, biopsy should not be performed.

Additional Differential Diagnoses

- **Milk of calcium.** Milk of calcium is liquid calcium that sediments in tiny benign cysts. Because of its fluid nature, its morphology varies depending on the position of the cysts. When viewed in the lateral projection, the milk of calcium within the cysts appears linear, discoid, layering, or meniscoid. When viewed in the craniocaudal projection, the milk of calcium appears round, amorphous, or smudgy.
- **Fibrocystic change.** Fibrocystic change is a normal spectrum of breast physiology, likely related to hormonal influences. It commonly occurs in premenopausal women. It can give rise to calcifications with various appearances. Some calcifications of fibrocystic change are characteristically benign in morphology (e.g., round or punctate) or distribution (e.g., bilateral and diffuse), whereas others are indeterminant (e.g., clustered and amorphous) and require biopsy to exclude malignancy.

Diagnosis

Ductal carcinoma in situ, high grade

✓ Pearls

- Spot compression magnification views are used to evaluate the morphology/distribution of calcifications.
- Calcifications with linear distribution and linear, branching morphology are suspicious for cancer.
- Indeterminant calcifications require biopsy to determine whether they are malignant or benign.

Suggested Readings

Al-Attar MA, Michell MJ, Ralleigh G, et al. The impact of image guided needle biopsy on the outcome of mammographically detected indeterminate microcalcification. Breast 2006;15(5):635–639

Berg WA, Arnoldus CL, Teferra E, Bhargavan M. Biopsy of amorphous breast calcifications: pathologic outcome and yield at stereotactic biopsy. Radiology 2001;221(2):495–503

Kopans DB. Breast Imaging. 3rd ed. Philadelphia: Lippincott Williams & Wilkins; 2007

Linden SS, Sickles EA. Sedimented calcium in benign breast cysts: the full spectrum of mammographic presentations. AJR Am J Roentgenol 1989;152(5):967–971

Sickles EA. Breast calcifications: mammographic evaluation. Radiology 1986;160(2):289–293

Case 282

Boon Chye Ching

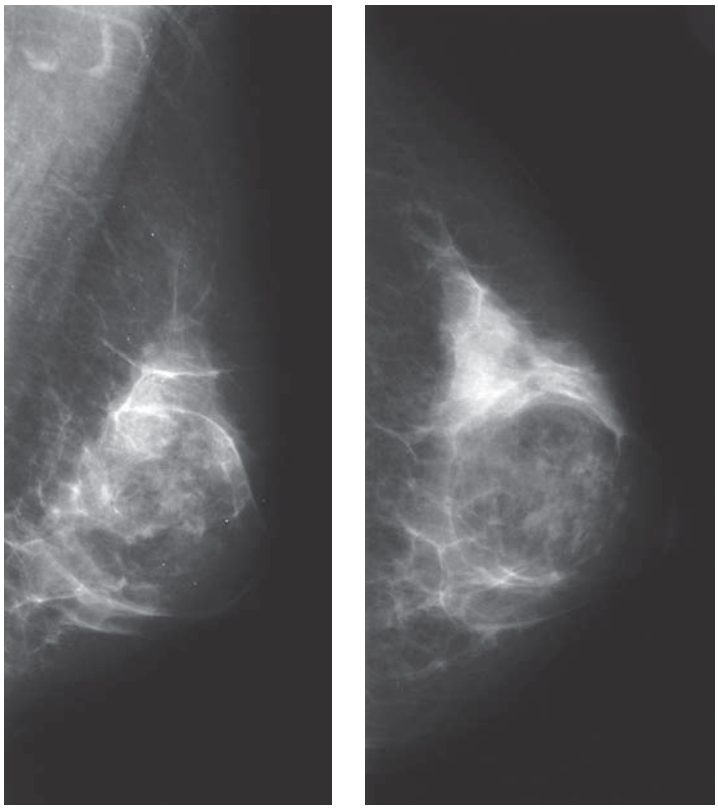


Fig. 282.1 Mammograms in **(A)** the medial-lateral oblique and **(B)** craniocaudal projections show an oval circumscribed mass with a pseudocapsule in the retroareolar breast. The mass is primarily radiolucent (fatty) at mammography, but it also contains a few soft tissue densities. (Courtesy of Jill S. L. Wong, MB, ChB, FACR [UK], National Cancer Centre, Singapore.)

Clinical Presentation

A 45-year-old woman presents for screening mammography (**Fig. 282.1**).

Key Imaging Finding

Fatty breast lesion

Top 3 Differential Diagnoses

- **Hamartoma (fibroadenolipoma).** Hamartoma is an uncommon (incidence of <1%) circumscribed benign mass composed of variable amounts of glandular tissue, fat, and fibrous connective tissue. It is usually asymptomatic but can sometimes present as a palpable mass. Distinct mammographic features include circumscribed margins and a combination of fatty and soft tissue densities surrounded by a thin radiopaque capsule or pseudocapsule (which may be complete or partial). On ultrasound, it typically appears as a circumscribed oval mass with heterogeneous internal echoes. It is usually diagnostic at mammography with a "breast within a breast" appearance. A classical hamartoma is benign and does not need to be biopsied. However, because it contains breast elements and ducts, carcinoma can develop within a hamartoma, so any suspicious mass or microcalcifications arising within a hamartoma should be biopsied.
- **Lipoma.** Lipoma is a fatty, radiolucent mass that may or may not have a thin, discrete rim separating it from the surrounding glandular tissue. Lipoma can present as a palpable lump. Unlike fat necrosis, it does not calcify. Ultrasound shows a well-circumscribed mass that is nearly isoechoic or slightly hyperechoic to the subcutaneous fat.
- **Galactocele.** A galactocele is a benign cyst containing thick, inspissated milk caused by ductal obstruction in patients with a history of lactation. Patients usually present with a painless, mobile, palpable lump. Mammography will show single or multiple masses with density similar or less than the surrounding fibroglandular tissue. However, if the fat content is very high, a galactocele can be completely radiolucent and simulate a lipoma. When in doubt, the diagnosis can be made by aspirating milk-like fluid with resolution of the lesion.

Additional Differential Diagnoses

- **Fat necrosis.** Fat necrosis occurs when intracellular fat escapes the damaged cells into the surrounding tissue and causes the body to react by forming granulation tissue. Because there are different stages of this process, the manifestations of fat necrosis are varied. Fat necrosis can present with very benign-appearing to very worrisome imaging features. It can present as lipid cyst, microcalcifications, coarse calcifications, spiculated areas of increased asymmetry, or focal masses. As a lipid cyst, it would be radiolucent at mammography, and dystrophic calcifications would appear over time. There may or may not be a history of trauma or surgery.
- **Oil cyst.** An oil cyst is a focal form of fat necrosis. The causes are varied, and the patient may not recall a history of trauma or surgery. It is usually clinically occult. Fat necrosis is commonly seen at sites of reduction mammoplasty or lumpectomy postradiation.

Diagnosis

Hamartoma (fibroadenolipoma)

✓ Pearls

- Hamartoma presents as a circumscribed fatty and soft tissue mass with a thin capsule or pseudocapsule.
- The mammographic appearance of a hamartoma is classically referred to as "breast within a breast."
- Lipomas are fatty, radiolucent masses that may or may not have a thin, discrete rim; they do not calcify.
- A clinical history of lactation is crucial in the diagnosis of a galactocele.

Suggested Readings

Ikeda DM. Breast Imaging: The Requisites. Philadelphia: Elsevier; 2004

Kopans DB. Breast Imaging. 3rd ed. Philadelphia: Lippincott Williams & Wilkins; 2007

Wahner-Roedler DL, Sebo TJ, Gisvold JJ. Hamartomas of the breast: clinical, radiologic, and pathologic manifestations. Breast J 2001;7(2):101–105

Case 283

Chloe M. Chhor

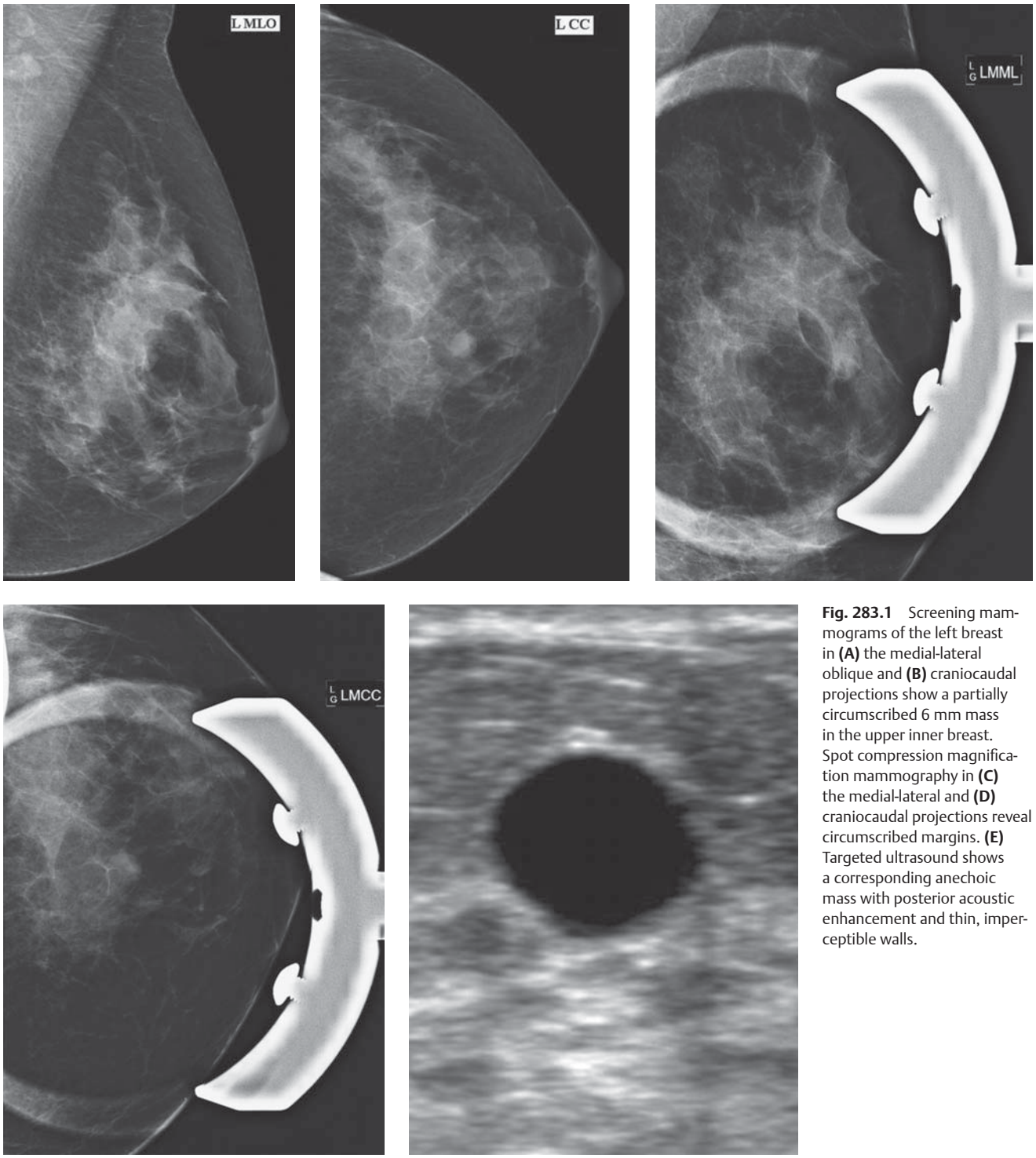


Fig. 283.1 Screening mammograms of the left breast in **(A)** the medial-lateral oblique and **(B)** craniocaudal projections show a partially circumscribed 6 mm mass in the upper inner breast. Spot compression magnification mammography in **(C)** the medial-lateral and **(D)** craniocaudal projections reveal circumscribed margins. **(E)** Targeted ultrasound shows a corresponding anechoic mass with posterior acoustic enhancement and thin, imperceptible walls.

Clinical Presentation

A 46-year-old woman is recalled from screening mammography for a mass in the upper inner left breast (**Fig. 283.1**).

Key Imaging Finding

Well-circumscribed mass in a premenopausal woman

Top 3 Differential Diagnoses

- **Fibroadenoma.** Fibroadenoma is the most common benign solid mass in young women. It can have a variable appearance at ultrasound, but classically it appears as a circumscribed or gently lobulated, mildly hypoechoic, thinly encapsulated, elliptically shaped mass that is oriented parallel to the chest wall (wider than tall). Fibroadenoma can be mistaken for a cyst when it is homogeneously hypoechoic with posterior acoustic enhancement. If there is significant fibrosis or calcifications associated with the fibroadenoma, posterior acoustic shadowing may be seen at ultrasound, and suspicion for malignancy may be erroneously raised. Correlation with mammography may reveal dystrophic calcifications and contribute to the correct diagnosis of a benign fibroadenoma.
- **Cyst.** Cyst is the most common breast mass in women over age 35. It is benign and not associated with an increased risk of breast cancer. At mammography, cysts may appear as asymmetries or masses. Ultrasound is used to distinguish a simple cyst from a solid mass. A simple cyst appears as an anechoic mass with posterior acoustic enhancement and thin, imperceptible walls. A complicated cyst is hypoechoic with homogeneous diffuse internal echoes. A complicated cyst is also benign; however, aspiration may be necessary to distinguish it from a hypoechoic solid mass. Most cysts are asymptomatic. Symptomatic cysts often present with pain correlating to menstrual cycles; they can be treated with aspiration.
- **Intramammary lymph node.** An intramammary lymph node may present as a mammographic or palpable finding. At mammography, an intramammary lymph node classically appears as a well-circumscribed, isodense, ovoid, reniform, or lobulated mass with a fatty hilum. At sonography, it is an ovoid or gently lobulated hypoechoic reniform mass with an echogenic fatty hilum that contains a vascular pedicle on Doppler imaging. If an intramammary lymph node maintains its characteristic shape and does not reach pathologic size criteria, no further follow-up is required.

Additional Differential Diagnoses

- **Breast carcinoma.** The majority of newly diagnosed well-circumscribed, round or oval masses in the breast are benign, but 2 to 5% of such masses are new cancers. Breast carcinomas can have variable appearances on mammograms and ultrasound scans, which can make it difficult to distinguish a benign solid mass from cancer. Medullary carcinoma is a classic example of an invasive carcinoma mimicking a cyst on ultrasound. If there is any uncertainty, percutaneous core biopsy is recommended to exclude malignancy.
- **Papilloma.** Papilloma is a benign fibroepithelial tumor of the breast that can be detected at screening mammography or present with a palpable lump or nipple discharge. Ultrasound and ductography are used to further evaluate nipple discharge and to assess for the presence and extent of papillomas. At sonography, papilloma may appear as an intraductal, intracystic, or solid mass. Papilloma is often surgically excised because of the difficulty in differentiating it from papillary carcinoma.

Diagnosis

Simple cyst

✓ Pearls

- Ultrasound is used to evaluate a palpable lump and to distinguish a simple cyst from a solid mass.
- Fibroadenoma is the most common solid mass in young women; a cyst is the most common mass after age 35.
- Lymph nodes are classically reniform in shape with a fatty hilum that contains a vascular pedicle.

Suggested Readings

Ikeda DM. Breast Imaging: The Requisites. Philadelphia: Elsevier; 2004

Kopans DB. Breast Imaging. 3rd ed. Philadelphia: Lippincott Williams & Wilkins; 2007

Stavros AT. Breast Ultrasound. Philadelphia: Lippincott Williams & Wilkins; 2004

Case 284

Frederick R. Margolin

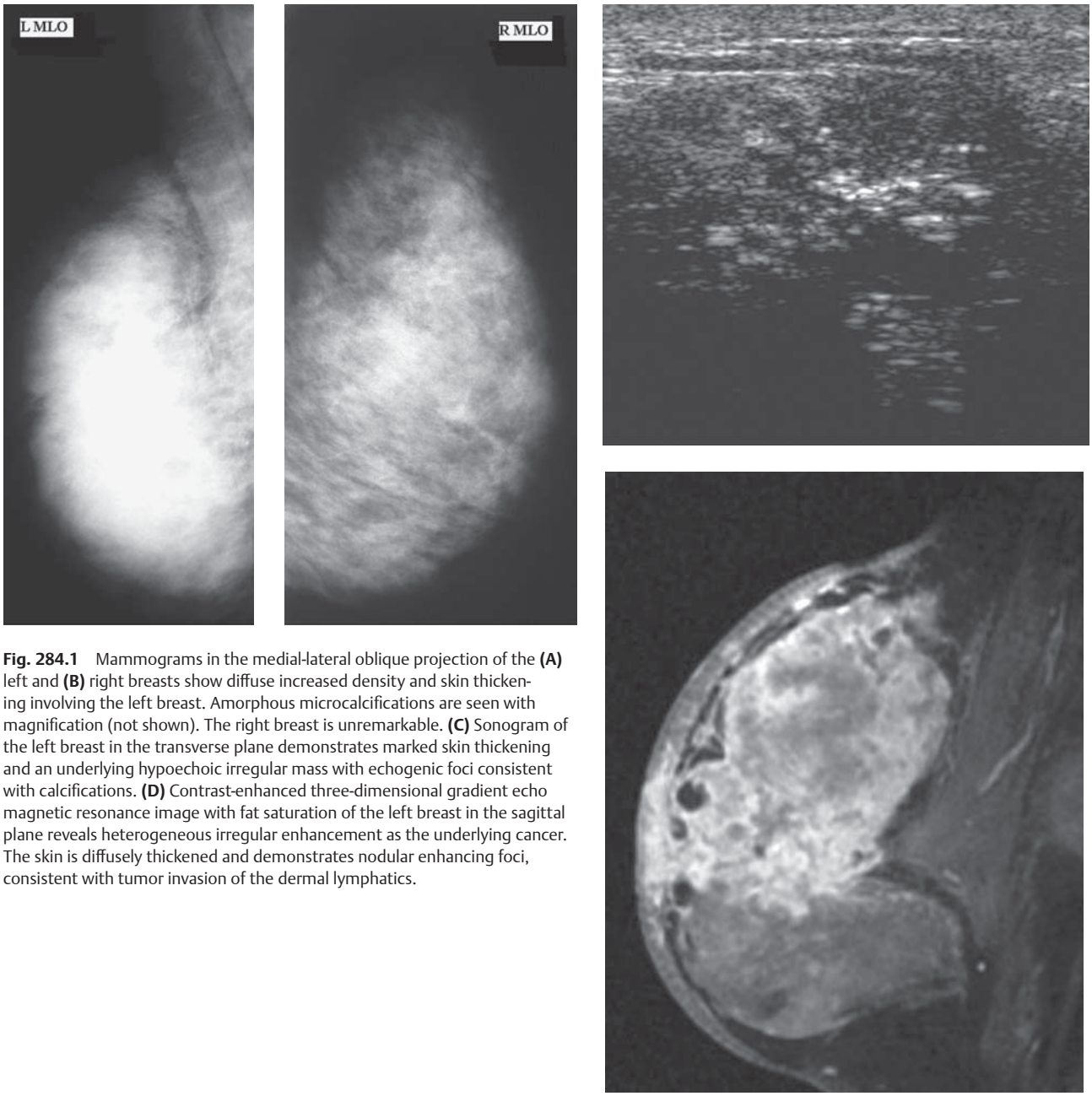


Fig. 284.1 Mammograms in the medial-lateral oblique projection of the **(A)** left and **(B)** right breasts show diffuse increased density and skin thickening involving the left breast. Amorphous microcalcifications are seen with magnification (not shown). The right breast is unremarkable. **(C)** Sonogram of the left breast in the transverse plane demonstrates marked skin thickening and an underlying hypoechoic irregular mass with echogenic foci consistent with calcifications. **(D)** Contrast-enhanced three-dimensional gradient echo magnetic resonance image with fat saturation of the left breast in the sagittal plane reveals heterogeneous irregular enhancement as the underlying cancer. The skin is diffusely thickened and demonstrates nodular enhancing foci, consistent with tumor invasion of the dermal lymphatics.

Clinical Presentation

A 38-year-old woman presents with erythema and tenderness of the left breast of 2 weeks' duration. Upon physical examination, findings consistent with peau d'orange are seen. The contralateral breast was unremarkable (**Fig. 284.1**).

Key Imaging Finding

Unilateral skin thickening

Top 3 Differential Diagnoses

- **Inflammatory breast cancer.** Inflammatory breast carcinoma is breast cancer (ductal or lobular) with invasion of the dermal lymphatics, resulting in skin thickening, erythema, pain, and swelling. The skin of the affected breast resembles the thick rind of an orange, giving rise to the description peau d'orange. Inflammatory breast cancer is biologically aggressive; metastasis to axillary lymph nodes at the time of diagnosis is often present. Bacterial superinfection is also common, such that affected patients may present with signs of mastitis. Diagnosis is made through punch biopsy of the skin, demonstrating tumor invasion of the dermal lymphatics. Imaging findings include diffuse skin thickening and increased density. An underlying malignancy, such as a spiculated mass or pleomorphic microcalcifications, may be seen. Overall, the prognosis is poor. Neoadjuvant (preoperative) chemotherapy is the usual treatment.
- **Mastitis.** Mastitis is infection of the breast, usually caused by bacterial organisms such as *Staphylococcus*. Patients often present with fever, an elevated white blood cell count, swelling, erythema, warmth, and tenderness. Patients should be followed to resolution, as mastitis may be clinically indistinguishable from inflammatory breast cancer. At imaging, diffuse skin thickening and increased density may be seen. Abscess formation often requires surgical or percutaneous drainage in addition to antibiotic therapy.
- **Invasive breast cancer.** Invasive breast cancer (ductal or lobular) may involve the skin by local extension, resulting in focal skin thickening, erythema, and warmth. In contrast to inflammatory breast cancer, this is a focal rather than diffuse process. At imaging, the underlying cancer is seen with adjacent skin involvement. Local invasion of the skin carries a better prognosis than dermal lymphatic invasion.

Additional Differential Diagnoses

- **Postsurgical or postradiation changes.** Skin thickening may be seen after surgery or, more commonly, after radiation. This is a unilateral finding affecting the treated breast. Postsurgical skin thickening is usually focal, whereas radiation results in diffuse skin thickening. Skin thickening may decrease over time.
- **Superior vena cava (SVC) syndrome.** SVC syndrome occurs secondary to external compression and thrombosis, usually from lung cancer. Increased venous pressure results in stasis of fluids and edema, manifesting as skin thickening. Thickening of the breast trabeculae may also be present.
- **Lymphedema.** Axillary lymph node dissection may be complicated by disruption of the lymphatic drainage of the ipsilateral breast. This results in edema, manifesting as skin and trabeculae thickening.

Diagnosis

Inflammatory breast carcinoma

✓ Pearls

- Inflammatory breast carcinoma is diffuse with clinical and imaging findings involving the entire breast.
- Skin involvement by local tumor extension has a better prognosis than inflammatory breast cancer.
- Mastitis may be indistinguishable from inflammatory breast cancer based on clinical and imaging findings.
- Postsurgical skin thickening is usually focal, whereas postradiation skin thickening is often diffuse.

Suggested Readings

Ikeda DM. Breast Imaging: The Requisites. Philadelphia: Elsevier; 2004

Kopans DB. Breast Imaging. 3rd ed. Philadelphia: Lippincott Williams & Wilkins; 2007

Kushwaha AC, Whitman GJ, Stelling CB, Cristofanilli M, Buzdar AU. Primary inflammatory carcinoma of the breast: retrospective review of mammographic findings. AJR Am J Roentgenol 2000;174(2):535–538

Merajver SD, Sabel MS. Inflammatory breast cancer. In: Harris JR, Lippman ME, Morrow M, Osborne CK, eds. Diseases of the Breast. 3rd ed. Philadelphia: Lippincott Williams & Wilkins; 2004

Case 285

Frederick R. Margolin

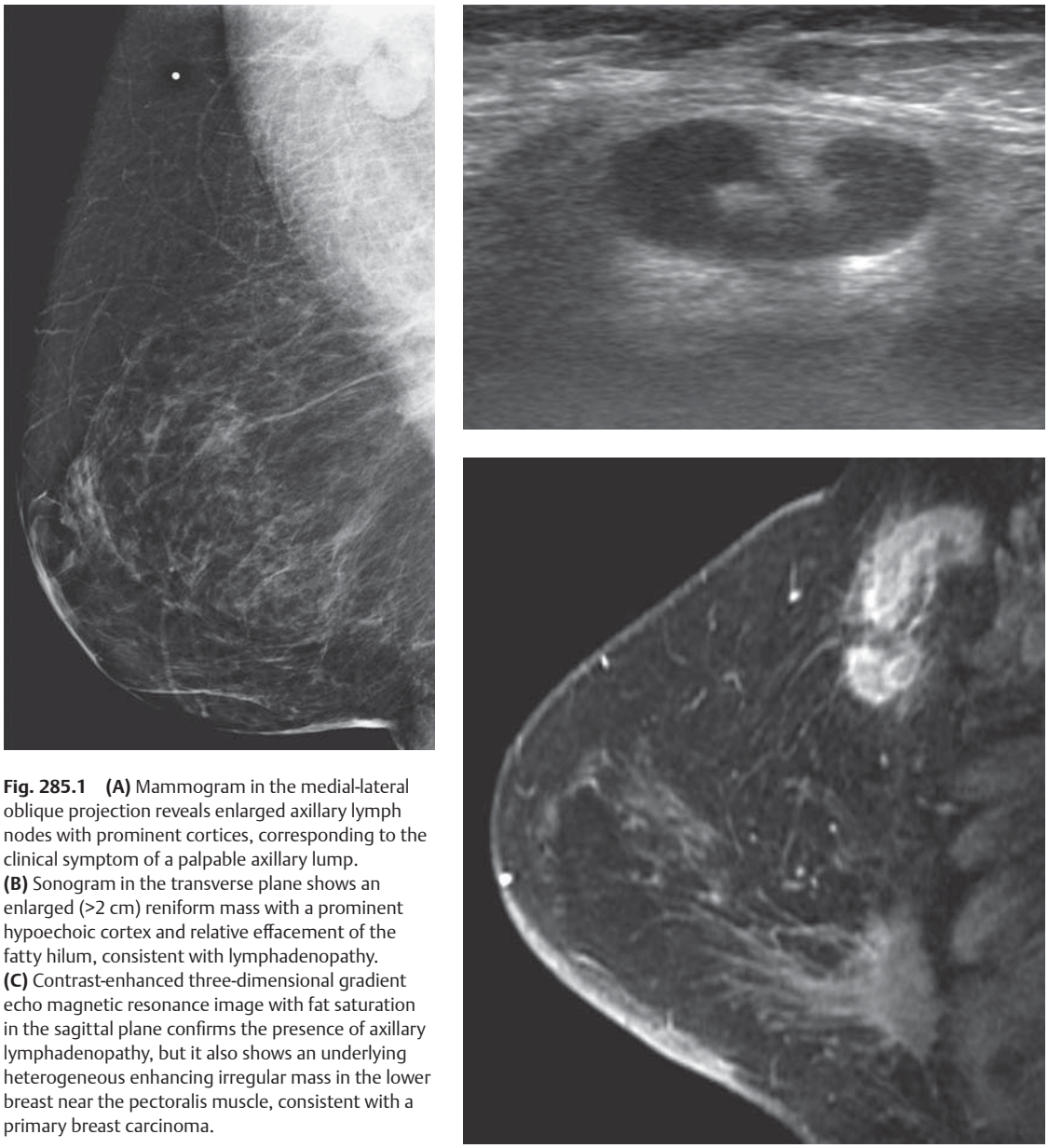


Fig. 285.1 **(A)** Mammogram in the medial-lateral oblique projection reveals enlarged axillary lymph nodes with prominent cortices, corresponding to the clinical symptom of a palpable axillary lump. **(B)** Sonogram in the transverse plane shows an enlarged (>2 cm) reniform mass with a prominent hypoechoic cortex and relative effacement of the fatty hilum, consistent with lymphadenopathy. **(C)** Contrast-enhanced three-dimensional gradient echo magnetic resonance image with fat saturation in the sagittal plane confirms the presence of axillary lymphadenopathy, but it also shows an underlying heterogeneous enhancing irregular mass in the lower breast near the pectoralis muscle, consistent with a primary breast carcinoma.

Clinical Presentation

A 73-year-old woman presents with a palpable lump in the left axilla of 2 months' duration (**Fig. 285.1**).

Key Imaging Finding

Axillary lymphadenopathy

Top 3 Differential Diagnoses

- **Breast cancer with lymph node spread.** When breast cancer spreads to the ipsilateral axillary node(s), this is considered locoregional disease and not systemic metastatic disease. Depending on staging, the prognosis is still relatively good, and the patient can potentially be cured. When sufficiently large, lymphadenopathy may be seen at mammography, ultrasound, or magnetic resonance imaging (MRI). However, imaging cannot exclude disease in nodes that are not enlarged and that retain their normal morphology. Sentinel node biopsy is now the standard of care in evaluating for axillary node involvement. If the sentinel nodes are negative for cancer, axillary nodal dissection would not be indicated. In women with adenocarcinoma of the axillary nodes but who have no identifiable primary cancer, the ipsilateral breast is the likely source. MRI has been shown to be a useful tool in identifying breast malignancies that are otherwise occult at mammography and ultrasound.
- **Lymphoma.** Systemic lymphoma (either Hodgkin or non-Hodgkin lymphoma) may present as bilateral axillary lymphadenopathy. Patients most often have lymphadenopathy elsewhere in the body as well. Patients may report systemic symptoms, such as weight loss and malaise. Diagnosis is made through correlation with the clinical history, identification of lymphadenopathy elsewhere in the body, and biopsy.
- **Reactive lymphadenopathy.** Reactive lymphadenopathy in the axilla is generally due to an infection of the upper extremity. The involved nodes may be tender. Cat scratch fever is one cause of painful regional lymphadenopathy. Correlation with the clinical history and physical examination is important in making this diagnosis. Reactive lymphadenopathy is generally unilateral and should resolve with time. Human immunodeficiency virus may cause bilateral reactive axillary lymphadenopathy.

Additional Differential Diagnoses

- **Metastases from a remote primary cancer.** Metastases from a remote primary cancer may present in the axilla. Reported primary cancers include thyroid, ovary, pancreas, and head and neck region. Lymphadenopathy may be unilateral or bilateral. Patients with such nodal disease have a poor prognosis. Diagnosis is often made with a clinical and imaging work-up for malignancy, as well as biopsy.
- **Connective tissue and granulomatous disorders.** Systemic diseases, including rheumatoid arthritis and sarcoidosis, may result in axillary lymphadenopathy. When this occurs, the lymphadenopathy is usually bilateral. Sarcoidosis classically manifests with concomitant mediastinal and hilar lymphadenopathy.
- **Castleman disease.** Castleman disease is a rare inflammatory lymphoproliferative disorder of unknown etiology. It most commonly presents as mediastinal lymphadenopathy, but rarely it may present as axillary lymphadenopathy (bilateral or unilateral).

Diagnosis

Breast cancer with axillary lymph node spread

✓ Pearls

- MRI is useful in demonstrating occult breast malignancies in the setting of axillary lymphadenopathy.
- Patients with lymphoma often have systemic symptoms, bilateral involvement, and involvement elsewhere.
- Reactive lymphadenopathy secondary to infection is most often unilateral and resolves with time.

Suggested Readings

Chang YW, Noh HJ, Hong SS, Hwang JH, Lee DW, Moon JH. Castleman's disease of the axilla mimicking metastasis. Clin Imaging 2007;31(6):425–427

Ikeda DM. Breast Imaging: The Requisites. Philadelphia: Elsevier; 2004

Ko EY, Han BK, Shin JH, Kang SS. Breast MRI for evaluating patients with metastatic axillary lymph node and initially negative mammography and sonography. Korean J Radiol 2007;8(5):382–389

Kopans DB. Breast Imaging. 3rd ed. Philadelphia: Lippincott Williams & Wilkins; 2007

Case 286

Boon Chye Ching

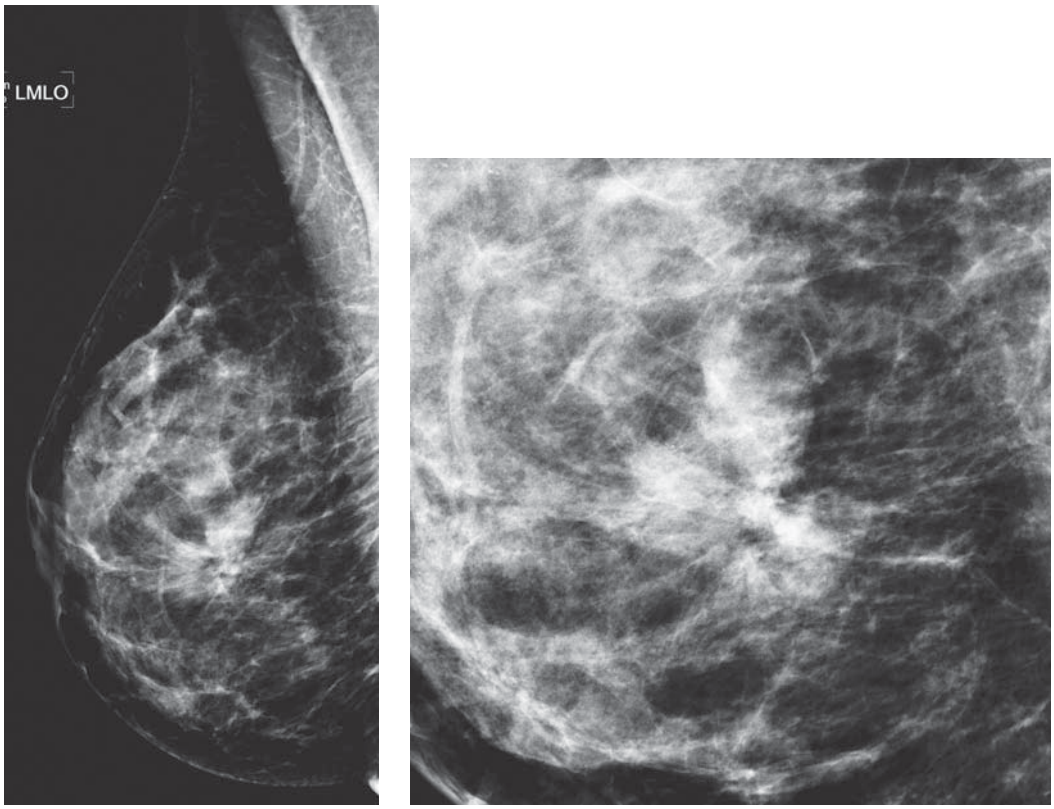


Fig. 286.1 **(A)** Screening mammogram in the medial-lateral oblique (MLO) projection suggests a spiculated mass with central lucency in the middle left breast. **(B)** Subsequent spot compression mammography in the MLO projection confirms the presence of this mass. A hypoechoic mass was identified at sonography (not shown). Ultrasound-guided core biopsy was performed.

Clinical Presentation

A 44-year-old woman presented for screening mammography (**Fig. 286.1**).

Key Imaging Finding

Mass with central lucency

Top 3 Differential Diagnoses

- **Radial scar.** A radial scar, also known as a complex sclerosing lesion when >1 cm, is a benign but high-risk lesion. About 33% of radial scars are associated with atypical or malignant conditions. The term *radial scar* is a misnomer because it is not a scar at all and is not related to prior surgery or trauma. It is usually nonpalpable. A radial scar at mammography appears as a focal asymmetry or architectural distortion with central radiolucent areas representing fat. It has long, thin radiating spicules against a backdrop of radiolucent fat ("black star" appearance). A radial scar is usually better seen on one of the two standard mammographic projections. At sonography, it usually appears as an area of architectural distortion or a hypoechoic mass. Sometimes a radial scar has to be completely excised for diagnosis.
- **Invasive ductal carcinoma.** Invasive ductal carcinoma can present at mammography as a dense mass with central lucency and short, truncated spicules (in contrast to a radial scar, where there are usually long, curvilinear spicules). The spiculated margin is usually the result of desmoplastic reaction, although in some cases it is the result of tumor infiltration. Invasive ductal carcinoma may present as a palpable lump; a radial scar is usually asymptomatic. At sonography, invasive ductal carcinoma typically presents as a hypoechoic irregular mass associated with nonparallel orientation and posterior acoustic shadowing.
- **Tubular carcinoma.** Tubular carcinoma is usually seen as a central mass with spiculated margins. It is typically <1 cm in diameter and is very slow growing. There is a bilateral incidence of 12 to 40%. Pure tubular carcinoma is extremely well differentiated. Less pure tubular carcinomas are known as mixed tubular carcinomas; those with lobular elements are known as tubulolobular carcinomas. These histologic distinctions are clinically important because there is a higher chance of multifocality and metastatic spread as the nontubular elements increase. The prognosis for pure tubular carcinoma is excellent.

Additional Differential Diagnoses

- **Fat necrosis.** Fat necrosis occurs when intracellular fat escapes the damaged cells into the surrounding tissues and causes the body to react by forming granulation tissue and thus a boundary. The imaging manifestations are varied based on the stage of fat necrosis, ranging from very benign to very malignant features. There may or may not be an identifiable history of trauma or surgery.
- **Postsurgical scar.** A postsurgical scar mimics breast carcinoma in that a spiculated mass or asymmetry may be present. At sonography, a postsurgical scar may manifest as an irregular hypoechoic mass with posterior acoustic shadowing. There should be distortion of the subcutaneous tissue extending from the skin overlying the scar in the plane of incision down to the spiculated mass. Comparison with previous studies and careful imaging follow-up are needed to detect subtle findings that may indicate malignancy.

Diagnosis

Radial scar

✓ Pearls

- Long radiating spicules with intervening lucency and absent central mass are suggestive of a radial scar.
- Invasive ductal carcinoma classically presents as a dense mass with spiculated margins and short spicules.
- Tubular carcinoma is a slow-growing cancer with an excellent prognosis.

Suggested Readings

Alleva DQ, Smetherman DH, Farr GH Jr., Cederbom GJ. Radial scar of the breast: radiologic-pathologic correlation in 22 cases. Radiographics 1999; 19(Spec Issue):S27–S35, discussion S36–S37

Cooper HS, Patchefsky AS, Krall RA. Tubular carcinoma of the breast. Cancer 1978;42(5):2334–2342

Hogge JP, Robinson RE, Magnant CM, Zuurbier RA. The mammographic spectrum of fat necrosis of the breast. Radiographics 1995;15(6):1347–1356

Case 287

Natasha Brasic

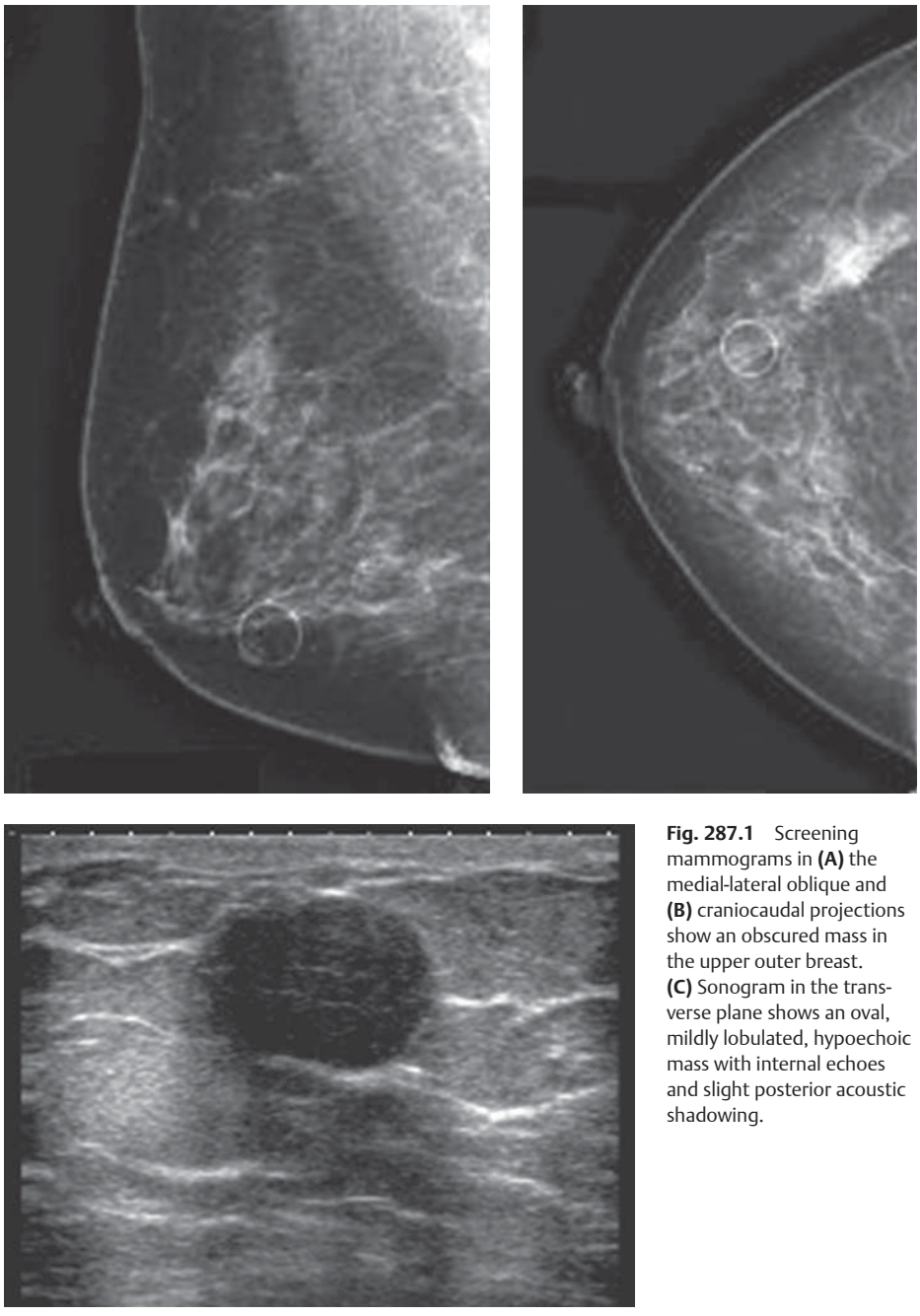


Fig. 287.1 Screening mammograms in **(A)** the medial-lateral oblique and **(B)** craniocaudal projections show an obscured mass in the upper outer breast. **(C)** Sonogram in the transverse plane shows an oval, mildly lobulated, hypoechoic mass with internal echoes and slight posterior acoustic shadowing.

Clinical Presentation

A 62-year-old woman presents for screening mammography (**Fig. 287.1**).

Key Imaging Finding

Well-circumscribed solid breast mass

Top 3 Differential Diagnoses

- **Fibroadenoma.** Fibroadenoma is the result of idiopathic overgrowth of connective tissue. Most studies suggest that fibroadenoma carries no significant risk for the subsequent development of breast cancer, although cancer can occur in fibroadenoma, just as in any other breast epithelium. At mammography, fibroadenoma typically appears as a well-circumscribed, round or oval mass with or without coarse "popcorn" calcifications. At sonography, it is classically hypoechoic, well circumscribed, gently lobulated, round or oval, and oriented parallel to the chest wall (wider than tall). Posterior sound transmission is variable.
- **Intramammary lymph node.** An intramammary lymph node is typically reniform in shape with a radiolucent notch due to fat in the hilum. There may be multiple nodes, and most are seen in the upper outer breast. On Doppler imaging, a vascular pedicle is seen at the hilum. If an intramammary lymph node shows a circumscribed, reniform morphology and is not of enlarged size, then no further work-up is needed.
- **Hamartoma (fibroadenolipoma).** Hamartoma is a benign mass of normal but disorganized ducts and lobules admixed with stroma and adipose tissue. It presents as a circumscribed, smoothly marginated, fat-containing mass. At mammography, various mixtures of fat and soft tissue are seen within a fibrous capsule. Sonography of these lesions is often confounding: fibrous elements produce specular reflections, and adenomatous elements appear heterogeneously hypoechoic.

Additional Differential Diagnoses

- **Circumscribed breast carcinoma.** There are a few cancers that are round, oval, or lobulated with circumscribed margins. The most common cancer that grows as a circumscribed mass is infiltrating ductal carcinoma, not otherwise specified. The medullary subtype of breast carcinoma is often circumscribed, although indistinct margins may be seen. Lymphoma, colloid carcinoma, and papillary carcinoma can appear as round, smoothly marginated masses. Metastases to the breast are often well circumscribed, but they are also usually multiple and bilateral, and the presence of an extramammary primary carcinoma is usually known.
- **Papilloma.** Occurring in the major ducts, solitary benign papilloma consists of epithelial proliferations on a fibrovascular stalk. It is typically sub- or periareolar in location and may produce serous or sanguineous nipple discharge. Intraductal papilloma may be associated with solitary duct enlargement due to duct obstruction. It usually extends within the lumen of the duct and may not be evident at conventional mammography. When visible at mammography, papilloma may appear as a circumscribed mass.

Diagnosis

Fibroadenoma

✓ Pearls

- Fibroadenoma is a common benign solid mass that is characteristically circumscribed and wider than tall.
- Intramammary lymph node has a reniform shape with a fatty hilum and is usually in the upper outer breast.
- Hamartoma is a circumscribed, smoothly marginated fat-containing mass with a fibrous capsule.
- Hamartomas are diagnosed at mammography; sonographic evaluation may confound the work-up.

Suggested Readings

Ikeda DM. Breast Imaging: The Requisites. Philadelphia: Elsevier; 2004

Kopans DB. Breast Imaging. 3rd ed. Philadelphia: Lippincott Williams & Wilkins; 2007

Sklair-Levy M, Sella T, Alweiss T, Craciun I, Libson E, Mally B. Incidence and management of complex fibroadenomas. AJR Am J Roentgenol 2008;190(1):214–218

Case 288

Jessica W. T. Leung

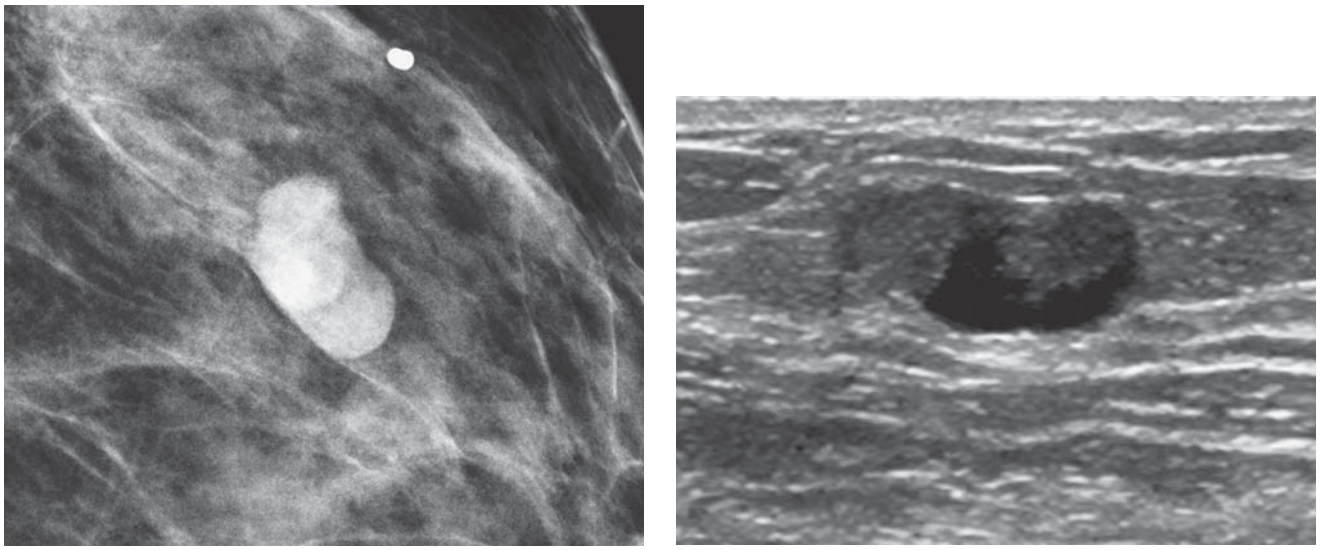


Fig. 288.1 **(A)** Spot compression mammogram in the craniocaudal projection shows a circumscribed lobulated mass. **(B)** Sonogram in the transverse plane shows a lobulated mass with cystic and solid components.

Clinical Presentation

A 60-year-old woman is recalled from screening mammography for a breast mass (**Fig. 288.1**).

Key Imaging Finding

Well-circumscribed cystic breast mass

Top 3 Differential Diagnoses

- **Papilloma/papillary carcinoma.** Papilloma is a benign breast mass that grows on a fibrovascular stalk. It may secrete fluid and form a surrounding cyst, resulting in intracystic papilloma with an appearance of a circumscribed cystic mass. It may also undergo necrosis with bloody nipple discharge. Pathologically, papilloma is often associated with atypia. Hence it may be difficult to distinguish benign papilloma from papillary carcinoma with core biopsy; surgical excision may be needed. Intracystic papillary carcinoma is similar in biologic behavior as in situ carcinoma. Invasive papillary carcinoma is rare. At mammography, papillary lesions may appear as circumscribed masses. At sonography, hypoechoic solid and cystic components may be present. Doppler signal may be present within the solid component, distinguishing it from cystic debris. Percutaneous core biopsy should include the solid component. A marker clip should be placed, as the lesion may be difficult to identify after biopsy if the cystic fluid component ruptures.
- **Seroma.** Seroma is a benign fluid collection that forms as a result of surgery. It usually appears as a well-circumscribed or partially circumscribed mass on mammograms. It appears cystic on sonography: the degree of anechoic versus hypoechoic components varies depending on the age of the seroma and the amount and type of fluid (bloody, proteinaceous, or simple). The collections may be complex with loculations. If the patient is symptomatic (with pain), ultrasound-guided aspiration may be performed.
- **Cyst with debris.** Cysts may contain cholesterol, protein, hemorrhage, or other debris, giving rise to hypoechoic components within a cystic lesion. At mammography, it may appear as a well-circumscribed or partially circumscribed mass. On ultrasound, a cystic mass with hypoechoic components is seen. The debris may be adherent or freely shifting. Doppler interrogation should not reveal blood flow. Aspiration may be necessary to differentiate a cyst with debris (which is benign) from other cystic masses.

Additional Differential Diagnoses

- **Hematoma.** Hematomas appear as well-circumscribed, partially circumscribed, obscured, or ill-defined masses on mammograms. They have various sonographic appearances, depending on the evolution of the clotting process, ranging from anechoic to hypoechoic to predominantly hyperechoic. Fluid–fluid levels reflecting different stages of blood may be seen. A hematoma is usually preceded by a history of trauma or anticoagulation use.
- **Abscess.** An abscess appears as an irregular or circumscribed mass, often associated with signs of mastitis (e.g., skin thickening and edema). On ultrasound, it is seen as a complex mass with various features, including cystic components, fluid–fluid levels, loculations, and debris. Ultrasound may be used to guide percutaneous aspiration or drainage catheter placement. The clinical history contributes to making the diagnosis.

Diagnosis

Papilloma (intracystic)

✓ Pearls

- Biopsy of a papilloma should include the solid component; place a marker clip to later identify the lesion.
- Doppler signal in a hypoechoic portion of a cystic mass supports papilloma over other cystic lesions.
- Seroma and a cyst with debris are both benign; aspiration is indicated for symptoms or if the diagnosis is unclear.

Suggested Readings

Berg WA, Campassi CI, Ioffe OB. Cystic lesions of the breast: sonographic-pathologic correlation. Radiology 2003;227(1):183–191

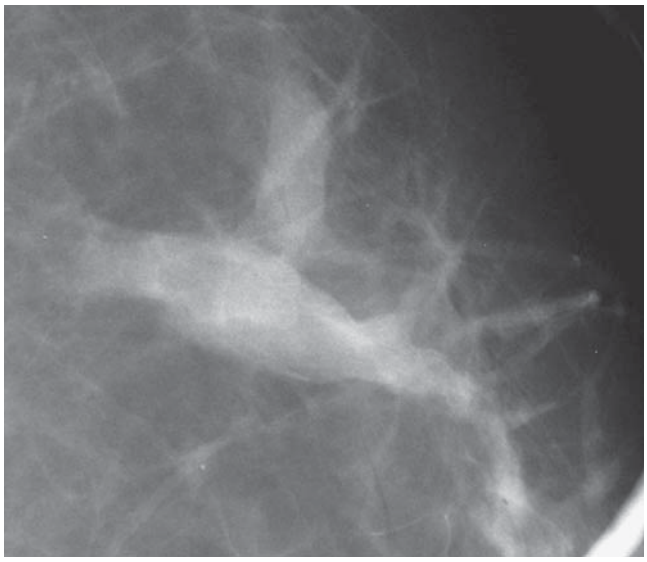
Doshi DJ, March DE, Crisi GM, Coughlin BF. Complex cystic breast masses: diagnostic approach and imaging-pathologic correlation. Radiographics 2007;27(Suppl 1):S53–S64

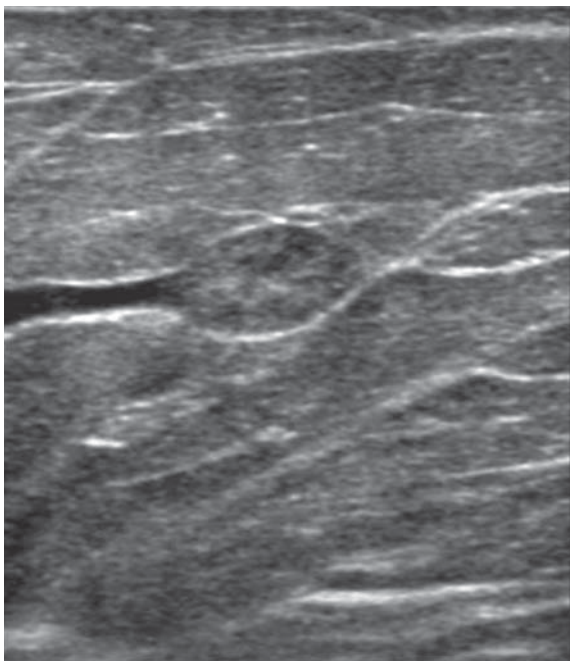
Ganesan S, Karthik G, Joshi M, Damodaran V. Ultrasound spectrum in intraductal papillary neoplasms of breast. Br J Radiol 2006;79(946):843–849

Kopans DB. Breast Imaging. 3rd ed. Philadelphia: Lippincott Williams & Wilkins; 2007

Case 289

Jessica W. T. Leung





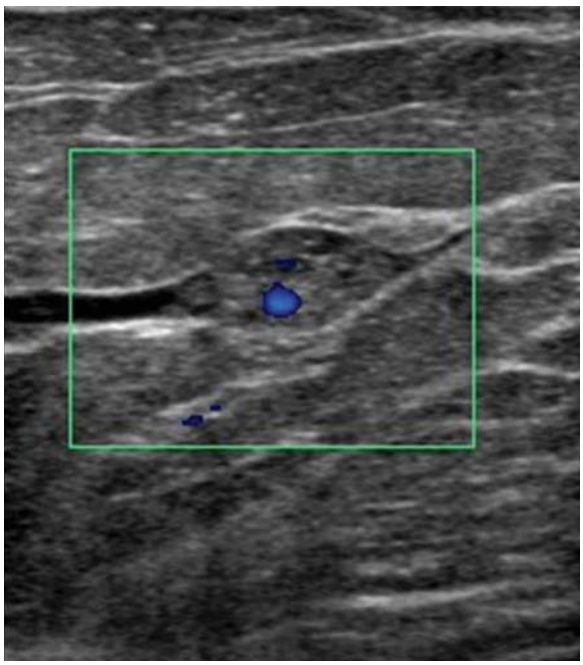


Fig. 289.1 **(A)** Spot compression mammogram of the retroareolar breast in the medial-lateral oblique projection shows a dilated duct, which was new since the prior screening mammogram 1 year ago. **(B)** Sonogram in the transverse plane shows a dilated duct containing an oval, slightly hypoechoic (nearly isoechoic) mass. **(C)** Doppler interrogation reveals blood flow within the slightly hypoechoic mass, suggesting that it is indeed solid tissue and not debris.

Clinical Presentation

A 57-year-old woman presents with a dilated duct detected at screening mammography, new since a prior examination 1 year ago (**Fig. 289.1**).

Key Imaging Finding

Ductal mass

Top 3 Differential Diagnoses

- **Intraductal papilloma.** A papilloma is a benign breast mass that grows on a fibrovascular stalk. It may grow into the duct lumen and cause distal obstruction, resulting in a dilated duct. It may twist upon its fibrovascular stalk or outgrow its blood supply, resulting in necrosis, bleeding, and the symptom of bloody nipple discharge. Pathologically, a papilloma is characterized by complex architecture consisting of infolding and redundancy of epithelium, which is often associated with atypia. Hence it may be difficult to distinguish a benign papilloma from papillary carcinoma on percutaneous core biopsy; surgical excision may be needed. At mammography, papilloma may appear as a circumscribed mass. At sonography, hypoechoic solid and cystic components may be present. Doppler signal may be present within the hypoechoic solid component, thus distinguishing it from hypoechoic debris. If duct obstruction is present, a dilated duct may be seen on a mammogram and ultrasound image. On percutaneous core biopsy, care should be given to sampling the solid component. A marker clip should be placed, as the lesion may be difficult to identify after biopsy if the cystic fluid component was ruptured (and the lesion may then appear isoechoic and difficult to identify).
- **Intracystic papillary carcinoma.** Intracystic papillary carcinoma is a low-grade form of papillary carcinoma. Because a papillary lesion (either benign or malignant) may secrete fluid, cyst formation may occur. If malignant, this may result in intracystic papillary carcinoma. A complex mass (with both cystic and solid components) is present at sonography. Intracystic papillary carcinoma is similar in biologic behavior as in situ carcinoma and generally does not metastasize. Invasive papillary carcinoma is rare.
- **Ductal carcinoma in situ (DCIS).** DCIS is most commonly diagnosed as calcifications at mammography. There are other less common manifestations, including a hypoechoic mass within a dilated duct. Doppler signal may be detected in this hypoechoic mass, differentiating it from a dilated duct with debris. Sonography cannot be used to distinguish among intraductal papilloma, intracystic papillary carcinoma, and DCIS. Biopsy is indicated to differentiate the various intraductal solid masses.

Additional Differential Diagnoses

- **Dilated duct with debris.** A dilated duct with debris may be seen in a variety of benign conditions, such as mammary ectasia, fibrocystic change, and lactation. A dilated duct with a hypoechoic intraductal component is often present, mimicking a benign intraductal papilloma or malignancy. Doppler signal is absent, as the intraductal hypoechoic component is debris and not a solid mass.

Diagnosis

Intraductal papilloma

✓ Pearls

- Doppler signal supports the diagnosis of an intraductal solid mass rather than nonsolid hypoechoic debris.
- Most intraductal masses are papillomas; they are benign and grow on fibrovascular stalks.
- Intracystic papillary carcinoma is a low-grade tumor with biologic behavior similar to that of DCIS.
- DCIS most commonly presents as malignant calcifications; it uncommonly presents as a ductal mass.

Suggested Readings

Ikeda DM. Breast Imaging: The Requisites. Philadelphia: Elsevier; 2004

Kopans DB. Breast Imaging. 3rd ed. Philadelphia: Lippincott Williams & Wilkins; 2007

Mercado CL, Hamele-Bena D, Oken SM, Singer CI, Cangiarella J. Papillary lesions of the breast at percutaneous core-needle biopsy. Radiology 2006;238(3):801–808

Case 290

Boon Chye Ching

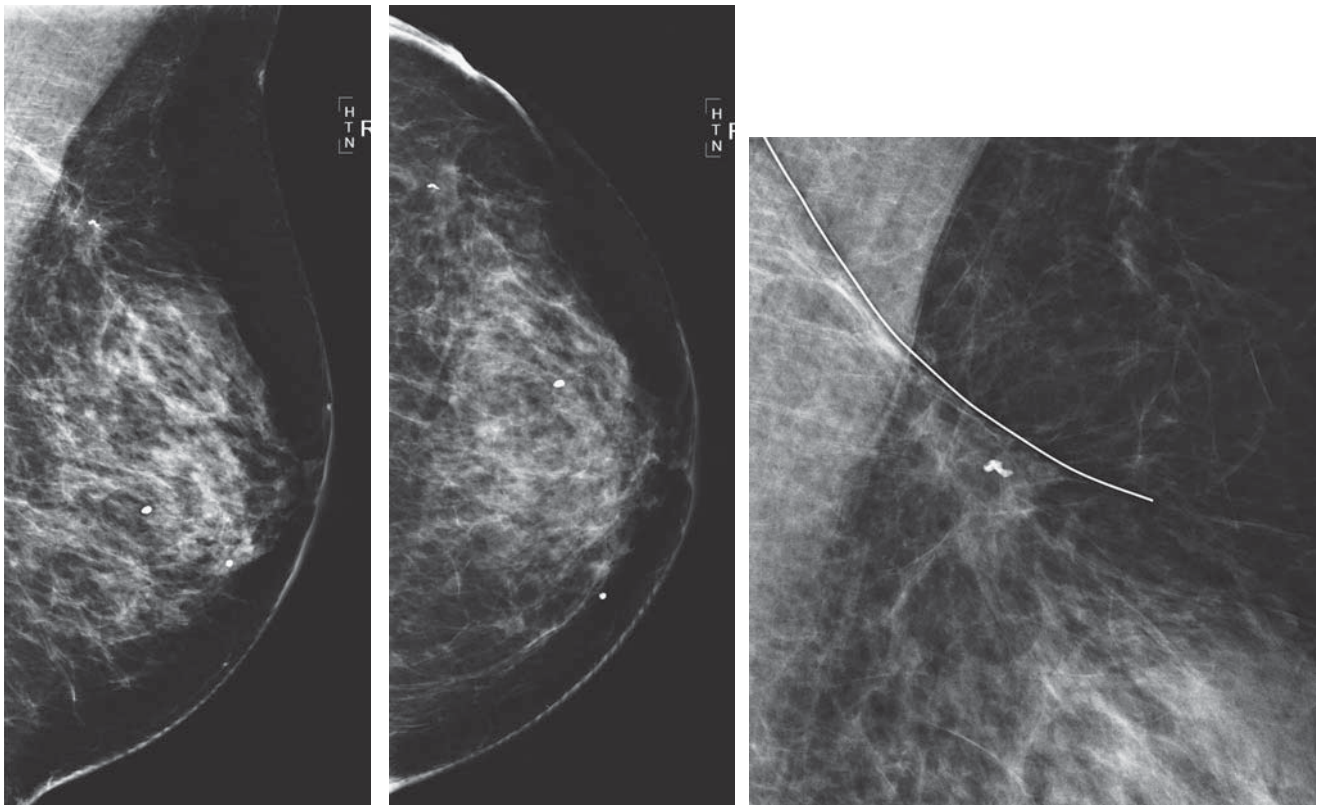


Fig. 290.1 Mammograms in **(A)** the medial-lateral oblique (MLO) and **(B)** craniocaudal (CC) projections show an area of architectural distortion in the posterior upper outer breast, consistent with a postsurgical scar. This scar is better seen on the MLO than the CC projection. The CC view shows overlying skin thickening. **(C)** Spot compression magnification mammography with a scar marker confirms that the scar seen on the skin of the patient corresponds to the architectural distortion identified at mammography. Spot compression magnification mammography further demonstrates the coarse morphology of the associated calcifications, indicating that they are benign dystrophic calcifications.

Clinical Presentation

A 46-year-old woman presents with a previous history of lumpectomy (**Fig. 290.1**).

Key Imaging Finding

Postoperative changes

Top 3 Differential Diagnoses

- **Postsurgical architectural distortion.** An established history of prior surgery is crucial for the diagnosis of architectural distortion as a result of postsurgical scarring. Tissue distortion can be seen at mammography or sonography, with the distortion extending all the way to the overlying skin. A marker placed on the scar is often helpful to confirm that the architectural distortion corresponds to the site of surgery. Initial postsurgical changes at sonography may include a complex cystic mass. The cystic portion may be subsequently resorbed, leaving a nonspecific irregular, hypoechoic mass that may mimic cancer. Postoperative changes will stabilize or decrease over time. At mammography, dystrophic calcifications may develop. Sonography is somewhat limited in evaluating postsurgical sites, as scarring often results in intense posterior acoustic shadowing. Most scars will not enhance on magnetic resonance imaging after 18 months, although some may enhance for a longer period of time.
- **Recurrent cancer.** Recurrent cancer usually occurs at or adjacent to the surgical site. There may be new suspicious microcalcifications (fine linear or pleomorphic microcalcifications in clustered, linear, or segmental distribution), developing asymmetry, a new mass, or increasing architectural distortion. Except for dystrophic calcifications, imaging findings that increase over time require immediate biopsy to exclude recurrent cancer.
- **Fat necrosis.** Fat necrosis occurs when intracellular fat escapes from damaged cells into the surrounding tissue, causing the body to react by forming granulation tissue. It is often due to surgery or trauma. Because there are different stages, the imaging manifestations of fat necrosis range from benign appearing to suspicious. It may present as lipid cysts, microcalcifications, coarse calcifications, focal asymmetries, or focal masses. Initially, the calcifications of fat necrosis may appear suspicious, but they coarsen over time.

Additional Differential Diagnoses

- **Radial scar.** A radial scar is a benign proliferative lesion, but it may be associated with atypical and malignant conditions. Classically, a radial scar appears at mammography as an area of architectural distortion with central lucent areas representing fat. There is no central mass. A radial scar is usually better seen on one of the two standard mammographic projections (usually better seen on the craniocaudal projection) and can have varying appearances on orthogonal imaging. At sonography, it usually appears as an area of architectural distortion, but a hypoechoic mass or posterior acoustic shadowing may be seen.
- **Tubular carcinoma.** On a mammogram, tubular carcinoma classically appears as a central mass with spiculated margins and thus simulates architectural distortion. It is generally <1 cm in diameter. It is usually very slow growing. It can be associated with amorphous or pleomorphic microcalcifications in up to 50% of cases. At sonography, tubular carcinoma typically presents as an irregular hypoechoic mass with spiculated or indistinct margins. Pure tubular carcinoma has a very good prognosis.

Diagnosis

Postsurgical architectural distortion

✓ Pearls

- Postsurgical architectural distortion stabilizes or decreases in size and/or conspicuity over time.
- Recurrent cancer often presents as increasing mass/architectural distortion or new suspicious calcifications.
- Microcalcifications seen in fat necrosis should coarsen over time; asymmetries should decrease with time.

Suggested Readings

Berg WA, Birdwell RL. Diagnostic Imaging. Breast. Salt Lake City, UT: Amirsys; 2006

Ikeda DM. Breast Imaging: The Requisites. Philadelphia: Elsevier; 2004

Mendelson EB. Evaluation of the postoperative breast. Radiol Clin North Am 1992;30(1):107–138

Case 291

Natasha Brasic

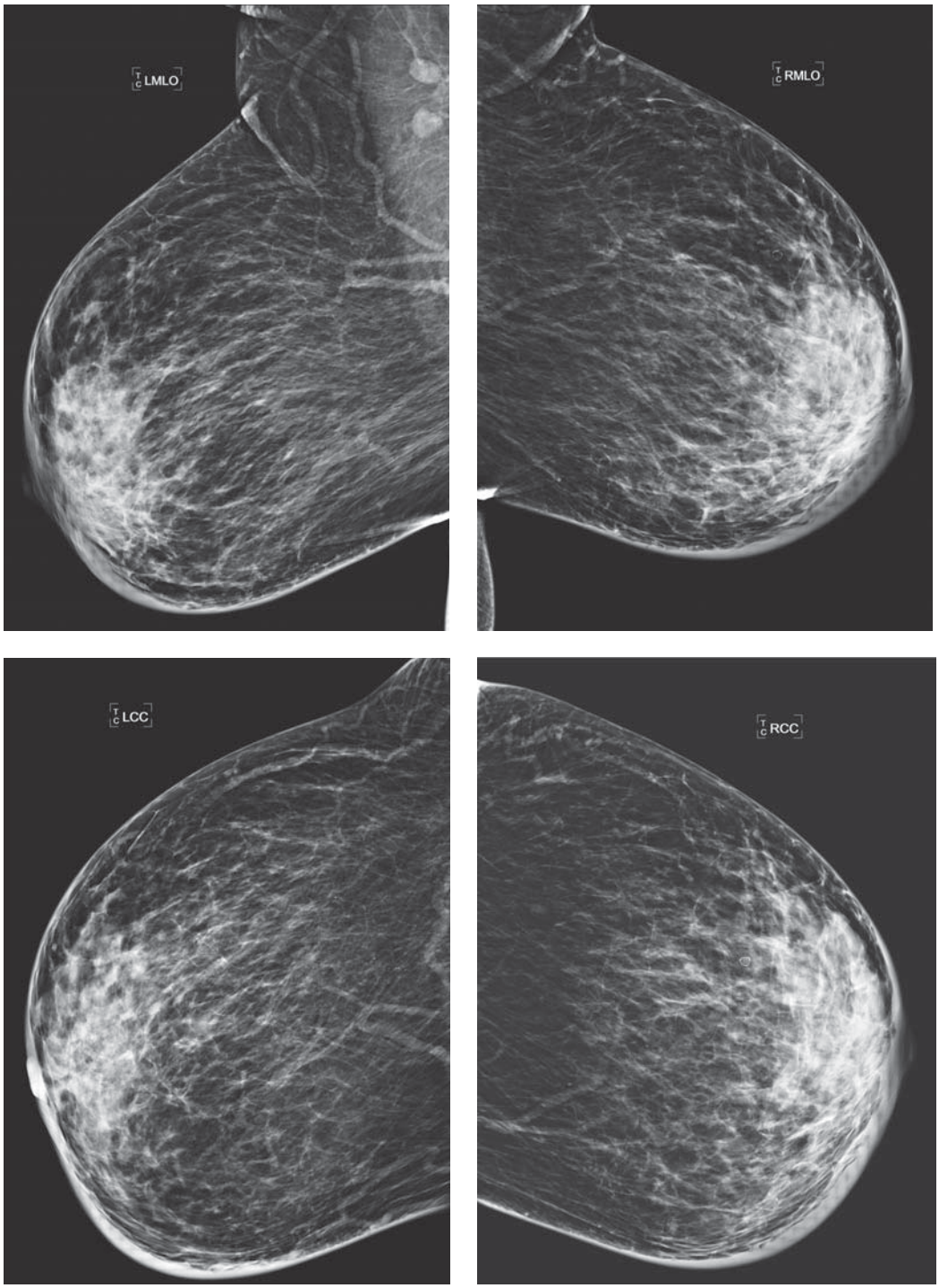


Fig. 291.1 **(A,B)** Bilateral medial-lateral oblique and **(C,D)** craniocaudal mammograms demonstrate bilateral diffuse skin thickening, increased retroareolar densities, and thickened trabeculae. (Courtesy of Amy Argus, MD, University of Cincinnati.)

Clinical Presentation

A 58-year-old woman presents for screening mammography (**Fig. 291.1**).

Key Imaging Finding

Bilateral skin thickening

Top 3 Differential Diagnoses

- **Congestive heart failure.** With elevated intracardiac pressures and impaired venous drainage in congestive heart failure, edema most commonly occurs in the lower extremities, but it also may occur in the breasts. Impaired venous return results in increased capillary hydrostatic pressures, resulting in soft tissue edema. This is seen as skin thickening at mammography (normal skin thickness measures up to ~2 mm). Trabecular thickening in the breast parenchyma may also be present.
- **Superior vena cava (SVC) obstruction.** Obstruction of the SVC is usually due to a thoracic tumor such as lung cancer. External compression coupled with thrombosis results in obstruction of the SVC. Subsequently, venous return to the heart is impaired, and increased venous pressure with elevated intracapillary hydrostatic pressure occurs. This results in edema of the breasts, visualized as skin thickening. If long-standing, collateral vessels will form, resulting in multiple dilated veins that may be visualized at mammography.
- **Bilateral lymphedema.** Lymphatic drainage of the skin is contiguous with the lymphatics that pass through the breasts. In up to 50% of axillary lymph node dissections, the lymphatic drainage is disrupted enough to result in lymphatic congestion of the skin. Often, there may be subtle or pronounced thickening of the breast trabeculae as defined by Cooper ligaments. Lymphedema may result in significant morbidity. This complication has significantly decreased with the advent of sentinel node biopsy techniques. In breast cancer cases where the sentinel node is free of cancer, full axillary lymph node dissection may be safely obviated, thus reducing patient morbidity.

Additional Differential Diagnoses

- **Psoriasis.** Psoriasis is a chronic disease of unknown etiology that leads to dry, scaly plaques and skin thickening. Patients are affected to varying degrees. Although a relatively uncommon cause of skin thickening of the breasts, psoriasis should be considered when skin thickening occurs in both breasts. Other systemic diseases with skin involvement are scleroderma, dermatomyositis, and congenital absence of the lymphatics. These conditions rarely affect the breasts.
- **Renal failure and volume overload.** Renal failure, whether acute or chronic, leads to volume overload and increased capillary hydrostatic pressures. The end result is skin and trabecular thickening caused by the same mechanism as congestive heart failure.

Diagnosis

Congestive heart failure

✓ Pearls

- Normal skin overlying the breast measures up to 2 mm in thickness.
- Volume overload or venous drainage obstruction leads to elevated hydrostatic pressure and edema.
- Disruption of lymphatic drainage from bilateral axillary lymph node dissection may cause skin thickening.
- Psoriasis may present with bilateral dry, scaly plaques and skin thickening.

Suggested Readings

Kopans DB. Breast Imaging. 3rd ed. Philadelphia: Lippincott Williams & Wilkins; 2007

Oraedu CO, Pinnapureddy P, Alrawi S, Acinapura AJ, Raju R. Congestive heart failure mimicking inflammatory breast carcinoma: a case report and review of the literature. Breast J 2001;7(2):117–119

Rönkä RH, Pamilo MS, von Smitten KA, Leidenius MH. Breast lymphedema after breast conserving treatment. Acta Oncol 2004;43(6):551–557

Case 292

Matthew R. Denny and Jessica W. T. Leung

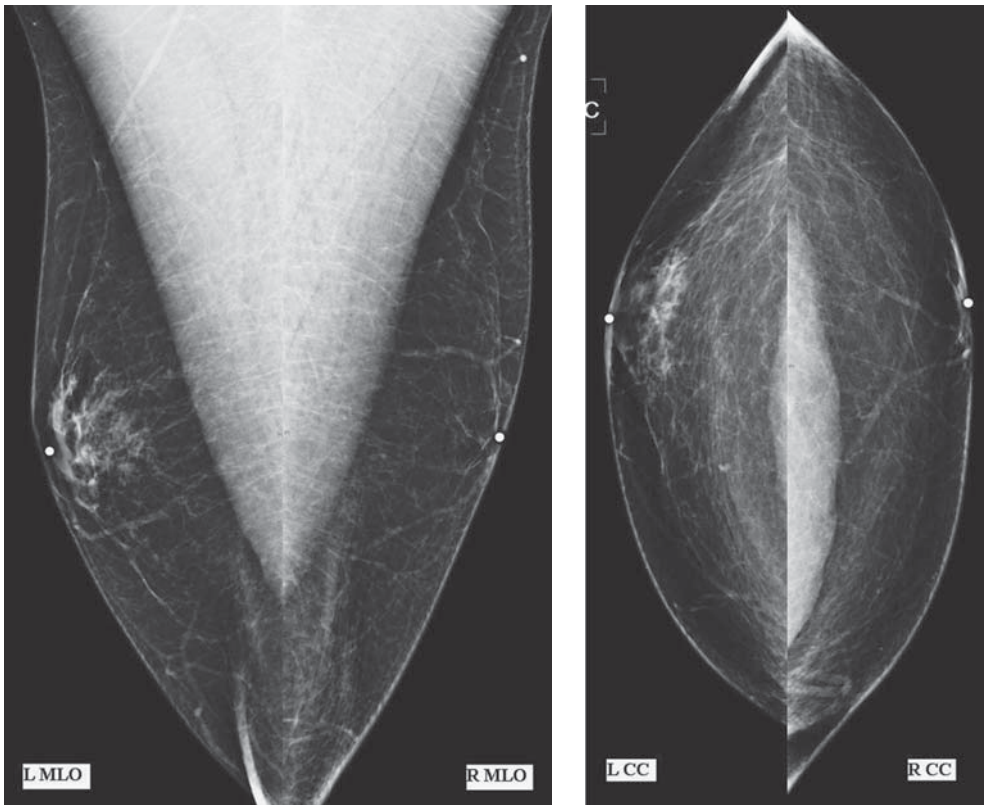


Fig. 292.1 Mammograms of both breasts in **(A)** the medial-lateral oblique and **(B)** craniocaudal projections reveal asymmetric breast tissue with a "flame-shaped" appearance in the retroareolar region of the left breast. No mass or calcifications are identified. The remainder of the left breast and the entire right breast are fatty but otherwise unremarkable. Prominent pectoralis muscles are present bilaterally.

Clinical Presentation

A 45-year-old man presents with a painful palpable lump in the left retroareolar breast of 2-months' duration (**Fig. 292.1**).

Key Imaging Finding

Breast lesion in a man

Top 3 Differential Diagnoses

- **Gynecomastia.** Gynecomastia is a benign condition of men in which breast tissue is stimulated and becomes prominent. Causative etiologies are idiopathic, drug use (e.g., marijuana, cimetidine, omeprazole, or spironolactone), and hormonal stimulation, either exogenous (antiandrogens or gonadotropin-releasing hormone agonists for treatment of prostate cancer) or endogenous (testicular and adrenal tumors). Physiologic gynecomastia may occur in newborns, at puberty, and in elderly or obese men. Patients present with a painful palpable lump in the retroareolar region. At mammography, gynecomastia appears as "flame-shaped" tissue in the retroareolar region without an associated mass or calcifications. It is usually unilateral but may be bilateral and asymmetric. In the absence of a mass at mammography, sonography need not be performed. In fact, ultrasound findings may be confusing and lead to unnecessary follow-up or biopsy.
- **Breast cancer.** Male breast cancer constitutes ~1% of all breast cancers. Because of the lack of lobular differentiation, all male breast cancers are of ductal (and not lobular) histology. Male breast cancer usually presents with a palpable lump, hard or fixed breast tissue, skin/nipple changes, or lymphadenopathy. A history of gynecomastia has been noted in up to 40% of patients with male breast cancer. At mammography, male breast cancer usually manifests as a discrete mass. Calcifications are less common than in female breast cancer, but they may be present. Ultrasound findings consist of a hypoechoic solid mass. Treatment is similar to female breast cancer; however, men tend to present at a later stage.
- **Lipoma.** Lipoma is a fat-containing mass. It appears lucent and circumscribed at mammography. Its sonographic appearance may be variable, ranging from a hypoechoic solid mass to a mass of mixed echogenicity. This benign diagnosis is made at mammography, and biopsy is generally not needed.

Additional Differential Diagnoses

- **Hematoma.** Hematoma appears as a high-density mass on a mammogram. It is usually preceded by a history of trauma or anticoagulation use. Upon visual inspection, ecchymosis of the overlying soft tissues is often present. Hematomas are benign but should be followed to resolution.
- **Abscess.** An abscess appears as an irregular or circumscribed mass, often associated with signs of mastitis (e.g., skin thickening and edema). Focal or diffuse pain is often present. The clinical history contributes to making this diagnosis. Percutaneous or surgical drainage may be necessary, along with antibiotic therapy.
- **Metastases.** Metastases to male breasts are rare. When present, they usually present as multiple bilateral, round or oval, partially circumscribed masses (as opposed to multicentric primary breast cancer, which is often irregular or spiculated). Melanoma and lymphoma are the most common metastases.

Diagnosis

Gynecomastia

✓ Pearls

- Gynecomastia presents as unilateral or bilateral, asymmetric, "flame-shaped", retroareolar breast tissue.
- Male breast cancer is of ductal (and not lobular) origin; the treatment is similar to breast cancer in women.
- Hematomas and abscesses are suggested by the clinical history; they should be followed to resolution.

Suggested Readings

Chen L, Chantra PK, Larsen LH, et al. Imaging characteristics of malignant lesions of the male breast. Radiographics 2006;26(4):993–1006

Kopans DB. Breast Imaging. 3rd ed. Philadelphia: Lippincott Williams & Wilkins; 2007

Mathew J, Perkins GH, Stephens T, Middleton LP, Yang WT. Primary breast cancer in men: clinical, imaging, and pathologic findings in 57 patients. AJR Am J Roentgenol 2008;191(6):1631–1639

Niewoehner CB, Schorer AE. Gynaecomastia and breast cancer in men. BMJ 2008;336(7646):709–713

Case 293

Natasha Brasic

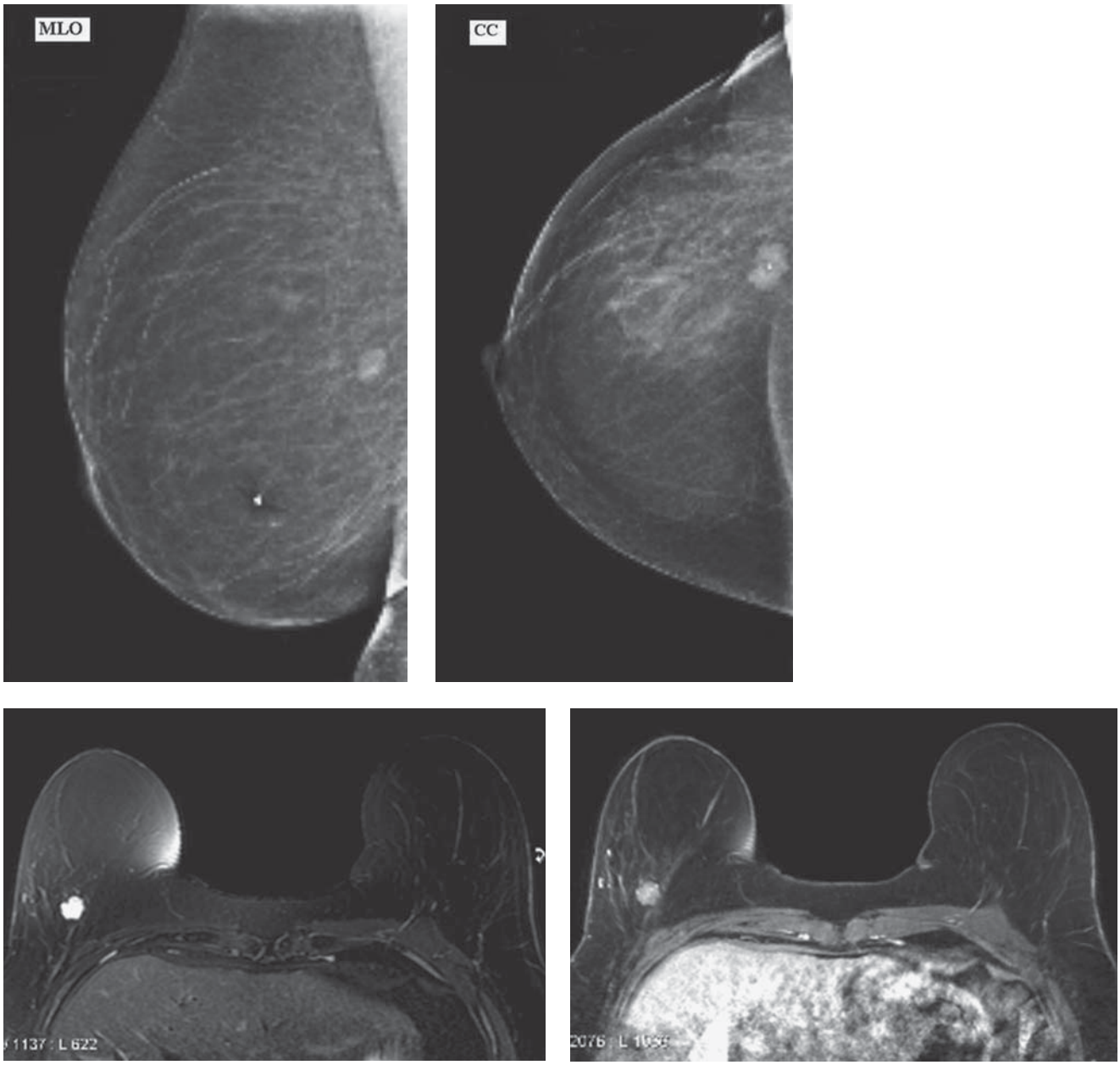


Fig. 293.1 Mammograms of the right breast in **(A)** the medial-lateral oblique and **(B)** craniocaudal projections show a circumscribed, lobulated mass in the outer central right breast. **(C)** T2-weighted fast spin echo magnetic resonance (MR) image with fat saturation and **(D)** contrast-enhanced, three-dimensional gradient echo MR image with fat saturation in the axial plane show that this mass is intrinsically hyperintense on T2-weighted imaging and enhances homogeneously.

Clinical Presentation

A 58-year-old woman presents with known breast carcinoma within the right breast (**Fig. 293.1**).

Key Imaging Finding

Well-circumscribed breast cancer

Top 3 Differential Diagnoses

- **Invasive ductal carcinoma, not otherwise specified (NOS).** The majority of invasive breast cancers are nonspecific forms that originate in the ductal epithelium, likely at the terminal duct at its junction with the lobule. The majority (65%) of ductal malignancies fall into the general category of undifferentiated lesions that have no particular distinguishing histologic features. Invasive ductal carcinoma, NOS elicits a fairly vigorous desmoplastic response with resultant fibrosis, producing a spiculated mass at mammography and a hard mass on palpation. However, it may at times present as a well-circumscribed mass. Given that invasive ductal carcinoma, NOS is the majority of breast cancers, a well-circumscribed cancer is most likely of invasive ductal carcinoma, NOS histology.
- **Mucinous carcinoma.** Also known as colloid carcinoma, mucinous carcinoma accounts for 2 to 3% of all invasive breast cancers. The abundant production of mucin by this cancer is felt to reflect its high degree of differentiation, which may account for the better prognosis of patients with this form of cancer. There are no mammographic features distinguishing mucinous carcinoma from other breast cancers. At sonography, these lesions have a nonspecific hypoechoic appearance with posterior acoustic characteristics that depend on the tumor architecture. On magnetic resonance (MR) images, mucinous carcinoma is characterized by intrinsically hyperintense T2 signals, possibly reflecting the mucin content.
- **Medullary carcinoma.** Medullary carcinoma constitutes ~3% of all breast cancers. It is distinctive in that it frequently grows quite large before it is detected. Classically, medullary carcinoma is described as well circumscribed, smooth, round, or ovoid at mammography. Although these lesions frequently exhibit necrosis, calcification is an uncommon feature. At sonography, medullary carcinoma usually appears as a well-circumscribed, lobulated, hypoechoic mass with homogeneous internal echoes. Posterior acoustic enhancement may be present. On MR images, medullary carcinomas enhance diffusely.

Additional Differential Diagnoses

- **Papillary carcinoma.** Papillary cancer is primarily an intraductal malignancy and represents <1% of invasive cancers. Relative frequency increases with age. When mammographically visible, papillary carcinoma may appear as a well-circumscribed mass.
- **Ductal carcinoma in situ (DCIS).** DCIS is most commonly detected as calcifications at mammography. However, DCIS may also present as a mammographic or sonographic mass (which is often well circumscribed), giving rise to the nodular form of DCIS. The prognosis is the same for all forms of DCIS.

Diagnosis

Mucinous carcinoma

✓ Pearls

- Most well-circumscribed breast cancers are invasive ductal carcinoma, NOS.
- Mucinous carcinoma has circumscribed margins and is intrinsically hyperintense on T2 MR sequences.
- Medullary carcinoma is typically large with well-circumscribed margins and a round or ovoid shape.

Suggested Readings

Ikeda DM, Andersson I. Ductal carcinoma in situ: atypical mammographic appearances. Radiology 1989;172(3):661–666
Kopans DB. Breast Imaging. 3rd ed. Philadelphia: Lippincott Williams & Wilkins; 2007
Okafuji T, Yabuuchi H, Sakai S, et al. MR imaging features of pure mucinous carcinoma of the breast. Eur J Radiol 2006;60(3):405–413
Ridolfi RL, Rosen PP, Port A, Kinne D, Mike V. Medullary carcinoma of the breast: a clinicopathological study with 10-year follow up. Cancer 1977;40:1365–1385
Stalsberg H, Thomas DB. Age distribution of histologic types of breast carcinoma. Int J Cancer 1993;54(1):1–7

Case 294

Jessica W. T. Leung

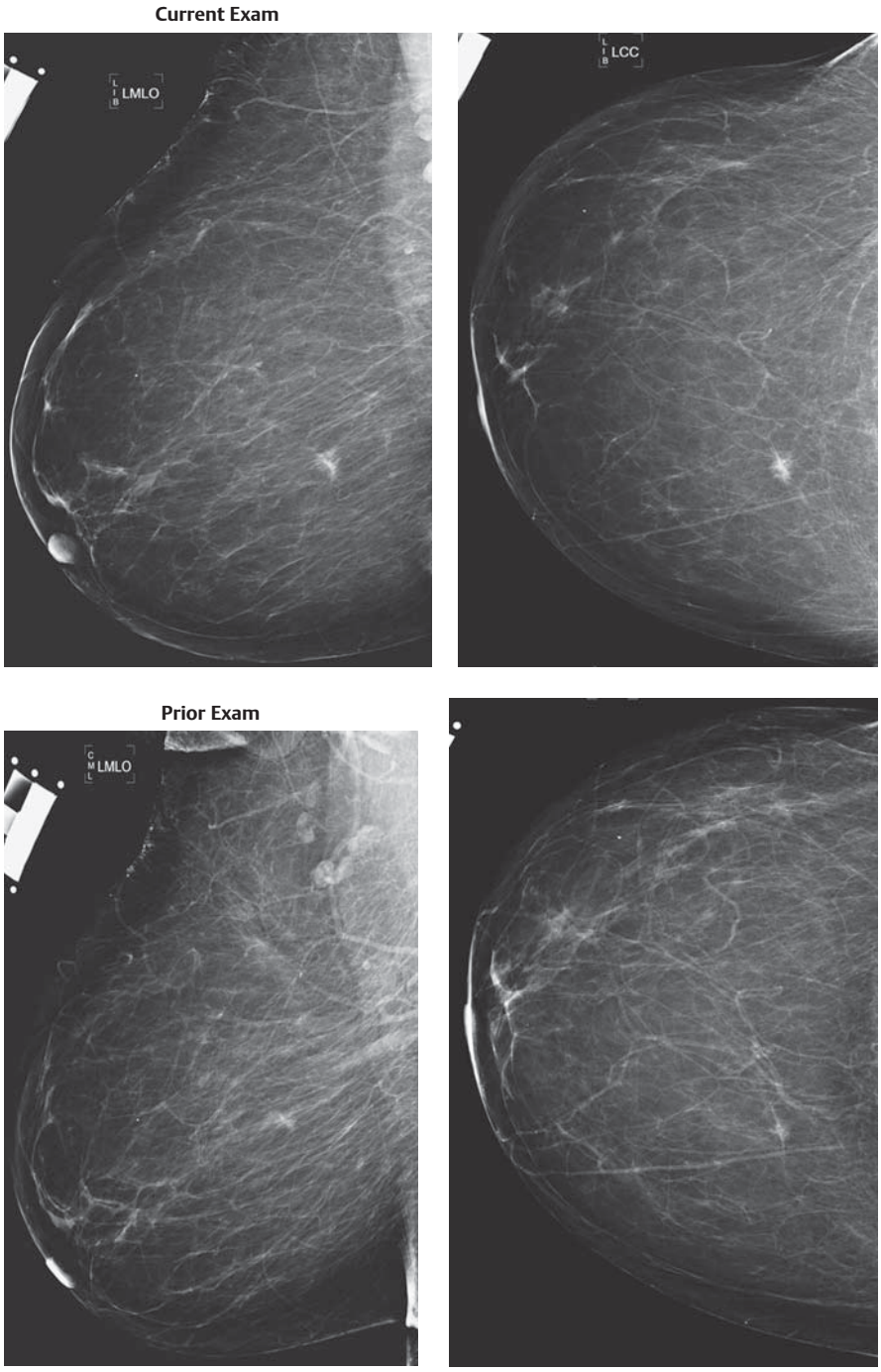


Fig. 294.1 Screening current mammograms in **(A)** the medial-lateral oblique (MLO) and **(B)** cranio-caudal (CC) projections show a spiculated focal asymmetry in the upper inner breast. When compared with the prior mammograms in **(C)** the MLO and **(D)** CC projections of 1 year ago, the focal asymmetry has shown interval increase. Hence it is a developing asymmetry and a sign of malignancy.

Clinical Presentation

A 69-year-old woman presents for screening mammography (**Fig. 294.1**).

Key Imaging Finding

Developing asymmetry

Top 3 Differential Diagnoses

- **Invasive ductal carcinoma.** Although uncommon, developing asymmetry is a mammographic sign of malignancy. It is a focal asymmetry that is new or increasing when compared with a prior examination. In contrast to an enlarging mass, developing asymmetry lacks a central density, and its margins are not necessarily convex. One study showed that the probability of malignancy in developing asymmetry is 13% at screening and 27% at diagnostic mammography. Because the probability is >2% (threshold for the American College of Radiology's Breast Imaging Reporting and Data System, third edition, probably benign lesions that can be safely followed), biopsy is indicated, regardless of whether there is a sonographic correlate. Among malignancies identified, invasive ductal carcinoma is the most common.
- **Invasive lobular carcinoma.** Invasive lobular carcinoma constitutes ~10% of invasive cancers. However, in one study of developing asymmetry, invasive lobular carcinoma constituted ~16% of the cancers identified. Hence invasive lobular carcinoma is disproportionately represented in developing asymmetry, which corresponds to its "single-file" growth pattern (rather than forming a central tumor mass). Stage for stage, invasive lobular carcinoma carries the same prognosis as invasive ductal carcinoma. However, invasive lobular carcinoma tends to be diagnosed at a later, more advanced stage. Targeted sonography and magnetic resonance imaging are helpful in diagnosing invasive lobular carcinoma.
- **Pseudoangiomatous stromal hyperplasia (PASH).** PASH is a benign proliferative stromal lesion that consists of fibroblasts. It responds to hormonal stimulus and is usually found in premenopausal women or postmenopausal women on hormone replacement therapy. PASH may present as a mass or developing asymmetry. It is considered a benign concordant diagnosis in core biopsy of a developing asymmetry.

Additional Differential Diagnoses

- **Asymmetric breast tissue.** Benign breast tissue may develop over time, particularly in response to hormonal stimulation. An increase in breast density is usually diffuse, but it may also be focal. If the increase in density is focal, then malignancy needs to be considered. Biopsy may be needed to exclude cancer.
- **Stromal fibrosis.** Stromal fibrosis is a benign condition that may present as a developing asymmetry. When a sonographic correlate is present, posterior acoustic shadowing may be seen and mimic malignancy. Core biopsy is helpful in making this diagnosis when the imaging findings are nonspecific. Stromal fibrosis is considered a benign concordant diagnosis in core biopsy of a developing asymmetry.
- **Fat necrosis.** Fat necrosis has varied imaging appearances, including developing asymmetry. Correlation with mammography is helpful, particularly when classic mammographic features of fat necrosis are present (e.g., coarse calcifications and oil cyst). Sonographic features are nonspecific and may mimic malignancy. Fat necrosis is considered a benign concordant diagnosis in core biopsy of a developing asymmetry.

Diagnosis

Invasive ductal carcinoma, moderately differentiated

✓ Pearls

- Biopsy is indicated for developing asymmetry, as the chance of malignancy is >2%.
- Invasive lobular carcinoma presents as a developing asymmetry because of its growth in "single files."
- PASH is a benign stromal lesion that responds to hormonal stimulus.

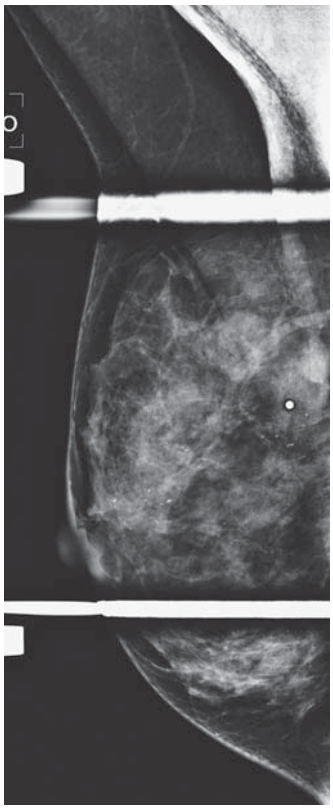
Suggested Readings

Kopans DB. Breast Imaging. 3rd ed. Philadelphia: Lippincott Williams & Wilkins; 2007

Leung JW, Sickles EA. Developing asymmetry identified on mammography: correlation with imaging outcome and pathologic findings. AJR Am J Roentgenol 2007;188:667–675

Case 295

Boon Chye Ching



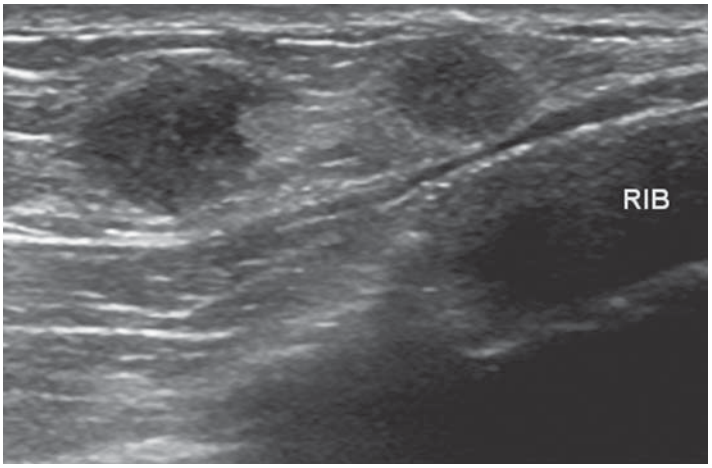


Fig. 295.1 **(A)** Spot compression mammogram in the medial-lateral oblique projection shows two irregular, ill-defined masses in the axillary tail, corresponding to the palpable nodularity as indicated by the metallic BB. **(B)** Sonogram in the transverse plane shows two corresponding ill-defined hypoechoic masses with echogenic rim adjacent to the pectoralis muscle, corresponding to the palpable nodularity and mammographic masses.

Clinical Presentation

A 56-year-old woman presents with palpable nodularity in the axillary tail of 6 weeks' duration (**Fig. 295.1**).

Key Imaging Finding

Ill-defined, infiltrative breast mass

Top 3 Differential Diagnoses

- **Invasive ductal carcinoma.** Invasive ductal carcinoma is the most common invasive breast cancer, accounting for >90% of all cases. It arises from the ductal epithelium and typically presents as an irregular mass with ill-defined spiculated margins. These imaging features reflect the infiltrative growth of invasive cancers. There may be associated malignant microcalcifications, representing concomitant ductal carcinoma in situ. At sonography, it usually manifests as an irregular hypoechoic mass with posterior acoustic shadowing. However, approximately one third of invasive ductal carcinomas may be associated with posterior acoustic enhancement, which reflects that the cancer is composed of uniform cells and likely poorly differentiated. An echogenic rim may be present, representing tumor reaction upon adjacent tissues.
- **Invasive lobular carcinoma.** Invasive lobular carcinoma arises from the breast lobules. The cancer cells grow in a single file; thus they are difficult to detect on imaging or physical examination. Invasive lobular carcinoma may be seen at mammography as a mass, calcifications, architectural distortion, or developing asymmetry. Sonographic findings range from subtle tissue distortion to an obvious spiculated mass. In general, the extent of invasive lobular carcinoma is underestimated at mammography and ultrasound because of its infiltrative nature. When compared with invasive ductal carcinoma, it has a higher rate of having multiple and bilateral disease. Magnetic resonance imaging (MRI) is a useful diagnostic tool in determining the extent of disease in cases of invasive lobular carcinoma.
- **Postsurgical scar.** For the diagnosis of a postsurgical scar to be made, a history of prior surgery is crucial. It may be seen at mammography or sonography as architectural distortion extending all the way to the overlying skin. It may also present as an irregular spiculated mass. Posterior acoustic shadowing is often present at sonography in scars. It is often useful to put a marker on the skin corresponding to the scar to confirm that the imaging finding actually corresponds to the site of the surgery. Temporal change is vital in diagnosing or excluding malignancy at postsurgical sites, as scars should remain stable or decrease over time. Although an increasing scar may be the result of benign fat necrosis, biopsy is needed to exclude recurrent cancer. Most scars will not enhance on MRI after 18 months, although some may enhance for a longer period of time.

Additional Differential Diagnoses

- **Fibrosis.** Fibrosis is a common incidentally detected benign finding that may have suspicious features at mammography and sonography. It may present as an irregular mass or developing asymmetry at mammography and may appear hypoechoic or echogenic at sonography. Core biopsy is helpful in making this diagnosis.

Diagnosis

Invasive ductal carcinoma (multifocal and poorly differentiated)

✓ Pearls

- Invasive ductal carcinoma (>90% of breast cancers) classically presents as an irregular spiculated mass.
- Imaging underestimates the extent of invasive lobular carcinoma because it grows in a “single file.”
- Comparison with prior imaging studies and temporal assessment are crucial in assessing postsurgical scars.

Suggested Readings

Evans WP, Warren Burhenne LJ, Laurie L, O’Shaughnessy KF, Castellino RA. Invasive lobular carcinoma of the breast: mammographic characteristics and computer-aided detection. Radiology 2002;225(1):182–189

Kopans DB. Breast Imaging. 3rd ed. Philadelphia: Lippincott Williams & Wilkins; 2007

Onesti JK, Mangus BE, Helmer SD, Osland JS. Breast cancer tumor size: correlation between magnetic resonance imaging and pathology measurements. Am J Surg 2008;196(6):844–848, discussion 849–850

Case 296

Matthew R. Denny and Jessica W. T. Leung

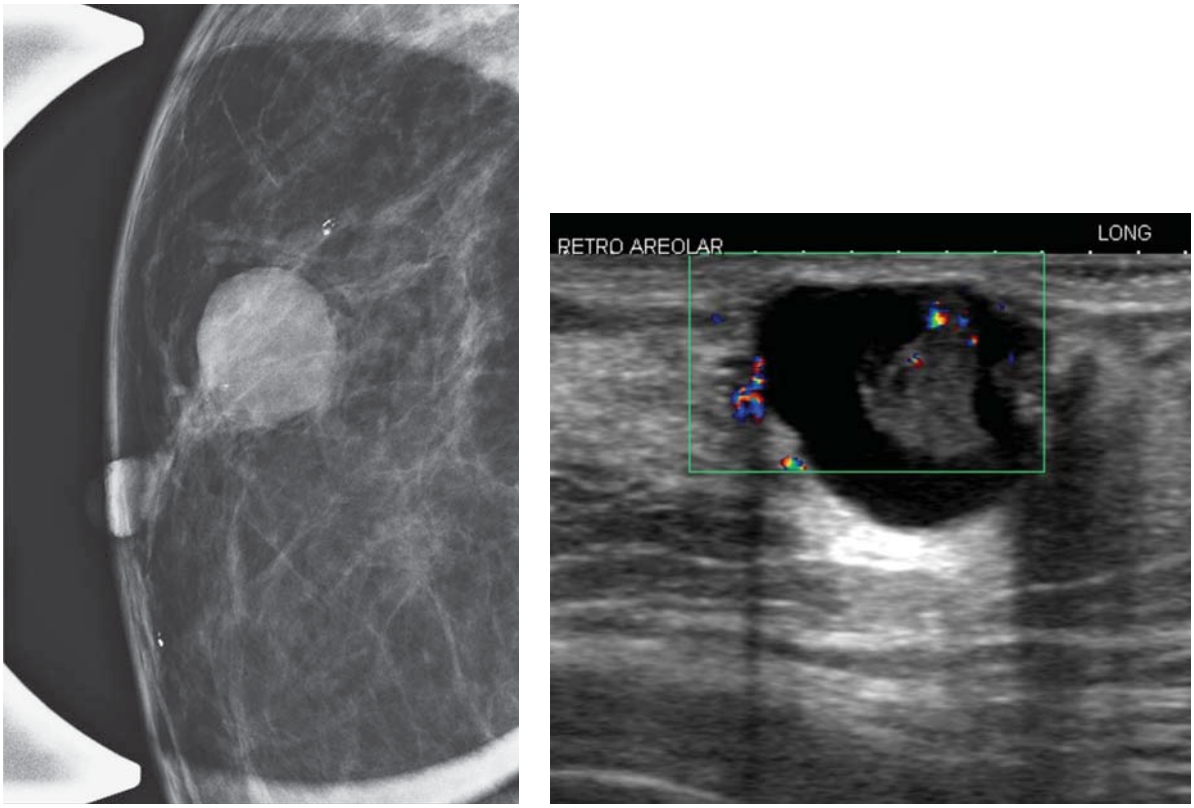


Fig. 296.1 **(A)** Spot compression magnification mammogram of the retroareolar breast in the craniocaudal projection shows a circumscribed mass. **(B)** Sonogram in the longitudinal plane shows a corresponding complex mass with both cystic and solid components. Doppler interrogation shows blood flow within the hypoechoic component, suggesting that the hypoechoic component is indeed solid tissue and not hypoechoic debris.

Clinical Presentation

A 50-year-old woman presents with spontaneous bloody nipple discharge of 3 months' duration (**Fig. 296.1**).

Key Imaging Finding

Breast lesion with nipple discharge

Top 3 Differential Diagnoses

- **Intraductal papilloma.** Papilloma is a benign breast mass that grows on a fibrovascular stalk. It may secrete fluid and form a surrounding cyst, resulting in intracystic papilloma with an appearance of a circumscribed cystic mass. It may also undergo necrosis with bloody nipple discharge. Pathologically, papilloma is often associated with atypia. Hence it may be difficult to distinguish benign papilloma from papillary carcinoma with core biopsy, and surgical excision may be needed. Intracystic papillary carcinoma is similar in its biologic behavior to in situ carcinoma. Invasive papillary carcinoma is rare. At mammography, papillary lesions may appear as circumscribed masses. At sonography, hypoechoic solid and cystic components may be present. Doppler signal may be present within the solid component, distinguishing it from cystic debris. Percutaneous core biopsy should include the solid component. A marker clip should be placed, as the lesion may be difficult to identify after biopsy if the cystic fluid component ruptures (the lesion may then appear isoechoic and difficult to identify).
- **Mammary duct ectasia.** Mammary duct ectasia results when a duct in the retroareolar breast becomes inflamed, dilated, or obstructed. Whitish, greenish, or blackish nipple discharge may result. Etiologies include hormonal changes, smoking, and a newly inverted nipple. This condition is benign and usually self-limiting. Mammography is usually negative. Nonspecific dilated duct(s) may be seen at ultrasound.
- **Breast carcinoma (ductal or papillary).** Nipple discharge that is the result of a malignancy is usually bloody and originates from a single duct. The underlying malignancy is most often intraductal carcinoma, such as ductal carcinoma in situ (DCIS). Other malignancies that can give rise to bloody nipple discharge are intracystic papillary carcinoma and invasive carcinomas (of either ductal or lobular histology). Mammography and ultrasound may show signs of malignancy, such as a mass or calcifications. Paget disease of the breast or DCIS affecting the nipple–areolar complex classically presents with bloody nipple discharge and crusting of the nipple. Calcifications may be seen in Paget disease.

Additional Differential Diagnoses

- **Fibrocystic change.** Fibrocystic change is within the spectrum of normal physiologic changes in the breast. On clinical exam, lumpy, tender breasts are found. A clear yellow or light green discharge may be expressed from both breasts. This is benign and usually self-limiting. Imaging is usually negative.
- **Galactorrhea.** Galactorrhea is a benign condition in which there is milky nipple discharge, usually from multiple ducts in both breasts. It may be a result of medication or disorders of the hypothalamus or pituitary gland, such as a prolactinoma. Mammography and ultrasound are usually negative.

Diagnosis

Intraductal papilloma

✓ Pearls

- Bloody nipple discharge may be benign (papilloma) or malignant (Paget disease and breast carcinoma).
- Imaging is often negative in the setting of nipple discharge due to fibrocystic change or galactorrhea.
- Patients with Paget disease present with bloody nipple discharge and nipple crusting.

Suggested Readings

Ballesio L, Maggi C, Savelli S, et al. Adjunctive diagnostic value of ultrasonography evaluation in patients with suspected ductal breast disease. Radiol Med (Torino) 2007;112(3):354–365

Doshi DJ, March DE, Crisi GM, Coughlin BF. Complex cystic breast masses: diagnostic approach and imaging-pathologic correlation. Radiographics 2007;27(Suppl 1):S53–S64

Ganesan S, Karthik G, Joshi M, Damodaran V. Ultrasound spectrum in intraductal papillary neoplasms of breast. Br J Radiol 2006;79(946):843–849

Kopans DB. Breast Imaging. 3rd ed. Philadelphia: Lippincott Williams & Wilkins; 2007

Case 297

Chloe M. Chhor

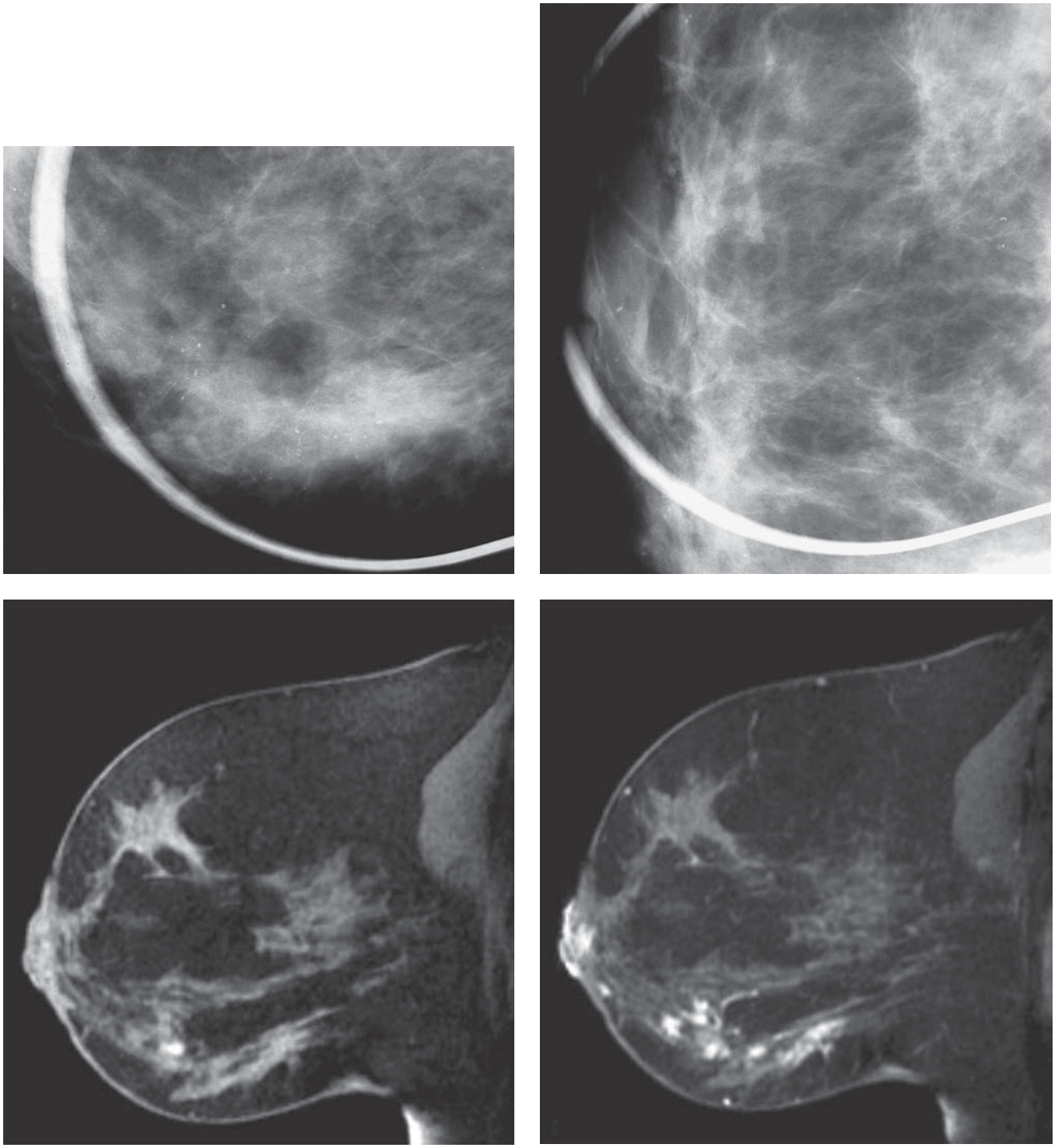


Fig. 297.1 Spot compression magnification mammograms in the lateral projection **(A)** of the lower breast and **(B)** of the nipple region reveal segmentally arrayed pleomorphic microcalcifications extending to the nipple. Three-dimensional gradient echo magnetic resonance images with fat saturation in the sagittal plane **(C)** prior to and **(D)** after contrast administration show nodular segmental nonmass enhancement in the lower breast with extension to the nipple. Although the nipple–areolar complex normally enhances, the nodular-enhancing focus immediately posterior to the nipple is abnormal.

Clinical Presentation

A 78-year-old woman presents with bloody crusting of the nipple of 4 months' duration (**Fig. 297.1**).

Key Imaging Finding

Unilateral nipple/skin changes

Top 3 Differential Diagnoses

- **Paget disease of the nipple.** Paget disease of the nipple is breast cancer affecting the nipple–areolar complex. Cancer cells extend into the large ducts and out into the skin of the nipple, manifesting as an eczematous, crusty nipple. Paget disease typically occurs in older women. Most commonly, ductal carcinoma in situ (DCIS) is the underlying malignancy, though an invasive component may be present. Clinically, the patient presents with bloody nipple discharge and crusting of the nipple. Malignant calcifications representing DCIS may be seen at mammography. Mastectomy is the usual treatment. On magnetic resonance imaging (MRI), either mass or nonmass enhancement may be present with extension to the nipple–areolar complex. MRI is also helpful in identifying an invasive component of the disease that is otherwise occult.
- **Mastitis.** Mastitis is cellulitis of the breast, usually bacterial in origin. Common bacterial agents are *Streptococcus* and *Staphylococcus*. The affected breast is erythematous, swollen, warm, and tender. Predisposing factors include lactation and trauma. Mammography may show increased density and skin thickening. Sonography may show skin thickening and edema and is useful in evaluating for abscess formation in patients with mastitis. If symptoms do not resolve following antibiotic treatment, carcinoma (especially inflammatory breast carcinoma) must be excluded promptly with biopsy.
- **Inflammatory breast carcinoma.** Inflammatory breast carcinoma is a relatively infrequent but very aggressive form of breast carcinoma that invades the dermal lymphatics. It may be of ductal or lobular histology. Clinically, patients present with rapid onset of warmth, erythema, and edema of the breast. The skin can have a pitted, thickened appearance similar to an orange skin (hence the label peau d'orange). Inflammatory breast carcinoma is primarily a clinical diagnosis, although skin punch biopsy is often helpful. Mammography, ultrasound, or MRI may reveal signs of cancer diffusely. Alternatively, the underlying cancer may be occult at imaging, and only skin thickening is identified. This disease carries a poor prognosis.

Additional Differential Diagnoses

- **Nipple adenoma.** Also known as florid papillomatosis or papillary adenoma, nipple adenoma is a benign tumor of the lactiferous ducts that develops in the superficial portion of the nipple and can present as a well-circumscribed, nonencapsulated mass. Symptoms may resemble those of Paget disease with serosanguineous nipple discharge, skin ulceration, erythema, and nipple enlargement.
- **Eczema of the breast.** Eczema of the breast may mimic Paget disease; it is characterized by an erythematous, crusty nipple with pruritic patches. This diagnosis is made when the signs and symptoms resolve with treatment, such as topical steroids.

Diagnosis

Paget disease of the nipple

✓ Pearls

- Though most commonly only DCIS is present, Paget disease can be associated with an invasive cancer.
- Cellulitis and inflammatory carcinoma can have similar clinical manifestations.
- If mastitis or eczema of the breast does not resolve with treatment, malignancy should be considered.

Suggested Readings

Frei KA, Bonel HM, Pelte MF, Hylton NM, Kinke lK. Paget disease of the breast: findings at magnetic resonance imaging and histopathologic correlation. Invest Radiol 2005;40(6):363–367

Kopans DB. Breast Imaging. 3rd ed. Philadelphia: Lippincott Williams & Wilkins; 2007

Kushwaha AC, Whitman GJ, Stelling CB, Cristofanilli M, Buzdar AU. Primary inflammatory carcinoma of the breast: retrospective review of mammographic findings. AJR Am J Roentgenol 2000;174(2):535–538

Morrogh M, Morris EA, Liberman L, Van Zee K, Cody HS III, King TA. MRI identifies otherwise occult disease in select patients with Paget disease of the nipple. J Am Coll Surg 2008;206(2):316–321

Case 298

Frederick R. Margolin

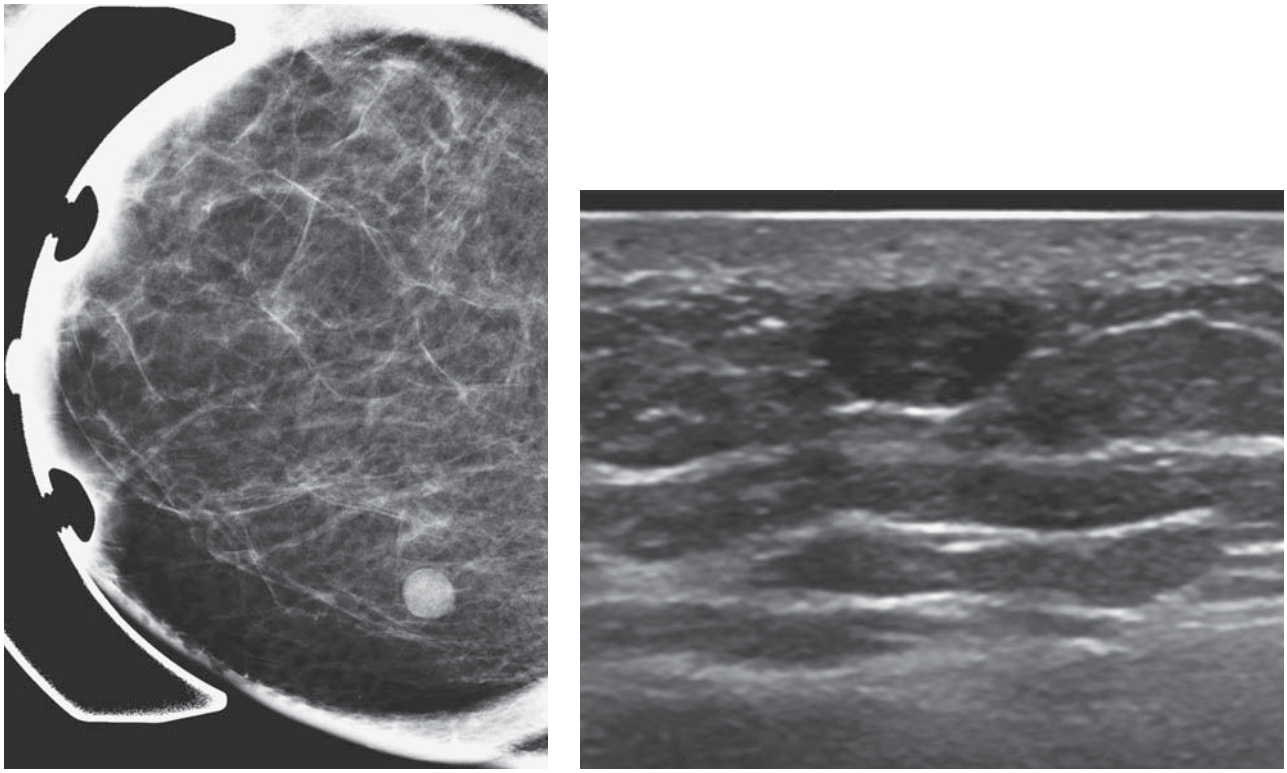


Fig. 298.1 **(A)** Spot compression magnification mammogram of the inner breast in the craniocaudal projection shows a circumscribed mass. **(B)** Sonogram in the transverse plane shows a corresponding circumscribed oval hypoechoic mass with orientation parallel to the chest wall and with posterior acoustic enhancement, contiguous with the skin.

Clinical Presentation

A 50-year-old woman presents with a small pea-shaped palpable lump in her breast, close to the skin surface (**Fig. 298.1**).

Key Imaging Finding

Superficial breast mass

Top 3 Differential Diagnoses

- **Sebaceous cyst.** A sebaceous cyst forms as a result of blockage of a sebaceous gland. It is benign and usually self-limiting. It may be umbilicated and express sebum centrally. Unless infected, it is usually nontender. Tangential views with a skin marker placed on the lesion will demonstrate that the finding is in or closely related to the skin. This should exclude breast cancer that arises from breast tissue deep to the skin. Sonography employing a stand-off pad will allow optimal imaging of the skin and subcutaneous tissues. A sebaceous cyst will be seen as a circumscribed, near anechoic or hypoechoic oval mass, contiguous with or causing interruption of the subdermal skin layer. Extension to the skin surface may be demonstrated. Posterior acoustic enhancement is often present. Clinical examination is important to corroborate the imaging findings, as a sebaceous cyst is usually evident at this time.
- **Epidermal inclusion cyst.** An epidermal inclusion cyst is the result of inclusion of keratinizing squamous epithelium within the dermis. A cyst filled with lamellated keratin is seen, which may give rise to an "onion ring" appearance of alternating concentric echogenic and hypoechoic rings at sonography, representing multiple layers of keratin. More commonly, an epidermal inclusion cyst resembles a sebaceous cyst at mammography and sonography. The diagnosis of an epidermal inclusion cyst is made if there is an antecedent history of surgery or percutaneous core biopsy at the affected site.
- **Focal infection.** Mastitis may result in a focal inflammatory collection near the skin, which may present as a tender, palpable lump. The imaging appearance often resembles sebaceous or epidermal inclusion cysts, except that the margins are more likely to be irregular or poorly defined. Additionally, inflammation is seen in the adjacent skin and subcutaneous tissues, particularly on clinical examination.

Additional Differential Diagnoses

- **Breast carcinoma.** Breast carcinoma uncommonly presents near the skin surface. When it occurs, the mammographic or sonographic appearance will be similar to breast cancer elsewhere in the breast. Diagnosis can be made via core biopsy.
- **Lymphoma.** Lymphoma of the breast is generally of the non-Hodgkin subtype and may present as diffuse breast enlargement or as one or multiple partially circumscribed masses in the breast. Uncommonly, focal deposits of lymphoma can be seen involving the skin and subcutaneous tissues of the breast.
- **Steatocystoma multiplex.** Steatocystoma multiplex is a rare autosomal dominant disorder involving the pilosebaceous unit, resulting in numerous dermal cysts that contain sebum. Multiple circumscribed lucent masses are seen in both breasts. The torso and upper extremities are also commonly involved.

Diagnosis

Sebaceous cyst

✓ Pearls

- Sebaceous cysts occur within the skin and are best diagnosed with tangential views or targeted sonography.
- Epidermal inclusion cysts may have an "onion ring" appearance at sonography.
- Focal infection is characterized by concomitant inflammatory changes.

Suggested Readings

Crystal P, Shaco-Levy R. Concentric rings within a breast mass on sonography: lamellated keratin in an epidermal inclusion cyst. AJR Am J Roentgenol 2005; 184(3, Suppl)S47–S48
Ikeda DM. Breast Imaging: The Requisites. Philadelphia: Elsevier; 2004
Kim HS, Cha ES, Kim HH, Yoo JY. Spectrum of sonographic findings in superficial breast masses. J Ultrasound Med 2005;24(5):663–680
Kopans DB. Breast Imaging. 3rd ed. Philadelphia: Lippincott Williams & Wilkins; 2007

Case 299

Boon Chye Ching

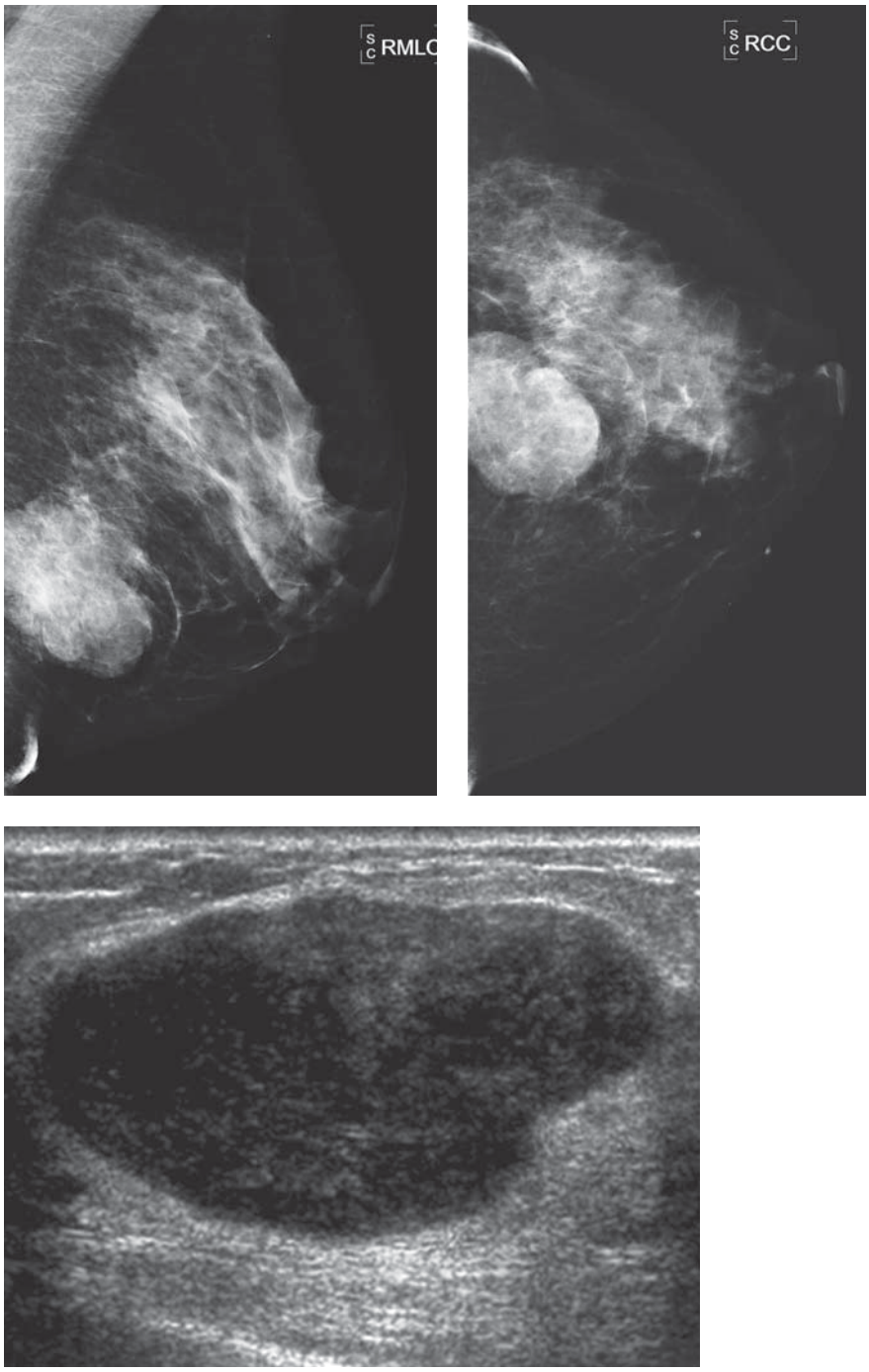


Fig. 299.1 Mammograms in **(A)** the medial-lateral oblique and **(B)** craniocaudal projections show a large lobulated mass in the lower breast. **(C)** Sonogram in the transverse plane demonstrates a corresponding lobulated hypoechoic solid mass.

Clinical Presentation

A 45-year-old woman presents with a palpable lump that has increased in size over several months (**Fig. 299.1**).

Key Imaging Finding

Large breast mass

Top 3 Differential Diagnoses

- **Phyllodes tumor.** *Phyllodes* comes from a Greek word meaning "leaflike." Under microscopy, papillary protuberances of epithelial-lined stroma may be seen. Like fibroadenoma, a phyllodes tumor is a fibroepithelial lesion. Thus cellular fibroadenoma is difficult to distinguish from phyllodes tumor. A phyllodes tumor appears as a dense, circumscribed mass that is hypoechoic on a sonogram. It is seldom associated with calcifications. The spectrum of phyllodes tumor ranges from low to high grade. High-grade tumors tend to have intramural cystic spaces. Benign tumors are locally aggressive, necessitating wide surgical margins. Imaging is not reliable in differentiating fibroadenomas from phyllodes tumors; a phyllodes tumor should be expected with a history of a rapidly enlarging, circumscribed mass.
- **Fibroadenoma.** Fibroadenoma is a solid benign mass. It is the most common mass in young women and the most common palpable mass in women in their 30s. At mammography, it appears as a circumscribed or lobulated, round or oval mass, possibly associated with dystrophic calcifications. At sonography, it is a circumscribed, hypoechoic mass with homogeneous internal echoes. There may be two or three gentle lobulations. A fibroadenoma may increase in size with hormonal stimulation, such as pregnancy. If increased to a large size, it may undergo necrosis and develop cystic areas.
- **Circumscribed breast carcinoma.** Because of the aggressive growth of cancers across tissue planes and because cancers may elicit desmoplastic reaction, cancers are generally poorly defined, irregular, or spiculated. Thus <10% of breast carcinomas are circumscribed. The most common circumscribed breast carcinoma is invasive ductal carcinoma, not otherwise specified (NOS). Other circumscribed breast carcinomas are mucinous, medullary, and papillary carcinomas.

Additional Differential Diagnoses

- **Hematoma.** Hematoma most often occurs in the setting of trauma, surgery, or anticoagulants. Imaging appearance varies depending on early or late presentation. At sonography, hematoma may present as a hypoechoic mass, a mass with heterogeneous echoes (especially as more clots develop), or a cystic lesion with a fluid–debris level. Hematomas should decrease in size and resolve over time without intervention.
- **Abscess.** An abscess typically presents as a tender, palpable mass near the subareolar region. It is usually associated with lactation or a recent surgical procedure. A breast abscess is painful and thus better imaged with ultrasound than mammography. Sonographic findings include a hypoechoic mass with internal heterogeneous echoes. There may be cystic areas, septations, or air. Surrounding edema may be seen in adjacent breast tissue. When superficial, skin thickening may be demonstrated. Hyperemia can also be detected on Doppler imaging. Abscesses should be followed to resolution.

Diagnosis

Phyllodes tumor

✓ Pearls

- Phyllodes tumor is a fibroepithelial lesion that is typically large; wide surgical margins are necessary.
- Imaging findings alone are not reliable in differentiating fibroadenomas from phyllodes tumors.
- Common circumscribed carcinomas include invasive ductal, NOS; mucinous; medullary; and papillary.
- Clinical history is helpful in diagnosing hematomas and abscesses; these should be followed to resolution.

Suggested Readings

Berg WA, Birdwell RL. Diagnostic Imaging: Breast. Salt Lake City, UT: 2006

Goel NB, Knight TE, Pandey S, Riddick-Young M, de Paredes ES, Trivedi A. Fibrous lesions of the breast: imaging-pathologic correlation. Radiographics 2005;25(6):1547–1559

Ikeda DM. Breast Imaging: The Requisites. Philadelphia: Elsevier; 2004

Case 300

Frederick R. Margolin

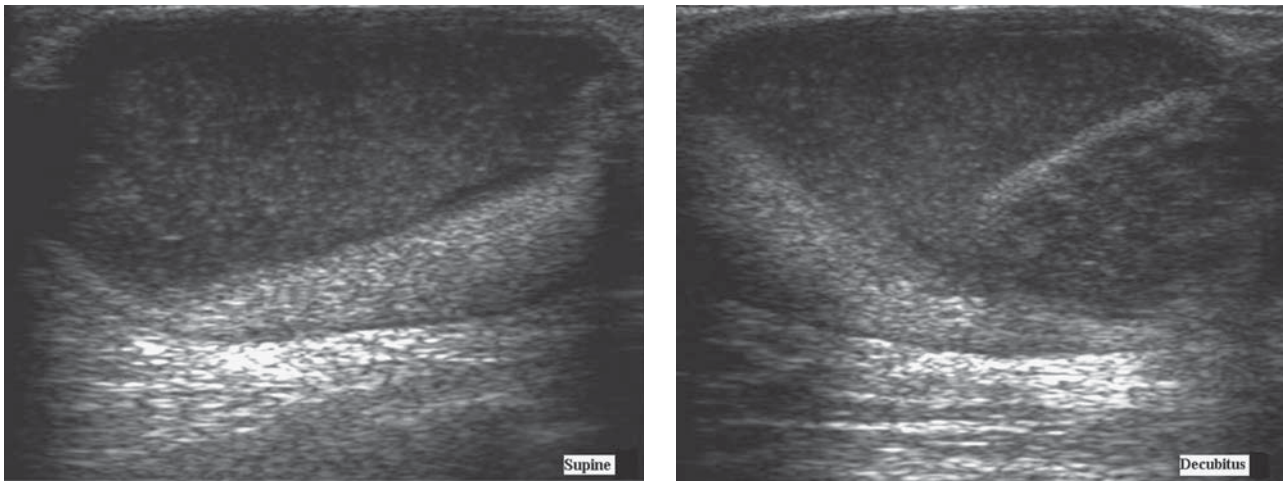


Fig. 300.1 **(A)** Sonogram in the transverse plane shows a complex cystic mass with a fluid–fluid level, hypoechoic debris, and a thick wall. **(B)** Sonogram in the transverse plane after changing the patient's position from supine to decubitus shows that the fluid–fluid level shifts with varying patient position. Additional thick septations are also identified.

Clinical Presentation

A 32-year-old lactating woman presents with erythema, warmth, swelling, and tenderness of the breast of 5 days' duration (**Fig. 300.1**).

Key Imaging Finding

Complex cystic mass

Top 3 Differential Diagnoses

- **Abscess.** Breast abscesses are most commonly seen in postpartum and lactating women as complications of mastitis. At sonography, a complex fluid collection is present, consisting of fluid–fluid levels, thick walls, septations, loculations, hypoechoic adherent debris resembling solid mural nodules, and internal echoes that may "float" during real-time examination. The diagnosis of an abscess is made in the proper clinical setting of mastitis and in conjunction with signs of infection and inflammation. Ultrasound may be used to guide percutaneous aspiration and drainage.
- **Hematoma.** Hematoma may closely resemble an abscess on a sonogram. It is the clinical presentation that distinguishes the two entities. Clinical signs of infection and inflammation are usually absent, and a history of trauma, surgery, or anticoagulation may be elicited. Hematomas should be followed to resolution to exclude an underlying lesion.
- **Cystic neoplasm.** A tumor arising within a cyst (i.e., intracystic papillary carcinoma) or a solid cancer that has undergone necrosis may exhibit sonographic features similar to an abscess. However, clinical signs of infection and inflammation are absent, distinguishing a cystic neoplasm from an abscess. Typically, poorly differentiated invasive carcinoma grows so rapidly that it outgrows its blood supply and undergoes ischemic necrosis. A complex mass is seen at sonography, containing both solid and cystic components. The presence of Doppler signal representing blood flow distinguishes the solid component in a cystic neoplasm from the pus or blood clots present in an abscess or a hematoma, respectively.

Additional Differential Diagnoses

- **Fat necrosis.** Fat necrosis results from various injuries to the breast, including ischemia and trauma. It has various appearances, including that of a complex cystic mass. Correlation with mammography is important to identify classic benign mammographic features of fat necrosis that may be present, such as coarse calcifications and oil cyst formation. In the absence of such classic mammographic signs, ultrasound-guided core biopsy may be needed to exclude malignancy.
- **Cyst with debris.** A cyst is a benign mass most commonly seen in premenopausal women. Hemorrhage, protein, and cholesterol deposits may be present within a cyst, resulting in a complex-appearing mass at sonography. Debris may be differentiated from solid tissue by ultrasound-guided aspiration.

Diagnosis

Abscess

✓ Pearls

- Breast abscesses are usually seen in postpartum and lactating women as complications of mastitis.
- Hematomas often occur in the setting of trauma or anticoagulation; they should be followed to resolution.
- Tumors arising within a cyst or large tumors undergoing necrosis can resemble benign cystic lesions.
- Benign cysts with debris can be differentiated from carcinomas through aspiration.

Suggested Readings

Berg WA, Campassi CI, Ioffe OB. Cystic lesions of the breast: sonographic-pathologic correlation. Radiology 2003;227(1):183–191

Kopans DB. Breast Imaging. 3rd ed. Philadelphia: Lippincott Williams & Wilkins; 2007

Section XIII Roentgen Classics

Case 301

Jeffrey P. Tan

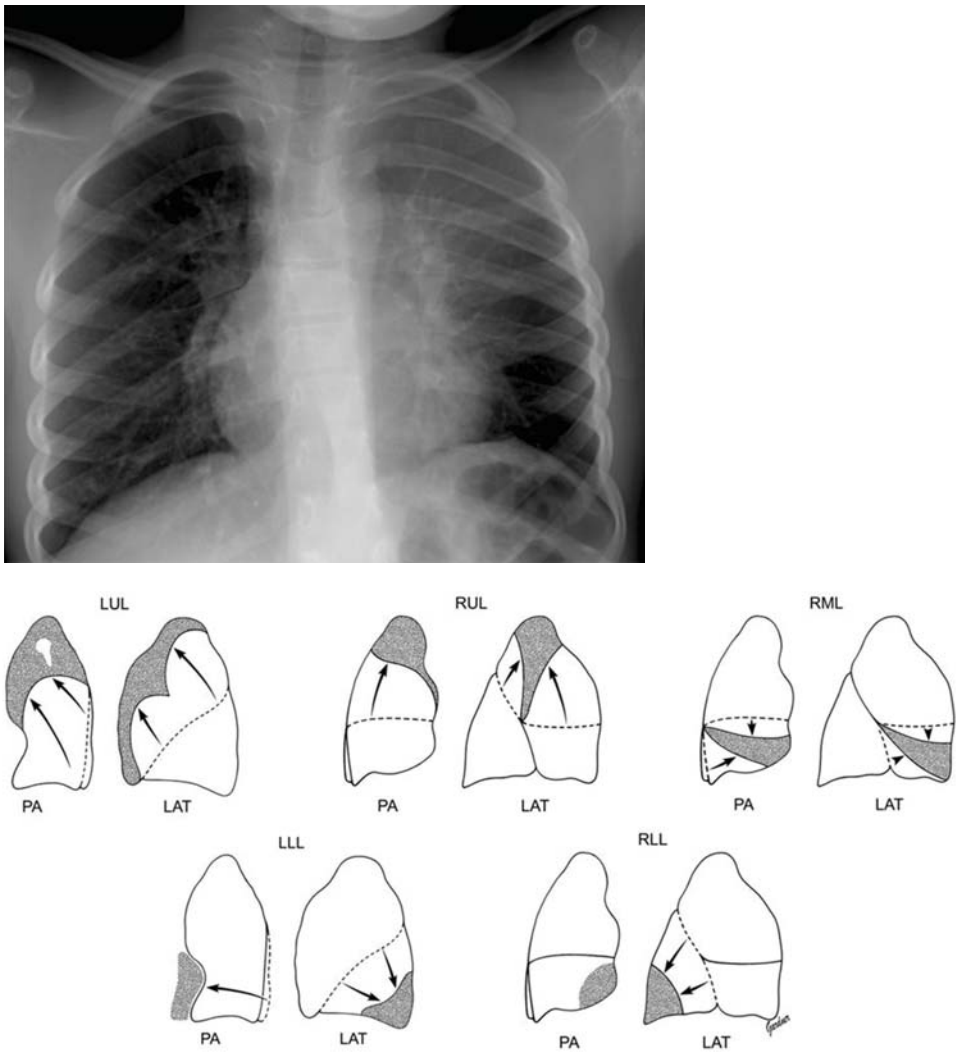


Fig. 301.1 **(A)** Frontal chest radiograph demonstrates veil-like opacification of the left lung with an elevated hilum, volume loss, and left diaphragmatic juxtaphrenic peak. Increased lucency adjacent to the aortic knob is consistent with a luftsichel (air crescent) sign. **(B)** Alternate patterns of lobar collapse. LAT, lateral; LLL, left lower lobe; LUL, left upper lobe; PA, posteroanterior; RLL, right lower lobe; RML, right middle lobe; RUL, right upper lobe.

Clinical Presentation

A 7-year-old boy presents with difficulty breathing (**Fig. 301.1**).

Key Imaging Finding

Veil-like opacification involving the left lung with volume loss

Diagnosis

- **Left upper lobe collapse.** Lobar collapse (atelectasis) results from decreased aeration of the lung, which may be due to an obstructing endobronchial lesion, extrinsic compression from an adjacent neoplastic process, or scarring. Common signs of lobar collapse are opacification with volume loss; shift of the mediastinum, fissure, or hilum toward the collapsed lobe; and compensatory hyperinflation of the remaining lobes. There are a few specific signs for certain patterns of lobar collapse, such as the luftsichel sign (German for "air sickle"), in which the left upper lobe collapses anterosuperiorly, and the hyperinflated superior segment of the left lower lobe causes an area of increased lucency adjacent to the aortic knob. When left upper lobe collapse occurs, a juxtaphrenic peak can result from tenting of the diaphragm along the inferior accessory fissure.

Whenever there is lobar collapse, it is important to evaluate the central airways for an obstructing lesion. Computed tomography and endoscopy may be used to localize the lesion. Possible lesions are bronchogenic carcinoma, carcinoid, lymphoma, scarring, salivary gland tumors, a foreign body, and mucus.

Notably, right upper lobe collapse secondary to a centrally obstructing mass is characterized by the "S sign of Golden," occurring when the right upper lobe collapses superomedially, and the minor fissure assumes an S shape with a medial convexity and a peripheral concavity due to a centrally obstructing hilar mass. For other patterns of lobar collapse, see **Fig. 301.1B.**

✓ Pearls

- Patterns of lobar collapse should be recognized by their characteristic features.
- Evaluation for a central endobronchial lesion is necessary when there is unexplained lobar collapse.
- Imaging findings include volume loss, hilar retraction, and fissure displacement.

Suggested Readings

Ashizawa K, Hayashi K, Aso N, Minami K. Lobar atelectasis: diagnostic pitfalls on chest radiography. Br J Radiol 2001;74(877):89–97

Blankenbaker DG. The luftsichel sign. Radiology 1998;208(2):319–320

Gupta P. The Golden S sign. Radiology 2004;233(3):790–791

Case 302

Jeffrey P. Tan

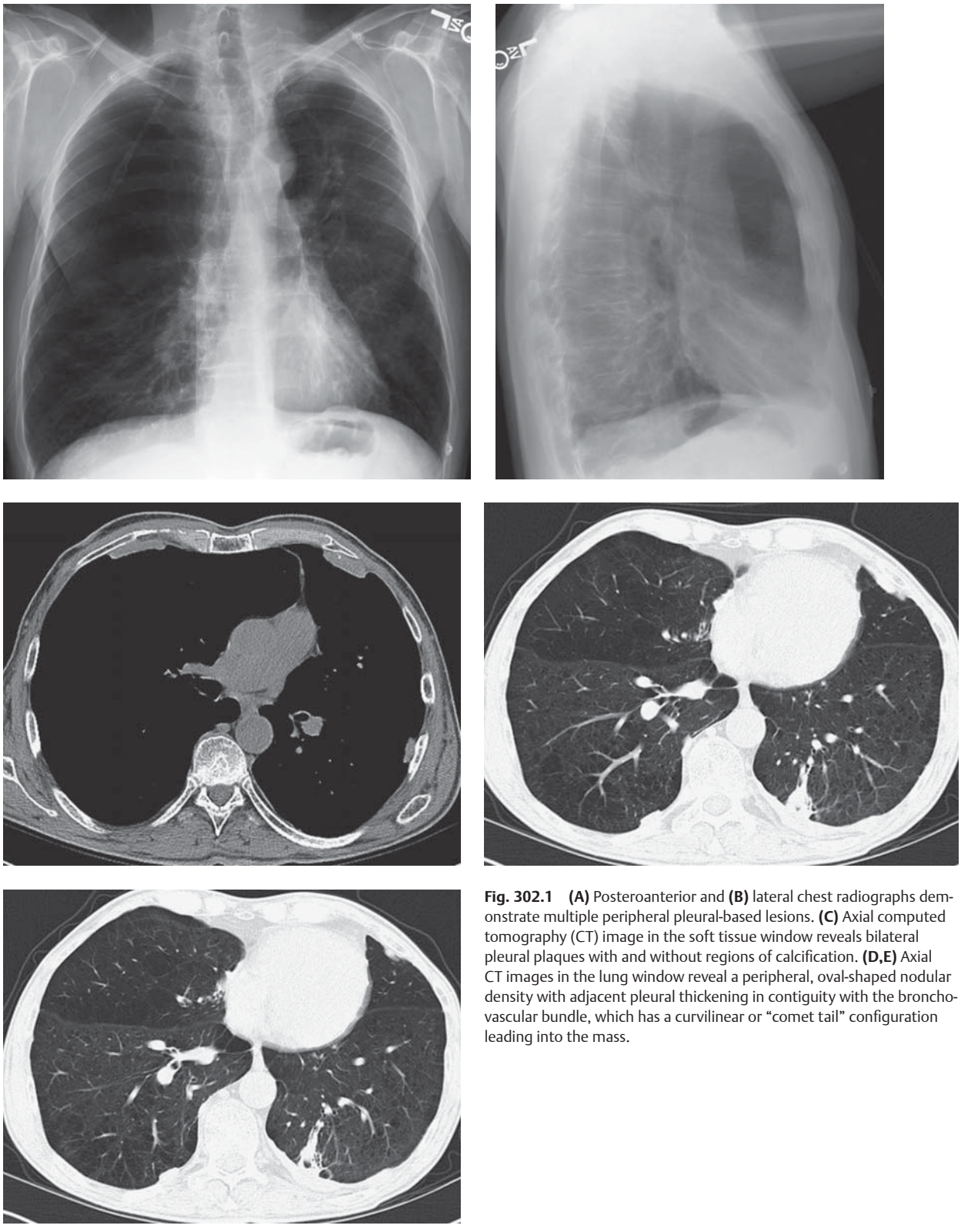


Fig. 302.1 **(A)** Posteroanterior and **(B)** lateral chest radiographs demonstrate multiple peripheral pleural-based lesions. **(C)** Axial computed tomography (CT) image in the soft tissue window reveals bilateral pleural plaques with and without regions of calcification. **(D,E)** Axial CT images in the lung window reveal a peripheral, oval-shaped nodular density with adjacent pleural thickening in contiguity with the bronchovascular bundle, which has a curvilinear or "comet tail" configuration leading into the mass.

Clinical Presentation

A 63-year-old man presents with shortness of breath (**Fig. 302.1**).

Key Imaging Finding

Pleural-based lesion adjacent to pleural thickening with volume loss

Diagnosis

- **Round atelectasis.** Round atelectasis is a chronic focal peripheral region of atelectatic lung adjacent to a region of underlying pleural disease. It is commonly identified in patients with asbestos-related pleural disease; however, any underlying pleural disease may cause round atelectasis. It is most commonly seen in the posterior lower lobes, although it can occur wherever there is pleural disease. It may range in size from 1 to 10 cm.

  On computed tomography, round atelectasis usually is round, oval, or wedge-shaped with angular margins along the pleura and adjacent pleural thickening. There is an indistinct margin along the side oriented toward the hilum with a curvilinear shape of the bronchovascular bundle, commonly referred to as the "comet tail" sign. Other suggestive findings are air bronchograms and volume loss within the affected lobe.

  Round atelectasis is a benign entity; however, if there is concern for an underlying neoplastic process, 18F-fluorodeoxyglucose positron emission tomography (FDG PET) may be useful, as many types of lung cancer may be metabolically active in contrast to round atelectasis.

✓ Pearls

- Round atelectasis occurs adjacent to underlying pleural disease and has angular margins and volume loss.
- A curvilinear bronchovascular bundle leading into the mass is referred to as the "comet tail" sign.
- Round atelectasis is most commonly associated with asbestos-related pleural disease.
- FDG PET may be useful in evaluating for an underlying neoplasm in equivocal cases.

Suggested Readings

Hansell DM, Armstrong P, Lynch DA, et al. Imaging of the Diseases of the Chest. 4th ed. Philadelphia: Elsevier-Mosby; 2005

Stathopoulos GT, Karamessini MT, Sotiriadi AE, Pastromas VG. Rounded atelectasis of the lung. Respir Med 2005;99(5):615–623

Case 303

Jeffrey P. Tan

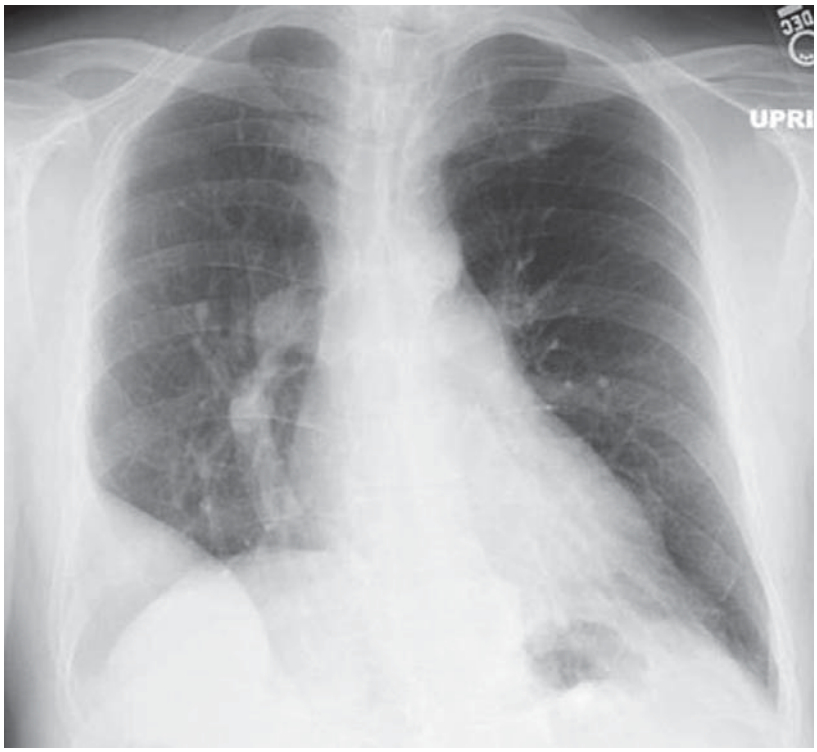


Fig. 303.1 Posteroanterior chest radiograph demonstrates right lung volume loss with a curvilinear opacity coursing inferiorly from the right hilum below the diaphragm. Incidentally, there is a right-sided pleural-based lesion, consistent with a known lipoma.

Clinical Presentation

A 42-year-old man presents with a cough (**Fig. 303.1**).

Key Imaging Finding

Right lung volume loss with a curvilinear opacity descending below the diaphragm

Diagnosis

- **Scimitar syndrome.** Scimitar syndrome, also known as hypogenetic lung syndrome or pulmonary venolobar syndrome, is characterized by right-sided pulmonary hypoplasia and partial anomalous pulmonary venous return. The anomalous pulmonary vein is typically a curvilinear opacity that resembles a scimitar (Turkish sword). The anomalous pulmonary venous drainage results in a left-to-right shunt. Other associated findings may include dextroposition of the heart, a small right pulmonary artery, and an abnormal bronchovascular pattern in the right hilum. Diaphragmatic and skeletal deformities may also be seen.

  Most patients with scimitar syndrome are asymptomatic; however, symptoms may be present in the setting of other associated anomalies, such as cardiac septal defects, bronchiectasis, and tracheal diverticula. Evaluation of scimitar syndrome and associated anomalies can be performed with contrast-enhanced computed tomography (CT) or magnetic resonance imaging (MRI). In addition, CT may demonstrate a rare associated anomaly, the horseshoe lung, in which the right and left lungs are fused posteriorly by an isthmus of lung tissue.

  The anomalous vein usually drains into the inferior vena cava (IVC) below the right hemidiaphragm. Less commonly, the anomalous vein drains into the suprahepatic portion of the IVC, hepatic veins, portal vein, azygos vein, coronary sinus, or right atrium. Rarely, it may empty into the left atrium, in which case it is referred to as the "meandering" pulmonary vein.

✓ Pearls

- Scimitar syndrome is characterized by a hypoplastic lung and partial anomalous pulmonary venous return.
- Patients are usually asymptomatic, except with a hemodynamically significant left-to-right shunt.
- CT or MRI can be used to evaluate for associated cardiac, pulmonary, and vascular anomalies.

Suggested Readings

Hansell DM, Armstrong P, Lynch DA, et al. Imaging of the Diseases of the Chest. 4th ed. Philadelphia: Elsevier-Mosby; 2005

Holt PD, Berdon WE, Marans Z, Griffiths S, Hsu D. Scimitar vein draining to the left atrium and a historical review of the scimitar syndrome. Pediatr Radiol 2004;34(5):409–413

Woodring JH, Howard TA, Kanga JF. Congenital pulmonary venolobar syndrome revisited. Radiographics 1994;14(2):349–369

Case 304

Grant E. Lattin Jr.

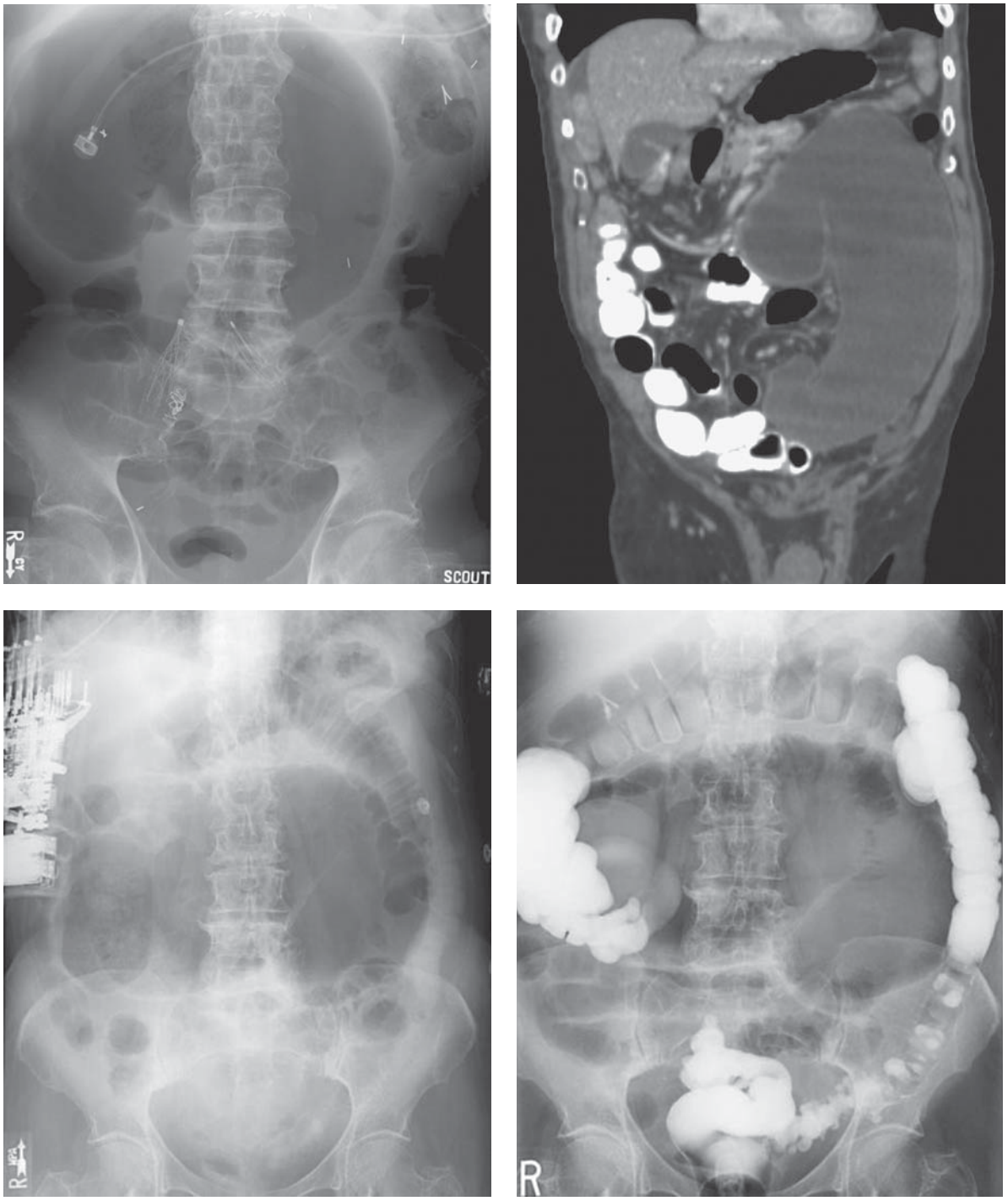


Fig. 304.1 **(A)** Plain radiograph of the abdomen demonstrates a coffee bean–shaped, dilated loop of bowel that points toward the left upper quadrant. **(B)** Reformatted coronal computed tomography image confirms a dilated cecum that has twisted on the axis of the right colon. **(C)** Plain radiograph and **(D)** barium enema in another patient with the same disease process display a gas-filled, dilated cecum with "beaking" of contrast within the midascending colon.

Clinical Presentation

A 63-year-old man presents with severe abdominal pain (**Fig. 304.1**).

Key Imaging Finding

Dilated, gas-filled cecum pointing toward the left upper quadrant of the abdomen

Diagnosis

- **Cecal volvulus.** Cecal volvulus occurs less commonly than sigmoid volvulus, accounting for 10 to 15% of all cases of volvulus. Seen usually in younger men between 20 and 40 years of age, cecal volvulus is due to rotation about the axis of the right colon, often due to a redundant mesentery with narrow fixation.

  Plain radiographs demonstrate a dilated, gas-filled cecum directed toward the left upper quadrant of the abdomen. Often referred to as having a "kidney bean" or "coffee bean" appearance, cecal volvulus may contain only one air–fluid level, rather than two, as can be observed in sigmoid volvulus. Contrast enema will show "beaking" of the contrast column at the midascending colon. Computed tomography will show tapering of the ends of the dilated cecum with "whirling" of adjacent mesenteric vessels.

  Although cecal volvulus may present classically with an acute abdomen, an initial differential diagnosis may include cecal bascule, acute ileus, Ogilvie syndrome (mechanical pseudo-obstruction), or toxic megacolon, in addition to sigmoid volvulus. Anatomical distribution of the dilated bowel as well as patient history may assist in making the diagnosis.

  Treatment options include reduction via colonoscopy or surgery, depending on the patient's condition. Delayed diagnosis and treatment may lead to bowel necrosis, sepsis, bowel perforation, and subsequent death. Prognosis, therefore, depends on the degree of complications associated with the volvulus.

✓ Pearls

- Cecal volvulus appears as a "coffee bean" configuration of a dilated cecum oriented in the left upper quadrant.
- On barium enema, there is "beaking" of the contrast column within the midascending colon.

Suggested Readings

Delabrousse E, Sarlième P, Sailley N, Aubry S, Kastler BA. Cecal volvulus: CT findings and correlation with pathophysiology. Emerg Radiol 2007;14(6):411–415

Feldman D. The coffee bean sign. Radiology 2000;216(1):178–179

Case 305

Grant E. Lattin Jr.

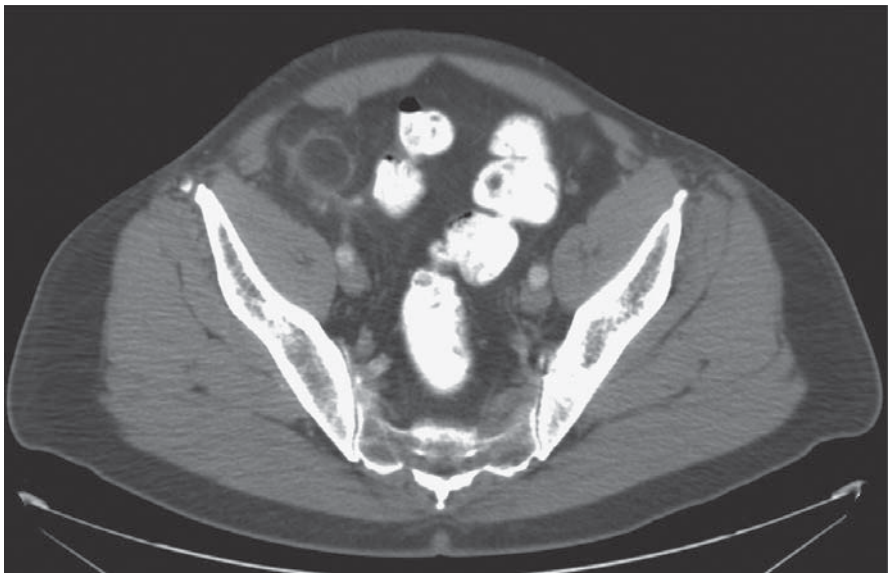


Fig. 305.1 Contrast-enhanced axial computed tomography image through the pelvis demonstrates inflammatory change around a focus of fat attenuation located along the right colon. The appendix (not shown) was normal in appearance.

Clinical Presentation

A 53-year-old man presents with right lower quadrant (RLQ) pain (**Fig. 305.1**).

Key Imaging Finding

Inflammatory fatty focus within the RLQ of the abdomen

Diagnosis

- **Epiploic appendagitis.** Epiploic appendagitis is a condition characterized by inflammatory change surrounding an epiploic appendage of the colon. These appendages are peritoneal outpouchings that arise from the colonic serosa and consist of fat and vessels. Venous occlusion or torsion may contribute to the localized abdominal pain experienced by patients.

  Computed tomography (CT) characteristics include an oval fatty lesion along the serosa of the colon with a hyperdense ring of inflammatory change seen most commonly along the anterior sigmoid colon. Care should be taken to identify a normal appendix and exclude any adjacent inflamed diverticula. Other intra-abdominal, inflammatory, fat-containing lesions to consider initially within the differential diagnosis are omental infarction, mesenteric panniculitis, trauma, and neoplasm, such as liposarcoma.

  Location and appearance by CT allow for differentiation of epiploic appendagitis from omental infarction. Omental infarction typically occurs deep to the anterior abdominal musculature within the right abdomen and may lack the hyperdense ring of inflammatory change surrounding central fat attenuation.

  Treatment for epiploic appendagitis is conservative with pain medication, but inflammatory change may evolve and persist for as long as 6 months.

✓ Pearls

- Epiploic appendagitis occurs most commonly along the anterior sigmoid colon.
- CT appearance is an ovoid fatty lesion with surrounding inflammatory change.
- Treatment of epiploic appendagitis is conservative pain management.
- CT changes may persist for as long as 6 months.

Suggested Readings

Sandrasegaran K, Maglinte DD, Rajesh A, Akisik FM. Primary epiploic appendagitis: CT diagnosis. Emerg Radiol 2004;11(1):9–14

Singh AK, Gervais DA, Hahn PF, Rhea J, Mueller PR. CT appearance of acute appendagitis. AJR Am J Roentgenol 2004;183(5):1303–1307

Case 306

Cam Chau and Rebecca Stein-Wexler

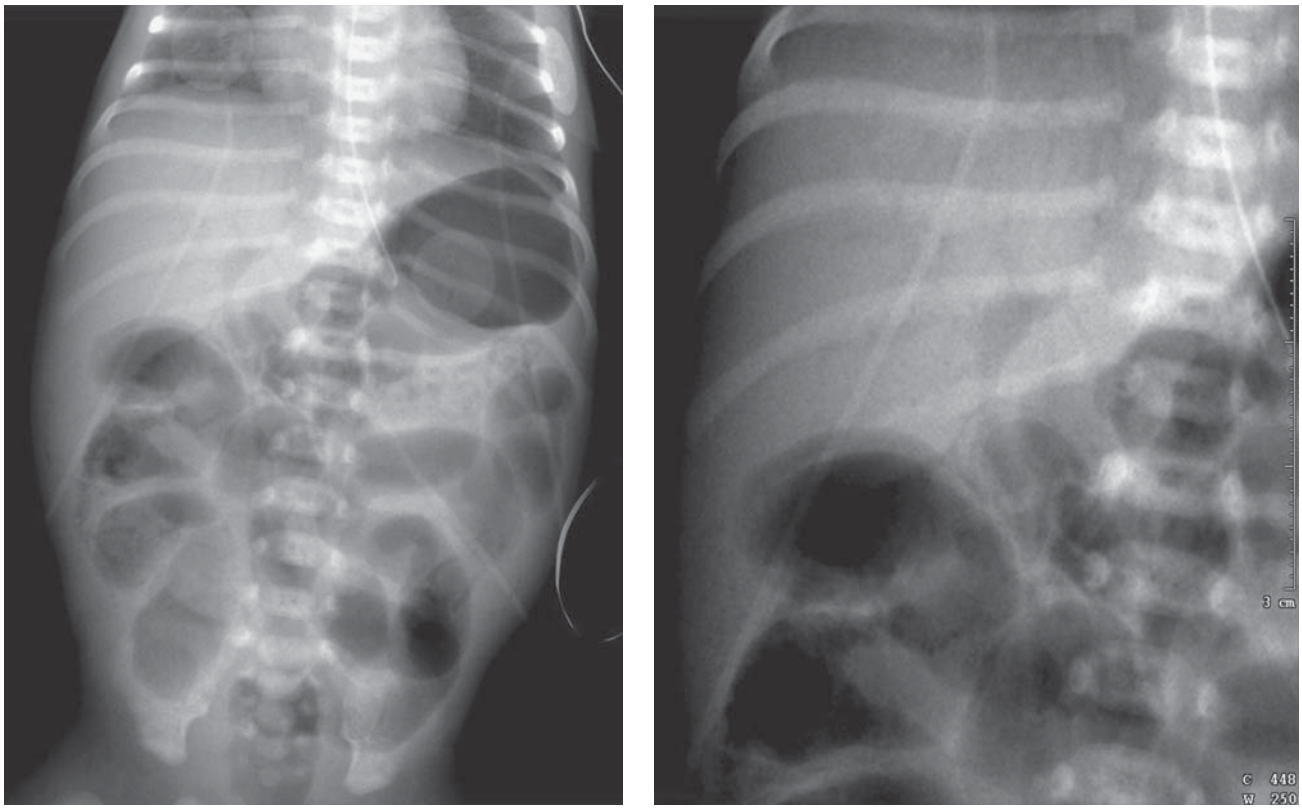


Fig. 306.1 **(A)** Supine anteroposterior abdominal radiograph demonstrates generalized bowel distention, along with linear and rounded lucencies along the bowel wall. Branching lucencies are also seen over the liver. **(B)** A coned-down view over the right upper quadrant better depicts the pneumatosis within gas-distended loops of the bowel, as well as portal venous gas over the liver.

Clinical Presentation

A 7-day-old premature infant presents with respiratory distress, abdominal distention, and bloody diarrhea (**Fig. 306.1**).

Key Imaging Finding

Pneumatosis and portal venous gas in a premature infant

Diagnosis

- **Necrotizing enterocolitis (NEC).** NEC is the most common gastrointestinal (GI) emergency in premature infants. It usually occurs in infants in the neonatal intensive care unit weighing <1000 g at birth, although ~10% of neonates with NEC are born at term (cardiac disease or maternal cocaine use is often present). The peak incidence is during the 1st or 2nd week of life, although NEC may occur later in extremely premature infants. The etiology of NEC is multifactorial and is associated with prematurity, intestinal ischemia/mucosal damage caused by bacterial colonization, inflammatory mediators, and early feeding. Bowel wall coagulative and hemorrhagic necrosis and inflammation result.

  NEC may occur anywhere in the GI tract but is found most often in the right colon and terminal ileum. Clinical symptoms include feeding intolerance, vomiting, diarrhea, bloody stools, and abdominal distention. Respiratory distress, acidosis, sepsis, shock, and temperature instability are associated sequelae.

  Infants with clinical suspicion of NEC are followed with serial supine and often also left lateral decubitus radiographs of the abdomen. The earliest finding is fixed bowel distention. Bowel wall pneumatosis constitutes definitive radiographic evidence of NEC and is seen in 50 to 70% of patients with this disease. The pneumatosis appears as bubbly or curvilinear lucencies within the bowel wall, depending on whether the gas is submucosal or subserosal. Portal venous gas may be seen as branching lucencies over the liver, with more peripheral extension than occurs with biliary gas. Free intraperitoneal air most often occurs due to perforation of the distal ileum or proximal colon and is the only universally accepted indication for surgical intervention. Radiographic findings of free air include increased lucency over the liver, gas outlining the falciform ligament, and gas on both sides of the bowel wall (Rigler sign) on supine radiographs; additional findings on left lateral decubitus views include triangular lucencies at the nondependent portion of the abdomen, along with larger collections of extraluminal gas.

  When there is strong clinical suspicion of NEC, or if the diagnosis has been established radiographically, infants are monitored with serial abdominal radiographs. Treatment includes bowel rest and decompression, broad spectrum antibiotics, parenteral nutrition, oxygen, and intravenous fluids. Long-term sequelae include intestinal strictures, malabsorption, fistulae formation, and short gut syndrome. Overall mortality for NEC is ~20 to 30%.

✓ Pearls

- NEC most commonly occurs in premature infants weighing <1000 g at birth.
- Pneumatosis most commonly occurs in the right lower quadrant.
- Portal venous gas is depicted as linear branching lucencies over the peripheral margin of the liver.
- Free intraperitoneal air necessitates surgical intervention.

Suggested Readings

Donnelly LF. Diagnostic Imaging: Pediatrics. Salt Lake City, UT: Amirsys; 2005

Epelman M, Daneman A, Navarro OM, et al. Necrotizing enterocolitis: review of state-of-the-art imaging findings with pathologic correlation. Radiographics 2007;27(2):285–305

Moss RL, Dimmitt RA, Barnhart DC, et al. Laparotomy versus peritoneal drainage for necrotizing enterocolitis and perforation. N Engl J Med 2006;354(21):2225–2234

Case 307

Cam Chau and Rebecca Stein-Wexler

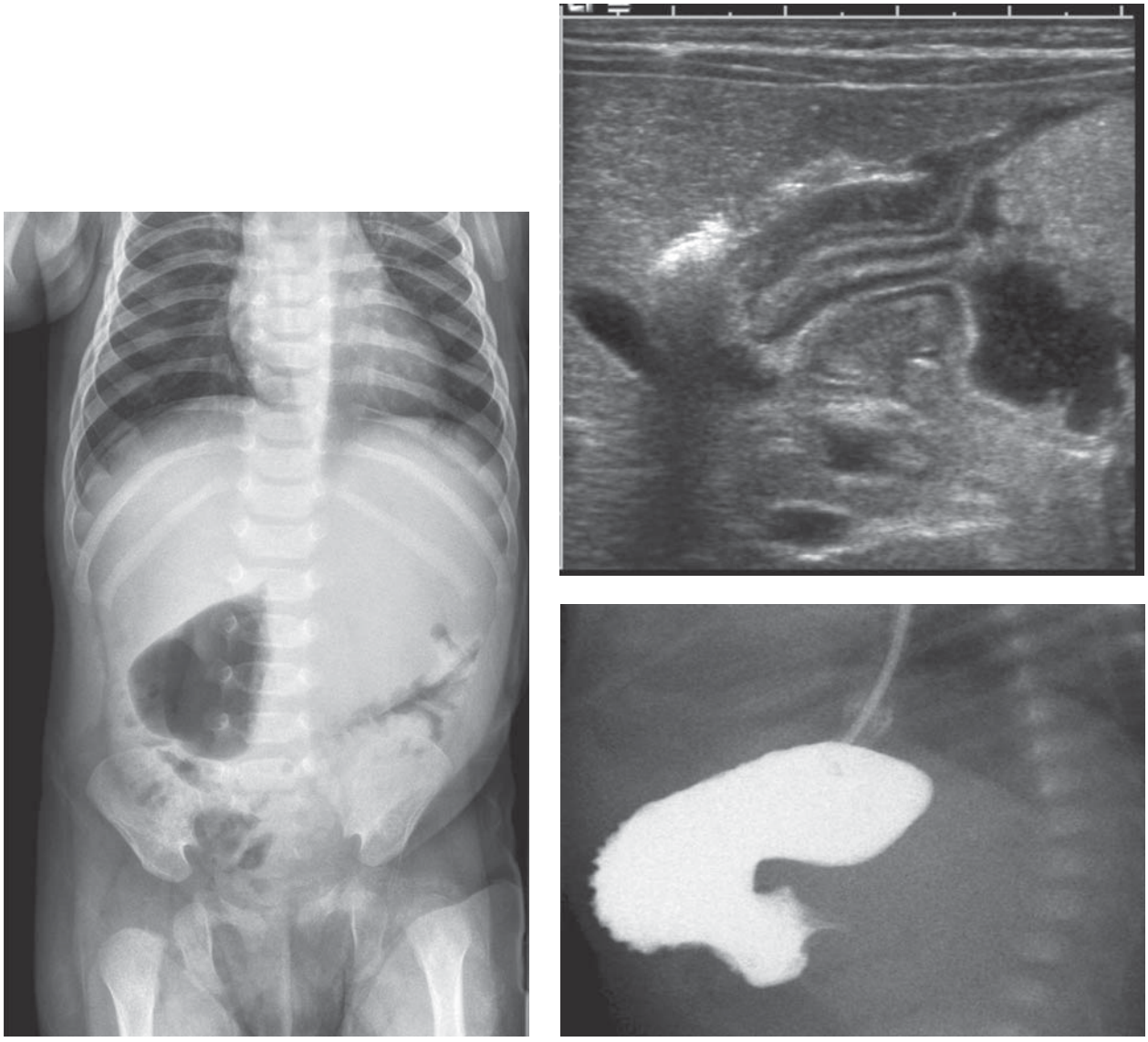


Fig. 307.1 **(A)** Left lateral decubitus radiograph of the abdomen demonstrates a distended stomach and minimal distal bowel gas. **(B)** Axial oblique ultrasound image shows elongation of the pyloric channel and thickening of the hypoechoic muscular wall. **(C)** A lateral view from an upper gastrointestinal examination shows shouldering of the gastric antrum and partial visualization of the elongated and narrowed pyloric channel resulting in the "string" sign. (Courtesy of Children's Hospital and Research Center, Oakland, California.)

Clinical Presentation

A 6-week-old infant presents with a 4-day history of nonbilious vomiting after feedings (**Fig. 307.1**).

Key Imaging Finding

Gastric outlet obstruction with enlarged pylorus

Diagnosis

- **Hypertrophic pyloric stenosis (HPS).** HPS develops in early infancy, presenting in infants between 2 and 12 weeks of age. It occurs in 2 to 5 per 1000 births per year, and the male-to-female ratio is 4 to 5:1. Most common among first-born Caucasian male children, HPS is not truly inherited but does have a familial link. Its true etiology remains unclear.

  Clinical symptoms include nonbilious vomiting that begins as occasional regurgitation but may progress to projectile vomiting after most feedings. Examiners may palpate an olive-shaped mass in the midepigastrium; if found, this sign is 97% specific. Other presentations are hypochloremic, hypokalemic metabolic alkalosis and weight loss, although these are encountered infrequently due to a relatively early diagnosis.

  Ultrasound is the examination of choice when HPS is suspected. The patient is positioned supine or right lateral decubitus, and glucose water may be administered to facilitate identification of the pylorus and assess gastric emptying. Peristaltic waves are absent from the thickened, elongated circular pyloric muscle, and the pyloric channel does not open to allow passage of gastric contents. When the pylorus is viewed in cross section, single-wall thickness of >3 mm is generally considered abnormal, as is length >14 mm (these standards do vary slightly among researchers). Pylorospasm may mimic HPS and is diagnosed when the configuration of the pylorus alters, allowing fluid to traverse the channel. Occasionally HPS is identified on an upper gastrointestinal (GI) examination. Exaggerated gastric motility results in a "caterpillar" appearance of the stomach. Barium within the elongated and narrowed pyloric channel results in the "string" sign. Mass effect from the hypertrophied muscle causes shouldering of the antrum and a "mushroom" appearance of the duodenum.

  Nonsurgical treatment of HPS includes administration of atropine and frequent small feedings. Pyloromyotomy is the surgical management of choice, whether open or laparoscopic. The thickened muscle is split longitudinally and the edges closed transversely, relieving the stricture.

✓ Pearls

- HPS is most common among first-born Caucasian male children and occurs between 2 and 12 weeks of age.
- Ultrasound demonstrates a thickened and elongated pylorus (≥3 mm single-wall thickness; ≥ 14 mm length).
- Upper GI examination demonstrates the "string" sign and shouldering at the gastric antrum.

Suggested Readings

Donnelly LF. Diagnostic Imaging: Pediatrics. Salt Lake City, UT: Amirsys; 2005

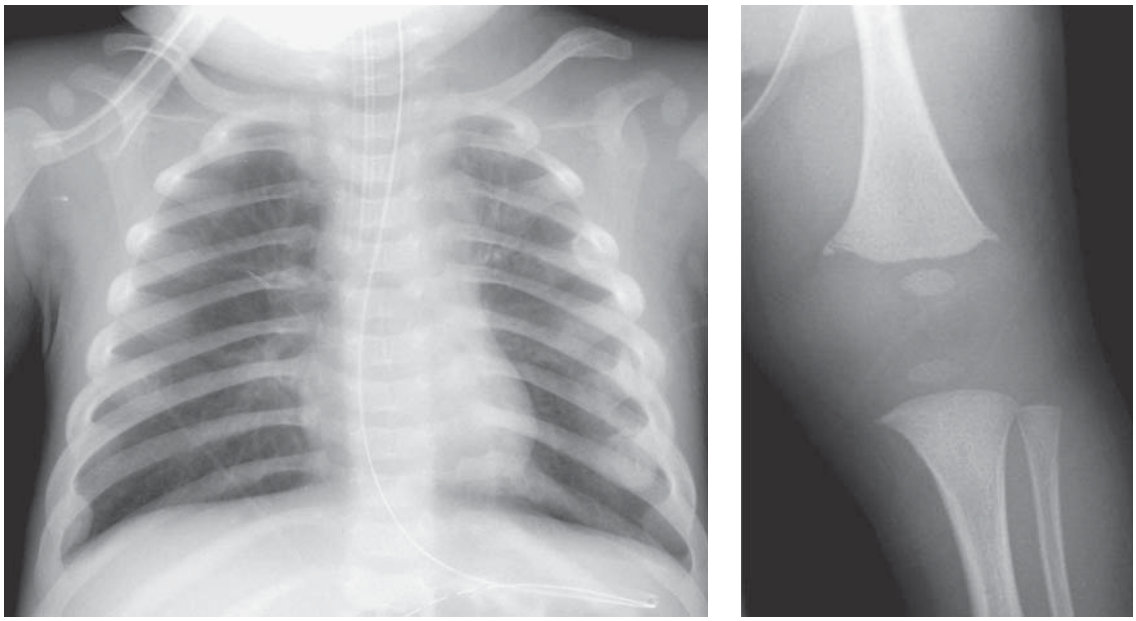
Hernanz-Schulman M. Infantile hypertrophic pyloric stenosis. Radiology 2003;227(2):319–331

Hernanz-Schulman M, Lowe LH, Johnson J, et al. In vivo visualization of pyloric mucosal hypertrophy in infants with hypertrophic pyloric stenosis: is there an etiologic role? AJR Am J Roentgenol 2001;177(4):843–848

van der Bilt JD, Kramer WL, van der Zee DC, Bax NM. Laparoscopic pyloromyotomy for hypertrophic pyloric stenosis: impact of experience on the results in 182 cases. Surg Endosc 2004;18(6):907–909

Case 308

Cam Chau and Rebecca Stein-Wexler



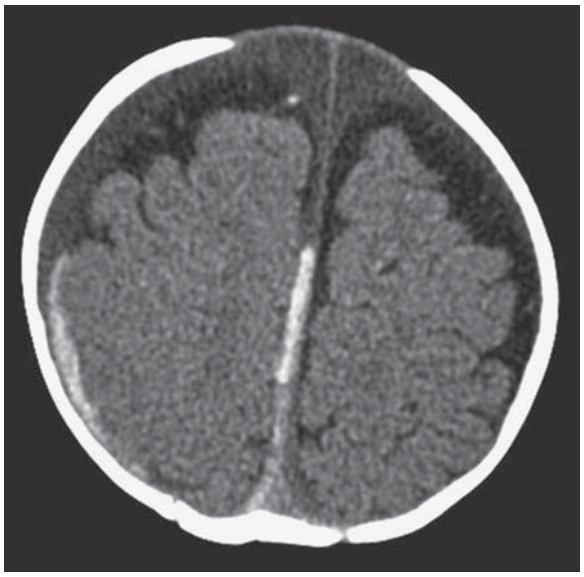


Fig. 308.1 **(A)** Frontal radiograph of the chest demonstrates multiple bilateral healing posterior and lateral rib fractures. There are endotracheal and enteric tubes. **(B)** Frontal radiograph of the left knee reveals a metaphyseal corner fracture of the distal femur. **(C)** Noncontrast head computed tomography image demonstrates acute extra-axial hemorrhages along the parafalcine region and right posterior convexity, as well as older bilateral frontoparietal subdural hematomas/hygromas.

Clinical Presentation

A 6-month-old female infant is brought to the emergency room by her mother, having lost consciousness after rolling off the bed (**Fig. 308.1**).

Key Imaging Finding

Multiple high-specificity fractures and injuries of varying ages

Diagnosis

- **Nonaccidental trauma.** Over 3 million cases of child abuse and neglect were reported in 2005 in the United States, and 30% were eventually substantiated. Over 15% of these cases involved physical abuse. Suspicion for nonaccidental trauma (NAT) must arise when characteristic fractures are encountered in infants, older children present with injuries that are not consistent with the clinical history, multiple injuries are noted in various stages of healing, or there are multiple types of coexisting injuries.

  Rib fractures are common in abused infants, representing an estimated 48% of bony injuries. Infants' ribs are pliable and do not readily fracture from a direct blow; such fractures in abused infants occur when the child is held by the chest and shaken. Posterior rib fractures, which overlie the adjacent transverse process, are highly specific for NAT due to the nature of the fracture, although anterior and lateral fractures are also common. Acute fractures are difficult to visualize, and callous formation results in increased conspicuity. Follow-up views at 2 weeks can be helpful.

  Corner metaphyseal lesions (CMLs) are also highly specific for child abuse. Also known as "corner" or "bucket handle" fractures, they result from torsional stress and shear, when an infant is shaken and the limbs flail, or when an extremity is twisted or pulled. The most immature and thus vulnerable region in a growing bone is the paraphyseal metaphysis; this fractures to form the CML. Viewed tangentially, the bone fragment resembles a corner; viewed obliquely, the larger curved fragment resembles a bucket handle. Sternal, scapular, and spinous process fractures also suggest NAT in infants.

  Intracranial injury is also common in abused infants and may be lethal. Subdural hematomas are suggestive, as are hemorrhages of varying ages. Parenchymal hemorrhage is usually relatively mild, but hypoxic-ischemic injury may be significant. Retinal hemorrhages provide a clinical clue for "shaken baby" syndrome.

  The skeletal survey is the study of choice for assessing suspected child abuse. Up to the age of 2 years, all bones are radiographed; in older children, a more selective survey is performed. Follow-up radiographs after 2 weeks may reveal additional fractures.

  If the radiologist suspects child abuse, the findings must be promptly reported to the referring clinician and, when necessary, to the appropriate governmental body.

✓ Pearls

- Posterior rib and metaphyseal corner fractures are common high-specificity fractures in NAT.
- Multiple fractures of different ages or a discordant clinical history should raise suspicion for NAT.
- Work-up for NAT typically includes a skeletal survey and noncontrast head computed tomography.

Suggested Readings

Kemp AM, Butler A, Morris S, et al. Which radiological investigations should be performed to identify fractures in suspected child abuse? Clin Radiol 2006;61(9):723–736

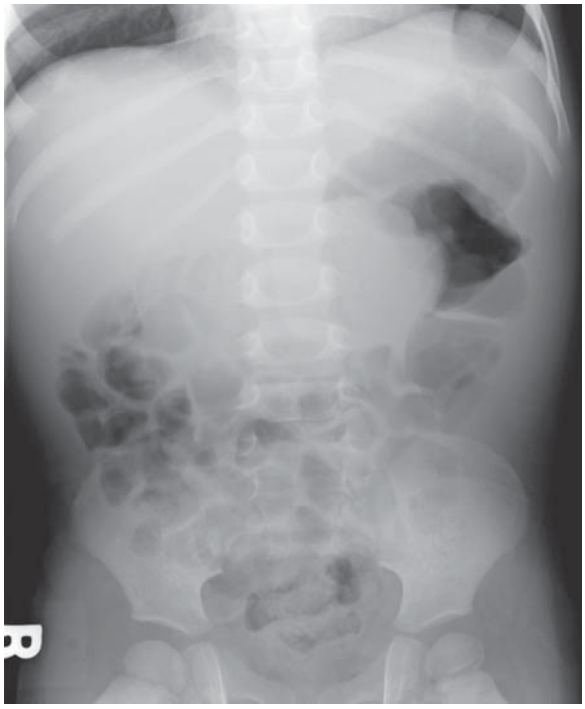
Kocher MS, Kasser JR. Orthopaedic aspects of child abuse. J Am Acad Orthop Surg 2000;8(1):10–20

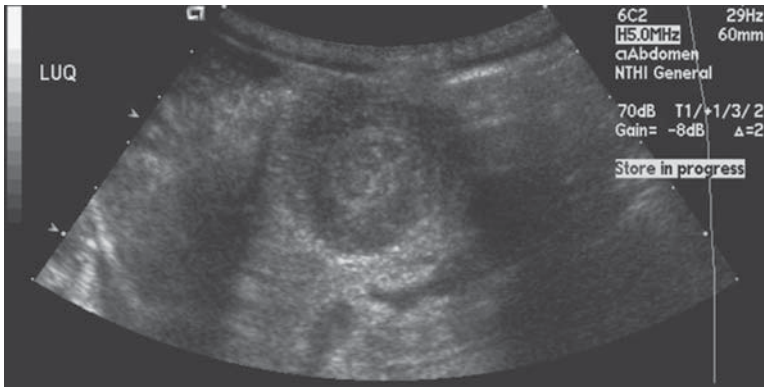
Jenny C; Committee on Child Abuse and Neglect. Evaluating infants and young children with multiple fractures. Pediatrics 2006;118(3):1299–1303

Donnelly LF. Diagnostic Imaging: Pediatrics. Salt Lake City, UT: Amirsys; 2005

Case 309

William T. O'Brien Sr.





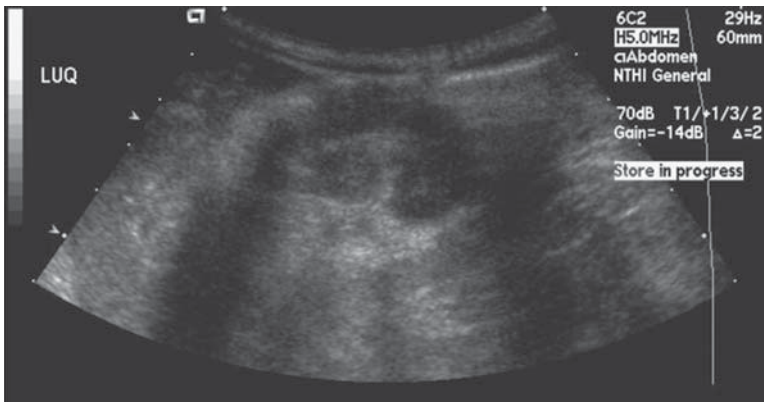


Fig. 309.1 **(A)** Plain radiograph of the abdomen demonstrates a meniscus of soft tissue projecting distally into the bowel lumen of the transverse colon within the left upper abdomen. **(B)** Sonographic evaluation through this region in the transverse plane reveals the bowel wall signature with central concentric rings of increased and decreased echotexture. **(C)** Longitudinal sonographic evaluation reveals a circumferential hypoechoic bowel wall with a central region of increased echotexture and distal bowel wall shadowing, an appearance referred to as the "pseudokidney" sign.

Clinical Presentation

A 3-year-old boy presents with severe intermittent abdominal pain and diarrhea (**Fig. 309.1**).

Key Imaging Finding

Intraluminal mass with bowel signature on ultrasound

Diagnosis

- **Intussusception.** Intussusception is a common and important cause of intestinal obstruction in children. The peak incidence occurs between 5 and 9 months of age, with nearly all idiopathic cases occurring before 3 years of age. More than 90% of cases are idiopathic with an antecedent viral infection. If intussusception occurs in a child older than 3 years of age, a pathologic lead point from entities such as lymphoma, Meckel diverticulum, and bowel hemorrhage (Henoch–Schönlein purpura) should be investigated.

  With regards to location, 90% of cases of intussusception are ileocolic, with the remainder either ileoileal or colocolic. The clinical symptoms include abdominal pain, vomiting, blood per rectum, a palpable abdominal mass, fever, and "currant jelly" stools. Differential diagnosis includes appendicitis and Meckel diverticulum.

  Plain radiographs demonstrate a meniscus of soft tissue protruding into the distal bowel lumen with the location dependent upon the type of intussusception. Most cases involve the cecum or ascending colon. On ultrasound, transverse images demonstrate alternating concentric rings of increased and decreased echotexture in a typical target appearance. Longitudinal scanning reveals a peripheral hypoechoic bowel wall with a central region of increased echotexture referred to as the "pseudokidney" sign.

  When intussusception is suspected based on imaging findings, a diagnostic and therapeutic examination such as an air enema may be performed. Air insufflation is performed via the rectum with a tight seal under fluoroscopic guidance, maintaining a pressure of <120 mm of mercury. Once reduced, air will reflux into the small bowel through the ileocecal valve. A follow-up film should demonstrate intraluminal bowel gas without free intraperitoneal air. Pediatric surgery should be readily available in the event of an adverse outcome during reduction, such as perforation, which occurs in <0.5% of cases. Contraindications to reduction include peritoneal signs on physical examination and free intraperitoneal air on imaging studies.

✓ Pearls

- Over 90% of cases of intussusception occur before 3 years of age and are idiopathic in nature.
- A pathologic lead point should be suspected in patients older than 3 years of age.
- Imaging findings include a meniscus of soft tissue on plain films and target and pseudokidney signs on ultrasound.
- When using the air reduction technique, pressures should not exceed 120 mm of mercury.

Suggested Readings

Applegate KE. Clinically suspected intussusception in children: evidence-based review and self-assessment module. AJR Am J Roentgenol 2005; 185(3, Suppl)S175–S183

Donnelly LF. Fundamentals of Pediatric Radiology. Philadelphia: WB Saunders; 2001

Case 310

Grant E. Lattin Jr.

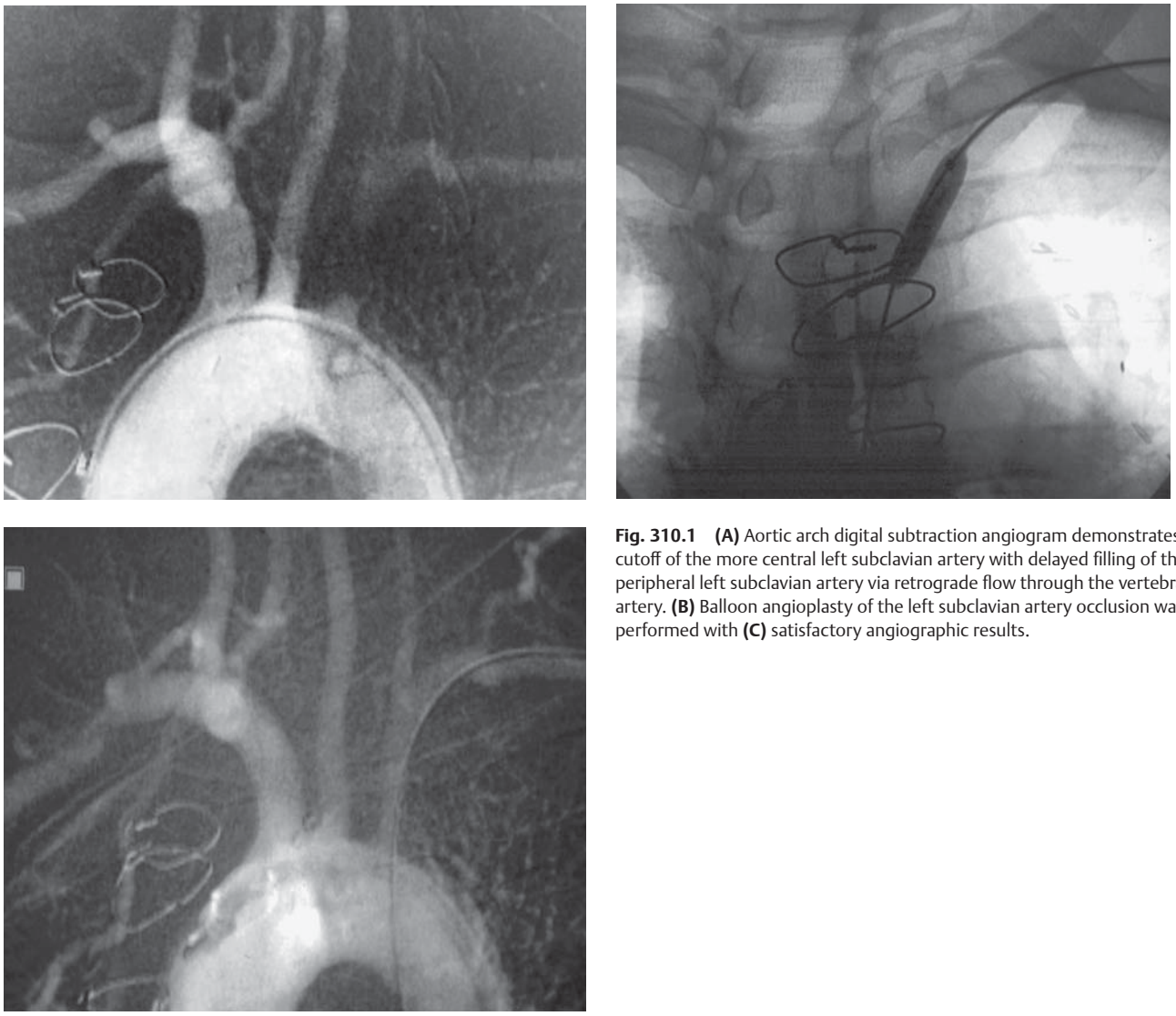


Fig. 310.1 **(A)** Aortic arch digital subtraction angiogram demonstrates cutoff of the more central left subclavian artery with delayed filling of the peripheral left subclavian artery via retrograde flow through the vertebral artery. **(B)** Balloon angioplasty of the left subclavian artery occlusion was performed with **(C)** satisfactory angiographic results.

Clinical Presentation

A 60-year-old man experiences vertebrobasilar symptoms with exercise (**Fig. 310.1**).

Key Imaging Finding

Left subclavian artery occlusion with retrograde filling distally from the vertebral artery

Diagnosis

- **Subclavian steal.** Subclavian steal is a phenomenon that occurs secondary to subclavian artery stenosis or occlusion central to the origin of the vertebral artery. The distal subclavian arterial supply comes from retrograde flow via the vertebral artery. Subclavian steal most commonly occurs secondary to atherosclerotic disease in elderly men, although other congenital and acquired etiologies do exist. Patients may be asymptomatic, have decreased blood pressure or a weak pulse in the affected arm, or experience vertebrobasilar symptoms, often associated with exercise of the upper extremity.

  Conventional angiography shows cutoff or stenosis of the subclavian artery with lack of antegrade opacification within the vertebral artery, followed by delayed retrograde filling of the distal subclavian artery via the vertebral artery. Computed tomography may show an area of stenosis, but associated calcification may be obscured by contrast or streak artifact. Magnetic resonance (MR) phase contrast imaging will display flow reversal in the vertebral artery. Gadolinium MR angiography will also demonstrate the area of stenosis. Duplex ultrasound of the ipsilateral vertebral artery may show complete reversal of flow, although diminished peak systolic velocities may be an early sign. Additionally, markedly increased contralateral vertebral artery peak systolic flow or a parvus-tardus waveform in the peripheral ipsilateral subclavian artery may support the diagnosis, especially following exercise of the upper extremity.

  Treatment options include endovascular balloon angioplasty with possible stent placement and surgery. Surgical options include a common carotid or innominate artery to subclavian artery bypass, depending on the anatomical location of the lesion.

✓ Pearls

- Subclavian steal is characterized by proximal stenosis/occlusion and distal filling via the vertebral artery.
- Patients commonly present with vertebrobasilar insufficiency when exercising the affected arm.
- MR phase contrast imaging will show flow reversal within the ipsilateral vertebral artery.
- Treatment options include angioplasty with possible stent placement versus surgical bypass procedures.

Suggested Readings

Henry M, Amor M, Henry I, Ethevenot G, Tzvetanov K, Chati Z. Percutaneous transluminal angioplasty of the subclavian arteries. J Endovasc Surg 1999;6(1):33–41

Kliewer MA, Hertzberg BS, Kim DH, Bowie JD, Courneya DL, Carroll BA. Vertebral artery Doppler waveform changes indicating subclavian steal physiology. AJR Am J Roentgenol 2000;174(3):815–819

Sueoka BL. Percutaneous transluminal stent placement to treat subclavian steal syndrome. J Vasc Interv Radiol 1996;7(3):351–356

Case 311

Jeffrey P. Tan

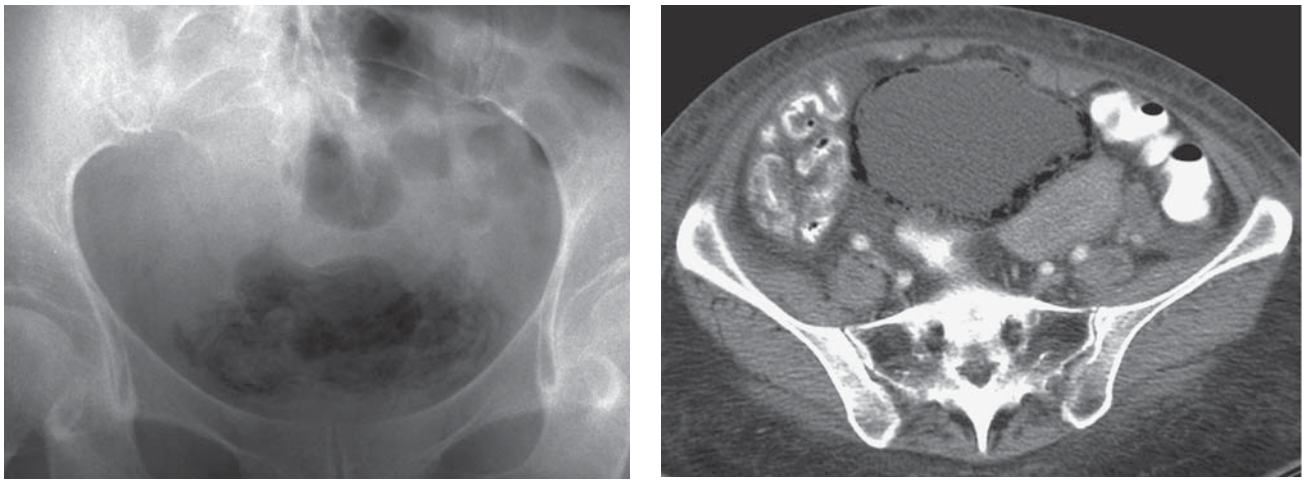


Fig. 311.1 **(A)** Anteroposterior radiograph of the pelvis reveals several small linear areas of lucency projecting over the bladder, distinct from gas within the rectum. **(B)** Contrast-enhanced axial computed tomography image through the pelvis reveals multiple foci of gas within the bladder wall.

Clinical Presentation

A 63-year-old woman presents with dysuria and pelvic pain (**Fig. 311.1**).

Key Imaging Finding

Gas within the bladder wall

Diagnosis

- **Emphysematous cystitis.** Emphysematous cystitis is an inflammatory condition characterized by gas in the bladder mucosa and underlying muscular tissue. This condition is most commonly identified in middle-aged diabetic women. Other predisposing conditions include neurogenic bladder, recurrent urinary tract infections, and urinary stasis from bladder outlet obstruction.

  Clinical presentation is variable, ranging from asymptomatic to dysuria, pneumaturia, or abdominal pain with sepsis. The infection is usually caused by a gas-forming organism. The most common bacterial infection is *Escherichia coli* followed by *Klebsiella pneumoniae*, *Pseudomonas aeruginosa*, and *Proteus mirabilis.* Noninfectious causes may include bladder instrumentation, vesicocolic or vesicovaginal fistulas, and trauma.

  Management of emphysematous cystitis is primarily medical. Therapy may include antibiotics, bladder drainage, and correction of hyperglycemia and any other comorbid conditions. Evaluation with computed tomography (CT) is useful to assess for perforation, fistula, abscess, or emphysematous pyelonephritis. The latter condition is an important entity to exclude, as the mortality for emphysematous pyelonephritis has been reported to be >50% as opposed to 7% for emphysematous cystitis. Management of emphysematous pyelonephritis typically requires surgical intervention.

✓ Pearls

- Emphysematous cystitis is characterized by gas within the bladder wall and is typically managed medically.
- Emphysematous cystitis most commonly occurs in older diabetic women.
- *E. coli* is the most common infectious organism.
- CT is useful in evaluating for potential complications, such as perforation or emphysematous pyelonephritis.

Suggested Readings

Grayson DE, Abbott RM, Levy AD, Sherman PM. Emphysematous infections of the abdomen and pelvis: a pictorial review. Radiographics 2002;22(3):543–561

Thomas AA, Lane BR, Thomas AZ, Remer EM, Campbell SC, Shoskes DA. Emphysematous cystitis: a review of 135 cases. BJU Int 2007;100(1):17–20

Case 312

Grant E. Lattin Jr.

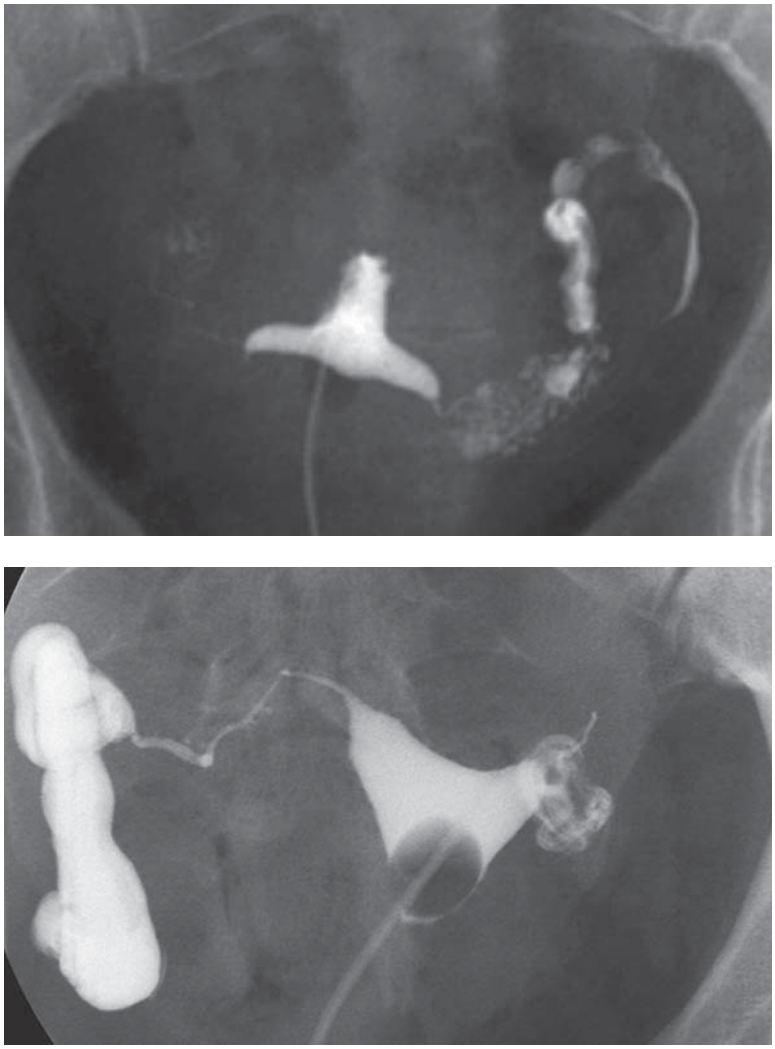


Fig. 312.1 **(A)** Early image from a hysterosalpingogram (HSG) demonstrates multiple small diverticula confined to the isthmic portion of the left fallopian tube and occlusion of the right fallopian tube. **(B)** HSG image from a different patient with the same disease process reveals fallopian tube diverticula, as well as resultant right hydrosalpinx.

Clinical Presentation

Two young women with infertility (**Fig. 312.1**).

Key Imaging Finding

Multiple small diverticula affecting the proximal portion of the fallopian tube

Diagnosis

- **Salpingitis isthmica nodosa (SIN).** SIN, or tubal diverticulosis, is a condition that affects the proximal fallopian tubes and is often associated with prior inflammation and pelvic infection. This condition is characterized by multiple small diverticula seen extending from the isthmus of the fallopian tube. Infertility and tubal pregnancy are known associations. Hydrosalpinx is a common secondary finding.

  Hysterosalpingography is the imaging modality that will best assist in making this diagnosis. Often SIN is diagnosed while the patient is undergoing a comprehensive workup for infertility. Although classic imaging findings are diagnostic of SIN, tubal endometriosis or tuberculosis may have thickening or irregularity of the isthmus as well. Usually, tubal endometriosis will have isthmic thickening with a somewhat honeycombed appearance, whereas tuberculous salpingitis may have calcifications within the wall.

  Treatment for infertility associated with SIN may include fallopian tube microcatheter recanalization prior to other options, such as tubal microsurgery or in vitro fertilization.

✓ Pearls

- SIN is characterized by multiple small diverticula confined to the proximal portion of the fallopian tube.
- Associations may include previous pelvic infection, infertility, and tubal pregnancy.
- Fallopian tube microcatheter recanalization may assist in reversing the patient's infertility.

Suggested Readings

Creasy JL, Clark RL, Cuttino JT, Groff TR. Salpingitis isthmica nodosa: radiologic and clinical correlates. Radiology 1985;154(3):597–600

Thurmond AS, Burry KA, Novy MJ. Salpingitis isthmica nodosa: results of transcervical fluoroscopic catheter recanalization. Fertil Steril 1995;63(4):715–722

Case 313

Grant E. Lattin Jr.

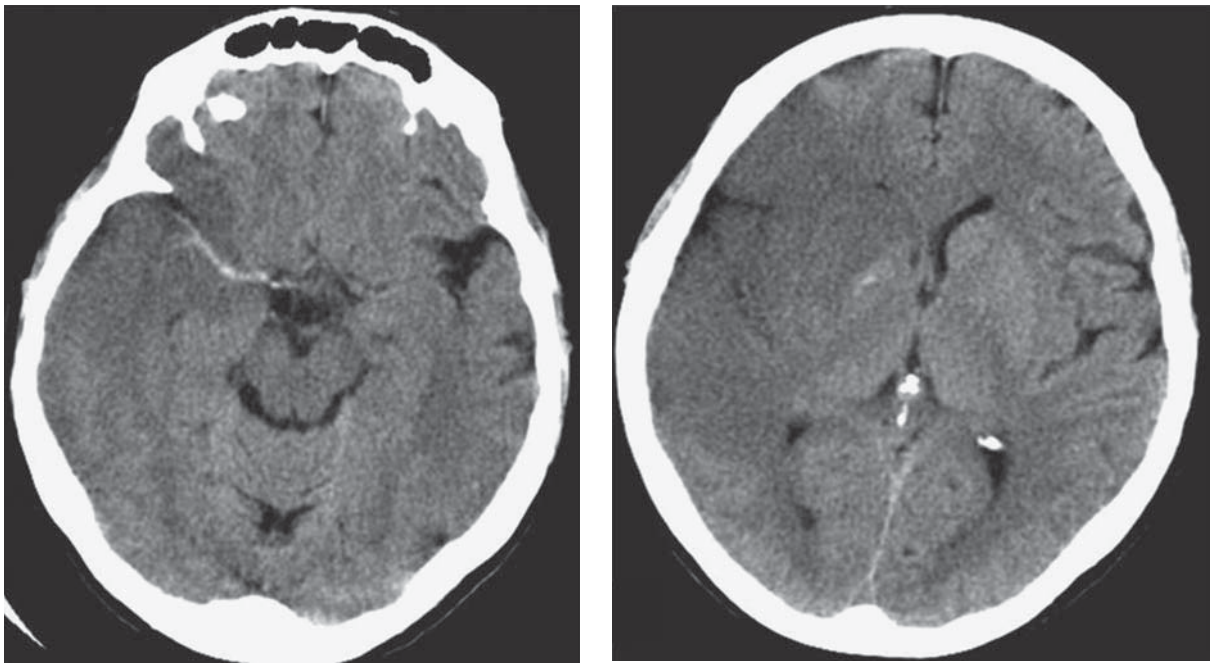


Fig. 313.1 **(A,B)** Axial computed tomography images of the head without contrast demonstrate a hyperdense right middle cerebral artery with a region of hypoattenuation affecting the majority of the right middle cerebral artery vascular distribution. Sulcal effacement, loss of the gray-white matter differentiation, and mass effect on the right lateral ventricular horn are also present.

Clinical Presentation

A 62-year-old man presents with left-sided weakness (**Fig. 313.1**).

Key Imaging Finding

Hyperdense middle cerebral artery (MCA) (with additional findings consistent with infarction)

Diagnosis

- **Middle cerebral artery distribution cerebral infarction.** Cerebral infarction is the result of loss of blood flow to the brain parenchyma, often associated with atherosclerosis or thromboembolic disease in older adults. An early sign of ischemia/infarction that has high specificity but low sensitivity is a hyperdense vessel, commonly the M1 segment of the MCA, also referred to as the "dense MCA" sign. More peripheral branches may display a focus of hyperattenuation described as the "dot" sign.

  Computed tomography findings of stroke also include loss of the cortical ribbon (gray-white matter junction) within the first 3 hours, subsequent parenchymal hypoattenuation, and sulcal effacement with gyral swelling within 12 to 24 hours. Hemorrhagic transformation may also occur at 24 to 48 hours. Acute strokes are hyperintense on diffusion-weighted imaging with corresponding low signal on the apparent diffusion coefficient (ADC) map. This pattern remains from minutes after the infarction begins to ~10 days following. Diffusion-weighted imaging sequences can be obtained very quickly in less than a minute.

  Acute treatment may include intravenous (IV) or catheter-directed intra-arterial fibrinolytic therapy within 3 or 6 hours of symptom onset, respectively, in appropriate nonhemorrhagic acute strokes. Mechanical clot retrieval devices may also be a treatment option.

✓ Pearls

- The "dense MCA" sign or MCA "dot" is an early, highly specific marker of acute ischemia.
- DWI-weighted magnetic resonance imaging and ADC map can confirm an acute ischemic event.
- IV or catheter-directed intra-arterial thrombolysis are possible treatment options in specific clinical settings.

Suggested Readings

Barber PA, Demchuk AM, Hudon ME, Pexman JH, Hill MD, Buchan AM. Hyperdense sylvian fissure MCA "dot" sign: A CT marker of acute ischemia. Stroke 2001;32(1):84–88

Bourekas EC, Slivka AP, Shah R, Sunshine J, Suarez JI. Intraarterial thrombolytic therapy within 3 hours of the onset of stroke. Neurosurgery 2004;54(1):39–44, discussion 44–46

Leary MC, Kidwell CS, Villablanca JP, et al. Validation of computed tomographic middle cerebral artery "dot"sign: an angiographic correlation study. Stroke 2003;34(11):2636–2640

Case 314

Grant E. Lattin Jr.

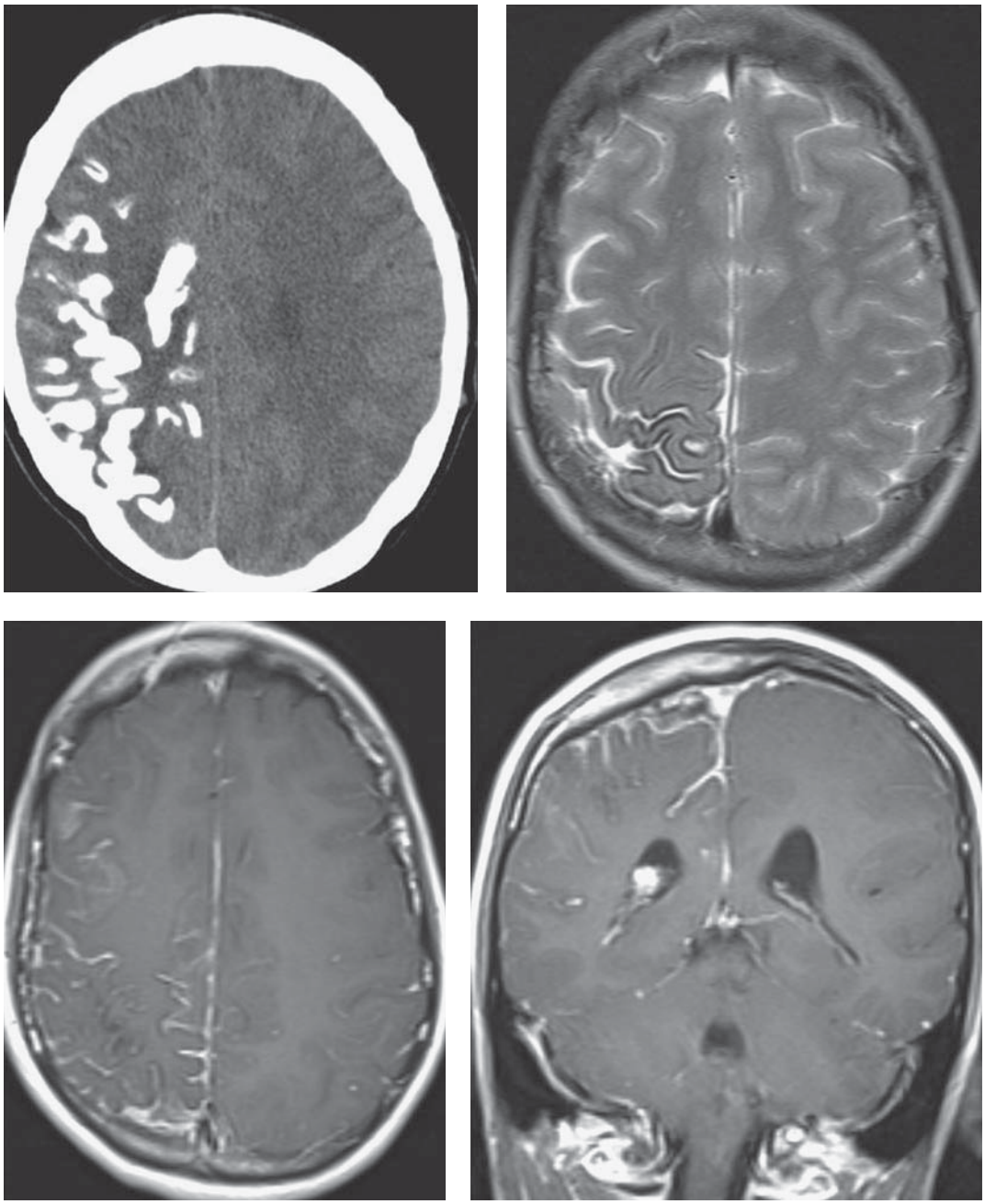


Fig. 314.1 **(A)** Axial noncontrast computed tomography image of the head demonstrates "tram track" cortical calcifications and underlying parenchymal atrophy primarily along the right frontal and parietal lobes. **(B)** Axial T2-weighted image shows linear hypointensity in a similar distribution. **(C)** Axial and **(D)** coronal postgadolinium T1-weighted images demonstrate pial enhancement involving predominantly the right parietal and frontal lobes, with underlying parenchymal atrophy and enlargement of the ipsilateral choroid plexus.

Clinical Presentation

A pediatric patient presents with seizures (**Fig. 314.1**).

Key Imaging Finding

"Tram track" calcifications, pial angiomatosis, and cerebral parenchymal atrophy

Diagnosis

- **Sturge–Weber syndrome.** Sturge–Weber syndrome or encephalotrigeminal angiomatosis is a phakomatosis that commonly presents with a nevus flammeus (port-wine stain) in the ophthalmic distribution of the fifth cranial nerve and seizures within the first year of life. This syndrome is due to a congenital malformation of fetal cortical veins/pial angiomatosis, which leads to chronic venous ischemia and subsequent gyriform calcifications. Choroidal angiomas also occur, leading to glaucoma.

  Computed tomography findings typically are characterized by "tram track" cortical calcifications that proceed from posterior to anterior. Associated parenchymal atrophy is common, and ipsilateral choroid plexus enlargement is also frequently seen. Late findings may include ipsilateral calvarial thickening and enlargement of the paranasal sinuses, as can be seen in Dyke–Davidoff–Masson syndrome.

  Magnetic resonance imaging will show the leptomeningeal enhancement due to pial angiomatosis most effectively, with parenchymal atrophy as well. Venous occlusion may progress with associated areas of ischemia or infarction. Magnetic resonance venography may show decreased superficial cortical veins with increased deep medullary collaterals.

  Treatment includes management of the seizure activity with possible resection of the affected cerebral lobes. Facial nevi may be treated with laser therapy.

✓ Pearls

- Sturge–Weber syndrome is characterized by a facial nevus flammeus, pial angiomatosis, and seizures.
- Imaging findings include cortical calcifications, parenchymal atrophy, and leptomeningeal enhancement.

Suggested Readings

Akpinar E. The tram-track sign: cortical calcifications. Radiology 2004;231(2):515–516

Lin DD, Barker PB, Kraut MA, et al. Early characteristics of Sturge–Weber syndrome shown by perfusion MR imaging and proton MR spectroscopic imaging. AJNR Am J Neuroradiol 2003;24:1912–1915

Smirniotopoulos JG, Murphy FM. The phakomatoses. AJNR Am J Neuroradiol 1992;13(2):725–746

Case 315

Grant E. Lattin Jr.

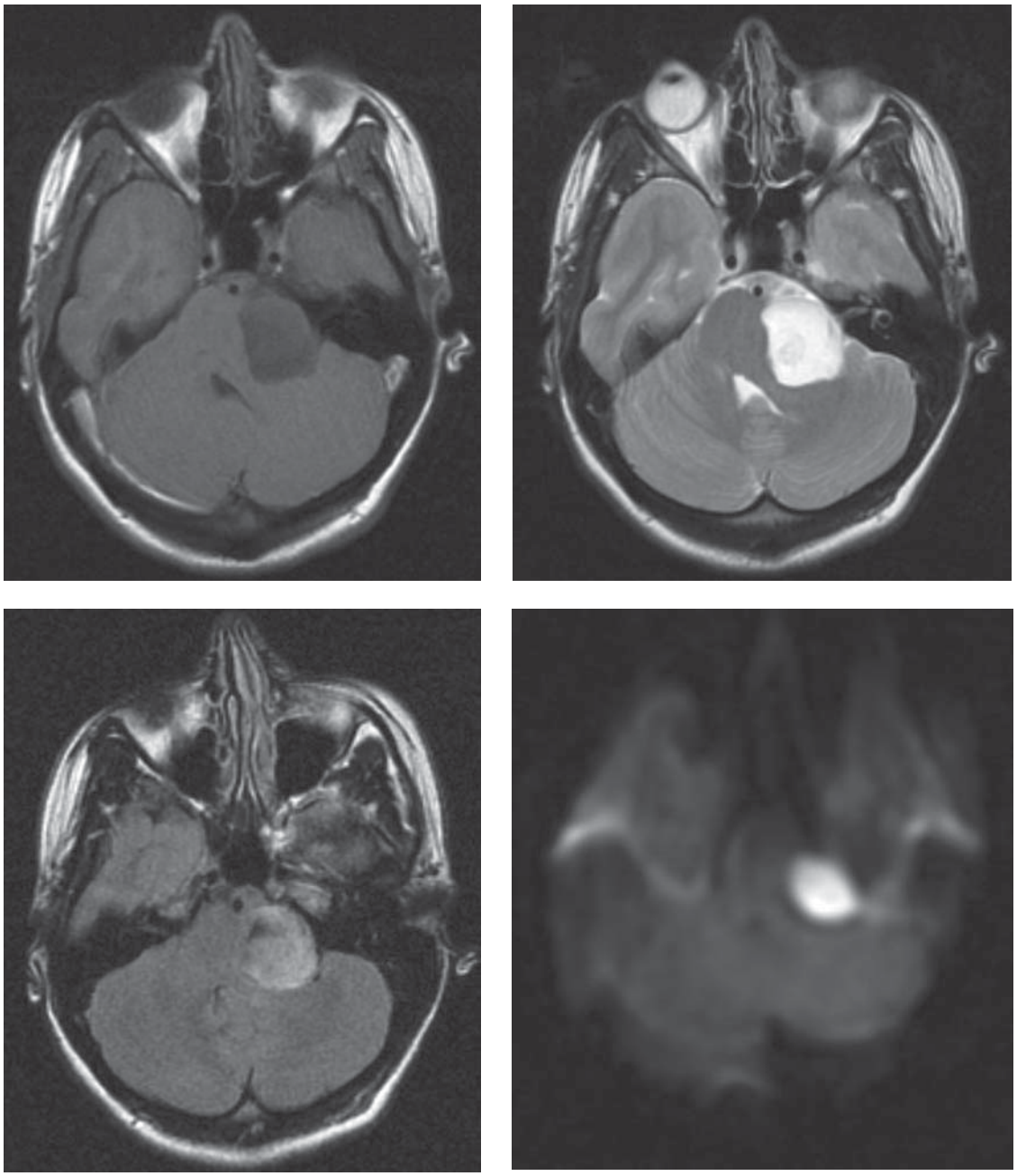


Fig. 315.1 **(A)** Axial T1- and **(B)** T2-weighted images demonstrate a left cerebellopontine angle mass that is isointense to slightly hyperintense to cerebrospinal fluid signal. **(C)** Fluid-attenuated inversion recovery imaging demonstrates mixed signal intensity without complete signal loss. **(D)** On diffusion-weighted imaging, there is restricted diffusion characterized by increased signal.

Clinical Presentation

A 23-year-old woman presents with headache (**Fig. 315.1**).

Key Imaging Finding

Left cerebellopontine angle (CPA) mass with similar signal to cerebrospinal fluid (CSF) and restricted diffusion on diffusion-weighted imaging

Diagnosis

- **Epidermoid.** Epidermoid tumor is the third most common CPA cisternal mass, with vestibular schwannomas and meningiomas being the two most common. Epidermoids contain epithelial elements due to inclusion during neural tube closure. They account for 1% of all intracranial tumors and occur most frequently between the ages of 20 and 40, with an equal distribution between men and women. Symptoms are usually minor.

  Classically, epidermoids occur in the posterior fossa, most commonly at the CPA, with an insinuating appearance. Unlike other CPA masses, such as arachnoid cysts, epidermoids engulf cranial nerves and vessels rather than displacing them. Their margins are scalloped and irregular, and occasionally they may be invasive. On computed tomography, epidermoids are isodense to CSF. Peripheral enhancement may occur. Calcification is seen in ~20% of cases.

  On T1-weighted imaging, epidermoids are isointense to slightly hyperintense to CSF, resulting in the descriptor "dirty CSF." On T2-weighted imaging, they are isointense to hyperintense to CSF. Peripheral enhancement can sometimes be seen. Mixed signal on fluid-attenuated inversion recovery (FLAIR) images and diffusion restriction (hyperintense on diffusion-weighted imaging) essentially confirm the diagnosis of epidermoid.

  Considering only the T1- and T2-weighted signal characteristics, an arachnoid cyst would still be within the differential diagnosis. However, an arachnoid cyst will follow CSF on all pulse sequences with low signal on T1- and high signal on T2-weighted imaging. Also, FLAIR images of an arachnoid cyst will show signal isointense to CSF, and there should be no restricted diffusion on diffusion-weighted imaging.

  Complete tumor removal is the surgical goal, with smaller lesions having better postoperative results.

✓ Pearls

- Epidermoids most commonly occur at the CPA; they are the third most common CPA mass.
- Epidermoids have similar signal to CSF on T1- and T2-weighted imaging; they are hyperintense to CSF on FLAIR.
- Restricted diffusion is the key differentiating characteristic of epidermoids.
- Epidermoids engulf vessels, rather than displace them, as is seen with arachnoid cysts.

Suggested Readings

Bonneville F, Sarrazin JL, Marsot-Dupuch K, et al. Unusual lesions of the cerebellopontine angle: a segmental approach. Radiographics 2001;21(2):419–438

Dutt SN, Mirza S, Chavda SV, Irving RM. Radiologic differentiation of intracranial epidermoids from arachnoid cysts. Otol Neurotol 2002;23(1):84–92

Case 316

Grant E. Lattin Jr.

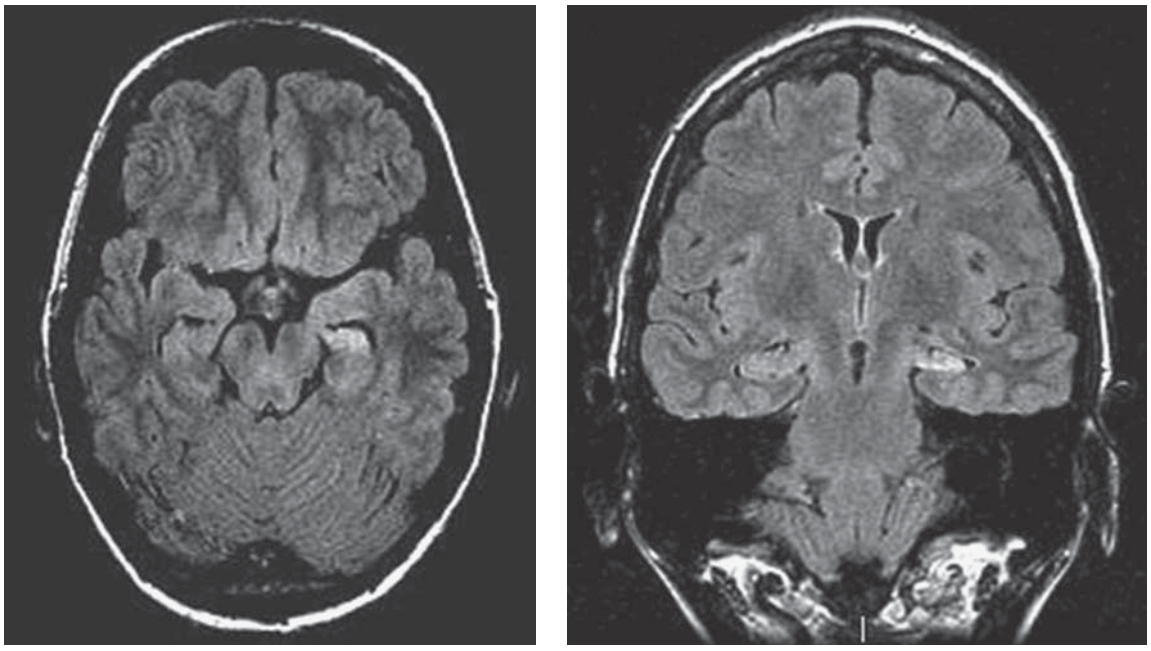


Fig. 316.1 **(A)** Axial and **(B)** coronal fluid-attenuated inversion recovery images demonstrate abnormal increased signal intensity and associated atrophy within the left mesial temporal lobe. There was no associated mass or abnormal enhancement on contrast-enhanced images (not shown). (Courtesy of Robert Luken, MD, University of Cincinnati.)

Clinical Presentation

A 23-year-old man presents with complex partial seizures (**Fig. 316.1**).

Key Imaging Finding

Atrophy and increased T2-weighted signal intensity of the mesial temporal lobe

Diagnosis

- **Mesial temporal sclerosis (MTS).** MTS is a condition that typically affects children and young adults, resulting in complex partial seizures. It is thought to represent the most common identifiable cause of temporal lobe seizures. Debate exists as to whether the etiology is acquired or developmental.

  Magnetic resonance imaging is the mainstay in the work-up of seizure disorders; computed tomography is often normal. Atrophy of the mesial temporal lobe is present along with hyperintensity on prolonged T2 sequences, most commonly affecting the hippocampus. Coronal, high-resolution T2-weighted sequences of the temporal lobes are often helpful in evaluation. Magnetic resonance spectroscopy shows decreased n-acetyl-aspartate in the affected temporal lobe and may be helpful in localizing certain cases. Decreased radiopharmaceutical activity is seen in the affected lobe on 18F-fluorodeoxyglucose positron emission tomography.

  Medical treatment is successful in only ~25% of cases of MTS. Anterior temporal lobe resection is often necessary for persistent seizure activity.

✓ Pearls

- MTS is thought to represent the most common identifiable cause of temporal lobe seizures.
- MTS is characterized by atrophy and increased T2/ fluid-attenuated inversion recovery signal intensity within the hippocampus.

Suggested Readings

Bocti C, Robitaille Y, Diadori P, et al. The pathological basis of temporal lobe epilepsy in childhood. Neurology 2003;60(2):191–195

Castillo M, Smith JK, Kwock L. Proton MR spectroscopy in patients with acute temporal lobe seizures. AJNR Am J Neuroradiol 2001;22(1):152–157

Case 317

Grant E. Lattin Jr.

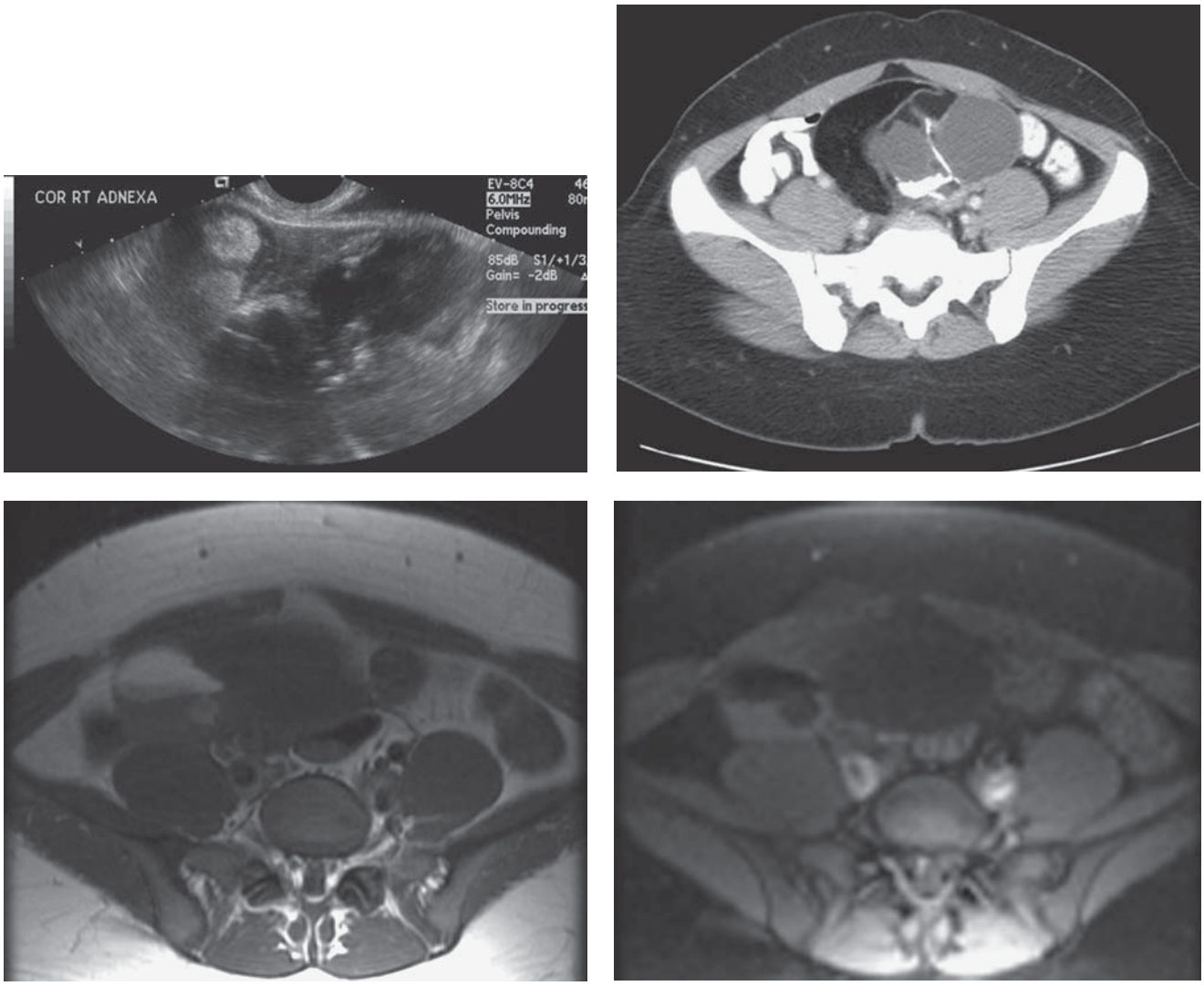


Fig. 317.1 **(A)** Endovaginal ultrasound image through the pelvis demonstrates a partially hyperechoic cystic mass that has posterior shadowing and adjacent specular reflectors, consistent with the "tip of the iceberg" sign. **(B)** Axial computed tomography image through the pelvis confirms a multiloculated cystic midline mass, which contains calcium and macroscopic fat. Findings are consistent with an ovarian dermoid originating from the left ovary. **(C)** Axial T1 and **(D)** T2 fat-suppressed images in the same patient demonstrate a smaller right ovarian cystic mass with macroscopic fat, also consistent with an ovarian dermoid.

Clinical Presentation

A 25-year-old woman presents with pelvic fullness (**Fig. 317.1**).

Key Imaging Finding

Ovarian cystic mass with the "tip of the iceberg" sign and macroscopic fat

Diagnosis

- **Ovarian dermoid.** Ovarian dermoid or teratoma is the most common benign ovarian tumor of young women. Occasionally, the dermoids may be bilateral, which is an extremely important finding if surgical excision is contemplated. Often these tumors are incidentally found, but they may become more symptomatic, especially as they increase in size.

  Classically, the ovarian dermoid appears as a cystic adnexal mass with a shadowing hyperechoic component by ultrasound. A hyperechoic nodule that projects into the lumen of the mass is known as a Rokitansky or dermoid plug. An echogenic component with posterior shadowing is known as the "tip of the iceberg" sign. However, if central linear or dotlike echogenic reflectors are present, then the term *dermoid mesh* is applicable. Based on ultrasound findings alone, the initial differential diagnosis may include an endometrioma, a hemorrhagic cyst, or a pedunculated lipoleiomyoma.

  Noncontrast computed tomography (CT) or magnetic resonance imaging (MRI) confirms the diagnosis by identifying the presence of macroscopic fat within the lesion. Commonly, teeth or calcifications may also be present, allowing the diagnosis to be suggested on radiographs. T1-weighted fat saturation techniques confirm the presence of fat as opposed to hemorrhage, which may also be hyperintense on T1-weighted images but will not suppress.

  Treatment for smaller dermoids is often nonsurgical, given their slow growth. Lesions >6 cm are usually excised due to the increased risk of ovarian torsion. A small portion (2%) of dermoids may also develop malignant degeneration later in life, usually in the 6th or 7th decade.

✓ Pearls

- Dermoids are the most common benign ovarian tumor in young women.
- Characteristic ultrasound findings include the Rokitansky plug and "tip of the iceberg" sign.
- The presence of fat on CT or MRI confirms the diagnosis of an ovarian dermoid.
- Larger dermoids (>6 cm) are excised due to the increased risk of ovarian torsion.

Suggested Readings

Hurwitz JL, Fenton A, McCluggage WG, McKenna S. Squamous cell carcinoma arising in a dermoid cyst of the ovary: a case series. BJOG 2007;114(10):1283–1287

Jung SE, Lee JM, Rha SE, Byun JY, Jung JI, Hahn ST. CT and MR imaging of ovarian tumors with emphasis on differential diagnosis. Radiographics 2002;22(6):1305–1325

Rim SY, Kim SM, Choi HS. Malignant transformation of ovarian mature cystic teratoma. Int J Gynecol Cancer 2006;16(1):140–144

Case 318

Grant E. Lattin Jr.

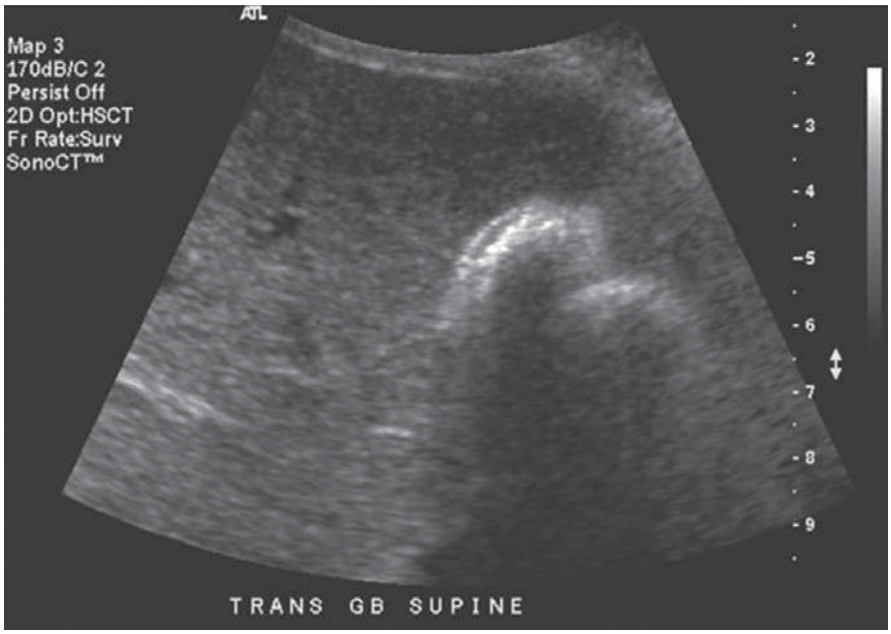


Fig. 318.1 Sonographic image of the gallbladder demonstrates the gallbladder wall (linear hyperechoic focus) with a second thin curvilinear hyperechoic focus just deep to this and posterior acoustic shadowing. The appearance of two curvilinear echogenic lines with an intervening area of decreased echotexture is commonly described as the "wall-echo-shadow" sign.

Clinical Presentation

A 47-year-old woman presents with right upper quadrant pain (**Fig. 318.1**).

Key Imaging Finding

Wall-echo-shadow (WES) sign

Diagnosis

- **Cholelithiasis.** The WES sign is characterized by two curvilinear echogenic lines created by the gallbladder wall and a gallbladder lumen filled with stones. These hyperechoic foci are separated by an intervening sonolucent region of bile within the gallbladder lumen. The gallstones cause posterior acoustic shadowing.

  Gallstones commonly present in women in their 40s with right upper quadrant discomfort following a fatty meal. The evaluation of gallstones is best performed by ultrasound. Decubitus imaging should be performed to look for mobility, as impacted stones may result in concurrent cholecystitis. Likewise, the common bile duct should be imaged as well to exclude choledocholithiasis. Ultrasound findings that may indicate associated cholecystitis include pericholecystic fluid, a gallbladder wall measuring >3 mm in diameter, and a sonographic Murphy sign.

  Computed tomography (CT) is less sensitive than ultrasound in the evaluation of gallstones. T2-weighted magnetic resonance imaging will show the stones as areas of signal void surrounded by hyperintense bile. Hepatobiliary scintigraphy may be of benefit if concern exists for an obstructing stone, and ultrasound findings are equivocal for cholecystitis.

  Although the WES sign is classic for cholelithiasis, care should be taken to exclude potential mimickers, such as emphysematous cholecystitis and porcelain gallbladder. Emphysematous cholecystitis presents with gas within the gallbladder wall and associated "dirty" posterior shadowing, as opposed to the "clean" shadowing seen with calcifications. Porcelain gallbladder is characterized by calcification within the gallbladder wall with posterior shadowing. Because the calcification is within the wall and not the gallbladder lumen, there is absence of the second hyperechoic focus that makes up the WES sign. If uncertain, CT will help evaluate for gas or calcifications within the gallbladder wall.

  Treatment of cholelithiasis may be conservative if asymptomatic. If symptomatic, surgical removal of the gallbladder is usually performed.

✓ Pearls

- The WES sign is caused by a gallbladder lumen full of gallstones.
- Ultrasound is more sensitive than CT in the evaluation of gallbladder pathology.
- Exclude mimickers of the WES sign, such as emphysematous cholecystitis and porcelain gallbladder.

Suggested Readings

Bortoff GA, Chen MY, Ott DJ, Wolfman NT, Routh WD. Gallbladder stones: imaging and intervention. Radiographics 2000;20(3):751–766

Rosenthal SJ, Cox GG, Wetzel LH, Batnitzky S. Pitfalls and differential diagnosis in biliary sonography. Radiographics 1990;10(2):285–311

Case 319

Grant E. Lattin Jr.

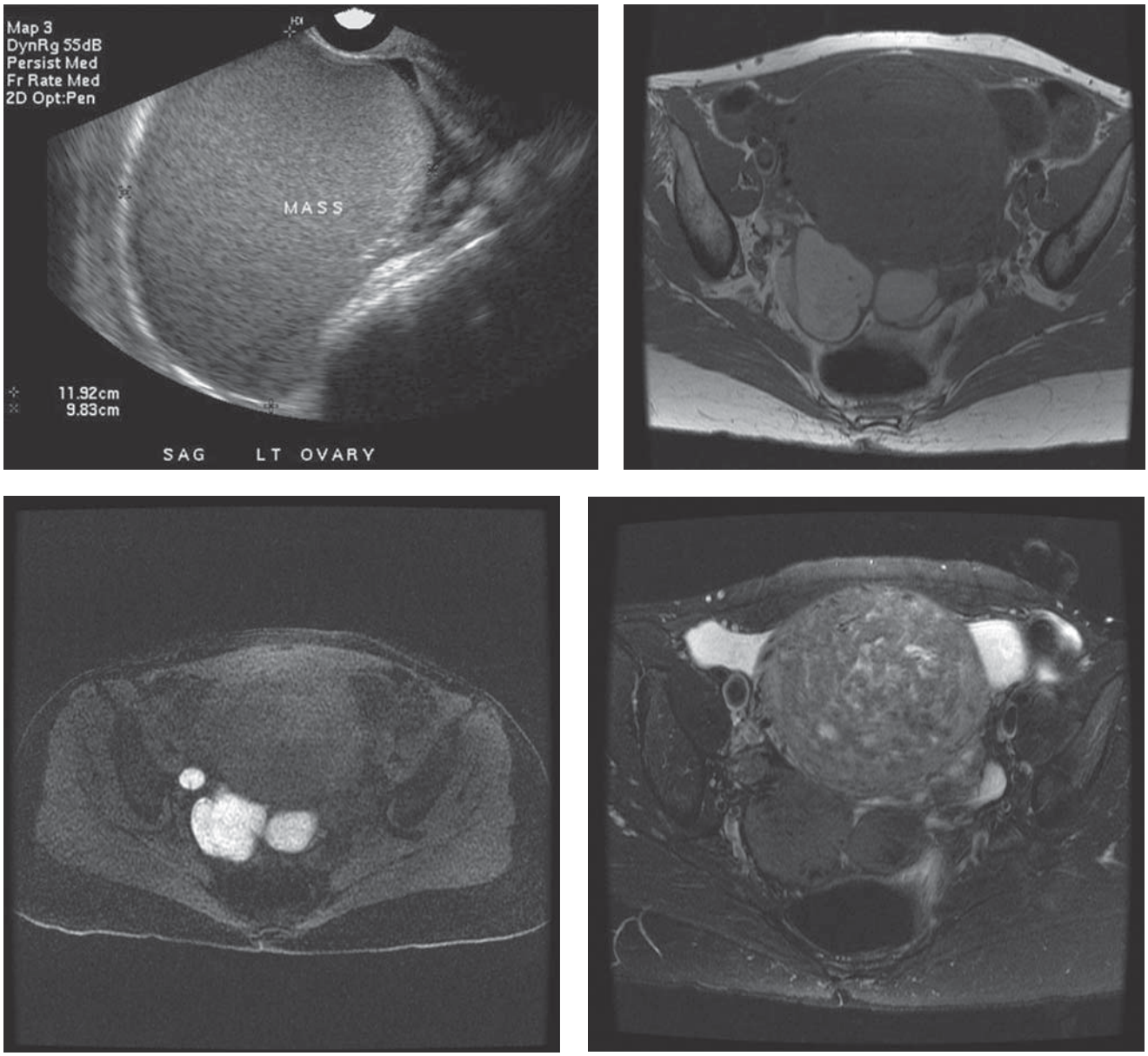


Fig. 319.1 **(A)** Sonographic image of the left ovary demonstrates a homogeneous mass with low-level internal echoes and increased through transmission, suggestive of a "chocolate cyst" appearance. **(B,C)** T1-weighted images of the pelvis in the second patient show T1 hyperintense masses posterior to the uterus that remain hyperintense with fat suppression. **(D)** These same foci demonstrate T2 "shading" or hypointensity on T2-weighted imaging. Secondary findings of adenomyosis are noted in the second patient.

Clinical Presentation

Two young women present with pelvic pain. **Fig. 319.1A** is of the first patient, and images in **Fig. 319.1B–D** are of the second patient.

Key Imaging Finding

Adnexal mass with increased through transmission and homogeneous low-level echoes.

Diagnosis

- **Endometrioma.** Endometriomas are cysts that contain functioning endometrium outside the uterus, resulting in contained cyclical hemorrhage. Endometriomas are seen within the spectrum of endometriosis and are associated with infertility and pelvic pain. Commonly, they may be multiple and are found in the ovaries and throughout the pelvis.

  When unilocular with homogeneous low-level echoes centrally, ultrasound findings are essentially diagnostic. Peripheral echogenic foci within the wall of such a mass are also suggestive of endometrioma. However, endometriomas with features such as true nodularity, fluid–fluid levels, and dense calcifications may be less clear. Magnetic resonance imaging (MRI) may then be useful to differentiate between an endometrioma and other ovarian masses, such as hemorrhagic cysts, teratomas (dermoids), and ovarian cystic neoplasms.

  On MRI, endometriomas appear T1 hyperintense (secondary to hemorrhage), which may increase in conspicuity with fat suppression. Conversely, a teratoma (dermoid) would decrease in signal intensity with fat suppression. On T2-weighted imaging, endometriomas will appear hypointense, an appearance sometimes referred to as T2 "shading," which can vary in degree of decreased intensity. Thick septations and nodularity should raise the suspicion of an ovarian cystic neoplasm, especially if unilateral.

  Treatment options include medical management or varying degrees of surgery, depending on the patient's desire for fertility. With time, the symptoms associated with endometriosis will often dissipate with menopause.

✓ Pearls

- Endometriomas are a form of endometriosis and commonly present with pain and occasionally infertility.
- Classic ultrasound findings of endometrioma are homogeneous low-level echoes and through transmission.
- MRI findings include T1 hyperintensity (secondary to hemorrhage) and T2 shading.

Suggested Readings

Alborzi S, Zarei A, Alborzi S, Alborzi M. Management of ovarian endometrioma. Clin Obstet Gynecol 2006;49(3):480–491

Woodward PJ, Sohaey R, Mezzetti TP, Jr. Endometriosis: radiologic-pathologic correlation. Radiographics 2001;21(1):193–216, 288–294

Case 320

Michael A. Mahlon

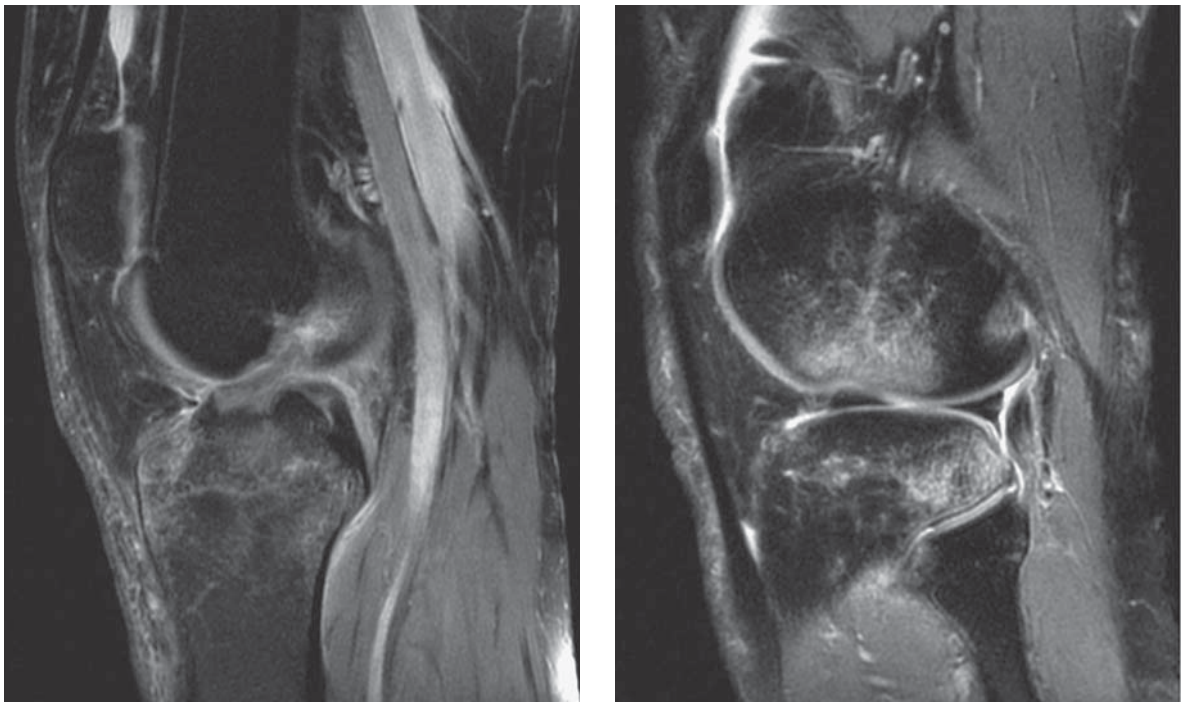


Fig. 320.1 **(A)** Fat-saturated sagittal T2weighted image of the knee reveals high signal intensity within and disruption of the anterior cruciate ligament. **(B)** Another image from the same sequence demonstrates "kissing contusions" of the lateral femoral condyle and proximal tibia. A deep lateral femoral sulcus, anterior translation of the tibia, and a small suprapatellar effusion are also seen.

Clinical Presentation

A 26-year-old man presents with knee pain following a loud pop while exercising (**Fig. 320.1**).

Key Imaging Finding

Disruption of the anterior cruciate ligament (ACL) with "kissing contusions"

Diagnosis

- **Anterior cruciate ligament tear.** The ACL attaches to the inner aspect of the lateral femoral condyle proximally and fans out to attach to the anterior aspect of the intercondylar eminence of the tibia distally. It runs from the femur to the tibia anteriorly, medially, and inferiorly within the intercondylar notch. It is intra-articular and extrasynovial throughout its course. The primary role of the ACL is to provide stability to the knee joint. It resists anterior translocation and internal rotation of the tibia over the femur. The ACL also limits hyperextension and both valgus and varus forces on the knee.

  Most ACL tears (~70%) occur in the middle aspect of the ligament, 20% occur proximally near its origin, and only 10% occur distally at the tibial attachment. Primary signs of an ACL tear include nonvisualization, focal or diffuse increased T2 signal intensity within the ligament, focal discontinuity, acute angulation, and a wavy contour of the ligament.

  Secondary signs of an ACL tear are a joint effusion, "kissing contusions" involving the lateral femoral condyle and lateral tibia, an angle between the lateral tibial plateau and the ACL <45 degrees, posterior displacement of the lateral meniscus >3.5 mm, anterior displacement of the tibia >7 mm, and a lateral femoral sulcus deeper than 1.5 mm. Coexisting internal derangements of the knee that may occur with an ACL tear include medial collateral ligament tears, posterolateral corner injuries, meniscal tears, cartilage damage, lateral tibial plateau fractures (Segond fracture), posterior cruciate ligament tears, and extensor mechanism injuries.

✓ Pearls

- ACL tears present as increased signal, abnormal contour, or discontinuity of the ligament.
- "Kissing contusions," anterior tibial displacement, and the deep sulcus sign are secondary indications of ACL injury.
- ACL tears are associated with internal derangement of other ligaments, menisci, cartilage, and fractures.

Suggested Readings

Gentili A, Seeger LL, Yao L, Do HM. Anterior cruciate ligament tear: indirect signs at MR imaging. Radiology 1994;193(3):835–840

Hall FM. Radiographic features of anterior cruciate ligament tear. Radiology 2002;222(2):576

Tung GA, Davis LM, Wiggins ME, Fadale PD. Tears of the anterior cruciate ligament: primary and secondary signs at MR imaging. Radiology 1993;188(3):661–667

Case 321

Michael A. Mahlon

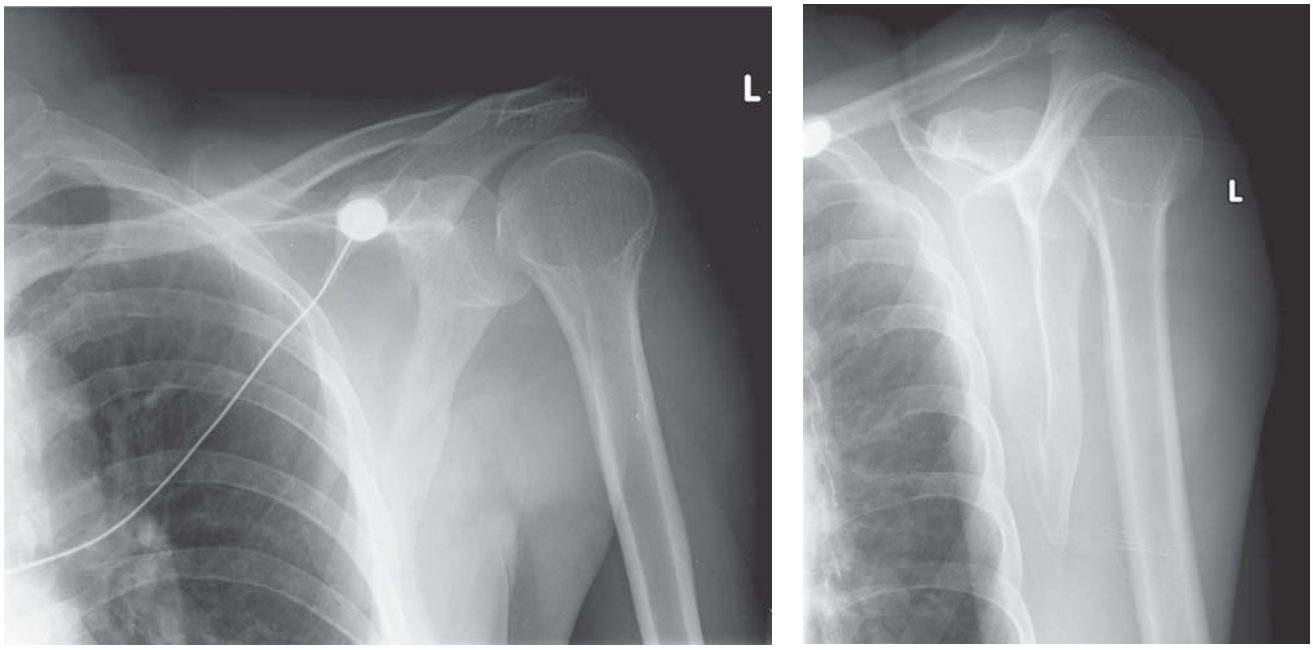


Fig. 321.1 **(A)** Anteroposterior view of the shoulder reveals a high-riding humeral head in relation to the glenoid, with linear sclerosis and a cortical cleft of the medial humeral head, consistent with a "trough line" sign. **(B)** Scapular Y view shows posterior displacement of the humeral head in relation to the glenoid. On both views, the humeral head is fixed in internal rotation, referred to as the "lightbulb" sign.

Clinical Presentation

A 35-year-old man presents with left shoulder pain (**Fig. 321.1**).

Key Imaging Finding

Posterior displacement and fixed internal rotation of the humeral head

Diagnosis

- **Posterior dislocation of the shoulder.** Posterior shoulder dislocation accounts for <5% of all shoulder dislocations. Acute traumatic posterior shoulder dislocation most commonly results from axial loading of the adducted internally rotated arm, as can be seen in convulsive seizures, violent muscle contraction, or electric shock. Posterior dislocations are clinically apparent ~95% of the time.

  Radiographically, the anteroposterior (AP) view may show a focus of linear sclerosis paralleling the medial border of the humeral head, known as the "trough line" sign. In a patient without a dislocation, the humeral head should overlap the glenoid on the AP view, forming what has been described as a "crescent" or "half moon" sign. In patients with posterior shoulder dislocations, this overlap is usually absent. A "rim" sign may also be identified on the AP view. This sign is present when the distance from the anterior glenoid rim to the medial humeral head measures >6 mm. To diagnose a posterior dislocation, a scapular Y or axillary view of the shoulder should be obtained, although the axillary view may be difficult to obtain, as patients may experience pain with abduction. On all views, the humeral head is commonly fixed in internal rotation, resulting in a "lightbulb" appearance of the humeral head.

  Associated injuries of the shoulder include reverse Hill–Sachs lesions, reverse Bankart lesions, avulsed posterior labrum injuries with posterior labrocapsular periosteal sleeve avulsion, rotator cuff tears, dislocation of the biceps tendon, intra-articular loose bodies, and impaction fractures of the humerus and glenoid. These injuries are often better appreciated on magnetic resonance imaging (MRI).

✓ Pearls

- Findings of posterior dislocation include the "trough line" sign, "rim" sign, and loss of the "crescent" sign.
- The humeral head is fixed in internal rotation with posterior dislocation, referred to as the "lightbulb" sign.
- Scapular Y and axillary views are helpful in confirming posterior dislocation radiographically.
- MRI is useful in evaluating for associated injuries of the shoulder.

Suggested Readings

Brant WE, Helms CA. Fundamentals of Diagnostic Radiology. Philadelphia: Lippincott Williams & Wilkins; 1999

Saupe N, White LM, Bleakney R, et al. Acute traumatic posterior shoulder dislocation: MR findings. Radiology 2008;248(1):185–193

Case 322

Michael A. Mahlon

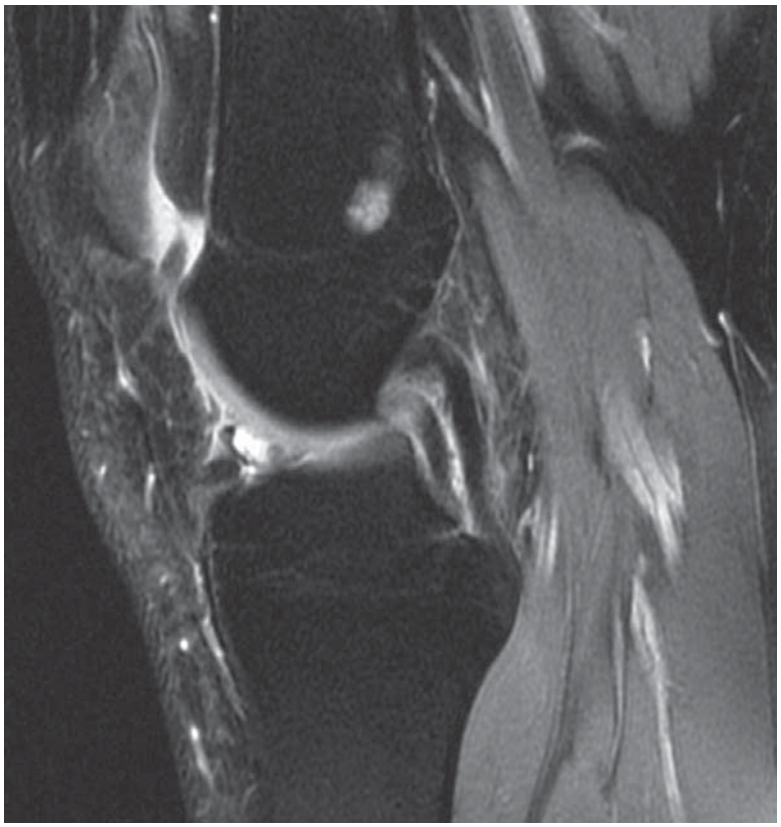


Fig. 322.1 Sagittal fat-saturated T2-weighted image reveals a crescent-shaped, linear, low-signal structure anterior to and paralleling the posterior cruciate ligament (PCL), referred to as the double PCL sign, along with a small joint effusion.

Clinical Presentation

A 31-year-old woman presents with knee pain after injury (**Fig. 322.1**).

Key Imaging Finding

Double posterior cruciate ligament (PCL) sign

Diagnosis

- **"Bucket handle" tear of the medial meniscus.** The double PCL sign is associated with a so-called bucket handle tear of the medial meniscus that occurs in the presence of an intact anterior cruciate ligament (ACL). A bucket handle tear is a longitudinal tear of a meniscus that results in a displaced but attached meniscal fragment. The fragment may become displaced into the notch between the PCL and the medial tibial eminence along the midline, with the fragment orientated parallel to the PCL. The intact ACL serves as a barrier that prevents further lateral displacement of the meniscal fragment.

  Because ligaments and menisci demonstrate a hypointense signal on all pulse sequences, the displaced fragment will mimic a second PCL that is anterior and inferior to the true ligament; hence the term *double PCL sign*. The double PCL sign remains a highly specific indicator of a bucket handle tear, with a specificity range of 98 to 100% and a positive predictive value of ~93%. A potential pitfall of the double PCL sign is the presence of an anterior meniscofemoral ligament, which is known as the ligament of Humphrey, and the oblique meniscomeniscal ligament, a normal variant.

  Bucket handle tears involve the medial meniscus more commonly than the lateral meniscus by a ratio of ~2:1. Displaced bucket handle tears can cause substantial symptoms, including knee locking or a lack of full extension. Arthroscopy is required to excise or reattach the free fragment.

✓ Pearls

- Double PCL sign occurs when there is a bucket handle medial meniscal tear with an intact ACL.
- Potential mimickers include the ligament of Humphrey and the oblique meniscomeniscal ligament.

Suggested Readings

Camacho MA. The double posterior cruciate ligament sign. Radiology 2004;233(2):503–504

Watt AJ, Halliday T, Raby N. The value of the absent bow tie sign in MRI of bucket-handle tears. Clin Radiol 2000;55(8):622–626

Weiss KL, Morehouse HT, Levy IM. Sagittal MR images of the knee: a low-signal band parallel to the posterior cruciate ligament caused by a displaced bucket-handle tear. AJR Am J Roentgenol 1991;156(1):117–119

Wright DH, De Smet AA, Norris M. Bucket-handle tears of the medial and lateral menisci of the knee: value of MR imaging in detecting displaced fragments. AJR Am J Roentgenol 1995;165(3):621–625

Case 323

Jeffrey P. Tan

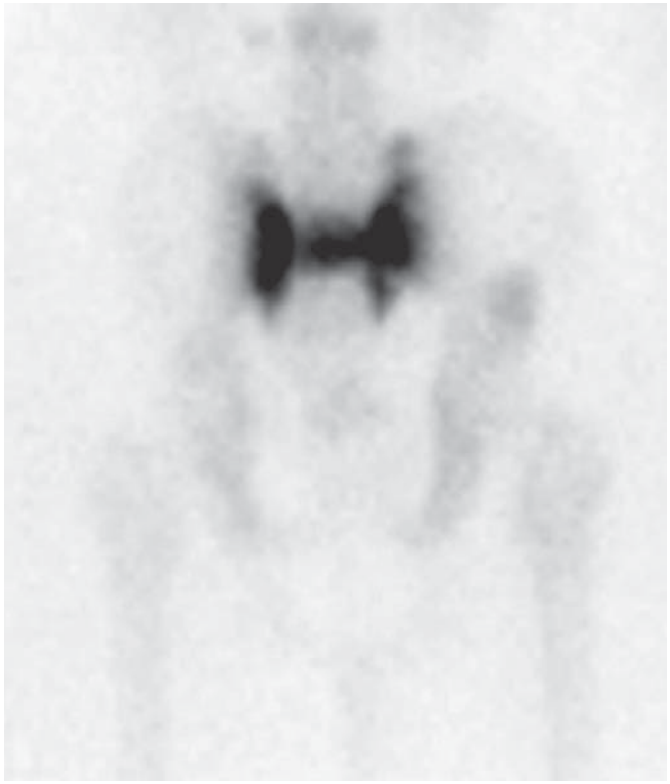


Fig. 323.1 Planar image over the pelvis from a technetium 99m hydroxymethylene diphosphonate bone scan reveals intense uptake within the sacrum in an H-shaped configuration.

Clinical Presentation

A 64-year-old woman presents with low back pain (**Fig. 323.1**).

Key Imaging Finding

Intense sacral uptake in an H-shaped configuration on a bone scan

Diagnosis

- **Sacral insufficiency fracture.** Sacral insufficiency fractures are due to normal stresses on weakened bone. Most commonly, these occur in elderly women with osteoporosis. Other predisposing factors are rheumatoid arthritis, chronic corticosteroid use, and pelvic radiation therapy. Clinical symptoms typically include low back pain, which is exacerbated by movement, with radiation to the hip or groin. There may be point tenderness over the sacrum.

  On nuclear medicine imaging, the classic findings include uptake vertically along the sacral alae bilaterally with a transverse line between them in an H configuration, which resembles the Honda symbol. It is therefore referred to as the Honda sign. Other variants of the Honda sign are the half butterfly pattern, in which the superior aspects of the vertical lines are absent; the bar pattern, in which the transverse line is thickened; and the tramline pattern, in which the transverse component of the H is absent.

  Evaluation with conventional radiography may demonstrate the lucent fracture line, cortical disruption, or sclerotic bands; however, it is usually limited by overlying bowel gas. Computed tomography may demonstrate the fracture lines or sclerosis with greater sensitivity. Magnetic resonance imaging (MRI) may reveal a T1 hypointense fracture line with increased T2 signal intensity in the marrow from underlying edema from the sacral insufficiency fracture. In addition, MRI is useful in evaluating for an underlying neoplastic process.

  Management of sacral insufficiency fractures consists of rest, analgesia, antiinflammatory therapy, limited weight bearing, and physical therapy.

✓ Pearls

- Sacral insufficiency fractures are usually due to osteoporosis.
- On a bone scan, there is a typical H-shaped configuration, known as the Honda sign.
- It is important to consider MRI in the evaluation of an underlying neoplastic process.

Suggested Readings

Blake SP, Connors AM. Sacral insufficiency fracture. Br J Radiol 2004;77(922):891–896

Fujii M, Abe K, Hayashi K, et al. Honda sign and variants in patients suspected of having a sacral insufficiency fracture. Clin Nucl Med 2005;30(3):165–169

White JH, Hague C, Nicolaou S, Gee R, Marchinkow LO, Munk PL. Imaging of sacral fractures. Clin Radiol 2003;58(12):914–921

Case 324

Jeffrey P. Tan

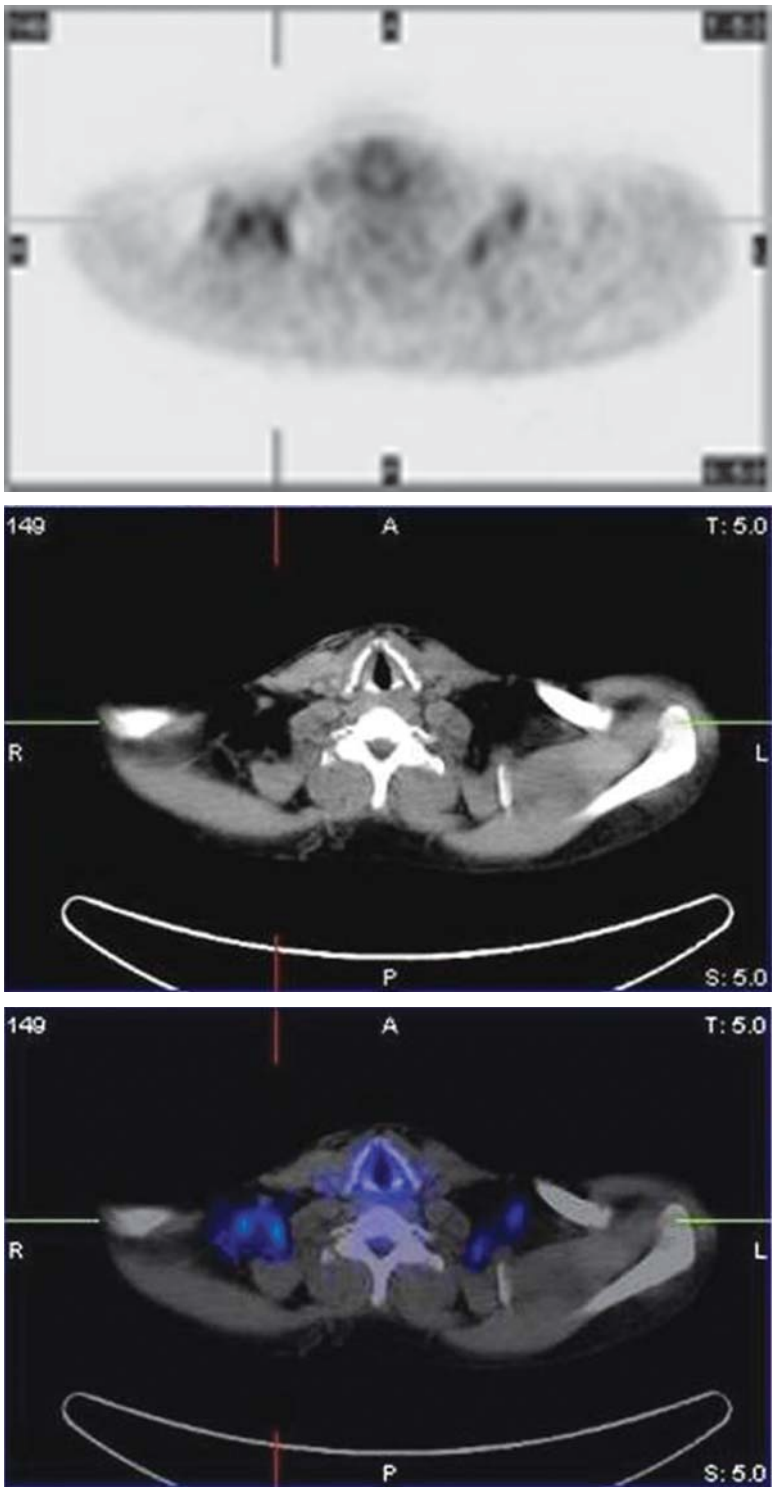


Fig. 324.1 **(A)** 18F-fluorodeoxyglucose positron emission tomography (PET) image demonstrates bilateral symmetric uptake in the supraclavicular soft tissues. **(B)** Noncontrast axial computed tomography (CT) scan of the same region reveals primarily fat within the supraclavicular soft tissues. **(C)** PET/CT fusion image confirms uptake in regions of fat tissue.

Clinical Presentation

A 52-year-old woman presents with a history of lymphoma (**Fig. 324.1**).

Key Imaging Finding

18F-fluorodeoxyglucose (FDG) uptake in supraclavicular fat

Diagnosis

- **Brown fat.** There are two types of adipose tissue in the human body: white and brown. White adipose, or white fat, is the primary type of adipose tissue that is used as energy storage. In contrast, brown adipose, or brown fat, is metabolically active and is used to generate heat. Brown fat is found in abundance in newborns and decreases with aging. The most common location of brown fat is within the supraclavicular soft tissues. Other typical locations are the neck, axilla, perivascular regions in the chest, perinephric spaces, intercostal spaces, along the spine, and in the para-aortic regions.

  Brown fat contains a mitochondrial protein that causes the uncoupling of oxidative phosphorylation. This results in heat generation instead of the production of adenosine triphosphate. Brown fat is active primarily in cold conditions and during food ingestion. Although glucose is not the primary source of energy for brown fat, during cold conditions, there is increased uptake of glucose in brown fat. When FDG positron emission tomography (PET) imaging is used, brown fat may increase its glucose metabolism, which results in uptake of FDG. With the advent of combined PET/computed tomography (CT) scanners, fusion imaging can demonstrate that regions of uptake correlate to fat tissue. It is important to exclude other causes of uptake, such as metastatic lymph nodes, primary neoplasms such as lymphoma, and inflammatory lesions.

✓ Pearls

- Brown fat is metabolically active with FDG PET imaging.
- The most common locations of brown fat are the supraclavicular soft tissues.
- PET/CT fusion images can confirm uptake within fat rather than a suspicious underlying lesion.

Suggested Readings

Cohade C, Osman M, Pannu HK, Wahl RL. Uptake in supraclavicular area fat ("USA-Fat"): description on 18F-FDG PET/CT. J Nucl Med 2003;44(2):170–176

Yeung HW, Grewal RK, Gonen M, Schöder H, Larson SM. Patterns of (18)F-FDG uptake in adipose tissue and muscle: a potential source of false-positives for PET. J Nucl Med 2003;44(11):1789–1796

Case 325

Grant E. Lattin Jr.

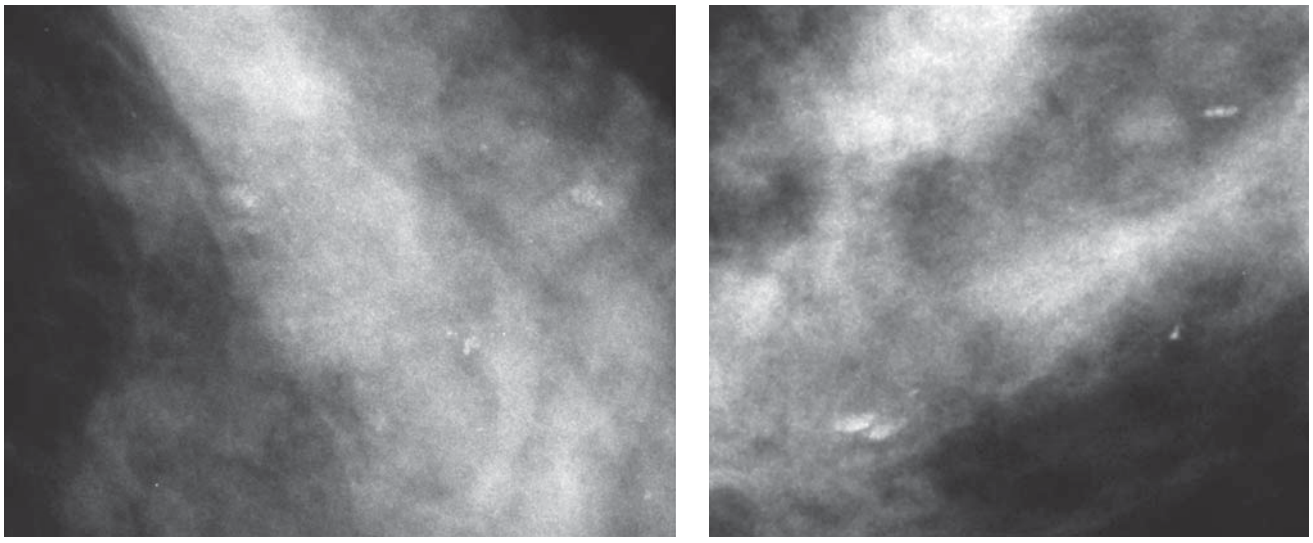


Fig. 325.1 **(A)** Coned-down magnified craniocaudal mammographic view reveals calcifications with a somewhat amorphous appearance. **(B)** A subsequent horizontal beam magnification view shows that these calcifications are now more linear or crescentic in configuration, suggestive of a "teacup" appearance.

Clinical Presentation

A 43-year-old woman presents with amorphous calcifications on a mammogram (**Fig. 325.1**).

Key Imaging Finding

Amorphous calcifications on the craniocaudal (CC) view that appear crescentic on the lateral view

Diagnosis

- **Milk of calcium.** Milk of calcium is a descriptor used when calcium accumulates in benign cysts. Also referred to as sedimented calcium, the calcium appears smudgy or amorphous on CC mammographic views. Horizontal beam views will show these calcifications to have a crescentic or linear appearance secondary to layering within the cysts. This appearance is commonly referred to as a "teacup" configuration.

  Often, on the true lateral view, not all of the amorphous calcifications will change in morphology. In these cases, a prone pendent view can be obtained and may help to make the diagnosis. As the patient leans forward, gravity and patient positioning will help the sedimented calcium to change in morphology. This change in appearance will confirm the diagnosis of milk of calcium.

  Milk of calcium is a benign finding and requires no further work-up. However, care should be taken to identify any other suspicious calcifications that may exist adjacent to milk of calcium.

✓ Pearls

- Amorphous calcifications on CC views should be evaluated with magnification horizontal beam views.
- "Teacup" appearance on medial-lateral oblique or lateral views is diagnostic of milk of calcium, a benign finding.
- Prone pendent view may be helpful in identifying milk of calcium if unclear on traditional views.

Suggested Readings

American College of Radiology. Breast Imaging Reporting and Data System: BI-RADS, Mammography. 4th ed. Reston, VA: Author; 2003

Moy L, Slanetz PJ, Yeh ED, et al. The pendent view: an additional projection to confirm the diagnosis of milk of calcium. AJR Am J Roentgenol 2001;177(1):173–175

Appendix: Differential Diagnoses by Case

I Chest and Cardiac Imaging

1 Solitary pulmonary nodule

Top 3 diagnoses
- Granuloma
- Neoplasm (bronchogenic carcinoma or solitary metastasis)
- Hamartoma

Additional diagnostic considerations
- Round pneumonia (under 8)
- Arteriovenous malformation

2 Multiple pulmonary nodules

Top 3 diagnoses
- Metastatic disease
- Granulomatous disease (TB or fungal)
- Septic emboli

Additional diagnostic considerations
- Wegener disease
- Rheumatoid arthritis

3 Cavitary pulmonary nodule

Top 3 diagnoses
- Tuberculosis
- Fungal disease
- Squamous cell carcinoma (primary or metastatic)

Additional diagnostic considerations
- Pyogenic infection (pulmonary abscess, septic emboli)
- Wegener disease
- Rheumatoid arthritis

4 Miliary pulmonary nodules

Top 3 diagnoses
- Tuberculosis
- Fungal disease
- Metastatic disease

Additional diagnostic considerations
- Pneumoconioses
- Healed varicella

5 Centrilobular pulmonary nodules

Top 3 diagnoses
- Infectious bronchiolitis (MAC, TB)
- Hypersensitivity pneumonitis
- Endobronchial spread of tumor

Additional diagnostic considerations
- Respiratory bronchiolitis associated interstitial lung disease
- Pneumoconioses

6 Cystic lung disease

Top 3 diagnoses
- Emphysema
- Lymphangioleiomyomatosis
- Langerhans cell histiocytosis

Additional diagnostic considerations
- Pneumocystis pneumonia
- Lymphocytic interstitial pneumonitis

7 Lower lobe interstitial disease

Top 3 diagnoses
- Idiopathic pulmonary fibrosis/Usual interstitial pneumonia
- Collagen vascular disease (scleroderma)
- Asbestos-related lung disease

Additional diagnostic considerations
- Drug toxicity

8 Upper lobe interstitial disease

Top 3 diagnoses
- Tuberculosis
- Sarcoidosis
- Cystic fibrosis

Additional diagnostic considerations
- Pneumoconioses
- Langerhans cell histiocytosis

9 Hyperlucent lung

Top 3 diagnoses
- Chest wall abnormality (mastectomy, Poland syndrome)
- Swyer-James syndrome
- Acute asthmatic attack

Top 3 Diagnoses You Cannot Miss
- Airway obstruction
- Pulmonary embolism
- Pneumothorax

10 Anterior mediastinal mass

Top 3 diagnoses
- Lymphoma
- Thymic lesion
- Thyroid lesion

Additional diagnostic considerations
- Germ cell neoplasm

11 Middle mediastinal mass

Top 3 diagnoses
- Lymphadenopathy
- Vascular abnormality (aortic or pulmonary artery aneurysm)
- Congenital cyst (bronchogenic cyst)

Additional diagnostic considerations
- Hiatal hernia

12 Posterior mediastinal mass

Top 3 diagnoses
- Neurogenic tumor
- Lymphoma
- Developmental cyst (neuroenteric cyst)

Additional diagnostic considerations
- Extramedullary hematopoiesis
- Mediastinal hematoma

13 Chronic air space disease

Top 3 diagnoses
- Cryptogenic organizing pneumonia
- Pulmonary alveolar proteinosis
- Bronchioloalveolar cell carcinoma

Additional diagnostic considerations
- Chronic eosinophilic pneumonia
- Lipoid pneumonia

14 Peripheral air space disease

Top 3 diagnoses
- Cryptogenic organizing pneumonia
- Eosinophilic pneumonia
- Pulmonary Infarct

Additional diagnostic considerations
- Pulmonary contusion
- Alveolar sarcoidosis

15 Ground glass opacification

Top 3 diagnoses
- Pulmonary edema
- Atypical infection
- Pulmonary hemorrhage

Additional diagnostic considerations
- Acute respiratory distress syndrome
- Alveolar proteinosis
- Vasculitis

16 Mediastinal/Hilar lymphadenopathy

Top 3 diagnoses
- Infection
- Lymphoma
- Sarcoidosis

Additional diagnostic considerations
- Metastatic disease
- Pneumoconioses

17 Calcified pleural disease

Top 3 diagnoses
- Asbestos related pleural disease
- Fibrothorax (prior infection or hemorrhage)
- Iatrogenic (pleurodesis)

18 Bronchiectasis

Top 3 diagnoses
- Postinfectious (bacterial, TB, MAC)
- Cystic Fibrosis
- Allergic bronchopulmonary aspergillosis

Additional diagnostic considerations
- Obstructive lesion/mass
- Ciliary dyskinesia

19 Perilymphatic pulmonary nodules

Top 3 diagnoses
- Sarcoidosis
- Lymphangitic spread of tumor
- Pneumoconioses

Additional diagnostic considerations
- Lymphoproliferative disorder

20 Pleural-based mass

Top 3 diagnoses
- Pleural-based metastatic disease
- Empyema
- Mesothelioma

Additional diagnostic considerations
- Fibrous tumor of the pleura
- Fibrothorax

21 Parenchymal disease in an HIV patient

Top 3 diagnoses
- Pneumocystis pneumonia
- Tuberculosis
- Fungal infection

Additional diagnostic considerations
- Invasive aspergillosis
- Kaposi sarcoma
- Pulmonary lymphoma

22 Abnormal left ventricular contour

Top 3 diagnoses
- True left ventricular aneurysm
- False left ventricular aneurysm
- Pericardial cyst/mass

Additional diagnostic considerations
- Calcific pericarditis

23 Cardiac mass

Top 3 diagnoses
- Thrombus
- Metastatic disease
- Benign cardiac neoplasm (atrial myxoma, rhabdomyoma)

Additional diagnostic considerations
- Malignant cardiac neoplasm (sarcoma, lymphoma)

24 Delayed myocardial enhancement

Top 3 diagnoses
- Infarction/Scar
- Myocarditis
- Cardiac mass

Additional diagnostic considerations
- Infiltrative disease (granulomatous, amyloidosis)

25 Cardiac wall fatty deposition

Top 3 diagnoses
- Lipoma
- Lipomatous hypertrophy of the interatrial septum
- Arrhythmogenic right ventricular dysplasia

II Gastrointestinal Imaging

26 Dense liver

Top 3 diagnoses
- Iron deposition (hemosiderosis, hemochromatosis)
- Amiodarone therapy
- Glycogen storage disease

Additional diagnostic considerations
- Gold therapy
- Thoratrast

27 Nodular liver contour

Top 3 diagnoses
- Cirrhosis
- Treated metastatic disease
- Budd-Chiari syndrome

Additional diagnostic considerations
- Schistosoma japonicum
- Confluent hepatic fibrosis

28 Esophageal diverticulum

Top 3 diagnoses
- Proximal esophageal pulsion diverticulum (Zenker, Killian-Jamison)
- Distal esophageal pulsion diverticulum (epiphrenic)
- Midesophageal traction diverticulum

Additional diagnostic considerations
- Intramural pseudodiverticulosis

29 Solitary hypodense, hypovascular liver mass

Top 3 diagnoses
- Hepatic cyst
- Solitary metastasis
- Abscess

Additional diagnostic considerations
- Peripheral cholangiocarcinoma
- Biliary cystadenoma
- Hepatic laceration (trauma)

30 Multiple hypodense hepatic lesions

Top 3 diagnoses
- Hepatic cysts
- Metastatic disease
- Multiple hepatic abscesses

Additional diagnostic considerations
- Cholangiocarcinoma

31 Right upper quadrant cystic mass in a child

Top 3 diagnoses
- Choledochal anomaly
- Pancreatic pseudocyst
- GI duplication cyst/diverticulum

Additional diagnostic considerations
- Ovarian cystic lesion
- Mesenteric cyst

32 Esophageal submucosal masses/thickened folds

Top 3 diagnoses
- Varices
- Reflux esophagitis
- Varicoid esophageal carcinoma

Additional diagnostic considerations
- Lymphoma

33 Esophageal dilatation

Top 3 diagnoses
- Achalasia
- Scleroderma
- Esophageal/gastric carcinoma

Additional diagnostic considerations
- Esophagitis with stricture
- Post surgical changes (vagotomy)

34 Esophageal pseudodiverticuli

Top 3 diagnoses
- Reflux esophagitis
- Candida esophagitis
- Superficial spreading carcinoma

Additional diagnostic considerations
- Drug-induced esophagitis

35 Esophageal ulcers

Top 3 diagnoses
- Reflux esophagitis
- Viral esophagitis (CMV, HIV, HSV)
- Drug-induced esophagitis

Additional diagnostic considerations
- Caustic esophagitis
- Esophageal carcinoma

36 Solid pancreatic mass

Top 3 diagnoses
- Pancreatic adenocarcinoma
- Islet cell tumor
- Solid and papillary epithelial neoplasm

Additional diagnostic considerations
- Lymphoma
- Metastatic disease

37 Linitis plastica

Top 3 diagnoses
- Gastric carcinoma
- Metastatic disease
- Lymphoma

Additional diagnostic considerations
- Crohn disease

38 Gastric ulcer

Top 3 diagnoses
- Peptic ulcer disease
- Gastric carcinoma
- Lymphoma

Additional diagnostic considerations
- Metastatic disease
- Zollinger-Ellison syndrome

39 Gastric fold thickening

Top 3 diagnoses
- Hypertrophic gastritis
- Gastric carcinoma
- Lymphoma

Additional diagnostic considerations
- Metastatic disease
- Menetrier disease

40 Cecal mass

Top 3 diagnoses
- Appendicitis/appendiceal abscess
- Cecal/appendiceal carcinoma
- Mucocele of appendix

Additional diagnostic considerations
- Lymphoma
- Adnexal mass

41 Mesenteric mass

Top 3 diagnoses
- Metastatic disease
- Carcinoid tumor
- Desmoid tumor/Fibrosing mesenteritis

Additional diagnostic considerations
- Reactive lymphadenopathy (Tuberculosis, MAC, Whipple)
- Abdominal mesothelioma

42 Terminal ileal wall thickening

Top 3 diagnoses
- Inflammatory bowel disease
- Infection (bacterial, Tuberculosis)
- Lymphoma

Additional diagnostic considerations
- Ischemia
- Metastatic disease

43 Colonic wall thickening

Top 3 diagnoses
- Infectious colitis
- Inflammatory bowel disease
- Colon carcinoma

Additional diagnostic considerations
- Ischemic colitis

44 Small bowel wall thickening

Top 3 diagnoses
- Crohn disease
- Lymphoma
- Small bowel hemorrhage

Additional diagnostic considerations
- Metastatic disease
- Amyloidosis
- Whipple disease

45 Esophageal stricture

Top 3 Diagnoses for Short Segment Strictures
- Reflux esophagitis
- Drug-induced stricture
- Esophageal carcinoma

Top 3 Diagnoses for Long Segment Strictures
- Iatrogenic (nasogastric tube)
- Caustic ingestion
- Radiation changes

46 Small bowel dilatation

Top 3 diagnoses
- Small bowel obstruction
- Adynamic Ileus
- Celiac sprue

Additional diagnostic considerations
- Scleroderma

47 Cystic pancreatic mass

Top 3 diagnoses
- Pancreatic pseudocyst
- Mucinous cystadenoma
- Serous cystadenoma

Additional diagnostic considerations
- Intraductal papillary mucinous neoplasm
- Solid and papillary epithelial neoplasm

48 Hypervascular liver mass

Top 3 diagnoses
- Hemangioma
- Focal nodular hyperplasia
- Hepatocellular carcinoma (including the fibrolamellar variant)

Additional diagnostic considerations
- Hepatic adenoma
- Hypervascular metastatic disease

49 Multiple splenic masses

Top 3 diagnoses
- Metastatic disease
- Lymphoma/leukemia
- Microabscesses

Additional diagnostic considerations
- Granulomatous disease (TB, sarcoid)
- Multiple splenic infarcts

50 Intrahepatic biliary ductal strictures

Top 3 diagnoses
- Primary sclerosing cholangitis
- Ascending cholangitis
- Acquired immunodeficiency syndrome cholangiopathy

Additional diagnostic considerations
- Neoplasm (cholangiocarcinoma, Metastatic disease)
- Post-transplant arterial ischemia

III Genitourinary Imaging

51 Solid Renal Mass

Top 3 diagnoses
- Renal cell carcinoma
- Oncocytoma
- Angiomyolipoma

Additional diagnostic considerations
- Transitional cell carcinoma
- Lymphoma

52 Multiple bilateral renal masses

Top 3 diagnoses
- Lymphoma
- Renal infection
- Renal cell carcinoma

Additional diagnostic considerations
- Angiomyolipomas
- Metastatic disease

53 Cystic renal mass

Top 3 diagnoses
- Complex renal cyst
- Cystic neoplasm (RCC in adult; Wilms in child)
- Multilocular cystic nephroma

Additional diagnostic considerations
- Multicystic dysplastic kidney (focal)
- Abscess

54 Retroperitoneal mass

Top 3 diagnoses
- Retroperitoneal hemorrhage
- Lymphadenopathy
- Retroperitoneal abscess

Additional diagnostic considerations
- Retroperitoneal fibrosis
- Retroperitoneal sarcoma

55 Cortical nephrocalcinosis

Top 3 diagnoses
- Acute renal cortical necrosis
- Chronic glomerulonephritis
- Oxalosis

Additional diagnostic considerations
- Chronic transplant rejection
- Alport syndrome

56 Medullary nephrocalcinosis

Top 3 diagnoses
- Hypercalcemia
- Medullary sponge kidney
- Renal tubular acidosis (Type 1)

Additional diagnostic considerations
- Papillary necrosis (analgesic nephropathy)
- Furosemide (newborn)
- Tuberculosis

57 Striated nephrogram

Top 3 diagnoses
- Pyelonephritis
- Urinary obstruction
- Renal vein thrombosis

Additional diagnostic considerations
- Renal contusion
- Hypotension

58 Papillary necrosis

Top 3 diagnoses
- Diabetes
- Analgesic nephropathy
- Pyelonephritis (especially TB)

Additional diagnostic considerations
- Sickle cell anemia
- Urinary obstruction
- Renal vein thrombosis

59 Staghorn calculus

Top 3 diagnoses
- Xanthogranulomatous pyelonephritis
- Pyonephrosis with obstructing stone
- Calcified neoplasm (RCC, treated lymphoma)

60 Renal cortical defect

Top 3 diagnoses
- Reflux nephropathy
- Chronic pyelonephritis
- Renal infarct

Additional diagnostic considerations
- Vasculitis
- Partial nephrectomy

61 Renal pelvic mass

Top 3 diagnoses
- Transitional cell carcinoma
- Multilocular cystic nephroma
- Medullary carcinoma

Additional diagnostic considerations
- Renal cell carcinoma

62 Medial deviation of the ureters

Top 3 diagnoses
- Retroperitoneal fibrosis
- Psoas muscle hypertrophy
- Pelvic lipomatosis

Additional diagnostic considerations
- Postoperative changes (lymph node dissection)
- Retrocaval ureter (unilateral deviation)

63 Ureteral filling defect

Top 3 diagnoses
- Transitional cell carcinoma
- Radiolucent calculi
- Pyeloureteritis cystica

Additional diagnostic considerations
- Blood clot
- Fungus ball
- Metastatic disease

64 Renal migration anomalies

Top 3 diagnoses
- Horseshoe kidney
- Cross fused ectopia
- Ectopic kidney

Additional diagnostic considerations
- Renal duplication

65 Bladder filling defect

Top 3 diagnoses
- Transitional cell carcinoma
- Fungus ball
- Blood clot

Additional diagnostic considerations
- Radiolucent calculi
- Extrinsic compression

66 Bilateral renal cysts

Top 3 diagnoses
- Autosomal dominant polycystic kidney disease
- Endstage renal disease (hemodialysis)
- von Hippel-Lindau disease

Additional diagnostic considerations
- Tuberous sclerosis

67 Perinephric fluid collection

Top 3 diagnoses
- Perinephric hemorrhage
- Urine leak/urinary extravasation
- Pyelonephritis/perinephric infection

68 Pear-shaped bladder

Top 3 diagnoses
- Pelvic hematoma
- Lymphadenopathy
- Pelvic lipomatosis

Additional diagnostic considerations
- Psoas hypertrophy
- Iliac artery aneurysms

69 Prostate enlargement

Top 3 diagnoses
- Prostate adenocarcinoma
- Benign prostatic hypertrophy
- Prostatitis

70 Bladder rupture

Top 3 diagnoses
- Extraperitoneal bladder rupture
- Intraperitoneal bladder rupture
- Intra- and extraperitoneal bladder rupture

Additional diagnostic considerations
- Urethral injury

71 Bladder wall calcifications

Top 3 diagnoses
- Transitional cell carcinoma
- Schistosomiasis
- Cystitis (Cytoxin or radiation)

Additional diagnostic considerations
- Tuberculosis
- Urachal carcinoma

72 Adrenal mass

Top 3 diagnoses
- Adrenal adenoma
- Metastatic disease
- Hemorrhage

Additional diagnostic considerations
- Pheochromocytoma
- Adrenal myelolipoma
- Adrenal cortical carcinoma

73 Fatty retroperitoneal mass

Top 3 diagnoses
- Angiomyolipoma
- Adrenal myelolipoma
- Retroperitoneal liposarcoma

Additional diagnostic considerations
- Renal cell carcinoma

74 Dilated ureter

Top 3 diagnoses
- Ureteral obstruction
- Reflux
- Primary megaureter

Additional diagnostic considerations
- Prune-belly syndrome

75 Urethral stricture

Top 3 diagnoses
- Urethral trauma
- Postinfectious/Postinflammatory stricture
- Urethral carcinoma

IV Musculoskeletal Imaging

76 Multiple lytic foci

Top 3 diagnoses in an adult
- Metastatic disease
- Multiple myeloma
- Lymphoma

Top 3 diagnoses in a child
- Langerhans cell histiocytosis (in patient less than 30)
- Fibrous dysplasia
- Multifocal osteomyelitis

77 Sequestrum

Top 3 diagnoses
- Osteomyelitis
- Langerhans cell histiocytosis
- Osteoid osteoma

Additional diagnostic considerations
- Lymphoma
- Fibrosarcoma

78 Newborn periosteal reaction

Top 3 diagnoses
- Physiologic periosteal reaction
- Trauma
- Infection (osteomyelitis, TORCH, TB, syphilis)

Additional diagnostic considerations
- Prostaglandin therapy
- Caffey disease (infantile cortical hyperostosis)

79 Rugger jersey spine

Top 3 diagnoses
- Renal osteodystrophy
- Osteopetrosis
- Paget disease

Additional diagnostic considerations
- Metastatic disease
- Myelofibrosis

80 Sacroiliitis

Top 3 Diagnoses for bilateral symmetric disease
- Ankylosing spondylitis
- Inflammatory bowel disease
- Rheumatoid arthritis

Top 3 Diagnoses for unilateral or bilateral asymmetric disease
- Psoriatic or reactive arthopathy
- Osteoarthritis
- Septic arthritis

81 Proximal arthritis

Top 3 diagnoses
- Rheumatoid arthritis
- Crystalline arthropathy (CPPD, gout)
- Collagen vascular disease (SLE)

Additional diagnostic considerations
- Hemochromatosis
- Infection

82 Distal arthritis

Top 3 diagnoses
- Osteoarthritis
- Erosive osteoarthritis
- Psoriatic arthritis

Additional diagnostic considerations
- Reactive arthritis
- Rheumatoid arthritis

83 Erosive arthropathy involving the foot

Top 3 diagnoses
- Rheumatoid arthritis
- Gout
- Reactive arthritis

Additional diagnostic considerations
- Infection (septic joint)
- Psoriatic arthritis

84 Chondrocalcinosis

Top 3 diagnoses
- CPPD arthropathy
- Hyperparathyroidism
- Hemochromatosis

Additional diagnostic considerations
- Wilson disease

85 Vertebra plana in a child

Top 3 diagnoses
- Langerhans cell histiocytosis
- Leukemia/Lymphoma
- Osteomyelitis

Additional diagnostic considerations
- Metastatic disease

86 Wormian bones

Top 3 diagnoses
- Idiopathic Wormian bones
- Osteogenesis imperfecta
- Cleidocranial dysostosis

Additional diagnostic considerations
- Down syndrome
- Metabolic disease (rickets, hypothyroidism)

87 Madelung deformity

Top 3 diagnoses
- Idiopathic Madelung deformity
- Turner syndrome
- Skeletal dysplasia (multiple epiphyseal dysplasia, dyschondrosteosis)

Additional diagnostic considerations
- Trauma
- Infection/Septic arthritis

88 Lucent metaphyseal bands

Top 3 diagnoses
- Leukemia
- Rickets
- Osteomyelitis

Additional diagnostic considerations
- Neuroblastoma metastatic disease
- Scurvy
- Syphilis

89 Medullary/Chondroid lesion

Top 3 diagnoses
- Enchondroma
- Bone infarct
- Chondrosarcoma

Additional diagnostic considerations
- Chronic osteomyelitis

90 Acro-osteolysis

Top 3 diagnoses
- Hyperparathyroidism
- Scleroderma
- Trauma (thermal or cold injury)

Additional diagnostic considerations
- Psoriasis
- Hajdu-Cheney syndrome

91 Dense effusion

Top 3 diagnoses
- Hemarthrosis (hemophilia, post-traumatic)
- Juvenile chronic arthritis
- Pigmented villonodular synovitis

Additional diagnostic considerations
- Septic arthritis
- Crystalline arthropathy (Gout, CPPD)

92 Loose bodies with erosions

Top 3 diagnoses
- Synovial (osteo)chondromatosis
- Pigmented villonodular synovitis
- Rheumatoid arthritis

93 Expansile rib lesion in a child

Top 3 diagnoses
- Fibrous dysplasia
- Bone cyst
- Enchondroma

Additional diagnostic considerations
- Langerhans cell histiocytosis
- Ewing sarcoma
- Metastatic disease

94 Posterior element lytic lesion

Top 3 diagnoses
- Aneurysmal bone cyst
- Osteoblastoma
- Infection (Tuberculosis)

Additional diagnostic considerations
- Metastatic disease
- Langerhans cell histiocytosis

95 Carpal dislocation

Top 3 diagnoses
- Perilunate dislocation
- Lunate dislocation
- Midcarpal fracture-dislocation

96 Periarticular soft tissue calcifications

Top 3 diagnoses
- Hemangioma
- Myositis ossificans
- Scleroderma

Additional Diagnostic Considerations
- Arthropathy with calcified soft tissue nodule
- Soft tissue sarcoma
- Tumoral calcinosis

97 Benign expansile lytic lesion

Top 3 diagnoses
- Fibrous dysplasia
- Unicameral bone cyst
- Aneurysmal bone cyst

Additional diagnostic considerations
- Giant cell tumor
- Eosinophilic granuloma

98 Sclerotic lesions in pelvis

Top 3 diagnoses
- Bone island/Osteopoikilosis
- Metastatic disease (breast, prostate)
- Paget disease

99 Vertebral body wedge fracture

Top 3 diagnoses
- Traumatic fracture
- Insufficiency fracture
- Pathologic fracture

100 Epiphyseal equivalent lesion

Top 3 diagnoses
- Chondroblastoma
- Giant cell tumor
- Langerhans cell histiocytosis

Additional diagnostic considerations
- Intraosseous ganglion cyst

V Head and Neck Imaging

101 Enhancing orbital mass

Top 3 diagnoses
- Hemangioma
- Lymphangioma
- Meningioma

Additional diagnostic considerations
- Metastatic disease
- Lymphoma

102 Orbital rim fracture

Top 3 diagnoses
- Orbital wall blowout fracture
- Tripod fracture
- Lefort fracture

103 Cavernous sinus mass/enhancement

Top 3 diagnoses
- Meningioma
- Schwannoma
- Carotid-cavernous fistula

Additional diagnostic considerations
- Tolosa-Hunt syndrome
- Sarcoidosis
- Perineural spread of tumor

104 Aggressive sinus disease with bony destruction

Top 3 diagnoses
- Invasive fungal sinusitis
- Wegener granulomatosis
- Sinonasal carcinoma

Additional diagnostic considerations
- Lymphoma
- Cocaine nose

105 Unilateral parotid mass

Top 3 diagnoses
- Pleomorphic adenoma
- Warthin tumor
- Parotid carcinoma (mucoepidermoid, adenoid cystic carcinoma)

Additional diagnostic considerations
- Lymphadenopathy
- Branchial cleft cyst (Type 1)

106 Bilateral parotid masses

Top 3 diagnoses
- Lymphoepithelial lesions
- Sjogren syndrome
- Warthin tumors

Additional diagnostic considerations
- Lymphadenopathy
- Sarcoidosis

107 Orbital muscle enlargement

Top 3 diagnoses
- Thyroid associated orbitopathy
- Orbital pseudotumor
- Lymphoma

Additional diagnostic considerations
- Infectious myositis
- Sarcoidosis

108 Pharyngeal mucosal mass

Top 3 diagnoses
- Squamous cell carcinoma
- Lymphoma
- Infection/abscess

Additional diagnostic considerations
- Minor salivary gland tumor
- Thornwaldt cyst

109 Masticator space mass

Top 3 diagnoses
- Infection/abscess
- Sarcoma
- Venolymphatic malformation

Additional diagnostic considerations
- Nerve sheath tumor

110 Carotid space mass

Top 3 diagnoses
- Paraganglioma
- Nerve sheath tumor
- Vascular abnormality

Additional diagnostic considerations
- Lymphadenopathy

111 Retropharyngeal mass

Top 3 diagnoses
- Infection/abscess
- Nodal metastases
- Lymphoma

Additional diagnostic considerations
- Venolymphatic malformation
- Tortuous ICA

112 Clival mass

Top 3 diagnoses
- Metastatic disease
- Chordoma
- Chondrosarcoma

Additional diagnostic considerations
- Invasive pituitary macroadenoma
- Plasmacytoma

113 Vascular injury to the neck

Top 3 diagnoses
- Dissection
- Psuedoaneurysm
- Arteriovenous fistula

Additional diagnostic considerations
- Thrombosis

114 Globe lesion in a child

Top 3 diagnoses
- Retinoblastoma
- Persistent hyperplastic primary vitreous
- Coats disease

Additional diagnostic considerations
- Retinopathy of prematurity
- Toxocariasis

115 Optic nerve enlargement and enhancement

Top 3 diagnoses
- Optic nerve glioma
- Optic neuritis
- Optic nerve sheath meningioma

Additional diagnostic considerations
- Leukemia/Lymphoma
- Sarcoidosis

116 Pachymeningeal enhancement

Top 3 diagnoses
- Intracranial hypotension
- Metastatic disease
- Pachymeningitis

Additional diagnostic considerations
- Subdural hemorrhage
- Sarcoidosis

117 Middle ear mass

Top 3 diagnoses
- Cholesteatoma
- Facial nerve schwannoma
- Glomus tympanicum

Additional diagnostic considerations
- Normal variant vasculature (aberrant ICA, dehiscent jugular bulb)
- Cholesterol granuloma

118 Temporal bone trauma with mastoid fluid

Top 3 diagnoses
- Longitudinal temporal bone fracture
- Transverse temporal bone fracture
- Mixed temporal bone fracture

119 Inner ear congenital malformation

Top 3 diagnoses
- Large vestibular aqueduct syndrome
- Cystic cochleovestibular anomaly
- Cystic common cavity

Additional diagnostic considerations
- Cochlear aplasia
- Labyrinthine ossificans

120 Floor of the mouth mass

Top 3 diagnoses
- Squamous cell carcinoma
- Infection/Abscess
- Ranula

Additional diagnostic considerations
- Congenital thyroid lesion
- Venolymphatic malformation
- Dermoid/Epidermoid cyst

121 Aggressive nasal mass in an adolescent

Top 3 diagnoses
- Juvenile angiofibroma
- Enthesioneuroblastoma
- Hemangioma

Additional diagnostic considerations
- Rhabdomyosarcoma
- Inverted papilloma
- Polyps

122 Cystic neck mass

Top 3 diagnoses
- Congenital cystic lesion (thyroglossal duct cyst, branchial cleft cyst)
- Abscess
- Necrotic lymph node

Additional diagnostic considerations
- Venolymphatic malformation
- Cystic nerve sheath tumor

123 Jugular foramen mass

Top 3 diagnoses
- Meningioma
- Schwannoma
- Paraganglioma

Additional diagnostic considerations
- Metastatic disease
- Dehiscent jugular bulb

124 Petrous apex mass

Top 3 diagnoses
- Cholesterol granuloma
- Mucocele
- Congenital cholesteatoma

Additional diagnostic considerations
- Apical petrositis
- Neoplasm (metastatic disease, chondrosarcoma)

125 Leptomeningeal enhancement

Top 3 diagnoses
- Leptomeningeal carcinomatosis
- Meningitis
- Neurosarcoidosis

Additional diagnostic considerations
- Subacute infarction
- Subarachnoid hemorrhage

VI Brain and Spine Imaging

126 Confluent white matter lesions in an adult

Top 3 diagnoses
- Demyelinating disease
- Neoplasm (gliomatosis cerebri, lymphoma, infiltrating primary)
- Progressive multifocal leukoencephalopathy

Additional diagnostic considerations
- Microvascular ischemic disease
- Autoimmune mediated vasculitis

127 Confluent white matter lesions in a child

Top 3 diagnoses
- Acute disseminating encephalomyelitis
- Multiple sclerosis
- Dysmyelinating disease (leukodystrophy)

Additional diagnostic considerations
- Atypical infection (PML)

128 Ring enhancing lesion

Top 3 diagnoses
- Neoplasm (GBM, lymphoma, metastatic disease)
- Subacute infarction
- Abscess

Additional diagnostic considerations
- Demyelinating disease
- Resolving contusion

129 Pineal gland mass

Top 3 diagnoses
- Pineal cyst
- Germ cell tumor (germinoma)
- Pineal cell tumor (pineoblastoma, pineocytoma)

Additional diagnostic considerations
- Meningioma
- Tectal plate glioma

130 Sellar/Suprasellar mass in a child

Top 3 diagnoses
- Craniopharyngioma
- Germ cell tumor
- Rathke cleft cyst

Additional diagnostic considerations
- Hypothalamic/Optic glioma
- Hypothalamic hamartoma

131 Posterior fossa mass in a child

Top 3 diagnoses
- Medulloblastoma
- Juvenile pilocystic astrocytoma
- Ependymoma

Additional diagnostic considerations
- Brain stem glioma

132 Posterior fossa mass in an adult

Top 3 diagnoses
- Infarction
- Metastatic disease
- Hemangioblastoma

Additional diagnostic considerations
- Vascular malformation
- Hypertensive hemorrhage

133 Posterior fossa cyst

Top 3 diagnoses
- Mega cisterna magna
- Arachnoid cyst
- Dandy-Walker malformation

Additional diagnostic considerations
- Joubert syndrome (vermian hypoplasia)

134 Cerebellopontine angle mass

Top 3 diagnoses
- Vestibular schwannoma
- Meningioma
- Arachnoid cyst

Additional diagnostic considerations
- Epidermoid

135 Tonsillar herniation

Top 3 diagnoses
- Arnold-Chiari malformation
- Ependymoma
- Posterior fossa mass

Additional diagnostic considerations
- Intracranial hypotension

136 CSF-lined cortical cleft

Top 3 diagnoses
- Prior infarct with encephalomalacia
- Schizencephaly
- Porencephalic cyst

137 Enhancing intramedullary spinal mass

Top 3 diagnoses
- Ependymoma
- Astrocytoma
- Hemangioblastoma

Additional diagnostic considerations
- Metastatic disease
- Demyelinating disease

138 Intradural extramedullary spinal mass

Top 3 diagnoses
- Nerve sheath tumor
- Meningioma
- CSF metastatic disease

139 Diffuse temporal lobe mass

Top 3 diagnoses
- Herpes encephalitis
- Ischemia/infarction
- Gliomatosis cerebri

Additional diagnostic considerations
- Limbic encephalitis
- Status epilepticus

140 Increased T2 signal intensity in basal ganglia/thalami in a child

Top 3 diagnoses
- Ischemia
- Carbon monoxide poisoning
- Wilson disease

Additional diagnostic considerations
- Mitochondrial disorder (MELAS, Leigh disease)
- Kernicterus
- Osmotic demyelination (extrapontine myelinolysis)

141 Hemorrhagic mass

Top 3 diagnoses
- Vascular malformation
- Hemorrhagic infarct
- Neoplasm (primary, hemorrhagic metastatic disease)

Additional diagnostic considerations
- Contusion
- Cerebral amyloid angiopathy

142 Corpus callosal lesion

Top 3 diagnoses
- Glioblastoma multiformans
- Lymphoma
- Demyelinating disease

Additional diagnostic considerations
- Diffuse axonal injury
- Marchiafava Bignami

143 Subependymal nodules/masses

Top 3 diagnoses
- Tuberous sclerosis
- Heterotopic gray matter
- TORCH infection

Additional diagnostic considerations
- Metastatic disease

144 Massive supratentorial CSF collection in a newborn

Top 3 diagnoses
- Hydrocephalus
- Hydranencephaly
- Holoprosencephaly

Additional diagnostic considerations
- Agenesis of the corpus callosum
- Bilateral open-lip schizencephaly

145 Intraventricular mass

Top 3 diagnoses
- Meningioma
- Choroid plexus tumor
- Central neurocytoma

Additional diagnostic considerations
- Ependymoma/Subependymoma
- Colloid cyst
- Subependymal giant cell astrocytoma

146 Cerebellar atrophy

Top 3 diagnoses
- Alcohol abuse
- Anti-convulsant therapy
- Paraneoplastic syndrome

Additional diagnostic considerations
- Sporadic olivopontocerebellar atrophy
- Cerebello-olivary atrophy
- Friedreich ataxia (spinocerebellar ataxia)

147 Spinal cord signal abnormality

Top 3 diagnoses
- Demyelinating disease
- Cord contusion
- Cord neoplasm

Additional diagnostic considerations
- Transverse myelitis
- Cord ischemia

148 Cortically-based enhancing neoplasm

Top 3 diagnoses
- Oligodendroglioma
- Astrocytoma
- Ganglioglioma

Additional diagnostic considerations
- Dysembryoplastic neuroectodermal tumor
- Desmoplastic infantile glioma

149 Epidural spinal mass

Top 3 diagnoses
- Disc extrusion
- Epidural hematoma
- Epidural abscess

Additional diagnostic considerations
- Metastatic disease
- Epidural lipomatosis
- Synovial cyst

150 Prominent periventricular/basal ganglia cystic lesions

Top 3 diagnoses
- Virchow-Robin spaces
- Lacunar infarctions
- Infection (neurocysticercosis, cryptococcus)

Additional diagnostic considerations
- Cystic neoplasm
- Neuroglial cyst

VII Pediatric Imaging

151 Neonatal lung disease with low lung volumes

Top 3 diagnoses
- Surfactant deficiency (respiratory distress syndrome)
- Beta-hemolytic streptococcal pneumonia
- Pulmonary hypoplasia

152 Neonatal lung disease with increased lung volumes

Top 3 diagnoses
- Transient tachypnea of the newborn
- Meconium aspiration
- Neonatal pneumonia

Additional diagnostic considerations
- Congenital heart disease

153 Cyanotic infant with decreased pulmonary flow

Top 3 diagnoses
- Tetralogy of Fallot
- Pulmonary atresia
- Tricuspid atresia

Additional diagnostic considerations
- Double outlet right ventricle
- Ebstein anomaly

154 Cyanotic infant with increased pulmonary vascularity

Top 3 diagnoses
- Transposition of the great arteries
- Truncus arteriosus
- Total anomalous pulmonary venous return

Additional diagnostic considerations
- Tricuspid atresia
- Single ventricle

155 Shunt vascularity

Top 3 diagnoses
- Ventricular septal defect
- Atrial septal defect
- Patent ductus arteriosus

Additional diagnostic considerations
- Atrioventricular canal defect

156 Solid pulmonary mass

Top 3 diagnoses
- Round pneumonia
- Congenital cystic adenomatoid malformation
- Sequestration

Additional diagnostic considerations
- Bronchogenic cyst
- Plasma cell granuloma

157 Liver mass in an infant

Top 3 diagnoses
- Hepatoblastoma
- Hemangioendothelioma
- Mesenchymal hamartoma

Additional diagnostic considerations
- Metastatic disease
- Abscess
- Hematoma

158 Suprarenal mass in a child

Top 3 diagnoses
- Neuroblastoma
- Adrenal hemorrhage
- Pheochromocytoma

Additional diagnostic considerations
- Subdiaphragmatic sequestration
- Congenital adrenal hyperplasia
- Adrenal cortical carcinoma

159 Solid renal mass

Top 3 diagnoses
- Wilms tumor
- Mesoblastic nephroma
- Nephroblastomatosis

Additional diagnostic considerations
- Lymphoma
- Renal cell carcinoma

160 Cystic renal lesion

Top 3 diagnoses
- Hydronephrosis
- Multicystic dysplastic kidney
- Multilocular cystic nephroma

Additional diagnostic considerations
- Cystic Wilms tumor
- Polycystic kidney disease
- Renal abscess

161 Subglottic narrowing

Top 3 diagnoses
- Laryngotracheobronchitis (Croup)
- Epiglottitis
- Retropharyngeal abscess

Additional diagnostic considerations
- Bacterial tracheitis
- Aspirated foreign body
- Hemangioma

162 Distal bowel obstruction in a neonate

Top 3 diagnoses
- Functional immaturity of the colon
- Hirschsprung disease
- Ileal atresia/stenosis

Additional diagnostic considerations
- Meconium ileus
- Anal atresia-anorectal malformations

163 Bowel wall thickening in an immunocompromised child

Top 3 diagnoses
- Pseudomembranous colitis
- Neutropenic colitis/thyphlitis
- Graft-versus-host disease

Additional diagnostic considerations
- Post-transplant lymphoproliferative disorder
- Shock bowel

164 Skeletal dysplasia

Top 3 diagnoses
- Achondroplasia
- Thanatophoric dysplasia
- Jeune Syndrome

Additional diagnostic considerations
- Ellis-van Creveld syndrome
- Chondrodysplasia punctata

165 Double-bubble sign

Top 3 diagnoses
- Malrotation with midgut volvulus
- Duodenal atresia/stenosis
- Annular pancreas

Additional diagnostic considerations
- Duodenal web
- Preduodenal portal vein

166 Posterior vertebral body scalloping

Top 3 diagnoses
- Dural ectasia (connective tissue disorders, neurofibromatosis)
- Mucopolysaccharidosis
- Dwarfism/Achondroplasia

Additional diagnostic considerations
- Spinal tumor
- Normal variant

167 Presacral mass

Top 3 diagnoses
- Sacrococcygeal teratoma
- Anterior meningocele
- Rectal duplication cyst

Additional diagnostic considerations
- Lymphangioma
- Germ cell tumor
- Adnexal mass

168 Long bone aggressive lesion

Top 3 diagnoses
- Osteosarcoma
- Ewing sarcoma
- Osteomyelitis

Additional diagnostic considerations
- Langerhans cell histiocytosis
- Metastatic disease

169 Endobronchial lesion in a child

Top 3 diagnoses
- Foreign body
- Papilloma
- Carcinoid tumor

Additional diagnostic considerations
- Inflammatory polyp
- Salivary gland neoplasm

170 Erlenmeyer flask deformity

Top 3 diagnoses
- Osteopetrosis
- Fibrous dysplasia
- Gaucher disease

Additional diagnostic considerations
- Hemoglobinopathy
- Multiple hereditary exostoses

171 Lytic skull lesion in a child

Top 3 diagnoses
- Langerhans cell histiocytosis
- Epidermoid cyst
- Neoplasm (leukemia, Ewing sarcoma, neuroblastoma, metastatic disease)

Additional diagnostic considerations
- Infection/Osteomyelitis
- Leptomeningeal cyst

172 Avascular necrosis of the femoral head

Top 3 diagnoses
- Legg-Calve-Perthes
- Trauma
- Sickle cell disease

Additional diagnostic considerations
- Corticosteroid use
- Gaucher disease
- Meyer dysplasia

173 Vascular anomaly with esophageal and tracheal compression

Top 3 diagnoses
- Aberrant right subclavian artery
- Double aortic arch
- Right aortic arch with aberrant left subclavian artery

Additional diagnostic considerations
- Pulmonary sling
- Innominate artery compression syndrome

174 Cystic pulmonary mass

Top 3 diagnoses
- Congenital lobar emphysema
- Congenital cystic adenomatoid malformation
- Congenital diaphragmatic hernia

Additional diagnostic considerations
- Necrotizing pneumonia

175 Esophageal obstruction in a neonate

Top 3 diagnoses
- Tracheoesophageal fistula/Esophageal atresia
- Foreign body
- Esophageal duplication cyst

Additional diagnostic considerations
- Vascular ring

VIII Ultrasound Imaging

176 Enlarged ovary

Top 3 diagnoses
- Ovarian torsion
- Ovarian neoplasm
- Pelvic inflammatory disease/Tubo-ovarian abscess

Additional diagnostic considerations
- Hemorrhagic cyst

177 Enlarged ovary with multiple peripheral follicles

Top 3 diagnoses
- Ovarian torsion
- Polycystic ovarian syndrome (Stein-Leventhal syndrome)
- Ovarian Hyperstimulation Syndrome

178 Hyperechoic liver mass

Top 3 diagnoses
- Hemangioma
- Focal fatty infiltration
- Hepatocellular carcinoma

Additional diagnostic considerations
- Metastatic disease
- Focal nodular hyperplasia
- Hepatic adenoma

179 Complex extra-testicular fluid collection

Top 3 diagnoses
- Varicocele
- Hematocele
- Pyocele

180 Hyperechoic renal mass

Top 3 diagnoses
- Angiomyolipoma
- Renal cell carcinoma
- Complex cyst

181 Complex cystic adnexal mass with positive HCG

Top 3 diagnoses
- Ectopic pregnancy
- Corpus luteal cyst
- Hemorrhagic cyst

182 Heterogeneous uterus

Top 3 diagnoses
- Diffuse leiomyomas
- Adenomyosis
- Endometrial carcinoma

183 Thickened endometrial stripe

Top 3 diagnoses
- Endometrial hyperplasia
- Endometrial polyps
- Endometrial carcinoma

Additional diagnostic considerations
- Submucosal fibroids
- Retained products of conception
- Gestational trophoblastic disease

184 Uterine anomaly

Top 3 diagnoses
- Bicornuate uterus
- Didelphus uterus
- Septated uterus

Additional diagnostic considerations
- Arcuate uterus

185 Starry sky liver

Top 3 diagnoses
- Acute hepatitis
- Hepatic congestion
- Infiltrating neoplasm (HCC, diffuse metastatic disease)

Additional diagnostic considerations
- Toxic shock syndrome
- Biliary or portal venous gas

186 "Target" lesions in the liver

Top 3 diagnoses
- Hepatocellular carcinoma
- Metastatic disease
- Lymphoma

Additional diagnostic considerations
- Hepatic abscesses
- Hepatic pseudotumor from focal fatty sparing

187 Portal vein thrombosis

Top 3 diagnoses
- Tumor thrombus (primary or metastatic disease)
- Hepatic cirrhosis with portal hypertension
- Periportal infection/inflammation (pancreatitis)

Additional diagnostic considerations
- Hypercoagulable conditions
- Trauma/iatrogenic

188 Cystic adnexal mass with negative HCG

Top 3 diagnoses
- Ovarian neoplasm
- Hemorrhagic cyst
- Tubo-ovarian abscess

Additional diagnostic considerations
- Endometrioma

189 Multiple hypoechoic liver masses

Top 3 diagnoses
- Neoplasm (multifocal HCC, metastatic disease, lymphoma)
- Multifocal abscesses
- Candidiasis

Additional diagnostic considerations
- Hematoma
- Diffuse fatty infiltration with focal fatty sparing

190 Hypoechoic renal mass

Top 3 diagnoses
- Simple or complex renal cyst
- Lymphoma
- Renal abscess

Additional diagnostic considerations
- Renal cell carcinoma
- Metastatic disease

191 Hyperechoic foci in gallbladder wall

Top 3 diagnoses
- Porcelain gallbladder
- Emphysematous cholecystitis
- Adenomyomatosis

192 Enlarged painful testicle

Top 3 diagnoses
- Testicular torsion
- Epididymo-orchitis
- Testicular hematoma/fracture

193 Gallbladder wall thickening

Top 3 Diagnoses for Diffuse Gallbladder Wall Thickening
- Acute cholecystitis
- Gallbladder wall edema (CHF)
- Secondary inflammation (HIV, hepatitis)

Top 3 Diagnoses for Focal Gallbladder Wall Thickening
- Gallbladder carcinoma
- Gallbladder polyp
- Adenomyomatosis

194 Right lower quadrant mass in a child

Top 3 diagnoses
- Appendicitis
- Intussusception
- Enteric duplication cyst

Additional diagnostic considerations
- Adnexal mass in a female
- Meckel diverticulum
- Mesenteric adenitis

195 Thyroid mass

Top 3 diagnoses
- Benign thyroid nodule
- Thyroid carcinoma
- Parathyroid adenoma

Additional diagnostic considerations
- Thyroglossal duct cyst

196 Multiple splenic hypoechoic foci

Top 3 diagnoses
- Fungal abscess (Candidiasis)
- Diffuse lymphoma
- Granulomatous disease

Additional diagnostic considerations
- Metastatic disease

197 Periventricular cysts

Top 3 diagnoses
- Periventricular leukomalacia
- Subependymal cysts
- Infection (TORCH, parasitic)

Additional diagnostic considerations
- Choroid plexus cysts
- Porencephaly

198 Periventricular hyperechoic foci

Top 3 diagnoses
- Germinal matrix hemorrhage
- Intraventricular/Intraparenchymal hemorrhage
- Early periventricular leukomalacia

Additional diagnostic considerations
- Hypoxic-ischemic brain injury
- CNS infection

199 Common bile duct dilatation

Top 3 diagnoses
- Choledocholithiasis
- Malignancy (pancreatic adenocarcinoma, cholangiocarcinoma)
- Chronic pancreatitis

Additional diagnostic considerations
- Cholangitis
- Choledochal anomaly

200 Enlarged painless testicle

Top 3 Diagnoses
- Testicular neoplasm
- Lymphoma/leukemia
- Testicular cysts

IX Fetal Imaging

201 Nuchal translucency

Top 3 diagnoses
- Trisomy 21
- Turner Syndrome
- Trisomy 18

Additional diagnostic considerations
- Trisomy 13

202 Sacral mass

Top 3 diagnoses
- Sacrococcygeal teratoma
- Myelomeningocele and variants
- Rhabdomyosarcoma

Additional diagnostic considerations
- Duplication cyst

203 Posterior fossa malformation

Top 3 diagnoses
- Chiari malformation
- Dandy-Walker malformation
- Joubert Syndrome

204 Hyperechoic thoracic mass

Top 3 diagnoses
- Congenital cystic adenomatoid malformation
- Sequestration
- Congenital lobar emphysema

Additional diagnostic considerations
- Congenital diaphragmatic hernia

205 Twin development-chorionicity

Top 3 diagnoses
- Dichorionic/diamnionic twin pregnancy
- Monochorionic/diamnionic twin pregnancy
- Monochorionic/monoamnionic twin pregnancy

206 Asymmetric fetal size

Top 3 diagnoses
- Twin-twin transfusion syndrome
- Fetal demise
- Normal variation

207 Enlarged bladder (megacystis)

Top 3 diagnoses
- Posterior urethral valves
- Prune-belly syndrome
- Megacystis-microcolon-intestinal hypoperistalsis syndrome

Additional diagnostic considerations
- Marked vesicoureteral reflux

208 Umbilical cord vascular abnormality

Top 3 diagnoses
- Two-vessel Cord
- Cord hematoma
- Cord hemangioma

Additional diagnostic considerations
- Wharton jelly cyst
- Umbilical cord varix

209 "Double bubble" sign

Top 3 diagnoses
- Congenital duodenal obstruction (duodenal atresia/stenosis)
- Annular pancreas
- Intestinal malrotation with volvulus

210 Hyperechoic intracardiac focus

Top 3 diagnoses
- Echogenic intracardiac focus/papillary muscle calcification
- Rhabdomyoma
- Fibroma

Additional diagnostic considerations
- Teratoma
- Hemangioma

211 CNS ventriculomegaly

Top 3 diagnoses
- Ventriculomegaly
- Congenital aqueductal stenosis
- Arnold-Chiari Malformation

Additional diagnostic considerations
- Agenesis of the corpus callosum
- Dandy-Walker malformation
- Holoprosencephaly

212 Cardiac outflow anomalies

Top 3 diagnoses
- Tetralogy of Fallot
- Transposition of the great arteries
- Truncus arteriosus

Additional diagnostic considerations
- Double outlet right ventricle
- Hypoplastic left heart syndrome

213 Cystic posterior neck mass

Top 3 diagnoses
- Cystic hygroma
- Occipital encephalocele/cervical myelomeningocele
- Cystic teratoma

214 Enlarged hyperechoic kidneys

Top 3 diagnoses
- Autosomal recessive polycystic kidney disease
- Trisomy 13
- Meckel-Gruber syndrome

Additional diagnostic considerations
- Autosomal dominant polycystic kidney disease (rare)

215 Oligohydramnios

Top 3 diagnoses
- Bilateral renal failure/outlet obstruction
- Premature rupture of membranes
- Intrauterine growth restriction

Additional diagnostic considerations
- Fetal demise

216 Polyhydramnios

Top 3 diagnoses
- Fetal gastrointestinal anomalies
- Fetal CNS anomalies
- Maternal diabetes

Additional diagnostic considerations
- Idiopathic polyhydramnios
- Fetal hydrops

217 Placental location abnormality

Top 3 diagnoses
- Placenta previa
- Placenta accrete/increta/percreta
- Marginal insertion of the cord

Additional diagnostic considerations
- Velamentous insertion of the cord

218 Abdominal wall defect

Top 3 diagnoses
- Omphalocele
- Gastroschisis
- Limb-body wall complex

Additional diagnostic considerations
- Pentalogy of Cantrell
- Bladder and cloacal exstrophy

219 Cranial/Calvarial defect

Top 3 diagnoses
- Anencephaly
- Acrania
- Amniotic band syndrome

Additional diagnostic considerations
- Encephalocele/myelomeningocele

220 Diaphragm abnormality

Top 3 diagnoses
- Congenital diaphragmatic hernia
- Congenital cystic adenomatoid malformation
- Sequestration

Additional diagnostic considerations
- Diaphragmatic eventration

221 Fetal hydrops

Top 3 diagnoses
- Cardiovascular anomalies
- Chromosomal abnormalities
- Infection (viral, TORCH)

Additional diagnostic considerations
- Immune hydrops

222 Linear echoes within amniotic fluid

Top 3 diagnoses
- Amniotic band syndrome
- Synechiae/amniotic shelf
- Chorioamniotic separation

Additional diagnostic considerations
- Hemorrhage

223 Placental abnormality/mass

Top 3 diagnoses
- Subchorionic/Retroplacental hematoma
- Placental venous lakes
- Succenturiate lobe

Additional diagnostic considerations
- Circumvallate placenta

224 Choroid plexus cyst

Top 3 diagnoses
- Normal variant/Incidental finding
- Trisomy 18
- Trisomy 21 (debatable)

225 Ventricular septal defect

Top 3 diagnoses
- Ventricular septal defect
- Endocardial cushion defect
- Normal foramen ovale

X Vascular and Interventional Radiology

226 Post procedure arterial abnormality

Top 3 diagnoses
- Hematoma
- Pseudoaneurysm
- Arteriovenous fistula

227 Carotid artery stenosis

Top 3 diagnoses
- Atherosclerosis
- Fibromuscular dysplasia
- Dissection

Additional diagnostic considerations
- Iatrogenic

228 Failing renal transplant

Top 3 diagnoses
- Acute tubular necrosis
- Renal artery stenosis
- Urinary obstruction

Additional diagnostic considerations
- Transplant rejection
- Renal vein thrombosis
- Cyclosporine toxicity

229 Digital artery occlusion/ischemia

Top 3 diagnoses
- Raynaud syndrome
- Vasculitis (SLE, Buerger disease)
- Embolic disease

Additional diagnostic considerations
- Thoracic outlet syndrome
- Trauma
- Atherosclerosis

230 Subclavian vein occlusion

Top 3 diagnoses
- Prior instrumentation/catheter placement
- Hypercoagulable state
- Paget-von Schrotter syndrome/Effort thrombosis

231 Great vessel stenosis

Top 3 diagnoses
- Atherosclerosis
- Vasculitis (GCA, Takayasu arteritis)
- Dissection

Additional diagnostic considerations
- Radiation

232 Renal artery stenosis

Top 3 diagnoses
- Atherosclerosis
- Fibromuscular dysplasia
- Dissection

233 Intraparenchymal renal artery aneurysms

Top 3 diagnoses
- Vasculitis (polyarteritis nodosa)
- Mycotic/Septic emboli
- Trauma

Additional diagnostic considerations
- Ehlers-Danlos
- Speed kidney

234 Hypervascular pulmonary mass

Top 3 diagnoses
- Arteriovenous malformation
- Bronchogenic carcinoma
- Hypervascular metastasis

Additional diagnostic considerations
- Pulmonary carcinoid
- Pulmonary artery aneurysm

235 Infrarenal aortic occlusion

Top 3 diagnoses
- Atherosclerosis
- Thrombus/Embolus
- Vasculitis (Takayasu arteritis)

Additional diagnostic considerations
- Dissection

236 Popliteal artery occlusion

Top 3 diagnoses
- Atherosclerosis
- Embolism
- Trauma

Additional diagnostic considerations
- Thrombosed popliteal artery aneurysm
- Popliteal artery entrapment syndrome
- Cystic adventitial disease

237 Extratesticular mass

Top 3 diagnoses
- Varicocele
- Pyocele/Hematocele
- Hydrocele

238 Inferior vena cava vascular anomaly/abnormality

Top 3 diagnoses
- Circumaortic/Retroaortic left renal vein
- Megacava
- Duplicated inferior vena cava

Additional diagnostic considerations
- Inferior vena cava thrombosis

239 Hypervascular renal mass

Top 3 diagnoses
- Renal cell carcinoma
- Angiomyolipoma
- Oncocytoma

Additional diagnostic considerations
- Arteriovenous malformation/fistula

240 Prominent paraspinal flow voids

Top 3 diagnoses
- Spinal dural arteriovenous fistula
- Spinal cord arteriovenous malformation
- Collateral venous flow from IVC occlusion

Additional diagnostic considerations
- Spinal cord neoplasm with increased vascular flow
- CSF pulsations

241 Suprasellar mass in an adult

Top 3 diagnoses
- Pituitary macroadenoma
- Craniopharyngioma
- Aneurysm

Additional diagnostic considerations
- Meningioma

242 Hypervascular cerebral mass/abnormality

Top 3 diagnoses
- Arteriovenous malformation
- Hypervascular tumor (GBM, meningioma)
- Aneurysm

Additional diagnostic considerations
- Moyamoya

243 Aortic dissection

Top 3 diagnoses
- Hypertension
- Trauma
- Connective tissue disease

Additional diagnostic considerations
- Annuloaortic ectasia
- Bicuspid aortic valve
- Coarctation of the aorta

244 Lower gastrointestinal bleeding

Top 3 diagnoses
- Diverticulosis
- Neoplasm
- Angiodysplasia

Additional diagnostic considerations
- Focal colitis

245 Vascular ring/sling

Top 3 diagnoses
- Aberrant right subclavian artery
- Double aortic arch
- Right arch with aberrant left subclavian artery

Additional diagnostic considerations
- Pulmonary sling

246 Urinary obstruction

Top 3 diagnoses
- Nephrolithiasis
- Neoplasm (TCC)
- Blood clot

Additional diagnostic considerations
- Fungus ball
- Sloughed papillae

247 TIPSS dysfunction

Top 3 diagnoses
- Neointimal hyperplasia
- Thrombosis
- Technical error

248 Biliary duct occlusion

Top 3 diagnoses
- Choledocholithiasis
- Cholangiocarcinoma
- Pancreatic adenocarcinoma

Additional diagnostic considerations
- Chronic pancreatitis
- Primary sclerosing cholangitis
- Parasitic infection (Ascariasis, Clonorchis)

249 Traumatic aortic injury

Top 3 diagnoses
- Pseudoaneurysm
- Aortic dissection
- Intramural hematoma

Additional diagnostic considerations
- Aortic transection

250 Occlusion of celiac axis

Top 3 diagnoses
- Atherosclerosis
- Thromboembolic disease
- Vasculitis (Takayasu, PAN)

Additional diagnostic considerations
- Median arcuate ligament syndrome
- Fibromuscular dysplasia
- Radiation

XI Nuclear Medicine

251 Transient ischemic dilatation

Top 3 diagnoses
- Multi-vessel coronary artery disease
- Subendocardial ischemia
- Systolic dysfunction

Additional diagnostic considerations
- Misaligned SPECT images

252 Symmetric "tram-track" cortical uptake of long bones

Top 3 diagnoses
- Hypertrophic osteoarthropathy
- Shin/quadriceps splints
- Chronic venous stasis

253 Poor quality bone scan

Top 3 diagnoses
- Off-peak Gamma camera
- Incorrect radiopharmaceutical administration
- Poor radiopharmaceutical preparation

Additional diagnostic considerations
- Infiltrated dose

254 Extrapulmonary activity on lung perfusion scan

Top 3 diagnoses
- Free Tc-99m
- Right-to-left shunt
- Retained activity from a different radiotracer study

255 Superscan

Top 3 diagnoses
- Metastatic disease (prostate, breast, lung)
- Metabolic disease (renal osteodystrophy, hyperthyroidism, osteomalacia)
- Paget disease

Additional diagnostic considerations
- Myeloproliferative/marrow infiltrative disorder

256 Increased activity and osseous expansion in the pelvis

Top 2 diagnoses in adults
- Paget disease
- Metastatic disease (prostate, breast)

Top 3 diagnoses in children
- Ewing sarcoma
- Lymphoma
- Fibrous dysplasia

257 Three-phase positive bone scan

Top 3 diagnoses
- Trauma
- Osteomyelitis
- Bone tumor

Additional diagnostic considerations
- Reflex sympathetic dystrophy

258 Nonvisualization of gallbladder on hepatobiliary imaging

Top 3 diagnoses
- Acute cholecystitis
- Chronic cholecystitis
- Inadequate patient preparation

Additional diagnostic considerations
- Severe hepatocellular disease
- High grade biliary obstruction

259 Focal intra-abdominal activity on pertechnetate imaging

Top 3 diagnoses
- Meckel diverticulum
- Focal intra-abdominal infectious or inflammatory process
- Physiologic renal/urinary activity

260 Persistent hepatogram on neonatal hepatobiliary imaging

Top 3 diagnoses
- Biliary atresia
- Neonatal hepatitis
- Intrahepatic cholestasis from severe parenchymal disease

261 Persistent focal cervical uptake on delayed Sestamibi imaging

Top 3 diagnoses
- Parathyroid adenoma
- Thyroid adenoma or carcinoma
- Metastatic lymphadenopathy

262 Intra-abdominal activity on Tc-RBC scan

Top 3 diagnoses
- Active GI bleed
- Neoplasm or inflammatory bowel disease
- Genitourinary activity

Additional diagnostic considerations
- Free technetium

263 Decreased cortical FDG activity in the setting of dementia

Top 3 diagnoses
- Alzheimer disease
- Pick disease
- Multi-infarct dementia

Additional diagnostic considerations
- Parkinson disease

264 Unilateral absent lung perfusion

Top 3 Diagnoses for Perfusion worse than Ventilation
- External compression (bronchogenic CA, fibrosing mediastinitis)
- Pulmonary artery anomalies or corrected congenital heart disease
- Massive unilateral PE

Top 3 Diagnoses for Ventilation worse than Perfusion
- Mucus plug
- Unilateral diffuse parenchymal disease
- Endobronchial lesion (mass or foreign body)

265 Worsening renal function on MAG-3 renal scan post-Captopril administration

Top 3 diagnoses
- Renal artery stenosis
- Unilateral urinary obstruction
- False positive scan in patients on calcium channel blocker

266 Cold nodule on I-123 thyroid scan

Top 3 diagnoses
- Thyroid carcinoma
- Colloid cyst
- Non-functioning adenoma

267 Focal abdominal uptake on Octreoscan

Top 3 diagnoses
- Neuroendocrine tumor
- Metastatic disease
- Granulomatous disease

268 Absent intracranial activity on Tc-99 HMPAO scan

Top 2 Diagnoses
- Brain death
- Quality control-poor radiopharmaceutical bolus

269 Focal neck uptake on I-131 post-ablation scan

Top 3 diagnoses
- Residual thyroid tissue
- Cervical nodal metastases
- Physiologic pharyngeal/esophageal activity

270 Increased mediastinal uptake on Gallium scan

Top 3 diagnoses
- Malignancy (lymphoma, bronchogenic carcinoma)
- Granulomatous disease (TB, Sarcoid)
- Non-specific inflammatory/infectious process

271 Focal increased hepatic uptake on sulfur colloid scan

Top 3 diagnoses
- Focal nodular hyperplasia
- Regenerating nodular cirrhosis
- Budd-Chiari syndrome

Additional diagnostic considerations
- Superior vena cava syndrome

272 Focal bowel uptake on In-111 labeled WBC scan

Top 3 diagnoses
- Infectious enteritis/colitis
- Inflammatory bowel disease
- GI bleed

Additional diagnostic considerations
- Swallowed activity from sinusitis/pharyngitis

273 Focal defect on QC images

Top 3 diagnoses
- Photomultiplier tube failure
- Crystal defect
- Collimator defect

Additional diagnostic considerations
- Electronic artifact

274 Focal increased activity within an extremity on bone scan

Top 3 diagnoses
- Stress fracture
- Osteomyelitis
- Neoplasm (benign and malignant-osteoid osteoma)

Additional diagnostic considerations
- Fibrous dysplasia

275 Solitary hypermetabolic pulmonary lesion on PET scan

Top 3 diagnoses
- Malignancy (bronchogenic carcinoma, metastatic disease)
- Active granulomatous disease
- Pulmonary infection/inflammation

XII Breast Imaging

276 Implant defect

Top 3 diagnoses
- Intracapsular rupture
- Extracapsular rupture
- Radial fold

Additional diagnostic considerations
- Gel bleed
- Herniation

277 MRI enhancement patterns

Top 3 diagnoses
- Type 1 persistent kinetics
- Type 2 plateau kinetics
- Type 3 wash-out kinetics

Additional diagnostic considerations
- Initial phase

278 Complex cystic mass in a lactating woman

Top 3 diagnoses
- Galactocele
- Abscess
- Fibroadenoma

Additional diagnostic considerations
- Hematoma
- Lactating adenoma
- Fibrocystic change

279 Coarse calcifications in a partially circumscribed mass

Top 3 diagnoses
- Degenerating fibroadenoma
- Fat necrosis
- Oil cyst

Additional diagnostic considerations
- Hematoma
- Abscess

280 Benign-appearing calcification; rim, punctate, and round forms

Top 3 diagnoses
- Calcified oil cyst
- Dystrophic calcifications
- Dermal calcifications

Additional diagnostic considerations
- Fibrocystic change
- Hyalinized fibroadenoma calcifications

281 Malignant-appearing calcifications; linear, branching forms

Top 3 diagnoses
- Ductal carcinoma in situ/Invasive ductal carcinoma
- Vascular calcifications
- Secretory calcifications

Additional diagnostic considerations
- Milk of calcium
- Fibrocystic change

282 Fatty breast lesion

Top 3 diagnoses
- Hamartoma (fibroadenolipoma)
- Lipoma
- Galactocele

Additional diagnostic considerations
- Fat necrosis
- Oil cyst

283 Well-circumscribed mass in a premenopausal woman

Top 3 diagnoses
- Fibroadenoma
- Cyst
- Intramammary lymph node

Additional diagnostic considerations
- Breast carcinoma
- Papilloma

284 Unilateral skin thickening

Top 3 diagnoses
- Inflammatory breast cancer
- Mastitis
- Invasive breast cancer

Additional diagnostic considerations
- Postsurgical or postradiation changes
- Superior vena cava syndrome
- Lymphedema

285 Axillary lymphadenopathy

Top 3 diagnoses
- Breast cancer with lymph node spread
- Lymphoma
- Reactive lymphadenopathy

Additional diagnostic considerations
- Metastatic disease from remote primary
- Connective tissue and granulomatous disorders
- Castleman disease

286 Mass with central lucency

Top 3 diagnoses
- Radial scar
- Invasive ductal cancer
- Tubular carcinoma

Additional diagnostic considerations
- Fat necrosis
- Postsurgical scar

287 Well-circumscribed solid breast mass

Top 3 diagnoses
- Fibroadenoma
- Intramammary lymph node
- Hamartoma (fibroadenolipoma)

Additional diagnostic considerations
- Circumscribed breast carcinoma
- Papilloma

288 Well-circumscribed cystic breast mass

Top 3 diagnoses
- Papilloma/papillary carcinoma
- Seroma
- Cyst with debris

Additional diagnostic considerations
- Hematoma
- Abscess

289 Ductal mass

Top 3 diagnoses
- Intraductal papilloma
- Intracystic papillary carcinoma
- Ductal carcinoma in situ

Additional diagnostic considerations
- Dilated duct with debris

290 Post-operative changes

Top 3 diagnoses
- Postsurgical architectural distortion
- Recurrent cancer
- Fat necrosis

Additional diagnostic considerations
- Radial scar
- Tubular carcinoma

291 Bilateral skin thickening

Top 3 diagnoses
- Congestive heart failure
- Superior vena cava obstruction
- Bilateral lymphedema

Additional diagnostic considerations
- Psoriasis
- Renal failure and volume overload

292 Breast mass in male

Top 3 diagnoses
- Gynecomastia
- Breast cancer
- Lipoma

Additional diagnostic considerations
- Hematoma
- Abscess
- Metastatic disease

293 Well-circumscribed cancer

Top 3 diagnoses
- Invasive ductal carcinoma, NOS
- Mucinous carcinoma
- Medullary carcinoma

Additional diagnostic considerations
- Papillary carcinoma
- Ductal carcinoma in situ

294 Developing asymmetry

Top 3 diagnoses
- Invasive ductal carcinoma
- Invasive lobular carcinoma
- Pseudoangiomatous stromal hyperplasia

Additional diagnostic considerations
- Asymmetric breast tissue
- Stromal fibrosis
- Fat necrosis

295 Ill-defined, infiltrative breast mass

Top 3 diagnoses
- Infiltrating ductal carcinoma
- Infiltrating lobular carcinoma
- Postsurgical scar

Additional diagnostic considerations
- Fibrosis

296 Breast lesion with nipple discharge

Top 3 diagnoses
- Intraductal papilloma
- Mammary duct ectasia
- Breast carcinoma (ductal or papillary)

Additional diagnostic considerations
- Fibrocystic change
- Galactorrhea

297 Unilateral nipple/skin changes

Top 3 diagnoses
- Paget disease of the nipple
- Mastitis
- Inflammatory breast carcinoma

Additional diagnostic considerations
- Nipple adenoma
- Eczema of the breast

298 Superficial breast mass

Top 3 diagnoses
- Sebaceous cyst
- Epidermal inclusion cyst
- Focal infection

Additional diagnostic considerations
- Breast carcinoma
- Lymphoma
- Steatocystoma multiplex

299 Large breast mass

Top 3 diagnoses
- Phyllodes tumor
- Fibroadenoma
- Circumscribed breast carcinoma

Additional diagnostic considerations
- Hematoma
- Abscess

300 Complex cystic mass

Top 3 diagnoses
- Abscess
- Hematoma
- Cystic neoplasm

Additional diagnostic considerations
- Fat necrosis
- Cyst with debris

XIII Roentgen Classics

301 Left upper lobe collapse
302 Round atelectasis
303 Scimitar syndrome
304 Cecal volvulus
305 Epiploic appendagitis
306 Necrotizing enterocolitis
307 Hypertrophic pyloric stenosis
308 Nonaccidental trauma
309 Intussusception
310 Subclavian steal
311 Emphysematous cystitis
312 Salpingitis isthmica nodosa
313 MCA distribution cerebral infarction
314 Sturge-Weber syndrome
315 Epidermoid
316 Mesial temporal sclerosis
317 Ovarian dermoid
318 Cholelithiasis
319 Endometrioma
320 ACL tear
321 Posterior dislocation of the shoulder
322 Bucket-handle tear of the medial meniscus
323 Sacral insufficiency fracture
324 Brown fat
325 Milk of calcium

Index of Differential Diagnoses, by Case

A
Aberrant internal carotid artery, 117
Aberrant right subclavian artery, 173, 175, 245
Abscess
  appendiceal, 40
  breast, 278, 279, 288, 292, 299, 300
  CNS, 128, 149
  dental, 109
  hepatic, 29, 30, 157, 186, 189
  neck, 122
  oral cavity, 120
  pharyngeal, 108
  pulmonary, 3
  renal, 52, 53, 160, 190
  retroperitoneal, 54
  retropharyngeal, 111, 161
Achalasia, 33
Achondroplasia, 164, 166
ACL tear, 320
Acquired immunodeficiency syndrome cholangiopathy, 50
Acrania, 219
Acro-osteolysis, 90
Acute disseminated encephalomyelitis, 126, 127, 128, 147
Acute renal cortical necrosis, 55
Acute respiratory distress syndrome, 15
Acute tubular necrosis, 228
Adenoid cystic carcinoma, 105, 169
Adenomyomatosis, 191, 193
Adenomyosis, 182
Adnexal mass, 31, 40, 167, 188, 194, 317
Adrenal adenoma, 72
Adrenal hemorrhage, 72, 158
Adrenal myelolipoma, 72, 73
Adrenocortical carcinoma, 72, 158
Adynamic ileus, 46
Agenesis of the corpus callosum, 144, 211
Airway obstruction, 9
Alcohol abuse, 146
Allergic bronchopulmonary aspergillosis, 18
Alport syndrome, 55
Alveolar proteinosis, 13, 15
Alveolar sarcoidosis, 14
Alzheimer disease, 263
Amiodarone therapy, 26
Amniotic band syndrome, 219, 222
Amniotic shelves, 222
Amphetamine abuse, 233
Amyloid angiopathy, 141
Amyloidosis, 24, 44
Anal atresia, 162
Analgesic nephropathy, 56, 58
Anaplastic astrocytoma, 126
Anencephaly, 219
Aneurysmal bone cyst, 93, 94, 97
Angiodysplasia, 244
Angiomyolipoma, 51, 52, 73, 180, 239
Angiosarcoma, 23
Ankylosing spondylitis, 80
Annular pancreas, 165, 209
Annuloaortic ectasia, 243
Anorectal malformation, 162
Anterior meningocele, 167
Anticonvulsant therapy, 146
Aortic aneurysm, 11
Aortic occlusion, 235
Aortic transection, 249
Apical petrositis, 124
Appendiceal carcinoma, 40
Appendicitis, 40, 194
Aqueductal stenosis, 211
Arachnoid cyst, 133, 134
Arcuate uterus, 184
Arnold-Chiari malformation, 135, 203, 211
Arrhythmogenic right ventricular dysplasia, 25
Arteriovenous fistula, 113, 226, 239, 240
Arteriovenous malformation, 1, 132, 135, 141, 234, 239, 240, 242
Asbestosis, 7, 17
Ascariasis, 248
Aspergillosis, 15, 18, 21
Asphyxiating thoracic dysplasia, 164
Aspirated foreign body, 161, 169, 175
Asthmatic attack, 9
Astrocytoma, 137, 147, 148, 150, 166
Asymmetric breast tissue, 294
Atherosclerosis, 227, 229, 231, 232, 235, 236, 250
Atrial myxoma, 23
Atrial septal defect, 155
Atrioventricular canal defect, 155, 225
Autosomal dominant polycystic kidney disease, 66, 160, 214
Autosomal recessive polycystic kidney disease, 214

B
Bacterial tracheitis, 161
Benign prostatic hypertrophy, 69
Beta-hemolytic streptococcal pneumonia, 151
Bicornuate uterus, 184
Bicuspid aortic valve, 243
Biliary atresia, 260
Biliary cystadenoma, 29
Biliary obstruction, 248, 258
Bladder exstrophy, 218
Bladder rupture, 70
Blood clot (GU), 63, 65, 246
Bone cyst, 93
Bone infarct, 89
Brain death, 268
Brainstem glioma, 131
Branchial cleft cyst, 105, 122
Breast calcifications, 279, 280, 281
Breast carcinoma, 281, 283, 284, 285, 286, 287, 290, 292, 293, 295, 296, 297, 298, 299, 300
Breast cyst, 283, 288, 300
Breast MRI enhancement patterns, 277
Bronchial obstruction, 18
Bronchioloalveolar cell carcinoma, 13
Bronchogenic carcinoma, 1, 234, 264, 270, 275
Bronchogenic cyst, 11, 156
Brown fat, 324
Budd-Chiari syndrome, 27, 271
Buerger disease, 229

C
Caffey disease, 78
Candida, 34, 49, 63, 65, 189, 196
Carbon monoxide poisoning, 140
Carcinoid tumor, 41, 169, 234, 267
Cardiac fibroma, 210
Cardiac mass, 23, 24
Carotid artery aneurysm, 110, 241, 242
Carotid artery pseudoaneurysm, 110, 113

Carotid artery stenosis, 227
Carotid body tumor, 110
Carotid-cavernous fistula, 103
Castleman disease, 11, 285
Cavernous malformation, 132, 135, 141
Cecal carcinoma, 40
Cecal volvulus, 304
Celiac sprue, 46
Central neurocytoma, 145
Cerebello-olivary degeneration, 146
Cerebellopontine angle mass, 134
Chest wall abnormality, 9
Chiari malformation, 135, 203, 211
Cholangiocarcinoma, 29, 30, 50, 199, 248
Cholangitis, 50, 199
Cholecystitis, 193, 258
Choledochal anomaly, 31, 199
Choledocholithiasis, 199, 248
Cholelithiasis, 318
Cholesteatoma, 117, 124
Cholesterol granuloma, 117, 124
Chondroblastoma, 100
Chondrocalcinosis, 81, 84
Chondrodysplasia punctata, 164
Chondrosarcoma, 89, 109, 112, 124
Chordoma, 112
Chorioamniotic separation, 222
Choroid plexus carcinoma, 145
Choroid plexus cyst, 197, 224
Choroid plexus papilloma, 145
Choroid plexus tumor, 145
Chronic eosinophilic pneumonia, 13
Chronic glomerulonephritis, 55
Chronic transplant rejection, 55
Chronic venous stasis, 252
Ciliary dyskinesia, 18
Circumaortic left renal vein, 238
Circumcaval ureter, 62
Circumvallate placenta, 223
Cirrhosis, 27, 187, 271
Cleidocranial dysostosis, 86
Clonorchis, 248
Coarctation of the aorta, 243
Coats disease, 114
Cocaine abuse, 104
Coccidioidomycosis, 1, 2, 3, 4, 11, 16
Cochlear aplasia, 119
Colitis, 43, 244, 272
Collagen vascular disease, 7, 81, 229
Collimator defect, 273
Colloid cyst, 145, 266
Colon carcinoma, 43, 244
Confluent hepatic fibrosis, 27
Congenital adrenal hyperplasia, 158
Congenital cystic adenomatoid malformation, 156, 174, 204, 220
Congenital diaphragmatic hernia, 174, 204, 220
Congenital heart disease, 152, 153, 154, 155
Congenital lobar emphysema, 174, 204
Congenital pulmonary airway malformation, 156, 174, 204, 220
Congestive heart failure, 15, 291
Connective tissue disorder, 233, 243, 285
Contusion (CNS), 128, 141
Cord contusion, 147
Cord ischemia, 147
Corpus callosal lesion, 142
Corpus luteal cyst, 181
Cortical nephrocalcinosis, 55
Corticosteroid use, 172
CPPD arthropathy, 81, 84, 91
Craniopharyngioma, 130, 241
Crohn disease, 37, 42, 43, 44
Cross-fused renal ectopia, 64
Croup, 161
Cryptococcosis, 150
Cryptogenic organizing pneumonia, 13, 14
Crystal defect, 273
Crystalline arthropathy, 81, 91
CSF pulsations, 240
Cyclosporine toxicity, 228
Cystic adventitial disease, 236
Cystic cochleovestibular anomaly, 119
Cystic common cavity, 119
Cystic fibrosis, 8, 18, 162
Cystic hygroma, 122, 213
Cystic medial necrosis, 243
Cystitis, 71
Cytomegalovirus, 15

D

Dandy-Walker malformation, 133, 203, 211
Dehiscent jugular bulb, 117, 123
Demyelinating disease, 126, 127, 128, 137, 142, 147
Dermal calcifications, 280
Dermoid, 120, 167, 317
Desmoid tumor, 41
Desmoplastic infantile glioma, 148
Developing asymmetry, 294
Diabetes, 58
Diaphragmatic eventration, 220
Dichorionic/diamnionic twin pregnancy, 205
Didelphus uterus, 184
Diffuse axonal injury, 142
Disc extrusion, 149
Dissection, 113, 227, 231, 232, 235, 243, 249
Distal esophageal pulsion diverticulum, 28
Diverticulitis, 43, 244, 272
Diverticulosis, 244
Double aortic arch, 173, 175, 245
Double outlet right ventricle, 153, 212
Down syndrome, 86, 201, 224
Drop metastasis, 138
Drug toxicity, 7
Ductal carcinoma in situ, 281, 289, 293, 296
Duodenal atresia/stenosis, 165, 209
Duodenal web, 165
Duplicated inferior vena cava, 238
Duplication cyst (GI), 31, 167, 175, 194, 202
Dural arteriovenous fistula, 240
Dural ectasia, 166
Dwarfism, 164, 166
Dysembryoplastic neuroectodermal tumor, 148
Dysmyelinating disease, 127
Dystrophic breast calcifications, 280

E

Ebstein anomaly, 153
Echogenic intracardiac focus, 210
Ectopic kidney, 64
Ectopic pregnancy, 181
Eczema of the breast, 297
Edward syndrome, 201, 224
Effort thrombosis, 230
Ehlers-Danlos syndrome, 233, 243
Electronic artifact, 273
Ellis-van Creveld syndrome, 164
Embolic disease (non-septic), 229, 235, 236, 250
Emphysema, 6
Emphysematous cholecystitis, 191
Emphysematous cystitis, 311
Empyema, 20
Encephalocele, 213, 219
Encephalomalacia, 136
Enchondroma, 89, 93
Endobronchial lesion, 264
Endobronchial spread of tumor, 5
Endocardial cushion defect, 155, 225
Endometrial carcinoma, 182, 183
Endometrial hyperplasia, 183
Endometrial polyps, 183

Endometrioma, 188, 319
Endstage renal disease (hemodialysis), 66
Enteritis, 272
Enthesioneuroblastoma, 121
Eosinophilic pneumonia, 13, 14
Ependymoma, 131, 135, 137, 145, 147, 166, 240
Epidermal inclusion cyst, 298
Epidermoid cyst, 120, 134, 171, 315
Epididymo-orchitis, 192
Epidural abscess, 149
Epidural hematoma, 149
Epidural lipomatosis, 149
Epiglottitis, 161
Epiphrenic diverticulum, 28
Epiploic appendagitis, 305
Erosive osteoarthritis, 82
Esophageal atresia, 175
Esophageal carcinoma, 32, 33, 34, 35, 45
Esophageal pseudodiverticuli, 28, 34
Esophageal stricture, 33
Esophageal ulcers, 35
Esophageal varices, 32
Esophagitis
Candida, 34
caustic, 35, 45
drug-induced, 34, 35, 45
iatrogenic, 45
radiation, 45
reflux, 32, 33, 34, 35, 45
viral, 35
Ewing sarcoma, 93, 109, 168, 171, 256
Extracapsular implant rupture, 276
Extradural spinal mass, 149
Extramedullary hematopoiesis, 12
Extraperitoneal bladder rupture, 70
Extrinsic bladder compression, 65

F
Facial nerve schwannoma, 117
Fat necrosis, 279, 282, 286, 290, 294, 300
Fatty infiltration of the liver, 178, 189
Fetal central nervous system (CNS) anomalies, 216
Fetal demise, 206, 215
Fetal gastrointestinal (GI) anomalies, 216
Fetal hydrops, 216, 221
Fibroadenoma, 278, 279, 280, 283, 287, 299
Fibrocystic change, 278, 280, 281, 296
Fibroid, 182, 183
Fibrolamellar hepatocellular carcinoma, 48
Fibromuscular dysplasia, 227, 232, 250
Fibrosarcoma, 77
Fibrosing mediastinitis, 264
Fibrosing mesenteritis, 41
Fibrosis, 295
Fibrothorax, 17, 20
Fibrous dysplasia, 76, 93, 97, 170, 256, 274
Fibrous tumor of the pleura, 20
Focal nodular hyperplasia, 48, 178, 271
Foramen ovale, 225
Foreign body aspiration, 9, 161, 169, 175
Free technetium 99m, 254, 262
Friedreich ataxia, 146
Frostbite, 229
Functional immaturity of the colon, 162
Fungal disease, 1, 2, 3, 4, 11, 16, 21, 49, 196, 267, 270, 275
Fungal sinusitis, 104
Fungus ball, 63, 65, 246
Furosemide therapy (newborn), 56

G
Galactocele, 278, 282
Galactorrhea, 296
Gallbladder carcinoma, 193
Gallbladder polyp, 193
Gallbladder wall edema, 193
Gallbladder wall inflammation, 193
Gallium scan, 270
Ganglioglioma, 148
Ganglion cyst, 100
Ganglioneuroma, 12
Gastric carcinoma, 33, 37, 38, 39
Gastric ulcer, 37
Gastritis, 39
Gastroschisis, 218
Gaucher disease, 170, 172
Gel bleed, 276
Genitourinary activity, 259, 262
Germ cell tumor, 10, 129, 130, 167
Germinal matrix hemorrhage, 198
Germinoma, 129
Gestational trophoblastic disease, 183
GI bleed, 262, 272
GI duplication cyst, 31, 167, 175, 194, 202
Giant cell arteritis, 231, 235, 250
Giant cell tumor, 97, 100
Glioblastoma multiforme, 128, 141, 142, 242
Gliomatosis cerebri, 126, 139
Glomerulonephritis, 55
Glomus jugulare, 123
Glomus tumor, 110, 117, 123
Glomus tympanicum, 117
Glomus vagale, 110
Glycogen storage disease, 26
Gold therapy, 26
Gout, 81, 83, 91, 96
Gradenigo syndrome, 124
Graft-*versus*-host disease, 163
Granulomatous disease, 1, 2, 3, 4, 11, 49, 196, 267, 270, 275, 285
Gynecomastia, 292

H
Hajdu-Cheney syndrome, 90
Hamartoma, 1, 282, 287
Hemangioblastoma, 132, 135, 137, 240
Hemangioendothelioma, 157
Hemangioma, 48, 96, 101, 109, 111, 120, 121, 161, 178, 210
Hemarthrosis, 91
Hematocele, 179, 237
Hematoma
breast, 278, 279, 288, 292, 299, 300
groin, 226
hepatic, 157, 189
Hemochromatosis, 26, 81, 84
Hemoglobinopathy, 170
Hemorrhagic ovarian cyst, 176, 181, 188
Hemosiderosis, 26
Henoch-Schonlein purpura, 44
Hepatic adenoma, 48, 178
Hepatic congestion, 185
Hepatic cyst, 29, 30
Hepatic fibrosis, 27
Hepatic laceration (trauma), 29
Hepatic pseudotumor, 186
Hepatic schistosomiasis, 27
Hepatitis, 185
Hepatobiliary imaging, 258, 260
Hepatoblastoma, 157
Hepatocellular carcinoma, 48, 178, 185, 186, 189
Herpes encephalitis, 139
Heterotopic gray matter, 143
Hiatal hernia, 11
Hirschsprung disease, 162
Histoplasmosis, 1, 2, 3, 4, 11, 16, 49, 196
Holoprosencephaly, 144, 211
Horseshoe kidney, 64

Hydranencephaly, 144
Hydrocele, 237
Hydrocephalus, 144, 211
Hydronephrosis, 160
Hypercalcemia, 56
Hypercoagulable states, 187, 230
Hyperparathyroidism, 84, 90
Hypersensitivity pneumonitis, 5
Hypertensive hemorrhage, 132, 135
Hyperthyroidism, 255
Hypertrophic gastritis, 39
Hypertrophic osteoarthropathy, 252
Hypertrophic pyloric stenosis, 307
Hypoplastic left heart syndrome, 212
Hypotension, 57
Hypothalamic glioma, 130
Hypothalamic hamartoma, 130
Hypothenar hammer syndrome, 229
Hypothyroidism, 86
Hypoxic-ischemic encephalopathy, 140, 198

I
Idiopathic Madelung deformity, 87
Idiopathic pulmonary fibrosis, 7
Idiopathic Wormian bones, 86
Ileal atresia, 162
Ileus, 46
Iliac artery aneurysms, 68
Immune hydrops, 221
Implant herniation, 276
Implant rupture, 276
Indium 111-labeled WBC scan, 272
Infantile cortical hyperostosis, 78
Infarct (CNS), 125, 128, 132, 135, 136, 139, 140, 141, 150
Infectious bronchiolitis, 5
Infectious colitis, 43, 244, 272
Inferior vena cava occlusion, 238, 240
Infiltrated dose, 253
Inflammatory bowel disease, 42, 43, 80, 262, 272
Inflammatory breast cancer, 284, 297
Inflammatory colitis, 244
Inflammatory polyp, 169
Innominate artery compression syndrome, 173
Insufficiency fracture, 99
Internal jugular venous thrombosis, 110
Intracapsular implant rupture, 276
Intracranial hypotension, 116, 135
Intraductal papillary mucinous tumor, 47
Intraductal papilloma, 283, 287, 288, 289, 296
Intradural extramedullary spinal mass, 138
Intrahepatic cholestasis, 260
Intramammary lymph node, 283, 287
Intramedullary spinal mass, 137
Intramural hematoma, 249
Intraosseous ganglion cyst, 100
Intraperitoneal bladder rupture, 70
Intrauterine growth restriction, 215
Intraventricular hemorrhage, 198
Intussusception, 194, 309
Invasive ductal carcinoma, 281, 284, 286, 293, 294, 295, 296
Invasive lobular carcinoma, 284, 294, 295
Inverted papilloma, 121
Iodine thyroid scan, 266
Iron deposition, 26
Ischemia (biliary), 50
Ischemic colitis, 43, 244
Ischemic enteritis, 42
Islet cell tumor, 36, 267

J
Jeune syndrome, 164
Joubert syndrome, 133, 203
Juvenile angiofibroma, 121
Juvenile chronic arthritis, 91
Juvenile pilocystic astrocytoma, 131, 135

K
Kaposi sarcoma, 21
Kernicterus, 140
Killian-Jamison diverticulum, 28

L
Labyrinthine ossificans, 119
Lactating adenoma, 278
Lacunar infarction, 150
Langerhans cell histiocytosis, 8, 76, 77, 85, 93, 94, 97, 100, 168, 171
Large vestibular aqueduct syndrome, 119
Laryngotracheal papillomatosis, 169
Laryngotracheobronchitis, 161
Lasix therapy (newborn), 56
Lateral hypopharyngeal diverticulum, 28
Le Fort fracture, 102
Left upper lobe collapse, 301
Left ventricular aneurysm, 22
Legg-Calve-Perthes disease, 172
Leigh syndrome, 140
Leiomyoma, 182, 183
Leptomeningeal carcinomatosis, 125
Leptomeningeal cyst, 171
Leukemia, 49, 85, 88, 115, 171, 185, 200
Leukodystrophy, 127
Limb-body wall complex, 218
Limbic encephalitis, 139
Lingual thyroid, 120
Lipoid pneumonia, 13
Lipoma, 25, 282, 292
Lipomatosis, 62, 68, 149
Lipomatous hypertrophy, interatrial septum, 25
Ludwig angina, 120
Lunate dislocation, 95
Lung perfusion scan, 254, 264
Lymphadenopathy
- abdominopelvic, 41, 54, 68, 267
- axillary, 285
- mediastinal, 11, 16
- neck, 110, 122, 261, 269
- parotid, 105, 106
- retropharyngeal, 111

Lymphangioleiomyomatosis, 6
Lymphangioma, 101, 109, 111, 120, 122, 167
Lymphangitic spread of tumor, 19
Lymphedema, 284, 291
Lymphocytic interstitial pneumonitis, 6, 19
Lymphoepithelial lesions, 106
Lymphoma
- bone, 76, 77, 85, 256
- breast, 285, 298
- cecum, 40
- chest, 10, 11, 12, 16, 19, 21, 270
- CNS, 126, 128, 142
- esophageal, 32
- gastric, 37, 38, 39
- hepatic, 185, 186, 189
- neck, 108, 111, 124
- orbital, 101, 107, 115
- pancreatic, 36
- parotid, 105
- renal, 51, 52, 159, 190
- retroperitoneal, 54
- sinuses, 104
- small bowel, 40, 42, 44
- splenic, 49, 196
- testicular, 200

Lymphoproliferative disorder, 19

M
Madelung deformity, 87
MAG 3 renal scan, 265
Malrotation, 165, 209

Mammary ductal ectasia, 289, 296
Marchiafava-Bignami disease, 142
Marginal insertion of the cord, 217
Mastectomy, 9
Mastitis, 284, 297, 298
Maternal diabetes mellitus, 216
MCA distribution cerebral infarction, 313
Meckel diverticulum, 194, 259
Meckel-Gruber syndrome, 214
Meconium aspiration, 152
Meconium ileus, 162
Median arcuate ligament syndrome, 250
Mediastinal hematoma, 12
Mediastinal lymphadenopathy, 11, 16
Mediastinal mass
anterior, 10
middle, 11
posterior, 12
Medullary carcinoma, 61, 293
Medullary nephrocalcinosis, 56
Medullary sponge kidney, 56
Medulloblastoma, 131, 135
Mega cisterna magna, 133
Megacava, 238
Megacystis-microcolon-intestinal hypoperistalsis (MMIH) syndrome, 207
MELAS, 140
Ménétrier disease, 39
Meningioma, 101, 103, 115, 123, 129, 134, 138, 145, 241, 242
Meningitis, 116, 125
Meningocele, 167
Meniscal tear ("bucket handle"), 322
Mesenchymal hamartoma, 157
Mesenteric adenitis, 194
Mesenteric cyst, 31
Mesial temporal sclerosis, 316
Mesoblastic nephroma, 159
Mesothelioma, 20, 41
Metabolic disease, 86, 255
Metastatic disease, 267
adrenal, 72
biliary, 50
bone, 76, 79, 85, 88, 93, 94, 98, 168, 255, 256
breast, 285, 292
cardiac, 23
CNS, 116, 126, 128, 132, 135, 137, 138, 141, 143, 149
gastric, 37, 38, 39
hepatic, 27, 29, 30, 157, 178, 185, 186, 189
hypervascular, 48, 234
mesenteric, 41
neck, 110, 122, 261, 269
nodal, 111
orbital, 101
pancreas, 36
pulmonary, 1, 2, 3, 4, 11, 16, 20, 234, 275
renal, 52, 190
skull base, 112, 123, 124
small bowel, 42, 44
splenic, 49, 196
ureteral, 63
Meyer dysplasia, 172
Microabscesses, 49
Microvascular ischemic disease, 126
Midcarpal dislocation, 95
Midgut volvulus, 165, 209
Milk of calcium, 281, 325
Misaligned SPECT images, 251
Mitochondrial disorder, 140
Monochorionic/diamnionic twin pregnancy, 205
Monochorionic/monoamnionic twin pregnancy, 205
Moyamoya disease, 242
Mucinous carcinoma, 293
Mucinous cystadenoma, 47
Mucocele, 40, 124
Mucoepidermoid, 105, 108, 169
Mucopolysaccharidosis, 166
Mucus plug, 264
Multicystic dysplastic kidney, 53, 160
Multi-infarct dementia, 263
Multilocular cystic nephroma, 53, 61, 160
Multiple hereditary exostoses, 170
Multiple myeloma, 76
Multiple sclerosis, 126, 127, 128, 142, 147
Multivessel coronary artery disease, 251
Mycobacterium avium complex, 5, 18
Mycotic emboli, 233
Myelofibrosis, 79
Myelomeningocele, 202, 213, 219
Myeloproliferative disorder, 255
Myocardial infarction/scar, 24
Myocarditis, 24
Myositis (orbital), 107
Myositis ossificans, 96

N

Necrotizing enterocolitis, 306
Necrotizing pneumonia, 174
Neointimal hyperplasia, 247
Neonatal hepatitis, 260
Neonatal pneumonia, 152
Nephrectomy, 60
Nephroblastomatosis, 159
Nephrolithiasis, 63, 65, 246
Nerve sheath tumor, 103, 109, 110, 122, 138
Neuroblastoma, 12, 158, 267
Neuroblastoma metastases, 88, 171
Neurocystocercosis, 150
Neuroendocrine tumor, 267
Neuroenteric cyst, 12
Neurofibroma, 109, 110, 138
Neurogenic tumor, 12
Neuroglial cyst, 150
Neutropenic colitis, 163
Nipple adenoma, 297
Nipple discharge, 296
Nodal metastases, 111
Nonaccidental trauma, 308

O

Obstruction (urinary), 57, 58, 74, 246
Octreoscan, 267
Off-peak gamma camera, 253
Oil cyst, 279, 280, 282
Oligodendroglioma, 148
Oligohydramnios, 215
Omphalocele, 218
Oncocytoma, 51, 239
Optic nerve glioma, 115, 130
Optic nerve sheath meningioma, 115
Optic neuritis, 115
Orbital pseudotumor, 107
Orbital wall blowout fracture, 102
Osmotic demyelination, 140
Osteoarthritis, 80, 81, 82
Osteoblastoma, 94
Osteogenesis imperfecta, 86
Osteoid osteoma, 77, 257, 274
Osteomalacia, 255
Osteomyelitis, 76, 77, 78, 85, 88, 89, 94, 168, 171, 257, 274
Osteopetrosis, 79, 170
Osteopoikilosis, 98
Osteosarcoma, 109, 168
Ovarian cyst, 31, 167, 176, 181, 188
Ovarian dermoid, 167, 317
Ovarian hyperstimulation syndrome, 177
Ovarian neoplasm, 176, 188
Ovarian torsion, 176, 177
Oxalosis, 55

P

Pachymeningitis, 116

Paget disease, 79, 98, 255, 256
Paget disease of the nipple, 297
Paget-von Schroetter syndrome, 230
Pancreatic adenocarcinoma, 36, 37, 199, 248
Pancreatic pseudocyst, 31, 47
Pancreatitis, 199, 248
Papillary carcinoma, 278, 289, 293, 296
Papillary necrosis, 56, 58, 246
Papilloma, 169, 283, 287, 288, 289, 296
Paraganglioma, 110, 117, 123, 267
Paraneoplastic syndrome, 146
Parasitic infection, 248
Parathyroid adenoma, 195, 261
Parkinson disease, 263
Parotid carcinoma, 105
Patau syndrome, 201
Patent ductus arteriosus, 155
Pathologic fracture, 99
Pelvic hematoma, 68
Pelvic inflammatory disease, 176
Pentalogy of Cantrell, 218
Peptic ulcer disease, 38
Pericardial cyst, 11, 22
Pericarditis, 22
Perilunate dislocation, 95
Perinephric hemorrhage, 67
Perineural spread of tumor, 103
Periosteal reaction, 78
Periportal infection/inflammation, 187
Periventricular leukomalacia, 197, 198
Persistent hyperplastic primary vitreous, 114
PET scan, 275, 324
Petrositis, 124
Pheochromocytoma, 72, 158, 267
Photomultiplier tube failure, 273
Phyllodes tumor, 299
Physiologic periosteal reaction, 78
Pick disease, 263
Pigmented villonodular synovitis, 91, 92
Pineal cell tumor, 129
Pineal cyst, 129
Pineoblastoma, 129
Pineocytoma, 129
Pituitary macroadenoma, 112, 241
Placenta accreta, 217
Placenta increta, 217
Placenta percreta, 217
Placenta previa, 217
Placental venous lakes, 223
Plasma cell granuloma, 156
Plasmacytoma, 112
Pleomorphic adenoma, 105, 108, 169
Pleurodesis, 17
Pneumobilia, 185
Pneumoconiosis, 4, 5, 8, 16, 19
Pneumocysitis pneumonia, 6, 15, 21
Pneumonia, 1, 15, 275
Pneumothorax, 9
Poland syndrome, 9
Polyarteritis nodosa, 233
Polycystic ovarian syndrome, 177
Polyhydramnios, 216
Poor radiopharmaceutical preparation, 253
Popliteal artery aneurysm, 236
Popliteal artery entrapment syndrome, 236
Popliteal artery occlusion, 236
Porcelain gallbladder, 191
Porencephalic cyst, 136, 197
Portal hypertension, 187
Portal venous gas, 185
Posterior shoulder dislocation, 321
Posterior urethral valves, 207, 215
Postinfectious urethral stricture, 75
Postsurgical changes (breast), 284, 286, 290, 295
Postsurgical changes (ureter), 62
Postsurgical changes (vagotomy), 33
Post-transplant arterial ischemia, 50
Post-transplant lymphoproliferative disorder, 19, 163
Preduodenal portal vein, 165
Premature rupture of membranes, 215
Primary megaloureter, 74
Primary sclerosing cholangitis, 50, 248
Progressive multifocal leukoencephalopathy, 126, 127
Prostaglandin therapy, 78
Prostate adenocarcinoma, 69
Prostatitis, 69
Proximal esophageal pulsion diverticulum, 28
Prune-belly syndrome, 74, 207
Pseudoaneurysm, 113, 226, 249
Pseudoangiomatous stromal hyperplasia, 294
Pseudodiverticulosis (esophageal), 28, 34
Pseudomembranous colitis, 163
Psoas muscle hypertrophy, 62, 68
Psoriasis, 291
Psoriatic arthropathy, 80, 82, 83, 90
Pulmonary artery aneurysm, 11, 234
Pulmonary artery atresia, 264
Pulmonary artery hypertension, 11
Pulmonary artery stenosis, 264
Pulmonary atresia, 153
Pulmonary contusion, 14
Pulmonary edema, 15
Pulmonary embolism, 9, 264
Pulmonary hemorrhage, 15
Pulmonary hypoplasia, 151
Pulmonary infarct, 14
Pulmonary nodule
  cavitary, 3
  centrilobular, 5
  miliary, 4
  multiple, 2
  perilymphatic, 19
  solitary, 1
Pulmonary sling, 173, 175, 245
Pyelonephritis, 52, 57, 58, 60, 67
Pyeloureteritis cystica, 63
Pyocele, 179, 237
Pyonephrosis, 59

R
Radial fold, 276
Radial scar, 286, 290
Radiation injury, 231, 250, 284
Radiolucent calculi, 63, 65
Ranula, 120
Rathke cleft cyst, 130
Raynaud disease, 229
Reactive arthropathy, 80, 82, 83
Reflex sympathetic dystrophy, 257
Reflux esophagitis, 32, 33, 34, 35, 45
Reflux nephropathy, 60
Regenerating nodular cirrhosis, 271
Renal agenesis, 215
Renal artery aneurysm, 233
Renal artery stenosis, 228, 265
Renal calculi, 63, 65, 246
Renal cell carcinoma, 51, 52, 53, 59, 61, 73, 159, 180, 190, 239
Renal contusion, 57
Renal cyst, 53, 180, 190
Renal duplication, 64
Renal failure, 291
Renal infarct, 60
Renal osteodystrophy, 79, 255
Renal tubular acidosis, 56
Renal vein thrombosis, 57, 58, 228
Respiratory bronchiolitis-associated interstitial lung disease, 5
Respiratory syncytial virus, 15
Retained activity, 254
Retained products of conception, 183

Retinoblastoma, 114
Retinopathy of prematurity, 114
Retroaortic left renal vein, 238
Retrocaval ureter, 62
Retroperitoneal fibrosis, 54, 62
Retroperitoneal hemorrhage, 54
Retroperitoneal liposarcoma, 54, 73
Retroperitoneal sarcoma, 54, 73
Retroplacental hematoma, 223
Rhabdomyoma, 23, 210
Rhabdomyosarcoma, 23, 109, 121, 202
Rheumatoid arthritis, 2, 3, 7, 80, 81, 82, 83, 92
Rickets, 86, 88
Right aortic arch with aberrant left subclavian artery, 173, 175, 245
Right-to-left shunt, 254
Ring enhancing lesion, 128
Round atelectasis, 302
Round pneumonia, 1, 156
“Rugger jersey” spine, 79

S

Sacral insufficiency fracture, 323
Sacrococcygeal teratoma, 167, 202
Sacroiliitis, 80
Salivary gland neoplasm, 105, 108, 169
Salpingitis isthmica nodosa, 312
Sarcoidosis, 8, 11, 14, 16, 19, 24, 27, 49, 103, 106, 107, 115, 116, 125, 267, 270, 275
Sarcoma (retroperitoneal), 54, 73
Sarcoma (soft tissue), 96, 109
Schistosomiasis, 27, 71
Schizencephaly, 136, 144
Schwannoma, 103, 109, 110, 117, 122, 123, 134, 138, 240
Scimitar syndrome, 303
Scleroderma, 7, 33, 46, 90, 96
Scurvy, 88
Sebaceous cyst, 298
Septated uterus, 184
Septic arthritis, 80, 83, 87, 91
Septic emboli, 2, 3, 233
Sequestration, 156, 158, 204, 220
Sequestrum, 77
Seroma, 288
Serous cystadenoma, 47
Sestamibi imaging, 261
Severe hepatocellular disease, 258, 260
Shin/quadriceps splints, 252
Shock bowel, 163
Sickle cell anemia, 58, 170, 172
Silicosis, 8, 16
Single ventricle, 154
Sinonasal carcinoma, 104
Sinonasal polyps, 121
Sjögren syndrome, 106
Skeletal dysplasia, 87
Skin thickening, 284, 291
Small bowel hemorrhage, 44
Small bowel obstruction, 46
Solid and papillary epithelial neoplasm, 36, 47
Speed kidney, 233
Spinocerebellar ataxia, 146
Splenic infarcts, 49
Sporadic olivopontocerebellar atrophy, 146
Squamous cell carcinoma, 3, 108, 109, 120, 124
Staghorn calculus, 59
Status epilepticus, 139
Steatocystoma multiplex, 298
Stress fracture, 274
Striated nephrogram, 57
Stroke, 125, 128, 132, 135, 136, 139, 140, 141, 150
Stromal fibrosis, 294
Sturge-Weber syndrome, 314
Subarachnoid hemorrhage, 125
Subchorionic hematoma, 223
Subclavian steal, 310
Subclavian vein occlusion, 230
Subdural hemorrhage, 116
Subendocardial ischemia, 251
Subependymal cyst, 197
Subependymal giant cell astrocytoma, 145
Subependymoma, 145
Succenturiate lobe, 223
Sulfur colloid scan, 271
Superior vena cava syndrome, 271, 284, 291
Superscan, 255
Suprasellar mass, 130, 241
Surfactant deficiency, 151
Swyer-James syndrome, 9
Synovial (osteo)chondromatosis, 92, 96
Synovial cyst, 149
Syphilis, 88
System lupus erythematosis, 7, 81
Systolic dysfunction, 251

T

Tagged Tc-RBC scan, 262
Takayasu arteritis, 231, 235, 250
Tc99m-HMPAO scan, 268
Temporal bone fracture, 118
Teratoma, 10, 167, 202, 210, 213
Terminal ileitis, 42, 43
Testicular cyst, 200
Testicular fracture, 192
Testicular hematoma, 192
Testicular neoplasm, 200
Testicular torsion, 192
Tetralogy of Fallot, 153, 212
Thalassemia, 170
Thanatophoric dysplasia, 164
Thoracic outlet syndrome, 229
Thoratrast, 26
Thornwaldt cyst, 108
Thromboangiitis obliterans, 229
Thrombus (cardiac), 23
Thymic lesion, 10
Thyroglossal duct cyst, 120, 122, 195
Thyroid adenoma, 261, 266
Thyroid associated orbitopathy, 107
Thyroid carcinoma, 195, 261, 266, 267
Thyroid lesion, 10, 195, 261
Thyroid nodule, 195
TIPS dysfunction, 247
TIPS thrombosis, 247
Tolosa-Hunt syndrome, 103
TORCH infections, 78, 143, 197, 198
Tortuous internal carotid artery, 111
Total anomalous pulmonary venous return, 154
Toxic shock syndrome, 185
Toxocariasis, 114
Tracheoesophageal fistula, 175
Traction diverticulum (midesophagus), 28
Transient ischemic dilatation, 251
Transient tachypnea of the newborn, 152
Transitional cell carcinoma, 51, 59, 61, 63, 65, 71, 246
Transplant rejection, 55, 228
Transposition of the great arteries, 154, 212
Transverse myelitis, 147
Trauma, 78, 87, 90, 99, 172, 187, 229, 233, 236, 243, 257
Tricuspid atresia, 153, 154
Tripod fracture, 102
Trisomy 13, 201, 214
Trisomy 18, 201, 224
Trisomy 21, 86, 201, 224
Truncus arteriosus, 154, 212
Tuberculosis, 1, 2, 3, 4, 5, 8, 11, 16, 18, 21, 42, 49, 56, 58, 71, 94, 196, 267, 270, 275

Tuberous sclerosis, 66, 143
Tubo-ovarian abscess, 176, 188
Tubular carcinoma, 286, 290
Tumor thrombus (portal vein), 187
Tumoral calcinosis, 96
Turner syndrome, 87, 201
Twin-to-twin transfusion syndrome, 206
Two-vessel umbilical cord, 208
Typhlitis, 163

U
Ulcerative colitis, 42, 43
Umbilical cord hemangioma, 208
Umbilical cord hematoma, 208
Umbilical cord varix, 208
Unicameral bone cyst, 93, 97
Urachal carcinoma, 71
Ureteral obstruction, 74, 246
Urethral carcinoma, 75
Urethral injury, 70, 75
Urethral stricture, 75
Urethral trauma, 75
Urinary extravasation, 67
Urinary obstruction, 57, 58, 74, 215, 228, 246, 265
Usual interstitial pneumonia, 7
Uterine synechiae, 222

V
Vagotomy, 33
Varicella (healed), 4
Varices (esophageal), 32
Varicocele, 179, 237
Vascular breast calcifications, 281
Vascular malformation, 1, 132, 135, 141, 234, 239, 240, 242
Vascular ring, 173, 175
Vascular thrombosis, 110, 113
Vasculitis, 15, 60, 126, 229, 231, 233, 235, 250
Velamentous insertion of the cord, 217
Venolymphatic malformation, 109, 111, 120, 121, 122
Venous stasis, 252
Ventricular septal defect, 155, 225
Ventriculomegaly, 144, 211
Vermian hypoplasia, 133
Vertebra plana, 85
Vertebral body scalloping, 166
Vesicoureteral reflux, 74, 207
Vestibular schwannoma, 134
Virchow-Robin spaces, 150
von Hippel-Lindau disease, 66

W
Warthin tumor, 105, 106
Wegener disease, 2, 3, 104, 233
Wharton jelly cyst, 208
Whipple disease, 44
Wilms tumor, 53, 159, 160
Wilson disease, 84, 140
Wormian bones, 86

X
Xanthogranulomatous pyelonephritis, 59

Z
Zenker diverticulum, 28
Zollinger-Ellison syndrome, 38

Index of Key Findings

Note: The index is ordered by case number within each section.

I Chest and Cardiac Imaging

1—Solitary pulmonary nodule
2—Multiple pulmonary nodules
3—Cavitary pulmonary nodule
4—Miliary pulmonary nodules
5—Centrilobular pulmonary nodules
6—Cystic lung disease
7—Lower lobe interstitial disease
8—Upper lobe interstitial disease
9—Hyperlucent lung
10—Anterior mediastinal mass
11—Middle mediastinal mass
12—Posterior mediastinal mass
13—Chronic air space disease
14—Peripheral air-space disease
15—Ground-glass opacification
16—Mediastinal/hilar lymphadenopathy
17—Calcified pleural disease
18—Bronchiectasis
19—Perilymphatic pulmonary nodules
20—Pleural-based mass
21—Parenchymal disease in an HIV patient
22—Abnormal left ventricular contour
23—Cardiac mass
24—Delayed myocardial enhancement
25—Cardiac wall fat deposition

II Gastrointestinal Imaging

26—Hyperdense liver
27—Nodular liver contour
28—Esophageal diverticulum
29—Solitary hypodense, hypovascular liver mass
30—Multiple hypoattenuating hepatic lesions
31—Right upper quadrant cystic mass in a child
32—Esophageal submucosal masses/thickened folds
33—Esophageal dilatation
34—Esophageal pseudodiverticula
35—Esophageal ulcers
36—Solid pancreatic mass
37—Linitis plastica
38—Gastric ulcer
39—Gastric fold thickening
40—Cecal mass
41—Mesenteric mass
42—Terminal ileal wall thickening
43—Colonic wall thickening
44—Small bowel wall thickening
45—Esophageal stricture
46—Small bowel dilatation
47—Cystic pancreatic mass
48—Hypervascular liver mass
49—Multiple splenic masses
50—Intrahepatic biliary ductal strictures

III Genitourinary Imaging

51—Solid renal mass
52—Multiple bilateral renal lesions/masses
53—Cystic renal mass
54—Retroperitoneal mass
55—Cortical nephrocalcinosis
56—Medullary nephrocalcinosis
57—Striated nephrogram
58—Papillary necrosis
59—Staghorn calculus
60—Renal cortical defect
61—Renal pelvic mass
62—Medial deviation of the ureters
63—Ureteral filling defect
64—Renal migration anomaly
65—Bladder filling defect
66—Bilateral renal cysts
67—Perinephric fluid collection
68—Pear-shaped bladder
69—Prostate enlargement
70—Bladder rupture
71—Bladder wall calcifications
72—Adrenal mass
73—Fatty retroperitoneal mass
74—Dilated ureter
75—Urethral stricture

IV Musculoskeletal Imaging

76—Multiple lytic foci
77—Sequestrum
78—Periosteal reaction in a newborn/infant
79—"Rugger jersey" spine
80—Sacroiliitis
81—Proximal arthropathy affecting primarily the metacarpophalangeal (MCP) joints
82—Distal arthritis affecting primarily the interphalangeal joints
83—Erosive arthropathy involving the foot
84—Chondrocalcinosis
85—Vertebra plana in a child
86 –Wormian bones
87—Madelung deformity
88—Lucent metaphyseal bands
89—Medullary/chondroid lesion
90—Acro-osteolysis
91—Dense joint effusion
92—Loose bodies with erosions
93—Expansile rib lesion in a child
94—Posterior element lytic lesion
95—Carpal dislocation
96—Periarticular soft tissue calcifications
97—Benign expansile lytic lesion
98—Multiple sclerotic foci in the pelvis
99—Vertebral body wedge fracture
100—Epiphyseal equivalent lucent lesion

V Head and Neck Imaging

101—Enhancing orbital mass
102—Orbital rim fracture
103—Cavernous sinus mass/enhancement
104—Aggressive sinus disease with bony destruction
105—Unilateral parotid mass
106—Bilateral parotid masses
107—Orbital muscle enlargement
108—Pharyngeal mucosal mass
109—Masticator space mass
110—Carotid space mass
111—Retropharyngeal mass
112—Clival mass
113—Vascular injury to the neck
114—Globe lesion in a child
115—Optic nerve enlargement and enhancement
116—Pachymeningeal (dural) enhancement
117—Middle ear mass
118—Temporal bone trauma with mastoid fluid
119—Inner ear congenital malformation

120—Floor of the mouth mass
121—Aggressive nasal mass in an adolescent
122—Cystic neck mass
123—Jugular foramen mass
124—Petrous apex lesion
125—Leptomeningeal enhancement

VI Brain and Spine Imaging
126—Confluent white matter lesions in an adult
127—Confluent white matter lesions in a child
128—Ring-enhancing lesion
129—Pineal region mass
130—Sellar/suprasellar mass in a child
131—Posterior fossa mass in a child
132—Posterior fossa mass in an adult
133—Posterior fossa cyst
134—Cerebellopontine angle (CPA) mass
135—Cerebellar tonsillar herniation
136—CSF-lined cortical cleft
137—Enhancing intramedullary spinal mass
138—Intradural extramedullary spinal mass
139—Diffuse temporal lobe mass
140—Increased T2 signal intensity in basal ganglia/thalami in a child
141—Intraparenchymal hemorrhage
142—Corpus callosal lesion
143—Subependymal nodules
144—Massive supratentorial CSF collection in a newborn
145—Intraventricular mass
146—Cerebellar atrophy
147—Spinal cord signal abnormality
148—Cortically based enhancing neoplasm
149—Epidural spinal mass
150—Prominent periventricular/basal ganglia cystic lesions

VII Pediatric Imaging
151—Neonatal lung disease with low lung volumes
152—Neonatal lung disease with increased lung volumes
153—Cyanotic infant with decreased pulmonary flow
154—Cyanotic infant with increased pulmonary vascularity
155—Shunt vascularity
156—Solid pulmonary mass
157—Liver mass in an infant
158—Suprarenal mass in a child
159—Solid renal mass
160—Cystic renal lesion
161—Subglottic airway narrowing
162—Distal bowel obstruction in a neonate
163—Bowel wall thickening in an immunocompromised child
164—Skeletal dysplasia
165—"Double bubble" sign
166—Posterior vertebral body scalloping
167—Presacral mass
168—Long bone aggressive lesion
169—Endobronchial lesion in a child
170—Erlenmeyer flask deformity
171—Lytic skull lesion in a child
172—Avascular necrosis (AVN) of the femoral head
173—Vascular anomaly with esophageal and tracheal compression
174—Cystic pulmonary mass
175—Esophageal obstruction in a neonate

VIII Ultrasound Imaging
176—Enlarged ovary
177—Enlarged ovary with multiple peripheral follicles
178—Hyperechoic liver mass
179—Complex extratesticular fluid collection
180—Hyperechoic renal mass
181—Complex cystic adnexal mass with positive HCG
182—Enlarged heterogeneous uterus
183—Thickened endometrial stripe
184—Uterine anomaly
185—"Starry sky" liver
186—"Target" lesions in the liver
187—Portal vein thrombosis
188—Cystic adnexal mass with negative HCG
189—Multiple hypoechoic liver masses
190—Hypoechoic renal mass
191—Hyperechoic foci in gallbladder wall
192—Enlarged painful testicle
193—Gallbladder wall thickening
194—Right lower quadrant mass in a child
195—Thyroid mass
196—Multiple splenic hypoechoic foci
197—Periventricular cysts
198—Periventricular hyperechoic foci
199—Common bile duct (CBD) dilatation
200—Enlarged painless testicle

IX Fetal Imaging
201—Nuchal translucency
202—Sacral mass
203—Posterior fossa malformation
204—Hyperechoic thoracic mass
205—Twin development (chorionicity)
206—Twin pregnancy with asymmetric fetal size
207—Enlarged bladder (megacystis)
208—Umbilical cord vascular abnormality
209—"Double bubble" sign
210—Hyperechoic intracardiac focus
211—CNS ventriculomegaly
212—Cardiac outflow anomalies
213—Cystic posterior neck mass
214—Enlarged hyperechoic kidneys
215—Oligohydramnios
216—Polyhydramnios
217—Placental location abnormality
218—Abdominal wall defect
219—Cranial/calvarial defect
220—Diaphragm abnormality
221—Fetal hydrops
222—Linear echoes within the amniotic fluid
223—Placental abnormality/mass
224—Choroid plexus cyst
225—Ventricular septal defect

X Vascular and Interventional Radiology
226—Postprocedure arterial abnormality
227—Carotid artery stenosis
228—Failing renal transplant
229—Digital artery occlusion/ischemia
230—Subclavian vein occlusion
231—Great vessel stenosis
232—Renal artery stenosis
233—Intraparenchymal renal artery aneurysms
234—Hypervascular pulmonary mass
235—Infrarenal aortic occlusion
236—Popliteal artery occlusion
237—Extratesticular mass
238—Inferior vena cava vascular anomaly/abnormality
239—Hypervascular renal mass

240—Prominent paraspinal flow voids
241—Suprasellar mass in an adult
242—Hypervascular cerebral mass/abnormality
243—Aortic dissection
244—Lower GI bleeding
245—Vascular ring/sling
246—Urinary obstruction
247—TIPS dysfunction
248—Biliary duct occlusion
249—Traumatic aortic injury
250—Celiac axis stenosis/occlusion

XI Nuclear Medicine
251—Transient ischemic dilatation
252—Symmetric "tram track" cortical uptake of the long bones
253—Poor-quality bone scan
254—Extrapulmonary activity on a lung perfusion scan
255—Superscan
256—Increased activity and osseous expansion in the pelvis
257—Three-phase positive bone scan
258—Nonvisualization of gallbladder on hepatobiliary imaging
259—Focal intra-abdominal activity on pertechnetate imaging
260—Persistent hepatogram on neonatal hepatobiliary imaging
261—Persistent focal cervical uptake on delayed sestamibi imaging
262—Intra-abdominal activity on Tc99m-RBC scan
263—Decreased cortical FDG activity in the setting of dementia
264—Unilateral absent lung perfusion
265—Worsening renal function on MAG 3 renal scan following Captopril administration
266—Cold nodule on an I123 thyroid scan
267—Focal abdominal uptake on Octreoscan
268—Absent intracranial activity on Tc99m HMPAO scan
269—Focal neck uptake on an I131 postablation scan
270—Increased mediastinal uptake on a gallium scan
271—Focal increased hepatic uptake on sulfur colloid scan
272—Focal bowel uptake on an In111-labeled WBC scan
273—Focal defect on QC images
274—Focal increased activity within an extremity on bone scan
275—Solitary hypermetabolic pulmonary lesion on a PET scan

XII Breast Imaging
276—Implant defect
277—MRI enhancement patterns
278—Complex cystic mass in a lactating woman
279—Coarse calcifications in a partially circumscribed mass
280—Benign-appearing calcifications; rim, punctate, and round forms
281—Malignant-appearing calcifications; linear, branching forms
282—Fatty breast lesion
283—Well-circumscribed mass in a premenopausal woman
284—Unilateral skin thickening
285—Axillary lymphadenopathy
286—Mass with central lucency
287—Well-circumscribed solid breast mass
288—Well-circumscribed cystic breast mass
289—Ductal mass
290—Postoperative changes
291—Bilateral skin thickening
292—Breast lesion in a man
293—Well-circumscribed breast cancer
294—Developing asymmetry
295—Ill-defined, infiltrative breast mass
296—Breast lesion with nipple discharge
297—Unilateral nipple/skin changes
298—Superficial breast mass
299—Large breast mass
300—Complex cystic mass

XIII Roentgen Classics
301—Left upper lobe collapse
302—Round atelectasis
303—Scimitar syndrome
304—Cecal volvulus
305—Epiploic appendagitis
306—Necrotizing enterocolitis
307—Hypertrophic pyloric stenosis
308—Nonaccidental trauma
309—Intussusception
310—Subclavian steal
311—Emphysematous cystitis
312—Salpingitis isthmica nodosa
313—MCA distribution cerebral infarction
314—Sturge-Weber syndrome
315—Epidermoid
316—Mesial temporal sclerosis
317—Ovarian dermoid
318—Cholelithiasis
319—Endometrioma
320—ACL tear
321—Posterior dislocation of the shoulder
322—"Bucket handle" tear of the medial meniscus
323—Sacral insufficiency fracture
324—Brown fat
325—Milk of calcium